

Changsheng Liu  
Hongyan He *Editors*

# Developments and Applications of Calcium Phosphate Bone Cements

# Springer Series in Biomaterials Science and Engineering

Volume 9

**Series editor**

Prof. Min Wang

Department of Mechanical Engineering

The University of Hong Kong

Pokfulam Road, Hong Kong

e-mail: [memwang@hku.hk](mailto:memwang@hku.hk)

**Aims and scope**

The Springer Series in Biomaterials Science and Engineering addresses the manufacture, structure and properties, and applications of materials that are in contact with biological systems, temporarily or permanently. It deals with many aspects of modern biomaterials, from basic science to clinical applications, as well as host responses. It covers the whole spectrum of biomaterials – polymers, metals, glasses and ceramics, and composites/hybrids – and includes both biological materials (collagen, polysaccharides, biological apatites, etc.) and synthetic materials. The materials can be in different forms: single crystals, polycrystalline materials, particles, fibers/wires, coatings, non-porous materials, porous scaffolds, etc. New and developing areas of biomaterials, such as nano-biomaterials and diagnostic and therapeutic nanodevices, are also focuses in this series. Advanced analytical techniques that are applicable in R & D and theoretical methods and analyses for biomaterials are also important topics. Frontiers in nanomedicine, regenerative medicine and other rapidly advancing areas calling for great explorations are highly relevant.

The Springer Series in Biomaterials Science and Engineering aims to provide critical reviews of important subjects in the field, publish new discoveries and significant progresses that have been made in both biomaterials development and the advancement of principles, theories and designs, and report cutting-edge research and relevant technologies. The individual volumes in the series are thematic. The goal of each volume is to give readers a comprehensive overview of an area where new knowledge has been gained and insights made. Significant topics in the area are dealt with in good depth and future directions are predicted on the basis of current developments. As a collection, the series provides authoritative works to a wide audience in academia, the research community, and industry.

More information about this series at <http://www.springer.com/series/10955>

Changsheng Liu • Hongyan He  
Editors

# Developments and Applications of Calcium Phosphate Bone Cements

 Springer

*Editors*

Changsheng Liu  
Key Laboratory for Ultrafine Materials  
of Ministry of Education  
East China University of Science  
and Technology  
Shanghai, China

Hongyan He  
Engineering Research Center for  
Biomedical Materials of Ministry of  
Education  
East China University of Science  
and Technology  
Shanghai, China

ISSN 2195-0644

ISSN 2195-0652 (electronic)

Springer Series in Biomaterials Science and Engineering

ISBN 978-981-10-5974-2

ISBN 978-981-10-5975-9 (eBook)

DOI 10.1007/978-981-10-5975-9

Library of Congress Control Number: 2017954397

© Springer Nature Singapore Pte Ltd. 2018

This work is subject to copyright. All rights are reserved by the Publisher, whether the whole or part of the material is concerned, specifically the rights of translation, reprinting, reuse of illustrations, recitation, broadcasting, reproduction on microfilms or in any other physical way, and transmission or information storage and retrieval, electronic adaptation, computer software, or by similar or dissimilar methodology now known or hereafter developed.

The use of general descriptive names, registered names, trademarks, service marks, etc. in this publication does not imply, even in the absence of a specific statement, that such names are exempt from the relevant protective laws and regulations and therefore free for general use.

The publisher, the authors and the editors are safe to assume that the advice and information in this book are believed to be true and accurate at the date of publication. Neither the publisher nor the authors or the editors give a warranty, express or implied, with respect to the material contained herein or for any errors or omissions that may have been made. The publisher remains neutral with regard to jurisdictional claims in published maps and institutional affiliations.

Printed on acid-free paper

This Springer imprint is published by Springer Nature

The registered company is Springer Nature Singapore Pte Ltd.

The registered company address is: 152 Beach Road, #21-01/04 Gateway East, Singapore 189721, Singapore

# Preface

As automobile mechanics repair damaged cars with auto parts, biomaterial researchers thereby endeavor to repair the damaged body tissue through the appropriate “parts”. With the bionic concepts, they attempt to fabricate nonlife materials to participate in the process of life for achieving tissue regeneration and functional restoration. Therefore, exploring appropriate biomaterials is highly challenging and endless.

Typically, artificial bones can be used to restore bone defects after suffering comminuted fracture, osteoporotic compression fractures, or bone tumors by enucleating. In the 1980s, artificial bones have been the focus of most of the research related to biological ceramics. Although this material could imitate the composition and strength of human bones, the low plasticity limited its wide applications. Our group has started to study on the “biological calcium phosphate cement (CPC)” since the early 1990s. In the following two decades, my coworkers and I have made a series of in-depth exploration for this kind of self-setting CPCs: from powder preparation to curing process; from the preparation mechanism to process control; from the physicochemical properties to the biological performance; from cell experiments *in vitro* to animal study/clinic research *in vivo*; and from material development to enterprise establishment, clinical trial approval, clinical applications, and so on.

With the development of the novel materials and deep understanding of calcium phosphate-based materials and their biological performance, numerous researchers and scientists have made unremitting effort to further improve the biological performances and extend the potentials of the CPC materials according to the feedback from the clinical applications in recent years. By introducing functional materials into the CPC compositions, the various shapes of CPC were designed and fabricated for user-friendly operation and better properties according to different requirements. To improve the integration of artificial bone material and the bone, porous CPCs were successfully prepared at room temperature, allowing a quick ingrowth of cell and tissue into materials and a better degradation of the materials. Moreover, the combination of the growth factors and the bone repair materials further enhanced the osteoinduction activity of CPC and promoted the growth and differentiation of the cells/tissues, speeding up the degradation of materials and new bone formation.

Advanced manufacturing technologies as 3D printings were applied for producing the well-defined architecture, paving ways in bone tissue engineering and in personalized medicine of clinical orthopedic and orthodontic practices.

This book presents the state-of-the-art review of the latest advances in developing calcium phosphate bone cements and their applications. It includes 15 main chapters and covers the synthesis methods, characterization approaches, material modification, and novel binders, as well as the fabrication technologies of calcium phosphate-based biomaterials in regenerative medicine and their clinical applications. Methodologies for fabricating scaffolds and biofunctional surfaces/interfaces and subsequently modulating the host response to implantable/injectable materials are highlighted. This book integrates a series of discussions and knowledge of the calcium phosphate cements involving their physiochemical properties and biological performance *in vitro* and *in vivo*. Accordingly, the book not only covers the fundamentals but also opens new avenues for meeting future challenges in research and clinical applications.

I believe this book will be useful to current bone material developers who wish to have a complete view of the field, to newcomers who attempt to make the best choice between different technologies, and to academic researchers who engage in technology transfer activities and need to evaluate the hurdles from material development to clinic trials. I am especially grateful to the authors, my colleagues, who kindly accepted to undertake the absorbing task of writing a chapter. And, of course, the organizational support from Springer in the production of this book is gratefully acknowledged.

Shanghai, P.R. China

Changsheng Liu

# Contents

<b>1</b>	<b>Calcium Phosphate Bone Cements: Their Development and Clinical Applications.....</b>	<b>1</b>
	Fangping Chen, Xiaoyu Ma, Yuanman Yu, and Changsheng Liu	
<b>2</b>	<b>Self-Setting Calcium Orthophosphate (CaPO<sub>4</sub>) Formulations.....</b>	<b>41</b>
	Sergey V. Dorozhkin	
<b>3</b>	<b>Injectable Calcium Phosphate Cements for Hard Tissue Repair .....</b>	<b>147</b>
	Fangping Chen, Yuanman Yu, Xiaoyu Ma, and Changsheng Liu	
<b>4</b>	<b>Calcium Phosphate Composite Cement.....</b>	<b>187</b>
	Jing Wang and Changsheng Liu	
<b>5</b>	<b>Accelerating Biodegradation of Calcium Phosphate Cement.....</b>	<b>227</b>
	Hongyan He, Zhongqian Qiao, and Changsheng Liu	
<b>6</b>	<b>Bioactivation of Calcium Phosphate Cement by Growth Factors and Their Applications.....</b>	<b>257</b>
	Yifan Ma, Baolin Huang, Dan Lin, Yuan Yuan, and Changsheng Liu	
<b>7</b>	<b>Drug-Loading Calcium Phosphate Cements for Medical Applications .....</b>	<b>299</b>
	Shuxin Qu, Jie Weng, Ke Duan, and Yumei Liu	
<b>8</b>	<b>Biomimetic Ion-Substituted Calcium Phosphates.....</b>	<b>333</b>
	Jun Ma, Shenglong Tan, and Shengmin Zhang	
<b>9</b>	<b>Nanodimensional and Nanocrystalline Calcium Orthophosphates.....</b>	<b>355</b>
	Sergey V. Dorozhkin	



<b>10 Calcium Phosphate-Silk Fibroin Composites: Bone Cement and Beyond</b> .....	449
Fengxuan Han, Chen Shi, Huilin Yang, and Bin Li	
<b>11 Importance of Biomaterials In Vivo Microenvironment pH (<math>\mu</math>e-pH) in the Regeneration Process of Osteoporotic Bone Defects</b> .....	473
Wenlong Liu, Xiuli Dan, William Weijia Lu, and Haobo Pan	
<b>12 3D Printing of Calcium Phosphate Bio-scaffolds for Bone Therapy and Regeneration</b> .....	497
Hongshi Ma, Jiang Chang, and Chengtie Wu	
<b>13 Development of Biodegradable Bone Graft Substitutes Using 3D Printing</b> .....	517
Zhida Xia, Yunsong Shi, Hongyan He, Yuanzhong Pan, and Changsheng Liu	
<b>14 Preparation of Collagen/Calcium Phosphate Coatings and Evaluation of Their Biological Performances</b> .....	547
Cheng Kui, Jun Lin, and Wenjian Weng	
<b>15 Preclinical and Clinical Assessments of Calcium Phosphate Bone Cements</b> .....	597
Lingyan Cao, Deliang Zeng, Shuxian Lin, Xiao Wang, Xiangkai Zhang, Ao Zheng, Jie Wang, and Xinquan Jiang	

# Contributors

**Lingyan Cao** Department of Prosthodontics, Ninth People's Hospital, Shanghai JiaoTong University School of Medicine, Shanghai, China

Shanghai Key Laboratory of Stomatology & Shanghai Research Institute of Stomatology, National Clinical Research Center of Stomatology, Shanghai, China

**Jiang Chang** State Key Laboratory of High Performance Ceramics and Superfine Microstructure, Shanghai Institute of Ceramics, Chinese Academy of Sciences, Shanghai, China

**Fangping Chen** Engineering Research Center for Biomedical Materials of Ministry of Education, East China University of Science and Technology, Shanghai, China

**Xiuli Dan** School of Biomedical Sciences, Faculty of Medicine, The Chinese University of Hong Kong, Shatin, Hong Kong

**Sergey V. Dorozhkin** Kudrinskaja sq. 1-155, Moscow, Russia

**Ke Duan** Key Lab of Advanced Technologies of Materials, Ministry of Education, School of Materials Science and Engineering, Southwest Jiaotong University, Chengdu, China

**Fengxuan Han** Orthopedic Institute, Soochow University (South Campus), Suzhou, Jiangsu, China

Department of Orthopaedics, The First Affiliated Hospital of Soochow University, Suzhou, Jiangsu, China

**Hongyan He** Engineering Research Center for Biomedical Materials of Ministry of Education, East China University of Science and Technology, Shanghai, China

**Baolin Huang** Engineering Research Center for Biomedical Materials of Ministry of Education, East China University of Science and Technology, Shanghai, China

**Xinquan Jiang** Department of Prosthodontics, Ninth People's Hospital, Shanghai JiaoTong University School of Medicine, Shanghai, China

Shanghai Key Laboratory of Stomatology & Shanghai Research Institute of Stomatology, National Clinical Research Center of Stomatology, Shanghai, China

**Cheng Kui** School of Materials Science and Engineering, Zhejiang University, Hangzhou, China

**Bin Li** Orthopedic Institute, Soochow University (South Campus), Suzhou, Jiangsu, China

Department of Orthopaedics, The First Affiliated Hospital of Soochow University, Suzhou, Jiangsu, China

**Dan Lin** Engineering Research Center for Biomedical Materials of Ministry of Education, East China University of Science and Technology, Shanghai, China

**Jun Lin** School of Materials Science and Engineering, Zhejiang University, Hangzhou, China

**Shuxian Lin** Department of Prosthodontics, Ninth People's Hospital, Shanghai JiaoTong University School of Medicine, Shanghai, China

Shanghai Key Laboratory of Stomatology & Shanghai Research Institute of Stomatology, National Clinical Research Center of Stomatology, Shanghai, China

**Changsheng Liu** Key Laboratory for Ultrafine Materials of Ministry of Education, East China University of Science and Technology, Shanghai, China

**Wenlong Liu** Research Center for Human Tissue and Organs Degeneration, Institute of Biomedicine and Biotechnology, Shenzhen Institutes of Advanced Technology, Chinese Academy of Sciences, Shenzhen, China

**Yumei Liu** Key Lab of Advanced Technologies of Materials, Ministry of Education, School of Materials Science and Engineering, Southwest Jiaotong University, Chengdu, China

**William Weijia Lu** Department of Orthopaedics and Traumatology, Faculty of Medicine, The University of Hong Kong, Pok Fu Lam, Hong Kong

**Hongshi Ma** State Key Laboratory of High Performance Ceramics and Superfine Microstructure, Shanghai Institute of Ceramics, Chinese Academy of Sciences, Shanghai, China

**Jun Ma** Advanced Biomaterials and Tissue Engineering Center, Huazhong University of Science and Technology, Wuhan, China

**Xiaoyu Ma** Engineering Research Center for Biomedical Materials of Ministry of Education, East China University of Science and Technology, Shanghai, China

**Yifan Ma** Engineering Research Center for Biomedical Materials of Ministry of Education, East China University of Science and Technology, Shanghai, China

**Haobo Pan** Research Center for Human Tissue and Organs Degeneration, Institute of Biomedicine and Biotechnology, Shenzhen Institutes of Advanced Technology, Chinese Academy of Sciences, Shenzhen, China

**Yuanzhong Pan** Engineering Research Center for Biomedical Materials of Ministry of Education, East China University of Science and Technology, Shanghai, China

**Zhongqian Qiao** Engineering Research Center for Biomedical Materials of Ministry of Education, East China University of Science and Technology, Shanghai, China

**Shuxin Qu** Key Lab of Advanced Technologies of Materials, Ministry of Education, School of Materials Science and Engineering, Southwest Jiaotong University, Chengdu, China

**Chen Shi** Department of Chemical and Materials Engineering, University of Alberta, Edmonton, Canada

**Yunsong Shi** Centre for Nanohealth, Swansea University Medical School, Singleton Park, Swansea, UK

**Shenglong Tan** Advanced Biomaterials and Tissue Engineering Center, Huazhong University of Science and Technology, Wuhan, China

**Jie Wang** Department of Prosthodontics, Ninth People's Hospital, Shanghai JiaoTong University School of Medicine, Shanghai, China

Shanghai Key Laboratory of Stomatology & Shanghai Research Institute of Stomatology, National Clinical Research Center of Stomatology, Shanghai, China

**Jing Wang** Engineering Research Center for Biomedical Materials of Ministry of Education, East China University of Science and Technology, Shanghai, China

**Xiao Wang** Department of Prosthodontics, Ninth People's Hospital, Shanghai JiaoTong University School of Medicine, Shanghai, China

Shanghai Key Laboratory of Stomatology & Shanghai Research Institute of Stomatology, National Clinical Research Center of Stomatology, Shanghai, China

**Jie Weng** Key Lab of Advanced Technologies of Materials, Ministry of Education, School of Materials Science and Engineering, Southwest Jiaotong University, Chengdu, China

**Wenjian Weng** School of Materials Science and Engineering, Zhejiang University, Hangzhou, China

**Chengtie Wu** State Key Laboratory of High Performance Ceramics and Superfine Microstructure, Shanghai Institute of Ceramics, Chinese Academy of Sciences, Shanghai, China

**Zhidao Xia** Centre for Nanohealth, Swansea University Medical School, Singleton Park, Swansea, UK

**Huilin Yang** Orthopedic Institute, Soochow University (South Campus), Suzhou, Jiangsu, China

Department of Orthopaedics, The First Affiliated Hospital of Soochow University, Suzhou, Jiangsu, China

**Yuanman Yu** Engineering Research Center for Biomedical Materials of Ministry of Education, East China University of Science and Technology, Shanghai, China

**Yuan Yuan** Engineering Research Center for Biomedical Materials of Ministry of Education, East China University of Science and Technology, Shanghai, China

**Deliang Zeng** Department of Prosthodontics, Ninth People's Hospital, Shanghai JiaoTong University School of Medicine, Shanghai, China

Shanghai Key Laboratory of Stomatology & Shanghai Research Institute of Stomatology, National Clinical Research Center of Stomatology, Shanghai, China

**Shengmin Zhang** Advanced Biomaterials and Tissue Engineering Center, Huazhong University of Science and Technology, Wuhan, China

**Xiangkai Zhang** Department of Prosthodontics, Ninth People's Hospital, Shanghai JiaoTong University School of Medicine, Shanghai, China

Shanghai Key Laboratory of Stomatology & Shanghai Research Institute of Stomatology, National Clinical Research Center of Stomatology, Shanghai, China

**Ao Zheng** Department of Prosthodontics, Ninth People's Hospital, Shanghai JiaoTong University School of Medicine, Shanghai, China

Shanghai Key Laboratory of Stomatology & Shanghai Research Institute of Stomatology, National Clinical Research Center of Stomatology, Shanghai, China

# Chapter 1

## Calcium Phosphate Bone Cements: Their Development and Clinical Applications

Fangping Chen, Xiaoyu Ma, Yuanman Yu, and Changsheng Liu

**Abstract** Calcium phosphate cement (CPC) has opened up a new era in the construction of bone-related defects in biomedical fields. Such unique properties as the easy shaping, injectability in practical use, excellent biocompatibility, and biodegradability of CPC make it a perfect substitution material and maintain the research focus during the years. In this chapter, the brief history, classification, setting mechanism, and kinetics of CPC are introduced. A further understanding of the chemical, physical, and biological properties of CPC, along with the clinical applications, is also addressed to provide a deeper insight into the regulation mechanism between the material properties and the clinical uses.

**Keywords** Calcium phosphate cement • Hydration • Self-setting • Bone repair • Drug delivery • Clinical applications

### 1.1 Introduction

#### 1.1.1 Emergence of Calcium Phosphate Cements (CPC)

According to the latest statistics published by the World Health Organization (WHO), the human life expectancy has increased dramatically in recent years, the most rapid increase since the 1960s. However, together with the growth of human life-span, an increasing number of people are now suffering from various issues, especially aging-related diseases. Among all the diseases and disorders confronted,

---

F. Chen • X. Ma • Y. Yu

Engineering Research Center for Biomedical Materials of Ministry of Education, East China University of Science and Technology, Shanghai 200237, China

C. Liu (✉)

Key Laboratory for Ultrafine Materials of Ministry of Education, East China University of Science and Technology, Shanghai 200237, China

e-mail: [liucs@ecust.edu.cn](mailto:liucs@ecust.edu.cn)

© Springer Nature Singapore Pte Ltd. 2018

C. Liu, H. He (eds.), *Developments and Applications of Calcium Phosphate Bone Cements*, Springer Series in Biomaterials Science and Engineering 9, DOI 10.1007/978-981-10-5975-9\_1

bone-associated problems have become one of the most serious issues that need to be addressed. Trauma-induced fractures, worn joints, or osteoporosis due to the aging problem, as well as some disease-causing damages to the bone, have greatly hampered the daily life of people and lowered the life quality as well.

It is a great challenge to treat large bone defects, which cannot be healed on their own and require implantation of suitable bone grafts into the defect site. To fix the damaged bone, it is usually impossible to achieve the bone reparation without any additional guidance. Bone tissue substitutes are thus employed in surgeries, including autografts, allografts, and artificial bone substitutes. Autologous transplantation has been extensively applied at the beginning, due to excellent osteoinductive and osteoconductive capability. This strategy is considered as “golden standard” for bone repair. However, the repair of bones is achieved at the cost of sacrificing normal and healthy tissues. Additionally, for the defects that are larger than critical size, there are no sufficient tissues to take from the healthy part for the damaged areas. To broaden the source of bone repair materials, xenograft is also developed and used as a suboptimal alternative. Nevertheless, the use of xenografts from people or animals is limited, due to the lack of mechanical strength, easy deformation, immunological rejection, spread of diseases, and even ethical issues. These complications necessitate the pursuit of synthetic substitutes for treatment of these formidable defects. Therefore, people are calling for artificial materials that can mimic the properties of natural bone and avoid all the above problems. As a result, artificial materials for bone repairing have turned into the focus of scientists and researchers. A variety of materials have been developed to meet the clinical requirements. Meanwhile, considering the minimal secondary damage, shorter hospital stays, and flexibility in the operation process, bone cement came into its existence.

As one of the bone repairing materials, it was created, extensively and profoundly investigated, and then widely used. Bone cement is a material with easy shaping and self-setting properties. At the initial stage, the solid powders are poured into solution, forming a viscous liquid with good fluidity and injectability. Thus, it could be molded into specific shape or injected directly into the defects. After the paste is formed, the material continues its reactions and goes through the “self-setting” process, gaining its strength so as to be used as bone substitutes. Since all the process could be done at room or body temperature, and the material itself could acquire adequate mechanical strength within a relatively short time (usually several minutes), the bone cement opened a new era for the healing of bone defects.

### ***1.1.2 History and Development of CPC***

In the development of bone cements, polymethylmethacrylate (PMMA) cement was first invented as bone substitutes to improve the quality of humans. PMMA bone cement was firstly applied in the bone repair and had positive impulse to the advance in artificial joints [1, 2]. Initiated by radicals, the polymerization occurred at the defeat site and long chain polymers were formed during the “self-setting” process. The resulted polymers showed excellent mechanical property and flexibility in the

operation. However, great heat was also produced in the polymerization process and the temperature at the local sites could reach as high as above 100 °C, which may cause severe side effects. Meanwhile, PMMA did not have good compatibility with adjacent bone tissues, which may lead to loosening or dislocation. But even worse, the potential release of monomers would cause toxicity and should be strictly avoided.

To resolve the above obstacles brought by the employment of PMMA bone cements, calcium silicate-based and calcium phosphate-based bone cements were soon coming into being, which served as a major breakthrough in the development of bone cement for the reconstruction of bone defects. Calcium silicate could be made to bioglass and tricalcium silicate cement. Although both are characterized by high bioactivity, tunable composition, and adjustable functionality, the mechanical properties especially the brittleness and bending resistance are not always satisfying. Compound calcium silicate cement has already experienced significant progress and become quite attractive in the current scientific world, but it has not been used in clinics. Therefore, it will not be discussed in detail here.

Calcium phosphate cement, as the composition extremely similar to that of natural bones, is preferred in both the research field and clinical applications. Calcium phosphate cement, also named as hydroxyapatite cement, is majorly composed of calcium phosphate and can be set at physiological condition. The CPC system consists of two parts: liquid part and solid part. For the liquid part, water, diluted phosphoric acid, saline, or other solutions could be used. For the solid part, two or more than two calcium phosphate powders are usually involved, for example, calcium phosphate dihydrate + tetracalcium phosphate (CPD+TTCP), monocalcium phosphate monohydrate +  $\beta$ -tricalcium phosphate (MPCM +  $\beta$ -TCP), and  $\alpha$ -tricalcium phosphate + monocalcium phosphate monohydrate + calcium oxide + hydroxyapatite ( $\alpha$ -TCP + MPCM + CaO + HA). Upon mixing its solid part with the liquid part at a certain ratio, a paste could be formed with excellent injectability and plasticity. Under the room temperature or human body temperature, the paste could be self-set into compact solids through crystallization. The final product is of good mechanical strength and can participate in the body metabolism, thus promoting the ingrowth of new bones. Since calcium phosphate is the major inorganic composition in natural bones, the implanted CPC material is of great biocompatibility, high bioactivity, and fantastic biodegradability (depending on the formula). With the time going, CPC is gradually absorbed and degraded into nontoxic ions in the defect site and then gradually replaced by the new bones.

Calcium phosphate cement itself has also experienced great development throughout the years. As early as in the 1980s, it was the first time when the hydration of  $\alpha$ -TCP was reported [3], which may be considered to lead to the first calcium phosphate cement. Soon, the first self-setting calcium orthophosphate, consisting of TTCP and DCPA or DCPD, was developed with a powder-to-liquid ratio of 4:1 [4]. The subsequent paste was then hardened to compact solids in over 30 min. However, the paste before self-setting was highly viscous and unable to be injectable. Meanwhile, for practical operation in the clinic, the setting time of CPCs is too long. During the extended curing process, a series of risks appear and may lead to potential threat such as infections. As a result, a variety of combinations of calcium phosphate was then established to improve the early formula. For the subsequent new



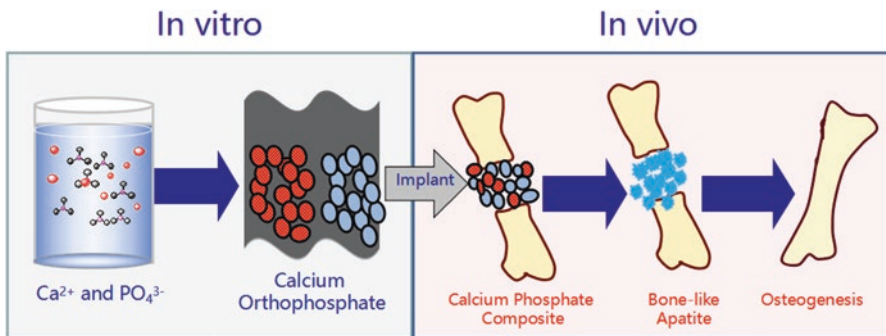
CPCs, the rheology properties and setting times could be tuned and thus made it viable and operative in the surgeries.

Up to now, hundreds of CPCs, with different combination of calcium orthophosphates, have already been developed and investigated. Composite materials made of CPCs and polymers have been widely investigated for the last decades. Since CPC alone suffers from the intrinsic disadvantages such as the lack of tensile strength and compressive strength, the corporation of fibers or polymers could offer better mechanical performance to the composite materials.

At the same time, a number of new functions have also been incorporated into CPC materials. For example, different ions have been added into CPCs to achieve special effects. Si [5], Mg [6], Sr [7], and several other cations were introduced into CPC system to adjust the speed of degradability or to improve the bioactivity of material. In addition, different proteins, especially growth factors, have also been loaded onto the CPCs to further promote the new bone formation, including bone morphogenetic protein (BMP) family [8] extensively used in the materials to strengthen the osteogenesis and osteoinduction or vascular endothelial growth factor (VEGF) [9, 10] employed to improve the vascularization in the bone formation process.

Besides, due to the non-exothermic setting reaction, CPCs can also serve as a good candidate as drug carrier since a variety of drugs can be loaded in the set cement with better controlled release profiles. The drugs can be mixed in the liquid, thus incorporated into the CPCs after self-curing and homogenously distributed inside the cement. The other way to load drugs into the CPCs is to use micro- or nano-spheres to encapsulate the drug and then disperse the drug-loaded spheres into the CPCs. By employing the method, drug release behaviors can be further regulated and adjusted, so as to lower the burst release of the drug. If the spheres can be degraded, then the degradation can produce pores, thus facilitating the ingrowth of cells and tissues into the materials (Fig. 1.1).

In summary, CPCs have already achieved great progress in the past few decades and will still on the way to better performance and multi-functionality. It is sure that the CPCs will play a more important role in bone reparation in the future.



**Fig. 1.1** The illustration of CPC implantation in vitro and in vivo

### 1.1.3 The Advantages of CPC

Calcium phosphate cement boasts a number of advantages, thus making it a favorable bone substitute in clinical applications.

*Easy Shaping* Since the bone defects vary from person to person, it is not possible to design the shape of the substitute in advance and then put it into use. In some cases, the shape of bone defect is quite complex; thus it is even more difficult to manufacture the precise and extricate substitute. Compared to traditional scaffolds or constructs, the CPCs, as a non-Newtonian fluid, can in situ form required shape and satisfy the restricted needs in manufacturing. At the same time, after hardening, the solid product can keep specific shape without deformation. Certainly, modifications could be made onto the solid CPC substitute, which is far easier than traditional ceramics.

*Biocompatibility* The final products after hydration reaction are hydroxyapatite or brushite for all the CPCs. In most of the commercial products, hydroxyapatite is usually employed as the final phase after self-setting reaction. Since hydroxyapatite is the major inorganic composition in natural bones, the hydration product of CPC exhibits excellent biocompatibility and biosafety. The substitutes coexist with surrounding tissues without any induction of tissue degeneration or necrosis and without notable inflammatory response or rejection. Meanwhile, the degradation products composed of  $\text{Ca}^{2+}$  and  $\text{PO}_4^{3-}$  are nontoxic, which will not lead to pathological changes or disorders in normal physiological courses.

*Biodegradability* As the hydration reaction is carried out in room temperature or body temperature, no sintering at high temperature is involved in the self-setting process. As a result, the final product of calcium phosphate, usually hydroxyapatite, is of relatively low crystallinity. For calcium phosphate materials, the solubility is closely related to the degree of crystallinity as the higher the crystallinity the lower the solubility. Therefore, the low degree of crystallinity of hydration products enables the materials to possess good degradability, which is an important factor in bone repairing area. By tuning the degradability of substitute, a delicate and intricate balance between new bone formation and CPC material adsorption could be achieved, which is beneficial to the patients' recovery.

*Osteoconductivity* As the degradation products of CPCs are composed of  $\text{Ca}^{2+}$  and  $\text{PO}_4^{3-}$ , the local enrichment of such ions will facilitate the growth of new bones onto the interface of CPC materials, thus boosting good osteoconductivity. At the same time, it can also promote mineralization by strengthening the binding between CPC implants and surrounding tissues.

*Injectability* The injectability is one of the most important factors for calcium phosphate cements. Due to its special rheological properties, the cement firstly forms a paste that could be molded into various shapes and then hardens to offer adequate mechanical strength. This gives us the opportunity to use the syringe to inject the paste into specific site, therefore to avoid secondary damage and associated injuries since there is no need for complicated preparation and handling. On the contrary, for traditional bone substitutes such as scaffolds and constructs, much

more painful surgeries are usually required since it is not easy enough to implant the substitutes into the defect site. During the operation, secondary injuries occur to the patients from time to time, thus prolonging the recovery time and extending the hospital stays for the patients.

## 1.2 Preparation of CPCs and Kinetics of Hydration Reaction

### 1.2.1 Classification of CPCs

In the development of calcium phosphate cements, hundreds of CPC formulas have been established and put into use. Different CPCs could be classified by phase composition of solid powders, the reaction process, phase composition of products, and so on.

*Phase Composition of Solid Powders* According to the phase composition of the solid powders, CPCs could be divided into TTCP cement,  $\alpha$ -TCP,  $\beta$ -TCP, and others. For example, the invented CPC system is majorly composed of TTCP with a small portion of DCP, thus could be classified as TTCP cement.

*Reaction Process* The classification of CPCs could also be based on reaction process. In short, it can be stated that there are generally two types of reaction processes involved in the self-setting. The first type is acid-base interaction. For example, a relatively acidic calcium phosphate, such as monocalcium phosphate monohydrate, reacts with a relatively basic one, such as TECP, to produce a relatively neutral compound. The second type of the reaction process could be identified as hydration of calcium phosphates in aqueous media, undergoing five periods including initiation, induction, acceleration, decelerating period, and termination. For instance, hydration of  $\alpha$ -TCP converts into hydroxyapatite as final products in water.

*Phase Composition of Products* Based on the phase composition of final hydration products, CPCs could be sorted into apatite-, brushite-, and amorphous calcium phosphate-forming cement. Since the amorphous calcium phosphate does not possess high stability, thus it could rapidly convert into apatite-like products. As a result, up to now, brushite and apatite cement remained the two dominant classifications. This is actually predictable because of the fact that apatite is the least soluble calcium orthophosphate when pH is approximately larger than 4.2, while brushite is the least soluble one when pH is approximately lower than 4.2, as reported by Ishikawa [11]. In other words, pH values determine the final products. Lower than 4.2, brushite is the most stable phase thermodynamically. However, when the pH is raised above 4.2, hydroxyapatite becomes the most stable phase.

Moreover, calcium phosphate cement has been proved by the FDA and has been commercially available in the 1990s. At present, a variety of CPCs are provided by different companies in the market, as summarized in Table 1.1 [12]. Meanwhile, one of the commercial products from Shanghai Rebone Company was exhibited in Fig. 1.2, to give a direct impression of CPC.

**Table 1.1** The list of commercially available CPC products

Company	Cement name	Components	End product
ETEX	$\alpha$ -BSM Embarc Biobon	Powder: ACP (50%), DCPD (50%)	Apatite
		Solution: H <sub>2</sub> O (unbuffered saline solution)	
Stryker-Leibinger Corp.	BoneSource	Powder: TetCP (73%), DCP (27%)	Apatite
		Solution: H <sub>2</sub> O, mixture of Na <sub>2</sub> HPO <sub>4</sub> and NaH <sub>2</sub> PO <sub>4</sub>	
Teknimed	Cementek®	Powder: $\alpha$ -TCP, TetCP, Na glycerophosphate	Apatite
	Solution: H <sub>2</sub> O, Ca(OH) <sub>2</sub> , H <sub>3</sub> PO <sub>4</sub>		
	Cementek® LV	Powder: $\alpha$ -TCP, TetCP, Na glycerophosphate, dimethylsiloxane	Apatite
	Solution: H <sub>2</sub> O, Ca(OH) <sub>2</sub> , H <sub>3</sub> PO <sub>4</sub>		
Biomet	Calcibon® (previously called "Biocement D")	Powder: $\alpha$ -TCP (61%), DCP (26%), CaCO <sub>3</sub> (10%), PHA (3%)	Apatite
		Solution: H <sub>2</sub> O, Na <sub>2</sub> HPO <sub>4</sub>	
	Mimix™	Powder: TetCP, $\alpha$ -TCP, C <sub>6</sub> H <sub>5</sub> O <sub>7</sub> Na <sub>3</sub> ·2H <sub>2</sub> O	Apatite
Solution: H <sub>2</sub> O, C <sub>6</sub> H <sub>8</sub> O <sub>7</sub>			
Mitsubishi Materials	Biopex®	Powder: $\alpha$ -TCP (75%), TetCP (20–18%), DCPD (5%), HA (0–2%)	Apatite
		Solution: H <sub>2</sub> O, sodium succinate (12–13%), sodium chondroitin sulfate (5–5.4%)	
	Biopex®-R	Powder: $\alpha$ -TCP, TetCP, DCPD, HA, Mg <sub>3</sub> (PO <sub>4</sub> ) <sub>2</sub> , NaHSO <sub>3</sub>	Apatite
Solution: H <sub>2</sub> O, sodium succinate, sodium chondroitin sulfate			
Kyphon	KyphOs™	Powder: $\alpha$ -TCP (77%), Mg <sub>3</sub> (PO <sub>4</sub> ) <sub>2</sub> (14%), MgHPO <sub>4</sub> (4.8%), SrCO <sub>3</sub> (3.6%)	Apatite
		Solution: H <sub>2</sub> O, (NH <sub>4</sub> ) <sub>2</sub> HPO <sub>4</sub> (3.5M)	
Skeletal kinetics	Callos™	Powder: nf	Apatite
		Solution: nf	
Shanghai Rebone Biomaterials Co., Ltd	Rebone®	Powder: TECP, DCP	Apatite
		Solution: H <sub>2</sub> O	

(continued)

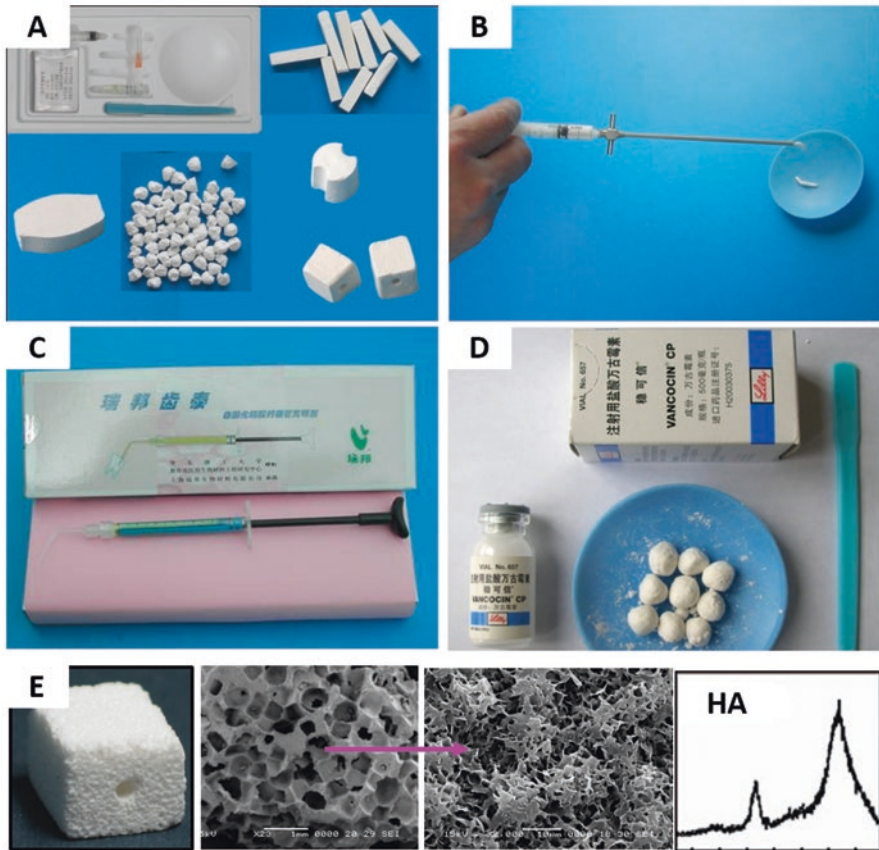
**Table 1.1** (continued)

Company	Cement name	Components	End product
Synthes-Norian	Norian <sup>®</sup> SRS	Powder: $\alpha$ -TCP (85%), CaCO <sub>3</sub> (12%) MCPM (3%)	Apatite
	Norian <sup>®</sup> CRS	Solution: H <sub>2</sub> O, Na <sub>2</sub> HPO <sub>4</sub>	
	Norian <sup>®</sup> SRS Fast Set Putty	Powder: nf	Apatite
	Norian <sup>®</sup> CRS Fast Set Putty	Solution: nf	
	chronOS <sup>™</sup> Inject	Powder: $\beta$ -TCP (73%), MCPM (21%), MgHPO <sub>4</sub> ·3H <sub>2</sub> O (5%), MgSO <sub>4</sub> (<1%), Na <sub>2</sub> H <sub>2</sub> P <sub>2</sub> O <sub>7</sub> (<1%) Solution: H <sub>2</sub> O, sodium hyaluronate (0.5%)	Brushite
Kasios	Eurobone <sup>®</sup>	Powder: $\beta$ -TCP (98%), Na <sub>4</sub> P <sub>2</sub> O <sub>7</sub> (2%)	Brushite
		Solution: H <sub>2</sub> O, H <sub>3</sub> PO <sub>4</sub> (3.0M), H <sub>2</sub> SO <sub>4</sub> (0.1M)	
CalciphOs	VitalOs	Component 1: $\beta$ -TCP (1.34 g), Na <sub>2</sub> H <sub>2</sub> P <sub>2</sub> O <sub>7</sub> (0.025 g), H <sub>2</sub> O, salts (0.05M pH 7.4 PBS solution)	Brushite
		Component 2: MCPM (0.78 g), CaSO <sub>4</sub> ·2H <sub>2</sub> O (0.39 g), H <sub>2</sub> O, H <sub>3</sub> PO <sub>4</sub> (0.05M)	

Reprinted from Ref. [12] with permission. Copyright © 2005 Elsevier Ltd  
*nf* not found

### 1.2.2 Preparation of CPCs

Since the formula of CPC varies, the preparation approach also differs from one to another. The preparation of CPC could be divided into two categories: powder preparation and liquid preparation. First of all, let's talk about the preparation of calcium phosphate salt powders. The high purity of powder is considered as the major control factor during the synthesis process. Thus, a series of methods have been developed to obtain powders with high quality. For example, TCP, DAP, DCPA, TECP, and Si/Mg-doped calcium phosphate-based biomaterials with high purity and high activity were successfully synthesized by controlling the nucleation and growth of the crystals and inhibiting the formation of by-products through optimizing the reactor design, use of micro-jet hybrid, heat treatment, and other engineering approaches [13, 14]. Meanwhile, amplification criterion for large-scale production was also explored, and the calcium phosphate-based powders have been successfully prepared at large scale, making an important guidance to prepare novel calcium phosphate-based biomaterials for clinical use and surgeries. On the other hand, for the liquid part, a variety of solutions have been applied in the formulations, depending on the choice of CPC systems, including water, citric acid aqueous

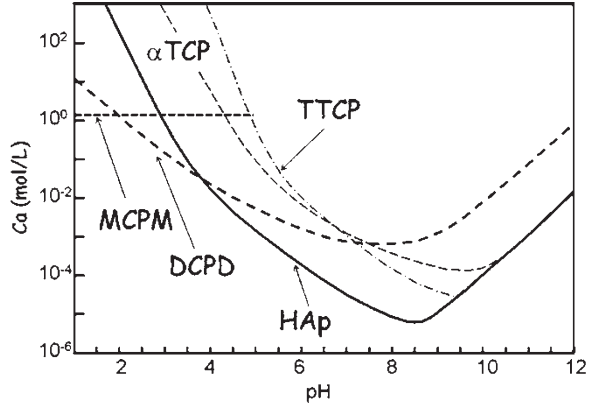


**Fig. 1.2** Self-setting CPC products (Rebone®). (a) CPCs with different shapes; (b) injectable CPCs; (c) tools for root canal filling; (d) drug-loaded CPCs; (e) porous CPCs and their microstructure

solution,  $\text{Na}_2\text{HPO}_4$  aqueous solution, and so on. For readers who are interested in the detailed synthesis and preparation of related calcium phosphate powders and engineering techniques, specific reports could be found elsewhere [15–18].

Based on this background, our group has carried out an intensive and extensive study on the development of CPC since 1993. In 1998, the products from Shanghai Rebone Biomaterials Co., Ltd. were granted the approval by China Food and Drug Administration (CFDA) on CPC (Rebone®). According to the feedbacks from clinical trials, a subsequent scale-up on the Rebone® production, technology integration, and second innovation was carried out. A series of self-setting calcium phosphate cements, including porous CPCs, drug-loading CPCs, injectable CPCs, high bioactive CPCs, CPC root canal fillers, and related equipment, has been developed to meet various clinical requirements. Up to now, these CPC commercial products have been employed in more than 300,000 cases, covering more than 500 hospitals in 30 provinces in China. The results demonstrated satisfactory curative effect for bone defect repair, spine surgery, and root canal filling.

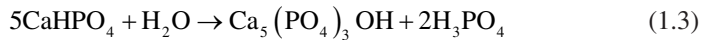
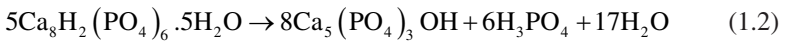
**Fig. 1.3** Phase diagram of the solubility of different calcium phosphates (Reprinted from Ref. [19] with permission. Copyright © 2014, Springer-Verlag Berlin Heidelberg)



### 1.2.3 Setting Mechanism and Kinetics of CPC Hydration

One of the most outstanding characteristics of calcium phosphate cements is the easy shaping and injectability. The key of the above advantages lies in the special hydration reaction and setting process of CPC materials.

The setting mechanism during hydration-hardening reaction of calcium phosphate compound is based on the different solubilities of sparingly soluble calcium phosphate salts in water. Figure 1.3 shows the phase diagram of the solubility of various calcium phosphates as a function of pH, where solubility is expressed as the concentration of calcium. In addition, several common hydration reaction processes are summarized as below:



According to Fig. 1.3, it could be inferred that most of calcium phosphates can be converted to hydroxyapatite. During the setting process, because of the difference in solubility among various calcium phosphate materials, they undergo a conversion into the most stable type, thus enabling the curing or setting of the paste-like form to the solid form. Basically, setting reaction of calcium phosphate cement is known as dissolution-precipitation reaction, followed by the growth of crystal and further entanglement of the crystals.

Although there appeared to be a great number of CPC systems, a general process of the self-setting process could be concluded and be applied to most systems [19].

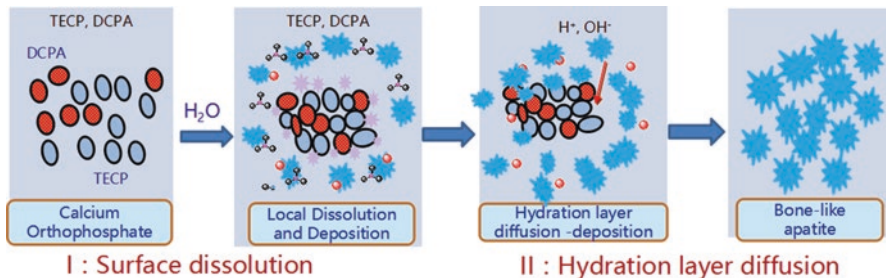


Fig. 1.4 The mechanism and kinetics of the hydration of TECP/DCPA system

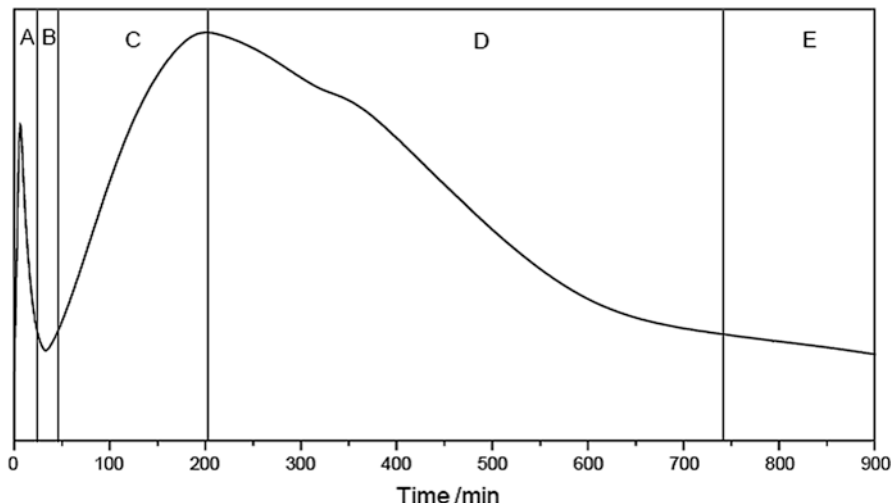
Take the TECP/DCPA system as an example. In the beginning, the hydration is controlled by dissolving DCPA powder surface. As the powder surfaces dissolve under the action of a liquid medium, the HA supersaturated solution is formed in micro-regions. After nucleation, small HA crystals are precipitated. With the hydration reaction, HA crystals continue to grow and cross-link covered with a cladding layer [20]. In the later stage of the hydration, the reaction rate is controlled by the diffusion of the product layers. The hydrations of TECP and DCPA produce excessive OH<sup>-</sup> and H<sup>+</sup> ions, which penetrate through the cladding layers to set until complete hydration. The hydration reaction within the particles depends on the penetration of the hydration product layers to the inner and the mutual diffusion of the ions (Fig. 1.4).

In another case, the self-setting process of α-tricalcium phosphate (α-TCP) system is also extensively investigated [21]. When α-TCP is mixed with water, it then dissolves and offers Ca<sup>2+</sup> and PO<sub>4</sub><sup>3-</sup>. The solution is usually in a state of equilibrium with calcium-deficient hydroxyapatite, whose solubility is lower than the solubility of α-TCP, leading to the precipitation of calcium-deficient HA crystals. As the calcium-deficient HA is precipitated in the water, an immediate undersaturation of the solution is achieved. In return, it will further promote the dissolution of α-TCP in the solution. These reactions continue successively, and the precipitated calcium-deficient HA crystals entangle each other to set. The self-setting process could be summarized as follows:



The hydration rate was also investigated. As reported [22], the exothermic hydration reaction of CPC containing TECP/DCPA was further studied, and a dynamic model has been established through calorimetric curve. The complete hydration of CPC could be summarized as five processes in Fig. 1.5, which were named as the

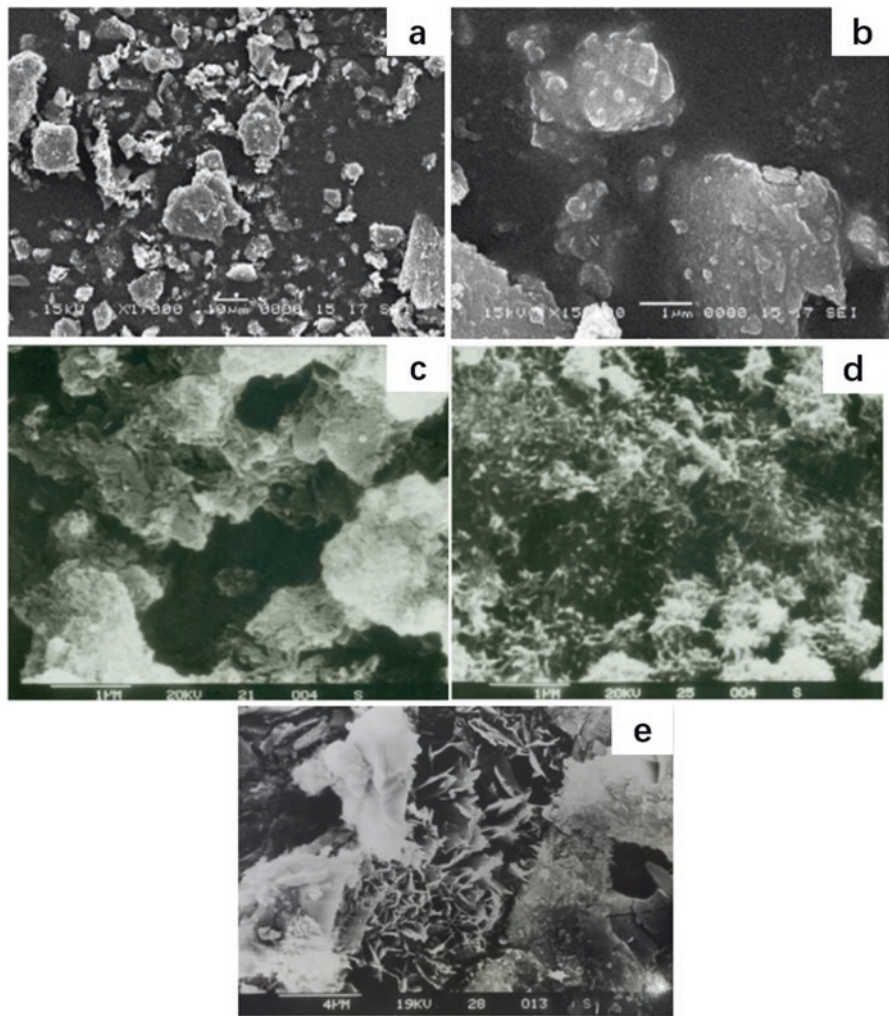




**Fig. 1.5** Calorimetric curve showing the rate of heat liberation of CPC with time. A, B, C, D, E: the start, induction, acceleration, deceleration, and termination period (Reprinted from Ref. [22] with permission. Copyright © 2003 Elsevier Ltd)

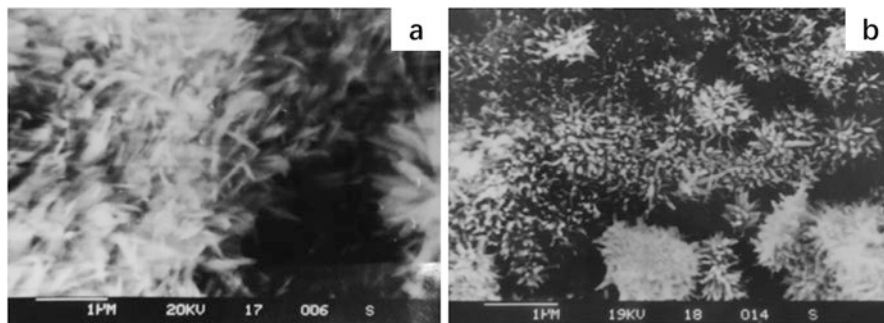
start, induction, acceleration, deceleration, and termination. The five periods could be divided to designate a specific reaction. The hydration rate could be tuned by properly controlling methods. Effects of various factors were further tested within the framework of the above five-period theory. Firstly, it was found that the introduction of a small amount of HA as crystal seed shortened induction, advanced on the reaction peak position, and reduced the activation energy of heterogeneous nucleation, thus accelerating hydration process while reducing the strength of the solidified materials [23]. It was also revealed that strong electrolyte accelerated the hydration reaction through reducing the system activity and improving the supersaturation. Otherwise, the addition of various additives changed the growth direction of the crystals and altered the morphology of hydration products, which provides the theoretic guidance for in situ reinforcement.

The microstructure development was also investigated [24, 25]. During the setting process of CPCs, including the dissolution and precipitation as well as the entanglement of gradually growing calcium phosphate crystals, the final solid product boosts the formation of porous structures, which is quite beneficial for subsequent biomedical applications. All types of hardened formulations will possess an intrinsic porosity within the nano- or micron-size ranges. Take the TECP/DCPA system as an example. After the initial dissolving and precipitation of calcium phosphate compounds, small HA crystals gradually enlarge and lead to the adherence and interlocking of the crystalline grains, resulting in hardening. The newly generated HA nuclei continue to grow, as we can observe more CPC materials formed at the interparticle spaces. With the proceeding of setting reactions, the CPC materials become very compacted with high density at some sites while with more porosity at



**Fig. 1.6** SEM micrographs of hydrated specimens at different time intervals. (a, b) At 0 min; (c) at 17 min; (d) at 70 min; (e) at 24 h (Reprinted from Ref. [25] with permission. Copyright © 2003 Elsevier Ltd)

interlocking areas. The development of the microstructures of CPC during hydration was directly observed under SEM in Fig. 1.6. Compared with the starting point (Fig. 1.6a, b), it was seen that the surfaces of the grains of the raw materials became rough and rugged, suggesting the dissolution of the grains. Thin ruffled products among the grains could also be observed, which endowed the cement a coagulate structure. After 70 min of hydration, many small petallike or needlelike crystals appeared, due to the binding of the grains from aggregation or crystallization.



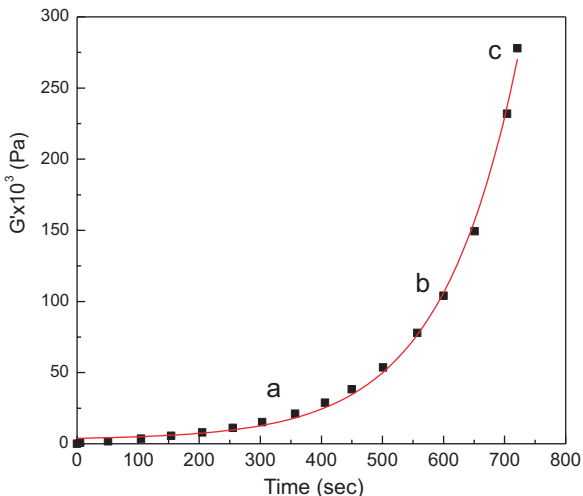
**Fig. 1.7** SEM micrographs of hydrated specimens with different additives. (a) 20% NaCl; (b) 20% CaSO<sub>4</sub>

Twenty-four hours later, grains further grew into plate- and flake-like shapes with larger-size and interlocking structures.

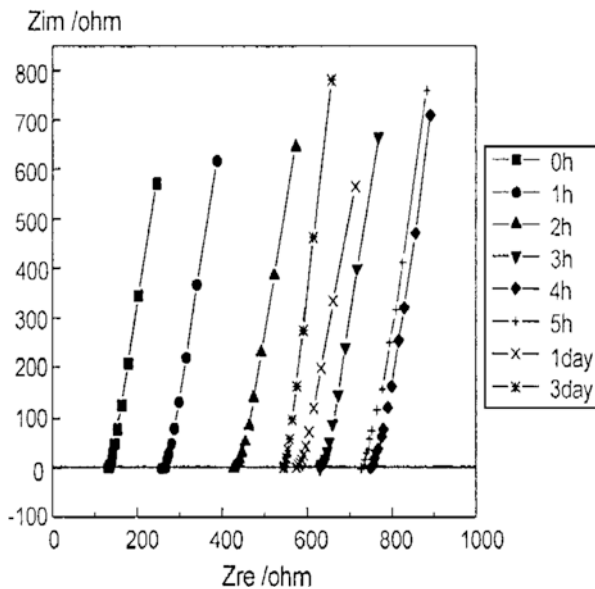
It is also worthy to note that various additives would greatly affect the microstructure evolution during hydration. As was shown in Fig. 1.7, the size and morphologies, as well as the growth direction of crystals, were altered after the addition of NaCl and CaSO<sub>4</sub>. In the 20% NaCl group, the subsequent hydration product was an agglomeration of HA debris. However, in the 20% CaSO<sub>4</sub> one, the final product was presented in the form of gathered short rods. It could be included that the morphology of the final hydration product was sensitive to the environment. Thus, a careful choice of additives could contribute to the favorable manipulation of the whole hydration process.

The physicochemical properties in the hydration process were also clarified to further investigate the microstructure development for the TECP/DCPA system [26]. At the initial stage of the hydration, the compressive strength increased accordingly with time, and the volume was slightly shrunken during the setting process. The porosity after hydration was about 30% with size below 0.1 μm, and the final product was low crystalline hydroxyapatite. Moreover, the relationship was established between the internal structure and material properties during the hydration reactions [27]. For example, as shown in Fig. 1.8, the change of G' could be measured along the setting of CPC. Generally, G' increased with a prolonged time sweep, exhibiting that the slurry was undergoing hydration reaction. However, from the curves, a coincident variational tendency with different rates of the inner structure formation process and the variation of the binding force could be observed. The region (a) of the curve in Fig. 1.8 demonstrated that the storage module, representing the network strength of the slurry, was low and grew in a relatively slow way. The regions (b) and (c), however, revealed that the storage module raised remarkably, indicating a rapid increase of the network strength of the slurry. By analyzing the dynamic rheological properties of CPC containing TECP/DCPA, it was found that the slurry developed from a flocculent structure to a net structure with increased strength, which can further demonstrate the mechanism of CPC setting. Meanwhile, the storage module of CPC during setting could help to forecast the setting time.

**Fig. 1.8** Variation of  $G'$  during the setting of CPC by time sweep. Strain, 1%;  $\omega$ , 1 rad  $s^{-1}$ . Particle match,  $D_2T_2$ ; P/L ratio, 2.0; T, 37 °C (Reprinted from Ref. [27] with permission. Copyright © 2006 Elsevier Ltd)



**Fig. 1.9** Impedance spectra of hydrating CPC at different times (Reprinted from Ref. [24] with permission. Copyright © 1999, John Wiley and Sons)



Apart from the mechanical properties, impedance spectra of hydrating CPC were also utilized at different times to further study the mechanism of hydration reaction. AC impedance spectroscopy is a favorable way to characterize the microstructure of CPC, due to its sensitivity to the change of the structure and its negligible effect on the hydration of the cement [22]. As illustrated in Fig. 1.9, the microstructure could be investigated qualitatively according to the intercepts and their variation. The lines of impedance spectra in the whole process were parallel to each other, and the value of the intercept increased evenly within the first 4 h of hydration, then decreased after 4 h, which was well accorded with the mechanical behavior during

CPC hydration. In detail, the compressive strength increased linearly along with the hydration time and reached the maximum after 4 h. However, the compressive strength decreased slightly after that, instead of continuing increasing. Hence, the impedance spectra once more confirmed the mechanism of hydration of CPC.

In summary, with the analysis for hydration rate and investigation for microstructure development, the whole self-setting process could be further clarified, thus contributing to a more extensive and profound understanding of the hydration reaction.

## 1.3 Properties of Calcium Phosphate Cements

### 1.3.1 *Physical/Chemical Properties and Their Influence Factors*

Human skeletal system is a complex stress microenvironment, and calcium orthophosphates used as orthopedic implants must possess sufficient mechanical strength to firmly combine with the host bone. Since both of them are remarkably biocompatible, bioresorbable, and osteoconductive, self-setting calcium orthophosphates appear to be promising biomaterials for bone grafting. Furthermore, such formulations possess excellent molding capabilities, easy manipulation, and nearly perfect adaptation to the complex shapes of bone defects, followed by gradual bioresorption and new bone formation. These involved characteristics of CPC due to the self-setting properties which attracted much attention in the medical applications, and more properties are being found during the clinic application.

*Self-Setting and Controllers* Self-setting is the most outstanding property of calcium phosphate cement in clinical applications. Setting reaction of CPC is a continuous process that is basically known as dissolution-precipitation reaction [27] described before. The reaction process always gives rise to the solid consists in three stages: dissolution of reactants, nucleation of the new phase, and crystal growth. This supplied ions of calcium and orthophosphate into the solution, where they chemically interact and precipitate in the form of either the final products or precursor phases, which causes the cement setting. During the first hours, the setting process is controlled by the dissolution kinetics of the raw materials, but once the new phase surrounds the reactants, the process is controlled by diffusion across the new phase. There are many factors influencing the self-setting efficiency of CPC. The formulations are blends of amorphous and crystalline calcium orthophosphate powders with an aqueous solution, which might be distilled water [28], phosphate buffer solution [29], aqueous solutions of sodium orthophosphates [30], ammonium orthophosphates [31], orthophosphoric acid [32], citric acid and its salts [33], sodium silicate [34], soluble magnesium orthophosphates [35], chitosan lactate in lactic acid [36], etc.

Without any improvement, CPCs normally have a relatively long setting time and hardening strength. A CPC with incompletely setting can cause problems. For instance, a long setting time of CPCs could not withstand the bone stress because of the belated development of mechanical strength, and a severe inflammatory response would occur when CPCs were unable to set or disintegrated [37]. In addition, fast-setting reaction is not conducive to the operation. Therefore, inducing setting controllers and regulating the setting reaction of CPCs seem particularly important. Since setting reaction of CPC is based on dissolution-precipitation reaction and entanglement of the precipitated calcium phosphate crystals, many strategies have been adopted to study the effects of particle size, temperature, crystalline, and various constituents on the setting time of CPCs.

Apatite cement has a relatively long setting time which may sustain 2–3 h, and the addition of the  $\text{PO}_4^{3-}$  such as  $\text{NaH}_2\text{PO}_4$  into the liquid phase could cause an accelerated HA formation. Kunio Ishikawa et al. [38] found that the setting time of a CPC consisting of TTCP and DCPA was reduced from 50 to 30 min by use of a liquid phase that contained a phosphate concentration of 0.25 mol/L or higher. And Tenhuisen and Brown [39] demonstrated that adding citric acids could strongly accelerate the formation of HA due to the increased solubility of the reactant phases at lower pH. Meanwhile, the particle size of the solid phase also has an influence on the self-setting process. This is attributed to the fact that larger particle has smaller specific surface area, and rate of rate of dissolution is slow. Additionally, the setting reaction of CPC also depends on the seed crystal. Liu and Shen [23] presented that the setting time of the CPC slurry was reduced from 150 to 7 min by introducing 5 wt% low crystalline HA. This improvement in the setting time was due to HA serving as a substrate for heterogeneous nucleation which accelerated nucleation.

However, the situation is contrary in case of brushite cement. The self-setting process of brushite cement is very rapid, and a retarder is needed to lengthen the setting time [19]. Sulfate, pyrophosphate, and citrate are proved as effective retarders. Bohner et al. [40] found that effectiveness at prolonging the setting time was in the order of pyrophosphate > citrate > sulfate. Basically, the mechanisms involved in extending the setting time using pyrophosphate and citrate ions were due to the inhibition of brushite crystallization.

*Mechanical Properties* The modern generation of biomedical materials should stimulate the body's own self-repairing abilities [41]. Therefore, during healing, a mature bone should replace the grafts, and this process must occur without transient loss of the mechanical support. The strength of initial synthetic calcium orthophosphate is relatively low and susceptible to brittle fracture, which have limited the use of CPC to only non-load-bearing applications [42, 43]. Therefore, attempts were made to increase the strength of CPC.

Firstly, the strength of CPC is closely related to the porosity, and the strength increases with decreasing porosity. Ishikawa [44] attempted to obtain the ideal mechanical strength by adjusting the critical porosity of CPC. CPCs at various porosities were made by packing CPC paste, at various powder-to-liquid (P/L) ratios

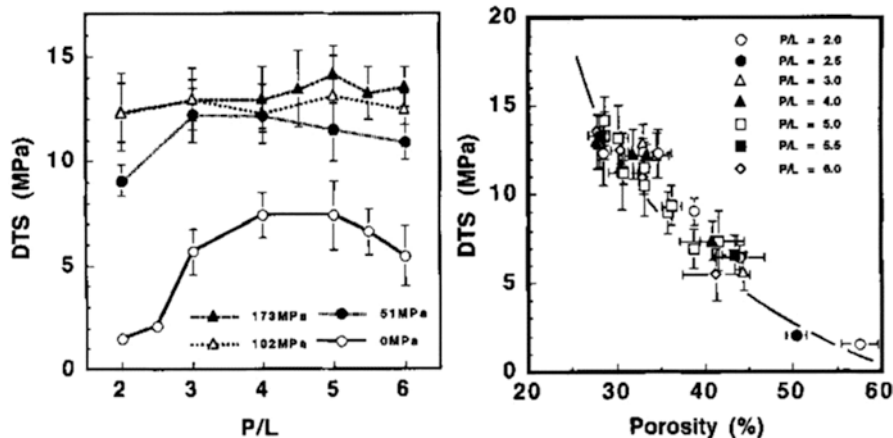


Fig. 1.10 Relationship between wet DTS and P/L and porosity (%) of CPC specimen (Reproduced from Ref. [44] with permission. Copyright © 1995 John Wiley & Sons, Inc.)

(2.0–6.0), into a mold under various pressures (0–173 MPa); the results were depicted in Fig. 1.10. The mechanical strength (diametral tensile strength, DTS) of CPCs increased with decreases in porosity. The ideal wet diametral tensile strength (DTS) and critical porosity of CPCs were estimated to be 102 MPa and 63%, respectively. The minimum porosity of the currently used CPCs was approximately 26–28%, even when it was packed under 173 MPa, and the maximum DTS value was thus approximately 13–14 MPa. However, an appropriate porosity is conducive to cell growth and survival, and the porosity should not blindly reduce for an increased strength.

Another approach to improve the mechanical properties of CPCs is to cover the items by polymeric coatings or infiltrate porous structures by polymers. Researchers found that the incorporation of fibers can improve the strength and fracture resistance of materials. In one study, four different fibers were used to reinforce CPCs [45]: aramid, carbon, E-glass, and polyglactin. The composite ultimate strength in MPa was  $(62 \pm 16)$  for aramid,  $(59 \pm 11)$  for carbon,  $(29 \pm 8)$  for E-glass, and  $(24 \pm 4)$  for polyglactin, with 5.7% volume fraction and 75 mm fiber length. In comparison, the strength of unreinforced CPCs was  $(13 \pm 3)$ . Additionally, fiber length and fiber volume fraction were also found to be key microstructural parameters that controlled the mechanical properties of CPC composites. The ultimate strength of CPC composite was intensified with the increase of the fiber length. In another study, Gorst [46] confirmed that the incorporation of resorbable polyglactin fibers and the compaction of the fiber/CPC paste mixture caused improved mechanical properties. The structure of the reinforcing fibers, random or regular, was shown to be crucial for resulting strength and modulus of elasticity. Random orientations led to a preserved modulus at a slight strength increase, whereas a regular fiber orientation led to increased strength at decreased modulus.

*Porosity* As mentioned above, the increase in the porosity will exponentially decrease the mechanical properties, whereas the permeability can be largely

**Table 1.2** A hierarchical pore size distribution that an ideal scaffold should exhibit

Pore sizes of a 3D scaffold	Biochemical effects or functions
<1 $\mu\text{m}$	Interaction with proteins
	Responsible for bioactivity
1–20 $\mu\text{m}$	Type of cells attracted
	Cellular development
	Orientation and directionality of cellular ingrowth
100–1000 $\mu\text{m}$	Cellular growth
	Bone ingrowth
	Predominant function in the mechanical strength
>1000 $\mu\text{m}$	Implant functionality
	Implant shape
	Implant esthetics

Reprinted from Ref. [48] with permission. Copyright © 2007 Elsevier B.V

increased with increased porosity. Hence, parameters such as the overall architecture, pore morphology, interconnectivity, and pore size distribution need to be balanced to guide proper tissue regeneration, which play a key role in allowing proper cell penetration, nutrient diffusion, as well as bone ingrowth [47], as shown in Table 1.2. A wide variety of techniques are processed to achieve a proper porosity of calcium phosphate cements.

Porogen addition is the simplest method to fabricate macroporous set CPC. Porogen should not dissolve during the mixing procedure and could be easily leached in an easy system. As a result, the macropores will be formed in the place where porogens occupied. Generally, the porogens should be nontoxic, and the popular examples comprise paraffin [49, 50], naphthalene [51, 52], sucrose [53, 54], mannitol [55],  $\text{NaHCO}_3$  [56, 57],  $\text{NaCl}$  [14, 58], and cellulose derivatives [59]. Xu [55] used mannitol as a porogen to develop an injectable, macroporous, and strong CPC. The injectable scaffolds with 30% and 40% mannitol possessed total porosity values of 77% and 83% (macroporosity of 36% and 51%), respectively. The macropore sizes ranged from 200 to 600  $\mu\text{m}$  [60]. Additionally, a mixture of frozen sodium phosphate solution particles and CPC powder were compacted at 106 MPa, and the sodium phosphate was allowed to melt and simultaneously set the cement [61]. The effect of the amount of porogen used during processing on the porosity, pore size distribution, and compressive strength of the scaffold was investigated. It was found that macroporous CPC could reliably be fabricated using cements – ice ratios as low as 5:2.

However, pores resulting from this method are often irregular in size and shapes are not fully interconnected with one another. The macropores on the surface of CPC are favorable for the rapid adsorption of nutrients and cells, but the disconnection of pores leads to a lack of nutrition and cells in the inner scaffold and reduces bone repair efficiency. Initially, a polymeric sponge method produces open-cell



porous ceramic scaffolds through replication of a porous polymer template. The scaffolds prepared by this approach have a controllable pore size, interconnected pores, and desired geometry [62]. The templates are easy to remove and foam molding; therefore, the common sponge templates contain PGA, chitosan, polyurethane, etc. Calcium phosphate slurry was homogeneously thick coated, while its viscosity directly affected the thickness of the hole wall. Sometimes, a binder-like polyvinyl alcohol is needed to adjust the viscoelasticity of the slurry. Sintering of the dried porous block exhibited the densest microstructure as well as the entire elimination of the organic additives. In some researches [63], dimethylformamide was added as a drying control chemical additive into a slurry to prevent the crack formation during drying.

At present, rapid prototyping and 3D printing are powerful tools to perform systematic studies on the effect of porosities through an extensive control over pore architecture [30]. Scaffolds have been designed with different pore morphologies and sizes, presenting a homogenous/heterogeneous, monomodal/bimodal, and random/organized pore distribution. All these parameters have a profound effect not only in the mechanical properties but also in the biological properties of the material.

The importance of porous structure (especially interconnected porous structure) is clear for calcium phosphate cements when they are intended to replace the bone. However, the ideal method for fabricating interconnected porous structure has not been established so far. It should be balanced between macropore fabrication and the decreased mechanical strength for the practical use of calcium phosphate cements.

*Degradability and Its Regulation* Degradation is the process caused by the action of microenvironment in vivo when calcium orthophosphate breaks down into its simpler components. The degradability of CaP phases is mainly affected by their chemical composition and crystal properties, which related to the dissolution characteristic of the CaP materials implanted [64]. The chemical composition influences the internal bonding strength of calcium phosphate cements which is reflected in the stability and solubility [17].  $\beta$ -TCP has been found to dissolve faster in physiological solutions, as well as exhibiting a greater rate of dissolution or degradation than HA. Additionally, the crystal size and crystal perfection also affect the extent and mode of dissolution of CPCs hardened at different conditions. Other factors involve pH and solution composition, which are related to the solution properties. The dissolution of CPC hardened block is also affected by the porosity. Increasing the porosity greatly enhances the surface area in contact with fluids and, thus, leads to a faster dissolution rate.

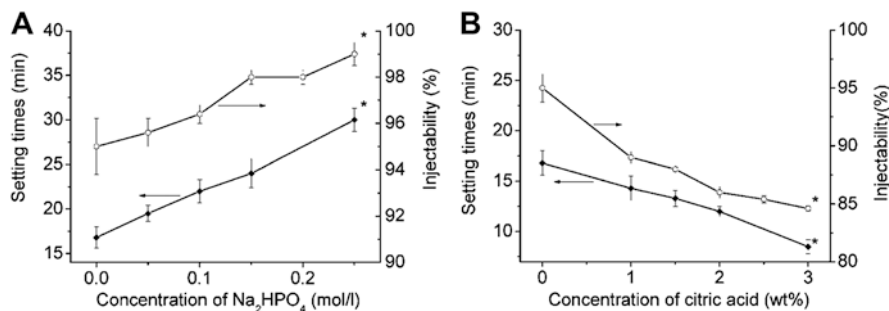
Dissolution property of the sparingly soluble synthetic or biological CaP compounds can be described by solubility product constants ( $K_{sp}$ ). Liu's group found that the solution property of CPC was influenced by the ratio of calcium to phosphate. When the ratios of calcium to phosphate were 1.67, 1.60, 1.55, and 1.50, the solubility products,  $-\log K_{sp}$ , were 99.2–102, 94.7–94.8, 89.6–90.5, and 85.5–86.4, respectively [20]. All these were significantly bigger than the values reported by the references due to the low crystallinity and calcium deficiency in the calcium phos-

phate cement hardening body. When CPC with Ca/P = 1.50 was immersed in fixed volumes of simulated blood plasma, both the calcium and phosphate concentrations in the solution increased, while for the samples with a ratio of 1.67, the concentrations decreased. These results showed that the simulated blood plasma was supersaturated to CPC with Ca/P = 1.67 while it was unsaturated to the CPC with Ca/P = 1.50. It was deduced that when CPC was implanted in the bodies, the specimen with the ratio of 1.5 was degraded faster than that with the sample of 1.67.

*Rheological Properties* Because of its good biocompatibility, excellent bioactivity, self-setting characteristic, low setting temperature, and easy shaping for any complicated geometry, CPC has been developed as an injectable bone substitute material in the noninvasive therapeutic approaches [65–69]. An injectable CPC is useful for fixation and augmentation of fractures, especially the osteoporotic bone fracture, such as femoral neck fracture, fractures of distal end of the radius, and the compression fracture of the spine.

The rheological properties such as the yield stress and viscosity play an important role in the process of cement delivery and infiltration into the cancellous bone cavities. For instance, the viscosity has to be kept sufficiently low and stable to ensure the low pressure required during injecting process; and the amount of solid particles in the suspension has to be maximized in order to ensure proper setting and mechanical strength of the final cement. Liu et al. [27] systematically described the rheological properties of concentrated aqueous injectable CPC slurry. The yield stress and hysteresis loop area were larger after 7 min of setting than those after 0.5 min, which indicate the increase of the resistance to flow or injection in CPC slurry and stability. The CPC slurry appeared to yield behavior at the low-strain and low-frequency range and presented the property of shear thinning. The changes of the storage modulus  $G'$ , the loss modulus  $G''$ , and the complex viscosity  $\eta^*$  reflect the flow property (or injection) and the internal structure development of the CPC slurry during the setting process. They increased with sweep time having the same trend and complied with the equation  $G' = A \exp . (Bt)$ , where the values of  $A$  and  $B$  were affected by technological parameters such as the P/L ratio, temperature, particle size matches, etc.

Obviously, viscous behavior evidently affected the rheological properties as well as the injectability of CPC. If the liquid phase is too viscous, the rheological properties of CPC will become inferior and increase the force for injection. Moreover, Wang et al. [70] concretely clarified the effects of additive on the rheological properties. In the work, the addition of disodium phosphate, PEG 200, glycerin, and citric acid remarkably influences the injectability and setting time of the ACP + DCPD bone cement, as shown in Fig. 1.11. With the increase of the disodium phosphate concentration to 0.25 mol/L, the viscosity of the paste was significantly reduced, and the injectability of the paste reached nearly 100%. It will be expedient for surgeons to put the cement into the internal treatment site and make the operation easier. With the increase of the citric acid concentration to 3.0 wt%, the setting time of the paste considerably decreased from  $16.8 \pm 1.2$  min to  $8.5 \pm 0.7$  min, while the injectability of the paste reduced to about 85%, which



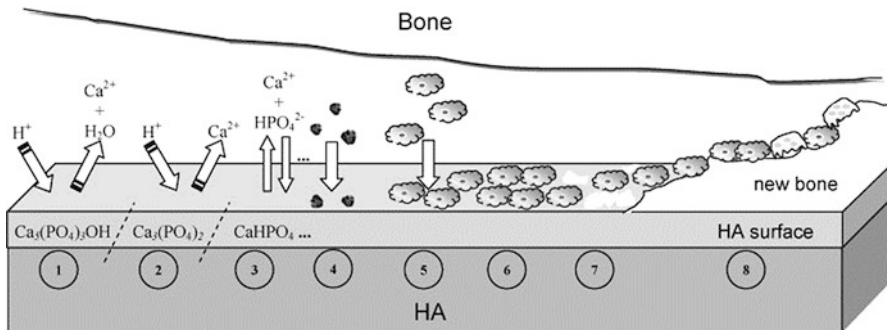
**Fig. 1.11** Influence of additives on the injectability and setting time of the pastes. (a) Influence of the concentration of  $\text{Na}_2\text{HPO}_4$  on the setting time and injectability of the pastes. (b) Influence of the concentration of citric acid on the setting time and injectability of the pastes. \* denotes statistical significant difference between the marked condition and deionized water ( $p < 0.05$ ) (Reproduced from Ref. [70] with permission. Copyright © 2005 Wiley Periodicals, Inc.)

seems still acceptable for clinical applications. The shortened setting time with acceptable injectability provides the surgeon an easy way to use such material in some urgent cases.

### 1.3.2 Biological Properties

**Biocompatibility and osteointegration** All CaP biomaterials have been found to be biocompatible. HA ceramics are considered as non-resorbable, while  $\beta$ -TCP is resorbable based on the amount of implant left as a function of time. To assess CPC biocompatibility, in vitro studies using the cement in a bulk form [71] or in a particle form with very large size [72] have been performed with different cell types. The phenomenon of mineralization always can be observed after CPC dipping in the simulated body fluid for several days. Alkaline phosphatase (ALP) and biomineralization of osteoblast on CPC can often be detected. Guo et al. [58] reported that Ca-deficient HA (CDHA) scaffolds from CPC exhibited no adverse effect on the growth, proliferation, and osteoblastic differentiation of marrow-derived mesenchymal stem cells (MSCs). Liu et al. systematically investigated the biocompatibility of CPC, including acute toxicity assay, cell culture cytotoxicity assay, gene mutation assay, chromosome aberration assay, and DNA damage assay. The results showed that CPC had no toxicity and all assays for mutagenicity and potential carcinogenicity of CPC extracts are negative [73].

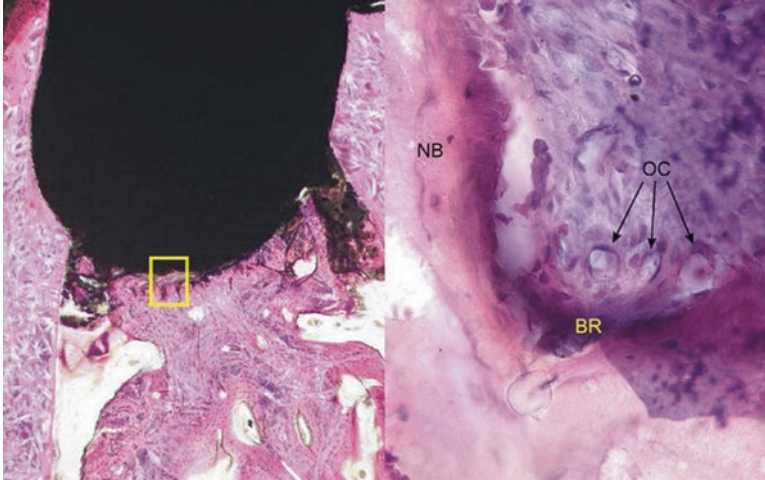
On the other hand, once calcium phosphate cements were implanted to the defect site in vivo, all interactions between implants and the surrounding tissues are dynamic processes [74]. Dissolved water and various biomolecules around the implant surface induce the change of pH value, and neutrophils will arrive at the area within initial few seconds after implantation, and the reactions occurring at the biomaterial/tissue interfaces lead to time-dependent changes in the surface charac-



**Fig. 1.12** A schematic diagram representing the phenomena that occur on HA surface after implantation: (1) beginning of the implant procedure, where a solubilization of the HA surface starts; (2) continuation of the solubilization of the HA surface; (3) the equilibrium between the physiological solutions and the modified surface of HA has been achieved (changes in the surface composition of HA does not mean that a new phase of DCPA or DCPD forms on the surface); (4) adsorption of proteins and/or other bioorganic compounds; (5) cell adhesion; (6) cell proliferation; (7) beginning of a new bone formation; (8) new bone has been formed (Reproduced from Ref. [75] with permission. Copyright © 2010 Elsevier B.V)

teristics of both the implanted biomaterials and the surrounding tissues. An inflammatory reaction was observed after implantation of calcium phosphate cements *in vivo*. The general conclusion on using calcium phosphates with Ca/P ionic ratio within 1.0–1.7 is that all types of implants (cements of various porosities and structures, powders, or granules) are not only nontoxic but also induce neither inflammatory nor foreign body reactions. Subsequently, osteoid is produced directly onto the surfaces of cements in the absence of a soft tissue interface. Consequently, the osteoid mineralizes and the resulting new bone undergoes remodeling. The biodegradation of CPCs is generally equivalent to bone formation. In 1997, our group implanted CPC into the femurs of rabbits under no-load condition. The results from histomorphology observation revealed that the implant tightly joined with the surrounding bone and the CPC is highly biocompatible [73] (Fig. 1.12).

**Osteoinductivity** Osteoinductivity is the ability of a material to induce osteogenesis and is demonstrated by bone formation in non-osseous (heterotopic) sites [19]. Bone morphogenetic proteins (BMPs) as osteoinductive factors have been verified that can significantly stimulate new bone formation [76, 77]. However, many studies have reported the osteoinductive properties associated with biomaterials only. The factors that affect the osteoinductive property of cements include the animal model, implantation sites, and the physicochemical properties of materials [78]. It is necessary to evaluate their ability to induce osteogenesis in ectopic sites. Zhang's group thought that calcium phosphate biomaterials have the property of osteoinduction when they exhibit specific chemical and structural characteristics [79]. In their experiments, calcium phosphate (HA, TCP/HA,  $\alpha$ -TCP,  $\beta$ -TCP, H-Cement, P-Cement)-induced osteogenesis was examined in dog muscle, while TiO<sub>2</sub> was used as a negative control. The following conclusions are obtained: (1) Porosity is a quite



**Fig. 1.13** (a) No inflammatory and infiltration is detectable (b) Zones of new developed bone and bone resorption can be observed (*BR* bone resorption, *NB* new bone, *OC* osteoclast) (Reproduced from Ref. [81] with permission. Copyright © 2006, Springer-Verlag)

important factor during osteogenesis; the absence of micropores resulted in the absence of bone induction. (2) Low sintering temperature is beneficial to calcium phosphate-induced osteogenesis. (3) Mild dissolution of the materials is more conducive to the ectopic bone formation. (4) Bone formation only occurred in the deep rugged surface of the cement and in pores into which soft tissue could grow. (5) Bone formation was only seen in calcium phosphate biomaterials, and osteoinduction could not be observed in  $\text{TiO}_2$  ceramics, although they had micropores on the macropore surface.

Moreover, a series of researches have already explored the effectiveness of CPC materials in dental applications. For example, Akiyoshi Sugawara [28] and Liu [80] have applied CPC material into root canal defeat as a sealer-filler. The results revealed that CPC could provide good sealing ability, in other words, providing an adequate seal of the canal without a separate sealer. In another case, TCP-based CPC was utilized to evaluate the inflammatory reactions and tissue responses when used as root canal fillers in dog model [81]. As was inferred from the results, the implantation of CPC material would not lead to inflammation and could facilitate the bone resorption and the growth of new bones. To further improve the performance of CPC, our group also introduced bismuth salicylate basic into CPC root canal filling. The radiopacity and sealability were largely improved compared to pure CPC. It was worth mentioning that the addition of bismuth led to strengthen the potent antimicrobial activity. It could be seen from the result that a uniform and tight adaptation to the root canal wall was formed (Fig. 1.13).

Recently, the osteoinductivity of CPCs was evaluated through investigating the ability to induce progenitor or undifferentiated cells like MSCs to differentiate toward the osteoblastic lineage in vitro. Common markers of the osteoblastic phe-

**Table 1.3** Key properties of CPCs that influence osteoblastic differentiation

CPC	Solubility ( $\sim K_{sp}$ )	Ca/P ratio	Osteoinductivity
HAP	Poor ( $10^{-58}$ )	1.67	+
TCP	Fair ( $10^{-25}$ – $10^{-29}$ )	1.5	++
ACP	High ( $10^{-23}$ – $10^{-25}$ )	1.15–1.67	+++
BCP	Variable (dependent on TCP/HAP ratio)	1.5–1.67	++++

Reprinted from Ref. [84] with permission. Copyright © 2013 Acta Materialia Inc. published by Elsevier Ltd

notype include type I collagen, ALP, BMP-2, osteopontin (OPN), osteocalcin (OCN), and bone sialoprotein (BSP) [82]. Through monitoring the expression of the relevant osteogenic genes, researchers found that CPC properties can significantly influence osteoinduction; detailed information are listed in Table 1.3.

However, the limited osteogenic capacity of calcium phosphate ceramics and CPCs mentioned above is attributed to their biomineralization that is often in direct and close contact to a matrix forming carbohydrate structure and adsorbing osteoinductive proteins like BMP-2. The osteoinduction of CPC is insufficient and cannot meet the conditions for the repair of large segment of bone defects. The introduction of BMP-2 to the materials can efficiently promote bone formation and accelerate the resorption of CPC [83].

## 1.4 Clinical Applications

### 1.4.1 Bone Repair

By now, CPCs have been widely used as bone replacement materials in orthopedic surgery. The most common use of CPC is as bone graft substitutes for filling of bone defects and subchondral voids in metaphyseal fractures, where it provides structural support and acts as an osteoconductive scaffold. A number of studies have been published that explore the possible use in different anatomic locations over the last several years. It is of great importance to have a review on the clinical applications of CPCs to confirm the superiority of CPC as artificial bone substitutes. Mohit Bhandari's group [77] adopted a meta-analysis of randomized trials to demonstrate whether the use of CPC improved outcomes in patients with metaphyseal fractures of the upper and lower extremities. The results suggested that the use of CPC for the treatment of fractures in patients was associated with a lower incidence of pain, a decreased risk of losing fracture reduction, lower infection rates in patients with radial fractures, and likely improved functional outcomes.

Based on the data we got in the past research, we also found that CPC used in bone defect repair didn't cause any allergic and toxic reactions. The radiological examination showed that the implanted CPC was directly bonded to the bone at the interface and the bone contour at the defect sites was successfully restored



**Fig. 1.14** X-ray images of the bone trauma repair. (a) Pre-operation of the left distal tibial comminuted fracture. (b) Post-operation of fracture reduction, plate fixation, and CPC filling in the defective site. (c) The patient recovered well in 1 year after surgery

(Fig. 1.14). From thousands of follow-up cases, the clinical results and feedbacks have demonstrated satisfactory treatments for bone tumor treatment, bone trauma repairing, or spine surgery.

Nowadays, calcium phosphate cements are attracting more and more interest; the properties of the materials are improving continually. Compared to the older generation of these products, new developments have improved wet-field properties, and newer products are much more resistant to shear forces. However, a major problem of calcium phosphate cements is the deficient osteoinductivity compared to autografts, which might cause delayed union or even nonunion in clinic for large bone defect. Infection caused during the operation is another mainly cause to limit its clinical applications.

### 1.4.2 Drug Delivery

Due to the non-exothermic setting reaction of CPC, CPC serves as an excellent carrier to encapsulate drugs, or proteins, leading to broad applications for local drug and biological molecule delivery devices to promote the healing of bone defects and treat some bone diseases [85, 86]. Unlike calcium phosphate ceramics employed as drug delivery systems, where the drugs are usually absorbed on the surface, in CPCs the drugs can be incorporated throughout the whole material volume, by incorporating them into the powder or liquid phase. Their ability to set at ambient condition when implanted within the body, giving a highly microporous material, allows the incorporation of many types of drugs and biologically bioactive molecules without losing activity and denaturalization.

The pore in CPC matrix is formed by a continuous dissolution-precipitation reaction after the mixtures of the composites of an aqueous phase and cement pow-

der. Appropriate porosity can retain the drugs and control its release. Nowadays, three basic strategies can be used for the drug incorporation into CPCs, including physically dispersing the drugs into cement solid phase or homogeneously dissolving the active substance in the liquid phase, impregnation of CPC with drug solution, or modifying the CPC with microencapsulated drug forms. For instance, Vorndran [87] proposed a controlled release system which combined a water-immiscible carrier liquid with suitable surfactants facilitating as discontinuous liquid exchange in CPC. The results demonstrated that this controlled release system appeared an initial burst release of ~7 to 28% antibiotics, followed by constant release rates. Uniquely, two antibiotics in this system exhibited two different release kinetics, which may be attributed to participation of the sulfate counter ion in the cement setting reaction altering the drug solubility. Additionally, Lopez-Heredia and his coworkers [88] have developed a local drug delivery system using a CPC as carrier of paclitaxel (PX). The results indicated that PX released from CPC remained active to influence cell viability and demonstrated that CPC is a feasible delivery vector for chemotherapeutic agents.

*Antibiotics* One of the key factors affecting the success of surgical interventions is to implant the osteoconductive material prevented from bacterial infections. Wound contamination or postoperative infections can cause serious contamination problems. For this reason, major attention has been paid to antibiotics due to their wide areas of applications [89], either as the treatment of bone infections or as the prophylactics to prevent infections produced during surgical interventions.

Due to the slow degradation rate and high mechanical strength, as an antibiotic carrier, CPC shows great advantages in the application of bone repair. Moreover, non-exothermic setting reaction of CPC is also a major advantage when used as a carrier of drug delivery systems since temperature-sensitive drug such as biological molecule will be inactive in the set cement [89]. However, the introduction of drugs will affect the hydration and hardening of CPC, such as prolonging the setting times and reducing the mechanical strength [89]. Meanwhile, the hydration process of CPC is often associated with drug inactivation. Therefore, when CPC is used as a carrier for sustained release of drugs, these factors should be considered for screening appropriate drugs and the dosage. As shown in Table 1.4, it summarizes the possible drugs that could be used in CPC system, which indicated the ratio of drugs to CPC and the setting time of CPC.

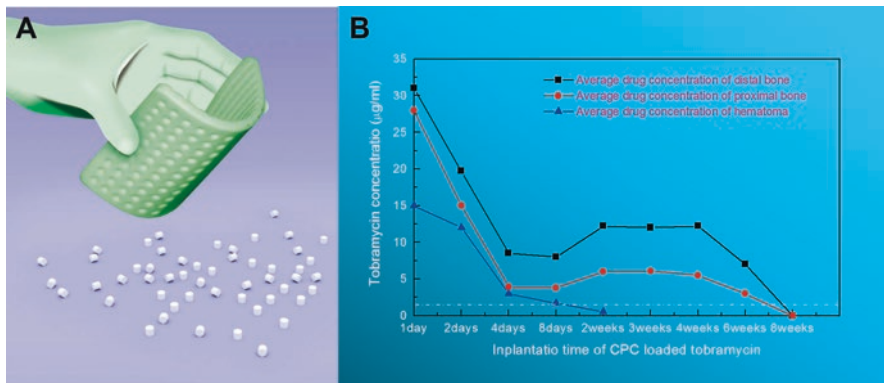
The release behavior of drug from CPC matrix is also important for effective treatment. During the drug loading process, the components of CPCs, P/L ratio, porosity, and additives will affect the release kinetics of antibiotic [83, 90]. For different indications, multiple CPC formulations need to be established for drug release. For prophylaxis, it is important that drug release from the CPC matrix is fast enough to reach concentrations above minimum inhibitory and avoid subinhibitory concentrations for long times, which may lead to bacterial resistance. Besides, the treatment of infectious pathologies such as osteomyelitis or periodontitis requires longer and sustained release of the antibiotic.



**Table 1.4** Reference of the usage compatibility of different drugs with CPC

Drug name	Content	Solid/liquid ratio	Setting time (min)	Classification	Remarks
Tobramycin	5%	5	14	Antibiotics –aminoglycosides	Maximum drug-loaded CPC usage: 40 g
Vancomycin	5%	3.5	10	Antibiotics	Maximum drug-loaded CPC usage: 100 g
Taineng (imipenem and cilastatin sodium)	5%	3.2	14	Antibiotics- $\beta$ -lactam	Maximum drug-loaded CPC usage: 200 g
Junbizhi (ceftriaxone, ceftriaxone sodium)	5%	6.6	12	Cephalosporin (third and fourth generation)	Maximum drug-loaded CPC usage: 200 g
Pipemidic acid	5%	3.1	5	Antibiotics – quinolones	
Metronidazole (Miediling)	5%	3.3	6	Antibiotics – nitrate imidazoles	
Methotrexate (MTX)	5%	5	5	Antitumor drugs – antimetabolites	
Adriamycin (ADM)	5%	4	10	Antitumor drugs – antitumor antibiotics	
Fluorouracil (5-FU)	5%	4	14	Antitumor drugs – antitumor antimetabolites	
Flutamide	5%	4	5	Antitumor drugs- antitumor hormonal drugs	
Lomustine	5%	5	18	Antitumor drugs – alkylating agent	
Naproxen sodium	5%	3	4	Anti-inflammatory agents	
Indometacin	5%	3.5	6	Anti-inflammatory agents	
Rifampicin	10%	3.5	8	Antitubercular agent	

The representative Rebone<sup>®</sup> drug-loaded CPC was presented in Fig. 1.15a, and the drug of tobramycin exhibited sustained release behaviors from CPC in vivo animal study (Fig. 1.15b). The results depicted that the tobramycin-incorporated CPC can maintain the effective concentration of drug up to 6–8 weeks, which is very important to the treatment of chronic osteomyelitis. On the basis of the results, our group further investigated the repair capacity of tobramycin-loaded CPC in the



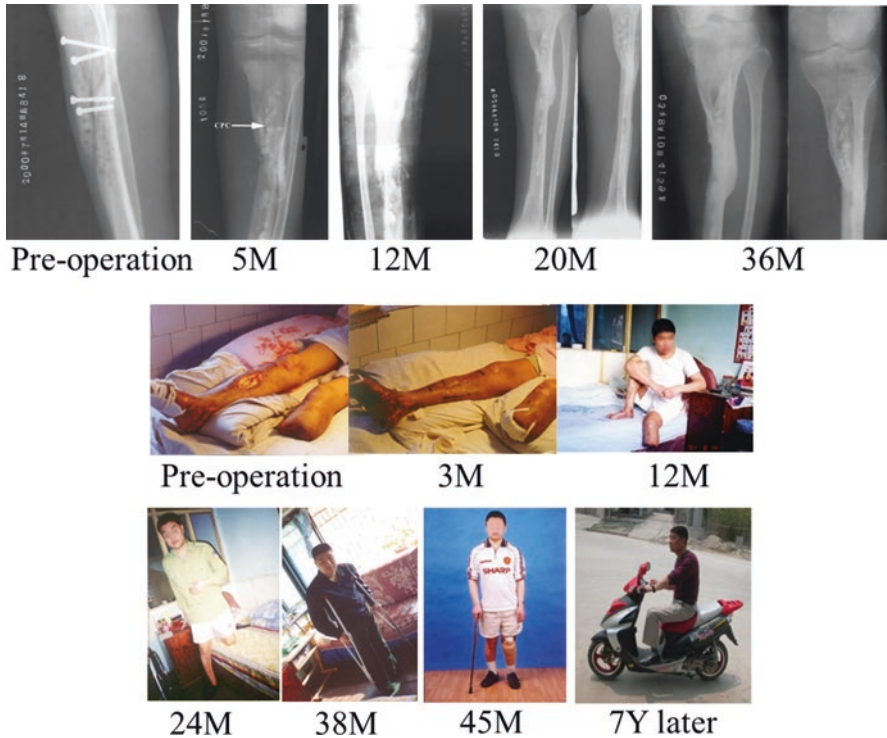
**Fig. 1.15** The product drug-impregnated CPC and the release curves of tobramycin. (a) Representative drug-impregnated CPC products. (b) The changes of drug concentration at implanted site over time. The white dot line represents the effective antimicrobial concentration of tobramycin (Reproduced from Ref. [91] by permission)

femora of rabbits. The CPC with a tobramycin dose of 6.5% did not show a side effect on the bone formation. Drug-loaded CPC bars were partially absorbed and new bone formed in bars without obvious inflammatory 3 months later after operation [91] (Table 1.4).

In Fig. 1.16, it is the situation that a 29-year-old male patient underwent the treatment of CPC implantation. His left leg was amputated after dropped out the hurt, and his right tibia defection was infected by *Pseudomonas aeruginosa* after open fractures. After the local debridement, clearing away the dead bone and tibial medullary cavity expansion, 10 g CPC powder with 0.5 g vancomycin, 0.5 g piperacillin, and some autogenous iliac graft bone were applied to fill the bone defection with negative pressure drainage. The patient had good postoperative conditions without irritation locally. After 3–5 months, X-ray images started to show a small amount of callus growth. 1 year later, the graft bone healed well and the lesions did not relapse. There was no recurrence of lesions at 24 months and 36 months after operation, and the patient could support the fields. The left leg was installed with artificial limb. The patient could re-walk after 45 months. The above results fully confirmed the performance of CPC.

**Bone Morphogenetic Protein-2 (BMP-2)** It is a highly potent osteoinductive growth factor and has been considered as the most notable cytokine to enhance bone formation and bone tissue reconstruction. Recombinant human BMP-2 (rhBMP-2)-loaded absorbable collagen sponge has been approved by the FDA in 2002 for interbody fusion surgeries, and its osteogenic capacity has been validated in numerous studies [92].

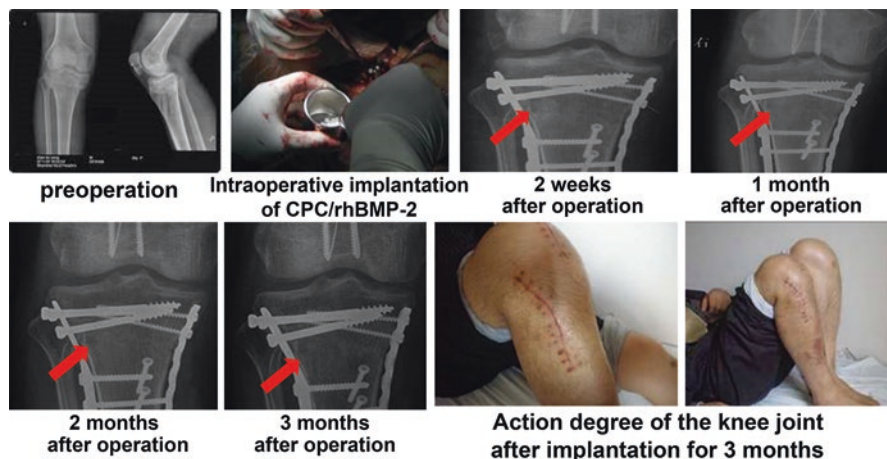
To address the drawbacks of low osteogenetic capacity and the prolonged regeneration time associated with the materials currently applied in clinic, highly active artificial bone repair materials, loaded with rhBMP-2, have been developed. In the past clinical application case, the CPC/rhBMP-2 scaffold exhibited an excellent



**Fig. 1.16** X-ray images (*up*) and bone growth conditions (*down*) of the patient with amputated leg, where *M* means month and *Y* means year

therapeutic capacity in tibial plateau fracture. In the case of CPC/rhBMP-2 bone-repair material by our group, a male patient suffered from fracture of tibial plateau. At 1 month after operation, the density of the material was similar to the normal bone tissue, and the shape of particles disappeared. After 3 months, trabecular bone has appeared and matured; the patient acquired a good active degree of the knee joint (Fig. 1.17).

The clinical studies demonstrated the superior overall performances of CPC/rhBMP-2 scaffold for enhancing bone regeneration in treatment of the bone fracture and would also provide an excellent candidate to treat the bone nonunion, delay unions, and vertebral fusion. Due to the high cost and the underlying side effect of high dose of growth factor, a controlled release profile is particularly important. Some researchers proposed that CPC can be modified by employing another drug delivery system in cement. By employing other systems, drug release profile can be regulated. For example, the growth factor incorporated with biodegradable microspheres containing drug mixed with the cement can significantly avoid burst release of the drug. Also, dissolved polymer can be used to create pores; thereafter cells and bone tissue can be penetrated into the pores [85].



**Fig. 1.17** Clinic application of CPC in a tibial plateau fracture case

**Cancer** Various antitumor drugs or antibiotics in setting solution are usually incorporated into the cement by blending the solution with solid powders of CPC and thus achieve a homogenous distribution in CPC, filling in diseased sites. Drugs will be located between the entangled crystals after self-setting, kept at specific site, and can be released in a continuous way via diffusion, which could maintain a high dose at local positions to effectively control and cure the cancer while reducing side effects. For example, Liu et al. has explored the optimal ratio between CPC and cisplatin [93]. The results revealed that CPC/cisplatin complex was not only beneficial to the repairing of bone defect but also limited the growth of tumor when the loading of cisplatin reached 0.1%. In another case, an injectable CPC was established for the local delivery of paclitaxel to the bone [88]. Both the in vitro experiment and chemotherapeutic loading model indicated that the burst release of paclitaxel was reduced and the drug released remained active to induce the apoptosis of cancer cells.

Compared to traditional therapies, the non-exothermic setting reaction of CPC is a major advantage when it is used as a carrier of drug delivery systems since temperature-sensitive drug and biological molecules can be loaded in the set cement [88]. Drug-loaded CPCs could concentrate the drugs at local sites for a much longer and more sustainable release. Such release profile could promote the antitumor efficacy of the system while decreasing the side effects. Drug-loaded CPC is now successfully and widely used in bone repair and casts new light on the effective treatment of chronic osteomyelitis. In addition, when CPC is loaded with current drug delivery system, such as polymer microspheres or silicon particle, more complicated and delicate tune of one or multidrugs could be achieved.

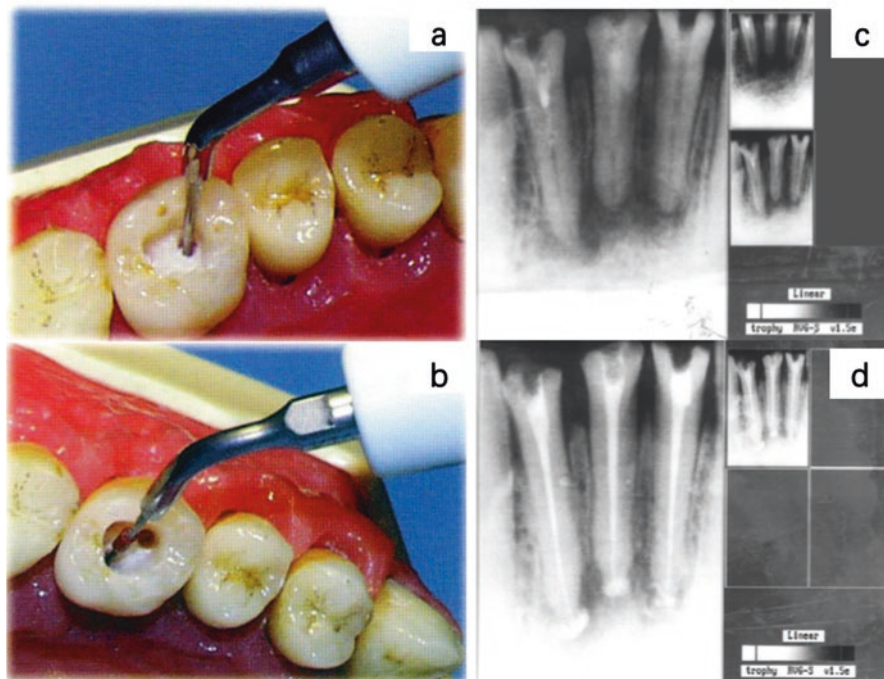
### 1.4.3 Dental Applications

Due to its specific strength in injectability and shaping properties, CPC is also widely employed in oral and dental applications, such as root canal fillers, pulpotomy, and periodontal bone defect repair. Naturally, calcium phosphates serve as the main component of oral and dental hard tissues and alveolar. To resolve commonly appeared problems, including pathological calcification, periodontal diseases, demineralization of dental tissues, and so on, therapeutic applications of CPC are possible.

Pulpotomy is an excellent platform for displaying the advantage of CPCs. Bijimole Jose employed CPC as an ideal pulpotomy material considering its biocompatibility and dentinogenic properties, exploring its suitability for pulpotomy in children within 8–12 years old, compared with form oculosol, which indicated that CPC offered more favorable results, showing low pulpal inflammation [94]. Meanwhile, CPC contributed to better formation of dentine bridge both in quantity and quality.

Root canal therapy is the most effective treatment for dental pulp diseases and periapical disease. The selected filler materials could determine the success and failure of the treatment. The CPC materials have already substantiated its effectiveness in root canal therapy. The cement is of great mobility, thus easy to be injected into root canal. Meanwhile, an appropriate curing time and suspension stability ensure its flexibility in the operation. After setting, the material boosts good compression strength and good integration with surrounding tissues. Figure 1.18 demonstrated the typical case of the CPC injection in pulpitis. CPC was injected into the hollow sites in the tooth during operation. Figure 1.18 (d) showed that no adverse response occurred even the overfilling of CPC due to the high biocompatibility of the material. No gutta-percha point was needed during treatment. The utilization of CPC in root canal therapy is of great effectiveness and promising resulting from the outperformed efficacy compared to the traditional methods.

Alveolar repairing is another area where CPCs could demonstrate its superiority. The defect in alveolar bone is a progressive pathological process, usually induced by periodontal diseases, and has long been the focus of clinicians. In one of the *in vivo* cases, Gutai (porous CPC commercial product) provided by Rebone Company was utilized to observe its effectiveness in alveolar repairing [95]. As it could be seen from the results, the introduction of CPC into defect sites could promote the formation of new tissues. The CPC can provide Ca and P with high concentration at local sites and facilitate the growth of new bone as the supporting scaffold. In another example, CPC was further tested in patients with alveolar defects [96]. The CPCs could be easily injected and impacted into defect sites with minimal invasion. Wound healing, clinical periodontal parameters, and the distal alveolar bone height of mandibular second molars were evaluated, and the conditions were significantly improved with an increase in both bone density and alveolar bone height after the usage of CPCs. To sum up, CPCs serve as one of the promising candidates in alveolar repairing.



**Fig. 1.18** The treatment of pulpitis by root canal filling using CPC. The pretreatment of root canal (a, b); X-ray film of the teeth before operation (c); X-ray film after treatment (d). CPC was injected into the root canal, showing no adverse response even overfilling of material

In addition, self-setting CPCs were applied as adjunctive supportive agents in restoration of enamel carious cavities and in other oral and dental areas. With decades of practice, encouraging results in clinical use corroborate that the CPC acts as a promising selection in the dental areas, for its biocompatibility, good sealing property, and promoting effects on new bone formation.

In spite of the above advantages, several issues still have to be addressed, such as the search of an appropriate curing time and the flexible control over degradation rate. It is expected that with the deepening on the research of CPC, the physical and chemical properties, as well as biological behaviors, will be further enhanced to meet with the increasing needs in dental applications.

## 1.5 Summary and Perspectives

In this chapter, the history and development of CPCs are described. It requires generational improvements to bring the materials into clinical applications. With the joint efforts of scientists, the materials now boost fantastic features, such as easy

shaping, self-setting properties, controlled biodegradability, and excellent biocompatibility, which could largely facilitate the uses in biomedical areas and bring great benefits to patients.

To fully understand and further explore the CPC materials, it is also necessary to dig into the setting mechanism and kinetics. The fundamental principle of the hydration-hardening of calcium phosphate compounds is based on their various solubilities in water. The different factors affecting the hydration-hardening process have been investigated, which can offer a guide for future material improvement.

The physical, chemical, and biological properties are also discussed. Mechanical properties are largely dependent on porosity and could be strengthened by polymeric coatings or infiltration of polymers. Degradability of CPC materials is mainly related to the chemical composition, porosity, and particle size, which could be tuned to satisfy the patient's needs as far as possible. Meanwhile, to achieve practical use as injectable biomaterials, rheological properties are also studied. Biologically, CPC materials boost excellent biocompatibility, osteointegration, and osteoinductivity. The implanted CPC facilitates the bone healing and possesses good integrity with surrounding tissues without severe side effects.

Up to now, the CPCs have been extensively applied in clinic application attributing to their versatility and flexibility, and the results are quite encouraging. However, there still are a number of issues that should be addressed [97]. Firstly, the current available products still cannot satisfy every need of the patients. The formulations with more specific tuned mechanical and biological properties have remained a problem. Secondly, CPCs are not superior to traditional materials in compressive loading in load-bearing sites. Another concern in the use of CPCs is that inflammation and other adverse reactions still exist at surrounding sites due to the incomplete hydration and impurities [98]. Considering all the existing issues, there is a great potential for further improvements [99]. A more precise control over powder physical and chemical properties, tunable microstructures, and novel additives is expected to meet the increasing needs. Meanwhile, surgeons are still looking forward to ready-to-use formulations, which are more convenient to use clinically and at lower price. More researches are required, and the perfect substituting material is still on the way.

**Acknowledgments** This investigation was supported by National Key Research and Development Program of China (No.2016YFC1102900), National Natural Science Foundation of China (No.31370960), and Shanghai Pujiang Program (16PJD015).

## References

1. Mousa WF, Kobayashi M, Shinzato S, Kamimura M, Neo M, Yoshihara S, Nakamura T (2000) Biological and mechanical properties of PMMA-based bioactive bone cements. *Biomaterials* 21(21):2137–2146
2. Frazer RQ, Byron RT, Osborne PB, West KP (2005) PMMA: an essential material in medicine and dentistry. *J Long Term Eff Med* 15(6):629–639

3. Monma H, Ueno S, Kanazawa T (1981) Properties of hydroxyapatite prepared by the hydrolysis of tricalcium phosphate. *J Chem Technol and Biotechnol* 31(1):15–24
4. Brown WE, Chow LC (1985) Dental restorative cement pastes. US 4518430 A, 1985
5. Zhang J, Zhou H, Yang K, Yuan Y, Liu C (2013) RhBMP-2-loaded calcium silicate/calcium phosphate cement scaffold with hierarchically porous structure for enhanced bone tissue regeneration. *Biomaterials* 34(37):9381–9392
6. Zhang J, Ma X, Lin D, Shi H, Yuan Y, Tang W, Zhou H, Guo H, Qian J, Liu C (2015) Magnesium modification of a calcium phosphate cement alters bone marrow stromal cell behavior via an integrin-mediated mechanism. *Biomaterials* 53:251–264
7. Thormann U, Ray S, Sommer U, ElKhasawna T, Rehling T, Hundgeburth M, Henß A, Rohnke M, Janek J, Lips KS (2013) Bone formation induced by strontium modified calcium phosphate cement in critical-size metaphyseal fracture defects in ovariectomized rats. *Biomaterials* 34(34):8589–8598
8. Ding S, Zhang J, Tian Y, Huang B, Yuan Y, Liu C (2016) Magnesium modification up-regulates the bioactivity of bone morphogenetic protein-2 upon calcium phosphate cement via enhanced BMP receptor recognition and Smad signaling pathway. *Colloid Surf B* 145:140–151
9. Lode A, Wolf-Brandstetter C, Reinstorf A, Bernhardt A, König U, Pompe W, Gelinsky M (2007) Calcium phosphate bone cements, functionalized with VEGF: release kinetics and biological activity. *J Biomed Mater Res A* 81(2):474–483
10. Wang M, Yu Y, Dai K, Ma Z, Liu Y, Wang J, Liu C (2016) Improved osteogenesis and angiogenesis of magnesium-doped calcium phosphate cement via macrophage immunomodulation. *Biomater Sci* 4(11):1574–1583
11. Ishikawa K (2010) Bone substitute fabrication based on dissolution-precipitation reactions. *Materials* 3(2):1138–1155
12. Bohner M, Gbureck U, Barralet JE (2005) Technological issues for the development of more efficient calcium phosphate bone cements: a critical assessment. *Biomaterials* 26(33):6423–6429
13. Wei J, Chen F, Shin J-W, Hong H, Dai C, Su J, Liu C (2009) Preparation and characterization of bioactive mesoporous wollastonite–polycaprolactone composite scaffold. *Biomaterials* 30(6):1080–1088
14. Wei J, Jia J, Wu F, Wei S, Zhou H, Zhang H, Shin J-W, Liu C (2010) Hierarchically microporous/macroporous scaffold of magnesium–calcium phosphate for bone tissue regeneration. *Biomaterials* 31(6):1260–1269
15. Raynaud S, Champion E, Bernache-Assollant D, Thomas P (2002) Calcium phosphate apatites with variable Ca/P atomic ratio I. Synthesis, characterisation and thermal stability of powders. *Biomaterials* 23(4):1065–1072
16. Xu HHK, Carey LE, Simon CG Jr, Takagi S, Chow LC (2007) Premixed calcium phosphate cements: Synthesis, physical properties, and cell cytotoxicity. *Dent Mater* 23(4):433–441
17. Kalita SJ, Bhardwaj A, Bhatt HA (2007) Nanocrystalline calcium phosphate ceramics in biomedical engineering. *Mater Sci Eng C* 27(3):441–449
18. Ginebra MP, Espanol M, Montufar EB, Perez RA, Mestres G (2010) New processing approaches in calcium phosphate cements and their applications in regenerative medicine. *Acta Biomater* 6(8):2863–2873
19. Ben-Nissan B (2014) *Advances in Calcium Phosphate Biomaterials*. Springer, Berlin, pp 199–223
20. Liu C, Shen W, Chen J (1999) Solution property of calcium phosphate cement hardening body. *Mater Chem Phys* 58(1):78–82
21. Tenhuisen KS, Brown PW (1998) Formation of calcium-deficient hydroxyapatite from  $\alpha$ -tricalcium phosphate. *Biomaterials* 19(23):2209–2217
22. Liu C, Gai W, Pan S, Liu Z (2003) The exothermal behavior in the hydration process of calcium phosphate cement. *Biomaterials* 24(18):2995–3003
23. Liu C, Shen W (1997) Effect of crystal seeding on the hydration of calcium phosphate cement. *J Mater Sci-Mater M* 8(12):803–807



24. Liu C, Huang Y, Zheng H (1999) Study of the hydration process of calcium phosphate cement by AC impedance spectroscopy. *J Am Ceram Soc* 82(4):1052–1057
25. Liu C, Shao H, Chen F, Zheng H (2003) Effects of the granularity of raw materials on the hydration and hardening process of calcium phosphate cement. *Biomaterials* 24(23):4103–4113
26. Liu C, Huang Y, Chen J (2004) The physicochemical properties of the solidification of calcium phosphate cement. *J Biomed Mater Res B* 69(1):73–78
27. Liu C, Shao H, Chen F, Zheng H (2006) Rheological properties of concentrated aqueous injectable calcium phosphate cement slurry. *Biomaterials* 27(29):5003–5013
28. Sugawara A, Chow LC, Takagi S, Chohayeb H (1990) In vitro evaluation of the sealing ability of a calcium phosphate cement when used as a root canal sealer-filler. *J Endodont* 16(4):162–165
29. Cheng HC, Chu KT, Teng NC, Tsai HL, Ou KL, Ou SF (2014) The effect of pH value on phase transformation of calcium phosphate cement. *Int J Appl Ceram Tec* 11(2):364–370
30. Espanol M, Perez R, Montufar E, Marichal C, Sacco A, Ginebra M (2009) Intrinsic porosity of calcium phosphate cements and its significance for drug delivery and tissue engineering applications. *Acta Biomater* 5(7):2752–2762
31. Chen C-K, Ju C-P, Lin J-HC (2012) Setting solution concentration effect on properties of a TTCP/DCPA-derived calcium phosphate cement. *J Mater Sci-Mater M* 23(9):2109–2114
32. Grover LM, Hofmann MP, Gbureck U, Kumarasami B, Barralet JE (2008) Frozen delivery of brushite calcium phosphate cements. *Acta Biomater* 4(6):1916–1923
33. Cama G, Barberis F, Capurro M, Di Silvio L, Deb S (2011) Tailoring brushite for in situ setting bone cements. *Mater Chem Phys* 130(3):1139–1145
34. Generosi A, Rau JV, Komlev VS, Albertini VR, Fedotov AY, Barinov SM (2009) Anomalous hardening behavior of a calcium phosphate bone cement. *J Phys Chem B* 114(2):973–979
35. Smirnov VV, Rau JV, Generosi A, Albertini VR, Ferro D, Barinov SM (2010) Elucidation of real-time hardening mechanisms of two novel high-strength calcium phosphate bone cements. *J Biomed Mater Res B* 93(1):74–83
36. Paduraru G, Aelenei N, Luca D, Cimpoeșu N (2011) New brushite cements analysis. *Optoelectron Adv Mater Rapid Commun* 5:465–468
37. Ueyama Y, Ishikawa K, Mano T, Koyama T, Nagatsuka H, Matsumura T, Suzuki K (2001) Initial tissue response to anti-washout apatite cement in the rat palatal region: Comparison with conventional apatite cement. *J Biomed Mater Res* 55(4):652–660
38. Ishikawa K, Takagi S, Chow LC, Ishikawa Y (1995) Properties and mechanisms of fast-setting calcium phosphate cements. *J Mater Sci-Mater M* 6(9):528–533
39. Tenhuisen K, Brown P (1994) The effects of citric and acetic acids on the formation of calcium-deficient hydroxyapatite at 38 C. *J Mater Sci-Mater M* 5(5):291–298
40. Bohner M, Lemaître J, Ring TA (1996) Effects of sulfate, pyrophosphate, and citrate ions on the physicochemical properties of cements made of  $\beta$ -tricalcium phosphate-phosphoric acid-water mixtures. *J Am Ceram Soc* 79(6):1427–1434
41. Hench LL, Polak JM (2002) Third-generation biomedical materials. *Science* 295(5557):1014–1017
42. Moore WR, Graves SE, Bain GI (2001) Synthetic bone graft substitutes. *ANZ J Surg* 71(6):354–361
43. Costantino PD, Friedman CD (1994) Synthetic bone graft substitutes. *Otolaryng Clin N Am* 27(5):1037–1074
44. Ishikawa K, Asaoka K (1995) Estimation of ideal mechanical strength and critical porosity of calcium phosphate cement. *J Biomed Mater Res* 29(12):1537–1543
45. Xu HH, Eichmiller FC, Giuseppetti AA (2000) Reinforcement of a self-setting calcium phosphate cement with different fibers. *J Biomed Mater Res* 52(1):107–114
46. Gorst N, Perrie Y, Gbureck U, Hutton A, Hofmann M, Grover L, Barralet J (2006) Effects of fibre reinforcement on the mechanical properties of brushite cement. *Acta Biomater* 2(1):95–102

47. Perez RA, Mestres G (2016) Role of pore size and morphology in musculo-skeletal tissue regeneration. *Mater Sci Eng C* 61:922–939
48. Sánchez-Salcedo S, Arcos D, Vallet-Regí M (2008) Upgrading calcium phosphate scaffolds for tissue engineering applications. In: *Key engineering materials*. Trans Tech Publ, Durnten-Zurich, pp 19–42
49. Ribeiro GB, Trommer RM, dos Santos LA, Bergmann CP (2011) Novel method to produce  $\beta$ -TCP scaffolds. *Mater Lett* 65(2):275–277
50. Silva TSN, Primo BT, Júnior S, Novaes A, Machado DC, Viezzer C, Santos LA (2011) Use of calcium phosphate cement scaffolds for bone tissue engineering: in vitro study. *Acta Cir Bras* 26(1):7–11
51. Li SH, Wijn JR, Layrolle P, Groot K (2003) Novel method to manufacture porous hydroxyapatite by dual-phase mixing. *J Am Ceram Soc* 86(1):65–72
52. De Oliveira J, De Aguiar P, Rossi A, Soares G (2003) Effect of process parameters on the characteristics of porous calcium phosphate ceramics for bone tissue scaffolds. *Artif Organs* 27(5):406–411
53. Pal K, Pal S (2006) Development of porous hydroxyapatite scaffolds. *Mater Manuf Process* 21(3):325–328
54. Tas A (2008) Preparation of porous apatite granules from calcium phosphate cement. *J Mater Sci-Mater M* 19(5):2231–2239
55. Xu HH, Quinn JB, Takagi S, Chow LC, Eichmiller FC (2001) Strong and macroporous calcium phosphate cement: effects of porosity and fiber reinforcement on mechanical properties. *J Biomed Mater Res* 57(3):457–466
56. Hesaraki S, Sharifi D (2007) Investigation of an effervescent additive as porogenic agent for bone cement macroporosity. *Biomed Mater Eng* 17(1):29–38
57. Hesaraki S, Moztarzadeh F, Sharifi D (2007) Formation of interconnected macropores in apatitic calcium phosphate bone cement with the use of an effervescent additive. *J Biomed Mater Res A* 83(1):80–87
58. Guo H, Su J, Wei J, Kong H, Liu C (2009) Biocompatibility and osteogenicity of degradable Ca-deficient hydroxyapatite scaffolds from calcium phosphate cement for bone tissue engineering. *Acta Biomater* 5(1):268–278
59. Liu W, Zhang J, Weiss P, Tancret F, Bouler J-M (2013) The influence of different cellulose ethers on both the handling and mechanical properties of calcium phosphate cements for bone substitution. *Acta Biomater* 9(3):5740–5750
60. Xu HH, Weir MD, Burguera EF, Fraser AM (2006) Injectable and macroporous calcium phosphate cement scaffold. *Biomaterials* 27(24):4279–4287
61. Barralet J, Grover L, Gaunt T, Wright A, Gibson I (2002) Preparation of macroporous calcium phosphate cement tissue engineering scaffold. *Biomaterials* 23(15):3063–3072
62. Ramay HR, Zhang M (2003) Preparation of porous hydroxyapatite scaffolds by combination of the gel-casting and polymer sponge methods. *Biomaterials* 24(19):3293–3302
63. Park Y-S, Kim K-N, Kim K-M, Choi S-H, Kim C-K, Legeros RZ, Lee Y-K (2006) Feasibility of three-dimensional macroporous scaffold using calcium phosphate glass and polyurethane sponge. *J Mater Sci* 41(13):4357–4364
64. Dorozhkin SV (2012) Calcium orthophosphates: applications in nature, biology, and medicine. Taylor & Francis, Danvers
65. Yuan H, Li Y, De Bruijn J, De Groot K, Zhang X (2000) Tissue responses of calcium phosphate cement: a study in dogs. *Biomaterials* 21(12):1283–1290
66. Liu C, Gai W. Injectable in-situ setting inorganic bone cement and its application in minimally invasive treatment. Chinese patent number: ZL2003 1 15250.3
67. Liu C, Chen F, Mao Y. Injectable calcium phosphate bone cement with high suspension stability and its preparation method and application. Chinese patent number: ZL2009 1 0197934.8
68. Liu C, Chen F, Wei J. Injectable calcium magnesium bone cement and its preparation method and application. Chinese patent number: ZL 201010205094.8

69. Liu C, Hong H. A preparation method of developed and inflatable balloons for percutaneous kyphoplasty. Chinese patent number: ZL 2011 1 0107501.6
70. Wang X, Ye J, Wang H (2006) Effects of additives on the rheological properties and injectability of a calcium phosphate bone substitute material. *J Biomed Mater Res B* 78(2):259–264
71. Oreffo RO, Driessens FC, Planell JA, Triffitt JT (1998) Growth and differentiation of human bone marrow osteoprogenitors on novel calcium phosphate cements. *Biomaterials* 19(20):1845–1854
72. Pioletti DP, Takei H, Lin T, Van Landuyt P, Ma QJ, Kwon SY, Sung K-LP (2000) The effects of calcium phosphate cement particles on osteoblast functions. *Biomaterials* 21(11):1103–1114
73. Liu C, Wang W, Shen W, Chen T, Gu Y, Chen Z (1997) Evaluation of the biocompatibility of a nonceramic hydroxyapatite. *J Endodontics* 23(8):490–493
74. Dorozhkin SV (2015) Calcium orthophosphate bioceramics. *Ceram Int* 41(10):13913–13966
75. Bertazzo S, Zambuzzi WF, Campos DD, Ogeda TL, Ferreira CV, Bertran CA (2010) Hydroxyapatite surface solubility and effect on cell adhesion. *Colloid Surf B* 78(2):177–184
76. Zhou H, Qian J, Wang J, Yao W, Liu C, Chen J, Cao X (2009) Enhanced bioactivity of bone morphogenetic protein-2 with low dose of 2-N, 6-O-sulfated chitosan in vitro and in vivo. *Biomaterials* 30(9):1715–1724
77. Tang W, Lin D, Yu Y, Niu H, Guo H, Yuan Y, Liu C (2016) Bioinspired trimodal macro/micro/nano-porous scaffolds loading rhBMP-2 for complete regeneration of critical size bone defect. *Acta Biomater* 32:309–323
78. Barradas A, Yuan H, Blitterswijk CA, Habibovic P (2011) Osteoinductive biomaterials: current knowledge of properties, experimental models and biological mechanisms. *Eur Cells Mater* 21:407–429
79. Yuan H, Yang Z, Li Y, Zhang X, De Bruijn J, De Groot K (1998) Osteoinduction by calcium phosphate biomaterials. *J Mater Sci-Mater M* 9(12):723–726
80. Liu C, Chen J. Self-setting calcium phosphate root canal filling agent. Chinese Patent number: ZL 03115251.1
81. Noetzel J, Özer K, Reissbauer B-H, Anil A, Rössler R, Neumann K, Kielbassa AM (2006) Tissue responses to an experimental calcium phosphate cement and mineral trioxide aggregate as materials for furcation perforation repair: a histological study in dogs. *Clin Oral Invest* 10(1):77–83
82. Albrektsson T, Johansson C (2001) Osteoinduction, osteoconduction and osseointegration. *Eur Spine J* 10(2):S96–S101
83. Liu C, Chen F, Yang G. Self-setting calcium phosphate cement with high in-situ osteogenetic activity and its preparation method and application. Chinese patent number: ZL 2002150885.2
84. Samavedi S, Whittington AR, Goldstein AS (2013) Calcium phosphate ceramics in bone tissue engineering: a review of properties and their influence on cell behavior. *Acta Biomater* 9(9):8037–8045
85. Ginebra M-P, Canal C, Espanol M, Pastorino D, Montufar EB (2012) Calcium phosphate cements as drug delivery materials. *Adv Drug Deliv Rev* 64(12):1090–1110
86. Verron E, Boulter J, Guicheux J (2012) Controlling the biological function of calcium phosphate bone substitutes with drugs. *Acta Biomater* 8(10):3541–3551
87. Vorndran E, Geffers M, Ewald A, Lemm M, Nies B, Gbureck U (2013) Ready-to-use injectable calcium phosphate bone cement paste as drug carrier. *Acta Biomater* 9(12):9558–9567
88. Lopez-Heredia MA, Kamphuis GB, Thüne PC, Öner FC, Jansen JA, Walboomers XF (2011) An injectable calcium phosphate cement for the local delivery of paclitaxel to bone. *Biomaterials* 32(23):5411–5416
89. Ginebra M-P, Traykova T, Planell JA (2006) Calcium phosphate cements: competitive drug carriers for the musculoskeletal system? *Biomaterials* 27(10):2171–2177
90. Ginebra M-P, Traykova T, Planell J (2006) Calcium phosphate cements as bone drug delivery systems: a review. *J Control Release* 113(2):102–110

91. Wang CJ, Chen TY, Zhang J, Liu CS (2001) An in vivo study of tobramycin-impregnated calcium phosphate cement as an artificial bone material repairing bone defect. *J Fudan Univ* 28(6):473–475
92. Bessa PC, Casal M, Reis R (2008) Bone morphogenetic proteins in tissue engineering: the road from laboratory to clinic, part II (BMP delivery). *J Tissue Eng Regen M* 2(2–3):81–96
93. Liu Y, Liu M, Ren P (2009) Drug delivery of CPC/cisplatin complex in vitro and its ability to repair bone defect and eliminate tumor in vivo. *J Cent South Univ* 34(10):991–997
94. Jose B, Ratnakumari N, Mohanty M, Varma H, Komath M (2013) Calcium phosphate cement as an alternative for formocresol in primary teeth pulpotomies. *Indian J Dent Res* 24(4):522
95. Zhao J, Wang LH, Bi LJ, Wang N, Li SW, Hu CY, Bao HX (2008) Experimental study on repairing alveolar bone defect of dogs with the compound of placenta tissue injection and CPC. *Chin J Conserv Dent* 18(7):375–380
96. Yang XQ, Chen J, Ma WQ, Wang ZP, Zheng JF (2014) Injectable calcium phosphate ceramics suspension to restore alveolar bone defect after extraction of impacted mandibular third molar. *Sichuan J Physiol Sci* 36(3):105–108
97. Naito K, Obayashi O, Mogami A, Itoi A, Kaneko K (2008) Fracture of the calcium phosphate bone cement which used to enchondroma of the hand: a case report. *Eur J Orthop Surgery Traumatol* 18(5):405–408
98. Wong RK, Gandolfi BM, St-Hilaire H, Wise MW, Moses M (2011) Complications of hydroxyapatite bone cement in secondary pediatric craniofacial reconstruction. *J Craniofac Surg* 22(1):247–251
99. Dorozhkin SV (2013) Self-setting calcium orthophosphate formulations. *J Funct Biomater* 4(4):209–311

## Chapter 2

# Self-Setting Calcium Orthophosphate ( $\text{CaPO}_4$ ) Formulations

Sergey V. Dorozhkin

**Abstract** In the early 1980s, researchers discovered self-setting calcium orthophosphate ( $\text{CaPO}_4$ ) cements, which are bioactive and biodegradable grafting bioceramics in the form of a powder and a liquid. After mixing, both phases form pastes of variable viscosity, which set and harden forming most commonly a non-stoichiometric calcium-deficient hydroxyapatite (CDHA) or brushite and rarely monetite with possible admixtures of unreacted compounds. As CDHA, brushite and monetite appear to be biocompatible, bioresorbable, and osteoconductive (therefore, in vivo they can be replaced with a newly forming bone), self-setting  $\text{CaPO}_4$  formulations come out to be very promising bioceramics for bone grafting. Furthermore, due to their moldability, such formulations possess an easy manipulation and a nearly perfect adaptation to the complex shapes of bone defects, followed by gradual bioresorption and new bone formation, which are additional distinctive advantages. Unfortunately, the mechanical properties of the ordinary self-setting  $\text{CaPO}_4$  formulations are poor; therefore, reinforced ones have been introduced. The latter might be described as  $\text{CaPO}_4$  concretes. In addition, porous formulations have been developed. The discovery of self-setting properties opened up a new era in the medical application of  $\text{CaPO}_4$ , and many commercial trademarks have been introduced as a result. Many more formulations are still in experimental stages. Currently such formulations are widely used as synthetic bone grafts, with several advantages, such as moldability, pourability, and injectability. Moreover, their low-temperature setting reactions and intrinsic porosity allow loading by drugs, biomolecules, and even cells for tissue engineering purposes. In this chapter, an insight into the self-setting  $\text{CaPO}_4$  formulations, as excellent bioceramics suitable for both dental and bone grafting applications, has been provided.

**Keywords** Calcium orthophosphates • Hydroxyapatite • Self-setting • Self-hardening • Cements • Bioceramics • Bone grafts • Scaffolds • Tissue engineering

---

S.V. Dorozhkin (✉)  
Kudrinskaja sq. 1-155, Moscow 123242, Russia  
e-mail: [sedorozhkin@yandex.ru](mailto:sedorozhkin@yandex.ru)

## 2.1 Introduction

According to the statistics, approximately half of the population sustains at least one bone fracture during their lifetime [1], and, as a result, surgery might be necessary. Luckily, among the surgical procedures available, minimally invasive techniques are able to offer special benefits for patients such as fewer associated injuries, quicker recovery, and less pain. In addition, shorter hospital stays are needed, often allowing outpatient treatments that cheapen the expenses [2]. However, these techniques require biomaterials able to be implanted through small (the smaller, the better) incisions, e.g., by means of syringes with needles and/or laparoscopic devices. To fulfill such requirements, the potential implants should be in a liquid or an injectable state, such as pastes. On the other hand, since all types of the calcified tissues are in the solid state, the bone repair biomaterials must be solid. Therefore, potential bone grafts applicable to the minimally invasive surgery must combine injectability with solidness. Such formulations are known as self-setting (self-hardening, self-curing) formulations because, together with an initial softness and injectability, they possess an ability to solidify in the appropriate period, giving strength to the implantation sites. Since the inorganic part of the mammalian calcified tissues is composed of calcium orthophosphates ( $\text{CaPO}_4$ ) of a biological origin [3], self-setting formulations based on  $\text{CaPO}_4$  appear to be excellent candidates for bone repair [4, 5]. The list of all known  $\text{CaPO}_4$ , including their chemical formulae, standard abbreviations, and the major properties, is summarized in Table 2.1 [6, 7].

Although the entire subject of  $\text{CaPO}_4$  has been investigated since the 1770s [8, 9], historically, Kingery appears to be the first who contributed to their self-setting abilities. Namely, in 1950, he published a paper on the chemical interactions between oxides and hydroxides of various metals ( $\text{CaO}$  was among them) with  $\text{H}_3\text{PO}_4$ , in which he mentioned that some of the reaction products were set [10]. However, the  $\text{CaPO}_4$  formulations were just a very small section of that study. Afterward, self-setting abilities of some  $\text{CaPO}_4$  formulations were described by Driskell et al. in 1975 [11], as well as Monma and Kanazawa in 1976 [12]. Namely, the latter researchers found that  $\alpha$ -TCP was set to form CDHA when  $\alpha$ -TCP was hydrated in water at 60–100 °C and pH between 8.1 and 11.4 [12]. Since the reactions took a long time and did not offer any clinical application, the results of those early studies were not noticed by coevals. Then, in the early 1980s, scientists from the American Dental Association such as LeGeros et al. [13], as well as Brown and Chow [14–17], published results of their studies. Since then, this subject became known as *calcium phosphate cements* (commonly referred to as CPC) [18], and due to their suitability for repair, augmentation, and regeneration of bones, such formulations were also named as calcium phosphate *bone* cements (occasionally referred to as CPBC) [19–21]. In order to stress the fact that these formulations consist either entirely or essentially from  $\text{CaPO}_4$ , this chapter is limited to the consideration of  $\text{CaPO}_4$ -based compositions only. The readers interested in self-setting formulations based on other types of calcium phosphates are requested to read the original publications [22, 23].

**Table 2.1** Existing CaPO<sub>4</sub> and their major properties [6, 7]

Ca/P molar ratio	Compound	Formula	Solubility at 25 °C, -log(K <sub>s</sub> )	Solubility at 25 °C, g/L	pH stability range in aqueous solutions at 25 °C
0.5	Monocalcium phosphate monohydrate (MCPM)	Ca(H <sub>2</sub> PO <sub>4</sub> ) <sub>2</sub> ·H <sub>2</sub> O	1.14	~18	0.0–2.0
0.5	Monocalcium phosphate anhydrous (MCPA or MCP)	Ca(H <sub>2</sub> PO <sub>4</sub> ) <sub>2</sub>	1.14	~17	<sup>a</sup>
1.0	Dicalcium phosphate dihydrate (DCPD), mineral brushite	CaHPO <sub>4</sub> ·2H <sub>2</sub> O	6.59	~0.088	2.0–6.0
1.0	Dicalcium phosphate anhydrous (DCPA or DCP), mineral monetite	CaHPO <sub>4</sub>	6.90	~0.048	<sup>a</sup>
1.33	Octacalcium phosphate (OCP)	Ca <sub>8</sub> (HPO <sub>4</sub> ) <sub>2</sub> (PO <sub>4</sub> ) <sub>4</sub> ·5H <sub>2</sub> O	96.6	~0.0081	5.5–7.0
1.5	α-Tricalcium phosphate (α-TCP)	α-Ca <sub>3</sub> (PO <sub>4</sub> ) <sub>2</sub>	25.5	~0.0025	<sup>b</sup>
1.5	β-Tricalcium phosphate (β-TCP)	β-Ca <sub>3</sub> (PO <sub>4</sub> ) <sub>2</sub>	28.9	~0.0005	<sup>b</sup>
1.2–2.2	Amorphous calcium phosphates (ACP)	Ca <sub>n</sub> H <sub>y</sub> (PO <sub>4</sub> ) <sub>z</sub> ·nH <sub>2</sub> O, n = 3–4.5; 15–20% H <sub>2</sub> O	<sup>c</sup>	<sup>c</sup>	~ 5–12 <sup>d</sup>
1.5–1.67	Calcium-deficient hydroxyapatite (CDHA or ca-def HA) <sup>e</sup>	Ca <sub>10-x</sub> (HPO <sub>4</sub> ) <sub>x</sub> (PO <sub>4</sub> ) <sub>6-x</sub> (OH) <sub>2-x</sub> (0 < x < 1)	~85	~0.0094	6.5–9.5
1.67	Hydroxyapatite (HA, HAp, or OHAp)	Ca <sub>10</sub> (PO <sub>4</sub> ) <sub>6</sub> (OH) <sub>2</sub>	116.8	~0.0003	9.5–12
1.67	Fluorapatite (FA or FAp)	Ca <sub>10</sub> (PO <sub>4</sub> ) <sub>6</sub> F <sub>2</sub>	120.0	~0.0002	7–12
1.67	Oxyapatite (OA, OAp, or OXA) <sup>f</sup> , mineral voelckerite	Ca <sub>10</sub> (PO <sub>4</sub> ) <sub>6</sub> O	~69	~0.087	<sup>b</sup>
2.0	Tetracalcium phosphate (TTCP or TetCP), mineral hilgenstockite	Ca <sub>4</sub> (PO <sub>4</sub> ) <sub>2</sub> O	38–44	~0.0007	<sup>b</sup>

<sup>a</sup>Stable at temperatures above 100 °C<sup>b</sup>These compounds cannot be precipitated from aqueous solutions<sup>c</sup>Cannot be measured precisely. However, the following values were found: 25.7 ± 0.1 (pH = 7.40), 29.9 ± 0.1 (pH = 6.00), 32.7 ± 0.1 (pH = 5.28). The comparative extent of dissolution in acidic buffer is ACP ≫ α-TCP ≫ β-TCP > CDHA ≫ HA > FA<sup>d</sup>Always metastable<sup>e</sup>Occasionally, it is called “precipitated HA (PHA)”<sup>f</sup>Existence of OA remains questionable

Due to a good bioresorbability, all self-setting  $\text{CaPO}_4$  formulations belong to the second generation of bone substitute biomaterials [24]. These formulations represent blends of amorphous and/or crystalline  $\text{CaPO}_4$  powder(s) with an aqueous solution, which might be distilled water [13–17], phosphate buffer solution (PBS) [18], aqueous solutions of sodium orthophosphates [25–39], ammonium orthophosphates [40],  $\text{H}_3\text{PO}_4$  [41–48], citric acid [26, 49] and its salts [50], sodium silicates [51–53], soluble magnesium orthophosphates [54], chitosan lactate in lactic acid [55], etc. Due to the presence of other ions in a number of solutions, some of such formulations are set with formation of ion-substituted  $\text{CaPO}_4$ .

Briefly, the self-setting  $\text{CaPO}_4$  formulations are used as follows. After the  $\text{CaPO}_4$  powder(s) and the solution have been mixed together, a viscous and moldable paste is formed that sets to a firm mass within a few minutes. When the paste becomes sufficiently stiff, it can be placed into a defect as a substitute for the damaged part of the bone, where it hardens in situ within the operating theater. The proportion of solid-to-liquid or the powder-to-liquid (P/L) ratio is a very important characteristic because it determines both bioresorbability and rheological properties. As the paste is set and hardened at room or body temperature, direct application in healing of bone defects became a new and innovative treatment modality by the end of the twentieth century. Moreover, self-setting  $\text{CaPO}_4$  formulations can be injected directly into the fractures and bone defects, where they intimately adapt to the bone cavity regardless its shape. More to the point, they were found to promote development of osteoconductive pathways, possess sufficient compressive strengths, be noncytotoxic, create chemical bonds to the host bones, restore contour, and have both the chemical composition and X-ray diffraction patterns similar to those of the bone [56]. Finally, but yet importantly, the self-setting  $\text{CaPO}_4$  formulations are osteoconductive, i.e., after implantation, the hardened formulations are replaced by a new bone tissue [57–59].

Since the hardened  $\text{CaPO}_4$  intend to reproduce the composition, structure, morphology, and crystallinity of bone crystals, the initial self-setting formulations might be considered as biomimetic ones [60, 61]. The aim of such formulations is to disturb bone functions and properties as little as possible and, until a new bone has been grown, to behave temporarily in a manner similar to that of the bone. Therefore, they provide surgeons with a unique ability of manufacturing, shaping, and implanting the bioactive bone substitute biomaterials on a patient-specific base in real time in the surgery room. Implanted bone tissues also take benefits from the self-setting formulations that give, in an acceptable clinical time, a suitable mechanical strength for a shorter tissue functional recovery. Thus, the major advantages of the self-setting  $\text{CaPO}_4$  formulations include a fast setting time, an excellent moldability, an outstanding biocompatibility, and an easy manipulation; therefore, they are more versatile in handling characteristics than prefabricated granules or blocks. Besides, like any other types of  $\text{CaPO}_4$  bioceramics, the self-setting formulations provide an opportunity for bone grafting using alloplastic materials, which are unlimited in quantity and provide no risk of infectious diseases [62–64].

Since self-setting  $\text{CaPO}_4$  formulations have been developed for use as implant biomaterials for parenteral application, for their chemical composition one might



employ all ionic compounds of oligoelements occurring naturally in a human body. The list of possible additives comprises (but is not limited to) the following cations, namely, Na<sup>+</sup>, K<sup>+</sup>, Mg<sup>2+</sup>, Ca<sup>2+</sup>, Sr<sup>2+</sup>, Zn<sup>2+</sup>, and H<sup>+</sup>, and anions, namely, PO<sub>4</sub><sup>3-</sup>, HPO<sub>4</sub><sup>2-</sup>, H<sub>2</sub>PO<sub>4</sub><sup>-</sup>, P<sub>2</sub>O<sub>7</sub><sup>4-</sup>, CO<sub>3</sub><sup>2-</sup>, HCO<sub>3</sub><sup>-</sup>, SO<sub>4</sub><sup>2-</sup>, HSO<sub>4</sub><sup>-</sup>, Cl<sup>-</sup>, OH<sup>-</sup>, F<sup>-</sup>, and silicates [57]. Therefore, mixed-type self-setting formulations consisting of CaPO<sub>4</sub> and other calcium salts, such as calcium sulfate [65–74], calcium pyrophosphate [75–77], calcium polyphosphates [78, 79], calcium carbonates [18, 29, 31–36, 61, 80–83], calcium oxide [84–89], calcium hydroxide [90–92], calcium aluminates [54, 93, 94], calcium silicates [95–102], bioactive glass [103], etc., are available. In addition, other chemicals such as Sr-containing compounds [21, 104–107], Mg-containing compounds [107–114], Zn-containing compounds [115, 116], etc. may be added to CaPO<sub>4</sub> as well. Furthermore, the self-setting formulations might be prepared from various types of ion-substituted CaPO<sub>4</sub> such as Ca<sub>2</sub>KNa(PO<sub>4</sub>)<sub>2</sub>, NaCaPO<sub>4</sub>, Na<sub>3</sub>Ca<sub>6</sub>(PO<sub>4</sub>)<sub>5</sub> (so-called calcium alkaline orthophosphates) [117–122], magnesium-substituted CDHA, strontium-substituted CDHA, etc. [123–128]. More to the point, self-setting formulations might be prepared in the reaction-setting mixture of Ca(OH)<sub>2</sub>-KH<sub>2</sub>PO<sub>4</sub> system [129], as well as by treatment of calcium carbonate or calcium hydroxide with orthophosphate solutions [130, 131]. In addition, if a self-setting formulation consisting of CaPO<sub>4</sub> only is set in a chemically reactive environment (e.g., in the presence of CO<sub>2</sub>), ion-substituted CaPO<sub>4</sub>, such as carbonate apatite, are formed [132]. Finally, self-setting CaPO<sub>4</sub>-based formulations possessing special properties, such as magnetic ones due to incorporation of iron oxides [133, 134], have been developed as well. However, with a few important exceptions, the ion-substituted formulations have not been considered in this chapter, but the interested readers are suggested to study the aforementioned publications.

The purpose of this chapter is to evaluate the chemistry, physical, mechanical, and biomedical properties of the available self-setting CaPO<sub>4</sub> formulations with the specific reference to their applications in surgery and dentistry.

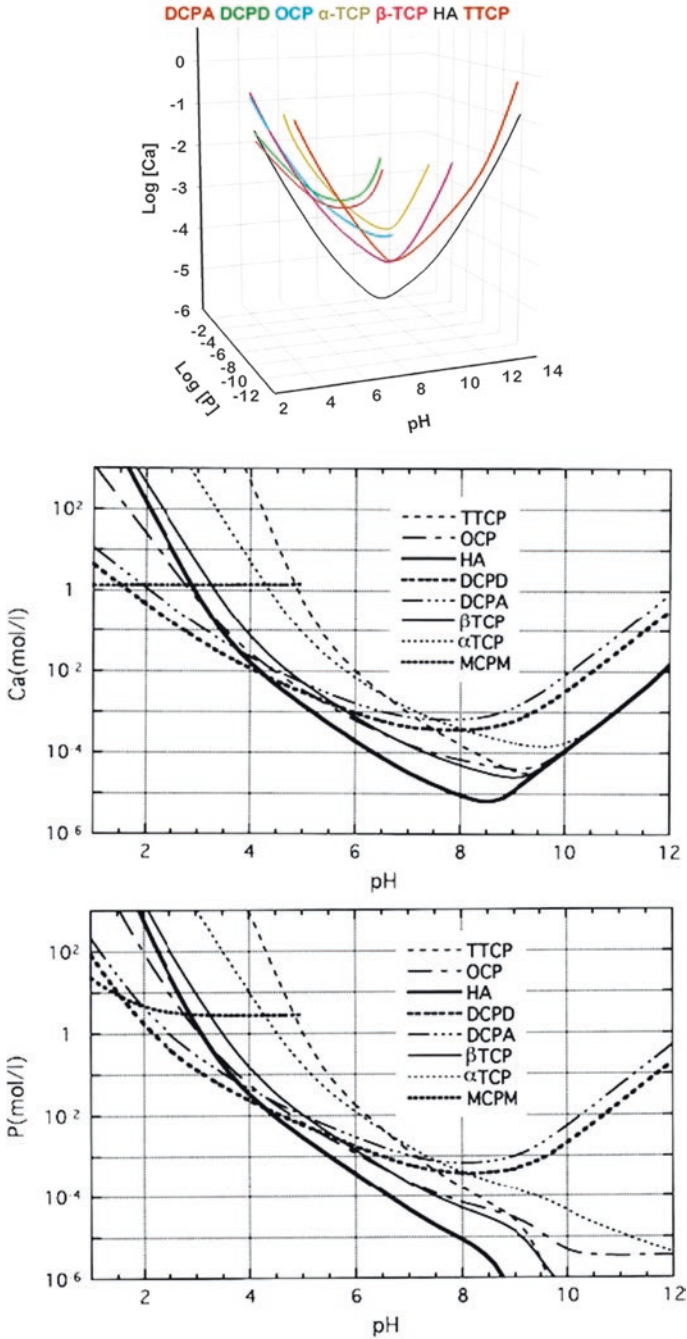
## 2.2 General Information and Knowledge

According to Wikipedia, the free encyclopedia, “In the most general sense of the word, *cement* is a binder, a substance that sets and hardens independently and can bind other materials together. The name ‘cement’ goes back to the Romans who used the term ‘*opus caementicium*’ to describe masonry, which resembled concrete and was made from crushed rock with burnt lime as binder. The volcanic ash and pulverized brick additives, which were added to the burnt lime to obtain a hydraulic binder, were later referred to as *cementum*, *cimentum*, *cäment* and *cement*” [135]. Thus, *CaPO<sub>4</sub> cement* appears to be a generic term to describe chemical formulations in the ternary system Ca(OH)<sub>2</sub>-H<sub>3</sub>PO<sub>4</sub>-H<sub>2</sub>O which can experience a transformation from a liquid or a pasty state to a solid state and in which the end product of the chemical reactions is a CaPO<sub>4</sub>.

The first self-setting  $\text{CaPO}_4$  formulation consisted of the equimolar mixture of TTCP and dicalcium phosphate (DCPA or DCPD) which was mixed with water at a P/L ratio of 4:1; the paste hardened in about 30 min and formed CDHA. These highly viscous and non-injectable pastes could be molded and, therefore, were used mainly as a contouring material in craniofacial surgery. Later studies revealed some differences between TTCP + DCPD and TTCP + DCPA formulations. Namely, due to a higher solubility of DCPD (Table 2.1 and Fig. 2.1), TTCP + DCPD mixtures set faster than TTCP + DCPA ones. Besides, injectability of TTCP + DCPD formulations is better [136–140]. In the 1990s, it was established that there were about 15 different binary combinations of  $\text{CaPO}_4$ , which gave self-setting pastes upon mixing with water or aqueous solutions. The list of these combinations is available in literature [141–143]. From those basic systems, secondary self-setting formulations were derived containing additional or even nonreactive compounds [19, 57, 86, 141, 144–157]. In terms of their viscosity, both pasties [158–163] and putties [164] of a very high viscosity [164–167] are known.

According to the classical solubility data of  $\text{CaPO}_4$  (Fig. 2.1), depending upon the pH value of a self-setting paste, after hardening, all formulations can form only two major end products: a precipitated poorly crystalline HA or CDHA at  $\text{pH} > 4.2$  and DCPD (also called “brushite”) at  $\text{pH} < 4.2$  [168]. Here one should notice that, in the vast majority cases, terms “a precipitated poorly crystalline HA” and “CDHA” are undistinguishable and might be considered as synonyms [6, 7], while the term “brushite” was coined to honor an American mineralogist George Jarvis Brush (1831–1912), who was a professor at Yale University, USA. However, in the real self-setting formulations, the pH border of 4.2 might be shifted to higher pH values. Namely, DCPD might be crystallized at the solution pH up to  $\sim 6$ , while CDHA normally is not formed at pH below 6.5–7 (Table 2.1).

In the early 1990s, depending on the type of  $\text{CaPO}_4$  formed after the setting, five groups of self-setting formulations were thought to exist: DCPD, CDHA, HA, ACP, and OCP [143, 169]. However, the results of the only study on an ACP-forming formulation demonstrated that it was rapidly converted into CDHA [155]; thus, it appeared to belong to apatite-forming formulations. With the OCP-forming formulations [170–173], the situation looks as follows. Contrary to the reports in the late 1980s [170] and early 1990s [171], in which OCP formation was claimed to be detected (however, no phase analysis was performed, just initial reagents were mixed in proportions to get the Ca/P ratio around 1.33), in recent papers, either simultaneous formation of OCP and CHDA was detected [173] or no phase analysis was performed [172]. Strong experimental evidences of the existence of a transient OCP phase during setting were found in still another study; however, after a few hours, the OCP phase disappeared giving rise to the final CDHA phase [52]. Therefore, OCP-forming formulations also appeared to belong to apatite-forming ones. Finally, according to the aforementioned, CDHA and HA are the synonyms. Thus, within the end of the 1990s to the beginning of the 2010s, the amount of the groups of the self-setting formulations was shortened to just two groups: apatite-forming and brushite-forming formulations [174, 175]. This is a predictable situation since, in aqueous solutions, HA is the least soluble  $\text{CaPO}_4$  at  $\text{pH} > 4.2$  and

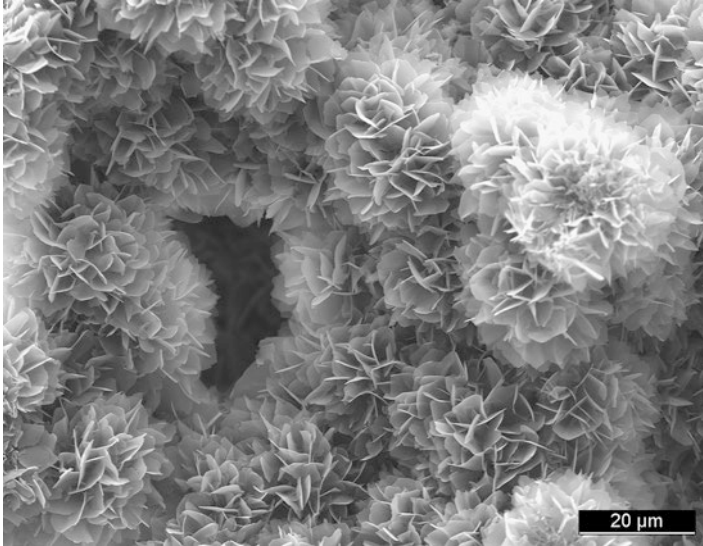


**Fig. 2.1** *Top*: A 3D version of the classical solubility phase diagrams for the ternary system Ca(OH)<sub>2</sub>-H<sub>3</sub>PO<sub>4</sub>-H<sub>2</sub>O (Reprinted from Ref. [136] with permission. Copyright © 2009 Elsevier Ltd). *Middle and bottom*: Solubility phase diagrams in two-dimensional graphs, showing two logarithms of the concentrations of (a) calcium and (b) orthophosphate ions as a function of the pH in solutions saturated with various salts (Reprinted from Ref. [137] with MDPI permission)

brushite is the least soluble one at  $\text{pH} < 4.2$  (Fig. 2.1). However, in the end of the 2000s, self-setting monetite (DCPA)-forming formulations were introduced (see Sect. 2.3.3 “Monetite-Forming Formulations”). Thus, one can claim that, depending on the type of  $\text{CaPO}_4$  formed after the setting, three groups of the self-setting formulations currently exist: apatite-, brushite-, and monetite-forming ones. The final hardened product of the formulations is of paramount importance because it determines the solubility and, therefore, *in vivo* bioresorbability. Since the chemical composition of mammalian bones is similar to an ion-substituted CDHA, apatite-forming formulations have been more extensively investigated. Nevertheless, many research papers on brushite-forming formulations have been published as well, while just a few publications on monetite-forming ones are currently available.

All self-setting  $\text{CaPO}_4$  formulations are made of an aqueous solution and fine powders of one or several types of  $\text{CaPO}_4$ . Here, dissolution of the initial  $\text{CaPO}_4$  (quickly or slowly depending on the chemical composition and solution  $\text{pH}$ ) and mass transport appear to be the primary functions of an aqueous environment, in which the dissolved reactants form a supersaturated (very far away from the equilibrium) microenvironment with regard to precipitation of the final product(s) [176, 177]. The relative stability and solubility of various  $\text{CaPO}_4$  (see Table 2.1) is the major driving force of the setting reactions occurred. Therefore, mixing of a dry powder with an aqueous solution induces various chemical transformations, in which crystals of the initial  $\text{CaPO}_4$  rapidly dissolve and precipitate into crystals of CDHA (precipitated HA), DCPD, or DCPA with possible formation of intermediate precursor phases (e.g., ACP [33, 155] and OCP [40, 170–173]). During precipitation, the newly formed crystals grow and form a web of intermingling microneedles or microplatelets of CDHA, DCPD, or DCPA, thus providing a mechanical rigidity to the hardened cements. In other words, entanglement of the newly formed crystals is the major reason of setting (Fig. 2.2). For the majority of apatite-forming formulations, water is not a reactant in the setting reactions; it is just a medium for reactions to occur. Therefore, the quantity of water, actually needed for setting of such formulations, is very small [24, 176, 179]. Similar is valid for apatite-forming ones. However, for brushite-forming formulations, water always participates in the chemical transformations because it is necessary for DCPD formation. Due to this reason, the brushite-forming formulations are always hydraulic, while this term is associated with neither apatite- nor monetite-forming ones.

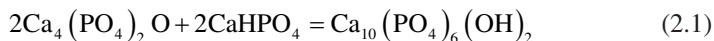
Setting of  $\text{CaPO}_4$  formulations is a continuous process that always starts with dissolution of the initial compounds in an aqueous system. This supplies ions of calcium and orthophosphate into the solution, where they chemically interact and precipitate in the form of either the final products or precursor phases, which causes setting [15, 180, 181]. This was confirmed by Ishikawa and Asaoka, who showed that when TTCP and DCPA powders were mixed in double-distilled water, both powders were dissolved. The dissolved ions were then precipitated in the form of CDHA on the surface of unreacted powders [182]. Since the physical state of the precipitates can be either a gel or a conglomerate of crystals, the hardening mechanism is either a sol-gel transition of ACP [33, 155] or entanglement of the precipitated crystals of the final products [57]. Thus, all types of hardened formulations



**Fig. 2.2** A typical microstructure of a  $\text{CaPO}_4$  formulation after hardening. The mechanical stability is provided by the physical entanglement of crystals (Reprinted from Ref. [178] with permission. Copyright © 2010 Elsevier Ltd)

possess an intrinsic porosity within the nano-/submicron size ranges (Fig. 2.2). For example, for the classical Brown-Chow formulation, after the initial setting, petal or needlelike crystals enlarge epitaxially and are responsible for the adherence and interlocking of the crystalline grains, which result in hardening. After  $\sim 2$  h, the newly formed crystals become rodlike, resulting from higher crystallinity with the observation of more material at the interparticle spaces. During this period, the setting reactions proceeded at a near-constant rate, suggesting that the reaction rate was limited by factors that are unrelated to the amounts of the starting materials and the reaction products present in the system. Such factors could be related to the surface area of DCPA or TTCP or to the diffusion distances over which the ions should migrate to form CDHA [183–185]. At  $\sim 24$  h, the crystals were completely formed, being very compacted in some areas of high density, and well separated in areas with more porosity [148, 153, 154].

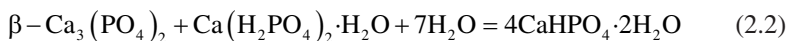
The chemical reactions occurring during setting depend on the chemical composition of  $\text{CaPO}_4$  formulations. However, it can be stated that there are only two major chemical types of the setting reactions. The first type occurs according to the classical rules of the acid-base interaction, i.e., a relatively acidic  $\text{CaPO}_4$  reacts with a relatively basic one to produce a relatively neutral compound. The first cement by Brown and Chow is a typical example of this type because TTCP (basic) reacts with DCPA (slightly acidic) in an aqueous suspension to form a poorly crystalline precipitated HA (slightly basic) [15, 16]:



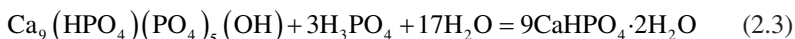
Initially, it was believed that DCPA and TTCP reacted upon mixing with water to form the stoichiometric HA [14–17]. However, further investigations have shown that only the first nuclei consist of a nearly stoichiometric HA, whereas further growth of these nuclei occurs in the form of CDHA [186]. Besides, there is a study demonstrating that the initially formed stoichiometric HA further interacts with remaining DCPD to form CDHA [187].

According to Eq. 2.1, formation of precipitated HA releases neither acidic nor basic by-products. Thus, the liquid phase of the formulation remains at a near-constant pH of ~7.5 for the TTCP + DCPD and ~8.0 for the TTCP + DCPA mixtures, respectively [183–185]. Various deviations from the stoichiometry of chemical Eq. 2.1 were studied in details, and various types of CDHA with Ca/P ionic ratio within 1.5–1.67 were found as the final product [188]. The effect of mixing ratio and pH on the reaction between TTCP and DCPA is well described elsewhere [189]. Furthermore, the influence of Ca/P ionic ratio of TTCP on the properties of the TTCP + DCPD cement was studied as well [190].

A blend proposed by Lemaître et al. [191, 192] is another example of the acid-base interaction in which  $\beta$ -TCP (almost neutral) reacts with MCPM (acidic) to form DCPD (slightly acidic):



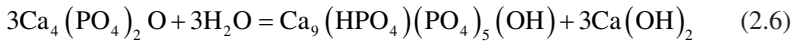
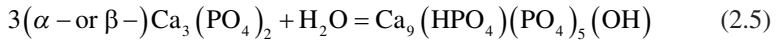
In chemical Eq. 2.2, MCPM may easily be substituted by  $\text{H}_3\text{PO}_4$  [41–47] or MCPA, while  $\beta$ -TCP may be replaced by  $\alpha$ -TCP [193, 194], CDHA [195, 196], HA [197, 198], or even  $\text{Ca}(\text{OH})_2$  [32, 38, 44] and CaO. For example,



Furthermore, self-setting formulations based on mixtures of ACP +  $\alpha$ -TCP [199, 200], ACP + DCPD [201, 202], DCPA +  $\alpha$ -TCP [194], OCP + TTCP [203], OCP +  $\alpha$ -TCP [46, 204, 205], and unspecified “partially crystallized calcium phosphate” (presumably, CDHA) + DCPA [206–208] as the initial reagents are also available. In addition, multiphase self-setting compositions such as  $\alpha$ -TCP + TTCP + DCPA [209], DCPA +  $\alpha$ -TCP +  $\beta$ -TCP + CDHA [210], and DCPA +  $\alpha$ -TCP +  $\beta$ -TCP + CDHA +  $\text{CaCO}_3$  [34, 35] have been developed as well.

The second type of the setting reaction might be defined as hydrolysis of metastable  $\text{CaPO}_4$  in aqueous media. As a result, both the initial components and final products have the same Ca/P ionic ratio. Due to the fact that only one  $\text{CaPO}_4$  is used, the solid part of such formulations might be called a single-phase (or single-component) formulation [211]. Namely, self-setting formulations made of ACP + an aqueous solution [212, 213],  $\alpha$ -TCP + an aqueous solution [25–27, 30, 39, 214–226],  $\beta$ -TCP + an aqueous solution [218, 227], DCPA + an aqueous solution [51, 228], CDHA + an aqueous solution [52], OCP + an aqueous solution [53], TTCP +

an aqueous solution [54, 229, 230], or  $\gamma$ -radiated TTCP + an aqueous solution [231–233] are the examples; the majority of them are recrystallized to CDHA during setting:



As seen from the amount of publications,  $\alpha$ -TCP is the most popular compound to produce self-setting single-phase CaPO<sub>4</sub> formulations.

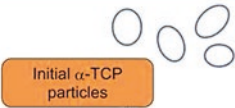


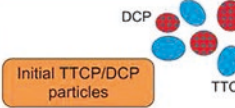


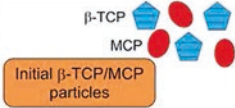

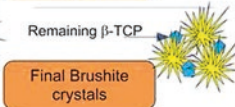
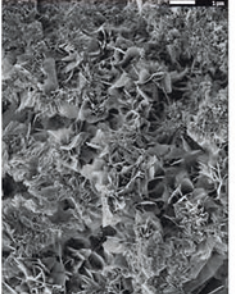
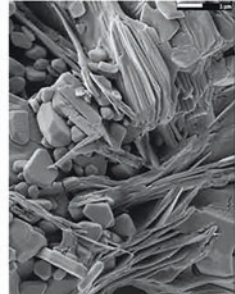
An interesting study was performed on the microstructure, mechanical, and setting properties of CaPO<sub>4</sub> formulations with variable Ca/P ratio within  $1.29 < \text{Ca/P} < 1.77$  [234]. The results showed that:

- (a) Only the reactant with Ca/P = 1.50 was monophasic and consisted of  $\alpha$ -TCP, which transformed during the setting into CDHA.
- (b) Reactants with Ca/P < 1.50 were composed of calcium pyrophosphate,  $\alpha$ -TCP, and  $\beta$ -TCP blends, while those with Ca/P > 1.50 were composed of  $\alpha$ -TCP, HA, and TTCP blends.
- (c) Formulations with Ca/P ratio other than 1.50 had longer setting and lower hardening properties.
- (d) The formulations' reactivity was clearly affected by the Ca/P ratio of the starting reactant.
- (e) Depending on the Ca/P ratio of the starting reactant, the hardened formulations developed different crystal microstructures with specific features [234].

Similarly, a self-setting formulation might be prepared from the thermal decomposition products of HA [235]. In addition, there is a study, in which  $\beta$ -TCP powders were mixed with 1.0 M CaCl<sub>2</sub> solution and 0.6 NaH<sub>2</sub>PO<sub>4</sub> solution consecutively. The ratio of the powder to CaCl<sub>2</sub> solution to NaH<sub>2</sub>PO<sub>4</sub> solution was 4:1:1 (g/ml/ml), while the total P/L was 2.0 g/ml and the Ca/P ratio of the mixing liquids was 1.67 [236].

The experimental details on TTCP hydrolysis under a near-constant composition condition are available elsewhere [237]. The details on  $\alpha$ -TCP hydrolysis are also available. The results indicated that setting of  $\alpha$ -TCP was initially controlled by surface dissolution; therefore, it depended on the surface area of the reactants [238–241]. Hydrolysis of DCPD to CDHA was studied as well [242]. Addition of ~2 wt. % of a precipitated poorly crystalline HA (i.e., CDHA) as a seed to  $\alpha$ -TCP powder phase might be useful to accelerate the kinetics of reaction (2.5) [243]. Similar results were obtained in another study [244]. The aforementioned information is summarized in Fig. 2.3 [245].

Further, there is a single-phase formulation consisting of K- and Na-containing CDHA (with the Ca/P ionic ratio of  $1.64 \pm 0.02$ ) that sets and hardens after mixing

		Apatite cements		Brushite cements
		Single Component	Multiple Components	
Reactives	$\alpha$ -TCP	TTCP + DCPA/DCPD	$\beta$ -TCP + MCPM/MCPA	
Reaction	$3\alpha\text{-Ca}_3(\text{PO}_4)_2 + \text{H}_2\text{O} \rightarrow \text{Ca}_9(\text{HPO}_4)(\text{PO}_4)_5(\text{OH})$	$2\text{Ca}_4(\text{PO}_4)_2\text{O} + 2\text{CaHPO}_4 \rightarrow \text{Ca}_{10}(\text{PO}_4)_6(\text{OH})_2$	$\beta\text{-Ca}_3(\text{PO}_4)_2 + \text{Ca}(\text{H}_2\text{PO}_4)_2 \cdot \text{H}_2\text{O} + 7\text{H}_2\text{O} \rightarrow 4\text{CaHPO}_4 \cdot 2\text{H}_2\text{O}$	
Type of Reaction	Hydrolysis	Acid-Base	Acid-Base	
Setting mechanism and crystal morphology	 <p>Initial <math>\alpha</math>-TCP particles</p>  <p>Dissolution - Precipitation</p>  <p>Final CDHA crystals</p>	 <p>Initial TTCP/DCP particles</p>  <p>Dissolution - Precipitation</p>  <p>Final HA crystals</p>	 <p>Initial <math>\beta</math>-TCP/MCP particles</p>  <p>Dissolution - Precipitation</p> <p>Remaining <math>\beta</math>-TCP</p>  <p>Final Brushite crystals</p>	
	SEM		<p>← APATITE</p> <p>BRUSHITE →</p>	

**Fig. 2.3** Classification of  $\text{CaPO}_4$  formulations with examples of the most common compositions. Scanning electron micrographs of set apatite and brushite cements obtained by the hydrolysis of  $\alpha$ -TCP and by reaction of  $\beta$ -TCP with MCPM, respectively, are also shown (Reprinted from Ref. [245] with permission. Copyright © 2012 Elsevier Ltd)

with an aqueous solution of sodium citrate and sodium orthophosphate [246]. After setting, this formulation gives rise to the formation of a weak cement (the compressive strength of  $15 \pm 3$  MPa) consisting of the ion-substituted CDHA again (presumably, with smaller Ca/P ionic ratio), mimicking the bone mineral. Unfortunately, neither the setting reaction nor the setting mechanism of this cement was disclosed [246].

The hydration process of  $\text{CaPO}_4$  formulations is slightly exothermic and undergoes five periods: initiating period, induction period, accelerating period, decelerating period, and terminating period [247]. For the classical Brown-Chow formulation, the activation energy of the hydration reaction is 176 kJ/mol [248]. The rate of heat



**Table 2.2** Some self-setting CaPO<sub>4</sub> formulations having the 510(k) clearance from the FDA [19, 179, 254]

Product <sup>a</sup>	Manufacturer	Applications <sup>a</sup>
BoneSource™ <sup>b</sup>	Stryker Howmedica Osteonics (Rutherford, NJ)	Craniofacial
α-Bone substitute material (α-BSM®) <sup>c</sup>	Etex Corporation (Cambridge, MA)	Filling of bone defects and voids, dental, craniofacial
Skeletal repair systems (SRS®)	Norian Corporation (Cupertino, CA)	Skeletal distal radius fractures, craniofacial

The technical data on these cements might be found in literature [24]

<sup>a</sup>In Europe, other applications may apply, and the materials may be sold with a different commercial name

<sup>b</sup>In Europe, it is distributed by Biomet Merck (Zwijndrecht, The Netherlands) as Biobon® [160], while in North America, it is marketed by Walter Lorenz Surgical (Jacksonville, FL) as Embarc® [22]

<sup>c</sup>BoneSource™ is the original formulation of CaPO<sub>4</sub> cement developed by Brown and Chow

liberation during the solidification of CaPO<sub>4</sub> formulations is low. The results of adiabatic experiments showed that the temperature rise reached the highest value of 37 °C 3 h later, which would cause no harm to surrounding tissues [249]. The results showed that the hardening process of that formulation was initially controlled by dissolution of the reactants in a 4 h period and subsequently by diffusion through the product layer of CDHA around the grains [154]. In general, setting of CaPO<sub>4</sub> formulations occurs mostly within the initial ~6 h, yielding ~80% conversion to the final products with the volume almost constant during setting (i.e., shrinkage is small). However, after hardening, the formulations always form brittle bioceramics with the tensile strength of 5–20 times lower than the compression strength [249, 250]. Since this biomaterial is weak under tensile forces, such formulations can only be used either in combination with metal implants or in non-load-bearing (e.g., craniofacial) applications [4, 5, 179, 251]. This is confirmed by the mechanical characterization of a bone defect model filled with bioceramic cements [252].

To conclude this part, one must stress that chemical Eqs. 2.1, 2.2, 2.3, 2.4, 2.5 and 2.6 for setting processes are valid for the *in vitro* conditions only. There are evidences that samples of CaPO<sub>4</sub> formulations retrieved 12 h after hardening *in vivo* already contained carbonate apatite, even though the initial mixtures did not contain carbonate as one of the solid components [253]. The mass fraction of carbonate in the 12 h samples was about 1%. The results suggest that under the *in vivo* conditions, carbonate is readily available and this allows formation of carbonate apatite in favor of carbonate-free CDHA [253].

By the end of the previous millennium, the United States Food and Drug Administration (FDA) approved several self-setting CaPO<sub>4</sub> formulations (Table 2.2) for clinical use [24, 254]. The same formulations also received a Conformité Européenne (CE) mark for certain maxillofacial indications and for use as bone-void fillers in the specific non-load-bearing orthopedic indications [179]. The major properties of these formulations are available in literature [24]. An extended list of the available formulations is presented in Table 2.3 [167], while even more formula-

**Table 2.3** A list of the commercial self-setting  $\text{CaPO}_4$  formulations with the producer, product name, composition (when available), and main end product. The end product of the reactions can be either an apatite (CDHA, carbonate apatite, etc.) or brushite (DCPD) [167]

Producer	Commercial name	Composition (when available)	Product
Aap Implantate (GER)	OsteoCem <sup>®</sup>	Powder: calcium orthophosphates (details unknown); Solution: unknown	Apatite
Berkeley advanced biomaterials (US)	Cem-Ostetic <sup>™</sup>	Powder: calcium orthophosphates (details unknown); Solution: water	Apatite
	Tri-Ostetic <sup>™</sup>	Powder: calcium orthophosphates (details unknown); Solution: water	Apatite
Biomatlante (FR)	MCPC	Powder: mainly $\alpha$ -TCP, ACP, BCP (HA + $\beta$ -TCP); Solution: phosphate-buffered solution	Apatite
Biomet (US) Interpore (US)	Calcibon <sup>®</sup>	Powder: $\alpha$ -TCP (61%), DCPA (26%), $\text{CaCO}_3$ (10%), CDHA (3%); Solution: $\text{H}_2\text{O}$ , $\text{Na}_2\text{HPO}_4$	Apatite
Walter Lorenz surgical (GER)	Mimix <sup>™</sup>	Powder: TTCP, $\alpha$ -TCP, trisodium citrate; Solution: citric acid aqueous solution	Apatite
	Quick set Mimix <sup>™</sup>	Powder: calcium orthophosphate powders, trisodium citrate; Solution: citric acid aqueous solution	Apatite
Calcitec (US)	Osteofix	Powder: calcium orthophosphate and calcium oxide powders; Solution: phosphate buffer	Apatite
ETEX (US)	$\alpha$ -BSM <sup>®</sup> ; Embarc; biobon	Powder: ACP (50%), DCPD (50%); Solution: un-buffered aqueous saline solution	Apatite
	$\beta$ -BSM <sup>®</sup>	Composition: could not be found (it has apparently a higher compressive strength and better injectability than $\alpha$ -BSM <sup>®</sup> )	Apatite
	$\gamma$ -BSM <sup>®</sup>	Composition: could not be found (putty consistency)	Apatite
	OssiPro	Composition: could not be found; the cement is claimed to be macroporous after hardening	Apatite
	CarriGen	Composition: synthetic calcium orthophosphate, sodium carboxymethylcellulose, sodium bicarbonate, and sodium carbonate	Apatite
Graftys (FR)	Graftys <sup>®</sup> HBS	Powder: $\alpha$ -TCP (78%), DCPD (5%), MCPM (5%), CDHA (10%), hydroxypropylmethylcellulose (2%); Solution: 5% $\text{Na}_2\text{HPO}_4$ aqueous solution	Apatite
	Graftys <sup>®</sup> quickset	Composition: calcium orthophosphate salts, hydroxypropylmethylcellulose, and orthophosphate-based aqueous solution	Apatite
INNOTERE (GER)	Velox <sup>®</sup>	Powder: $\alpha$ -TCP (60%), DCPA (26%), $\text{CaCO}_3$ (10%), CDHA (4%); Solution: short-chain triglyceride, tween 80, Amphisol A	Apatite

(continued)

**Table 2.3** (continued)

Producer	Commercial name	Composition (when available)	Product
Kasios (FR)	Jectos Eurobone <sup>®</sup>	Powder: $\beta$ -TCP (98%), Na <sub>2</sub> P <sub>2</sub> O <sub>7</sub> (2%); Solution: H <sub>2</sub> O, H <sub>3</sub> PO <sub>4</sub> (3.0 M), H <sub>2</sub> SO <sub>4</sub> (0.1 M)	Brushite
	Jectos+	Composition: could not be found (likely to be close to that of Jectos)	Brushite
Kuraray Noritake Dental (J)	Teethmate <sup>TM</sup>	Powder: TTCP, DCPA; Solution: water, preservative	Apatite
Kyphon (US)	KyphOs <sup>TM</sup>	Powder: $\beta$ -TCP (77%), Mg <sub>3</sub> (PO <sub>4</sub> ) <sub>2</sub> (14%), MgHPO <sub>4</sub> (4.8%), SrCO <sub>3</sub> (3.6%); Solution: H <sub>2</sub> O, (NH <sub>4</sub> ) <sub>2</sub> HPO <sub>4</sub> (3.5 M)	Apatite
Merck (GER) Biomet (US)	Bio cement D	Powder: 58% $\alpha$ -TCP, 24% DCPA, 8.5% CaCO <sub>3</sub> , 8.5% CDHA; Solution: 4 wt% Na <sub>2</sub> HPO <sub>4</sub> in water	Apatite
Mitsubishi Materials (J)	Biopex <sup>®</sup>	Powder: $\alpha$ -TCP (75%), TTCP (20–18%), DCPD (5%), HA (0–2%); Solution: H <sub>2</sub> O, Na succinate (12–13%), Na chondroitin sulfate (5–5.4%)	Apatite
	Biopex <sup>®</sup> -R	Powder: $\alpha$ -TCP, TTCP, DCPD, HA, Mg <sub>3</sub> (PO <sub>4</sub> ) <sub>2</sub> , NaHSO <sub>3</sub> ; Solution: H <sub>2</sub> O, Na succinate, Na chondroitin sulfate	Apatite
NGK spark plug (J)	Cerapaste <sup>®</sup>	Powder: TTCP + DCPA; Solution: sodium dextran sulfate sulfur 5	Apatite
	Primafix <sup>®</sup>	Powder: TTCP + DCPD; Solution: sodium dextran sulfate sulfur 5	Apatite
Produits Dentaires SA (CH), CalciphOs (CH)	VitalOs <sup>®</sup>	Solution 1: $\beta$ -TCP (1.34 g), Na <sub>2</sub> H <sub>2</sub> P <sub>2</sub> O <sub>7</sub> (0.025 g), H <sub>2</sub> O, salts (0.05 M PBS solution, pH 7.4); solution 2: MCPM (0.78 g), CaSO <sub>4</sub> ·2H <sub>2</sub> O (0.39 g), H <sub>2</sub> O, H <sub>3</sub> PO <sub>4</sub> (0.05 M)	Brushite
Shanghai Rebone Biomaterials (CN)	Rebone	Powder: TTCP, DCPA; Solution: H <sub>2</sub> O	Apatite
Skeletal Kinetics (US)	Callos <sup>TM</sup>	Powder: $\alpha$ -TCP, CaCO <sub>3</sub> , MCPM; Solution: sodium silicate	Apatite
	Callos Inject <sup>TM</sup>	Composition: $\alpha$ -TCP and unknown compounds (likely to be close to that of Callos <sup>TM</sup> )	Apatite
	SKaffold <sup>TM</sup>	Powder: $\alpha$ -TCP, CaCO <sub>3</sub> , MCPM; Solution: sodium silicate	Apatite
	SKaffold ReNu <sup>TM</sup>	The same as SKaffold <sup>TM</sup> but with a porogen to create macroporosity	Apatite
	CAAP	Probably similar to SKaffold <sup>TM</sup>	Apatite
	OsteoVation EX inject	Probably similar to Callos inject <sup>TM</sup> (product produced by SK but sold by OsteoMed)	Apatite

(continued)

**Table 2.3** (continued)

Producer	Commercial name	Composition (when available)	Product
Stryker (US) Leibinger (GER)	BoneSource™	Powder: TTCP (73%), DCPD (27%); Solution: H <sub>2</sub> O, mixture of Na <sub>2</sub> HPO <sub>4</sub> and NaH <sub>2</sub> PO <sub>4</sub>	Apatite
Stryker (US)	HydroSet™	Powder: TTCP, DCPD, trisodium citrate; Solution: H <sub>2</sub> O, polyvinylpyrrolidone, Na orthophosphate	Apatite
Surgiwear (India)	G-bone cement	Powder: TCP, TTCP; Solution: sodium and calcium salts in aqueous solution	Apatite
DePuy Synthes (US)	Norian® SRS Norian® CRS	Powder: α-TCP (85%), CaCO <sub>3</sub> (12%), MCPM (3%); Solution: H <sub>2</sub> O, Na <sub>2</sub> HPO <sub>4</sub>	Apatite
	Norian® SRS fast set putty, Norian® CRS fast set putty	Composition: could not be found (likely to be close to that of Norian SRS/CRS)	Apatite
	Norian drillable	Composition: calcium orthophosphate powder, bioresorbable fibers, and Na hyaluronate solution	Apatite
	ChronOS™ inject	Powder: β-TCP (73%), MCPM (21%), MgHPO <sub>4</sub> ·3H <sub>2</sub> O (5%), MgSO <sub>4</sub> (<1%), Na <sub>2</sub> H <sub>2</sub> P <sub>2</sub> O <sub>7</sub> (<1%); Solution: H <sub>2</sub> O, Na, hyaluronate (0.5%)	Brushite
Teknimed (FR)	Cementek®	Powder: α-TCP, TTCP, Na glycerophosphate; Solution: H <sub>2</sub> O, ca(OH) <sub>2</sub> , H <sub>3</sub> PO <sub>4</sub>	Apatite
	Cementek® LV	Powder: α-TCP, TTCP, Na glycerophosphate, dimethylsiloxane; Solution: H <sub>2</sub> O, ca(OH) <sub>2</sub> , H <sub>3</sub> PO <sub>4</sub>	Apatite

tions are in experimental stages. Other lists of the commercially available injectable bone cements with their chemical composition (when obtainable) might be found elsewhere [5, 185, 255–257]. A general appearance of two randomly chosen commercial CaPO<sub>4</sub> cements is shown in Fig. 2.4.

## 2.3 Three Major Types of The Self-Setting CaPO<sub>4</sub> Formulations

### 2.3.1 Apatite-Forming Formulations

As indicated by its name, apatite-forming formulations have a poorly crystalline precipitated HA and/or CDHA as the final product of setting reactions (chemical Eqs. 2.1, 2.4, 2.5 and 2.6), although traces of unreacted starting compounds can be present [148]. Self-setting FA-forming formulations are also known; they can be prepared by the same way but in the presence of soluble F<sup>-</sup> ions [258–260]. Due to



Fig. 2.4 A presentation of two randomly chosen commercial  $\text{CaPO}_4$  cements

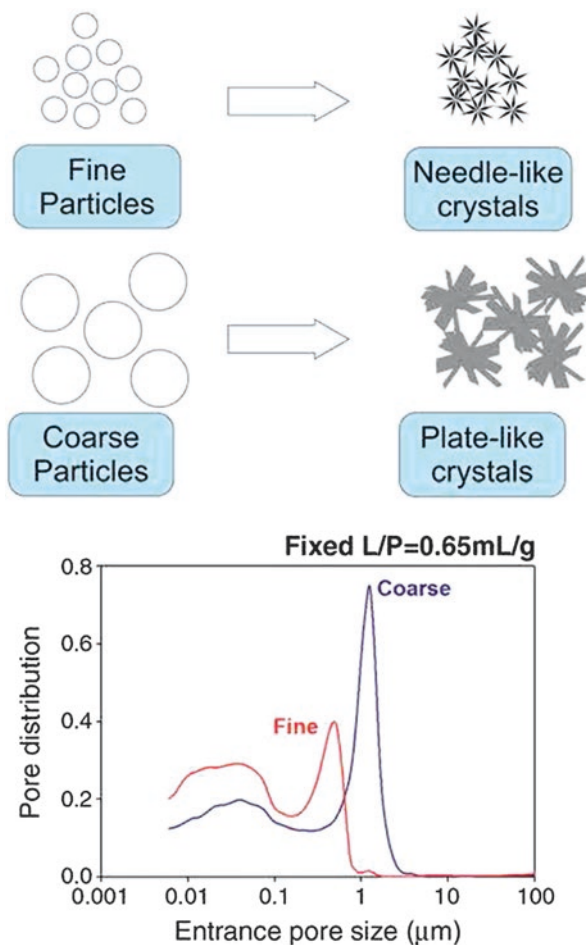
the initial presence of carbonates, commercial formulations such as Norian SRS<sup>®</sup> and Biocement D<sup>®</sup> (Table 2.3) form a non-stoichiometric carbonate apatite or dahlite ( $\text{Ca}_{8.8}(\text{HPO}_4)_{0.7}(\text{PO}_4)_{4.5}(\text{CO}_3)_{0.7}(\text{OH})_{1.3}$ ) as the end product [80, 261]. As both CDHA and carbonate apatite are formed in an aqueous environment and have a low crystallinity, they appear to be rather similar to the biological apatite of bones and teeth. These properties are believed to be responsible for their excellent *in vivo* resorption characteristics. Conventional apatite-forming formulations contain TCP and/or TTCP phases in their powder components [256], while a single-component formulation consisting of K- and Na-containing CDHA is also available [246]. The reactivity of TCP-based apatite-forming formulations was found to vary as a function of TCP crystal phase, crystallinity, and particle size [262, 263]. Generally, a higher reactivity is observed with a thermodynamically less stable phase (from  $\beta$ -TCP to  $\alpha$ -TCP and further to ACP) and with a smaller particle size [200, 218]. Nominally, it might be stated that formation of apatites through self-setting reactions is a sort of a biomimetic process because it occurs in a physiological environment and at body temperature [64]; however, both the crystallization kinetics and a driving force are very far away from the biomimeticity. A unique feature of the hardened apatite-forming formulations is that the force linking the newly formed crystals (of both CDHA and carbonate apatite) is weak; therefore, the crystals can be easily detached from the bulk of hardened formulations, especially after dissolution has partly occurred. When this happens, osteoclasts and other cells can easily ingest the apatite crystals [264].

Immediately after implantation, any formulation becomes exposed to blood and other tissue fluids that delays the setting time. Intrinsic setting time for apatite-forming formulations was extensively studied, and it appeared to be rather long. For example, for the original formulation by Brown and Chow, it ranges from 15 to 22 min [15, 16]. This may result in procedural complications. To remedy this, the amount of liquid could be reduced to a possible minimum. In such cases, all

apatite-forming formulations look like viscous and easily moldable pastes, which tend to be difficult to inject. Besides playing with the P/L ratio, the setting time also could be reduced by using additives to the liquid phase (which is distilled water in the Brown-Chow formulation [15, 16]). The list of possible additives includes  $\text{H}_3\text{PO}_4$ , MCPM, and other soluble orthophosphates. These additives promote dissolution of the initial solid  $\text{CaPO}_4$  by lowering the solution pH. In such cases, a setting time in the range of 10–15 min can be obtained [212–220, 265]. The influence of soluble orthophosphates (e.g.,  $\text{Na}_2\text{HPO}_4$  or  $\text{NaH}_2\text{PO}_4$ ) on the setting time is explained by the fact that dissolution of DCPA and formation of CDHA during setting occur in a linear fashion, thus avoiding early formation of CDHA. This is important because too early formation of CDHA might engulf unreacted DCPA, which slows down DCPA dissolution and thus the setting kinetics becomes slower, while the presence of sodium orthophosphates prevents DCPA particles from being isolated [266]. Particle size [243, 267, 268], temperature, and initial presence of HA powders as seeds in the solid phase are other factors that influence the setting time [15, 16, 64, 243, 262, 263]; however, *in vitro* studies demonstrated that these parameters did not affect significantly [148]. On the other hand, particle size reduction was found to result in a significant decrease in both initial and final setting times [243, 267, 268], an acceleration of the hardening rate [243], and hydration kinetics of the hardening formulation [268]. In general, smaller crystals or particles result in a higher supersaturation degrees achieved in the self-setting  $\text{CaPO}_4$  pastes, which favors crystal nucleation and results in the precipitation of greater many and smaller needlelike crystals, instead of the larger platelike crystals formed when bigger particles are used (Fig. 2.5) [245]. These different microstructures give rise to different pore size distributions in the set formulations (bottom part of Fig. 2.5). Besides, the crystallite sizes of the final products can be strongly reduced by increasing the specific surface of the starting powders, which allows developing formulations with tailored structures at the micro- and nanoscale levels [243]. Unfortunately, an unclear correlation was found between the particle dimensions of the initial  $\text{CaPO}_4$  and mechanical properties of the hardened products: namely, a significant increase in compressive strength and storage modulus was reported for some formulations [267, 268], but a minor effect on compressive strength was discovered for other ones [243]. This inconsistency is not surprising because the manufacturing methods used to produce test samples varied from one author to the other. Therefore, the only remaining fact is that the hardened formulations are brittle and hence worthless for load-bearing applications [4, 5].

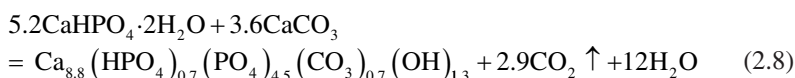
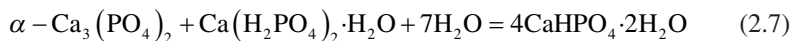
Setting process of the most types of apatite-forming formulations occurs according to just one chemical reaction (see chemical Eqs. 2.1, 2.4, 2.5 and 2.6) and at near the physiological pH, which might additionally contribute to the high biocompatibility [183–185]. Namely, for the classical formulation by Brown and Chow, the transmission electron microscopy results suggested the process for early-stage apatite formation as follows: when TTCP and DCPA powders were mixed in an orthophosphate-containing solution, TTCP powder quickly dissolved due to its higher solubility in acidic media. Then the dissolved ions of calcium and orthophosphate, along with ions already existing in the solution, were precipitated

**Fig. 2.5** A schematic drawing of the influence of the particle dimensions on the properties of self-setting formulations (Reprinted from Ref. [245] with permission. Copyright © 2012 Elsevier Ltd)



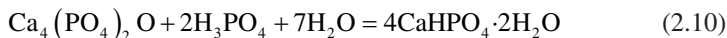
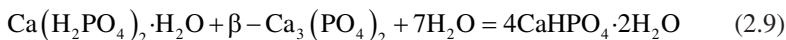
predominantly onto the surface of DCPA particles. Few apatite crystals were observed on the surface of TTCP powder. At a later stage of the reaction, an extensive growth of apatite crystals or whiskers effectively linked DCPA particles together and bridged the larger TTCP particles causing the setting [269].

However, Norian SRS<sup>®</sup> and Cementek<sup>®</sup> (Table 2.3) were found to set according to two chemical reactions: precipitation of DCPD, followed by precipitation of either CDHA or carbonate apatite:

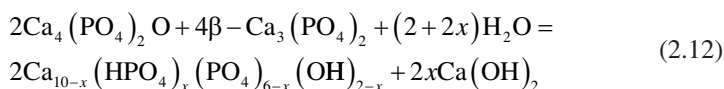
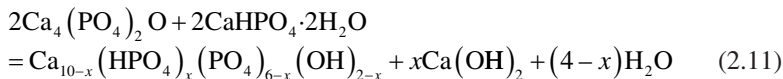


The initial chemical reaction (2.7) was very fast and provoked DCPD formation and initial setting within seconds. The second step was slower: DCPD reacted completely within several hours with remaining  $\alpha$ - $\text{Ca}_3(\text{PO}_4)_2$  and  $\text{CaCO}_3$  forming carbonate apatite according to Eq. 2.8. The latter step caused the hardening. A similar two-step hardening mechanism was established for a formulation consisting of MCPM and  $\text{CaO}$ : in the first step, during the mixing time, MCPM reacted with  $\text{CaO}$  immediately to give DCPD, which, in the second step, reacted more slowly with the remaining  $\text{CaO}$  to give CDHA [86].

In addition, the setting mechanism of an apatite-forming formulation was investigated in details for a three-component mixture of TTCP,  $\beta$ -TCP, and MCPM dry powders in convenient proportions and with the overall atomic  $\text{Ca/P}$  ratio equal to 1.67. Two liquid phases in a row were used to damp the cement powder; initially it was water + ethanol (ethanol was added to slow down the hardening) and afterward  $\text{H}_3\text{PO}_4$  and sodium glycerophosphate were added to water to prepare a reactive liquid [176]. At the very beginning, DCPD was found to form according to two chemical equations:



The formation reactions of DCPD were fast and corresponded to the initial setting. Afterward, TTCP reacted with the previously formed DCPD and with  $\beta$ -TCP to give CDHA according to the equations:



The reaction kinetics of the CDHA phase formation was quite slow and corresponded to the hardening stage. Although OCP was not detected in that study, its formation as an intermediate phase was postulated [176]. A similar suggestion on the intermediate formation of OCP was made for the setting mechanism of Brown-Chow classical formulation [143, 148]; however, reliable evidences for its presence are still lacking [215, 270]. Strong experimental evidences of the existence of a transient OCP phase during setting were found in still another study; however, that system contained sodium silicates [52]. In all cases, OCP was suggested to appear as an intermediate because it was a faster forming phase than CDHA. This hypothesis is based upon the classical studies performed by Prof. W. E. Brown et al., about the precursor phase formation during chemical crystallization of apatites in aqueous solutions [271–273].



Solubility of the hardened apatite-forming formulations in aqueous solutions is expected to be rather similar to that of the bone mineral. This means that they are relatively insoluble at neutral pH and increasingly soluble as pH drops down; this is an important characteristic of normal bone mineral that facilitates controlled dissolution by osteoclasts [261].

To conclude this part, one should mention, that in 2000 the US bone substitute market for Norian SRS<sup>®</sup> accounted for ~15% of the total sales, followed by BoneSource<sup>™</sup> at ~13%, and  $\alpha$ -BSM<sup>®</sup> at ~8.5% [179].

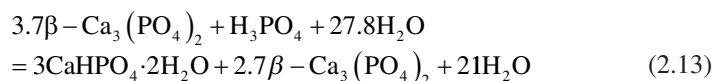
### 2.3.2 Brushite-Forming Formulations

As indicated by its name, DCPD is the major product of the setting reaction for brushite-forming formulations (chemical Eqs. 2.2 and 2.3), although traces of the unreacted starting compounds can be present. Mirtchi and Lemaître [191] and independently Bajpai et al. [41] introduced this type of the cements in 1987. Up to now, several formulations have been already proposed, e.g.,  $\beta$ -TCP + MCPM [191, 192],  $\beta$ -TCP + H<sub>3</sub>PO<sub>4</sub> [41–43], and TTCP + MCPM + CaO [274]. The full list of brushite-forming formulations is available in a topical review on the subject [275]. As seen from the chemical composition, all types of the brushite-forming formulations are set by the acid-base interaction only. As DCPD can only be precipitated at the solution pH <6 (Table 2.1), the pastes of the self-setting brushite-forming formulations are always acidic during hardening [43, 276]. For example, during setting of a  $\beta$ -TCP + MCPM formulation, the formulation pH varies from very acidic pH values of ~2.5 to almost neutral pH values of ~6.0 [43]. Replacing MCPM by H<sub>3</sub>PO<sub>4</sub> renders the paste very acidic for the initial ~30 s but then the pH profile follows that obtained with MCPM. It is important to notice that  $\beta$ -TCP + H<sub>3</sub>PO<sub>4</sub> formulations have several advantages over  $\beta$ -TCP + MCPM ones, namely, (i) easier and faster preparation, (ii) a better control of the chemical composition and reactivity, and (iii) improved physicochemical properties, such as longer setting times and larger tensile strengths due to a higher homogeneity. However, the use of H<sub>3</sub>PO<sub>4</sub> might impair the biocompatibility of the formulations, due to low pH values during setting [43].

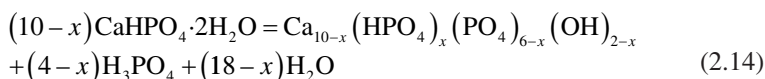
As the solubility of CaPO<sub>4</sub> generally decreases with increasing of their basicity (Table 2.1 and Fig. 2.1), the setting time of brushite-forming formulations much depends on the solubility of a basic phase: the higher its solubility, the faster the setting time. Therefore, the setting time of formulations made of MCPM + a basic CaPO<sub>4</sub> increases in the order of HA >  $\beta$ -TCP >  $\alpha$ -TCP [4, 5]. For example, HA + MCPM mixtures have a setting time of several minutes,  $\beta$ -TCP + MCPM mixtures of 30–60 s, and  $\alpha$ -TCP + MCPM mixtures of a few seconds [191, 192]. Furthermore, if brushite-forming formulations contain an excess of a basic phase, the equilibrium pH will be given by the intersection of the solubility isotherms of the basic phase with that of DCPD. For example, the equilibrium pH values of  $\beta$ -TCP + MCPM, HA + MCPM, and TTCP + MCPM mixtures were found to be 5.9, 4.2, and 7.6, respectively [4, 5]. Follow-up of the chemical composition by <sup>31</sup>P solid-state NMR

enabled to show that the chemical setting process for  $\beta$ -TCP + MCPM formulation reached the end after  $\sim 20$  min [277]. Nevertheless, despite this initial high reactivity, the hardening reaction of brushite-forming formulations typically lasts 1 day until completion [262, 263]. Additives that inhibit the crystal growth of DCPD have successfully been used to increase the setting time of  $\beta$ -TCP + MCPM mixtures [278]. Interestingly, contrary to apatite-forming formulations, the brushite-forming ones can be initially liquid and still set within a short period of time [4, 5].

By itself, brushite is remarkably biocompatible and bioresorbable [276]. Due to both a better solubility of DCPD if compared to that of CDHA (Table 2.1 and Fig. 2.1) and metastability of DCPD under physiological conditions [279], after implantation, brushite-forming formulations degrade faster than apatite-forming ones [280–282]. They are quickly resorbed in vivo and suffered from a rapid decrease in strength (although the mechanical properties of the healing bone increase as bone ingrowth occurs [62]). Short setting times, low mechanical strength, and limited injectability seem to prevent brushite-forming formulations from a broader clinical application. However, the major reason why they are not more widespread is probably not related to the mechanical issues but just to a later arrival on the market. Use of sodium citrate or citric acid as setting retardants is an option to get more workable and less viscous pastes of brushite-forming formulations [49, 283–286]. Similar effect could be achieved by addition of chondroitin 4-sulfate [287] and glycolic acid [288]. For the formulations with  $H_3PO_4$  as the initial reactant (chemical Eq. 2.3), acid-deficient formulations were also found to improve the workability. In this case, the setting reaction might be described by the following chemical equation [286]:



Although several studies revealed that too much of DCPD in a given volume was not detrimental to the biological properties of brushite-forming formulations [62, 261, 274], occasionally, when large quantities of them were used, a certain degree of tissue inflammation during the first weeks of in vivo implantation was reported [282, 286, 289]. Further investigations indicated that the inflammation could be due to a partial transformation of DCPD into CDHA with release of orthophosphoric acid [290]:



Transformation of DCPD into CDHA was found to occur via two successive processes, dissolution and precipitation [291], and could be retarded by adding magnesium ions to the formulations, thus reducing the possibility of inflammation [4, 5]. The aforementioned case of acid-deficient formulations (chemical Eq. 2.13)

is the second option, because it reduces the amount of unreacted acid [286] with an option to consume liberating in chemical Eq. 2.14 H<sub>3</sub>PO<sub>4</sub> by the excess of β-TCP. Implantation of previously set brushite-forming formulations might be the third option, because a solid bioceramics was found to be better tolerated than paste implants. Besides, more bones were formed at the solid implant contact and the solid material degraded not so rapidly [292]. For the hardened brushite formulations, a linear degradation rate of 0.25 mm/week was reported [293]. This rapid degradation rate might lead to the formation of an immature bone. Adding β-TCP granules to the self-setting pastes could solve this problem because the granules might act as bone anchors and encourage formation of a mature bone [293, 294].

Additional details on the self-setting brushite-forming formulations might be found in a special review on the subject [247].

### 2.3.3 *Monetite-Forming Formulations*

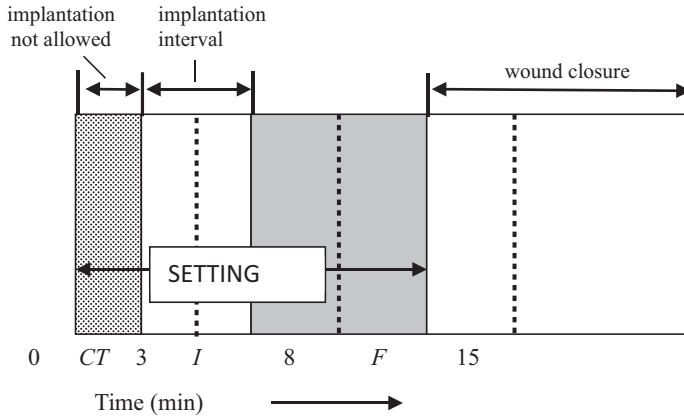
The term “monetite” belongs to a CaPO<sub>4</sub> mineral, which was first described in 1882 in rock-phosphate deposits from the Moneta (now Monito) Island (archipelago of Puerto Rico) [295]. It is well known that DCPA (monetite) is crystallized under the same conditions as DCPD (brushite) but either from aqueous solutions at elevated ( $t \gtrsim 90$  °C) temperatures or at ambient conditions but in water-deficient environments [276, 296]. Therefore, self-setting monetite-forming formulations could exist. Indeed, there are several publications, in which formation of monetite instead of brushite was detected as the final product [32, 44, 131, 297–302]. For example, addition of a big amount of NaCl to a self-setting β-TCP + MCPM formulation was found to result in monetite formation at ambient conditions [300, 301]. Furthermore, DCPA was prepared by a chemical interaction between Ca(OH)<sub>2</sub> and H<sub>3</sub>PO<sub>4</sub> [131]. Moreover, there are self-setting CaPO<sub>4</sub> formulations, in which the final product strongly depends on the reaction temperature. Namely, setting at different temperatures showed that mainly brushite was formed at 5 °C, a mixture of brushite and monetite was formed at 21 °C, and mainly monetite was formed at 37 °C [299]. Interestingly, that for MCPM + β-TCP formulations, an excess of β-TCP resulted in brushite formation, while an excess of MCPM resulted in monetite formation [299]. In addition, there are formulations, which, after setting, resulted in the formation of a complicated mixture of the products, such as DCPA, DCPD, CDHA, and traces of the unreacted initial components [303]. Finally, monetite might be formed during a prolonged storage of dry powders of brushite-forming formulations in normal laboratory atmosphere (~60% relative humidity) [304].

## 2.4 Various Properties

### 2.4.1 *Setting and Hardening*

Generally, self-setting  $\text{CaPO}_4$  formulations must set slowly enough to provide sufficient time to a surgeon to perform implantation but fast enough to prevent delaying the operation. Ideally, good mechanical properties should be reached within minutes after initial setting. Two main experimental approaches are used to study the setting process: a batch approach and a continuous approach. In the batch approach, the setting reaction is stopped at various times, and the resulting samples are analyzed to determine, e.g., the composition and compressive strength of the samples [262, 263]. There are currently two standardized methods to apply this approach, namely, Gillmore needle method (ASTM C266-89) [305] and Vicat needle method (ASTM C191-92) [306]. The idea of both methods is to examine visually the sample surfaces to decide whether the formulation has already set, i.e., if no mark can be seen on the surface after indentation. Besides, the setting process might be monitored in real time by nondestructive methods (the continuous approach), e.g., using pulse-echo ultrasound technique [307, 308], isothermal differential scanning calorimetry [217, 218, 309–315], and alternating current (AC) impedance spectroscopy [316]. For example, calorimetry measurements suggested that in Eq. 2.2 the endothermic MCPM dissolution and the highly exothermic  $\beta$ -TCP dissolution occurred simultaneously, followed by the exothermic crystallization of DCPD [313]. Thus, brushite-forming formulations usually warm upon final setting [309]. Moreover, acid-base reactions (2.1–2.3) can be and have been analyzed by measuring the pH evolution of diluted pastes [262]. In addition, nondestructive methods of Fourier transform infrared spectroscopy [51, 52, 54, 314, 317], solid-state NMR [277], embedded sensors [318], X-ray diffraction [51, 54, 77, 193, 319], and energy-dispersive X-ray diffraction [51–54, 320–322] can be applied as well. The latter techniques proved to be powerful even though they have limitations such as the time required for each measurement (250 s for an X-ray diffraction scan is a problem for fast setting reactions). In addition, the analysis is often located at the sample surfaces where evaporation and thermal effects can modify the reaction rates if compared to those in the bulk. Furthermore, the continuous approaches are indirect, which markedly complicates an interpretation of the collected data, particularly in complex formulations [262].

A way to assess the hardening kinetics is to measure its setting time, which means the time required to reach a certain compressive strength, generally close to 1 MPa. The most straightforward approach is to prepare self-setting samples with a well-controlled geometry (e.g., cylinders), incubating those samples for various times in the right environment (temperature, humidity) and assessing the composition and mechanical properties of the samples as a function of time [262]. One should stress that setting time for  $\text{CaPO}_4$  formulations often corresponds to an earlier stage in the overall setting reaction, typically 5–15% of the overall reaction, while the end of the hardening process is typically reached after several days [148,



**Fig. 2.6** A diagram of the setting parameters relevant for a self-setting CaPO<sub>4</sub> formulation: *CT* cohesion time, *I* initial setting time, *F* final setting time (Adapted from Ref. [6] with permission)

215]. Gillmore needles have been used with success to measure the initial (*I*) and final (*F*) setting times of CaPO<sub>4</sub> cements [141]. Namely, a light and thick needle is used to measure the initial setting time *I* while a heavy and thin needle for the final setting time *F* [169]. The clinical meaning is that the cement paste should be implanted before time *I* and that the wound can be closed after time *F* (Fig. 2.6).

The implanted formulations should not be deformed between times *I* and *F* because in that stage of the setting any deformation could induce cracks [57]. The following handling requirements have been formulated for CaPO<sub>4</sub> cements, as a result [169, 323]:

$$3 \text{ min} \leq I < 8 \text{ min}$$

$$I - CT \geq 1 \text{ min}$$

$$F \leq 15 \text{ min}$$

These parameters are represented schematically in Fig. 2.6. The second requirement means that the cohesion time (*CT*) must be at least 1 min before *I*, so that a clinician has at least 1 min to apply and to mold the material. *CT* is the time from which a formulation no longer disintegrates when immersed in Ringer's solution [169]. As the mixing in a mortar is about 1 min, the shortest *CT* that can be allowed is about 2 min, so that a clinician has at least 1 min to collect the paste from the mortar and put it on a pallet knife or into a syringe with which it is to be transferred to the wound after *CT* and before *I* [169]. For dental applications, time *I* must be close to 3 min, whereas for orthopedic applications it must be close to 8 min. However, in no case it will be tolerable for the clinicians if time *F* becomes greater than 15 min [57, 169].

### 2.4.2 Phase Mixing






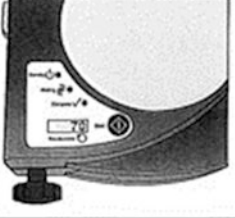
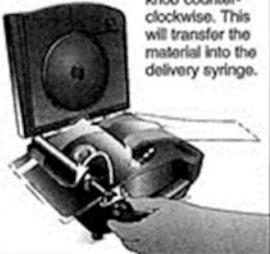


In the clinical situation, self-setting  $\text{CaPO}_4$  formulations can be either applied by the fingertips of a surgeon or injected from a syringe to the defect area of a bone. The first type of the application requires formulation of high-viscous self-setting pastes and putties, which can be applied manually as dough, while the second type requires formulation of low-viscosity compositions, which can be applied by injection from a syringe [169]. Currently, injection appears to be the preferred method between these two major options. Thus, a compromise must be found between a high viscosity leading to too high injection forces and a low viscosity increasing the risk of extravasations. Thus, viscosity values in the range of 100–2000 Pa·s are generally considered to be adequate [324].

In any case, before using, a surgeon needs to have a powder and a liquid mixed properly and thoroughly (to avoid the powder/liquid encapsulation) within the prescribed time. This process must be performed in a sterile environment. Therefore, a mixing procedure is very important because prior to be injected, a self-setting paste must be transferred from a mixing chamber into a syringe. Ideally, this should be done without trapping air bubbles by the formulation [325]. Earlier, most  $\text{CaPO}_4$  formulations were manually mixed with aqueous solutions using a mortar and either a pestle or a spatula. That time, some concerns were raised about an insufficient and inhomogeneous mixing thus compromising the implant strength, as well as on inconsistencies between operators causing unpredictable variations in graft performance [326]. Mechanical mixing (such as an electrically powered mixing machine of Norian SRS/CRS<sup>®</sup> (Fig. 2.7) or Minimalax<sup>®</sup> mixing system for Cementek<sup>®</sup>, produced by Teknimed SA) is the modern approach. It allows mixing the pastes within 60–80 s and enables a rapid and reliable filling of the application syringe [256]. Besides, a powder and a solution could be placed into a syringe and mixed inside a shaker to produce a consistent self-setting paste of the desired viscosity [325]. A mechanical mixing was found to decrease both the mean viscosity of the curing pastes and variability in the viscosity at a given time [327]. However, it did not improve the mechanical strength of the hardened formulations [4, 5].

Of the commercial formulations listed in Table 2.2, Norian SRS<sup>®</sup> is sold as a reactant pack containing two components: a mixture of dry powders (MCPM +  $\alpha$ -TCP +  $\text{CaCO}_3$ ) and a liquid (aqueous solution of  $\text{Na}_2\text{HPO}_4$ ). The components are mixed in the operating room. The paste that is formed is malleable and injectable for ~5 min; it hardens within ~10 min after injection [24, 261]. However, data are available that out of 4.5 ml Norian SRS<sup>®</sup> cement paste ~3 ml is injectable only, whereas up to 1.5 ml of the paste might remain uninjectable from the syringe [57]. This phenomenon is prescribed to the formulation rheology and its interaction with the hydraulic forces of the syringe.  $\alpha$ -BSM<sup>®</sup> (Table 2.2) is also a two-component system; it is prepared from a mixture of ACP and DCPD powders and a saline solution [212]. Biopex<sup>®</sup> consists of four different types of  $\text{CaPO}_4$ : 75 wt. %  $\alpha$ -TCP, 18 wt. % TTCP, 5 wt. % DCPD, and 2 wt. % HA (Table 2.3). The aqueous solution contains 12 wt. % sodium succinate and 5 wt. % sodium chondroitin sulfate [328].

# Demo Rotary Mixer Pack

## Mixing Instructions

<p><b>1</b> Open the mixer lid by depressing the thumb latch located at the right corner of the lid. Position the reactants pack on the Norian® Rotary Mixer by aligning the arrows on the pack and mixer.</p> 	<p><b>2</b> Remove the solution syringe from the foil pouch. Remove the protective cap from the tip of the syringe.</p> 	<p><b>3</b> Remove the protective cap from the injection port on the reactants pack. Connect the solution syringe to the port and fully dispense the solution. Once the solution is injected, complete steps 4–9 immediately.</p> 
<p><b>4</b> Remove the pouch clip and unfold the reactants pack with the delivery syringe to the right.</p> 	<p><b>5</b> Close the lid and depress the thumb latch to lock the lid in place. The mixer is now ready to mix.</p> 	<p><b>6</b> Depress the Start button to initiate mixing. Mixing is complete after 70 cycles. The "Complete" indicator will flash and the mixer will beep until the lid is opened.</p> 
<p><b>7</b> Open the mixer lid and lift the pack from the mixer center post. Feed the reactants pack through the rollers by turning the knob counterclockwise. This will transfer the material into the delivery syringe.</p> 	<p><b>8</b> Remove the reactants pack by turning the knob clockwise.</p> 	<p><b>9</b> Open the outer pouch to access the delivery syringe. Disconnect the syringe from the reactants pack with 1/4 turn counterclockwise. Attach the appropriate delivery needle and begin injecting.</p> 

20-2016 Rev A  
2/04 J5153-A

Fig. 2.7 Mixing instructions for a Norian rotary mixer

Effects of liquid phase on the basic properties of Biopex® were investigated. When mixed with neutral sodium hydrogen orthophosphate or succinic acid disodium salt solution, the initial setting times of the cement were  $19.4 \pm 0.55$  and  $11.8 \pm 0.45$  min, respectively. These setting times were much shorter than that of distilled water,  $88.4 \pm 0.55$  min [329]. Biopex® is mixed with a spatula inside a syringe that can be opened from the front. After mixing, the front part is closed, a needle is inserted into this front part, and the cement paste can be manually injected [4, 5].

Several systematic studies on the influence of composition and concentration of the liquids used in preparing of self-setting  $\text{CaPO}_4$  formulations were performed as well [49, 283, 284]. Unfortunately, the results appeared to be rather unclear. For example, for several formulations, mixing with sodium citrate or citric acid resulted in some effects on the initial setting time [49, 284], while for other ones the effect was insignificant [283]. Concentration increasing of sodium citrate solution resulted in initial setting time increase [49, 283], although the injectability variations of the cement pastes were inconsistent [49, 284].

### 2.4.3 Rheological Properties

In terms of the rheological properties, all types of self-setting  $\text{CaPO}_4$  formulations belong to non-Newtonian fluids. The latter means that the viscosity of such fluids is dependent on shear rate or shear rate history. Nevertheless, good injectability, adequate viscosity, and satisfactory cohesion are required for the successful biomedical applications [330, 331]. Among them, injectability was defined as an ability of a formulation to be extruded through a small hole of a long needle (e.g., 2 mm diameter and 10 cm length) [332, 333] (other needles were also applied [334, 335]), and for certain applications, injectability is even a prerequisite. However, other definitions are possible. For example, injectability of a paste was also defined as its ability to stay homogeneous (without filter pressing) during injection, independently on the injection force [332]. Injectability is measured by the weight percentage of the formulation that could be injected without demixing from a standard syringe by either a hand or a force of 100 N maximum. The numerical values are calculated by the following equation [336]:

$$Inj = (W_F - W_A) / (W_F - W_E) \times 100\%,$$

where *Inj* is the percentage injectability,  $W_E$  is the weight of the empty syringe,  $W_F$  is the weight of the full syringe, and  $W_A$  is the weight of the syringe after the injection.

Usually, injectability of  $\text{CaPO}_4$  formulations are varied inversely with their viscosity, the P/L ratio, as well as the time after starting the mixing of liquid and powder [84, 333, 337]. In addition, powder reactivity was shown to influence the injectability. Namely, significant differences were observed between the injection



behaviors of the nonhardening  $\beta$ -TCP pastes and self-hardening  $\alpha$ -TCP pastes,  $\alpha$ -TCP being less injectable than  $\beta$ -TCP and requiring higher injection loads. What is more, the parameters affecting powder reactivity were shown also to affect injectability. Thus, whereas powder calcination resulted in increased injectability, an addition of setting accelerants tended to reduce the injectability [336]. Furthermore, injectability is improved with smaller particle sizes, with shorter and larger diameter cannula, as well as at smaller flow rates [332]. Moreover, particle shape of the powder is also expected to have effects on the injectability. Namely, powders with spherical shape or round particles are easy to roll, and thus good handling properties and injectability are found when pastes are prepared from such materials. Besides, it should be noted that the pastes could become fluid with less amount of liquid phase since no captured liquid exists in the case of spherical powder [338].

Unfortunately, when a self-setting formulation, which is a biphasic blend of a finely divided ceramic (powder, granules) and a liquid, is submitted to a pressure gradient, the liquid may flow faster than the solid, resulting in local changes of the paste composition. Specifically, the paste present in the region of the highest pressure (e.g., close to the plunger of a syringe) may become so depleted in liquid that the biphasic blend in this zone is no longer a paste but a wet powder [332, 334]. Contrarily, the paste in the zone of the lowest pressure (e.g., at the cannula tip) is enriched in liquid. As these effects are dynamic, the size of the zone depleted in liquid (wet powder) increases during injection, eventually reaching the tip of the injection device and plugging it. The phenomenon, in which the pressure applied to the paste provokes a phase separation after a certain injection time, is generally referred as filter pressing, phase separation, or phase migration [167] (see the aforementioned example for Norian SRS<sup>®</sup> [57], in which a thick mass remained inside a syringe).

Possible mechanisms underlying the limited injectability of the self-setting CaPO<sub>4</sub> formulations have been discussed in literature [335, 339]. In the case of demixing, the exact composition of the extruded part of the paste becomes unknown. Moreover, due to a deviation from the initial P/L ratio, it becomes unclear whether the setting behavior and the mechanical and histological properties of the extruded part are still clinically acceptable. Therefore, a good cohesion of the paste is necessary in order to avoid these problems [340].

Cohesion (cohesiveness, “non-decay”) is the ability of a paste to keep its geometrical integrity in an aqueous solution [167]. It is evaluated by measuring the amount of solid particles released from the formulation prior to its final setting. For self-setting formulations, a bad cohesion may prevent setting and may lead to negative in vivo reactions due to the release of microparticles [341]. Since a high cohesion is the result of strong attractive forces among the particles, factors enhancing van der Waals forces (attractive) and decreasing electrostatic forces (repulsive) can be used to improve cohesion [167]. For example, an appropriate cohesion was achieved when no disintegration of the paste was observed in the fluid [169, 340]. This can be accomplished by keeping a high viscosity for self-setting pastes [24] or using cohesion promoters (e.g., 1–3% aqueous solution of sodium alginate [219, 342–344], as well as other chemicals [219, 345–348]). Some CaPO<sub>4</sub> formulations

fulfill both criteria, e.g., Norian SRS<sup>®</sup>, but others fulfill only one or even none of these requirements. For example, BoneSource<sup>™</sup> [145] and Cementek<sup>®</sup> (Table 2.3) are not injectable, and blood must be kept away from the implanting site until setting [4, 5]. A poor cohesion has been associated to a poor biocompatibility that might lead to inflammatory reactions [341]. Further details on the cohesion properties of various CaPO<sub>4</sub> pastes are available in literature [340].

Viscosity is a measure of the resistance of a fluid, which is being deformed by either shear stress or tensile stress. Generally, the viscosity in the range of 100–1000 Pa·s appears to be ideal [349], and, if possible, a self-setting formulation should have a constant viscosity in the indicated range. Unfortunately, viscosity of self-setting formulations is not a constant value, which, after a decrease in the first seconds after mixing, increases considerably during curing, eventually leading to hardening. Furthermore, viscosity should be high enough to prevent extravasation; therefore, it is very important to define an adequate injection window [349].

#### 2.4.4 *Properties Improving*

As written above, the properties of the existing self-setting CaPO<sub>4</sub> formulations are not ideal. Several ways can be adopted to improve them. The first approach consists of injectability improvement. There are numerous options for this. Firstly, the injection device can be modified. For example, shorter cannulas with a larger diameter, as well as smaller injection rates, favor a good injectability. The last option is not so straightforward: for example, data are available that large injection rates are not detrimental to injectability because of the shear-thinning behavior of many self-setting formulations [335]. Secondly, an external energy might be applied. For example, injectability was improved by ultrasonication, which was believed to result from a reduction in the injection force versus the filtration force as a result of a lesser reduction in the particle interaction and the paste flowability [350]. Thirdly, the composition can also be adapted. Namely, a decrease of the particle size, the P/L ratio, and the plastic limit was found to contribute to a better injectability [332, 337]. For example, injectability was found to be unaffected by P/L ratio within the range of 3.85–4.50 g/ml but drops by nearly 100% between P/L ratio of 4.50 and 5.00 g/ml [49]. However, a decrease in P/L ratio leads to a decrease in the mechanical properties of the self-setting formulations and cohesion might be destroyed. Furthermore, both the initial and final setting times decreased markedly with the P/L ratio increasing [283, 351]. Therefore, variations in the P/L ratio appear to be valid to a certain extent only. That is why the manufacturer of Biopex<sup>®</sup> suggests using a P/L ratio of 2.8 or 3.3 g/ml.

Particle size decreasing of CaPO<sub>4</sub> crystals is one more approach of the injectability improvement. For example,  $\alpha$ -BSM<sup>®</sup> is well injectable because it consists of small crystals. Even though small particles require a larger amount of mixing liquid to obtain a paste, injectability and cohesion of such formulations are generally very good [4, 5]. An indirect approach is to add CaPO<sub>4</sub> crystals that act as spacers

between other particles. For example, DCPA is added to the formulation of Biocement D<sup>®</sup> to improve injectability [4, 5]. Similarly, there is an apatite-forming formulation containing spherical particles of TTCP to improve injectability [352].

Using various chemical additives is the second way to improve the properties of the self-setting formulations [353]. For example, water demand can be reduced by ionically modifying the liquid component, e.g., by adding nontoxic sodium salts of  $\alpha$ -hydroxy di- and tri-acids [354, 355]. A list of additives that have been already studied includes fluidificants, air-entraining agents, porogens, workability-improvement agents, setting time controllers, and reinforcing additives [201, 257, 356]. Besides, various radiopacifiers could be used to simplify an un-invasive in vivo monitoring of the implanted cements [357–362]. The main role of fluidificants is to reduce a mixing time of the formulations. Citric acid is an example of this reagent; it retards the dissolution-precipitation reactions, decreases the compressive strength during initial setting, but increases its strength in the final stages of hardening [284]. Furthermore, data are available that citric acid decreases the setting time and improves the mechanical properties of the hardened formulations [363]. Adding of surfactants to the self-setting formulations was found to have two different meanings: they might act as both air-entraining agents by lowering the surface tension [364, 365] and interaction modifiers by shifting the isoelectric point [366].

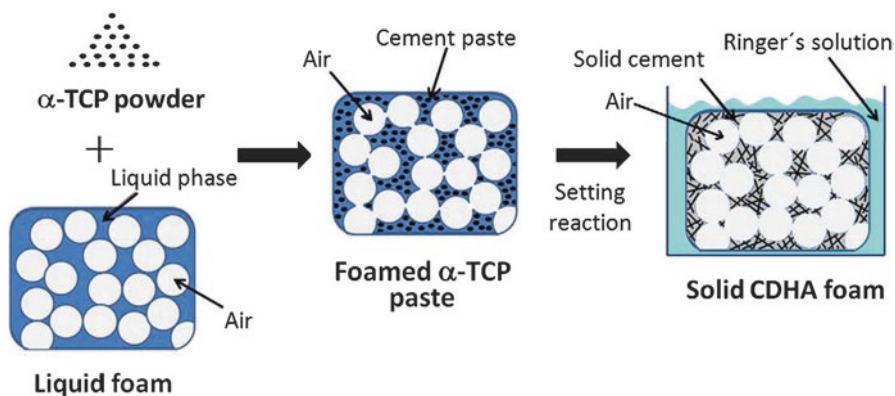
In addition, studies are available, in which self-setting CaPO<sub>4</sub> formulations were modified by various bioorganic compounds in attempts to influence the bone healing process [367–370]. For example, there is a study, in which a self-setting formulation was set in the presence of cocarboxylase, glucuronic acid, tartaric acid,  $\alpha$ -glucose-1-phosphate, L-arginine, L-aspartic acid, and L-lysine, respectively, with the aim to influence the formation and growth of CDHA crystals through the functional groups of these biomolecules [370]. Except for glucuronic acid, all these modifications were found to result in the formation of smaller and more agglomerated CDHA particles, which had a positive impact on the biological performance indicated by first experiments with the human osteoblast cell line hFOB 1.19. Moreover, initial adhesion of human bone marrow-derived mesenchymal stem cells was improved on the formulations containing cocarboxylase, arginine, and aspartic acid. Furthermore, cell proliferation was enhanced on the formulations modified with cocarboxylase and arginine, whereas osteogenic differentiation remained unaffected. Besides, the formulations with arginine and aspartic acid, but not with cocarboxylase, led to a higher BMP-2 binding [370].

Since a good adhesion to bones and other structures allows better transmission of forces at the implant/bone interfaces, a proper adhesion between the set formulations and bones is very important for many surgical procedures. Chemical additives might also improve adhesive properties of the self-setting CaPO<sub>4</sub> formulations. For example, it was observed that brushite-forming formulations set with pyrophosphoric acid in the liquid phase had an increased adherence to various surfaces such as bone, alumina, sintered HA, and stainless steel [371].

Porosity is a very important property to provide good in vivo bioresorption of implanted biomaterials [372]. Thus, various air-entraining agents and porogens are commonly used to induce macroporosity of self-setting CaPO<sub>4</sub> formulations,

ideally, without affecting their normal setting. For example, crystals of mannitol,  $\text{CH}_2\text{OH}(\text{CHOH})_4\text{CH}_2\text{OH}$ , were tested as an air-entraining agent; however, both loss of workability during mixing and severe depreciation of mechanical properties were discovered simultaneously [373–379]. Other porogenic agents were also tested to create porosity. The examples include hydrogen peroxide in the liquid phase [380] and/or iced [381], crystals of  $\text{NaHCO}_3$  and  $\text{Na}_2\text{HPO}_4$  [382], calcium sulfate [69], calcite [274] and  $\text{NaCl}$  [383–385], poly(D,L-lactic-co-glycolic acid) microparticles [386–395], microspheres of pectin [396] and gelatin [397–399], vesicants [400], cetyltrimethyl ammonium bromide [401], polytrimethylene carbonate [402], sucrose [385], as well as some immiscible liquids. These additives could be applied on preset formulations only, while the solubility degree of the solid porogens during setting influences both the content and dimensions of the macroporosity. After hardening, dissolution of the remaining soluble porogens in either water or body fluids produces macropores with the dimensions and shapes of the dissolved crystals. One important limitation that can be envisaged from this route is the need to add a large amount of porogenic agents to guarantee pore interconnectivity, thus compromising not only the excellent biocompatibility and bioactivity of self-setting  $\text{CaPO}_4$  formulations but also their injectability. Another shortcoming is a lack of strength of the resulting bioceramics, especially if particulates dissolve quickly, greatly limiting its applications. An innovative approach that aims at overcoming the lack of interconnectivity and initial strength consists in using resorbable fibers [39, 403–411]. These fibers have the function of initial reinforcing, providing the needed short-term strength and toughness, and gradually dissolving afterward, leaving behind macropores suitable for bone ingrowth. One interesting advantage of long fibers over particulates and short fibers is the fact that once resorbed they can form interconnected pores inside the solid structure facilitating bone tissue regeneration [412].

One more approach to create porosity consists in adding solid  $\text{NaHCO}_3$  to the starting powder and using two different liquids: first, a basic liquid to form the paste, and second, an acid liquid to obtain  $\text{CO}_2$  bubbles to create porosity [413]. Besides, pore-forming  $\text{CO}_2$  bubbles appear at the hardening of apatite-forming formulations, consisting of an acidic  $\text{CaPO}_4$ , such as MCPM or DCPD, and either  $\text{CaCO}_3$  [33, 61, 80–82] or  $\text{NaHCO}_3$  [414–416]. Furthermore, addition of an effervescent porogen formulation comprised from  $\text{NaHCO}_3$  (54.52%) and citric acid monohydrate (45.48%) has been suggested [417]. More to the point, the liquid phase of a self-setting formulation might be initially foamed (commonly, addition of some accessory reagents, such as emulsifiers, foaming agents, and/or surfactants, appear to be necessary) and subsequently mixed with  $\text{CaPO}_4$  powders. In this case, the setting reactions transform the liquid foam into a solid, which ideally maintains the geometry, size, and shape of the bubbles (Fig. 2.8). Thus, the liquid foam acts as a template for the macroporosity of the solid foam [380, 418–423]. In addition, several other porosity creation techniques for self-setting  $\text{CaPO}_4$  formulations are known and, for further details on the subject, the interested readers are referred to an excellent review [412]. Finally, there is a study devoted to evaluation of methods to determine the porosity of the self-setting  $\text{CaPO}_4$  formulations [424].



**Fig. 2.8** A schematic drawing of CDHA foam preparation. Initially a liquid was formed by mechanical agitation of an aqueous solution of a soluble surfactant. Then, the foam was mixed with  $\alpha$ -TCP powder, producing a foamed paste, which was either cast or directly injected into the molds. The setting reaction produced hydrolysis of  $\alpha$ -TCP to CDHA, which resulted in foam hardening (Reprinted from Ref. [419] with permission. Copyright © 2009 Acta Materialia Inc. and Published by Elsevier Ltd)

The major examples of workability-improvement agents, which are added to the self-setting formulations, include water-soluble (bio)polymers. Specifically, polysaccharides [138, 150, 425–428], gelatin [225, 351, 429–435], and polyacrylic acid [436–438] are of interest due to their biocompatibility and good rheological properties. Only small amounts (a few weight %) are needed to dramatically increase the viscosity of the pastes. Besides, the pastes become more cohesive and highly resistant to washout immediately after mixing. For example, a 5 wt. % sodium chondroitin sulfate solution is used as mixing liquid in Biopex® [4, 5]. In the case of gelatin, more than a 50% improvement of the compressive strength was detected [431]. The gelatin-containing formulations after setting were found to exhibit reduced crystallinity, much smaller CDHA crystals, and a more compact microstructure; all these phenomena might be accounted for the improved mechanical properties [432]. In addition, the presence of gelatin improved mechanical properties of the formulations; in particular, the formulations containing 2 wt. % gelatin were found to harden in an acceptable time and were recommended for clinical applications [435]. In some cases, addition of a gelling agent might cause an increase in hardening time [439], but this was remedied by the use of a sodium orthophosphate solution as the liquid phase [184, 185]. Most polysaccharide solutions are thixotropic, i.e., the viscosity of the solution decreases as the shear rate increases. Certain polysaccharides, such as sodium alginate, pectate in contact with calcium ions. This property can be used to make putty-like cement pastes [24]. However, only few polysaccharides are accepted for parenteral use [4, 5]. Nevertheless, the use of gelling agents widened a possible application of the self-setting  $\text{CaPO}_4$  formulations because such formulations can be used even when complete homeostasis is difficult.

Of the three groups of the self-setting formulations, monetite- and brushite-forming formulations react generally much faster than apatite-forming ones. As a result, to satisfy the clinical requirements (Fig. 2.6), setting time of monetite- and brushite-forming formulations has to be prolonged, whereas that of apatite-forming ones has to be shortened [4, 5]. According to the aforementioned, setting reactions of any self-setting  $\text{CaPO}_4$  formulation consists of three successive stages: (1) dissolution of reactants to saturate the mixing liquids by calcium and orthophosphate ions, (2) nucleation of crystals from the supersaturated solutions, and (3) growth of crystals. Therefore, experimental approaches to modify the setting kinetics are to be targeted to these three stages. The available approaches have been summarized in Table 2.4 [262]. Furthermore, seven strategies have been described to decrease the setting time of  $\text{CaPO}_4$  formulations [263]. They are:

- (i) Mean particle size decreasing of the initial powders
- (ii) The P/L ratio increasing
- (iii) pH drop of the mixing liquid to increase  $\text{CaPO}_4$  solubility and hence accelerate the chemical transformations
- (iv) A nucleating phase addition, such as a nano-sized HA powder
- (v) Adding orthophosphate and/or calcium ions into the mixing liquid to accelerate the setting reaction according to the common ion effect
- (vi) Solubility reducing of the reaction end product, for example, by adding fluoride ions into the mixing liquid
- (vii) Solubility increasing of the starting material by amorphization, e.g., by prolonged milling

For further details on these strategies and approaches, as well as for application examples, the interested readers are referred to the original publications [262, 263].

Various setting time controllers (accelerators and retardants) are used to influence the setting time. They include sodium hydrogen pyrophosphate ( $\text{Na}_2\text{H}_2\text{P}_2\text{O}_7$ ) and magnesium sulfate which are added in amounts  $<1$  wt. % [440]. According to other studies, ions of citrate, sulfate, and pyrophosphate are necessary [278, 441, 442]. Application of biocompatible  $\alpha$ -hydroxylated organic acids (glycolic, lactic, malic, tartaric, and citric acids) and their calcium and sodium salts for modification of both rheological and setting properties of  $\text{CaPO}_4$  formulations is well described elsewhere [443, 444]. Besides, aqueous solutions of sodium orthophosphates [138, 266, 304, 391, 445–447] and gelatinized starch [448] are also known as setting time accelerators. An extensive list of the compounds, which might be suitable as accelerators, retarders, additives, or reactants in  $\text{CaPO}_4$  cement formulations, might be found in literature [141]. Interestingly that in some cases, a simple thermal treatment of the initial reagents (in that particular case,  $\alpha$ -TCP powder) at  $\sim 500$  °C could extend the initial part of the setting reaction from a few minutes to a few hours hence providing a potential approach to better control the setting process [449, 450].

The subject of the reinforcing additives is discussed in details in Sect. 2.7 “Reinforced  $\text{CaPO}_4$  Formulations and Concretes.”

Concerning storage stability and shelf life, the factors, significantly influencing those properties for the initial dry powders of  $\text{CaPO}_4$  formulations, were found to be

**Table 2.4** List of strategies and approaches to modify reactivity of the self-setting CaPO<sub>4</sub> formulations [262]

Strategy	Approach	Sub-approaches
1. Dissolution rate	1.1. Change contact area between reagent and mixing liquid	1.1.1. Change milling duration
		1.1.2. Use nano- or micron-sized powders
	1.2. Change solubility in the mixing liquid	1.2.1. Use more/less soluble phase
		1.2.2. Change of reaction pH
	1.3. Change saturation of the mixing liquid	
	1.4. Use dissolution inhibitors in the mixing liquid	
1.5. Modify reagent surface	1.5.1. Chemical change (pre-reaction)	
	1.5.2. Physical change (dissolution pits)	
2. Nucleation rate	2.1. Use crystallization nuclei	
	2.2. Change the saturation of the reaction product in the mixing liquid	2.2.1. Change of saturation
		2.2.2. Change of end product solubility
2.3. Use nucleation inhibitors		
3. Growth rate	3.1. Change the saturation of the reaction product in the mixing liquid	3.1.1. Change of saturation
		3.1.2. Change of end product solubility
	3.2. Use crystal growth inhibitors	

temperature, humidity, and a mixing regime of the powders. Various storage conditions appeared to be effective in prolonging the stability of dry brushite-forming formulations. In the order of effectiveness, they were ranged as follows: adding solid citric acid retardant > dry argon atmosphere  $\approx$  gentle mixing (minimal mechanical energy input)  $\gg$  low temperature [304]. Finally, before a clinical use, the self-setting formulations must be sterilized. A detailed description of the sterilization techniques might be found elsewhere [451].

## 2.5 Bioresorption and Replacement of the Self-Setting CaPO<sub>4</sub> Formulations by Bones

Due to the excellent bioresorbability of DCPA, DCPD, and CDHA, a newly forming woven bone might substitute the hardened CaPO<sub>4</sub> formulations. Namely, the implants made of hardened BoneSource™ (an apatite-forming formulation) were found to be partly resorbed and replaced by natural bone, depending upon the size of the cranial defect [145]. Replacement of BoneSource™ by bone with a minimal invasion of connective tissue was detected in another study, while ChronOS™ Inject

(a brushite-forming formulation) samples exhibited a higher rate of connective tissue formation and an insufficient osseointegration [452].  $\alpha$ -BSM<sup>®</sup> was evaluated in a canine femoral slot model. New bone was found to form in 3 weeks via an osteoconductive pathway. After 4 weeks, only ~1.7% of the implanted material was observed. The hybrid bone possessed the strength of normal, unoperated bone after 12 weeks. In 26 weeks, the boundary between old and new bones was virtually indistinguishable, with only ~0.36% of the implant recognizable [212]. Neither influence on general health, limb-specific function and pain, nor associated complications with  $\alpha$ -BSM<sup>®</sup> application were found past 2 years in another study [453]. Norian SRS<sup>®</sup> was evaluated in canine tibial and femoral metaphyseal defects. The hardened formulation appeared to be gradually remodeled over time, with blood vessels penetrating through it. However, some amounts of Norian SRS<sup>®</sup> were detected in the medullary area as long as 78 weeks after being implanted in dog femurs [60]. An interesting study on the *in vitro* resorption of three apatite-forming formulations (conventional, fast setting, and anti-washout) by osteoclasts if compared with a similar resorption of sintered HA and a cortical bone revealed an intermediate behavior of the formulations: they were resorbed slower than bone but faster than HA [454]. Furthermore, bone neoformation was seen 7 days after implantation of a self-setting  $\alpha$ -TCP formulation [455]. The biodegradation rate of the formulations might be influenced by ionic substitutions in CaPO<sub>4</sub> [456]. Evidences of the direct contact of bone and a hardened CaPO<sub>4</sub> formulation without soft tissue interposition might be found in literature [457, 458].

Different studies reported on both bioresorption and the progress of bone formation around hardened CaPO<sub>4</sub> formulations which in certain cases demonstrated both osteoconductive and osteoinductive properties [459]. However, there are studies in which the osteoinductive properties of self-setting CaPO<sub>4</sub> formulations were not confirmed [460]. Besides, inflammatory reactions were noticed when the formulation did not set [341]. Since the solubility of a non-stoichiometric CDHA is higher than that of stoichiometric HA and  $\alpha$ - and  $\beta$ -TCP (Table 2.1), while the particle dimensions of a precipitated CDHA is smaller than that of sintered CaPO<sub>4</sub>, the biodegradability of apatite-forming formulations is always better than that of dense bioceramics made of sintered stoichiometric CaPO<sub>4</sub>. For example, histologically, at 2 weeks, spicules of living bone with normal bone marrow and osteocytes in lacunae could be seen in implanted formulations. At 8 weeks, the formulation was almost totally surrounded by mature bone. At this stage, no resorption was observed [461]. Only ~30% decrease of the implanted amount of Norian SRS<sup>®</sup> was reported after 24 months in a rabbit femur [462]. Moreover, several differences could be expected depending on the formulation type. For example, as the product of BoneSource<sup>™</sup> and Cementek<sup>®</sup> is a crystalline CDHA, both commercial formulations are expected to resorb slower than other apatite-forming formulations. Indeed no resorption of BoneSource<sup>™</sup> was observed after several years implantation, though some resorption of Biobon<sup>®</sup> was detected. However, porosity appears to be the main biodegradability factor at play: the more porous (for cells) hardened formulations degrade faster than the less porous ones [463, 464]. For example, as Biobon<sup>®</sup> is more porous than BoneSource<sup>™</sup>, the discovered diversity could be due to the differences in



porosity [4, 5]. The latter conclusion is confirmed by the results of other studies: a positive influence of the porosity on resorption rates was found [343]. The interested readers are referred to a study on the suitability of hardened and porous CaPO<sub>4</sub> formulations as scaffolds for bone regeneration, using a rabbit model [465].

The bioresorption properties of bioceramics are generally believed to relate to the solubility of their constitutive phases. The implanted CaPO<sub>4</sub> might be bioresorbed by two possible mechanisms, namely, an active resorption, mediated by the cellular activity of macrophages, osteoclasts, and other types of living cells (so called phagocytosis or literally “cell-eating”) [302, 466–468], and a passive resorption due to either dissolution [6, 7] or chemical hydrolysis (valid for brushite- and monetite-forming formulations only, because both DCPD and DCPA appear to be metastable phases at the physiological pH) [198, 286] in the body fluids. For example, a layer of OCP was found to appear on the surface of hardened brushite formulation [469]. Sometimes, an active resorption is further subdivided into macrophages engulfing of CaPO<sub>4</sub> debris and osteoclast-mediated resorption [275, 470]. Interestingly, that contrary to the brushite-forming formulations, the monetite-forming ones do not hydrolyze into a more chemically stable CaPO<sub>4</sub>, such as CDHA, but conserve their chemical composition and degradability, allowing replacement by the newly formed bone tissue [385].

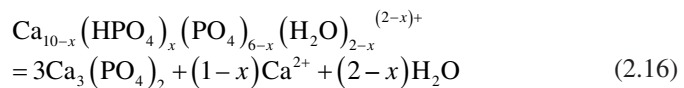
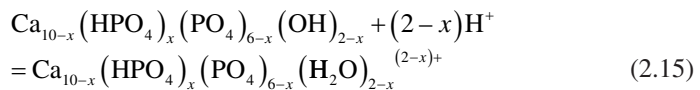
Dissolution might be both chemical and physical. The former occurs with CaPO<sub>4</sub> of a low solubility (those with Ca/P ratio  $\gtrsim 1.3$ ) in acidic environments, while the latter occurs with CaPO<sub>4</sub> of a high solubility (those with Ca/P ratio  $\lesssim 1.3$ ). For example, for MCPM, MCPA, DCPD, and DCPA the solubility product are several times higher than the corresponding ion concentrations in the surrounding body fluids; therefore, they might be physically dissolved *in vivo*, which is not the case for  $\alpha$ -TCP,  $\beta$ -TCP, CDHA, HA, FA, OA, and TTCP since the surrounding body fluids are already supersaturated with regard to these compounds. Therefore, biodegradation of the latter materials is only possible by osteoclastic bone remodeling and is limited to surface degradation since cells cannot penetrate the microporous ceramic structure. Osteoclastic cells resorb CaPO<sub>4</sub> with Ca/P ratio  $\gtrsim 1.3$  by providing a local acidic environment which results in chemical dissolution. In order to investigate two bioresorption mechanisms separately, experiments should be performed by incubating the samples in a cell culture medium without cells to study the passive resorption, whereas the active resorption should be determined during cell culturing on the sample surfaces [470]. Unfortunately, the factors concerning the biodegradation of CaPO<sub>4</sub> biomaterials have not been completely elucidated yet. The chemical composition, physical characteristics, and crystal structures certainly play an important role in their biological behavior. In addition, biodegradation may be influenced by the investigational conditions, such as experimental models, implantation sites, and animal species [467].

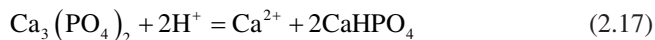
The data are available that macrophages and giant cells decompose quickly resorbed CaPO<sub>4</sub> (e.g., brushite-forming formulations) [282], while slowly (from months to years) resorbed apatite-forming formulations are decomposed by osteoclast-type cells [58, 264, 471]. Clearly, a fast resorption of brushite-forming formulations can only be achieved if the resorption occurs before conversion DCPD

to CDHA according to Eq. 2.14 [75]. Both types of the resorption mechanisms (active + passive) might occur almost simultaneously, if a hardened formulation consists of two different types of  $\text{CaPO}_4$ , e.g., from DCPD and  $\beta$ -TCP. For example, the biphasic brushite-forming ChronOS™ Inject was found to resorb by dissolution with cement disintegration and particle formation followed by the phagocytosis of the cement particles through macrophages [472]. Similar formulation was found to be degraded through a dissolution process associated with a cellular process. The observations suggested that cell activities could be influenced by a small particle size, without close correlation between the particle size and the cell activities but with a correlation between particle concentration and the cell activities [467]. To get further details on this topic, the interested readers are referred to an interesting review on the cellular degradation mechanisms of  $\text{CaPO}_4$  bioceramics [473].

The summary of studies on brushite-forming formulations implantation in various animal models and defect locations is available in literature [286]. Generally, in the same animal model, a degradation rate decreases with an increase in the sample size, as does DCPD to CDHA conversion time. Data are available that hardened brushite-forming formulations experience an initial linear degradation rate of  $\sim 0.25$  mm/week [293], which slightly overwhelms the bone regeneration capacity, resulting in small bone material gaps and a reduction in mechanical properties [62]. In addition, an *in vivo* degradation was found to depend on porosity. Namely, the hardened brushite formulations of higher porosity were found to be quantitatively transformed into crystalline OCP after 10 months of implantation, while lower porosity ones appeared to be chemically stable with the absence of reprecipitate formation and minor resorption from the implant surface [474]. Additional details on the compositional changes of brushite-forming formulations after implantation in sheep are well described elsewhere [440, 475].

The kinetics of passive resorption depends on porosity of the samples, ionic substitutions in  $\text{CaPO}_4$  (when applicable), crystallinity, and pH at the tissue interfaces. The active resorption is due to cellular activity; however, it is also related to the passive one. Namely, the solution pH near macrophages and osteoclasts can drop to  $\sim 5$  by excretion of lactic acid, which increases the solubility (Fig. 2.1), whereas near osteoblasts (bone-forming cells) solution pH can become as high as 8.5 by excretion of ammonia [57]. Dissolution chemistry of CDHA (therefore, of hardened apatite-forming formulations) in acidic media ( $\text{CaPO}_4$  are almost insoluble in alkaline solutions (Fig. 2.1)) might be described as a slightly modified sequence of four successive chemical equations [476, 477]:



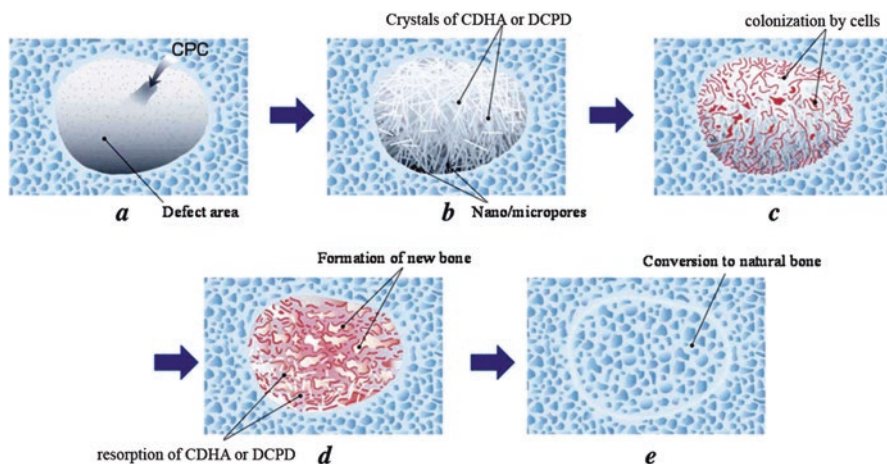


Obviously, the dissolution chemistry of DCPA and DCPD (therefore, of hardened monetite- and brushite-forming formulations, respectively) in acidic media is described by Eq. 2.18. One should stress, that in Eq. 2.18 water is omitted for simplicity. Therefore, dissolution of DCPA is written only.

Nevertheless, the situation with biodegradation mechanisms appears to be more difficult. Namely, in a special study, brushite-forming MCPM/HA and MCPM/ $\beta$ -TCP formulations were compared to test the hypothesis that DCPD chemistry affected both degradation properties and cytocompatibility of the self-setting formulations [478]. Using simple in vitro models, the authors found that brushite-forming MCPM/ $\beta$ -TCP formulations degraded primarily by DCPD dissolution, which was associated with a slight pH drop and relatively low mass loss. Cytocompatibility testing revealed no significant change in cell viability relative to the negative control for all of the MCPM/ $\beta$ -TCP formulations. In contrast, the brushite-forming MCPM/HA formulations were prone to undergo rapid conversion of DCPD to CDHA, resulting in a sharp pH drop and extensive mass loss. A stoichiometric excess of HA in initial formulations was found to accelerate the conversion process, and significant cytotoxicity was observed. Presumably, the initial excess of HA promoted DCPD  $\rightarrow$  CDHA transformation. The authors concluded that, although the product of the setting reaction was the same, brushite-forming formulations produced from MCPM/HA and MCPM/ $\beta$ -TCP differed significantly in their degradation properties and cytocompatibility [478].

The mechanism of bone healing caused by self-setting CaPO<sub>4</sub> formulations is very multifactorial because the surface of the formulations is rapidly colonized by cells. Several types of these cells degrade CaPO<sub>4</sub> by either phagocytotic mechanisms (fibroblasts, osteoblasts, monocytes/macrophages) or an acidic mechanism with a proton pump to reduce the pH of the microenvironment and resorb the hardened bioceramics (osteoclasts) [473, 479]. Various types of mesenchymal cells located at the implantation sites can induce solubilization of CaPO<sub>4</sub>. Upon the cell's arrival, various types of active enzymes, such as acid phosphatase, are secreted that causes dissolution of the hardened cements [480–482]. Much more biology, than chemistry and material science altogether, is involved into this very complex process, and many specific details still remain unknown. Nevertheless, the entire process of bone defect healing by self-setting CaPO<sub>4</sub> formulation might be schematically represented by Fig. 2.9 [483].

It is well known that various polypeptides and growth factors present in bone matrix might be adsorbed onto HA [484–486] and modulate the local milieu of cells. This is supported by many purification protocols of growth factors and bone morphogenetic proteins/osteogenins involving HA chromatography [487, 488]. However, osteoblasts are not found in direct contact with CaPO<sub>4</sub>. A complex proteinaceous layer, usually osteoid, directly contacts the osteoblasts. After implanta-



**Fig. 2.9** A schematic drawing of bone defect regeneration by means of a self-setting  $\text{CaPO}_4$  cement (CPC): (a) filling of a bone defect with a viscous formulation; (b) formulation setting with formation of the end product (CDHA or DCPD); (c) colonization by cells; (d) resorption of CDHA or DCPD by osteoclasts and bone formation by osteoblasts; (e) bone regeneration (Reprinted from Ref. [483] with permission. Copyright © 2013 The Royal Society of Chemistry)

tion of self-setting  $\text{CaPO}_4$  formulations, mitogenic events could occur either during the initial mesenchymal cell contact or after osteoid degradation by osteoblast collagenase. In a dense, mineralized biomaterials such as hardened  $\text{CaPO}_4$  formulations, which provide a barrier to the free diffusion of circulating hormones, growth factors, and cytokines, it is questionable whether the local responses at the periphery of the material regulate osteoconduction [24]. The tissue response to injectable  $\text{CaPO}_4$  formulations is well described in literature [414, 454, 471, 489, 490]. The results of histological and mechanical evaluations in a sheep vertebral bone void model are available elsewhere [491]. The interested readers are also advised to get through a paper on the *in vitro* biodegradation of hardened brushite-forming formulations by a macrophage cell line [168].

To conclude this part, one should note that self-setting  $\text{CaPO}_4$  formulations are able to provide short-term biologically desirable properties and then be replaced by a new bone, which is very important [492]. In general, the growth rate of a newly forming bone depends on age, sex, and general metabolic health of the recipient as well as on the anatomic site, porosity, bulk site, crystallinity, chemical composition (monetite, brushite or apatite), particle sizes, and P/L ratio of the mixture. Considering all these factors, it might take from 3 to 36 months for different formulations to be completely resorbed and replaced by bones [254]. However, additional sound scientific data to determine the exact degree of biodegradability are still needed, *viz.*, animal studies performed in a critical-size defect model. One must stress that the resorption kinetics should be balanced with the rate of new bone formation to avoid collapse at the fracture site, which might occur if the resorption is too fast. Interestingly that to advance self-setting  $\text{CaPO}_4$  formulations as bioabsorb-

able bone replacement materials, it is essential to utilize the patient's own blood in combination with the formulations [493].

## 2.6 The Mechanical Properties

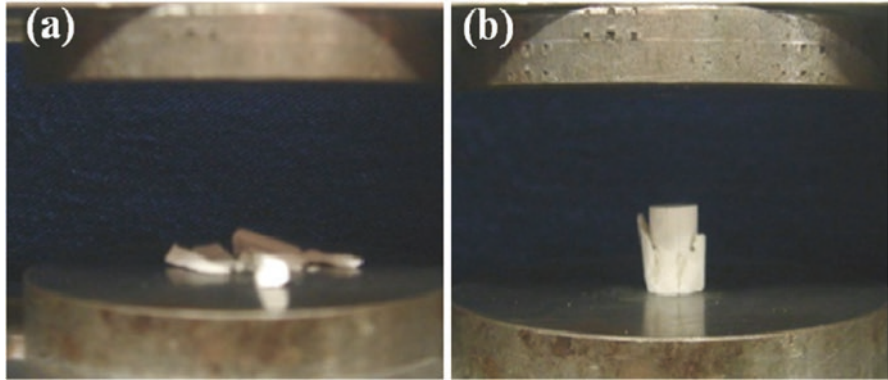
In general, investigations of the mechanical properties of the hardened CaPO<sub>4</sub> formulations revealed that they exhibited large sample-to-sample deviation due to the presence of pores, possibility of inhomogeneous mixing, and small specimen size. This situation generates difficulties for obtaining accurate results and creates obstacles for testing different compositions where only a small batch size is available. In this respect, specimen shape, whether being injected, porosity ratio, and surface quality, bearing support design, appear to have significant matter on variability in terms of the mechanical tests [494].

### 2.6.1 Nonporous Formulations

As in most clinical applications self-setting CaPO<sub>4</sub> formulations are applied in direct contact with human trabecular bones, it may be stated as a mechanical requirement that the strength of the formulations must be at least as high as that of trabecular bones, which is close to 10 MPa [495]. Due to a combination of different forces that may include bending, torsion, tension, and compression, three-dimensional (3D) complex load is normally applied to human bones. Unfortunately, ordinary CaPO<sub>4</sub> cements are strong enough at compression only [249]. In theory, after setting, they can reach the mechanical properties comparable to those of CaPO<sub>4</sub> blocks with the same porosity. However, in practice, their strength is lower than that of bones, teeth, or sintered CaPO<sub>4</sub> bioceramics [185].

Two types of mechanical assessments are usually performed with the hardened self-setting CaPO<sub>4</sub> formulations: compressive strength and tensile strength tests. Compressive strength measurements are performed on cylindrical samples with an aspect ratio of 2 until fracture occurs (Fig. 2.10) [496]. On the other hand, direct tensile strength is difficult to measure in such brittle materials. Therefore, in many studies, the alternative method of measuring the diametric tensile strength has been used, despite the fact that this technique gives results that underestimate the true tensile strength by a factor of 85% [497].

Having the ceramic origin, the set products of all CaPO<sub>4</sub> formulations are brittle and have both a low-impact resistance and a low tensile strength (within 1–10 MPa), whereas the compression strength varies within 10–100 MPa [182, 249, 250]. The latter value exceeds the maximum compression strength of human trabecular bones. Furthermore, at 12 weeks after implantation, the compressive strength of the hardened formulations was found to be still significantly higher (60–70 MPa) than that of normal bone [62]. In general, hardened brushite-forming formulations are slightly



**Fig. 2.10** Pictorial representation of specimens post critical loading for (a) the control and (b) the same formulation reinforced by 5 wt. % of bovine collagen fibers (Reprinted from Ref. [496] with permission. Copyright © 2012 Acta Materialia Inc and Published by Elsevier Ltd)

weaker than hardened apatite-forming ones. Namely, a tensile strength of  $\sim 10$  MPa and a compressive strength of  $\sim 60$  MPa were obtained for brushite-forming formulations [498]. In comparison, apatite-forming ones can reach a tensile strength of  $\sim 16$  MPa [499] and a compressive strength of  $\sim 83$  MPa [500]. However, due to the inherent brittleness of ceramics, those values are close to be meaningless. Namely, the indication of a mean compressive strength of, say, 50 MPa measured on well-prepared (e.g., under vibrations and pressure) and perfectly shaped samples does not inform the readers with which probability this formulation will fail in situ under a cyclic load of, e.g., 10 MPa. Furthermore, a comparison of the compressive strength of hardened formulations with that of cancellous bone is not very helpful either because cancellous bone is much less brittle than ceramics [167].

Moreover, the mechanical properties of hardened  $\text{CaPO}_4$  formulations are not narrowly distributed around a mean value (as for metals) but widespread over a very large range of values, which strongly reduces their clinical application [501]. In vivo, the difference between the hardened apatite- and brushite-forming formulations boosts: namely, the mechanical properties of the former were found to increase [447], whereas those of the latter decreased [62]. This is attributed to a higher solubility of DCPD when compared with that of CDHA (Table 2.1). However, the mechanical properties of the hardened formulations may vary with implantation time. For example, animal studies indicated that the mechanical properties of apatite-forming formulations tended to increase continually [447], in contrast to those of brushite-forming ones, which initially decreased and again increased when bone was growing [62]. Furthermore, shear and tensile forces play a very important role. Thus, these parameters should also be considered, for example, using the Mohr circle approach [497]. Besides, it is difficult to compare the mechanical properties of different formulations. For example, the following numeric values of the compression strength and setting time were obtained: (i) Norian SRS<sup>®</sup> ( $\sim 50\%$  porosity),  $33 \pm 5$  MPa and  $8.5 \pm 0.5$  min; (ii) Cementek<sup>®</sup>,  $8 \pm 2$  MPa and  $17 \pm 1$  min; (iii)

Biocement D<sup>®</sup> (~40% porosity),  $83 \pm 4$  MPa and  $6.5 \pm 0.5$  min; and (iv)  $\alpha$ -BSM<sup>®</sup> (~80% porosity),  $4 \pm 1$  MPa and  $19 \pm 1$  min, respectively [500]. Among them, Biocement D<sup>®</sup> has the highest compressive strength but the lowest porosity, and a high compressive strength does not necessarily mean that Biocement D<sup>®</sup> is the least breakable implant [4]. Additional details on the major properties of Norian SRS<sup>®</sup> are available elsewhere [257, 502]. Besides, the interested readers are suggested to get through the mechanical characterization of a bone defect model filled with ceramic cements [252].

To improve the mechanical properties of the self-setting CaPO<sub>4</sub> formulations, addition of water-soluble polymers might be considered. For example, in the early 1990s, Miyazaki et al. [503, 504] used a number of polymers, including polyacrylic acid and polyvinyl alcohol, to improve the properties of a TTCP + DCPD formulation. They noted marked increases (up to threefold) in mechanical properties but with an unacceptable reduction of workability and setting time. Later, another research group reported similar results using sodium alginate and sodium polyacrylate [505]. Afterward, other researchers added several polyelectrolytes, polyethylene oxide, and a protein bovine serum albumin into  $\alpha$ -BSM<sup>®</sup> cement pastes to create CaPO<sub>4</sub>-polymer biocomposites [506]. Biocomposites of  $\alpha$ -BSM<sup>®</sup> with polycations (polyethylenimine and polyallylamine hydrochloride) exhibited compressive strengths up to six times greater than that of pure  $\alpha$ -BSM<sup>®</sup> material. Biocomposites of  $\alpha$ -BSM<sup>®</sup> with bovine serum albumin developed compressive strengths twice than that of the original  $\alpha$ -BSM<sup>®</sup> [506]. Similar strengthening effect was achieved by addition of some commercial superplasticizers [507]. The results showed that small additions, i.e., 0.5 vol. %, in the aqueous liquid phase improved the maximum compressive strength (35 MPa) of Biocement-H© by 71%, i.e., till ~60 MPa. Moreover, the addition of high amounts of superplasticizers, i.e., 50 vol. %, allowed for a significant increasing of the P/L ratio from 3.13 to 3.91 g/ml, without affecting the maximum strength and/or the workability [507]. This effect was explained by an inhibiting effect of the aforementioned additives on the crystal growth kinetics of newly forming crystals of CaPO<sub>4</sub>, which resulted in smaller crystallites and, hence, a denser and more interdigitated microstructure. However, the increased strength was attributed mainly to the polymer's capacity to bridge between multiple crystallites (thus forming a more cohesive composite) and to absorb energy through a plastic flow [506]. Other factors affecting strength are the materials used in the solid phase, particle sizes, incorporation of fillers (see Sect. 2.7 "Reinforced CaPO<sub>4</sub> Formulations and Concretes" for details), the P/L ratio, and various additives to the liquid phase [148].

The strength of the cement-prosthesis interface might be studied by a pullout test. The details are available elsewhere [93].

## 2.6.2 Porous Formulations

As the presence of pores simplifies for cracks to run throughout the ceramic mass, the mechanical properties of the hardened formulations were found to decrease exponentially with porosity increasing [223, 508]. In theory, self-setting  $\text{CaPO}_4$  formulations can be made with almost any porosity. However, for most commercial formulations, the pores are of 8–12  $\mu\text{m}$  in diameter, and, after setting, porosity occupies about 40–50% of the entire volume [509]. To reduce porosity of the hardened formulations, pressure can be applied [185, 510, 511]. Usually, the pore dimensions in hardened formulations are too small to allow a fast bone ingrowth. Thus, there is a lack of macroporosity. Besides, unless special efforts have been performed, the available pores are not interconnected. Due to these reasons, after injection, osteoclastic cells are able to degrade the hardened  $\text{CaPO}_4$  layer by layer only, starting at the bone/implant interface throughout its inner part (in other words, from the outside to the inside). This is the main drawback of the classical self-setting formulations when compared to  $\text{CaPO}_4$  ceramic scaffolds with an open macroporosity [4, 5].

Since strength is reciprocally proportional to porosity [463], the former might be adjusted by varying the P/L ratio in the hardening mixtures. At high P/L (i.e., low L/P) ratios, the space between particles in self-setting pastes decreases. Considering that precipitation of new crystals takes place surrounding the initial powder particles, this leads to a more compact structure of the crystal agglomerates (Fig. 2.11) [245]. Elevated compression strength would be applicable in cranioplasty for regions requiring significant soft tissue support. For small bone defects, such as root canal fillings, formulations of low compression strength might be used [179]. Concerning the tensile strength of self-setting  $\text{CaPO}_4$  formulations, as a rule of thumb, it appears to increase twofold with each 10 vol. % decrease of the porosity, i.e., 5, 10, 20, 40, and 80 MPa for 80%, 70%, 60%, 50%, and 40% porosity, respectively [4, 5]. The effect of porosity on the compressive modulus of self-setting  $\text{CaPO}_4$  formulations is shown in Fig. 2.4 in Ref. [511]. Ishikawa and Asaoka showed a linear relation ( $R^2 = 0.94$ ) between the natural logarithm of diametral tensile strength and porosity of self-setting  $\text{CaPO}_4$  formulations where porosity was controlled by compaction pressure (up to 173 MPa) [182]. Besides, an empirical relationship between strength,  $S$ , and porosity,  $P$ , has been introduced in another study:

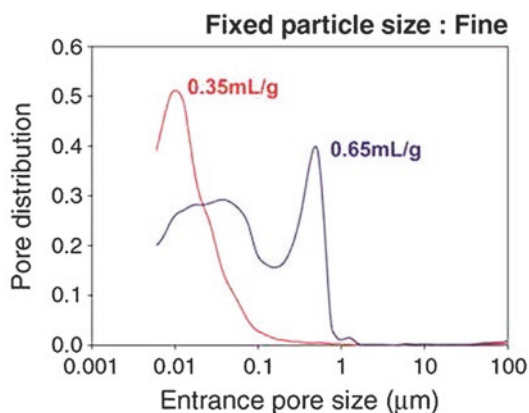
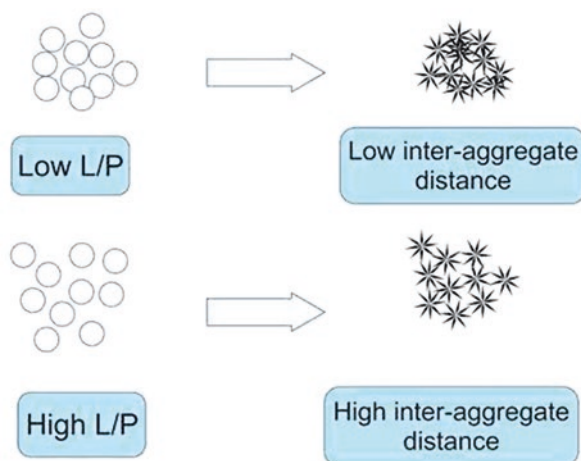
$$S = S_0 e^{-bP},$$

where  $S_0$  is the theoretical strength at  $P = 0$  (fully dense) and  $b$  is an empirical constant [512].

As the porosity is mainly due to an excess of water used in the self-setting formulations, attempts were made to reduce the amount of water. However, the amount of water determines the rheological properties of self-setting pastes: a decrease in water content leads to a large increase in viscosity, eventually leading to non-flowable pastes. As  $\text{CaPO}_4$  formulations are set at an almost constant volume, the final porosity can be predicted from the initial composition [4, 5]. A shrinkage



**Fig. 2.11** A schematic drawing of the influence of the L/P ratio on the properties of self-setting formulations (Reprinted from Ref. [245] with permission. Copyright © 2012 Elsevier Ltd)



degree of ~1% causes no restrictions on clinical use [247]. Studies on the in vivo evaluation of an injectable macroporous  $\text{CaPO}_4$  formulations revealed a higher bioresorption rate due to both a higher surface contact with body fluids (which increases dissolution) and enhancing cellular activity due to particle degradation [343, 414].

Besides the addition of porogens [373–402], the porosity level of the self-setting  $\text{CaPO}_4$  formulations might be controlled to a certain extent by adjusting particle sizes and the P/L ratio. When the P/L ratio is high, the porosity of the hardened formulations is low [4, 5]. According to calculations, the tensile strength of the formulations with zero porosity could be as high as 103 MPa [182]. However, a high density and a lack of pores decreases bioresorbability because a newly forming bone appears to be unable to grow into the implant; it might grow only simultaneously with dissolution of the hardened formulations. Thus, porosity of self-setting  $\text{CaPO}_4$  formulations is a very important factor for their biodegradability [4, 5].

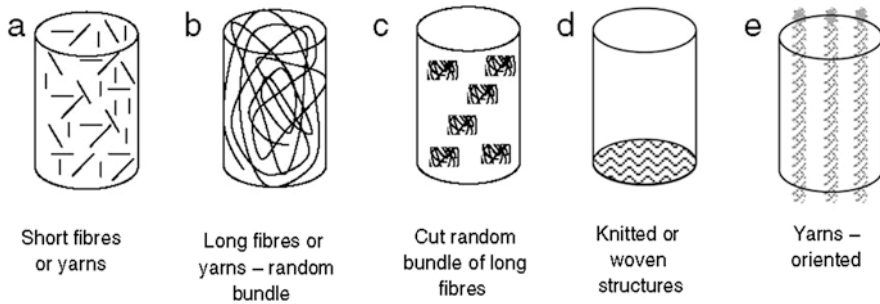
## 2.7 Reinforced CaPO<sub>4</sub> Formulations and Concretes

Being aware on the excellent bioresorbability of DCPA, DCPD, and CDHA, researchers are focused on attempts to overcome the mechanical weakness of the self-setting CaPO<sub>4</sub> formulations [513]. Among them, an approach devoted to adding of various fillers, fibers, and reinforcing additives, giving rise to formation of various multiphasic biocomposite formulations, appears to be the most popular one [146, 147, 151, 251, 328, 509, 514–527]. Even carbon nanotubes have been successfully tested to reinforce the self-setting CaPO<sub>4</sub> formulations [32, 528–531]. Although the biomaterials community does not use this term (just one paper has been published [532]), a substantial amount of such formulations might be defined as CaPO<sub>4</sub> concretes. According to Wikipedia, the free encyclopedia, “Concrete is a construction material that consists of a cement (commonly Portland cement), aggregates (generally gravel and sand) and water. It solidifies and hardens after mixing and placement due to a chemical process known as hydration. The water reacts with the cement, which bonds the other components together, eventually creating a stone-like material.” [533]. The idea behind the concretes is simple: if a strong filler is present in the matrix, it might stop crack propagation. In such formulations, the load is transferred through the matrix to the fillers by shear deformation at the matrix/filler interfaces. Both fillers and matrix are assumed to work altogether providing a synergism needed to make an effective composite. However, adding fillers always reduced porosity, which negatively influenced the ability of the concretes to allow bone ingrowth into the pores. Hence, denser formulations have slower resorption rates and thus a slower bone substitution [182]. Moreover, due to the presence of fillers, injectability and other rheological properties of the reinforced formulations and concretes frequently appear to be worse than the same properties of the ordinary formulations [534]. Thus, it is difficult to increase strength of the self-setting formulations without having a negative influence on the other properties.

The reinforced formulations and concretes can be prepared from any type of self-setting CaPO<sub>4</sub> formulations [513]. For example, in an attempt to improve the mechanical properties, investigators prepared concretes by adding human cadaveric femur bone chips in amounts of 25, 50, and 75% (w/w) to  $\alpha$ -BSM<sup>®</sup> cement [515]. The mechanical tests revealed that the specimens of pure cement exhibited a relatively high stiffness but a low ductility. However, for the concretes, an increase of bone content was found to result in the decrease of elastic modulus and increase in the ductility; however, the ultimate strength showed only small changes with no apparent trend [515]. A concrete of Biopex<sup>®</sup> cement with allografts taken from femurs and tibiae of rabbits is also available. Unfortunately, nothing is written on the improvement of the mechanical properties, but, surprisingly, by the addition of allografts, the hydrolysis process of Biopex<sup>®</sup> was significantly changed [328]. By adding polymers, other researchers succeeded in improving the mechanical strength of the formulations up to ~30 MPa; however, both the kinetics of CDHA formation and, thus, the bioactivity were decreased [152, 535]. Xu et al. reported that incorporation of long carbon fibers at a volume fraction of 5.7% increased the flexural

strength about four times and work of fracture  $\sim 100$  times, if compared to unreinforced formulations [536]. In another study, DCPD-forming formulations were reinforced by poly(propylene fumarate) and, if compared with non-reinforced controls, flexural strength improved from  $1.80 \pm 0.19$  to  $16.1 \pm 1.7$  MPa, flexural modulus increased from  $1073 \pm 158$  to  $1304 \pm 110$  MPa, maximum displacement during testing increased from  $0.11 \pm 0.04$  to  $0.51 \pm 0.09$  mm, and work of fracture improved from  $2.7 \pm 0.8$  to  $249 \pm 82$  J/m<sup>2</sup> [537]. The reinforcement mechanisms were found to be crack bridging and fiber pullout, while fiber length and volume fraction were key microstructural parameters that determined the concrete properties [538]. Although addition of polypropylene, nylon, and carbon fibers was found to reduce the compression strength of a double-setting CaPO<sub>4</sub> formulation due to increased porosity, it strongly increased the fracture toughness and tensile strength, relative to the values for the unreinforced formulations [516]. A knitted two-dimensionally oriented polyglactin fiber-mesh was found to be effective in improving load-bearing behavior of self-setting formulations for potential structural repair of bone defects [251]. To make the material stronger, fast setting, and anti-washout, chitosan was added [47, 131, 221, 379, 434, 503, 538–548]. Furthermore, anti-washout properties might appear by adding sodium alginate [549]. CaPO<sub>4</sub> concretes containing SiO<sub>2</sub> and TiO<sub>2</sub> particles showed a significant ( $\sim 80$ – $100$  MPa) increase in the compressive strength, while no change in the mechanical behavior was observed when ZrO<sub>2</sub> particles were added [550]. Additional examples of the properties improving comprise addition of silica [38], silk fibroin [83], calcium silicates [95, 525], calcium carbonate [82, 550], polypeptide copolymers [551], gelatinized starches [552], fibrin glue [553], magnesium wires [554], and collagen [496, 555–564]. Fig. 2.10 shows specimens of a hardened unreinforced CaPO<sub>4</sub> formulation (a) and the same formulation reinforced by 5 wt. % of bovine collagen fibers (b) after compression loading up to  $\sim 15$  % level of strain. The characteristic brittle behavior of the set unreinforced formulation can be observed, as the specimen exhibited catastrophic failure after critical loading and subsequently broke into fragments. Observing a typical compression specimen of the set reinforced formulation after testing clearly displays that the failure mechanism was very different, as the specimen maintains a degree of cohesive structure and remains capable of supporting a load [496]. Additionally, strength improvement was found when DCPA and TiO<sub>2</sub> crystals were used as fillers for mechanically activated  $\alpha$ -TCP formulations [565].

The blending of fibers with the self-setting pastes or precursor powders can be carried out using different structures of the fibrous materials, as shown in Fig. 2.12 [566], and the effects of varying fiber type, fiber length, and volume fraction of fiber-reinforced CaPO<sub>4</sub> formulations were investigated [539, 567]. Four fiber types were studied: aramid, carbon, E-glass, and polyglactin. Fiber length ranged within 3–200 mm and fiber volume fraction ranged within 1.9–9.5%. The results indicated that self-setting formulations were substantially strengthened via fiber reinforcement. Aramid contributed to the largest increase in strength, followed by carbon, E-glass, and polyglactin. Fiber length, fiber volume fraction, and fiber strength were found to be key microstructural parameters that controlled the mechanical properties of the concretes [539, 567]. Fiber reinforcement of porous formulations (man-



**Fig. 2.12** Different ways of fiber disposition in the fiber-reinforced  $\text{CaPO}_4$  self-setting formulations. As seen from this figure, fibers can be introduced as short staple ones (a) or as long fibers forming a random bundle (b). The random bundles can also be cut into small pieces and dispersed inside the self-setting matrix (c). If fibers are spun into yarns, the latter can also be cut and introduced randomly into the formulation (a, b), oriented (e) or may be woven or knitted into laminar textile structures (d) (Reprinted from Ref. [566] with permission. Copyright © 2011 Elsevier Ltd)

nitrol was used as a porogen) was performed as well [568]. Namely, reinforcement by aramid fibers (volume fraction of 6%) was found to improve the properties of a  $\text{CaPO}_4$  concrete with the strength increasing threefold at 0% mannitol, sevenfold at 30% mannitol, and nearly fourfold at 40% mannitol. Simultaneously, the work of fracture increased by nearly 200 times; however, the modulus was not changed as a result of fiber reinforcement [568]. Addition of 20 wt. % of acrylamide and 1 wt. % ammonium polyacrylate to the liquid increased the compressive and tensile strength of  $\alpha$ -TCP formulation by 149% and 69% (55 and 21 MPa), respectively, due to a dual-setting mechanism (in which a dissolved monomer is simultaneously cross-linked during setting of the  $\text{CaPO}_4$  components) [569]. Other types of the dual-setting  $\text{CaPO}_4$ -containing formulations are known as well [570–574]. The advantages of the dual-setting strategy comprise the possibility of a high polymer loading into the self-setting  $\text{CaPO}_4$  formulations without compromising the rheological properties of the freshly prepared pastes. This is related to the fact that the dissolved monomers represent water-miscible liquids of a low viscosity; therefore, even high monomer concentrations are not strongly altering the initial rheology [513]. A positive influence of polyamide fibers [575], polyhydroxyalkanoate fibers [576], and bioactive glass [577–580] is also known. Interestingly that reinforcement of self-setting formulations could be performed by infiltration of a preset composition by a reactive polymer and then cross-linking the polymer in situ [581].

The reinforcement of self-setting  $\text{CaPO}_4$  formulations by resorbable or biodegradable fillers responds to a different strategy. In this case, the rationale is to provide strength augmentation at the initial stages and, subsequently to filler degradation, to facilitate bone ingrowth into the macropores [39, 403–411, 554]. For example, the initial strength of a concrete was threefold higher than that of the unreinforced control [403]. The work of fracture (toughness) was found to increase by two orders of magnitude for other biocomposites of  $\text{CaPO}_4$  with resorbable fibers, such as Vicryl polyglactin 910 (Ethicon, Somerville, NJ) [404] and a mesh of

copolymer of polyglycolic and polylactic acids [408]. The addition of fillers with higher bioresorption rate than the hardened CaPO<sub>4</sub> matrix allows creating macropores to favor cell colonization, angiogenesis, and eventually fostering bone regeneration. Ideally, the loss of strength produced by filler degradation should be compensated by the formation of new bone. One important advantage of long fibers over particulates and short fibers is the fact that once resorbed they form a network of interconnected channels inside the set structures, which could facilitate bone ingrowth into implants [184, 185, 403, 408]. For example, interconnected macropores were formed in a hardened formulation at 84 days of immersion in a physiological solution [408]. One should note that, apart from the mechanical properties of the reinforcing materials, the structure of the incorporated fibers, regular or random, appears to be crucial for the resulting flexural strength and modulus of elasticity [406]. A higher strength might help extending the use of CaPO<sub>4</sub> formulations to larger stress-bearing repairs, while the macropores might facilitate tissue ingrowth and integration of the hardened formulations with adjacent bones. To extend this idea further, several types of fibers with different rates of bioresorbability might be simultaneously incorporated into self-setting formulations.

Besides the aforementioned, it is important to mention on the reinforced formulations and concretes, after hardening consisting of CaPO<sub>4</sub> only [293, 294, 472, 582–590]. The first biphasic concrete consisting of a hardened DCPD matrix filled with  $\beta$ -TCP granules was introduced in 1992 [583]. Further development of this formulation was well described in other papers [293, 472]; unfortunately, neither mechanical nor rheological properties of that concrete were disclosed. Nevertheless, the results of still another study showed that, by addition of 20 wt. % the as-prepared  $\beta$ -TCP aggregates, the compressive strength of the self-setting concrete was increased by about 70%, while the paste itself still maintained injectable, while the heat release in the hydration process decreased by ~25% [586].

At physiological pH, the *in vitro* solubility of DCPD is approximately 100 times higher than that of  $\beta$ -TCP (Table 2.1 and Fig. 2.1); roughly, the same order of magnitude applies for the *in vivo* resorption kinetics of these types of CaPO<sub>4</sub>. Thus, a new bone is formed in the space left after resorption of the DCPD matrix, while  $\beta$ -TCP granules act as guiding structures. This feature of the cement can be considered an inverse scaffolding effect [591]. Another research group invented a formulation that incorporated as major powder components  $\alpha$ -TCP, ACP, and BCP (HA +  $\beta$ -TCP in various HA/ $\beta$ -TCP ratios) [514]. It was believed that after setting such a formulation could provide a porous bioceramics *in vivo* due to preferential dissolution of a better soluble ACP component compared to the other CaPO<sub>4</sub> in the matrix. Further, this combination was extended to a multiphase concrete composition consisting of 70% w/w settable matrix (mixture of 45%  $\alpha$ -TCP, 5% MCPM, and 25% of ion-substituted ACP) with the average particle dimensions of 15  $\mu$ m and 30% BCP (HA +  $\beta$ -TCP) granules (ranging between 80 and 200  $\mu$ m) as a filler [582]. The role of BCP granules is quite interesting: after implantation of a formulation without BCP granules, the quality of newly formed bone was not identical to the host bone, while implantation of a concrete with BCP granules resulted in formation of a new bone identical to the host bone. The reason of this phenomenon is

not clear yet, but, perhaps, it correlates with similar results for  $\beta$ -TCP granules, which act as bone anchors and encourage formation of a mature bone [293, 294]. Other ACP-containing formulations were elaborated as well [592].

Effects of added  $\alpha$ -TCP and  $\beta$ -TCP were investigated to shed light on the setting reactions of apatite-forming formulations consisting of TTCP and DCPA [585]. Added  $\beta$ -TCP showed no reactivity, and thus resulted in extended setting time and decreased mechanical strength. Similar results were obtained in another study [589]. In contrast,  $\alpha$ -TCP dissolved to supply calcium and orthophosphate ions after initial apatite crystal formation by the chemical reaction (2.1). Although setting time was delayed because  $\alpha$ -TCP was involved only in the latter reaction of apatite cement, larger apatite crystals were formed due to its addition. Due to larger apatite crystal formation, the mechanical strength of the  $\alpha$ -TCP-added formulations increased by approximately 30%, as compared to  $\alpha$ -TCP-free ones [585]. In another study, HA whiskers were used as the reinforcement phase to prepare concretes and the maximum strength was achieved when HA whiskers were added in amount of 4% (wt.) [587]. Besides, self-setting  $\text{CaPO}_4$  formulations might be reinforced by calcium polyphosphate fibers [593, 594]. Additional details on this topic might be found in special reviews [566, 595].

To conclude this part, one should briefly mention on the reverse situation: there are bone concretes made of various polymeric cements, reinforced by  $\text{CaPO}_4$  powders or granules to establish a compromise between the desired mechanical and biological properties [596–602]. The  $\text{CaPO}_4$  presented in such formulations act as fillers, which are necessary to both improve the mechanical properties and impart bioactivity; however, they do not participate in the hardening mechanisms. For example, the higher the amount of HA was in bioactive acrylic bone cements, the higher were the compressive and tensile moduli. Furthermore, as the percentage of HA increased to 20 wt. %, the heterogeneity of the material was higher [597]. Polymerization of monomers is primarily responsible for setting of such types of biocomposites and concretes. However, that is another story.

## 2.8 Biomedical and Clinical Applications

Injectable and self-setting  $\text{CaPO}_4$  formulations have been introduced as adjuncts to internal fixation for treating selected fractures. Different studies have already shown that they are highly biocompatible and osteoconductive materials, which can stimulate tissue regeneration [24, 603]. The main purpose of the self-setting  $\text{CaPO}_4$  formulations is to fill voids in metaphyseal bones, thereby reducing the need for bone graft, although such formulations might also improve the holding strength around metal devices in osteoporotic bone. Bone augmentation (i.e., a reinforcement of osteoporotic bone through injection) appears to be a very promising application field of the self-setting  $\text{CaPO}_4$  formulations. Such procedures ease the fixation of screws in mechanically poor bone (e.g., for osteosynthesis) and decrease pains associated with unstable vertebrae. The combination of a self-setting nature,

biocompatibility, lack of any by-products, and a great potential for replacement by bones makes CaPO<sub>4</sub> formulations very promising materials for clinical and medical applications. In addition, they can easily be used by bone remodeling cells for reconstruction of damaged parts of bones [144, 145, 282, 490, 604–606]. The ability to be molded in place also is a very important property because these formulations can easily be delivered into the desired place and can be fitted perfectly with bone defects [145]. Besides, some formulations were found to possess an antimicrobial activity [84, 87, 89, 96, 607], as well as promote osteoblast cell adhesion and gene expression in vitro [608].

Numerous studies reported optimistic results on the clinical application of the self-setting CaPO<sub>4</sub> formulations. For example, the data on cytocompatibility and early osteogenic characteristics are available in literature [609]. The ratio of the cases determined to be “effective” or “better” among the 74 cases we found to be 97.3% [610]. Besides, the results of intra-articular degradation and resorption kinetics of these formulations revealed no signs of pronounced acute or chronic inflammation [611]. Injected Norian SRS® cement was mainly found as a single particle, anterior to the cruciate ligaments. Synovial tissues surrounded the cement within 4 weeks and signs of superficial resorption were found [611]. However, disintegration or washout of self-setting CaPO<sub>4</sub> formulations has been reported as a potential clinical problem [182, 265]. Perhaps, this problem could be solved by putting pressure on the paste during the setting period. In addition, sodium alginate could be added; however, the mechanical properties (strength) of this formulation are still poor [150].

According to the available information, the earliest attempts for biomedical applications of the self-setting CaPO<sub>4</sub> formulations occurred in 1984 and were related to dentistry [612, 613]. However, those were in vitro studies, while the earliest animal studies were performed in 1987 [41]. Afterward, in 1991, a TTCP + DCPA cement was investigated histologically by implanting disks within the heads of nine cats [614]. Simultaneously, another research group evaluated the tissue reactions to this cement in the teeth of monkeys [615]. Some important examples of medical applications of the self-setting CaPO<sub>4</sub> formulations are given below.

### ***2.8.1 Dental Applications***

A group of investigators extracted all mandibular premolar teeth from beagles [616]. After 1 month of healing, alveolar bone was reduced to make space for a previously fabricated CaPO<sub>4</sub> cement block. One more month later, 8 mm HA implants were placed in such a manner that the apical half was embedded into alveolar bone and the coronal half in the CaPO<sub>4</sub> cement block. The investigators observed that the cement block was gradually replaced by bone and histopathologic features of the cement area were similar to that of natural bone. Moreover, the coronal half of the implants, previously surrounded by the CaPO<sub>4</sub> cement, was firmly attached by natural bone [616]. In another study, the same researchers used fluorescent labeling

analysis and electron microanalysis to measure the extent of new bone formation and elemental (Ca, P, Mg) distribution [617]. The results indicated the presence of newly formed bone at ~1 month after surgery and similar elemental distributions in the CaPO<sub>4</sub> cement and natural bone areas at ~6 months after surgery [254].

A self-setting CaPO<sub>4</sub> was injected as a bone filler for gaps around oral implants placed on the medial femoral condyles of six goats and found excellent bone formation around the graft material. Unfortunately, the degradation rate of the formulation appeared to be very slow, and no resorption was observed [618]. In another study, a self-setting formulation was placed on artificially created periodontal defects, but no significant difference was found between the hardened formulation and control. However, the formulation acted as a scaffold for bone formation and provided histocompatible healing of periodontal tissues [619]. Still other investigators used a self-setting formulation for direct pulp capping [620, 621] and compared it to calcium hydroxide. Both materials were found to be equally capable of producing a secondary dentin at ~24 weeks [621]. Positive results were obtained in other studies [172, 622, 623]. Besides, self-setting CaPO<sub>4</sub> formulations were tried as root canal fillers [87, 624, 625] and for pulpotomy [626] and restoration of enamel carious cavities [260]. Namely, a high alkaline pH value of the setting reaction of single-phase TTCP formulations provides a strong antimicrobial potency which is of interest for dental applications, e.g., as pulp capping agents or root canal fillers. The studies demonstrated a higher potency compared to commercial Ca(OH)<sub>2</sub>/salicylate formulations against various oral microbial strains, e.g., *Streptococcus salivarius* and *Staphylococcus epidermidis*, or a clinically isolated plaque mixture [607]. Finally, self-setting CaPO<sub>4</sub> formulations can be used as adjunctive supportive agents for dental implants [627]. Further details on the dental applications of CaPO<sub>4</sub> are available in a topical review [628].

### 2.8.2 Oral, Maxillofacial and Craniofacial Applications

Bone regeneration in oral, maxillofacial and craniofacial surgery can be divided into two main types of procedures: bone augmentation and bone defect healing. The use of self-setting CaPO<sub>4</sub> formulations for such purposes seems logical, as there is little or no stress generated under these conditions. Moreover, the ability to mold the material at placement is an enormous advantage from a cosmetics standpoint [254]. For example, BoneSource™ is indicated for the repair of neurosurgical burr holes, contiguous craniotomy cuts, and other cranial defects with a surface area no larger than 25 cm<sup>2</sup> per a defect. In addition, it may be used in the sinus region for facial augmentation [145, 629], and the formulation can be supported by metal hardware [145]. In dogs, BoneSource™ was employed to supplement the supraorbital ridge and to augment skull base defects [630]. Another group performed trials to ascertain the inflammation around the site and the degree of loss of the implanted BoneSource™. The material was found to be osteoconductive with both periosteal and endosteal bone formation [631]. Still another group presented excellent results using the



material combined with an underlying resorbable mesh in calvarian defects of Yorkshire pigs. They found progressive bone ingrowths in all defects at 180 days, with nearly complete replacement by host bone [409]. Besides, excellent results for over 100 human patients were reported when a self-setting CaPO<sub>4</sub> formulation was used in cranial defects. The success rate after 6 years was 97% [134]. Furthermore, self-setting CaPO<sub>4</sub> formulations are used in orbital reconstructions [159, 161, 632]. The results of still other medical trials are available elsewhere [275, 633–647].

To conclude this part, one should stress that complications still occur: namely, two cases of apatite-forming cement resorption and subsequent seroma formation have been reported for patients who had undergone retrosigmoid craniotomy [648]. Furthermore, another study describes complications occurred with 17 patients who underwent secondary forehead cranioplasty with Norian® CRS [649]. Of 17 patients, 10 (59%) ultimately had infectious complications. Infection occurred on a mean of 17.3 months after surgery, and of the ten patients with complications, nine required surgical debridement and subsequent delayed reconstruction. The authors concluded that although apatite-forming cements could yield excellent aesthetic results, their use in secondary reconstruction yielded unacceptably high infection rates leading to discontinuation of their use in this patient population [649].

### ***2.8.3 Orthopedic Applications***

Self-setting CaPO<sub>4</sub> formulations have successfully been used for the treatment of the distal radius fracture [261, 650, 651]. Besides, other successful attempts have been made to use these formulations for calcaneal fractures [652], hip fractures [653, 654], augmentation of osteoporotic vertebral bodies [655], distal radius fractures [656], tibial plateau fractures [61, 656–661], restoration of pedicle screw fixation [662, 663], reinforcement of thoracolumbar burst fractures [664], cancellous bone screws [665, 666], vertebral body fillings [667], wrist arthrodesis [668], and fixation of titanium implants [669]. A study on a cement augmentation of the femoral neck defect might be found elsewhere [670]. Considering their properties, self-setting CaPO<sub>4</sub> formulations might potentially be applied to reinforce osteoporotic vertebral bodies [655, 671]. Further details and additional examples on this topic are available elsewhere [275, 672–674]. Besides, the self-setting formulations appear to be a reliable subchondral replacement biomaterial when the bone defect is adjacent to the articular cartilage [675].

### ***2.8.4 Vertebroplasty and Kyphoplasty***

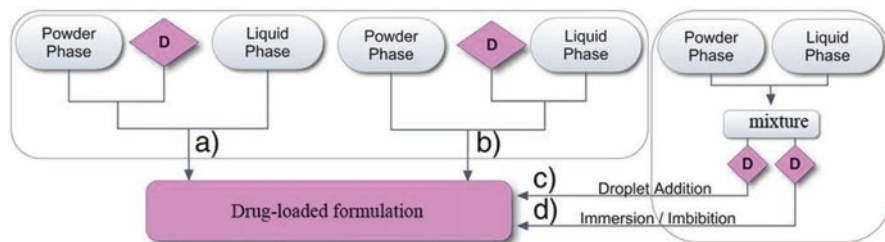
Vertebroplasty and kyphoplasty are two surgical procedures that recently have been introduced to medically manage osteoporosis-induced vertebral compression fractures. Particularly, both procedures aim to augment the weakened vertebral body,

stabilize it, and/or restore it to as much of its normal height and functional state as possible. Both procedures involve injection of self-setting  $\text{CaPO}_4$  pastes into the fractured vertebral body, which resulted in a faster healing [134, 257, 675–683]. Furthermore, prophylactic injections of such formulations also have been performed.

### 2.8.5 Drug Delivery

In general, a potential substrate to be used as a drug carrier must have the ability to incorporate a drug, retain it in a specific target site, and deliver it progressively with time in the surrounding tissues. Therefore, a certain level of porosity is mandatory. Additional advantages are provided if the biomaterial is injectable, is biodegradable, sets at ambient temperature, and has both near-neutral pHs and a large surface area [63, 64]. These properties make self-setting  $\text{CaPO}_4$  formulations very attractive candidates as drug carriers for therapeutic peptides [684], antibiotics [29, 422, 685–697], anticancer [698–702] and anti-inflammatory [703, 704] agents, cytokines [705], hormones [706], bone morphogenetic proteins [546, 707–711], and other biologically active compounds [712–721]. For example, a “growth factor cement” was reported [722]. In that study, a combination of bone morphogenetic protein-2 (BMP-2), transforming growth factor-beta (TGF- $\beta$ 1), platelet-derived growth factor, and basic fibroblast growth factor (bFGF) was used in a  $\text{CaPO}_4$  cement for treatment of peri-implant defects in a dog model. The findings indicated a significant effect of the “growth factor cement” on increased bone-to-implant contact and amount of bone per surface area if compared with both the cement-only and no-cement treatment groups [722]. Similar data were found for a combination of a self-setting formulation with an exogenous nerve growth factor [723]. Even more complicated combination of deproteinized osteoarticular allografts integrated with a  $\text{CaPO}_4$  cement and recombinant human vascular endothelial cell growth factor plus recombinant human BMP-2 (rhBMP-2) has been studied as well [724]. The drug delivery properties of the self-setting  $\text{CaPO}_4$  formulations might be influenced by crystal morphology, porosity, and microstructure [725].

For the self-setting formulations, the first issue that has to be considered and which will determine a drug distribution and its interaction with the matrix is the incorporation method of the drug. In principle, drugs (as well as hormones, cells, and other biomedical or biological compounds) might be incorporated into both liquid and powder phases before phase mixing, as well as into the self-setting formulations obtained after both phases have been mixed. This process is schematically shown in Fig. 2.13 [245]. After setting, the drugs appear to be distributed within a porous solid matrix. According to a topical review on the subject [245], there are three options of drug existence inside the matrix: (a) dissolved in the remaining liquid phase within the existing pores among the newly formed inorganic crystals, (b) adsorbed or chemically bound on the surface of the crystals, or (c) in a solid form inside pores (Fig. 2.14).



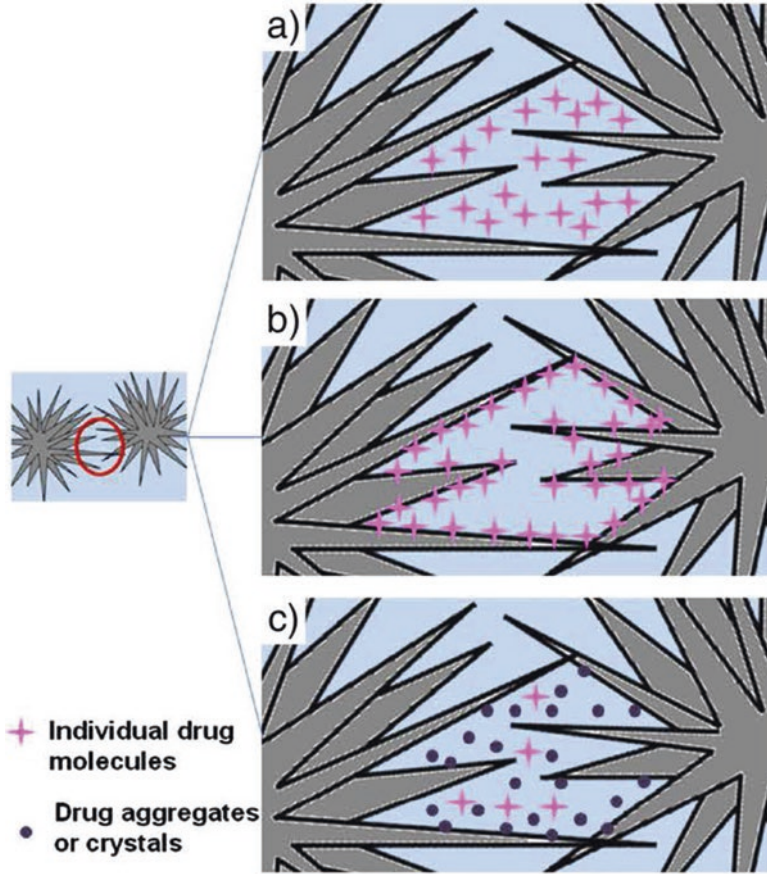
**Fig. 2.13** A schematic drawing of the possible ways of drug (denoted as *D*) incorporation into the self-setting formulations. Prior phase mixing a drug can either be distributed within the powder phase (a) or solubilized in the liquid phase (b). Drug loading can also be made after setting by droplet addition (c) or by imbibition (immersion) in the drug-containing solution (d). The procedures (c, d) do not allow injection since they require formulation pre-setting (Reprinted from Ref. [245] with permission. Copyright © 2012 Elsevier Ltd)

Studies on drug release are the second most important topic on drug incorporation into the self-setting formulations [265, 687–690, 726, 727]. This process is regulated by the microstructure of the set formulations (i.e., their porosity), as well as by the presence or absence of additives able to influence the movement of drug molecules within the solid matrix. For example, it was observed that hardened formulations with very low porosity showed much slower drug release patterns than those with higher porosities [688]. Moreover, drugs that inhibit the setting reactions and reduce the porosity have a slower rate of release. This phenomenon has been observed with gentamicin sulfate. The presence of sulfate ions in this drug inhibits brushite crystal growth, resulting in a finer solid microstructure with lower porosity that slows down drug release [685]. In another study, investigators added flomoxef sodium to a self-setting formulation and found that the release of antibiotic could be easily controlled *in vivo* by adjusting the content of sodium alginate [265]. *In vitro* elution of vancomycin from a hardened cement has been studied as well [727]. Concerning the possible mechanisms of drug releases, a topical review on the subject [245] describes three reasonable scenarios:

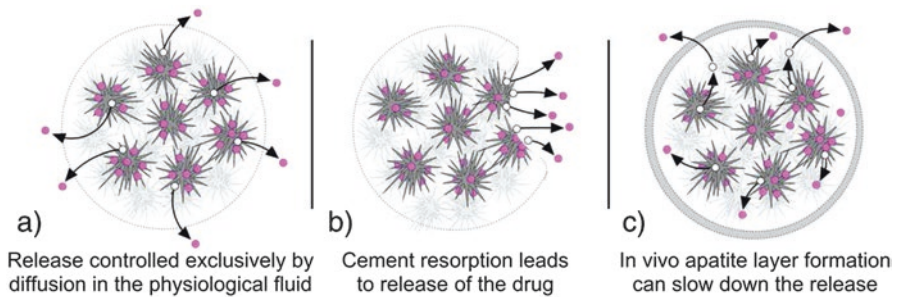
- If the rate of the matrix degradation is slower than drug diffusion, drug release is controlled by diffusion of the drug through the liquid permeating the set formulation (might be valid for apatite-forming formulations).
- If the rate of matrix degradation is faster than drug diffusion, the former controls drug release (might be valid for monetite- and brushite-forming formulations).
- In some cases, an apatite layer can be formed on the surface after implantation, thus hindering the diffusion of the drug to the surrounding tissue (Fig. 2.15).

Finally, various types of surface coatings might be applied as well to slow down the kinetics of drug release.

Studies on drug adsorption appear to be the third most important topic. In general, adsorption of any type of bioorganic molecules is related to chemical interactions between their functional groups and the CaPO<sub>4</sub> matrix, and the strength of this



**Fig. 2.14** A schematic drawing of the different ways a drug can be found within a solid matrix: (a) as individual molecules dissolved in the remaining liquid within the pores; (b) adsorbed or chemically bound to the crystals surface; (c) in a solid form, as drug crystals or aggregates (Reprinted from Ref. [245] with permission. Copyright © 2012 Elsevier Ltd)



**Fig. 2.15** A schematic drawing of the different ways a drug release from hardened formulations (Reprinted from Ref. [245] with permission. Copyright © 2012 Elsevier Ltd)

interaction influences the release pattern of drugs. Accordingly, bioorganic substances with adherent functional groups show a slow release pattern, whereas those that do not adhere well to CaPO<sub>4</sub> matrices will be more rapidly released. For instance, vancomycin release from 3D-printed brushite matrices is complete within 1–2 days, while only 25% of tetracycline loaded on the same matrix is released after 5 days of incubation [728]. Therefore, in order to obtain adequate release patterns, adsorption of bioorganic molecules to the self-setting matrix needs to be tuned. This can be done by either selecting the most appropriate drug for the matrix or modifying the self-setting matrix itself. For instance, doping brushite-forming formulations with Sr was found to reduce the antibiotic adsorption capacity, resulting in an increase in the fraction of drug released and in a faster release rate [729].

The laboratory studies on drug incorporation into the self-setting CaPO<sub>4</sub> formulations cover different aspects. Firstly, it is necessary to verify that addition of a drug does not influence the setting reaction not only in terms of the setting and hardening mechanisms but also with respect to the rheological behavior and injectability. Secondly, it is necessary to determine the *in vitro* kinetics of drug release. Thirdly, the drug delivery properties of the formulation must be studied *in vivo*. Finally, but still importantly, the clinical performance of the drug delivery system must be evaluated as well [63, 64]. For example, recombinant human transforming growth factor  $\beta$ 1 (rhTGF- $\beta$ 1) was added to a CaPO<sub>4</sub> cement [730–733]. This resulted in the formation of a bioactivated formulation that could be used as a bone filler and bone replacement [730]. It appeared that after 8 weeks, the addition of growth factors stimulated and increased bone formation (50% volume) and bone contact (65%) in comparison to control calvarian defects in an animal study. Besides, the growth factor group reduced the remaining volume of the cement by 20% [731]. Examples of rhBMP-2 release from a loaded porous CaPO<sub>4</sub> cement might be found elsewhere [733, 734], while an experimental study on a self-setting formulation impregnated with dideoxy-kanamycin B is also available [735]. In addition, self-setting CaPO<sub>4</sub> formulations could be loaded by other bioactive and/or biological compounds, such as ascorbic [736] and nucleic [737] acids. Further details and additional examples are well described elsewhere [57, 63, 64, 245]. Thus, the possibility of using injectable and self-setting CaPO<sub>4</sub> formulations as drug delivery systems offers an attractive and efficient solution for the treatment of various bone diseases, e.g., tumors, osteoporosis, and osteomyelitis, which normally require long and painful therapies.

### 2.8.6 *Brief Conclusions on the Biomedical Applications*

To conclude the biomedical part, one should stress that despite several encouraging results, not every surgeon's expectation has been met yet [735]. First, self-setting CaPO<sub>4</sub> formulations are not superior to autografts, despite offering primary stability against compressive loading [738, 739]. One of the main concerns of clinicians is to reach higher rates of bioresorption, an improvement of bone reconstruction,

and, to a lesser extent, higher mechanical resistance [61]. Besides, clinical application of the self-setting formulations in comminuted fractures revealed penetration of the viscous paste into the joint space [740–742]. The interested readers are referred to a paper on cement leakage during vertebroplasty [743]. To date, cadaveric studies have already shown that use of the self-setting  $\text{CaPO}_4$  formulations with conventional metal fixation in certain fractures of the distal radius, tibial plateau, proximal femur, and calcaneus can produce better stability, stiffness, and strength than metal fixation alone. Early clinical results have revealed a reduced time to full load bearing when the formulations were used for augmentation of tibial plateau and calcaneal fractures, more rapid gain of strength, and range of motion when used in distal radius fractures and improved stability in certain hip fractures [605, 650]. However, surgeons reported on difficulties in filling the vertebral bodies (a bad injectability of present formulations) and other problems, such as filter pressing and decohesion, observed during vertebral body injection that resulted in bone instability due to low mechanical strength as well as long setting times of the cements [744]. This happens due to not only poor mechanical properties of the self-setting formulations but also some difficulties of filling vertebral bodies. In order to maintain a good cohesion and reduce filter pressing, the  $\text{CaPO}_4$  formulations need to be more viscous (hence, less injectable) [4, 5]. For example, they might be modified by addition of polysaccharides [138, 150, 425–428] and/or gelatin [225, 351, 429–434].

Another type of concerns has been raised that the use of self-setting  $\text{CaPO}_4$  formulations for the augmentation of fractured and osteoporotic bones might aggravate cardiovascular deterioration in the event of pulmonary cement embolism by stimulating coagulation [745]. To investigate these potential problems, 2.0 ml of either  $\text{CaPO}_4$  or polymethylmethacrylate (PMMA) cement was injected intravenously in 14 sheep. Intravenous injection of  $\text{CaPO}_4$  cement resulted in a more severe increase in pulmonary arterial pressure and decrease in arterial blood pressure compared to the PMMA cement. Disintegration of the  $\text{CaPO}_4$  cement seemed to be the reason for more severe reaction that represents a risk of cardiovascular complications. The authors concluded that further research efforts should aim at improving cohesion of self-setting  $\text{CaPO}_4$  formulations in an aqueous environment for future clinical applications such as vertebral body augmentation [745].

The third type of concerns is related to inflammation and other adverse reactions from the surrounding tissues. Although such cases are rare, all of them must be considered in differential diagnosis of the side effects [648, 649, 746–749]. For example, there was a patient who experienced an allergic reaction to Biopex® [748]. A patch test was performed and a positive reaction to magnesium orthophosphate was obtained. Since Biopex® contains magnesium orthophosphate, that case was diagnosed as an allergic reaction. Two publications [648, 649] have been described above in Sect. 2.8.2 “Oral, Maxillofacial and Craniofacial Applications.” In addition, there are cases, such as cochlear implantation surgery [749], in which self-setting  $\text{CaPO}_4$  formulations appear to be unsuitable.

To conclude the biomedical part of this chapter, one should mention that, although the long-term outcomes are still poorly documented, currently there are no doubts concerning a very great potential of the clinical applications of self-setting CaPO<sub>4</sub> formulations for healing of bone and dental defects. For example, a bioresorbable CaPO<sub>4</sub> cement was once found to be a better choice, at least in terms of the prevention of subsidence, than autogenous iliac bone graft for the treatment of sub-articular defects associated with unstable tibial plateau fractures [750]. Furthermore, BoneSource™ was found to be safe and effective when used to fill traumatic metaphyseal bone voids and appeared to be at least as good as autograft for treatment of these defects [751]. However, in other studies, autologous cancellous grafts were demonstrated to lead to a significantly better bone regeneration compared to the application of CaPO<sub>4</sub> granules produced from a self-setting CaPO<sub>4</sub> formulation after 6 weeks [752]. As this text is intended to be read mainly by chemists and materials researchers, the biological, medical, and clinical aspects of self-setting CaPO<sub>4</sub> formulations have not been discussed in many details. For additional biomedical details, the interested readers are referred to other papers and reviews [24, 57, 63, 64, 179, 605, 610, 738, 753].

## 2.9 Non-biomedical Applications

Since a non-biomedical topic is beyond the general subject of current review, this section is brief. In literature, there are some reports on brushite cement-based biosensors, one for phenol detection by combining the cement with the enzyme tyrosinase [754] and another for the detection of glucose using the enzyme glucose oxidase [755]. Both biosensors have faster signaling and higher sensitivity than traditional biosensor systems based on polymeric or clay matrices, opening up many possibilities for the future development of these devices.

## 2.10 Recent Achievements and Future Developments

As the self-setting CaPO<sub>4</sub> formulations represent an intriguing group of new biomaterials for bone augmentation and reconstruction, there is a great potential for further improvement of their properties, in which the ideal characteristics (Table 2.5) should be approached by manipulations with the chemical composition, powder particle size and distribution, as well as by means of various additives. Several commercial formulations have been already approved for the clinical applications (Tables 2.2 and 2.3). New compositions are expected to appear in the market soon. The forthcoming commercial products will need to be improved in order to take the advantage of a variety of possibilities offered by the self-setting properties. New formulations will include (i) injectable and open macroporous compositions to

**Table 2.5** Major advantages and disadvantages of the self-setting CaPO<sub>4</sub> formulations [63, 64, 254]

Advantages	Disadvantages
1. Self-setting ability in vivo	1. Mechanical weakness: limited use due to potential collapse of material followed by soft tissue formation instead of bone formation (loaded areas). Until cements with adequate shear strength are available, most complex fractures that can be repaired with cement also will require metal supports
2. Good injectability that allows cement implantation by minimally invasive surgical techniques, which are less damageable than the traditional surgical techniques	2. Can be washed out from surgical defect if excess of blood
3. Good osteoconductivity and occasional osteoinductivity: the initial biological properties of the hardened cements are similar to those of CDHA or brushite	3. Lack of macroporosity (especially interconnected pores), which prevents fast bone ingrowth and the cements degrade layer by layer from the outside to the inside only
4. Can be replaced by newly formed bone after a period of time (osteotransductivity)	4. The in vivo biodegradation of many formulations is slower than the growth rate of a newly forming bone
5. Moldability: the perfect fit to the implant site, which assures good bone-material contact, even in geometrically complex defects	
6. Excellent biocompatibility and bioactivity	
7. No toxicity	
8. Low cost	
9. Ease of preparation and handling	
10. Setting at body temperature	
11. Form chemical bonds to the host bone	
12. Clinically safe materials in their powder components	
13. Can be used to deliver antibiotics, anti-inflammatory drugs, growth factors, morphogenic proteins, etc. at local sites, which are able to stimulate certain biological responses <sup>a</sup>	

<sup>a</sup>Further studies are necessary

optimize their osteoconduction [351], (ii) formulations containing only one CaPO<sub>4</sub> (single-phase powders) [246], and (iii) drug-loaded and hormone-loaded formulations for the treatment of bone diseases [57, 63, 64]. Furthermore, incorporation of autologous or allogenic osteo-progenitor cells into the self-setting formulations will be favorable [756–758]. Obviously, the first two directions deal with both chemistry and material science, while the last two directions are more related to biology and medicine.



Concerning the material point of view, an innovative approach of so-called ready-to-use self-setting formulations was introduced relatively recently. The concept was shown to work with both single-phase CaPO<sub>4</sub> powders and mixtures of several components. For example, the ready-to-use formulations can be obtained by stabilizing the CaPO<sub>4</sub> reactants as separated liquid or pasty components, with at least one of them containing an aqueous liquid, which is needed to initiate the setting reactions after mixing. Such formulations consist of two injectable pastes to be mixed together and injected at the time of implantation [759, 760]. The preparation process is fast and reproducible since two liquid phases can be mixed more homogeneously than powder with liquid as performed for conventional self-setting formulations. This strategy allows usage of dual-chamber syringes equipped with a mixing device (e.g., by a static twin-chambered mixer incorporated in the injection cannula that allows injection of the paste immediately after mixing), meaning reduced paste processing/handling time, lesser contamination risks, enhanced reproducibility, and immediate injection of the mixture into the bone defects [761]. In such formulations, a wide range of possibilities appears by changing the CaPO<sub>4</sub> components. Furthermore, such formulations can also be modulated by adjoining different additives such as setting retardants, polymeric adjuvants, visco-enhancing agents, suspension stabilizers, osteoinductive agents, radiopaque fillers, or macropore-forming agents [412, 483]. For example, aqueous pastes of  $\alpha$ -TCP powder were found to be stabilized for up to a year at room temperature by using of 0.1 M MgCl<sub>2</sub> solution (it was believed that chemical reaction (2.5) was suppressed by sorption of Mg cations on the  $\alpha$ -TCP surface; therefore, wet  $\alpha$ -TCP formulations were not set). Then, adding of a CaCl<sub>2</sub> solution in a 1:4 volume ratio activated wet  $\alpha$ -TCP pastes and the formulations were set. This was explained by displacement of adsorbed Mg cations from the surface of  $\alpha$ -TCP particles by Ca cations, which initiated  $\alpha$ -TCP transformation to CDHA according to reaction (2.5) [762].

Another preparation approach of the ready-to-use self-setting formulations comprises a water-reactive paste such as a mixture of TTCP and DCPD powders dispersed in a nonaqueous but water-miscible liquid (e.g., glycerol, polyethylene glycol, N-methyl-2-pyrrolidone) + a gelling agent (e.g., hydroxypropylmethylcellulose, carboxymethylcellulose, chitosan, sodium alginate) + a hardening accelerator (e.g., MCPM, Na<sub>2</sub>HPO<sub>4</sub>, tartaric, malic, malonic, citric or glycolic acids) to form a stable paste that can be directly injected into bone defects [299, 694, 763–771]. In literature, this type of self-setting pastes is called “premixed calcium phosphate cements” (occasionally referred to as PCPC), in which the paste preparation is done under defined conditions, while the pastes remain stable during storage and harden only after placement into the defect. The pastes can be obtained of different consistencies, from low-viscosity ones to putty-like plastic pastes [164–166]. Setting occurs *in vivo* upon a contact with body fluids or *in vitro* in a physiological solution. Since hardening occurs solely after the paste has been injected into a bone defect, this approach works with any formulation. In addition, premixed CaPO<sub>4</sub> formulations eliminate the powder-liquid mixing stage during surgery, which might improve their performance and allow shortening the surgical time. Besides, a risk of operator-induced error is considerably reduced. On the negative side, the setting reaction of

the premixed formulations is difficult to control, and the mechanical properties of the hardened  $\text{CaPO}_4$  are poor. Commonly, a hardening process is both slow and volume dependent because it relies on the exchange or replacement of a nonaqueous liquid by water. Furthermore, the use of additional components makes both production and certification more difficult, while the release of large amounts of a foreign liquid during injection may result in adverse biological reactions. In addition, premixed  $\text{CaPO}_4$  formulations must be protected from the environmental moisture during storage [772, 773]. Besides, little attention has been paid to the problem that the presence of water impurities in the nonaqueous liquid and/or the powdered solid can compromise the stability of the paste. The composition of some premixed  $\text{CaPO}_4$  formulations might be found in literature [412].

The earliest premixed self-setting  $\text{CaPO}_4$  formulations were formed apatite as the final product and had a setting time of longer than 1 h and a low mechanical strength [763]. Afterward, improved formulations were developed. They exhibited a rapid setting when immersed in a physiological solution, yielding a hardened bioceramics with a higher mechanical strength, approached the reported strengths of sintered porous HA implants and cancellous bone [764–766]. Such formulations are produced commercially, e.g., VELOX<sup>®</sup> by INNOTERE GmbH (Radebeul, Germany). Brushite-forming premixed self-setting formulations have been introduced as well [759, 760, 772, 774–776]; they have shorter setting times than the aforementioned apatite-forming ones. In addition, studies appeared on preparation of the premixed monetite-forming formulations [297–299], as well as on premixed macroporous  $\text{CaPO}_4$  scaffolds reinforced by slow-dissolving fibers (in other words, premixed macroporous concretes) [410]. Similar to the common self-setting  $\text{CaPO}_4$  formulations, the premixed ones could be also used for drug delivery applications [777]. Furthermore, antimicrobial properties could be created as well [778, 779].

The third approach to manufacture the ready-to-use self-setting  $\text{CaPO}_4$  formulations applies very low temperatures [45]. According to this approach, powder and liquid components of the self-setting formulations are mixed, and the prepared pastes are immediately frozen. Thus, premixed frozen  $\text{CaPO}_4$  “slabs” are obtained, which are stored in freezers or even in liquid nitrogen. By freezing, the setting reactions are slowed down or even inhibited (this depends on the temperature), but when the formulations have to be applied, the “slabs” are defrosted and the softened pastes are molded by hands at ambient temperatures. When frozen and stored at  $t = -80\text{ }^\circ\text{C}$  or less, significant degradation in compression strength did not occur for the duration of the study (28 days). Interestingly, that in the case of the brushite-forming formulations prepared from a combination of  $\beta$ -TCP with 2 M  $\text{H}_3\text{PO}_4$  solution, freezing the paste had the effect of increasing mean compressive strength fivefold (from 4 to 20 MPa), which was accompanied by a reduction in the setting rate of the cement. This strength improvement was attributed to a modification of crystal morphology and a reduction in damage caused to the cement matrix during manipulation [45].

Using biphasic  $\text{CaPO}_4$  formulations (such as  $\alpha$ -TCP +  $\beta$ -TCP simultaneously) instead of  $\alpha$ - or  $\beta$ -TCP alone as the initial component of the self-setting formulation appears to be the next innovative approach [34, 35, 37, 210]. Due to the differences between  $\alpha$ - and  $\beta$ -TCP in both the reaction kinetics and reactivity in interactions

with other chemicals, depending on the  $\alpha$ -TCP/ $\beta$ -TCP ratio in the precursor blends, the variability of the handling behavior, physicochemical properties, and degradation characteristics of the hardened formulations was observed. Namely, after hydrolysis of  $\alpha$ -TCP phase according to Eq. 2.15, the  $\alpha$ -TCP +  $\beta$ -TCP blend transforms to a partially nonabsorbable CDHA and a completely resorbable  $\beta$ -TCP phase, providing new properties. In general, biphasic  $\alpha$ -TCP +  $\beta$ -TCP formulations revealed longer setting and injectability times as compared to monophasic ones. During hardening, the amount of apatite formation was found to be inversely proportional to the extent of  $\beta$ -TCP, whereas the predominant morphology of the precipitated crystals changed from platelets to needles with increasing of the  $\beta$ -TCP content. The hardening process appeared to be controlled by the transformation reaction of  $\alpha$ -TCP into a mixed matrix consisting of CDHA and  $\beta$ -TCP. In vitro degradation studies indicated that the degradation rates of biphasic  $\alpha$ -TCP +  $\beta$ -TCP formulations containing sufficient amounts of  $\beta$ -TCP were more than twice as high if compared to just  $\alpha$ -TCP-containing formulations [34, 35, 37, 210]. Furthermore, if  $\alpha$ -TCP +  $\beta$ -TCP blend is used as a single-phase (or single-component) cement powder, hydrolysis of  $\alpha$ -TCP phase into CDHA and stability of  $\beta$ -TCP phase results in formation of solid BCP (CDHA +  $\beta$ -TCP) formulations [37]. Therefore, this approach could be considered as a new preparation technique of multiphasic CaPO<sub>4</sub> formulations [780].

A lack of macropores is a substantial disadvantage of many current self-setting CaPO<sub>4</sub> formulations [343]. As a result, biodegradation takes place layer by layer on the surface, from outside to inside. To solve this problem, various types of porogens are used [373–402]. Using a hydrophobic liquid instead of soluble particles could be an alternative. At the turn of the millennium, an open macroporous structure was obtained using a mixture of oil and a self-setting paste [781]; however, since then no research papers on this subject have been published. Besides, by means of surfactants, air bubbles might be incorporated into the bulk of the formulations [365]. Unfortunately, the mechanical strength and porosity are conflicting requirements. As porosity of the CaPO<sub>4</sub> formulations appears to be of paramount importance to achieve an excellent bioresorbability, other experimental approaches have to be developed [782].

In the case of CaPO<sub>4</sub>-reinforced formulations and concretes, future studies could combine in one formulation porogens and biodegradable fibers of different shapes and dissolution rates to form after in vivo hardening scaffolds with sustained strength. In such a system, one porogen is quickly dissolved, which creates macropores to start a bone ingrowth process, while the second type of fibers provides the required strength to the implant. After significant bone ingrowth into the initial pores increased the implant strength, the second set of fibers would then be dissolved to create additional macropores for bone ingrowth [403]. Such complicated formulations have already been developed. For example, chitosan, sodium orthophosphate, and hydroxypropylmethylcellulose were used to render CaPO<sub>4</sub> formulations fast setting and resistant to washout, while absorbable fibers and mannitol porogen were incorporated for strength and macropores, respectively. Both strength and fracture resistance of this concrete were substantially increased and approached

those values for sintered porous HA implants [783]. Turning on a bit of imagination, one might predict development of polymeric forms of drugs (already available [784, 785]), hormones, growth factors, etc. (e.g., prepared by either incorporation into or cross-linking with either water-soluble or bioresorbable polymers). Coupled with reinforcing biodegradable fibers and porogens, such types of “healing fibers” might be added to self-setting  $\text{CaPO}_4$  formulations, which not only will accelerate the remedial process but also will allow simultaneous improvement in both their strength and injectability. In addition, graded structures are possible. For example, a layered structure was designed by combining a macroporous layer of  $\text{CaPO}_4$  cement with a strong fiber-reinforced  $\text{CaPO}_4$  concrete layer. The rationale for such construction was for the macroporous layer to accept tissue ingrowth, while the fiber-reinforced strong layer would provide the needed early strength [786].

Stability (insolubility) in normal physiological fluid environment and resorbability under acidic conditions produced by osteoclasts appears to be among the most important *in vivo* characteristics of modern types of  $\text{CaPO}_4$  bioceramics. For some clinical applications, such as cranioplasty, a relatively slow resorption and replacement by bone is quite acceptable, whereas in other applications, such as periodontal bone defects repair, sinus lift, etc., the ability of the hardened formulations to be replaced quickly by bone is crucial. Experimental results suggest that a number of parameters of the self-setting  $\text{CaPO}_4$  formulations, such as the Ca/P ionic ratio, carbonate content, ionic substitution, crystallinity, etc., might affect the dissolution characteristics in slightly acidic solutions. This gives an opportunity to formulate compositions, possessing different resorption rates, which is suited for different biomedical applications [184, 185].

Furthermore, the discovery of self-setting  $\text{CaPO}_4$  formulations has already opened up new perspectives in synthesis of bioceramic scaffolds, possessing sufficient mechanical properties and suitable for tissue engineering purposes [375, 380, 381, 512]. In the past, strong scaffolds could only be manufactured by the sintering route at elevated temperatures [787]. Therefore, until recently it was impossible to produce resorbable preset low-temperature hydrated 3D bioceramics for various applications, e.g., scaffolds and granules, from low-temperature  $\text{CaPO}_4$ , such as ACP, DCPA, DCPD, OCP, and CDHA. Currently, using the appropriate techniques (e.g., 3D powder printing [728, 788, 789], plotting [721, 790] or robocasting [225]), open macroporous 3D scaffolds [208, 374, 412, 418–423, 512, 721, 790–793] and/or other objects [794, 795] consisting of the aforementioned low-temperature phases (currently, excluding ACP and OCP) can be produced via cementitious reactions, thus, dramatically widening the biomedical applications of low-temperature  $\text{CaPO}_4$ . It is important to stress, that bulk  $\text{CaPO}_4$  materials produced at or close to room temperature commonly have the specific surface areas that are often close to the ones of bone mineral ( $\sim 80 \text{ m}^2/\text{g}$ ) which is up to two orders of magnitude higher than the values exhibited by sintered  $\text{CaPO}_4$  bioceramics (typically below  $1 \text{ m}^2/\text{g}$ ). Such high values of the specific surface are believed to stimulate protein adsorption, which is a very important event in bone healing. Therefore, the low-temperature  $\text{CaPO}_4$  bioceramics could be very promising for tissue engineering applications,

and, among them, CDHA is of a special interest due to its chemical similarity to bone material.

Nevertheless one should stress that the most promising direction of the future developments of the self-setting CaPO<sub>4</sub> formulations is obviously seen in their functionalization by incorporation of (or impregnation by) various hormones, growth factors, drugs, other bioorganic compounds, as well as incorporation of living cells and/or other tiny biological objects [796–810]. For example, silk fibroin can make the mineralization process regular and bond with HA to form fibroin/HA nanodimensional biocomposites with increased gelation properties and, thus, it can be used as an additive to improve cohesion of CaPO<sub>4</sub> formulations and decrease a risk of cardiovascular complications in its application in vertebroplasty and kyphoplasty [803].

While the simplicity in the processing of self-setting formulations encourages the incorporation of cells, the principal difficulty remains to ensure cell survival. The harsh environment in terms of pH and high ionic strength together with the high stiffness achieved upon hardening can be thought as the principal threats for cell endurance. The initial attempts have already been performed but without a great success yet. For example, researchers have already found that unset CaPO<sub>4</sub> formulations might have toxic effects when placed on cell monolayers, while the set formulations are biocompatible for the same type of cells (MC3T3-E1 osteoblast-like cells were tested). A gel encapsulation in alginate beads was found to be a possible solution to protect living cells for seeding into self-setting pastes [757, 811]. In vitro cytotoxic effect of  $\alpha$ -TCP-based self-setting formulation was also observed [812]. In light of these results, the encapsulation approach [390] could potentially be used to seed a patient's ex vivo expanded stem cells into the formulations to create osteoinductive bone grafts those could be used to treat that patient. However, this becomes more related to tissue engineering and biology, rather than to chemistry and material science. A first possibility would be designing self-setting formulations that have setting reactions close to the physiological pH or by adding additives into the self-setting pastes able to neutralize the acidic or basic ions released during the chemical reactions.

In addition, besides the aforementioned chemical, material, and biomedical improvements of the self-setting CaPO<sub>4</sub> formulations, one should not forget on a better design of both the mixing equipment and delivery (injection) techniques. As an example, the interested readers are referred to a new cannula to ease cement injection during vertebroplasty [813]; however, this subject is beyond the scope of current review.

Finally, one should not forget on the recent progress in self-setting formulations used as construction materials. Due to the ceramic nature, industrial concretes are very sensitive to crack formation because of their limited tensile strength. Therefore, self-healing formulations are developed [814–817]; presumably, some of these principles and approaches might be applied for the biomedical formulations as well.

## 2.11 Conclusions

Thus, among the diverse range of bone replacement biomaterials, self-setting  $\text{CaPO}_4$  formulations undoubtedly represent a distinct group because they are relatively simple biomaterials formed by combining of a  $\text{CaPO}_4$  mixture with an aqueous solution [818]. However, they symbolize an important breakthrough in the field of bone repair bioceramics, since they offer the possibility of obtaining thermally unstable  $\text{CaPO}_4$  in a monolithic form at room or body temperature by means of a cementation reaction. This particular fabrication technique implies that the self-setting formulations are moldable and therefore can adapt easily to the bone cavity providing a good fixation and the optimum tissue-biomaterial contact, necessary for stimulating bone ingrowth into them and their subsequent osteotransduction [57].

Unfortunately, the perfect grafting material does not exist. The self-setting  $\text{CaPO}_4$  formulations are not an exception to this statement. While possessing excellent biological properties (osteoconduction and, occasionally, osteoinduction), adequate setting time, excellent moldability, and the capability to deliver different bone-enhancing proteins/antibiotics at a local level, unfortunately, the biomaterial lacks adequate mechanical properties for applications other than non-loaded surgical sites (see Table 2.5 for other details). Nevertheless, even in its present state, the self-setting  $\text{CaPO}_4$  formulations appear to be suitable for a number of applications. They can be injected into osteoporotic bone to reinforce it or can be used to make granules and blocks out of low-temperature  $\text{CaPO}_4$ . Several types of the self-setting formulations are now on the market (Tables 2.2 and 2.3), while scaffolds made of low-temperature  $\text{CaPO}_4$  are being tested. The use of slightly different chemical compositions and various dopants affects both the setting time and tensile strength that enables further improvements. In addition, new trials are conducted with the reinforced formulations and concretes, which represent additional attempts to improve the existing products.

It is anticipated that the use of self-setting  $\text{CaPO}_4$  formulations will enable a faster and more aggressive rehabilitation, as the strength of the hardened concretes makes it possible to allow full weight bearing earlier than when bone graft is used. Although preliminary clinical trials have already confirmed the great potential of this novel therapeutic product, the self-setting  $\text{CaPO}_4$  formulations need to be improved further; in particular, their bioresorption needs to be accelerated as well as their injectability and mechanical properties need to get better. Besides, extra clinical studies are required to define the most appropriate indications and limitations of  $\text{CaPO}_4$  formulations for fracture repair.

In the author's humble opinion, mentioning Prof. James M. Anderson's opinion on the history of biomaterials field would be the best way to conclude this subject. According to Prof. Anderson, within 1950–1975 researchers studied biMATERIALS, within 1975–2000 they studied BIOMATERIALS, and since 2000 the time for BIOMaterials has come [819]. Here, the capital letters emphasize the major direction of the research efforts in the complex subject of biomaterials. Since the real history of self-setting  $\text{CaPO}_4$  formulations started only in 1983, the aforemen-

tioned periods appeared to be shifted along the time scale. Certainly, the biomATERIALS epoch for the self-setting CaPO<sub>4</sub> formulations is over (every possible combination of CaPO<sub>4</sub> has been already studied and tested), while the BIOMaterials era (where cells are the key factor) is just at the very beginning. Most likely, current state of the art of the self-setting CaPO<sub>4</sub> formulations corresponds to the final stages of the BIOMATERIALS phase with an approximately equal contribution of the biological and materials directions. Therefore, still there is much room for versatile ideas and approaches.

## References

1. Brinker MR, O'Connor DP (2004) The incidence of fractures and dislocations referred for orthopaedic services in a capitated population. *J Bone Joint Surg Am* 86A:290–297
2. Smith ZA, Fessler RG (2012) Paradigm changes in spine surgery – evolution of minimally invasive techniques. *Nat Rev Neurol* 8:443–450
3. Glimcher MJ (2006) Bone: nature of the calcium phosphate crystals and cellular, structural, and physical chemical mechanisms in their formation. *Rev Mineral Geochem* 64:223–282
4. Bohner M (2000) Calcium orthophosphates in medicine: from ceramics to calcium phosphate cements. *Injury* 31(Suppl 4):S-D37–S-D47
5. Bohner M (2001a) Physical and chemical aspects of calcium phosphates used in spinal surgery. *Eur Spine J* 10:S114–S121
6. Dorozhkin SV (2013a) Self-Setting calcium orthophosphate formulations. *J Funct Biomater* 4:209–311
7. Dorozhkin SV (2016a) Calcium orthophosphates (CaPO<sub>4</sub>): occurrence and properties. *Prog Biomater* 5:9–70
8. Dorozhkin SV (2012a) Calcium orthophosphates and human beings A historical perspective from the 1770s until 1940. *Biomater* 2:53–70
9. Dorozhkin SV (2013b) A detailed history of calcium orthophosphates from 1770-s till 1950. *Mater Sci Eng C* 33:3085–3110
10. Kingery WD II (1950) Cold setting properties. *J Am Ceram Soc* 33:242–246
11. Driskell TD, Heller AL, Koenigs JF (1975) Dental treatments. US Patent No 3913229, Oct 21
12. Monma H, Kanazawa T (1976) The hydration of  $\alpha$ -tricalcium phosphate. *J Ceram Soc Jpn* 84:209–213
13. LeGeros RZ, Chohayeb A, Shulman A (1982) Apatitic calcium phosphates: possible dental restorative materials. *J Dent Res* 61(Spec Iss):343
14. Brown WE, Chow LC (1983) A new calcium phosphate setting cement. *J Dent Res* 62(Spec Iss):672
15. Brown WE, Chow LC (1986) A new calcium phosphate water-setting cement. In: Brown PW (ed) *Cements research progress*. Westerville, American Ceramic Society
16. Brown WE, Chow LC (1985) Dental restorative cement pastes. US Patent No 4518430, May 21
17. Gruninger SE, Siew C, Chow LC, O'Young A, Tsao NK, Brown WE (1984) Evaluation of the biocompatibility of a new calcium phosphate setting cement. *J Dent Res* 63(Spec Iss):200
18. Cheng HC, Chu KT, Teng NC, Tsai HL, Ou KL, Ou SF (2014) The effect of pH value on phase transformation of calcium phosphate cement. *Int J Appl Ceram Technol* 11:364–370
19. Driessens FCM, Planell JA, Gil FJ (1995) Calcium phosphate bone cements. In: Wise DL, Trantolo DJ, Altobelli DE, Yaszemski MJ, Gresser JD, Schwarz ER (eds) *Encyclopedic handbook of biomaterials and bioengineering, part B, applications*. Marcel Dekker, New York

20. Tofighi A (2012) Calcium phosphate bone cement (CPBC): development, commercialization and future challenges. *Key Eng Mater* 493–494:349–354
21. Schumache M, Henß A, Rohnke M, Gelinsky MA (2013) novel and easy-to-prepare strontium (II) modified calcium phosphate bone cement with enhanced mechanical properties. *Acta Biomater* 9:7536–7544
22. Bolarinwa A, Gbureck U, Purnell P, Bold M, Grover LM (2010) Cement casting of calcium pyrophosphate based bioceramics. *Adv Appl Ceram* 109:291–295
23. Grover LM, Wright AJ, Gbureck U, Bolarinwa A, Song J, Liu Y, Farrar DF, Howling G, Rose J, Barralet JE (2013) The effect of amorphous pyrophosphate on calcium phosphate cement resorption and bone generation. *Biomaterials* 34:6631–6637
24. Schmitz JP, Hollinger JO, Milan SB (1999) Reconstruction of bone using calcium phosphate bone cements: a critical review. *J Oral Maxillofac Surg* 57:1122–1126
25. Espanol M, Perez RA, Montufar EB, Marichal C, Sacco A, Ginebra MP (2009) Intrinsic porosity of calcium phosphate cements and its significance for drug delivery and tissue engineering applications. *Acta Biomater* 5:2752–2762
26. Cardoso HAI, Motisuke M, Zavaglia CAC (2012a) The influence of three additives on the setting reaction kinetics and mechanical strength evolution of  $\alpha$ -tricalcium phosphate cements. *Key Eng Mater* 493–494:397–402
27. Vieira RS, Coelho WT, Thürmer MB, Fernandes JM, Santos LA (2012) Evaluation of  $\alpha$ -tricalcium phosphate cement obtained at different temperatures. *Mater Sci Forum* 727–728:1187–1192
28. Varma NP, Garai S, Sinha A (2012) Synthesis of injectable and cohesive nano hydroxyapatite scaffolds. *J Mater Sci Mater Med* 23:913–919
29. Rabiee SM (2013) Development of hydroxyapatite bone cement for controlled drug release via tetracycline hydrochloride. *Bull Mater Sci* 36:171–174
30. Matsuya S, Maruta M, Tsuru K, Ishikawa K (2013) Preparation of carbonate apatite cement based on  $\alpha$ -TCP. *Key Eng Mater* 529–530:197–201
31. Cahyanto A, Maruta M, Tsuru K, Matsuya S, Ishikawa K (2013a) Basic properties of carbonate apatite cement consisting of vaterite and dicalcium phosphate anhydrous. *Key Eng Mater* 529–530:192–196
32. Boroujeni NM, Zhou H, Luchini TJF, Bhaduri SB (2013) Development of multi-walled carbon nanotubes reinforced monetite bionanocomposite cements for orthopedic applications. *Mater Sci Eng C* 33:4323–4330
33. Chen SY, Ou SF, Teng NC, Kung CM, Tsai HL, Chu KT, Ou KL (2013a) Phase transformation on bone cement: monocalcium phosphate monohydrate into calcium-deficient hydroxyapatite during setting. *Ceram Int* 39:2451–2455
34. Sariibrahimoglu K, Wolke JGC, Leeuwenburgh SCG, Jansen JA (2013) Characterization of  $\alpha/\beta$ -TCP based injectable calcium phosphate cement as a potential bone substitute. *Key Eng Mater* 529–530:157–160
35. Sariibrahimoglu K, Wolke JGC, Leeuwenburgh SCG, Yubao L, Jansen JA (2014) Injectable biphasic calcium phosphate cements as a potential bone substitute. *J Biomed Mater Res B Appl Biomater* 102B:415–422
36. Cahyanto A, Maruta M, Tsuru K, Matsuya S, Ishikawa K (2015) Fabrication of bone cement that fully transforms to carbonate apatite. *Dent Mater J* 34:394–401
37. Gallinetti S, Canal C, Ginebra MP (2014) Development and characterization of biphasic hydroxyapatite/ $\beta$ -TCP cements. *J Am Ceram Soc* 97:1065–1073
38. Zhou H, Luchini TJ, Agarwal AK, Goel VK, Bhaduri SB (2014) Development of monetite–nanosilica bone cement: a preliminary study. *J Biomed Mater Res B Appl Biomater* 102B:1620–1626
39. Irbe Z, Loca D, Bistрова I, Berzina-Cimdina L (2014a) Calcium phosphate bone cements reinforced with biodegradable polymer fibres for drug delivery. *Key Eng Mater* 604:184–187
40. Chen CK, Ju CP, Lin JHC (2012a) Setting solution concentration effect on properties of a TTCP/DCPA-derived calcium phosphate cement. *J Mater Sci Mater Med* 23:2109–2114



41. Bajpai P, Fuchs C, McCullum D (1987) Development of tricalcium orthophosphate ceramic cement. In: Lemons J (ed) Quantitative characterization and performance of porous implants for hard tissue applications. ASTM STP 953 Am Soc Test Mater, Philadelphia
42. Bohner M, Lemaître J, Ring TA (1996) Effects of sulfate, pyrophosphate and citrate ions on the physicochemical properties of cements made of  $\beta$ -tricalcium phosphate – phosphoric acid – water mixtures. *J Am Ceram Soc* 79:1427–1434
43. Bohner M, van Landuyt P, Merkle HP, Lemaître J (1997a) Composition effects on the pH of a hydraulic calcium orthophosphate cement. *J Mater Sci Mater Med* 8:675–681
44. Desai TR, Bhaduri SB, Tas AC (2007) A self-setting, monetite (CaHPO<sub>4</sub>) cement for skeletal repair. In: Lara-Curzio E, Mizuno M, Wereszczak A (eds) Advances in bioceramics and bio-composites II, ceramic engineering and science proceedings. Wiley, Hoboken, pp 61–69
45. Grover LM, Hofmann MP, Gbureck U, Kumarasami B, Barralet JE (2008) Frozen delivery of brushite calcium phosphate cements. *Acta Biomater* 4:1916–1923
46. Komlev VS, Fadeeva IV, Barinov SM, Rau JV, Fosca M, Gurin AN, Gurin NA (2012) Phase development during setting and hardening of a bone cement based on  $\alpha$ -tricalcium and octacalcium phosphates. *J Biomater Appl* 26:1051–1068
47. Tonoli MS, Beppu MM (2014) In situ X-ray diffraction study of phase development during hardening of  $\beta$ -tricalcium phosphate bone cements with chitosan. *Key Eng Mater* 587:109–114
48. Otsuka Y, Takeuchi M, Otsuka M, Ben-Nissan B, Grossin D, Tanaka H (2015) Effect of carbon dioxide on self-setting apatite cement formation from tetracalcium phosphate and dicalcium phosphate dehydrate: ATR-IR and chemoinformatics analysis. *Colloid Polym Sci* 293:2781–2788
49. Gbureck U, Barralet JE, Spatz K, Grover LM, Thull R (2004a) Ionic modification of calcium phosphate cement viscosity Part I: hypodermic injection and strength improvement of apatite cement. *Biomaterials* 25:2187–2195
50. Cama G, Barberis F, Capurro M, di Silvio L, Deb S (2011) Tailoring brushite for in situ setting bone cements. *Mater Chem Phys* 130:1139–1145
51. Generosi A, Rau JV, Komlev VS, Albertini VR, Fedotov AY, Barinov SM (2010) Anomalous hardening behavior of a calcium phosphate bone cement. *J Phys Chem B* 114:973–979
52. Rau JV, Generosi A, Komlev VS, Fosca M, Barinov SM, Albertini VR (2010) Real-time monitoring of the mechanism of poorly crystalline apatite cement conversion in the presence of chitosan, simulated body fluid and human blood. *Dalton Trans* 21:11412–11423
53. Fosca M, Komlev VS, Fedotov AY, Caminiti R, Rau JV (2012) Structural study of octacalcium phosphate bone cement conversion in vitro. *ACS Appl Mater Interfaces* 4:202–210
54. Smirnov VV, Rau JV, Generosi A, Albertini VR, Ferro D, Barinov SM (2010) Elucidation of real-time hardening mechanisms of two novel high-strength calcium phosphate bone cements. *J Biomed Mater Res B Appl Biomater* 93B:74–83
55. Paduraru GD, Aelenei N, Luca D, Cimpoesu N (2011) New brushite cements analysis. *Optoelectron Adv Mater Rapid Comm* 5:465–468
56. Driessens FCM, Boltong MG, Khairoun I, de Maeyer EAP, Ginebra MP, Wenz R, Planell JA, Verbeeck RMH (2000a) Applied aspects of calcium phosphate bone cement. In: Wise DL, Trantolo DJ, Lewandrowski KU, Gresser JD, Cattaneo MV (eds) Biomaterials engineering and devices: human applications. Humana Press, Totowa, pp 253–260
57. Driessens FCM, Planell JA, Boltong MG, Khairoun I, Ginebra MP (1998) Osteoconductive bone cements. *Proc Inst Mech Eng H: J Eng Med* 212:427–435
58. Frankenburg EP, Goldstein SA, Bauer TW, Harris SA, Poser RD (1998) Biomechanical and histological evaluation of a calcium phosphate cement. *J Bone Joint Surg Am* 80A:1112–1124
59. Frayssinet P, Gineste L, Conte P, Fages J, Rouquet N (1998) Short-term implantation effects of a DCPD-based calcium phosphate cement. *Biomaterials* 19:971–977
60. Rey C, Tofighi A, Mounic S, Combes C, Lee D (2002) Biomimetic and calcium phosphate cements. In: Mainard D, Louis JP (eds) Actualités en Biomatériaux. Editions Romilla, Paris, pp 27–37

61. Combes C, Bareille R, Rey C (2006) Calcium carbonate-calcium phosphate mixed cement compositions for bone reconstruction. *J Biomed Mater Res A* 79A:318–328
62. Ikenaga M, Hardouin P, Lemaître J, Andrianjatovo H, Flautre B (1998) Biomechanical characterization of a biodegradable calcium phosphate hydraulic cement: a comparison with porous biphasic calcium phosphate ceramics. *J Biomed Mater Res* 40:139–144
63. Ginebra MP, Traykova T, Planell JA (2006a) Calcium phosphate cements: competitive drug carriers for the musculoskeletal system? *Biomaterials* 27:2171–2177
64. Ginebra MP, Traykova T, Planell JA (2006b) Calcium phosphate cements as bone drug delivery systems: a review. *J Control Release* 113:102–110
65. Bohner M (2004) Hydraulic cements based on  $\alpha$ -tricalcium phosphate – calcium sulfate dihydrate mixtures. *Biomaterials* 25:741–749
66. Fernández E, Vlad MD, Gel M, Lopez J, Torres R, Cauch JV, Bohner M (2005a) Modulation of porosity in apatitic cements by the use of  $\alpha$ -tricalcium phosphate – calcium sulphate dihydrate mixtures. *Biomaterials* 26:3395–3404
67. Hu G, Xiao L, Fu H, Bi D, Ma H, Tong P (2010a) Degradable and bioactive scaffold of calcium phosphate and calcium sulphate from self-setting cement for bone regeneration. *J Porous Mater* 17:605–613
68. Hu G, Xiao L, Fu H, Bi D, Ma H, Tong P (2010b) Study on injectable and degradable cement of calcium sulphate and calcium phosphate for bone repair. *J Mater Sci Mater Med* 21:627–634
69. Nilsson M, Fernández E, Sarda S, Lidgren L, Planell JA (2002a) Characterization of a novel calcium phosphate/sulphate bone cement. *J Biomed Mater Res* 61:600–607
70. Vlad MD, Şindilar EV, Mariñoso ML, Poeată I, Torres R, López J, Barracó M, Fernández E (2010) Osteogenic biphasic calcium sulphate dihydrate/iron-modified  $\alpha$ -tricalcium phosphate bone cement for spinal applications: in vivo study. *Acta Biomater* 6:607–616
71. Ju CP, Hung SH, Chen CK, Chen WL, Lee JW, Lin RM, Chen WC, Chern JHL (2011) Immersion-induced changes in structure and properties of a TTCP/DCPA/CSH cement. *Mater Chem Phys* 130:303–308
72. Zhou W, Xue Y, Ji X, Yin G, Zhang N, Ren Y (2011) A novel injectable and degradable calcium phosphate/calcium sulfate bone cement. *African J Biotechnol* 10:19449–19457
73. Lin JHC, Hung SH, Chen WL, Chen CK, Lin JL, Ju CP (2012) Properties of TTCP/DCPA/CSH cement immersed in Hanks' solution. *J Med Biol Eng* 32:201–204
74. Zima A, Paszkiewicz Z, Siek D, Czechowska J, Ślósarczyk A (2012) Study on the new bone cement based on calcium sulfate and Mg, CO<sub>3</sub> doped hydroxyapatite. *Ceram Int* 38:4935–4942
75. Grover LM, Gbureck U, Wright AJ, Tremaynec M, Barralet JE (2006a) Biologically mediated resorption of brushite cement in vitro. *Biomaterials* 27:2178–2185
76. Grover LM, Gbureck U, Wright AJ, Barralet JE (2005a) Cement formulations in the calcium phosphate H<sub>2</sub>O – H<sub>3</sub>PO<sub>4</sub> – H<sub>4</sub>P<sub>2</sub>O<sub>7</sub> system. *J Am Ceram Soc* 88:3096–3103
77. Grover LM, Gbureck U, Young AM, Wright AJ, Barralet JE (2005b) Temperature dependent setting kinetics and mechanical properties of  $\beta$ -TCP – pyrophosphoric acid bone cement. *J Mater Chem* 46:4955–4962
78. Oh KS, Jeong YK, Yu JP, Chae SK, Kim HY, Lee HY, Jeun SS (2005) Preparation and in vivo studies of  $\beta$ -TCP based bone cement containing polyphosphate. *Key Eng Mater* 284–286:93–96
79. Lilley KJ, Gbureck U, Wright AJ, Knowles JC, Farrar DF, Barralet JE (2007) Brushite cements from polyphosphoric acid, calcium phosphate systems. *J Am Ceram Soc* 90:1892–1898
80. Fernández E, Planell JA, Best SM (1999a) Precipitation of carbonated apatite in the cement system  $\alpha$ -Ca<sub>3</sub>(PO<sub>4</sub>)<sub>2</sub> – Ca(H<sub>2</sub>PO<sub>4</sub>)<sub>2</sub> – CaCO<sub>3</sub>. *J Biomed Mater Res* 47:466–471
81. Calafiori AR, di Marco G, Martino G, Marotta M (2007) Preparation and characterization of calcium phosphate biomaterials. *J Mater Sci Mater Med* 18:2331–2338
82. Kon M, Hirakata LM, Miyamoto Y, Kasahara H, Asaoka K (2005) Strengthening of calcium phosphate cement by compounding calcium carbonate whiskers. *Dent Mater J* 24:104–110

83. Qu Y, Yang Y, Li J, Chen Z, Li J, Tang K, Man Y (2011) Preliminary evaluation of a novel strong/osteoinductive calcium phosphate cement. *J Biomater Appl* 26:311–325
84. Serraj S, Michailesco P, Margerit J, Bernard B, Boudeville P (2002) Study of a hydraulic calcium phosphate cement for dental applications. *J Mater Sci Mater Med* 13:125–131
85. Nurit L, Margerit J, Terol A, Boudeville P (2002) pH-metric study of the setting reaction of monocalcium phosphate monohydrate/calcium oxide-based cements. *J Mater Sci Mater Med* 13:1007–1014
86. Boudeville P, Serraj S, Leloup JM, Margerit J, Pauvert B, Terol A (1999) Physical properties and self-setting mechanism of calcium phosphate cements from calcium bis-dihydrogenophosphate monohydrate and calcium oxide. *J Mater Sci Mater Med* 10:99–109
87. Michailesco P, Kouassi M, Briak HE, Armynot A, Boudeville P (2005) Antimicrobial activity and tightness of a DCPD – CaO-based hydraulic calcium phosphate cement for root canal filling. *J Biomed Mater Res B Appl Biomater* 74B:760–767
88. Briak HE, Durand D, Nurit J, Munier S, Pauvert B, Boudeville P (2002) Study of a hydraulic dicalcium phosphate dihydrate/calcium oxide-based cement for dental applications. *J Biomed Mater Res Appl Biomater* 63:447–453
89. Briak HE, Durand D, Boudeville P (2008) Study of a hydraulic DCPA/CaO-based cement for dental applications. *J Mater Sci Mater Med* 19:737–744
90. Takagi S, Chow LC, Ishikawa K (1998) Formation of hydroxyapatite in new calcium phosphate cements. *Biomaterials* 19:1593–1599
91. Yang Q, Troczynski T, Liu DM (2002) Influence of apatite seeds on the synthesis of calcium phosphate cement. *Biomaterials* 23:2751–2760
92. Hsu HC, Chiu CY, Tuan WH, Lee HY (2008) Structural stability of calcium phosphate cement during aging in water. *Mater Sci Eng C* 28:429–433
93. Roemhildt ML, McGee TD, Wagner SD (2003) Novel calcium phosphate composite bone cement, strength and bonding properties. *J Mater Sci Mater Med* 14:137–141
94. Roemhildt ML, Wagner SD, McGee TD (2006) Characterization of a novel calcium phosphate composite bone cement: flow, setting, and aging properties. *J Mater Sci Mater Med* 17:1127–1132
95. Wang X, Ye J, Wang Y, Chen L (2007a) Self-setting properties of a  $\beta$ -dicalcium silicate reinforced calcium phosphate cement. *J Biomed Mater Res B Appl Biomater* 82B:93–99
96. Huan Z, Chang J (2007) Novel tricalcium silicate/monocalcium phosphate monohydrate composite bone cement. *J Biomed Mater Res B Appl Biomater* 82B:352–359
97. Huan Z, Chang J (2009a) Calcium-phosphate-silicate composite bone cement, self-setting properties and in vitro bioactivity. *J Mater Sci Mater Med* 20:833–841
98. Huan Z, Chang J (2009b) Novel bioactive composite bone cements based on the  $\beta$ -tricalcium phosphate – monocalcium phosphate monohydrate composite cement system. *Acta Biomater* 5:1253–1264
99. Shen Q, Sun J, Wu J, Liu C, Chen F (2010) An in vitro investigation of the mechanical-chemical and biological properties of calcium phosphate/calcium silicate/bismutite cement for dental pulp capping. *J Biomed Mater Res B Appl Biomater* 94:141–148
100. Morejón-Alonso L, Ferreira OJB, Carrodegua RG, dos Santos LA (2012) Bioactive composite bone cement based on  $\alpha$ -tricalcium phosphate/tricalcium silicate. *J Biomed Mater Res B Appl Biomater* 100B:94–102
101. Zhou S, Ma J, Shen Y, Haapasalo M, Ruse ND, Yang Q, Troczynski T (2013) In vitro studies of calcium phosphate silicate bone. *J Mater Sci Mater Med* 24:355–364
102. de Aza PN, Zuleta F, Velasquez P, Vicente-Salar N, Reig JA (2014)  $\alpha$ 'H -Dicalcium silicate bone cement doped with tricalcium phosphate: characterization, bioactivity and biocompatibility. *J Mater Sci Mater Med* 25:445–452
103. Kent NW, Hill RG, Karpukhina N (2016) A new way of forming a calcium phosphate cement using bioactive glasses as a reactive precursor. *Mater Lett* 162:32–36
104. Guo D, Xu K, Zhao X, Han Y (2005) Development of a strontium-containing hydroxyapatite bone cement. *Biomaterials* 26:4073–4083

105. Wang X, Ye J (2008) Variation of crystal structure of hydroxyapatite in calcium phosphate cement by the substitution of strontium ions. *J Mater Sci Mater Med* 19:1183–1186
106. Pina S, Torres PM, Goetz-Neunhoeffler F, Neubauer J, Ferreira JMF (2010a) Newly developed Sr-substituted  $\alpha$ -TCP bone cements. *Acta Biomater* 6:928–935
107. Pina S, Torres PMC, Ferreira JMF (2010b) Injectability of brushite-forming Mg-substituted and Sr-substituted  $\alpha$ -TCP bone cements. *J Mater Sci Mater Med* 21:431–438
108. Wu F, Su JC, Wei J, Guo H, Liu CS (2008a) Injectable bioactive calcium-magnesium phosphate cement for bone regeneration. *Biomed Mater* 3:044105. (7 pages)
109. Wu F, Wei J, Guo H, Chen FP, Hong H, Liu CS (2008b) Self-setting bioactive calcium-magnesium phosphate cement with high strength and degradability for bone regeneration. *Acta Biomater* 4:1873–1884
110. Pina S, Olhero SM, Gheduzzi S, Miles AW, Ferreira JMF (2009) Influence of setting liquid composition and liquid-to-powder ratio on properties of a Mg-substituted calcium phosphate cement. *Acta Biomater* 5:1233–1240
111. Klammert U, Reuther T, Blank M, Reske I, Barralet JE, Grover LM, Kübler AC, Gbureck U (2010) Phase composition, mechanical performance and in vitro biocompatibility of hydraulic setting calcium magnesium phosphate cement. *Acta Biomater* 6:1529–1535
112. Alkhraisat MH, Cabrejos-Azama J, Rodríguez CR, Jerez LB, Cabarcos EL (2013) Magnesium substitution in brushite cements. *Mater Sci Eng C* 33:475–481
113. Jia J, Zhou H, Wei J, Jiang X, Hua H, Chen F, Wei S, Shin JW, Liu C (2010) Development of magnesium calcium phosphate biocement for bone regeneration. *J Royal Soc Interf* 7:1171–1180
114. Lu J, Wei J, Yan Y, Li H, Jia J, Wei S, Guo H, Xiao T, Liu C (2011) Preparation and preliminary cytocompatibility of magnesium doped apatite cement with degradability for bone regeneration. *J Mater Sci Mater Med* 22:607–615
115. Pina S, Vieira SI, Rego P, Torres PMC, da Cruz E Silva OAB, da Cruz E Silva EF, Ferreira JMF (2010c) Biological responses of brushite-forming Zn- and ZnSr- substituted beta-tricalcium phosphate bone cements. *Eur Cell Mater* 20:162–177
116. Pina S, Vieira SI, Torres PMC, Goetz-Neunhoeffler F, Neubauer J, da Cruz E Silva OAB, da Cruz E Silva EF, Ferreira JMF (2010d) In vitro performance assessment of new brushite-forming Zn- and ZnSr-substituted  $\beta$ -TCP bone cements. *J Biomed Mater Res B Appl Biomater* 94B:414–420
117. Doi Y, Shimizu Y, Moriwaki Y, Aga M, Iwanaga H, Shibutani T, Yamamoto K, Iwayama Y (2001) Development of a new calcium phosphate cement that contains sodium calcium phosphate. *Biomaterials* 22:847–854
118. Gbureck U, Knappe O, Grover LM, Barralet JE (2005a) Antimicrobial potency of alkali ion substituted calcium phosphate cements. *Biomaterials* 26:6880–6886
119. Gbureck U, Thull R, Barralet JE (2005b) Alkali ion substituted calcium phosphate cement formation from mechanically activated reactants. *J Mater Sci Mater Med* 16:423–427
120. Dombrowski F, Hoffmann R, Ploska U, Marx H, Berger G (2012a) Investigations on degradable and figuline calcium alkaline phosphate cements with multimodal particle size distribution. *Key Eng Mater* 493–494:355–360
121. Dombrowski F, Marx H, Ploska U, Nicolaidis D, Stiller M, Knabe C, Berger G (2012b) Solubility and ingrowth behaviour of degradable and figuline calcium alkaline phosphate cements. *Key Eng Mater* 493–494:387–390
122. Tanaka M, Takemoto M, Fujibayashi S, Kawai T, Tsukanaka M, Takami K, Motojima S, Inoue H, Nakamura T, Matsuda S (2014) Development of a novel calcium phosphate cement composed mainly of calcium sodium phosphate with high osteoconductivity. *J Mater Sci Mater Med* 25:1505–1517
123. Lilley J, Gbureck U, Knowles JC, Farrar DF, Barralet JE (2005a) Cement from magnesium substituted hydroxyapatite. *J Mater Sci Mater Med* 16:455–460

124. Ni GX, Lu WW, Tang B, Ngan AHW, Chiu KY, Cheung KMC, Li ZY, Luk KDK (2007) Effect of weight-bearing on bone-bonding behavior of strontium-containing hydroxyapatite bone cement. *J Biomed Mater Res A* 83A:570–576
125. Alkhraisat MH, Mariño FT, Rodríguez CR, Jerez LB, Cabarcos EL (2008) Combined effect of strontium and pyrophosphate on the properties of brushite cements. *Acta Biomater* 4:664–670
126. Yao ZP, Liu WG, Ni GX (2008) Biology characteristics and clinical application of strontium substituted hydroxyapatite bone cement. *J Clin Rehabil Tissue Eng Res* 12:7151–7154
127. Pina S, Ferreira JMF (2010) Brushite-forming Mg-, Zn- and Sr-substituted bone cements for clinical applications. *Materials* 3:519–535
128. Ni GX, Lin JH, Chiu PKY, Li ZY, Lu WW (2010) Effect of strontium-containing hydroxyapatite bone cement on bone remodeling following hip replacement. *J Mater Sci Mater Med* 21:377–384
129. Fadeeva IV, Barinov SM, Komlev VS, Fedotov DA, Durisin J, Medvecky L (2004) Apatite formation in the reaction-setting mixture of Ca(OH)<sub>2</sub> – KH<sub>2</sub>PO<sub>4</sub> system. *J Biomed Mater Res A* 70A:303–308
130. Tas AC (2008a) Use of vaterite and calcite in forming calcium phosphate cement scaffolds. *Ceram Eng Sci Proc* 28:135–150
131. Boroujeni NM, Zhou H, Luchini TJF, Bhaduri SB (2014) Development of monetite/phosphorylated chitosan composite bone cement. *J Biomed Mater Res B Appl Biomater* 102B:260–266
132. Cahyanto A, Tsuru K, Ishikawa K (2013b) Carbonate apatite formation during the setting reaction of apatite cement. *Ceram Eng Sci Proc* 33:7–10
133. Fernández E, Vlad MD, Hamcerencu M, Darie A, Torres R, Lopez J (2005b) Effect of iron on the setting properties of  $\alpha$ -TCP bone cements. *J Mater Sci* 40:3677–3682
134. Vlad MD, del Valle LJ, Poeta I, Barracó M, López J, Torres R, Fernández E (2008) Injectable iron-modified apatitic bone cement intended for kyphoplasty, cytocompatibility study. *J Mater Sci Mater Med* 19:3575–3583
135. <http://en.wikipedia.org/wiki/Cement>. Accessed in Dec 2016
136. Chow LC (2009) Next generation calcium phosphate-based biomaterials. *Dent Mater J* 28:1–10
137. Ishikawa K (2010) Bone substitute fabrication based on dissolution-precipitation reactions. *Materials* 3:1138–1155
138. Burguera EF, Xu HHK, Weir MD (2006) Injectable and rapid-setting calcium phosphate bone cement with dicalcium phosphate dehydrate. *J Biomed Mater Res B Appl Biomater* 77B:126–134
139. Burguera EF, Guitian F, Chow LC (2004) A water setting tetracalcium phosphate-dicalcium phosphate dihydrate cement. *J Biomed Mater Res A* 71A:275–282
140. Kim SY, Jeon SH (2012) Setting properties, mechanical strength and in vivo evaluation of calcium phosphate-based bone cements. *J Ind Eng Chem* 18:128–136
141. Driessens FCM, Boltong MG, Bermudez O, Planell JA (1993) Formulation and setting times of some calcium orthophosphate cements, a pilot study. *J Mater Sci Mater Med* 4:503–508
142. Chow LC, Markovic M, Takagi S (1998) Calcium phosphate cements. In: Struble LJ (ed) *Cements research progress*. American Ceramic Society, Westerville, pp 215–238
143. Driessens FCM, Boltong MG, Bermudez O, Planell JA, Ginebra MP, Fernández E (1994) Effective formulations for the preparation of calcium phosphate bone cements. *J Mater Sci Mater Med* 5:164–170
144. Kurashina K, Hirano M, Kotani A, Klein CPAT, de Groot K (1997) In vivo study of calcium phosphate cements, implantation of an  $\alpha$ -tricalcium phosphate/dicalcium phosphate dibasic/tetracalcium phosphate monoxide cement paste. *Biomaterials* 18:539–543
145. Friedman CD, Costantino PD, Takagi S, Chow LC (1998) BoneSource™ hydroxyapatite cement, a novel biomaterial for craniofacial skeletal tissue engineering and reconstruction. *J Biomed Mater Res* 43:428–432

146. Khairoun I, Boltong MG, Driessens FCM, Planell JA (1997) Effect of calcium carbonate on the compliance of apatitic calcium phosphate bone cement. *Biomaterials* 18:1535–1539
147. Fernández E, Gil FJ, Best SM, Ginebra MP, Driessens FCM, Planell JA (1998a) Improvement of the mechanical properties of new calcium phosphate bone cements in the  $\text{CaHPO}_4 - \alpha\text{-Ca}_3(\text{PO}_4)_2$  system, compressive strength and microstructural development. *J Biomed Mater Res* 41:560–567
148. Fukase Y, Eanes ED, Takagi S, Chow LC, Brown WE (1990) Setting reactions and compressive strengths of calcium phosphate cements. *J Dent Res* 69:1852–1856
149. Xie L, Monroe EA (1991) Calcium phosphate dental cements. *Mat Res Soc Symp Proc* 179:25–39
150. Ishikawa K, Miyamoto Y, Kon M, Nagayama M, Asaoka K (1995a) Non-decay type fast-setting calcium orthophosphate cement composite with sodium alginate. *Biomaterials* 16:527–532
151. Xu HHK, Quinn JB, Takagi S, Chow LC (2002) Processing and properties of strong and non-rigid calcium phosphate cement. *J Dent Res* 81:219–224
152. Lee YK, Lim BS, Kim CW (2003) Mechanical properties of calcium phosphate based dental filling and regeneration materials. *J Oral Rehabil* 30:418–425
153. Ginebra MP, Fernández E, de Mayer EAP, Verbeeck RMH, Boltong MG, Ginebra J, Driessens FCM, Planell JA (1997) Setting reaction and hardening of an apatitic calcium phosphate cement. *J Dent Res* 76:905–912
154. Liu C, Shen W, Gu Y, Hu L (1997) Mechanism of the hardening process for a hydroxyapatite cement. *J Biomed Mater Res* 35:75–80
155. Driessens FCM, de Mayer EAP FE, Boltong MG, Berger G, Verbeeck RMH, Ginebra MP, Planell JA (1996) Amorphous calcium phosphate cements and their transformation into calcium deficient hydroxyapatite. *Bioceramics* 9:231–234
156. Lemaître J (1995) Injectable calcium phosphate hydraulic cements: new developments and potential applications. *Inn Tech Biol Med* 16:109–120
157. Neira IS, Kolen'ko YV, Lebedev OI, van Tendeloo G, Gupta HS, Matsushita N, Yoshimura M, Guitián F (2009) Rational synthesis of a nanocrystalline calcium phosphate cement exhibiting rapid conversion to hydroxyapatite. *Mater Sci Eng C* 29:2124–2132
158. Kawakami T, Antoh M, Hasegawa H, Yamagishi T, Ito M, Eda S (1992) Experimental study on osteoconductive properties of a chitosan-bonded hydroxyapatite self-hardening paste. *Biomaterials* 13:759–763
159. Tañag MA, Yano K, Hosokawa K (2004) Orbital floor reconstruction using calcium phosphate cement paste: an animal study. *Plast Reconstr Surg* 114:1826–1831
160. Hatoko M, Tada H, Tanaka A, Yurugi S, Niitsuma K, Iioka H (2005) The use of calcium phosphate cement paste for the correction of the depressed nose deformity. *J Craniofac Surg* 16:327–331
161. Tañag MA, Madura T, Yano K, Hosokawa K (2006) Use of calcium phosphate cement paste in orbital volume augmentation. *Plast Reconstr Surg* 117:1186–1193
162. Meng D, Xie QF, Xiao JJ (2009) Effects of two calcium phosphate cement pastes on osteoblasts during solidification. *J Clin Rehabil Tiss Eng Res* 13:471–474
163. Chen F, Liu C, Wei J, Chen X, Zhao Z, Gao Y (2011) Preparation and characterization of injectable calcium phosphate cement paste modified by polyethylene glycol-6000. *Mater Chem Phys* 125:818–824
164. Ishikawa K, Miyamoto Y, Takechi M, Toh T, Kon M, Nagayama M, Asaoka K (1997) Non-decay type fast-setting calcium phosphate cement: hydroxyapatite putty containing an increased amount of sodium alginate. *J Biomed Mater Res* 36:393–399
165. Ishikawa K, Miyamoto Y, Takechi M, Ueyama Y, Suzuki K, Nagayama M, Matsumura T (1999a) Effects of neutral sodium hydrogen phosphate on setting reaction and mechanical strength of hydroxyapatite putty. *J Biomed Mater Res* 44:322–329
166. Momota Y, Miyamoto Y, Ishikawa K, Takechi M, Yuasa T, Tatehara S, Nagayama M (2004) Effects of neutral sodium hydrogen phosphate on the setting property and hemostatic ability

- of hydroxyapatite putty as a local hemostatic agent for bone. *J Biomed Mater Res B Appl Biomater* 69B:99–103
167. Bohner M (2010a) Design of ceramic-based cements and putties for bone graft substitution. *Eur Cell Mater* 20:1–12
  168. Xia Z, Grover LM, Huang Y, Adamopoulos IE, Gbureck U, Triffitt JT, Shelton RM, Barralet JE (2006) In vitro biodegradation of three brushite calcium phosphate cements by a macrophage cell-line. *Biomaterials* 27:4557–4565
  169. Khairoun I, Boltong MG, Driessens FCM, Planell JA (1998a) Limited compliance of some apatitic calcium phosphate bone cements with clinical requirements. *J Mater Sci Mater Med* 9:667–671
  170. Monma H, Makishima A, Mitomo M, Ikegami T (1988) Hydraulic properties of the tricalcium phosphate – dicalcium phosphate mixture. *J Ceram Soc Jpn* 96:878–880
  171. Bermudez O, Boltong MG, Driessens FCM, Planell JA (1994) Development of an octacalcium phosphate cement. *J Mater Sci Mater Med* 5:144–146
  172. Sena M, Yamashita Y, Nakano Y, Ohgaki M, Nakamura S, Yamashita K, Takagi Y (2004) Octacalcium phosphate-based cement as a pulp-capping agent in rats. *Oral Surg Oral Med Oral Pathol Oral Radiol Endod* 97:749–755
  173. Markovic M, Chow LC (2010) An octacalcium phosphate forming cement. *J Res Natl Inst Stand Technol* 115:257–265
  174. Dorozhkin SV (2008) Calcium orthophosphate cements for biomedical application. *J Mater Sci* 43:3028–3057
  175. Dorozhkin SV (2009) Calcium orthophosphate cements and concretes. *Materials* 2:221–291
  176. Lacout J, Mejdoubi E, Hamad M (1996) Crystallization mechanisms of calcium orthophosphate cement for biological uses. *J Mater Sci Mater Med* 7:371–374
  177. Song Y, Feng Z, Wang T (2007) In situ study on the curing process of calcium phosphate bone cement. *J Mater Sci Mater Med* 18:1185–1193
  178. Bohner M (2010b) Resorbable biomaterials as bone graft substitutes. *Mater Today* 13:24–30
  179. Weiss DD, Sachs MA, Woodard CR (2003) Calcium phosphate bone cements: a comprehensive review. *J Long Term Eff Med Implants* 13:41–47
  180. Fernández E, Gil FJ, Ginebra MP, Driessens FCM, Planell JA, Best SM (1999b) Calcium phosphate bone cements for clinical applications Part I: solution chemistry. *J Mater Sci Mater Med* 10:169–176
  181. Hatim Z, Freche M, Keribech A, Lacout JL (1998) The setting mechanism of a phosphocalcium biological cement. *Ann Chim Sci Mat* 23:65–68
  182. Ishikawa K, Asaoka K (1995) Estimation of ideal mechanical strength and critical porosity of calcium phosphate cement. *J Biomed Mater Res* 29:1537–1543
  183. Chow LC (1991) Development of self-setting calcium phosphate cements. *J Ceram Soc Jpn* 99:954–964
  184. Chow LC (2000) Calcium phosphate cements: chemistry, properties and applications. *Mat Res Soc Symp Proc* 599:27–37
  185. Chow LC (2001) Calcium phosphate cements. In: Chow LC, Eanes ED (eds) Octacalcium phosphate, monographs in oral science. Karger, Basel, pp 148–163
  186. Brown PW, Fulmer MT (1991) Kinetics of hydroxyapatite formation at low temperature. *J Am Ceram Soc* 74:934–940
  187. TenHuisen KS, Brown PW (1994) The formation of hydroxyapatite-ionomer cements at 38 °C. *J Dent Res* 3:598–606
  188. Ishikawa K, Takagi S, Chow LC, Suzuki K (1999b) Reaction of calcium phosphate cements with different amounts of tetracalcium phosphate and dicalcium phosphate anhydrous. *J Biomed Mater Res* 46:504–510
  189. Matsuya S, Takagi S, Chow LC (2000) Effect of mixing ratio and pH on the reaction between Ca<sub>4</sub>(PO<sub>4</sub>)<sub>2</sub>O and CaHPO<sub>4</sub>. *J Mater Sci Mater Med* 11:305–311

190. Burguera EF, Guitian F, Chow LC (2008a) Effect of the calcium to phosphate ratio of tetracalcium phosphate on the properties of calcium phosphate bone cement. *J Biomed Mater Res A* 85A:674–683
191. Lemaître J, Mirtchi AA, Mortier A (1987) Calcium phosphate cements for medical use: state of the art and perspectives of development. *Silic Ind* 9–10:141–146
192. Mirtchi AA, Lemaître J, Terao N (1989) Calcium phosphate cements: study of the  $\beta$ -tricalcium phosphate – monocalcium phosphate system. *Biomaterials* 10:475–480
193. Fernández E, Gil FJ, Best SM, Ginebra MP, Driessens FCM, Planell JA (1998b) The cement setting reaction in the  $\text{CaHPO}_4 - \alpha\text{-Ca}_3(\text{PO}_4)_2$  system: an X-ray diffraction study. *J Biomed Mater Res* 42:403–406
194. Fernández E, Gil FJ, Ginebra MP, Driessens FCM, Planell JA, Best SM (1999c) Production and characterisation of new calcium phosphate bone cements in the  $\text{CaHPO}_4 - \alpha\text{-Ca}_3(\text{PO}_4)_2$  system: pH, workability and setting times. *J Mater Sci Mater Med* 10:223–230
195. Barralet JE, Lilley KJ, Grover LM, Farrar DF, Ansell C, Gbureck U (2004a) Cements from nanocrystalline hydroxyapatite. *J Mater Sci Mater Med* 15:407–411
196. Lilley KJ, Gbureck U, Wright AJ, Farrar DF, Barralet JE (2005b) Cement from nanocrystalline hydroxyapatite: effect of calcium phosphate ratio. *J Mater Sci Mater Med* 16:1185–1190
197. Alge DL, Cruz GS, Goebel WS, Chu TMG (2009) Characterization of dicalcium phosphate dihydrate cements prepared using a novel hydroxyapatite-based formulation. *Biomed Mater* 4:025016
198. Alge DL, Goebel WS, Chu TMG (2012a) In vitro degradation and cytocompatibility of dicalcium phosphate dihydrate cements prepared using the monocalcium phosphate monohydrate/hydroxyapatite system reveals rapid conversion to HA as a key mechanism. *J Biomed Mater Res B Appl Biomater* 100B:595–602
199. Wang X, Ye J, Wang Y, Wu X, Bai B (2007b) Control of crystallinity of hydrated products in a calcium phosphate bone cement. *J Biomed Mater Res A* 81A:781–790
200. Hurlle K, Neubauer J, Bohner M, Doebelin N, Goetz-Neunhoffer F (2014) Effect of amorphous phases during the hydraulic conversion of  $\alpha$ -TCP into calcium-deficient hydroxyapatite. *Acta Biomater* 10:3931–3941
201. Wang X, Ye J, Wang H (2006) Effects of additives on the rheological properties and injectability of a calcium phosphate bone substitute material. *J Biomed Mater Res B Appl Biomater* 78B:259–264
202. Tofighi A, Schaffer K, Palazzolo R (2008) Calcium phosphate cement (CPC): a critical development path. *Key Eng Mater* 361–363:303–306
203. de Maeyer EAP, Verbeeck RMH, Vercruyse CWJ (2000) Conversion of octacalcium phosphate in calcium phosphate. *J Biomed Mater Res* 52:95–106
204. Nakano Y, Ohgaki M, Nakamura S, Takagi Y, Yamashita K (1999) In vitro and in vivo characterization and mechanical properties of  $\alpha$ -TCP/OCF settings. *Bioceramics* 12:315–318
205. Nakano Y (2000) Preparation and characterization of porous octacalcium phosphate setting improved by  $\alpha$ -tricalcium phosphate additive. *J Dent Mater* 19:65–76
206. Wang X, Ye J, Wang Y (2008a) Hydration mechanism of a novel PCCP + DCPA cement system. *J Mater Sci Mater Med* 19:813–816
207. Wang X, Ye J (2009) Exothermal behavior during the hydration of the PCCP + DCPA system cement. *Mater Sci Forum* 610–613:1255–1258
208. He F, Ye J (2013) Bi-layered calcium phosphate cement-based composite scaffold mimicking natural bone structure. *Sci Technol Adv Mater* 14:045010. (11 pages)
209. Kim YB, Lee BM, Lee MC, Noh I, Lee SJ, Kim SS (2013) Preparation and characterization of calcium phosphate cement of  $\alpha$ -tricalcium phosphate-tetracalcium phosphate-dicalcium phosphate system incorporated with poly( $\gamma$ -glutamic acid). *Macromol Res* 21:892–898
210. Lopez-Heredia MA, Bongio M, Bohner M, Cuijpers V, Winnubst LA, van Dijk N, Wolke JG, van den Beucken JJ, Jansen JA (2012a) Processing and in vivo evaluation of multiphasic calcium phosphate cements with dual tricalcium phosphate phases. *Acta Biomater* 8:3500–3508



211. Zoulgami M, Lucas A, Briard P, Gaudé J (2001) A self-setting single-component calcium phosphate cement. *Biomaterials* 22:1933–1937
212. Knaack D, Goad ME, Aiolovala M, Rey C, Tofighi A, Chakravarthy P, Lee DD (1998) Resorbable calcium phosphate bone substitute. *J Biomed Mater Res* 43:399–409
213. Tofighi A, Mounic S, Chakravarthy P, Rey C, Lee D (2001) Setting reactions involved in injectable cements based on amorphous calcium phosphate. *Key Eng Mater* 192–195:769–772
214. Monma H, Kanazawa T (2000) Hydration of  $\alpha$ -tricalcium phosphate. *J Ceram Soc Jpn* 108:575–580
215. Fernández E, Ginebra MP, Boltong MG, Driessens FCM, Ginebra J, de Maeyer EAP, Verbeeck RMH, Planell JA (1996) Kinetic study of the setting reaction of a calcium phosphate bone cement. *J Biomed Mater Res* 32:367–374
216. Gbureck U, Barralet JE, Radu L, Klinger HG, Thull R (2004b) Amorphous  $\alpha$ -tricalcium phosphate, preparation and aqueous setting reaction. *J Am Ceram Soc* 87:1126–1132
217. Bohner M, Malsy AK, Camire CL, Gbureck U (2006a) Combining particle size distribution and isothermal calorimetry data to determine the reaction kinetics of  $\alpha$ -tricalcium phosphate – water mixtures. *Acta Biomater* 2:343–348
218. Brunner TJ, Grass RN, Bohner M, Stark WJ (2007a) Effect of particle size, crystal phase and crystallinity on the reactivity of tricalcium phosphate cements for bone reconstruction. *J Mater Chem* 38:4072–4078
219. Alves HLR, dos Santos LA, Bergmann CP (2008) Injectability evaluation of tricalcium phosphate bone cement. *J Mater Sci Mater Med* 19:2241–2246
220. Jack V, Buchanan FJ, Dunne NJ (2008) Particle attrition of  $\alpha$ -tricalcium phosphate, effect on mechanical, handling, and injectability properties of calcium phosphate. *Proc Inst Mech Eng H: J Eng Med* 222:19–28
221. Oh SA, Lee GS, Park JH, Kim HW (2010) Osteoclastic cell behaviors affected by the  $\alpha$ -tricalcium phosphate based bone cements. *J Mater Sci Mater Med* 21:3019–3027
222. Cardoso HAI, Motisuke M, Rodas ACD, Higa OZ, Zavaglia CAC (2012b) pH evolution and cytotoxicity of [alpha]-tricalcium phosphate cement with three different additives. *Key Eng Mater* 493–494:403–408
223. Zhang JT, Tancret F, Bouler JM (2012) Mechanical properties of calcium phosphate cements (CPC) for bone substitution: influence of fabrication and microstructure. *Key Eng Mater* 493–494:409–414
224. Ishikawa K, Tsuru K, Pham TK, Maruta M, Matsuya S (2012) Fully-interconnected pore forming calcium phosphate cement. *Key Eng Mater* 493–494:832–835
225. Maazouz Y, Montufar EB, Guillem-Marti J, Fleps I, Ohman C, Persson C, Ginebra MP (2014) Robocasting of biomimetic hydroxyapatite scaffolds using self-setting inks. *J Mater Chem B* 2:5378–5386
226. Sugiura Y, Tsuru K, Ishikawa K (2016) Fabrication of carbonate apatite foam based on the setting reaction of  $\alpha$ -tricalcium phosphate foam granules. *Ceram Int* 42:204–210
227. Gbureck U, Grolms O, Barralet JE, Grover LM, Thull R (2003a) Mechanical activation and cement formation of  $\beta$ -tricalcium phosphate. *Biomaterials* 24:4123–4131
228. Zhou H, Luchini TJ, Boroujeni NM, Agarwal AK, Goel VK, Bhaduri SB (2015) Development of nanosilica bonded monetite cement from egg shells. *Mater Sci Eng C* 50:45–51
229. Gbureck U, Barralet JE, Hofmann MP, Thull R (2004c) Nanocrystalline tetracalcium phosphate cement. *J Dent Res* 83:425–428
230. Gbureck U, Barralet JE, Hofmann MP, Thull R (2004d) Mechanical activation of tetracalcium phosphate. *J Am Ceram Soc* 87:311–313
231. Tsai CH, Ju CP, Lin JHC (2008a) Morphology and mechanical behavior of TTCP-derived calcium phosphate cement subcutaneously implanted in rats. *J Mater Sci Mater Med* 19:2407–2415
232. Tsai CH, Lin RM, Ju CP, Lin JHC (2008b) Bioresorption behavior of tetracalcium phosphate-derived calcium phosphate cement implanted in femur of rabbits. *Biomaterials* 29:984–993

233. Tsai CH, Lin JHC, Ju CP (2007)  $\gamma$ -radiation-induced changes in structure and properties of tetracalcium phosphate and its derived calcium phosphate cement. *J Biomed Mater Res B Appl Biomater* 80B:244–252
234. Vlad MD, Gómez S, Barracó M, López J, Fernández E (2012) Effect of the calcium to phosphorus ratio on the setting properties of calcium phosphate bone cements. *J Mater Sci Mater Med* 23:2081–2090
235. Koshino T, Kubota W, Morii T (1995) Bone formation as a reaction to hydraulic hydroxyapatite thermal decomposition product used as bone cement in rabbits. *Biomaterials* 16:125–128
236. Bae J, Ida Y, Sekine K, Kawano F, Hamada K (2015) Effects of high-energy ball-milling on injectability and strength of  $\beta$ -tricalcium-phosphate cement. *J Mech Behav Biomed Mater* 47:77–86
237. Chow LC, Markovic M, Frukhtbeyn SA, Takagi S (2005) Hydrolysis of tetracalcium phosphate under a near-constant composition condition – effects of pH and particle size. *Biomaterials* 26:393–401
238. TenHuisen KS, Brown PW (1998) Formation of calcium-deficient hydroxyapatite from  $\alpha$ -tricalcium phosphate. *Biomaterials* 19:2209–2217
239. Ginebra MP, Fernández E, Driessens FCM, Planell JA (1999) Modeling of the hydrolysis of  $\alpha$ -TCP. *J Am Ceram Soc* 82:2808–2812
240. Durucan C, Brown PW (2000)  $\alpha$ -tricalcium phosphate hydrolysis to hydroxyapatite at and near physiological temperature. *J Mater Sci Mater Med* 11:365–371
241. Durucan C, Brown PW (2002) Kinetic model for  $\alpha$ -tricalcium phosphate hydrolysis. *J Am Ceram Soc* 85:2013–2018
242. Fulmer MT, Brown PW (1998) Hydrolysis of dicalcium phosphate dihydrate to hydroxyapatite. *J Mater Sci Mater Med* 9:197–202
243. Ginebra MP, Driessens FCM, Planell JA (2004) Effect of the particle size on the micro and nanostructural features of a calcium phosphate cement: a kinetic analysis. *Biomaterials* 25:3453–3462
244. Tsuru K, Ruslin K, Maruta M, Matsuya S, Ishikawa K (2015) Effects of the method of apatite seed crystals addition on setting reaction of  $\alpha$ -tricalcium phosphate based apatite cement. *J Mater Sci Mater Med* 26:244. 8 pp
245. Ginebra MP, Canal C, Espanol M, Pastorino D, Montufar EB (2012) Calcium phosphate cements as drug delivery materials. *Adv Drug Deliv Rev* 64:1090–1110
246. Tas AC (2007) Porous, biphasic  $\text{CaCO}_3$ -calcium phosphate biomedical cement scaffolds from calcite ( $\text{CaCO}_3$ ) powder. *Int J Appl Ceram Technol* 4:152–163
247. Liu C, Huang Y, Chen J (2004) The physicochemical properties of the solidification of calcium phosphate cement. *J Biomed Mater Res B Appl Biomater* 69B:73–78
248. Liu C, Gai W, Pan S, Liu Z (2003a) The exothermal behavior in the hydration process of calcium phosphate cement. *Biomaterials* 24:2995–3003
249. Charrière E, Terrazzoni S, Pittet C, Mordasini P, Dutoit M, Lemaître J, Zysset P (2001) Mechanical characterization of brushite and hydroxyapatite cements. *Biomaterials* 22:2937–2945
250. Morgan H, Dauskardt RH (2003) Notch strength insensitivity of self-setting hydroxyapatite bone cements. *J Mater Sci Mater Med* 14:647–653
251. von Gonten AS, Kelly JR, Antonucci JM (2000) Load-bearing behavior of a simulated craniofacial structure fabricated from a hydroxyapatite cement and bioresorbable fiber-mesh. *J Mater Sci Mater Med* 11:95–100
252. Gisep A, Kugler S, Wahl D, Rahn B (2004) The mechanical characterization of a bone defect model filled with ceramic cements. *J Mater Sci Mater Med* 15:1065–1071
253. Takagi S, Chow LC, Markovic M, Friedman CD, Costantino PD (2001) Morphological and phase characterizations of retrieved calcium phosphate cement implants. *J Biomed Mater Res Appl Biomater* 58:36–41
254. Ambard AJ, Mueninghoff L (2006) Calcium phosphate cement: review of mechanical and biological properties. *J Prosthodont* 15:321–328

255. Kenny SM, Buggy M (2003) Bone cements and fillers: a review. *J Mater Sci Mater Med* 14:923–938
256. Bohner M, Gbureck U, Barralet JE (2005) Technological issues for the development of more efficient calcium phosphate bone cements: a critical assessment. *Biomaterials* 26:6423–6429
257. Lewis G (2006) Injectable bone cements for use in vertebroplasty and kyphoplasty, state-of-the-art review. *J Biomed Mater Res B Appl Biomater* 76B:456–468
258. Takagi S, Frukhtbeyn S, Chow LC, Sugawara A, Fujikawa K, Ogata H, Hayashi M, Ogiso B (2010) In vitro and in vivo characteristics of fluorapatite-forming calcium phosphate cements. *J Res Natl Inst Stand Technol* 115:267–276
259. Wei J, Wang J, Shan W, Liu X, Ma J, Liu C, Fang J, Wei S (2011a) Development of fluorapatite cement for dental enamel defects repair. *J Mater Sci Mater Med* 22:1607–1614
260. Wei J, Wang J, Liu X, Ma J, Liu C, Fang J, Wei S (2011b) Preparation of fluoride substituted apatite cements as the building blocks for tooth enamel restoration. *Appl Surf Sci* 257:7887–7892
261. Constantz BR, Ison IC, Fulmer MT, Poser RD, Smith ST, van Wagoner M, Ross J, Goldstein SA, Jupiter JB, Rosenthal DI (1995) Skeletal repair by in situ formation of the mineral phase of bone. *Science* 267:1796–1799
262. Bohner M (2007) Reactivity of calcium phosphate cements. *J Mater Chem* 38:3980–3986
263. Bohner M, Brunner TJ, Stark WJ (2008) Controlling the reactivity of calcium phosphate cements. *J Mater Chem* 8:5669–5675
264. Yuan H, Li Y, de Bruijn JD, de Groot K, Zhang X (2000) Tissue responses of calcium phosphate cement, a study in dogs. *Biomaterials* 21:1283–1290
265. Takechi M, Miyamoto Y, Ishikawa K, Toh T, Yuasa T, Nagayama M, Suzuki K (1998) Initial histological evaluation of anti-washout type fast-setting calcium phosphate cement following subcutaneous implantation. *Biomaterials* 19:2057–2063
266. Fulmer MT, Brown PW (1993) Effects of Na<sub>2</sub>HPO<sub>4</sub> and NaH<sub>2</sub>PO<sub>4</sub> on hydroxyapatite formation. *J Biomed Mater Res* 27:1095–1102
267. Otsuka M, Matsuda Y, Suwa Y, Fox JL, Higuchi WI (1995) Effect of particle size of metastable calcium phosphates on mechanical strength of a novel self-setting bioactive calcium phosphate cement. *J Biomed Mater Res* 29:25–32
268. Liu C, Shao H, Chen F, Zheng H (2003b) Effects of granularity of raw materials on the hydration and hardening process of calcium phosphate cement. *Biomaterials* 24:4103–4113
269. Chen WC, Lin JHC, Ju CP (2003) Transmission electron microscopic study on setting mechanism of tetracalcium phosphate/dicalcium phosphate anhydrous-based calcium phosphate cement. *J Biomed Mater Res* 64:664–671
270. Fernández E, Gil FJ, Ginebra MP, Driessens FCM, Planell JA, Best SM (1990) Calcium phosphate bone cements for clinical applications Part II: precipitate formation during setting reactions. *J Mater Sci Mater Med* 10:177–183
271. Brown WE (1966) Crystal growth of bone mineral. *Clin Orthop Rel Res* 44:205–220
272. Tung MS, Brown WE (1983) An intermediate state in hydrolysis of amorphous calcium phosphate. *Calcif Tissue Int* 35:783–790
273. Brown WE, Eidelman N, Tomazic BB (1987) Octacalcium phosphate as a precursor in biomineral formation. *Adv Dent Res* 1:306–313
274. Constantz BR, Barr BM, Ison IC, Fulmer MT, Baker J, McKinney LA, Goodman SB, Gunasekaran S, Delaney DC, Ross J, Poser RD (1998) Histological, chemical and crystallographic analysis of four calcium phosphate cements in different rabbit osseous sites. *J Biomed Mater Res Appl Biomater* 43:451–461
275. Tamimi F, Sheikh Z, Barralet J (2012) Dicalcium phosphate cements: brushite and monetite. *Acta Biomater* 8:474–487
276. Elliott JC (1994) Structure and chemistry of the apatites and other calcium orthophosphates. Elsevier, Amsterdam

277. Legrand AP, Sfihi H, Lequeux N, Lemaître J (2009)  $^{31}\text{P}$  solid-state NMR study of the chemical setting process of a dual-paste injectable brushite cements. *J Biomed Mater Res B Appl Biomater* 91B:46–54
278. Bohner M, Merkle HP, van Landuyt P, Trophardy G, Lemaître J (2000) Effect of several additives and their admixtures on the physico-chemical properties of a calcium phosphate cement. *J Mater Sci Mater Med* 11:111–116
279. Vereecke G, Lemaître J (1990) Calculation of the solubility diagrams in the system  $\text{Ca}(\text{OH})_2 - \text{H}_3\text{PO}_4 - \text{KOH} - \text{HNO}_3 - \text{CO}_2 - \text{H}_2\text{O}$ . *J Cryst Growth* 104:820–832
280. Klein CP, de Groot K, Driessen AA, van der Lubbe HB (1985) Interaction of biodegradable  $\beta$ -whitlockite ceramics with bone tissue, an in vivo study. *Biomaterials* 6:189–192
281. Liu C, Shen W, Chen J (1999a) Solution property of calcium phosphate cement hardening body. *Mater Chem Phys* 58:78–83
282. Apelt D, Theiss F, El-Warrak AO, Zlinszky K, Bettschart-Wolfsberger R, Bohner M, Matter S, Auer JA, von Rechenberg B (2004) In vivo behavior of three different injectable hydraulic calcium phosphate cements. *Biomaterials* 25:1439–1451
283. Barralet JE, Grover LM, Gbureck U (2004b) Ionic modification of calcium phosphate cement viscosity Part II: hypodermic injection and strength improvement of brushite cement. *Biomaterials* 25:2197–2203
284. Sarda S, Fernández E, Nilsson M, Balcells M, Planell JA (2002) Kinetic study of citric acid influence on calcium phosphate bone cements as water-reducing agent. *J Biomed Mater Res* 61:653–659
285. Qi X, Ye J, Wang Y (2008) Improved injectability and in vitro degradation of a calcium phosphate cement 2008. *Acta Biomater* 4:1837–1845
286. Grover LM, Knowles JC, Fleming GJP, Barralet JE (2003) In vitro ageing of brushite calcium phosphate cement. *Biomaterials* 24:4133–4141
287. Mariño FT, Mastio J, Rueda C, Blanco L, Cabarcos EL (2007a) Increase of the final setting time of brushite cements by using chondroitin 4-sulfate and silica gel. *J Mater Sci Mater Med* 18:1195–1201
288. Mariño FT, Torres J, Hamdan M, Rodríguez CR, Cabarcos EL (2007b) Advantages of using glycolic acid as a retardant in a brushite forming cement. *J Biomed Mater Res B Appl Biomater* 83B:571–579
289. Flautre B, Delecourt C, Blary M, van Landuyt P, Lemaître J, Hardouin P (1999) Volume effect on biological properties of a calcium phosphate hydraulic cement, experimental study on sheep. *Bone* 25:S35–S39
290. Bohner M (2001b) pH variations of a solution after injecting brushite cements. *Key Eng Mater* 192–195:813–816
291. Xie J, Riley C, Chittur K (2001) Effect of albumin on brushite transformation to hydroxyapatite. *J Biomed Mater Res* 57:357–365
292. Frayssinet P, Roudier M, Lerch A, Ceolin JL, Depres E, Rouquet N (2000) Tissue reaction against a self-setting calcium phosphate cement set in bone or outside the organism. *J Mater Sci Mater Med* 11:811–815
293. Ohura K, Bohner M, Hardouin P, Lemaître J, Pasquier G, Flautre B (1996) Resorption of and bone formation from new  $\beta$ -tricalcium phosphate – monocalcium phosphate cements: an in vivo study. *J Biomed Mater Res* 30:193–200
294. Flautre B, Maynou C, Lemaître J, van Landuyt P, Hardouin P (2002) Bone colonization of  $\beta$ -TCP granules incorporated in brushite cements. *J Biomed Mater Res Appl Biomater* 63:413–417
295. Shepard CU (1982) On two new minerals, monetite and monite, with a notice of pyroclasilite. *Am J Sci* 23:400–405
296. Tas AC (2009) Monetite ( $\text{CaHPO}_4$ ) synthesis in ethanol at room temperature. *J Am Ceram Soc* 92:2907–2912
297. Åberg J, Engqvist H (2008) Non-aqueous, hydraulic cement useful for producing hardened cement, as biomaterials composition comprises non-aqueous mixture of Brushite or

- Monetite-forming calcium phosphate powder composition, and nonaqueous water-miscible liquid. US Patent NoWO2010055483-A2
298. Åberg J, Brisby H, Henriksson HB, Lindahl A, Thomsen P, Engqvist H (2010) Premixed acidic calcium phosphate cement: characterization of strength and microstructure. *J Biomed Mater Res B Appl Biomater* 93B:436–441
  299. Åberg J, Unosson JE, Engqvist H (2013a) Setting mechanisms of an acidic premixed calcium phosphate cement. *Bioceram Dev Appl* 3:070. (6 pages)
  300. Cama G, Gharibi B, Sait MS, Knowles JC, Lagazzo A, Romeed S, di Silvio L, Deb S (2013) A novel method of forming micro- and macroporous monetite cements. *J Mater Chem B* 1:958–969
  301. Şahin E, Çiftçiöğlü M (2013) Monetite promoting effect of NaCl on brushite cement setting kinetics. *J Mater Chem B* 1:2943–2950
  302. Montazerolghaem M, Ott MK, Engqvist H, Melhus H, Rasmusson AJ (2015) Resorption of monetite calcium phosphate cement by mouse bone marrow derived osteoclasts. *Mater Sci Eng C* 52:212–218
  303. Irbe Z, Vecbiškėna L, Bērziņa-Cimdiņa L (2011) Setting properties of brushite and hydroxyapatite compound cements. *Adv Mater Res* 222:239–242
  304. Gbureck U, Dembski S, Thull R, Barralet JE (2005c) Factors influencing calcium phosphate cement shelf-life. *Biomaterials* 26:3691–3697
  305. Standard test method for time of setting of hydraulic cement paste by Gillmore needles ASTM C266-89 (1993) Annual book of ASTM standards, vol 0401. Cement, Lime, Gypsum American Society for Testing and Materials, Philadelphia, pp 189–191
  306. Standard test method for time of setting of hydraulic cement paste by Vicat needle ASTM C191-92 (1993) Annual book of ASTM standards, vol 0401. Cement, Lime, Gypsum American Society for Testing and Materials, Philadelphia, pp 158–160
  307. Nilsson M, Carlson J, Fernández E, Planell JA (2002b) Monitoring the setting of calcium-based bone cements using pulse-echo ultrasound. *J Mater Sci Mater Med* 13:1135–1141
  308. Carlson J, Nilsson M, Fernández E, Planell JA (2003) An ultrasonic pulse-echo technique for monitoring the setting of CaSO<sub>4</sub>-based bone cement. *Biomaterials* 24:71–77
  309. Hofmann MP, Nazhat SN, Gbureck U, Barralet JE (2006a) Real-time monitoring of the setting reaction of brushite-forming cement using isothermal differential scanning calorimetry. *J Biomed Mater Res B Appl Biomater* 79B:360–364
  310. Martin RI, Brown PW (1997) The effects of magnesium on hydroxyapatite formation in vitro from CaHPO<sub>4</sub> and Ca<sub>4</sub>(PO<sub>4</sub>)<sub>2</sub>O at 374 °C. *Calcif Tissue Int* 60:538–546
  311. Brunner TJ, Bohner M, Dora C, Gerber C, Stark WJ (2007b) Comparison of amorphous TCP nanoparticles to micron-sized  $\alpha$ -TCP as starting materials for calcium phosphate cements. *J Biomed Mater Res B Appl Biomater* 83B:400–407
  312. Gao WY, Wang YW, Dong LM, Yu ZW (2006) Thermokinetic analysis of the hydration process of calcium phosphate cement. *J Therm Anal Calorim* 85:785–789
  313. Bohner M, Gbureck U (2008) Thermal reactions of brushite cements. *J Biomed Mater Res B Appl Biomater* 84B:375–385
  314. Hofmann MP, Young AM, Nazhat SN, Gbureck U, Barralet JE (2006b) Setting kinetics observation of a brushite cement by FTIR and DSC. *Key Eng Mater* 309–311:837–840
  315. Mohn D, Doebelin N, Tadier S, Bernabei RE, Luechinger NA, Stark WJ, Bohner M (2011) Reactivity of calcium phosphate nanoparticles prepared by flame spray synthesis as precursors for calcium phosphate cements. *J Mater Chem* 21:13963–13972
  316. Liu C, Huang Y, Zheng H (1999b) Study of the hydration process of calcium phosphate cement by AC impedance spectroscopy. *J Am Ceram Soc* 82:1052–1057
  317. Hofmann MP, Young AM, Gbureck U, Nazhat SN, Barralet JE (2006c) FTIR-monitoring of a fast setting brushite bone cement: effect of intermediate phases. *J Mater Chem* 16:3199–3206
  318. Bimis A, Karalekas D, Bouropoulos N, Mouzakis D, Zaoutos S (2016) Monitoring of hardening and hygroscopic induced strains in a calcium phosphate bone cement using FBG sensor. *J Mech Behav Biomed Mater* 60:195–202

319. Hsu HC, Tuan WH, Lee HY (2009) *In-situ* observation on the transformation of calcium phosphate cement into hydroxyapatite. *Mater Sci Eng C* 29:950–954
320. Rau JV, Generosi A, Smirnov VV, Ferro D, Rossi AV, Barinov SM (2008) Energy dispersive X-ray diffraction study of phase development during hardening of calcium phosphate bone cements with addition of chitosan. *Acta Biomater* 4:1089–1094
321. Generosi A, Smirnov VV, Rau JV, Rossi AV, Ferro D, Barinov SM (2008) Phase development in the hardening process of two calcium phosphate bone cements: an energy dispersive X-ray diffraction study. *Mater Res Bull* 43:561–571
322. Rau JV, Fosca M, Komlev VS (2013) In situ time-resolved energy dispersive X-ray diffraction studies of calcium phosphate based bone cements. *Key Eng Mater* 541:115–120
323. Ginebra MP, Fernández E, Driessens FCM, Boltong MG, Muntasell J, Font J, Planell JA (1995a) The effects of temperature on the behaviour of an apatitic calcium phosphate cement. *J Mater Sci Mater Med* 6:857–860
324. Baroud G, Bohner M, Heini P, Steffen T (2004a) Injection biomechanics of bone cements used in vertebroplasty. *Biomed Mater Eng* 14:487–504
325. Leung KS, Siu WS, Li SF, Qin L, Cheung WH, Tam KF, Po P, Lui Y (2006) An in vitro optimized injectable calcium phosphate cement for augmenting screw fixation in osteopenic goats. *J Biomed Mater Res B Appl Biomater* 78B:153–160
326. Eames WB, Monroe SD, Roan JD, Oneal SJ (1977) Proportioning and mixing of cements – comparison of working times. *Oper Dent* 2:97–104
327. Baroud G, Matsushita C, Samara M, Beckman L, Steffen T (2004b) Influence of oscillatory mixing on the injectability of three acrylic and two calcium phosphate bone cements for vertebroplasty. *J Biomed Mater Res B Appl Biomater* 68B:105–111
328. Nomoto T, Haraguchi K, Yamaguchi S, Sugano N, Nakayama H, Sekino T, Niihara K (2006) Hydrolyses of calcium phosphates-allografts composite in physiological solutions. *J Mater Sci Mater Med* 17:379–385
329. Od M, Takeuchi A, Lin X, Matsuya S, Ishikawa K (2008) Effects of liquid phase on basic properties of  $\alpha$ -tricalcium phosphate-based apatite cement. *Dent Mater J* 27:672–677
330. Sarda S, Fernández E, Llorens J, Martínez S, Nilsson M, Planell JA (2001) Rheological properties of an apatitic bone cement during initial setting. *J Mater Sci Mater Med* 12:905–909
331. Liu C, Shao H, Chen F, Zheng H (2006a) Rheological properties of concentrated aqueous injectable calcium phosphate cement slurry. *Biomaterials* 27:5003–5013
332. Bohner M, Baroud G (2005) Injectability of calcium phosphate pastes. *Biomaterials* 26:1553–1563
333. Khairoun I, Boltong MG, Driessens FCM, Planell JA (1998b) Some factors controlling the injectability of calcium phosphate bone cements. *J Mater Sci Mater Med* 9:425–428
334. Burguera EF, Xu HHK, Sun L (2008b) Injectable calcium phosphate cement: effects of powder-to-liquid ratio and needle size. *J Biomed Mater Res B Appl Biomater* 84B:493–502
335. Habib M, Baroud G, Gitzhofer F, Bohner M (2008) Mechanisms underlying the limited injectability of hydraulic calcium phosphate paste. *Acta Biomater* 4:1465–1471
336. Montufar EB, Maazouz Y, Ginebra MP (2013) Relevance of the setting reaction to the injectability of tricalcium phosphate pastes. *Acta Biomater* 9:6188–6198
337. Baroud G, Cayer E, Bohner M (2005) Rheological characterization of concentrated aqueous beta-tricalcium phosphate suspensions: the effect of liquid-to-powder ratio, milling time and additives. *Acta Biomater* 1:357–363
338. Ishikawa K (2003) Effects of spherical tetracalcium phosphate on injectability and basic properties of apatitic cement. *Key Eng Mater* 240–242:369–372
339. Habib M, Baroud G, Gitzhofer F, Bohner M (2010) Mechanisms underlying the limited injectability of hydraulic calcium phosphate paste Part II: particle separation study. *Acta Biomater* 6:250–256
340. Bohner M, Doebelin N, Baroud G (2006b) Theoretical and experimental approach to test the cohesion of calcium phosphate pastes. *Eur Cell Mater* 12:26–35

341. Miyamoto Y, Ishikawa K, Takechi M, Toh T, Yuasa T, Nagayama M, Suzuki K (1999) Histological and compositional evaluations of three types of calcium phosphate cements when implanted in subcutaneous tissue immediately after mixing. *J Biomed Mater Res Appl Biomater* 48:36–42
342. Bermudez O, Boltong MG, Driessens FCM, Planell JA (1993) Compressive strength and diametral tensile strength of some calcium-orthophosphate cements, a pilot study. *J Mater Sci Mater Med* 4:389–393
343. del Valle S, Miño N, Muñoz F, González A, Planell JA, Ginebra MP (2007) In vivo evaluation of an injectable macroporous calcium phosphate cement. *J Mater Sci Mater Med* 18:353–361
344. Coelho WT, Fernandes JM, Vieira RS, Thurmer MB, Santos LA (2012) Effect on mechanical strength of tricalcium phosphate cement by additions of sodium alginate. *Mater Sci Forum* 727–728:1181–1186
345. Khairoun I, Driessens FCM, Boltong MG, Planell JA, Wenz R (1999) Addition of cohesion promoters to calcium orthophosphate cements. *Biomaterials* 20:393–398
346. Alkhraisat MH, Rueda C, Mariño FT, Torres J, Jerez LB, Gbureck U, Cabarcos EL (2009) The effect of hyaluronic acid on brushite cement cohesion. *Acta Biomater* 5:3150–3156
347. Alkhraisat MH, Rueda C, Jerez LB, Mariño FT, Torres J, Gbureck U, Cabarcos EL (2010a) Effect of silica gel on the cohesion, properties and biological performance of brushite cement. *Acta Biomater* 6:257–265
348. An J, Wolke JGC, Jansen JA, Leeuwenburgh SCGI (2016a) Influence of polymeric additives on the cohesion and mechanical properties of calcium phosphate cements. *J Mater Sci Mater Med* 27:58
349. Low KL, Tan SH, Zein SHS, Roether JA, Mouriño V, Boccaccini AR (2010) Calcium phosphate-based composites as injectable bone substitute materials. *J Biomed Mater Res B Appl Biomater* 94B:273–286
350. Habib M, Baroud G, Galea L, Bohner M (2012) Evaluation of the ultrasonication process for injectability of hydraulic calcium phosphate pastes. *Acta Biomater* 8:1164–1168
351. Bigi A, Bracci B, Panzavolta S (2004a) Effect of added gelatin on the properties of calcium phosphate cement. *Biomaterials* 25:2893–2899
352. Ishikawa K, Matsuya S, Nakagawa M, Udoh K, Suzuki K (2004) Basic properties of apatite cement containing spherical tetracalcium phosphate made with plasma melting method. *J Mater Sci Mater Med* 15:13–17
353. Wang X, Ye J, Wang Y (2008b) Effect of additives on the morphology of the hydrated product and physical properties of a calcium phosphate cement. *J Mater Sci Technol* 24:285–288
354. Barralet JE, Hofmann M, Grover LM, Gbureck U (2003) High strength apatitic cement by modification with  $\alpha$ -hydroxy acid salts. *Adv Mater* 15:2091–2095
355. Barralet JE, Duncan CO, Dover MS, Bassett DC, Nishikawa H, Monaghan A, Gbureck U (2005a) Cortical bone screw fixation in ionically modified apatite cements. *J Biomed Mater Res B Appl Biomater* 73B:238–243
356. Ginebra MP, Boltong MG, Fernández E, Planell JA, Driessens FCM (1995b) Effect of various additives and temperature on some properties of an apatitic calcium phosphate cement. *J Mater Sci Mater Med* 6:612–616
357. Acarturk O, Lehmicke M, Aberman H, Toms D, Hollinger JO, Fulmer MT (2008) Bone healing response to an injectable calcium phosphate cement with enhanced radiopacity. *J Biomed Mater Res B Appl Biomater* 86B:56–62
358. Wang X, Ye J, Wang Y (2007c) Influence of a novel radiopacifier on the properties of an injectable calcium phosphate cement. *Acta Biomater* 3:757–763
359. Chen F, Liu C, Mao Y (2010) Bismuth-doped injectable calcium phosphate cement with improved radiopacity and potent antimicrobial activity for root canal filling. *Acta Biomater* 6:3199–3207
360. Romieu G, Garric X, Munier S, Vert M, Boudeville P (2010) Calcium-strontium mixed phosphate as novel injectable and radio-opaque hydraulic cement. *Acta Biomater* 6:3208–3215

361. Åberg J, Henriksson HB, Engqvist H, Palmquist A, Brantsing C, Lindahl A, Thomsen P, Brisby H (2012) Biocompatibility and resorption of a radiopaque premixed calcium phosphate cement. *J Biomed Mater Res A* 100A:1269–1278
362. López A, Montazerolghaem M, Ott MK, Persson C (2014) Calcium phosphate cements with strontium halides as radiopacifiers. *J Biomed Mater Res B Appl Biomater* 102B:250–259
363. Watanabe M, Tanaka M, Sakurai M, Maeda M (2006) Development of calcium phosphate cement. *J Eur Ceram Soc* 26:549–552
364. Bercier A, Gonçalves S, Lignon O, Fitremann J (2010) Calcium phosphate bone cements including sugar surfactants: part one – porosity, setting times and compressive strength. *Materials* 3:4695–4709
365. Sarda S, Nilsson M, Balcells M, Fernández E (2003) Influence of surfactant molecules as air-entraining agent for bone cement macroporosity. *J Biomed Mater Res A* 65A:215–221
366. Friberg J, Fernández E, Sarda S, Nilsson M, Ginebra MP, Martínez S, Planell JA (2001) An experimental approach to the study of the rheology behavior of synthetic bone calcium phosphate cements. *Key Eng Mater* 192–195:777–780
367. Reinstorf A, Hempel U, Olgemöller F, Domaschke H, Schneiders W, Mai R, Stadlinger B, Rösen-Wolff A, Rammelt S, Gelinsky M, Pompe W (2006) O-phospho-L-serine modified calcium phosphate cements-material properties, in vitro and in vivo investigations. *Mat-Wiss u Werkstofftech* 37:491–503
368. Lode A, Reinstorf A, Bernhardt A, Wolf-Brandstetter C, König U, Gelinsky M (2008) Heparin modification of calcium phosphate bone cements for VEGF functionalization. *J Biomed Mater Res A* 86A:749–759
369. Mai R, Lux R, Proff P, Lauer G, Pradel W, Leonhardt H, Reinstorf A, Gelinsky M, Jung R, Eckelt U, Gedrange T, Stadlinger B (2008) O-phospho-L-serine: a modulator of bone healing in calcium-phosphate cements. *Biomed Tech* 53:229–233
370. Vater C, Lode A, Bernhardt A, Reinstorf A, Nies B, Gelinsky M (2010) Modifications of a calcium phosphate cement with biomolecules – influence on nanostructure, material, and biological properties. *J Biomed Mater Res A* 95A:912–923
371. Grover LM, Gbureck U, Farrar DF, Barralet JE (2006b) Adhesion of a novel calcium phosphate cement to cortical bone and several common biomaterials. *Key Eng Mater* 309-311:849–852
372. Pastorino D, Canal C, Ginebra MP (2015a) Multiple characterization study on porosity and pore structure of calcium phosphate cements. *Acta Biomater* 28:205–214
373. Markovic M, Takagi S, Chow LC (2001) Formation of macropores in calcium phosphate cements through the use of mannitol crystals. *Key Eng Mater* 192–195:773–776
374. Tajima S, Kishi Y, Oda M, Maruta M, Matsuya S, Ishikawa K (2006) Fabrication of biporous low-crystalline apatite based on mannitol dissolution from apatite cement. *Dent Mater J* 25:616–620
375. Xu HHK, Weir MD, Burguera EF, Fraser AM (2006) Injectable and macroporous calcium phosphate cement scaffold. *Biomaterials* 27:4279–4287
376. Cama G, Barberis F, Botter R, Cirillo P, Capurro M, Quarto R, Scaglione S, Finocchio E, Mussi V, Valbusa U (2009) Preparation and properties of macroporous brushite bone cements. *Acta Biomater* 5:2161–2168
377. Vazquez D, Takagi S, Frukhtbeyn S, Chow LC (2010) Effects of addition of mannitol crystals on the porosity and dissolution rates of a calcium phosphate cement. *J Res Natl Inst Stand Technol* 115:225–232
378. Shimogoryo R, Eguro T, Kimura E, Maruta M, Matsuya S, Ishikawa K (2009) Effects of added mannitol on the setting reaction and mechanical strength of apatite cement. *Dent Mater J* 28:627–633
379. Liu H, Liu XQ, Liang JS (2012) Basic properties of calcium phosphate cement scaffold. *Adv Mater Res* 531:354–357
380. Almirall A, Larrecq G, Delgado JA, Martínez S, Planell JA, Ginebra MP (2004) Fabrication of low temperature macroporous hydroxyapatite scaffolds by foaming and hydrolysis of an  $\alpha$ -TCP paste. *Biomaterials* 25:3671–3680



381. Barralet JE, Grover L, Gaunt T, Wright AJ, Gibson IR (2002a) Preparation of macroporous calcium phosphate cement tissue engineering scaffold. *Biomaterials* 23:3063–3072
382. Takagi S, Chow LC (2001) Formation of macropores in calcium phosphate cement implants. *J Mater Sci Mater Med* 12:135–139
383. Tas AC (2008b) Preparation of porous apatite granules from calcium phosphate cement. *J Mater Sci Mater Med* 19:2231–2239
384. Tas AC (2006) Preparation of self-setting cement-based micro- and macroporous granules of carbonated apatitic calcium phosphate. *Ceram Eng Sci Proc* 27:49–60
385. Cama G, Gharibi B, Knowles JC, Romeed S, di Silvio L, Deb S (2014) Structural changes and biological responsiveness of an injectable and mouldable monetite bone graft generated by a facile synthetic method. *J R Soc Interface* 11:20140727
386. Simon CG Jr, Khatri CA, Wight SA, Wang FW (2002) Preliminary report on the biocompatibility of a moldable, resorbable, composite bone graft consisting of calcium phosphate cement and poly(lactide-*co*-glycolide) microspheres. *J Orthop Res* 20:473–482
387. Ruhe PQ, Hedberg EL, Padron NT, Spauwen PHM, Jansen JA, Mikos AG (2005) Biocompatibility and degradation of poly(D,L-lactic-*co*-glycolic acid)/calcium phosphate cement composites. *J Biomed Mater Res A* 74A:533–544
388. Habraken WJEM, Wolke JGC, Mikos AG, Jansen JA (2006) Injectable PLGA microsphere/calcium phosphate cements, physical properties and degradation characteristics. *J Biomater Sci Polym Ed* 17:1057–1074
389. Link DP, van den Dolder J, Jurgens WJFM, Wolke JGC, Jansen JA (2006) Mechanical evaluation of implanted calcium phosphate cement incorporated with PLGA microparticles. *Biomaterials* 27:4941–4947
390. Habraken WJEM, Wolke JGC, Mikos AG, Jansen JA (2008a) PLGA microsphere/calcium phosphate cement composites for tissue engineering, *in vitro* release and degradation characteristics. *J Biomater Sci Polym Ed* 19:1171–1188
391. Link DP, van den Dolder J, van den Beucken JJJP, Cuijpers VM, Wolke JGC, Mikos AG, Jansen JA (2008a) Evaluation of the biocompatibility of calcium phosphate cement/PLGA microparticle composites. *J Biomed Mater Res A* 87A:760–769
392. Lanao RPF, Leeuwenburgh SC, Wolke JG, Jansen JA (2011) *In vitro* degradation rate of apatitic calcium phosphate cement with incorporated PLGA microspheres. *Acta Biomater* 7:3459–3468
393. Lopez-Heredia MA, Sariibrahimoglu K, Yang W, Bohner M, Yamashita D, Kunstar A, van Apeldoorn AA, Bronkhorst EM, Lanao RPF, Leeuwenburgh SCG, Itatani K, Yang F, Salmon P, Wolke JGC, Jansen JA (2012b) Influence of the pore generator on the evolution of the mechanical properties and the porosity and interconnectivity of a calcium phosphate cement. *Acta Biomater* 8:404–414
394. Zhong ML, Chen XQ, Fan HS, Zhang XD (2012) Incorporation of salmon calcitonin-loaded poly(lactide-*co*-glycolide) (PLGA) microspheres into calcium phosphate bone cement and the biocompatibility evaluation *in vitro*. *J Bioact Compat Polym* 27:133–147
395. van Houdt CIA, Preethanath RS, van Oirschot BAJA, Zwarts PHW, Ulrich DJO, Anil S, Jansen JA, van den Beucken JJJP (2016) Toward accelerated bone regeneration by altering poly(D,L-lactic-*co*-glycolic) acid porogen content in calcium phosphate cement. *J Biomed Mater Res A* 104:483–492
396. Fullana SG, Ternet H, Freche M, Lacout JL, Rodriguez F (2010) Controlled release properties and final macroporosity of a pectin microspheres-calcium phosphate composite bone cement. *Acta Biomater* 6:2294–2300
397. Li M, Liu X, Liu X, Ge B, Chen K (2009) Creation of macroporous calcium phosphate cements as bone substitutes by using genipin – crosslinked gelatin microspheres. *J Mater Sci Mater Med* 20:925–934
398. Habraken WJEM, de Jonge LT, Wolke JGC, Yubao L, Mikos AG, Jansen JA (2008b) Introduction of gelatin microspheres into an injectable calcium phosphate cement. *J Biomed Mater Res A* 87A:643–655

399. Matsumoto G, Sugita Y, Kubo K, Yoshida W, Ikada Y, Sobajima S, Neo M, Maeda H, Kinoshita Y (2014) Gelatin powders accelerate the resorption of calcium phosphate cement and improve healing in the alveolar ridge. *J Biomater Appl* 28:1316–1324
400. Tang PF, Li G, Wang JF, Zheng QJ, Wang Y (2009) Development, characterization, and validation of porous carbonated hydroxyapatite bone cement. *J Biomed Mater Res B Appl Biomater* 90B:886–893
401. Wang XP, Ye JD, Li X, Dong H (2008c) Production of in-situ macropores in an injectable calcium phosphate cement by introduction of cetyltrimethyl ammonium bromide. *J Mater Sci Mater Med* 19:3221–3225
402. Habraken WJEM, Zhang Z, Wolke JGC, Grijpma DW, Mikos AG, Feijen J, Jansen JA (2008c) Introduction of enzymatically degradable poly(trimethylene carbonate) microspheres into an injectable calcium phosphate cement. *Biomaterials* 29:2464–2476
403. Xu HHK, Simon CG Jr (2004a) Self-hardening calcium phosphate composite scaffold for bone tissue engineering. *J Orthop Res* 22:535–543
404. Burguera EF, Xu HHK, Takagi S, Chow LC (2005) High early strength calcium phosphate bone cement: effects of dicalcium phosphate dihydrate and absorbable fibers. *J Biomed Mater Res A* 75A:966–975
405. Xu HHK, Quinn JB (2002) Calcium phosphate cement containing resorbable fibers for short-term reinforcement and macroporosity. *Biomaterials* 23:193–202
406. Gorst NJS, Perrie Y, Gbureck U, Hutton AL, Hofmann MP, Grover LM, Barralet JE (2006) Effects of fiber reinforcement on the mechanical properties of brushite cement. *Acta Biomater* 2:95–102
407. Zuo Y, Yang F, Wolke JGC, Li Y, Jansen JA (2010) Incorporation of biodegradable electrospun fibers into calcium phosphate cement for bone regeneration. *Acta Biomater* 6:1238–1247
408. Xu HHK, Simon CG Jr (2004b) Self-hardening calcium phosphate cement-mesh composite: reinforcement, macropores, and cell response. *J Biomed Mater Res A* 69A:267–278
409. Losee JE, Karmacharya J, Gannon FH, Slemple AE, Ong G, Hunenko O, Gorden AD, Bartlett SP, Kirschner RE (2003) Reconstruction of the immature craniofacial skeleton with a carbonated calcium phosphate bone cement, interaction with bioresorbable mesh. *J Craniofac Surg* 14:117–124
410. Xu HHK, Carey LE, Simon CG Jr (2007a) Premixed macroporous calcium phosphate cement scaffold. *J Mater Sci Mater Med* 18:1345–1353
411. Vasconcelos LA, dos Santos LA (2013) Calcium phosphate cement scaffolds with PLGA fibers. *Mater Sci Eng C* 33:1032–1040
412. Ginebra MP, Espanol M, Montufar EB, Perez RA, Mestres G (2010) New processing approaches in calcium phosphate cements and their applications in regenerative medicine. *Acta Biomater* 6:2863–2873
413. del Real RP, Wolke JGC, Vallet-Regi M, Jansen JA (2002) A new method to produce macropores in calcium phosphate cements. *Biomaterials* 23:3673–3680
414. del Real RP, Ooms E, Wolke JGC, Vallet-Regi M, Jansen JA (2003) In vivo bone response to porous calcium phosphate cement. *J Biomed Mater Res A* 65A:30–36
415. Hesarakı S, Moztarzadeh F, Sharifi D (2007) Formation of interconnected macropores in apatitic calcium phosphate bone cement with the use of an effervescent additive. *J Biomed Mater Res A* 83A:80–87
416. Hesarakı S, Zamanian A, Moztarzadeh F (2008) The influence of the acidic component of the gas-foaming porogen used in preparing an injectable porous calcium phosphate cement on its properties, acetic acid versus citric acid. *J Biomed Mater Res B Appl Biomater* 86B:208–216
417. Hesarakı S, Moztarzadeh F, Solati-Hashjin M (2006) Phase evaluation of an effervescent-added apatitic calcium phosphate bone cement. *J Biomed Mater Res B Appl Biomater* 79B:203–209
418. Ginebra MP, Delgado JA, Harr I, Almirall A, del Valle S, Planell JA (2007) Factors affecting the structure and properties of an injectable self-setting calcium phosphate foam. *J Biomed Mater Res A* 80A:351–361

419. Montufar EB, Aguirre A, Gil C, Engel E, Traykova T, Planell JA, Ginebra MP (2010) Foamed surfactant solution as a template for self-setting injectable hydroxyapatite scaffolds for bone regeneration. *Acta Biomater* 6:876–885
420. Montufar EB, Traykova T, Planell JA, Ginebra MP (2011) Comparison of a low molecular weight and a macromolecular surfactant as foaming agents for injectable self setting hydroxyapatite foams: polysorbate 80 versus gelatin. *Mater Sci Eng C* 31:1498–1504
421. de Oliveira RC, Pereta NC, Bertran CA, Motisuke M, de Sousa E (2014) Study of in vitro degradation of brushite cements scaffolds. *J Mater Sci Mater Med* 25:2297–2303
422. Pastorino D, Canal C, Ginebra MP (2015b) Drug delivery from injectable calcium phosphate foams by tailoring the macroporosity–drug interaction. *Acta Biomater* 12:250–259
423. Zhang J, Liu W, Gauthier O, Source S, Pilet P, Rethore G, Khairoun K, Bouler JM, Tancret F, Weiss PA (2016) simple and effective approach to prepare injectable macroporous calcium phosphate cement for bone repair: syringe-foaming using a viscous hydrophilic polymeric solution. *Acta Biomater* 31:326–338
424. Unosson JE, Persson C, Engqvist H (2015) An evaluation of methods to determine the porosity of calcium phosphate cements. *J Biomed Mater Res B Appl Biomater* 103B:62–71
425. Andrianjatovo H, Lemaître J (1995) Effects of polysaccharides on the cement properties in the monocalcium phosphate/ $\beta$ -tricalcium phosphate system. *Innov Tech Biol Med* 16:140–147
426. Cherng A, Takagi S, Chow LC (1997) Effects of hydroxypropylmethylcellulose and other gelling agents on the handling properties of calcium phosphate cement. *J Biomed Mater Res* 35:273–277
427. Yokoyama A, Matsuno H, Yamamoto S, Kawasaki T, Kohgo T, Uo M, Watari F, Nakasu M (2003) Tissue response to a newly developed calcium phosphate cement containing succinic acid and carboxymethyl-chitin. *J Biomed Mater Res A* 64A:491–501
428. Jyoti MA, Thai VV, Min YK, Lee BT, Song HY (2010) In vitro bioactivity and biocompatibility of calcium phosphate cements using hydroxy-propyl-methyl-cellulose (HPMC). *Appl Surf Sci* 257:1533–1539
429. Bigi A, Torricelli P, Fini M, Bracci B, Panzavolta S, Sturba L, Giardino RA (2004b) Biomimetic gelatin-calcium phosphate bone cement. *Int J Artif Organs* 27:664–673
430. Bigi A, Panzavolta S, Sturba L, Torricelli P, Fini M, Giardino R (2006) Normal and osteopenic bone-derived osteoblast response to a biomimetic gelatin – calcium phosphate bone cement. *J Biomed Mater Res A* 78A:739–745
431. Fujishiro Y, Takahashi K, Sato T (2001) Preparation and compressive strength of  $\alpha$ -tricalcium phosphate/gelatin gel composite cement. *J Biomed Mater Res* 54:525–530
432. Bigi A, Panzavolta S, Rubini K (2004c) Setting mechanism of a biomimetic bone cement. *Chem Mater* 16:3740–3745
433. Panzavolta S, Torricelli P, Sturba L, Bracci B, Giardino R, Bigi A (2008) Setting properties and in vitro bioactivity of strontium-enriched gelatin-calcium phosphate bone cements. *J Biomed Mater Res A* 84A:965–972
434. Xu LX, Shi XT, Wang YP, Shi ZL (2008a) Performance of calcium phosphate bone cement using chitosan and gelatin as well as citric acid as hardening liquid. *J Clin Rehabil Tissue Eng Res* 12:6381–6384
435. Shie MY, Chen DCH, Wang CY, Chiang TY, Ding SJ (2008) Immersion behavior of gelatin-containing calcium phosphate cement. *Acta Biomater* 4:646–655
436. Majekodunmi AO, Deb S, Nicholson JW (2003) Effect of molecular weight and concentration of poly(acrylic acid) on the formation of a polymeric calcium phosphate cement. *J Mater Sci Mater Med* 14:747–752
437. Majekodunmi AO, Deb S (2007) Poly(acrylic acid) modified calcium phosphate cements, the effect of the composition of the cement powder and of the molecular weight and concentration of the polymeric acid. *J Mater Sci Mater Med* 18:1883–1888
438. Chen WC, Ju CP, Wang JC, Hung CC, Lin JHC (2008) Brittle and ductile adjustable cement derived from calcium phosphate cement/polyacrylic acid composites. *Dent Mater* 24:1616–1622

439. Komath M, Varma HK (2003) Development of a fully injectable calcium phosphate cement for orthopedic and dental applications. *Bull Mater Sci* 26:415–422
440. Bohner M, Theiss F, Apelt D, Hirsiger W, Houriet R, Rizzoli G, Gnos E, Frei C, Auer JA, von Rechenberg B (2003) Compositional changes of a dicalcium phosphate dihydrate cement after implantation in sheep. *Biomaterials* 24:3463–3474
441. Chavez GSC, Alge DL, Chu TMG (2011) Additive concentration effects on dicalcium phosphate dihydrate cements prepared using monocalcium phosphate monohydrate and hydroxyapatite. *Biomed Mater* 6:065007
442. Engstrand J, Persson C, Engqvist H (2014) The effect of composition on mechanical properties of brushite cements. *J Mech Behav Biomed Mater* 29:81–90
443. Leroux L, Hatim Z, Freche M, Lacout JL (1999) Effects of various adjuvants (lactic acid, glycerol and chitosan) on the injectability of a calcium phosphate cement. *Bone* 25:S31–S34
444. Barralet JE, Tremayne MJ, Lilley KJ, Gbureck U (2005b) Chemical modification of calcium phosphate cements with  $\alpha$ -hydroxy acids and their salts. *Chem Mater* 17:1313–1319
445. Driessens FCM, Boltong MG, de Maeyer EAP, Verbeeck RMH, Wenz R (2000b) Effect of temperature and immersion on the setting of some calcium phosphate cements. *J Mater Sci Mater Med* 11:453–457
446. Ishikawa K, Takagi S, Chow LC, Ishikawa Y (1995b) Properties and mechanisms of fast-setting calcium phosphate cements. *J Mater Sci Mater Med* 6:528–533
447. Miyamoto Y, Ishikawa K, Fukao K, Sawada M, Nagayama M, Kon M, Asaoka K (1995) In vivo setting behavior of fast-setting calcium phosphate cement. *Biomaterials* 16:855–860
448. Kawai T, Fujisawa N, Suzuki I, Ohtsuki C, Matsushima Y, Unuma H (2010) Control of setting behavior of calcium phosphate paste using gelatinized starch. *J Ceram Soc Jpn* 118:421–424
449. Bohner M, Luginbühl R, Reber C, Doebelin N, Baroud G, Conforto E (2009) A physical approach to modify the hydraulic reactivity of  $\alpha$ -tricalcium phosphate powder. *Acta Biomater* 5:3524–3535
450. Egli RJ, Gruenenfelder S, Doebelin N, Hofstetter W, Luginbuehl R, Bohner M (2011) Thermal treatments of calcium phosphate biomaterials to tune the physico-chemical properties and modify the in vitro osteoclast response. *Adv Eng Mater* 13:B102–B107
451. Takechi M, Miyamoto Y, Momota Y, Yuasa T, Tatehara S, Nagayama M, Ishikawa K (2004) Effects of various sterilization methods on the setting and mechanical properties of apatite cement. *J Biomed Mater Res B Appl Biomater* 69B:58–63
452. Schneider G, Blechschmidt K, Linde D, Litschko P, Körbs T, Beleites E (2010) Bone regeneration with glass ceramic implants and calcium phosphate cements in a rabbit cranial defect model. *J Mater Sci Mater Med* 21:2853–2859
453. Johal HS, Buckley RE, Le ILD, Leighton RK (2009) A prospective randomized controlled trial of a bioresorbable calcium phosphate paste ( $\alpha$ -BSM) in treatment of displaced intra-articular calcaneal fractures. *J Trauma Injury Infect Crit Care* 67:875–882
454. Yuasa T, Miyamoto Y, Ishikawa K, Takechi M, Suzuki K (2001) In vitro resorption of three apatite cements with osteoclasts. *J Biomed Mater Res* 54:344–350
455. Puricelli E, Corsetti A, Ponzoni D, Martins GL, Leite MG, Santos LA (2010) Characterization of bone repair in rat femur after treatment with calcium phosphate cement and autogenous bone graft. *Head Face Med* 6:10
456. Zhao X, Lib F, Lic S (2010) Degradation characteristic of strontium-containing calcium phosphate cement in vivo. *Adv Mater Res* 105–106:553–556
457. Khairoun I, Magne D, Gauthier O, Bouler JM, Aguado E, Daculsi G, Weiss P (2002) In vitro characterization and in vivo properties of a carbonated apatite bone cement. *J Biomed Mater Res* 60:633–642
458. Mao K, Yang Y, Li J, Hao L, Tang P, Wang Z, Wen N, Du M, Wang J, Wang Y (2009) Investigation of the histology and interfacial bonding between carbonated hydroxyapatite cement and bone. *Biomed Mater* 4:045003

459. Sanzana ES, Navarro M, Macule F, Suso S, Planell JA, Ginebra MP (2008) The in vivo behavior of calcium phosphate cements and glasses as bone substitutes. *Acta Biomater* 4:1924–1933
460. Bodde EWH, Cammaert CTR, Wolke JGC, Spauwen PHM, Jansen JA (2007) Investigation as to the osteoinductivity of macroporous calcium phosphate cement in goats. *J Biomed Mater Res B Appl Biomater* 83B:161–168
461. Miyamoto Y, Ishikawa K, Takeshi M, Toh T, Yoshida Y, Nagayama M, Kon M, Asaoka K (1997) Tissue response to fast-setting calcium phosphate cement in bone. *J Biomed Mater Res* 37:457–464
462. Young S, Holde M, Gunasekaran S, Poser R, Constantz BR (1998) The correlation of radiographic, MRI and histological evaluations over two years of a carbonated apatite cement in a rabbit model. In: *Proceedings of the 44th annual meeting, Orthopedic Research Society, New Orleans, USA*, pp 846
463. Feng B, Guolin M, Yuan Y, Liu C, Zhen W, Jian L (2010) Role of macropore size in the mechanical properties and in vitro degradation of porous calcium phosphate cements. *Mater Lett* 64:2028–2031
464. An J, Liao H, Kucko NW, Herber RPC, Wolke JGC, van den Beucken JJJP, Jansen JA, Leeuwenburgh SCG (2016b) Long-term evaluation of the degradation behavior of three apatite-forming calcium phosphate cements. *J Biomed Mater Res A* 104A:1072–1081
465. Kroese-Deutman HC, Wolke JGC, Spauwen PHM, Jansen JA (2006) Closing capacity of cranial bone defects using porous calcium phosphate cement implants in a rabbit animal model. *J Biomed Mater Res A* 79A:503–511
466. Bourgeois B, Laboux O, Obadia L, Gauthier O, Betti E, Aguado E, Daculsi G, Bouler JM (2003) Calcium-deficient apatite: a first in vivo study concerning bone ingrowth. *J Biomed Mater Res A* 65A:402–408
467. Lu J, Descamps M, Dejoui J, Koubi G, Hardouin P, Lemaître J, Proust JP (2002) The biodegradation mechanism of calcium phosphate biomaterials in bone. *J Biomed Mater Res Appl Biomater* 63:408–412
468. Wenisch S, Stahl JP, Horas U, Heiss C, Kilian O, Trinkaus K, Hild A, Schnettler R (2003) In vivo mechanisms of hydroxyapatite ceramic degradation by osteoclasts, fine structural microscopy. *J Biomed Mater Res A* 67A:713–718
469. Ajaxon I, Öhman C, Persson C (2015) Long-term in vitro degradation of a high-strength brushite cement in water, PBS, and serum solution. *BioMed Res Int* 2015:575079
470. Grossardt C, Ewald A, Grover LM, Barralet JE, Gbureck U (2010) Passive and active in vitro resorption of calcium and magnesium phosphate cements by osteoclastic cells. *Tissue Eng A* 16:3687–3695
471. Ooms EM, Wolke JGC, van der Waerden JP, Jansen JA (2002) Trabecular bone response to injectable calcium phosphate (Ca-P) cement. *J Biomed Mater Res* 61:9–18
472. Theiss F, Apelt D, Brand B, Kutter A, Zlinszky K, Bohner M, Matter S, Frei C, Auer JA, von Rechenberg B (2005) Biocompatibility and resorption of a brushite calcium phosphate cement. *Biomaterials* 26:4383–4394
473. Heymann D, Pradal G, Benahmad M (1999) Cellular mechanisms of calcium phosphate degradation. *Histol Histopathol* 14:871–877
474. Kanter B, Geffers M, Ignatius A, Gbureck U (2014) Control of in vivo mineral bone cement degradation. *Acta Biomater* 10:3279–3287
475. Penel LN, van Landuyt P, Flautre B, Hardouin P, Lemaître J, Leroy G (1999) Raman microspectrometry studies of brushite cement: in vivo evolution in a sheep model. *Bone* 25(Suppl 2):81S–84S
476. Dorozhkin SV (1999) Inorganic chemistry of the dissolution phenomenon, the dissolution mechanism of calcium apatites at the atomic (ionic) level. *Comment Inorg Chem* 20:285–299
477. Dorozhkin SV (2012b) Dissolution mechanism of calcium apatites in acids: a review of literature. *World J Methodol* 2:1–17

478. Alge DL, Goebel WS, Chu TMG (2013) Effects of DCPD cement chemistry on degradation properties and cytocompatibility: comparison of MCPM/ $\beta$ -TCP and MCPM/HA formulations. *Biomed Mater* 8:025010
479. Knabe C, Driessens FCM, Planell JA, Gildenhaar R, Berger G, Reif D, Fitzner R, Radlanski RJ, Gross U (2000) Evaluation of calcium phosphates and experimental calcium phosphate bone cements using osteogenic cultures. *J Biomed Mater Res* 52:498–508
480. Teitelbaum SL (2000) Bone resorption by osteoclasts. *Science* 289:1504–1508
481. Mostov K, Werb Z (1997) Journey across the osteoclast. *Science* 276:219–220
482. Rodan GA, Martin TJ (2000) Therapeutic approaches to bone diseases. *Science* 289:1508–1514
483. Sugawara A, Asaoka K, Ding SJ (2013) Calcium phosphate-based cements: clinical needs and recent progress. *J Mater Chem B* 1:1081–1089
484. Midy V, Hollande E, Rey C, Dard M, Plouët J (2001) Adsorption of vascular endothelial growth factor to two different apatitic materials and its release. *J Mater Sci Mater Med* 12:293–298
485. Hossain M, Irwin R, Baumann MJ, McCabe LR (2005) Hepatocyte growth factor (HGF) adsorption kinetics and enhancement of osteoblast differentiation on hydroxyapatite surfaces. *Biomaterials* 26:2595–2602
486. Sun L, Berndt CC, Gross KA, Kucuk A (2001) Material fundamentals and clinical performance of plasma-sprayed hydroxyapatite coatings, a review. *J Biomed Mater Res B Appl Biomater* 58:570–592
487. Renault F, Chabriere E, Andrieu JP, Dublet B, Masson P, Rochu D (2006) Tandem purification of two HDL-associated partner proteins in human plasma, paraoxonase (PON1) and phosphate binding protein (HPBP) using hydroxyapatite chromatography. *J Chromatogr B* 836:15–21
488. Yoshitake T, Kobayashi S, Ogawa T, Okuyama T (2006) Hydroxyapatite chromatography of guanidine denatured proteins: 1 guanidine containing phosphate buffer system. *Chromatography* 27:19–26
489. Ooms EM, Egglezos EA, Wolke JGC, Jansen JA (2003a) Soft-tissue response to injectable calcium phosphate cements. *Biomaterials* 24:749–757
490. Ooms EM, Wolke JGC, van de Heuvel MT, Jeschke B, Jansen JA (2003b) Histological evaluation of the bone response to calcium phosphate cement implanted in cortical bone. *Biomaterials* 24:989–1000
491. Kobayashi N, Ong K, Villarraga M, Schwardt J, Wenz R, Togawa D, Fujishiro T, Turner AS, Seim HB III, Bauer TW (2007) Histological and mechanical evaluation of self-setting calcium phosphate cements in a sheep vertebral bone void model. *J Biomed Mater Res A* 81A:838–846
492. Wen CY, Qin L, Lee KM, Chan KM (2009) The use of brushite calcium phosphate cement for enhancement of bone-tendon integration in an anterior cruciate ligament reconstruction rabbit model. *J Biomed Mater Res B Appl Biomater* 89B:466–474
493. Musha Y, Umeda T, Yoshizawa S, Shigemitsu T, Mizutani K, Itatani K (2010) Effects of blood on bone cement made of calcium phosphate: problems and advantages. *J Biomed Mater Res B Appl Biomater* 2010(92B):95–101
494. Altundal S, Gross KA, Ohman C, Engqvist H (2015) Improving the flexural strength test of brushite cement. *Key Eng Mater* 631:67–72
495. Fernández E, Ginebra MP, Bermudez O, Boltong MG, Driessens FCM, Planell JA (1995) Dimensional and thermal behaviour of calcium phosphate cements during setting compared to PMMA bone cements. *J Mater Sci Lett* 14:4–5
496. O'Hara RM, Orr JF, Buchanan FJ, Wilcox RK, Barton DC, Dunne NJ (2012) Development of a bovine collagen-apatitic calcium phosphate cement for potential fracture treatment through vertebroplasty. *Acta Biomater* 8:4043–4052
497. Pittet C, Lemaître J (2000) Mechanical characterization of brushite cements: a Mohr circles approach. *J Biomed Mater Res Appl Biomater* 53:769–780

498. Andrianjatovo H, Jose F, Lemaître J (1996) Effect of  $\beta$ -TCP granulometry on setting time and strength of calcium orthophosphate hydraulic cements. *J Mater Sci Mater Med* 7:34–39
499. Ishikawa K, Takagi S, Chow LC, Ishikawa Y, Eanes ED, Asaoka K (1994) Behavior of a calcium orthophosphate cement in simulated blood plasma in vitro. *Dent Mater* 10:26–32
500. Driessens FCM (1999) Chemistry and applied aspects of calcium orthophosphate bone cements. In: *Concepts and clinical applications of ionic cements*, 15th European conference on biomaterials Arcachon, Bordeaux, France
501. Yamamoto H, Niwa S, Hori M, Hattori T, Sawai K, Aoki S, Hirano M, Takeuchi H (1998) Mechanical strength of calcium phosphate cement in vivo and in vitro. *Biomaterials* 19:1587–1591
502. Morgan EF, Yetkinler DN, Constantz BR, Dauskardt RH (1997) Mechanical properties of carbonated apatite bone mineral substitute: strength, fracture and fatigue behavior. *J Mater Sci Mater Med* 8:559–570
503. Miyazaki K, Horibe T, Antonucci JM, Takagi S, Chow LC (1993a) Polymeric calcium phosphate cements, analysis of reaction products and properties. *Dent Mater* 9:41–45
504. Miyazaki K, Horibe T, Antonucci JM, Takagi S, Chow LC (1993b) Polymeric calcium phosphate cements: setting reaction modifiers. *Dent Mater* 9:46–50
505. dos Santos LA, de Oliveira LC, Rigo ECS, Carrodegua RG, Boschi AO, de Arruda ACF (1999) Influence of polymeric additives on the mechanical properties of  $\alpha$ -tricalcium phosphate cement. *Bone* 25:99S–102S
506. Mickiewicz RA, Mayes AM, Knaack D (2002) Polymer – calcium phosphate cement composites for bone substitutes. *J Biomed Mater Res* 61:581–592
507. Fernández E, Sarda S, Hamcerencu M, Vlad MD, Gel M, Valls S, Torres R, López J (2005c) High-strength apatitic cement by modification with superplasticizers. *Biomaterials* 26:2289–2296
508. Takahashi T, Yamamoto M, Ioku K, Goto S (1997) Relationship between compressive strength and pore structure of hardened cement pastes. *Adv Cement Res* 9:25–30
509. Costantino PD, Friedman CD, Jones K, Chow LC, Sisson GA (1992) Experimental hydroxyapatite cement cranioplasty. *Plast Reconstr Surg* 90:174–185
510. Chow LC, Hirayama S, Takagi S, Parry E (2000) Diametral tensile strength and compressive strength of a calcium phosphate cement, effect of applied pressure. *J Biomed Mater Res Appl Biomater* 53:511–517
511. Barralet JE, Gaunt T, Wright AJ, Gibson IR, Knowles JC (2002b) Effect of porosity reduction by compaction on compressive strength and microstructure of calcium phosphate cement. *J Biomed Mater Res Appl Biomater* 63:1–9
512. Zhang Y, Xu HHK, Takagi S, Chow LC (2006) In situ hardening hydroxyapatite-based scaffold for bone repair. *J Mater Sci Mater Med* 17:437–445
513. Geffers M, Groll J, Gbureck U (2015a) Reinforcement strategies for load-bearing calcium phosphate biocements. *Materials* 8:2700–2717
514. Khairoun I, LeGeros RZ, Daculsi G, Bouler JM, Guicheux J, Gauthier O (2008) Macroporous, resorbable and injectable calcium phosphate-based cements (MCPC) for bone repair: augmentation, regeneration and osteoporosis treatment. US patent No 7351280
515. Speirs AD, Oxland TR, Masri BA, Poursartip A, Duncan CP (2005) Calcium phosphate cement composites in revision hip arthroplasty. *Biomaterials* 26:7310–7318
516. dos Santos LA, Carrodegua RG, Boschi AO, de Arruda ACF (2003a) Fiber-enriched double-setting calcium phosphate bone cement. *J Biomed Mater Res A* 65A:244–250
517. Gbureck U, Spatz K, Thull R (2003b) Improvement of mechanical properties of self-setting calcium phosphate bone cements mixed with different metal oxides. *Mat-Wiss u Werkstofftech* 34:1036–1040
518. Zhang Y, Xu HHK (2005) Effects of synergistic reinforcement and absorbable fiber strength on hydroxyapatite bone cement. *J Biomed Mater Res A* 75A:832–840
519. Buchanan F, Gallagher L, Jack V, Dunne N (2007) Short-fibre reinforcement of calcium phosphate bone cement. *Proc Inst Mech Eng H: J Eng Med* 221:203–212

520. Guo H, Wei J, Song W, Zhang S, Yan Y, Liu C, Xiao T (2012) Wollastonite nanofiber-doped self-setting calcium phosphate bioactive cement for bone tissue regeneration. *Int J Nanomed* 7:3613–3624
521. Srakaew N, Rattanachan ST (2012) Effect of apatite wollastonite glass ceramic addition on brushite bone cement containing chitosan. *Adv Mater Res* 506:106–109
522. Mohammadi M, Hesaraki S, Hafezi-Ardakani M (2014) Investigation of biocompatible nano-sized materials for development of strong calcium phosphate bone cement: comparison of nano-titania, nano-silicon carbide and amorphous nano-silica. *Ceram Int* 40:8377–8387
523. Wu TY, Zhou ZB, He ZW, Ren WP, Yu XW, Huang Y (2014) Reinforcement of a new calcium phosphate cement with RGD-chitosan-fiber. *J Biomed Mater Res A* 102A:68–75
524. Maenz S, Kunisch E, Mühlstädt M, Böhm A, Kopsch V, Bossert J, Kinne RW, Jandt KD (2014) Enhanced mechanical properties of a novel, injectable, fiber-reinforced brushite cement. *J Mech Behav Biomed Mater* 39:328–338
525. Motisuke M, Santos VR, Bazanini NC, Bertran CA (2014) Apatite bone cement reinforced with calcium silicate fibers. *J Mater Sci Mater Med* 25:2357–2363
526. Maenz S, Hennig M, Mühlstädt M, Kunisch E, Bungartz M, Brinkmann O, Bossert J, Kinne RW, Jandt KD (2016) Effects of oxygen plasma treatment on interfacial shear strength and post-peak residual strength of a PLGA fiber-reinforced brushite cement. *J Mech Behav Biomed Mater* 57:347–358
527. Yu W, Wang X, Zhao J, Tang Q, Wang M, Ning X (2015) Preparation and mechanical properties of reinforced hydroxyapatite bone cement with nano-ZrO<sub>2</sub>. *Ceram Int* 41:10600–10606
528. Wang X, Ye J, Wang Y, Chen L (2007d) Reinforcement of calcium phosphate cement by biomineralized carbon nanotube. *J Am Ceram Soc* 90:962–964
529. Chew KK, Low KL, Zein SHS, McPhail DS, Gerhardt LC, Roether JA, Boccaccini AR (2011) Reinforcement of calcium phosphate cement with multi-walled carbon nanotubes and bovine serum albumin for injectable bone substitute applications. *J Mech Behav Biomed Mater* 4:331–339
530. Low KL, Tan SH, Zein SHS, McPhail DS, Boccaccini AR (2011) Optimization of the mechanical properties of calcium phosphate/multi-walled carbon nanotubes/bovine serum albumin composites using response surface methodology. *J Mater Des* 32:3312–3319
531. Lin B, Zhou H, Leaman DW, Goel VK, Agarwal AK, Bhaduri SB (2014) Sustained release of small molecules from carbon nanotube-reinforced monetite calcium phosphate cement. *Mater Sci Eng C* 43:92–96
532. Vélez D, Arita IH, García-Garduño MV, Castaño VM (1994) Synthesis and characterization of a hydroxyapatite-zinc oxide-polyacrylic acid concrete. *Mater Lett* 19:309–315
533. <http://en.wikipedia.org/wiki/Concrete>, Accessed in Dec 2016
534. Tadier S, Galea L, Charbonnier B, Baroud G, Bohner M (2014) Phase and size separations occurring during the injection of model pastes composed of  $\beta$ -tricalcium phosphate powder, glass beads and aqueous solutions. *Acta Biomater* 10:2259–2268
535. Dickens-Venz SH, Takagi S, Chow LC, Bowen RL, Johnston AD, Dickens B (1994) Physical and chemical properties of resin-reinforced calcium phosphate cements. *Dent Mater* 10:100–106
536. Xu HHK, Eichmiller FC, Barndt PR (2001a) Effects of fiber length and volume fraction on the reinforcement of calcium phosphate cement. *J Mater Sci Mater Med* 12:57–65
537. Alge DL, Bennett J, Treasure T, Voytik-Harbin S, Goebel WS, Chu TMG (2012b) Poly(propylene fumarate) reinforced dicalcium phosphate dihydrate cement composites for bone tissue engineering. *J Biomed Mater Res A* 100A:1792–1802
538. Takagi S, Chow LC, Hirayama S, Eichmiller FC (2003a) Properties of elastomeric calcium phosphate cement-chitosan composites. *Dent Mater* 19:797–804
539. Xu HHK, Quinn JB, Takagi S, Chow LC (2004a) Synergistic reinforcement of in situ hardening calcium phosphate composite scaffold for bone tissue engineering. *Biomaterials* 25:1029–1037



540. Yokoyama A, Yamamoto S, Kawasaki T, Kohgo T NM (2002) Development of calcium phosphate cement using chitosan and citric acid for bone substitute materials. *Biomaterials* 23:1091–1101
541. Xu HHK, Simon CG Jr (2005) Fast setting calcium phosphate-chitosan scaffold: mechanical properties and biocompatibility. *Biomaterials* 26:1337–1348
542. Sun L, Xu HHK, Takagi S, Chow LC (2007) Fast setting calcium phosphate cement – chitosan composite, mechanical properties and dissolution rates. *J Biomater Appl* 21:299–316
543. Pan ZH, Jiang PP, Fan QY, Ma B, Cai HP (2007) Mechanical and biocompatible influences of chitosan fiber and gelatin on calcium phosphate cement. *J Biomed Mater Res B Appl Biomater* 82B:246–252
544. Liu H, LiH CW, Yang Y, Zhu M, Zhou C (2006b) Novel injectable calcium phosphate/chitosan composites for bone substitute materials. *Acta Biomater* 2:557–565
545. Pan ZH, Cai HP, Jiang PP, Fan QY (2006) Properties of a calcium phosphate cement synergistically reinforced by chitosan fiber and gelatin. *J Polymer Res* 13:323–327
546. Weir MD, Xu HHK (2008) High-strength, in situ-setting calcium phosphate composite with protein release. *J Biomed Mater Res A* 85A:388–396
547. Lian Q, LiDC HJK, Wang Z (2008) Mechanical properties and in-vivo performance of calcium phosphate cement – chitosan fibre composite. *Proc Inst Mech Eng H: J Eng Med* 222:347–353
548. Wang X, Chen L, Xiang H, Ye J (2007e) Influence of anti-washout agents on the rheological properties and injectability of a calcium phosphate cement. *J Biomed Mater Res B Appl Biomater* 81B:410–418
549. Tanaka S, Kishi T, Shimogoryo R, Matsuya S, Ishikawa K (2003) Biopex acquires anti-washout properties by adding sodium alginate into its liquid phase. *Dent Mater J* 22:301–312
550. Sariibrahimoglu K, Leeuwenburgh SCG, Wolke JGC, Yubao L, Jansen JA (2012) Effect of calcium carbonate on hardening, physicochemical properties, and in vitro degradation of injectable calcium phosphate cements. *J Biomed Mater Res A* 100A:712–719
551. Lin J, Zhang S, Chen T, Liu C, Lin S, Tian X (2006) Calcium phosphate cement reinforced by polypeptide copolymers. *J Biomed Mater Res B Appl Biomater* 76B:432–439
552. Liu H, Guan Y, Wei D, Gao C, Yang H, Yang L (2016) Reinforcement of injectable calcium phosphate cement by gelatinized starches. *J Biomed Mater Res B Appl Biomater* 104:615–625
553. Lopez-Heredia MA, Pattipeilohy J, Hsu S, Grykien M, van der Weijden B, Leeuwenburgh SCG, Salmon P, Wolke JGC, Jansen JA (2013) Bulk physicochemical, interconnectivity, and mechanical properties of calcium phosphate cements-fibrin glue composites for bone substitute applications. *J Biomed Mater Res A* 101A:478–490
554. Krüger R, Seitz JM, Ewald A, Bach FW, Groll J (2013) Strong and tough magnesium wire reinforced phosphate cement composites for load-bearing bone replacement. *J Mech Behav Biomed Mater* 20:36–44
555. Miyamoto Y, Ishikawa K, Takechi M, Toh T, Yuasa T, Nagayama M, Suzuki K (1998) Basic properties of calcium phosphate cement containing atelocollagen in its liquid or powder phases. *Biomaterials* 19:707–715
556. Knepper-Nicolai B, Reinstorf A, Hofinger I, Flade K, Wenz R, Pompe W (2002) Influence of osteocalcin and collagen I on the mechanical and biological properties of Biocement D®. *Biomol Eng* 19:227–231
557. Hempel U, Reinstorf A, Poppe M, Fischer U, Gelinsky M, Pompe W, Wenzel KW (2004) Proliferation and differentiation of osteoblasts on Biocement D® modified with collagen type I and citric acid. *J Biomed Mater Res B Appl Biomater* 71B:130–143
558. Reinstorf A, Ruhnnow M, Gelinsky M, Pompe W, Hempel U, Wenzel KW, Simon P (2004) Phosphoserine – a convenient compound for modification of calcium phosphate bone cement collagen composites. *J Mater Sci Mater Med* 15:451–455

559. Otsuka M, Kuninaga T, Otsuka K, Higuchi WI (2006) Effect of nanostructure on biodegradation behaviors of self-setting apatite/collagen composite cements containing vitamin K<sub>2</sub> in rats. *J Biomed Mater Res B Appl Biomater* 79B:176–184
560. Moreau JL, Weir MD, Xu HHK (2009) Self-setting collagen – calcium phosphate bone cement: mechanical and cellular properties. *J Biomed Mater Res A* 91A:605–613
561. Otsuka M, Nakagawa H, Ito A, Higuchi WI (2010) Effect of geometrical structure on drug release rate of a three-dimensionally perforated porous apatite/collagen composite cement. *J Pharm Sci* 99:286–292
562. Dunne N, O’Gara R, Buchanan F, Orr J (2012) Effect of liquid/powder ratio on the setting, handling and mechanical properties of collagen-apatitic cements. *Key Eng Mater* 493–494:415–421
563. Perez RA, Ginebra MP (2013) Injectable collagen/ $\alpha$ -tricalcium phosphate cement: collagen-mineral phase interactions and cell response. *J Mater Sci Mater Med* 24:381–393
564. Palmer I, Nelson J, Schatton W, Dunne NJ, Buchanan FJ, Clarke SA (2016) Biocompatibility of calcium phosphate bone cement with optimized mechanical properties. *J Biomed Mater Res B Appl Biomater* 104:308–315
565. Gbureck U, Spatz K, Thull R, Barralet JE (2005d) Rheological enhancement of mechanically activated  $\alpha$ -tricalcium phosphate cements. *J Biomed Mater Res B Appl Biomater* 73B:1–6
566. Canal C, Ginebra MP (2011) Fibre-reinforced calcium phosphate cements: a review. *J Mech Behav Biomed Mater* 4:1658–1671
567. Xu HHK, Eichmiller FC, Giuseppetti AA (2000) Reinforcement of a self-setting calcium phosphate cement with different fibers. *J Biomed Mater Res* 52:107–114
568. Xu HHK, Quinn JB, Takagi S, Chow LC, Eichmiller FC (2001b) Strong and macroporous calcium phosphate cement: effects of porosity and fiber reinforcement on mechanical properties. *J Biomed Mater Res* 57:457–466
569. dos Santos LA, Carrodegus RG, Boschi AO, de Arruda ACF (2003b) Dual-setting calcium phosphate cement modified with ammonium polyacrylate. *Artif Organs* 27:412–418
570. Rigo ECS, dos Santos LA, Vercik LCO, Carrodegus RG, Boschi AO (2007)  $\alpha$ -tricalcium phosphate- and tetracalcium phosphate/dicalcium phosphate-based dual setting cements. *Lat Am Appl Res* 37:267–274
571. Barounian M, Hesaraki S, Kazemzadeh A (2012) Development of strong and bioactive calcium phosphate cement as a light-cure organic-inorganic hybrid. *J Mater Sci Mater Med* 23:1569–1581
572. Christel T, Kuhlmann M, Vorndran E, Groll J, Gbureck U (2013) Dual setting  $\alpha$ -tricalcium phosphate cements. *J Mater Sci Mater Med* 24:573–581
573. Geffers M, Barralet JE, Groll J, Gbureck U (2015b) Dual-setting brushite–silica gel cements. *Acta Biomater* 11:467–476
574. Hurlé K, Christel T, Gbureck U, Moseke C, Neubauer J, Goetz-Neunhoffer F (2016) Reaction kinetics of dual setting  $\alpha$ -tricalcium phosphate cements. *J Mater Sci Mater Med* 27:1
575. dos Santos LA, de Oliveira LC, da Silva Rigo EC, Carrodéguas RG, Boschi AO, de Arruda ACF (2000) Fiber reinforced calcium phosphate cement. *Artif Organs* 24:212–216
576. Ogasawara T, Sawamura T, Maeda H, Obata A, Hirata H, Kasuga T (2016) Enhancing the mechanical properties of calcium phosphate cements using short-length polyhydroxyalkanoate fibers. *J Ceram Soc Jpn* 124:180–183
577. Liu CS, Chen CW, Ducheyne P (2008a) In vitro surface reaction layer formation and dissolution of calcium phosphate cement-bioactive glass composites. *Biomed Mater* 3:034111. (11 pages)
578. Renno ACM, van de Watering FCJ, Nejadnik MR, Crovace MC, Zanotto ED, Wolke JGC, Jansen JA, van den Beucken JJJP (2013a) Incorporation of bioactive glass in calcium phosphate cement: an evaluation. *Acta Biomater* 9:5728–5739
579. Renno ACM, Nejadnik MR, van de Watering FCJ, Crovace MC, Zanotto ED, Hoefnagels JPM, Wolke JGC, Jansen JA, van den Beucken JJJP (2013b) Incorporation of bioactive glass

- in calcium phosphate cement: material characterization and in vitro degradation. *J Biomed Mater Res A* 101A:2365–2373
580. Yu L, Li Y, Zhao K, Tang Y, Cheng Z, Chen J, Zang Y, Wu J, Kong L, Liu S, Lei W, Wu Z (2013) A novel injectable calcium phosphate cement-bioactive glass composite for bone regeneration. *PLoS ONE* 8:e62570
581. Alge DL, Chu TMG (2010) Calcium phosphate cement reinforcement by polymer infiltration and in situ curing: a method for 3D scaffold reinforcement. *J Biomed Mater Res A* 94A:547–555
582. Julien M, Khairoun I, LeGeros RZ, Delplace S, Pilet P, Weiss P, Daculsi G, Bouler JM, Guicheux J (2007) Physico-chemical-mechanical and in vitro biological properties of calcium phosphate cements with doped amorphous calcium phosphates. *Biomaterials* 28:956–965
583. Lemaître J, Munting E, Mirtchi AA (1992) Setting, hardening and resorption of calcium phosphate hydraulic cements. *Rev Stomatol Chir Maxillofac* 93:163–165
584. Müller FA, Gbureck U, Kasuga T, Mizutani Y, Barralet JE, Lohbauer U (2007) Whisker-reinforced calcium phosphate cements. *J Am Ceram Soc* 90:3694–3697
585. Nakagawa A, Matsuya S, Takeuchi A, Ishikawa K (2007) Comparison of the effects of added  $\alpha$ - and  $\beta$ -tricalcium phosphate on the basic properties of apatite cement. *Dent Mater J* 26:342–347
586. Gu T, Shi H, Ye J (2012) Reinforcement of calcium phosphate cement by incorporating with high-strength  $\beta$ -tricalcium phosphate aggregates. *J Biomed Mater Res B Appl Biomater* 100B:350–359
587. Zhao P, Zhao S, Zhao T, Ren X, Wang F, Chen X (2012) Hydroxyapatite whisker effect on strength of calcium phosphate bone cement. *Adv Mater Res* 534:30–33
588. Chu B, Xiong J, Wang MB, Li XL, She ZD (2013) Study on hydroxyapatite fibers with strontium reinforced calcium phosphate cement. *Adv Mater Res* 788:119–126
589. Srakaew N, Rattanachan ST (2014) The pH-dependent properties of the biphasic calcium phosphate for bone cements. *J Biomim Biomater Biomed Eng* 21:3–16
590. Sarkar SK, Lee BY, Padalhin AR, Sarker A, Carpena N, Kim B, Paul K, Choi HJ, Bae SH, Lee BT (2016) Brushite-based calcium phosphate cement with multichannel hydroxyapatite granule loading for improved bone regeneration. *J Biomater Appl* 30:823–837
591. Gisep A, Wieling R, Bohner M, Matter S, Schneider E, Rahn B (2003) Resorption patterns of calcium-phosphate cements in bone. *J Biomed Mater Res A* 66A:532–540
592. van den Vreken NMF, Pieters IY, Declercq HA, Cornelissen MJ, Verbeeck RMH (2010) Characterization of calcium phosphate cements modified by addition of amorphous calcium phosphate. *Acta Biomater* 6:617–625
593. Zhou L, Yan JL, Hu CJ (2007) Degradation of bone repairing composite of calcium polyphosphate fiber, calcium phosphate cement and micromorselized bone in vitro. *J Clin Rehabil Tiss Eng Res* 11:33–36
594. Xu LX, Shi XT, Wang YP, Shi ZL (2009) Mechanical effect of calcium polyphosphate fiber on reinforcing calcium phosphate bone cement composites. *J Clin Rehabil Tiss Eng Res* 13:7474–7476
595. Krüger R, Groll J (2012) Fiber reinforced calcium phosphate cements – on the way to degradable load bearing bone substitutes? *Biomaterials* 33:5887–5900
596. Xu HHK, Quinn JB (2001) Whisker-reinforced bioactive composites containing calcium phosphate cement fillers: effects of filler ratio and surface treatments on mechanical properties. *J Biomed Mater Res* 57:165–174
597. Espigares I, Elvira C, Mano JF, Vázquez B, San Román J, Reis RL (2002) New partially degradable and bioactive acrylic bone cements based on starch blends and ceramic fillers. *Biomaterials* 23:1883–1895
598. Pek YS, Kurisawa M, Gao S, Chung JE, Ying JY (2009) The development of a nanocrystalline apatite reinforced crosslinked hyaluronic acid-tyramine composite as an injectable bone cement. *Biomaterials* 30:822–828

599. Lopez-Heredia MA, Sa Y, Salmon P, de Wijn JR, Wolke JGC, Jansen JA (2012c) Bulk properties and bioactivity assessment of porous polymethylmethacrylate cement loaded with calcium phosphates under simulated physiological conditions. *Acta Biomater* 8:3120–3127
600. Jayasree R, Kumar TSS (2015) Acrylic cement formulations modified with calcium deficient apatite nanoparticles for orthopaedic applications. *J Compos Mater* 49:2921–2933
601. Sa Y, Yang F, de Wijn JR, Wang Y, Wolke JGC, Jansen JA (2016) Physicochemical properties and mineralization assessment of porous polymethylmethacrylate cement loaded with hydroxyapatite in simulated body fluid. *Mater Sci Eng C* 61:190–198
602. Baldino L, Naddeo F, Cardea S, Naddeo A, Reverchon E (2015) FEM modeling of the reinforcement mechanism of hydroxyapatite in PLLA scaffolds produced by supercritical drying, for tissue engineering applications. *J Mech Behav Biomed Mater* 51:225–236
603. Claes L, Höllen I, Ignatius A (1997) Resorbable bone cements. *Orthopäde* 26:459–462
604. Jansen JA, de Ruijter JE, Schaeken HG, van der Waerden JPC, Planell JA, Driessens FCM (1995) Evaluation of tricalciumphosphate/hydroxyapatite cement for tooth replacement, an experimental animal study. *J Mater Sci Mater Med* 6:653–657
605. Larsson S, Bauer TW (2002) Use of injectable calcium phosphate cement for fracture fixation: a review. *Clin Orthop Rel Res* 395:23–32
606. Oshtory R, Lindsey DP, Giori NJ, Mirza FM (2010) Bioabsorbable tricalcium phosphate bone cement strengthens fixation of suture anchors. *Clin Orthop Rel Res* 468:3406–3412
607. Gbureck U, Knappe O, Hofmann N, Barralet JE (2007a) Antimicrobial properties of nanocrystalline tetracalcium phosphate cements. *J Biomed Mater Res B Appl Biomater* 83B:132–137
608. Sethuraman S, Nair LS, El-Amin S, Nguyen MTN, Greish YE, Bender JD, Brown PW, Allcock HR, Laurencin CT (2007) Novel low temperature setting nanocrystalline calcium phosphate cements for bone repair: osteoblast cellular response and gene expression studies. *J Biomed Mater Res A* 82A:884–891
609. Link DP, van den Dolder J, Wolke JGC, Jansen JA (2007) The cytocompatibility and early osteogenic characteristics of an injectable calcium phosphate cement. *Tissue Eng* 13:493–500
610. Oda H, Nakamura K, Matsushita T, Yamamoto S, Ishibashi H, Yamazaki T, Morimoto S (2006) Clinical use of a newly developed calcium phosphate cement (XSB-671D). *J Orthop Sci* 11:167–174
611. Braun C, Rahn B, Fulmer MT, Steiner A, Gisepp A (2006) Intra-articular calcium phosphate cement, its fate and impact on joint tissues in a rabbit model. *J Biomed Mater Res B Appl Biomater* 79B:151–158
612. Krell KV, Wefel JS (1984) A calcium phosphate cement root canal sealer – scanning electron microscopic analysis. *J Endod* 10:571–576
613. Krell KV, Madison S (1985) Comparison of apical leakage in teeth obturated with a calcium phosphate cement or Grossman's cement using lateral condensation. *J Endod* 8:336–339
614. Costantino P, Friedman C, Jones K, Chow LC, Pelzer H, Sisson G (1991) Hydroxyapatite cement I Basic chemistry and histologic properties. *Arch Otolaryngol Head Neck Surg* 117:379–384
615. Hong YC, Wang JT, Hong CY, Brown WE, Chow CY (1991) The periapical tissue reactions to a calcium phosphate cement in the teeth of monkeys. *J Biomed Mater Res* 25:485–498
616. Sugawara A, Fujikawa K, Kusama K, Nishiyama M, Murai S, Takagi S, Chow LC (2002) Histopathologic reaction of calcium phosphate cement for alveolar ridge augmentation. *J Biomed Mater Res* 61:47–52
617. Fujikawa K, Sugawara A, Kusama K, Nishiyama M, Murai S, Takagi S, Chow LC (2002) Fluorescent labeling analysis and electron probe microanalysis for alveolar ridge augmentation using calcium phosphate cement. *Dent Mater J* 21:296–305
618. Comuzzi L, Ooms E, Jansen JA (2002) Injectable calcium phosphate cement as a filler for bone defects around oral implants, an experimental study in goats. *Clin Oral Implants Res* 13:304–311

619. Shirakata Y, Oda S, Kinoshita A, Kikuchi S TH, Ishikawa I (2002) Histocompatible healing of periodontal defects after application of injectable calcium phosphate bone cement A preliminary study in dogs. *J Periodontol* 73:1043–1053
620. Lee SK, Lee SK, Lee SI, Park JH, Jang JH, Kim HW, Kim EC (2010a) Effect of calcium phosphate cements on growth and odontoblastic differentiation in human dental pulp cells. *J Endod* 36:1537–1542
621. Chaung HM, Hong CH, Chiang CP, Lin SK, Kuo YS, Lan WH, Hsieh CC (1996) Comparison of calcium phosphate cement mixture and pure calcium hydroxide as direct pulp-capping agents. *J Formos Med Assoc* 95:545–550
622. Zhang W, Walboomers XF, Jansen JA (2008) The formation of tertiary dentin after pulp capping with a calcium phosphate cement, loaded with PLGA microparticles containing TGF- $\beta$ 1. *J Biomed Mater Res A* 85A:439–444
623. Coutinho VB, Silva JA, Santos LA, Fook MVL (2012) Primary implant stability in calcium phosphate cement: clinical, radiographic and histological analysis. *Mater Sci Forum* 727–728:1131–1135
624. Sugawara A, Chow LC, Takagi S, Chohayeb H (1990) In vitro evaluation of the sealing ability of a calcium phosphate cement when used as a root canal sealer-filler. *J Endod* 16:162–165
625. Noetzel J, Özer K, Reissbauer BH, Anil A, Rössler R, Neumann K, Kielbassa AM (2006) Tissue responses to an experimental calcium phosphate cement and mineral trioxide aggregate as materials for furcation perforation repair, a histological study in dogs. *Clin Oral Invest* 10:77–83
626. Tagaya M, Goto H, Iinuma M, Wakamatsu N, Tamura Y, Doi Y (2005) Development of self-setting Te-Cp/ $\alpha$ -TCP cement for pulpotomy. *Dent Mater J* 24:555–561
627. Arisan V, Anil A, Wolke JG, Özer K (2010) The effect of injectable calcium phosphate cement on bone anchorage of titanium implants: an experimental feasibility study in dogs. *Int J Oral Maxillofac Surg* 39:463–468
628. Dorozhkin SV (2016b) Calcium orthophosphates (CaPO<sub>4</sub>) and dentistry. *Bioceram Dev Appl* 6:96
629. Aral A, Yalçın S, Karabuda ZC, Anil A, Jansen JA, Mutlu Z (2008) Injectable calcium phosphate cement as a graft material for maxillary sinus augmentation: an experimental pilot study. *Clin Oral Implants Res* 19:612–617
630. Sliindo ML, Costantino PD, Friedman CD, Chow LC (1993) Facial skeletal augmentation using hydroxyapatite cement cranioplasty. *Arch Otolaryngol Head Neck Surg* 119:185–190
631. Bifano CA, Edgin WA, Colleton C, Bifano SL, Constantino PD (1998) Preliminary evaluation of hydroxyapatite cement as an augmentation device in the edentulous atrophic canine mandible. *Oral Surg* 85:512–516
632. Ciprandi MTO, Primo BT, Gassen HT, Closs LQ, Hernandez PAG, Silva AN Jr (2012) Calcium phosphate cement in orbital reconstructions. *J Craniofac Surg* 23:145–148
633. Friedman CD, Constantino PD, Jones K, Chow LC, Pelzer H, Sisson G (1991) Hydroxyapatite cement II Obliteration and reconstruction of the cat frontal sinus. *Arch Otolaryngol Head Neck Surg* 117:385–389
634. Sinikovic B, Kramer FJ, Swennen G, Lubbers HT, Dempf R (2007) Reconstruction of orbital wall defects with calcium phosphate cement: clinical and histological findings in a sheep model. *Int J Oral Maxillofac Surg* 36:54–61
635. Smartt JM, Karmacharya J, Gannon FH, Ong G, Jackson O, Bartlett SP, Poser RD, Kirschner RE (2005) Repair of the immature and mature craniofacial skeleton with a carbonated calcium phosphate cement: assessment of biocompatibility, osteoconductivity and remodeling capacity. *Plast Reconstr Surg* 115:1642–1650
636. Reddi SP, Stevens MR, Kline SN, Villanueva P (1999) Hydroxyapatite cement in craniofacial trauma surgery, indications and early experience. *J Cran Maxillofac Trauma* 5:7–12
637. Friedman CD, Costantino PD, Synderman CH, Chow LC, Takagi S (2000) Reconstruction of the frontal sinus and frontofacial skeleton with hydroxyapatite cement. *Arch Facial Plast Surg* 2:124–129

638. Kuemmerle JM, Oberle A, Oechslin C, Bohner M, Frei C, Boecken I, von Rechenberg B (2005) Assessment of the suitability of a new brushite calcium phosphate cement for cranioplasty – an experimental study in sheep. *J Cran Maxillofac Surg* 33:37–44
639. Luaces-Rey R, García-Rozado A, Crespo-Escudero JL, Seijas BP, Arenaz-Búa J, López-Cedrún JL (2009) Use of carbonated calcium phosphate bone cement and resorbable plates for the treatment of frontal sinus fractures: two case reports. *J Plastic Reconstr Aesthetic Surg* 62:272–273
640. Tamimi F, Torres J, Cabarcos EL, Bassett DC, Habibovic P, Luceron E, Barralet JE (2009) Minimally invasive maxillofacial vertical bone augmentation using brushite based cements. *Biomaterials* 30:208–216
641. Lee DW, Kim JY, Lew DH (2010b) Use of rapidly hardening hydroxyapatite cement for facial contouring surgery. *J Craniofac Surg* 21:1084–1088
642. Singh KA, Burstein FD, Williams JK (2010) Use of hydroxyapatite cement in pediatric craniofacial reconstructive surgery: strategies for avoiding complications. *J Craniofac Surg* 21:1130–1135
643. Bambakidis NC, Munyon C, Ko A, Selman WR, Megerian CA (2010) A novel method of translabyrinthine cranioplasty using hydroxyapatite cement and titanium mesh: a technical report. *Skull Base* 20:157–161
644. Abe T, Anan M, Kamida T, Fujiki M (2009) Surgical technique for anterior skull base reconstruction using hydroxyapatite cement and titanium mesh. *Acta Neurochirur* 151:1337–1338
645. Sanada Y, Fujinaka T, Yoshimine T, Kato A (2011) Optimal reconstruction of the bony defect after frontotemporal craniotomy with hydroxyapatite cement. *J Clin Neurosci* 18:280–282
646. Araki K, Tomifuji M, Suzuki H, Shiotani A (2012) Vocal fold injection with calcium phosphate cement (BIOPEX). *Jpn J Logop Phoniatr* 53:187–193
647. Chung SB, Nam DH, NamPark K, Kim JH, Kong DS (2012) Injectable hydroxyapatite cement patch as an on-lay graft for the sellar reconstructions following endoscopic endonasal approach. *Acta Neurochir* 154:659–664
648. Benson AG, Djalilian HR (2009) Complications of hydroxyapatite bone cement reconstruction of retrosigmoid craniotomy: two cases. *Ear Nose Throat J* 88:E1–E4
649. Wong RK, Gandolfi BM, St-Hilaire H, Wise MW, Moses M (2011) Complications of hydroxyapatite bone cement in secondary pediatric craniofacial reconstruction. *J Craniofac Surg* 22:247–251
650. Liverneaux P (2005) Osteoporotic distal radius curettage-filling with an injectable calcium phosphate cement A cadaveric study. *Eur J Orthop Surg Traumatol* 15:1–6
651. Liverneaux P, Vernet P, Robert C, Diacono P (2006) Cement pinning of osteoporotic distal radius fractures with an injectable calcium phosphate bone substitute, report of 6 cases. *Eur J Orthop Surg Traumatol* 16:10–16
652. Thordarson D, Hedman T, Yetkinler D, Eskander E, Lawrence T, Poser R (1999) Superior compressive strength of a calcaneal fracture construct augmented with remodelable cancellous bone cement. *J Bone Joint Surg Am* 81A:239–246
653. Stankewich CJ, Swiontkowski MF, Tencer AF, Yetkinler DN, Poser RD (1996) Augmentation of femoral neck fracture fixation with an injectable calcium-phosphate bone mineral cement. *J Orthop Res* 14:786–793
654. Goodman S, Bauer T, Carter D, Casteleyn PP, Goldstein SA, Kyle RF, Larsson S, Stankewich CJ, Swiontkowski MF, Tencer AF, Yetkinler DN, Poser RD (1998) Norian SRS® cement augmentation in hip fracture treatment. *Clin Orthop Rel Res* 348:42–50
655. Bai B, Jazrawi L, Kummer F, Spivak J (1999) The use of an injectable, biodegradable calcium orthophosphate bone substitute for the prophylactic augmentation of osteoporotic vertebrae and the management of vertebral compression fractures. *Spine* 24:1521–1526
656. Ryf C, Goldhahn S, Radziejowski M, Blauth M, Hanson B (2009) A new injectable brushite cement: first results in distal radius and proximal tibia fractures. *Eur J Trauma Emerg Surg* 35:389–396

657. Horstmann WG, Verheyen CCPM, Leemans R (2003) An injectable calcium phosphate cement as a bone-graft substitute in the treatment of displaced lateral tibial plateau fractures. *Injury* 34:141–144
658. Simpson D, Keating JF (2004) Outcome of tibial plateau fractures managed with calcium phosphate cement. *Injury* 35:913–918
659. Welch RD, Zhang H, Bronson DG (2003) Experimental tibial plateau fractures augmented with calcium phosphate cement or autologous bone graft. *J Bone Joint Surg Am* 85A:222–231
660. Keating JF, Hajducka CL, Harper J (2003) Minimal internal fixation and calcium-phosphate cement in the treatment of fractures of the tibial plateau. *J Bone Joint Surg Br* 85B:68–73
661. Yin X, Li J, Xu J, Huang Z, Rong K, Fan C (2013) Clinical assessment of calcium phosphate cement to treat tibial plateau fractures. *J Biomater Appl* 28:199–206
662. Moore D, Maitra R, Farjo L, Graziano G, Goldstein S (1997) Restoration of pedicle screw fixation with an in situ setting calcium orthophosphate cement. *Spine* 22:1696–1705
663. Cho W, Wu C, Erkan S, Kang MM, Mehbod AA, Transfeldt EE (2011) The effect on the pullout strength by the timing of pedicle screw insertion after calcium phosphate cement injection. *J Spinal Disord Tech* 24:116–120
664. Mermelstein LE, McLain RF, Yerby SA (1998) Reinforcement of thoracolumbar burst fractures with calcium phosphate cement. *Spine* 23:664–671
665. Mermelstein LE, Chow LC, Friedman C, Crisco J (1996) The reinforcement of cancellous bone screws with calcium orthophosphate cement. *J Orthop Trauma* 10:15–20
666. Stadelmann VA, Bretton E, Terrier A, Procter P, Pioletti DP (2010) Calcium phosphate cement augmentation of cancellous bone screws can compensate for the absence of cortical fixation. *J Biomech* 43:2869–2874
667. Daculsi G, Durand M, Hauger O, Seris E, Borget P, LeGeros R, le Huec JC (2012) Self hardening macroporous biphasic calcium phosphate bone void filler for bone reconstruction; animal study and human data. *Key Eng Mater* 493–494:709–713
668. Liverneaux P, Khallouk R (2006) Calcium phosphate cement in wrist arthrodesis: three cases. *J Orthop Sci* 11:289–293
669. Ooms EM, Wolke JGC, van der Waerden JPCM, Jansen JA (2003c) Use of injectable calcium phosphate cement for the fixation of titanium implants: an experimental study in goats. *J Biomed Mater Res B Appl Biomater* 66B:447–456
670. Strauss EJ, Pahk B, Kummer FJ, Egol K (2007) Calcium phosphate cement augmentation of the femoral neck defect created after dynamic hip screw removal. *J Orthop Trauma* 21:295–300
671. Schildhauer TA, Bennett AP, Wright TM, Lane JM, O’Leary PF (1999) Intravertebral body reconstruction with an injectable in situ-setting carbonated apatite: biomechanical evaluation of a minimally invasive technique. *J Orthop Res* 17:67–72
672. Jansen JA, Ooms E, Verdonschot N, Wolke JGC (2005) Injectable calcium phosphate cement for bone repair and implant fixation. *Orthop Clin North Am* 36:89–95
673. Maestretti G, Cremer C, Otten P, Jakob RP (2007) Prospective study of standalone balloon kyphoplasty with calcium phosphate cement augmentation in traumatic fractures. *Eur Spine J* 16:601–610
674. van der Stok J, Weinans H, Kops N, Siebelt M, Patka P, van Lieshout EM (2013) Properties of commonly used calcium phosphate cements in trauma and orthopaedic surgery. *Injury* 44:1368–1374
675. Hisatome T, Yasunaga Y, Ikuta Y, Fujimoto Y (2002) Effects on articular cartilage of subchondral replacement with polymethylmethacrylate and calcium phosphate cement. *J Biomed Mater Res* 59:490–498
676. Lim TH, Brebach GT, Renner SM, Kim WJ, Kim JG, Lee RE, Andersson GB, An HS (2002) Biomechanical evaluation of an injectable calcium phosphate cement for vertebroplasty. *Spine* 27:1297–1302
677. Belkoff SM, Mathis JM, Jasper LE, Deramond H (2001) An *ex vivo* biomechanical evaluation of a hydroxyapatite cement for use with vertebroplasty. *Spine* 26:1542–1546

678. Heini PF, Berlemann U, Kaufmann M, Lippuner K, Fankhauser C, van Landuyt P (2001) Augmentation of mechanical properties in osteoporotic vertebral bones—a biomechanical investigation of vertebroplasty efficacy with different bone cements. *Eur Spine J* 10:164–171
679. Tomita S, Kin A, Yazu M, Abe M (2003) Biomechanical evaluation of kyphoplasty and vertebroplasty with calcium phosphate cement in a simulated osteoporotic compression fracture. *J Orthop Sci* 8:192–197
680. Libicher M, Hillmeier J, Liegibel U, Sommer U, Pyerin W, Vetter M, Meinzer HP, Grafe I, Meeder P, Nöldge G, Nawroth P, Kasperk C (2006) Osseous integration of calcium phosphate in osteoporotic vertebral fractures after kyphoplasty: initial results from a clinical and experimental pilot study. *Osteoporos Int* 17:1208–1215
681. Khanna AJ, Lee S, Villarraga M, Gimbel J, Steffey D, Schwardt J (2008) Biomechanical evaluation of kyphoplasty with calcium phosphate cement in a 2-functional spinal unit vertebral compression fracture model. *Spine J* 8:770–777
682. Zhu XS, Zhang ZM, Mao HQ, Geng DC, Wang GL, Gan MF, Yang HL (2008) Biomechanics of calcium phosphate cement in vertebroplasty. *J Clin Rehabil Tissue Eng Res* 12:8071–8074
683. Nakano M, Hirano N, Zukawa M, Suzuki K, Hirose J, Kimura T, Kawaguchi Y (2012) Vertebroplasty using calcium phosphate cement for osteoporotic vertebral fractures: Study of outcomes at a minimum follow-up of two years. *Asian Spine J* 6:34–42
684. Otsuka M, Matsuda Y, Suwa Y, Fox JL, Higuchi WI (1994a) A novel skeletal drug-delivery system using a self-setting calcium orthophosphate cement 3 Physicochemical properties and drug-release rate of bovine insulin and bovine albumin. *J Pharm Sci* 83:255–258
685. Bohner M, Lemaître J, van Landuyt P, Zambelli P, Merkle HP, Gander B (1997b) Gentamicin-loaded hydraulic calcium orthophosphate bone cement as antibiotic delivery system. *J Pharm Sci* 86:565–572
686. Kisanuki O, Yajima H, Umeda T, Takakura Y (2007) Experimental study of calcium phosphate cement impregnated with dideoxy-kanamycin. *B J Orthop Sci* 12:281–288
687. McNally A, Sly K, Lin S, Bourges X, Daculsi G (2008) Release of antibiotics from macroporous injectable calcium phosphate cement. *Key Eng Mater* 361–363:359–362
688. Hofmann MP, Mohammed AR, Perrie Y, Gbureck U, Barralet JE (2009) High-strength resorbable brushite bone cement with controlled drug-releasing capabilities. *Acta Biomater* 5:43–49
689. Tamimi F, Torres J, Bettini R, Ruggera F, Rueda C, López-Ponce M, Cabarcos EL (2008) Doxycycline sustained release from brushite cements for the treatment of periodontal diseases. *J Biomed Mater Res A* 85A:707–714
690. Young AM, Ng PYJ, Gbureck U, Nazhat SN, Barralet JE, Hofmann MP (2008) Characterization of chlorhexidine-releasing, fast-setting, brushite bone cements. *Acta Biomater* 4:1081–1088
691. Hesaraki S, Nemati R (2009) Cephalexin-loaded injectable macroporous calcium phosphate bone cement. *J Biomed Mater Res B Appl Biomater* 89B:342–352
692. van Staden AD, Dicks LMT (2012) Calcium orthophosphate-based bone cements (CPCs): applications, antibiotic release and alternatives to antibiotics. *J Appl Biomater Funct Mater* 1:2–11
693. Canal C, Pastorino D, Mestres G, Schuler P, Ginebra MP (2013) Relevance of microstructure for the early antibiotic release of fresh and pre-set calcium phosphate cements. *Acta Biomater* 9:8403–8412
694. Vorndran E, Geffers M, Ewald A, Lemm M, Nies B, Gbureck U (2013) Ready-to-use injectable calcium phosphate bone cement paste as drug carrier. *Acta Biomater* 9:9558–9567
695. Mestres G, Kugiejko K, Pastorino D, Unosson J, Öhman C, Karlsson OM, Ginebra MP, Persson C (2016) Changes in the drug release pattern of fresh and set simvastatin-loaded brushite cement. *Mater Sci Eng C* 58:88–96
696. Cabrejos-Azama J, Alkhraisat MH, Rueda C, Torres J, Pintado C, Blanco L, López-Cabarcos E (2016) Magnesium substitution in brushite cements: efficacy of a new biomaterial loaded with vancomycin for the treatment of *Staphylococcus aureus* infections. *Mater Sci Eng C* 61:72–78



697. Noukrati H, Cazalbou S, Demnati I, Rey C, Barroug A, Combes C (2016) Injectability, microstructure and release properties of sodium fusidate-loaded apatitic cement as a local drug-delivery system. *Mater Sci Eng C* 59:177–184
698. Sakamoto Y, Ochiai H, Ohsugi I, Inoue Y, Yoshimura Y, Kishi K (2013) Mechanical strength and in vitro antibiotic release profile of antibiotic-loaded calcium phosphate bone cement. *J Craniofac Surg* 24:1447–1450
699. Otsuka M, Matsuda Y, Suwa Y, Fox JL, Higuchi WI (1994b) A novel skeletal drug delivery system using a self-setting calcium orthophosphate cement 5 Drug release behavior from a heterogeneous drug-loaded cement containing an anticancer drug. *J Pharm Sci* 83:1565–1568
700. Tahara Y, Ishii Y (2001) Apatite cement containing cis-diamminedi chloroplatinum implanted in rabbit femur for sustained release of the anticancer drug and bone formation. *J Orthop Sci* 6:556–565
701. Tani T, Okada K, Takahashi S, Suzuki N, Shimada Y, Itoi E (2006) Doxorubicin-loaded calcium phosphate cement in the management of bone and soft tissue tumors. *Vivo* 20:55–60
702. Tanzawa Y, Tsuchiya H, Shirai T, Nishida H, Hayashi K, Takeuchi A, Kawahara M, Tomita K (2011) Potentiation of the antitumor effect of calcium phosphate cement containing anticancer drug and caffeine on rat osteosarcoma. *J Orthop Sci* 16:77–84
703. Otsuka M, Matsuda Y, Suwa Y, Fox JL, Higuchi WI (1994c) A novel skeletal drug delivery system using a self-setting calcium orthophosphate cement 2 Physicochemical properties and drug release rate of the cement-containing indomethacin. *J Pharm Sci* 83:611–615
704. Panzavolta S, Torricelli P, Bracci B, Fini M, Bigi A (2009) Alendronate and pamidronate calcium phosphate bone cements, setting properties and in vitro response of osteoblast and osteoclast cells. *J Inorg Biochem* 103:101–106
705. le Nihouannen D, Hacking SA, Gbureck U, Komarova SV, Barralet JE (2008) The use of RANKL-coated brushite cement to stimulate bone remodeling. *Biomaterials* 29:3253–3259
706. Li DX, Fan HS, Zhu XD, Tan YF, Xiao WQ, Lu J, Xiao YM, Chen JY, Zhang XD (2007) Controllable release of salmon-calcitonin in injectable calcium phosphate cement modified by chitosan oligosaccharide and collagen polypeptide. *J Mater Sci Mater Med* 18:2225–2231
707. Kamegai A, Shimamura N, Naitou K, Nagahara K, Kanematsu N, Mori M (1994) Bone formation under the influence of bone morphogenetic protein/self-setting apatite cement composite as delivery system. *Biomed Mater Eng* 4:291–307
708. Fei Z, Hu Y WD, Wu H, Lu R, Bai J, Song H (2008) Preparation and property of a novel bone graft composite consisting of rhBMP-2 loaded PLGA microspheres and calcium phosphate cement. *J Mater Sci Mater Med* 19:1109–1116
709. Ruhé PQ, Kroese-Deutman HC, Wolke JGC, Spauwen PHM, Jansen JA (2004) Bone inductive properties of rhBMP-2 loaded porous calcium phosphate cement implants in cranial defects in rabbits. *Biomaterials* 25:2123–2132
710. Bodde EWH, Boerman OC, Russel FGM, Mikos AG, Spauwen PHM, Jansen JA (2008) The kinetic and biological activity of different loaded rhBMP-2 calcium phosphate cement implants in rats. *J Biomed Mater Res A* 87A:780–791
711. Perrier M, Lu Y, Nemke B, Kobayashi H, Peterson A, Markel M (2008) Acceleration of second and fourth metatarsal fracture healing with recombinant human bone morphogenetic protein-2/calcium phosphate cement in horses. *Vet Surg* 37:648–655
712. Lopez-Heredia MA, Kamphuis BGI, Thüne PC, Öner CF, Jansen JA, Walboomers FX (2011) An injectable calcium phosphate cement for the local delivery of paclitaxel to bone. *Biomaterials* 32:5411–5416
713. Schnitzler V, Fayon F, Despas C, Khairoun I, Mellier C, Rouillon T, Massiot D, Walcarius A, Janvier P, Gauthier O, Montavon G, Bouler JM, Bujoli B (2011) Investigation of alendronate-doped apatitic cements as a potential technology for the prevention of osteoporotic hip fractures: critical influence of the drug introduction mode on the in vitro cement properties. *Acta Biomater* 7:759–770
714. Irbe Z, Loca D, Vempere D, Berzina-Cimdina L (2012) Controlled release of local anesthetic from calcium phosphate bone cements. *Mater Sci Eng C* 32:1690–1694

715. Thein-Han W, Liu J, Xu HHK (2012) Calcium phosphate cement with biofunctional agents and stem cell seeding for dental and craniofacial bone repair. *Dent Mater* 28:1059–1070
716. Otsuka M, Hamada H, Otsuka K, Ohshima H (2012) Dissolution medium responsive simvastatin release from biodegradable apatite cements drug delivery system, -the therapeutically effect and their histology in osteoporosis rats. *Key Eng Mater* 493–494:684–688
717. Ko CL, Chen WC, Chen JC, Wang YH, Shih CJ, Tyan YC, Hung CC, Wang JC (2013) Properties of osteoconductive biomaterials: calcium phosphate cement with different ratios of platelet-rich plasma as identifiers. *Mater Sci Eng C* 33:3537–3544
718. Forouzandeh A, Hesarak S, Zamanian A (2014) The releasing behavior and in vitro osteoinductive evaluations of dexamethasone-loaded porous calcium phosphate cements. *Ceram Int* 40:1081–1091
719. Perez RA, Kim TH, Kim M, Jang JH, Ginebra MP, Kim HW (2013) Calcium phosphate cements loaded with basic fibroblast growth factor: delivery and in vitro cell response. *J Biomed Mater Res A* 101A:923–931
720. Mestres G, Santos CF, Engman L, Persson C, Ott MK (2015) Scavenging effect of Trolox released from brushite cements. *Acta Biomater* 11:459–466
721. Akkineni AR, Luo Y, Schumacher M, Nies B, Lode A, Gelinsky M (2015) 3D plotting of growth factor loaded calcium phosphate cement scaffolds. *Acta Biomater* 27:264–274
722. Meraw SJ, Reeve CM, Lohse CM, Sioussat TM (2000) Treatment of perimplant defects with combination growth factor cement. *J Periodont* 71:8–13
723. Liu H, Zang XF, Zhao ZP, Wang JL, Mi L (2008b) Co-transplantation of exogenous nerve growth factor and calcium phosphate cement composite for repairing rabbit radial bone defects. *J Clin Rehabil Tissue Eng Res* 12:8037–8041
724. Qu XY, Jiang DM, Li M, Zhang DW, Qin JQ, Liu CK (2008) Deproteinized osteoarticular allografts integrated with calcium phosphate cement and recombinant human vascular endothelial cell growth factor plus recombinant human bone morphogenetic protein-2, an immunological study. *J Clin Rehabil Tissue Eng Res* 12:8067–8070
725. Yu T, Ye J, Gao C, Yu L, Wang Y (2010) Synthesis and drug delivery property of calcium phosphate cement with special crystal morphology. *J Am Ceram Soc* 93:1241–1244
726. Stallmann HP, de Roo R, Faber C, Amerongen AVN, Wuisman PIJM (2008) In vivo release of the antimicrobial peptide hLFi-11 from calcium phosphate cement. *J Orthop Res* 26:531–538
727. Sasaki T, Ishibashi Y, Katano H, Nagumo A, Toh S (2005) In vitro elution of vancomycin from calcium phosphate cement. *J Arthroplasty* 20:1055–1059
728. Gbureck U, Vorndran E, Muller FA, Barralet JE (2007b) Low temperature direct 3D printed bioceramics and biocomposites as drug release matrices. *J Control Release* 122:173–180
729. Alkhraisat MH, Rueda C, Cabrejos-Azama J, Lucas-Aparicio J, Mariño FT, García-Denche JT, Jerez LB, Gbureck U, Cabarcos EL (2010b) Loading and release of doxycycline hyclate from strontium-substituted calcium phosphate cement. *Acta Biomater* 6:1522–1528
730. Blom EJ, Klein-Nulend J, Wolke JGC, van Waas MAJ, Driessens FCM, Burger EH (2002) Transforming growth factor- $\beta$ 1 incorporation in a calcium phosphate bone cement, Material properties and release characteristics. *J Biomed Mater Res* 59:265–272
731. Blom EJ, Klein-Nulend J, Yin L, van Waas MAJ, Burger EH (2001) Transforming growth factor- $\beta$ 1 incorporated in calcium phosphate cement stimulates osteotransductivity in rat calvarial bone defects. *Clin Oral Implants Res* 12:609–616
732. Link DP, van den Dolder J, van den Beucken JJ, Wolke JGC, Mikos AG, Jansen JA (2008b) Bone response and mechanical strength of rabbit femoral defects filled with injectable CaP cements containing TGF- $\beta$ 1 loaded gelatin microparticles. *Biomaterials* 29:675–682
733. Habraken WJEM, Boerman OC, Wolke JGC, Mikos AG, Jansen JA (2009) In vitro growth factor release from injectable calcium phosphate cements containing gelatin microspheres. *J Biomed Mater Res A* 91A:614–622
734. Ruhé PQ, Boerman OC, Russel FGM, Mikos AG, Spauwen PHM, Jansen JA (2006) In vivo release of rhBMP-2 loaded porous calcium phosphate cement pretreated with albumin. *J Mater Sci Mater Med* 17:919–927

735. Naito K, Obayashi O, Mogami A, Itoi A, Kaneko K (2008) Fracture of the calcium phosphate bone cement which used to enchondroma of the hand, a case report. *Eur J Orthop Surg Traumatol* 18:405–408
736. Hemmati K, Hesaraki S, Nemati A (2014) Evaluation of ascorbic acid-loaded calcium phosphate bone cements: physical properties and in vitro release behavior. *Ceram Int* 40:3961–3968
737. Ito T, Koyama Y, Otsuka M (2012) DNA complex-releasing system by injectable self-setting apatite cement. *J Gene Med* 14:251–261
738. Blatter TR, Delling G, Weckbach A (2003) Evaluation of an injectable calcium phosphate cement as an autograft substitute for transpedicular lumbar interbody fusion: a controlled, prospective study in the sheep model. *Eur Spine J* 12:216–223
739. Cavalcanti SC, Santos SC, Pereira CL, Mazzonetto R, de Moraes M, Moreira RWF (2008) Histological and histomorphometric analyses of calcium phosphate cement in rabbit calvaria. *J Cran Maxillofac Surg* 36:354–359
740. Sanchez-Sotelo J, Munuera L, Madero R (2000) Treatment of fractures of the distal radius with a remodelable bone cement: a prospective, randomised study using Norian SRS®. *J Bone Joint Surg Br* 82B:856–863
741. Lobenhoffer P, Gerich T, Witte F, Tscherne H (2002) Use of an injectable calcium phosphate bone cement in the treatment of tibial plateau fractures: a prospective study of twenty-six cases with twenty-month mean follow-up. *J Orthop Trauma* 16:143–149
742. Cassidy C, Jupiter JB, Cohen M, Delli-Santi M, Fennell C, Leinberry C, Husband J, Ladd A, Seitz WR, Constantz BR (2003) Norian SRS® cement compared with conventional fixation in distal radial fractures, a randomized study. *J Bone Joint Surg Am* 85A:2127–2137
743. Schmidt R, Cakir B, Mattes T, Wegener M, Puhl W, Richter M (2005) Cement leakage during vertebroplasty, an underestimated problem? *Eur Spine J* 14:466–473
744. Vlad MD, Torres R, López J, Barracó M, Moreno JA, Fernández E (2007) Does mixing affect the setting of injectable bone cement? An ultrasound study. *J Mater Sci Mater Med* 18:347–352
745. Krebs J, Aebli N, Goss BG, Sugiyama S, Bardyn T, Boecken I, Leamy PJ, Ferguson SJ (2007) Cardiovascular changes after pulmonary embolism from injecting calcium phosphate cement. *J Biomed Mater Res B Appl Biomater* 82B:526–532
746. Poetker DM, Pytynia KB, Meyer GA, Wackym PA (2004) Complication rate of transtemporal hydroxyapatite cement cranioplasties: a case series review of 76 cranioplasties. *Otol Neurotol* 25:604–609
747. Ridenour JS, Poe DS, Roberson DW (2008) Complications with hydroxyapatite cement in mastoid cavity obliteration. *Otolaryngol Head Neck Surg* 139:641–645
748. Mizowaki T, Miyake S, Yoshimoto Y, Matsuura Y, Akiyama S (2013) Allergy of calcium phosphate cement material following skull reconstruction: a case report. *Neurol Surg* 41:323–327
749. Gaskin JA, Murphy J, Marshall AH (2013) Complications of hydroxyapatite bone cement use in cochlear implantation? *Cochlear Implants Int* 14:174–177
750. Russell TA, Leighton RK (2008) Comparison of autogenous bone graft and endothermic calcium phosphate cement for defect augmentation in tibial plateau fractures A multicenter, prospective, randomized study. *J Bone Joint Surg Am* 90A:2057–2061
751. Dickson KF, Friedman J, Buchholz JG, Flandry FD (2002) The use of BoneSource™ hydroxyapatite cement for traumatic metaphyseal bone void filling. *J Trauma* 53:1103–1108
752. Jungbluth P, Hakimi M, Grassmann JP, Schnependahl J, Kessner A, Sager M, Hakimi AR, Becker J, Windolf J, Wild M (2010) The progress of early phase bone healing using porous granules produced from calcium phosphate cement. *Eur J Med Res* 15:196–203
753. Bongio M, van den Beucken JJ, Leeuwenburgh SC, Jansen JA (2015) Preclinical evaluation of injectable bone substitute materials. *J Tissue Eng Regen Med* 9:191–209
754. Lopez MSP, Tamimi F, Lopez-Cabarcos E, Lopez-Ruiz B (2009) Highly sensitive amperometric biosensor based on a biocompatible calcium phosphate cement. *Biosens Bioelectron* 24:2574–2579

755. Lopez MSP, Lopez-Ruiz B (2011) A sensitive glucose biosensor based on brushite, a biocompatible cement. *Electroanalysis* 23:280–286
756. Yoshikawa T, Suwa Y, Ohgushi H, Tamai S, Ichijima K (1996) Self-setting hydroxyapatite cement as a carrier for bone-forming cells. *Biomed Mater Eng* 6:345–351
757. Simon CG Jr, Guthrie WF, Wang FW (2004) Cell seeding into calcium phosphate cement. *J Biomed Mater Res A* 68A:628–639
758. Xu HHK, Weir MD, Simon CG Jr (2008b) Injectable and strong nano-apatite scaffolds for cell/growth factor delivery and bone regeneration. *Dent Mater* 24:1212–1222
759. Lemaître J, Pittet C, Brendlen D (2008) Pasty or liquid multiple constituent compositions for injectable calcium phosphate cements. US Patent No 7407542
760. Chow LC, Takagi S (2007) Dual-phase cement precursor systems for bone repair. US Patent Application No 20070092580
761. Heinemann S, Rössler S, Lemm M, Ruhnnow M, Nies B (2013) Properties of injectable ready-to-use calcium phosphate cement based on water-immiscible liquid. *Acta Biomater* 9:6199–6207
762. Bohner M, Tainen H, Michel P, Döbelin N (2015) Design of an inorganic dual-paste apatite cement using cation exchange. *J Mater Sci Mater Med* 26:63
763. Takagi S, Chow LC, Hirayama S, Sugawara A (2003b) Premixed calcium phosphate cement pastes. *J Biomed Mater Res B Appl Biomater* 67B:689–696
764. Carey LE, Xu HHK, Simon CG Jr, Takagi S, Chow LC (2005) Premixed rapid-setting calcium phosphate composites for bone repair. *Biomaterials* 26:5002–5014
765. Xu HHK, Carey LE, Simon CG Jr, Takagi S, Chow LC (2007b) Premixed calcium phosphate cements: synthesis, physical properties, and cell cytotoxicity. *Dent Mater* 23:433–441
766. Shimada Y, Chow LC, Takagi S, Tagami J (2010) Properties of injectable apatite-forming premixed cements. *J Res Natl Inst Stand Technol* 115:233–241
767. Sugawara A, Fujikawa K, Hirayama S, Takagi S, Chow LC (2010) In vivo characteristics of premixed calcium phosphate cements when implanted in subcutaneous tissues and periodontal bone defects. *J Res Natl Inst Stand Technol* 115:277–290
768. Rajzer I, Castañó O, Engel E, Planell JA (2010) Injectable and fast resorbable calcium phosphate cement for body-setting bone grafts. *J Mater Sci Mater Med* 21:2049–2056
769. Wu F, Ngohai Y, Wei J, Liu C, O'Neill B, Wu Y (2012a) Premixed, injectable PLA-modified calcium deficient apatite biocement (cd-AB) with washout resistance. *Colloids Surf B* 92:113–120
770. Chen F, Mao Y, Liu C (2013b) Premixed injectable calcium phosphate cement with excellent suspension stability. *J Mater Sci Mater Med* 24:1627–1637
771. Irbe Z, Krieke G, Salma-Ancane K, Berzina-Cimdina L (2014b) Fast setting pre-mixed calcium phosphate bone cements based on  $\alpha$ -tricalcium phosphate. *Key Eng Mater* 604:204–207
772. Han B, Ma PW, Zhang LL, Yin YJ, Yao KD, Zhang FJ, Zhang YD, Li XL, Nie W (2009)  $\beta$ -TCP/MCPM-based premixed calcium phosphate cements. *Acta Biomater* 5:3165–3177
773. Chow LC, Takagi S (2006) Premixed self-hardening bone graft pastes. US Patent Application No 20060263443
774. Aberg J, Henriksson HB, Engqvist H, Palmquist A, Lindahl A, Thomsen P, Brisby H (2011) In vitro and in vivo evaluation of an injectable premixed calcium phosphate cement; cell viability and immunological response from rat. *Int J Nano Biomater* 3:203–221
775. Engstrand J, Åberg J, Engqvist H (2013) Influence of water content on hardening and handling of a premixed calcium phosphate cement. *Mater Sci Eng C* 33:527–531
776. Åberg J, Engstrand J, Engqvist H (2013b) Influence of particle size on hardening and handling of a premixed calcium phosphate cement. *J Mater Sci Mater Med* 24:829–835
777. Montazerolghaem M, Ott MK (2014) Sustained release of simvastatin from premixed injectable calcium phosphate cement. *J Biomed Mater Res A* 102A:340–347
778. Akashi A, Matsuya Y, Unemori M, Akamine A (2001) Release profile of antimicrobial agents from  $\alpha$ -tricalcium phosphate cement. *Biomaterials* 22:2713–2717

779. Ewald A, Hösel D, Patel S, Grover LM, Barralet JE, Gbureck U (2011) Silver-doped calcium phosphate cements with antimicrobial activity. *Acta Biomater* 7:4064–4070
780. Dorozhkin SV (2016c) Multiphasic calcium orthophosphate (CaPO<sub>4</sub>) bioceramics and their biomedical applications. *Ceram Int* 42:6529–6554
781. Bohner M (2001c) Calcium phosphate emulsions: possible applications. *Key Eng Mater* 192–195:765–768
782. Troczynski T (2004) A concrete solution. *Nat Mater* 3:13–14
783. Xu HHK, Takagi S, Quinn JB, Chow LC (2004b) Fast-setting calcium phosphate scaffolds with tailored macropore formation rates for bone regeneration. *J Biomed Mater Res A* 68A:725–734
784. Ginebra MP, Rilliard A, Fernández E, Elvira C, san Roman J, Planell JA (2001) Mechanical and rheological improvement of a calcium phosphate cement by the addition of a polymeric drug. *J Biomed Mater Res* 57:113–118
785. García-Fernández L, Halstenberg S, Unger RE, Aguilar MR, Kirkpatrick CJ, San Román J (2010) Anti-angiogenic activity of heparin-like polysulfonated polymeric drugs in 3D human cell culture. *Biomaterials* 31:7863–7872
786. Xu HHK, Burguera EF, Carey LE (2007c) Strong, macroporous and in situ-setting calcium phosphate cement-layered structures. *Biomaterials* 28:3786–3796
787. Andriotis O, Katsamenis OL, Mouzakis DE, Bouropoulos N (2010) Preparation and characterization of bioceramics produced from calcium phosphate cements. *Cryst Res Technol* 45:239–243
788. Gbureck U, Hozel T, Klammert U, Wurzler K, Muller FA, Barralet JE (2007c) Resorbable dicalcium phosphate bone substitutes prepared by 3D powder printing. *Adv Funct Mater* 17:3940–3945
789. Habibovic P, Gbureck U, Doillon CJ, Bassett DC, van Blitterswijk CA, Barralet JE (2008) Osteoconduction and osteoinduction of low-temperature 3D printed bioceramic implants. *Biomaterials* 29:944–953
790. Lode A, Meissner K, Luo Y, Sonntag F, Glorius S, Nies B, Vater C, Despang F, Hanke T, Gelinsky M (2014) Fabrication of porous scaffolds by three-dimensional plotting of a pasty calcium phosphate bone cement under mild conditions. *J Tissue Eng Regen Med* 8:682–693
791. Steffen T, Stoll T, Arvinte T, Schenk RK (2001) Porous tricalcium phosphate and transforming growth factor used for anterior spine surgery. *Eur Spine J* 10:S132–S140
792. Guo H, Su J, Wei J, Kong H, Liu C (2009) Biocompatibility and osteogenicity of degradable Ca-deficient hydroxyapatite scaffolds from calcium phosphate cement for bone tissue engineering. *Acta Biomater* 5:268–278
793. Guo H, Wei J, Kong H, Liu C, Pan K (2008) Biocompatibility and osteogenesis of calcium phosphate cement scaffolds for bone tissue engineering. *Adv Mater Res* 47-50:1383–1386
794. Park JH, Lee GS, Shin US, Kim HW (2011) Self-hardening microspheres of calcium phosphate cement with collagen for drug delivery and tissue engineering in bone repair. *J Am Ceram Soc* 94:351–354
795. Moseke C, Bayer C, Vorndran E, Barralet JE, Groll J, Gbureck U (2012) Low temperature fabrication of spherical brushite granules by cement paste emulsion. *J Mater Sci Mater Med* 23:2631–2637
796. Weir MD, Xu HHK, Simon CG Jr (2006) Strong calcium phosphate cement-chitosan-mesh construct containing cell-encapsulating hydrogel beads for bone tissue engineering. *J Biomed Mater Res A* 77A:487–496
797. Xu JH, Tan WQ, Lin J (2007d) Repair of mandibular bone defect by combining calcium phosphate cement with bone morphogenetic protein composite as a bone graft material. *Chin J Biomed Eng* 26:153–156
798. Niikura T, Tsujimoto K, Yoshiya S, Tadokoro K, Kurosaka M, Shiba R (2007) Vancomycin-impregnated calcium phosphate cement for methicillin-resistant staphylococcus aureus femoral osteomyelitis. *Orthopedics* 30:320–321

799. Lode A, Wolf-Brandstetter C, Reinstorf A, Bernhardt A, König U, Pompe W, Gelinsky M (2007) Calcium phosphate bone cements, functionalized with VEGF: release kinetics and biological activity. *J Biomed Mater Res A* 81A:474–483
800. Yoshikawa M, Toda T (2004) In vivo estimation of periapical bone reconstruction by chondroitin sulfate in calcium phosphate cement. *J Eur Ceram Soc* 24:521–531
801. Wang JL, Mi L, Hou GH, Zheng Z (2008d) Repair of radial defects using calcium phosphate cements/poly lactic-co-glycolic acid materials combined with mesenchymal stem cells in rabbits. *J Clin Rehabil Tissue Eng Res* 12:8001–8005
802. Zhao L, Weir MD, Xu HHK (2010a) Human umbilical cord stem cell encapsulation in calcium phosphate scaffolds for bone engineering. *Biomaterials* 31:3848–3857
803. Ding T, Yang H, Maltenfort M, Xie R (2010) Silk fibroin added to calcium phosphate cement to prevent severe cardiovascular complications. *Case Reports Clin Pract Rev* 16:23–26
804. Panzavolta S, Torricelli P, Bracci B, Fini M, Bigi A (2010) Functionalization of biomimetic calcium phosphate bone cements with alendronate. *J Inorg Biochem* 104:1099–1106
805. Xu HHK, Zhao L, Detamore MS, Takagi S, Chow LC (2010) Umbilical cord stem cell seeding on fast-resorbable calcium phosphate bone cement. *Tiss Eng A* 16:2743–2753
806. Li M, Liu X, Liu X, Ge B (2010) Calcium phosphate cement with BMP-2-loaded gelatin microspheres enhances bone healing in osteoporosis: a pilot study. *Clin Orthop Rel Res* 468:1978–1985
807. Weir MD, Xu HHK (2010) Human bone marrow stem cell-encapsulating calcium phosphate scaffolds for bone repair. *Acta Biomater* 6:4118–4126
808. Chen W, Zhou H, Tang M, Weir MD, Bao C, Xu HHK (2012b) Gas-foaming calcium phosphate cement scaffold encapsulating human umbilical cord stem cells. *Tiss Eng A* 18:816–827
809. Wang P, Zhao L, Chen W, Liu X, Weir MD, Xu HHK (2014) Stem cells and calcium phosphate cement scaffolds for bone regeneration. *J Dent Res* 93:618–625
810. Perez RA, Shin SH, Han CM, Kim HW (2015) Bone-bioactive injectables based on calcium phosphates for the delivery of drugs and cells in hard tissue engineering: a recent update. *Tiss Eng Reg Med* 12:1–12
811. Zhao L, Weir MD, Xu HHK (2010b) An injectable calcium phosphate-alginate hydrogel-umbilical cord mesenchymal stem cell paste for bone tissue engineering. *Biomaterials* 31:6502–6510
812. dos Santos LA, Carrodéguas RG, Rogero SO, Higa OZ, Boschi AO, de Arruda AC (2002) Alpha-tricalcium phosphate cement: “in vitro” cytotoxicity. *Biomaterials* 23:2035–2042
813. Baroud G, Steffen T (2005) A new cannula to ease cement injection during vertebroplasty. *Eur Spine J* 14:474–479
814. Joseph C, Gardner D, Jefferson T, Isaacs B, Lark B (2011) Self-healing cementitious materials: a review of recent work. *Proc Inst Civil Eng Constr Mater* 164:29–41
815. Wu M, Johannesson B, Geiker M (2012b) A review: self-healing in cementitious materials and engineered cementitious composite as a self-healing material. *Constr Build Mater* 28:571–583
816. Mihashi H, Nishiwaki T (2012) Development of engineered self-healing and self-repairing concrete – state-of-the-art report. *J Adv Concrete Technol* 10:170–184
817. van Tittelboom K, de Belie N (2013) Self-healing in cementitious materials – a review. *Materials* 6:2182–2217
818. Zhang J, Liu W, Schnitzler V, Tancret F, Bouler JM (2014) Calcium phosphate cements for bone substitution: chemistry, handling and mechanical properties. *Acta Biomater* 10:1035–1049
819. Anderson JM (2006) The future of biomedical materials. *J Mater Sci Mater Med* 17:1025–1028

# Chapter 3

## Injectable Calcium Phosphate Cements for Hard Tissue Repair

Fangping Chen, Yuanman Yu, Xiaoyu Ma, and Changsheng Liu

**Abstract** Injectable self-setting biomaterials are conducive to repair the complex-shaped bone voids by an invasive technique. With the combination of good injectability, fast setting in situ, easy shaping to complicated geometries, and excellent biocompatibility, injectable calcium phosphate cement (ICPC) has become an urgent need to repair the hard tissue. This chapter reviews the history and development, classification, properties (including injectability, rheological properties, fast setting, anti-washout, radiopacity, suspension stability, sealability), and their influence factors, as well as the applications of ICPC in hard tissue repair.

**Keywords** Injectable calcium phosphate cement • Minimally invasive treatment • Root canal filling • Sealability • Bone repairing

### 3.1 Introduction

The large number of orthopedic procedures performed each year has led to great interest in injectable biodegradable materials for bone regeneration. Osteoporosis is one of the three major diseases in the elderly, of which the incidence increases sharply year by year. It is estimated that over 100 million people in China suffer from osteoporosis, and the number of patients is expected to more than 200 million by 2050. Of these, the incidence of women and men over the age of 60 were 68.9% and 33% in year 2015, respectively. Additionally, high morbidity and mortality due to the increase of accidents and sports injuries bring a heavy burden to individuals and society. According to the latest statistics of the World Health Organization,

---

F. Chen • Y. Yu • X. Ma

Engineering Research Center for Biomedical Materials of Ministry of Education, East China University of Science and Technology, Shanghai 200237, China

C. Liu (✉)

Key Laboratory for Ultrafine Materials of Ministry of Education, East China University of Science and Technology, Shanghai 200237, China

e-mail: [liucs@ecust.edu.cn](mailto:liucs@ecust.edu.cn)

dental diseases have been classified as the third major disease after cancer and cerebrovascular disease. The prevalence of caries in deciduous teeth of Chinese 5-year-old children was 66%, and 98.4% for 65–74 years old. Root canal therapy is currently the world's most common treatment of "pulpitis and apical periodontitis." Therefore, suitable biomaterials have become in great need for hard tissue repairing.

The repair of hard tissue defects is always an intractable problem perplexing surgeons and patients. Owing to their biological and physiochemical similarities to human bone and teeth, calcium phosphate cements (CPCs) have been extensively used in hard tissue repair and replacement. The biomaterials for replacement are available as powders, granules, or blocks. However, these forms are of limited effectiveness when cavities are not easily accessible. Some fractures in orthopedics, such as in distal radius, tibial plateau, and vertebral compression, only need to be treated by percutaneous injection without open surgery. In addition, nearly 60% of root canal filling materials causes the failure of endodontic surgery, especially for some small narrow and spindly apical foramens, clearances between root canal walls, and lateral accessory root canal. Therefore, injectable biomaterials are excellent candidates for bone grafting treatments in orthopedic and dental clinical.

Currently, the most commonly used injectable bone cement is poly(methyl methacrylate) (PMMA). Because of low viscosity and good injectability, PMMA can be applied to improve vertebral intensity and rigidity. Nevertheless, abundant clinic evidences show that there still remain many disadvantages including strong heat release, toxic monomers, and nondegradability when PMMA is applied in percutaneous vertebroplasty. For these reasons, there are views against applications of PMMA for vertebra only if it is used for palliative care of vertebral metastatic tumors.

With the combination of good injectability, fast setting in situ, easy shaping to complicated geometries, and excellent biocompatibility, injectable calcium phosphate cement (ICPC) has become an urgent need to repair the hard tissue. In addition, the strengthening and the stabilization of an osteoporotic bone tissue can be carried out solely by injection without excision or destruction of the residual bone matrix. Injectable cement has been attempted to use in paste form to minimize the invasiveness of surgical procedures and reduce the site of scars and postoperative pain. This chapter will provide an overview of injectable calcium phosphate cement for use in bone and teeth regeneration.

## 3.2 History and Development of ICPC

Injectable biphasic calcium phosphate (BCP) bone cement was first studied by Frenchman Daculsi et al. in 1996 [1]. The cement was easily injectable with the addition of a 2% methyl cellulose carrier gel in BCP particles (60/40 HA/ $\beta$ -TCP weight ratio). After 10 weeks implantation in rabbit distal femurs, bone ingrowth proceeded from the perimeter inward at a greater rate than in BCP blocks alone [2]. However, the low initial mechanical properties of BCP directly lead to difficulty in maintenance of the composite within the defect during surgery.



Since 1997, many kinds of injectable cements have been investigated. Knaack et al. [3] studied injectable calcium phosphate bone substitute (ABS) (a-BSM™, ETEX Corporation, Cambridge, MA), which was prepared from calcium phosphate precursor powders with an unbuffered physiological saline solution. The result showed that the autograft and ABS were associated with similar new bone growth and defect filling characteristics, and materials were nearly absorbed after implantation for 26 weeks.

ChronOS Inject (Synthes AG, Switzerland) consists of a powder mixture of brushite-based calcium phosphate and a sodium hyaluronate solution. The chronOS Inject as bone void filler was injected in fresh fractures of follow-up for 1 year. High patient satisfaction (92%) with treatment was achieved, despite the loss of reduction being described in 11% of proximal tibia and 2% of distal radius fractures. Overall, the material showed good outcome in the majority of patients and adequate resorption characteristics. However, stable internal fixation and sufficient bone quality are essential requirements for chronOS Inject [4].

Matsumine et al. [5] injected ICPC after bone excision and carried out X-ray tracing in 56 patients, showing that ICPC was adaptable to surrounding tissue. The HA and  $\beta$ -calcium phosphate complex was developed as an injectable, bone marrow-containing, and two-phase bone repair material with improved osteoconductive property. In vivo histological studies have also demonstrated that nanocrystal HA has better osteogenic property and vascular regeneration performance [6].

Our group developed CPC, composed of TECP and DCPA, as an injectable biomaterial (Injectable CaP, Rebone®) in 1998. Injectable CaP was firstly used in percutaneous vertebroplasty in 2003 [7–9]. Then the biodegradable injectable CaP was scaled up for wide clinic applications, and now it has been widely used for more than 20,000 cases in 300 hospitals. Clinical studies have shown that the injectable CaP can enhance vertebral body strength and stiffness, restore spinal function characteristics, and at the same time significantly reduce the potential serious side effects such as intraoperative blood pressure drop, pulmonary embolism, spinal cord and nerve root injury, etc.

Zhu XS and Yang HL [10] compared the properties of Injectable CaP, CaS (calcium sulfate), and PMMA by injecting them into the defect vertebrae L2–L5 in 24 adult female sheep. Animals were sacrificed after 2, 12, and 24 weeks of the bone filler augmentation, respectively. The vertebrae of L2–L6 were collected, and their biomechanical strength/stiffness, osseointegration activity, and biodegradability were evaluated. At all three time points tested, the PMMA-augmented lumbar vertebra had the highest biomechanical strength and stiffness, followed by the intact vertebra L6. Injectable CaP (Rebone®) and CaS significantly improved the strength, but did not yet restore it to the normal level. Osteogenesis occurred in the injectable CaP (Rebone®)-augmented defect vertebrae at 12 and 24 weeks. The result indicated that injectable CaP (Rebone®) and CaS were effective enough to strengthen the fractured lumbar vertebrae in a time-dependent manner [10]. Although these materials were reported to have good compatibility and excellent injectability, initial mechanical properties were still low to support the tissue growth. Xu [11] studied the clinical effect of thoracic and lumbar fractures treated by pedicle screw

fixation and vertebroplasty with calcium phosphate cement with the help of C-shaped arm X-ray machine. The result showed that all the 21 cases were treated successfully without postoperative infection, neurologic symptoms, and internal fixation complications. During the period of follow-up, outcomes were satisfactory and no injured vertebral lost its height obviously. Furthermore, Xu found that the vertebroplasty treated by injectable calcium phosphate cement contributed to the reconstruction of the injured vertebra, and the biomechanics of postoperative vertebral body restored to the level before fracture [12].

SRS (skeletal repair system; Norian Company, USA) is a typical injectable calcium phosphate bone cement, mainly composed of TCP, calcium phosphate, calcium carbonate, and sodium phosphate. To inject the cement into the porous structure easily, an injection gun was applied especially in the osteoporotic vertebral body. Carbonated hydroxyapatite was formed after setting for 10 min. The result showed that SRS bound closely with surrounding bone, with compressive strength of 10 MPa and up to 55 MPa after 12 h. Serraj Siham et al. [13] injected Norian SRS in the subchondral bone defect. 15.3% of reduction of the fracture required revision surgery after surgery for 8 weeks due to partial bone loss. All other patients had complications, and fractures were healed without any displacement. The high mechanical strength of the cement allowed early weight bearing after a mean postoperative period of 4.5 weeks.

Many existing calcium phosphate materials degrade very slowly and have low strength, leading to the decreased bone regeneration at the site of the implant [14]. In an effort to address these concerns, researchers have chosen to investigate polymeric materials for use. Examples of naturally occurring biopolymers used include chitosan, alginate acid and hyaluronic acid, polyesters, and PMMA. The frangibility and mechanical property of calcium hydrogen phosphate were significantly improved by adding PMMA molecules. Compared to macroporous biphasic calcium phosphate, the composites of hydroxypropyl methyl cellulose and calcium phosphate as injectable bone materials had improved biological activity at the early implantation stage. The poly(propylene fumarate) and calcium phosphate composites can be injectably used for the treatment of femoral head necrosis. The results showed that the mechanical properties of the composites were enhanced with the increase of calcium phosphate content in the composites [15, 16].

Some elements or components can improve the bone repair ability of the ICPC. The CPC containing strontium carbonate had better injectability and compressive strength, which had an effect on the distribution of pores in the cement [17]. The mixture of calcium phosphate and calcium sulfate had not only good injectability, appropriate setting time, and mechanical property but also improved degradability and osteogenic ability [18]. Studies found that after hydration, biphasic bone substitute materials mixed by calcium sulfate and tricalcium phosphate could form calcium sulfate dihydrate and decalcified hydroxyapatite simultaneously [19]. The mechanical strength of composite IBS matches the human cancellous bone. Therefore, it is suitable for the treatment of the vertebral body and cystic cavities.

In addition to SRS, commercially available injectable bone cements are shown in Table 3.1.

**Table 3.1** Examples of commercially available injectable bone cements

	Company	Commercially available product	Composition	Commercially available forms	Current proof
Bone repair	AlloSource	AlloFuse™	Heat-sensitive copolymer with DBM	Injectable gel and putty	Case reports
					Animal studies
					Cell culture
	Biomet Osteobiologics	BonePlast®	Calcium sulfate with or without HA/CC composite granules	Various volumes of powder and setting solution	Case reports
					Animal studies
	Exactech	Optefil®	DBM suspended in gelatin carrier	Injectable bone paste dry powder ready to be hydrated	Human studies
					Case reports
		Opteform®	DBM and cortical cancellous chips suspended in gelatin carrier	Formable putty or dry powder ready to be hydrated	Animal studies
					Every lot tested in vivo for osteoinduction
	Integra Orthobiologics/ IsoTis OrthoBiologics	Accell Connexus®	DBM, accell bone matrix, reverse phase medium	Injectable putty	Human studies
Case reports					
Animal studies					
Accell Evo3™		DBM, accell bone matrix, reverse phase medium	Injectable putty	Every DBM lot tested for osteoinduction	
				Animal studies	
DynaGraft II	DBM, reverse phase medium	Injectable putty	Every DBM lot tested for osteoinduction		
			Human studies		
			Case reports		

(continued)

**Table 3.1** (continued)

Company	Commercially available product	Composition	Commercially available forms	Current proof
	OrthoBlast II	DBM, cancellous bone, reverse phase medium	Injectable putty	Human studies Case reports Animal studies Every DBM lot tested for osteoinduction
	Integra Mozaik™	80% highly purified b-TCP/20% highly purified type 1 collagen	Strip and putty	Human studies Case reports Animal studies
LifeNet Health	Optium DBM®	DBM combined with glycerol carrier	Formable putty (bone fibers) and injectable gel (bone particles)	Human studies Case reports Animal studies
Medtronic Spinal & Biologics	MasterGraft® putty	Biphasic calcium phosphate and collagen	Moldable putty	Animal studies
	Osteofil® DBM	DBM in porcine gelatin	Injectable paste and moldable strips	Animal studies Case reports
	Progenix™ plus	DBM in type 1 bovine collagen and sodium alginate	Putty with demineralized cortical bone chips	Animal studies Case reports
	Progenix™ putty	DBM in type 1 bovine collagen and sodium alginate	Ready to use injectable putty	Animal studies Case reports
MTF/Synthes	DBX®	DBM in sodium hyaluronate carrier	Paste, putty mix and strip	Human studies Case reports Animal studies
Orthovita	Vitoss®	100% β-TCP and 80% β-TCP/20% collagen and 70% β-TCP/20% collagen/10% bioactive glass	Putty, strip, flow, morsels and shapes	Published human studies (level I and III) Case reports Animal studies

(continued)

**Table 3.1** (continued)

	Company	Commercially available product	Composition	Commercially available forms	Current proof
	Osteotech	Grafton®	DBM fibers with demineralized cortical cubes	Packable graft	Peer-reviewed published human studies (incl. level I–II prospective studies)
		Crunch®			Case reports
	Animal studies	Every lot tested in vivo for osteoinduction			
		Grafton® gel	DBM in a syringe	MIS and percutaneous injectable graft	Peer-reviewed published human studies (incl. level I–II prospective studies)
Case reports	Animal studies	Every lot tested in vivo for osteoinduction			
	Grafton® orthoblend large defect	DBM fibers with crushed cancellous chips	Packable graft	Peer-reviewed published human studies (incl. level I–II prospective studies)	
Case reports	Animal studies	Every lot tested in vivo for osteoinduction			
	Grafton® orthoblend small defect	DBM fibers with larger cancellous chips	Packable moldable graft	Peer-reviewed published human studies (incl. level I–II prospective studies)	
Case reports	Animal studies	Every lot tested in vivo for osteoinduction			

(continued)

**Table 3.1** (continued)

Company	Commercially available product	Composition	Commercially available forms	Current proof
Osteotech	Grafton Plus® paste	DBM in a syringe	Injectable MIS graft, resists irrigation	Peer-reviewed published human studies (incl. level I–II prospective studies) Case reports Animal studies Every lot tested in vivo for osteoinduction
	Grafton® putty	DBM fiber technology	Packable moldable graft	Peer-reviewed published human studies (incl. level I–II prospective studies) Case reports Animal studies Every lot tested in vivo for osteoinduction
Regeneration Technologies	BioSet™	DBM combined with natural gelatin carrier	Injectable paste, injectable putty, strips and blocks with cortical cancellous chips	Human studies Case reports Animal studies Every lot tested in vivo for osteoinduction
Smith & Nephew	Viagraf	DBM combined with glycerol	Putty, paste, gel, crunch and flex	Animal studies
Synthes	Norian® SRS®	Calcium phosphate	Injectable paste	Human studies Case reports Animal studies
	Norian® SRS® fast set putty	Calcium phosphate	Moldable putty	Human studies Case reports Animal studies

(continued)

**Table 3.1** (continued)

Company	Commercially available product	Composition	Commercially available forms	Current proof
Wright Medical Technology	Allomatrix®	DBM with/without CBM in surgical grade calcium sulfate powder	Various volumes of injectable/formable putty	Human studies Case reports Animal studies Cell culture
	Allomatrix® RCS	DBM with Caciplex™ technology in surgical grade calcium sulfate powder	Various volumes of formable putty	Animal studies
	MIIG® X3	High strength surgical grade calcium sulfate	Minimally invasive injectable graft for compression fractures	Human studies Case reports Animal studies
	PRO-DENSE® injectable regenerative graft	75% calcium sulfate and 25% calcium phosphate	Procedure kits, various volumes of injectable paste	Human studies Case reports Animal studies
	PRO-STIM™ injectable inductive graft	50% calcium sulfate, 10% calcium phosphate, and 40% DBM by weight	Procedure kits, various volumes of injectable paste/formable putty	Case reports Animal studies
Zimmer	CopiOs® bone void filler	Dibasic calcium phosphate and type 1 collagen	Sponge and paste	Case reports Animal studies
	Puros® DBM	Allograft DBM putty (putty with chips includes allograft chips from the same donor)	Putty and putty with chips	Every lot tested in an in vivo rat assay for osteoinductive potential demonstrating bone formation in an ectopic model

(continued)

**Table 3.1** (continued)

	Company	Commercially available product	Composition	Commercially available forms	Current proof
Root canal	Morita	Vitapex	30% calcium hydroxide, 40.4% triiodomethane, 22.4% silicone oil, 6.9% filler	Alone (temporarily) or in conjunction with the Gutta Perch (permanent). Paste	
	Meta	Metapex	Barium sulfate, calcium hydroxide	Exposed pulp of pulp capping and pulpotomy	
				Root canal leakage	
				Apexification	
				Hard tissue barrier formation	
Rebone	ReboneGutai™	Superfine calcium phosphate paste	Sponge and paste Bone defect repair and root canal filling	Human studies Case reports Animal studies	
PD	Pro-Pul-Pan	Powder: zinc oxide 9.0%, thymol iodine 22.5% solution: eugenol	Root canal filling paste		

A. *CaP* calcium phosphate, *DCPD* dicalcium phosphate dihydrate, *TCP* tricalcium phosphate, *TTCP* tetracalcium phosphate, *HA* hydroxyapatite, *DCP* dicalcium phosphate, *MCPM* monocalcium phosphate monohydrate, *Bis-GMA* 2,2-bis[4-(2-hydroxymethacryloxypropyl)phenyl] propane, *Bis-EMA* 2,2-bis[4-(2-methacryloxyethoxy)]phenyl propane, *TEGDMA* triethylene glycol dimethacrylate, *3MPS* 3-methylacryloxy-propyltrimethoxysilane, *BPO* benzoyl peroxide, *DHEPT* di(hydroxy-ethyl)-p-toluidine

### 3.3 Classification of ICPC

Ideally, ICPC can be injected into the damaged tissues and then mold to the shape of the bone cavity in situ filling in the defects. Before injection, the ICPC should remain stable, be easy to inject through the percutaneous or small bone window, and set rapidly after implantation in defects.

Conventional injectable CPC, taking a variety of aqueous media (e.g., distilled water, phosphate-buffered saline solution, sodium phosphate, citrate buffer solution, carbonate buffer solution, or saline solution) as setting liquid, has proven to be an alternative bone substitute [20]. The aqueous phase ICPC has combined characteristics of biocompatibility, osteoconductivity, fast solidifying, high initial mechanical strength, and easy shaping for any complicated contours of bone defects [21].



However, several drawbacks of ICPC prevent them from gaining universal acceptance. It is worthwhile to note that the aqueous phase ICPC has to be prepared just before implantation, since setting starts from the moment that the powder comes in contact with water. Clearly, it is difficult for the clinician to mix the powder with liquid thoroughly and hard to inject the aqueous phase ICPC into the defect within a prescribed time as well. In addition, the operation of on-site powder-liquid mixing prolongs the surgical time. It may degrade physical and chemical properties of ICPC and even cause potential side effects on tissue repairing because of inhomogeneous mixing and insufficient filling stemming from the limited mixing time [22]. In order to overcome herein before shortages, ICPCs can be prepared as being aqueous injectable calcium phosphate cement (a-ICPC) or nonaqueous injectable calcium phosphate cement (n-ICPC) on the basis of the nature of the liquid phase.

Takagi and Xu [23] made nonaqueous phase setting liquid from nontoxic organic liquids which were immiscible with water, such as glycerol, polypropylene glycol, and low molecular weight polyethylene glycol (PEG) liquid. The n-ICPC can be mixed in advance in a controlled environment to keep the system anhydrous. It avoids the temporary mixture of solid-liquid two-phase to shorten the operation time and shows the characteristic of long-term preservation.

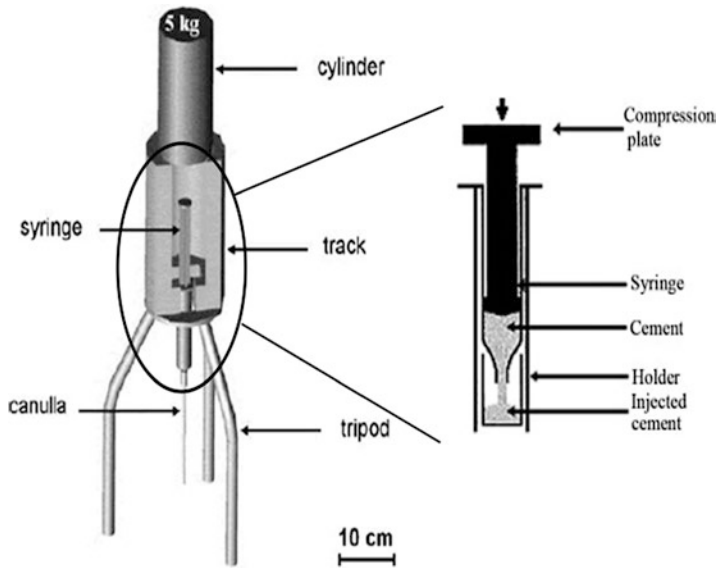
Premixed acidic CPC was formed by mixing the powder phases with glycerol as a delivery system for water-solubilized simvastatin. The lower doses of SVA showed an approximately fourfold increase in mineralization as compared to the control. The results also demonstrated that premixed acidic CPC is a good option for local delivery of SVA leading to a prolonged stimulation of osteogenesis [24]. The cements with smaller particle sizes showed higher compressive strength and more difficulty to inject. The addition of granules made the cements easier to inject, but prolonged the setting time and reduced the strengths. Therefore, the particle size can be used to control the handling and physical properties of premixed cements [25].

Our group has developed the n-ICPC root canal paste by well-premixed ultrafine calcium phosphate powders with nonaqueous phase organic setting liquid since the year of 2003. n-ICPC has a series of excellent properties including good injectability, self-setting, excellent biocompatibility, controllable degradation, and proper compressive strength. Moreover, the paste can seal root canal effectively and be compatible with apical surrounding tissues without root canal filling reaction. The success rate of surgery with n-ICPC in clinic applications reached over 98.6%. More importantly, it did not need gutta-percha point to close the root canal, indicating the great potential of ICPC in root canal treatment.

### 3.4 Properties of ICPC

The ultimate goal of injectable calcium phosphate cement is to offer an ideal bone substitute for better clinic performance. Nowadays, the main disadvantages of ICPC are:

1. Anti-washout property of ICPC is so poor that the slurry is easily dispersed by blood or tissue fluid.



**Fig. 3.1** Devices for evaluating the injectability of paste

2. Poor injectability for some cements and solid-liquid separation issue.
3. Contradiction between injectability and setting time still remains. ICPC with good injectability has long setting time, while ICPC with short setting time is difficult to inject.

Therefore, the improvement of the biomaterial properties or the development of related products should obey the clinical demands. ICPC should satisfy the required properties as follows.

### 3.4.1 *Injectability*

Injectable cement not only has the potential to fill the lesions and stabilizes the osteoporotic bone at risk for fracture but also conforms to the defect area such as periodontal bone repair and tooth root canal fillings. Injectability is related to the ability of a paste to extrude through a syringe or to be filled into the bone defects under pressure keeping the homogeneity. It is generally measured by correlating either to the force required for complete extrusion or to the quantity of the cement extruded during a certain period. Different techniques and parameters were applied to measure and quantify injectability of bone cements. However, there is no unified standard for measuring injectability. Generally speaking, injectability is measured by the percentage of a paste that could be injected from a syringe under a constant compressive load. Figure 3.1 shows the device for evaluating the injectability used in our group.

The injectability of paste is affected by many factors, such as the size and shape of particles, the ratio of solid phase to liquid phase, the additives and injection force, etc. It has been reported that small crystals favored a good injectability of  $\alpha$ -BSM<sup>®</sup>. Although a larger amount of liquid was required to form a paste with small particles, injectability and cohesion of  $\alpha$ -BSM were generally very good [26, 27]. Ishikawa found that the cements with round particles, regular shape, and higher ratio of liquid to powder could be injected easily.

The lack of inherent viscosity limits the fabrication of injectable cements. When injected from a delivery system, the pastes will undergo “filter pressing” or phase separation, in which the liquid part gets expelled leaving behind the solid phase [28]. An effective method to break through the bottleneck is to incorporate gelling agents or viscous media. The choice, however, is limited because of the requirement of biocompatibility, as the complex interaction between the ions of the additives may lead to the formation of toxic moieties. Moreover, the additives can adversely affect the setting and mechanical properties of the cement. Typically, ICPCs with good injectability have been successfully fabricated with the use of low quantities of glycerol phosphate, chitosan, alginate, cellulose, glycerol, lactic acid, citric acid, etc., which have reasonable biocompatibility. These additives not only decreased the interactions between particles or increased the viscosity of liquid phase but also prevent the phase separation between the solid and liquid. Our experiments have demonstrated that the white dextrin, Xanthan gum, and PEG-6000 promoted the injectability of ICPC to a certain extent [29, 30].

When the paste was injected into the bone defects, the injection resistance would increase due to the pressure inside the body cavity. Therefore, the injectable cement was propelled by motor pushers. Obviously, the better the injectability of ICPC is, the smaller the propelling force or the injection pressure will be. Moreover, the parameters of the injection device also affect the injectability. Namely, shorter canulas with a larger diameter, as well as smaller injection rates were found to contribute to a better injectability. More importantly, the injectability is time dependent, which decreases with the advance of the hydration of CPC. That is the reason that injectability should be calculated from the starting point of mixing the solid with the liquid.

### ***3.4.2 Rheological Properties***

During the whole injection process, the flow characteristics of ICPC are quite important. The slurry should be injectable with low resistance, and there is no powder-liquid phase separation. These requirements mainly depend on a suitable rheological property of ICPC. In this sense, rheological parameters are suitable to quantitatively describe the flow or injection process. In such a reactive system of ICPC, the internal microstructure changes with the time. These changes affect not only the flow and workability but also the mechanical properties of the cement after hydration. Therefore, the investigation of the rheological properties of ICPC would be beneficial to improve the performance characteristics of the ICPC slurry.

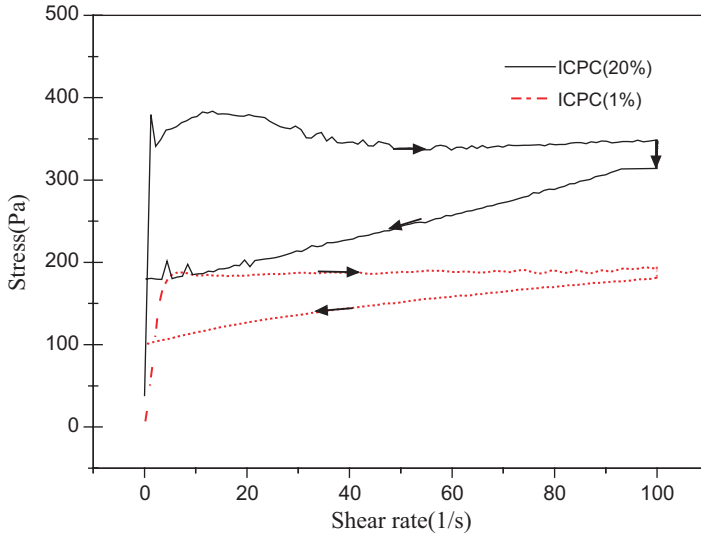
**Table 3.2** Thixotropy loop area and stress slowdown rate of ICPC with different PEG-6000 contents

Content (wt%)	$A_{\tau}(\text{Pa s}^{-1})$	$\Delta\tau(\%)$
ICPC (0)	5100.2	15.61
ICPC (0.5%)	5998.7	9.54
ICPC (1%)	6521.0	8.78
ICPC (5%)	8860.4	11.70
ICPC (10%)	1.208E+04	11.74
ICPC (20%)	1.479E+04	12.61

Rheologies include the steady rheology and dynamic rheology. The steady rheology is to measure the shear stresses under consecutive linear increasing and decreasing in the rotational shear rates. Viscosity is an indicator of a fluidic resistance to flow, describing internal friction in a moving fluid. Low viscosity favors the injectability of cement. Yield stress is the critical strength that must be applied to a material allowing it to flow. The bigger the yield stress, the more difficult a cement is to inject. Thixotropy, a phenomenon in steady rheology, is defined as the continuous decrease of apparent viscosity with the time under shear and subsequent recovery of viscosity when the flow is discontinued. This parameter reflects the complex interaction forces of particles and the formation of isolated large flocs or single particulate structure throughout the whole materials.

Thixotropic hysteresis loop area was used to evaluate the magnitude of thixotropy of the paste during motion, which is proportional to the energy required to break down the thixotropic structure. The larger the thixotropic hysteresis loop area, the more energy is required to break down the thixotropic structure. Liu et al. explored the steady rheological properties in ICPC reactive system. The results indicated that the yield stress and the area of the thixotropic hysteresis loop were enlarged as the setting process progressed. With the increase of the ratio of solid to liquid, structural strength, viscosity within the ICPC improved, and the corresponding thixotropy became larger. It also revealed the microstructure development of ICPC during the whole setting process, and the factors affected the rheological properties [31]. Chen reported that the change of the hysteresis loop area and stress slowdown rate with the increased PEG-6000 content (Table 3.2). The degree of thixotropy is judged from the area between the up and down curves. By adding PEG-6000 to the cement liquid, the thixotropy loop area of the pastes notably increased, thus enhance the stability of ICPC paste. Among these ICPC pastes, the ICPC (20%) is with the highest thixotropy, and the pure ICPC paste is least in thixotropy. In addition, the addition of PEG-6000 reduced the  $\Delta\tau$  of the ICPC pastes till 1 wt%. But above 1 wt%, the  $\Delta\tau$  would keep almost constant. It is also clear that the stability of the ICPC paste can be improved by introducing proper content of PEG-6000 (Fig. 3.2).

Dynamic rheology is the dynamic mechanical oscillatory strain applied to a sample, allowing the sample to be subjected to a strain and viscous and elastic properties of the sample and to be measured simultaneously to explore the internal structure

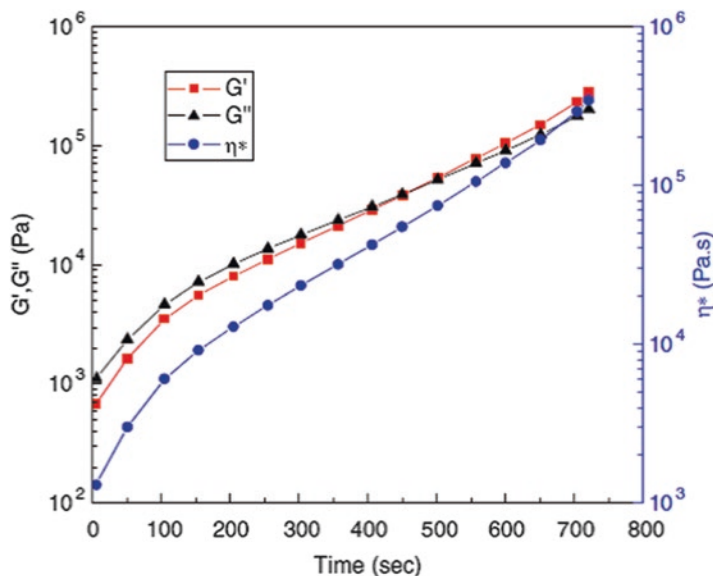


**Fig. 3.2** Thixotropy loop curves of ICPC pastes (Reproduced from Ref. [29] by permission. Copyright © 2010 Elsevier B.V)

of the sample. The recovery of the material after deformation was characterized by the storage modulus  $G'$  and loss modulus  $G''$ .  $G'$  represents the ability of the material to store the energy of deformation, while  $G''$  refers to the ability of materials to consume the energy of deformation. Figure 3.3 showed that all the storage modulus  $G'$ , loss modulus  $G''$  and complex viscosity  $\eta^*$  increased with hydration time, further verifying that the recovery of ICPC after deformation was involved with the components of solids materials [29].

Rheological properties are related to the particle size, distribution of the components, the ratio of powder to liquid, and the surface charge of the particles in contact with the liquid phase [32]. Gbureck et al. improved the injectability of activated  $\alpha$ -tricalcium phosphate ( $\alpha$ -TCP)-based cement by adding several fine-particle-sized fillers and showed that the introduction of inert filler reduced the viscosity significantly [33]. Baroud et al. found that P/L, milling time, and additives significantly affected the rheological characterization of concentrated aqueous  $\beta$ -TCP suspensions, such as the viscosity and yield stress [34].

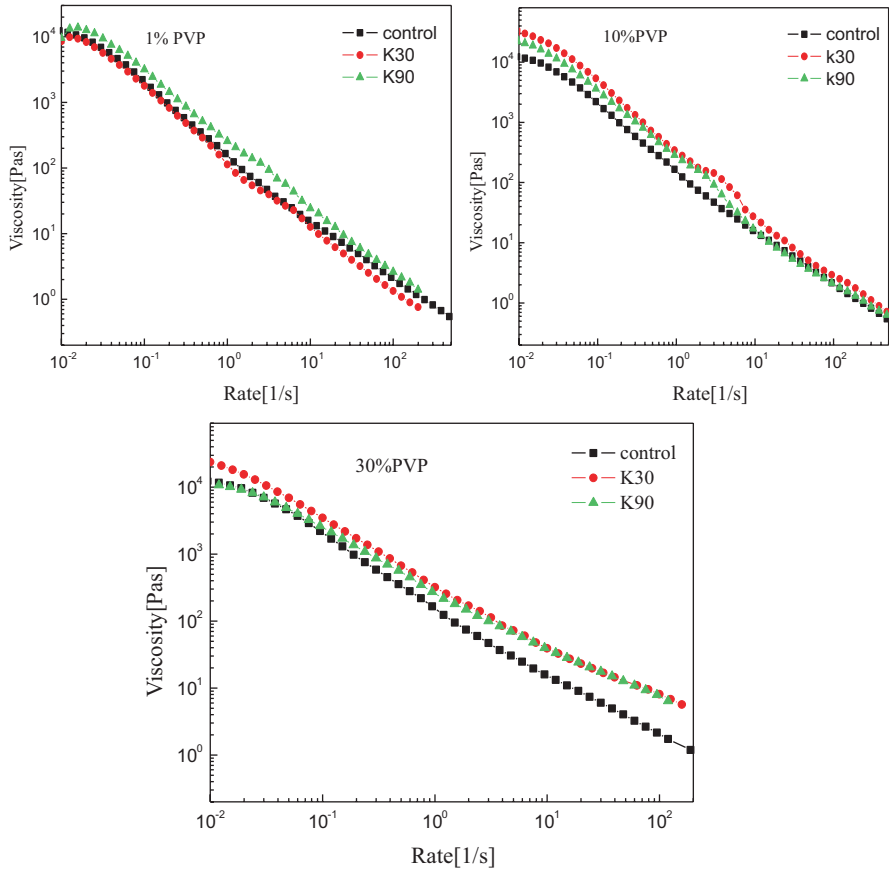
To make ICPC easy to operate in the clinic, some rheological additives are added to improve the thixotropy and the stability of the slurry, the fluidity, water resistance, the coagulation time, and so on. The effect of lactic acid, glycerol, acetyl chitin, glycerin, and sodium phosphate on the ICPC was studied, but the comprehensive performance was still not satisfied [35]. Jin et al. [36] investigated the influence of polyvinylpyrrolidone (PVP) on the rheological characteristics of ICPC through an advanced rheometric expansion system (ARES). By introducing the PVP with different value of K and different quantity into the setting liquid, the rheological behaviors of CPC slurry could be improved greatly. The results showed that



**Fig. 3.3** Time-sweep curves of CPC slurry at 1 min after mixing. Stain, 1%;  $\omega$ , 1 rad  $s^{-1}$ ; P/L ratio, 2.0 (Reproduced from Ref. [31] by permission. Copyright © 2006 Elsevier B.V)

the CPC slurry was a typical non-Newtonian shear-thinning fluid, and the addition of PVP could not change this property of CPC slurry. But due to the existence of PVP, the viscosity of CPC slurry and the area of thixotropic loop were increased, and the restorability was also improved (Fig. 3.4), leading to the improved stability of CPC slurry. These results were also explained in Tables 3.3 and 3.4. The study showed that the 20% PVPK90 and 30% PVPK30 improved the rheological properties of ICPC slurry, which makes the ICPC more suitable as an injectable material.

In addition, the effect of water-soluble polymer PEG on ICPC was also investigated. Viscosity curves showed that the ICPC containing PEG had obvious shear-thinning behavior. With the increase of additive concentration, the viscosity of ICPC gradually increased. Curve slope remains unchanged, which illustrates different concentrations of additive had the same effect on the shear thinning of the system. Thixotropic loop curve showed that the ICPC is characterized with thixotropy. One percent PEG would not give much benefit on thixotropy of ICPC. Further increasing the PEG content up to 30% and 50%, the area of thixotropic loop significantly increased, and the thixotropy enhanced greatly. Therefore, the improvement of the structure strength of ICPC lies to the formation of network composed of particles and polymer with the interactions between PEG and water. Obviously, the thickening effect of PEG can increase the viscosity and the stability of the system (Fig. 3.5).



**Fig. 3.4** Effect of K30 and K90 on viscosity curves of ICPC with 1%, 10%, and 30% PVP (Reproduced from Ref. [36] by permission)

**Table 3.3** Results of thixotropic loop test of CPC slurry with PVP K30

Concentration/%	Area of loop	Degradation of strain/%
0 (control)	5100.2	15.61
1	6756.1	18.78
5	8297.9	12.61
10	13380.0	15.39
20	15440.0	15.30
30	21740.0	10.57

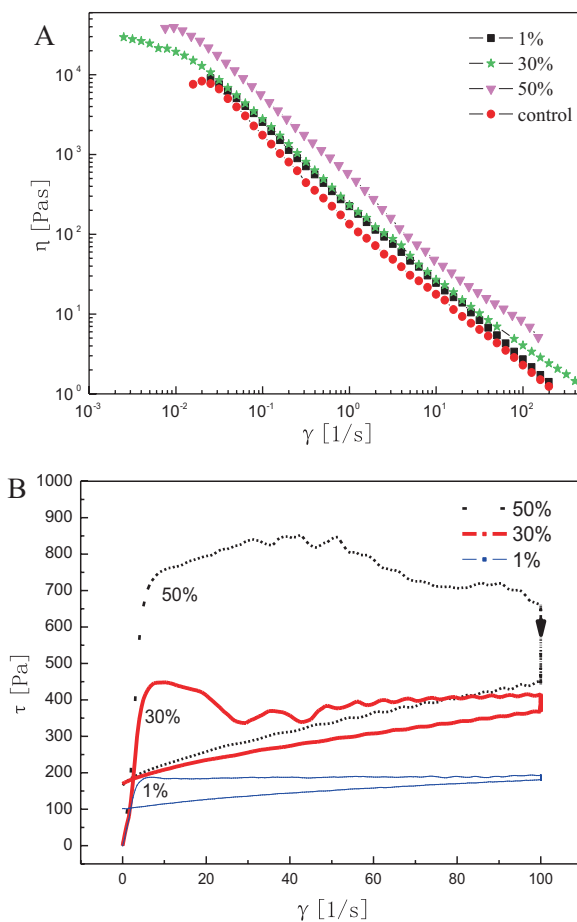
Reproduced from Ref. [36] by permission

**Table 3.4** Results of thixotropic loop test of ICPC with PVP K90

Concentration/%	Area of loop	Degradation of strain/%
0 (control)	5100.2	15.61
1	7538.0	9.97
5	9250.2	12.57
10	11850.0	13.03
20	11320.0	9.78
30	19000.0	17.40

Reproduced from Ref. [36] by permission

**Fig. 3.5** Viscosity curves (a) and thixotropic loop (b) with PEG2000 (1%, 30%, 50%)





### 3.4.3 Fast Setting

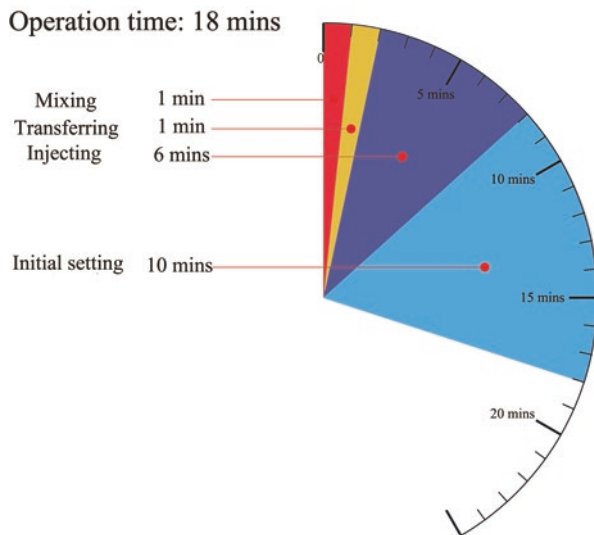
A good injectability is an important property required for ICPC applications. Furthermore, ICPC must set slowly enough to provide sufficient time for a surgeon to perform implantation. However, it also required fast setting enough to prevent washout and delayed operation. Therefore, setting time should be in a suitable range. The environment of ICPC implanted will also affect the setting time. For instance, magnesium ions in blood along with many organic materials will inhibit the setting of ICPC and thus make the setting time longer in serum than in distilled water. In addition, if the liquid phase of nonaqueous ICPC needs to exchange with the water or tissue liquid, the setting time thus becomes longer than those of aqueous ICPC. Therefore, it is necessary to shorten the setting time for the nonaqueous ICPC.

The Gillmore needle test and Vicat needle test define the setting time according to such standards as ASTM C266-89 and ASTM C191-92. The initial (I) and final (F) setting time are determined using the time required for the penetration of the needle into a paste specimen of specific consistency to a specific depth. In particular, a light and thick needle is used to measure the initial setting time I, while a heavy and thin needle for the final setting time F. The clinical meaning is that the cement paste should be implanted before time I and that the wound can be closed after time F.

In recent years, nondestructive methods have been attempted to online monitor the setting process, e.g., using electrical resistivity, ultrasonic, isothermal differential scanning calorimetry, dynamic rheological test and alternating current (AC) impedance spectroscopy, Fourier-transform infrared spectroscopy, solid-state NMR, X-ray diffraction, and energy-dispersive X-ray diffraction. An ultrasound through transmission is a novel method to analyze the entire setting process in situ about the nonaqueous injectable cement (glycerol as setting liquid) changes in body fluids. The material constants including the Young's modulus ( $E$ ), the Poisson ratio ( $\nu$ ), and the shear modulus ( $G$ ) at each step of the set process were monitored, as well as for the comprehensive systematic tracking of changes in the cement paste during the setting and hardening process of the cement, starting from the moment of immersion of cement in body fluids to a final product in the form of a hardened cement, and even the subsequent degradation process [37]. According to the clinic experience, 5–15 min is the reasonable range for the setting of ICPC (Fig. 3.6). Longer setting time would be conducive to the doctor's operation, but longer setting than necessary tends to make ICPC crumble upon early contact with blood or other fluids. Therefore, it is necessary to regulate the setting time of ICPC in a proper range.

The setting time of ICPC was affected by many factors. Previous literature reported that setting time was significantly shortened by decreasing the particle size of TECP and DCPA or introduction of HA crystal seeds [38]. The dissolution of phosphate or calcium salts (e.g.,  $\text{Na}_2\text{HPO}_4$  and  $\text{CaCl}_2$  solutions) increased the supersaturation of  $\text{Ca}^{2+}$  and  $\text{PO}_4^{3-}$  in the solution during hydration, thus improving the impetus of the reaction and accelerating the setting. Citric acid can provide pair

**Fig. 3.6** The reasonable time range of ICPC



electrons and calcium ions have electron vacancies. Thus, citric acid can react with calcium in the solution and transform into a chelate compound through chelation, accelerating the setting of ICPC.

The shortened setting time with acceptable injectability provides an easy way for the surgeon to use such materials in some urgent cases. Related studies showed that the injectability and the setting time can be balanced, and ICPC with satisfied fluidity and injectability for clinical operation can be prepared by introducing the additives and regulating concentration, particle sizes, ratio of powder to liquid, and so on.

#### 3.4.4 *Anti-washout*

Injectable cement washout can occur in vivo when it comes in contact with physiological fluids or when bleeding occurs due to difficulty in achieving complete hemostasis. Some cements would be washed out completely when immersed in simulated body fluid immediately after mixing. In percutaneous vertebroplasty, particles are ready to fall off the pastes and enter the cardiovascular system along with the blood, which often cause vascular blockage to thrombus, pulmonary embolism, or other complications. In this sense, it is necessary to improve the anti-washout property of the injectable cements.

Anti-washout property was usually estimated by qualitative analysis and quantitative analysis. Qualitative analysis of the washout resistance for injectable calcium phosphate cement relies mainly on the naked-eye observation, such as the disintegration of the pastes and the turbidity of the soaked liquid. Quantitative analysis

refers to calculate the washout mass loss rate of the paste during the period of immersion according to Eq. 3.1. Anti-washout property is affected by the hydration rate, the formation of waterproof membrane, the temperature of the simulated body fluid, and the speed of the shaker.

$$\text{Washout mass loss\%} = \frac{\text{Mass lost during immersion}}{\text{Total mass before immersion}} \times 100\% \quad (3.1)$$

The higher ratio of the liquid to solid and the prolonged setting time tend to make ICPCs crumble easily by plasma or other body fluids before the paste hardens. The bad resistance to water of ICPCs further prolongs the setting time. All these restrict the wide clinic applications of injectable cements. Thus, great efforts have been made to improve the washout resistance of ICPC.

Preventing the fluids from spreading to the cement paste is an effective strategy to improve the anti-washout property of injectable cement. To attain this goal, gelling agents have been utilized to impart viscosity to cement. Ishikawa [39] revealed that sodium alginate in the liquid could prevent the injectable cements from collapse and could be set normally. The reason is that calcium ions can react with sodium alginate to form insoluble calcium alginate hydrogel, which protect the CPC from being washed out. Takechi [40] showed that carboxymethyl cellulose, chitosan acetate, and chitosan lactate improved the operation performances of injectable cements, but prolonged the setting time. Although the detailed mechanisms of washout resistance for injectable cements with gelling agents have not been fully clarified at present, the improvement in anti-washout properties can be attributed to the adhesive property and negative charge of gel, which serves as a “glue” to fuse the particles together. Wang evaluated the water resistance, setting time, compressive strength, and biocompatibility of ICPC with cellulose as additives [41]. In addition, modified starch [42], white dextrin, and locust bean gum [43] have been tried to prepare the anti-washout type cement. Inositol phosphate was added to improve the anti-washout properties by virtue of the strong chelating capability to calcium ions in novel CPC system [44]. The development of versatile additives improves the anti-washout performance, but they may deteriorate other properties of injectable cements.

Speeding up the setting process of ICPC is another alternative way to improve the anti-washout property. An amount of wollastonite promoted the hydration reaction and shortened the setting time of ICPC, thus improving the anti-washout. The amorphous silica layer was formed by the wollastonite dissolution and absorbed on the surface of the CPC particles, which keeps the paste from being eroded by liquid [45]. Magnesium phosphate cement (MPC), consisting of magnesium oxide (MgO) and calcium biphosphate ( $\text{Ca}(\text{H}_2\text{PO}_4)_2$ ), is of special interest due to its rapid setting and high initial mechanical strength in comparison with the phosphate cement [46]. The major components of MPC could react in aqueous environment to form magnesium phosphate ( $\text{Mg}_3(\text{PO}_4)_2$ ) and calcium triphosphate ( $\text{Ca}_3(\text{PO}_4)_2$ ) as final products. Chen et al. [47] developed a fast-setting calcium-MPC by introducing MPC

into CPC, which enhanced the anti-washout ability. The reaction may prohibit the liquid penetration to the cement, thereafter improving its washout properties, thus endowing the CPC/MPC with anti-washout ability.

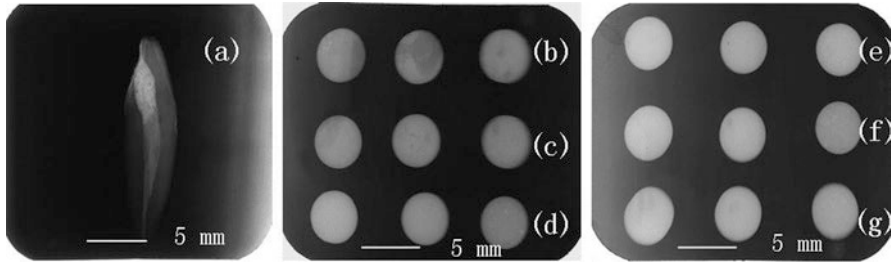
### 3.4.5 Radiopacity

Cement leakage needs to be of concern when using injectable bone substitutes. Up to 70 distal radius cases on cement leakage have been reported. Thus, the radiological evaluation is necessary. Radiopacity refers to the relative resistance for electromagnetic radiation, such as X-rays, to pass through a material. The radiopacity assists in positioning of injectable implants in the body, detecting of injected implant over time, and forecasting possible failure. However, the intrinsic radiopacity of CPCs is limited, and typically the addition of a contrast agent is required for certain applications. Although ICPC approval for uses in vertebroplasty is considered intrinsically radiopaque, the radiopacity is sometimes not enough, and it can be troublesome to distinguish them from bone. Furthermore, both over-filling and under-filling of ICPC into the root canal often occur, causing serious problems during endodontic treatment. To fully fill the root canal, the obturation procedures are performed visually with close fluoroscopic monitoring. Radiography enables the filling of the canal to be monitored at later stages during root canal therapy and improves the clinical performance.

Radiopacifying agents are typically included in injectable biomaterial formulations to improve the radiopaque properties for radiography, computed tomography, and/or real-time fluoroscopy. Organic radiopaque agents can be ionic or nonionic compounds with covalently bonded iodine. Examples of organic compounds currently used as contrast agents include diatrizoic acid, metrizoic acid, iopamidol, and iohexol. Organic radiopaque agents are administered orally for visualization of the organs, but their use is limited due to high cost and side effects.

Inorganic radiopaque agents (e.g., barium sulfate and zirconium dioxide) were also used in bone cements. However, they were not recommended due to the noted negative effects, such as causing bone resorption, decreasing the mechanical properties, and damaging biological functions [48]. Strontium ions have been reported to be used as radiopaque agents. Strontium fluoride and strontium chloride are mostly used for dental applications; however, they have a very low solubility and decrease the mechanical properties of the hardened end product significantly.

Accordingly, a resorbable radiopacifying agent in combination with high mechanical strength and biocompatibility is highly desirable for bone repair. Patent WO 2014/016707 A2 claimed that  $\text{SrBr}_2$  and  $\text{SrI}_2$  provided a better radiopaque effect than other strontium halides in injectable cement because of their higher molecular mass. This would result in the lower-amount uses of  $\text{SrBr}_2$  and  $\text{SrI}_2$  necessary to give the same radiopacity as other radiopaque has. Along with the higher intrinsic radiopaque and better water solubility,  $\text{SrBr}_2$  and  $\text{SrI}_2$  were biocompatible and favored the cell viability.



**Fig. 3.7** Radiographic images of extracted human tooth, pure ICPC, and BD-ICPCs with different contents of bismuth salicylate basic: (a) extracted human tooth filling with pure ICPC, (b) pure ICPC, (c) BD-ICPC (5%), (d) BD-ICPC (10%), (e) BD-ICPC (15%), (f) BD-ICPC (20%), (g) BD-ICPC (25%) (Reproduced from Ref. [49] by permission. Copyright © 2010 Elsevier Ltd)

Bismuth salicylate basic was also introduced as an alternative radiopaque agent to ICPC in root canal fillings. The results showed that the radiopacity and sealability of ICPC were improved with the addition of bismuth salicylate basic due to its good radiopacity, stability, and insolubility (Fig. 3.7). It was noteworthy that this reagent also imparted the potent antimicrobial activity [49].

Radiopacity was always assessed by an X-ray device. After samples were exposed to X-ray for a period, the film was imaged in an automatic processor. The relative X-ray radiopacities of samples and the control group (e.g., extracted tooth) were judged visually. The image contrast between the sample region and the surrounding black region was used to evaluate the X-ray radiopacity of cement, which can be calculated according to Eq. 3.2 [50]. The image process software Adobe Photoshop® was adopted to test the grayscale of the sample region and the surrounding black region [51]. Ten pairs of regions, scattered as far as possible, were selected by random in both the sample and the black surrounding to measure their gray-scales. Each region was averaged over an area of  $5 \times 5$  pixels:

$$V = \frac{G_1 - G_2}{G_1} \quad (3.2)$$

As shown in Fig. 3.5, the radiographic image of pure ICPC was inhomogeneous and doped with some large drop shadows. The result indicated that the brightness of all radiographic images of BD-ICPC cements was increased, and the drop shadow areas were lessened, which indicated that the addition of BSB helped to improve the radiopacity of ICPC. In addition, contrasts were produced between the extracted human teeth and BD-ICPC. Measured contrasts of radiographs of pure ICPC and BD-ICPC were  $0.55 \pm 0.027$  and  $0.89 \pm 0.008$ .

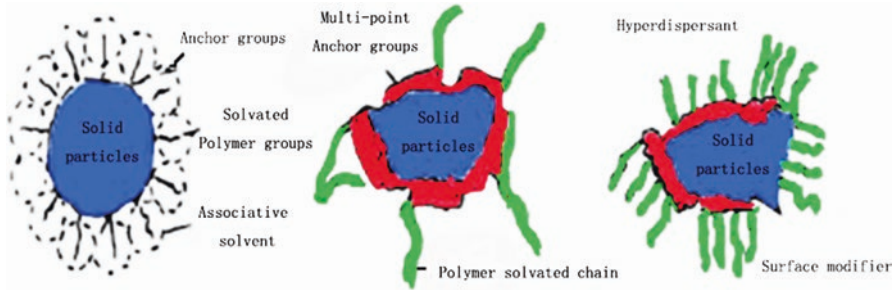
### 3.4.6 Suspension Stability

As stated earlier, nonaqueous ICPC facilitates the direct operation without the need of mixing on the spot and avoids the uneven performances caused by different operations. During this minimally invasive injection process, a well-dispersed suspension, with high solid loading of reasonably low viscosity to facilitate ICPC injected to the defect, is required. It was considered to be kinetically stable if the destabilization rate of the ICPC suspension is low enough during the expected lifespan. However, nonaqueous ICPC is a coexistent suspension system with solid and liquid phase. The interfacial energy between two phases is great; thus, the nonaqueous ICPC is an unstable system. In addition, CPC powders are easily aggregated in the nonaqueous solution due to the small particle size and large specific surface energy, which feed directly into inhomogeneity, flocculation, or precipitation of the ICPC suspension system. All these affect the injectability and the self-setting of ICPC and greatly limit the applications of ICPC in the clinic. Therefore, how to improve the long-term suspension stability of ICPC while maintaining the good slurry injection is an important issue to be addressed during the storage, transportation, and clinical application and the key to realize the large-scale production and applications in clinic.

Nonaqueous ICPC is a multicomponent, high viscosity, and opaque concentrated suspension, and it is sensitive to temperature and dilution. Two strategies are mainly conducted to study on the stable behavior. One is the measurement of the zeta potential of the particle surface to predict the stability of the dispersion [52]. This predictive method is effective for relatively simple preparations, but it cannot give information about the effects of the multiple components dissolved in the continuous phase on the flocculation behavior of particles. Aging tests are often performed. The products are evaluated for a long time under specific conditions (temperature, light, etc.). However, it is time consuming and cannot obtain objective and accurate data.

An instrument called Turbiscan LA-b<sup>Expert</sup> (Formulation Co., Ltd., France) can directly measure the dynamic stability of suspension without dilution based on multiwavelength reflection. Compared with microscopy, particle size, and zeta potential analysis, the Turbiscan presents the advantage of being a nondestructive tool. It gives kinetic information on the process leading to phase separation and allows to detect two kinds of destabilization phenomena: particle migration which is often reversible by mechanical agitation and particle size variations (coalescence, flocculation). At the same time, the Turbiscan analyzes the unstable mechanism and speed at the beginning of the unstable phenomenon and measures the concentration change in the middle and bottom of the suspension with time [53].

The following are three behaviors (flocculation, coalescence, and subsidence) of thick suspension. The steady state of suspension indicates the particle size and solution concentration without change. Particle movement (emulsion oil rise or the solid particles settle) caused changes in the concentrations of the sample and the strength of the backscattering and transmission. Particle sizes change due to agglomeration



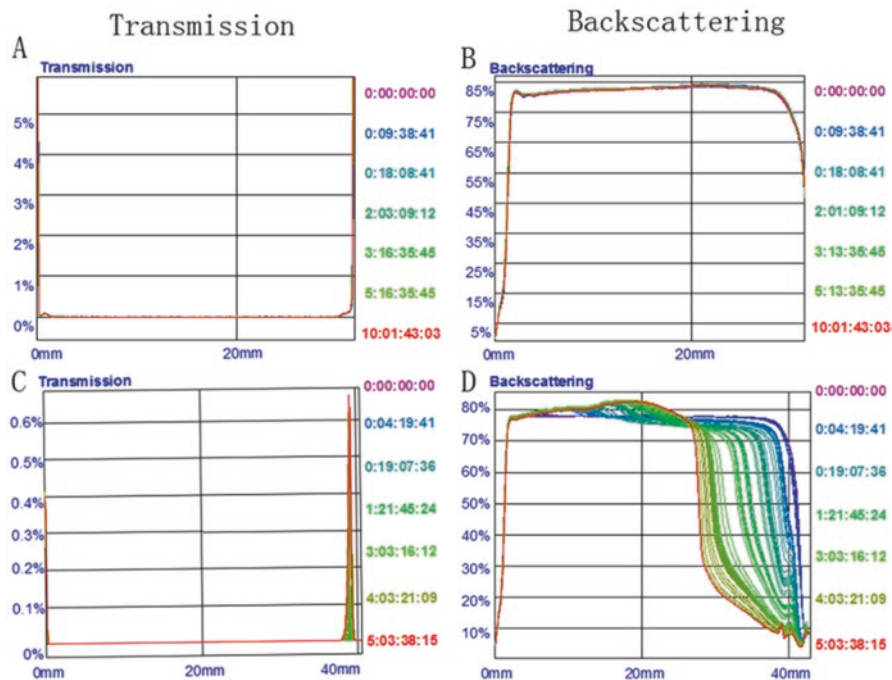
**Fig. 3.8** Interactions of dispersant with particles in suspension system

of particles or droplets of flocculation, causing strength change of the backscattering and transmission. Therefore, the transmission and backscattering profiles contain overall (sedimentation and aggregation) kinetics information and the relative migration speed of the particles.

The suspension of ICPC is affected by agglomeration, dissolution, and thermal motion of the suspended particles. The rate of particle movement, thickness of precipitation phase, average particle size, the volume concentration of the disperse system, and a series of changes of the suspension system such as flocculation, emulsification, and sedimentation can be calculated according to changes in the transmission light of curve and the intensity of backscattered light. There are several ways to improve the suspension stability:

1. Constructing wettable surface of solid particles by the medium (Fig. 3.8). Solid particles are separated by the disperse medium to avoid agglomeration and sedimentation. Solid particles have a good dispersion effect in an aqueous medium, while they are poor in a nonaqueous phase. Therefore, new dispersants with anchoring groups and solvated chains for nonaqueous system should be explored.
2. Reducing the density difference between the dispersing medium and suspended substance. Sedimentation velocity is directly proportional to the density difference. Therefore, reducing sedimentation velocity is favored to enhance the suspension stability. A range of dispersants were added to modify stability. The result showed that polyacrylates, Darvan C, and Dispex A40 were the most effective dispersants for HA in water. Solsperser 3000 at low levels and Atsurf 3222 were the most effective among the 10 dispersants in alcohol. Solsperser 3000, a carboxylic acid-terminated polyester, was also the most effective dispersant in hexadecane [54].
3. Increasing viscosity and reducing relative molecular weight and particle diameter by grinding, homogeneity, or enzymatic hydrolysis is a common method to improve suspension stability. Sedimentation velocity is in proportion to the square of the radius of dispersed particles. To be more specific, the larger the particles are, the faster the sedimentation velocity is and vice versa.

Furthermore, the kinetic suspension stability can be attained by adding thixotropic agents [55–57]. Fumed silica formed the network structure when it was incor-



**Fig. 3.9** (a) Transmission light curves of p-ICPC with sample height, (b) backscattered light curves of p-ICPC with sample height, (c) transmission light curves of n-ICPC with sample height, (d) backscattered light curves of n-ICPC with sample height (Reproduced from Ref. [58] by permission. Copyright © 2013 Springer Science + Business Media New York)

porated into n-ICPC pastes as a thixotropic agent. The suspension stability of p-ICPC was performed on the Turbiscan LA-b<sup>Expert</sup>, and n-ICPC was used as a control. After a period of storage, tiny particles tend to settle down to the bottom of the sample cell due to the gravitation, which lead to the suspension destabilization. Interestingly, no sedimentation occurred in p-ICPC at room temperature (Fig. 3.9) even scanning for 10 days. Both T and BS in p-ICPC remained close to zero all through the sample cell, even at the top. On the contrary, the n-ICPC under the same condition stratified rapidly in two phases. The apparition of the nonaqueous phase was reflected by an increase in the T signals. Obviously, the suspension stability of p-ICPC was effectively improved. It is mainly due to the formation of the network structure [58].

### 3.4.7 Sealability

As root canal sealers, n-ICPC fills the narrow and irregular root canal. However, inadequate filling could lead to the fluid penetrant to the filling defects causing a periapical chronic inflammatory reaction and compromising the treatment success.



Therefore, the detection of leakage *in vitro* is widely used to evaluate the sealing efficiency with high clinical significance.

The leakage testing has a long history, and the first study on leakage was conducted in 1961 [59]. Based on the principles of leakage testing in other dental fields, leakage test were adopted and modified to test for implants leakage as well. Evaluation of the gap at the interface level with radiographs, SEM, or other optical means is a simple method to detect inadequacies in the connection. However, this testing is less reliable and could not reflect the real situation as the continuity and depth of the gap cannot be evaluated. Other accepted testing techniques are microbial leakage or bacterial seal testing [60], endotoxin or other molecular microleakage tests [61], spectrophotometric determination of dye penetration [62], electrochemical [63], glucose penetration model [64], and the gas permeability test [65]. The latter method not only provides information whether the implant leaks or not but also provides the leakage amount over time allowing for quantitative comparison among different implants systems.

Dye penetration was the most common method due to its simplicity [66] and intuitively observation of the linear penetration of the dye between the root canal filling and the walls. Methylene blue dye was used as a leakage marker because it is readily detectable under visible light, soluble in water, and easy to diffuse. Torabinejad et al. [67] stated that a material that prevents the small molecule's (dye) penetration should prevent larger substances like bacteria and their by-products. Camps and Pashley [68] reported that the dye penetration method saved much time. Ethylene blue microleakage was also used to estimate the sealability of ICPC in our study. The microleakage distance of methylene blue was measured directly with vernier calipers from the end of the root filling material to the end point of the dye in the canal. The result showed that the mean microleakage lengths of bismuth-doped ICPC were lower than that of pure ICPC, indicating that the former possessed better resistance against methylene blue dye penetration [69]. The good sealability was probably attributed to the improved injectability and formation of the gap-filling apatite deposits. On one hand, BSB enhanced the injectability of BD-ICPC and made BD-ICPC fill up any gaps induced during the material shrinkage phase and the dentinal tubules. On the other hand, the hydration product of ICPC wrapped a small amount of fine BSB, formed a closely packed structure, and made the BD-ICPC denser.

Rhodamine B was another dye to evaluate the sealability without suffering discoloration from filling materials, as occurs with methylene blue. Furthermore, the authors used vacuum to eliminate the air bubbles and make the dye easy to penetrate [70]. The result showed Rhodamine B was an effective method to evaluate the sealability of MTA and calcium hydroxide.

Bacteria are microorganisms that cause the infection of the root canal. To better simulate the oral environment, bacteria model *in vitro* is established closer to the clinical than the dye and the radioactive elements. Mortensen [71] proposed that microleakage can be measured by bacteria in place of dyes and radionuclides as a marker. Radionuclide penetration takes radionuclide-labeled particles as a penetration marker. Particles are protein, salt, urea, and other molecules. The labeled materials were introduced together with the solution for penetration and finally using the

self-development of the radioactive isotope. The depth of penetration usually displays in the X-ray. The biggest advantage of the liquid flow, microscope, and computer 3D reconstruction is to observe the microgap of the sample repeatedly and directly. Lyroudia [72] scanned the cross section of the root canal, studied the microseepage by the computer three-dimensional image reconstruction, and obtained the results from different visual angles.

## **3.5 Applications of ICPC in Hard Tissue Repair**

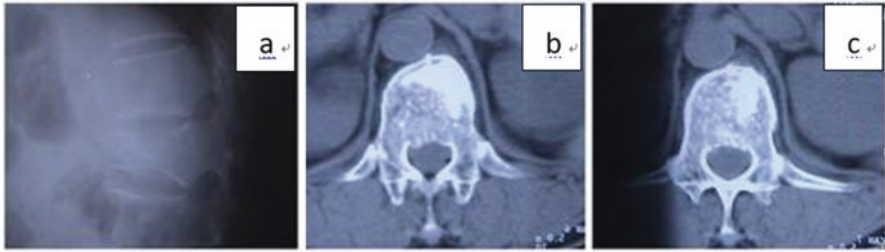
### ***3.5.1 Applications of ICPC in Bone Repairing***

Due to the intrinsic biocompatibility, degradability of the material itself, and flexibility in shaping and injectability in practical use, CPCs serve as a promising candidate in bone tissue repairing and have already been proven as suitable substitutes in tissue engineering. Considering the specific chemical composition of CPCs, the combination of Ca and P boosts excellent osteoconductivity, which could stimulate further tissue regeneration, especially in hard tissue repairing areas such as spinal repair, root canal filler, or periodontal defect filling in physically damaged or pathological bone sites. In addition, the better understanding of setting behaviors of CPCs enables us to load drugs into the material in a tunable way to achieve a controlled release at the local site.

With the coming of aging society, the number of patients with vertebral compression fractures, vertebral metastasis, radius fracture, etc., triggered by osteoporosis is on the rise. The long-term pain or incapability to sit down has severely disturbed the normal life of people. Considering the low efficacy of medical treatment and unsuitability of internal screw fixation in patients with decreasing bone mechanical properties, percutaneous vertebroplasty by the use of ICPC to strengthen diseased vertebra could serve as a good therapeutic option.

A number of researchers have explored the superiority of ICPC in the field of bone repair. For example, Libicher [73] and coworkers applied resorbable CPCs in osteoporotic vertebral fractures and investigated the osseous integration. It was observed that the cured CPC materials demonstrated good integration with surrounding tissues and were gradually replaced by autologous bone tissue via osteonal ingrowth. Shigeo Ishiguro [74] applied ICPC in percutaneous vertebroplasty for osteoporotic compression fractures. Totally, 36 patients with osteoporotic fractures underwent percutaneous vertebroplasty using CPC. The clinical results showed that immediate pain relief was achieved, and the risk of vertebral body collapse and pseudarthrosis was reduced, demonstrating the effectiveness of ICPC.

Since 2003, our group [75] has carried out the minimally invasive therapy research of injectable and degradable calcium phosphate-based inorganic cements on vertebral fractures. It was found in the clinical use that ICPC boosted excellent



**Fig. 3.10** Compression fracture treatment by injection of ICPCs (a) before surgery, (b) after injection, and (c) one month after surgery

injectability. The pastes could easily pass the syringe needle with 0.33 mm inner diameter, and the force needed to inject into centrum was less than that needed for PMMA. With synergetic modification of various compositions, the curing time of ICPC could be controlled under 18 min to achieve the initial strength and completely cured at body temperature (37 °C) after 24 h to achieve the highest strength, which could satisfy the requirements of surgeries. Meanwhile, the material possessed good water resistance, with the anti-washout rate of above 98%. The strength and tenacity were enhanced, with the increase of compressive strength from 22 MPa after 1 h to 47 MPa after 24 h, which was higher than the mechanical strength of similar imported products MIIG.

ICPC of TECP/DCPA system prepared by our group has been used in clinical trials. The mechanical strength of ICPC is 20 MPa higher than the average commercial products, ranging from natural spongy bone and cortical bone, self-set within 3–15 min, and achieves 85% of the highest compression strength after 4 h. Meanwhile, the ICPC system exhibits an outstanding injectability with excellent bonding to bone tissues after setting.

In one case, ICPC was employed in percutaneous vertebroplasty. As it was inferred from the CT image (Fig. 3.10), ICPC materials were well filled into the damaged cavity and demonstrated good adhesion to surrounding bone tissues, greatly promoting the therapeutic effect.

ICPC was also injected into the vertebral bone trabecular gap of fresh bodies to further investigate biomechanics. Only 8–10 psi was needed during the injection, which was greatly lower than that of PMMA (20–40 psi), proving again its excellent injectability. The CPCs could self-set within 8–15 min at the gap. After injection, the loading capacity has increased to 8000 N, 52.4% higher than the original centrum, showing that the mechanical property could satisfy the clinical need.

To sum up, the ICPC could be considered as an outstanding material, especially in spinal repairing such as percutaneous vertebroplasty. Of course, to meet with clinical requirements, injectable bone cements whose viscosity versus time from commencement of mixing characteristics are consistent with the aforementioned requirements of various patients still have to be developed [74]. In addition, more clinical trials are needed to further identify the effectiveness of ICPC materials.

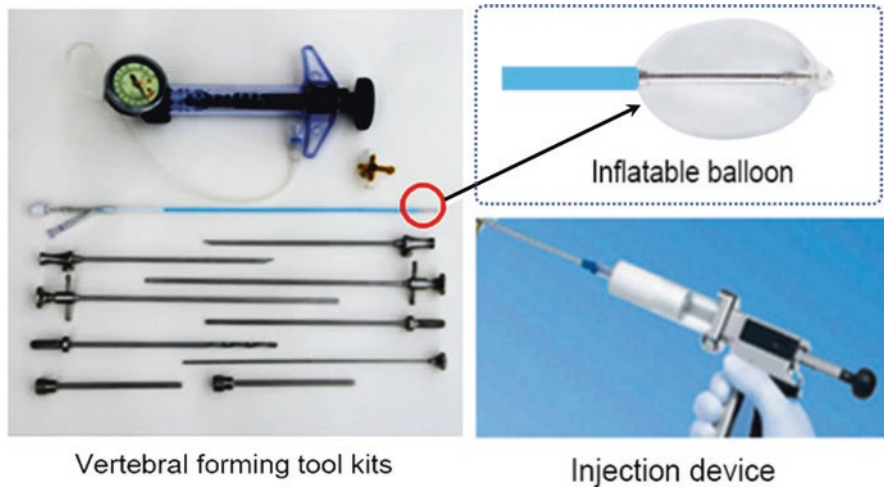


Fig. 3.11 Operating process of percutaneous kyphoplasty

### 3.5.2 Percutaneous Vertebral Device for Minimally Invasive Treatment of ICPC

In minimally invasive vertebral body forming technology, designing reasonable supporting equipment and establishing an effective working channel are the keys to ensure the point injection of bone cement and restore the vertebral body height. In recent years, percutaneous kyphoplasty (PKP) rapidly developed, that is, the percutaneous and pedicle firstly imbedded the inflatable balloon into the vertebral body, expanding the balloon and squeezing the damaged vertebral body to reduce the fracture vertebrae with a safe and effective space, followed by venting out of the balloon and filling the bone cement at a low pressure (Fig. 3.11). Using the technology of PKP can restore the vertebral height, enhance the vertebral strength, and reduce postoperative pain. More importantly, filling CPC into the vertebrae under low pressure can effectively lessen the leakage of cement to reduce complications. However, obtaining a miniature, thin-walled balloon and ensuring the sealing connection between balloon and catheter is very difficult. The existing cardiovascular dilatation balloon cannot withstand the high pressure above 350 psi which is considered to be the minimum pressure of vertebral minimally invasive surgery. Additionally, the deformation of balloon should be limited to keep stable dimensions under the desired high pressure. And the cardiovascular dilatation balloon cannot meet this requirement.

In order to meet the special requirements of inflatable balloon in the process of vertebral minimally invasive treatment, our group invented the process technology of multistage ring-shaped rotary expansion and radial double-sided tensile to prepare high-resistive tear balloon [76]. On account of thermoplastic property of polyurethane (TPU) elastomer, our group produced the isotropic TPU materials through multiple bidirectional expansion orientation techniques. The rotational expansion and radial stretching of TPU lead to the orderly alignment of polymer chains in a circumferential and radial direction, respectively. This process enhances and stabilizes the tear strength and dimensional stability of the thin-walled balloon. The balloon can still withstand the pressure environment more than 350 psi when the wall thickness is about 0.2  $\mu\text{m}$ , and the balloon possesses excellent mechanical strength

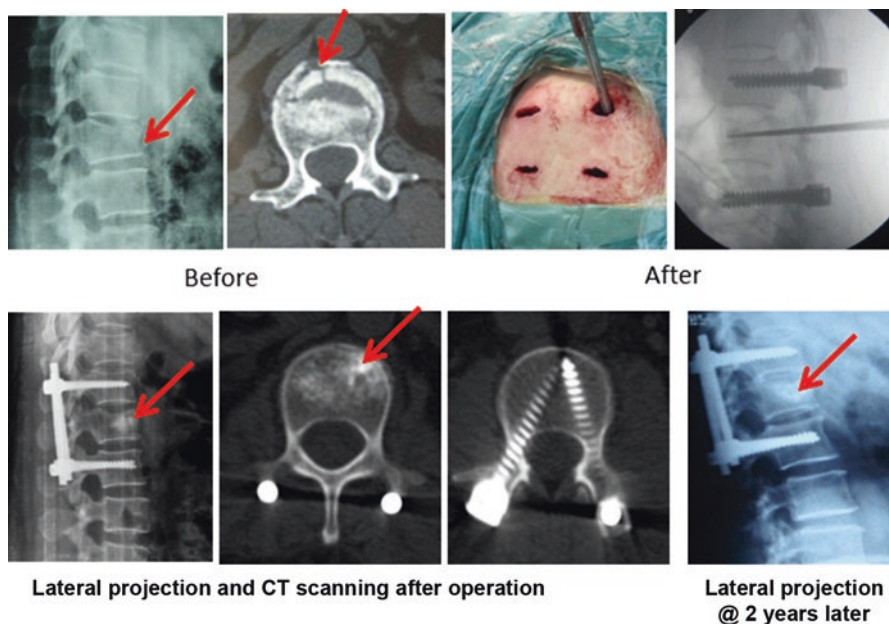


**Fig. 3.12** The devices and tools for percutaneous kyphoplasty

which can withstand the sharp contact pressure like bone fragments without damage. Moreover, the balloon can rebound back to the size before expansion for facilitating removal. On the other hand, the high-frequency (>100 kHz) welding technology was utilized to achieve the seal connection between the balloon and the catheter (Fig. 3.12). The finally prepared balloon catheter has a maximum tolerated pressure of no less than 400 psi, which can meet the requirements of PKP operation.

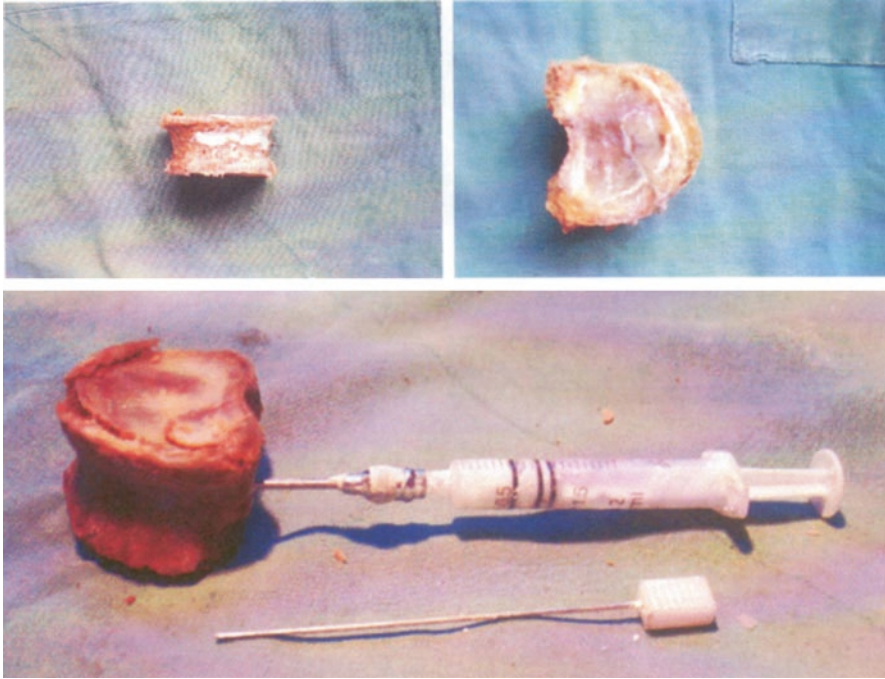
### ***3.5.3 Operational Techniques for Centrum Minimal Invasive Treatment in Clinical Use***

Posterior pedicle screw is one of the common methods employed in the treatment of thoracic and lumbar fractures. However, due to the osteoporosis of elderly patients, the implant could suffer from the poor stability, enlarged porosity after resetting of fracture, and collapse of the centrum after recovery. All the above defeats could induce the rapid increase of stress on the posterior pedicle screw, thus leading to the high failure of the fixation due to the loosening and rupture of screw. Meanwhile, the screw expands the fixation sites, and only the cortical bones surrounding the centrum are restored. By combining the centrum minimal invasive treatment with pedicle screw fixation, a new clinical operational technique has been proposed and reduced stress of pedicle screw when working alone, lowered the failure rate of inner fixation, and maintained better restoration of fractured part. Compared with PMMA, ICPC has less influence on the near intervertebral disc after centrum strengthening, thus significantly improving the load distribution of spinal stress field and displacement field.



**Fig. 3.13** 45-year-old female, vertebral pedicle screw fixation, and PVP (ICPC from Rebone, Shanghai, China) (Reproduced from Ref. [77] by permission. Copyright © 2017)

Patients with fresh single-segment thoracolumbar burst fracture and without neurological symptoms are selected for pedicle screw fixation and percutaneous vertebroplasty. The clinical results reveal that the combination of centrum minimal invasive treatment with pedicle screw fixation cannot only improve the restoration of fractured centrum but also maintain the height after operation to prevent any losses that lead to fixation failure. Compared with traditional methods, the new approach reduces the operation time and accelerates the recovery, thus opening up a new door for the safe and effective treatment of osteoporotic vertebral fractures and thoracolumbar vertebral burst fractures. In one typical case (Fig. 3.13), a 45-year-old female with first lumbar vertebral burst fracture has taken the combined treatment of vertebral pedicle screw fixation and percutaneous vertebroplasty (ICPC produced by Rebone, Shanghai). Pain score dropped to 2 points immediately and fell to 0 after treatment for 3 months. ICPC had a lower occurrence rate of pulmonary fat embolism than PMMA. The central and anterior vertebral body height significantly increased, and the strength of catagmatic vertebra restored to two times, while rigidity increased 15–20%. It kept shapes and internal structure of the vertebra, preventing micromotion in the vertebra and providing a stable internal environment for recovery. The results confirmed that percutaneous vertebroplasty with ICPC is a good choice for the treatment of acute thoracolumbar osteoporotic vertebral compression fractures.



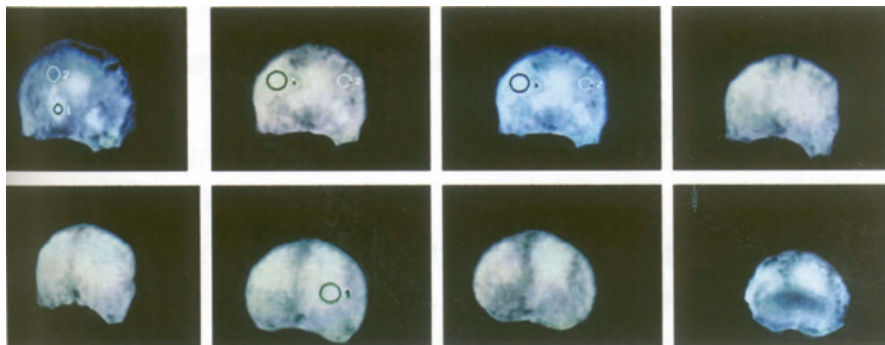
**Fig. 3.14** Injection of ICPC into centrum (Which is reproduced from Ref. [78] by permission)

Biomechanics in percutaneous vertebroplasty after fracture was also investigated. During the trials on fresh bodies, ICPC was injected into gaps resulted from fracture, and cavity formed after the removal of the centrum (Fig. 3.14). After the injection of ICPC and thereafter hardening process, the load-bearing capacity of the repaired site was 2275 N, a 16.7% increase compared to 1950 N of the original one. Meanwhile, the stiffness also increased by 11.1% after the injection of ICPC materials. As we can see from the CT images in Fig. 3.15, the materials presented good adhesion to the surrounding bone tissues.

### **3.5.4 Application of ICPC as Root Canal Fillers**

Root canal filler serves as a good therapeutic method for dental-related diseases, including periapical or pulposus problems. A careful choice of filler material and a good performance in filling process remain the most important factors in clinical applications. ICPC, with excellent biocompatibility and osteoconductivity, has also been extensively employed in dental field.

An ideal root canal filler is required to be nontoxic, no stimulation, and no obvious postoperative inflammatory reaction when it contacts with periapical tissue. It



**Fig. 3.15** CT images of ICPC filling areas (Which is reproduced from Ref. [78] by permission)

should offer adherence to dentinal walls of the retrograde preparation, periradicular tissue tolerance, and bioactive promotion of healing. Meanwhile, the filling material should not corrode or be electrochemically active. It should also be kept in mind that easiness to manipulate, dimensional stability, non-absorbability, as well as no penetration by bacteria must be considered during the selection of materials [79].

A DCPD-CaO-based hydraulic CPC was investigated for its antimicrobial activity and tightness in root canal filling [80]. In the following studies, it was found that in comparison to traditional calcium hydroxide pastes, the CPC material demonstrated better mechanical properties and provided a fluid-tight sealing [81]. Sealing property is considered as one of the most important parameter in root canal filler and to some degree determines the final therapeutic effect [82]. As a result, the performance in sealing ability of different fillers was also evaluated in the report. It was shown that CPC paste containing dicalcium phosphate anhydrous and dicalcium phosphate dihydrate exhibited good sealing ability against dye penetration, suggesting the capability to provide adequate seal of the canal. BD-ICPC exhibited improved plasticity, self-setting, radiopacity, sealability, and potent antimicrobial activity. In addition, BD-ICPCs afforded a uniform and tight adaptation to the root canal wall. It is expected to be used as a novel root canal filling material.

The tissue response of CPC was studied [83]. The results illustrated that, in the histological study in dogs, varying tissue reactions in contact with CPCs after implantation did not lead to severe inflammation, confirming the biocompatibility and nontoxicity of the materials. Hong CY [84] injected ICPC into monkeys' incisor and overbrimmed it to periapical tissues. Only mild stimulation reaction was observed after 1 month of treatment and no adverse reaction after 5 months. Goodel [85] made CPC into sealer of root canals and filled the gutta-percha point with Grossman's cement by high pressure. The control group only sealed gutta-percha points with Grossman's cement in pressure. The results of linear dye penetrant test in two groups showed that the experimental group had less dye infiltration than the control group in the root canal. Then the team used CPC to carry on leak proofness tests with zinc oxide eugenol sealer (ZOE) and gutta-percha points sealed with



Grossman's cement, respectively, proving that CPC as root filling material has good properties of sealing [86, 87]. Tchaou [88] compared six kinds of dental materials, such as CPC, formaldehyde cresol (FC), calcium hydroxide, zinc oxide, etc., for antibacterial effect against 21 kinds of bacteria in the root canal. The results indicated that the material containing CPC and FC has the strongest antibacterial ability, especially for anaerobic gram-negative bacteria.

Though ICPC has a series of comprehensive advantages and has already been applied in practical use, there is still a long way to go to further understand the in vivo behaviors and further confirm the therapeutic effect.

### 3.5.5 *Periodontal Defect Filling*

The periodontium is a complex anatomical structure composed of both hard (bone and cementum) and soft (periodontal ligament) connective tissues [89]. A periodontal wound is always created along with a series of periodontal lesions which have shown to be a high risk of disease progression in subjects who had not received systematic therapy [90], while deep intraosseous defects represent a major challenge for the clinician.

CPCs are identified as an emerging bone substitute materials for osseous augmentation due to its unique combination of osteoconductivity, biocompatibility, and mouldability. Moreover, the injectable CPC is important for minimally invasive surgery and optimal defect filling in clinical applications of periodontal defect to provide intimate adaptation to the bone lesions and cracks.

Nowadays, the technologies of periodontal defect repair have become increasingly mature, and a series of preclinical or clinical evaluation criteria and models were proposed such as socket healing, supra-alveolar periodontal defects, and furcation and fenestration defects [91]. ICPC was treated for pulpal and periapical diseases. The researchers suggested that the materials could close root canal and prevent bacteria invasion without adverse reactions. There was no side effects including tooth discoloration, volume change, postoperative pain, local gums bleeding, edema, and so on [92]. Yoshinori Shirakata et al. [93] concluded that the filling volume and stiffness of CPC may compromise the clinical outcomes for periodontal intrabony defects. However, the study failed to demonstrate any superior clinical outcomes for the CPC group compared to the open flap debridement group, whereas radiographs revealed more favorable results in the CPC group. In addition, the purpose of periodontal regeneration procedures is not just to obtain a bone filling of the defect, but a regeneration of all the periodontium. To improve the injectability of materials and their stability in the osseous defects, researches developed a composite based on silanized hydroxypropyl methyl cellulose (Si-HPMC) and biphasic calcium phosphate (HA and  $\beta$ -TCP), which obtained an exciting repair results in dog's critical size furcation defects [93].

Although injectable CPC has been used in clinical for a long time, however, drawbacks still existed such as easy to collapse and low osteogenesis. To address these issues, CPC-based composites were developed: some were studied in vivo experiments, and some were assessed by preclinical evaluations.

### 3.6 Summary and Perspectives

Injectable calcium phosphate cements have received much attention in recent years due to their numerous potential advantages such as in situ self-setting, precision injection, no exothermic heat release during the hydration process, minimal damages to tissues, and great relief of patients' suffering.

However, there are still many issues that restrict their wider clinical applications. For instance, the requirements regarding viscosity are conflicting. Ideally, the viscosity of ICPCs should be low and easy for injection through the cannula but high enough after implantation in bone defect to prevent from the tissue fluid to washout. Future research should focus on the improvement of the strength and in the meantime the injectability. A injectable cement with good injectability possesses the higher ratio of liquid to solid, thereafter having lower strength after setting. Potential solutions to overcome the shortcoming are to introduce some setting accelerators. Developing an injectable biomaterial for the encapsulation of viable cells and mimicking the 3D structure of natural bones are the potentially fruitful direction of injectable cements for hard tissue repair. Furthermore, a comprehensive internationally accepted standard should be developed to characterize the injectable bone cements. This standard should document procedures for determining not only the properties of ICPCs but also the guidance on how to use them in clinical applications.

### References

1. Gaculsi O, Bouler JM, Weiss P et al (1999) Kinetic study of bone ingrowth and ceramic resorption associated with the implantation of different injectable calcium phosphate substitutes. *J Biomed Mater Res* 47:28–35
2. Dupraz A, Delecryn J, Moreau A, Pilet P, Passuti N (1998) Long-term bone response to particulate injectable ceramic. *J Biomed Mater Res* 42:368–375
3. Knaack D, Goad MEP, Aiolova M et al (1998) Resorbable calcium phosphate bone substitute. *J Biomed Mater Res* 43:399–409
4. Ryf C, Goldhahn S, Radziejowski M et al (2009) A new injectable brushite cement: first results in distal radius and proximal tibia fractures. *Eur J Trauma Emerg S* 35(4):389–396
5. Matsumine A, Kusuzaki K, Matsubara T et al (2006) Calcium phosphate cement in musculoskeletal tumor surgery. *J Surg Oncol* 93(3):212–220
6. Laschke MW, Witt K, Pohlemann T et al (2007) Injectable nanocrystalline hydroxyapatite paste for bone substitution: in vivo analysis of biocompatibility and vascularization. *J Biomed Mater Res B* 82(2):494–505

7. Xu B (2001) Study on vertebroplasty and its clinical research. Dissertation thesis, The first affiliated Hospital of Soochow University
8. Li Z, Zhu H, Long H (2002) Preliminary report in treating thoracolumbar vertebrae fractures with filling with auto solidification calcium phosphate cement from percutaneous vertebroplasty. *J Bone Jt Injury* 17(2):86–88
9. Liu CS, Gai W. Injectable self-setting in situ inorganic bone cement and its application in minimally invasive treatment. Chinese Patent ZL2003115250.3
10. Zhu XS, Chen XQ, Chen CM, Wang GL, Gu Y, Geng DC, Mao HQ, Zhang ZM, Yang HL (2012) Evaluation of calcium phosphate and calcium sulfate as injectable bone cements in sheep vertebrae. *J Spinal Disord Tech* 25(6):333–337
11. Xu B, Tang T, Ni C et al (2003) Posterior open reduction short segmental pedicle internal fixation and vertebral plasty in the treatment of thoracolumbar fractures. *Chin J Orthop Trauma* 19(5):264–266
12. Xu B, Tang T, Hu Y, Ni C, Yang H (2002) Therapeutic potential of vertebroplasty in the treatment of thoracolumbar burst fracture. *Chin J Orthop* 22(12):738–740
13. Lobenhoffer P, Gerich T, Witte F, Tscherne H (2002) Use of injectable calcium phosphate bone cement in the treatment of tibial plateau fractures: a prospective study of twenty-six cases with twenty-month mean follow-up. *J Orthop Trauma* 16(3):143–149
14. Frankenburg EP, Goldstein SA, Bauer TW, Harris SA, Poser RD (1998) Biomechanical and histological evaluation of a calcium phosphate cement. *J Bone Jt Surg* 80A:1112–1124
15. Chen ZG, Zhang XL, Kang LZ, Xu F, Wang ZL, Cui FZ, Guo ZW (2015) Recent progress in injectable bone repair materials research. *Front Mater Sci* 9(4):332–345
16. Aghyarian S, Rodriguez LC, Chari J et al (2014) Characterization of a new composite PMMA-HA/brushite bone cement for spinal augmentation. *J Biomater Appl* 29:688–698
17. Wang X, Ye J, Wang Y (2007) Influence of a novel radiopacifier on the properties of an injectable calcium phosphate cement. *Acta Biomater* 3(5):757–763
18. Hu G, Xiao L, Fu H et al (2010) Study on injectable and degradable cement of calcium sulphate and calcium phosphate for bone repair. *J Mater Sci Mater M* 21(2):627–634
19. Iooss P, Ray AML, Grimandi G et al (2001) A new injectable bone substitute combining poly(caprolactone) microparticles with biphasic calcium phosphate granules. *Biomaterials* 22(20):2785–2794
20. Friedman CD, Costantino PD, Takagi S, Chow LC (1998) Bone-Source™ hydroxyapatite cement: a novel biomaterial for craniofacial skeletal tissue engineering and reconstruction. *J Biomed Mater Res B* 43:428–432
21. Chow LC (2000) Calcium phosphate cements: chemistry, properties, and applications. *Mater Res Soc Symp Proc* 599:27–37
22. Xu HHK, Careya LE, Takagi S, Chow LC (2007) Premixed calcium phosphate cements: synthesis, physical properties, and cell cytotoxicity. *Dent Mater* 23:433–441
23. Shozo T, Chow LC, Hirayama SA, Sugawara A (2003) Premixed calcium-phosphate cement pastes. *J Biomed Mater Res* 67B:689–696
24. Montazerolghaem M, Engqvist H, Karlsson Ott M (2014) Sustained release of simvastatin from premixed injectable calcium phosphate cement. *J Biomed Mater Res A* 102A:340–347
25. Åberg J, Engstrand J, Engqvist H (2013) Influence of particle size on hardening and handling of a premixed calcium phosphate cement. *J Mater Sci Mater M* 24:829–835. from ceramics to calcium phosphate cements. *Injury* 31: 37–47
26. Knaack D, MEP G, Aiolova M, Rey C, Tofighi A, Chakravarthy P, Lee DD (1998) Resorbable calcium phosphate bone substitute. *J Biomed Mater Res A* 43(4):399–409
27. Bohner M (2001) Physical and chemical aspects of calcium phosphates used in spinal surgery. *Eur Spine J* 10:S114–S121
28. Zhao L, Weir MD, Xu HHK (2010) An injectable calcium phosphate-alginate hydrogel-umbilical cord mesenchymal stem cell paste for bone tissue engineering. *Biomaterials* 31:6502–6510

29. Chen FP, Liu CS, Wei J, Chen X, Gao YL, Zhao Z (2011) Preparation and characterization of injectable calcium phosphate cement paste modified by polyethylene glycol-6000. *Mater Chem Phys* 125:818–824
30. Chen FP, Liu CS, Wei J, Chen XL (2012) Physicochemical properties and biocompatibility of white dextrin modified injectable calcium-magnesium phosphate cement. *Int J Appl Ceram Technol* 9(5):979–990
31. Liu CS, Shao HF, Chen FY, Zheng HY (2006) Rheological properties of concentrated aqueous injectable calcium phosphate cement slurry. *Biomaterials* 27(29):5003–5013
32. Bacchi A, Pfeifer CS (2016) Rheological and mechanical properties and interfacial stress development of composite cements modified with thio-urethane oligomers. *Dent Mater* 32(8):978–986
33. Gbureck U, Spatz K, Thull R, Barralet JE (2005) Rheological enhancement of mechanically activated  $\alpha$ -tricalcium phosphate cements. *J Biomed Mater Res B* 73B:1–6
34. Baroud G, Cayer E, Bohner M (2005) Rheological characterization of concentrated aqueous beta-tricalcium phosphate suspensions: the effect of liquid-to-powder ratio, milling time, and additives. *Acta Biomater* 1(3):357–363
35. Leroux L, Hatim Z, Freche M et al (1999) Effects of various adjuvants on the injectability of a calcium phosphate cement. *Bone* 25(2):31–34
36. Jin J, Gai W, Liu C (2005) The influence of additives on calcium phosphate bone cement rheological properties I. Polyvinyl pyrrolidone. *J East China Univ Sci Technol* 31(1):83–87
37. Rajzer I, Piekarczyk W, Castaño O (2016) An ultrasonic through-transmission technique for monitoring the setting of injectable calcium phosphate cement. *Mater Sci Eng C* 67:20–25
38. Brown PW, Fulmer M (1991) Kinetics of hydroxyapatite formation at low temperature. *J Am Ceram Soc* 74(5):934–940
39. Ishikawa K, Miyamoto Y, Takechi M (1997) Non-decay type fast-setting calcium phosphate cement: hydroxyapatite putty containing all increased amount of sodium alginate. *J Biomed Mater Res* 36(3):393–399
40. Takechi M, Miyamoto Y, Ishikawa K et al (1996) Non-decay type fast-setting calcium phosphate cement using chitosan. *J Mater Sci Mater M* 7(6):317–322
41. Wang Y, Wei J, Guo H, Liu CS (2006) Water resistance, calcium phosphate cement bioactive bone repair materials research. *J Inorg Mater* 21(6):1435–1442
42. Wang XP, Ye JD, Wang YJ (2008) Effect of additives on the morphology of the hydrated product and physical properties of a calcium phosphate cement. *J Mater Sci Technol* 24(2):285–288
43. Liu JQ, Li JY, Ye JD (2016) Properties and cytocompatibility of anti-washout calcium phosphate cement by introducing locust bean gum. *J Mater Sci Technol* 32(10):1021–1026
44. Konishi T, Takahashi S, Zhuang Z et al (2013) Biodegradable b-tricalcium phosphate cement with anti-washout property based on chelate-setting mechanism of inositol phosphate. *J Mater Sci Mater M* 24:1383–1394
45. Liu JQ, Li JY, Ye JD, He FP (2016) Setting behavior, mechanical property and biocompatibility of anti-washout wollastonite/calcium phosphate composite cement. *Ceram Int* 42:13670–13681
46. Liu C, Chen F, Wei J. Injectable calcium magnesium bone cement and its preparation method and application. Authorized Chinese patent number ZL 201010205094.8
47. Chen FP, Song ZY, Liu CS (2015) Fast setting and anti-washout injectable calcium-magnesium phosphate cement for minimally invasive treatment of bone defects. *J Mater Chem B* 3:9173–9181
48. López A, Engqvist H (2014) Compositions comprising injectable biomaterial cement and radiopacity improving agent. WO 2014/016707 A2, PCT/IB 2013/002575, 30 Jan 2014
49. Chen FP, Mao YH, Liu CS (2010) Bismuth-doped injectable calcium phosphate cement with improved radiopacity and potent antimicrobial activity for root canal filling. *Acta Biomater* 6(8):3199–3207
50. Wang XP, Ye JD, Wang YJ (2007) Influence of a novel radiopacifier on the properties of injectable calcium phosphate cement. *Acta Biomater* 3:757–763

51. Kjellson F, Almen T, Tanner KE, McCarthy ID, Lidgren L (2004) Bone cement X-ray contrast media: a clinically relevant method of measuring their efficacy. *J Biomed Mater Res Part B Appl Biomater* 70:354–361
52. Depraetere P (1983) *Potentiel Zeta des emulsions*. Galenica, vol 5. Elsevier Edition, pp 373–407
53. Balsamo V, Nguyen D, Phan J (2014) Non-conventional techniques to characterize complex SAGD emulsions and dilution effects on emulsion stabilization. *J Pet Sci Eng* 122:331–345
54. Gao F, Yang S, Hao P et al (2010) Suspension stability and fractal patterns: a comparison using hydroxyapatite. *J Am Ceram Soc* 94(3):704–712
55. Bossis G, Volkova O, Lacis S, Meunier A, Odenbach S (eds) (2002) *Ferrofluids*. Springer, Berlin. Chap. 11
56. de Vicente J, Lopez-Lopez MT, Gonzalez-Caballero F, Duran JDG (2003) Rheological study of the stabilization of magnetizable colloidal suspensions by addition of silica nanoparticles. *J Rheol* 47:1093–1109
57. Volkova O, Bossis G, Guyot M, Bashtovoi V, Reks A (2000) Magnetorheology of magnetic holes compared to magnetic particles. *J Rheol* 144:91–104
58. Chen F, Mao Y, Liu C (2013) Premixed injectable calcium phosphate cement with excellent suspension stability. *J Mater Sci Mater Med* 7:1627–1637
59. Swartz ML, Phillips RW (1961) In vitro studies on the marginal leakage of restorative materials. *J Am Dent Assoc* 62:141
60. Meleo D, Baggi L, Di Girolamo M et al (2012) Fixture-abutment connection surface and micro-gap measurements by 3D micro-tomographic technique analysis. *Ann Ist Super Sanita* 48:53–58
61. Assenza B, Tripodi D, Scarano A et al (2012) Bacterial leakage in implants with different implant abutment connections: an in vitro study. *J Periodontol* 83:491–497
62. Azem M, Mahjour F, Dianat O, Fallahi S, Jahankhah M (2013) Root-end filling with cement-based materials: an in vitro analysis of bacterial and dye microleakage. *J Dent Res* 10:46–51
63. Arruda RA, Cunha RS, Miguita KB, Silveira CF, De Martin AS, Pinheiro SL et al (2012) Sealing ability of mineral trioxide aggregate (MTA) combined with distilled water, chlorhexidine, and doxycycline. *Eur J Oral Sci* 54:233–239
64. Hohenfeldt PR, Aurelio JA, Gerstein H (1985) Electrochemical corrosion in the failure of apical amalgam. Report of two cases. *Oral Surg Oral Med Oral Pathol Oral Radiol Endod* 60:658–660
65. Souza EM, Wu MK, Shemesh H, Bonetti-Filho I, Wesselink PR (2008) Comparability of results from two leakage models. *Oral Surg Oral Med Oral Pathol Oral Radiol Endod* 106:309–313
66. Torres JH, Mechali M, Romieu O et al (2011) Development of a new quantitative gas permeability method for dental implant-abutment connection tightness assessment. *Biomed Eng Online* 10:28
67. Claus PE, Pia G, Brita W, Bernd H (2008) Marginal integrity of class V restorations: SEM versus dye penetration. *Dent Mater* 24:319–327
68. Torabinejad M, Watson TF, Pitt Ford TR (1993) Sealability of a mineral trioxide aggregate when used as root end filling material. *J Endod* 19:591–595
69. Camps J, Pashley DH (2003) Reliability of the dye penetration studies. *J Endod* 29:592–594
70. Gomes-Filho JE, Moreira JV, Watanabe S et al (2012) Sealability of MTA and calcium hydroxide containing sealers. *J Appl Oral Sci* 20(3):347–351
71. Mortensen DW, Boucher NE Jr, Ryge G (1965) A method of testing for marginal leakage of dental restorations with bacteria. *J Dent Res* 44(1):58–62
72. Lyroudia K, Pantelidou O, Mikrogeorgis G et al (2008) Three-dimensional reconstruction: a new method for the evaluation of apical microleakage. *J Endod* 26(1):36–42
73. Libicher M, Hillmeier J, Liegibel U et al (2006) Osseous integration of calcium phosphate in osteoporotic vertebral fractures after kyphoplasty: initial results from a clinical and experimental pilot study. *Osteoporos Int* 17(8):1208–1215

74. Ishiguro S, Kasai Y, Sudo A et al (2010) Percutaneous vertebroplasty for osteoporotic compression fractures using calcium phosphate cement. *J Orthop Surg* 18(3):346–351
75. Liu C, Gai W (2005) Injectable in-situ setting inorganic bone cement and its application in minimally invasive treatment. Authorized Chinese patent number ZL2003 1 15250.3
76. Liu C, Hong H (2011) A preparation method on developed inflatable balloons for kyphoplasty. Authorized Chinese patent number ZL 2011 1 0107501.6
77. Gu Y, Zhu D, Liu H, Zhang F, McGuire R (2015) Minimally invasive pedicle screw fixation combined with percutaneous vertebroplasty for preventing secondary fracture after vertebroplasty. *J Orthop Surg Res* 10:31–42
78. Zhang L, Chen T, Chen Z (2004) Comparison of effect of vertebroplasty assisted with different volume of auto-setting calcium phosphate cement. *Fudan Univ J Med Sci* 31(3):263–266
79. Jou Y, Pertl C (1997) Is there a best retrograde filling material? *Dent Clin N Am* 41(3):555
80. Michăilescu P, Kouassi M, El Briak H, Armynot A, Boudeville P (2005) Antimicrobial activity and tightness of a DCPD-CaO-based hydraulic calcium phosphate cement for root canal filling. *J Biomed Mater Res B* 74(2):760–767
81. Pradhan PK, Das S, Patri G, Patil AB, Sahoo KC, Pattanaik S (2015) Evaluation of sealing ability of five different root end filling material: an in vitro study. *J Int Oral Health* 7(11):11
82. Sugawara A, Chow LC, Takagi S, Chohayeb H (1990) In vitro evaluation of the sealing ability of a calcium phosphate cement when used as a root canal sealer-filler. *J Endod* 16(4):162–165
83. Noetzel J, Özer K, Reisschauer B-H, Anil A, Rössler R, Neumann K, Kielbassa AM (2006) Tissue responses to an experimental calcium phosphate cement and mineral trioxide aggregate as materials for furcation perforation repair: a histological study in dogs. *Clin Oral Investig* 10(1):77–83
84. Hong YC, Lin SK, Kok SH et al (1990) Histologic reaction to a newly developed calcium phosphate cement implant in the periodontal tissues. *J Formos Med Assoc* 89(4):297–302
85. Goodel GG, Mork TO, Hutter JW et al (1997) Linear dye penetration of a calcium phosphate cement apical barrier. *J Endod* 23(3):174–178
86. Yoshikawa M, Inamoto T, Hakata T et al (1996) Apical canal sealing ability of calcium phosphate based cements. *J Osaka Dent Univ* 30(1–2):1–13
87. Sugawara A, Chow LC, Takagi S et al (1990) In vitro evaluation of the sealing ability of a calcium phosphate cement when used as a root canal sealer diller. *J Endod* 16(4):162–164
88. Tchaou WS, Tummy BF, Minah GE et al (1996) Inhibition of pure culture of oral bacteria by root canal filling material. *Pediatr Dent* 18(7):444–447
89. Yang Y, Rossi FM, Putnins EE (2010) Periodontal regeneration using engineered bone marrow mesenchymal stromal cells. *Biomaterials* 31(33):8574–8582
90. Trombelli L, Heitz-Mayfield LJ, Needleman I, Moles D, Scabbia A (2002) A systematic review of graft materials and biological agents for periodontal intraosseous defects. *J Clin Periodontol* 29(s3):117–135
91. Bongio M, Beucken JJ, Leeuwenburgh SC, Jansen JA (2015) Preclinical evaluation of injectable bone substitute materials. *J Tissue Eng Regen M* 9(3):191–209
92. Dai HL, Yan YH, Cao XY, Li SP, Jia L, Dong WL (2002) Calcium phosphate sealing performance study of root canal material. *Biomed Eng Mag* 19(4):552–555
93. Shirakata Y, Setoguchi T, Machigashira M, Matsuyama T, Furuichi Y, Hasegawa K, Yoshimoto T, Izumi Y (2008) Comparison of injectable calcium phosphate bone cement grafting and open flap debridement in periodontal intrabony defects: a randomized clinical trial. *J Periodontol* 79(1):25–32

# Chapter 4

## Calcium Phosphate Composite Cement

Jing Wang and Changsheng Liu

**Abstract** Calcium phosphate cement (CPC) has shown great promise for bone regeneration. However, optimizations are still required to improve its comprehensive performance, including mechanical strength, biodegradation rate, cell affinity, etc. This chapter gives a general view on modifications of CPCs using the composite strategy. Development on elemental doping method, fiber incorporation tactics, and inorganic-polymeric hybrid system are elaborated. The chapter will offer inspiration on designing novel calcium phosphate-based cements.

**Keywords** Calcium phosphate cement • Composite • Fiber • Degradation • Interpenetrating Network (IPN)

### 4.1 Introduction

#### 4.1.1 Requirements of Bone Regeneration

Bone defects and nonunion caused by trauma, resection, or abnormal development pose a significant health problem worldwide [1–5]. It is estimated that by the year 2020, approximately 6.6 million orthopedic surgeries will be performed annually [6]. Currently, the best approaches for bone reconstruction are bone grafts either from autografts of the patient or allograft provided by the donor [7–10]. However, serious disadvantages are associated with the use of bone grafts. Considering the limited supply, donor site morbidity, risk of immune rejection, and chronic immune response owing to the second surgery at the donor site, strategies have prompted interest in artificial bone substitutes. By far, bone substitution is still an unsolved

---

J. Wang (✉)

Engineering Research Center for Biomedical Materials of Ministry of Education, East China University of Science and Technology, Shanghai 200237, China  
e-mail: [wangjing08@ecust.edu.cn](mailto:wangjing08@ecust.edu.cn)

C. Liu

Key Laboratory for Ultrafine Materials of Ministry of Education, East China University of Science and Technology, Shanghai 200237, China

problem, and there is a growing interest in the development of bone-like materials which allow for osteointegration into native tissue.

Since discovered in 1982–1983, calcium phosphate cements (CPCs) have been successfully used as bone substitute for more than 20 years due to their close semblance to the mineral phase and crystalline structure of natural bone, as well as their excellent biocompatibility and osteoconductivity [11–17]. Conventional CPC systems consist of a precursor powder containing one or several calcium phosphates and an aqueous solution. After mixing with specific ratio, the calcium phosphate precursors can transform into a less soluble nanocrystalline hydroxyapatite (HA) through a dissolution and re-precipitation reaction procedure, and the self-setting paste is formed. Both bulk scaffold and injectable paste can be fabricated [18–20].

Although CPC is highly promising for orthopedic applications, it has inferior mechanical properties and can hardly subject to the mechanical loading [21–25]. Periodic dynamic loading would lead to cracking and displacement of the surrounding bone fragments, which would delay or inhibit bone formation and thus impair healing. The relatively low strength and susceptibility to brittle fracture have limited its use to only non-stress-bearing applications. In comparison, the cortical bone has a true fracture toughness over 20 MPa. Besides low strength, there are still other shortcomings with the conventional CPC during the practical application, involving its prolonged setting time and washout upon early contact with physiological fluids or when bleeding occurs because of the difficulty in some cases to achieve complete hemostasis. In addition, its resorbability is comparatively lower, which is difficult to match the new bone formation [26–31]. Thus, current studies related to the development of “ideal” CPC are focused on the achievement of optimum balance between resorbability, porosity, and mechanical properties.

Much attention has been drawn to the optimizations of CPCs, especially the availability of novel load-bearing CPC cements. Nevertheless, combination of high strength and toughness is rare in engineered materials because these properties are antagonistic; single-phase materials are normally either strong and brittle or ductile and weak. Moreover, modification with biodegradability is even more challenging because biodegradability generally implies weak chemical bonds, which are in consequence rarely mechanically strong.

#### ***4.1.2 Strategy of Composite Cement Designing***

Since it seems difficult to fulfill all requirements such as load-bearing, degradation, fast setting, and anti-washout by single material, the focus of researchers has shifted toward composite materials, which combine properties of materials of different nature. In fact, bone is a complex nanocomposite of organic / inorganic structures where the inorganic component consists of nanoscaled HA crystals embedded between the precisely arranged organic collagen (Col I) fibers [32–37]. Col I builds the basic three-dimensional framework of the bone matrix for mineralization and remodeling. Thus, different composites with favorable physical, mechanical, and biological properties have been investigated as bone substitutes and regenerative materials.



Therefore, extensive studies have been performed to circumvent such problems in recent years, aiming at mechanical reinforcement, degradation promotion, and endowing some biological properties. This chapter provides an overview on current development of various composite strategies, including the reinforcement through addition of either inorganic granules or polymeric compositions, improvement of biological properties by doping with bioactive elements, as well as modification of resorption capability [38]. The aim of this chapter is to give a critical look on the Ca-P-based hybrids, which may pave the way for design of optimized CPC cements.

## 4.2 Silicate-Substituted Calcium Phosphate Cement

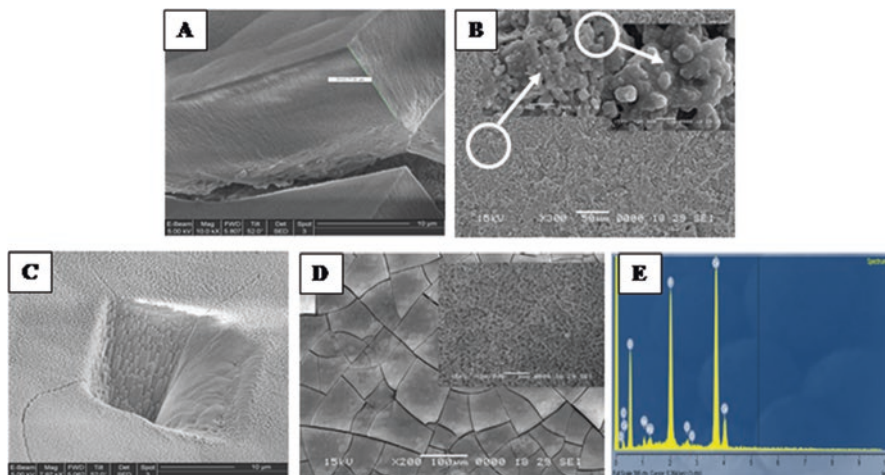
As abovementioned, an ideal substrate for the bone regeneration should not only have adaptive mechanical strength but also can promote bone repairing. Numerous works have been carried out about the Si-containing CPC since silicon is considered to be relevant to the initiation of mineralization and has positive effect on bone repairing [39–44]. Hence, both bioactive glass composite cements and silicate calcium phosphate have produced an impressive number of studies, which would supply better biological properties compared to pure calcium phosphates.

### 4.2.1 Bioactive Glass-Calcium Phosphate Composite Cement

It has been suggested that bioactive glass (BG) would make good bone forming either alone or in combination. Ducheyne et al. reported that mesenchymal stem cell (MSC)-seeded BG released Ca, P, and Si ions as part of the cascade of reactions that included the calcium phosphate layer formation and the preferential absorption of proteins such as fibronectin [45–48]. The latter step is an intermediary step preceding osteoblast cell attachment to the material surface, which affects the osteogenic phenotype expression and alkaline phosphatase (ALP) activity. So, it is rational that addition of BG to CPC is useful for the design and optimization of degradable implant materials in bone tissue repair and regeneration procedures.

#### 4.2.1.1 Fabrication and In Vitro Bioactivity

Generally, the composite BG-CPC cement consists of binary bioglass and calcium phosphate powder and liquid phase. In a representative research in Liu's group [49–51], calcium phosphate cements have the composition of tetracalcium phosphate (TTCP,  $\text{Ca}_4(\text{PO}_4)_2\text{O}$ ) and dicalcium phosphate anhydrous (DCPA,  $\text{CaHPO}_4$ ) in an equivalent molar ratio; hydroxyapatite (HA) was used as the hydration crystal seed. The Ca/P ratios of CPCs were 1.67, 1.60, 1.50, and 1.40, which were obtained by changing the ratio of TTCP and DCPA, and were coded as CPC<sub>1.67</sub>, CPC<sub>1.60</sub>, CPC<sub>1.50</sub>,



**Fig. 4.1** (A) SEM images of the thickness of the surface layers for cement-bioactive glass composite CPC<sub>1.5</sub>BG after differential immersion for 14 days. (B) SEM images of the surface of CPC<sub>1.5</sub>BG after differential immersion in Tris buffer solution (containing 10% newborn bovine serum) for 14 days. (C) Crystal morphology of CPC<sub>1.5</sub>BG layer. (D) Surface images of CPC<sub>1.50</sub>BG after immersion for 7 days. The inserted magnification revealed the external superficial granular apatite layer. (E) EDX spectrum of the surface of CPC<sub>1.50</sub>BG after immersion for 14 days (Reprinted with permission from Ref. ([49]). Copyright © 2008 *Biomedical Materials*. Rights Managed by IOP)

and CPC<sub>1.40</sub>. The silicon of the materials comes from traditional bioactive glass (BG) 45S5 granules (Wt%: 45% SiO<sub>2</sub>, 24.5% Na<sub>2</sub>O, 24.5% CaO, and 6% P<sub>2</sub>O<sub>5</sub>). Composite CPC-BG powders were prepared by mixing both CPC and BG at certain weight ratio. For example, composite materials that contained 80% CPC and 20% BG (W/W) were termed as CPC<sub>1.67</sub>BG. Deionized water was employed as the cement liquid; setting condition was set with 100% relative humidity at 37 °C for 48 h.

After the composite BG-CPC composites were immersed in Tris buffer, changes in microstructure could be observed. Poorly crystallized carbonate apatite could be found in the FT-IR spectrum. SEM examinations (Fig. 4.1) revealed that the surface of the samples was fully and uniformly covered by densely packed calcium phosphate precipitates. At a higher magnification, small crystallites were revealed in the granular apatite layer, verifying the formation of apatite layer on the surface, which was different from the parent glass. The representative CPC<sub>1.50</sub>BG sample showed a similar crystalline layer which possessed a subtle morphology of rodlike texture with directional arrangement apatite as formed during immersion. Further survey using ion beam bombardment demonstrated the surface formation of apatite layer. With longer immersion periods, microcracks of a tortoise shell character appeared on the fresh surface, which was resulted from the contraction during drying process.

A further confirmation conducted by EDX spectrum (Fig. 4.1E) indicated that the surface was a calcium phosphate with a Ca/P ratio of about 1.51. Thus, during immersion, the bioactive composite CPC dissolved and a new surface formed by precipitation and transformation reactions, leading to a poorly crystallized, Ca-deficient carbonated apatite. Such result is compatible with supersaturating conditions of the various ions in solution.

#### 4.2.1.2 Effects of Silica Content on Degradation

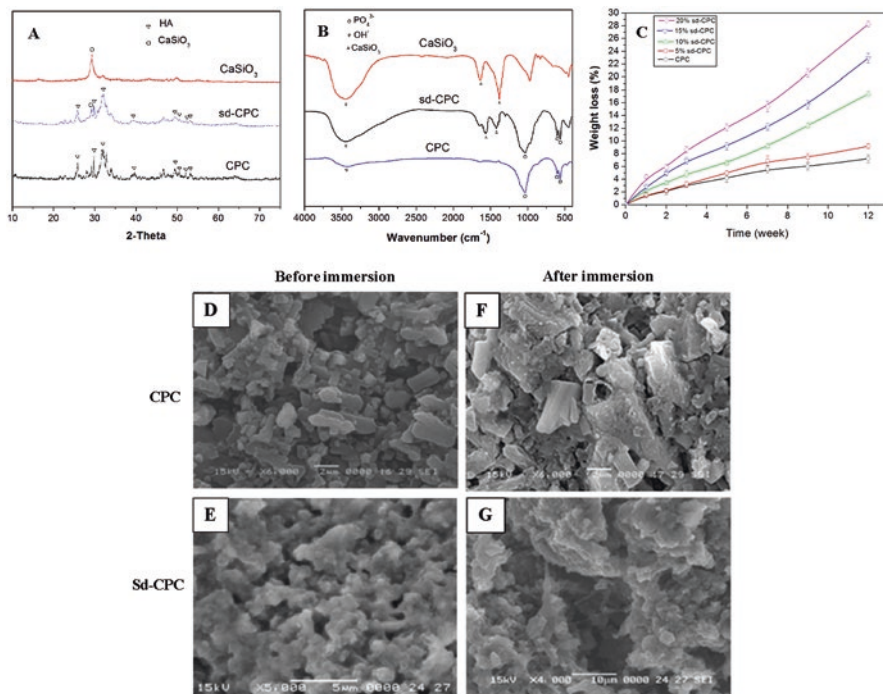
It is well known that proper degradation in a physiological environment is one of the most important characteristics of bone substitute biomaterials. The present study demonstrated that CPC-BG composites exhibited noticeable weight loss in Tris buffer solution over time, which indicated its improved degradability. As expected, the formation of Ca-deficient carbonated apatite with imperfect crystallization will be beneficial to degradation [52]. It was clear that the degradation rate of CPC-BG composite increased with the reducing of Ca/P ratio. In contrast, the CPC had lost only 7.23% of its initial weight at the end of the experiment, and pure active bio-glass was recognized as nondegradable material. But, surprisingly, the hybridization gave rise to the lower-crystallized Ca-deficient apatite, which had the specialty of degradation. In addition, thanks to the microcracks and micropores caused by the discrepant contraction between the different phases, which enlarged the surface of CPC-BG composite in contact with the liquid, the degradation ratio was improved. This cooperative effect is instructive for designing the biodegradable materials and can be modulated by varying the Ca/P ratio.

### 4.2.2 Silicate-Substituted Calcium Phosphate Cements

It is generally noted that Ca and Si ions play an important role in the nucleation and growth of apatite and influence the biological metabolism of osteoblastic cells in the mineralization process and bone bonding mechanism. In addition, wollastonite (naturally occurring calcium silicate) composites as plasma-sprayed coating on titanium alloy substrates or polymeric matrix showed good bioactivity and biocompatibility. As a result, preparation of Si-containing composite cement by doping with calcium silicates became a common approach [53–55].

#### 4.2.2.1 Effect of Silicate on Degradation Rate

In a typical research of silicate-doped calcium phosphate cement [52, 56] (termed as sdCPC), the existence of calcium silicate can be confirmed from the XRD and FTIR spectrum (Fig. 4.2). In addition, HA can be observed in the composites, indicating the occurrence of hydration of CPC. Compared with pure CPC which was

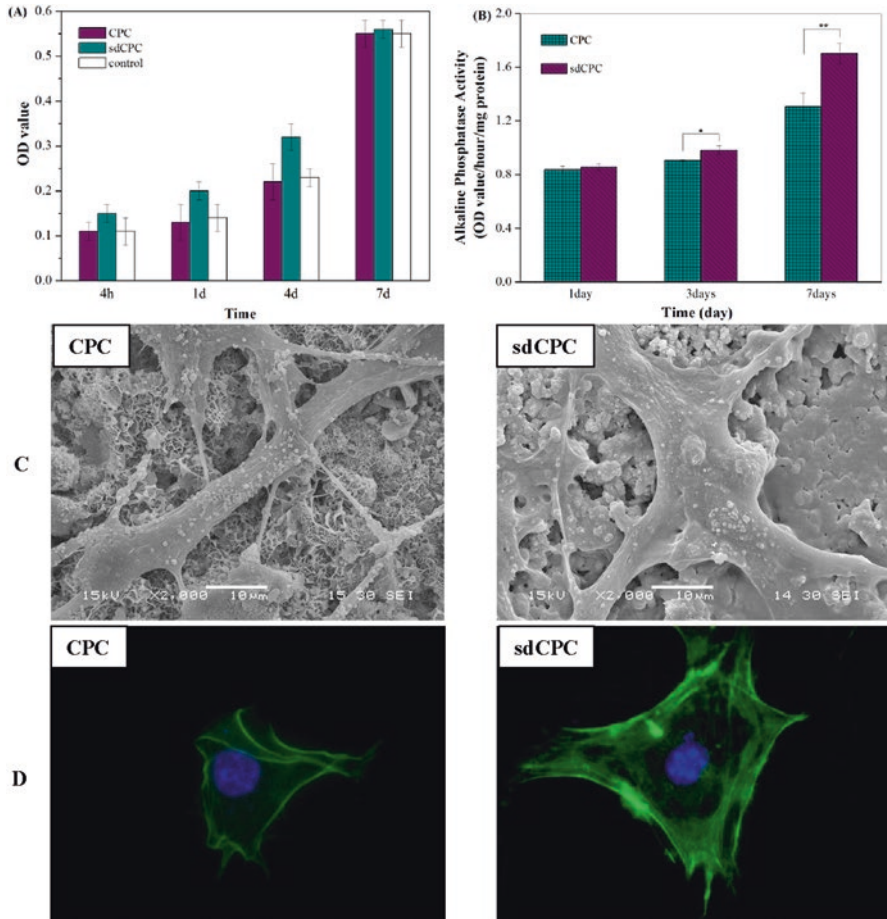


**Fig. 4.2** (A–B) XRD, FTIR spectrum of calcium silicate, CPC, and sdCPC (10 wt% silicate). (C) Weight loss of CPC and sdCPC soaking in Tris-HCl solution for various periods. (D–G) SEM micrographs of CPC and sdCPC before and after immersion in Tris-HCl for 5 weeks

composed of many particle-like crystal of HA, the sdCPC formed web structure. It looks like that HA crystal particle was completely embedded with calcium silicate xerogel. Mentionable, the *in vitro* weight loss of sdCPCs can be regulated flexibly by the amount of silicate. Increasing silicate content leads to accelerated degradation. Further evidence of many micropores can be found in sdCPC in SEM, indicating the accelerated degradation rate of sdCPC.

#### 4.2.2.2 Cell Affinity

More attentions have been paid to the Si-doped CPC since Si was reported to have positive effect on bone metabolism. As for silicate-doped CPC, superior cell attachment of sdCPC can be obtained compared with CPC, suggesting that introduction of Si will facilitate cell adhesion on their surfaces. Since the superficial specialty plays a key role in the cell response and behavior [57–59], the improved cell attaching is consistent with the liable formation of apatite layer on the sdCPC surface. Moreover, attachment is part of the first phase of cell-material interactions, which will influence the capacity for growth, morphology, proliferation, and



**Fig. 4.3** Effect of CPC and CPC-BG on proliferation (A) and differentiation (B) of C2C12 with different culturing time. Morphology observation (C) and cytoskeleton organization (D) of MC3T3-E1 cells on CPC and sdCPC surface (C, D) (Reprinted with permission from Ref. [56]. Copyright © 2010 *Biomedical Materials*. Rights Managed by IOP)

differentiation upon contacting with the implant. As a result, proliferation of C2C12 cells revealed the highest OD values of sdCPC specimen which was significantly higher than CPC and control after 1 and 4 days ( $p < 0.05$ , Fig. 4.3A).

Cell morphology observation under SEM micrographs (Fig. 4.3C) exhibited different morphology of MC3T3-E1 cells cultured onto the CPC and sdCPC disks after incubated for 24 h [56]. Cells located on the sdCPC spread better and were more closely adapted to the surface compared with CPC. As shown in Fig. 4.3D, after cultured for 24 h, MC3T3-E1 cells on the sdCPC disks displayed unique and limpid F-actin including microfilaments. In contrast, cells on the CPC disks exhibited mild and poorly F-actin fragment. Moreover, in accordance with the SEM

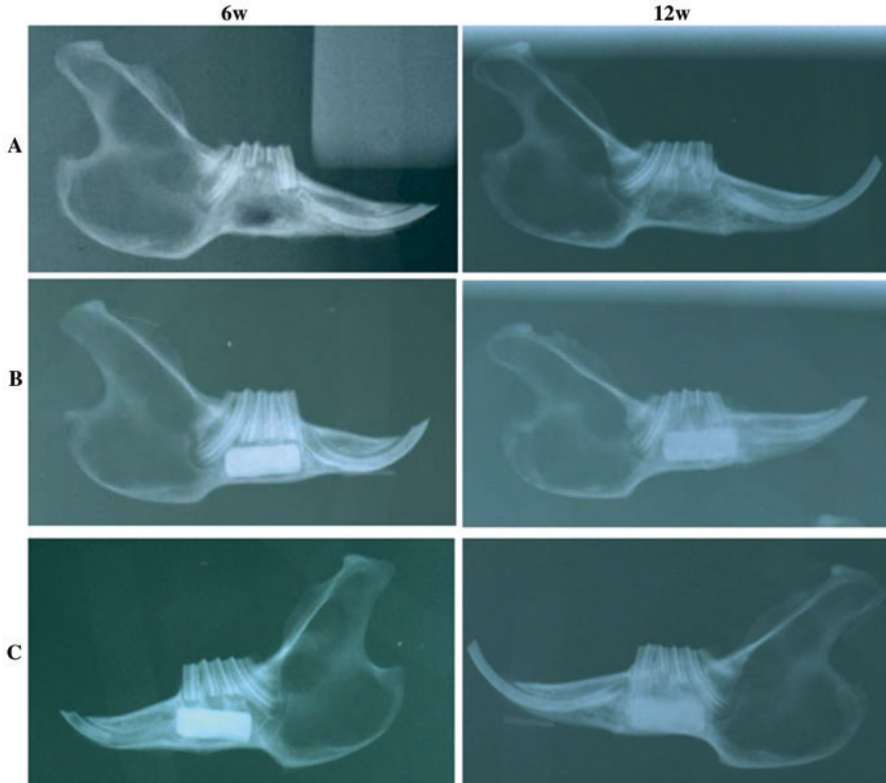
observation, cells cultured on sdCPC revealed better spread behavior since highly organized cytoskeleton with stress fibers is often associated with strong cell adhesion. These results suggest that Si-doping has positive effect on promoting cell growth and cell proliferation. Silicon is proven to stimulate the proliferation of bone cells and enhance osteogenesis through direct control over genes that regulate cell cycle induction and progression. With regard to the sdCPC, cell differentiation was evaluated in terms of the ALP activities of MC3T3-E1 cells cultured on both CPC and sdCPC at 1, 3, and 7 days (Fig. 4.3B). It was found that both two materials supported MC3T3-E1 cells differentiation. Obviously, as the culture time progressed, significantly greater activity was observed. However, ALP activity significantly increased compared with CPC, when cells were cultured on the sdCPC disks at 3 and 7 days.

#### 4.2.2.3 In Vivo Implantation for Bone Regeneration

In vivo osteogenesis was evaluated through a critical-sized ( $15 \times 6 \times 4$  mm) mandible defect of New Zealand white rabbits. For each animal, sdCPC sample was implanted in the left side, while either controlled CPC or blank was inserted in the right side.

From the X-ray radiographs [52], regeneration failed in the blank group; little new bone was formed at 12 weeks except partial regeneration at the edge of the defect. In CPC group, due to the slower resorption, no evident density decreasing of the implanted CPC was observed even after implanting for 12 weeks. Despite the vacancy length had been almost disappeared, the easier distinguished marginal area between material and tissue suggested the weak bony connection. In contrast, the density of the defect area in sdCPC group was enhanced, closed to the normal bony tissue. The disorganized trabecula was observed after 6 weeks, and some callus as well as osteoid tissue had formed at the extremities of the implants. At 12 weeks, mass callus had formed and the implanted material was partly degraded. A tendency of decreasing could be found around the edge of material, which was more close to the density of peripheral bony tissue. Especially, partial boundary between newly formed and normal bone disappeared, the bony fusion could be deduced and the defects were repaired on the verge of the ambient hard tissues (Fig. 4.4A–C).

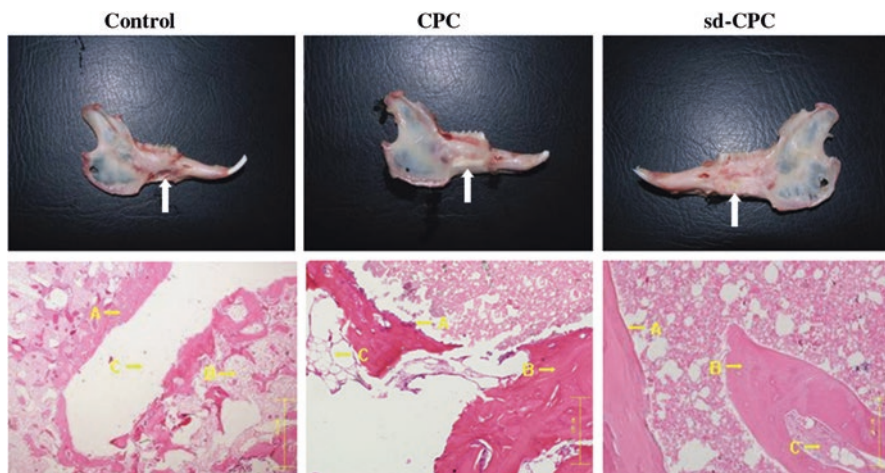
The gross inspection revealed that no synostosis but fibrous structure was predominantly observed at the defect area in controlled blank group. Though the penetrating defect was partially filled with newly bony structure, the defective area had not been repaired exactly, remaining the concave of about 6–8 mm. Repairing with CPC alone had the similar aspect to the sdCPC. The edge of defect had been covered with lamella neoformative callus, and a small part of the implanted material was degraded. However, bony union only appeared at the extremities of the implanted material, and the integration between material and defective tissue was not tight enough. In agreement with the radiographic analyses, the gross view of the jaw repaired with the sdCPC constructs showed that complete bony union was achieved at 12 weeks after surgery (Fig. 4.5). Although part of the implanted mate-



**Fig. 4.4** X-ray radiographs of different samples for 6 weeks and 12 weeks: (A) blank, (B) CPC, (C) sdCPC

rial remained at 12 weeks after surgery, bony union was achieved, and the shapes of the repaired mandible closely resembled those of the normal tissue. Locked-in integration was found between the interface on materials and new bone.

Histological analysis [52] of hematoxylin-eosin staining revealed that there was no bony tissue in the specimens from controlled blank group at 6-week time point, and the defects were filled with fibrous-like tissue. No obvious formation of bone at the central region of the implants had been found even after 12 weeks. This illustrated that addition of bone substitute was beneficial to the repairing of massive defect. In groups of CPC and sdCPC composite, new bone formation was observed in the central and peripheral regions. Especially in group sdCPC, the boundary between material and host bone was unclear due to the sufficient formation of mature bone tissues. Central osteogenesis could be observed, while scarcely ingrowth of new bone was found in the CPC group by contrast, except the coexistence of bony union and fibroblasts (Fig. 4.5). This suggested the osteoconductive ability of sdCPC was better than that of pure CPC cement [60–63].



**Fig. 4.5** General observation and histological analysis of the middle plane of the implanted constructs in postoperative 12 weeks ( $\times 10$ , A: bone healing, B: flaked new bone around material, C: marrow cavity)

### 4.2.3 Summary

The endeavor of Si-doping calcium phosphate cement modified apatite-forming ability, which seems to be a favorable surface reaction in forming a bond between tissue and materials and plays an important role in the process of attachment, spreading, and proliferation of cells on the interface of material. Moreover, Si-doped composite system has an improved resorption rate and accelerated bone formation.

## 4.3 Magnesium-Doped Calcium Phosphate Cement

### 4.3.1 Design of Magnesium-Doped Calcium Phosphate Bone Cement

A typical CPC that initially contains an equimolar mixture of tetracalcium phosphate (TECP) and dicalcium phosphate anhydrous (DCPA) can transform into hydroxylapatite as final product in about 30 min. However, its poor mechanical properties, lower biodegradation rate in vivo, and relatively prolonged setting time limit further applications. Particularly, in clinical applications, a long setting time may cause the cement to crumble when it comes into contact with physiological fluids or when bleeding occurs due to the difficulty in performing entire hemostasis in some cases, and a more rapid resorption and replacement by newly formed bone is desirable in some clinical situations as well.



The magnesium (Mg) is the fourth most abundant cations in the human body and is naturally found in the skeleton. In contrast, magnesium phosphate cement (MPC) composed of magnesium oxide (MgO) and ammonium phosphate ( $\text{NH}_4\text{H}_2\text{PO}_4$ ) is a kind of fast-setting phosphate cement [64–66]. Moreover, MPC has high initial strength and accelerated resorption rate [67–69]. Thus, it is rational that a combination of MPC with CPC might result in a novel magnesium-doped calcium phosphate complex with improved properties.

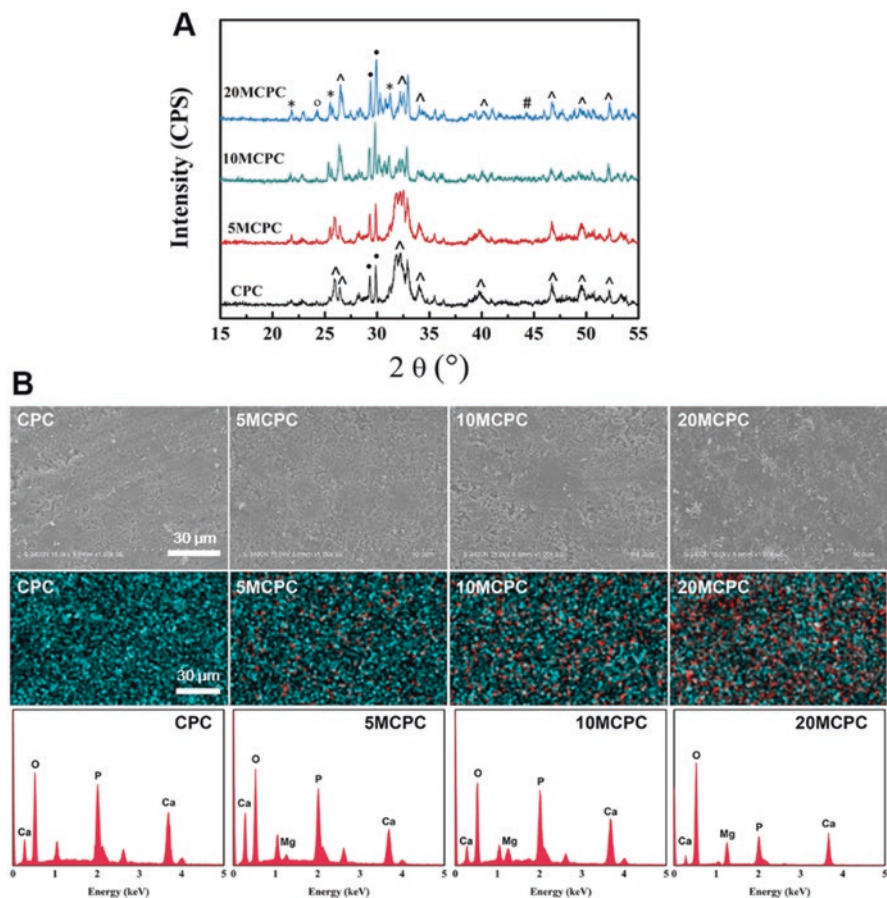
### 4.3.2 Effects of Magnesium Content on Properties [70–72]

MCPC can be obtained expediently by mix CPC powder, MPC powder, and cement liquid, such as ultrapure water. In a typical XRD analysis (Fig. 4.6A) after setting for 24 h in 100% relative humidity at 37 °C, both characteristic diffraction peaks of HA, magnesium phosphate, and the residuals of phosphates appeared in the composite. For example, CPC showed classical HA peaks and peaks for unhydrated TTCP. For MCPCs, the HA peaks shifted toward wide angles, indicating the formation of Mg-substituted hydroxyapatite (MgHA). Composite samples with lower Mg content (i.e., 5MCPC, which has 5 wt% of MPC) exhibited a similar composition phase with CPC except slight MgHA and  $\text{Mg}_3(\text{PO}_4)_2$ . But with the increasing of the MPC, the relative intensities of HA peaks decreased, and the intensities of several additional peaks corresponding to  $\beta$ -TCP and  $\text{Mg}_3(\text{PO}_4)_2$  increased, especially for the 20MCPC (containing 20 wt% MPC), which could be attributed to the hydration of magnesium phosphate cement.

Subtle microstructural difference existed among MPC, CPC, and Mg-doped CPC (MCPC) [72]. In SEM micrographs, MPC formed a xerogel-like dense, solid network, while CPC formed a particle-like structure with many micropores. In addition, MCPC exhibited a compact surface morphology, and the MPC xerogel seemed to fill into the microporous of CPC matrix (Fig. 4.6B). Lower content of MCPC exhibited a similar surface morphology like CPC and a significant surface roughness. Further intuitive survey of Ca and Mg distribution on CPC and MCPC surfaces detected by EDS exhibited similarly well-distributed Ca (shown as blue dots). For MCPC groups, magnesium (shown as red dots) was uniformly distributed. With the increase of MPC content, the distribution of Mg on the surfaces was more intense. The specific EDS spectrum showed the distinct peaks for Mg on MCPCs.

Moreover, superficial properties are influenced by Mg incorporation. Surface roughness by AFM analysis showed a relatively higher average of roughness (Ra) and increased hydrophobicity (Fig. 4.7). Mentionable, the *in vitro* degradation rate of MCPC can be accelerated and be modulated by MPC content. Higher percentage of MPC leads to faster degradation rate [73].

As to the mechanical strength, the composite MCPC samples have obvious higher compressive strength either than MPC or CPC after setting for 24 h. In addition, setting time of MCPC was shorter than those separate CPC or MPC. Specially,  $\text{MCPC}_{1/1}$  (MPC/CPC = 1:1) attained the highest compressive strength (of about 91 MPa) and the shortest setting time of approximately 6 min [70].

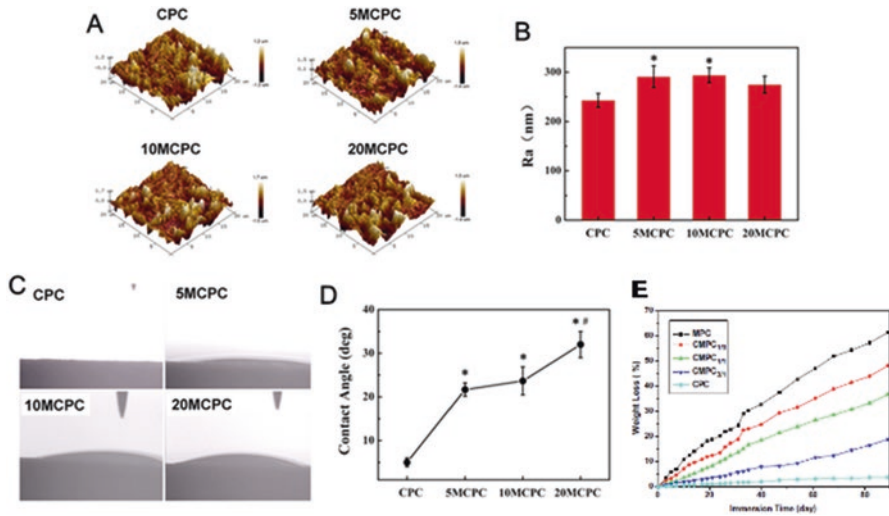


**Fig. 4.6** XRD patterns (A), superficial properties (B), and EDS analysis (C) of CPC and MCPC. (^: HA/MgHA. black dot: TTCP. o: beta- $\text{Ca}_3(\text{PO}_4)_2$ . #:  $\text{Mg}_3(\text{PO}_4)_2$ ). EDS mapping of Ca element (shown as blue dots) and Mg element (shown as red dots) distribution on CPC and MCPC surfaces (Reprinted with permission from Ref. ([73]. Copyright © 2015 *Biomaterials*. Rights Managed by Elsevier)

### 4.3.3 Effects on Cell Response

#### 4.3.3.1 Cell Compatibility

Cells showed well growth and stretched sufficiently on the surface of the 50MCPC samples, without any abnormal morphology. After 7 days, cells spread well and formed a confluent layer in intimate contact with the sample surface, while maintaining physical contact with each other. Results from the MTT assay indicated normal cell affinity on the CPC, MPC, and composite 50MCPC. In fact, 50MCPC exhibited superior proliferation than the other two pure samples.

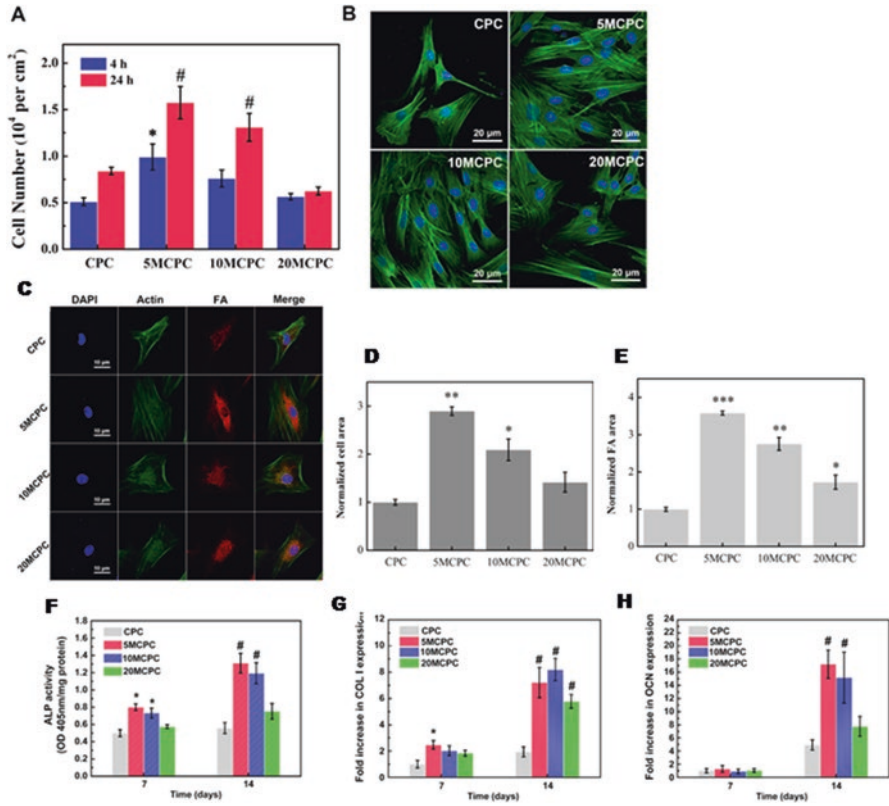


**Fig. 4.7** Effects of the MPC component on physiochemical properties of CPC. (A–B) The average roughness (Ra) of the CPC and MCPC surfaces analyzed by AFM images. (C–D) Contact angles of MCPC cements with different MPC content. (E) Weight loss ratio of various CPC and MCPC samples after immersing in SBF (Reprinted with permission from Ref. ([73]. Copyright © 2015 *Biomaterials*. Rights Managed by Elsevier)

#### 4.3.3.2 Influence on Adhesion Behavior of BMSCs

It is worthwhile to note that lower content of Mg has a positive effect on the attachment of cells [74–77]. Under fluorescence staining exploration, obvious differences could be observed in terms of the cell amount and morphology on MCPC with varied Mg content. Zhang et al. investigated MCPC-induced adhesion and osteogenic differentiation of BMSCs [73]. They found the highest cell attachment of BMSCs was observed on 5MCPC, which has lower Mg content, and the cells spread better. However, higher MPC contents in CPC seemed to be harmful to cell adhesion and spreading (Fig. 4.8A, B). Further study on spatial distribution of focal adhesion contacts and actin cytoskeleton of BMSCs exhibited a better spread morphology and more cytoplasmic extensions on 5(10)MCPC surfaces with significantly larger average cell area and enriched FA dots (Fig. 4.8C). More FA complexes were formed in those lower Mg-contented 5(10)MCPC groups, as well as greatly activated intracellular actin filaments. Nevertheless, the increase might be suppressed in higher Mg content; substantially reduced actin filaments were detected in 20MCPC group.

Intriguing results showed lower content of Mg might have an influence on the downstream signaling events to upregulate the osteogenic-related marker gene expression [73, 78, 79]. As a result, expression of both COL I and OCN was significantly upregulated on 5(10)MCPC compared to CPC. Moreover, ALP activity on 5(10)MCPC was significantly higher than that of CPC.

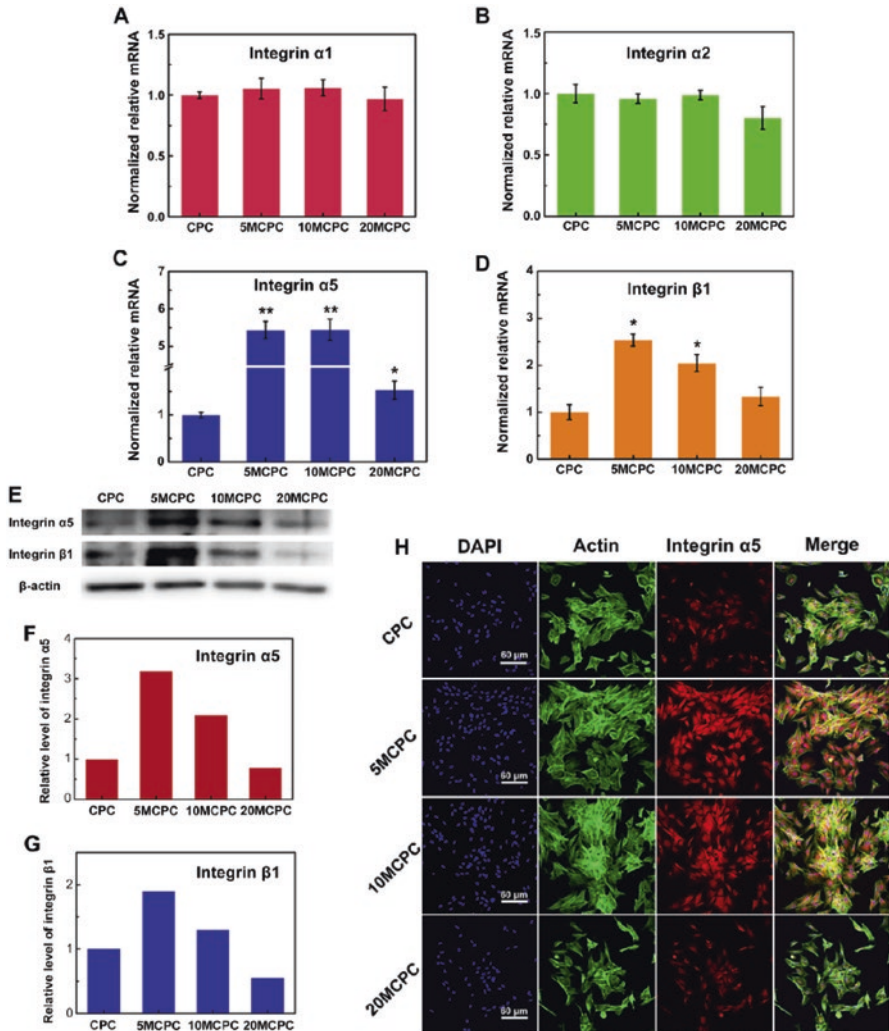


**Fig. 4.8** (A) BMSCs adhesion on CPC and MCPC. (B) Initial spread and cytoskeletal arrangement of BMSCs after 24 h seeded onto the CPC and MCPC surfaces. (C) Fluorescence images of FA formation through vinculin (red) and actin cytoskeleton filaments (green) of BMSCs. (D, E) Quantitative analysis data for cell area and FA area. (F–H) Effect of MCPC on the ALP activity and gene expression of major osteogenic differentiation makers of BMSCs (Reprinted with permission from Ref. [73]. Copyright © 2015 *Biomaterials*. Rights Managed by Elsevier)

Similar trend in immunofluorescence staining demonstrated the enhanced signal intensity of integrin  $\alpha 5$  in the 5MCPC and 10MCPC groups, indicating that the 5(10)MCPC could mediate cell adhesion and intracellular events through the Fn-integrin  $\alpha 5 \beta 1$  interactions (Fig. 4.9).

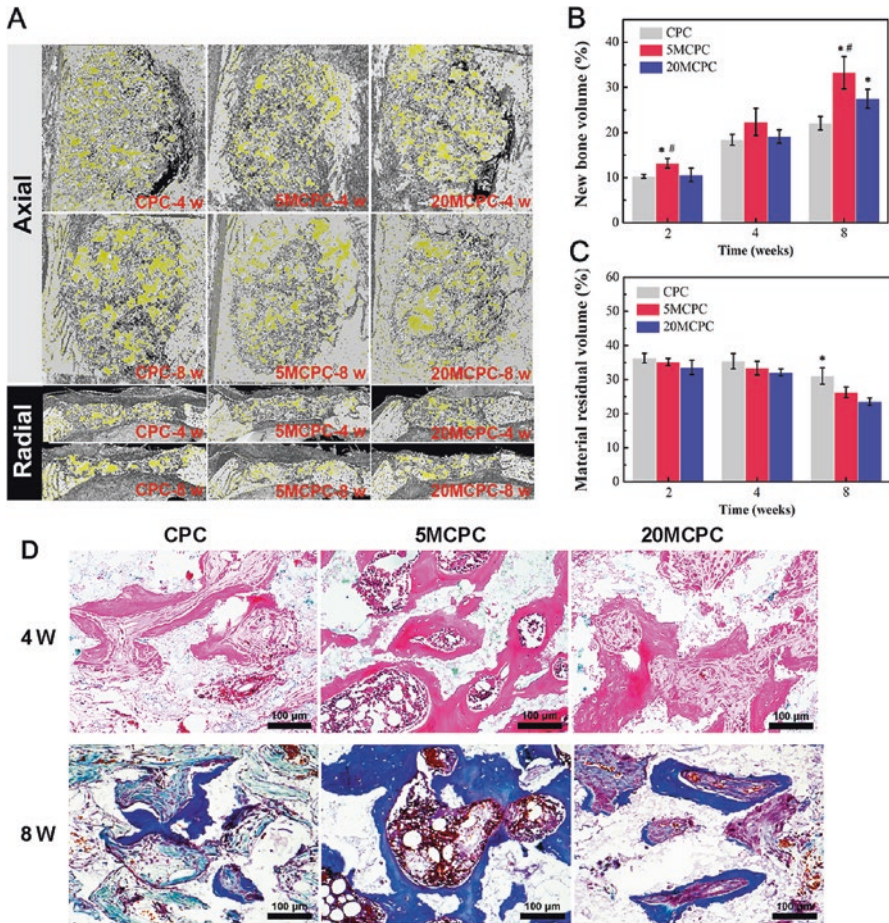
### 4.3.4 In Vivo Animal Test

In a critical-sized calvarial defect model of SD rats, obviously more new bone formation was acquired in 5MCPC from the reconstructed 3D images of implanted scaffolds by micro-CT at both 4 weeks and 8 weeks, with extensive bone ingrowth



**Fig. 4.9** Cell adhesion-related gene/protein expression on CPC and MCPCs. (A–D) Real-time PCR results of integrin subunit gene expressions. Results were standardized using GAPDH as a housekeeping gene. (E–G) Western blotting of integrin  $\alpha 5$  and  $\beta 1$  in cells cultured for 24 h on the cements. (H) Immunofluorescence analysis of integrin  $\alpha 5$  expression (red) in BMSCs on CPC and MCPCs surfaces (Reprinted with permission from Ref. ([73]. Copyright © 2015 *Biomaterials*. Rights Managed by Elsevier)

and nearly no gap left between the host bone and the material, and enhanced osteo-integration was achieved. These results were supported by histological evaluation. Obviously more trabecular bone formed in 5MCPC group was generated, suggesting the formation of medullary cavity. Noticeably those Mg-doped CPC scaffolds and prominent resorption of materials at the bone interface occurred, suggesting the accelerated degradation of the materials (Fig. 4.10).



**Fig. 4.10** Bone regeneration in a calvarial defect in SD rats: (A) 3D reconstruction images of the defect sites by SR $\mu$ CT (*white*: bone tissue, *yellow*: material residue). (B, C) Quantitative analysis of the new bone volume and material residual volume after 2, 4, and 8 weeks of surgery by SR $\mu$ CT. (D) Histological evaluation of orthotopic bone formation (H-E and Masson trichrome staining) (Reprinted with permission from Ref. ([73]. Copyright © 2015 *Biomaterials*. Rights Managed by Elsevier)

Based on these results, it can be inferred that lower Mg-containing 5(10) MCPC could mediate the adhering behavior of Fn and upregulate the expression of integrin  $\alpha 5 \beta 1$  on the cell membrane, which thereby not only promoted adhesion of BMSCs but also stimulated the osteogenic differentiation, leading to enhanced bone regeneration [80–83].

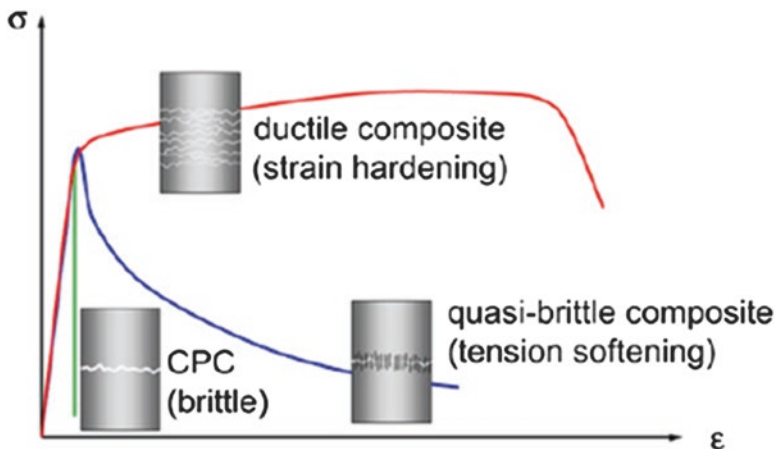
### 4.3.5 Summary

Mg-doped CPC composite cements had a shorter setting time and higher compressive strength compared with pure CPC. The degradation rate of the MCPC was higher than that of CPC both in vitro and in vivo and can be regulated by MPC content. The MCPC could support the well attachment and proliferation of cells. Furthermore, lower Mg content was considered to mediate desirable adhering behaviors of Fn and upregulated the osteogenic expressions, thus led to accelerated new bone formation.

## 4.4 Fiber-Modified Calcium Phosphate Composite Cement

CPC has been widely used in orthopedic surgery and dental procedures, including the reconstruction of osseous defects and frontal sinus, augmentation of craniofacial skeletal defects, and repairing of periodontal bone defects and tooth defects owing to its excellent biocompatibility. However, its relatively low strength and susceptibility to brittle catastrophic fracture have limited its applications in many stress-bearing locations and unsupported defects. There is a popular belief that the use of CPC is limited to the reconstruction of non-load-bearing applications.

Fibers are widely used for mechanical reinforcement of materials [84–89]. For example, poly(methyl methacrylate) bone cements have been reinforced with carbon fibers, titanium fibers, and polymeric fibers [90]. Predictably, incorporation of fibers can improve the strength and fracture resistance of CPC (Fig. 4.11). Various



**Fig. 4.11** Typical stress-strain curves for brittle behaving CPC and fiber-reinforced cementitious composites showing either quasibrittle tension softening or strain hardening behavior (Reprinted with permission from Ref. [91]. Copyright © 2012 *Biomaterials*. Rights Managed by Elsevier)

**Table 4.1** Examples for the reinforcement of calcium phosphate cements with either degradable or nondegradable fibers

Composition fiber/additive/matrix	Fiber volume fraction	Strength [MPa]	Work of fracture [KJ/m <sup>2</sup> ]	Test method
<b>Degradable fibers</b>				
HA matrix (TTCP + DCPA (+Na <sub>2</sub> HPO <sub>4</sub> -solution))	–	10–15	0.032–0.05	3 p.b.
Polyglactin 910/-/HA (TTCP+DCPA)	25 vol%	17.5–25	2.6–3.6	3 p.b.
Polyglactin 910/-/HA (TTCP+DCPA)	Mesh multilayer	8.5–24.5	0.75–3.1	3 p.b.
Polyglactin 910/chitosan lactate/HA (TTCP+DCPA)	45 vol%	41	11	3 p.b.
Polyglactin 910/chitosan lactate/HA (TTCP+DCPA)	Mesh multilayer	43	9.8	3 p.b.
Polyglactin 910/polycaprolactone/brushite ( $\beta$ -TCP+H <sub>3</sub> PO <sub>4</sub> )	24 vol% random short	7.5–20	n.a.	4 p.b.
	6–25 long fibers UD <sup>#</sup>			
<b>Nondegradable fibers</b>				
Carbon/-/HA (TTCP+DCPA)	2–10 vol%	32–60	3.5–6.5	3 p.b.
CNT/-/HA ( $\alpha$ -TCP+HA)	0.2–1.0 wt%	8.2–10.5	n.a.	3 p.b.
Aramid/-/macroporous HA (TTCP+DCPA+Na <sub>2</sub> HPO <sub>4</sub> )	6 vol%	7.5–13.5	0.8–6.5	3 p.b.
HA <sub>w</sub> /-/HA(TTCP+DCPA)	10–40 vol%	5.4–7.4	57–102	4 p.b.

Reprinted with permission from Ref. [38]. Copyright © 2015 *Materials*. Rights Managed by MDPI

3 p. b three-point bending, 4 p. b four-point bending, # UD unidirectional fibers, TTCP tetracalcium phosphate, HA<sub>w</sub> hydroxyapatite whiskers

types of fibers can be used, including both degradable and nondegradable types, as presented in Table 4.1 [38, 91–94]. The reinforcement depends on the matrix composition, strength, and fiber properties, such as fiber volume fraction, orientation, aspect ratio, etc., as well as the interface features between matrix and fibers [95, 96].

#### 4.4.1 Effects of Different Fibers on CPC

Hockin Xu summarized two different fiber reinforcement strategies commonly used [97]. One is introduction of short fiber for reinforcement in which the fibers had lengths much shorter than the matrix size. Fibers were randomly distributed in the matrix, resulting in composites with relatively isotropic properties. The other is incorporation of continuous fiber in which the fibers were nearly as long as the specimen size and were aligned in the matrix in certain directions (e.g., unidirectional). The crack resistance can be highly enhanced in the direction perpendicular



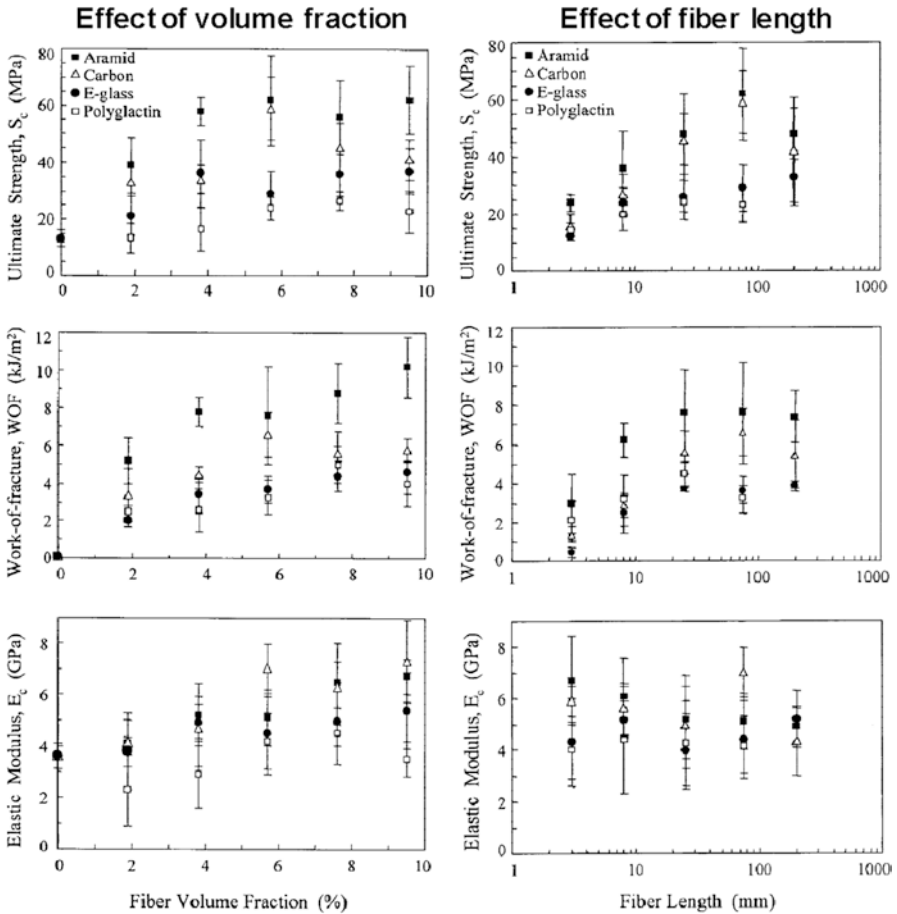
to the fibers; nevertheless, the fracture resistance of the composite is anisotropic so that the crack can propagate easily in the direction parallel to the fibers.

In a representative study, four different fibers with a wide range of properties, aramid, carbon, E-glass, and polyglactin, were used to reinforce CPC [98]. Fiber length ranged from 3 to 200 mm, and fiber volume fraction ranged from 1.9 to 9.5%. The influences of parameters of fibers, such as fiber type, length, and volume fraction, on the mechanical properties of composite CPCs were investigated. Fiber types were demonstrated to have significant effects on composite properties. The composite ultimate strength (MPa) was  $62 \pm 16$  for aramid,  $59 \pm 11$  for carbon,  $29 \pm 8$  for E-glass, and  $24 \pm 4$  for polyglactin, with 5.7% volume fraction and 75 mm fiber length. For each fiber, the ultimate strength generally increased with volume fraction. In comparison, all fiber-modified groups were improved significantly higher than unreinforced CPC ( $13 \pm 3$  MPa). The work-of-fracture (WOF) and elastic modulus values also increased with volume fraction for each fiber (Fig. 4.12).

Fiber length also played an important role [99–101]. For each fiber, increasing the fiber length generally increased the composite ultimate strength and work-of-fracture. Comparing the four fibers, aramid fiber composites generally had the highest strength and work-of-fracture, followed by those with carbon fibers; E-glass and polyglactin fiber composites had lower strengths. For composites containing 5.7% aramid fibers, the ultimate strength was ( $24 \pm 3$ ) for 3 mm fibers, ( $36 \pm 13$ ) for 8 mm fibers, ( $48 \pm 14$ ) for 25 mm fibers, and ( $62 \pm 16$ ) for 75 mm fibers. At 25 mm fiber length, the ultimate strength of CPC composite was found to be linearly proportional to fiber strength (Fig. 4.12). However, two competing factors existed: the higher reinforcement associated with longer fibers and the decreased distribution uniformity of longer fibers in the CPC composite. Similar condition lies in the effect of fiber volume fractions. Increased fiber volume fraction always leads to higher reinforcement; however, greater difficulty occurs in mixing and wetting more fibers with the CPC paste.

Different from CPCs which are apt to fail by a single crack, fibers can keep the multiple-cracked specimen intact (Fig. 4.13). Parallel fibers are embedded in the matrix and appeared nearly perpendicular to the fracture surface, consuming energy during frictional pullout and the creation of new surfaces. In comparison, the fracture surfaces of CPC control were observed to be relatively flat, as is typical for brittle materials. Interestingly, the embedded fibers did not affect the hydration process and formation of bone-like apatite of CPC during setting. Both CPC and CPC composites have the similar attaching HA crystallites.

Besides the polymeric fibers, inorganic nanofibers can also be introduced into CPCs. Guo et al. reported incorporation of wollastonite nanofibers (WNFs) into CPC [102]. According to their research, addition of lower content (<10 wt%) of WNFs into CPC had no obvious effect on the setting time or the compressive strength of wnf-CPC. However, the hydrophilicity and degradability were significantly improved. The preferred dissolution of WNFs caused the formation of microporosity and promoted degradation of the wnf-CPC. In addition, cell affinity and in vivo new bone formation on the wnf-CPC were superior to that on the CPC, suggesting improved osteogenesis.

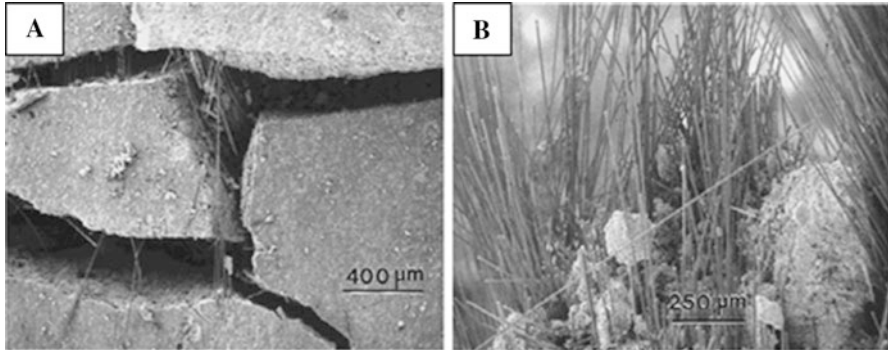


**Fig. 4.12** Effect of fiber volume fraction and fiber length. The *top* graph shows composite ultimate strength; the *middle* graph shows work-of-fracture; and the *bottom* graph shows modulus, as a function of fiber volume fraction. Each datum is mean with error bar showing one standard deviation (SD);  $n = 6$  (Reprinted with permission from Ref. ([98]). Copyright © 2000 *J Biomed Mater Res*. Rights Managed by John Wiley & Sons)

### 4.4.2 Effects of Resorbable Fibers on CPC

The composite ultimate strength increased linearly with fiber strength, suggesting the vital function of fiber reinforcement. Apart from the traditional polymeric fibers, more attentions had been paid on the absorbable fibers, which would endow reinforcement and biodegradation simultaneously.

Biodegradable poly-lactic-co-glycolic acid (PLGA) is one of the most frequently used reinforcement fibers. Plenty of works have been carried out by Xu’s group [103–105]. They investigated the effects of commercial absorbable suture fibers

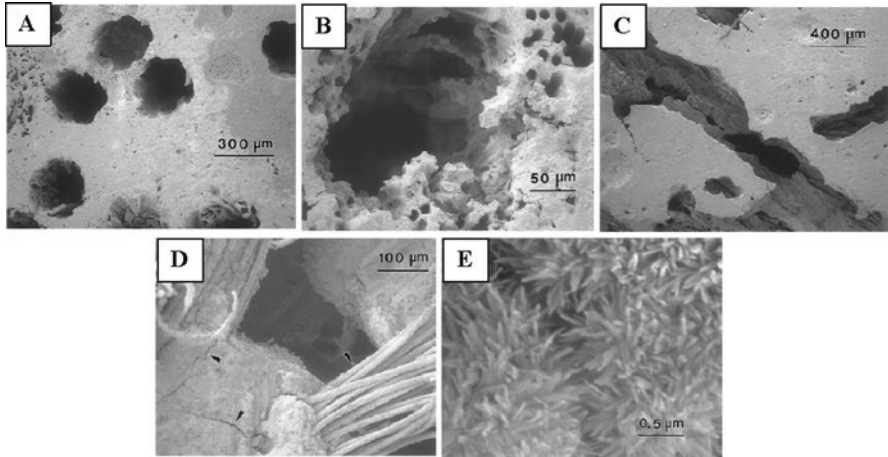


**Fig. 4.13** SEM images of (A) the polished surface of a specimen with 5.7% carbon fibers at 75 mm length. The surface shown was placed in tension during flexure. The fibers kept the multiple-cracked specimen intact. (B) Fracture surface and fiber pullout, with substantial energy consumption during fiber pullout and creation of new surfaces (Reprinted with permission from Ref. [98]. Copyright © 2000 *J Biomed Mater Res*. Rights Managed by John Wiley & Sons)

(Vicryl), which possessed a relatively high strength, on mechanical properties and biological features of macroporous scaffold. Herein, the large-diameter absorbable fibers would supply initial strength and toughness and then dissolve to form long cylindrical macropores for spreading and ingrowth by osteoblasts. Undoubtedly, increasing the absorbable fiber volume fraction would significantly increase the initial mechanical strength and the volume fraction of macropore.

According to their research, fiber volume fraction had significant effects on strength and work-of-fracture, but not on modulus. Macropores were formed in composite CPC from fiber dissolution. The macropore volume fractions were consistent with the fiber volume fractions incorporated into CPC. In elaborated SEM image (Fig. 4.14B, C), macropore channels can be observed, indicating the gradual absorption of bundles of fibers. Higher magnification suggests that the smaller holes might be created from the dissolution of the individual fiber in the bundle. The macropores are nearly parallel to the specimen surface resulting from fiber dissolution (Fig. 4.14D). HA crystallites can be seen, which appeared similar to CPC without fibers, indicating that incorporating fibers had not interfered with hydration of CPC (Fig. 4.14E).

As to cell affinity, the CPC-fiber formulation was non-cytotoxic and supported the adhesion, spreading, proliferation, and viability of osteoblast-like cells. From the live-dead survey, the live cells on CPC-fiber appeared to have adhered and attained a normal, polygonal morphology on all three materials. Few dead cells were visible, similar to both control groups of CPC and TCPS [105]. The enhanced osteogenic differentiation and mineralization of stem cells was attributed to the high surface area and biomimetic features of the CPC-fiber scaffold. Moreover, in a representative in vivo test of repairing fractured canine radii carried out by Lian, composites showed better load-bearing capability than the CPC control samples (Fig. 4.15). Macropores evolved from degraded chitosan fibers, and new callus and bone formation were observed [91].



**Fig. 4.14** (A–C) Macropores in CPC-fiber composite after fiber dissolution in immersion in a physiological solution for 12 weeks. (A) Shows holes intercepting the specimen surface. (B) A higher magnification of pores indicates the smaller holes are created from the dissolution of the individual fibers in the bundle perpendicular to specimen surface that was completely empty. (C) Shows macropores nearly parallel to the surface resulting from fiber dissolution. (D) The tensile surface of a specimen with Vicryl™ fibers bridging the crack, keeping the multiple-cracked specimen intact. One braided fiber bundle appeared to have been separated (*long arrow*). (E) Higher magnification SEM showing hydroxyapatite crystallites in the composite specimen, which appeared similar to CPC without fibers, indicating that the fibers had not interfered with hydroxyapatite crystallization (Reprinted with permission from Ref. ([104]. Copyright © 2002 *Biomaterials*. Rights Managed by Elsevier)

#### 4.4.3 Synergistic Reinforcement of Mesh and Chitosan

Cements may also be modified by using fiber meshes instead of single fibers. A promising work is dealing with co-incorporation of both chitosan and commercial absorbable fiber mesh (Vicryl™) [106, 107]. The mesh fibers appeared to be wetted by the CPC paste during mixing, since the fiber mesh can be firmly held by the CPC matrix. In fact, the mesh fibers can bridge the cracks to resist their opening and propagation. By contrast, the CPC control without mesh failed catastrophically in a single crack. The synergistic reinforcement from mesh and chitosan together would be more effective than the reinforcement from mesh or chitosan alone; the mechanism of synergistic reinforcement for the dramatic strengthening might be a stronger support for the fiber meshes and more efficient crack bridging. Moreover, the absorbable meshes would provide strength and then dissolve to create macropores (Fig. 4.16A, B). After immersion, numerous cracks were found in CPC+mesh, although the specimens were still intact due to mesh reinforcement. In contrast, the CPC+chitosan+mesh had few cracks after extensive deformation (Fig. 4.16C, D). As a result, the novel CPC scaffold had a flexural strength 39% higher and WOF

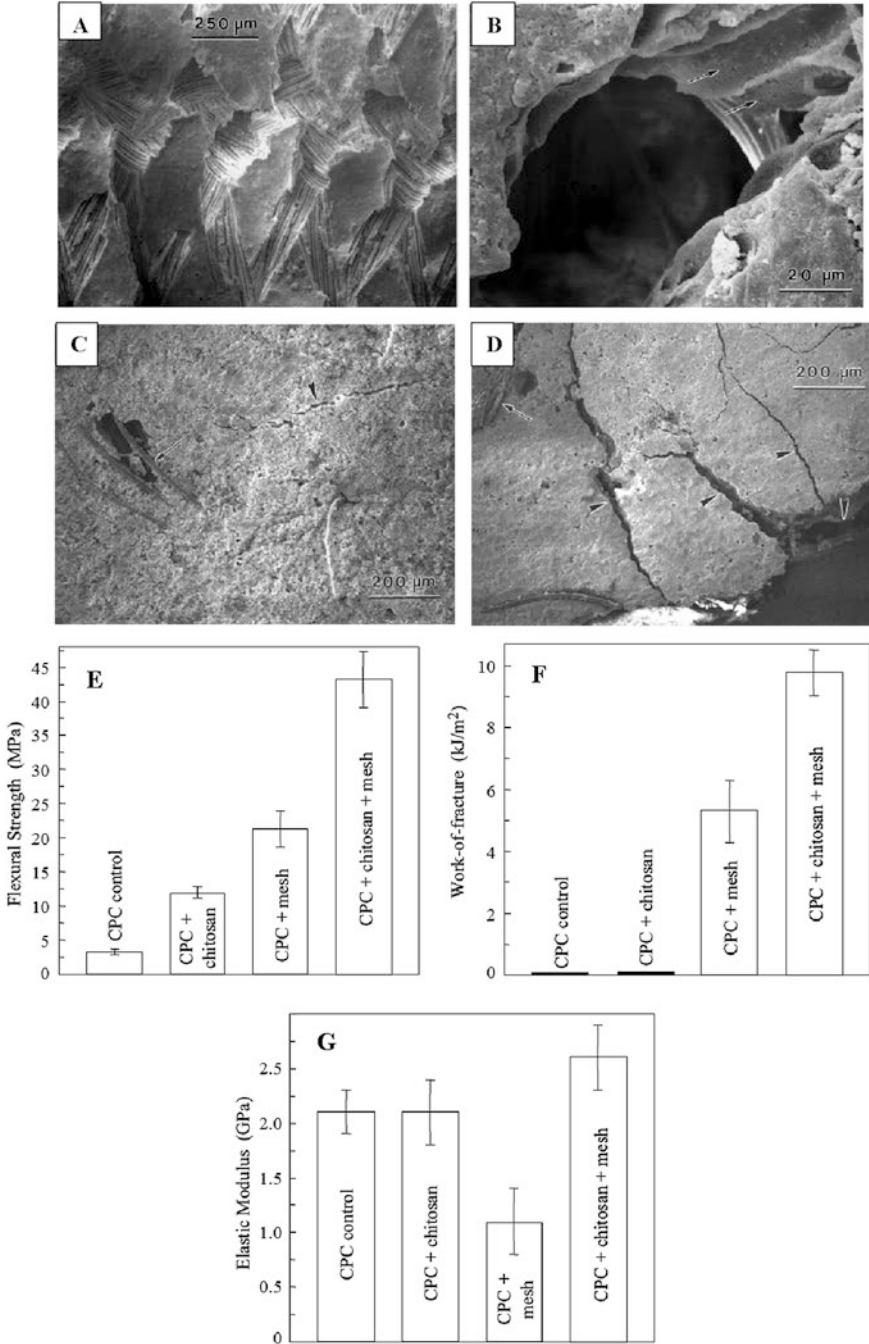


**Fig. 4.15** Radiographic observation after 20 weeks in vivo: (A) CPC-fiber implant; (B) CPC control (Reprinted with permission from [91]. Copyright © 2012 *Biomaterials* Rights Managed by Elsevier)

256% higher than the conventional CPC without macropores. For example, the flexural strength of the reinforced macropores CPC co-incorporated with chitosan and mesh can be increased to 43.2 MPa, significantly stronger than either the chitosan-modified group (11.9 MPa) or mesh-modified group (21.3 MPa). The work-of-fracture (WOF) (toughness) was also increased by two orders of magnitude (Fig. 4.16E–G). The composite CPC had an elastic modulus within the range for cortical bone and cancellous bone and a flexural strength higher than those for cancellous bone and sintered porous hydroxyapatite implants.

#### 4.4.4 Summary

Fiber reinforcement imparted substantial improvements in mechanical properties. Parameters of fibers play the vital role in enhancing the effect. In addition to reinforcement, biodegradable fibers contribute to the microstructural modification by the gradual dissolution and formation of macropores. The strong and macroporous CPC scaffold may be useful in stress-bearing craniofacial and orthopedic repairs.



**Fig. 4.16** (A) SEM micrograph of macropore channels in CPC+chitosan+mesh created dissolution of mesh. (B) Higher magnification of a macropore. *Arrows* indicate connections to a neighboring pore. (C, D) Specimen tensile surfaces of CPC+chitosan+mesh (C) and CPC+mesh

## 4.5 Double-Network Hybrid Cements

A major obstacle for development of more efficient CPC is its relative lower mechanical strength and susceptibility to brittle fracture. Extensive studies have been performed to solve the problems, including addition of polymers. A critical challenge is the mixing and interfacial bonding between the two dissimilar matrixes. Physical mixtures of organic polymers and inorganic particles may lead to separation in discrete phases, resulting in small benefit for mechanical performance. Recently, a novel dual-setting hybrid has been developed based on the in situ cross-linking polymerization and hydration process of CPC synchronously.

### 4.5.1 Formation of Hybrid Interpenetrating Network

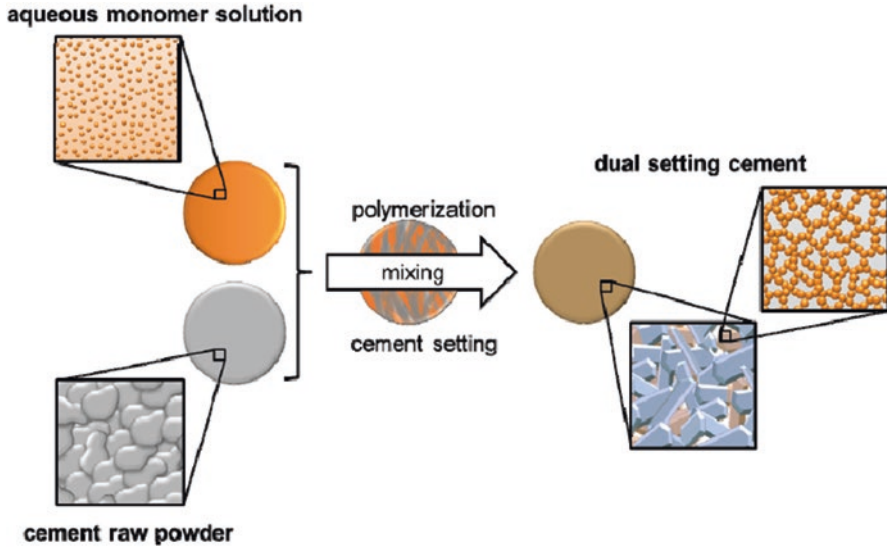
Distinct from the addition of nonreactive polymers, reactive monomer systems are used in this dual-setting system. These monomers can be dissolved in the liquid phase of CPC cement and simultaneously polymerize during hydration of calcium phosphates. Aqueous monomers having reactive groups, e.g., acrylic group, maleic anhydride, or polymeric compounds which can be cross-linked by binding calcium ions, can be competent for this process.

Polymerization occurs first, antecedent to the hydration of phosphates, depending on the initiation of chain polymerization, and forms the hydrogel shelter rapidly. The inorganic phosphate particles are embedded in the hydrogels, which undergo subsequent conversion via continuous dissolution-precipitation reaction. Thus, in this system, besides the polymerization of organic moiety, hydration of calcium phosphates proceeds simultaneously to form the hybrid double-network system. Thus, the hybrid interpenetration network comes into being. The “hard” moiety of CPC cement and “soft” hydrogel segment would incorporate each other to make the hybrid cement stiff and ductile.

A major concern about this strategy is the forming mechanism of the double network. In fact, both chain polymerization and setting of CPCs are concomitant in the complex system. The formation of the binary networks is carried out by a sequential two-step process. Distinct from the pure CPC system, setting time of the dual-setting system can be regulated by either polymerization conditions or hydration conditions. Rapid formation of hydrogel avoids the macroscopic disentanglement. Furthermore, the initial compressive strength generally originated from the

---

←  
**Fig. 4.16** (continued) **(D)** after 1 d immersion and then loading in flexure to a displacement of 3.5 mm. Numerous cracks were found in CPC+mesh, although the specimens were still intact due to mesh reinforcement. In contrast, the CPC+chitosan+mesh had few cracks after extensive deformation. The *short arrows* indicate cracks, and the *long arrows* point to the mesh fibers. **(E–G)** Flexural strength, WOF (toughness), and elastic modulus of each group (Reprinted with permission from Ref. [106]. Copyright © 2004 *Biomaterials*. Rights Managed by Elsevier)



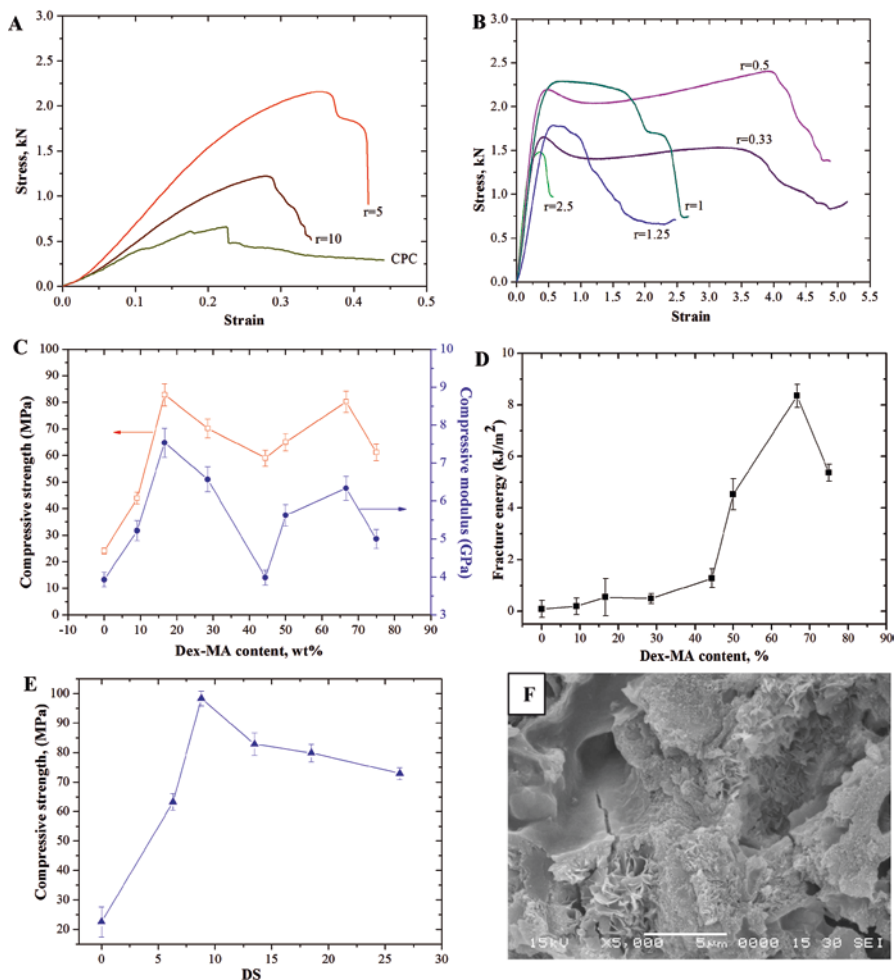
**Fig. 4.17** Hardening mechanism of dual-setting cements with the formation of interconnected matrices of hydrogel and precipitated cement crystals (Reprinted with permission from Ref. ([38]. Copyright © 2015 *Materials*. Rights Managed by MDPI)

polymeric network is supplied during the earlier stage. Most of calcium phosphate particles subsequently go through hydration in situ and convert into HA crystalline in the hydrogel matrix gradually, serving as the inorganic skeleton. The remainders disperse therein, acting as the thickening fillers, which cause the elevated viscosity of slurry and faster gelation behavior than pure hydrogel (Fig. 4.17).

#### 4.5.2 *Effects of Polymeric Network on Hybrid Cement*

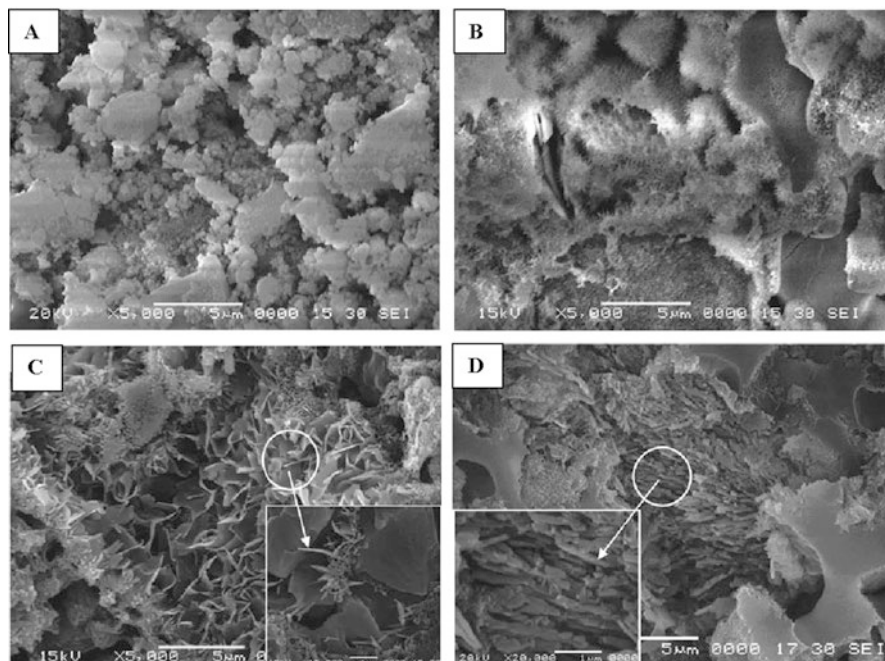
It is worth noting that introduction of the dual network into CPC possibly can be used to improve the mechanical properties of the cement, i.e., overcome brittleness, as a higher strain-at-yield can be obtained with an increasing percentage of polymeric moieties. In addition, the toughness increases as composites do not fracture after reaching the yield strength but keep together by the elongated hydrogel network. A representative work in Liu's group developed a dual-setting hybrids based on glycidyl methacrylate derivatized dextran (Dex-MA) and a cement matrix of tetracalcium phosphate/dicalcium [108]. They changed the ratio of the binary components from 10:1 to 1:3 (CPC/dextran). As a result, the hybrid cement possessed characteristics of both components and displayed ductility but not softness according to the ratio of the compositions. The appearance of typical yielding flats revealed that the brittle deformation had converted to toughness (Fig. 4.18A, B). Interestingly, bimodal fluctuation was observed in compressive strength, and the second peak has





**Fig. 4.18** (A, B) Typical compressive stress-strain curves of CPC and CPC/Dex with different Dex content. (C, D) Influence of Dex-MA content on compressive strength, modulus, and fracture energy of CPC/Dex hybrid. (E) Dependence of compressive strength on the degree of substitution. (F) Cross-section morphology at fracture interface of CPC/Dex ( $r = 0.5$ ) hybrid (Reprinted with permission from Ref. ([108]. Copyright © 2010 *Adv. Func. Mater.* Mater Rights Managed by John Wiley & Sons)

the higher compressive strength of about 80 MPa, exceeding the CPC without polymeric additives, which was brittle with lower compressive strength at about 24 MPa. And the fracture energy was improved by nearly two orders of magnitude from  $0.084$  to  $8.35 \text{ kJ m}^{-2}$  (Fig. 4.18C, D). Further the survey of microstructure displays under high compression CPC/Dex-MA did not fracture into separate smaller pieces. The specimens were still intact, although numerous microcracks appeared in the matrix (Fig. 4.18F). Despite of the cracks that occurred, the propagation was



**Fig. 4.19** SEM micrographs of CPC (A) and CPC/Dex-MA composite with different contents (B)  $r = 10$ ; (C)  $r = 5$ , The inset bottom right showed that the crystals had grown on the surface of the flask; (D)  $r = 0.33$ , the magnificent images in the insert showed the arrayed of blade-like crystals (arrow) (Reprinted with permission from Ref. ([108]. Copyright © 2010 *Adv. Func. Mater* Rights Managed by John Wiley & Sons)

retarded, and the crack opening displacement did not grow straightly, but changed direction into the Dex-MA moiety, where the crack tip could be absorbed owing to the toughness.

Moreover, the substitution degree of methyl acrylate group influences the compressive strength. According to the study, increasing the substitution degree of MA from 0 to 8.8 resulted in a dramatic enhancement of compressive strength from 22.56 MPa to the highest 98.33 MPa (Fig. 4.18E). This is reasonable, because neither the cross-linked structure nor interpenetrating network can be formed without the double bond on MA groups, thus leading to the loss of strength. Nevertheless, further increase in DS leads to a gradual decline of mechanical strength.

The incorporated ratio of the inorganic and polymeric moiety can be varied over a wide range, from inorganic-based to polymeric-based hybrid. The mass ratio not only directly influences the mechanical properties but also has a crucial influence on the microstructures. As shown in morphology observation, different micro-architectures appeared, such as fluffy agglomerates, needle crystals, flower cluster, entrapped blade shaped, etc. (Fig. 4.19). Thus, the polysaccharide hydrogel serves as the matrix used for the in situ growth of HA crystalline. The nucleation of apatite crystals generates onto its surface, forming a linear growth of apatite crystals (sur-

face control process) and a potential growth of apatite crystals (diffusion control process). As a result, both polymerization and hydration process an entangled network, which is responsible for the mechanical properties.

Due to the introduction of cross-linked hydrogel moiety, CPC/Dex hybrids show distinct feature of swelling. The noticeable volumetric shrinkage during deswelling process was thought to be crucial. The external layer contracts prior to the inside layers, generating the shrinkage force from outside and applying on the inside of the hybrid. Therefore, the CPC/Dex can be self-reinforced by behavior of shrinkage in the process of drying. This accidental behavior is beneficial to the mechanical strength, acting as radial compact.

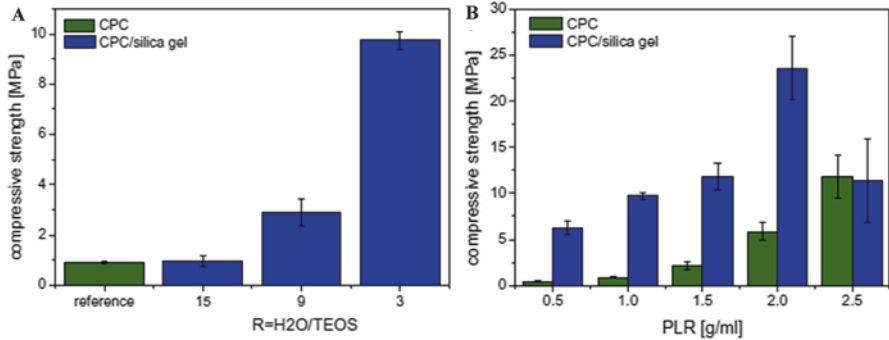
Similar research by T Christel et al. modified the CPC with 2-hydroxyethylmethacrylate (HEMA) to obtain a mechanically stable polymer-ceramic composite with interpenetrating organic and inorganic networks [109]. Setting time of the hybrid CPC was decreased, and four-point bending strength was increased from 9 MPa to more than 14 MPa. The addition of 50% HEMA reduced the brittle fracture behavior of the cements and resulted in an increase of the work of fracture by more than an order of magnitude.

### 4.5.3 Dual Inorganic Network

Apart from using organic monomers to form a second network in cements, it is also possible to apply the concept of dual-setting cements to entirely inorganic materials. Geffers et al. modified a brushite-forming cement paste with a second inorganic silica-based precursor, which was obtained by pre-hydrolyzing tetraethyl orthosilicate (TEOS) under acidic conditions [110]. The addition of the cement powder provoked an increased pH value of the silica precursor, so that cement setting by a dissolution-precipitation process and the condensation reaction of the hydrolyzed TEOS occurred simultaneously. Thus, an interpenetrating hybrid CPC is generated, in which the macropores of the cement (pore sizes in  $\mu\text{m}$  range) were infiltrated by the microporous silica gel (pore sizes in nm range), leading to a higher density and a compressive strength approximately five to ten times higher than the CPC (Fig. 4.20).

### 4.5.4 Summary

In dual-setting system, the inorganic cement network has a relatively higher modulus but rather brittle. Under compression, stress could easily develop locally inside the network to form cracks. The loosely cross-linked hydrogel effectively dissipate the crack energy by deforming the network conformation and/or sliding the physical entanglement points along the chains to prevent the crack growing to a macroscopic level. Such a strategy is highly desirable for bone regeneration and provides insight into hybrid cement designing.



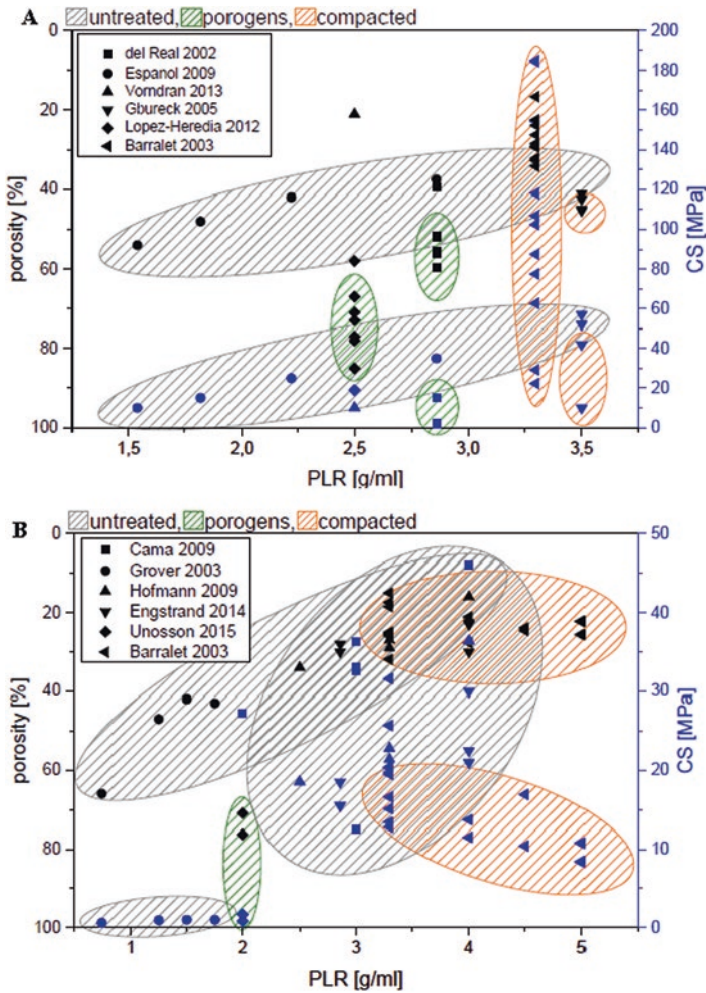
**Fig. 4.20** Compressive strength of CPC reference and CPC-silica gel composite. (A) Effect of H<sub>2</sub>O/TEOS ratio, a PLR of 1 g/mL was used. (B) Effect of PLR and H<sub>2</sub>O/TEOS ratio was constant 3 (Reprinted with permission from Ref. ([110]). Copyright © 2014 *Acta Biomaterialia* Rights Managed by Elsevier)

## 4.6 Others

### 4.6.1 Porosity Reduction for Reinforcement Using Inorganic Granules

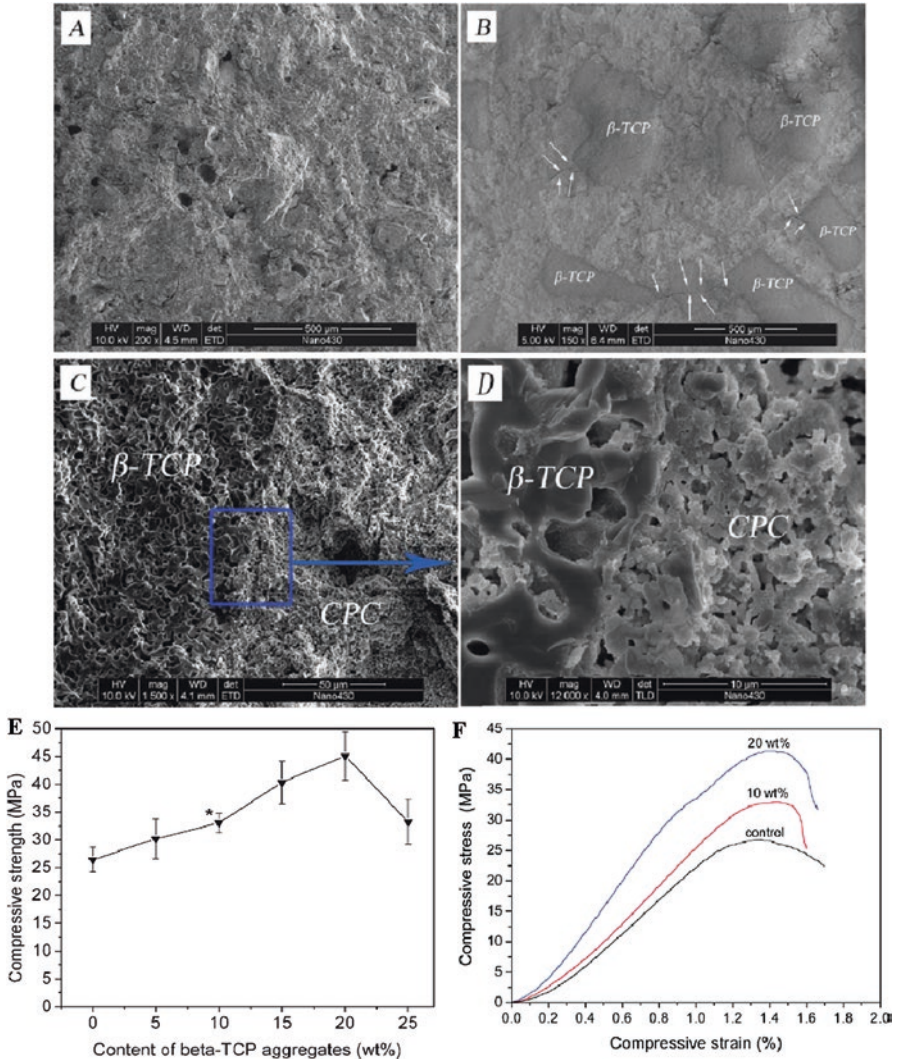
The low fracture toughness restricts the use of CPC to non-load-bearing defects. CPC is set by a dissolution-precipitation reaction of the supersaturated phosphate solutions and forms an entangled cementitious crystal matrix. Hence, porosity that originates from the heterogeneous reactants located in the voids of the slurry plays an important role in the mechanical strength. In fact, porosity considerably decreases the strength and stiffness of the cements. It is known from literature that porosity reduction in cements from 50 to 31% by compression can increase compressive strength by nearly an order of magnitude. Gbureck et al. summarized the correlation between the integrant powder to liquid ratio and the resulting porosity/compressive strength for both HA and brushite cements [111–113] (Fig. 4.21).

It is regularly believed that using multimodal size distribution of raw materials and modifying the superficial properties with higher  $\zeta$ -potential are efficient methods to decrease porosity. Apart from this, porosity can be reduced by filling with hard agglomerates using composite methods. In a representative study by Gu et al. the dispersion of 20% high-strength  $\beta$ -tricalcium phosphate granules with a size of 200–450  $\mu\text{m}$  in the cement showed an increase of the compressive strength by 70% while maintaining the rheological properties [114] (Fig. 4.22). The high strength or high rigidity of the TCP aggregates and good interfacial bonding between the aggregates and the CPC matrix seemed to contribute to the significant improvement in the mechanical performance. Another study by Engstrand et al. investigated the effect of  $\beta$ -TCP filler particles on the mechanical properties of a brushite-forming cement



**Fig. 4.21** Correlation between powder to liquid ratio and porosity/compressive strength from different studies: (A) Hydroxyapatite cement; (B) Brushite cement. Cements were either set without compacting manipulation, processed by pre-compactation, or porogens were added to create artificial macroporosity (Reprinted with permission from Ref. ([38]. Copyright © 2015 *Materials*. Rights Managed by MDPI)

( $\beta$ -TCP-MCPM system) [115]. The results showed that the addition of low amounts of a filler (up to 10%) in combination with 0.8 M citric acid solution effectively increased the powder to liquid ratio and hence decreased porosity from ~30 to ~23%. This strongly affects compressive strength of the cements with an increase from ~23 MPa (no filler and citric acid) to ~42 MPa.



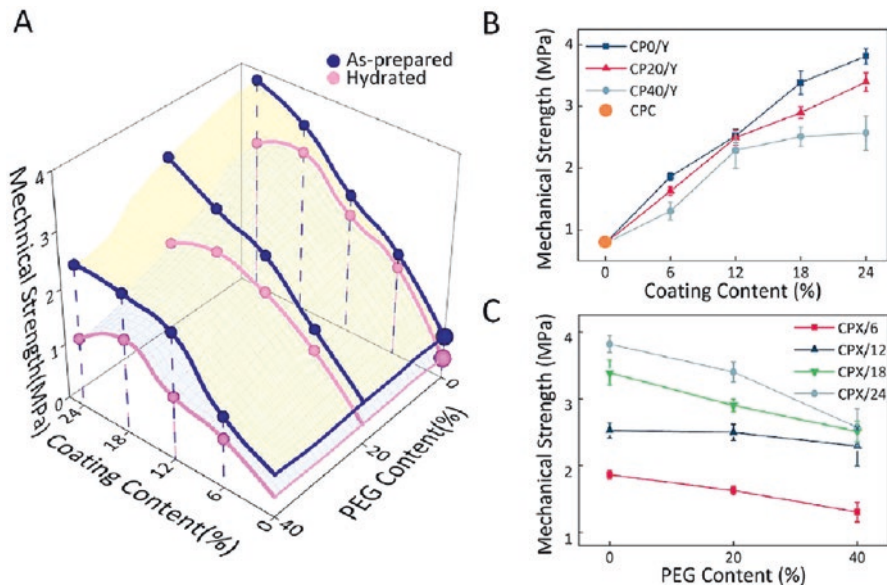
**Fig. 4.22** (A–D) SEM images of the surface of CPC after hardening for 3 days: (A) CPC without  $\beta$ -TCP aggregates; (B) CPC containing 20 wt% of  $\beta$ -TCP aggregates; (C, D) Higher magnification images of the cross section of the CPC- $\beta$ -TCP aggregate interface; (e) Influence of  $\beta$ -TCP content on the compressive strength of the cement; (F) Compressive stress vs. compressive strain curves of the CPC concretes with different content of  $\beta$ -TCP aggregates (Reprinted with permission from Ref. ([114]. Copyright © 2012 *J Biomed Res Part B* Rights Managed by John Wiley & Sons)

### 4.6.2 Elastomers as Enhancers of CPC

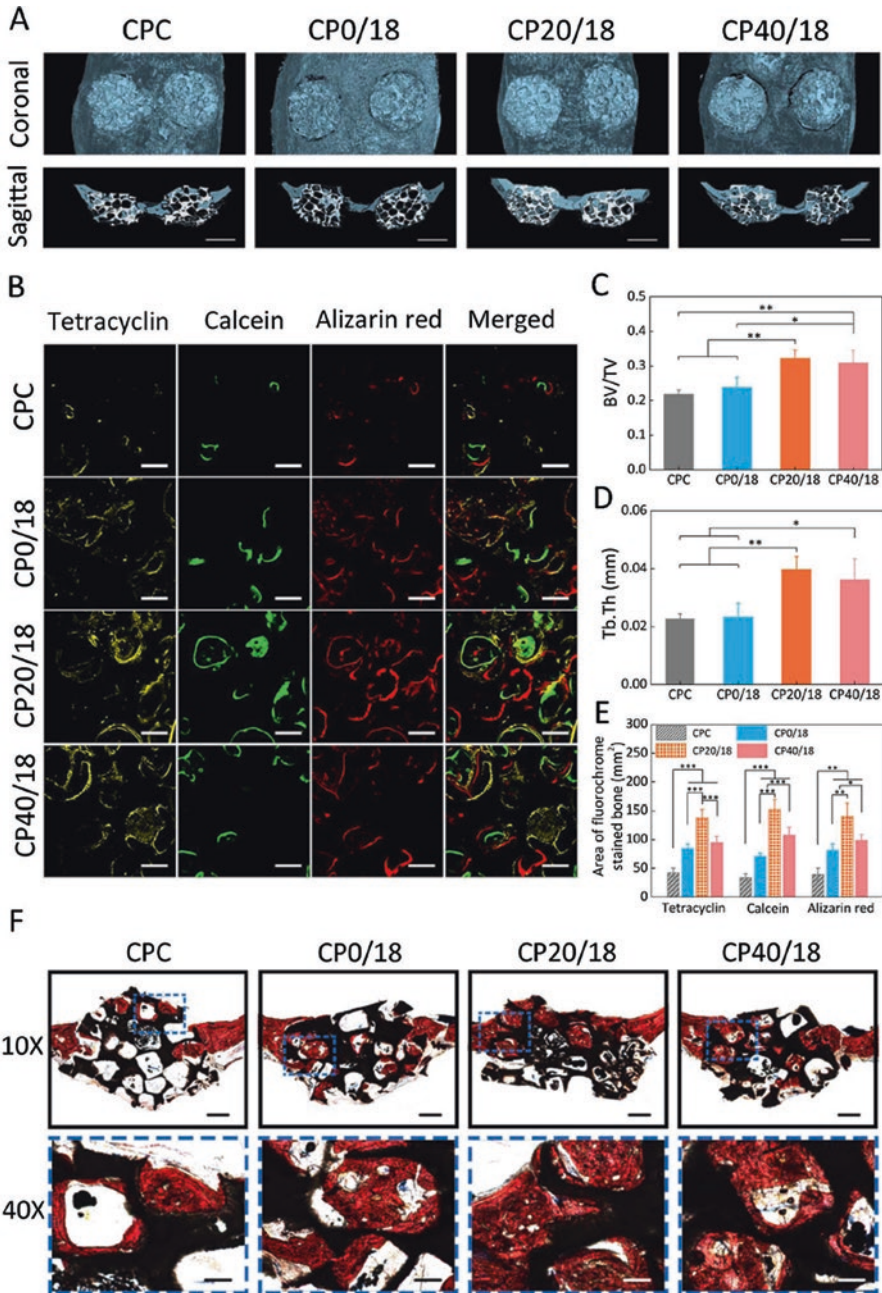
One of the limitations of CPC is its insufficient mechanical robustness. More recently, novel modification method about incorporation with polymeric elastomer has been reported [116–118]. PEGylated poly(glycerol sebacate) (PEGS), a hydrophilic elastomer, was used to modify a model CPC scaffold. The PEGS pre-polymer was coated onto the CPC scaffolds by infiltration and thermal cross-link process [119]. Enhanced compression strength and toughness were exhibited as to the CPC/PEGS composite scaffold, around fivefold and threefold improvement compared to the CPC (Fig. 4.23). In addition, *in vitro* cell affinity indicated the facilitated cell attachment and proliferation in a dose-dependent manner. Particularly, osteogenic differentiation of BMSCs on PEGS/CPC scaffold was strongly enhanced. In rat critical-sized calvarial defect repairing, osteogenic efficacy of PEGS/CPC further demonstrated the potential for applications in bone tissue regeneration (Fig. 4.24).

### 4.6.3 Summary

Improvement of mechanical strength and degradability are both required for development of novel CPCs. Introduction of polymeric compositions is one of the convenient approaches for optimizing. Future work should be done on the adjusted



**Fig. 4.23** (A) Relationship between scaffold mechanical strength and PEG content/polymer coating amount in as-prepared (yellow surface) and hydrated condition (blue surface). (B, C) Effects of coating and PEG content on mechanical strength (Reprinted with permission from Ref. ([119]). Copyright © 2016 *Acta Biomaterialia*. Rights Managed by Elsevier)



**Fig. 4.24** Bone regeneration in a calvarial defect in SD rats after various porous CPC and CPX/18 group implantations in 8 weeks. **(A)** 3D reconstruction images depicted the different reparative effects of CPC, CP0/18, CP20/18, and CP40/18. **(B)** New bone formation and mineralization were determined histomorphometrically by tetracycline, calcein, and alizarin red-labeling analysis.



degradation and retain strengthening and toughening effect over the entire degradation period of CPC.

## 4.7 Conclusions and Perspectives

This chapter depicts the composite strategy of CPCs, aiming at the reinforcement, superficial improvement, and modification for the cell affinity. Ionic effects, including doping with Mg and Si, are discussed for degradation and cell behaviors. Moreover, cellular behaviors can be modulated for better osteogenesis. Desired mechanical properties can be acquired by incorporation with fibers. Especially, subtle designing of in situ formation of dual-setting system can provide the obvious improvement of mechanical strength. The coordination between the “hard” calcium phosphate-based network and “soft” hydrogel network can create a hybrid CPC network which is stiff but not brittle, ductile but not soft. In summary, the application of CPC composites is still immature, and many important questions have yet to be resolved. Future success of these CPC composites can be expected.

**Acknowledgments** The authors wish to express their gratitude for financial supports from the National Natural Science Foundation of China (No.31330028, No.31470923), Major Basic Research Foundation of Shanghai Science and Technique Committee (14JC1490800), and International Cooperation Project of Shanghai Science and Technique Committee (15520711100). This study was also supported by the Key Project of Logistic Scientific Research of PLA (BWS13C014) and 111 Project (B14018).

## References

1. Stephanie L, Jelena R-K, Daniel F et al (2014) Silk as a bioadhesive sacrificial binder in the fabrication of hydroxyapatite load bearing scaffolds. *Biomaterials* 35:6941–6953
2. Gugala Z, Lindsey RW, Gogolewski (2007) New approaches in the treatment of critical-size segmental defects in long bones. *Macromol Symp* 253:147–161
3. Gruskin E, Doll BA, Futrell FW et al (2012) Demineralized bone matrix in bone repair: history and use. *Adv Drug Deliv Rev* 64:1063–1077
4. Taimoor H, Mooney D, Pumberger M et al (2015) Biomaterials based strategies for skeletal muscle tissue engineering: existing technologies and future trends. *Biomaterials* 53:502–521

**Fig. 4.24** (continued) Column 1 (*yellow*) represents tetracycline at week 2; column 2 (*green*) represents calcein at week 4; column 3 (*red*) represents alizarin red at week 6; column 4 represents merged images of three fluorochromes for the same group. (C–E) Morphometric analysis of bone volume/total volume (BV/TV), trabecular number (Tb. N), and the percentage of each fluorochrome area for different groups. (F) Histological images of newly formed bone in calvarial defects after operation (Reprinted with permission from Ref. [118]. Copyright © 2016 *Acta Biomaterialia*. Rights Managed by Elsevier)

5. Henkel J, Woodruff M, Epari D et al (2013) Bone regeneration based on tissue engineering conceptions – a 21st century perspective. *Bone Res* 3:216–248
6. Biomedical Market Newsletter (EBSCO) (2011) Datamonitor reports epidemiology: major orthopedic surgery on the rise as the global elderly population continues to grow. p 1–27
7. Laurencin CT, Ambrosio AMA, Borden MD et al (1999) Tissue engineering: orthopedic applications. *Annu Rev Biomed Eng* 1:19–46
8. Lichte P, Pape HC, Pufe T et al (2011) Scaffolds for bone healing: concepts, materials, and evidence. *Injury* 42:569–573
9. Lauren C, Ashish T, Nima J et al (2016) Nanoengineered biomaterials for repair and regeneration of orthopedic tissue interfaces. *Acta Biomater* 42:2–17
10. Klazen C, Lohle P, Vries J et al (2010) Vertebroplasty versus conservative treatment in acute osteoporotic vertebral compression fractures (vertos II): an open-label randomized trial. *Lancet* 376:1085–1092
11. LeGeros Z (2002) Properties of osteoconductive biomaterials: calcium phosphates. *Clin Orthop* 395:81–98
12. Masashi T, Mitsuru T, Shunsuke F et al (2014) Development of a novel calcium phosphate cement composed mainly of calcium sodium phosphate with high osteoconductivity. *J Mater Sci Mater Med* 25:1505–1517
13. Galea L, Alexeev D, Bohner M et al (2015) Textured and hierarchically structured calcium phosphate ceramic blocks through hydrothermal treatment. *Biomaterials* 67:93–103
14. Egli P, Muller W, Schenk K (1988) Porous hydroxyapatite and tricalcium phosphate cylinders with two different pore size ranges implanted in the cancellous bone of rabbits. A comparative histomorphometric and histologic study of bony ingrowth and implant substitution. *Clin Orthop* 232:127–138
15. Ginebra P, Espanol M, Montufar B et al (2010) New processing approaches in calcium phosphate cements and their applications in regenerative medicine. *Acta Biomater* 6:2863–2873
16. Dorozhkin SV (2008) Calcium orthophosphate cements for biomedical application. *J Mater Sci* 43:3028–3057
17. Barradas A, Yuan H, Stok J et al (2012a) The influence of genetic factors on the osteoinductive potential of calcium phosphate ceramics in mice. *Biomaterials* 33:5696–5705
18. Bohner M (2010) Design of ceramic-based cements and putties for bone graft substitution. *Eur Cells Mater* 20:1–12
19. Liu C, Shao H, Chen F et al (2003a) Effects of the granularity of raw materials on the hydration and hardening process of calcium phosphate cement. *Biomaterials* 24:4103–4113
20. Liu C, Gai W, Pan S et al (2003b) The exothermal behavior in the hydration process of calcium phosphate cement. *Biomaterials* 24:995–3003
21. Bohner M, Gbureck U, Barralet JE (2005) Technological issues for the development of more efficient calcium phosphate bone cements: a critical assessment. *Biomaterials* 26:6423–6429
22. Gbureck U, Spatz K, Thull R et al (2005) Rheological enhancement of mechanically activated alpha-tricalcium phosphate cements. *J Biomed Mater Res Biomater* 73(B):1–6
23. Charriere E, Terrazon S, Pittet C et al (2001) Mechanical characterization of brushite and hydroxyapatite cements. *Biomaterials* 22:2937–2945
24. Dorozhkin S (2009) Calcium orthophosphate-based biocomposites and hybrid biomaterials. *J Mater Sci* 44:2343–2387
25. Von G, Kelly R, Antonucci M (2000) Load-bearing behavior of a simulated craniofacial structure fabricated from a hydroxyapatite cement and bioresorbable fiber-mesh. *J Mater Sci Mater Med* 11:95–100
26. Bohner M (2000) Calcium orthophosphates in medicine: from ceramics to calcium phosphate cements. *Injury* 31:D37–D47
27. Habraken W, Jonge L, Wolke J et al (2008) Introduction of gelatin microspheres into an injectable calcium phosphate cement. *J Biomed Mater Res* 87A:643–655
28. Ruhé Q, Hedberg L, Padron T et al (2005) Biocompatibility and degradation of poly (DL-lactic-co-glycolic acid)/calcium phosphate cement composites. *J Biomed Mater Res* 74A:533–544

29. Habraken W, Liao H, Zhang Z et al (2010) In vivo degradation of calcium phosphate cement incorporated into biodegradable microspheres. *Acta Biomater* 6:2200–2211
30. Lanao R, Leeuwenburgh S, Wolke J et al (2011) In vitro degradation rate of apatitic calcium phosphate cement with incorporated PLGA microspheres. *Acta Biomater* 7(9):3459–3468
31. Real R, Wolke J, Vallet-Regi M et al (2002) A new method to produce macropores in calcium phosphate cements. *Biomaterials* 23(17):3673–3680
32. Rho J, Kuhn-Spearing L, Peter Z (1998) Mechanical properties and the hierarchical structure of bone. *Med Eng Phys* 20:92–102
33. Weiner S, Traub W (1992) Bone structure: from angstroms to microns. *FASEB* 6:879–885
34. Landis W (1995) The strength of a calcified tissue depends in part on the molecular structure and organization of its constituent mineral crystals in their organic matrix. *Bone* 16:533–544
35. Reilly T, Burstein H, Frankel H (1974) The elastic modulus of bone. *J Biomech* 7:271–275
36. Choi K, Kuhn JL, Ciarelli MJ et al (1990) The elastic moduli of human subchondral trabecular, and cortical bone tissue and the size-dependency of cortical bone modulus. *J Biomech* 23:1103–1113
37. Rho JY, Tsui TY, Pharr GM (1997) Elastic properties of human cortical and trabecular lamellar bone measured by nanoindentation. *Biomaterials* 18:1325–1330
38. Geffers M, Groll J, Gbureck U et al (2015a) Reinforcement strategies for load-bearing calcium phosphate biocements. *Materials* 8:2700–2717
39. Bohner M (2009) Silicon-substituted calcium phosphates – a critical view. *Biomaterials* 30:6403–6406
40. Wu C, Jiang C (2013) A review of bioactive silicate ceramics. *Biomed Mater* 8:032001
41. Wu C, Fan W, Zhou Y et al (2012a) 3D-printing of highly uniform CaSiO<sub>3</sub> ceramic scaffolds: preparation, characterization and in vivo osteogenesis. *J Mater Chem* 22:12288–12295
42. Ruys AJ (1993) Silicon-doped hydroxyapatite. *J Aust Ceram Soc* 29:71–80
43. Patel N, Best SM, Bonfield W (2005) Characterisation of hydroxyapatite and substituted -hydroxyapatites for bone grafting. *J Aust Ceram Soc* 41:1–22
44. Vallet-Regi M, Arcos D (2005) Silicon substituted hydroxyapatites. A method to upgrade calcium phosphate based implants. *J Mater Chem* 15:1509–1516
45. Hench L, Xynos D, Polak M (2004) Bioactive glasses for in situ tissue regeneration. *J Biomater Sci Polym Ed* 15:543–562
46. Reilly C, Radin S, Chen T et al (2007) Differential alkaline phosphatase responses of rat and human bone marrow derived mesenchymal stem cells to 45S5 bioactive glass. *Biomaterials* 28:409–4097
47. Silva A, Coutinho P, Ducheyne P et al (2007) The effect of starch and starch-bioactive glass composite microparticles on the adhesion and expression of the osteoblastic phenotype of a bone cell line. *Biomaterials* 28:326–334
48. Radin S, Chen T, Ducheyne P (2009) The controlled release of drugs from emulsified, sol gel processed silica microspheres. *Biomaterials* 30:850–858
49. Liu C, Chen W, Ducheyne P (2008) In vitro surface reaction layer formation and dissolution of calcium phosphate cement – bioactive glass composites. *Biomed Mater* 3:034111
50. Liu C, Shao H, Chen F et al (2006) Rheological properties of concentrated aqueous injectable calcium phosphate cement slurry. *Biomaterials* 27:5003–5013
51. Radin S, Ducheyne P et al (1997) The effect of in vitro modeling conditions on the surface reactions of bioactive glass. *J Biomed Mater Res* 37:363–375
52. Guo H (2008) A study on degradable calcium-phosphorous based self-setting materials for hard tissue repair. Ph.D. thesis, East China University of Science and Technology
53. Linez-Bataillon P, Monchau F, Bigerelle M et al (2002) In vitro MC3T3 osteoblast adhesion with respect to surface roughness of Ti6Al4V substrates. *Biomol Eng* 19:133–141
54. Refitt DM, Ogston N, Jugdaohsingh R et al (2003) Orthosilicic acid stimulates collagen type 1 synthesis and osteoblastic differentiation in human osteoblast-like cells in vitro. *Bone* 32:127–135

55. Matsuda T, Davies JE (1987) The in vitro response of osteoblasts to bioactive glass. *Biomaterials* 8:275–284
56. Zhao Q, Qian J, Zhou H et al (2010) In vitro osteoblast-like and endothelial cells response to calcium silicate-substituted calcium phosphate cements. *Biomed Mater* 5:035004
57. Beck GR, Sullivan EC, Moran E et al (1998) Relationship between alkaline phosphatase levels, osteopontin expression, and mineralization in differentiating MC3T3-E1 osteoblasts. *J Cell Biochem* 68:269–280
58. Anselme K, Bigerelle M, Noel B et al (2000) Qualitative and quantitative study of human osteoblast adhesion on materials with various surface roughnesses. *J Biomed Mater Res* 49:155–166
59. Anselme K, Linez P, Bigerelle M et al (2000) The relative influence of the topography and chemistry of TiAl6V4 surfaces on osteoblastic cell behaviour. *Biomaterials* 21:1567–1577
60. Kaigler D, Krebsbach P, Polverini P et al (2003) Role of vascular endothelial growth factor in bone marrow stromal cell modulation of endothelial cells. *Tissue Eng* 9:95–103
61. Yu H, Vande V, Mao L et al (2009) Improved tissue-engineered bone regeneration by endothelial cell mediated vascularization. *Biomaterials* 30:508–517
62. Zhang X, Wu C, Chang J et al (2014) Stimulation of osteogenic protein expression for rat bone marrow stromal cells involved in the ERK signalling pathway by the ions released from  $\text{Ca}_7\text{Si}_2\text{P}_2\text{O}_{16}$  bioceramics. *J Mater Chem B* 2:885–891
63. Wang C, Xue Y, Lin K, Lu J, Chang J, Sun J (2012) The enhancement of bone regeneration by a combination of osteoconductivity and osteostimulation using beta- $\text{CaSiO}_3$ /beta- $\text{Ca}_3(\text{PO}_4)_2$  composite bioceramics. *Acta Biomater* 8(1):350–360
64. Bei J (1987) The properties of hardened MPC mortar and concrete relevant to the requirements of rapid repair of concrete pavements. *Concrete* 21:25–31
65. Seehra S, Gupta S, Kumar S (1993) Rapid setting magnesium phosphate cement for quick repair of concrete pavements – characterisation and durability aspects. *Cem Concr Res* 23:254–266
66. Abdelrazig B, Sharp J, Siddy P et al (1984) Chemical reactions in magnesia-phosphate cement. *Proc Br Ceram Soc* 35:141–154
67. Yang Q, Wu X (1999) Factors influencing properties of phosphate cement-based binder for rapid repair of concrete. *Cem Concr Res* 29:389–396
68. Jia J, Zhou H, Wei J et al (2010) Development of magnesium calcium phosphate bio cement for bone regeneration. *J R Soc Interface* 7:1171–1180
69. Yu Y, Wang J, Liu C et al (2010) Evaluation of inherent toxicology and biocompatibility of magnesium phosphate bone cement. *Colloid Surf B* 2010(76):496–5044
70. Wu F, Wei J, Guo H et al (2008) Self-setting bioactive calcium–magnesium phosphate cement with high strength and degradability for bone regeneration. *Acta Biomater* 4:1873–1884
71. Klammert U, Reuther T, Blank M et al (2010) Phase composition, mechanical performance and in vitro biocompatibility of hydraulic setting calcium magnesium phosphate cement. *Acta Biomater* 6:1529–1535
72. Lilley K, Gbureck U, Knowles J et al (2005) Cement from magnesium substituted hydroxyapatite. *J Mater Sci Mater M* 16:455–460
73. Zhang J, Ma X, Lin D et al (2015) Magnesium modification of a calcium phosphate cement alters bone marrow stromal cell behavior via an integrin-mediated mechanism. *Biomaterials* 53:251–264
74. Barradas A, Fernandes H, Groen N et al (2012) A calcium-induced signaling cascade leading to osteogenic differentiation of human bone marrow-derived mesenchymal stromal cells. *Biomaterials* 33:3205–3215
75. Yoshizawa S, Brown A, Barchowsky A et al (2014) Role of magnesium ions on osteogenic response in bone marrow stromal cells. *Connect Tissue Res* 55:155–159
76. Luthringer BJC, Willumeit R (2016) Effect of magnesium degradation products on mesenchymal stem cell fate and osteoblastogenesis. *Gene* 575:9–20

77. Yoshizawa S, Brown A, Barchowsky A et al (2014) Magnesium ion stimulation of bone marrow stromal cells enhances osteogenic activity, simulating the effect of magnesium alloy degradation. *Acta Biomater* 10:2834–2842
78. Hynes RO (1992) Integrins: versatility, modulation, and signaling in cell adhesion. *Cell* 69:11–25
79. Zreiqat H, Howlett CR, Zannettino A et al (2002) Mechanisms of magnesium-stimulated adhesion of osteoblastic cells to commonly used orthopaedic implants. *J Biomed Mater Res* 62:175–184
80. Treiser MD, Yang EH, Gordonov S et al (2010) Cytoskeleton-based forecasting of stem cell lineage fates. *Proc Natl Acad Sci U S A* 107:610–615
81. Liu H, Peng H, Wu Y et al (2013) The promotion of bone regeneration by nanofibrous hydroxyapatite/chitosan scaffolds by effects on integrin-BMP/Smad signaling pathway in BMSCs. *Biomaterials* 34:4403–4417
82. Ohmori T, Kashiwakura Y, Ishiwata A et al (2010) Vinculin is indispensable for repopulation by hematopoietic stem cells, independent of integrin function. *J Biol Chem* 285:31763–31773
83. Humphries J, Wang P, Streuli C et al (2007) Vinculin controls focal adhesion formation by direct interactions with talin and actin. *J Cell Biol* 179:1043–1057
84. De G, Corbijn AJ (1989) Metal fibre reinforced hydroxy-apatite ceramics. *J Mater Sci* 24:3411–3415
85. Suchanek W, Yashima M, Kakihana M et al (1996) Processing and mechanical properties of hydroxyapatite reinforced with hydroxyapatite whiskers. *Biomaterials* 17:1715–1723
86. Dorner-Reisel A, Müller E, Tomandl G (2004) Short fiber reinforced hydroxyapatite based bioceramics. *Adv Eng Mater* 6:572–577
87. Knepper M, Moricca S, Milthrope B (1997) Stability of hydroxyapatite while processing short-fibre reinforced hydroxyapatite ceramics. *Biomaterials* 18:1523–1529
88. Dorner-Reisel A, Klemm V, Irmer G et al (2002) Nano- and microstructure of short fibre reinforced and unreinforced hydroxyapatite. *Biomed Tech* 47:397–400
89. Knepper M, Milthrope BK, Moricca S (1998) Interdiffusion in short-fiber reinforced hydroxyapatite ceramics. *J Mater Sci Mater Med* 9:589–596
90. Ahern BJ, Harten RD, Gruskin EA et al (2010) Evaluation of a fiber reinforced drillable bone cement for screw augmentation in a sheep model-mechanical testing. *Clin Transl Sci J* 3:112–115
91. Krüger R, Groll J (2012) Fiber reinforced calcium phosphate cements – on the way to degradable load bearing bone substitutes? *Biomaterials* 33:5887–5900
92. Callister W, Rethwisch D (2009) *Materials science and engineering: an introduction*. Wiley, Hoboken
93. Ramay HRR, Zhang M (2004) Biphasic calcium phosphate nanocomposite porous scaffolds for load-bearing bone tissue engineering. *Biomaterials* 25:5171–5180
94. Santos LA, Oliveira LC, Silva EC et al (2000) Fiber reinforced calcium phosphate cement. *Artif Organs* 24:212–216
95. Li VC (2003) On engineered cementitious composites (ECC) – a review of the material and its applications. *J Adv Concr Technol* 1:215–230
96. Karihaloo BL, Wang J (1997) Micromechanical modelling of strain hardening and tension softening in cementitious composites. *Comput Mech* 19:453–462
97. Xu H, Quinn J, Takagi S et al (2001) Strong and macroporous calcium phosphate cement: effects of porosity and fiber reinforcement on mechanical properties. *J Biomed Mater Res* 57:457–466
98. Xu H, Eichmiller F, Giuseppetti A (2000) Reinforcement of a self-setting calcium phosphate cement with different fibers. *J Biomed Mater Res* 52:107–114
99. Xu H (1993) Crack-bridging toughening in ceramic fiber composites at ambient and elevated temperatures. Ph.D. thesis, University of Maryland at College Park
100. Xu H, Braun L, Ostertag C et al (1995) Failure modes of SiC-fiber/Si<sub>3</sub>N<sub>4</sub>-matrix composites at elevated temperatures. *J Am Ceram Soc* 78:389–394

101. Muller F, Gbureck U, Kasuga T et al (2007) Whisker-reinforced calcium phosphate cements. *J Am Ceram Soc* 90:3694–3697
102. Guo H, Wei J, Song W et al (2012) Wollastonite nanofiber-doped self-setting calcium phosphate bioactive cement for bone tissue regeneration. *Int J Nanomed* 7:3613–3624
103. Zhang Y, Xu H (2005) Effects of synergistic reinforcement and absorbable fiber strength on hydroxyapatite bone cement. *J Biomed Mater Res* 75A:832–840
104. Xu H, Quinn J (2002) Calcium phosphate cement containing resorbable fibers for short-term reinforcement and macroporosity. *Biomaterials* 23:193–202
105. Xu H, Simon Jr (2004) Self-hardening calcium phosphate composite scaffold for bone tissue engineering. *J Orthop Res* 22:535–543
106. Weir M, Xu H, Simon C et al (2006) Strong calcium phosphate cement-chitosan- mesh construct containing cell-encapsulating hydrogel beads for bone tissue engineering. *J Biomed Mater Res* 77A:487–496
107. Xu H, Quinn J, Takagi S et al (2004) Synergistic reinforcement of in situ hardening calcium phosphate composite scaffold for bone tissue engineering. *Biomaterials* 25:1029–1037
108. Wang J, Liu C, Liu Y, Zhang S (2010) Double-network interpenetrating bone cement via in situ hybridization protocol. *Adv Funct Mater* 20:3997–4011
109. Christel T, Kuhlmann M, Vorndran E et al (2013) Dual setting a-tricalcium phosphate cements. *J Mater Sci Mater Med* 24:573–581
110. Geffers M, Barralet J, Groll J et al (2015b) Dual-setting brushite-silica gel cements. *Acta Biomater* 11:467–476
111. Vorndran E, Geffers M, Ewald A et al (2013) Ready-to-use injectable calcium phosphate bone cement paste as drug carrier. *Acta Biomater* 9:9558–9567
112. Engstrand J, Persson C, Engqvist H (2014) The effect of composition on mechanical properties of brushite cements. *J Mech Behav Biomed Mater* 29:81–90
113. Hofmann M, Mohammed A, Perrie Y et al (2009) High-strength resorbable brushite bone cement with controlled drug-releasing capabilities. *Acta Biomater* 5:43–49
114. Gu T, Shi H, Ye J (2012) Reinforcement of calcium phosphate cement by incorporating with high-strength b-tricalcium phosphate aggregates. *J Biomed Mater Res* 100B:350–359
115. Johanna E, Cecilia P, Håkan E (2014) The effect of composition on mechanical properties of brushite cements. *J Mech Behav Biomed* 29:81–90
116. Wu F, Yung N, Wei J et al (2012) Premixed, injectable PLA-modified calcium deficient apatite biocement (cd-AB) with washout resistance. *Colloid Surf* 92B:113–120
117. Maazouz Y, Montufar E, Malbert J et al (2017) Self-hardening and thermoresponsive alpha tricalcium phosphate/pluronic pastes. *Acta Biomater* 49:563–574
118. Brückner T, Schamel M, Kübler A et al (2016) Novel bone wax based on poly (ethylene glycol)-calcium phosphate cement mixtures. *Acta Biomater* 33:252–263
119. Ma Y, Zhang W, Wang Z et al (2016) PEGylated poly(glycerol sebacate)-modified calcium phosphate scaffolds with desirable mechanical behavior and enhanced osteogenic capacity. *Acta Biomater* 44:110–124

# Chapter 5

## Accelerating Biodegradation of Calcium Phosphate Cement

Hongyan He, Zhongqian Qiao, and Changsheng Liu

**Abstract** Calcium phosphate cements (CPCs) are extensively used for bone replacement and regeneration in orthopedic, dental, and maxillofacial surgical applications. Despite their natural bone-like compositions, excellent biocompatibility and osteoconductivity, and superior clinical handling, they exhibit brittle nature, low bending/tensile strength, and poor degradability, prohibiting their use in load-bearing sites and limiting bone ingrowth into the implant. In order to accelerate the degradation of these biomaterials effectively, the major factors including cement composition and porosity are first discussed in this chapter. Small alterations to these factors substantially affect the degradation rate of the cement and thus the formation of new bone. To face the challenge in the biodegradation investigation on CPC without reducing the mechanical strength and losing the self-setting ability, several strategies are then proposed to speed up the biodegradation of calcium phosphate cements. Especially, the proposed combination strategies allow the CPC replacement to achieve the multifunctions.

**Keywords** Biodegradation • Calcium phosphate cement • Resorption • Macroporosity • Ion doping • Biodegradable polymer microsphere

---

H. He (✉) • Z. Qiao

Engineering Research Center for Biomedical Materials of Ministry of Education, East China University of Science and Technology, Shanghai 200237, China  
e-mail: [hyhe@ecust.edu.cn](mailto:hyhe@ecust.edu.cn)

C. Liu

Key Laboratory for Ultrafine Materials of Ministry of Education, East China University of Science and Technology, Shanghai 200237, China

© Springer Nature Singapore Pte Ltd. 2018

C. Liu, H. He (eds.), *Developments and Applications of Calcium Phosphate Bone Cements*, Springer Series in Biomaterials Science and Engineering 9, DOI 10.1007/978-981-10-5975-9\_5

## 5.1 Introduction

Annually, numerous patients worldwide are treated for skeletal complications in the areas of orthopedic surgery, dental implantology, maxillofacial surgery, neurosurgery, etc. The use of autologous bone grafts is the gold standard in treating these bone defects because they are osteoconductive, osteoinductive, and osteogenic. However, they require invasive surgery techniques, and the resource of graft material is limited. Alternatives based on the synthetic biomaterials for autologous grafts become more attractive from the last decades. Within the different materials (i.e., bioactive glass, polymers), calcium phosphate (CaP)-based ceramics or cements are one of the most desirable candidates for bone replacement and other applications [1]. According to the crystal phase, CaP can be classified, e.g., hydroxyapatite (HA),  $\beta$ -tricalcium phosphate ( $\beta$ -TCP), biphasic calcium phosphate (BCP), amorphous calcium phosphate (ACP), carbonated apatite (CA), and calcium-deficient hydroxyapatite (CDHA) [2]. Based on the composition criteria, CaP cements are classified into apatite cements, apatite-forming cements, and dicalcium phosphate dihydrate (brushite) cements [3]. A list of existing calcium phosphate compounds and their abbreviations is summarized in Table 2.1 of Chap. 2.

CaP-based materials have been widely used for the bone tissue engineering and regenerative therapies because of their natural bone-like compositions, nontoxicity, biocompatibility, excellent osteoconductivity, and good processibility [4–8]. A desirable bone substitute may require the following characteristics: (1) good mechanical properties, which allow bone remodeling within the porous structure [9]; (2) appropriate degradation rate, which should ideally match with the osteogenic rate [10]; (3) osteoconductive, thus able to guide bone tissue growth along the surface and into pores [11]; and (4) osteoinductive, inducing the differentiation of pluripotent stem cells into bone-forming osteoprogenitor cells [12, 13]. All these characteristics of the materials are very crucial for bone tissue engineering purposes, and we will focus on the biodegradation properties of biomaterials in this chapter.

After injection/implantation, it requires the enough space that the bone and vascular tissues can grow into. Hence, the material biodegradation is necessary and critical. Typically, “degradation” represents the decomposition of a compound, especially complex substances such as polymers and proteins. The degradation mechanism can be summarized as simple hydrolysis, enzymatic degradation, or their combination [14]. Biodegradation can be considered as an *in vivo* process. A material breaks down into biologically acceptable molecules that are metabolized and removed from the body via normal metabolic pathways. Some researchers have proposed the mechanism of biodegradation of CaP based via solution-driven extracellular liquid dissolution and cell-mediated resorption processes [15]. The term “resorption” is often used to describe the breakdown of CPC, essentially signifying the biodegradation taking place via cellular mechanisms. The fate of implanted CaP biomaterials *in vivo* is dependent on various mechanisms and processes. Therefore,



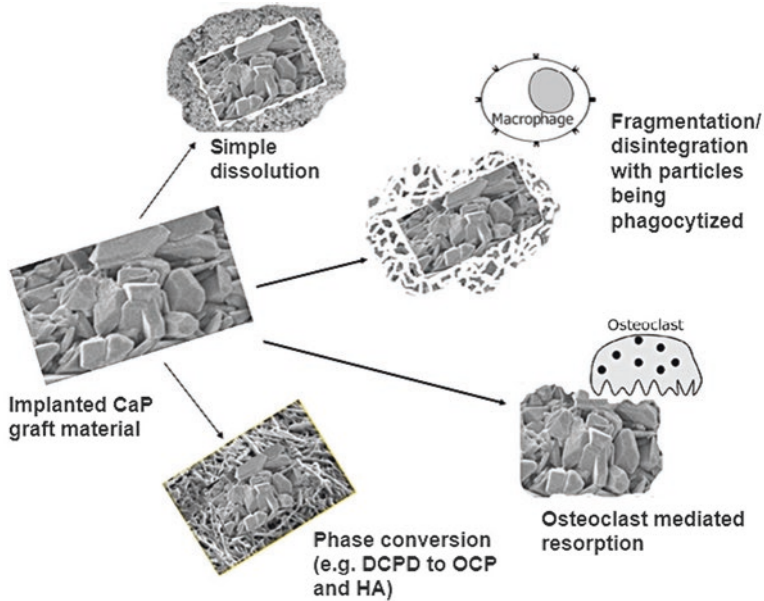
their biodegradation behavior can be regulated via physic-chemical properties of materials, the environment conditions around the implanted materials (i.e., pH level, ionic concentration, implanted locations), and the patient's health conditions. To make the strategies for accelerating biodegradation of materials, there is a great need to get a thorough understanding of the factors influencing the biodegradation.

## 5.2 Degradation of Calcium Phosphate Cements

As we all know, calcium phosphate cements (CPCs) consist of a powder phase and a liquid phase. The powder phase comprises one or more CaP compounds, while water or a calcium- or phosphate-containing solution is used as the liquid and may contain chitosan, alginate, hyaluronate, gelatin, chondroitin sulfate, succinate, or citric acid to allow the dissolution of the initial CaP compounds [16]. The attractive property of CPC lies on the self-setting reaction at room/body temperature in which a calcium phosphate precipitate is formed. The CPC mixture can self-solidify in the simulated *in vivo* environment in minutes. The solidification process is not exothermal without excitant odors and is harmless to the surrounding tissues. Another advantage is the easy shaping. When the CPC fills into bone defects, it is easy to meet the requirements of various shapes of wounds, achieving optimal tissue-to-implant contact and fast operation. Generally, CaP cements can be divided into two subgroups: apatite cements (i.e., HA, CA, or CDHA) and brushite cements (i.e., dicalcium phosphate dihydrate (DCPD)). According to the literatures, microporous apatite cements show slow degrading and good mechanical stability, while brushite cements exhibit a lower mechanical strength but a faster biodegradability than the apatite cements [17]. As contacting with body fluids, brushite cements will eventually change into apatite.

Generally, CPC products can be formulated with different CaP compounds. To achieve the desirable replacement for bones from the clinical view, the property requirements of CPC materials are very critical, especially for the degradation behavior. The rate of material degradation should optimally match the rate of new bone formation, allowing a gradual takeover of mechanical strength by newly formed bone tissue. When the CPC materials are injected/ implanted into the specific site, the extracellular liquid and surrounding cells/tissues will influence the resorption processes of CPC and directly mediate the degradation performances. Compared with other common materials, the CaP-based materials show various mechanisms and processes (Fig. 5.1).

According to these proposed mechanisms for CaP biomaterials, their biodegradation may be a combination of the following processes: (1) physical effects (i.e., abrasion, fracture, disintegration), (2) chemical reactions (dissolution, increases of Ca and P locally at the surface), and (3) reductions in pH values due to cellular and phagocytic activities [18]. Typically, these activities will promote the rate of biodegradation due to the dissolution of the CaP biomaterials. First, the biodegradation of



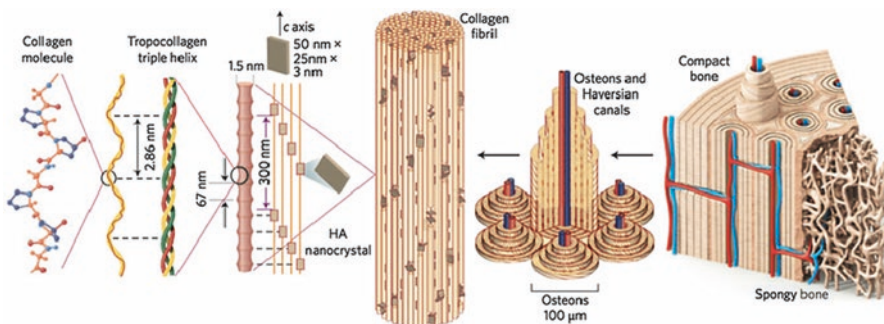
**Fig. 5.1** The degradation fate of CaP biomaterials after implantation. Here, *CaP* calcium phosphate, *DCPD* dicalcium phosphate dihydrate, *OCP* octacalcium phosphate, *HA* hydroxyapatite (Reproduced from Ref. ([18] by permission of MDPI, Basel, Switzerland)

CPC is influenced by the cement properties, which include chemical composition, setting reaction, porosity, crystallinity, and particle size of the calcium phosphate compounds [19, 20]. These factors affect each other and are influenced by the chemical composition of the material. The patient conditions also play an important role in material degradation. Depending on the patient's age, sex, type of the bone, hormone levels, genetic predisposition, and other metabolic health conditions, the speed of degradation can be different [21, 22]. Furthermore, the implantation site influences the biodegradation and bone formation. The implanted materials are exposed to the microenvironment around, in which the tissues, blood/nutrient supply, and other conditions may play a role in degradation of the materials. In this chapter, different factors that influence the biodegradation of calcium phosphate cements are discussed. These factors also have impacts on the mechanical properties of CPC. Typically, the better biodegradation of materials means poor mechanical strength. However, as a fact, bone implants are required to provide adequate short- and long-term mechanical support in the defect site in clinical applications. Therefore, the feasible strategies are proposed not only for promoting the degradation of CPC, but also for maintaining/improving the stress of the bone.

## 5.3 Major Factors Influencing CPC Biodegradation

### 5.3.1 Composition and Structure of Bones

Since the degradation of CPC materials as bone alternatives always occurs after implantation, it is necessary to understand the composition and structure of bones and the surrounding tissues. The bone (Fig. 5.2) in the human body can be defined as a composite of hydroxyapatite, type I collagen, water, cells, and lipids [23]. As can be seen, natural bone derives its unique combination of mechanical properties from an architectural design that spans macroscopic to nanoscale dimensions, with precisely and carefully engineered interfaces [24]. The bone is comprised of two distinct forms: dense cortical bone and porous cancellous bone. Cortical bone is the outer layer, which gives the support for the shape and form of the bone. Eighty percent of the skeleton is composed of cortical bone [25]. Cancellous bone has a lower Young's modulus and is more elastic compared to cortical bone. Its porous structure consists of pore sizes in the range of 200–500  $\mu\text{m}$ , and 30–90% of the porosity, which depends on the load, age, and health situation of the bone [26]. More importantly, the bone is a nanomaterial composed of organic (mainly collagen) and inorganic (mainly nano-hydroxyapatite) components, with a hierarchical structure ranging from nanoscale to macroscale. To design and produce the desirable bone replacement, many research groups have tried to manipulate the mechanical properties (e.g., stiffness, strength, and toughness) of scaffolds through the design of nanostructures (e.g., the inclusion of nanoparticles or nanofiber reinforcements) to mimic bone's natural nanocomposite architecture [27, 28]. However, the good mechanical properties are not the only objective for realizing the desirable bone replacement. Its biodegradation has to be matchable for the new bone, allowing a gradual takeover of mechanical strength. Therefore, it is necessary to balance the mechanical and biodegradable properties during the designing and fabricating of nanomaterials.



**Fig. 5.2** Hierarchical organization of vascularized bone, from single collagen molecules to compact and spongy bone (Reproduced from Ref. ([24] with permission. Copyright © 2014, Rights Managed by Nature Publishing Group)

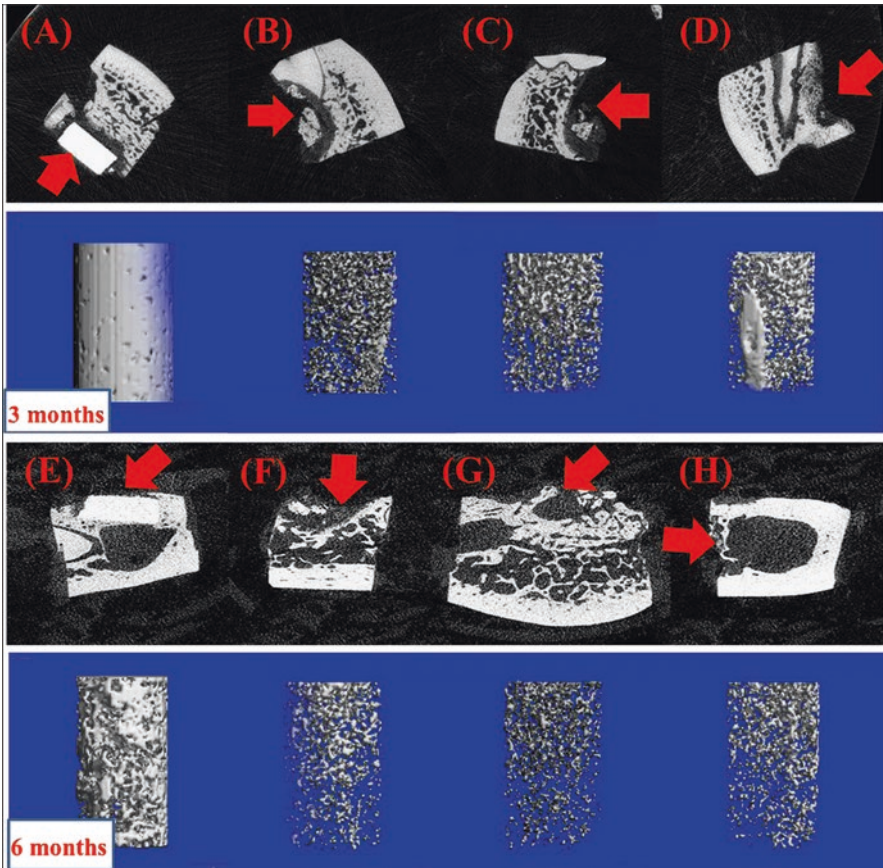
### 5.3.2 *Effect of Porous Architecture on CPC Biodegradation*

Porosity is a parameter that refers to fraction of the void volume filled with liquid phase within a solid matrix. Unlike porosity, pore size directly refers to geometry of pores. Surrounding implanted materials, cell adhesion and motility depend on size of the pores, rather than porosity. Mean pore size has correlation with porosity for many synthetic polymers of simple composition. However, for natural polymers like collagenous gels, there is no direct correlation, since the diameter of collagen fibrils can vary from few nanometers to a few hundred nanometers [29].

In bone regeneration, permeability for fluid flow and molecular diffusion is important, since low permeability may result in a lack of nutrients and ischemia [30]. The permeability in vitro and in vivo depends on the porous structure of implants, including pore size, size distribution, porous morphology, interconnectivity, and surface area-to-volume ratio [31]. Each of these factors not only influences biological response (i.e., cell migration, proliferation, and thus tissue regeneration), but also plays roles in the resorption of implanted materials including CPCs. As a bone substitute material, CPC also contains an intrinsic high nano-/submicron-sized porosity, which may be related with the particle size of the powder phase [19] and liquid/powder ratio [20]. Typically, the porous size of dense materials is classified in three different types by biomaterial scientists: macropores ( $>50\ \mu\text{m}$ ), micropores ( $0.1\text{--}50\ \mu\text{m}$ ), and mesopores ( $2\text{--}50\ \text{nm}$ ). Therefore, we will distinguish these three different types of pores and discuss their effects on the material biodegradation and the bone ingrowth throughout this section.

#### 5.3.2.1 **Effect of Macroporosity**

Macroporosity plays a critical role in the regeneration of damaged tissues, allowing cell penetration and tissue/blood vessel ingrowth [32]. At the same time, it is the key factor for controlling CPC biodegradation/resorbability, the important property of implanted materials for clinical usage. Ideally, the CPC will degrade in a short period of time matching new bone formation. Suitable pore size and an adequate interconnectivity should be required [33, 34]. However, there exist debates about the proper pore size for bone repairing materials. Some researchers claimed that a pore size larger than  $100\ \mu\text{m}$  is sufficient for tissue ingrowth, since macropore size determines the efficiency at which cells seed into the scaffold [33], whereas other studies suggested that the larger pores (up to  $500\ \mu\text{m}$ ) are preferred [34]. It is generally acknowledged that the materials with larger pores will lead to a faster degradation. However, the structural/functional integrity of materials should be considered for different uses. Generally, the optimum pore size for scaffolds lies in the range between  $100$  and  $400\ \mu\text{m}$  [35]. This will allow cell ingrowth and vascularization and promote metabolite transport. A scaffold with an open and interconnected pore network and a high degree of porosity ( $>90\%$ ) is ideal for the scaffold to interact and



**Fig. 5.3** Micro-CT images of reconstructed cross section of beagle's molar region and the residual materials implanted samples at 3 months (a–d) and 6 months (e–h); (a) and, (e) CPC control; (b) and, (f) CPCC; (c) and, (g) CPCCB; (d), and (h) CPCCBV; Note: CPC control, dense CPC; CPCC, macroporous CPC with collagen; CPCCB, CPCC with recombinant human bone morphogenetic protein-2 (rhBMP-2); CPCCBV, CPCC with VEGF (Reproduced from [37] by permission. Copyright © 2014 Elsevier Ltd. and Techna Group S.r.l)

integrate with the host tissue [36]. Figure 5.3 describes the typical degradation behavior of CPC/biodegradable polymer in vivo [37].

As can be seen, Fig. 5.3 shows the precise micro-CT scan results about the material degradation and osteogenesis performance in vivo at each determined time. Obviously, all the samples exhibited varying degrees of degradation ability in vivo with the time passing. Specifically, the dense CPC group with several microns or less pore size still maintained the original shape and structure after 6 months of implantation. Lack of macroporous structure is the main reason. In comparison, CPCC groups with average pore size of 250  $\mu\text{m}$  and macroporosity of 45% presented a certain amount of new bone formation [37]. The implanted materials had

been partly absorbed and replaced by newly formed bone trabeculae on its peripheral portion. CPCCBV group showed the best new bone formation at both peripheral and central areas of the cement. After 6 months, the residual CPC material volume fraction of CPCCBV was about 20%, further indicating the fastest degradation speed among four groups. These behaviors were attributed to the encouraging effect of macroporous structure and macroporosity.

Some other researchers mentioned that CPC products had superiority over sintered HA because CPC could form macroporous HA in situ in the bone site without machining [38]. The pores of diameter  $\sim 20$  to  $50\ \mu\text{m}$  are expected to provide favorable functionality for physiological liquid exchange, while pores of diameter  $\sim 100$  to  $350\ \mu\text{m}$  are suitable for cell colonization and vascularization [39]. Thus, pristine CPC cannot allow vascular permeation and cell ingrowth. Such bone cement is very stable in the body, and the absorption and degradation usually occur only on the surface and the absorption rate is very slow [40]. To speed up the degradation rate of CPC, one of the feasible ways is to create macropores within CPC by using foaming agents or degradable polymer microparticles.

The degree of macropore interconnectivity is also considered to be critically important in a manner similar to pore size. In biodegradable porous ceramics, the degree of interconnectivity was noted to be seemingly more important than the pore size, while in nonbiodegradable materials (i.e., CPC), interconnectivity and pore size were observed to be equally important. Under in vivo conditions, the penetration of cells and chondroid tissue formation inside macropores occurred when the interconnectivity dimensions were greater than  $\sim 20\ \mu\text{m}$ , while mineralized bone formation occurred when the interconnectivity size exceeded  $50\ \mu\text{m}$  [41]. The interconnectivity of pores ensures availability of higher surface area for fast resorption, enhanced cell adhesion, and proliferation. For bone tissue engineering, the optimal pore size for the resorption and osteoblast activity within the material matrix is still controversial and undermined.

### 5.3.2.2 Effects of Microscopic Features (Micropores and Grain Size)

While macropores with pore sizes and interconnections are in the range of hundreds of microns, microporous features in the range of nanometers up to several microns also play pivotal roles in tissue engineering. It was in 1984 that Klein et al. [23] underlined the fact that not only macropores but also micropores (typically close to  $0.1\text{--}10\ \mu\text{m}$ ) were essential to provide a fast resorption. In 1993, Langer and Vacanti [42] devoted to the control of the architecture of CaP bone graft substitutes and to the understanding of the relationship between implant architecture and biological response. Since then, a number of researchers have investigated the effects of microscopic features such as micropores or grain size on the resorption behavior of CPCs (listed in Table 5.1) [43].

For example, Wei et al. [51] implanted magnesium-CaP macroporous scaffolds with 9% and 27% microporosity and found that the presence of micropores increased the degradation rate and accelerated bone formation. A similar result was found by

**Table 5.1** List of several studies devoted to the effect of architectural factors on the in vivo performance of resorbable CPC scaffolds (sintered HA is considered to be non-resorbable). Various aspects were considered: micro- and macropore size, micro- and macroporosity, grain size, and interconnection pore size

Animal study	Material	Investigated factor(s)	Resorption	Bone formation	Remarks
Rabbits (1, 2, 4, 8 w)	$\beta$ -TCP	Macropore size: 300–400, 400–500, 500–600, 600–700 $\mu\text{m}$ ; interconnection: from 72 to 198 $\mu\text{m}$ ; porosity: 67–79%	NA	NA	Increase of blood vessel ingrowth with an increase of macropore and interconnection size [44]
Rabbits (2, 4w, 4, 6 m)	$\beta$ -TCP	Macropore size: 50–100, 200–400 $\mu\text{m}$	2/3 and 5/6 resorbed after 6 months for groups I and II, resp.	$\approx 2\times$ faster in group I than group II at 2 and 4 weeks	Very limited material characterization [32]
Rabbits (8 w)	BCP	Grain size Two groups produced according to the same method but with two different raw materials	Fourfold increase of resorption rate with an increase of grain size	No difference	Grain size: G1 roughly 1 $\mu\text{m}$ ; G2 0.1–0.2 $\mu\text{m}$ . Not the same raw material for the two groups [45]
Dogs (45, 90 day)	BCP	Grain size (two groups): Group 1 ( $86 \pm 20$ nm) and group 2 ( $768 \pm 321$ nm)	NA	10–20% more bone formation in group 1	Refer to [46]
Rabbits (16 m)	$\beta$ -TCP	Microporosity and macroporosity Four groups without or with macropores and with a small (<5%) and large (50–60%) amount of micropores	Faster resorption of the microporous samples	More bone ingrowth in the macroporous samples	Only one histological time point (16 months). Only XRD to assess resorption within the first months of implantation [47]
Rabbits (3, 6, 12 m)	$\beta$ -TCP	Microporosity and macroporosity Five groups; microporosity between 40% and 55%; macroporosity between 0% and 20%	Faster with more macroporosity and microporosity	No difference	Only qualitative results [48]

(continued)

**Table 5.1** (continued)

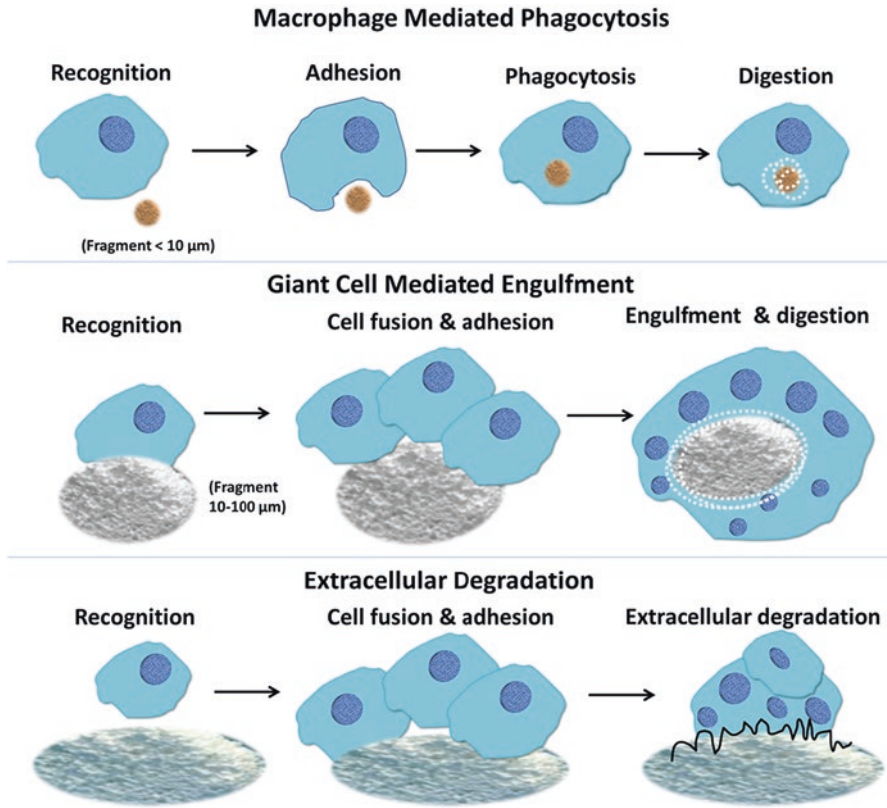
Animal study	Material	Investigated factor(s)	Resorption	Bone formation	Remarks
Rabbits (4, 12, 24 w)	$\beta$ -TCP	Microporosity	~30% in ceramic area at 24w for group 1; ~2% for group 2	No difference	Not clear how a ceramic with 0% microporosity can have a SSA value of 2 m <sup>2</sup> /g. No XRD data demonstrating that both ceramics are pure $\beta$ -TCP. Not the same raw materials for the two groups [49]
		Group 1: $\mu$ Por $\approx$ NA; $\mu$ Por size $\approx$ 0.2–0.5 $\mu$ m; porosity $\approx$ 60%; MPor size: 150–400 $\mu$ m; SSA = 10 m <sup>2</sup> /g; group 2: $\mu$ Por $\approx$ 0%; porosity $\approx$ 57%; MPor size: 150–400 $\mu$ m; SSA = 2 m <sup>2</sup> /g		Very small amount of bone	
Rabbits (4, 20 w)	$\beta$ -TCP	Macroporosity and growth factor	Faster resorption for samples with 200–300 $\mu$ m macropores at 20 weeks, 52.5% of materials loss	Higher new bone formation and faster resorption for samples loaded with BMP-2	Refer to [50]

NA not applicable/no response, MPor macroporosity,  $\mu$ Por microporosity [43]

other several groups [23, 47, 49, 52]. Klein et al. [47] reported that changes of microporosity played a more important role in the resorption process than changes in macroporosity. Recently, the presence of micropores was associated with the biological response of cells and osteoinductive potential for bone ingrowth [53–56]. These pores are usually few microns in size and are involved mainly on the initial adsorption of proteins on the surface of the materials, thus regulating the cell behavior on the implant surfaces as well as cell-material interactions. Some groups have revealed that microporosity that incorporated into CaP biomaterials can enhance the protein adsorption and cell adhesion due to the larger surface area, the tight interlock between material and tissue. Take an example, the cells spread and adhered better on membranes with smaller micropores (0.2  $\mu$ m diameter) [53]. Once various proteins (soluble growth factor, serum proteins, and extracellular matrix proteins) and cells are adsorbed onto the surfaces, the interfacial properties will be changed, resulting in enhanced degradation in vivo [57, 58].

The influence of grain size on the CPC resorption might be related to the resorption mechanism. It has been proposed that the biodegradation of CaP-based biomaterial takes place via solution-driven extracellular liquid dissolution and cell-mediated resorption processes [21]. The dissolution is heavily influenced by the solubility of the implanted CaP materials, while the cell-mediated CaP resorption is due to the particle formation as a result of disintegration [59]. It has been reported that the grain size of the CaP materials affects the rate and effectiveness of cellular





**Fig. 5.4** Macrophage response to biomaterials depending on the size of the implanted materials. Macrophages respond to small fragments and particles ( $<10 \mu\text{m}$  in diameter) by internalization and intracellular digestion. If the particle size is larger than  $10 \mu\text{m}$  and smaller than  $100 \mu\text{m}$ , the macrophages fuse together forming giant cells which in turn engulf the particles and digest them. If the particles are larger, the bulk digestion is carried out via extracellular degradation by macrophages and macrophage-fused giant cells (Reproduced from Ref. ([18, 62] by permission of MDPI, Basel, Switzerland)

resorption activity [60]. Typically, the resorption rate increased with a decrease in grain size [11, 47, 48, 61], which can be schematically explained by Fig. 5.4 [62]. It was noted that the macrophages and giant cells actively participate in the resorption process for rapidly resorbing cements [63]. When the fragments and particles are  $<10 \mu\text{m}$  in diameter, they are easily internalized in macrophages and rapidly intracellularly digested. For larger biomaterials ( $>100 \mu\text{m}$  in diameter), the bulk digestion is carried out via extracellular degradation by macrophages and giant cells.

Most studies devoted to microscopic features suggest that an increase of microporosity and a decrease of grain size accelerate resorption. However, there still exist the contradictory results and the difficulty to draw conclusions about the influences of microscopic features, since it is impossible to vary one parameter without

changing other parameters. Here, we only discussed the effect of porous architectures on the *in vivo* resorption behavior of CPCs quantitatively. Recently, more attentions have been paid on the hierarchy structure of tissue scaffolds incorporating mesoporous materials ranging within 2–50 nm. With regard to the biomedical applications, mesoporous materials can easily host drug molecules and, therefore, could be useful to improve the drug adsorption ability and enhance bone-forming properties, as well as promoting resorption of CPCs.

### ***5.3.3 Effect of CPC Composition on Biodegradation***

Since commercial CaP bone graft substitutes have been launched for 40 years, many different formulations have been commercially available or are still being developed. Within various CaP compounds, HA,  $\beta$ -TCP,  $\alpha$ -TCP, and DCPD can be the typical compositions forming CPCs. Among these compounds, HA is the most biocompatible. An important *in vivo* characteristic of HA-forming CPC is that it does not dissolve spontaneously in a normal physiological fluid environment, yet is resorbable under cell-mediated acidic conditions.  $\beta$ -TCP is the material more suitable for promoting synthetic osteoconduction, but its resorption remains slow *in vivo*, which can be regulated via cell-mediated processes. It has a lower strength and poorer mechanical properties than other CaPs. Although  $\alpha$ -TCP has the same chemical composition as  $\beta$ -TCP, the difference in crystallinity makes it much more soluble than  $\beta$ -TCP. Therefore, early efforts to speed up the resorption of a CaP material were focused on  $\alpha$ -TCP. CaP cements made of  $\alpha$ -TCP powder have shown the excellent biocompatibility and biodegradability [64, 65]. Also, some studies have reported the positive performance of implanted  $\alpha$ -TCP granules [66]. However,  $\alpha$ -TCP is considered to be resorbed too fast and has hardly been investigated as raw material for larger granules and shaped blocks. DCPD is the most easily synthesized CaP compound. DCPD is biocompatible and osteoconductive and is reabsorbed faster than the  $\beta$ -TCP/HA-forming CPCs, allowing faster bone formation. However, the conversion process of DCPD into HA easily releases amounts of acid, leading to a severe inflammatory response.

Rapid resorption does not always indicate better bone formation. Under certain clinical situation, rapid resorption was reported to lead to lower quality bone formation [66]. In order to achieve optimum clinical performance, an appropriate CPC resorption rate needs to be modulated by tuning the composition of CPCs for the intended clinical applications. For periodontal bone defect repairs and sinus lift, the rapid replacement of the implant cement is highly desirable. To promote the resorption rate of certain CPCs with slow degradation, one of the feasible ways is to add the compounds with rapid resorption. These compounds could be small molecules (i.e., basic/acidic compounds, specific ions), degradable polymers, or other additives. For instance, calcium sulfate is biocompatible; however, it is less suitable for bone substitution because of its rapid resorption. Interestingly, mixing calcium sulfate with TTCP and DCPA leads to a good biocompatibility, enhanced degradability,

and bone ingrowth as compared to CPC consisting of only TTCP and DCPA [22]. Small acidic compound also plays a role in the active resorption of the cement. It has been reported that a cement produced by a mixture of sodium calcium phosphate, tetracalcium phosphate and  $\beta$ -TCP powder, and malic acid or citric acid showed an increased number of osteoclasts on the cement [67], which indirectly indicates the cement mixed with malic acid has better resorption and is more promising for bone substitution than the cement mixed with citric acid.

### 5.3.3.1 Effects of Ions on CPC Degradation

The incorporation of some specific ions plays an important role in the biochemistry of bone substitutes, improving some properties such as the stability, solubility, porosity, or cytocompatibility of the bone remodeling process [68, 69]. Numerous studies have revealed that doping inorganic ions including calcium ( $\text{Ca}^{2+}$ ), silicate (Si), magnesium ( $\text{Mg}^{2+}$ ), zinc ( $\text{Zn}^{2+}$ ), strontium ( $\text{Sr}^{2+}$ ), manganese ( $\text{Mn}^{2+}$ ), copper ( $\text{Cu}^{2+}$ ), or ( $\text{Fe}^{3+}$ ) may trigger bone cell response, change CPC resorption behavior, and show important impact on bone healing strategies.

Calcium is the most abundant mineral in the human body. About 99% of the calcium in the body is found in bones and teeth [70].  $\text{Ca}^{2+}$  is a mineral that the body needs for numerous functions, especially for bone formation. The mineral phase of the bone also contains Si, an essential trace element for metabolic processes associated with the development of the bone and connective tissues. This mineral is responsible for the depositing of minerals into the bones, especially calcium. It has been reported that Si can speed up the healing of fractures and also reduce scarring at the site of a fracture. Both Ca and Si ions play an important role in the nucleation and growth of apatite and then influence the biological metabolism of osteoblastic cells in the mineralization process and bone-bonding mechanism. Therefore, both ions can make the important contributions for the clinical field of bone regeneration, as well as material resorption.

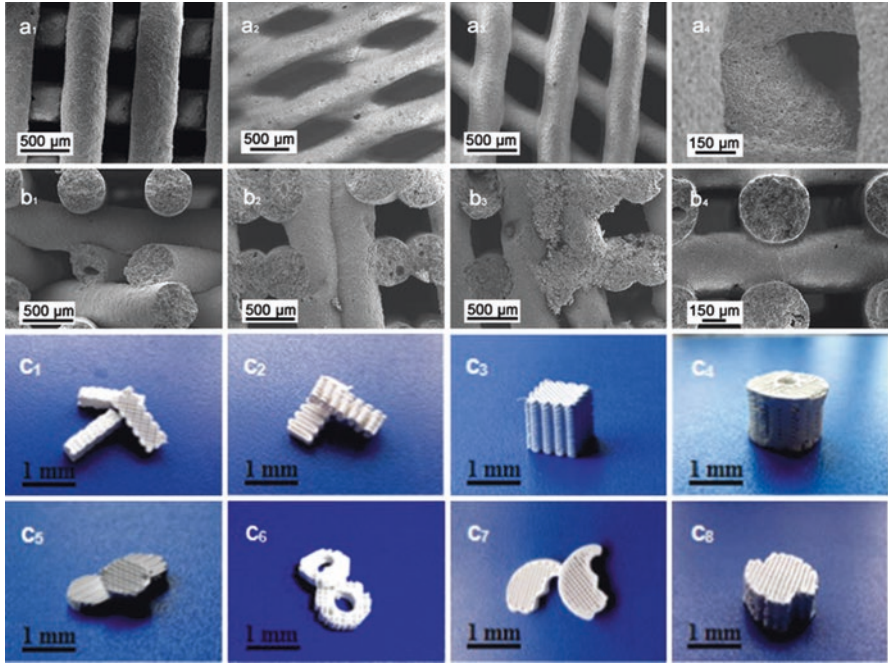
Si has been substituted in different CPC formulations (i.e., HA,  $\alpha$ -TCP, HA-based cements,  $\beta$ -TCP) to enhance in vivo implant degradation favoring their osteotransduction [71]. In the early stages of mineralization, Si content is higher, while decreasing at advanced stages with the increase of the Ca/P ratio toward that of HA [72]. Pietak et al. [73] have demonstrated that aqueous Si solutions enhanced osteoblast proliferation, differentiation, and collagen synthesis in vitro. They also reported that Si levels below 30 ppm could stimulate the development of osteoclasts, whereas higher levels inhibit osteoclast formation. The degradability of the Si-TCP scaffold was 90–80% after 1 year of implantation, and its complete resorption and replacement by new bone tissue had been achieved after 2 years [71]. Alkraishat et al. developed a silica-gel-modified CPC that increased the amount of remaining graft after implantation in rabbit calvaria [74]. To reveal the in vivo resorption of silicon-substituted CPCs, Aparicio et al. [75] prepared the sintered silicon-doped  $\beta$ -TCP powder first. By well controlling the constant Ca/(P + Si) ratio, a powder/liquid ratio, and the powder size, the physicochemical properties

and *in vivo* degradation of the Si-CPC properties were evaluated. The cement porosity was about 40% with a shift of the average pore diameter to the nanometric range, whereas the degree of absorption was lower with increasing Si content. Interestingly, this Si-CPC provides a high specific surface area of up to  $29 \text{ m}^2 \text{ g}^{-1}$  and an enhancement of cell proliferation and cell attachment. Moreover, this bone substitute made of Si-CPC with lower Si content could interact efficiently with the surrounding bone and induce the formation of bone tissue *in vivo*.

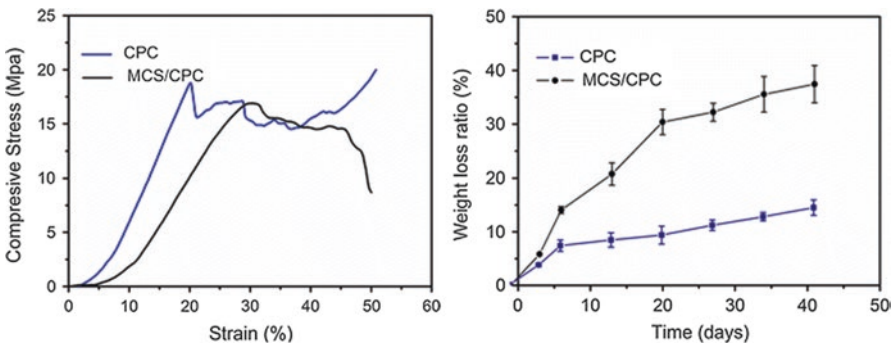
Some evidences have suggested the body cannot assimilate calcium without the presence of silica [76]. Therefore, to improve the bioactivity and degradability of CPC, calcium silicate (CS) was added to CPC. Low-crystalline CS prepared by heat treatment at low temperature had excellent bioactivity and degradability. Adding CS to CPC did not affect the phase composition and chemical structure of CPC and had a little effect on the setting time and compressive strength of the composite cement. However, CS could effectively improve the *in vitro* and *in vivo* bioactivity and biodegradation of CPC and enhance the cell proliferation on the CPC material [77]. For designing the ideal bone substitutes, it is more challenging to achieve rapid biodegradability with maintaining/enhancing the mechanical strength. Liu group has explored the development of bioactive mesoporous calcium silicate/calcium phosphate cement (MCS/CPC) scaffolds (shown in Fig. 5.5) with high mechanical strength and fast degradation rate by micro-droplet jetting [78].

Figure 5.5 illustrates the MCS/CPC scaffolds with various architectures and pore structures. The inner pore shape was controlled by adjusting the angle of the process pattern. It could be clearly seen that the macropores in the scaffolds were uniform and completely open. In addition, scaffolds with different pore structures in Z direction were prepared precisely (b1–b4). To meet a wide range of individual needs, MCS/CPC scaffolds with different outer architectures were also designed and fabricated successfully. Moreover, addition of MCS to CPC not only exhibited outstanding printability of MCS/CPC paste but also achieved high mechanical strength and fast degradation rate (Fig. 5.6). Therefore, Si/Ca doping is a potential way to speed up the biodegradation and promote the bone repairing of CPCs.

The magnesium and zinc are also important foreign ions into the structure of synthetic calcium phosphate phases used as starting powders. The presence of  $\text{Mg}^{2+}$  and  $\text{Zn}^{2+}$  can alter a series of structural, physicochemical, and biological properties of CPC, such as crystallinity, solubility in the setting liquid, resorption, and bone-bonding capability [79, 80]. Incorporation of ions into  $\alpha$ ,  $\beta$ -TCP structures has been experimentally proven through quantitative phase analysis and structural refinement of the powders. Several groups have reported that the incorporation of  $\text{Mg}^{2+}$  and  $\text{Zn}^{2+}$  into  $\beta$ -TCP structure led to a decreasing trend in the lattice parameter values and a contraction of cell volumes [81, 82]. The reason for this contraction in refined parameters is due to the lower ionic radii of Mg ( $0.72 \text{ \AA}$ ) and Zn ( $0.745 \text{ \AA}$ ) than Ca ion. Since the degree of lattice disturbance by the substituted ions had implications in terms of thermal stability of the  $\beta$ -TCP phase,  $\text{Mg}^{2+}$  has been also reported to have a stabilizing role of noncrystalline CaPs, preventing crystallization into other more stable CaP phases. Therefore, the presence of Mg had a strong effect on cement composition and strength, namely, by increasing the proportion of brushite



**Fig. 5.5** SEM images of (a1–a4, b1–b4) and digital camera photographs (c1–c8) of MCS/CPC scaffolds (Reproduced from [78] by permission. Copyright © 2015 Springer)



**Fig. 5.6** The compressive stress–strain curve (left) and weight loss (right) in TrisHCl solution of CPC and MCS/CPC scaffolds (Reproduced from [78] by permission. Copyright © 2015 Springer)

and decreasing the compress strength. According to these authors [83], Mg could be used to adjust the composition and rate of hydration of the cement. For instance, magnesium phosphate cement (MPC) composed of magnesium oxide and ammonium phosphate is a kind of fast-setting phosphate cement. Moreover, MPC has high initial strength and rapid resorption rate. When combined MPC with CPC, a novel magnesium-doped calcium phosphate complex with improved properties was

achieved. For Mg-doped materials, the resorption process is closely related to the biological behavior of surrounding cells. Numerous research have reported that Mg has acted as a surrogate for Ca in transport and mineralization processes [84, 85], but it also exerts a large number of other actions, including enzyme co-factor function and modulation of the action of hormones, growth factors, and cytokines. Mg also has direct effects on the bone formation processes of resorption and mineral aggregation [86]. For example, our group has demonstrated that the C2C12 cells cultured on 5MCPC/rhBMP-2 substrates exhibited dramatically enhanced in vitro osteogenic differentiation, compared with CPC/rhBMP-2. Moreover, it was the Mg on the underlying substrates that became the main contributor to mediate the adsorption and conformation of rhBMP-2 bound on the matrix, thus enhancing osteogenic activity and the resorption of CPC matrix [87].

Besides the ions above, strontium is an alkaline earth metal accounting for approx. 0.02–0.03% of the earth's crust. Strontium was discovered to follow the metabolic pathways and signaling principles known for calcium, although the response to  $\text{Sr}^{2+}$  tends to be weaker. It has been reported that  $\text{Sr}^{2+}$  could exert a dual effect on bone remodeling.  $\text{Sr}^{2+}$  enhances protein binding capacity and osteoblast activity, increasing new bone formation, although the exact mechanism of how Sr affects bone cells remains unknown; at the same time,  $\text{Sr}^{2+}$  inhibits osteoclast activity and thus reduces cellular bone resorption [88, 89]. Recently, many researchers have focused on the systematic investigation of  $\text{Sr}^{2+}$  effect on the biological activities of CPC including resorption behavior. As we described before, the solubility of the cement components affects the CPC degradation. Integration of  $\text{Sr}^{2+}$  ions into CPCs could increase solubility, and consequently higher degradation was demonstrated for SrHA and SrHA-forming cements.  $\text{Sr}^{2+}$  ions were also introduced into  $\beta$ -TCP to produce brushite-forming cements. A zero-order release of Sr during immersion of SrTCP in water indicated that  $\text{Sr}^{2+}$  was released by bulk erosion [68]. In addition, several in vivo studies revealed an increased degradation of SrCPC compared to the respective Sr-free control groups and thus confirmed the above findings [90].

To be summarized, ion-substituted bone cements hold great potential for applications in repair of bony and periodontal defects, owing to their relevant excellent properties (i.e., setting time, injectability, good resorption for clinical uses), especially the Sr-containing cements that exhibited an overall better performance. However, there remains a great need for optimization and prospective studies of ionic-substituted cements regarding specific clinical applications.

### 5.3.3.2 Effect of Degradable Polymers on CPC Degradation

As discussed above, an ideal substrate for the bone regeneration should not only have adaptive mechanical strength, but also can promote bone repairing with good biodegradation. Adding biodegradable polymers into CPC matrix is a feasible strategy to improve the degradability of CPC and alter their mechanical/physical

**Table 5.2** Summary of major degradable polymers used in combination with CPCs [17]

Group	Polymers
Natural polymer	Collagen, gelatin, fibrin, peptides
Poly(lactic series)	Poly(lactic acid (PLA), polyglycolic acid (PGA), poly(lactic-co-glycolic acid) (PLGA), poly- $\epsilon$ -caprolactone (PCL)
Carbohydrates	Chitosan, cellulose, starch, alginate, hyaluronan, hydroxymethylpropyl cellulose (HPMC), amylopectin
Others	Polycarbonate, polyalkanoates, poly(ethylene glycol) (PEG), poly(ethylene oxide) PEO, polypropylene (PP), poly(allylamine hydrochloride) (PAH), poly-trimethylene carbonate (PTMC)

properties. A number of biodegradable polymers have been considered for CPC degradation promotion and mechanical reinforcement (as listed in Table 5.2).

Biodegradable polymers are processed in CPC materials with the specific form of wires, fibers, or microspheres. For instance, as abundant reinforcing materials, PLGA fibers or other degradable polymeric fibers were introduced into CPC to enhance the mechanical properties and improve the degradability. The best mechanical properties reported for fiber-reinforced CPC were achieved with PLGA fibers and HA matrix, which had a highest bending strength of 40–45 MPa [91]. In physiologic environment, the PLGA fibers degraded within 3–4 weeks, leading to a loss of reinforcing effect, while the HA matrix took months to years to degrade.

More interesting, the introduction of PLGA microspheres is proposed for mechanical reinforcement and degradation modulation. Adding PLGA microspheres inside CPCs was first done in 2002, and the resulting paste was moldable and showed good biocompatibility [92]. By well controlling the physical/chemical properties of PLGA microparticles via tuning the molecular weight, L/G ratio, and the content of PLGA, PLGA/CPC composites were successfully fabricated and held different degradability and mechanical strength [92–97]. Table 5.3 summarizes the degradable and mechanical properties of typical PLGA microspheres/CPC composites.

As can be seen, the presence of PLGA microspheres can enhance the early compressive strength of CPC [92, 94, 97, 98]. And the acidic degradation products of PLGA could accelerate the dissolution of CPC on account of the acidified surroundings [95]. Moreover, the generation of macropores by prior degradation of PLGA microspheres can provide channels for cell distribution and migration together with the ingrowth of blood vessels, promoting the new bone formation [93]. Therefore, tissues can easily grow into the PLGA/CPC composites along with the interconnections among pores formed after microsphere degradation.

Besides the advantages discussed above, these entrapped microspheres can be applied as drug delivery vehicles for osteoinductive growth factors or anti-inflammatory drugs. Combined these bioactive molecules and degradable microparticles with CPCs, multifunctional performances could be achieved for bone repairing including better resorption and new bone formation, which will be discussed later.

**Table 5.3** The degradable/mechanical properties of typical PLGA/CPC composites

Preparing method	Microsphere size/CPC	Degradation	Mechanical properties	Biological performance	Ref.
Mixing	PLGA 180–360 $\mu\text{m}$ ; TTCP	PLGA microspheres degraded in D90 to form macropores	Tensile strength: 6.4 MPa @ D 0	Biocompatible	[92]
Mixing	PLGA 20–40 $\mu\text{m}$ ; HA-based CPC	Mass loss and a pH decrease @ D40; total degradation and highly porous @ D90	CSth: 12.2 MPa @ D 90	NA	[93]
Mixing and dispersion	PLGA/gelatin/PTMC: 30–40 $\mu\text{m}$ ; HA-based CPC	MW: PLGA 55,000–4000 Da; gelatin/PLGA same @ W8. Complete degradation @ W12	CSth: PLGA 13.5–3.5 MPa; gelation 7.5–3.4 MPa; PTMC 4.3–3.4 MPa @ D 90	Capsule thickness ↓; inflammatory response ↑ over time	[94]
Mixing	PLGA 30–50 $\mu\text{m}$ with varying MW and content; $\alpha$ -TCP-DCPA-pHA	A pH decrease to 3.0 @ W12; porosity increased to 65% @ W4	NA	$\mu\text{CT}$ images for confirming the degradation	[95]
Mixing	PLGA 30–50 $\mu\text{m}$ ; CPC w/wo CMC and Bio-Oss®	Bio-Oss® 35%; PLGA/CPC 8%; PLGA/CPC-CMC 21% @ W26	NA	Bone formation: Bio-Oss® 25%; PLGA/CPC 44%; PLGA/CPC-CMC 32% @ W 26	[96]
Dripping-freezing	PLGA 50–100 $\mu\text{m}$ ; DCPA-calcium silicate	Weight loss: 20% CPC vs. 40% PLGA/CPC @ week 14	CSth: PLGA/CPC 3.7 MPa; CPC 1.2 MPa	Good for proliferation and differentiation of mBMSCs	[97]

Here, *D* means day, *W* refers to week, *CSth* means compressive strength, *MW* means molecular weight



Obviously, incorporation of PLGA microspheres is a promising way to design the resorption rate of bone graft matching for the rate of new bone formation in bone defect repair.

### 5.3.3.3 Effect of Other Additives on CPC Degradation

As mentioned before, one of the advantages of CPC is the low-temperature setting, which allows the incorporation of different useful additives/biomolecules: from antibiotics and anti-inflammatory drugs to growth factors. After implantation, these additives released from CPC cannot only treat the different skeletal diseases or speed up the bone repairing but also alter the microenvironment surrounding the implants, influencing the resorption behavior of implants.

In most cases, it is supposed that CPCs do not degrade while additive is released. However, some authors have shown certain degree of degradation of CPCs during drug liberation. For example, Otsuka [99] showed an increase of porosity in a carbonated HA cement during the release of indomethacin. Bai [50] revealed that the amount of newly formed bone and the rate of biodegradation were higher in porous CPC loaded with rhBMP-2, compared to the scaffolds without rhBMP-2. Therefore, it should not be neglected the effect of the additives on the resorption rate of CPC. Typically, the additives such as antibiotics, even growth factors, have the small size, and their release is considered to be excessively fast. Therefore, the additives may tend to improve the degradation rate of CPC. And the influences of additives on the CPC mechanical strength are still **controversial**: some researchers reported the minor variations of mechanical strength due to the antibiotic loading, while some found the enhanced mechanical properties due to the effect of loaded drugs with substantial interactions with CPCs. To prolong their release behavior and modify the properties of CPCs, one possible way is to entrap the polymeric microspheres loaded with additives/drugs into CPC matrix. Polymeric microspheres not only provide a carrier for controlled release and better bioactivity of drugs/proteins but also reinforce the mechanical strength of CPC as fillers. This has been confirmed by many research groups. Ruhe et al. [100] mixed hrBMP-2-loaded PLGA microspheres with a CPC. The release rate of rhBMP-2 in PLGA/CPC composite was much slower than the rate in the microspheres alone.

As we know, there are many additives available for CPC applications. Various additives/drugs have various effects on CPC properties, and this represents a serious issue for the implementation of this technology. A lot of work has still to be done to establish the general laws to regulate additives and modify the properties of CPC for different therapeutic needs.

## 5.4 Typical Strategies for Rapid Biodegradation of CaP-Based Cements

CPCs are frequently used as synthetic bone graft materials in view of their excellent osteocompatibility and clinical handling behavior. However, the degradation rate of plain CPC is limited, especially for HA-forming CPCs, thereby limiting complete bone regeneration. In the previous section, we have discussed many factors influencing the biodegradation of the CPC, mainly including porous architectures and intercompositions. Hence, there are many strategies available for achieving the faster biodegradation of CPCs. The most important one is the macroporosity, the key factor for controlling CPC biodegradation/resorbability. For a better bone regeneration, different approaches have been used to induce macroporosity in CPC, such as inclusion of water-soluble additives, foaming agents, a hydrophobic liquid (oil), and biodegradable polymeric microspheres. However, it is considered that macropores severely degraded the CPC strength. After macroporous materials were implanted in vivo, the strength significantly increased once new bone started to grow into the macropores [101]. Therefore, it is in the early stage of implantation when the macroporous implant is in the most need of strength [102].

### 5.4.1 Water-Soluble Additives for Macroporosity Enhancement

The inclusion of water-soluble molecules in CPC is a common approach to induce macroporosity. Also known as the particle leaching technique, it is often used to create porosity in bone substitute materials such as preset ceramics or polymeric scaffolds. Saccharides such as sucrose, chitosan, as well as the salts sodium chloride and sodium phosphate are water-soluble compounds to generate macroporosity in CPC. Depending on the solubility of these sacrificial materials, these are dissolved before implantation or gradually degraded in vivo. Sucrose is a disaccharide derived from glucose and fructose. Sucrose crystals with the size in the range of 125–250  $\mu\text{m}$  have been included in CPC, and macroporosity was readily generated after dissolution of the crystals during incubation of the samples in aqueous media. However, the mechanical strength of CPC decreased with increasing macroporosity [103]. Another approach is the creation of microspheres from a saccharide. As a linear polysaccharide, chitosan has been processed in the form of fibers and microspheres, embedded in or trapped on the CPC matrix in order to enhance its mechanical properties in an early stage and to generate porosity after the fiber degradation [104]. Several salts have also been used to induce porosity in CPC, such as sodium chloride crystals,  $\text{NaHCO}_3$ ,  $\text{CaSO}_4 \cdot 2\text{H}_2\text{O}$ , and  $\text{Na}_2\text{HPO}_4$ . Similarly to when saccharides are employed, porosity is generated after the salt is leached out from the CPC in an aqueous environment. The degree of solubility of the particular additives during the setting reaction of the cement is responsible for the content and dimension of the macroporosity [105]. However, the lack of strength of the resulting cement

(especially for the additives with quickly dissolving) and compromise requirements between CPC handling and its bioactivity due to a large amount of additives limit the applications of this technique.

### ***5.4.2 Foaming Agents for Macroporosity Enhancement***

The use of foaming agents is another way to generate gas bubbles and form macropores. Typical foaming agents involve hydrogen peroxide and carbon dioxide (CO<sub>2</sub>). CO<sub>2</sub> bubbles from sodium bicarbonate have been used during the cement setting to generate porosity [106]. Besides, citric acid was employed as porogens for CPC for good injectable properties and higher porosity [107]. Furthermore, citric acid has combined with sodium bicarbonate as effervescent agents to generate porosity [108]. Since no potentially toxic gas is released after implantation of the cement, this technique holds great potential for macroporosity enhancement and fast biodegradation. However, the low initial strength and poor reproducibility still remain the issues for this technique.

### ***5.4.3 CPC/Synthetic Degradable Polymers***

To overcome the issues including the initial strength, degradability, and lack of interconnectivity, synthetic degradable polymers in forms of fibers and microparticles have been added in cements. Typical degradable PCL and PLGA fibers entrapped in CPCs had the function of reinforcing the cement, providing the needed short-term strength and toughness and gradually dissolving afterward, leaving behind macropores suitable for bone ingrowth [109, 110]. The fiber parameters (i.e., length, volume fraction, type of fiber, and the mass percentage) affected the physicochemical properties of cements, especially the resorption behavior. The advantages of long fibers over particulates and short fibers are the fact that, once resorbed, they can form interconnected pores inside the CPC structure facilitating bone tissue regeneration [111]. In vivo results also proved that the introduction of ultrafine degradable fibers within a CPC matrix improved macroporosity efficiently and enhanced CPC degradation and bone ingrowth largely [110].

Of special interest are also the various works that incorporated PLGA microspheres within the cement paste [92–97]. The rationale was to create a macroporous structure through degradation of the PLGA microparticles/microspheres. The mechanical strength of the microspheres contributes to the initial strength of CPCs, and the degradable nature of microspheres offers the better resorption performance of CPCs. Since the degradation of PLGA by nonenzymatic hydrolysis of its ester linkages depends on its molecular weight, this allows the easy modulation of macropore formation.

These microspheres can be applied as delivery vehicles for osteoinductive growth factors or other biofunctional additives. Besides the mechanical enhancement, the microspheres could simultaneously release the osteogenic factors for accelerating the new bone formation. The *in vivo* results from subcutaneous implantation in rats showed that the PLGA microspheres were completely degraded after 12 weeks of implantation, allowing blood vessels to colonize the macropores [100, 112].

Other types of microspheres also showed the similar effects on cement properties. For examples, self-setting CPCs were produced upon the introduction of microspheres composed of gelatin [113] and poly(trimethylene carbonate) (PTMC) [114]. *In vitro* incubation of all these composites in phosphate-buffered saline or enzyme-containing media resulted in an interconnected, macroporous calcium phosphate matrix after microsphere degradation. Gelatin and PTMC microsphere/CPC composites were found to show gradual degradation of the microspheres from the outer to the inner parts, as the cement delayed enzyme diffusion through the material [113]. On the other hand, PLGA/CPC degraded simultaneously throughout the whole composite as a result of hydrolytic cleavage of the polymer chains. Furthermore, compared with the bulk erosion mechanism of PLGA and gelatin microspheres, surface erosion of the PTMC microspheres [114] resulted in a rapid decrease in compressive strength as they detached from the cement skeleton. This trend is also confirmed by subcutaneously implanting of CPC composite *in vivo* [94].

Acid-producing microparticles are also attractive to create macroporosity since CPCs degrade by acid dissolution. Félix Lanao et al. [115] incorporated glucono delta-lactone (GDL) into CPC for accelerating CPC degradation. After 2 weeks of implantation, CPC containing 10% of GDL degraded faster and was replaced by more bone tissue than CPCs containing either PLGA or gelatin microspheres. For matching the medical use, the degradation rate of CPCs was turned by formulating mixtures of PLGA microspheres and GDL microparticles [116]. The animal studies revealed that incorporation of 43% PLGA, 30% PLGA-5% GDL, and 30% PLGA-10% GDL in CPC significantly increased bone formation and resulted in higher bone height compared with both 10% GDL- and 20% GDL-containing CPC samples. Besides the biodegradable polymers listed in Table 5.2, there exist many potential additives, which can be used for tuning the CPC degradation, as well as other properties. More contributions should be made for fulfilling the therapeutic needs.

#### **5.4.4 Strategy Combinations**

In some studies, researchers combined the previously mentioned methods for accelerating the degradation behavior of CPCs. For example, CO<sub>2</sub> foaming has been used to induce porosity in combination with PLGA microparticles embedded in CPC for the creation of secondary porosity at a later time point [117]. Acid-producing GDL was formulated with PLGA microspheres within CPC matrix for adjusting the CPC

degradation [116]. Mannitol crystals were used to generate early macroporosity in combination with slower resorbable chitosan fibers, which improved the mechanical properties of the cement at initial time points [118].

Recently, it has already circumstantiated that both micrometer and nanometer scale features of a material have marked influence on cell behaviors *in vitro* and *in vivo*. Additionally, materials organized on multiple length scales have better conformity to biological matrices than those with single-scale features. Therefore, some attempts for fabricating synthetic scaffolds with hierarchical macro-/micro- or macro-/nano-architectures have been carried out by using properly mesostructured materials. The purpose of such scaffolds is twofold, as they combine the properties of traditional CPC-derived scaffolds, i.e., mechanical support in the defect zone, bioactivity, favored osteointegration, and bone tissue regeneration, with the unique features supplied by mesoporous materials, such as enhanced bioactivity and controlled drug adsorption/release ability for drug therapy *in situ*.

Our group developed the bioactive mesoporous calcium silicate/calcium phosphate cement (MCS/CPC) scaffolds by using micro-droplet jetting. The 3D printed MCS/CPC scaffolds with hierarchical architectures (350  $\mu\text{m}$  micropores and 10–20 nm mesopores) showed fast degradation rate, high mechanical strength, and good cytocompatibility [82]. Combined the growth factor rhBMP-2 with the mesoporous bioactive glass (MBG)/CPC composite, the resultant scaffold not only presented a hierarchical pore structure (interconnected pores of around 200  $\mu\text{m}$  and 2–10  $\mu\text{m}$ ) and a sufficient compressive strength (up to 1.4 MPa) but also exhibited excellent drug delivery behavior. Moreover, this composite scaffold presented a significant improvement of osteogenic efficiency, especially at the early stage *in vivo*. Moreover, better resorption was obtained in the rhBMP-2-loaded MBG/CPC scaffold compared to the others [119]. Obviously, it is very challenging to improve the properties of CPC satisfying all the requirements for clinical applications via altering one simple factor. Many research studies have demonstrated that the strategy combination will be feasible and hold great potentials.

## 5.5 Future Perspectives

The ultimate goal of bone reconstruction is the regeneration of the physiological bone that simultaneously fulfills both morphological and functional restorations. Within the different materials, CPCs are one of the most desirable candidates for bone replacement. However, the poor degradation and low mechanical strength limit their clinical applications. To overcome the limitations, especially for material degradation, different strategies (water-soluble additives, foaming agents, ions introduction, and biodegradable polymeric microspheres) can be applied. To meet the requirements for bone substitutes, strategy combinations are also suggested to obtain the attractive biological performances.

The injectability and moldability of the CPC are promising for less invasive and faster surgery as compared to other bone substitutes. The improvement of resorption

behavior of CPCs is still an “old new” topic. Many strategies including the introduction of polymeric wires, fibers, or microparticles have been applied for accelerating the CPC resorption with reinforcing their mechanical properties. Simultaneously, functional biomolecules are loaded/immobilized into the CPC matrix. However, the biocompatibility issues caused by the use of large volumes of degradable polymers and the difficulties to combine polymers with CPC without compromising the physicochemical properties with biological response still prevent the CPC applications for desirable clinical uses. Recent studies in the area of hierarchical scaffolds with immobilized growth factors have clearly revealed that the architecture of complicated design with well-defined structures has shown the excellent properties (i.e., mechanical, degradable, osteoconductive, osteoinductive features) and outstanding *in vivo* medical performances. However, *in vivo* studies and clinical trials have not yet been investigated to their maximum extent. There are still lots of optimization work to do for developing desirable CPC products, which have superior clinical performance and are easily applicable in clinical practice.

**Acknowledgments** This work was supported by grants from the National Natural Science Foundation of China (Grant No. 31570971 and No. 31330028), National Natural Science Foundation of China for Innovative Research Groups (No. 51621002), the Fundamental Research Funds for the Central Universities, State Administration of Foreign Experts Affairs P.R. China (Grant No. B14018), and Science and Technology Commission of Shanghai Municipality (Grant No. 14ZR1409800).

## References

1. van de Watering FCJ, van den Beucken JJJP, Lanao Felix PR, JGC W, Jansen JA (2012) Biodegradation of calcium phosphate cement composites. In: Eliaz N (ed) *Degradation of implant materials*. Springer, New York, pp 139–172
2. Habraken WJEM, Wolke JGC, Jansen JA (2007) Ceramic composites as matrices and scaffolds for drug delivery in tissue engineering. *Adv Drug Deliv Rev* 59(4–5):234–248
3. Bohner M (2000) Calcium orthophosphates in medicine: From ceramics to calcium phosphate cements. *Injury* 31:D37–D47
4. Dorozhkin SV (2009) Calcium orthophosphates in nature, biology and medicine. *Materials* 2:399–498
5. Dorozhkin SV, Epple M (2002) Biological and medical significance of calcium phosphates. *Angew Chem Int Ed* 41:3130–3146
6. Dorozhkin SV (2010) Bioceramics of calcium orthophosphates. *Biomaterials* 31:1465–1485
7. Combes C, Rey C (2010) Amorphous calcium phosphates: synthesis, properties and uses in biomaterials. *Acta Biomater* 6:3362–3378
8. Sanzana ES, Navarro M, Macule F, Suso S, Planell JA, Ginebra MP (2010) Of the *in vivo* behavior of calcium phosphate cements and glasses as bone substitutes. *Acta Biomater* 4(6):1924–1933
9. Khan Y, Yaszemski MJ, Mikos AG, Laurencin CT (2008) Tissue engineering of bone: material and matrix considerations. *J Bone Jt Surg* 90:36–42
10. Rezwan K, Chen Q, Blaker J, Boccaccini AR (2006) Biodegradable and bioactive porous polymer/inorganic composite scaffolds for bone tissue engineering. *Biomaterials* 27:3413–3431

11. LeGeros R (2002) Properties of osteoconductive biomaterials: calcium phosphates. *Clin Orthop Relat Res* 395:81–98
12. Chow L (2009) Next generation calcium phosphate-based biomaterials. *Dent Mater J* 28:1–10
13. Ambard A, Muenninghoff L (2006) Calcium phosphate cement: review of mechanical and biological properties. *J Prosthodont* 15(5):321–328
14. Achim G (1996) Mechanisms of polymer degradation and erosion. *Biomaterials* 17(2):103–114
15. Lu J, Descamps M, Dejou J, Koubi G, Hardouin P, Lemaitre J, Proust JP (2002) The biodegradation mechanism of calcium phosphate biomaterials in bone. *J Biomed Mater Res* 63:408–412
16. Xue Z, Zhang H, Jin A et al (2014) Correlation between degradation and compressive strength of an injectable macroporous calcium phosphate cement. *Acta Biomater* 10:1035–1049
17. Habraken WJEM (2008) Development of biodegradable calcium phosphate cement for bone tissue engineering. *Period Biomater* 36(12):3–6
18. Sheikh Z, Abdallah M-N, Hanafi A et al (2015) Mechanisms of in vivo degradation and resorption of calcium phosphate based biomaterials. *Materials* 8:7913–7925
19. Ginebra MP, Driessens FCM, Planell JA (2004) Effect of the particle size on the micro and nanostructural features of a calcium phosphate cement: a kinetic analysis. *Biomaterials* 25(17):3453–3462
20. Espanol M, Perez RA, Montufar EB et al (2009) Intrinsic porosity of calcium phosphate cements and its significance for drug delivery and tissue engineering applications. *Acta Biomater* 5(7):2752–2762
21. Lu J, Descamps M, Dejou J et al (2002) The biodegradation mechanism of calcium phosphate biomaterials in bone. *J Biomater Mater Res B* 63(4):408–412
22. Hu G, Xiao L, Fu H et al (2010) Study on injectable and degradable cement of calcium sulphate and calcium phosphate for bone repair. *J Mater Sci Mater Med* 21(2):627–634
23. Klein CP, de Groot K, Driessen AA, Van der Lubbe HBM (1985) Interaction of biodegradable -whitlockite with bone tissue: an in vivo study. *Biomaterials* 6(3):189–194
24. Wegst UG, Bai H, Saiz E, Tomsia AP, Ritchie RO (2015) Bioinspired structural materials. *Nat Mater* 14(1):23–36
25. Clarke B (2008) Normal bone anatomy and physiology. *Clin J Am Soc Nephrol* 3(Suppl 3):S131–S139
26. Prakasam M, Locs J, Salma-Ancane K et al (2015) Fabrication, properties and applications of dense hydroxyapatite: a review. *J Funct Biomater* 6(4):1099–1140
27. Gong T, Xie J, Liao J et al (2015) Nanomaterials and bone regeneration. *Bone Res* 3:15029. 7 pages
28. Agarwal S, Wendorff JH, Greiner A (2008) Use of electrospinning technique for biomedical applications. *Polymer* 49(26):5603–5621
29. Liu Y, Manjubala I, Roschger P, Epari DR, Schell H, Lienau J, Bail HJ, Duda GN, Fratzl P (2008) Characteristics of mineral particles in the callus during fracture healing in a sheep model. *Calcif Tissue Int* 82:S69–S70
30. Ramanujan S, Pluen A, McKee TD, Brown EB, Boucher Y, Jain RK (2002) Diffusion and convection in collagen gels: implications for transport in the tumor interstitium. *Biophys J* 83:1650–1660
31. Sabetrasekh R, Tiainen H, Lyngstadaas SP, Reseland J, Haugen H (2011) A novel ultra-porous titanium dioxide ceramic with excellent biocompatibility. *J Biomater Appl* 25(6):559–580
32. Egli P, Muller W, Schenk R (1988) Porous hydroxyapatite and tricalcium phosphate cylinders with two different pore size ranges implanted in cancellous bone of rabbits. *Clin Orthop Relat Res* 232:127–138
33. El-Ghannam A, Ducheyne P, Shapiro L (1995) Bioactive material template for in vitro synthesis of bone. *J Biomed Mater Res* 29:359–370
34. Chang BS, Lee CK, Hong KS et al (2000) Osteoconduction at porous hydroxyapatite with various pore configurations. *Biomaterials* 21(12):1291–1298

35. Cyster L, Grant D, Howdle S, Rose F, Irvine D, Freeman D, Scotchford C, Shakesheff K (2005) The influence of dispersant concentration on the pore morphology of hydroxyapatite ceramics for bone tissue engineering. *Biomaterials* 26:697–702
36. Freyman TM, Yannas IV, Gibson LJ (2001) Cellular materials as porous scaffolds for tissue engineering. *Prog Mater Sci* 46:273–282
37. Xiao Y, Yin Q, Wang L, Bao C (2014) Macro-porous calcium phosphate scaffold with collagen and growth factors for periodontal bone regeneration in dogs. *Ceram Int* 41(1):995–1003
38. Xu HHK, Quinn JB, Takagi S, Chow LC, Eichmiller FC (2001) Strong and macroporous calcium phosphate cement: effects of porosity and fiber reinforcement. *J Biomed Mater Res* 57A:457–466
39. Sun T, Donoghue PS, Higginson JR, Gadegaard N, Barnett SC, Riehle MO (2011) The interactions of astrocytes and fibroblasts with defined pore structures in static and perfusion cultures. *Biomaterials* 32(8):2021–2031
40. Bohner M, Gbureck U, Barralet JE (2005) Technological issues for the development of more efficient calcium phosphate bone cements: a critical assessment. *Biomaterials* 26:6423–6429
41. Lu JX, Flautre B, Anselme K, Hardouin P, Gallur A, Descamps M, Thierry B (1999) Role of interconnections in porous bioceramics on bone recolonization in vitro and in vivo. *J Mater Sci Mater Med* 10(2):111–120
42. Langer R, Vacanti JP (1993) Tissue engineering. *Science* 260(5110):920–926
43. Lapczynska H, Galea L, Wüst S et al (2014) Effect of grain size and microporosity on the in vivo behavior of  $\beta$ -tricalcium phosphate scaffolds. *Eur Cells Mater* 28:299–319
44. Bai F, Wang Z, Lu J et al (2010) The correlation between the internal structure and vascularization of controllable porous bioceramic materials in vivo: a quantitative study. *Tissue Eng A* 16:3791–3803
45. Gauthier O, Bouler JM, Aguado E et al (1999) Elaboration conditions influence physicochemical properties and in vivo bioactivity of macroporous biphasic calcium phosphate ceramics. *J Mater Sci Mater Med* 10:199–204
46. Hong Y, Fan H, Li B, Guo B, Liu M, Zhang X (2010) Fabrication, biological effects, and medical applications of calcium phosphate nanoceramics. *Mater Sci Eng R* 70:225–242
47. Klein CPAT, Driessen AA, De Groot K, Van den Hooff A (1983) Biodegradation behavior of various calcium phosphate materials in bone tissue. *J Biomed Mater Res* 17:769–784
48. Klein CPAT, De Groot K, Driessen AA, Van der Lubbe HBM (1986) A comparative study of different  $\beta$ -whitlockite ceramics in rabbit cortical bone with regard to their biodegradation behaviour. *Biomaterials* 7:144–146
49. Yokozeki H, Hayashi T, Nakagawa T, Kurosawa H, Shibuya K, Ioku K (1998) Influence of surface microstructure on the reaction of the active ceramics in vivo. *J Mater Sci Mater Med* 9:381–384
50. Bai F (2010) Role of macropores size of porous CPC with rhBMP-2 in bone formation and degradation. Dissertation, University of Science and Technology, China
51. Wei J, Jia J, Wu F, Wei S, Zhou H, Zhang H, Shin JW, Liu C (2010) Hierarchically microporous/macroporous scaffold of magnesium-calcium phosphate for bone tissue regeneration. *Biomaterials* 31:1260–1269
52. De Groot K (1988) Effect of porosity and physicochemical properties on the stability, resorption, and strength of calcium phosphate ceramics. *Ann N Y Acad Sci* 523:227–233
53. Lee JH, Lee SJ, Khang G, Lee HB (1999) Interaction of fibroblasts on polycarbonate membrane surfaces with different micropore sizes and hydrophilicity. *J Biomater Sci Polym Ed* 10(3):283–294
54. Perez RA, Mestres G (2016) Role of pore size and morphology in musculo-skeletal tissue regeneration. *Mater Sci Eng C Mater Biol Appl* 61:922–939
55. Chan O, Coathup MJ, Nesbitt A et al (2012) The effects of microporosity on osteoinduction of calcium phosphate bone graft substitute biomaterials. *Acta Biomater* 8:2788–2794
56. Yuan H, Fernandes H, Habibovic P et al (2010) Osteoinductive ceramics as a synthetic alternative to autologous bone grafting. *Proc Natl Acad Sci U S A* 107:13614–13619



57. Kim YW, Kim JJ, Kim YH, Rho JY (2002) Effects of organic matrix proteins on the interfacial structure the bone–biocompatible nacre interface in vitro. *Biomaterials* 23:2089–2096
58. Tamimi F, Sheikh Z, Barralet J (2012) Dicalcium phosphate cements: brushite and monetite. *Acta Biomater* 8:474–487
59. Rae T (1986) The macrophage response to implant materials—with special reference to those used in orthopedics. *CRC Crit Rev Biocompat* 2:97–126
60. Hannink G, Arts JC (2011) Bioresorbability, porosity and mechanical strength of bone substitutes: What is optimal for bone regeneration? *Injury* 42:S22–S25
61. LeGeros RZ, Parsons JR, Daculsi G et al (1988) Significance of the porosity and physical chemistry of calcium phosphate ceramics. Biodegradation–bioresorption. *Ann NY Acad Sci* 523:268–271
62. Xia Z, Triffitt JT (2006) A review on macrophage responses to biomaterials. *Biomed Mater* 1:R1
63. Ooms E, Wolke J, Van Der Waerden J, Jansen J (2002) Trabecular bone response to injectable calcium phosphate (ca-p) cement. *J Biomed Mater Res* 61:9–18
64. Constantz BR, Ison IC, Fulmer MT (1995) Skeletal repair by in situ formation of the mineral phase of bone. *Science* 267(5205):1796–1799
65. Constantz BR, Barr BM, Ison IC et al (1998) Histological, chemical, and crystallographic analysis of four calcium phosphate cements in different rabbit osseous sites. *J Biomed Mater Res* 43:451–461
66. Kummerle JM, Oberle A, Oechslin C et al (2005) Assessment of the suitability of a new brushite calcium phosphate cement for cranioplasty – an experimental study in sheep. *J Craniomaxillofac Surg* 33:37–44
67. Doi Y, Shimizu Y, Moriwaki Y et al (2001) Development of a new calcium phosphate cement that contains sodium calcium phosphate. *Biomaterials* 22(8):847–854
68. Alkhraisat MH, Moseke C, Blanco L et al (2008) Strontium modified bioceramics with zero order release kinetics. *Biomaterials* 29:4691–4697
69. Cabrejos-Azama J, Alkhraisat MH, Rueda C et al (2014) Magnesium substitution in brushite cements for enhanced bone tissue regeneration. *Mater Sci Eng C* 43:403–410
70. Rey C, Combes C, Drouet C, Glimcher MJ (2009) Bone mineral: update on chemical composition and structure. *Osteoporos Int* 20(6):1013–1021
71. Mastrogiacoma M, Corsi A, Francioso E et al (2006) Reconstruction of extensive long bone defects in sheep using resorbable bioceramics based on silicon stabilized tricalcium phosphate. *Tissue Eng* 12:261–273
72. Yamada MO, Tohno Y, Tohno S et al (2003) Silicon compatible with the height of human vertebral column. *Biol Trace Elem Res* 95:113–121
73. Pietak AM, Reid JW, Stott MJ, Sayer M (2007) Silicon substitution in the calcium phosphate bioceramics. *Biomaterials* 28:4023–4032
74. Alkhraisat MH, Rueda C, Jerez LB et al (2010) Effect of silica gel on the cohesion, properties and biological performance of brushite cement. *Acta Biomater* 6:57–65
75. Aparicio JL, Rueda C, Manchón A et al (2016) Effect of physicochemical properties of a cement based on silicocarnotite/calcium silicate on in vitro cell adhesion and in vivo cement degradation. *Biomed Mater* 11:045005
76. <http://www.regenerativenutrition.com/natural-supplements-cure-osteoporosis.asp>
77. Guo H, Wei J, Yuan Y, Liu C (2007) Development of calcium silicate/calcium phosphate cement for bone regeneration. *Biomed Mater* 2:S153–S159
78. Li C, Gao L, Chen F, Liu C (2015) Fabrication of mesoporous calcium silicate/calcium phosphate cement scaffolds with high mechanical strength by freeform fabrication system with micro-droplet jetting. *J Mater Sci* 50(22):7182–7191
79. Suchanek W, Byrappa K, Shuk P et al (2004) Mechanochemical hydrothermal synthesis of calcium phosphate powders with coupled magnesium and carbonate substitution. *J Sol St Chem* 177:793–799

80. Kannan S, Goetz-Neunhoeffler F, Neubauer J et al (2008) Ionic substitutions in biphasic hydroxyapatite and beta-tricalcium phosphate mixtures: structural analysis by rietveld refinement. *J Am Ceram Soc* 91:1–12
81. Enderle R, Goetz-Neunhoeffler F, Gobbels M, Muller FA, Greil P (2005) Influence of magnesium doping on the phase transformation temperature of beta-TCP ceramics examined by Rietveld refinement. *Biomaterials* 26:3379–3384
82. Kannan S, Goetz-Neunhoeffler F, Neubauer J, Ferreira JMF (2009) Synthesis and structure refinement of zinc-doped beta-tricalcium phosphate powders. *J Am Ceram Soc* 92:1592–1595
83. Lilley KJ, Gbureck U, Knowles JC et al (2005) Cement from magnesium substituted hydroxyapatite. *J Mater Sci Mater Med* 16:455–460
84. Arthur E (1993) Physiological functions of calcium, magnesium and mineral ion balance. In: Murray J (ed) *Primer on the metabolic bone diseases and disorders of mineral metabolism*. Lippincott Raven, New York, pp 41–46
85. Eisman J (1998) Pathogenesis of osteoporosis. In: Kippel J, Dieppe P (eds) *Rheumatology*. Mosby, London, p 8
86. Wallach S (1992) Relation of magnesium to osteoporosis and calcium urolithiasis. *Magn Trace Elem* 10:281–286
87. Ding S, Zhang J, Tian Y, Huang B et al (2016) Magnesium modification up-regulates the bioactivity of bone morphogenetic protein-2 upon calcium phosphate cement via enhanced BMP receptor recognition and Smad signaling pathway. *Colloids Surf B: Biointerfaces* 145:140–151
88. Braux J, Velard F, Guillaume C et al (2011) *Acta Biomater* 7:2593–2603
89. Schumacher M, Gelinsky M (2015) Strontium modified calcium phosphate cements – approaches towards targeted stimulation of bone turnover. *J Mater Chem B* 3:4626–4640
90. Kuang GM, Yau WP, Wu J et al (2014) *J Biomed Mater Res Part A* 00A:1552–4965
91. Zhang Y, Xu HHK (2005) Effects of synergistic reinforcement and absorbable fiber strength on hydroxyapatite bone cement. *J Biomed Mater Res Part B Appl Biomater* 75A:832–840
92. Simon CG Jr, Khatri CA, Wight SA, Wang FW (2002) Preliminary report on the biocompatibility of a moldable, resorbable, composite bone graft consisting of calcium phosphate cement and poly(lactide-co-glycolide) microspheres. *J Orthop Res* 20:473–482
93. Habraken WJEM, Wolke JGC, Mikos AG, Jansen JA (2006) Injectable PLGA microsphere/calcium phosphate cements: physical properties and degradation characteristics. *J Biomater Sci Polym Ed* 17(9):1057–1074
94. Habraken WJEM, Liao HB, Zhang Z, JGC W et al (2010) In vivo degradation of calcium phosphate cement incorporated into biodegradable microspheres. *Acta Biomater* 6:2200–2211
95. Felix Lanao RP, Leeuwenburgh SC, Wolke JG, Jansen JA (2011) In vitro degradation rate of apatitic calcium phosphate cement with incorporated PLGA microspheres. *Acta Biomater* 7:3459–3468
96. Grosfeld EC, Hoekstra JW, Herber R-P et al (2016) Long-term biological performance of injectable and degradable calcium phosphate cement. *Biomed Mater* 12(1):015009
97. Li H, Li J, Ye J (2016) Construction and properties of poly(lactic-co-glycolic acid)/calcium phosphate cement composite pellets with microspheres-in-pellet structure for bone repair. *Ceram Int* 42:5587–5592
98. Qi X, Ye J, Wang Y (2008) Improved injectability and in vitro degradation of a calcium phosphate cement containing poly(lactide-co-glycolide) micro-spheres. *Acta Biomater* 4:1837–1845
99. Otsuka M, Matsuda Y, Wang Z et al (1997) Effect of sodium bicarbonate amount on in vitro indomethacin release from self-setting carbonated-apatite cement. *Pharm Res* 14(4):444–449
100. Ruhe PQ, Hedberg EL, Padron NT (2003) rhBMP-2 release from injectable poly(DL-lactic-co-glycolic acid)/calcium-phosphate cement composites. *J Bone Jt Surg* 85:75–82
101. Martin RB, Chapman MW, Holmes RE et al (1989) Effects of bone ingrowth on the strength and non-invasive assessment of a coralline hydroxyapatite material. *Biomaterials* 10:481–488
102. Shors EC, Holmes RE (1993) Porous hydroxyapatite. In: Hench LL, Wilson J (eds) *An introduction to bioceramics*. World Scientific, New Jersey, pp 181–198

103. Takagi S, Chow LC (2001) Formation of macropores in calcium phosphate cement implants. *J Mater Sci Mater Med* 12(2):135–139
104. Lian Q, Li D, He J et al (2008) Mechanical properties and in vivo performance of calcium phosphate cement-chitosan fibre composite. *Proc Inst Mech Eng H* 222:347–353
105. Ginebra MP, Espanol M, Montufar EB et al (2010) New processing approaches in calcium phosphate cements and their applications in regenerative medicine. *Acta Biomater* 6:2863–2873
106. del Real R, Wolke J, Vallet-Regí M et al (2002) A new method to produce macropores in calcium phosphate cements. *Biomaterials* 23(17):3673–3680
107. Hesaraki S, Sharifi D (2007) Investigation of an effervescent additive as porogenic agent for bone cement macroporosity. *Biomed Mater Eng* 17(1):29–38
108. Saeed H, Ali Z, Fatollah M (2008) The influence of the acidic component of the gas-foaming porogen used in preparing an injectable porous calcium phosphate cement on its properties: acetic acid versus citric acid. *J Biomater Mater Res B* 86B(1):208–216
109. Zuo Y, Yang F, Wolke JGC, Li Y, Jansen JA (2010) Incorporation of biodegradable electrospon fibers into calcium phosphate cement for bone regeneration. *Acta Biomater* 6:1238–1247
110. Yang B, Zuo Y, Zou Q et al (2016) Effect of ultrafine poly( $\epsilon$ -caprolactone) fibers on calcium phosphate cement: in vitro degradation and in vivo regeneration. *Int J Nanomedicine* 11:163–177
111. Xu HHK, Eichmiller FC, Barndt PR (2001) Effects of fiber length and volume fraction on the reinforcement of calcium phosphate cement. *J Mater Sci Mater Med* 12:57–65
112. Ruhé PQ, Hadberg EL, Padron NT et al (2005) Biocompatibility and degradation of poly(DL-lactic-co-glycolic acid)/calcium phosphate cement composites. *J Biomed Mater Res A* 74:533–544
113. Habraken WJEM, Wolke JGC, Mikos AG, Jansen JA (2009) Porcine gelatin microsphere/calcium phosphate cement composites: in vitro degradation and drug release. *J Biomed Mater Res B Appl Biomater* 91B(2):555–561
114. Habraken WJEM, Zhang Z, Wolke JGC et al (2008) Introduction of enzymatically degradable poly(trimethylene carbonate) microspheres into an injectable calcium phosphate cement. *Biomaterials* 29(16):2464–2476
115. Félix Lanao RP, Sariibrahimoglu K, Wang H et al (2013) Accelerated calcium phosphate cement degradation due to incorporation of Glucono-Delta-Lactone microparticles. *Tissue Eng A* 20(1–2):378–388
116. Sariibrahimoglu Kemal AJ, van Oirschot Bart AJA, Nijhuis Arnold WG et al (2014) Tuning the degradation rate of calcium phosphate cements by incorporating mixtures of polylactic-co-glycolic acid microspheres and glucono-delta-lactone microparticles. *Tissue Eng Part A* 20(21–22):2870–2882
117. Ruhé P, Hedberg-Dirk E, Padron NT et al (2006) Porous poly(dl-lactic-co-glycolic acid)/calcium phosphate cement composite for reconstruction of bone defects. *Tissue Eng* 12(4):789–800
118. Xu HHK, Weir MD, Simon CG (2008) Injectable and strong nano-apatite scaffolds growth factor delivery and bone regeneration. *Dent Mater* 24(9):1212–1222
119. Li N, Jiang C, Zhang X et al (2015) Preparation of an rhBMP-2 loaded mesoporous bioactive glass/calcium phosphate cement porous composite scaffold for rapid bone tissue regeneration. *J Mater Chem B* 3:8558–8566

# Chapter 6

## Bioactivation of Calcium Phosphate Cement by Growth Factors and Their Applications

Yifan Ma, Baolin Huang, Dan Lin, Yuan Yuan, and Changsheng Liu

**Abstract** Calcium phosphate cement (CPC) scaffold has been widely used as bone graft substitutes. In order to deal with formidable defects in clinic, such as critical-sized bone defects or elderly patients with low regeneration capacity, a recombinant human bone morphogenetic protein-2 (rhBMP-2) was further loaded into CPC scaffold currently. In this chapter, effects of the surface properties, microstructure, and chemical composition on the bioactivity of rhBMP-2 were carried out. The osteogenic activity of CPC/rhBMP-2 in vitro and in vivo and the underlying mechanism were reported. Additionally, the clinical application of this active CPC/rhBMP-2 scaffold was also presented. These findings will provide insightful guide for the design and fabrication of rhBMP-2-based scaffolds/implants and further promote the clinical translation of growth factor-loaded porous scaffolds for bone regeneration.

**Keywords** rhBMP-2/CPC • Surface physicochemical properties • Microstructures • Ions incorporation • Clinical application

### 6.1 Introduction

As previously stated, calcium phosphate cement (CPC) has been an alternative to autologous and allogenic bone grafting for bone defects due to its similar composition to those of natural bones [1, 2] and was firstly reported in 1986 [3, 4]. In general, CPC cements are a mixture of powder and liquid and form a paste after mixing. The powders of calcium phosphate cements normally consist of the calcium

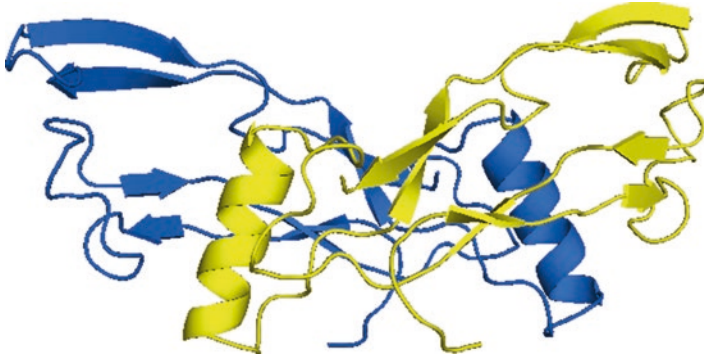
---

Y. Ma • B. Huang • D. Lin • Y. Yuan (✉)

Engineering Research Center for Biomedical Materials of Ministry of Education, East China University of Science and Technology, Shanghai 200237, China  
e-mail: [yyuan@ecust.edu.cn](mailto:yyuan@ecust.edu.cn)

C. Liu

Key Laboratory for Ultrafine Materials of Ministry of Education,  
East China University of Science and Technology, Shanghai 200237, China



**Fig. 6.1** Structures of BMP-2 molecule

phosphates precipitated from aqueous solutions at low temperatures (e.g., monocalcium phosphate monohydrate (MCPM), dicalcium phosphate (DCP), dicalcium phosphate dihydrate (DCPD), octacalcium phosphate (OCP), precipitated hydroxyapatite (PHA), amorphous calcium phosphate (ACP)) or calcium phosphates obtained only at high temperatures (e.g., anhydrous monocalcium phosphate (MCP), sintered hydroxyapatite (SHA),  $\alpha$ -tricalcium phosphate ( $\alpha$ -TCP),  $\beta$ -tricalcium phosphate ( $\beta$ -TCP), tetracalcium phosphate (TTCP)) [5–8]. Specifically, a typical CPC that initially contains an equimolar mixture of tetracalcium phosphate (TECP) and dicalcium phosphate anhydrous (DCPA) that can harden in about 30 min after mixing the powder with water to form a paste and ensuing changes into hydroxyapatite (HA) has been successfully applied in clinic since 1996 [3, 4]. As a preferred substrate for cell attachment and expression of osteoblast phenotype, the preformed CPC monoliths have been considered as a bone scaffold of choice. However, for critical-sized bone defects resulting from nonunion fractures, severe trauma, congenital deficiency, malignancy resection, or elderly patients with poor regeneration capacity, CPC often exhibited undesirable osteoinductivity and therapeutic efficacy. Therefore, improvement of the osteoactivity becomes the research focus of the CPC-based bone repair materials.

Besides the physicochemical properties of materials, another effective strategy to enhance the osteogenetic bioactivity is to incorporate/immobilize growth factors. Among the growth factors, bone morphogenetic protein-2 (BMP-2), belonging to the transforming growth factor- $\beta$  (TGF- $\beta$ ) superfamily, has been known for decades as a great osteoinductive growth factor (as shown in Fig. 6.1) [9–11]. In 1965, BMPs were first shown by Urist et al. to be implicated in bone formation when implanted at an ectopic site [12–14]. The ectopic bone was the result of osteogenic differentiation of circulating osteoblast progenitors or stem cells, which were locally exposed to the BMP-2. Subsequently, it was reported that BMP-2 induced bone regeneration in a dose-dependent manner, with higher doses of BMP-2 resulting in greater amounts of bone formation [9, 15, 16]. Moreover, BMP-2 has FDA approval for clinical applications (such as the treatment of acute tibial fractures) and is one of the most prevalent growth factors used in tissue regeneration. However, BMP-2 administered at a super physiological dose may also lead to unfavorable side effects,

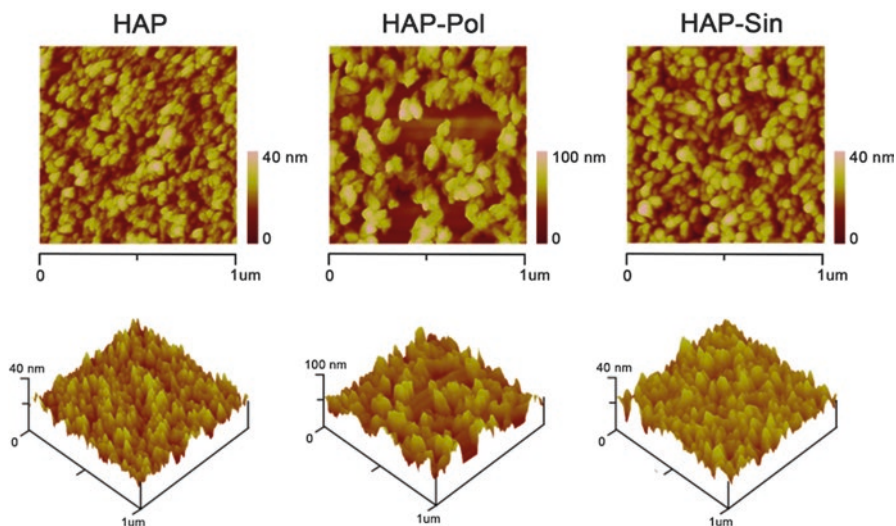
including excessive bone formation and adverse immune responses [9, 11, 17]. Strategies that are capable of locally delivering and then sustaining physiological levels of BMP-2 with sufficient bioactivity are still required.

With three dimensions of  $7 \times 3.5 \times 3$  nm, BMP-2 (Fig. 6.1) is a homodimer linked with interchain disulfide bridges in its biologically active form. BMP-2 exerts its function mainly through oligomerizing type I and type II receptors serine/threonine kinases on the cellular membranes [18, 19]. The “wrist” epitope assembled around the central  $\alpha$ -helix of BMP-2 binds the type IA and type IB receptors (BMPR-IA and BMPR-IB), whereas the “knuckle” epitope located at the back of the hand near the outer finger segment binds to BMP-2 receptors type II (BMPR-II) and active in receptors type II (ActR-II). After binding, the BMP-2/BMPR initiates the downstream signaling events. Therefore, from this viewpoint, to achieve a desirable osteogenic bioactivity of recombinant human BMP-2 (rhBMP-2), it is therefore necessary to ensure the accessibility of the “wrist” and “knuckle” epitopes of rhBMP-2 for ligand-receptor interactions.

Based on the above rationale, in the past few years, our group has endeavored to load BMP-2 into CPC to enhance the osteogenic bioactivity. The studies mainly include (1) the effect of the surface physicochemical properties on the adsorption dynamics, conformation, and bioactivity of BMP-2, (2) fabrication and property of rhBMP-2/CPC bioactivity scaffold, and (3) clinical application of rhBMP-2/CPC.

## 6.2 Surface-Mediated Conformation and Bioactivity of rhBMP-2

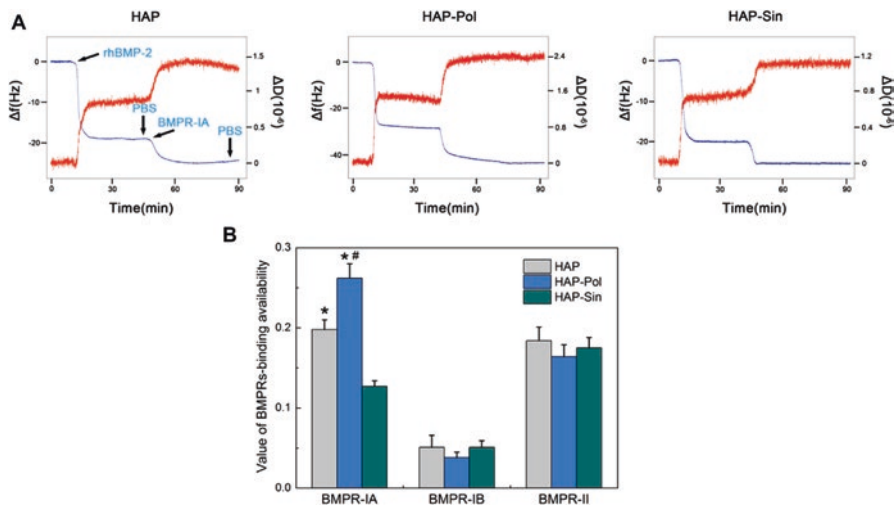
Currently, in the field of protein immobilization, nanoscaled surface-induced changes of conformation and bioactivity of protein have attracted great attentions [15, 20, 21]. It is well-recognized that the interface, especially in the range of nanoscale with comparable size of proteins, plays a critical role in the adsorption, conformation, and bioactivity of proteins. Moreover, these phenomena are not only related to the nature of adsorbed proteins but also are strongly dependent on the physicochemical characteristics of solid surfaces (especially the nanoscaled interface), including topography, chemistry, charge, hydrophilicity, and crystallinity [22–25]. For instance, Monkawa et al. found that fibrinogen exhibited different conformations and biological activities on gold, tantalum, and hydroxyapatite (HAP) surfaces (as shown in Fig. 6.2) with different surface roughness and crystal sizes at nanoscale. It was also reported that fibronectin intended to an open and highly unfolded conformation on the hydroxyapatite surfaces (HAPs) and thereby showed higher bioactivity than on the gold surface [5, 7]. Inspired by these previous studies, it is hypothesized that the nanoscaled surface properties would affect the way of rhBMP-2 binding and in turn influence the conformation and bioactivity of adsorbed rhBMP-2 molecules [9, 11]. Considering that the final transformation product of CPC is HAP, we first used HAP as substrate to explore the effect of the surface physicochemical properties on the adsorption, conformation, and bioactivity of rhBMP-2.



**Fig. 6.2** AFM images ( $1.0 \times 1.0 \mu\text{m}$ ) of HAPs employed in the QCM-D measurements. The largest z-range value is 100 nm for the HAP-Pol surface and 40 nm for the HAP and HAP-Sin surfaces (Reprinted with permission from Ref. [15]. Copyright © 2015 Acta Biomaterialia Inc. Published by Elsevier Ltd.)

### 6.2.1 Effect of Nanoscaled HAP Surface

The complex interactions between proteins and the CaP surface are primarily governed by physicochemical properties of the CaP surface, functional groups, and the protein conformations [15, 21, 26]. In general, the smaller the CaP particle sizes, the higher the total surface area and, thus, the greater the number of available binding sites for protein adhesion. Numerous studies have reported that CaP with a higher surface area could be fabricated by modulating the surface roughness, porosity, and pore size. Pore size and pore distribution have a significant impact on the total surface area of CaP and their protein adsorption capacities. Meanwhile, the effect of pore size on protein adsorption is size dependent. For example, if the pore size is larger than a protein molecule, the protein can enter into the pores, thereby increasing protein adsorption [10, 27]. Surface roughness and topography influence protein adsorption by affecting the spatial distribution of adsorption sites. Independent of the total surface area, increasing surface roughness on the nanometer scale can improve the protein adsorption [5, 22]. This increase is attributed to a change in the geometrical arrangement of protein molecules on the surface of materials, and it has been shown that the adsorption is less correlated to the roughness for globular proteins such as bovine serum albumin (BSA). Protein adsorption is less influenced by roughness on the micrometer scale as the surface topography may appear smooth to proteins. Furthermore, CaPs with lower crystallinity have higher solubility, which in turn causes an inevitable increase in ionic strength in the



**Fig. 6.3** (a)  $\Delta f$  (blue line) and  $\Delta D$  (red line) recorded against time for rhBMP-2 (*Escherichia coli*-derived) adsorption onto HAPs and subsequently BMPR-IA binding. The frequency and dissipation data presented are from the fifth overtone. (b) Calculated BMPRs binding availability for the rhBMP-2-adsorbed HAPs. Values are shown as mean  $\pm$  standard error of the mean from 5 data points ( $n = 5$ ). \* $p < 0.05$ , compared with the HAP-Sin surface, and # $p < 0.05$ , compared with the HAP surface (Reprinted with permission from Ref. [15]. Copyright © 2015 Acta Biomaterialia Inc. Published by Elsevier Ltd.)

surrounding medium [9, 28]. Proteins or drugs in solutions with high ionic strength undergo structural conformational changes, exposing more polar ionized charges on the surface of the protein, which promotes a higher adsorption rate onto the material surfaces. Also, proteins are known to favorably adsorb onto a hydrophobic surface, by unfolding their hydrophobic core, than a neutrally charged hydrophilic surface. Therefore, we systematically study the effect of the surface properties (roughness, crystallinity, etc.) of HAPs on the way of rhBMP-2 binding and thus the changes of conformation and bioactivity of the adsorbed rhBMP-2 molecules (as shown in Fig. 6.2).

To prepare HAP surface with distinct roughness and crystallinity, we strictly controlled the synthesis and deposition of HAPNs. By polishing the substrates and sintering the HAPN at low temperature, a series of HAPs with single difference in roughness and crystallinity were obtained and named as HAP, HAP-Pol, and HAP-Sin (Fig. 6.2). The HAP-Pol surface showed a remarkably increased surface roughness. For the HAP-Sin surface, due to the sintering process, apart from a significantly increased crystallinity, the WCA and zeta potential were slightly decreased and the sintered HAPN was obviously elongated.

The adsorption of rhBMP-2 and the availability of the binding epitopes of adsorbed rhBMP-2 for BMP receptors (BMPRs) on HAPs were determined by quartz crystal microbalance with dissipation (QCM-D). The results (Fig. 6.3) indicated that the alterations of surface roughness and crystallinity of HAPs exerted

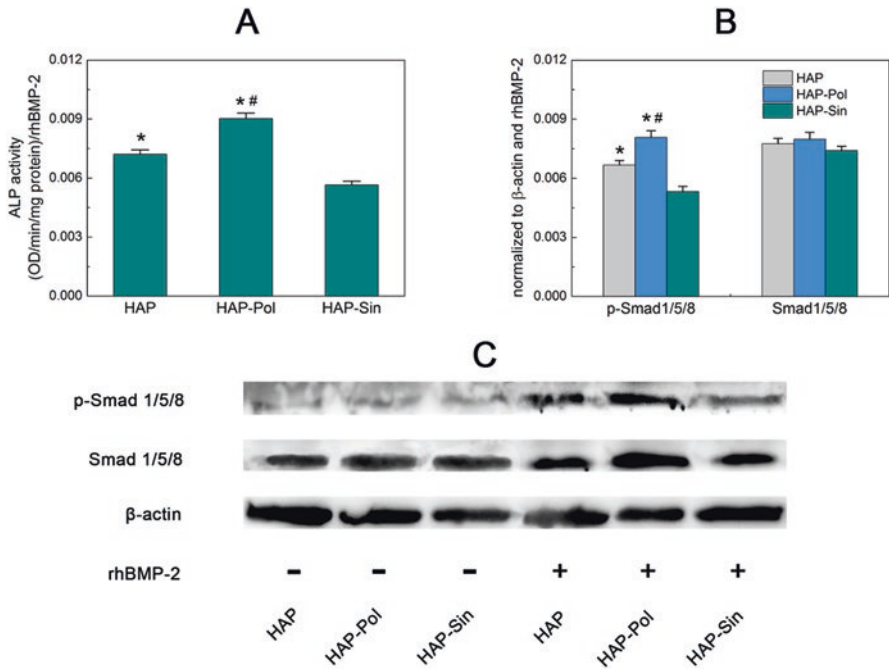


remarkable effect on the recruitment of BMPR-IA, but not BMPR-IB and BMPR-II [21, 26]. Specifically, compared to the HAP surface, the HAP-Pol surface showed a 1.5-fold improvement of mass uptake of rhBMP-2 and enhanced the recruitment of BMPR-IA by about two times. However, the HAP-Sin surface, although with slightly higher adsorption amount of rhBMP-2, significantly undermined this process [2, 29]. It can be hypothesized that the interaction of rhBMP-2 and BMPR-IA played a pivotal role in determining the bioactivity of rhBMP-2 upon HAPs. And the HAP-Pol surface favored the recruitment of BMPR-IA to adsorbed rhBMP-2, but the HAP-Sin surface displayed the opposite effect. This noticeable discrepancy of the interaction of rhBMP-2 on HAPs with the BMPR-IA should be related to the way of rhBMP-2 binding to HAPs. It is also worthwhile to note that, inconsistent with the previous report about the weak interaction of BMPR-II to rhBMP-2, the rhBMP-2 upon HAPs fabricated here all showed desirable affinity toward the BMPR-II, which may play some roles in the bioactivity of rhBMP-2 [9, 15]. This could be related to the binding of the N-terminal domain of rhBMP-2 to negatively charged HAPNs, which undermine the auto-inhibitory of N-terminal domain of rhBMP-2 to BMPR-II binding.

It is well-recognized that the primary interactions between proteins and substrate surfaces are dependent on the hydrophobic interaction, electrostatic potential, and contact area [17, 30]. For the HAP-Pol surface, the remarkably higher RMS induced a significantly larger specific surface area and thus led to a great deal of adsorption amount of rhBMP-2. For the HAP-Sin surface, with a slight reduction of WCA and zeta potential, the hydrophobic interaction and electrostatic interaction (zeta potential of rhBMP-2 is 8.1 at pH 7.4) between rhBMP-2 and the HAP-Sin surface were weakened, which undermined the adsorption of rhBMP-2 to some extent [15, 21]. However, the elongated sintered HAPN induced a slightly higher RMS and larger specific surface area, which is favorable for the adsorption of rhBMP-2. Collectively, the higher mass density of rhBMP-2 on the HAP-Sin surface should be contributable to the enhanced crystallinity and elongated morphology of the sintered HAPN.

The *in vitro* cell culture results revealed that the surface roughness and crystallinity exerted great effect on the bioactivity of rhBMP-2 upon HAPs [9, 31]. The *in vitro* cellular evaluations showed that the rhBMP-2 adsorbed onto rough surface (HAP-Pol) not only exhibited a higher expression of ALP but also showed an enhanced BMP-mediated Smad1/5/8 signaling. However, the increasing of the crystallinity (HAP-Sin) undermined the bioactivity of the rhBMP-2 to some extent. ALP activity and Smad1/5/8 signaling level showed a distinct surface roughness- and crystallinity-dependent trend: HAP-Sin < HAP < HAP-Pol (as shown in Fig. 6.4).

Besides the osteogenic differentiation, we have further investigated the effect of rhBMP-2 on the cellular adhesion. The results indicated that the adsorbed rhBMP-2 layers greatly facilitated cellular attachment and cytoskeleton organization. Specifically, the rhBMP-2-adsorbed HAP-Pol surface exhibited the greatest cellular area and cellular perimeter of C2C12 cells. Such phenomena signified that the presence of rhBMP-2 on HAPs and the surface roughness exert significant influence on the adhesion of C2C12 cells. Crouzier et al. [32] noticed that rhBMP-2 that presented in solution/matrix played crucial roles in early adhesive events, including



**Fig. 6.4** (a) ALP expressions of C2C12 cells cultured on rhBMP-2-adsorbed HAPs after 3 days of incubation. (b) Relative expressions of p-Smad1/5/8 and Smad1/5/8 signaling. (c) Western blotting of p-Smad1/5/8, Smad1/5/8, and  $\beta$ -actin for C2C12 cells cultured on the rhBMP-2-adsorbed and unadsorbed HAPs after 2 days of incubation (Reprinted with permission from Ref. [15]. Copyright © 2015 Acta Biomaterialia Inc. Published by Elsevier Ltd.)

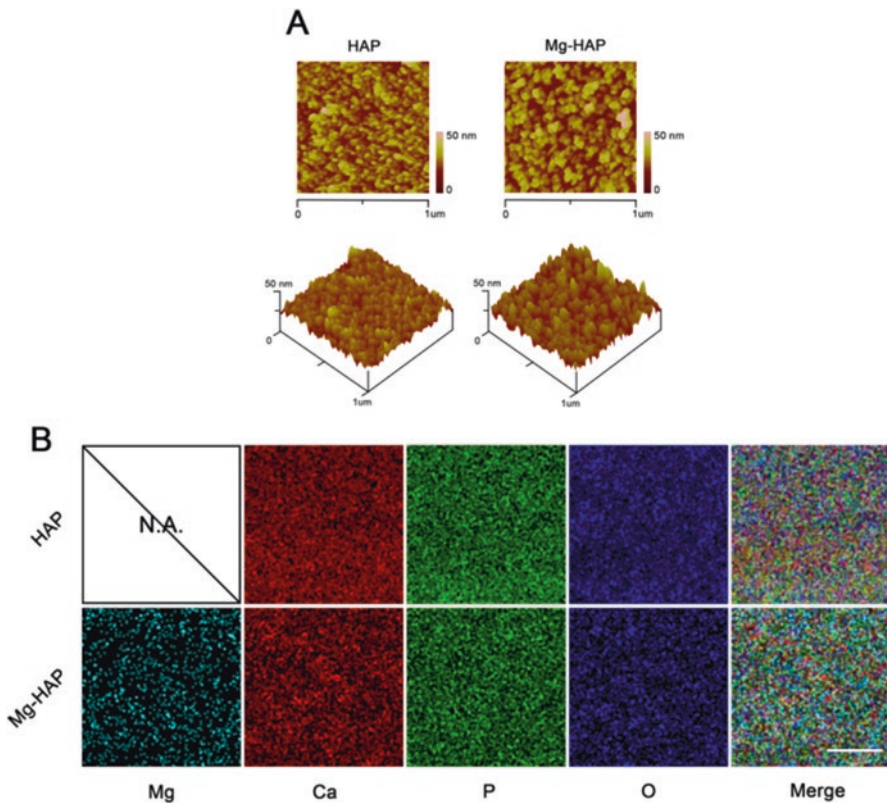
adhesion and migration. It is reported that nano-submicron hybrid roughed titanium surfaces could promote adhesion and differentiation of osteoblasts [33]. Therefore, it is plausible that the observed phenomenon may be associated with a synergistic effect between the roughness of the HAP-Pol surface ( $RMS = 17.4 \pm 0.8$  nm) and the adsorbed rhBMP-2 layer on the HAP-Pol surface. It can be found that the cell morphology, cellular area, and cellular perimeter on rhBMP-2-adsorbed HAP surface were significantly greater than those on rhBMP-2-adsorbed HAP-Sin surface, while the surface mass density of rhBMP-2 on the HAP surface is slightly low as compared to that on the HAP-Sin surface. This finding demonstrates that the density of rhBMP-2 did not affect cellular binding to HAPs, while the conformation of rhBMP-2 could actually affect.

Collectively, the above results revealed that the HAP-Pol surface exhibited an increased mass uptake of rhBMP-2 and an upregulated osteoactivity of rhBMP-2, while the HAP-Sin surface performed oppositely. Furthermore, the nanoscaled HAPs had obvious influences on the conformation and availability to BMPRs of the adsorbed rhBMP-2, which in turn governed the bioactivity of rhBMP-2.

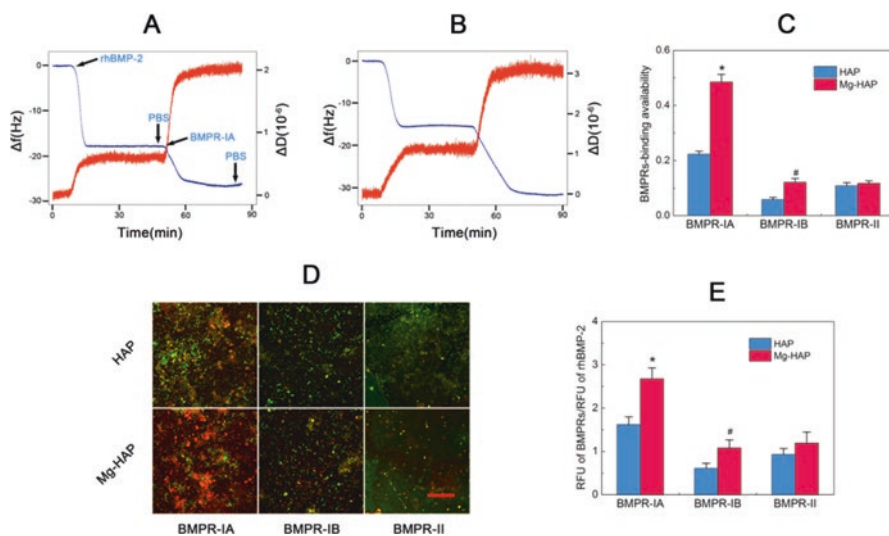
### 6.2.2 Mg-Substituted HAP Mediate Bioactivity of rhBMP-2

Magnesium is a vital and widely used component for the bone substitutes. Here, we further endeavored to systematically study the effects of the magnesium element on the conformation and bioactivity of rhBMP-2. To achieve this goal, we both investigated the adsorption, receptor recruitment, and bioactivity of rhBMP-2 on the HAP and Mg-HAP surfaces experimentally and numerically.

Surface topographies of the HAP and Mg-HAP surfaces were evaluated by atomic force microscopy (AFM, Fig. 6.5a). It can be found that the HAP and Mg-HAP surfaces consist of very delicate nanostructures. EDS patterns of the deposited coatings revealed similar element contents as compared to those of respective nanoparticles. In particular, the ratio of Mg/Ca was demonstrated as 2.2% for the Mg-HAP coatings. Moreover, the element distributions of the HAP and Mg-HAP surfaces are presented in Fig. 6.5b. It suggested that Mg, Ca, P, and O



**Fig. 6.5** (a) AFM images of the HAP and Mg-HAP surfaces. (b) Element distributions on the HAP and Mg-HAP surfaces. *N.A.* represents not available. Scale bar is 5 μm (Reprinted with permission from Ref. [13] Copyright © 2016 Scientific Reports. Rights managed by Nature Publishing Group)



**Fig. 6.6** Typical changes in  $\Delta f$  (blue line) and  $\Delta D$  (red line) recorded against time during the adsorption of rhBMP-2 and subsequent binding of BMPR-IA on (a) the HAP surface and (b) the Mg-HAP surface. (c) Calculated BMPR-binding availability by adsorbed rhBMP-2 on the HAP and Mg-HAP surfaces. Values are shown as mean  $\pm$  standard error of the mean from 5 data points ( $n = 5$ ). \* $p < 0.05$ , # $p < 0.05$ , compared with the HAP surface. (d) CLSM observation of the fluorescent staining of adsorbed rhBMP-2 (green). Scale bar is 50  $\mu\text{m}$ . (e) The RFU (relative fluorescence units) of BMPRs per RFU of rhBMP-2. Values are shown as mean  $\pm$  standard error of the mean from 50 data points ( $n = 50$ ). \* $p < 0.05$  and # $p < 0.05$ , compared with the HAP surface (Reprinted with permission from Ref. [13] Copyright © 2016 Scientific Reports. Rights managed by Nature Publishing Group)

were uniformly located on the respective surfaces. Notably, Mg was sparsely distributed on the Mg-HAP surface. Our results indicated that the HAP and Mg-HAP surfaces exhibited similar water contact angles, zeta potentials, and RMS values.

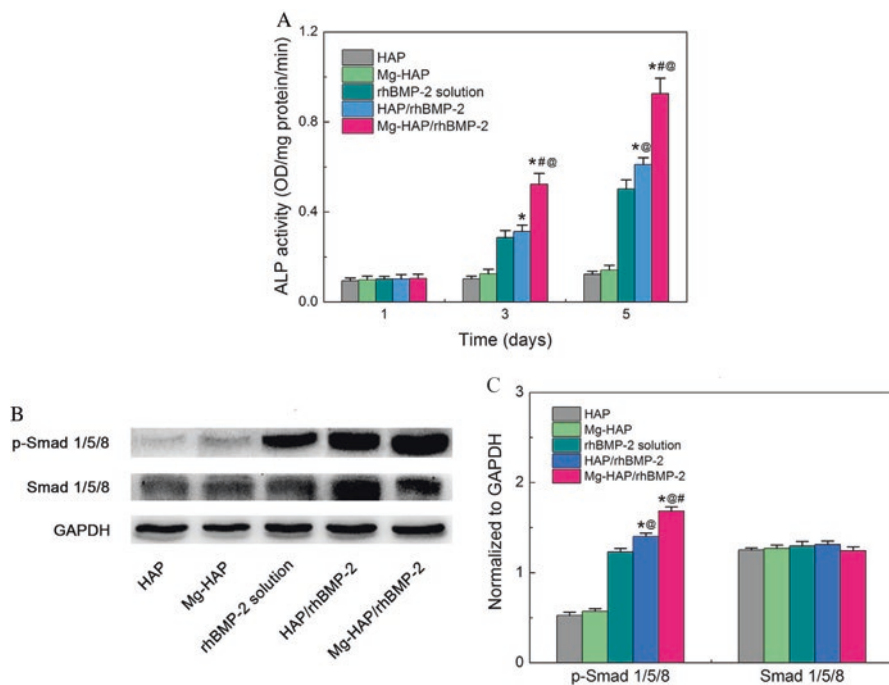
Next, we measured and compared the adsorption of rhBMP-2 and subsequent recognition of BMPRs on the HAP and Mg-HAP surfaces. Typical QCM-D shifts in frequency and dissipation for the adsorption of rhBMP-2 and subsequent binding of BMPR-IA are shown in Fig. 6.6. The adsorption amounts of rhBMP-2 and BMPRs were calculated with the Sauerbrey equation [34]. It was found that the Mg-HAP surface showed a slightly lower mass uptake of rhBMP-2 than the HAP surface. However, the adsorbed rhBMP-2 on the Mg-HAP surface induced an increased recruitment of BMPRs. For example, a nearly 1.9-fold mass uptake of BMPR-IA and 1.8-fold mass uptake of BMPR-IB were found. To further compare the capacity of the adsorbed rhBMP-2 for recruiting BMPRs, the “BMPR-binding availability” was calculated (Fig. 6.6c). As expected, a nearly 2.2-time availability of BMPR-IA and 2.1-time availability of BMPR-IB were achieved for adsorbed rhBMP-2 on the Mg-HAP surface. There was no significant difference ( $p > 0.05$ ) for the binding availability of BMPR-II by adsorbed rhBMP-2 on both surfaces [34, 35].

To further identify the recognition of BMPRs by adsorbed rhBMP-2 on the HAP and Mg-HAP surfaces, immunofluorescence staining of rhBMP-2 and BMPRs was measured (Fig. 6.6d). Compared with the HAP surface, large recognized BMPR-IA clusters were achieved on the Mg-HAP surface. The clusters of BMPR-IB on the HAP surface were small ( $<5 \mu\text{m}$ ) and uniformly dispersed, while that on the Mg-HAP surface exhibited large aggregations (10–15  $\mu\text{m}$ ). The clusters of BMPR-II on both surfaces were comparable (5–10  $\mu\text{m}$ ). In addition, the relative fluorescence units (RFU) of BMPRs per RFU of rhBMP-2 were calculated (Fig. 6.6e). It showed a similar trend as compared to the results of “BMPR-binding availability.” For instance, an almost 1.7-time recruitment of BMPR-IA per rhBMP-2, 1.8-time recruitment BMPR-IB per rhBMP-2, and comparable recruitment of BMPR-II per rhBMP-2 were achieved on the Mg-HAP surface as compared to those on the HAP surface. The result indicated that both the HAP/rhBMP-2 and Mg-HAP/rhBMP-2 samples exhibited no significant difference ( $p > 0.05$ ) in the adsorption stability of rhBMP-2: an initial burst release within the first 24 h and a gradual release after that. Notably, more than 85% of rhBMP-2 remained on the HAP and Mg-HAP surfaces, which indicated that the growth factors were tightly adsorbed and had good adsorption stability.

The osteogenetic bioactivity of adsorbed rhBMP-2 was determined by quantitating the ALP expressions of C2C12 cells (Fig. 6.7a). It was clearly found that the HAP and Mg-HAP samples (as negative control) exhibited little ALP expression. At days 3 and 5, the Mg-HAP/rhBMP-2 sample induced significantly ( $p < 0.05$ ) increased ALP activity of C2C12 cells compared to the HAP/rhBMP-2 sample. Importantly, the ALP expression normalized to rhBMP-2 amount (data not shown) was significantly higher ( $p < 0.05$ ) for C2C12 cells cultured on the Mg-HAP/rhBMP-2 surface than on the HAP/rhBMP-2 surface. Intriguingly, the bioactivity of adsorbed rhBMP-2 on the Mg-HAP surface was notably greater ( $p < 0.05$ ) than the theoretical positive control, most likely due to the contributing synergistic effects of the nanostructured Mg-HAP surface and desirable conformation of adsorbed rhBMP-2. Moreover, the enhanced bioactivity of rhBMP-2 on the Mg-HAP surface was also evidenced by the Western blot (Fig. 6.7b) and quantitative real-time PCR results showing significantly ( $p < 0.05$ ) promoted p-Smad1/5/8 and expression of Id1, Runx2, and OCN of C2C12 cells on the Mg-HAP/rhBMP-2 group.

By using immunofluorescence staining, the expression of various BMPRs on cellular surface of C2C12 cells cultured on the rhBMP-2-adsorbed surfaces was investigated. The results indicated that the expressed BMPRs are uniformly distributed on the cellular surface of C2C12 cells cultured on the HAP/rhBMP-2 and Mg-HAP/rhBMP-2 surfaces. Importantly, significant higher ( $p < 0.05$ ) BMPR-IA and BMPR-IB clusters and comparable BMPR-IB clusters are found on the C2C12 cells seeded on the Mg-HAP/rhBMP-2 sample than on the HAP/rhBMP-2 sample. In addition, the RFU of BMPRs revealed that the BMPR-IA and BMPR-IB were more expressed in the C2C12 cells cultured on the Mg-HAP/rhBMP-2 surface.

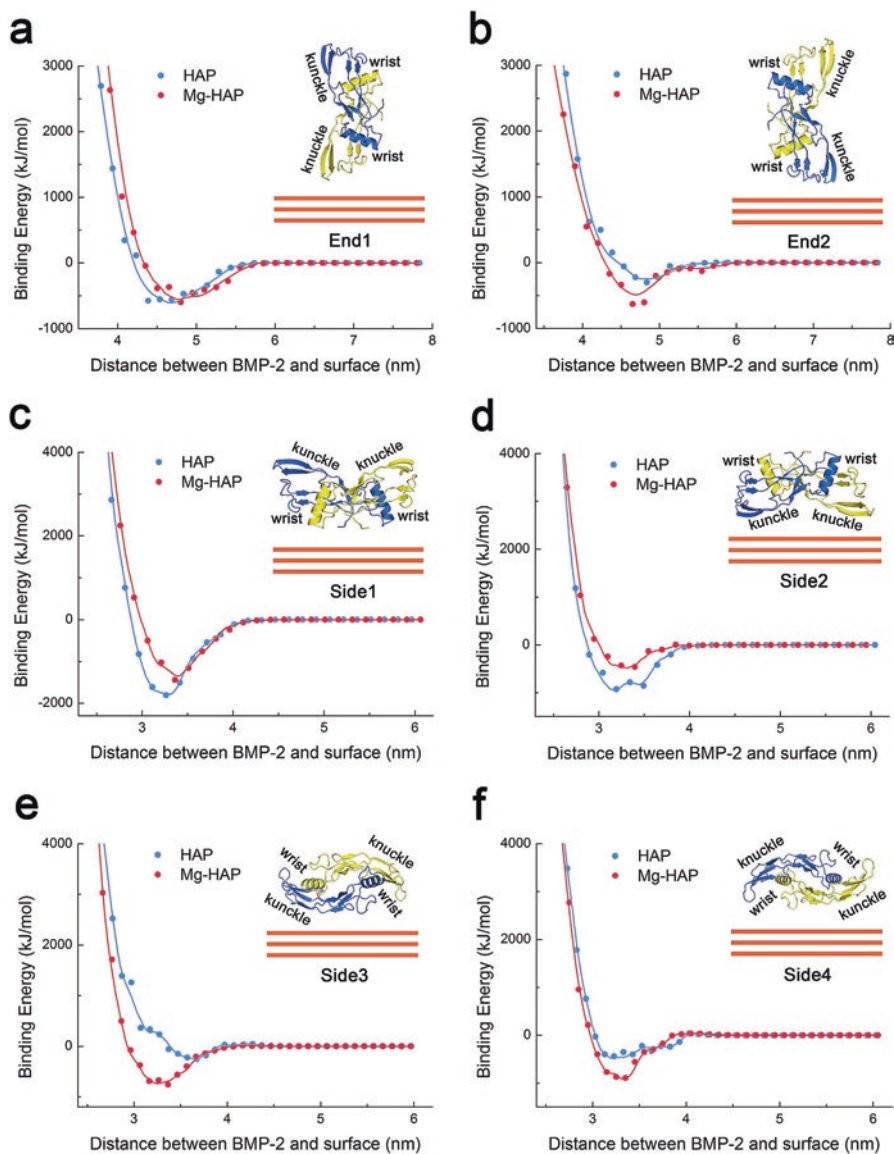
The cellular morphology, focal adhesion, and cytoskeleton organization of C2C12 cells on the respective surfaces were also investigated with an immunofluorescence staining of the actin, vinculin, and nucleus. The results revealed that



**Fig. 6.7** (a) ALP activity assay. The HAP and Mg-HAP surfaces without rhBMP-2 were acted as negative control. The rhBMP-2 solution represented culture medium contain fresh rhBMP-2 and was used as positive control. Values are shown as mean  $\pm$  standard error of the mean from 5 data points ( $n = 5$ ). \* $p < 0.05$ , compared with the corresponding surfaces without rhBMP-2; # $p < 0.05$ , compared with HAP/rhBMP-2; @ $p < 0.05$ , compared with rhBMP-2 solution. (b) Western blot of p-Smad1/5/8, Smad1/5/8, and GAPDH for C2C12 cells cultured on corresponding surfaces. (c) Relative expressions of p-Smad1/5/8 and Smad1/5/8 (data are normalized to the total GAPDH content). Values are shown as mean  $\pm$  standard error of the mean from 5 data points ( $n = 5$ ). Western blot of p-Smad1/5/8, Smad1/5/8, and GAPDH for C2C12 cells cultured on respective surfaces. Relative expressions of p-Smad1/5/8 and Smad1/5/8 (data are normalized to the total GAPDH content). Values are shown as mean  $\pm$  standard error of the mean from 5 data points ( $n = 5$ ) (Reprinted with permission from Ref. [13] Copyright © 2016 Scientific Reports. Rights managed by Nature Publishing Group)

C2C12 cells were well spread and had intimate contact with the surfaces, especially for the HAP/rhBMP-2 and Mg-HAP/rhBMP-2 samples. The cell amounts were obviously larger ( $p < 0.05$ ) on the HAP/rhBMP-2 and Mg-HAP/rhBMP-2 surfaces as compared to that on the respective HAP and Mg-HAP surfaces. Moreover, C2C12 cells cultured on the Mg-HAP/rhBMP-2 surface showed a better spread morphology and a well-organized actin cytoskeleton when compared to those of the HAP/rhBMP-2 surface.

In order to shed light on the dynamic adsorption of BMP-2 on the HAP and Mg-HAP surfaces at atomic level, we performed combined MD and SMD simulations. The binding energy against the distance between BMP-2 and the surface in the SMD process is provided in Fig. 6.8. In the End1 orientation, there is no



**Fig. 6.8** Binding energy against the distance between BMP-2 (central of mass) and surface (HAP and Mg-HAP) for End1 (a), End2 (b), Side1 (c), Side2 (d), Side3 (e), and Side4 (f) orientations. Inserts are illustrations of corresponding configurations of BMP-2 (with wrist and knuckle epitopes noted) toward surface (Reprinted with permission from [13]. Copyright © 2016 Scientific Reports. Rights managed by Nature Publishing Group)

significant difference between the binding energies for the HAP and Mg-HAP surfaces. In the Side1 and Side2 orientations, it was found that the binding energy for the HAP surface is lower than that for the Mg-HAP surface. However, in the End2, Side3, and Side4 orientations, a remarkably lower binding energy was observed on the Mg-HAP surface compared to that on the HAP surface. These findings suggest that BMP-2 adsorbed in different orientations toward the HAP and Mg-HAP surfaces exhibited distinct interactions with these surfaces. Moreover, we recorded the minimum binding energy and the separation distance of the adsorption state. Basically, the separation distances between BMP-2 and the surface for side-on orientations were notably shorter ( $p < 0.05$ ) than that for end-on orientations.

The simulation about the radius of gyrate (Rg) of BMP-2 with respect to simulation time indicated that the Rg values of BMP-2 for the whole process were significantly lower ( $p < 0.05$ ) in all end-on orientations, while it was notably higher ( $p < 0.05$ ) in all side-on orientations. This finding suggests that the configuration of BMP-2 was partly folded during the adsorption process in the end-on orientations, while it was partly loosened during the adsorption process in the side-on orientations. Moreover, various Rg shifts indicated that BMP-2 molecules were folded or loosened at different extents on the HAP and Mg-HAP models as compared to the initial configuration. In addition, the profile of root mean square deviation (RMSD) of BMP-2 against the simulation time exhibited a similar trend: a linear increase of RMSD from 0 to 600 ps, a rapid upregulation of RMSD from 600 to 750 ps, and a slight rise of RMSD in the MD procedure (750–2750 ps). The RMSDs of BMP-2 on the HAP and Mg-HAP models varied slightly.

The root mean square fluctuation (RMSF) of residues of BMP-2 was also calculated in the whole adsorption process. As expected, the values of RMSF are also varied on HAP and Mg-HAP surfaces in a same orientation of BMP-2. It was also found that a rash of residues showed a high value of RMSF for BMP-2 adsorbed on the HAP and Mg-rash HAP surface in the Side2 orientation. Regardless of the orientation of BMP-2, significantly more residues with a high value of RMSF on the Mg-HAP surface were found than that on the HAP surface. In particular, it was extremely high ( $>0.6$  nm) for the RMSFs of residues Phe23-Ala34 of BMP-2 in the Side2 orientation on the Mg-HAP surface, which might lead to denaturation of the adsorbed protein. In addition, the values of RMSF of cysteine knots of BMP-2 are relatively low. It can be found that the cysteine knots of BMP-2 show different stabilities in six orientations both on the HAP and Mg-HAP surfaces. Together, the results indicated that the cysteine knots of BMP-2 on the Mg-HAP surface are more stable than that on the HAP surface.

In summary, with experimental and numerical approaches, we have demonstrated that the recruitment of BMPRs and bioactivity of BMP-2 were remarkably increased on the Mg-HAP surface compared to those on the HAP surface. The presence of a low amount of Mg on the Mg-HAP surface not only induced a slightly loosened conformation of BMP-2 but also maintained the integrity of cysteine knots of the adsorbed BMP-2. The clear advantages of the Mg-HAP surface for loading BMP-2 highlight the potential of Mg-HAP biomaterials in being used as bone regeneration implants/scaffolds.



### 6.3 Fabrication and Property of rhBMP-2/CPC Scaffold

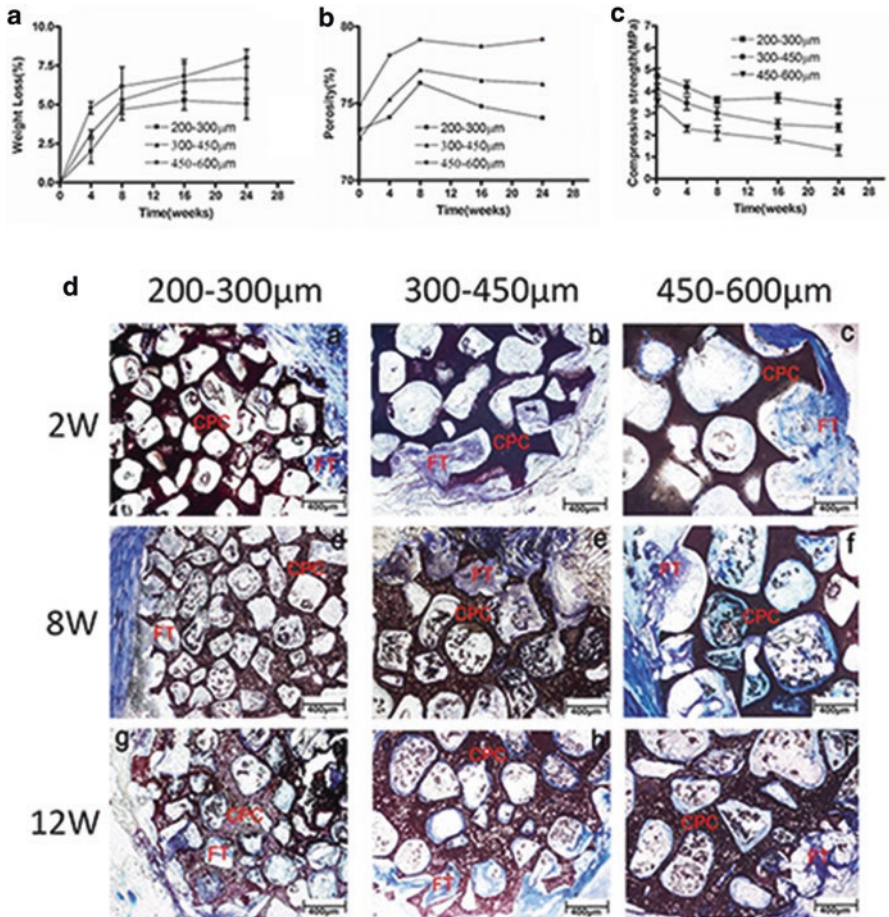
The design of biomaterials as scaffolds is a foundation for bone tissue engineering. An ideal scaffold should meet certain criteria to serve such functions as good biocompatibility, biodegradability at a rate commensurate with remodeling, osteoconductivity, osteoinductive, and mechanical properties similar to those of the bone repair site. To achieve this, rhBMP-2-loaded calcium phosphate cements (rhBMP-2/CPC) have been developed as grafts for bone regeneration. A series of researches have been launched, including porous structures of CPC substrate and incorporation of bioactive ions in CPC, to improve the efficacy of the rhBMP-2 on matrix.

#### 6.3.1 *Effect of Porous Structure on rhBMP-2/CPC Bioactivity*

It is well accepted that a scaffold with a porous structure favors tissue ingrowth, the mass transport of nutrients and osteointegration with the host bone, as well as long-term stable fixation of bone implants [36, 37]. Therein, the effect of macropore size of scaffolds as an important structural parameter on the degradation, initial cell attachment, and subsequently on the guidance of bone tissue formation has been widely addressed, but few literatures about the role of the important morphological feature in mechanical property and degradation of biomaterials are available.

CPC with different macropore sizes but unchangeable porosity was under assessment, and the degradation behavior was evaluated *in vitro* and *in vivo*. The results (Fig. 6.9) showed that the increase of macropore size of CPC resulted in a decrease in the compressive strength but increase in the degradation rate and porosity of CPC significantly *in vitro* simulation. But the rate of degradation of all porous CPC was lower *in vitro* simulation than that *in vivo*. In contrast to degradation *in vitro*, the decrease of macropore size of CPC resulted in an increase in the degradation rate of CPC significantly *in vivo*. These results suggest the possibility to the degradation rate, and compressive strength of biomaterials can be modulated by varying the macropore size while maintaining porosity unchanged. But the role of macropore size in degradation of porous CPC scaffold *in vitro* simulation is different compared to that *in vivo*.

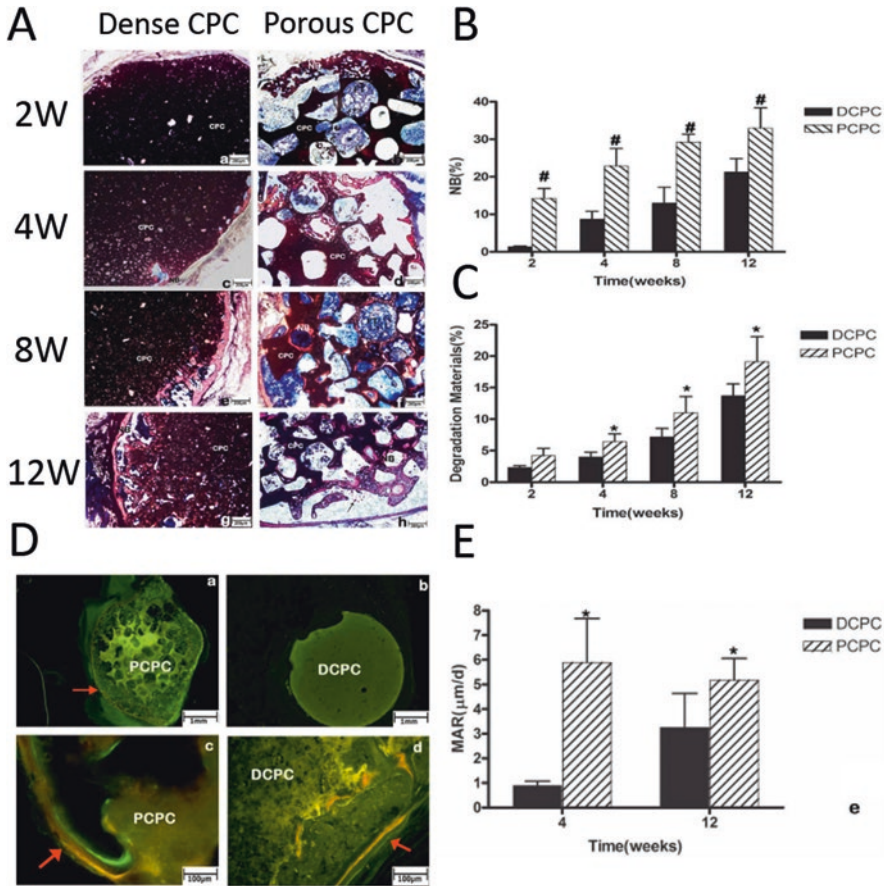
Next, the bone formation of porous CPC/rhBMP-2 and dense CPC/rhBMP-2 was compared *in vivo* in an ectopic bone formation model. As illustrated in Fig. 6.10, better ossification for each period could be observed in porous CPC/rhBMP-2 compared to dense CPC, including more newly formed bone tissue and higher rate of bone formation. The reason could be attributed to the appropriate porous structure plunking for the release of rhBMP-2, which would induce more bone formed. Moreover, porous structure was believed to induce the migration of mesenchymal cells as shown by histological analysis and thereby promoting the ingrowth of bone tissue. In addition to better ossification, faster degradation was observed in the porous CPC compare to dense one. After 12 weeks implanted *in vivo*, the mass loss



**Fig. 6.9** Changing of weight loss (a), porosity (b), and compressive strength (c) of the CPC porous scaffolds with three-pore size during 24 weeks soaked in PBS; histological observation of new bone formation in porous scaffolds at 2, 8, 12 weeks (d)

of porous CPC reached 19.6% while 13.6% in dense CPC. Such acceleration of degradation could benefit the renewal of bone tissue and improve the efficacy of rhBMP-2. Thereby, porous structure can regulate the effectiveness of osteoinductive growth factors loaded scaffolds and degradation of biomaterials.

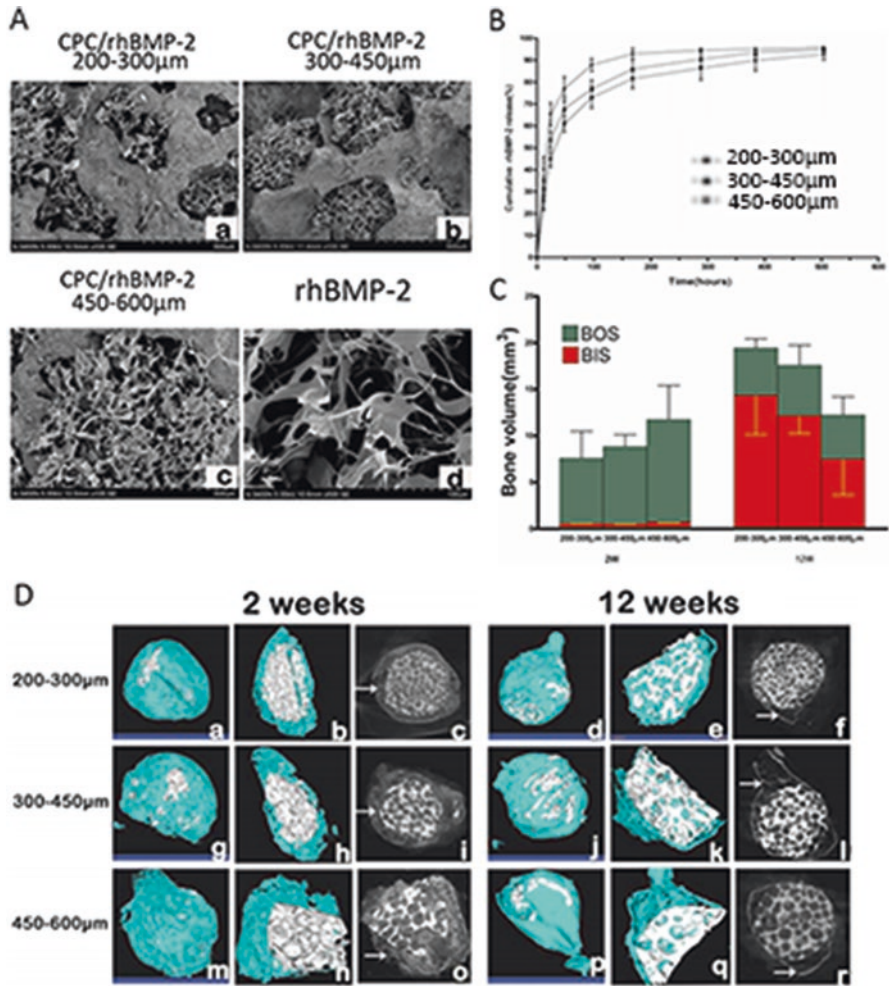
The introduction of porous CPC in various pore size and the comparison of porous CPC with dense CPC as mentioned above have indicated that porous structure plays a critical role in the mechanical behavior, degradation, and biological properties of biomaterials. Interestingly, optimal bone substitutes for regeneration are prone to be with specific porous structure as well. Considering the combination of rhBMP-2 and CPC, it is necessary to study the role of pore size of scaffolds in



**Fig. 6.10** Histological observation of new bone formation in dense and porous scaffolds at 2, 4, 8, and 12 weeks (a). Quantitative analysis of the new bone volume and material degradation after 2, 4, and 8 weeks of surgery by histomorphometric analysis (b, c). Sequential fluorescent labeling (d) of TE and CA at 4 (a, b) and 12 (c, d) weeks, respectively. The graph shows the rate of bone formation for each group

osteogenicity of rhBMP-2 and synergistic effect of pore size and rhBMP-2 on osteogenesis.

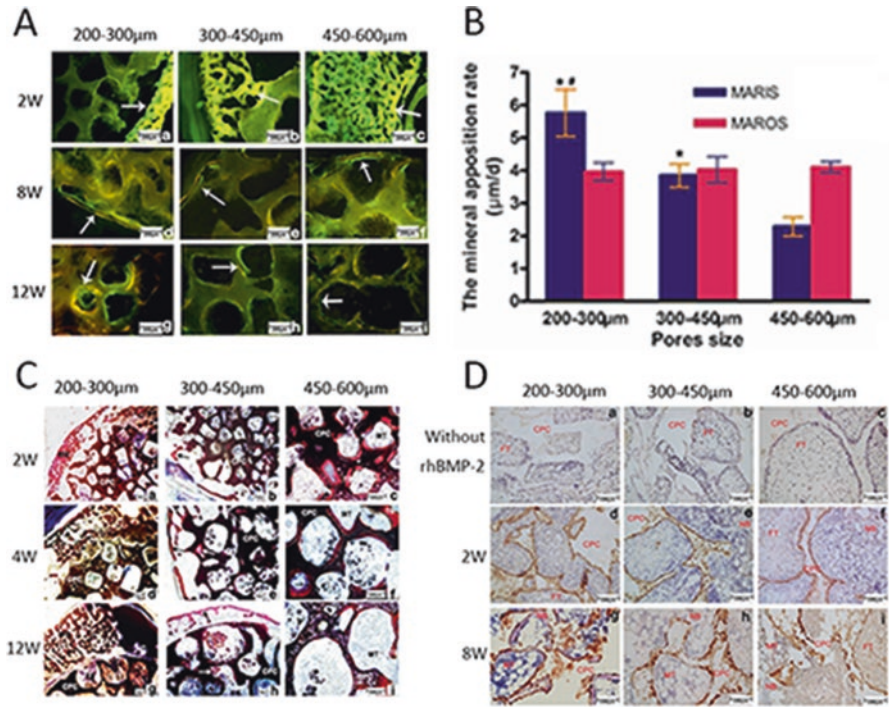
Furthermore, three CPC cylinders with three different macropore sizes (200–300, 300–450, and 450–600 μm) mentioned above were used as implanted substrates. The release of rhBMP-2 loaded to porous CPC with different macropore size was prior to be investigated in vitro simulation. The data displayed that accumulation release of rhBMP-2 in CPC with 450–600 μm pore size was almost 93% in 168 h, which was far ahead of the others. The releasing curves also showed that the rhBMP-2 loaded into the scaffold with larger macropore possessed a larger initial burst release than that in scaffold with smaller macropores. By contrast, the CPC delivery system with smaller macropores releases rhBMP-2 in a bioactive form for



**Fig. 6.11** CPC stimulated the ectopic bone formation induced by rhBMP-2 in vivo. SEM images (a) of porous scaffolds loaded with rhBMP-2. Cumulative release of rhBMP-2 (b) from three scaffolds with different size pore. The 3D reconstruction images depicted the different reparative effects of three CPC scaffolds with different size pore at 2 and 12 weeks (c, d)

a prolonged period, which indicates that macropore size plays an important role in the kinetics of rhBMP-2 liberation from porous CPC carriers.

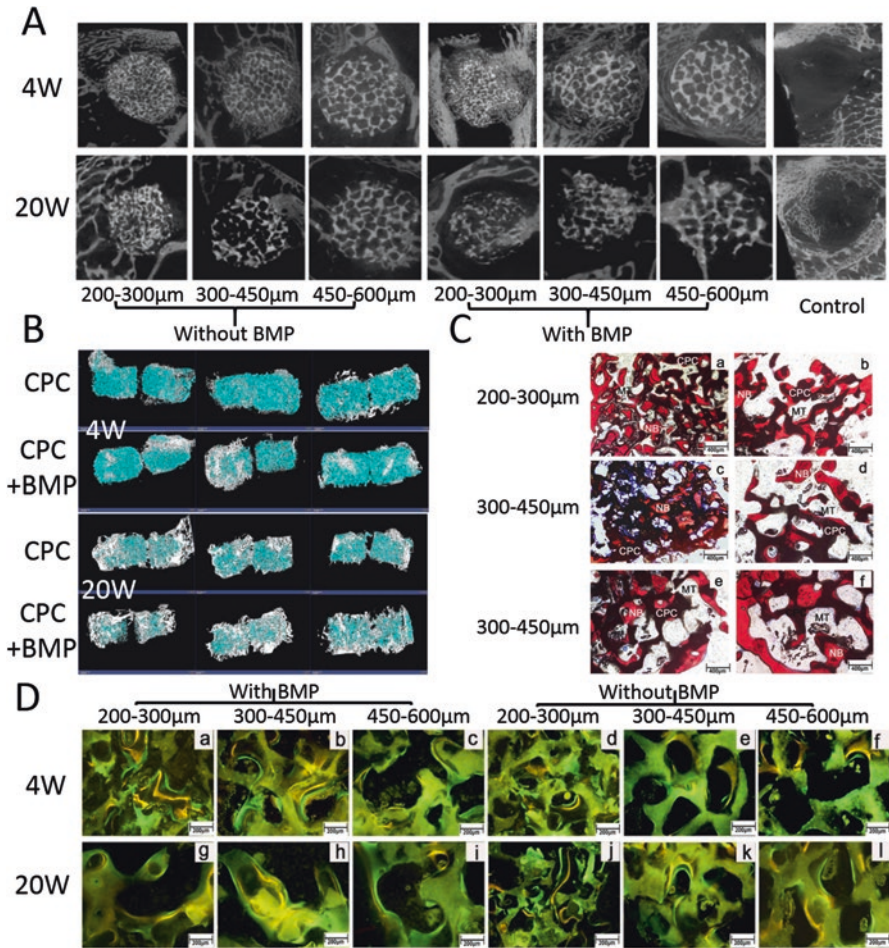
Then, CPC/rhBMP-2 with three different macropores size was discussed in ectopic osteoinductivity and orthotopic osteoregeneration, respectively. Three different CPCs were analyzed by micro-CT, histology, and histomorphometry. Bone formation outside the implant could be observed frequently in the initial stage of implantation shown in Figs. 6.11d and 6.12a, c. The increase of the macropore size resulted in a statistically significant increase in the total amounts of newly formed bone



**Fig. 6.12** Sequential fluorescent labeling (a) of TE and CA at 2, 8, and 12 weeks, respectively. The graph (b) shows the rate of bone formation for each group. Histological observation (c) of new bone formation in dense and porous scaffolds at 2, 4, and 12 weeks. Immunohistochemical analysis (d) of newly formed bone 2 and 8 weeks postoperation

mainly from outside scaffolds. In the later stage, the increase of macropore size resulted in a statistically significant decrease of the amounts of newly formed bone in pores of scaffolds. Compared to porous CPC/rhBMP-2 with larger macropores, the scaffold with smaller macropores showed higher rate of bone formation. These results suggested macropores size can regulate the release and bone inductive properties of rhBMP-2 loaded to scaffolds. Compared with porous CPC/rhBMP-2 with larger macropores, the CPC/rhBMP-2 with smaller macropores showed better bone inductive properties in vivo.

The role of macropores size in the osteoinductive properties and biodegradation of porous CPC loaded with rhBMP-2 was sequentially verified in femoral condyle defect model of rabbit (shown in Fig. 6.13). Three typical CPC cylinders with different macropore sizes were employed as discussed above. The scaffolds with or without rhBMP-2 were implanted into drill hole defects in cancellous bone of rabbit for 4, 12, and 20 weeks. The bone formation and degradation of different CPCs were analyzed by DR-X ray, micro-CT, histology, and histomorphometry as ectopic osteoinductivity. The results showed that the amount of newly formed bone tissue and material loss in all implants increased with time. Compared to the scaffolds



**Fig. 6.13** Bone regeneration in a cavity defect after various CPC/rhBMP-2 scaffolds implantation in the rabbit femur. The 3D reconstruction images (a, b) depicted the different reparative effects of three CPC scaffolds with different size pore at 4 and 20 weeks. Immunohistochemical analysis (c) of newly formed bones at 20 weeks postoperation. Sequential fluorescent labeling (d) of TE and CA at 12 and 20 weeks, respectively

without rhBMP-2, the amount of newly formed bone and the rate of biodegradation were higher in porous CPC loaded with rhBMP-2. Moreover, the decrease of the macropore size resulted in a statistically significant increase in the total amounts of newly formed bone and biodegradation. Samples with 200–300 µm macropores were resorbed significantly faster showed more bone formation than other samples. At 20 weeks after implantation, the percentage area of material loss in scaffolds with 200–300 µm macropores was about 52.5%. However, the area of bone formation in porous CPC loaded with rhBMP-2 decreased after 12 weeks, which may be caused by bone resorption and reconstitution. These results suggested macropore

sizes can regulate bone inductive properties of rhBMP-2 loaded to scaffolds and the rate of degradation of scaffolds in vivo. Moreover, the macropores size in coordination with rhBMP-2 contributes to the new bone formation and resorption of scaffolds.

With the investigation in vitro and in vivo, pore size of scaffolds would have great impact on the bone formation and degradation of materials in vivo. Additionally, osteoinductive efficiency of rhBMP-2 in vivo could also be dramatically influenced by the pore size of loading substrate. Interestingly, CPC with diverse pore size presented apparent difference in bone formation and degradation behaviors, especially with loaded of rhBMP-2. In a nutshell, pore size and embarkation of rhBMP-2 synergistically could modulate the bone formation and degradation of CPC/rhBMP-2 in vivo. The design of CPC/rhBMP-2 with controllable pore size exerts great influence on the bone formation, degradation of implanted scaffold, and efficacy of rhBMP-2, which can be extended to other scaffolds with pore structures and are expected to provide new thoughts on the development of future tissue engineering materials.

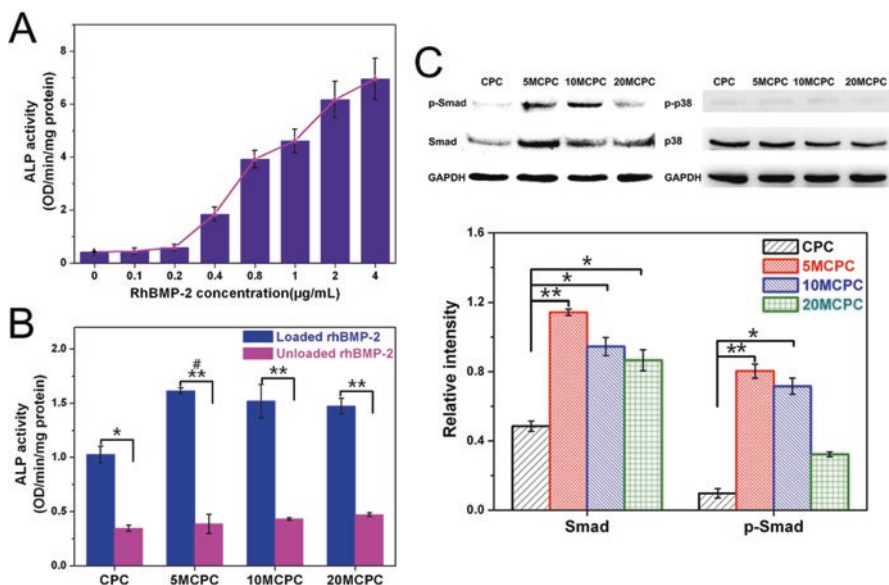
### **6.3.2 Effect of Bioactive Ions on rhBMP-2/CPC Scaffolds**

Generally, the chemical composition and microstructure play critical roles in the osteogenetic and osteoconductive activity of a scaffold. Incorporation of bioactive ions like Si, Mg, Ca, Zn, and Sr has been considered as an effective strategy to improve the bioactivity of biomaterials. As a matter of fact, cation ions (such as  $\text{La}^{3+}$ ,  $\text{Mg}^{2+}$ ) and interfacial properties of the support have been proven to have great effect on the conformation and bioactivity of proteins in recent years. However the surface-induced conformational and functional changes of rhBMP-2 onto CPC have seldom attracted attentions.

#### **6.3.2.1 Mg Modification Regulates Bioactivity of rhBMP-2/CPC Scaffolds**

Magnesium ion ( $\text{Mg}^{2+}$ ), the second most abundant intracellular divalent cation, has been known to be involved in diverse cellular functions and plays an essential positive role in bone biomineralization. The increasing of soluble  $\text{Mg}^{2+}$  could upregulate the gene expression of COL10A1 and VEGF in human bone marrow stromal cells (hBMSCs), consequently leading to the enhanced ECM mineralization [38]. Previous study also demonstrated that appropriate magnesium enhanced cell adhesion and osteogenic differentiation of hBMSCs by upregulation of integrin  $\alpha 5\beta 1$  expression [39]. Thereby, more attention was paid on the impact of Mg modification on the conformation and osteogenic bioactivity of rhBMP-2 loaded on the substrates.

With this respect, Mg modification-induced changes of conformation and osteogenic capacity of rhBMP-2 on CPC were focused. Due to the advantages of rapid



**Fig. 6.14** (a) Effect of concentrations of free rhBMP-2 on ALP activity in C2C12 cells. C2C12 cells were cultured for 3 days with different doses of soluble rhBMP-2. (b) Effect of different amounts of MPC into CPC loaded with rhBMP-2 on alkaline phosphatase activity in C2C12 cells for 3-day culture. Four rhBMP-2-loaded MCPCs induced significantly greater ALP activity than unloaded ones. Normalized ALP activity of cells seeded on 5MCPC/rhBMP-2 was the highest. (\* =  $p < 0.05$  compared to MCPCs; \*\* =  $p < 0.01$  compared to MCPCs; # =  $p < 0.05$  compared to CPC/rhBMP-2). (c) Magnesium-dependent effects on Smad signaling and p38 signaling were investigated in C2C12 cells exposed to various MCPC/rhBMP-2 samples for 12 h. The intensities of protein bands for Smad pathway were quantified and normalized to GAPDH levels. (\* =  $p < 0.05$  compared to CPC/rhBMP-2; \*\* =  $p < 0.01$  compared to CPC/rhBMP-2) (Reprinted with permission from Ref. [42]. Copyright © 2016 Colloids and Surfaces B: Biointerfaces Inc. published by Elsevier Ltd.)

setting, better mechanical properties, as well as significantly improved biodegradability [40], magnesium phosphate cement (MPC) was introduced to CPC precursor to obtain Mg-doped CPC (MCPC) with various Mg content (coded with 5MCPC, 10MCPC, 20MCPC). A specific amount of rhBMP-2 could load onto CPC substrate that stimulated ALP expression within the dynamic linear range of the pluripotent skeletal muscle myogenic progenitor C2C12 cells (Fig. 6.14a). The bioactivity of rhBMP-2 upon CPC and MCPC could be examined using an ALP activity assay on C2C12 cells as shown in Fig. 6.14b. Obviously, MCPC alone did not stimulate an increase in ALP activity compared to CPC. In rhBMP-2-loaded groups, ALP expression level depended greatly on the Mg/Ca ratio, and 5MCPC induced the highest ALP activity normalized to protein concentration (more than 1.5-fold increase compared to the CPC group). Interestingly, with more MPC added into CPC substrate, the ALP expression was attenuated slightly. The results suggested that pure magnesium contributed little to osteodifferentiation of C2C12 cells, which was different



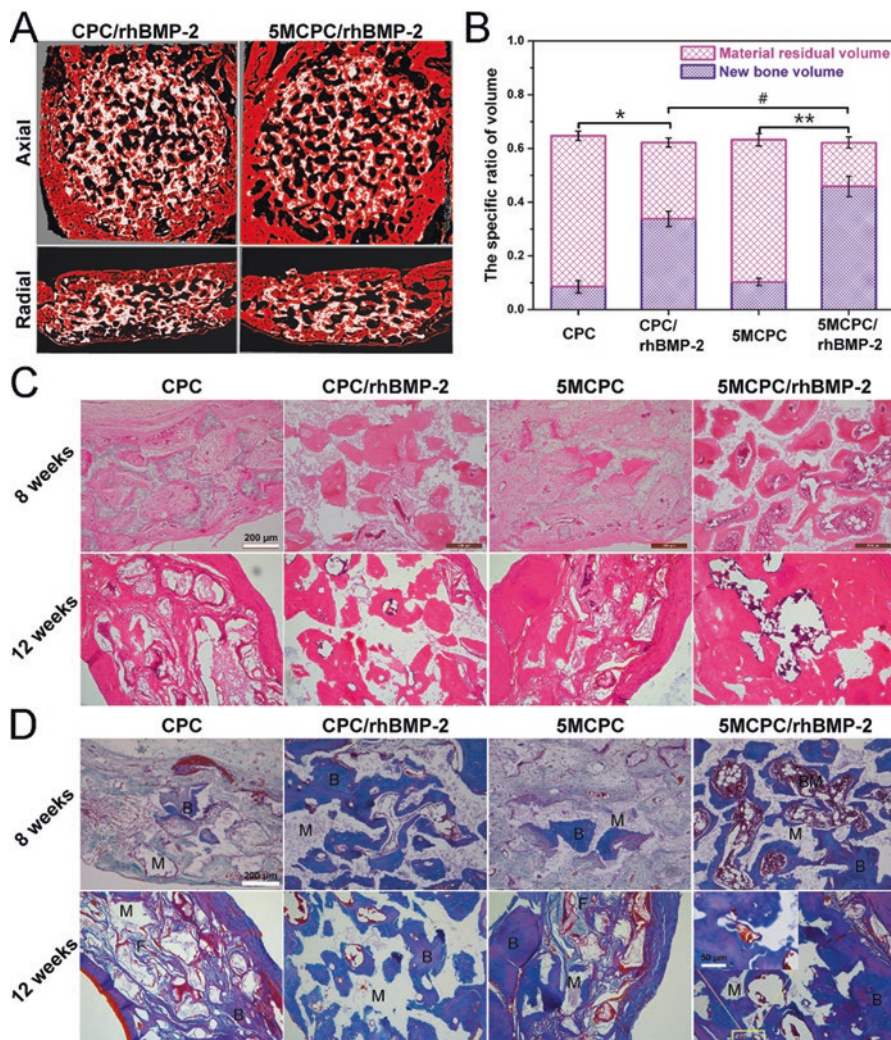
from other reports that moderating Mg ions could stimulate osteogenic responses in BMSCs [41].

To evaluate the effect of Mg ion on the key downstream targets (Smads and MAPK), total proteins extracted from C2C12 cells were subjected to the detection of Smad and MAPK signaling molecules and their phosphorylated forms, p-Smad1/5/8 and p-p38 by western blotting. As shown in Fig. 6.14c, rhBMP-2 adsorbed upon 5MCPC induced more robust phosphorylation of Smad1/5/8 as well as more expression of Smad1/5/8 protein. Phosphor-Smad levels were decreased when more MPC added to CPC precursor, which was similar to the trend of ALP expression. But for the phosphorylation of p38, no obvious expression was observed in all samples under the same conditions, either in C2C12 myoblasts (Fig. 6.14c). That is to say, the extracellular matrix-bound rhBMP-2 has a preference for the complex of BMPR-IA and BMPR-II on the cell surface, which leads to the canonical Smad transcriptional pathway.

It is well-recognized that BMP signaling is regulated by BMP ligand bioavailability, BMP receptor endocytosis, lateral movement and oligomerization of receptors, as well as the chemical composition and stiffness of the plasma membrane, and the underlying cortical actin cytoskeleton [43]. Generally, the two BMP pathways were linked to the same receptors, but the endocytic routes of receptors were different, including clathrin-dependent Smad pathway and caveolae-dependent non-Smad pathway [43]. Both BMPR-IA and BMPR-II undergo internalization via the clathrin-coated pits, while only BMPR-II can be endocytosed via caveolae. The phosphorylation of Smad1/5/8 takes place independently of endocytosis at the cell surface [44]. In our experiment, we speculated that CPC/MCPC samples might make for the clathrin-dependent internalization into endosomes and went against the caveolae-dependent internalization of C2C12 cells, which correspondingly facilitated the phosphorylation of Smad1/5/8, and weakened the phosphorylation of p38 protein. Furthermore, the presentation of rhBMP-2 upon MCPCs might affect the formation of active heteromeric complexes at the plasma membrane, thus regulating the signaling strength and dynamics of the pathway [23].

There might be various reasons contributing to the above positive osteoinductive activity. Generally, there are two existence forms of protein in the biological environment: a free form and a matrix-bound form, both of which play an integral role in regulating cell behaviors [32]. When seeded on the surface of MCPC, cells are supposed to interact with the released free rhBMP-2 and the bound rhBMP-2 on substrate simultaneously. In this study, the CPC and MCPC substrates were prepared by the same process and possessed comparable structure properties, and the main difference was the introduction of magnesium. Thus, the possible mechanism due to the Mg modification on the two states of rhBMP-2 could be explored and testified.

In vivo assessment, more new bone tissues were formed in rhBMP-2-loaded 5MCPC with extensive bone ingrowth throughout the entire volume of the implants. The regenerated bone volume and material residuals volume in the defects of the two groups were calculated, respectively, to evaluate the repair of bone defects more precisely (Fig. 6.15b). The result showed that rhBMP-2-loaded MCPC scaffolds



**Fig. 6.15** Bone regeneration in a calvarial defect in SD rats after various MCPC porous scaffolds implantation for 8 weeks and 12 weeks. (a) The tridimensional reconstruction images of the defect sites by micro-CT for 8 weeks (red bone tissue, white material residue). (b) Quantitative analysis of the new bone volume and the material residual volume after 8 weeks of surgery by micro-CT (\* =  $p < 0.05$  compared to CPC; \*\* =  $p < 0.01$  compared to 5MCPC; # =  $p < 0.05$  compared to CPC/rhBMP-2). (c) HE staining of new bone formation in porous scaffolds at 8 and 12 weeks. (d) Masson trichrome staining of new bone formation in porous scaffolds at 8 and 12 weeks (*M* materials, *B* bone, *BM* bone marrow, *F* fibrous tissue, *Yellow frame* blood vessel) (Reprinted with permission from Ref. [42]. Copyright © 2016 Colloids and Surfaces B: Biointerfaces Inc. published by Elsevier Ltd.)

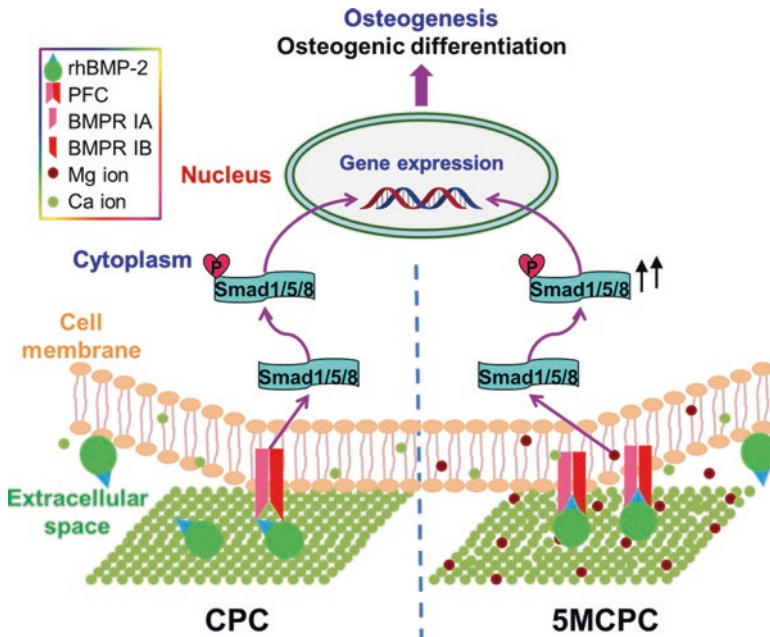
contained higher bone volumes in 8 weeks with less material residuals, indicating a faster biodegradation of magnesium-modified CPC. Furthermore, the newly formed bone volume for rhBMP-2-loaded 5MCPC increased by 35.73% compared with rhBMP-2-loaded CPC, while that percentage for 5MCPC and CPC was only 21.13%, indicating that the rhBMP-2 played an important role in the osteogenic regeneration. Moreover, the enhanced osteogenesis effect of MCPC/ rhBMP-2 was not just a sum of the effect of Mg and rhBMP-2, and Mg and rhBMP-2 promoted each other.

Figure 6.15c, d showed the histological evaluation of MCPC scaffolds implanted in the bone defects of rat calvaria. According to the HE and Masson trichrome staining results, it could be directly observed that there was hardly any new bone formation for 8 weeks implantation of both unloaded scaffolds. In contrast, some new bone regenerated and penetrated through the interconnected pores into the center of the loaded implants. For 5MCPC/rhBMP-2, obviously more trabecular bone formed than CPC/rhBMP-2 and the new bone was in direct contact with the material surface. Moreover, some red marrow and blood vessel (Yellow frame in Fig. 6.15d) were observed in 5MCPC group, suggesting the formation of medullary cavity and vasculogenesis. With increasing time, newly formed bone increased gradually both in quantity and maturation (12 weeks).

These analyses presented higher therapeutic efficacy (scored as more extensive *in vivo* bone formation) of 5MCPC/rhBMP-2 compared with CPC/rhBMP-2. Many causes would endow the positive outcomes. For one thing, 5MCPC was more favorable to the attachment and proliferation of cells, recruiting more osteoblasts to accelerate bone mineralization. For another, rhBMP-2-loaded 5MCPC promoted the new bone regeneration *in vivo*. In fact, it is more intriguing and complicated for the study of cell-material interactions *in vivo*. Further experiments will be investigated in the future.

The data obtained and discussed above led us to a proposed schematic illustration for the mechanism of Mg modification-promoted osteogenic efficacy of rhBMP-2, as shown in Fig. 6.16. Compared to the pure CPC, the addition of 5 wt% MPC did not interfere with the hydration of CPC and the formation of HAP, only a few Mg ions taking the place of Ca ions in the crystalline solid. As a consequence, magnesium modification of CPC neither affected the delivery of rhBMP-2 nor changed the secondary structure and the bioactivity of the released rhBMP-2. But the matrix-bound Mg anchored on 5MCPC not the soluble  $Mg^{2+}$  could mediate the adsorption way and spatial conformation of the rhBMP-2 physisorbed on the surface and in turn facilitated the recognition and binding of the preformed receptor complexes (PFCs) of BMPR-IA and BMPR-II with higher affinity on cell membrane, which thereby significantly triggered Smad signaling pathway, stimulated the osteogenic differentiation, and enhanced bone regeneration.

In summary, the effect of magnesium modification on the osteogenic bioactivity of rhBMP-2 with CPC and MCPC is impressive and crucial for the future study of rhBMP-2/CPC bioactivity scaffold. Compared with CPC/rhBMP-2, C2C12 cells cultured on 5MCPC/rhBMP-2 substrates exhibited dramatically enhanced *in vitro* osteogenic differentiation and phosphorylation of Smad1/5/8. The soluble  $Mg^{2+}$

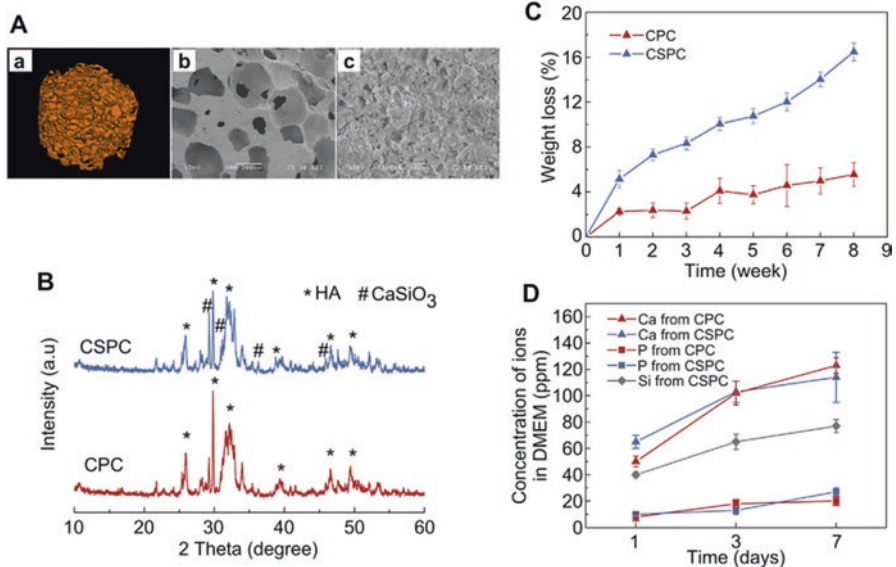


**Fig. 6.16** Schematic illustration of the mechanism for better osteogenic efficacy of rhBMP-2-loaded 5MCPC. The released rhBMP-2, both from CPC and 5MCPC, exhibited similar osteogenic bioactivity. However, matrix-bound Mg anchored on 5MCPC could mediate the spatial conformation of bioactive rhBMP-2 to bind preformed receptor complexes (PFCs) of BMPR-IA and BMPR-II with higher affinity on cell membrane in comparison with CPC, which significantly triggered Smad signaling pathway and thereby stimulated the osteogenic differentiation and bone regeneration (Reprinted with permission from Ref. [42]. Copyright © 2016 Colloids and Surfaces B: Biointerfaces Inc. published by Elsevier Ltd.)

made little difference to the osteogenic bioactivity of both released rhBMP-2 and bound rhBMP-2. It was the Mg on the underlying substrates that became the main contributor to mediate the adsorption and conformation of rhBMP-2 bound on the matrix, thus facilitating the recognition to BMPRs (type I and type II) and enhancing osteoactivity (Fig. 6.16). The present study had established that the synergy between matrix-bound rhBMP-2 and Mg might endow unanticipated biological functions as well as excellent bone tissue regeneration.

### 6.3.2.2 Si Modification Regulate Bioactivity of rhBMP-2/CPC Scaffolds

Previous study have revealed that incorporating 10–20% low crystalline calcium silicate (CS) into CPC could effectively improve the *in vitro* and *in vivo* bioactivity as well as degradability of CPC [45, 46]. Interestingly, CPC could be simply and operatively prepared with simultaneous macroporosity and microporosity by means of salting-out method. Loading of BMP-2 into CPC has been largely reported as

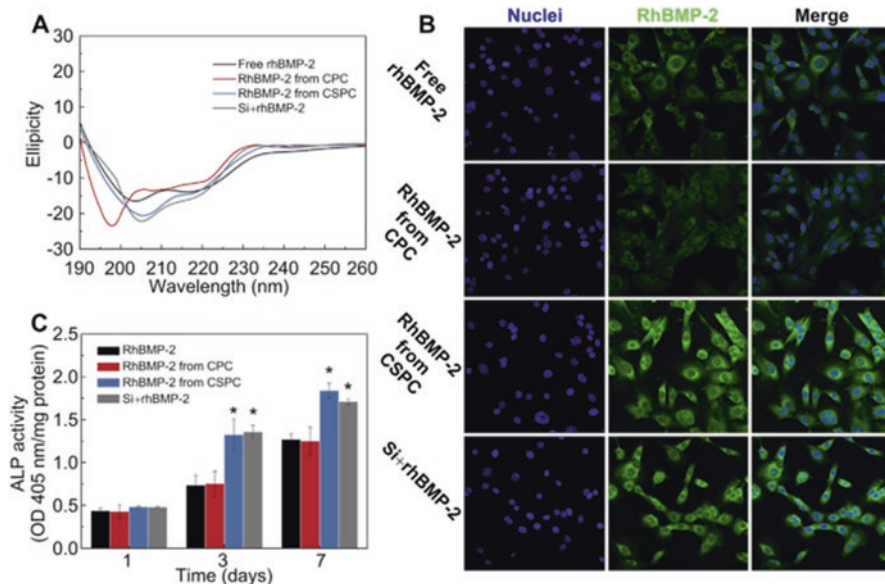


**Fig. 6.17** (a) 3D topology of the porous CSPC scaffold observed by micro-CT (a) and the surface morphology of the porous CSPC scaffolds by SEM (b  $\times 40$ , c  $\times 1000$ ). (b) XRD patterns of CPC and CSPC scaffolds (\*for peaks of HA and # for peaks of  $\text{CaSiO}_3$ ). (c) Degradation profiles of the CPC and CSPC scaffolds. (d) Ions released from the CPC and CSPC scaffolds (Reprinted with permission from Ref. [48]. Copyright © 2013 Biomaterials Inc. published by Elsevier Ltd.)

another efficient way to obtain osteoinductivity and enhance bone repair and reconstruction [47]. Thus, rhBMP-2-loaded calcium silicate phosphate cement scaffold for enhanced bone tissue regeneration was a concern.

The CSPC scaffold, fabricated by particles leaching method (as shown in Fig. 6.17a), were designed with specific amount of  $\text{CaSiO}_3$ , and such incorporation were not involved in the transformation of CPC to hydroxyapatite as the XRD shown in Fig. 6.17b. Then, a specific amount rhBMP-2 was anchored on the CSPC through lyophilization as mentioned in Sect. 6.3.2.1. The addition of CS into CPC scaffold favored the retention of secondary structure and bioactivity of rhBMP-2 (Fig. 6.18a). Compared with the CPC, CPC/rhBMP-2, and CSPC scaffolds, the rhBMP-2-loaded CSPC scaffold induced more enhanced osteogenic differentiation in vitro (Fig. 6.18c) and significantly promoted the ectopic bone formation (Fig. 6.19) and bone regeneration in a rabbit femur cavity defect model (Fig. 6.20). Such an impressive consequence is worthwhile for the further research and discussion.

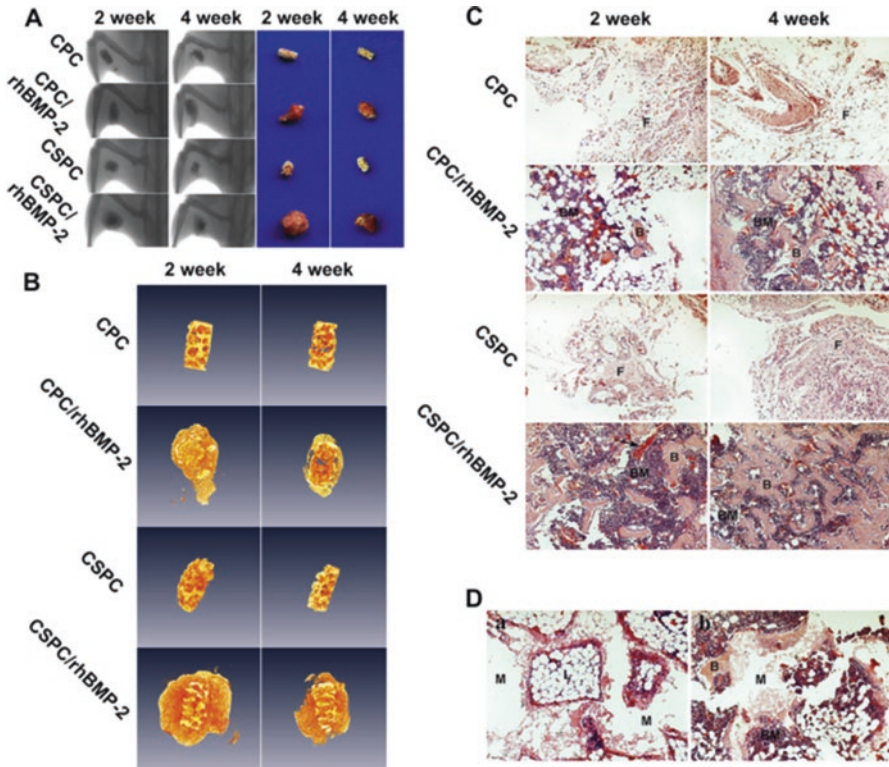
The crucial factor should be taken into account is the CSPC-induced desirable conformation and release behavior of rhBMP-2. It is known that hydrophobic interactions between a protein and the surface of an inorganic material sometimes result in deactivation of the protein due to the collapse of its secondary or tertiary structure [49, 50]. The CD spectra (Fig. 6.18a) revealed that the immobilization on the CPC and CSPC scaffolds indeed resulted in the changes of the secondary structure of



**Fig. 6.18** (a) Far-UV circular dichroism spectra of rhBMP-2 released from CPC and CSPC scaffolds in SBF (the positive peak head upward and the minus peak head downward) and the rhBMP-2 in presence of Si ion. (b) Effects of CPC and CSPC scaffolds and Si ions on localization of rhBMP-2 on cell layers. C2C12 cells were pretreated with free rhBMP-2, rhBMP-2 released from CPC and CSPC scaffolds in culture medium for 3 h and the rhBMP-2 in presence of Si ions. RhBMP-2 was detected with anti-BMP-2 antibody and FITC-labeled goat anti-mouse IgG (*green*), and cell nuclei were stained with DAPI (*blue*) for cell localization (400 $\times$ ). (c) ALP activity of C2C12 cells induced by rhBMP-2 released from CPC and CSPC scaffolds and in presence of Si ions (\*,  $p < 0.05$ , Si-rhBMP-2 vsRhBMP-2) (Reprinted with permission from [48]. Copyright © 2013 Biomaterials Inc. published by Elsevier Ltd.)

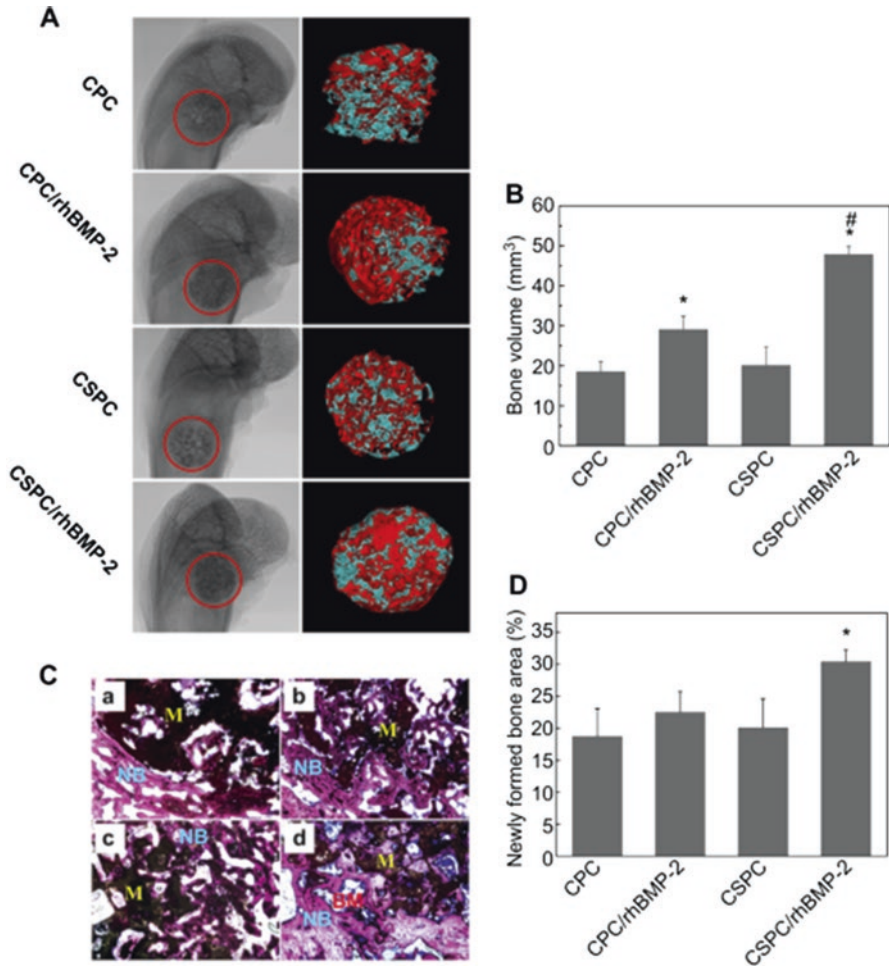
rhBMP-2, especially for the CPC scaffold. Based on the results from in vitro ALP activity (Fig. 6.18b), and in vivo ectopic and orthotopic bone formation, the addition of CS alone failed to alter the cellular response and osteogenic capacity of CPC, while the incorporation of rhBMP-2 could facilitate the osteoactivity of CPC to some extent. However, it is interesting to find that the combination of CSPC and rhBMP-2 exhibited markedly enhanced osteogenic differentiation in vitro and osteoinductive efficacy in vivo, which revealed a markedly synergistic action of CS and rhBMP-2.

The noticeable differences with regard to in vitro osteogenic differentiation, ectopic osteoinductivity, and orthotopic osteoregeneration between CPC/rhBMP-2 and CSPC/rhBMP-2 arouse our attention. The CPC and CSPC scaffolds were designed with similar surface structure. Therefore, it can be inferred that such differences between the bioactivity of rhBMP-2 from CPC and CSPC may originate from the existence of silicon in the scaffold or released into the culture medium. Previous studies have asserted that the rhBMP-2/ceramic interaction was thought to depend on hydroxyl, amine, and carboxyl groups in rhBMP-2 and the number of



**Fig. 6.19** CSPC stimulated the ectopic bone formation induced by rhBMP-2 in vivo. (a) X-ray images (left) and digital photos (right) of the ectopic bone. (b) 3D SRmCT reconstructed views of ectopic bone formation with different implants at 2 and 4 weeks. (c) Histological staining with H&E of the scaffolds and ectopic bone at 2 and 4 weeks postimplantation (*B* bone, *M* residual materials, *BM* bone marrow, *F* fibrous tissue, *Arrow* blood vessel). (d) Histological observation of bone formation over the residual material edges of CPC/rhBMP-2(a) and CSPC/rhBMP-2(b) at 4 weeks postimplantation (Reprinted with permission from Ref. [48]. Copyright © 2013 Biomaterials Inc. published by Elsevier Ltd.)

divalent ions present in the ceramic [51]. Additionally, some cation ions, such as  $Mg^{2+}$  mentioned in the above chapter, could significantly modulate the secondary structure and thereby change the catalytic activity of protein [52, 53]. Based on these previous reports, the silicon in the CSPC scaffold might interact directly with rhBMP-2 and the dissolved silicon ions in the culture medium might further modulate the bio-function of the released rhBMP-2. As speculated, the results showed the rhBMP-2 released from CSPC scaffolds exhibited similar CD spectra, comparable ALP expression and binding capacity to cellular receptor to the rhBMP-2 in the presence of Si ions at the same concentration of which released from CSPC at 7 days. These results confirmed that it was the Si ion extracted from the CSPC that plays critical role in maintaining the secondary structure and promoting the rhBMP-2-induced osteogenic differentiation.



**Fig. 6.20** Bone regeneration in a cavity defect after various CPC-based scaffolds implantation in the rabbit femur in 8 weeks. (a) Micro-CT images (left) of the bone regeneration in the defects (red circle) and tridimensional reconstruction images (right) of the defect sites (red: new bone formed, blue: scaffold residue). (b) Quantitative analysis of the new bone volume after 8 weeks of surgery by micro-CT (\* $p < 0.05$ , compared with CPC; # $p < 0.05$ , CSPC/rhBMP-2 vs CPC/rhBMP-2). (c) Histological observation of new bone formation in porous scaffolds (VG staining) (a CPC, b CPC/rhBMP-2, c CSPC, d CSPC/rhBMP-2, M materials, NB newly formed bone, BM bone marrow). (d) Quantitative analysis of the new bone area after 8 weeks of surgery by histological observation (\* $p < 0.05$ , compared with all the other groups) (Reprinted with permission from Ref. [48]. Copyright © 2013 Biomaterials Inc. published by Elsevier Ltd.)

Besides the preservation of the structural integrity and bioactivity, the controlled release of rhBMP-2 is another crux for the scaffolds to deliver rhBMP-2 in an efficient way. Many previous investigations reported that initial burst release followed by sustained release is better for promoting new bone formation and the initial burst

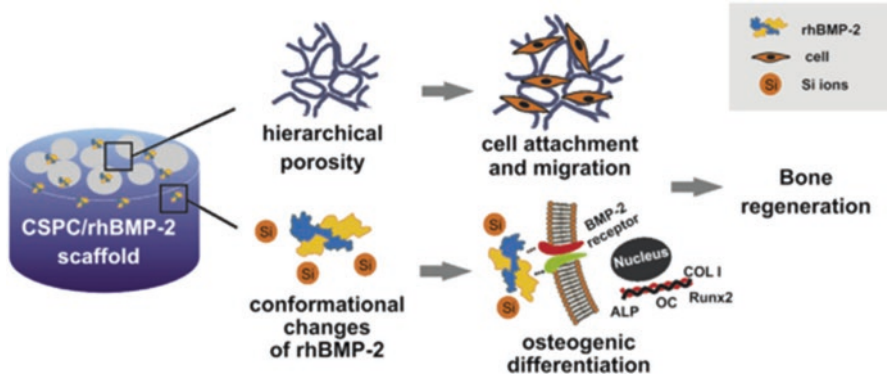


release of the growth factor from the implant acted as a chemotactic signal for the local recruitment of stem cells [54, 55]. For example, Li et al. evaluated the bone repair capacity of rhBMP-2 when delivered in polyurethane scaffolds possessing different release kinetics and found improved healing in scaffolds featuring an initial burst followed by sustained release [55]. Therefore, the release of rhBMP-2 from the CSPC scaffold with multiscale porosity exhibited typical initial burst and ensuing sustained release.

Moreover, the release of rhBMP-2 from CSPC scaffold exhibited the similar trend with polyurethanes (PUR)/PLGA large microspheres/rhBMP-2, which was confirmed to have better performance than other delivery systems [55]. We believe that this satisfactory release rate of rhBMP-2 from CSPC scaffold should be attributable to the combination of macroporous with microporous structures and the high affinity between negatively charged CSPC and the positively charged rhBMP-2. Although not fully understood, the above discussion highlighted the fact that CSPC could not only effectively maintain the microstructure and the bioactivity of rhBMP-2 but also control the release of BMP-2 for a sufficient period. From these viewpoints, the CSPC scaffold with multiscale porous structure is a suitable carrier for rhBMP-2 delivery.

Another significant factor contributing to the efficient bone regeneration is the absorbability of CSPC/rhBMP-2 scaffold *in vivo* [56]. The biomaterials used for bone regeneration should be degradable and gradually replaced by newly formed bone tissue [57]. The present CSPC scaffolds exhibited *in vitro* degradation in Tris-HCl solution and lost 16% of its initial weight after soaking for 8 weeks. 3D SR $\mu$ CT images and histological analysis of the implants and ectopic bone (Fig. 6.19) showed more materials absorbed in CSPC and CSPC/rhBMP-2 groups at 2 weeks and 4 weeks *in vivo*. Micro-CT and histological studies of scaffolds implanted in rabbit femur defect for 8 weeks (Fig. 6.20) also indicated much faster degradation in the CSPC group than that in CPC group. It was notable that the combination of rhBMP-2 with CSPC obviously enhanced the degradation rate of the implants when compared to the corresponding implants without rhBMP-2. According to the H&E and VG staining histological analysis, the surface of the residue materials was surrounded by a large amount of newly formed bone. Possible explanations might be (1) rhBMP-2 accelerates the expression of bone-related proteins and thus regulates the microenvironment conditions around the defect site, such as pH value, the concentration of enzymes, etc., and (2) the new marrow formation in the rhBMP-2-induced bone where a large number of osteoclastic precursors resided stimulates the cell-mediated resorption of materials.

The bone tissue scaffold should act not only as a biologically and mechanically compatible framework that enhances cell migration, bone ingrowth, and mechanical stability but also as an osteoinductive stimulus by delivering bioactive ions and growth factors such as rhBMP-2 within the therapeutic window to allow osteoprogenitor cells to differentiate into osteoblasts. Here, the fabricated CSPC/rhBMP-2 scaffold showed inspiring properties in terms of cellular attachment, osteoinductivity, and biodegradability. The results clearly demonstrated the significance of the



**Fig. 6.21** Schematic diagram of the combinatorial effect of CS and rhBMP-2 of CSPC/rhBMP-2 on bone regeneration. (1) The hierarchically porous structure of the scaffold favored the cell attachment and migration and promoted the transport of nutrient and waste and the bone ingrowth. (2) Si ions dissolved from CSPC was beneficial for the preservation of the secondary structure of the released rhBMP-2. The synergistic action of CS and rhBMP-2 contributed better binding capacity with BMP-2 receptors on cell membrane, which further stimulated the expression of osteogenic marker genes and the ALP activity. As a result, the enhanced cell adhesion and osteogenic differentiation lead to more efficient bone regeneration. Taken together, the hierarchical porosity and the synergistic effect of Si and rhBMP-2 enabled the micro/macroporous CSPC/rhBMP-2 scaffold to be an ideal substitute for bone repair (Reprinted with permission from Ref. [48]. Copyright © 2013 Biomaterials Inc. published by Elsevier Ltd.)

hierarchically porous structure, CS-mediated efficient rhBMP-2 immobilization, and proper biodegradability, which determined the osteogenetic ability of the CSPC/rhBMP-2 (Fig. 6.21).

## 6.4 Clinical Applications of rhBMP-2-Loaded CPC Scaffolds

### 6.4.1 Current Situation and Application of Bone Substitutes in Clinic

Considerable bone defects resulting from nonunion fractures, severe trauma, malignancy resection, or infection have raised great demands for clinical bone repair [58]. Large bone defects that cannot heal on its own require implantation of suitable bone grafts into the defect site [59]. Bone grafts include autografts, allografts, and artificial bone substitutes. Autograft remains the gold standard in orthopedic surgery due to its excellent osteoinductive and osteoconductive capability, yet limited tissue availability, donor site morbidity, and additional surgical pain restrict their clinical applications [60, 61]. As a suboptimal alternative, allografts have risks of immune rejection and disease transmission [62, 63]. These complications necessitate the pursuit of synthetic substitutes for treatment of these formidable defects [64].

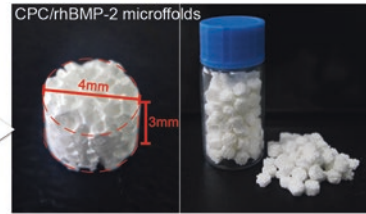
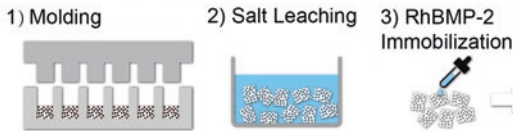
Bone tissue engineering scaffolds have been widely developed and are considered as the most perspective among all bone substitutes. Macroporosities of scaffolds, comparing to dense materials, have been demonstrated as a prerequisite for bone formation *in vivo*. Based on previous studies [65, 66], the minimum requirement of pore size is considered to be  $\sim 100\ \mu\text{m}$  for cell migration and nutritious transport, and pore sizes  $>300\ \mu\text{m}$  are recommended, due to enhanced new bone formation and formation of capillaries. To date, researchers have developed various biomaterials for porous scaffolds, and some of them have been successfully applied in clinic, such as  $\beta$ -tricalcium phosphate ( $\beta$ -TCP) and biphasic calcium phosphate (HA/TCP) scaffolds [67–69]. As a bioresorbable bone substitute, CPC has been widely reported *in vitro/in vivo* and applied in clinic due to its outstanding properties [70, 71]. However, a major problem of these artificial scaffolds is their deficient osteoinductivity compared to autografts, which might cause delayed union or even nonunion in clinic [72, 73]. Another challenging problem that needs to be addressed in the clinical translational process is the customization of the scaffold according to the defect size and shape of the patient, which often requires a long period and is hard to achieve.

Currently, a widely efficient and clinically applicable way to promote endogenous repair mechanism and enhance bone formation is the loading of growth factors into biomaterials [74, 75]. Among all growth factors, BMP-2 has been considered as the most notable cytokine to enhance bone formation and bone tissue reconstruction [76, 77]. rhBMP-2-loaded absorbable collagen sponge has been approved by FDA in 2002 for interbody fusion surgeries, and its osteogenic capacity has been validated in numerous studies [78–80]. However, due to the lack of sustained release, low dosage of rhBMP-2 with desirable therapeutic efficacy remains a challenge in the therapy of bone defects [81, 82]. High dosage not only increases the potential risks associated with excessive concentrations of rhBMP-2 but also raises the therapeutic costs to an unaffordable level that hampers further applications of rhBMP-2 [83, 84]. Although researchers have realized the sustained release of rhBMP-2 from different scaffolds, most of the BMP-2-loaded scaffolds are still confined to *in vitro* and animal experiments and still have a long way from bench to bedside [85].

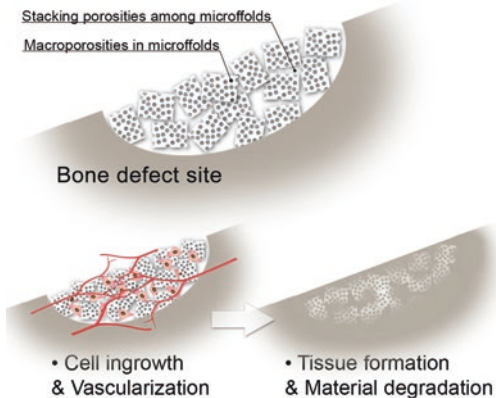
#### **6.4.2 Clinical Trials of rhBMP-2-Loaded CPC Scaffolds**

By combining CPC and rhBMP-2, two mature clinical applications of material and growth factor, Liu's group has successfully developed a pre-cured CPC/rhBMP-2 micro-scaffold and further applied it as an easy-to-operate filler for bone regeneration in clinic. The concept of "microfolds" (short for "micro-scaffolds") was proposed, which means the mass production in advance and easy handling during the surgery. The porous structure of microfold and the stacking macroporosities among the microfolds ensure the rapid ingrowth of tissues and fast degradation of the materials (Fig.6.22). Physicochemical properties and protein release kinetics of the

## Massive Production



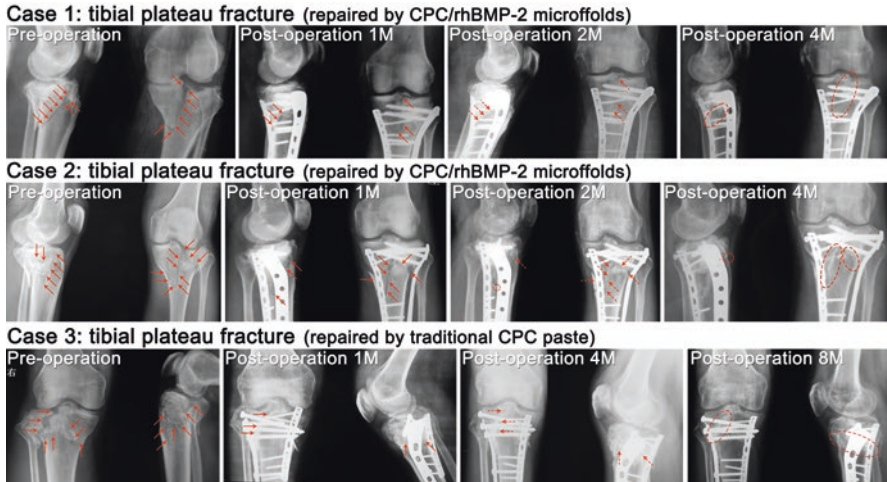
## Rapid Regeneration



**Fig. 6.22** Massive production route of rhBMP-2-loaded CPC scaffolds and illustration of the rapid regeneration process by the scaffolds. The route of CPC/rhBMP-2 microffolds includes molding, salt leaching, and rhBMP-2 immobilization; in contrast, traditional scaffolds involve the need of customization according to the defect size and shape, which is time-consuming and requires specific equipment. In the rapid regeneration process by CPC/rhBMP-2 microffolds, abundant porosities allow cell ingrowth and vascularization, which renders rapid formation of new bone tissue and synchronous degradation of materials; in contrast, traditional CPC paste undergoes bioresorption layer by layer slowly due to its high density and thus cannot be replaced by bone tissue until years later (Reprinted with permission from Ref. [86]. AJTR Copyright © 2016. Published by PubMed Central (PMC) site)

microffolds were characterized *in vitro* and *in vivo*. In a rabbit distal femur defect model, bone regeneration was achieved in three months after CPC/rhBMP-2 scaffold implantation, with regenerated tissue similar to normal tissue. A pilot clinical study was initiated in 81 patients to test safety and preliminary efficacy in humans (bone tissue repairing capacity) and to evaluate standard clinical and rehabilitation protocols that are not possible in animal models. Compared to traditional therapies by CPC paste, the average fracture healing time (for bony reunion) 0.5–2 months was shortened, and the repairing qualities were improved by CPC/rhBMP-2 microffolds. This bench-to-bedside translation represents a potential development of the clinical treatment of bone defects.

CPC microffolds could be designed to fill defect sites of different sizes and shape with easy operability and sufficient macroporosities for tissue ingrowth (Fig. 6.22). By a salt leaching and molding method, cylindrical CPC microffolds ( $\text{Ø} 4 \times 3 \text{ mm}$ ) were massively prepared and then sterilized, immobilized with rhBMP-2 by an adsorption and lyophilization process to achieve the final CPC/rhBMP-2 microffolds.



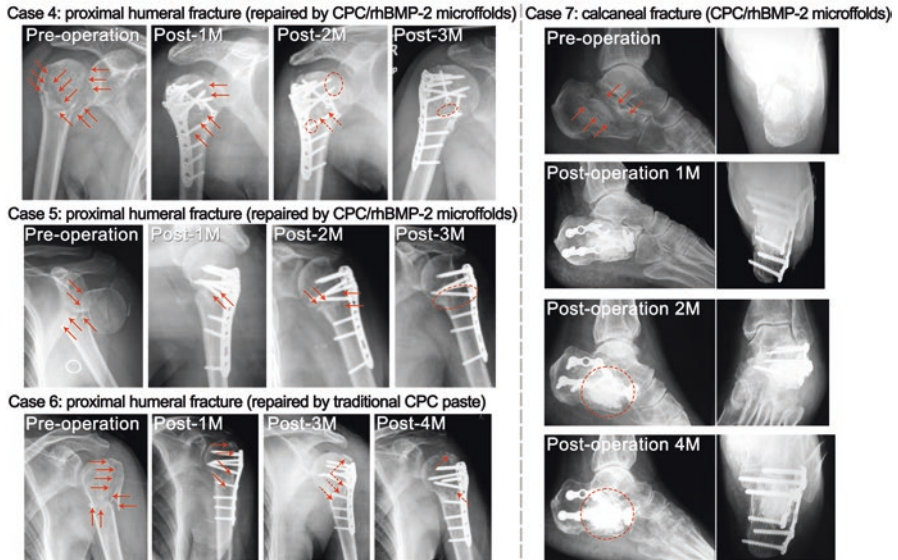
**Fig. 6.23** Typical cases of tibial plateau fractures: two cases (case 1 and case 2) repaired by CPC/rhBMP-2 microfolds and a comparable case (case 3) repaired by traditional CPC paste. *Red solid arrows* indicate the fracture lines; *red dashed arrows* indicate fuzzy fracture lines, which were considered as clinical healing; *red dashed circles* indicate the disappearance of the fracture lines, which was considered as bony reunion (Reprinted with permission from Ref. [86]. AJTR Copyright © 2016. Published by Pub Med Central (PMC) site)

The products have confirmed the good preservation for a long-term and doctor-friendly filler during surgeries.

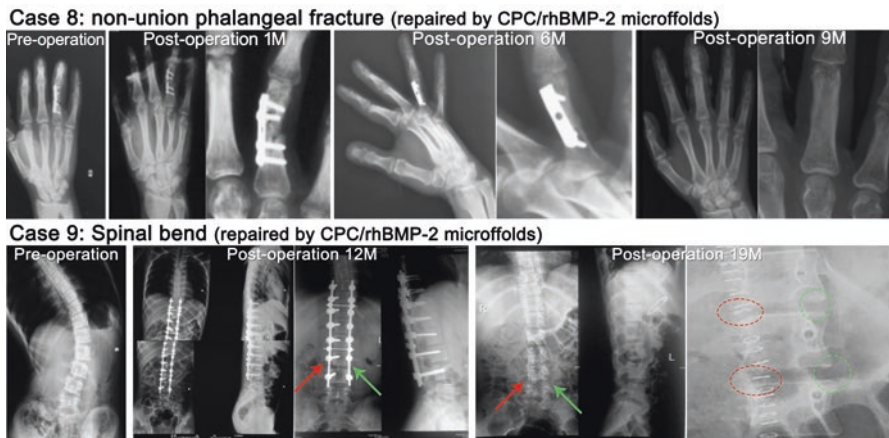
Despite that the great potential of porous scaffolds and growth factors in the field of bone repairing has been well-acknowledged, most porous scaffolds are still underdevelopment, and most growth factors have very limited clinical application due to the lack of proper carriers and the unaffordable cost.

Currently, scaffolds with specific size and shape can be prepared according to the protocol of the selected animal model, for example, long cylinder-shaped scaffolds for radius defect models [32], oblate scaffolds for cranial defect models [33], etc. However, bone defects of clinical patients come in various sizes and shapes, which cannot be accurately determined with current imaging techniques, and the duration from the occurrence of defect to surgical treatment is too short to order and customize. The concept of “microfolds” proposed could provide a trajectory to the clinical translation of porous scaffolds. The microfolds were designed not only to retain the advantageous macroporosities of traditional scaffolds but also for a better operability that is not restricted to the defect size and shape, which avoids the needs of customization and allows massive production and long-term preservation (Fig. 6.22).

The introduction of rhBMP-2 has greatly accelerated new bone formation and material degradation in vivo (Figs. 6.23, 6.24, and 6.25). Current rhBMP-2 productions for clinical use mainly adopted hydrogel as carrier. However, since hydrogels lacked osteoconductivity and controlled release, high doses of rhBMP-2 were required to achieve desirable osteogenic efficiency, which had raised the cost to an



**Fig. 6.24** Typical cases of proximal humeral fractures: two cases (case 4 and case 5) repaired by CPC/rhBMP-2 microffolds and a comparable case (case 6) repaired by traditional CPC paste. *Right*: typical case of calcaneal fracture (case 7) repaired by CPC/rhBMP-2 microffolds. *Red solid arrows* indicate the fracture lines; *red dashed arrows* indicate fuzzy fracture lines, which were considered as clinical healing; *red dashed circles* indicate the disappearance of the fracture lines, which was considered as bony reunion (Reprinted with permission from Ref. [86]. AJTR Copyright © 2016. Published by PubMed Central (PMC) site)



**Fig. 6.25** Two cases: nonunion phalangeal fracture (case 8) repaired by CPC/rhBMP-2 microffolds and scoliosis (case 9) implanted with CPC/rhBMP-2 microffolds and autografts. Case 9 applies CPC/rhBMP-2 microffolds (*red arrow*) and allografts (*green arrow*) to each side of the spine; *red dashed circle* indicated callus formation on the side of CPC/rhBMP-2 microffolds, while *green dashed circle* exhibited no callus formation on the side of allografts (Reprinted with permission from Ref. [86]. AJTR Copyright © 2016. Published by PubMed Central (PMC) site)

unaffordable level. In addition, since current artificial bone substitutes (e.g., traditional CPC paste) exhibited no notable advantage in the repairing efficiency comparing to autografts, most patients would rather choose autografts for its relatively low cost and high efficiency [34]. As a solvation and improvement to current substitutes, the CPC/rhBMP-2 microfolds combined the osteoconductivity of porous CPC scaffolds and the osteoinductivity of rhBMP-2 and thus achieved a rapid bone repair with relatively low dose of rhBMP-2. Compared to current clinical therapies (traditional CPC paste), the average fracture healing time was 0.5–2 months shorter after implanted CPC/rhBMP-2 microfolds, and the defect site could rapidly recover to a satisfactory functional level within 3–6 months postimplantation. Moreover, CPC/rhBMP-2 microfolds exhibited the potential in treating fractures that are most challenging for current therapies.

Eighty-one bone defect patients were randomly divided into two groups: treated by CPC/rhBMP-2 microfolds or traditional CPC paste (control group). In the CPC/rhBMP-2 group, 40 patients included 25 males and 15 females, with an average age of 46.7; the bone defects were located as follows: tibial plateau in 16 patients, proximal humerus in 11 patients, and calcaneus in 13 patients; the defects were repaired with CPC/rhBMP-2 microfolds. In the control group, 41 patients included 27 males and 14 females, with an average age of 44.3; the bone defects were located as follows: tibial plateau in 15 patients, proximal humerus in 12 patients, and calcaneus in 14 patients; the defects were repaired with traditional CPC paste.

Seven to twelve days after operation, skin wound healing by first intention of the surgical incisions was acquired in 78 cases; wound exudation occurred in one case of control group and two cases of CPC/rhBMP-2 group at 2 weeks postoperation, which were all healed after dressing change. These implant rejections were diagnosed as idiopathic noninfectious inflammatory, which might be related with blood supply deficiency, scar constitution, long time of limb fixation, or heterologous protein allergy. No toxic effect, skin rash, or high fever was found in all patients; liver and kidney functions, routine blood and urine tests, and C-reactive protein were normal. All cases were followed up for 12–24 months, average 15.3 months. During follow-up, no occurrence of osteomyelitis, fractures, or obvious collapses after the bone defect repair was observed; no plate and screw loosening or other complications occurred. The average time of clinical healing and bony reunion by CPC/rhBMP-2 microfolds was significantly shortened compared to the control group repaired by traditional CPC paste; and the average function scores and the excellent rates of function scores at each time point also indicated shortened repairing time and higher repairing qualities in CPC/rhBMP-2 microfolds group.

Typical cases were selected and shown in Figs. 6.23 and 6.24, including three cases of tibial plateau fractures, three cases of proximal humeral fractures, and one case of calcaneal fracture. The X-ray films intuitively indicated the acceleration of clinical healing (red dashed arrows) and bony reunion (red dashed circles) by CPC/rhBMP-2 microfolds. Take the typical cases of tibial plateau fractures as examples (Fig. 6.23): for 1 month postoperation, the anatomic shapes of the bone defects were all recovered after surgery; bone filler materials were closely connected with the host bone; there was no gap between the bone and the filling material at the inter-

face; and fracture lines were clearly visible in both groups. In the cases using CPC/rhBMP-2 microffolds (Fig. 6.23, case 1 and case 2), the fracture lines became fuzzy at month 2, progressively faded and total disappeared at week 4. The fuzziness of fracture lines together with other physical criteria was considered as clinical healing, and the disappearance of fracture line was considered as bony reunion. In contrast, in case of traditional CPC paste (Fig. 6.23, Case 3), the time of clinical healing and bony reunion were postponed to month 4 and month 8. Moreover, CPC/rhBMP-2 microffolds exhibited a similar density to the host bone due to its abundant porous structure, while traditional CPC paste showed a white shadow indicating high density, which results in slow degradation and clear vision of the material after bony reunion. Similar trends could be observed from the typical cases of proximal humeral fractures and calcaneal fracture (Fig. 6.24).

Furthermore, we had accepted two additional cases that could not be treated successfully by traditional treatment (Fig. 6.25). In case 8, a male patient of age 26, with bone nonunion of phalangeal fractures after internal fixation, was treated with tradition CPC paste filling therapy and implanted CPC/rhBMP-2 microffolds in revision. The X-ray films exhibited gradual degradation of material accompanied with trabecular bone ingrowth after one month; after six months, the microffolds were replaced by host bone tissue and clinical healing was achieved; after the removal of internal fixation at nine months postoperation, the affected finger was healed with complete bony reunion. In case 9, a 17-year-old male patient with scoliosis received orthopedic surgery of intervertebral fusion and pedicle screw fixation, using CPC/rhBMP-2 microffolds in the left side and autografts in the right side, respectively. The orthopedic outcome 12 months postoperation was satisfactory with internal fixation in place. After removal of internal fixation at 19 months postoperation, the X-ray films exhibited obvious callus formation in the side of CPC/rhBMP-2 microffolds (red dashed circle) and no callus formation in the side of autografts (green dashed circle), indicating a better therapeutic efficacy of CPC/rhBMP-2 microffolds than autografts.

These results demonstrated that CPC/rhBMP-2 microffolds were superior to traditional CPC paste in overall performances, with not only shortened repairing time but also improved repairing qualities. Moreover, CPC/rhBMP-2 microffolds exhibited the potential in treating fractures that are most challenging for current therapies.

## 6.5 Summary and Prospectives

The loading of rhBMP-2 has been commonly acknowledged as an efficient way for improving osteoinductivity and clinic therapeutic efficacy of bone regeneration materials/scaffolds. This chapter has systematically introduced the research development and clinical application of the rhBMP-2-loaded CPC scaffold. The interfacial surface, composition, and porous structure all played critical roles on bioactivity of rhBMP-2-loaded CPC porous scaffolds.



In future, efforts are still needed for further research and development of more efficient and better osteobioactivity of CPC/rhBMP-2 bone repairing materials. In addition to modulating the properties of the material, other approaches, including the combinational utilization of small molecular drugs or other growth factors, will be developed. Meanwhile, various formulations of the CPC/rhBMP-2 will be developed according to the clinic needs. The available evidence provided in this chapter and obtained from our clinical study could shed light on developing new strategies to enhance bone formation using CPC material with rhBMP-2 protein.

**Acknowledgments** This work was supported by grants from the National Basic Research Program of China (973 Program, No. 2012CB933600), the 111 Project (B14018), and the National Natural Science Foundation of China (Nos. 31100679, 31330028, and 31470924).

## References

1. Kuang G-M, Yau WP, Lu WW, Chiu KY (2014) Local application of strontium in a calcium phosphate cement system accelerates healing of soft tissue tendon grafts in anterior cruciate ligament reconstruction experiment using a rabbit model. *Am J Sports Med* 42:2996–3002
2. Thormann U, Ray S, Sommer U, ElKhassawna T et al (2013) Bone formation induced by strontium modified calcium phosphate cement in critical-size metaphyseal fracture defects in ovariectomized rats. *Biomaterials* 34:8589–8598
3. Dorozhkin SV, Epple M (2002) Biological and medical significance of calcium phosphates. *Angew Chem Int Ed* 41:3130–3146
4. Ginebra MP, Traykova T, Planell JA (2006) Calcium phosphate cements as bone drug delivery systems: a review. *J Control Release* 113:102–110
5. Guan J, Yang J, Dai J, Qin Y et al (2015) Bioinspired nanostructured hydroxyapatite/collagen three-dimensional porous scaffolds for bone tissue engineering. *RSC Adv* 5:36175–36184
6. Wang Y, Ren X, Ma X, Su W et al (2015) Alginate-intervened hydrothermal synthesis of hydroxyapatite nanocrystals with nanopores. *Cryst Growth Des* 15:1949–1956
7. Chen F, Lam WM, Lin CJ, Qiu GX et al (2007) Biocompatibility of electrophoretical deposition of nanostructured hydroxyapatite coating on roughen titanium surface: in vitro evaluation using mesenchymal stem cells. *J Biomed Mater Res B* 82B:183–191
8. Hu R, Lin CJ, Shi HY (2007) A novel ordered nano hydroxyapatite coating electrochemically deposited on titanium substrate. *J Biomed Mater Res A* 80A:687–692
9. Kim SE, Yun Y-P, Shim K-S, Park K et al (2015) Fabrication of a BMP-2-immobilized porous microsphere modified by heparin for bone tissue engineering. *Colloid Surf B* 134:453–460
10. Kisiel M, Klar AS, Ventura M, Buijs J et al (2013) Complexation and sequestration of BMP-2 from an ECM mimetic hyaluronan gel for improved bone formation. *Plos One* 8:e78551
11. Autefage H, Briand-Mesange F, Cazalbou S, Drouet C et al (2009) Adsorption and release of BMP-2 on nanocrystalline apatite-coated and uncoated hydroxyapatite/beta-tricalcium phosphate porous ceramics. *J Biomed Mater Res B* 91B:706–715
12. Yang F, Wang J, Hou J, Guo H et al (2013) Bone regeneration using cell-mediated responsive degradable PEG-based scaffolds incorporating with rhBMP-2. *Biomaterials* 34:1514–1528
13. Huang B, Yuan Y, Li T, Ding S et al (2016) Facilitated receptor-recognition and enhanced bioactivity of bone morphogenetic protein-2 on magnesium-substituted hydroxyapatite surface. *Sci Rep-UK* 6:24323
14. Huang RL, Chen G, Wang WJ, Herller T et al (2015) Synergy between IL-6 and soluble IL-6 receptor enhances bone morphogenetic protein-2/absorbable collagen sponge-induced bone regeneration via regulation of BMPRIA distribution and degradation. *Biomaterials* 67:308–322

15. Huang B, Yuan Y, Ding S, Li J et al (2015) Nanostructured hydroxyapatite surfaces-mediated adsorption alters recognition of BMP receptor IA and bioactivity of bone morphogenetic protein-2. *Acta Biomater* 27:275–285
16. Kim S, Kang Y, Krueger CA, Sen M et al (2012) Sequential delivery of BMP-2 and IGF-1 using a chitosan gel with gelatin microspheres enhances early osteoblastic differentiation. *Acta Biomater* 8:1768–1777
17. van de Watering FCJ, Molkenboer-Kueneen JDM, Boerman OC, van den Beucken JJJP et al (2012) Differential loading methods for BMP-2 within injectable calcium phosphate cement. *J Control Release* 164:283–290
18. Kirsch T, Sebald W, Dreyer MK (2000) Crystal structure of the BMP-2-BRIA ectodomain complex. *Nat Struct Biol* 7:492–496
19. Kirsch T, Nickel J, Sebald W (2000) BMP-2 antagonists emerge from alterations in the low-affinity binding epitope for receptor BMPR-II. *EMBO J* 19:3314–3324
20. Chandra P, Lee SJ (2015) Synthetic extracellular microenvironment for modulating stem cell behaviors. *Biomark Insights* 10:105–116
21. Riau AK, Mondal D, Yam GHF, Setiawan M et al (2015) Surface modification of PMMA to improve adhesion to corneal substitutes in a synthetic core-skirt keratoprosthesis. *ACS Appl Mater Interfaces* 7:21690–21702
22. Falconnet D, Csucs G, Grandin HM, Textor M (2006) Surface engineering approaches to micropattern surfaces for cell-based assays. *Biomaterials* 27:3044–3063
23. Schwab EH, Pohl TLM, Haraszti T, Schwaerzer GK et al (2015) Nanoscale control of surface immobilized BMP-2: toward a quantitative assessment of BMP-mediated signaling events. *Nano Lett* 15:1526–1534
24. Liu X, Li H, Jin Q, Ji J (2014) Surface tailoring of nanoparticles via mixed-charge monolayers and their biomedical applications. *Small* 10:4230–4242
25. Roach P, Farrar D, Perry CC (2006) Surface tailoring for controlled protein adsorption effect of topography at the nanometer scale and chemistry. *J Am Chem Soc* 128:3939–3945
26. Hassel S, Schmitt S, Hartung A, Roth M et al (2003) Initiation of Smad-dependent and Smad-independent signaling via distinct BMP-receptor complexes. *J Bone Joint Surg Am* 85A:44–51
27. Ishida K, Acharya C, Christiansen BA, Yik JHN et al (2013) Cartilage oligomeric matrix protein enhances osteogenesis by directly binding and activating bone morphogenetic protein-2. *Bone* 55:23–35
28. Sieber C, Kopf J, Hiepen C, Knaus P (2009) Recent advances in BMP receptor signaling. *Cytokine Growth F R* 20:343–355
29. Autefage H, Briand-Mesange F, Cazalbou S, Drouet C et al (2009) Adsorption and release of BMP-2 on nanocrystalline apatite-coated and uncoated hydroxyapatite/beta-tricalcium phosphate porous ceramics. *J Biomed Mater Res Part B Appl Biomater* 91:706–715
30. Liu Z, Qu S, Zheng X, Xiong X et al (2014) Effect of polydopamine on the biomimetic mineralization of mussel-inspired calcium phosphate cement in vitro. *Mater Sci Eng C Mater Biol Appl* 44:44–51
31. Jing Z, Xiaoyu M, Dan L, Hengsong S et al (2015) Magnesium modification of a calcium phosphate cement alters bone marrow stromal cell behavior via an integrin-mediated mechanism. *Biomaterials* 53:251–264
32. Crouzier T, Fourel L, Boudou T, Albiges-Rizo C et al (2011) Presentation of BMP-2 from a soft biopolymeric film unveils its activity on cell adhesion and migration. *Adv Mater* 23:H111–H118
33. Khang D, Choi J, Im YM, Kim YJ et al (2012) Role of subnano-, nano- and submicron-surface features on osteoblast differentiation of bone marrow mesenchymal stem cells. *Biomaterials* 33:5997–6007
34. Dolatshahi-Pirouz A, Jensen T, Foss M, Chevallier J et al (2009) Enhanced surface activation of fibronectin upon adsorption on hydroxyapatite. *Langmuir* 25:2971–2978
35. Boix T, Gomez-Morales J, Torrent-Burgues J, Monfort A et al (2005) Adsorption of recombinant human bone morphogenetic protein rhBMP-2m onto hydroxyapatite. *J Inorg Biochem* 99:1043–1050

36. Hollister SJ (2005) Porous scaffold design for tissue engineering. *Nat Mater* 4:524
37. Karageorgiou V, Kaplan D (2005) Porosity of 3D biomaterial scaffolds and osteogenesis. *Biomaterials* 26:5491
38. Yoshizawa S, Brown A, Barchowsky A, Sfeir C (2014) Magnesium ion stimulation of bone marrow stromal cells enhances osteogenic activity, simulating the effect of magnesium alloy degradation. *Acta Biomater* 10:2834–2842
39. Zhang J, Ma X, Lin D, Shi H et al (2015) Magnesium modification of a calcium phosphate cement alters bone marrow stromal cell behavior via an integrin-mediated mechanism. *Biomaterials* 53:251–264
40. Wu F, Wei J, Guo H, Chen F et al (2008) Self-setting bioactive calcium–magnesium phosphate cement with high strength and degradability for bone regeneration. *Acta Biomater* 4:1873–1884
41. Yang CX, Yuan GY, Zhang J, Tang Z et al (2010) Effects of magnesium alloys extracts on adult human bone marrow-derived stromal cell viability and osteogenic differentiation. *Biomed Mater* 5:045005
42. Ding S, Zhang J, Tian Y, Huang B et al (2016) Magnesium modification up-regulates the bioactivity of bone morphogenetic protein-2 upon calcium phosphate cement via enhanced BMP receptor recognition and Smad signaling pathway. *Colloids Surf B: Biointerfaces* 145:140–151
43. Kopf J, Paarmann P, Hiepen C, Horbelt D et al (2014) BMP growth factor signaling in a bio-mechanical context. *Biofactors* 40:171–187
44. Hartung A, Bitton-Worms K, Rechtman MM, Wenzel V et al (2006) Different routes of bone morphogenic protein (BMP) receptor endocytosis influence BMP signaling. *Mol Cell Biol* 26:7791–7805
45. Zhao QH, Qian JC, Zhou HJ, Yuan Y et al (2010) In vitro osteoblast-like and endothelial cells' response to calcium silicate/calcium phosphate cement. *Biomed Mater* 5:035004
46. Guo H, Wei J, Yuan Y, Liu CS (2007) Development of calcium silicate/calcium phosphate cement for bone regeneration. *Biomed Mater* 2:S153
47. Crouzier T, Sailhan F, Becquart P, Guillot R et al (2011) The performance of BMP-2 loaded TCP/HAP porous ceramics with a polyelectrolyte multilayer film coating. *Biomaterials* 32:7543–7554
48. Zhang J, Zhou HJ, Yang K, Yuan Y et al (2013) RhBMP-2-loaded calcium silicate/calcium phosphate cement scaffold with hierarchically porous structure for enhanced bone tissue regeneration. *Biomaterials* 34:9381–9392
49. Oliveira AF, Gemming S, Seifert G (2011) Conformational analysis of aqueous BMP-2 using atomistic molecular dynamics simulations. *J Phys Chem B* 115:1122–1130
50. Habibovic P, Sees TM, van den Doel MA, van Blitterswijk CA et al (2006) Osteoinduction by biomaterials – physicochemical and structural influences. *J Biomed Mater Res A* 77A:747–762
51. Lim TC, Chian KS, Leong KF (2010) Cryogenic prototyping of chitosan scaffolds with controlled micro and macro architecture and their effect on in vivo neo-vascularization and cellular infiltration. *J Biomed Mater Res Part A* 94:1303–1311
52. Guo S, Wang L, Lu A, Lu T et al (2010) Inhibition mechanism of lanthanum ion on the activity of horseradish peroxidase in vitro. *Spectrochim Acta A Mol Biomol Spectrosc* 75:936–940
53. Dong X, Wang Q, Wu T, Pan H (2007) Understanding adsorption-desorption dynamics of BMP-2 on hydroxyapatite (001) surface. *Biophys J* 93:750–759
54. Visser R, Arrabal PM, Becerra J, Rinas U et al (2009) The effect of an rhBMP-2 absorbable collagen sponge-targeted system on bone formation in vivo. *Biomaterials* 30:2032–2037
55. Li B, Yoshii T, Hafeman AE, Nyman JS et al (2009) The effects of rhBMP-2 released from biodegradable polyurethane/microsphere composite scaffolds on new bone formation in rat femora. *Biomaterials* 30:6768–6779
56. Dai C, Guo H, Lu J, Shi J et al (2011) Osteogenic evaluation of calcium/magnesium-doped mesoporous silica scaffold with incorporation of rhBMP-2 by synchrotron radiation-based  $\mu$ CT. *Biomaterials* 32:8506–8517
57. Hench LL, Polak JM (2002) Third-generation biomedical materials. *Science* 295:1014–1017

58. Yuan H, Fernandes H, Habibovic P, de Boer J et al (2010) Osteoinductive ceramics as a synthetic alternative to autologous bone grafting. *Proc Natl Acad Sci U S A* 107:13614–13619
59. Tagil M (2014) Bone substitutes, grafts and cement. In: Høve LM, Lindau T, Hølmer P (eds) *Distal radius fractures*. Springer, Berlin, pp 233–239
60. Smith CA, Richardson SM, Eagle MJ, Rooney P et al (2015) The use of a novel bone allograft wash process to generate a biocompatible, mechanically stable and osteoinductive biological scaffold for use in bone tissue engineering. *J Tissue Eng Regen Med* 9:595–604
61. Dumic-Cule I, Pecina M, Jelic M, Jankolija M et al (2015) Biological aspects of segmental bone defects management. *Int Orthop* 39:1005–1011
62. Aponte-Tinco L, Ayerza M, Muscolo DL, Farfalli G (2016) What are the risk factors and management options for infection after reconstruction with massive bone allografts? *Clin Orthop Relat Res* 474:669–673
63. Lee I, Chung C, Lee K, Kwon S-S et al (2015) Incidence and risk factors of allograft bone failure after calcaneal lengthening. *Clin Orthop Relat Res* 473:1765–1774
64. Yunus Basha R, Sampath Kumar TS, Doble M (2015) Design of biocomposite materials for bone tissue regeneration. *Mater Sci Eng C Mater Biol Appl* 57:452–463
65. Tian B, Liu J, Dvir T, Jin L et al (2012) Macroporous nanowire nanoelectronic scaffolds for synthetic tissues. *Nat Mater* 11:986–994
66. Kraehenbuehl TP, Langer R, Ferreira LS (2011) Three-dimensional biomaterials for the study of human pluripotent stem cells. *Nat Methods* 8:731–736
67. Cancedda R, Giannoni P, Mastrogiacomo M (2007) A tissue engineering approach to bone repair in large animal models and in clinical practice. *Biomaterials* 28:4240–4250
68. Shayesteh YS, Khojasteh A, Soleimani M, Alikhasi M et al (2008) Sinus augmentation using human mesenchymal stem cells loaded into a  $\beta$ -tricalcium phosphate/hydroxyapatite scaffold. *Oral Surg Oral Med Oral Pathol Oral Radiol Endod* 106:203–209
69. Kokemueller H, Spalthoff S, Nollf M, Tavassol F et al (2010) Prefabrication of vascularized bioartificial bone grafts in vivo for segmental mandibular reconstruction: experimental pilot study in sheep and first clinical application. *Int J Oral Maxillofac Surg* 39:379–387
70. Bose S, Tarafder S (2012) Calcium phosphate ceramic systems in growth factor and drug delivery for bone tissue engineering: a review. *Acta Biomater* 8:1401–1421
71. Pan W, Li D, Wei Y, Hu Y et al (2013) Tendon-to-bone healing using an injectable calcium phosphate cement combined with bone xenograft/BMP composite. *Biomaterials* 34:9926–9936
72. Vallet-Regi M, Ruiz-Hernandez E (2011) Biceramics: from bone regeneration to cancer nanomedicine. *Adv Mater* 23:5177–5218
73. Anderson JM, Patterson JL, Vines JB, Javed A et al (2011) Biphasic peptide amphiphile nanomatrix embedded with hydroxyapatite nanoparticles for stimulated osteoinductive response. *ACS Nano* 5:9463–9479
74. Facca S, Cortez C, Mendoza-Palomares C, Messadeq N et al (2010) Active multilayered capsules for in vivo bone formation. *Proc Natl Acad Sci U S A* 107:3406–3411
75. Schindeler A, McDonald MM, Bokko P, Little DG (2008) Bone remodeling during fracture repair: the cellular picture. *Semin Cell Dev Biol* 19:459–466
76. Hunziker EB, Enggist L, Kuffer A, Buser D et al (2012) Osseointegration: the slow delivery of BMP-2 enhances osteoinductivity. *Bone* 51:98–106
77. Li L, Zhou G, Wang Y, Yang G et al (2015) Controlled dual delivery of BMP-2 and dexamethasone by nanoparticle-embedded electrospun nanofibers for the efficient repair of critical-sized rat calvarial defect. *Biomaterials* 37:218–229
78. Bessa PC, Casal M, Reis RL (2008) Bone morphogenetic proteins in tissue engineering: the road from laboratory to clinic, part II (BMP delivery). *J Tissue Eng Regen Med* 2:81–96
79. Geiger M, Li RH, Friess W (2003) Collagen sponges for bone regeneration with rhBMP-2. *Adv Drug Deliv Rev* 55:1613–1629
80. Hsu WK, Wang JC (2008) The use of bone morphogenetic protein in spine fusion. *Spine J* 8:419–425
81. Jonkheijm P, Weinrich D, Schroder H, Niemeyer CM et al (2008) Chemical strategies for generating protein biochips. *Angew Chem Int Ed* 47:9618–9647

82. Lee JS, Suarez-Gonzalez D, Murphy WL (2011) Mineral coatings for temporally controlled delivery of multiple proteins. *Adv Mater* 23:4279–4284
83. Shah NJ, Hyder MN, Moskowitz JS, Quadir MA et al (2013) Surface-mediated bone tissue morphogenesis from tunable nanolayered implant coatings. *Sci Transl Med* 5:10
84. Kim RY, Oh JH, Lee BS, Seo YK et al (2014) The effect of dose on rhBMP-2 signaling, delivered via collagen sponge, on osteoclast activation and in vivo bone resorption. *Biomaterials* 35:1869–1881
85. Conde MCM, Chisini LA, Demarco FF, Nör JE et al (2015) Stem cell-based pulp tissue engineering: variables enrolled in translation from the bench to the bedside, a systematic review of literature. *Int Endod J* 49:543–550
86. Lin D, Zhang J, Bai F, Cao XH et al (2016) Fabrication and clinical application of easy-to-operate pre-cured CPC/rhBMP-2 micro-scaffolds for bone regeneration. *Am J Transl Res* 8:1379–1396

# Chapter 7

## Drug-Loading Calcium Phosphate Cements for Medical Applications

Shuxin Qu, Jie Weng, Ke Duan, and Yumei Liu

**Abstract** Calcium phosphate cements (CPCs) are uniquely promising drug carriers for orthopedic applications because of their room-temperature setting property and injectability. This chapter reviews the basics of CPCs, techniques used for preparing drug-loaded CPCs and composites, effects of drug incorporation on the physicochemical characteristics (i.e., strength, handling properties) of the cement, the drug release behaviors of drug-loaded CPCs, and medical applications of CPCs for the delivery of a variety of drugs. It becomes clear that, with from simple to latest techniques (e.g., mixing, 3D freedom fabrication), CPCs incorporating a large number of drugs have been developed including antibiotics, analgesics, anti-osteoporotic agents, anti-inflammatory compounds, and anticancer drugs. Composites with more advanced structures (e.g., polymer microspheres-in-cement design) have also been widely investigated to modulate drug release profiles and cement degradation. Additionally, although drug release almost routinely follows Higuchi's diffusion-controlled model, other situations exist and innovations in material design can open new possibilities in controlling the rate of drug release. Finally, we suggest that development of smarter and multifunctional CPC release systems, such as sequential release CPCs for meeting the requirements of each stage of bone healing, may be a promising direction for future research.

**Keywords** Calcium phosphate cement • Drug-loading technique • CPC-based composite • Mechanical properties • Handling properties • Release kinetics • Medical application • Musculoskeletal disorder • Therapeutic agents and bioactive substance • Multiple stimuli-responsive CPC release system

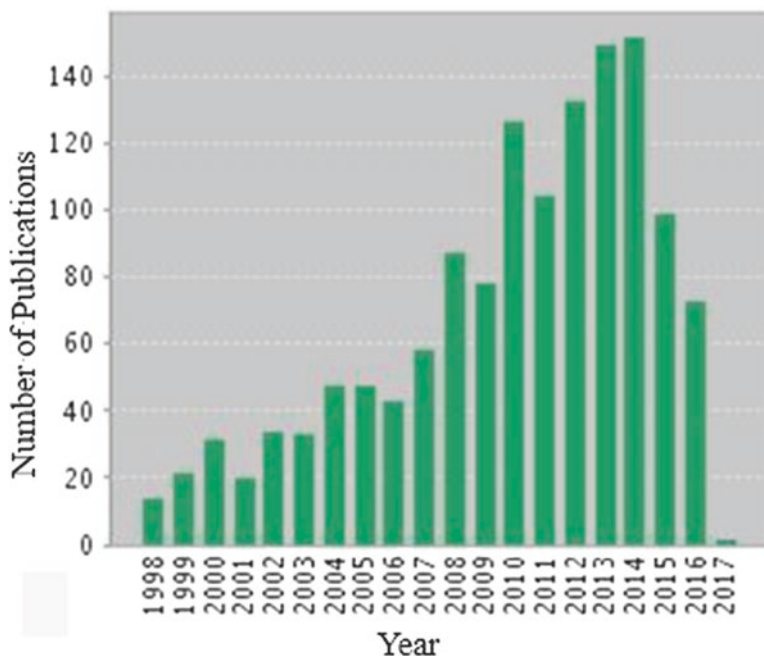
---

S. Qu • J. Weng (✉) • K. Duan • Y. Liu  
Key Lab of Advanced Technologies of Materials, Ministry of Education, School of Materials Science and Engineering, Southwest Jiaotong University, Chengdu 610031, China  
e-mail: [jweng@swjtu.edu.cn](mailto:jweng@swjtu.edu.cn)

## 7.1 Introduction

Because they are similar to human bone mineral in chemistry and phase structures [1], calcium phosphates (CaPs) are ideal biomaterials for bone repair. Currently, CaP-related biomaterials are used in clinics with a variety of forms, primarily including CaP bioceramics, CaP cements (CPCs), CaP-based bioglasses, CaP-based coatings on metallic implants, nano-sized CaP particles carrying drugs, and CaP/polymer composites [1]. Among these, CPCs are frequently used as bone defect fillers because of their excellent biocompatibility, biodegradability, self-setting property, and moldability [1–4]. CPCs are uniquely different from the other forms of CaP-related materials in that as settable materials, which can be conveniently molded into customized geometries to meet the individual requirement of each patient [2]. In addition, a critical advantage of CPCs is that they can be injected into the defect region to manage skeletal disorders in a minimally invasive manner. For example, they have been successfully used in stabilizing spinal fractures (i.e., vertebroplasty) [1]. Moreover, the degradation products of CPCs are simply inorganic ions constituting human bones [2]. In contrast, polymeric bone cements (e.g., polymethyl methacrylate bone cement) either are nondegradable or can only degrade into organic fragments not found in the human body [5]. CPCs were first commercialized in the 1990s for treatment of maxillofacial defects [6, 7] as well as bone fractures [8]. Subsequently, various cement formulations have been developed to fulfill specific requirements for other orthopedics applications, e.g., bone augmentation [9–13], reinforcement of osteoporotic bones [14, 15], fixation of metallic implants in weakened bone [16, 17], and stabilization of spinal fractures [18, 19].

Various bone defects can be created by musculoskeletal diseases and traumas, e.g., infection, arthritis, osteoporosis, osteonecrosis, tumor, and fracture [20]. However, human bones are generally poorly vascularized, and thus, drugs systematically administered to manage skeletal diseases (e.g., osteomyelitis) have only poor access to bones [21]. This problem is aggravated when vascularization at the target site is disrupted by trauma or surgical operation. Therefore, there is a great demand in orthopedics for local drug delivery at a site of injury or defect. It may be noted that, the concept of “drug” is not limited to traditional therapeutic agents, e.g., antibiotic, antitumor, and anti-inflammatory compounds. The scope of “drug’s” potential applications in orthopedics has expanded to include growth factors, bioactive proteins, enzymes, nonviral genes (DNAs and RNAs), and inorganic ions with biological activities, e.g.,  $\text{Sr}^{2+}$ ,  $\text{Mg}^{2+}$ ,  $\text{Zn}^{2+}$ ,  $\text{Cu}^{2+}$ ,  $\text{Ag}^{+}$ , and  $\text{F}^{-}$  [2, 22–25]. Even more, extracts from traditional Chinese herbal medicines were also studied as potential candidates for the treatment of bone disorders [26]. Various growth factors, bioactive biomolecules, ions, and drugs were used in bone tissue engineering to impart osteoinductivity to biomaterials, with the goal of accelerating healing process associated with musculoskeletal disorders [2, 22–26]. Thus, research into the application of drugs and bioactive substances in orthopedics is wide and growing rapidly. This further highlights the necessity of developing successful drug delivery systems for these musculoskeletal disorders.



**Fig. 7.1** Original research articles published between 1998 and 2017 by searching Web of Science using keywords “calcium phosphate cement” and “drug”

To successfully serve as a drug carrier, the vehicle material must be biocompatible, can incorporate drugs conveniently without destroying their activities, and degrade gradually. Importantly, it should control the rate of drug release in a desirable manner. CPCs can harden under physiological conditions, thus avoiding affecting the activities of many drugs that can be destroyed by harsh conditions (e.g., high temperature in ceramic sintering) [23]. Combined with versatility, biocompatibility, bioactivity, and tailorable biodegradability, CPCs are being increasingly explored as attractive candidates for orthopedic drug delivery [2, 23]. The concept of drug-loaded CPCs was first suggested by Chen and Monroe in 1991 [27]. Since that, numerous studies have demonstrated the feasibility of introducing drugs into CPCs, e.g., antibiotics, anti-inflammatory compounds, analgesic, anticancer drugs, proteins, growth factors, hormones, and Chinese medicines [2, 25, 28]. After simply mixing the drug with CPCs and subsequent setting, it readily forms a viscous moldable paste, which in some instances can be injected during surgery by using minimally invasive procedures [29, 30]. More importantly, CPC-based drug delivery can maximize the drug access to the target skeletal site while avoiding side effects associated with systemic administration [2]. To date, many studies have investigated incorporation of drugs in CPCs, and Fig. 7.1 depicts the number of research articles published between 1997 and 2016 related to drug-loaded CPCs retrieved by



searching Web of Science using keywords “calcium phosphate cement” and “drug.” The search shows a clear increasing trend between 2005 and 2014.

Different approaches have been explored to load drugs in CPCs. To fully utilize the advantages promised by this family of carriers, it is important to understand the effect of drugs on the microstructure, setting time, mechanical properties, and phase structure of CPCs. This review summarizes drug-loaded CPCs in terms of drug-loading approaches, physicochemical characteristics, drug-release kinetics, and medical applications. Challenges for future development of drug-loaded CPC products are also discussed.

## 7.2 Basic Concepts of CPCs

CPCs are composed of one or more kinds of CaP salts. When used, CPCs' powders are mixed with a liquid (e.g., phosphate buffer saline, deionized water, and blood serum) and then harden under the physical conditions [2]. Current CPCs use a variety of materials and proportions, resulting in different setting reactions, products, and physicochemical and biological properties.

In fact, the mineral in the bone is a poor crystalline carbonate and other substituent containing an analog of geologic apatite. Therefore, several substituents, both cations ( $\text{Mg}^{2+}$ ,  $\text{Sr}^{2+}$ ,  $\text{Fe}^{2+}$ ,  $\text{Zn}^{2+}$ ,  $\text{Na}^+$ ,  $\text{K}^+$ ) and anions ( $\text{CO}_3^{2-}$ ,  $\text{F}^-$ ,  $\text{HPO}_4^{2-}$ ,  $\text{H}_2\text{PO}_4^-$ ), are studied to be doped into CPCs to improve biocompatibility, antibacterial ability, and mechanical properties [1, 2]. Doping of some metal ions (e.g.,  $\text{Mg}^{2+}$ ,  $\text{Sr}^{2+}$ ,  $\text{Zn}^{2+}$ s) endows CaP the ability to stimulate osteoblast proliferation and differentiation and, thereby, bone formation. In addition, CPCs doped with antibacterial ions, e.g.,  $\text{Ag}^+$ ,  $\text{Zn}^{2+}$ , and  $\text{Cu}^{2+}$ , display excellent bactericidal effects. Substitution of  $\text{PO}_4^{3-}$  in the hydroxyapatite (HA) structure with anionic compounds has also been reported [1, 31, 32]. Table 7.1 lists the common raw materials for CPCs.

Broad possibilities to manipulate CPC compositions provide a unique opportunity to obtain materials with a wide range of physicochemical properties. Table 7.2 summarizes some typical CPC compositions and loaded drugs. The most adopted are  $\alpha$ -TCP-,  $\beta$ -TCP-, and DCP-based CaP materials, which have been demonstrated to be able to provide the suitable support for cells in a direct contact.

## 7.3 Preparation of CPCs for Drug Delivery Systems

Drug-loaded CPC delivery systems may be prepared by different approaches, primarily including blending with the powder and liquid phase, entrapment of encapsulated drug carriers, and chemical binding of drugs [2, 34, 35, 38, 39, 42, 44, 48, 49, 52–57]. The most convenient approach is directly blending; however, this often results in a heavy initial burst release. The other approaches were developed to overcome this limitation and produce a more sustained drug release. Various approaches

**Table 7.1** Various raw materials used for preparing CPCs as drug delivery systems

Phase name (most common)	Acronym	Chemical formula
Hydroxyapatite	HA or HAP	$\text{Ca}_{10}(\text{OH})_2(\text{PO}_3)_6$
Alpha, beta-tricalcium phosphate	$\alpha$ -TCP/ $\beta$ -TCP	$\alpha/\beta\text{-Ca}_3(\text{PO}_4)_2$
Tetracalcium phosphate	TTCP	$\text{Ca}_4(\text{PO}_4)_2\text{O}$
Dicalcium phosphate anhydrate	DCPA	$\text{CaHPO}_4$
Dicalcium phosphate dihydrate (brushite)	DCPD	$\text{CaHPO}_4 \cdot 2\text{H}_2\text{O}$
Monocalcium phosphate monohydrate	MCPM	$\text{Ca}(\text{H}_2\text{PO}_4)_2 \cdot \text{H}_2\text{O}$
Monocalcium phosphate anhydrate	MCPA	$\text{Ca}(\text{H}_2\text{PO}_4)_2$
Calcium carbonate	–	$\text{CaCO}_3$
Calcium-deficient hydroxyapatite	CDHA	$\text{Ca}_x\text{H}_y(\text{PO}_4)_z \cdot n\text{H}_2\text{O}$ , $n=3\text{--}4.5$
Amorphous calcium phosphate	ACP	$\text{Ca}_{10-x}(\text{HPO}_4)_x(\text{PO}_4)_{6-x}(\text{OH})_{2-x}$ ( $0 < X < 1$ )
Farringtonite	–	$\text{Mg}_3(\text{PO}_4)_2$
Calcium sulfate hemihydrate	CSH	$\text{CaSO}_4 \cdot 1/2\text{H}_2\text{O}$
Calcium pyrophosphate	–	$\text{Ca}_2\text{O}_7\text{P}_2$
Magnesium-doped $\beta$ -tricalcium phosphate	Mg- $\beta$ -TCP	$\beta\text{-Ca}_{2.96-x}\text{Mg}_x(\text{PO}_4)_2$

are associated with different loading efficiencies, which also affect subsequent drug release. In addition, various drugs may affect the physical and chemical properties of CPCs (e.g., mechanical strength, porosity, and setting time), handling characteristics (e.g., injectability and cohesion behavior), phase composition, and degradability.

### 7.3.1 Blending

#### 7.3.1.1 Addition to Powder Phase

Earlier studies incorporated drugs to CPCs by mixing with the powder phase through ball milling or manual milling. By this approach, Otsuka et al. developed CPCs containing a variety of drugs (e.g., indomethacin, bovine insulin, and bovine albumin). The pristine CPCs were based on an equimolar mixture of tetracalcium phosphate and dicalcium phosphate [35, 52]. The powder transformed into HA cement after mixing with a dilute phosphoric acid solution. The drug was embedded in the set mass, forming a homogeneous drug-loaded material [35, 52].

Otsuka et al. also prepared a self-setting bioactive cement based on  $\text{CaO-SiO}_2\text{-P}_2\text{O}_5$  glass [34]. Glass powders containing 2% and 5% indomethacin hardened within 5 min after mixing with a phosphate buffer [34]. Ding et al. develop an injectable cement based on  $6\text{Na}_2\text{O-8K}_2\text{O-8MgO-22CaO-54B}_2\text{O}_3\text{-2P}_2\text{O}_5$  borate

**Table 7.2** Common CPCs with various compositions to be used as drug delivery systems

Solid phase	Liquid phase	Drug loaded	Refs.
HAp, $\alpha$ -TCP	0.5 M $\text{Na}_2\text{HPO}_4$ , 0.5 M $\text{NaH}_2\text{PO}_4$ solutions	Vancomycin	[33]
CaO-SiO <sub>2</sub> -P <sub>2</sub> O <sub>5</sub> glass	PBS	Indomethacin, cephalexin	[34]
TTCP, DCPD, HAP	H <sub>3</sub> PO <sub>4</sub>	Indomethacin	[35]
$\beta$ -TCP, MCPM	Citric acid and polyacrylic acid	Chlorhexidine diacetate	[36]
HA/CS composite particles, Ca(OH) <sub>2</sub> , CaCO <sub>3</sub> , NaHCO <sub>3</sub>	Citric acid, acetic acid, NaH <sub>2</sub> PO <sub>4</sub> , CaCl <sub>2</sub> , poloxamer	Lysostaphin	[37]
6Na <sub>2</sub> O-8K <sub>2</sub> O-8MgO-22CaO-54B <sub>2</sub> O <sub>3</sub> -2P <sub>2</sub> O <sub>5</sub>	Chitosan, citric acid, glucose	Vancomycin	[38]
$\alpha$ -TCP, DCPA, CaCO <sub>3</sub> , HA, SrCO <sub>3</sub> , Sr-HA	Disodium hydrogen phosphate ( $\text{Na}_2\text{HPO}_4$ ) solution	Sr <sup>2+</sup>	[39]
Porous biphasic CaP granules, Calcium sulfate hemihydrates	Water/normal saline	Vancomycin hydrochloride and tobramycin sulfate	[40]
Mg <sub>3</sub> (PO <sub>4</sub> ) <sub>2</sub>	1% of hydroxypropyl methyl cellulose (HPMC, sigma) dissolved in 30% ethanol	Lysozyme	[41]
$\beta$ -TCP, MCPM	Deionized water	Gentamicin sulfate	[42]
$\alpha$ -TCP, CSH	4 wt.% $\text{Na}_2\text{HPO}_4$ solution	Ibuprofen	[43]
$\alpha$ -TCP, DCPA, pHA	2 wt.% $\text{Na}_2\text{HPO}_4$ solution	Paclitaxel	[44]
$\beta$ -TCP, MCPM, Na <sub>4</sub> P <sub>2</sub> O <sub>7</sub> , SPP,	Deionized water or hydrolyzed simvastatin solution	Simvastatin	[45]
CaCO <sub>3</sub> , MCPM, sodium alginate	1 M $\text{Na}_2\text{HPO}_4$	Gentamicin sulfate	[46]
DCPA, $\beta$ -TCP, MCPM, TTCP, CaCO <sub>3</sub>	Deionized water	Antibiotics (gentamicin sulfate and neomycin sulfate separately)	[47]
$\beta$ -TCP, $\alpha$ -TCP, DCHA, Ga-doped CDA, DCPA, HPMC	0.5 wt.% $\text{Na}_2\text{HPO}_4$ aqueous	Ga <sup>3+</sup>	[48]
$\alpha$ -TCP, DCPA, pHA	2.5 wt.% $\text{Na}_2\text{HPO}_4$ solution	Simvastatin	[49]
$\alpha$ -TCP, DCPD, MCPH, CDA	5 wt.% $\text{Na}_2\text{HPO}_4$ solution	Alendronate (AL)	[50]
CaCO <sub>3</sub> , DCPD	9 wt.% SF aqueous solution	Sodium fusidate	[51]

bioglass [38]. Borate bioglass particles were mixed with vancomycin powders, which bonded together after mixing with a liquid containing chitosan, citric acid, and glucose in the mass ratio 1:10:20 [38].

Inorganic ions with physiological functions (e.g., Mg<sup>2+</sup>, Sr<sup>2+</sup>, Ag<sup>+</sup>, and Ga<sup>3+</sup>) were incorporated into raw materials of CPCs by chemisorption or doping (substitution of Ca<sup>2+</sup>) [1, 31, 32, 39, 48, 53]. Sr<sup>2+</sup>, known to stimulate bone formation and used in systemic osteoporosis therapies, were incorporated into an HA-forming CPCs via

two simple approaches: incorporation of strontium carbonate crystals and substitution of  $\text{Ca}^{2+}$  by  $\text{Sr}^{2+}$  ions during cement setting [39]. Different options were explored to incorporate  $\text{Ga}^{3+}$ , a known bone resorption inhibitor, into apatitic CPCs. These ions were either chemisorbed onto calcium-deficient apatite (CDA) or inserted in the lattice of  $\beta$ -TCP [48, 53]. A new Ag-doped bioactive glass (Ag-BG) was incorporated into flowable dental composites to fabricate a new material combining bioactive and antibacterial properties [54]. Ag-BG was synthesized based on a sol-gel technique through incorporating  $\text{Ag}^+$  into the sol-gel bioactive glass in the solution stage. The resulting composite solution underwent a specific heat treatment: aging at 60 °C, drying at 180 °C, and final stabilization at 700 °C. The final sol-gel-derived Ag-BG was in the system  $\text{SiO}_2$  58.6-CaO 24.9- $\text{P}_2\text{O}_5$  7.2- $\text{Al}_2\text{O}_3$  4.2- $\text{Na}_2\text{O}$  1.5- $\text{K}_2\text{O}$  1.5- $\text{Ag}_2\text{O}$  2.1 wt.% [54].

Besides the blending with CaP and drugs, some studies also immobilized or adsorbed drugs on the CaP powder. Alendronate (AL)-doped CDA was obtained by suspending the desired CDA (1 g) in an ultrapure water solution of AL and was mechanically slowly rotated (16 rpm) for 5 days. After centrifugation, the solid was filtered and washed with ultrapure water and allowed to dry at room temperature. Cement samples were prepared by mixing solid phase with  $\text{Na}_2\text{HPO}_4$  aqueous solution. The composition of the solid phase is 78 wt.%  $\alpha$ -TCP, 5 wt.% DCPD, 5 wt.% monocalcium phosphate monohydrate ( $\text{Ca}(\text{H}_2\text{PO}_4)_2 \cdot \text{H}_2\text{O}$ ), 10 wt.% of CDA partially loaded with AL, and 2 wt.% hydroxypropyl methylcellulose [50].

### 7.3.1.2 Addition to CPC Paste or Liquid Phase

Drugs, especially aqueous soluble ones, can be easily added to CPCs paste or liquid phase to produce CPCs containing homogeneously distributed drugs. Otsuka et al. mixed bioactive bone cement powders with a phosphate buffer, and drug powders were mixed with the paste to prepare homogeneously drug-loaded CPCs [55]. Sugo et al. incorporated antibiotic drugs (vancomycin hydrochloride and gentamicin sulfate) by mixing the drug with the paste [56]. Brushite CPCs containing gentamicin were obtained by dissolving the drug in water before mixing with the powder phase [42]. Similarly, powdered zoledronate, an anti-osteoporotic drug, was dissolved in water before mixing with CPC powders to obtain CPCs containing zoledronate [57]. Furthermore, the introduction of an antibiotic, sodium fusidate (SF), into the liquid phase of calcium carbonate-calcium phosphate ( $\text{CaCO}_3$ -CaP) bone cement was studied by Noukrati et al. [51].

Nonaqueous soluble drugs were generally loaded in CPCs by dissolution in organic solvents before mixing with the liquid phase. For example, paclitaxel was dissolved in dimethyl sulfoxide (DMSO) and subsequently diluted in Dulbecco's Modified Eagle Media (DMEM) [44]. The solution was pipetted on the top of the CPC disks, and the liquid was allowed to be adsorbed for 30 min to accomplish drug loading [44].

### 7.3.2 *CPC-Based Composite*

Numerous studies introduced organic or inorganic materials into CPCs as additives to further control the drug release. Examples include chitosan, hyaluronan, poly(lactic-co-glycolic acid) (PLGA), and poly( $\epsilon$ -caprolactone)-co-polyethylene glycol (PCL-co-PEG). These polymers were added in CPCs either by blending or as microsphere, fibers, or coating on the CaP particles [37, 40, 46, 49, 58–66]. Other inorganic materials were also explored as carriers for loading drug (e.g., carbon nanotubes and biodegradable microsphere) [33, 47, 67–69]. Following their introduction, the drug release profiles were modified significantly.

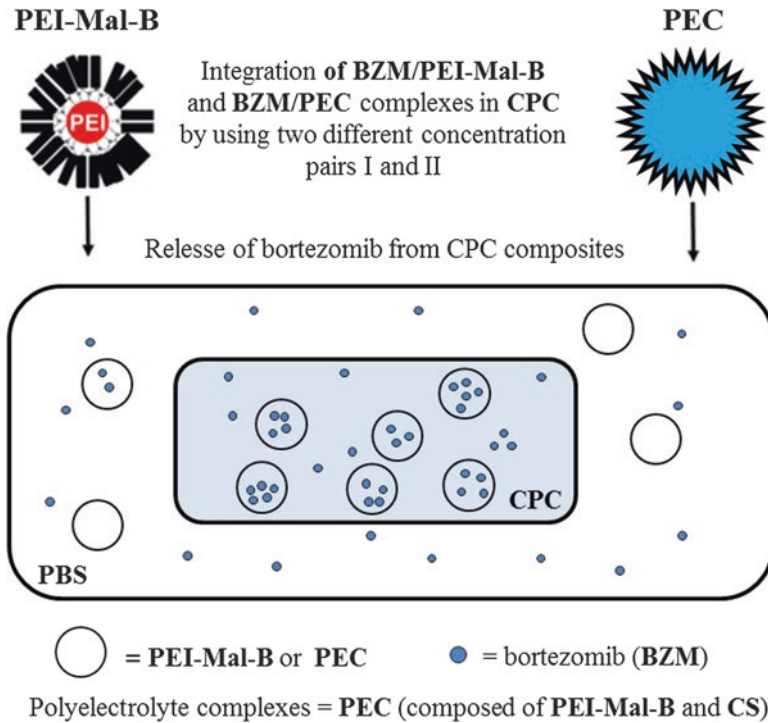
#### 7.3.2.1 *CPC/Polymer Composites*

Human bone is a composite of inorganic and organic components mainly composed of poorly crystallized and ion-substituted HA and collagen. Therefore, various biocompatible polymers were composited with CaP-based materials to mimic the human bone. For drug-delivering CPCs, these polymer additives also act as modifiers to control drug release [58].

$\beta$ -TCP and a thermoresponsive hyaluronan hydrogel were mixed to form a paste and further blended with 0.1% bovine serum albumin (BSA) solution containing the hyaluronan to produce a CPCs [59]. Xue et al. developed a lysostaphin-loaded, control-released porous bone cement [37]. The cement samples were made through cementitious reactions by mixing solid powder, mixture of HA/chitosan particles, lysostaphin,  $\text{Ca}(\text{OH})_2$ ,  $\text{CaCO}_3$ , and  $\text{NaHCO}_3$ . The mixture was set with a liquid containing citric acid, acetic acid,  $\text{NaH}_2\text{PO}_4$ ,  $\text{CaCl}_2$ , and poloxamer [37]. Chen et al. compared physicochemical properties and in vitro release behaviors of gentamicin-loaded CPCs with and without alginate [46]. The rate of gentamicin release from CPCs was retarded by the presence of alginate. The addition of gentamicin did not impair cell viability, and alginate actually enhanced the cell viability. Therefore, this CPC composite was not only useful as a source for antibiotic delivery but may also improve bone regeneration [46].

More complex and functional polymers are used to be prepared as nano- or microsphere or fiber for addition in CPCs to load and control the release of drugs. Striegler et al. presented two novel drug delivery systems (DDS), a weakly cationic dendritic glycopolymer and a cationic polyelectrolyte complex, composed of dendritic glycopolymer and cellulose sulfate, for the proteasome inhibitor bortezomib (BZM) [60]. Both DDS are able to induce short-term retarded release of bortezomib from CPCs in comparison to a burst release of the drug from CPCs alone. The schematic approach released BZM from various DDS/CPCs which is shown in Fig. 7.2. In addition, biocompatibility of CPCs, modified with the new drug delivery systems, was investigated using human mesenchymal stromal cells [60].

He et al. developed platelet-rich plasma (PRP)-PLGA/CPC composite scaffold [61]. It is prepared by incorporating PRP into PLGA/CPC scaffold with unidirectional



**Fig. 7.2** Schematic approach of the determination of BZM released from various DDS/CPC composites in PBS at pH 7.4. The same concentration pairs for BZM-/maltose-modified hyperbranched poly(ethylene imine) (PEI-Mal-B) and BZM/PEC complexes were used to prepare CPC composites: (i) concentration pair I with BZM/PEI-Mal-B 50 mg/100 mg and 100 mg/100 mg; (ii) concentration pair II with BZM/PEI-Mal-B 100 mg/100 mg and 100 mg/200 mg. Both drug carriers, PEI-Mal-B and PEC, possessed a cationic surface charge. Polyelectrolyte complexes consisted of PEI-Mal-B and CS (Modified from Ref. [60])

pore structure, which is fabricated by the unidirectional freeze casting of CPC slurry and the following infiltration of PLGA. The incorporation of PRP into scaffold showed more outstanding improvement in osteogenesis as the scaffolds were used to repair the segmental radial defects, especially at the early stage [61]. Babo et al. added platelet lysate (PL)-loaded hyaluronic acid (HAC) microparticles to CPCs to improve the degradation and biological performance [62]. Moreover, CPCs directly incorporating PL were also prepared. CPCs incorporating PL (with or without HAC microparticles) gave sustained PL release for 8 days. Moreover, the incorporation of HAC microparticles largely increased the loading ability and the sustained release of PL and significantly improved total porosity, interconnectivity, and weight loss of the cement structures [62]. Loca et al. prepared  $\alpha$ -TCP-based CPC modification with vancomycin-loaded poly(lactic acid) (PLA) microcapsules [33]. It was found the initial burst release of drug decreased down to 7.7%, with only 30.4% of drug transferred into medium over 43 days. In contrast, in pure vancomycin-loaded CPCs

(without microcapsules), 100% drug release occurred in 12 days [33]. Paraben nanoparticles were also used as antimicrobial compound in bone cements. They were embedded in various types of bone cements (poly(methyl methacrylate) [PMMA], hydroxyapatite, and brushite) [63].

Large osseous defects remain a difficult clinical problem in orthopedic surgery owing to the limited effective therapeutic options, and bone morphogenetic protein-2 (BMP-2) is useful for its potent osteoinductive properties in bone regeneration. Wu et al. reported a strategy to achieve prolonged duration time and help inducing new bone formation by using water-soluble polymers as a protective film [64]. In their study, CPC scaffolds were prepared as the matrix and combined with sodium carboxymethyl cellulose (CMC-Na), hydroxypropyl methylcellulose (HPMC), and polyvinyl alcohol (PVA) to prevent the digestion of the loaded recombinant human bone morphogenetic protein-2 (rhBMP-2). After implantation in mouse thigh muscles, the surface-modified composite scaffolds induced evident ectopic bone formation. A rabbit radius critical defect model indicated that the modified CPC scaffold may be the optimum combination for segmental bone regeneration [64]. Wang et al. also explored long hydrogel fibers encapsulating stem cells embedded in CPC scaffold for bone tissue engineering [65].

In addition, adsorption is generally used to load drug in CPC/polymer composites. Canal et al. investigated the use of biocompatible plasma polymers to provide a tool for controlled drug release from drug-loaded CaP scaffolds with complex surfaces and intricate 3D structures [49]. Two CaPs displaying great differences in microstructure were selected: low-temperature CaP (calcium-deficient HA cement, CDHA) and sintered CaP ceramic ( $\beta$ -TCP). PCL-co-PEG copolymer was deposited on CaPs by a low-pressure plasma process. The coating covered the micro- and nano-pores of the CaP surface and produced complex geometries presenting a nano- and micro-sized rough morphology, which produced a low wettability despite the hydrophilic nature of the copolymer. Simvastatin acid (SVA, a potential osteogenic and angiogenic drug) incorporation was accomplished by immersion in 200 mg SVA/mL solution. Plasma coating with PCL-co-PEG on scaffolds loaded with SVA delayed and modulated the drug release from the bone scaffolds depending on the thickness of the PCL-co-PEG deposited [49]. Mistry et al. soaked porous biphasic CaP granules (BCP) in solutions of vancomycin or tobramycin. Then, the granules were encapsulated separately with a 2.5% (w/v) PLGA solution and mixed with  $\alpha$ -CSH to form a gypsum cement carrying antibiotic-loaded granules. The cement was settable upon mixing with water or normal saline [40].

In another study, collagen membrane was used to wrap around CPCs containing methotrexate to reduce the side effects on soft tissue healing. Significantly improved healing was seen in samples wrapped by membrane compared to those without wrapping [66].

### 7.3.2.2 CaP/Inorganic Composite

Some inorganic vehicles are developed for loading drugs to incorporate into CPCs. Halloysite nanotubes (HNTs) are double-layered aluminosilicate tubes found naturally as raw mineral deposits [47]. When dehydrated 15–20 clay layers, they form a hollow tubule capable of hosting drugs. Using vacuum loading technique, HNTs were loaded with gentamicin and neomycin. Loaded HNTs were then mixed with different formulations of CaPs before setting with a liquid phase. Addition of HNTs to CPCs increased the compressive and flexural strengths, and gave sustained release profiles [47]. Mesoporous silica beads containing an iron oxide core were produced to enhance bone magnetic resonance (MR) contrast. The beads were functionalized with silane linkers for anchoring BMP-2 and further coated with CaP before embedding in CPCs [67].

Some metal ions with bioactivity have been added in CPCs. It is known that strontium increases the solubility of hydroxyapatite as well as exerts both anabolic and anticatabolic effects on bone. Therefore, tricalcium silicate ( $\text{Ca}_3\text{SiO}_5$ ) cement, a novel self-setting biomaterial, has been shown to exhibit good hydraulic properties and excellent bioactivity. Gentamicin sulfate was integrated into cement pastes. The results showed that the initial fast release of GS was restricted to a low level, and prolonged release of drugs was achieved in water and PBS. This prolonged GS release is attributed to the interaction of GS with the calcium silicate hydrate network and the formation of unique nano-to-microporous structure after hydration. The results suggested that  $\text{Ca}_3\text{SiO}_5$  cement might be used as bioactive bone implant materials with drug loading and prolonged release properties [68]. Lu et al. incorporate strontium into CPCs to accelerate the degradation rate and enhance the osteoconductivity. In conclusion, in the 10% Sr-CPC group, strontium exerts dual effects on CPCs: accelerating degradation rate and enhancing osteoconductivity both *in vitro* and *in vivo* [53]. A hollow mesoporous structure of silica ( $\text{SiO}_2$ ) microspheres was first synthesized and loaded with ibuprofen. Poly(1, 8-octanediol-co-citrate) (POC) and  $\beta$ -TCP, together with ibuprofen-loaded  $\text{SiO}_2$ , were fabricated by a 3D printing technique based on the freeform fabrication system with micro-droplet jetting (FFS-MDJ). The developed ibuprofen-loaded  $\text{SiO}_2/\beta$ -TCP/POC scaffolds presented a highly interconnected porous network and proper compressive modulus and biocompatibility. The result indicated that the present bone scaffold was promising for bone regeneration in the clinical case of infected bone defects [69]. A series of magnesium phosphate-modified CPCs (MCPCs) loaded with rhBMP-2 were prepared, and rhBMP-2 was physically absorbed onto MCPCs and dried overnight under vacuum. Results demonstrated that all MCPCs exhibited similar rhBMP-2 release rates and preserved comparable conformation and biological activity of the released rhBMP-2. Also, the ionic extracts of MCPCs made little difference to the bioactivity of rhBMP-2, either in soluble or in matrix-bound forms. *In vivo* results demonstrated a better bone regeneration capacity of rhBMP-2-loaded MCPCs containing 5% (w/w) magnesium phosphate. It provided a novel approach to addition of Mg in CPCs that tailored the way of rhBMP-2 bound on



MCPCs and thus facilitated the recognition of bone morphogenetic proteins (BMPs) to stimulate osteogenic differentiation [31].

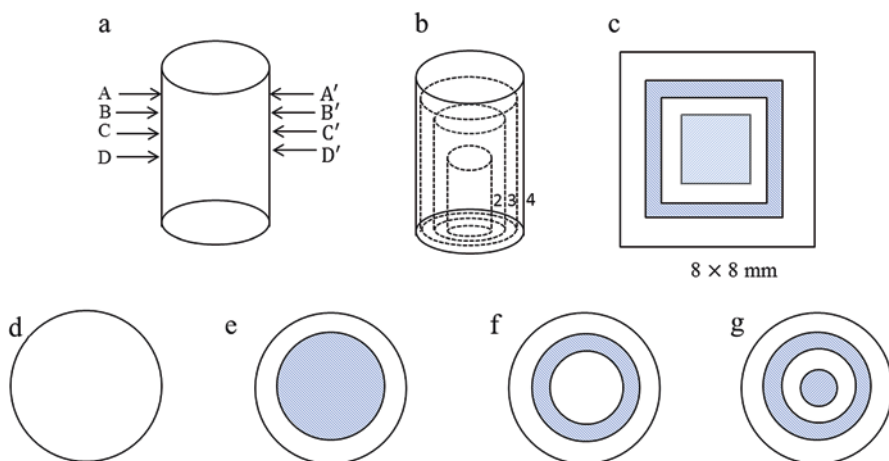
### 7.3.2.3 Dual or Multiple Drugs in CPCs

As known, many biomolecules are involved in the different processes of angiogenesis, inflammation, and tissue remodeling in a spatiotemporal manner. In addition, bone defect generally is associated with various bone disease, infection, tumor, and osteoporosis. Therefore, concurrent administration of multiple drugs counteracting infection, tumor, and osteoporosis is employed in clinics [70]. These biomolecules or drugs must have a specific localization and orchestration in order to guide a specific pathway. The use of a single biomolecule or drug via a delivery system would be insufficient for promoting such a complex regeneration process. To date, many studies fabricate the suitable vehicles with the ability to deliver multiple drugs or growth factors with different kinetics, which are considered to have more potential for mimicking or treating complex clinical situations [71–73].

Huang et al. prepared a dual-drug release system comprising of icariin, a flavonoid isolated from *Herba epimedii*, vancomycin, and CPCs [74]. The sample was filled in *Staphylococcus aureus*-contaminated bone defects in rabbits. Twelve weeks after filling, the defects healed completely with significantly improved formation of lamellar bone and recanalization of the marrow cavity compared with blank controls. These results demonstrate that this dual-drug release system has potential for the treatment of contaminated bone injury or infectious bone disease [74]. In a study by Lin et al., simvastatin and collagenase were loaded in CPCs for dental pulp applications [75]. Simvastatin can stimulate the differentiation of dental pulp stem cells. Collagenase is a matrix metalloproteinase (MMP) capable of removing the extracellular matrix and then allowing cells to return to the progenitor state. The collagenase and simvastatin were released via the micro-pinhole channels in the cement to regenerate dental pulp stem cells and stimulate the differentiation of pulp cells [75].

Geffers et al. prepared dual-mechanism-setting cement combining a brushite-forming cement paste with an inorganic silica-based precursor [76]. Materials were obtained by pre-hydrolyzing tetraethyl orthosilicate (TEOS) following addition of CPC powders (mixture of  $\beta$ -TCP and monocalcium phosphate). Cement setting occurred via a dissolution-precipitation process, and changes in pH during setting initiated the condensation of the hydrolyzed TEOS, producing an interpenetrated composite with an excellent mechanical strength. Additionally, the composite with the highest silicate content showed a similar cell proliferation to HA and a significantly higher activity per cell [76].

To address chronic osteomyelitis, Wu et al. manufactured implants carrying levofloxacin (LVFX) and tobramycin (TOB) with a multilayered structure by three-dimensional (3D) printing technology (Fig. 7.3) [77]. The implant exhibited a sustained and programmed drug release. The two drugs were found to act collaboratively in pharmacodynamic action [77].



**Fig. 7.3** The schematic illustration of the multidrug implant: (a) the external appearance; (b) three-dimensional perspective drawing; (c) longitudinal section; (d) cross sections AA'; (e) cross sections BB'; (f) cross sections CC'; (g) cross sections DD'. The four layers of the concentric rings were composed from the center to the periphery. The first and third layers (the *blue* part) contained LVFX, and the second and fourth layers (the *white* part) contained TOB (Modified from Ref. [77])

#### 7.3.2.4 3D Printing

Recently, addition manufacturing technologies are increasingly used for healthcare. Firstly, Gbureck et al. investigated the adsorption-desorption kinetics of antibiotics to microporous bioceramics manufactured by a low-temperature 3D powder printing process [78]. 3D printing CaP samples were immersed in the solution of dissolved antibiotics [78]. Vorndran et al. utilized a multijet 3D rapid prototyping machine to manufacture bioceramic implants while simultaneously depositing bioactive compounds with high spatial accuracy for localized delivery [79]. Solution of drugs and binder, stored in separate reservoirs, was injected in a controlled manner by software. Homogeneous, localized polymer incorporation during printing allowed the drug release kinetics to be retarded from first to zero order over a period of 3–4 days [79]. Lee et al. produced 3D porous magnesium phosphate (MgP) scaffolds with high drug load/release efficiency using a paste-extruding deposition (PED) system and cement chemistry [40]. Lysozyme was dissolved in 1% hydroxypropyl methylcellulose solution and blended with MgP powders to form a paste. In another implementation, the MgP scaffold was placed in 2 mL of PBS containing lysozyme (1 mg/mL) to allow adsorption [40]. Wu et al. confirmed that it was feasible and convenient to fabricate a multidrug implant with a complex construction by 3D printing technology (Fig. 7.3). The multidrug implant had a sustained and programmed drug release property. LVFX and TOB which were released from the multidrug implant worked in tandem to enhance pharmacodynamic action which was similar to a tumor chemotherapy program and was sufficient to treat chronic osteomyelitis [77]. Inzana et al. fabricated dual antibiotic (rifampin and

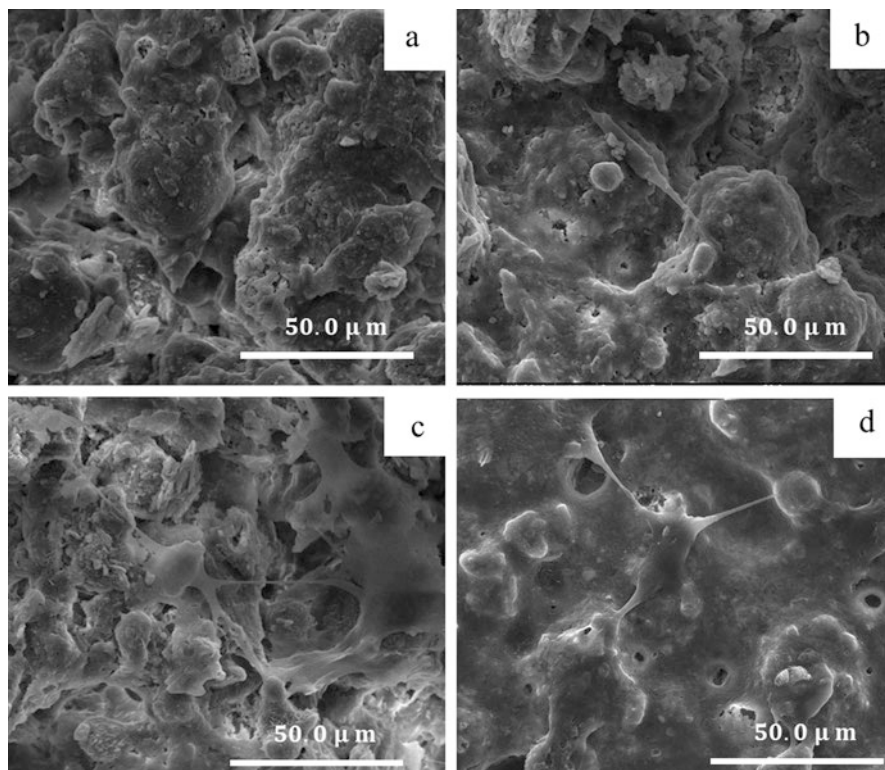
vancomycin) CaP scaffolds by 3D printing [80]. A phosphoric acid-based solution was selectively sprayed rastering over a layered bed of  $\alpha$ -TCP powders to initiate a dissolution-precipitation reaction. Repeated layer-by-layer binding formed the 3D scaffold. Drug loading was performed by premixing vancomycin or rifampin with the  $\alpha$ -TCP powders. Alternatively, it was accomplished by infusing an antibiotic solution in the scaffold [80]. Akkineni et al. fabricated CPC scaffolds by 3D plotting using water-immiscible carrier liquid. BSA and vascular endothelial growth factor (VEGF) were encapsulated in polymer microparticles and then mixed into the CPC paste [81].

### 7.3.3 *Extract of Herb or Chinese Medicine*

To improve the bone repair capability of bone scaffolds (e.g., CPCs), osteoinductive agents, e.g., growth factors and biological molecules, are usually loaded. However, the high cost and rapid degradation of such expensive GFs limit their widespread use, particularly in clinics. Therefore, there is an urgent need to develop alternative osteogenic products or drugs with higher efficacies and lower costs than GFs. Some herbal medicines have been widely used in the treatment of fractures and bone disorders for thousands of years in Asia [82]. The basic principles of traditional Chinese medicine for treating bone injuries are enhancing blood circulation, nourishing energy, and invigorating the kidney which regulates bone formation.

Icariin (IC) is a flavonoid isolated from *Herba epimedii*. IC and vancomycin are dissolved into ethanol- and phosphate-buffered solution (PBS, pH 8.0), respectively [74]. Then CPC powders were added into the mixture of IC-VA solution, subsequently casted and freeze-dried to obtain IC-VA/CPC composite [74]. In vivo results demonstrated that this dual-drug release system, with its concomitant antibiotic and osteoinductive properties, showed significant potential for the treatment of contaminated bone injury or infectious bone disease [74]. Danggui Buxue Tang (DBT) is a traditional Chinese herbal decoction containing *Radix Astragali* and *Radix Angelicae sinensis* [83]. Pharmacological results have indicated that DBT can stimulate bone cell proliferation and differentiation. DBT was incorporated into porous composites (GGT) of genipin-crosslinked gelatin and  $\beta$ -TCP as bone substitutes (GGTDBT). In vivo results revealed that the GGTDBT stimulated the innate regenerative capacity of bone, supporting their use in bone tissue regeneration [83]. Xu Duan (XD), traditional Chinese medicine for hundreds of years as an anti-osteoporotic, tonic, and antiaging agent, was incorporated into  $\beta$ -TCP/calcium silicate (CS). In vitro cell experiments showed that the amount of cells and osteogenesis protein was stimulated by XD released from  $\beta$ -TCP/CS composites [84, 85]. The present drug release strategy with CS-based cements may pave the way for future alternative bone repair therapy.

Qu et al. studied the effects of various Chinese medicines (xiangdan injection and drynaria) on the properties, such as setting, mechanical strength, and composition of CPCs. In vitro release of Chinese medicine increased with the increasing



**Fig. 7.4** SEM images of osteoblasts cultured on CPCs loaded with drynaria for 3 days. (a) CPC, blank; (b) CPC, 5% drynaria; (c) CPC, 10% drynaria; (d) CPC, 15% drynaria (Modified with permission from Ref. [87])

concentration of Chinese medicine in CPCs accompanied with the initial burst release, which was fit to the Higuchi's diffusion-controlled model. The effect of drynaria-loaded CPCs on osteoblasts was time and dose dependent (Fig. 7.4). CPCs loaded with 5 wt.% and 10 wt.% drynaria significantly promoted osteoblast proliferation after culture for 5 days [86, 87]. This CPC-loaded Chinese medicine may provide the promising candidate for bone graft.

## 7.4 Characterization of Drug-Loaded CPCs

### 7.4.1 Mechanical Properties

Mechanical properties are important considerations in the development and application of CPCs. As we expect for ceramics, CPCs are intrinsically brittle materials and thus not suitable for bearing major loads or complex stresses (e.g., severe tension

and torsion) [14]. Nevertheless, it is still desirable that CPCs can match the host bone in such mechanical properties as strength and elastic modulus. As a reference, the compressive strength of the human trabecular bone ranges approximately 4–12 MPa and cortical bone 130–180 MPa [88, 89].

A large number of studies have investigated the mechanical properties of blank and drug-loaded CPCs, and most studies evaluated compressive strengths because of the technical difficulty of reliably measuring the tensile strengths of CPCs [28, 90, 91]. Materials science teaches that the strength of a material is critically dependent on its microstructural characteristics such as porosity, grain size, crystal geometry, and the nature of defects. Therefore, the effects (or non-effects) of a drug on the compressive strength of its CPC matrix must be understood from the perspective of structure-property relations. Furthermore, it should be noticed that, strength is not an intrinsic property; instead, it is sensitive to experimental conditions such as sample geometry (e.g., size, height/diameter ratio), displacement rate, and defects (e.g., density and geometry of microcracks) before testing. Therefore, caution should be taken when comparing results from different studies.

Driven by a strong demand of skeletal infection control, numerous studies have investigated loading antibiotics in CPCs. Joosten et al. [92] added gentamicin at 16–32 mg/g to a commercial CPC product-based equimolar mixture of ACP and DCP, which hardens to form microporous HA. They tested the compressive strengths after hardening for 4 and 24 h. It was found that, compared with the blank cement (4 h: 5.2 MPa, 24 h: 7.7 MPa), all gentamicin-loaded samples exhibited only minor variations (generally  $\leq 1\%$ ) in compressive strength at 4 h and 24 h regardless of the drug concentration. Similarly, Hofmann et al. reported that addition of up to 2 wt% ciprofloxacin to a cement had no significant effect on the compressive strength. Typically, this non-effect may suggest a lack of substantial interactions between the drug and the hardened cement particles. These behaviors appear to be explained by the molecular structures of gentamicin and ciprofloxacin, which lack sufficient groups allowing bonding to  $\text{Ca}^{2+}$  on CaP particles [93]. Stigter et al. studied the interactions of seven antibiotics with HA and found that molecules carrying abundant carboxyl groups are more effectively incorporated in HA, presumably by complexing  $\text{Ca}^{2+}$  on their surface [94]. McNally et al. observed a different behavior of gentamicin-loaded CPCs [95]. They incorporated the drug in another commercial CPCs at 3% and tested samples after hardening for 24 h and 48 h in PBS. The gentamicin-loaded cement exhibited compressive strengths of 7.89 MPa at 24 h and 9.91 MPa at 48 h, both significantly higher than those recorded from the blank cement (5.55 MPa at 24 h and 3.87 MPa at 48 h). The strength of the blank cement decreased between 24 and 48 h obviously because samples were hardened in PBS (instead of air), experiencing dissolution of bonds between CaP particles [95]. Interestingly, the gentamicin-loaded samples reversed this strength decay, indicating that gentamicin effectively prevented this dissolution. This would suggest substantial interactions between gentamicin and the cement [95]. However, the study did not report morphological or structural characteristics of the CPCs; therefore, it is unclear whether these different behaviors were attributable to differences in cement composition, microstructure, or other experimental conditions. Nevertheless,

compressive strengths of CPCs in physiological status may provide potentially relevant information regarding their behaviors *in vivo*.

Other studies incorporated drugs with well-known strong interactions with CaPs in CPCs. Examples include tetracycline (a wide spectrum antibiotic) and bisphosphonates (a family of potent anti-osteoporotic compounds). Ratier et al. added tetracycline at 0–1% to the solid phase of a commercial CPCs based on tetracalcium phosphate (TTCP) and  $\alpha$ -TCP [96]. After air hardening for 1 h, samples were immersed in water for up to 21 days. Tests found that tetracycline reduced the compressive strength dose dependently and inhibited the hardening reaction strongly. Between 2 and 21 days, the strength of the blank cement varied only moderately (16.2–14.7 MPa), whereas the cement containing 1% tetracycline attained only 3.5 MPa on day 2 and subsequently increased to 6.7 MPa on day 21 [96]. This is readily explained by the strong adsorption of tetracycline on CaP crystals to block dissolution of the starting particles and growth of the product, preventing the formation of a satisfactorily cohesive structure [96]. Zhao et al. added 2–10% alendronate, the currently first-choice bisphosphonate drug used to treat osteoporosis, to the solid phase of CPCs based on TCP and TTCP [97]. After hardening for 24 h, all alendronate-loaded cements had significantly lower compressive strengths (range: 5.16–5.54 MPa) compared with the blank cement (13 MPa). It may be the reason that alendronate may have inhibited cementing product growth, but scanning electron microscopy (SEM) indicated that all hardened cements exhibited generally similar morphology [97]. Shen et al. similarly added alendronate at 0.1–3.0% to CPCs based on partially crystallized TCP and DCPA [98]. They found that addition of 0.1–1% alendronate, however, improved the compressive strength (31.62 MPa at 1%) compared with the blank (19.22 MPa), and further increase in alendronate fraction substantially reduced the strength to approaching the blank (17.57 MPa at 3%). According to the SEM images, alendronate reduced the crystal size of the cementing product to produce a more compact structure, and this effect was particularly evident at >1% alendronate [98]. Reduction of compressive strength was also reported for pamidronate, another bisphosphonate drug [99]. Collectively, these results indicate that the effects of drugs on mechanical properties of CPCs are highly dependent on the structural characteristics of the drugs and their concentrations. In some cases, the effects can be complicated and may involve more factors and structural features (e.g., interparticle bonding) that may be characterized at even smaller scales [99].

In addition to small antibiotics, studies also incorporated macromolecular drugs such as proteins and cytokines in CPCs for accelerating bone regeneration. Blom et al. incorporated human transforming growth factor- $\beta$ 1 (rhTGF- $\beta$ 1, co-dissolved in liquid with BSA) into CPCs based on  $\alpha$ -TCP and DCPA [100]. Mechanical testing was, however, performed on samples containing BSA alone, presumably because the rhTGF- $\beta$ 1 concentration was so low (vs. BSA) that its effect was deemed to be negligible. Nevertheless, the BSA-modified cement gave a significantly improved compressive strength only at 4 h (vs blank) during immersion in tissue culture fluid for 1 h to 8 weeks [100]. In addition to directly adding a biomolecular drug to CPCs, many studies pre-encapsulated the drugs in polymeric

microspheres before incorporating them in CPCs [81]. This was performed partly because cement setting creates a harsh environment (e.g., extreme pH, high ionic strength, and temperature elevation) easily causing denaturation-deactivation of biomolecules, and the microspheres would provide a physical barrier against these deleterious forces. In this microsphere-in-cement design, the mechanical properties are controlled by microspheres rather than the drug molecules.

### 7.4.2 Handling Properties

Besides the acceptable strength, a successful CPC product must have satisfying handling properties. Being self-settable and injectable are the two major advantages of CPCs; consequently, setting time and injectability are critical indicators of their handling properties [101].

Numerous studies have measured the initial and final setting times of CPCs by Gillmore needle method [102]. Frequently, drug introduction was found to delay CPC setting. Haghbin-Nazarpak et al. incorporated gentamicin in CPCs based on  $\beta$ -TCP [103]. It was found that the initial and final settings of the blank cement occurred at 8.5 and 23.5 min, respectively. When 8 mg gentamicin was added to the cement, they were accelerated to 5 min and 20 min, respectively. However, when the gentamicin dose was further increased to 16 and 24 mg, they were lengthened substantially, reaching  $\sim$ 20 min and  $>$ 40 min, respectively, at 24 mg [103]. The delayed setting at the higher doses was suggested to be attributed to the sulfate ions in gentamicin, while the significant decrease in setting at the low dose was not explained [103]. Alkhraisat et al. studied a  $\beta$ -TCP-based CPC and two Sr-doped counterparts set with doxycycline solutions [91]. The final setting of Sr-free CPCs was considerably delayed ( $\sim$ 12 min vs. 7.7 min) by doxycycline, but the samples did not follow a simple trend with the doxycycline concentration. In contrast, the final setting of Sr-doped counterparts was only slightly affected by doxycycline without a clear trend [91]. As would be expected, drugs interacting strongly with CaPs were found to substantially delay CPC setting. Alendronate addition (0–4.0%) increased the initial setting time from 9.3 to 17.3 min, and the final setting time from 29.3 to 44.2 min [97]. Pamidronate (1.0 mM in liquid phase) was observed to delay the initial and final setting of CPCs from 6 and 15 min to 10 and 27 min, respectively [99].

Injectability broadly indicates the handling performance during injecting a CPC through the syringe needle [101]. As opposed to setting times, no universal definition seems to have been given to injectability. Many studies measured by the force required to extrude CPCs from the syringe, and other weighed the percentage of mass extruded at a given pressure [33, 98]. However, these results reflect the flow property without caring for the quality of the extruded paste, such as liquid-solid separation during paste injection. Shen et al. reported that addition of 0.1–3.0% alendronate to CPCs improved the injectability (percentage of paste extruded a syringe needle in 2 min under 5 kg force) from  $\sim$ 70% to  $>$ 90% [98]. Haghbin-

Nazarpak et al. measured the injectability (force applied to drive paste flow) of gentamicin-loaded CPCs and did not notice major changes [33]. Injectability is intrinsically related to rheology, and small molecules are usually not strong modifiers of rheological properties [104]. This is analogous to the situation for OPC used in the construction industry, where rheological properties of cement slurry are routinely modified with polymers. For CPCs, as recently reviewed by Zhang et al., major factors affecting injectability are physical ones such as liquid/solid ratio, particle size distribution, particle morphology, and viscous component [104].

### 7.4.3 Release Kinetics

Release of drugs from CPCs can be affected by multiple factors, such as porosity of the CPCs, distribution of pore size, drug-CPC interactions, and CPC degradation [2]. However, in numerous studies, the release rate was found to follow Higuchi's Eq. 7.1 [28]:

$$Q = A \times M_0 \sqrt{(2C_0 - C_s) \times D \times C_s \times t} \quad (7.1)$$

where  $Q$  is the amount of drug released at moment  $t$ ,  $A$  is the surface area of the drug-releasing CPC sample,  $M_0$  is the total amount of drug,  $C_0$  is the initial concentration of the drug in the CPCs,  $D$  is the diffusion coefficient of the drug in the CPCs,  $C_s$  is the solubility of the drug in the CPC matrix, and  $t$  represents the time [28].

This famous equation was initially developed for the release of a drug from a polymer matrix based on the following assumptions: (1) the initial drug concentration in the matrix is higher than its solubility; thus, the drug is homogeneously dispersed in the matrix as solid particles; (2) the drug diffusion through the matrix is the rate-limiting step; (3) the diffusion coefficient of the drug is constant and independent of time or location; and (4) the matrix is not swelling or dissolving [105].

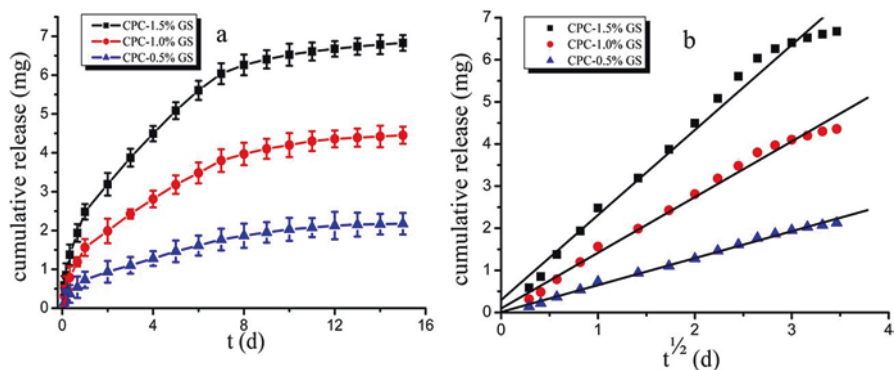
CPCs are intrinsically porous. The degree of porosity and characteristics of pores are also factors influencing drug release from CPCs. When pores in the matrix are taken in consideration, Eq. 7.1 is modified to Eq. 7.2 [28]:

$$Q = A \times M_0 \sqrt{(2C_0 - C_s) \times \frac{D\varepsilon}{\tau} \times C_s \times t} \quad (7.2)$$

where  $\varepsilon$  and  $\tau$  represent the porosity and tortuosity of the matrix, respectively.

Nevertheless, in both equations, the cumulative release ( $Q$ ) is proportion to the square root of time ( $t^{1/2}$ ). This relationship explains the ubiquitously observed biphasic release profile (fast initial release followed by a gradually slowed release toward a plateau, Fig. 7.5) in a large number of studies, as reviewed in other sections of this Chapter. Otsuka et al. [35, 52, 55] performed a series of studies on CPCs containing





**Fig. 7.5** (a) Cumulative release of gentamicin (GC) (0.5–1.5 wt.%) from CPC. (b) Same results plotted as cumulative release vs. square root of time (unpublished results)

a variety of drugs (e.g., indomethacin, bovine insulin, and BSA) and confirmed that the release rate was in accordance with Higuchi's equation.

As would be predicted by Higuchi's model, the porosity is a key influencing factor for the rate of drug release, and this has been confirmed by numerous studies. Otsuka et al. prepared CPC samples with a range of porosities by varying the liquid/solid ratio and found that the release rate increased progressively with the porosity [106]. Additionally, based on Eqs. 7.1 and 7.2, it may be tempting to think that drug release is independent of the chemistry of the drug or the material. However, careful observation indicates that this is incorrect, because the characteristics (e.g., solubility) of the drug and likely drug-material interactions may present additional kinetic limiting steps, violating the assumption (2) associated with Eq. 7.1. Under these conditions, drug release can be controlled by multiple factors. Yang et al. prepared CPCs containing 1% methotrexate (a nonaqueous soluble anticancer drug) and observed a continuous drug release lasting for 2–4 months, which is largely explained by the insolubility of this drug [107]. Zhao et al. reported that CPCs containing 2%, 5%, and 10% alendronate released only 33.2%, 24.4%, and 20.8% of the drug load over 21 days; this slow release is also attributed to the strong binding of phosphonate groups of the drug to  $\text{Ca}^{2+}$  on the surface of CPC particles [107]. Compared with organic polymers, drug incorporation in inorganic materials presents many challenges, such as the difficulty to tune their encapsulation properties and interactions with drugs. Despite this, Ghosh et al. recently discovered that the characteristics of the CPC powder, and drug-material interactions, can be used to tune the drug release behavior [108]. They synthesized two forms of HA that maintained their amorphous nature for different periods before final transformation to crystalline HA by controlling the precipitating conditions during synthesis [108]. The authors found that, by varying the ratios of the two forms in the CPCs, the release kinetics of vancomycin and ciprofloxacin were adjusted. Increasing the proportion of the form maintaining the amorphous state for a shorter period decreased the release rates for both drugs and vice versa [108]. These showed that, although

Higuchi's diffusion-controlled model dominates in the majority of cases, the drug release is controlled by additional factors, and innovation in materials development can open new opportunities in controlling drug release from CPCs.

## 7.5 Potential Applications of CPCs as Drug Delivery Systems

CPCs have been demonstrated to bond to bones and degrade progressively to allow substitution by newly formed bone tissue [2]. In many cases, it is developed in an injectable form to improve the ease of use and allow minimally invasive operations. Furthermore, CPC-based release systems can locally deliver drugs with improved bioavailability and controlled released profiles [2, 27]. Thus, the drug is retained locally at the site of implantation for a prolonged period to achieve desired purposes such as modulating the healing process [2, 27].

As mentioned above, drug release from CPCs implanted in vivo is generally believed to be Higuchi's diffusion-controlled model because the rate of CPC degradation is much lower than that of drug release [27]. Furthermore, drug release from the CPCs is affected by two major factors: the porosity of the CPCs and the characteristics of the drug incorporated [27]. Therefore, the use of CPCs in the musculoskeletal system for local-controlled drug release is an attractive option to accelerate bone fracture and defect healing. To date, in terms of the application of CPC-based drug release system, four major categories of CPC-based drug release systems have been developed for promoting bone regeneration, preventing bone infections, treating bone tumors, and managing osteoporosis. Furthermore, Ginebra et al. reviewed studies on CPCs as carriers for antibiotics, analgesics, anticancer, anti-inflammatory, and growth factors [2, 90].

### 7.5.1 Promotion of Bone Regeneration

A variety of growth factors have been found to stimulate bone regeneration and were therefore introduced into porous bioceramic scaffolds to enhance their osteoinductive and vascularization properties [109, 110]. Some extensively studied factors include bone morphogenic proteins (BMPs), transforming growth factors (TGFs), basic fibroblast growth factor (bFGF), insulin-like growth factor (IGF), and vascular endothelial growth factors (VEGFs) [27]. The same strategy has been applied to CPCs. Bose et al. reviewed approaches of delivering drugs and growth factors via various forms of CaP (particles, coatings, cements, scaffolds) for orthopedic and dental applications and then identified critical issues and challenges [25].

Ohura et al. incorporated BMP-2 to a resorbable CPC at two doses (1.26 or 6.28  $\mu\text{g}$ ) and implanted samples in critical-sized defects created in the femurs of rats [111]. Three weeks after implantation, samples carrying 6.28  $\mu\text{g}$  of recombinant human BMP-2 (rhBMP-2) resulted in osseous union; 9 weeks after implantation,

the experimental femurs recovered 99% of the failure torque and 141% of bone stiffness (vs. intact contralateral femurs), confirming an accelerated fracture consolidation [111]. Seeherman et al. performed a series of *in vivo* studies to compare the performances of different injectable CPC osteogenic factor combinations in large animal models [112–114]. Results showed that 10 weeks after operation, a commercial resorbable CPC carrying rhBMP-2 promoted bone healing in a nonhuman primate fibular osteotomy model. In their study, bone healing was accelerated by approximately 40%, as compared to untreated osteotomy sites [112–114]. Ventura et al. investigated the stages of bone healing of CPC scaffolds carrying BMP-2 with three controls (i.e., blank porous CPCs, dense CPCs, autografts) in a rat calvarial defect model by positron emission tomography (PET) and computed tomography [115]. Eight weeks after implantation, they recorded the highest  $^{18}\text{F}$  intensity in the BMP-2 group, followed by the controls (order: blank porous CPCs > dense CPCs > autograft). Histomorphometry (bone volume percentage) also indicated a significantly higher new bone formation in the BMP-2 group than the controls [115].

Kroese-Deutman et al. loaded rhBMP-2 on porous CPC disks and subcutaneously implanted them in the backs of rabbits for 10 weeks and found clear bone formation and vessel ingrowth into CPCs [116]. In comparison, no bone formation was found in blank CPC controls. No signs of CPC degradation were found, and all disks maintained their original shape and stability during the study [116]. Seeherman et al. loaded rhBMP-2 in CPCs at two levels (0.166 or 0.033 mg/mL CPCs) and injected samples into critical-size (20 mm) mid-diaphyseal defects in the radii or mature rabbits [117]. Eight weeks after operation, complete cortical bridging and reconstruction of the medullary canal were observed in all defects filled with CPCs containing 0.166 mg rhBMP-2/mL CPCs [117]. Link et al. mixed CPCs with gelatin microparticles containing TGF- $\beta$ 1 and injected the composite cement in circular defects in the femoral condyles of rabbits [118]. Twelve weeks after operation, defects filled with composite CPCs exhibited increased bone density, remodeling, and filler degradation [118].

Lee et al. also investigated CaP-alginate cement composites for drug delivery and tissue engineering applications [119]. They mixed a powder based on  $\alpha$ -tricalcium phosphate ( $\alpha$ -TCP) with a sodium alginate solution and injected the paste in a Ca-containing bath, forming submillimeter-diametered fibers. The fibers were subsequently press molded into different porous scaffolds with different porosities. Rat bone marrow-derived stromal cells (BMSCs) seeded on the scaffolds proliferated actively and permeated into the porous network, with the highly porous scaffolds exhibiting more favorable proliferation and osteogenic differentiation. Implantation of the porous scaffolds into rat calvarial defects for 6 weeks indicated bone formation inside scaffolds and a nearly complete defect closure [119]. Mause et al. studied CPC composite based on  $\beta$ -TCP for BMP-2 release [120]. CPCs containing rhBMP-2 (0.2 mg/cm<sup>3</sup>) were used to fill distal epiphyseal defects in bovine femurs, as compared with controls (i.e., autograft, blank TCP, unfilled defect). It was found that defects filled with blank TCP exhibited a significantly increased bone content compared with those filled with the composite or autograft. However,

the TCP/rhBMP-2 group showed significantly less cement particles compared with blank TCP, suggesting that incorporation of rhBMP-2 led to a faster remodeling of the defect [120].

In addition to drugs, cells actively participating in bone regeneration are another promising factor for incorporation in CPCs. Recently, Weir et al. studied the possibility of combining cells with CPCs [121]. They encapsulated human bone marrow-derived stromal cells (hBMSCs) in alginate hydrogel beads and then incorporated these beads in scaffolds prepared from CPCs, CPC composite reinforced with chitosan, and CPC composite reinforced with chitosan and polylactide-co-polyglycolide fibers. After cultured for 21 days, the percentage of viable cells and cell density inside CPC-based composites matched those in alginate without CPCs. Cells formed apatitic mineral deposits, indicating that CPC setting did not harm the viability and activity of hBMSCs encapsulated in the beads, and these composites may present an interesting option for bone regeneration [121]. Park et al. prepared CPC composites containing three different additives and/or viscosity modifiers (e.g., carboxymethyl cellulose, silk, and alginate) as vehicles for the delivery of cells (hBMSCs) and evaluated cell protection behaviors of the composites [122]. The CPCs modified with alginate produced the best cell proliferation, ALP and collagen production, and osteogenic transcript increase. These results suggested that, CPC-alginate composites may serve as delivery vehicles for cells involved in bone regeneration [122].

### 7.5.2 Bone Infection

Bacterial adherence and postoperative infection is one of the most frequent causes of bone implant failure. Local use of CPCs carrying antibacterial compounds has been proposed to control inflammatory response and reduce the risk of bone infection. The advantages of this strategy include a high delivery efficiency, sustained antibacterial action, and reduced toxicity.

Hamanashi et al. incorporated vancomycin in a CPC based on TTCP and DCPD [123]. They observed sustained release in PBS for 2–9 weeks from composites containing 1–5% vancomycin. It was noted that a composite containing 5% vancomycin maintained effective concentration (20 times minimum inhibitory concentration) in rabbit tibial condyle bone marrow for 3 weeks [123]. In addition to common antibiotics, Stallmann et al. studied the use of CPCs containing a broad-spectrum antimicrobial peptide (hLF 1–11) in preventing osteomyelitis with a rabbit femur model [124]. Cement containing 50 mg/g peptide was injected in femoral canals after inoculated with *Staphylococcus aureus*. Three weeks after operation, slices retrieved from peptide-treated CPCs formed significantly less bacterial colonies compared with the untreated control. Early bone ingrowth into CPCs was also detected [124].

Apatitic CPCs are typically degraded slowly in vivo, as a result of its thermodynamic stability [125]. This limits the degree of tissue ingrowth into the CPCs,

adverse affecting its replacement by a new bone. To overcome this disadvantage, a number of studies have explored compositing CPCs with polymers to modulate the degradability of the former [2, 27, 33, 90, 126]. The rationale is that, upon degradation, polymers release acidic monomers, which accelerate CPC degradation and increasing the drug release. Roy et al. incorporated vancomycin-loaded microspheres (40 or 100  $\mu\text{m}$  in diameter) in a CPC based on  $\alpha$ -TCP [126]. The composite cements showed controlled releases lasting for >10 weeks. The microsphere-laden CPCs produced decreasing pH profiles plateauing after ~400 h in PBS, whereas the blank CPCs yielded a slightly increasing pH trend. Porosity and morphological characterizations revealed that microsphere incorporation created pores between 15–30 days in PBS with pore sizes consistent with the microsphere diameters, supporting the starting rationale [126]. Loca et al. incorporated vancomycin-loaded PLA microcapsules, coated or uncoated with HA, in a CPC based on  $\alpha$ -TCP [33]. The composite cement released 7.7% (uncoated microcapsules) and 25.6% (HA-coated microcapsules) of vancomycin in 1 day and released 30.4% (uncoated) and 85.3% (coated) in 43 days [33]. However, this study did not investigate whether the incorporation of polymer microspheres affected the degradation of the CPC matrix.

### 7.5.3 Bone Tumors

The skeleton is a common site for tumor metastasis, or relocation of cancer cells from a primary solid tumor [127]. Tumors mostly frequently spread to bones include cancers of the lungs, breasts, and prostate. Bone metastases are regularly treated by surgical resection and chemotherapies [127]. After bone tumor resection, drug-loaded CPCs can be used to fill the void and serve as a source of chemotherapeutic agent release. Commonly used chemotherapeutic agents include the classical cyclophosphamide, methotrexate, and 5-fluorouracil and newer anthracyclines and hexanes such as epirubicin, doxorubicin, and paclitaxel [128].

Aimed at local delivery of paclitaxel to bone, Lopez-Heredia et al. developed a CPC based on  $\alpha$ -TCP,  $\text{CaHPO}_4$ , and HA [44]. Paclitaxel was loaded in hardened CPCs by adsorption. In vitro loading model indicated a high retention behavior by the CPCs, and cell viability assays indicated that paclitaxel released from CPCs remained active to influence the viabilities of osteosarcoma and breast cancer cells [128]. Yang et al. fabricated CPCs containing 0–1% methotrexate [107]. The in vitro and in vivo release profiles showed an initial burst release and subsequent slower release. Release rate was found faster in vivo than in vitro, and the authors suggested that methotrexate could be continuously released for 2–4 months at effective concentration without producing apparent toxicity on the host rabbits [107]. Tanzawa et al. investigated the possibility of co-delivering two drugs from CPCs [129]. They prepared CPCs containing cisplatin and caffeine, with the latter expected to enhance the cytotoxic effect of the former. In vitro growth inhibition assays using rat osteosarcoma cells (SOSN<sub>2</sub>) found that cisplatin and caffeine

released from the CPCs inhibited their proliferation and the degree of inhibition was greater than that produced by CPCs containing cisplatin alone, confirming the synergistic effect. In vivo effect was examined by transplanting SOSN<sub>2</sub> to rat tibias, tumor excision 3 days later, and implantation of CPCs. It was similarly found that CPCs simultaneously containing cisplatin and caffeine have the greatest tumor growth inhibition than that containing cisplatin alone [129]. In addition to numerous studies using CaPs as the setting phase, Doadrio et al. investigated gypsum-based cement containing apatite as a carrier for cephalexin [130]. They found that, pure gypsum cement rapidly released 80–90% of the drug load after immersion in simulated body fluid (SBF) for 8 h, whereas gypsum cement containing HA produced a more sustained release with only 25% released after 8 h and 90% after 1 week. Furthermore, the addition of HA to gypsum also reduced the viscosity of the past, offering an improved workability [130].

#### 7.5.4 Osteoporosis

Osteoporosis is an increasingly common skeletal disorder characterized by decrease of bone mineral density and accompanying loss of skeletal strength. It is a frequent cause of bone fractures, particularly in the elderly [131]. Osteoporosis is attributed to the disruption of homeostasis in the skeletal system. The bones are constantly remodeled by osteoclasts responsible for resorbing bone mass and osteoblasts producing new bony mass. In healthy adults, the two actions are normally balanced, thereby maintaining a stable bone mineral density. In an osteoporotic patient, however, the osteoclastic activity exceeds the osteoblastic activity, resulting in a net loss of bone mass [131].

The currently leading pharmaceutical treatment for osteoporosis is the systemic use of bisphosphonates [132]. Bisphosphonate drugs are a family of compounds with two phosphonate groups bonded to a carbon atom, which also bears a hydroxyl group. These drugs potently inhibit the activity of osteoclasts to arrest, and in some cases even reverse, the development of osteoporosis. Some commonly used bisphosphonates include alendronate, clodronate, pamidronate, and zoledronate [132]. A number of studies have studied CPCs containing bisphosphonates as a local treatment for osteoporosis. Panzavolta et al. developed two bisphosphonate-loaded CPCs based on a tri-CaP formulation (i.e., TCP, nanocrystalline HA, DCPD) [99, 133]. Alendronate and pamidronate were separately incorporated into the CPCs by dissolving in the liquid phase (water) at 0.4 or 1 mM. It was observed that either bisphosphonate did not affect the CPC setting, transformation to calcium-deficient HA, or the microstructure of the final product. Human osteoblast-like cells (MG63) cultured on bisphosphonate-loaded cements for 3–7 days exhibited normal morphology and improved osteoblastic proliferation. In comparison, human mononuclear cells cultured on all bisphosphonate-loaded samples exhibited significantly higher production of osteoprotegerin (a cytokine inhibitor of osteoclast genesis) and lower osteoclast counts compared with the blank CPC control. These results suggest

that bisphosphonate-loaded CPCs may be a biocompatible and anti-osteoporotic material for local use in orthopedics [99, 133]. Zhao et al. prepared CPCs containing 2–10 wt.% alendronate by blending the drug with the cement powder [90]. The alendronate-loaded samples exhibited a fast in vitro drug release for ~5 days, and a subsequent slow release up to day 21. At 21 days, samples carrying 2%, 5%, and 10% alendronate release only 33.2%, 24.4%, and 20.8% of the drug incorporated. This remarkably sustained release is expectable from the molecular structures of bisphosphonate drugs. With two phosphonate groups, these compounds are strong chelators for  $\text{Ca}^{2+}$ ; thus, all clinically used bisphosphonates have strong affinities to CaPs, including synthetic CaPs and human bone mineral, explaining the slow release of alendronate from the CPCs. Rat mesenchymal cells cultured on all samples proliferated between 1 and 7 days, and no significant difference was observed between cements containing different fractions of alendronate nor between a drug-loaded cement and the blank CPC control [90].

Estradiol is a female sex hormone but naturally present in both sexes [134]. It is essential for the development and maintenance of multiple organs such as the reproductive tissues, skin, and bone. At the cellular level, estradiol inhibits the differentiation toward osteoclasts, reducing their number. In adults, estradiol deficiency leads to accelerated bone resorption [134, 135]. Estradiol replacement therapy has been clinically used to prevent osteoporotic bone fracture in women. Therefore, estradiol is another potential anti-osteoporotic agent for local release. Otsuka et al. incorporated 0.5% estradiol in CPCs and investigated its release in SBF containing 0–100 mg/L  $\text{Ca}^{2+}$  [134, 135]. It was found that estradiol release decreased with increasing  $\text{Ca}^{2+}$  concentration. Subcutaneous implantation in normal and vitamin D-deficient rats (i.e., low plasma  $\text{Ca}^{2+}$  level) confirmed that estradiol release was significantly faster in the former than in the latter. These findings suggest that estradiol from this cement is responsive to the local  $\text{Ca}^{2+}$  level, which may be relevant to skeletal disorders involving abnormal calcium homeostasis such as osteoporosis [134, 135].

## 7.6 Challenges and Prospectives

The process of bone regeneration in a CPC-filled defect starts with the interactions between CPCs and the host tissues. Shortly after implantation, the CPC stimulates a cascade of biological responses, such as protein adsorption on the CPC surface, subsequent cellular adhesion, and migration of mesenchymal bone cells, their osteogenic differentiation to osteoblasts, the formation and penetration of new blood vessels, and finally the formation of new bony tissues [136]. This biological cascade recruits and activates the progenitors of inflammatory cell required for effective repair of the damaged tissue. On the other hand, it is critical to avoid any adverse response from the host, such as fibrous encapsulation of the CPCs [136]. It is generally accepted that bone regeneration occurs following a complex spatiotemporal profile. Inspired by this natural process, more advanced CPCs may be equipped

with smart release mechanisms to meet the requirement of bioactive agents during each stage of defect repair [136].

CPCs used for repairing bone defects should provide an effective structural and functional solution to the patient. However, bone defects can be caused by fractures, surgical excision of tumors, debridement of skeletal infection, or other disorders leading to bone damage. Faced with complex origins and pathological characteristics, even the newest purely inorganic (drug-free) CPCs may not address the demand of each situation satisfactorily [22]. Therefore, it is imperative to develop smarter and multifunctional CPC release systems incorporating a variety of drug carriers and functionalities responding to diverse clinical demands.

Stimulus-responsive polymers have been widely investigated as intelligent drug release systems that deliver drugs upon triggering by specific physical, chemical, or biological signals [137]. Moreover, multifunctional delivery platforms have established in polymeric control system to coordinate the timing, concentration, and spatial distribution of signal molecules (e.g., growth factors) to optimally accelerate tissue repair [138]. In the future, CPCs and the composite of CaP and functional biopolymer may be developed to produce spatial and sequential release of multiple drugs or signal factors targeting inflammatory response, angiogenesis, stem cell adhesion, osteoblastic differentiation, and bone matrix synthesis [138].

Inorganic nanoparticles with controlled size, shape, charge, surface chemistry, and properties have emerged as a new effective tool for drug delivery [139–142]. A variety of nanoparticles have been studied for delivering agents of orthopedic interests. For example, Slowing et al. synthesized mesoporous silica nanoparticles (MSNs) encapsulated with cytochrome c and demonstrated that these particles were internalized by HeLa cells and the protein cargo was released into the cytoplasm [143]. This suggests the opportunity of delivering signal molecules into living cells involved in bone regeneration. Moreover, when functionalized with folate groups, these particles also serve as promising carriers selectively targeting cancer cells, suggesting potential use in managing bone tumors [143]. Furthermore, because of the remarkable versatility of MSNs, they present the possibility of integrating multiple stimuli-responsive mechanisms in a single delivery system. Manzano et al. have reviewed the boom of multifunctional MSNs as delivery systems [144].

CPCs have been clinically used for over 40 years, and their applications as bone graft substitutes and as delivery vehicles have demonstrated very important successes. However, enormous applications of CPCs have not yet been explored to their maximum extent. The development of advanced technologies and the clinical demand will bring their research and development to next step.

## References

1. Vallet-Regí M, González-Calbet JM (2004) Calcium phosphates as substitution of bone tissues. *Prog Solid State Chem* 32:1–31



2. Ginebra MP, Canal C, Espanol M et al (2012) Calcium phosphate cements as drug delivery materials. *Adv Drug Deliv Rev* 64:1090–1110
3. Brown WE, Chow LC (1983) A new calcium phosphate setting cement. *J Dent Res* 62:672
4. LeGeros RZ, Chohayeb A, Shulman A (1982) Apatitic calcium phosphates: possible dental restorative materials. *J Dent Res* 61:343–347
5. Guelcher SA, Srinivasan A, Dumas JE et al (2008) Synthesis, mechanical properties, biocompatibility, and biodegradation of polyurethane networks from lysine polyisocyanates. *Biomaterials* 29:1762–1775
6. Friedman CD, Costantino PD, Takagi S et al (1998) BoneSource™ hydroxyapatite cement: a novel biomaterial for craniofacial skeletal tissue engineering and reconstruction. *J Biomed Mater Res A* 43:428–432
7. Kamerer DB, Hirsch BE, Snyderman CH et al (1994) Hydroxyapatite cement: a new method for achieving watertight closure in transtemporal surgery. *Am J Otol* 15:47–49
8. Constantz BR, Ison IC, Fulmer MT et al (1995) Skeletal repair by in situ formation of the mineral phase of bone. *Science* 267:1796–1799
9. Horstmann WG, Verheyen CCPM, Leemans R (2003) An injectable calcium phosphate cement as a bone-graft substitute in the treatment of displaced lateral tibial plateau fractures. *Injury* 34:141–144
10. Strauss EJ, Egol KA (2007) The management of ankle fractures in the elderly. *Injury* 38:2–9
11. Liverneaux PA (2004) Osteoporotic distal radius curettage-filling with an injectable calcium phosphate cement. A cadaveric study. *Eur J Orthop Surg Traumatol* 15:1–6
12. Welch RD, Zhang H, Bronson DG (2003) Experimental tibial plateau fractures augmented with calcium phosphate cement or autologous bone graft. *J Bone Joint Surg Am* 85:222–231
13. Aral A, Yalçın S, Karabuda ZC et al (2008) Injectable calcium phosphate cement as a graft material for maxillary sinus augmentation: an experimental pilot study. *Clin Oral Implants Res* 19:612–617
14. Maestretti G, Cremer C, Otten P et al (2007) Prospective study of standalone balloon kyphoplasty with calcium phosphate cement augmentation in traumatic fractures. *Eur Spine J* 16:601–610
15. Libicher M, Hillmeier J, Liegibel U et al (2006) Osseous integration of calcium phosphate in osteoporotic vertebral fractures after kyphoplasty: initial results from a clinical and experimental pilot study. *Osteoporos Int* 17:1208–1215
16. Mermelstein LE, Chow LC, Friedman CD et al (1996) The reinforcement of cancellous bone screws with calcium phosphate cement. *J Orthop Trauma* 10:15–20
17. Ooms EM, Wolke JGC, Van der Waerden JPCM et al (2003) Use of injectable calcium-phosphate cement for the fixation of titanium implants: an experimental study in goats. *J Biomed Mater Res B* 66:447–456
18. Takemasa R, Kiyasu K, Tani T et al (2007) Validity of calcium phosphate cement vertebroplasty for vertebral non-union after osteoporotic fracture with middle column involvement. *Spine J* 7:148S
19. Lewis G (2006) Injectable bone cements for use in vertebroplasty and kyphoplasty: state-of-the-art review. *J Biomed Mater Res B* 76:456–468
20. Drosse I, Volkmer E, Capanna R et al (2008) Tissue engineering for bone defect healing: an update on a multi-component approach. *Injury* 39:S9–S20
21. Weigand A, Beier JP, Arkudas A et al (2015) Comment on “Microsurgical techniques used to construct the vascularized and neurotized tissue engineered bone”. *Biomed Res Int* 2015:685412
22. Arcos D, Vallet-Regí M (2013) Bioceramics for drug delivery. *Acta Mater* 61:890–911
23. Verron E, Khairoun I, Guicheux J et al (2010) Calcium phosphate biomaterials as bone drug delivery systems: a review. *Drug Discov Today* 15:547–552
24. Luginbuehl V, Wenk E, Koch A et al (2005) Insulin-like growth factor I-releasing alginate-tricalcium phosphate composites for bone regeneration. *Pharm Res* 22:940–950

25. Bose S, Tarafder S (2012) Calcium phosphate ceramic systems in growth factor and drug delivery for bone tissue engineering: a review. *Acta Biomater* 8:1401–1421
26. Mukwaya E, Xu F, Wong MS et al (2014) Chinese herbal medicine for bone health. *Pharm Biol* 52:1223–1228
27. Chen WS, Monroe EA (1991) Phosphate glass cement bone graft. *Biomaterials* 12:561–564
28. Ginebra MP, Traykova T, Planell JA (2006) Calcium phosphate cements as bone drug delivery systems: a review. *J Control Release* 113:102–110
29. Ishikawa K, Karashima S, Takeuchi A et al (2008) Apatite foam fabrication based on hydrothermal reaction of  $\alpha$ -tricalcium phosphate foam. *Key Eng Mater* 361–363:319–322
30. Bohner M, Baroud G (2005) Injectability of calcium phosphate pastes. *Biomaterials* 26:1553–1563
31. Ding S, Zhang J, Tian Y et al (2016) Magnesium modification up-regulates the bioactivity of bone morphogenetic protein-2 upon calcium phosphate cement via enhanced BMP receptor recognition and Smad signaling pathway. *Colloids Surf B Biointerfaces* 145:140–151
32. Wu F, Wei J, Guo H et al (2008) Self-setting bioactive calcium-magnesium phosphate cement with high strength and degradability for bone regeneration. *Acta Biomater* 4:1873–1884
33. Loca D, Sokolova M, Locs J et al (2015) Calcium phosphate bone cements for local vancomycin delivery. *Mater Sci Eng C* 49:106–113
34. Otsuka M, Matsuda Y, Kokubo T et al (1994) A novel skeletal drug delivery system using self-setting bioactive glass bone cement. III: the in vitro drug release from bone cement containing indomethacin and its physicochemical properties. *J Control Release* 31:111–119
35. Otsuka M, Matsuda Y, Suwa Y et al (1994) A novel skeletal drug delivery system using self-setting calcium phosphate cement. 2. Physicochemical properties and drug release rate of the cement-containing indomethacin. *J Pharm Sci* 83:611–615
36. Xia W, Razi MRM, Ashley P et al (2014) Quantifying effects of interactions between polyacrylic acid and chlorhexidine in dicalcium phosphate-forming cements. *J Mater Chem B* 2:1673–1680
37. Xue B, Zhang C, Wang YH et al (2014) A novel controlled-release system for antibacterial enzyme lysostaphin delivery using hydroxyapatite/chitosan composite bone cement. *PLoS One* 9:e113797
38. Ding H, Zhao CJ, Cui X et al (2014) A novel injectable borate bioactive glass cement as an antibiotic delivery vehicle for treating osteomyelitis. *PLoS One* 9:e85472
39. Schumacher M, Lode A, Helth A et al (2013) A novel strontium (II)-modified calcium phosphate bone cement stimulates human-bone-marrow-derived mesenchymal stem cell proliferation and osteogenic differentiation in vitro. *Acta Biomater* 9:9547–9557
40. Mistry S, Roy S, Maitra NJ et al (2016) A novel, multi-barrier, drug eluting calcium sulfate/biphasic calcium phosphate biodegradable composite bone cement for treatment of experimental MRSA osteomyelitis in rabbit model. *J Control Release* 239:169–181
41. Lee J, Farag MM, Park EK et al (2014) A simultaneous process of 3D magnesium phosphate scaffold fabrication and bioactive substance loading for hard tissue regeneration. *Mater Sci Eng C* 36:252–260
42. Cox SC, Jamshidi P, Eisenstein NM et al (2016) Adding functionality with additive manufacturing: fabrication of titanium-based antibiotic eluting implants. *Mater Sci Eng C* 64:407–415
43. Alexopoulou M, Mystiridou E, Mouzakis D et al (2016) Preparation, characterization and in vitro assessment of ibuprofen loaded calcium phosphate/gypsum bone cements. *Cryst Res Technol* 51:41–48
44. Lopez-Heredia MA, Kamphuis GJB, Thüne PC et al (2011) An injectable calcium phosphate cement for the local delivery of paclitaxel to bone. *Biomaterials* 32:5411–5416
45. Mestres G, Kugiejko K, Pastorino D et al (2016) Changes in the drug release pattern of fresh and set simvastatin-loaded brushite cement. *Mater Sci Eng C* 58:88–96
46. Chen CHD, Chen CC, Shie MY et al (2011) Controlled release of gentamicin from calcium phosphate/alginate bone cement. *Mater Sci Eng C* 31:334–341

47. Tappa KK, Jammalamadaka UM, Mills DK (2014) Design and evaluation of a nanoenhanced anti-Infective calcium phosphate bone cements. Paper presented at the 36th annual international conference of the IEEE engineering in medicine and biology society, Sheraton Chicago Hotel and Towers, Chicago, 26–30 August 2014
48. Mellier C, Fayon F, Boukhechba F et al (2015) Design and properties of novel gallium-doped injectable apatitic cements. *Acta Biomater* 24:322–332
49. Canal C, Khurana K, Gallinetti S et al (2016) Design of calcium phosphate scaffolds with controlled simvastatin release by plasma polymerisation. *Polymer* 92:170–178
50. Verron E, Pissonnier ML, Lesoeur J et al (2014) Vertebroplasty using bisphosphonate-loaded calcium phosphate cement in a standardized vertebral body bone defect in an osteoporotic sheep model. *Acta Biomater* 10:4887–4895
51. Noukrati H, Cazalbou S, Demnati I et al (2016) Injectability, microstructure and release properties of sodium fusidate-loaded apatitic cement as a local drug-delivery system. *Mater Sci Eng C* 59:177–184
52. Otsuka M, Matsuda Y, Suwa Y et al (1994) A novel skeletal drug delivery system using self-setting calcium phosphate cement. 3. Physicochemical properties and drug-release rate of bovine insulin and bovine albumin. *J Pharm Sci* 83:255–258
53. Kuang GM, Yau WP, Wu J et al (2015) Strontium exerts dual effects on calcium phosphate cement: accelerating the degradation and enhancing the osteoconductivity both in vitro and in vivo. *J Biomed Mater Res A* 103:1613–1621
54. Chatzistavrou X, Velamakanni S, DiRenzo K et al (2015) Designing dental composites with bioactive and bactericidal properties. *Mater Sci Eng C* 52:267–272
55. Otsuka M, Nakahigashi Y, Matsuda Y et al (1994) A novel skeletal drug delivery system using self-setting calcium phosphate cement. 7. Effect of biological factors on indomethacin release from the cement loaded on bovine bone. *J Pharm Sci* 83:1569–1573
56. Sugo K, Kawashima R, Nakasu M et al (2016) Antibiotic elution profile and physical properties of a novel calcium phosphate cement material. *J Ceram Soc Jpn* 124:954–958
57. Wu CC, Wang CC, Lu DH et al (2012) Calcium phosphate cement delivering zoledronate decreases bone turnover rate and restores bone architecture in ovariectomized rats. *Biomed Mater* 7:035009
58. Hartgerink JD, Beniash E, Stupp SI (2001) Self-assembly and mineralization of peptide-amphiphile nanofibers. *Science* 294:1684–1688
59. Petta D, Fussell G, Hughes L et al (2016) Calcium phosphate/thermoresponsive hyaluronan hydrogel composite delivering hydrophilic and hydrophobic drugs. *J Orthop Transl* 5:57–68
60. Striegler C, Schumacher M, Effenberg C et al (2015) Dendritic glycopolymer as drug delivery system for proteasome inhibitor bortezomib in a calcium phosphate bone cement: first steps toward a local therapy of osteolytic bone lesions. *Macromol Biosci* 15:1283–1295
61. He FP, Chen Y, Li JY et al (2015) Improving bone repair of femoral and radial defects in rabbit by incorporating PRP into PLGA/CPC composite scaffold with unidirectional pore structure. *J Biomed Mater Res A* 103:1312–1324
62. Babo PS, Santo VE, Gomes ME et al (2016) Development of an injectable calcium phosphate/hyaluronic acid microparticles system for platelet lysate sustained delivery aiming bone regeneration. *Macromol Biosci* 16:1662–1677
63. Pemi S, Thenault V, Abdo P et al (2015) Antimicrobial activity of bone cements embedded with organic nanoparticles. *Int J Nanomed* 10:6317–6329
64. Wu Y, Hou J, Yin ML et al (2014) Enhanced healing of rabbit segmental radius defects with surface-coated calcium phosphate cement/bone morphogenetic protein-2 scaffolds. *Mater Sci Eng C* 44:326–335
65. Wang L, Wang P, Weir MD et al (2016) Hydrogel fibers encapsulating human stem cells in an injectable calcium phosphate scaffold for bone tissue engineering. *Biomed Mater* 11:065008
66. Uzun AS, Akman A, Demirkan AF et al (2014) Collagen membrane wrapping around methotrexate-containing calcium-phosphate cement reduces the side effects on soft tissue healing. *Eklemler Hast Cerrahisi* 25:96–101

67. Ventura M, Sun Y, Cremers S et al (2014) A theranostic agent to enhance osteogenic and magnetic resonance imaging properties of calcium phosphate cements. *Biomaterials* 35:2227–2233
68. Liu WN, Chang J (2009) In vitro evaluation of gentamicin release from a bioactive tricalcium silicate bone cement. *Mater Sci Eng C* 29:2486–2492
69. Chen FP, Song ZY, Gao L et al (2016) Hierarchically macroporous/mesoporous POC composite scaffolds with IBU-loaded hollow SiO<sub>2</sub> microspheres for repairing infected bone defects. *J Mater Chem B* 4:4198–4205
70. Farokhi M, Mottaghtalab F, Shokrgozar MA et al (2016) Importance of dual delivery systems for bone tissue engineering. *J Control Release* 225:152–169
71. Su Y, Li XQ, Liu SP et al (2009) Controlled release of dual drugs from emulsion electrospun nanofibrous mats. *Colloids Surf B Biointerfaces* 73:376–381
72. Cheng DX, Sefton MV (2009) Dual delivery of placental growth factor and vascular endothelial growth factor from poly (hydroxyethyl methacrylate-co-methyl methacrylate) microcapsules containing doubly transfected luciferase-expressing L929 cells. *Tissue Eng Part A* 15:1929–1939
73. Chapanian R, Amsden BG (2010) Combined and sequential delivery of bioactive VEGF<sub>165</sub> and HGF from poly (trimethylene carbonate) based photo-cross-linked elastomers. *J Control Release* 143:53–63
74. Huang JG, Pang L, Chen ZR et al (2013) Dual-delivery of vancomycin and icariin from an injectable calcium phosphate cement-release system for controlling infection and improving bone healing. *Mol Med Rep* 8:1221–1227
75. Lin WC, Hung PH, Lin CP (2016) Development of drug delivery bioceramics cement for vital pulp therapy. Paper presented at the 16th international conference on nanotechnology, Sendai International Center, Japan, 22–25 August 2016
76. Geffers M, Barralet JE, Groll J et al (2015) Dual-setting brushite-silica gel cements. *Acta Biomater* 11:467–476
77. Wu WG, Ye CY, Zheng QX et al (2016) A therapeutic delivery system for chronic osteomyelitis via a multi-drug implant based on three-dimensional printing technology. *J Biomater Appl* 31:250–260
78. Gbureck U, Vorndran E, Müller FA et al (2007) Low temperature direct 3D printed bioceramics and biocomposites as drug release matrices. *J Control Release* 122:173–180
79. Vorndran E, Klammert U, Ewald A et al (2010) Simultaneous immobilization of bioactives during 3D powder printing of bioceramic drug-release matrices. *Adv Funct Mater* 20:1585–1591
80. Inzana JA, Trombetta RP, Schwarz EM et al (2015) 3D printed bioceramics for dual antibiotic delivery to treat implant-associated bone infection. *Eur Cells Mater* 30:232–247
81. Akkineni AR, Luo YX, Schumacher M et al (2015) 3D plotting of growth factor loaded calcium phosphate cement scaffolds. *Acta Biomater* 27:264–274
82. Liu YR, Qu SX, Maitz MF et al (2007) The effect of the major components of *Salvia miltiorrhiza* Bunge on bone marrow cells. *J Ethnopharmacol* 111:573–583
83. Wang WL, Sheu SY, Chen YS et al (2015) Enhanced bone tissue regeneration by porous gelatin composites loaded with the Chinese herbal decoction Danggui Buxue Tang. *PLoS One* 10:e0131999
84. Huang MH, Kao CT, Chen YW et al (2015) The synergistic effects of Chinese herb and injectable calcium silicate/ $\beta$ -tricalcium phosphate composite on an osteogenic accelerator in vitro. *J Mater Sci Mater Med* 26:1–12
85. Chang NJ, Chen YW, Shieh DE et al (2015) The effects of injectable calcium silicate-based composites with the Chinese herb on an osteogenic accelerator in vitro. *Biomed Mater* 10:055004
86. Li MH, Qu SX, Yao N et al (2010) Properties of calcium phosphate cement with various concentration of Xiangdan injection. *J Inorg Mater* 25:507–511

87. Jiang XX, Qu SX, Lin SZ et al (2011) Influence of drynaria on physicochemical and in vitro biological properties of calcium phosphate cement. *J Inorg Mater* 26:29–37
88. Lee JS, Cha HD, Shim JH et al (2012) Effect of pore architecture and stacking direction on mechanical properties of solid freeform fabrication-based scaffold for bone tissue engineering. *J Biomed Mater Res A* 100:1846–1853
89. Espalin D, Arcaute K, Rodriguez D et al (2010) Fused deposition modeling of patient-specific polymethyl methacrylate implants. *Rapid Prototyp J* 16:164–173
90. Ginebra MP, Traykova T, Planell JA (2006) Calcium phosphate cements: competitive drug carriers for the musculoskeletal system? *Biomaterials* 27:2171–2177
91. Alkhraisat MH, Rueda C, Cabrejos-Azama J et al (2010) Loading and release of doxycycline hyclate from strontium-substituted calcium phosphate cement. *Acta Biomater* 6:1522–1528
92. Joosten U, Joist A, Frebel T et al (2004) Evaluation of an in situ setting injectable calcium phosphate as a new carrier material for gentamicin in the treatment of chronic osteomyelitis: studies in vitro and in vivo. *Biomaterials* 25:4287–4295
93. Hofmann MP, Mohammed AR, Perrie Y et al (2009) High-strength resorbable brushite bone cement with controlled drug-releasing capabilities. *Acta Biomater* 5:43–49
94. Stigter M, Bezemer J, de Groot K et al (2004) Incorporation of different antibiotics into carbonated hydroxyapatite coatings on titanium implants, release and antibiotic efficacy. *J Control Release* 99:127–137
95. McNally A, Sly K, Lin S et al (2008) Release of antibiotics from macroporous injectable calcium phosphate cement. *Key Eng Mater* 361–363:359–962
96. Ratier A, Gibson IR, Best SM et al (2001) Setting characteristics and mechanical behaviour of a calcium phosphate bone cement containing tetracycline. *Biomaterials* 22:897–901
97. Zhao JD, Tang H, Gu JC et al (2010) Evaluation of a novel osteoporotic drug delivery system in vitro: alendronate-loaded calcium phosphate cement. *Orthopedics* 33:546–561
98. Shen ZH, Yu T, Ye JD (2014) Microstructure and properties of alendronate-loaded calcium phosphate cement. *Mater Sci Eng C* 42:303–311
99. Panzavolta S, Torricelli P, Bracci B et al (2009) Alendronate and pamidronate calcium phosphate bone cements: setting properties and in vitro response of osteoblast and osteoclast cells. *J Inorg Biochem* 103:101
100. Blom EJ, Klein-Nulend J, Wolke JGC et al (2010) Transforming growth factor-1 incorporation in a calcium phosphate bone cement: material properties and release characteristics. *J Biomed Mater Res A* 59:265–272
101. Xu HHK, Weir MD, Burguera EF et al (2006) Injectable and macroporous calcium phosphate cement scaffold. *Biomaterials* 27:4279–4287
102. Buchanan F, Gallagher L, Jack V et al (2007) Short-fibre reinforcement of calcium phosphate bone cement. *Proc Inst Mech Eng H* 221:203–211
103. Haghbin-Nazarpak M, Moztaarazadeh F, Solati-Hashjin M et al (2011) Injectable and biore-sorbable calcium phosphate delivery system with gentamicin sulphate for treatment of bone diseases: in vitro study. *Adv Appl Ceram* 110:482–489
104. Zhang JT, Liu WZ, Schnitzler V et al (2014) Calcium phosphate cements for bone substitution: chemistry, handling and mechanical properties. *Acta Biomater* 10:1035–1049
105. Siepmann J, Peppas NA (2012) Modeling of drug release from delivery systems based on hydroxypropyl methylcellulose (HPMC). *Adv Drug Deliv Rev* 64:163–174
106. Otsuka M, Matsuda Y, Suwa Y et al (1994) A novel skeletal drug-delivery system using self-setting calcium phosphate cement. 4. Effects of the mixing solution volume on the drug-release rate of heterogeneous aspirin-loaded cement. *J Pharm Sci* 83:259–263
107. Yang ZP, Li D, Han J et al (2009) Incorporation of methotrexate in calcium phosphate cement: behavior and release in vitro and in vivo. *Orthopedics* 32:27
108. Ghosh S, Wu V, Pernal S et al (2016) Self-setting calcium phosphate cements with tunable antibiotic release rates for advanced antimicrobial applications. *ACS Appl Mater Interfaces* 8:7691–7708

109. Habraken WJEM, Wolke JGC, Jansen JA (2007) Ceramic composites as matrices and scaffolds for drug delivery in tissue engineering. *Adv Drug Deliv Rev* 59:234–248
110. Mouriño V, Boccaccini AR (2010) Bone tissue engineering therapeutics: controlled drug delivery in three-dimensional scaffolds. *J R Soc Interface* 7:209–227
111. Ohura K, Hamanishi C, Tanaka S et al (1999) Healing of segmental bone defects in rats induced by a  $\beta$ -TCP-MCPM cement combined with rhBMP-2. *J Biomed Mater Res A* 44:168–175
112. Seeherman H, Li R, Wozney J (2003) A review of preclinical program development for evaluating injectable carriers for osteogenic factors. *J Bone Joint Surg Am* 85:96–108
113. Edwards RB, Seeherman HJ, Bogdanske JJ et al (2004) Percutaneous injection of recombinant human bone morphogenetic protein-2 in a calcium phosphate paste accelerates healing of a canine tibial osteotomy. *J Bone Joint Surg Am* 86:1425–1438
114. Seeherman HJ, Bouxsein M, Kim H et al (2004) Recombinant human bone morphogenetic protein-2 delivered in an injectable calcium phosphate paste accelerates osteotomy-site healing in a nonhuman primate model. *J Bone Joint Surg Am* 86:1961–1972
115. Ventura M, Boerman OC, Franssen GM et al (2014) Monitoring the biological effect of BMP-2 release on bone healing by PET/CT. *J Control Release* 183:138–144
116. Kroese-Deutman HC, Ruhé PQ, Spauwen PHM et al (2005) Bone inductive properties of rhBMP-2 loaded porous calcium phosphate cement implants inserted at an ectopic site in rabbits. *Biomaterials* 26:1131–1138
117. Seeherman HJ, Azari K, Bidic S et al (2006) rhBMP-2 delivered in a calcium phosphate cement accelerates bridging of critical-sized defects in rabbit radii. *J Bone Joint Surg Am* 88:1553–1565
118. Link DP, van den Dolder J, van den Beucken JJ et al (2008) Bone response and mechanical strength of rabbit femoral defects filled with injectable CaP cements containing TGF- $\beta$ 1 loaded gelatin microparticles. *Biomaterials* 29:675–682
119. Lee GS, Park JH, Shin US et al (2011) Direct deposited porous scaffolds of calcium phosphate cement with alginate for drug delivery and bone tissue engineering. *Acta Biomater* 7:3178–3186
120. Maus U, Andereya S, Gravius S et al (2008) BMP-2 incorporated in a tricalcium phosphate bone substitute enhances bone remodeling in sheep. *J Biomater Appl* 22:559–576
121. Weir MD, Xu HHK (2010) Human bone marrow stem cell-encapsulating calcium phosphate scaffolds for bone repair. *Acta Biomater* 6:4118–4126
122. Park SH, Tofighi A, Wang XQ et al (2011) Calcium phosphate combination biomaterials as human mesenchymal stem cell delivery vehicles for bone repair. *J Biomed Mater Res B* 97:235–244
123. Hamanishi C, Kitamoto K, Tanaka S et al (1996) A self-setting TTCP-DCPD apatite cement for release of vancomycin. *J Biomed Mater Res A* 33:139–143
124. Stallmann HP, Faber C, Bronckers ALJJ et al (2004) Osteomyelitis prevention in rabbits using antimicrobial peptide hLF-11- or gentamicin-containing calcium phosphate cement. *J Antimicrob Chemother* 54:472–476
125. Malsy A, Bohner M (2005) Brushite conversion into apatite. *Eur Cells Mater* 10:28
126. Roy A, Jhunjhunwala S, Bayer E et al (2016) Porous calcium phosphate-poly (lactic-co-glycolic) acid composite bone cement: a viable tunable drug delivery system. *Mater Sci Eng C* 59:92–101
127. Mirra JM, Gold RH, Marcove RC (1980) Bone tumors, diagnosis and treatment: diagnosis and treatment. Lippincott Williams & Wilkins, Baltimore
128. Guarneri V, Conte PF (2004) The curability of breast cancer and the treatment of advanced disease. *Eur J Nucl Med Mol Imaging* 31:S149–S161
129. Tanzawa Y, Tsuchiya H, Shirai T et al (2011) Potentiation of the antitumor effect of calcium phosphate cement containing anticancer drug and caffeine on rat osteosarcoma. *J Orthop Sci* 16:77–84

130. Doadrio JC, Arcos D, Cabañas MV et al (2004) Calcium sulphate-based cements containing cephalixin. *Biomaterials* 25:2629–2635
131. Kanis JA, Melton LJ, Christiansen C et al (1994) The diagnosis of osteoporosis. *J Bone Miner Res* 9:1137–1141
132. Marx RE, Sawatari Y, Fortin M et al (2005) Bisphosphonate-induced exposed bone (osteonecrosis/osteopetrosis) of the jaws: risk factors, recognition, prevention, and treatment. *J Oral Maxil Surg* 63:1567–1575
133. Panzavolta S, Torricelli P, Bracci B et al (2010) Functionalization of biomimetic calcium phosphate bone cements with alendronate. *J Inorg Biochem* 104:1099–1106
134. Otsuka M, Yoneoka K, Matsuda Y et al (1998) Oestradiol release from self-setting apatitic bone cement responsive to plasma-calcium level in ovariectomized rats and its physicochemical mechanism. *J Pharm Pharmacol* 49:1182–1188
135. Otsuka M, Matsuda Y, Baig AA et al (2000) Calcium-level responsive controlled drug delivery from implant dosage forms to treat osteoporosis in an animal model. *Adv Drug Deliv Rev* 42:249–258
136. Zhang J, Zhou HJ, Yang K et al (2013) RhBMP-2-loaded calcium silicate/calcium phosphate cement scaffold with hierarchically porous structure for enhanced bone tissue regeneration. *Biomaterials* 34:9381–9392
137. Mano JF (2008) Stimuli-responsive polymeric systems for biomedical applications. *Adv Eng Mater* 10:515–527
138. Vo TN, Kasper FK, Mikos AG (2012) Strategies for controlled delivery of growth factors and cells for bone regeneration. *Adv Drug Deliv Rev* 64:1292–1309
139. Vallet-Regí M, Balas F, Arcos D (2007) Mesoporous materials for drug delivery. *Angew Chem Int Ed* 46:7548–7558
140. Manzano M, Colilla M, Vallet-Regí M (2009) Drug delivery from ordered mesoporous matrices. *Expert Opin Drug Del* 6:1383–1400
141. Manzano M, Vallet-Regí M (2010) New developments in ordered mesoporous materials for drug delivery. *J Mater Chem* 20:5593–5604
142. Ferrari M (2005) Cancer nanotechnology: opportunities and challenges. *Nat Rev Cancer* 5:161–117
143. Slowing II, Trewyn BG, Lin VSY (2007) Mesoporous silica nanoparticles for intracellular delivery of membrane-impermeable proteins. *J Am Chem Soc* 129:8845–8849
144. Manzano M, Vallet-Regí M (2012) Revisiting bioceramics: bone regenerative and local drug delivery systems. *Prog Solid State Chem* 40:17–30

# Chapter 8

## Biomimetic Ion-Substituted Calcium Phosphates

Jun Ma, Shenglong Tan, and Shengmin Zhang

**Abstract** Biomimetic approaches have been developed to produce calcium phosphate with similar composition and/or structure with bone tissues. Template regulation and ionic substitution can endow calcium phosphate special properties and improve their interactivity with bone tissues. In this chapter, the recent progress on biomimetic ion-substituted calcium phosphate and its applications as calcium phosphate cements are reviewed.

**Keywords** Biomimetic • Template regulation • Ion substitution • Calcium phosphate

### 8.1 Introduction

After several billion years of evolution, mineralized tissues of vertebrates present unique hierarchical structures which are assembled in a complicated way. Till now, the assembling mechanisms of these hard mineralized tissues remain mysterious and nobody can fully reveal the process of mineral formation in biological systems. In the past decade, the structure of mineralized hard tissues including bone and teeth has been extensively studied [1]. Through simulated mineralization reaction, the formation of hydroxyapatite regulated by biological molecules can reveal part of the mineralization process in biological systems [2, 3]. However, the fabrication of ideal augmentation biomaterials for bone regeneration is still a challenge for us nowadays [4].

Biomimetic methods of preparing calcium phosphate often refer to the imitation of the biological mineralization process. Because vertebrates have well-adapted bone structures through natural selection, the biomimetic approaches inspired by natural mineralization process have brought many novel solutions to produce better

---

J. Ma • S. Tan • S. Zhang (✉)

Advanced Biomaterials and Tissue Engineering Center, Huazhong University of Science and Technology, Wuhan 430074, China

e-mail: [smzhang@mail.hust.edu.cn](mailto:smzhang@mail.hust.edu.cn)

© Springer Nature Singapore Pte Ltd. 2018

C. Liu, H. He (eds.), *Developments and Applications of Calcium Phosphate Bone Cements*, Springer Series in Biomaterials Science and Engineering 9,  
DOI 10.1007/978-981-10-5975-9\_8

333



materials and devices for biomaterials and tissue engineering applications. In bone tissues, collagen fibrils are self-assembled into fibers and they regulate the formation of calcium phosphate as template. The calcium phosphate mineral in bone is mainly calcium-deficient hydroxyapatite phase. From the microscopic observations, the array of mineralized collagen fibrils with a periodicity of about 67 nm is well-organized. In the previous summary, such self-assembling mechanism has been well established in detail [5]. Inspired by the composition and hierarchical structure of bones, nanostructured biomaterials containing calcium phosphate have been paid great attention for fabricating bone graft materials, because such materials can promote cell adhesion and proliferation and stimulate new bone growth, which show inherent advantages compared to conventional materials [6].

In bone, the mineral is mainly carbonate hydroxyapatite with a platelet-like morphology. The bone mineral composes of 50–150 nm thick stacks of closely packed apatite platelets with a thickness of 2.5–4 nm [5]. It is worth noting that many impurity ions are found in bone minerals. The unit cell of hydroxyapatite is flexible to accept other ions besides calcium, phosphate, and hydroxyl ions. These ionic substitutions such as  $\text{Mg}^{2+}$  and  $\text{F}^-$  endow the hydroxyapatite materials special properties. In average, bone minerals contain 7.4% carbonate, 0.13%  $\text{Cl}^-$ , 0.72  $\text{Mg}^{2+}$ , 0.9%  $\text{Na}^+$ , and so on. Many other trace elements such as  $\text{Sr}^{2+}$ ,  $\text{Zn}^{2+}$ ,  $\text{Cu}^{2+}$ , and  $\text{Fe}^{3+}$  are also found in bone minerals. Bone is considered to be a reservoir for many metal ions; thus, some poisonous elements can be found in skeleton bone after many years. In general, these elements replace calcium, phosphate, and hydroxyl ions in hydroxyapatite besides the adsorption on the crystal surface or extracellular matrix. Cationic ions, such as  $\text{Sr}^{2+}$  and  $\text{Zn}^{2+}$ , prefer to replace  $\text{Ca}^{2+}$  because they have similar size and charge. Anionic ions such as  $\text{F}^-$  and  $\text{Cl}^-$  prefer to substitute  $\text{OH}^-$  in hydroxyapatite for the same reason. Silicate ions are considered to replace phosphate ions in hydroxyapatite due to the similarity between the silicate ions and phosphate ions [7]. Because silicate ions have one more negative charge compared to phosphate ions, the charge compensation is needed. The substitution mechanism of silicon in hydroxyapatite is influenced by the doping concentration and synthesis process [8]. Silicon-substituted phosphate and associated charge compensation occur by generating a more electronegative surface, which promotes biomimetic precipitation [9]. For carbonate ions, the substitution in hydroxyapatite has two possible positions: hydroxyl position for A-type and phosphate position for B-type [10]. Raman and infrared (IR) spectroscopy can be used to analyze the carbonate substitution in hydroxyapatite. For example, the A-type carbonate substitution can be recognized with a FT-IR band at  $1455\text{ cm}^{-1}$ , while the FT-IR band of the B-type carbonate substitution is at  $1425\text{ cm}^{-1}$  [11].

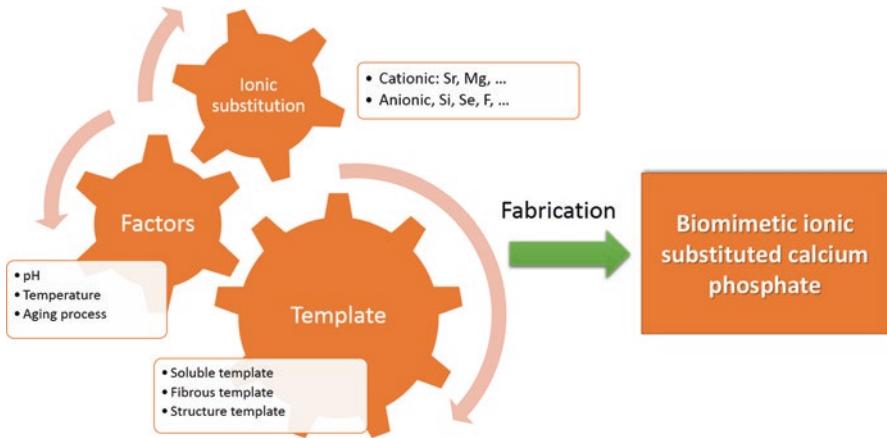
It is known that many ions play critical roles in the biological system. For example, bone is a reservoir of zinc ions which have diverse roles such as enzymatic activity, hormonal activity, and mineralization process [12]. Zinc-substituted hydroxyapatite has been paid much attention because it promotes bone formation around the implants. In addition,  $\text{Zn}^{2+}$  is considered to regulate the immunological response. The production of cytokines of monocyte cells is influenced by the  $\text{Zn}^{2+}$  released from the implants [13].  $\text{Sr}^{2+}$  and  $\text{Mg}^{2+}$  have been extensively studied

because their substitutions in hydroxyapatite can stimulate new bone formation [14–18]. In general, the effect of ion-substituted calcium phosphate is induced by the degradation and subsequent release of ionic ions. However, the role of silicon substitution in calcium phosphate is a little complicated and remains debated. The improved biological performance of silicon-substituted calcium phosphate does not fully correspond to the release of silicate ions [8]. Although the release of silicon does not reach the effective level, the silicon-substituted hydroxyapatite can still perform superior biological properties.

Besides hydroxyapatite, calcium phosphate has other phases. Although these phases do not have similar composition and structure with hydroxyapatite, they can transform into hydroxyapatite or calcium-deficient calcium phosphate in physiological conditions. Composed of calcium phosphate precursor powder and curing liquid, calcium phosphate cements (CPCs) can react with water and hydrolyze subsequently, forming apatite-like materials, which is called a setting process. According to the composition of final products, apatite and brushite can be formed after the setting process. For apatite cements,  $\alpha$ -TCP was used and formed calcium-deficient hydroxyapatite. The other forms of calcium phosphate such as tetracalcium phosphate (TTCP) and dicalcium phosphate anhydrous (DCPA) or dicalcium phosphate dehydrate (DCPD) can set at physiological environments. For brushite cements,  $\beta$ -TCP is the major component. One typical example is the mixture of  $\beta$ -TCP and monocalcium phosphate monohydrate. During the setting process, brushite crystals are precipitated and form stable cements. Compared to the traditional polymethyl methacrylate (PMMA) bone cement, the heat generation of CPC setting process is much less, which can be negligible. The unreacted monomer of PMMA cement is harmful to the surrounding tissues. For CPC, unreacted calcium phosphate seemed to be harmless to tissue.

The setting process of CPCs is important to the tissue response. CPCs have attracted so much interest because their setting products have similar composition to bone minerals and they have bioactivity with bone. The apatite-forming ability at the interface of the implant cement materials for bone repairing is critical to the performance for long-term applications. Many failures occur because of the interfacial loosening. Osteointegration is used to describe such direct interface between the bone implant and bone tissues. Higher apatite-forming ability means more reliable performance and good osteointegration. Fabrication of bone cement materials with similar composition and structure with bone tissues is a typical biomimetic approach. In order to fabricate better biomimetic biomaterials for bone repairing, we need to understand the details of bone remodeling process and the related bone structures.

Through mimicking the composition of natural bone, CPC materials have shown great potential in the orthopedic applications. In this chapter, biomimetic methods will be introduced to prepare calcium phosphate with ionic substitutions for bone repairing applications, especially as bone cement and defect filling materials. In the strategy of fabricating biomimetic ion-substituted calcium phosphate, template molecules (soluble, fibrous, structure template) and ionic substitutions (Sr, Mg, Si, Se, F, etc.) can be varied to adjust the properties of calcium phosphate obtained. In



**Fig. 8.1** The biomimetic approach for fabrication of ion-substituted calcium phosphate

addition, the reaction factors including pH, temperature, and aging process also have important roles in the fabrication process (Fig. 8.1).

## 8.2 Biomimetic Synthesis of Ion-Substituted Calcium Phosphate

Wet chemical precipitation is a typical facile process for the synthesis of calcium phosphate. For a typical reaction, calcium ions and phosphate ions are mixed and the supersaturation of calcium phosphate is reached in aqueous solution. Different calcium phosphate phases have different Ca/P molar ratios. The Ca/P ratio of stoichiometric hydroxyapatite is 1.667. For a typical synthesis of hydroxyapatite, 0.06 M sodium hydrogen phosphate solution is mixed with 0.1 M calcium chloride solution ( $P/Ca = 0.6$ ) and the pH value is adjusted to 9–11 by alkaline solution at 80 °C. After aging for 3–5 h, the precipitate in the slurry can be separated by centrifugation or filtration. Using the similar method, different calcium phosphate phases can be precipitated according to the conditions such as the Ca/P ratio, temperature, pH value, aging time, and template molecules. The template molecules can change the nucleation and crystal growth of calcium phosphate, including the phase transition process [1].

The Ca/P molar ratio of DCPD and DCPA is only 1.0. DCPD is obtained by mixing calcium and phosphate solution at room temperature to 60 °C and  $pH = 4-6$ . After heating above 100 °C, DCPD converts to DCPA. The Ca/P ratio of TCP is 1.5. TCP is produced by heat treatment of calcium phosphate.  $\beta$ -TCP can be fabricated by solid-state reaction of calcium carbonate with DCPD at 900 °C. Calcium-deficient hydroxyapatite can also be transformed to  $\beta$ -TCP. With the aid of surfactant, the phase transition temperature can be reduced through the biomimetic method.

For example, ovalbumin was used to regulate the formation of calcium-deficient hydroxyapatite and the resultant products can be converted to  $\beta$ -TCP at 550 °C [19]. At 1300 °C,  $\alpha$ -TCP can be converted from the  $\beta$ -TCP phase or other calcium phosphate phases. Compared to  $\beta$ -TCP,  $\alpha$ -TCP is more soluble and can more rapidly hydrolyze to calcium-deficient hydroxyapatite [20]. Other calcium phosphate salts can also be fabricated by controlling the reaction conditions [21]. In most studies, TCP was prepared by heat treatment at high temperature. Besides the sintering process, a sol-gel method could be used to prepare TCP at room temperature. In methanol, nanosized  $\beta$ -TCP was synthesized at room temperature for 8 h by the reaction between calcium acetate and  $H_3PO_4$  [22].

The preparation of ion-substituted hydroxyapatite and TCP can be realized by adding related ions. For example, nanostructured hydroxyapatite and Mg-substituted brushite and TCP were introduced by simply replacing the calcium salts with magnesium salts [23]. Detailed examples of ionic substitution in calcium phosphate will be further introduced in the following sections.

CPCs often contain one part of precursor powder and one part of liquid. Physical mixing of calcium phosphate salts is often used to produce CPC precursor powder. The curing liquid is mixed with the precursor powder before applying to the bone defects and implanted areas. The setting time of the paste mixture is of importance to the clinical applications. Typically, biomimetic calcium phosphate cement has a setting time from several minutes to half an hour. For example, 58 wt%  $\alpha$ -TCP, 25 wt% DCPA, 8.5% calcium carbonate, and 8.5% hydroxyapatite were intermixed using a mortar and pestle and a typical CPC precursor powder was produced. For strontium substitution, calcium carbonate can be replaced partially or fully by strontium carbonate. For the preparation of paste mixture, aqueous 4 wt% disodium hydrogen phosphate solution was mixed with the precursor powder and subsequent setting process occurred [24]. The precursor properties including crystal phases and particle size affect the solubility and setting process. The ratio of liquid chemical composition containing phosphate to the powder is critical to the property of the bone cement, such as setting time, mechanical strength, and injectability. Many studies focused on the optimized formulations of CPCs to achieve good mechanical properties and biological activity.

### 8.3 Cation-Substituted Calcium Phosphate

Here, four main types of cationic ions (Mg, Zn, Sr, and alkali ions) substituted in calcium phosphate are introduced, which show biological functions for bone tissues. According to the composition, three types of calcium phosphate bone cements are involved: brushite [25], apatite [26], and  $\alpha$ -TCP cement [27].  $Mg^{2+}$ ,  $Zn^{2+}$ , and  $Sr^{2+}$  ions are all divalent cations, which usually substitute into the Ca (II) site. For alkali ions such as  $K^+$  and  $Na^+$ , they substitute into the H (I) site in the structure of calcium phosphate. It is well known that ionic substitutions in the lattice of calcium phosphates have significant influence on the crystal structure, lattice parameters,

crystal shape, solubility, and thermal stability compared to calcium phosphate without substitution. Furthermore, degradability, self-setting characteristics, mechanical strength, injectability, and biological properties of CPCs are influenced after the cationic substitutions.

In general, there are four possible ways to produce cation-substituted CPCs: (a) add cationic ions or salts to an existing cement formulation, (b) substitute calcium ions in the cement precursor powder by their cationic analogues (e.g., substitution of  $\text{CaHPO}_4$  by  $\text{SrHPO}_4$ ), (c) use cation-substituted calcium phosphate phase as a component in the precursor powder (e.g., Sr-substituted  $\alpha$ -TCP), and (d) use a cationic salt-containing solution as liquid phase during the preparation of cement paste [14].

### 8.3.1 Strontium Substitutions

Strontium maintains almost entirely in bone as a level 100–1500  $\mu\text{g/g}$  of the ash mass, and it can substitute in many types of calcium phosphates, like amorphous calcium phosphate, TCP, hydroxyapatite, octacalcium phosphate (OCP), and DCPD. The reported Sr-substituted calcium phosphate contained Sr element in the range of 200–1000  $\mu\text{g/g}$ , which overlaps well with the Sr concentration in bone [28]. Strontium substitutions cause an increase of apatite lattice parameters and cell unit volume because the radius of strontium ions is greater than that of calcium ions [29]. The same effect can be found in brushite, apatite,  $\alpha$ -TCP, and  $\beta$ -TCP [30–33]. In addition, up to 80 mol.% of strontium can enter into the crystal structure of  $\beta$ -TCP [31]. The strontium substitution also induces the increased solubility of strontium-substituted apatite and brushite [32, 34]. It was reported that the solubility of strontium-substituted apatite increased with the increasing concentration of strontium [34]. Strontium-substituted CPC (SrCPC) can help to enhance in vitro degradability and, consequently, osteo-conductivity, as Kuang et al. reported [35].

The setting time of bone cement is important for clinical applications. The desired final setting time of bone cement is about 10–15 min [36]. Although the setting process of CPCs depends on the solubility, it is dramatically influenced by the physicochemical properties of the cement paste such as the Ca/P ratio, particle size, aggregation pattern, and pH value [37]. It was found that when adding nonreactive Sr-containing phases like  $\text{SrCl}_2$  to brushite and  $\alpha$ -TCP cement, the final setting time increased with the high concentration [32, 38]. Meanwhile, it decreased when the reactive Sr-containing phases like SrO were added [39]. Moreover, increasing strontium can reduce the reactivity of Sr- $\alpha$ -TCP and retard the hydration [30], thus increasing final setting time. In order to shorten the final setting time to a designed range, prolonged milling process with suitable reactants was adopted to increase the reactivity of reactants with decreased particle size [40]. Another method is the introduction of a fast chelate reaction by the addition of citric acid, which significantly reduced the setting time when 20 wt% citric acid was added [37].

The mechanical strength of bone cement is determined by the setting process. For  $\alpha$ -TCP, the more rapid the dissolution, the higher the supersaturation of the solution and the faster the reaction, which results in small platelike crystals. After adding strontium, Sr- $\alpha$ -TCP produces larger and needlelike crystals with larger voids. These differences of setting process can explain the lower compressive strength of Sr- $\alpha$ -TCP bone cement compared to the  $\alpha$ -TCP bone cement [30]. It was reported that there might exist an optimized Sr content which could improve the mechanical strength of Sr- $\alpha$ -TCP bone cement [38] or Sr-containing CPCs [24, 41]. The Sr content of 1.0 wt% exhibited a maximum value of 13.0 MPa after 7 days of soaking, while large Sr contents led to a reduction in compressive strength.

With the development of minimally invasive surgical techniques, controlled injectability of CPCs has stimulated much interest. The main factors to manipulate the CPC injectability are particle size [42], particle shape, viscosity of mixing liquid, L/P ratio, and rheology of the paste and additives [43]. S. Pina et al. reported that the Sr substitution increased the injectability of  $\alpha$ -TCP cement in a relatively low L/P ratio up to 0.36 ml/g and explained that Sr enhanced the reactivity of the cement. When the L/P ratio was larger than 0.36 ml/g, there was no influence on the injectability of  $\alpha$ -TCP cement after the Sr substitution [44]. It can be seen that the injectability was a result from the combined effects, and no general conclusion has been drawn by a single factor.

Sr-containing CPCs have been approved to enhance osteointegration and osteoconductivity both in vitro and in vivo [35, 45]. The in vitro cell cytotoxicity of Sr-containing hydroxyapatite bone cement was reported, and no low cytotoxicity was observed [46]. Another important merit of the strontium substitution was that it effectively attenuates osteoclastic resorption, but does not inhibit osteoclastogenesis [47] and osteogenic differentiation [48].

### 8.3.2 $Mg^{2+}$ Substitutes

$Mg^{2+}$  ions have a low content of 0.55 wt% in bone and 0.44 wt% in tooth enamel [49], which is much higher than the content of  $Sr^{2+}$  ions. Like  $Sr^{2+}$ ,  $Mg^{2+}$  can substitute  $Ca^{2+}$  in brushite bone cement [50], apatite bone cement [51–53], and  $\alpha$ -TCP bone cements [44]. The incorporation of  $Mg^{2+}$  into  $\beta$ -TCP has been reported to induce a decreasing trend in *a*- and *c*-axis parameter values and a contraction of calculated cell volume with increasing Mg concentration. The lattice change can be well explained by the different ionic size.  $Mg^{2+}$  ions (72 pm) are smaller than  $Ca^{2+}$  ions (100 pm) [49]. Furthermore, a decreased degree of crystallinity was confirmed from the X-ray diffraction (XRD) patterns after substitution [54]. The degree of crystallinity of Mg- $\beta$ -TCP decreased with the increasing of Mg content. It was found that low crystallinity caused decreased solubility for Mg-doped apatite. Moreover, it was interesting that through the low-temperature synthetic process, 5.7 wt% Mg-doped apatite seemed to perform well in terms of composition, morphology, and crystallinity. The low crystallinity and specific surface area of

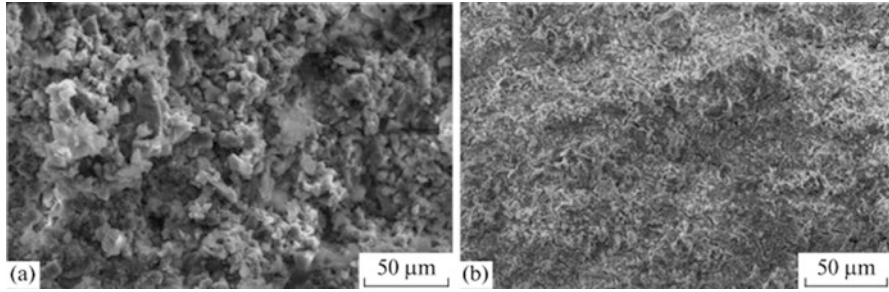
Mg-doped apatite may induce increased solubility [55]. The XRD patterns of the Mg-hydroxyapatite powder were similar to that of natural apatite.

Marc Bohner confirmed that the setting reaction of  $\alpha$ -TCP was inhibited with the increase of the  $\text{MgCl}_2$  concentration from 0.1 to 0.5 M and thus prolonged the setting time [56]. Further studies suggested that the ability of cations to block the hydrolysis of  $\alpha$ -TCP and the conversion to apatite is related to their cationic exchange ability with apatite [56, 57]. The increased setting time was also confirmed after the addition of magnesium-substituted  $\beta$ -TCP with the general formula  $\text{Mg}_x\text{Ca}_{(3-x)}(\text{PO}_4)_2$  with  $0 < x < 3$  to the brushite bone cement [58]. When Mg-substituted CPCs contained MgO phase, the setting time decreased with the increasing magnesium content [51] for the high reactivity of MgO [59, 60].

It seemed that both Mg-substituted  $\alpha$ -TCP cements, fabricated by mainly Mg-substituted  $\alpha$ -TCP [44] and the addition of  $\text{MgCl}_2$  solution [56], have no significant change in mechanical property. The same results were found in brushite bone cement with the addition of Mg-substituted  $\beta$ -TCP [58]. Although the Mg-substituted CPCs contained MgO phase, the mechanical strength did not significantly change for the Mg-substituted  $\alpha$ -TCP and brushite cements with the setting fluid  $\text{Na}_2\text{HPO}_4$ . Another literature reported that the compressive strength was slightly higher in the case of Mg-substituted CPC [61]. Moreover, when the setting fluid changed to  $\text{NaH}_2\text{PO}_4$ , the mechanical strength slightly increased with the substitution of  $\text{Mg}^{2+}$  [51], which may be related to the faster reaction [30] of MgO in a lower pH condition. Figure 8.2 shows the microstructure of the cement materials obtained using (a) liquid 1 ( $\text{Na}_2\text{HPO}_4$ ) and (b) liquid 2 ( $\text{NaH}_2\text{PO}_4$ ). The use of liquid 2 promoted a considerable increase in the cement density and the structure became more homogeneous. The amorphous phase predominated which led to enhancement of the mechanical properties of cement materials.

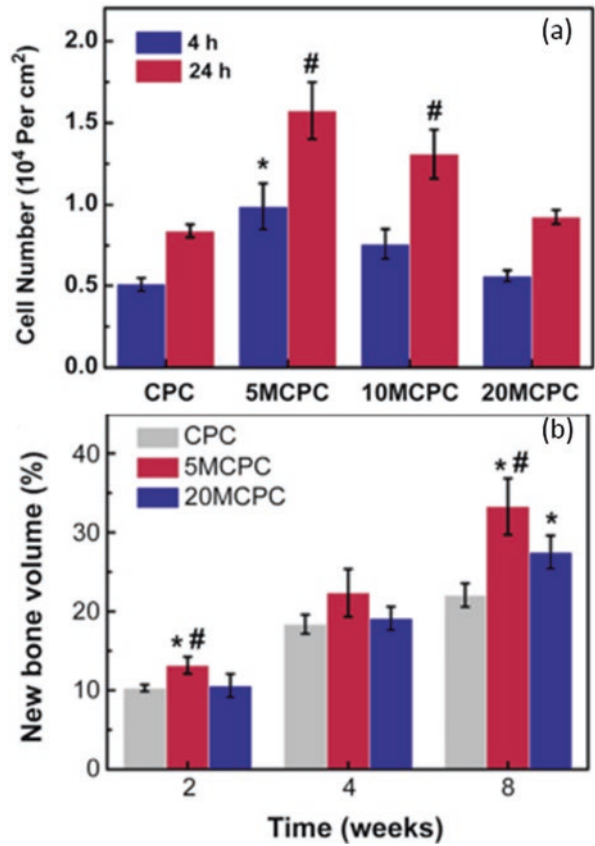
For lower liquid-to-powder ratios like 0.34 and 0.35 mL/g, Mg-substituted  $\alpha$ -TCP cement shows good injectability than Sr-substituted  $\alpha$ -TCP due to the specific role of Mg in delaying the setting process, while at the higher liquid-to-powder ratios like 0.38 mL/g, there was no significant change in injectability and full injectability was obtained as  $\alpha$ -TCP [44]. The similar result was found in Mg-doped brushite cement that the injectability increased with the increasing of Mg content [54].

A few literatures reported the biocompatibility evaluation of the Mg-substituted CPC. The *in vitro* cell testing of brushite cement mixed with Mg-substituted  $\beta$ -TCPs has shown slight cytotoxicity and enabled the osteoblast cells to proliferate [58]. Another *in vitro* rat BMSC cell adhesion and viability of magnesium-doped apatite cement showed that magnesium-doped apatite cement had a better cell adhesion than apatite cement in low magnesium content, but higher magnesium contents in CPC seemed to be harmful to cell adhesion and spreading [62]. The *in vivo* bone regeneration results also showed that magnesium-doped apatite cement with low magnesium content induced more new bone tissue than apatite cement or magnesium-doped apatite cement with high magnesium content [62]. Figure 8.3 shows that the low magnesium content doped apatite cement is good in biocompatibility *in vitro* (a) and bone regeneration *in vivo* (b).



**Fig. 8.2** Microstructure of the cement materials with 40 wt%  $Mg^{2+}$  substitution for  $Ca^{2+}$  obtained using (a) liquid 1 and (b) liquid 2 (Goldberg et al. [51]) (Reprinted with permission. Copyright © 2016, Pleiades Publishing, Ltd.)

**Fig. 8.3** The influence of magnesium content on the cell adhesion in vitro (a) and bone regeneration in vivo (b) of magnesium-doped apatite cement (Zhang et al. [62]) (Reprinted with permission. Copyright © 2015 Elsevier Ltd.)





### 8.3.3 $Zn^{2+}$ Substitutes

Zn is a trace metal element in bone. The average concentrations of Zn were about 30 ppm and 6 ppm in samples of human bone mineral and collagen matrix, respectively [63]. As a divalent ion, Zn can substitute Ca in  $\alpha$ -TCP bone cement [64, 65],  $\beta$ -TCP from brushite bone cement [31, 66, 67], and apatitic bone cement [68–70].  $Zn^{2+}$  has lower ionic radii (74.5 pm for sixfold coordination with O) than  $Ca^{2+}$  (100 pm for sixfold coordination with O sites in the  $\beta$ -TCP structure). The size difference leads to that zinc-substituted  $\beta$ -TCP or apatite has a decreased cell parameter and contraction in the unit cell volume [31, 67, 71]. It was interesting that neither magnesium nor zinc can replace calcium at an extent greater than 20% in the  $\beta$ -TCP structure, while  $\beta$ -TCP can host up to 80 atom% of strontium. These differences suggested that the incorporation of large ions such as  $Sr^{2+}$  does not induce a remarkable rearrangement of the unit cell of  $\beta$ -TCP. In contrast, the incorporation of small ions such as  $Zn^{2+}$  or  $Mg^{2+}$  induced significant rearrangements of the unit cell [31]. The limited Zn substitution concentration has also shown in Zn-doped apatite that the substitution limit of Zn was estimated at about 20 mol% for over which the precipitates lost their apatite structures and became amorphous phase [72]. The same study also showed that the crystal size and the crystallinity significantly decreased with an increasing Zn concentration which may distort the crystal structure of HA and hinder HA crystal growth. A few studies reported that the solubility of Zn-substituted TCP changed because of the ionic substitution. Atsuo Ito reported that the solubility of Zn-substituted  $\beta$ -TCP decreased steeply with an increase in the zinc content [64]. Zinc ions induced destabilization of the  $\alpha$ -TCP structure and led to an increase in solubility of the Zn-substituted  $\alpha$ -TCP phase [73].

Some studies focused on the comparison of Zn-substituted TCP and TCP on the setting time. Xia Li reported that  $\alpha$ -TCP bone cement incorporating 0.19 wt% zinc or less had no adverse effect on the hydrolysis rate of pure  $\alpha$ -TCP bone cement [65], while the hydrolysis of  $\alpha$ -ZnTCP was significantly retarded by incorporating zinc at more than 0.26 wt%. The formed apatite decreased significantly compared with the hydrolyzed from pure  $\alpha$ -TCP [73]. At the same time, the setting time was prolonged like  $Mg^{2+}$ -substituted  $\alpha$ -TCP [56]. Another literature studied the setting time of Zn substituted brushite bone cement, but they failed to study the influence of Zn addition on the setting time of brushite bone cement due to the use of additives like PEG [74].

Sahar Vahabzadeh reported that zinc-doped brushite cement with 0.25 wt% Zn resulted in a notable decrease in compressive strength compared with brushite cement after incubation in PBS at 37 °C for 1 day [75]. However,  $\alpha$ -TCP bone cement incorporating 0.19 wt% zinc or less has no adverse effect on the mechanical strength compared with pure  $\alpha$ -TCP [65]. These above results indicated that the compressive strength of Zn-substituted CPCs may decrease over certain zinc content.

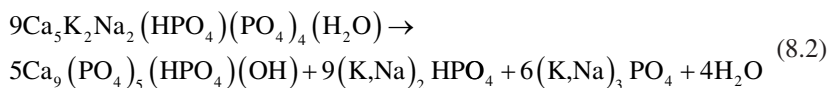
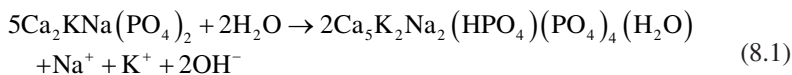
In general, limited  $Zn^{2+}$  release had no cytotoxic effect on cell in vitro. The in vitro cytocompatibility test of 0.11 Zn wt%  $\alpha$ -ZnTCP showed that no significant differences in cell density were found compared to pure  $\alpha$ -TCP [73]. The ZnTCP/

HAP composite ceramics promoted the proliferation of MC3T3-E1 cells without a cytotoxic effect up to a zinc content of 1.20 wt%, releasing zinc up to a concentration of 3.53 mg/L. The cytotoxicity was induced by more release of  $Zn^{2+}$  ions for the more soluble zinc oxide [66]. Another study reported that Zn- and ZnSr-substituted  $\beta$ -TCP cements with about  $2.4 \pm 0.1$  mol%  $Zn^{2+}$  showed nontoxicity to MC3T3-E1 cells. It also showed that ZnCPC or ZnSrCPC cements confirmed their biocompatibility and capability of induction of cellular proliferation [76]. The in vivo study about zinc-containing  $\alpha$ -TCP with different Zn contents from 0.03 to 0.08 wt% indicated that the optimum amount of zinc in the hard tissues is about 0.03 wt%, avoiding inflammatory reaction and significantly promoting more new bone formation than that without zinc [65]. The in vivo results showed that brushite cement with higher Zn content of 0.25 wt% can effectively enhance early-stage in vivo osteointegration and bone remodeling properties [75]. In summary, the suitable zinc concentration in the CPCs can bring positive effect to the bone integration.

### 8.3.4 Alkali Ionic Substitutes

Alkali ions like  $Na^+$  and  $K^+$  were detected mostly in human tendons and bone minerals as trace elements with concentrations of  $10^3$  and  $10^2$  ppm, respectively [63]. Alkali ions can substitute  $H^+$  ions in many types of calcium phosphates, like  $CaNaPO_4$  (CSP),  $CaKPO_4$  (CPP),  $Ca_2KNa(PO_4)_2$  (CPCP) [77], and  $Ca_2KNa(PO_4)_2$  (CPSP) [78, 79]. The available alkali ion-substituted CPC reactants were usually fabricated though a two-step process. The mixture of potassium or sodium carbonate and monetite was sintered to form element-substituted CPC reactants and then milled to produce suitable powder for cement preparation. The enough milling process induced not only decrease of particle size but also loss of crystallinity. The formation of amorphous phase in the products increased the solubility [78, 80]. Moreover, smaller particle size by milling process increased the rate of hydrolysis of alkali ion-substituted calcium phosphate cement and then shortened the setting time.

The setting process of such cements is considered to be a two-step reaction. At first, alkali ion containing apatite is formed according to Eq. (8.1), and this substituted apatite is converted to calcium-deficient hydroxyapatite (Eq. 8.2) with further release of basic by-products [80]:



A series of alkali ion-substituted calcium phosphate cements were fabricated and showed a setting time of approximately 5 min [77]. R. Gildenhaar fabricated a series of  $\text{Ca}_2\text{KNa}(\text{PO}_4)_2$  (CPSP) cements mixed with different additives and setting fluids. The results showed that the addition of sodium pyrophosphate led to a decreased viscosity, extended setting time, and change in solubility behavior [79].

The compressive strength of alkali ion-substituted CPCs was reported to be about 5–10 MPa [77, 81]. The addition of additives to the alkali ion-substituted calcium phosphate cements may improve the compressive strength up to 14–19 MPa [79].

The small particle size by milling also induced strong alkaline pH value of alkali ion-substituted CPC, which may provide antimicrobial properties. Uwe Gbureck reported that alkali ion containing cements showed a significantly higher and longer antimicrobial potency [77]. The inhibition zones around the potassium- and sodium-substituted cements increased to values of approximately 3–6 mm, which showed that the antimicrobial potency of the alkali containing CPC was significantly higher compared to that of the  $\text{Ca}(\text{OH})_2/\text{salicylate}$ .

## 8.4 Anion-Substituted Calcium Phosphate

The anionic substitutions in calcium phosphate contain fluoride, silicate, and carbonate ions. Compared to cation-substituted calcium phosphates, anionic substitutions have not been extensively studied because their effect on new bone formation is not very significant. However, the other effects induced by the anion-substituted CPC have been paid attention. Fluoride is used as an additive in toothpaste for many years because it can enhance the property of enamel. Fluorapatite-based CPCs were prepared by 62.8%  $\text{CaHPO}_4$ , 30.8%  $\text{CaCO}_3$ , and 6.4% NaF and then mixed with tricalcium silicate (TCS) to form cement materials, which were set by mixing with 1.5 M phosphate solution. The setting time was about 10 min and tensile strength was about 3.9 MPa [82]. The product showed highly crystalline apatite phase and the pH value was approximately 11.0. This formulation of fluorapatite-TCS cement is designed for endodontic applications.

Selenium can induce the apoptosis of cancer cells. The incorporation of selenium into calcium phosphate can produce a material for anticancer therapy, especially for filling bone defects after the removal of bone tumors. Selenite ions were incorporated into hydroxyapatite by wet chemical coprecipitation [83]. The obtained novel selenite-substituted hydroxyapatite can slowly release selenite ions and induce the apoptosis of osteosarcoma cells *in vitro* [84] and *in vivo* [85]. The selenite-substituted hydroxyapatite is potentially used as bone filler and cement component after the resection surgery of bone tumor tissues, which can not only improve the healing process of bone tissues but also reduce the recurrence of bone tumor.

Silicon plays important roles during the bone development. The incorporation of silicon into calcium phosphate can endow the material enhanced ability for stimu-

lating new bone formation. In the preparation process of silicon-doped calcium phosphate, many methods including co-sintering and coprecipitation can be applied. Silica-doped TCP was prepared by co-sintering at 1400 °C. The apatite deposition ability of TCP was enhanced after silica doping and degradation rate was reduced. The results showed that apatite covered the sample with >20% Si content and the weight loss was about 30% after immersing in SBF. The silica doping could also improve the hDPC proliferation and differentiation because of the silicon release [86]. Calcium silicate can be mixed with calcium phosphate to form precursor powder of bone cement. For example, monocalcium phosphate was added to calcium silicate cement to form the precursor powder. The setting rate and compressive strength decreased with the concentration of monocalcium phosphate in the cement. During the setting process, monocalcium phosphate reacted with the calcium hydroxide that was a hydrate product of calcium silicate and formed apatite. This process produced a porous microstructure. The composite cement materials showed no toxicity to osteoblast cells and promoted the cell proliferation. The animal test results suggested that the incorporation of monocalcium phosphate improved osteointegration and decreased the degradation rate [87].

In calcium phosphate, cationic and anionic ions can be doped at the same time; for example, silicon and zinc are together doped into the brushite cement. The results suggested that 0.5 wt% Si did not change the performance of cement such as setting time, TCP content, and compressive strength. However, the addition of zinc (0.25 wt%) ions greatly reduced the mechanical strength from 4.8 to 3.8 MPa. For dual doping of silicon and zinc, the mechanical strength decreased to about 3.3 MPa. According to the bone regeneration effect after implantation, silicon-substituted brushite cement showed the best performance, which could promote the early-stage osteointegration and bone remodeling process [75]. In order to improve the mechanical properties, carbon fibers were used to reinforce the calcium phosphate silicate bone cement, which was used to implant into the femoral defect and intramuscular pouches of beagle dogs. The incorporation carbon fibers significantly improved the mechanical strength, and the composite cement showed good osteo-conductivity and osteo-inductivity according to the in vivo results [88].

## 8.5 Bi-Phase Calcium Phosphate

The development of biphasic calcium phosphate (BCP) attracts much attention because of the optimum balance of hydroxyapatite and TCP. Hydroxyapatite is stable in human body, and TCP can gradually hydrolyze to calcium-deficient hydroxyapatite [89]. Gomes reported that silicon can be incorporated into BCP composed of a mixture hydroxyapatite and  $\beta$ -TCP and silicate ions prefer to substitute phosphate in hydroxyapatite [90]. In another study, a basic colloidal hydroxyapatite was mixed with silica and sintered over 800 °C, resulting in a mixture of TCP and hydroxyapatite with silicon substitution. Silicon was found in both TCP and hydroxyapatite lattice, and the doping concentration can regulate the phase transformation of  $\alpha$ -TCP to  $\beta$ -TCP [91].

Calcium silicate was mixed with calcium phosphate to form biphasic cement which contained TCP and DCDP. Human dental pulp cells cultured on this CaSi-TCP material showed upregulated ALP and OCN genes. Meanwhile, cells on CaSi-DCDP only showed upregulated OCN gene and no effect to ALP [92]. The BCP compound prepared by wet chemical precipitation method was mixed with calcium silicate as the precursor powder. Saline solution was used as curing liquid. The BCP could not harden, while calcium silicate showed good strength [93]. The setting process of the bone cement with good injectability can be utilized to produce porous scaffolds for bone defect repair by 3D printing. Li et al. reported that CPC was mixed with mesoporous calcium silicate to produce scaffolds with high mechanical strength. Various structures of the scaffolds can be designed and produced by 3D printing. In this process, the CPCs exhibited good properties for 3D printing [94]. The addition of polypeptide in bone materials regulates the bone formation. Casein phosphopeptide is proved to enhance the mineral adsorption from food. Amorphous calcium phosphate with casein phosphopeptide was added to produce calcium silicate-based cement. The addition of 0.5–1 wt% calcium phosphate did not influence the physical property, but prolonged the setting time. The Ca and P release from the cement increased when 1–3 wt% calcium phosphate was added [95]. Zinc acetate was selected as zinc source, and zinc-substituted BCP was prepared by a sol-gel method. The obtained Zn-BCP was implanted into a femoral defect of rabbit, and it was found that an optimum zinc content in BCP was 0.316 wt% to stimulate the bone formation [96].

## 8.6 Biomimetic Hybrid Calcium Phosphate Materials

The mineralization process is very complicated in the biological systems. Although we cannot produce bone tissues or a piece of tooth *in vitro*, many simplified reactions have been studied to reveal the mechanisms based on template regulations. Some soluble acidic molecules, such as citrate ions, are involved as inhibitors, which cover the surface of mineral crystals and stop the further growth of crystals. The recent studies suggest that citrate bridges the mineral plates [97]. The proposed bone mineral is a structure of thin hydroxyapatite platelets with octacalcium phosphate citrate like sandwich, which has been proved by solid-state NMR spectroscopy and XRD analysis. In addition, the soluble acidic molecules form calcium phosphate clusters in the initial stages of mineralization [3]. The calcium phosphate clusters enter the fibrils of collagen by diffusion and solidify into an amorphous phase. The mineralization process directed by collagen drives the phase transition from amorphous calcium phosphate to hydroxyapatite.

Collagen is often used to regulate the mineralization process, resulting in a composite of collagen and hydroxyapatite. The hydroxyapatite crystals in the composite are nanocrystalline and grow along the c-axis of collagen fibers, which is similar to the structure in natural bone. In addition, calcium-deficient hydroxyapatite is most frequently obtained in this process. The products are also called mineralized

collagen. The hybrid materials of hydroxyapatite and collagen produced using a biomimetic mineralization process are widely used as biomaterials because they show good biocompatibility to bone. The mineralized collagen can be mixed with calcium sulfate hemihydrate and produces an injectable bone cement [98]. By emulsification of a calcium phosphate cement paste with collagen, hybrid calcium-deficient hydroxyapatite microspheres are produced. These composite materials were evaluated in a femur bone defect model of rabbits. After 3 months of evaluation, new bone grew into the implants composed of microspheres with a tenfold increase compared to the normal cement materials. The microspheres formed macroporous networks, and the large surface area of hybrid microspheres enhanced the osteoconduction [99]. By using reverse microemulsion, calcium phosphate nanoparticles ( $\text{Ca/P} = 1.5$ ) can be produced. After heat treatment between 600 and 800 °C, calcium-deficient hydroxyapatite and  $\beta$ -TCP with different ratios were obtained [100].

Besides collagen, many kinds of proteins and macromolecules have been used as template molecules to regulate the formation of calcium phosphate [1]. Silk fibroin is a linear polypeptide which can also regulate the nucleation and crystal growth of hydroxyapatite. In the precipitation process of  $\text{CaCl}_2$  and  $(\text{NH}_4)_2\text{HPO}_4$ , silk fibroin was added to regulate the mineralization at  $\text{pH} = 7.4$ . After aging for 24 h, the obtained composite nanoparticle showed needle- or rodlike shapes with a length of 20–60 nm [101]. Silk fibroin solution was mixed with  $\text{H}_3\text{PO}_4$  solution, and the mixed solution was added to  $\text{Ca}(\text{OH})_2$  suspension at 70 °C. The precipitated nanomaterials are dispersible in water [102]. These hybrid nanomaterials containing hydroxyapatite and proteins can be used as the main components of CPCs.

The peptide amphiphile nanofibers were assembled into hydrogel scaffolds, which served as template to direct the formation of calcium phosphate [103]. The nanofibers have a diameter of 5–7 nm to mimic the nanofibrous structure of a collagen matrix. Bi-/multimolecular templates offer more nucleation sites and active centers in the mineralization process. Wang et al. combined silk fibroin and albumin as chimeric template, and the hydroxyapatite nanospheres produced by this bimolecular template promoted the osteoblastic differentiation of bone marrow stromal stem cells [104]. Ma et al. have used silk fibroin and alginate (acidic molecule) to regulate the formation of calcium phosphate, and the shape of hydroxyapatite nanoparticles changed into sheetlike with a thickness of about 3 nm and a size of more than 100 nm [105]. Zinc ions were also found to change the morphology and structure of the obtained hydroxyapatite nanocomposites. The synthetic bimolecular template was fabricated by polymerization of acrylic acid in chitosan, forming the spherical nanogels. These nanogels could also regulate the formation of hydroxyapatite. The obtained hybrid materials show promising applications as drug delivery systems for protein drugs [106]. An organic matrix composed of chitosan and cis-butenedioic acid (maleic acid, MAc) was used as structure template to guide the mineralization of monetite crystals. After phase transformation, bioinspired organized structures containing hydroxyapatite materials were obtained [107]. Amphiphilic nanogels of 30–40 nm prepared by self-assembling method were used as templates for calcium phosphate mineralization in a dilute hydroxyapatite solution. Hierarchical structures were constructed by nanogel-liposomes and calcium phosphate with a size of about 200 nm [108].

It is known that TCP bone cement changes into hydroxyapatite in the implanted area. The setting process was mediated by the environmental factors. The TCP bone cement was mixed with gelatin, which could control the setting process and improve the mechanical properties. DCPD is added to adjust the phase transition from TCP to calcium-deficient hydroxyapatite. The addition of DCPD prevented gelatin release during the setting process. Thus, the reported compressive strength reached 35 MPa [109].

Poly(methyl methacrylate) (PMMA)-based bone cement has been widely used in clinic for many years. Bone morphogenetic protein 2 (BMP-2) plays very important roles in the formation of new bone and cartilage tissues, which is involved in the signaling pathway of TGF- $\beta$ . BMP-2 is also considered as one of the most useful osteoinductive proteins. Polydopamine is positively charged, which can promote the mineralization process [110]. Immobilization of osteoinductive molecules can be realized using a bioinspired way. A thin layer of polydopamine is applied on the scaffold of polymer or ceramics. The polydopamine-modified surface can efficiently immobilize BMP-2 or similar proteins. In vivo bone formation using the polydopamine-BMP-2-modified PLGA scaffolds suggested that osteoinduction was improved by this biomimetic coating [111]. Hydroxyapatite nanoparticles have been decorated with polydopamine and BMP-2-like peptide (serine-serine-valine-proline-threonine). The modified nanoparticles were mixed with PMMA cement. The obtained composites exhibited excellent interfacial mechanical properties with bone tissues. The biomimetic decoration synergistically enhances the bioactivity for bone regeneration [112].

## 8.7 Conclusion and Perspective

Calcium phosphate cements possess many advantages because they show similar composition compared to bone tissues. Their integration with the surrounding tissues is fast and the biocompatibility is attractive. After the addition of functional element substitutions, the osteo-compatibility is enhanced or special unique properties are endowed. Sr<sup>2+</sup> and Mg<sup>2+</sup> substitutions in calcium phosphate cements have been paid much attention for their enhanced bone formation after implantation. The degradation rate matching the regeneration rate of bone tissues is still a challenge for us to design an ideal bone void-filling material. In addition, injectable calcium phosphate bone cement materials show promising applications. After setting, porous structures with enough mechanical properties formed in the bone defects or between the implants and bone tissues. The biomimetic designs are believed to be better because they provide similar microenvironments which can mimic the complex extracellular matrix for cells. The biomimetic material design following the hierarchical structure of bone tissues can create highly tailored environments for bone regeneration. The biomimetic ion-substituted calcium phosphate materials have great potential in the development of novel bone cement materials.

## References

1. Ma J, Wang J, Ai X et al (2014) Biomimetic self-assembly of apatite hybrid materials: from a single molecular template to bi-/multi-molecular templates. *Biotechnol Adv* 32:744–760
2. Nudelman F, Pieterse K, George A et al (2010) The role of collagen in bone apatite formation in the presence of hydroxyapatite nucleation inhibitors. *Nat Mater* 9:1004–1009
3. Colfen H (2010) Biomineralization: a crystal-clear view. *Nat Mater* 9:960–961
4. Place ES, Evans ND, Stevens MM (2009) Complexity in biomaterials for tissue engineering. *Nat Mater* 8:457–470
5. Cui FZ, Li Y, Ge J (2007) Self-assembly of mineralized collagen composites. *Mater Sci Eng R* 57:1–27
6. Pina S, Oliveira JM, Reis RL (2015) Natural-based nanocomposites for bone tissue engineering and regenerative medicine: a review. *Adv Mater* 27:1143–1169
7. Qiu ZY, Li G, Zhang YQ et al (2012) Fine structure analysis and sintering properties of Si-doped hydroxyapatite. *Biomed Mater* 7:045009
8. Bohner M (2009) Silicon-substituted calcium phosphates – a critical view. *Biomaterials* 30:6403–6406
9. Pietak AM, Reid JW, Stott MJ et al (2007) Silicon substitution in the calcium phosphate bioceramics. *Biomaterials* 28:4023–4032
10. Kubota T, Nakamura A, Toyoura K et al (2014) The effect of chemical potential on the thermodynamic stability of carbonate ions in hydroxyapatite. *Acta Biomater* 10:3716–3722
11. Antonakos A, Liarokapis E, Leventouri T (2007) Micro-Raman and FTIR studies of synthetic and natural apatites. *Biomaterials* 28:3043–3054
12. Tang YZ, Chappell HF, Dove MT et al (2009) Zinc incorporation into hydroxylapatite. *Biomaterials* 30:2864–2872
13. Grandjean-Laquerriere A, Laquerriere P, Jallot E et al (2006) Influence of the zinc concentration of sol-gel derived zinc substituted hydroxyapatite on cytokine production by human monocytes in vitro. *Biomaterials* 27:3195–3200
14. Schumacher M, Gelinsky M (2015) Strontium modified calcium phosphate cements – approaches towards targeted stimulation of bone turnover. *J Mater Chem B* 3:4626–4640
15. Ni GX, Chiu KY, Lu WW et al (2006) Strontium-containing hydroxyapatite bioactive bone cement in revision hip arthroplasty. *Biomaterials* 27:4348–4355
16. Hurlle K, Neubauer J, Goetz-Neunhoeffler F (2016) Influence of Sr<sup>2+</sup> on calcium-deficient hydroxyapatite formation kinetics and morphology in partially amorphized alpha-TCP. *J Am Ceram Soc* 99:1055–1063
17. Lu JX, Wei J, Yan YG et al (2011) Preparation and preliminary cytocompatibility of magnesium doped apatite cement with degradability for bone regeneration. *J Mater Sci-Mater Med* 22:607–615
18. Serre CM, Papillard M, Chavassieux P et al (1998) Influence of magnesium substitution on a collagen-apatite biomaterial on the production of a calcifying matrix by human osteoblasts. *J Biomed Mater Res* 42:626–633
19. Zhao HS, He W, Wang YJ et al (2008) Biomimetic synthesis and characterization of hydroxyapatite crystal with low phase transformation temperature. *J Chem Eng Data* 53:2735–2738
20. Carrodegua RG, De Aza S (2011) Alpha-Tricalcium phosphate: synthesis, properties and biomedical applications. *Acta Biomater* 7:3536–3546
21. Boanini E, Gazzano M, Bigi A (2010) Ionic substitutions in calcium phosphates synthesized at low temperature. *Acta Biomater* 6:1882–1894
22. Bow JS, Liou SC, Chen SY (2004) Structural characterization of room-temperature synthesized nano-sized beta-tricalcium phosphate. *Biomaterials* 25:3155–3161
23. Kumta PN, Sfeir C, Lee DH et al (2005) Nanostructured calcium phosphates for biomedical applications: novel synthesis and characterization. *Acta Biomater* 1:65–83
24. Schumacher M, Henss A, Rohnke M et al (2013) A novel and easy-to-prepare strontium(II) modified calcium phosphate bone cement with enhanced mechanical properties. *Acta Biomater* 9:7536–7544



25. Gisepp A, Wieling R, Bohner M et al (2003) Resorption patterns of calcium-phosphate cements in bone. *J Biomed Mater Res A* 66A:532–540
26. Li YW, Leong JCY, Lu WW et al (2000) A novel injectable bioactive bone cement for spinal surgery: a developmental and preclinical study. *J Biomed Mater Res* 52:164–170
27. Kirschner HJ, Obermayr F, Schaefer J et al (2012) Treatment of benign bone defects in children with silicate-substituted calcium phosphate (SiCaP). *Eur J Pediatr Surg* 22:143–147
28. Rokita E, Hermes C, Nolting HF et al (1993) Substitution of calcium by strontium within selected calcium phosphates. *J Cryst Growth* 130:543–552
29. Bigi A, Boanini E, Capuccini C et al (2007) Strontium-substituted hydroxyapatite nanocrystals. *Inorg Chim Acta* 360:1009–1016
30. Saintjean SJ, Camiré CL, Nevsten P et al (2005) Study of the reactivity and in vitro bioactivity of Sr-substituted  $\alpha$ -TCP cements. *J Mater Sci Mater M* 16:993–1001
31. Bigi A, Foresti E, Gandolfi M et al (1997) Isomorphous substitutions in  $\beta$ -tricalcium phosphate: the different effects of zinc and strontium. *J Inorg Biochem* 66:259–265
32. Chulián MF (2011) Strontium ions substitution in brushite crystals: the role of strontium chloride. *J Func Biomater* 2:31–38
33. Pan HB, Li ZY, Lam WM et al (2009) Solubility of strontium-substituted apatite by solid titration. *Acta Biomater* 5:1678–1685
34. Christoffersen J, Christoffersen MR, Kolthoff N et al (1997) Effects of strontium ions on growth and dissolution of hydroxyapatite and on bone mineral detection. *Bone* 20:47–54
35. Kuang GM, Yau WP, Wu J et al (2015) Strontium exerts dual effects on calcium phosphate cement: accelerating the degradation and enhancing the osteoconductivity both in vitro and in vivo. *J Biomed Mater Res Part A* 103:1613–1621
36. Ginebra MP, Fernández E, Boltong MG et al (1994) Compliance of an apatitic calcium phosphate cement with the short-term clinical requirements in bone surgery, orthopaedics and dentistry. *Clin Mater* 17:99–104
37. Guan-Ming K, Yau WP, Lam WM et al (2012) An effective approach by a chelate reaction in optimizing the setting process of strontium-incorporated calcium phosphate bone cement. *J Biomed Mater Res B* 100:778–787
38. Panzavolta S, Torricelli P, Sturba L et al (2008) Setting properties and in vitro bioactivity of strontium-enriched gelatin–calcium phosphate bone cements. *J Biomed Mater Res A* 84:965–972
39. Tao Y, Li DX, Li YB (2013) Effect of substitutional Sr ion on mechanical properties of calcium phosphate bone cement. *J Wuhan Univ Technol* 28:741–745
40. Gbureck U, Barralet JE, Radu L et al (2004) Amorphous  $\alpha$ -Tricalcium phosphate: preparation and aqueous setting reaction. *J Am Ceram Soc* 87:1126–1132
41. D’Onofrio A, Kent NW, Shahdad SA et al (2016) Development of novel strontium containing bioactive glass based calcium phosphate cement. *Dent Mater* 32:703–712
42. Torres PMC, Gouveia S, Olhero S et al (2015) Injectability of calcium phosphate pastes: effects of particle size and state of aggregation of beta-tricalcium phosphate powders. *Acta Biomater* 21:204–216
43. Low KL, Tan SH, Zein SHS et al (2010) Calcium phosphate-based composites as injectable bone substitute materials. *J Biomed Mater Res B* 94:273–286
44. Pina S, Torres PMC, Ferreira JMF (2010) Injectability of brushite-forming Mg-substituted and Sr-substituted alpha-TCP bone cements. *J Mater Sci Mater Med* 21:431–438
45. Baier M, Staudt P, Klein R et al (2012) Strontium enhances osseointegration of calcium phosphate cement: a histomorphometric pilot study in ovariectomized rats. *J Orthop Surg Res* 8:1–8
46. Guo D, Xu K, Zhao X et al (2005) Development of a strontium-containing hydroxyapatite bone cement. *Biomaterials* 26:4073–4083
47. Schumacher M, Wagner AS, Kokesch-Himmelreich J et al (2016) Strontium substitution in apatitic CaP cements effectively attenuates osteoclastic resorption but does not inhibit osteoclastogenesis. *Acta Biomater* 37:184–194

48. Schumacher M, Lode A, Helth A et al (2013) A novel strontium(II)-modified calcium phosphate bone cement stimulates human-bone-marrow-derived mesenchymal stem cell proliferation and osteogenic differentiation in vitro. *Acta Biomater* 9:9547–9557
49. Kannan S, Goetz-Neunhoeffler F, Neubauer J et al (2009) Rietveld structure and in vitro analysis on the influence of magnesium in biphasic (hydroxyapatite and  $\beta$ -tricalcium phosphate) mixtures. *J Biomed Mater Res B* 90B:404–411
50. Pina S, Ferreira JMF (2010) Brushite-forming Mg-, Zn- and Sr-substituted bone cements for clinical applications. *Dent Mater* 3:519–535
51. Goldberg MA, Smirnov VV, Antonova OS et al (2016) Magnesium-substituted calcium phosphate cements with (Ca + Mg)/P=2. *Dokl Chem* 467:100–104
52. Yu T, Ye JD, Zhang M (2013) Effect of magnesium doping on hydration morphology and mechanical property of calcium phosphate cement under non-calcined synthesis condition. *J Am Ceram Soc* 96:1944–1950
53. Teterina AY, Egorov AA, Fedotov AY et al (2016) Bone cements in the calcium phosphate-chitosan systems containing magnesium and zinc. *Dokl Chem* 468:199–201
54. Saleh AT, Ling LS, Hussain R (2016) Injectable magnesium-doped brushite cement for controlled drug release application. *J Mater Sci* 51:7427–7439
55. Landi E, Logroscino G, Proietti L et al (2008) Biomimetic Mg-substituted hydroxyapatite: from synthesis to in vivo behaviour. *J Mater Sci Mater Med* 19:239–247
56. Bohner M, Tiainen H, Michel P et al (2015) Design of an inorganic dual-paste apatite cement using cation exchange. *J Mater Sci Mater Med* 26:63
57. Suzuki T, Hatsushika T, Hayakawa Y (1981) Synthetic hydroxyapatites employed as inorganic cation-exchangers. *J Chem Soc Faraday Trans* 5:1059–1062
58. Klammert U, Reuther T, Blank M et al (2010) Phase composition, mechanical performance and in vitro biocompatibility of hydraulic setting calcium magnesium phosphate cement. *Acta Biomater* 6:1529–1535
59. Liu W, Dong Z, Huan Z et al (2015) Novel tricalcium silicate/magnesium phosphate composite bone cement having high compressive strength, in vitro bioactivity and cytocompatibility. *Acta Biomater* 21:217–227
60. Chen FP, Song ZY, Liu CS (2015) Fast setting and anti-washout injectable calcium-magnesium phosphate cement for minimally invasive treatment of bone defects. *J Mater Chem B* 3:9173–9181
61. Pina S, Olhero SM, Gheduzzi S et al (2009) Influence of setting liquid composition and liquid-to-powder ratio on properties of a Mg-substituted calcium phosphate cement. *Acta Biomater* 5:1233–1240
62. Zhang J, Ma XY, Lin D et al (2015) Magnesium modification of a calcium phosphate cement alters bone marrow stromal cell behavior via an integrin-mediated mechanism. *Biomaterials* 53:251–264
63. Spadaro JA, Becker RO, Bachman CH (1970) The distribution of trace metal ions in bone and tendon. *Calcif Tissue Res* 6:49–54
64. Ito A, Sogo Y, Kamo M et al (2003) Zinc-containing alpha-tricalcium phosphate cement for stimulating bone formation: a preliminary study. *J Dental Res* 82:B278
65. Li X, Sogo Y, Ito A et al (2009) The optimum zinc content in set calcium phosphate cement for promoting bone formation in vivo. *Mat Sci Eng C-Bio S* 29:969–975
66. Ito A, Ojima K, Naito H et al (2000) Preparation, solubility, and cytocompatibility of zinc-releasing calcium phosphate ceramics. *J Biomed Mater Res* 50:178–183
67. Kannan S, Goetz-Neunhoeffler F, Neubauer J et al (2009) Synthesis and structure refinement of zinc-doped  $\beta$ -tricalcium phosphate powders. *J Am Ceram Soc* 92:1592–1595
68. Hattori Y, Mori H, Chou J et al (2016) Mechanochemical synthesis of zinc-apatitic calcium phosphate and the controlled zinc release for bone tissue engineering. *Drug Dev Ind Pharm* 42:595–601
69. Horiuchi S, Asaoka K, Tanaka E (2009) Development of a novel cement by conversion of hopeite in set zinc phosphate cement into biocompatible apatite. *Biomed Mater Eng* 19:121–131

70. Walczyk D, Malina D, Krol M et al (2016) Physicochemical characterization of zinc-substituted calcium phosphates. *Bull Mater Sci* 39:525–535
71. Miyaji F, Kono Y, Suyama Y (2005) Formation and structure of zinc-substituted calcium hydroxyapatite. *Mater Res Bull* 40:209–220
72. Ren F, Xin R, Xiang G et al (2009) Characterization and structural analysis of zinc-substituted hydroxyapatites. *Acta Biomater* 5:3141–3149
73. Sogo Y, Ito A, Kamo M et al (2004) Hydrolysis and cytocompatibility of zinc-containing  $\alpha$ -tricalcium phosphate powder. *Mater Sci Eng C* 24:709–715
74. † SP, † SIV, Torres PMC et al (2010) In vitro performance assessment of new brushite-forming Zn- and ZnSr-substituted  $\beta$ -TCP bone cements. *J Biomed Mater Res B* 94B: 414–420
75. Vahabzadeh S, Bandyopadhyay A, Bose S et al (2015) IGF-loaded silicon and zinc doped brushite cement: physico-mechanical characterization and in vivo osteogenesis evaluation. *Integr Biol-Uk* 7:1561–1573
76. Pina S, Vieira SI, Rego P et al (2010) Biological responses of brushite-forming Zn- and ZnSr-substituted beta-tricalcium phosphate bone cements. *Eur Cell Mater* 20:162–177
77. Gbureck U, Knappe O, Grover LM et al (2005) Antimicrobial potency of alkali ion substituted calcium phosphate cements. *Biomaterials* 26:6880–6886
78. Gbureck U, Thull R, Barralet JE (2005) Alkali ion substituted calcium phosphate cement formation from mechanically activated reactants. *J Mater Sci-Mater Med* 16:423–427
79. Gildenhaar R, Berger G, Lehmann E et al (2008) Development of alkali containing calcium phosphate cements. In: Daculsi G, Layrolle P (ed) *Bioceramics* 20:331–334
80. Driessens FCM, Boltong MG, Maeyer EAPD et al (2002) The Ca/P range of nanoapatitic calcium phosphate cements. *Biomaterials* 23:4011–4017
81. Berger G, Ullner C, Neumann G et al (2006) New characterization of setting times of alkali containing calcium phosphate cements by using an automatically working device according to Gillmore needle test. In: Nakamura T, Yamashita K, Neo M (eds) *Bioceramics* 18:825–828
82. Suzuki Y, Hayashi M, Yasukawa T et al (2015) Development of a novel fluorapatite-forming calcium phosphate cement with calcium silicate: in vitro and in vivo characteristics. *Dent Mater J* 34:263–269
83. Ma J, Wang YH, Zhou L et al (2013) Preparation and characterization of selenite substituted hydroxyapatite. *Mat Sci Eng C Mater* 33:440–445
84. Wang YH, Ma J, Zhou L et al (2012) Dual functional selenium-substituted hydroxyapatite. *Interface focus* 2:378–386
85. Wang Y, Hao H, Liu H et al (2015) Selenite-releasing bone mineral nanoparticles retard bone tumor growth and improve healthy tissue functions in vivo. *Adv Healthc Mater* 4:1813–1818
86. Huang SH, Chen YJ, Kao CT et al (2015) Physicochemical properties and biocompatibility of silica doped beta-tricalcium phosphate for bone cement. *J Dental Sci* 10:282–290
87. Gong T, Wang Z, Zhang Y et al (2016) A comprehensive study of osteogenic calcium phosphate silicate cement: material characterization and in vitro/in vivo testing. *Adv Healthc Mater* 5:457–466
88. Zheng JJ, Xiao Y, Gong TX et al (2016) Fabrication and characterization of a novel carbon fiber-reinforced calcium phosphate silicate bone cement with potential osteo-inductivity. *Biomed Mater* 11:015003
89. Daculsi G (1998) Biphasic calcium phosphate concept applied to artificial bone, implant coating and injectable bone substitute. *Biomaterials* 19:1473–1478
90. Gomes S, Renaudin G, Mesbah A et al (2010) Thorough analysis of silicon substitution in biphasic calcium phosphate bioceramics: a multi-technique study. *Acta Biomater* 6:3264–3274
91. Reid JW, Pietak A, Sayer M et al (2005) Phase formation and evolution in the silicon substituted tricalcium phosphate/apatite system. *Biomaterials* 26:2887–2897
92. Gandolfi MG, Spagnuolo G, Siboni F et al (2015) Calcium silicate/calcium phosphate biphasic cements for vital pulp therapy: chemical-physical properties and human pulp cells response. *Clin Oral Investig* 19:2075–2089

93. Radwan MM, Abd El-Hamid HK, Mohamed AF (2015) Influence of saline solution on hydration behavior of beta-dicalcium silicate in comparison with biphasic calcium phosphate/hydroxyapatite bio-ceramics. *Mater Sci Eng C-Mater Biol Appl* 57:355–362
94. Li CD, Gao L, Chen FP et al (2015) Fabrication of mesoporous calcium silicate/calcium phosphate cement scaffolds with high mechanical strength by freeform fabrication system with micro-droplet jetting. *J Mater Sci* 50:7182–7191
95. Dawood AE, Manton DJ, Parashos P et al (2015) The physical properties and ion release of CPP-ACP-modified calcium silicate-based cements. *Aust Dent J* 60:434–444
96. Kawamura H, Ito A, Miyakawa S et al (2000) Stimulatory effect of zinc-releasing calcium phosphate implant on bone formation in rabbit femora. *J Biomed Mater Res* 50:184–190
97. Davies E, Muller KH, Wong WC et al (2014) Citrate bridges between mineral platelets in bone. *P Natl Acad Sci USA* 111:E1354–E1363
98. Liu X, Wang XM, Chen Z et al (2010) Injectable bone cement based on mineralized collagen. *J Biomed Mater Res B* 94:72–79
99. Cuzmar E, Perez RA, Manzanares MC et al (2015) In vivo osteogenic potential of biomimetic hydroxyapatite/collagen microspheres: comparison with injectable cement pastes. *PLoS One* 10
100. Dasgupta S, Bandyopadhyay A, Bose S (2009) Reverse micelle-mediated synthesis of calcium phosphate nanocarriers for controlled release of bovine serum albumin. *Acta Biomater* 5:3112–3121
101. Wang J, Yu F, Qu L et al (2010) Study of synthesis of nano-hydroxyapatite using a silk fibroin template. *Biomed Mater* 5:041002
102. Huang X, Liu X, Liu S et al (2014) Biomineralization regulation by nano-sized features in silk fibroin proteins: synthesis of water-dispersible nano-hydroxyapatite. *J Biomed Mater Res B* 102:1720–1729
103. Spoerke ED, Anthony SG, Stupp SI (2009) Enzyme directed templating of artificial bone mineral. *Adv Mater* 21:425–430
104. Wang JL, Yang GJ, Wang YF et al (2015) Chimeric protein template-induced shape control of bone mineral nanoparticles and its impact on mesenchymal stem cell fate. *Biomacromolecules* 16:1987–1996
105. Ma J, Qin J (2015) Graphene-like zinc substituted hydroxyapatite. *Cryst Growth Des* 15:1273–1279
106. Qin J, Zhong Z, Ma J (2016) Biomimetic synthesis of hybrid hydroxyapatite nanoparticles using nanogel template for controlled release of bovine serum albumin. *Mater Sci Eng C* 62:377–383
107. Ruan QC, Liberman D, Zhang YZ et al (2016) Assembly of layered monetite-chitosan nanocomposite and its transition to organized hydroxyapatite. *ACS Biomater Sci Eng* 2:1049–1058
108. Sugawara A, Yamane S, Akiyoshi K (2006) Nanogel-templated mineralization: polymer-calcium phosphate hybrid nanomaterials. *Macromol Rapid Commun* 27:441–446
109. Panzavolta S, Bracci B, Rubini K et al (2011) Optimization of a biomimetic bone cement: role of DCPD. *J Inorg Biochem* 105:1060–1065
110. Zhou YZ, Cao Y, Liu W et al (2012) Polydopamine-induced tooth remineralization. *ACS Appl Mater Interfaces* 4:6900–6909
111. Ko E, Yang K, Shin J et al (2013) Polydopamine-assisted osteoinductive peptide immobilization of polymer scaffolds for enhanced bone regeneration by human adipose-derived stem cells. *Biomacromolecules* 14:3202–3213
112. Kang T, Hua XL, Liang PQ et al (2016) Synergistic reinforcement of polydopamine-coated hydroxyapatite and BMP2 biomimetic peptide on the bioactivity of PMMA-based cement. *Compos Sci Technol* 123:232–240

# Chapter 9

## Nanodimensional and Nanocrystalline Calcium Orthophosphates

Sergey V. Dorozhkin

**Abstract** Nano-scaled particles and crystals play very important roles in biological systems. For example, calcium orthophosphates ( $\text{CaPO}_4$ ) with nano-size dimensions represent the basic inorganic building blocks of bones and teeth of mammals. According to recent discoveries in biomineralization, zillions of nanodimensional crystals of biological apatites are nucleated in body fluids, and afterward, they are self-assembled into these complex structures. In addition, both a greater viability and a better proliferation of various types of cells have been detected on smaller crystals of  $\text{CaPO}_4$ . All these effects are due to the higher surface-to-volume ratio, increased reactivity, and biomimetic morphologies of the nano-scaled particles. Thus, the nano-sized and nanocrystalline forms of  $\text{CaPO}_4$  have a great potential to revolutionize the hard tissue engineering field, starting from bone repair and augmentation to controlled drug delivery systems. Therefore, preparation and application of nanodimensional  $\text{CaPO}_4$  are the important topics in modern material science, and such formulations have been already tested clinically for various purposes. Currently, more efforts are focused on the possibility of combining nano-scaled  $\text{CaPO}_4$  with cells, drugs, and other biologically active substances for multipurpose applications. This chapter describes current state-of-the-art and recent developments on the subject, starting from synthesis and characterization to biomedical and clinical applications.

**Keywords** Calcium orthophosphates • Hydroxyapatite • Nano-scaled • Bone grafts • Tissue engineering

---

S.V. Dorozhkin (✉)  
Kudrinskaja sq. 1-155, Moscow 123242, Russia  
e-mail: [sedorozhkin@yandex.ru](mailto:sedorozhkin@yandex.ru)

## 9.1 Introduction

Living organisms can create the amazing ways to produce various high-performance materials, and over 60 different inorganic minerals of biological origin have already been revealed [1]. Among them, calcium orthophosphates ( $\text{CaPO}_4$ ) are of a special importance since they are the most important inorganic constituents of hard tissues in vertebrates [2, 3]. In the form of a poor crystalline, nonstoichiometric, ion-substituted CDHA (commonly referred to as “biological apatite”),  $\text{CaPO}_4$  are present in bones, teeth, deer antlers, and tendons of mammals to give these organs stability, hardness, and function [2, 4, 5]. Though we still do not exactly know why the highly intelligent animals use conformable  $\text{CaPO}_4$  as their crucial biomineral for survival [6], current biomedical questions of persistent pathological and physiological mineralization in the body force people to focus on the processes, including the occurrence, formation, and degradation of  $\text{CaPO}_4$  in living organisms [7–9].

Biomineralization is a process of *in vivo* formation of inorganic minerals [1, 2]. In the biomineralization processes, organized assemblies of organic macromolecules regulate nucleation, growth, morphology, and assembly of inorganic crystals. Biologically formed  $\text{CaPO}_4$  (biological apatite) are always nanodimensional and nanocrystalline, which have been formed *in vivo* under mild conditions [10]. According to many reports, dimensions of biological apatite in the calcified tissues always possess a range of a few to hundreds of nanometers with the smallest building blocks on the nanometer-sized scale [2, 4, 5, 11]. For example, tens to hundreds of nanometer-sized apatite crystals in a collagen matrix are combined into self-assembled structures during bone and teeth formation [2, 4, 5]. Recent advances suggest that this is a natural selection, since the nanostructured materials provide a better capability for the specific interactions with proteins [12].

Due to the aforementioned, nanodimensional and nanocrystalline forms of  $\text{CaPO}_4$  are able to mimic both the compositions and dimensions of constituent components of the calcified tissues. Thus, they can be utilized in biomineralization and as biomaterials due to their excellent biocompatibility [13, 14]. Further development of  $\text{CaPO}_4$ -based biomaterials obviously will stand to benefit mostly from nanotechnology [15], which offers unique approaches to overcome shortcomings of many conventional materials. For example, nano-sized ceramics can exhibit significant ductility before failure contributed by the grain-boundary phase. Namely, already in 1987, Karch et al. reported that, with nanodimensional grains, a brittle ceramic could permit a large plastic strain up to 100% [16]. In addition, nanostructured ceramics can be sintered at lower temperatures; thereby, major problems associated with a high-temperature sintering are also decreased. Thus, nanodimensional and nanocrystalline forms of bioceramics clearly represent a promising class of orthopedic and dental implant formulations with improved biological and biomechanical properties [17].

Many other advances have been made in biomaterial field due to a rapid growth of nanotechnology [18]. For example, a theory of “aggregation-based crystal growth” [19] and a concept of “mesocrystals” [20, 21] highlighted the roles of

nano-sized particles in biological crystal engineering. In this aspect, the study of  $\text{CaPO}_4$  is a specific area in nanotechnology, because they might be applied readily to repair hard skeletal tissues of mammals [22–24].

Herein, an overview of nano-scaled apatites and other  $\text{CaPO}_4$  in studies on biomineralization and biomaterials is given. The available  $\text{CaPO}_4$  are listed in Table 9.1. To narrow the subject of this chapter, with a few important exceptions, undoped and unsubstituted  $\text{CaPO}_4$  are considered and discussed only. The readers interested in various nanodimensional and nanocrystalline ion-substituted  $\text{CaPO}_4$  are referred to the original publications [25–51]. Furthermore, the details on  $\text{CaPO}_4$ -based nanodimensional biocomposites [52–66] or nanodimensional  $\text{CaPO}_4$ -based biocomposites [67–76] are available in literature [77].

This chapter is organized into several sections. After a brief introduction (current section), general information on “nano” is provided in the second section. The third section briefly compares the micron-sized and nano-scaled  $\text{CaPO}_4$ . The fourth section briefly discusses the presence of nano-scaled  $\text{CaPO}_4$  in normal calcified tissues of mammals. The structure of nano-scaled apatites is described in the fifth section. Synthesis of nano-scaled  $\text{CaPO}_4$  with various dimensions and shapes is reviewed in the sixth section, while biomedical applications are examined in the seventh section. Finally, the summary and reasonable future perspectives in this active research area are given in the last section.

## 9.2 General Information on “Nano”

The prefix “nano” specifically means a measure of  $10^{-9}$  units. Although it is widely accepted that the prefix “nano” specifically refers to  $10^{-9}$  units, in the context of nano-scaled materials, the units should only be those of dimensions, rather than of any other unit of the scientific measurements. Besides, for practical purposes, it appears to be unrealistic to consider the prefix “nano” to solely and precisely refer to  $10^{-9}$  m, just as it is not considered that “micro” specifically and solely concerns something with a dimension of precisely  $10^{-6}$  m [78]. Currently, there is a general agreement that the subject of nanoscience and nanotechnology started after the famous talk: “There’s plenty of room at the bottom” given by the Nobel Prize winner in physics Prof. Richard P. Feynman on December 26, 1959, at the annual meeting of the American Physical Society held at California Institute of Technology. This well-known talk has been widely published in various media (e.g., [79]).

In 2007, an extensive discussion about a framework for definitions presented to the European Commission took place. As the result, on November 29, 2007, the nanoscale has been defined as being of the order of 100 nm or less. Similarly, a nanomaterial has been defined as “any form of a material that is composed of discrete functional parts, many of which have one or more dimensions of the order of 100 nm or less” [80]. However, on October 18, 2011, the European Commission adopted another crosscutting definition of nanomaterials to be used for all regulatory purposes: “Nanomaterial means a natural, incidental or manufactured material

**Table 9.1** Existing calcium orthophosphates and their major properties [240, 241]

Ca/P molar ratio	Compounds and their typical abbreviations	Chemical formula	Solubility at 25 °C, -log(K <sub>s</sub> )	Solubility at 25 °C, g/L	pH stability range in aqueous solutions at 25 °C
0.5	Monocalcium phosphate monohydrate (MCPM)	Ca <sub>2</sub> (H <sub>2</sub> PO <sub>4</sub> ) <sub>2</sub> ·H <sub>2</sub> O	1.14	~18	0.0–2.0
0.5	Monocalcium phosphate anhydrous (MCPA or MCP)	Ca <sub>2</sub> (H <sub>2</sub> PO <sub>4</sub> ) <sub>2</sub>	1.14	~17	<sup>a</sup>
1.0	Dicalcium phosphate dihydrate (DCPD), mineral brushite	CaHPO <sub>4</sub> ·2H <sub>2</sub> O	6.59	~0.088	2.0–6.0
1.0	Dicalcium phosphate anhydrous (DCPA or DCP), mineral monetite	CaHPO <sub>4</sub>	6.90	~0.048	<sup>a</sup>
1.33	Octacalcium phosphate (OCP)	Ca <sub>8</sub> (HPO <sub>4</sub> ) <sub>2</sub> (PO <sub>4</sub> ) <sub>4</sub> ·5H <sub>2</sub> O	96.6	~0.0081	5.5–7.0
1.5	α-Tricalcium phosphate (α-TCP)	α-Ca <sub>3</sub> (PO <sub>4</sub> ) <sub>2</sub>	25.5	~0.0025	<sup>b</sup>
1.5	β-Tricalcium phosphate (β-TCP)	β-Ca <sub>3</sub> (PO <sub>4</sub> ) <sub>2</sub>	28.9	~0.0005	<sup>b</sup>
1.2–2.2	Amorphous calcium phosphates (ACP)	Ca <sub>n</sub> H <sub>n</sub> (PO <sub>4</sub> ) <sub>n</sub> ·nH <sub>2</sub> O, n = 3–4.5; 15–20% H <sub>2</sub> O	<sup>c</sup>	<sup>c</sup>	~5–12 <sup>d</sup>
1.5–1.67	Calcium-deficient hydroxyapatite (CDHA or Ca-def HA) <sup>e</sup>	Ca <sub>40-x</sub> (HPO <sub>4</sub> ) <sub>x</sub> (PO <sub>4</sub> ) <sub>6-x</sub> (OH) <sub>2-x</sub> (0 < x < 1)	~85	~0.0094	6.5–9.5
1.67	Hydroxyapatite (HA, HAp, or OHAp)	Ca <sub>10</sub> (PO <sub>4</sub> ) <sub>6</sub> (OH) <sub>2</sub>	116.8	~0.0003	9.5–12
1.67	Fluorapatite (FA or FAp)	Ca <sub>10</sub> (PO <sub>4</sub> ) <sub>6</sub> F <sub>2</sub>	120.0	~0.0002	7–12
1.67	Oxyapatite (OA, OAp, or OXA) <sup>f</sup> , mineral voelckerite	Ca <sub>10</sub> (PO <sub>4</sub> ) <sub>6</sub> O	~69	~0.087	<sup>b</sup>
2.0	Tetracalcium phosphate (TTCP) or TetCP), mineral hilgenstockite	Ca <sub>4</sub> (PO <sub>4</sub> ) <sub>2</sub> O	38–44	~0.0007	<sup>b</sup>

<sup>a</sup>Stable at temperatures above 100 °C<sup>b</sup>These compounds cannot be precipitated from aqueous solutions<sup>c</sup>Cannot be measured precisely. However, the following values were found: 25.7 ± 0.1 (pH = 7.40), 29.9 ± 0.1 (pH = 6.00), 32.7 ± 0.1 (pH = 5.28) [247]. The comparative extent of dissolution in acidic buffer is ACP >> α-TCP >> β-TCP >> CDHA >> HA > FA [90]<sup>d</sup>Always metastable<sup>e</sup>Occasionally, it is called “precipitated HA (PHA)”<sup>f</sup>Existence of OA remains questionable



containing particles, in an unbound state or as an aggregate or as an agglomerate and where, for 50% or more of the particles in the number size distribution, one or more external dimensions is in the size range 1 nm – 100 nm. In specific cases and where warranted by concerns for the environment, health, safety or competitiveness the number size distribution threshold of 50% may be replaced by a threshold between 1 and 50%” [81]. Thus, since 2011, the presence of coarser particles in amounts up to 50% is allowed in nanomaterials.

Other definitions logically follow this approach such as a nanocrystalline material is “a material that is comprised of many crystals, the majority of which have one or more dimensions of the order of 100 nm or less” (used to be with the presence of neither the micron-sized crystals nor an intergranular amorphous phase; however, this is not the case after October 18, 2011) and a nanocomposite is a “multi-phase material in which the majority of the dispersed phase components have one or more dimensions of the order of 100 nm or less” [78]. Similarly, nanostructured materials are defined as the materials containing structural elements (e.g., clusters, crystallites, or molecules) with dimensions in the 1–100 nm range [82], nanocoatings represent individual layers or multilayer surface coatings of 1–100 nm thick, nanopowders are extremely fine powders with an average particle size in the range of 1–100 nm, and nanofibers are the fibers with a diameter within 1–100 nm [83, 84]. It also has been proposed to extend the lower size limit to 0.1 nm [85], which would include all existing organic molecules, allowing chemists to rightly claim they have been working on nanotechnology for very many years [86].

Strictly speaking, there are serious doubts that the term “nanomaterial” has a reasonable meaning. For example, let me cite Prof. David F. Williams, the Editor in Chief of *Biomaterials*:

... some words which have no rational basis whatsoever become part of everyday language so rapidly, even if so illogically, that it is impossible to reverse the process and their common use has to be accepted, or perhaps, accommodated. Nanomaterial is one such word, where I have argued that it should not exist, but accept that it does through common usage and have to recognise its existence [78]. The discussion about nanomaterial provides a hint of the analysis of a biomaterial that follows, since a prefix, which is an indicator of scale, cannot specify the integer that follows (in this case a material) unless that integer can be qualified by that scale. In other words, it is very clear what a nanometre is because nano – means  $10^{-9}$  and a metre is a measure of length. In the case of nanomaterial, what is it about the material that is  $10^{-9}$ . Is it the dimension of a crystal within the material, or of a grain boundary, a domain, or a molecule, or is it a parameter of a surface feature of the sample, or perhaps of the resistivity or thermal conductivity of the material. Clearly this is nonsense, but one has to accept that nanomaterials are here to stay, with even some journal titles containing the word [87].

Following this logic, such terms as “nanocomposite,” “nanocoatings,” “nanopowders,” “nanofibers,” and “nanocrystals” are senseless either and should be replaced, for example, by “composites with nano-sized (or nanodimensional) dispersed phase(s),” “coatings of nano-sized (or nanodimensional) thickness,” “nano-sized (or nanodimensional) powders,” “fibers of nano-sized (or nanodimensional) thickness,” and “nano-sized (or nanodimensional) crystals,” respectively. At least, this has been done in this chapter.

According to their geometry, all nanodimensional materials can be divided into three major categories: equiaxed, one-dimensional (or fibrous), and two-dimensional (or lamellar) forms. Selected examples and typical applications of each category of nanodimensional materials and their use in biomedical applications are available in literature [88]. It is important to note that in the scientific literature on  $\text{CaPO}_4$ , there are cases when the prefix “nano” has been applied for the structures, with the minimum dimensions exceeding 100 nm [89–99].

As a rule, nanodimensional materials can be manufactured from nearly any substance. Of crucial importance, there are two major characteristics conferring the special properties of any nanodimensional material. These are the quantum effects associated with the very small dimensions (currently, this is not applicable to the biomaterial field) and a large surface-to-volume ratio that is encountered at these dimensions. For instance, specific surface areas for submicron-sized particles are typically 60–80  $\text{m}^2/\text{g}$ , while decreasing particle diameter to tens of nanometers increases the specific surface area up to five times more – an amazing amount of surface area per mass! Furthermore, all nanophase materials have unique surface properties, such as an increased number of grain boundaries and defects on the surface, huge surface area, and altered electronic structure, if compared to the micron-sized materials [78, 100]. While less than ~1% of a micron-sized particle’s atoms occupy the surface positions, over a tenth of the atoms in a 10-nm-diameter particle reside on its surface and ~60% in a 2-nm particle [101]. This very high surface-to-volume ratio of nanodimensional materials provides a tremendous driving force for diffusion, especially at elevated temperatures, as well as causes a self-aggregation into larger particles. Besides, solubility of many substances increases with particle size decreasing [102, 103]. What’s more, nanophase materials could have surface features (e.g., a higher amount of nanoscale pores) to influence the type and amount of adsorption of selective proteins that could enhance specific osteoblast adhesion [104]. Finally and yet importantly, the nanodimensional and nanocrystalline materials have different mechanical, electrical, magnetic, and optical properties if compared to the larger-grained materials of the same chemical composition [105–108].

Further, one should stress that there are both nano-sized biomaterials and nanostructured biomaterials, which should be differentiated from each other. The former ones refer to individual molecular level biomaterials such as single proteins (are not considered in this chapter), while the latter ones refer to any biomaterials whose structure or morphology can be engineered to get features with nanometer-scale dimensions [109]. Although both types of biomaterials constitute a bridge between single molecules and bulk material systems, this chapter is limited to  $\text{CaPO}_4$ -based nanostructured biomaterials only. In general, nanostructured materials can take the form of powders, dispersions, coatings, or even bulk materials. Furthermore, they usually contain a large volume fraction (greater than 50%) of defects such as grain boundaries, interphase boundaries, and dislocations, which strongly influence their chemical and physical properties. The great advantages of nanostructuring were first understood in electronic industry with the advent of thin film deposition processes. Other application areas have followed. For example, nanostructured bioceramics was found to improve friction and wear problems associated with joint

replacement components because it was tougher and stronger than coarser-grained bioceramics [110]. Furthermore, nanostructuring has allowed chemical homogeneity and structural uniformity to an extent, which was once thought to be impossible to achieve [111]. In  $\text{CaPO}_4$  bioceramics, the major target of nanostructuring is to mimic the architecture of bones and teeth [111, 112].

### 9.3 Micron- and Submicron-Sized $\text{CaPO}_4$ Versus the Nano-scaled Ones

The micron-sized  $\text{CaPO}_4$ -based bioceramic powders suffer from poor sinterability, mainly due to a low surface area (typically 2–5  $\text{m}^2/\text{g}$ ), while the specific surface area of nanodimensional  $\text{CaPO}_4$  exceeds 100  $\text{m}^2/\text{g}$  [113]. In addition, the resorption process of synthetic micron-sized  $\text{CaPO}_4$  was found to be quite different from that of bone mineral [114].

While the nano-scaled features of natural  $\text{CaPO}_4$  of bones and teeth had been known earlier [2, 115–120], the history of the systematic investigations of this field has started only in 1994. Namely, a careful search in scientific databases using various combinations of keywords “nano” + “calcium phosphate,” “nano” + “apatite,” “nano” + “hydroxyapatite,” etc. in the article title revealed five papers published in 1994 [121–125]. Although no papers published earlier than 1994 with the aforementioned keywords in the title were found, it is very likely that  $\text{CaPO}_4$  of nanoscale dimensions had been prepared long before; however, those samples just did not contain the “nano” prefix due to a lack of the modern fashion to “nano”-related terms.

Nanodimensional (size ~67 nm) HA was found to have a higher surface roughness of 17 nm if compared to 10 nm for the submicron-sized (~180 nm) HA, while the contact angles (a quantitative measure of the wetting of a solid by a liquid) were significantly lower for nano-sized HA (6.1) if compared to the submicron-sized HA (11.51). Additionally, the diameter of individual pores in nanodimensional HA compacts is several times smaller (pore diameter ~6.6 Å) than that in the submicron grain-sized HA compacts (pore diameter within 19.8–31.0 Å) [126]. A surface roughness is known to enhance the osteoblast functions, while a porous structure improves the osteoinduction compared with smooth surfaces and nonporous structure, respectively [104]. Furthermore, nanophase HA appeared to have ~11% more proteins of fetal bovine serum adsorbed per 1  $\text{cm}^2$  than submicron-sized HA [127]. Interestingly, that nano-sized HA was found to increase a thermal stability of pectate lyase from *Bacillus megaterium*, that is, this enzyme could retain a high activity at elevated temperatures (up to 90 °C) in the presence of nanodimensional HA [128]. Interfacial interactions between calcined HA nano-sized crystals and various substrates were studied, and a bonding strength appeared to be influenced not only by the nature of functional groups on the substrate but also by matching of surface roughness between the nano-sized crystals and the substrate [129]. More to the

point, incorporating of nanodimensional particles of HA into polyacrylonitrile fibers was found to result in their crystallinity degree rising by about 5% [130]. In a comparative study on the influence of incorporated micron-sized and nano-sized HA particles into poly-L-lactide matrixes, addition of nano-sized HA was found to influence both thermal and dynamic mechanical properties in greater extents [131].

The nanostructured  $\text{CaPO}_4$  offer much improved performances than their larger particle-sized counterparts due to their huge surface-to-volume ratio and unusual chemical synergistic effects. For instance, powders of nanocrystalline apatites [132–137] and  $\beta$ -TCP [138, 139] were found to exhibit an improved sinterability and enhanced densification due to a greater surface area. This is explained by the fact that the distances of material transport during the sintering become shorter for ultrafine powders with a high specific surface area, resulting in a densification at a low temperature. Therefore, due to low grain growth rates, a low-temperature sintering appears to be effective to produce fine-grained apatite bioceramics [140]. Furthermore, the mechanical properties (namely, hardness and toughness) of HA bioceramics appeared to increase as the grain size decreased from sub-micrometers to nanometers [141].

More to the point, nano-sized HA is also expected to have a better bioactivity than coarser crystals [142–144]. Namely, Kim et al. found that osteoblasts (bone-forming cells) attached to the nano-sized HA/gelatin biocomposites to a significantly higher degree than to micrometer-sized analog did [145]. An increased osteoblast and decreased fibroblast (fibrous tissue-forming cells) adhesion on nanophase ceramics [146–150], as well as on nanocrystalline HA coatings on titanium, if compared to traditionally used plasma-sprayed HA coatings, was also discovered by other researchers [151–153]. Furthermore, incorporation of nanoscale  $\text{CaPO}_4$  was found to result in improved mechanical properties and osteogenic behavior within the scaffold compared to the microscale  $\text{CaPO}_4$  additives [154]. Scientists also observed enhanced osteoclast (bone-resorbing cells) functions to show healthy remodeling of bone at the simulated implant surface [143]. Besides, the proliferation and osteogenic differentiation of periodontal ligament cells were found to be promoted when a nanophase HA was used, if compared to dense HA bioceramics [155]. Thus, the underlying material property, responsible for this enhanced osteoblast function, is the surface roughness of the nanostructured surface [18]. Interestingly, an increased osteoblast adhesion was discovered on nano-sized  $\text{CaPO}_4$  powders with higher Ca/P ratios [156], which points out to some advantages of apatites over other  $\text{CaPO}_4$ . Furthermore, a histological analysis revealed a superior biocompatibility and osteointegration of bone graft substitutes when nano-sized HA was employed in biocomposites [157–159]. However, data are available that nano-sized HA could inhibit growth of osteoblasts in a dose-dependent manner [160]. Furthermore, a cellular activity appeared to be affected by the shape and dimensions of nano-sized HA [161, 162]. Namely, the cellular activity of L929 mouse fibroblasts on nano-sized fibers with a diameter within 50–100 nm was significantly enhanced relative to that on a flat HA surface, while nanodimensional HA needles and sheets with a diameter/thickness of less than 30 nm inhibited cellular adhesion and/or subsequent activity because cells could not form focal adhesions of sufficient

size [161]. Studies are also available, in which nano-scaled  $\text{CaPO}_4$  did not show any significant improvement over the bigger ones [163].

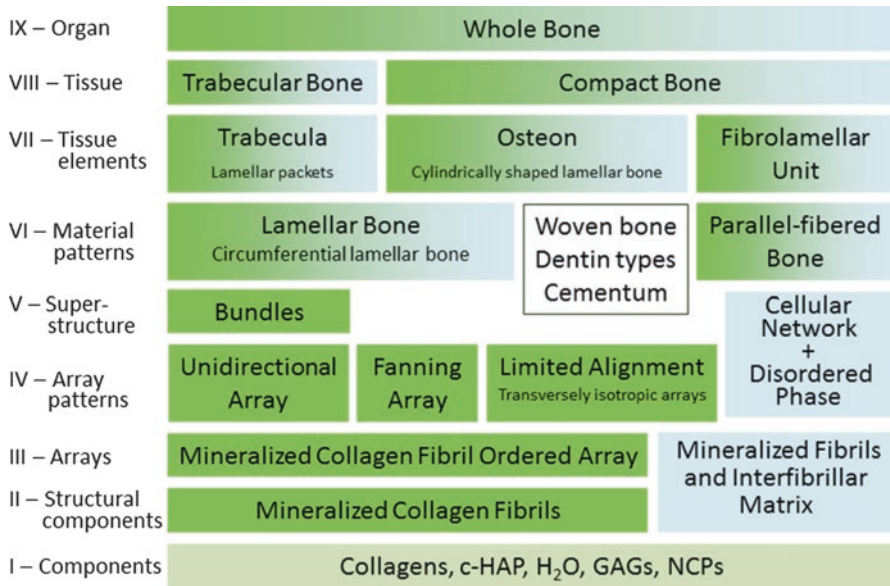
Obviously, the volume fraction of grain boundaries in nanodimensional  $\text{CaPO}_4$  is increased significantly leading to improved osteoblast adhesion, proliferation, and mineralization. Therefore, a composition of these biomaterials at the nanoscale emulates the bone's hierarchic organization, to initiate the growth of an apatite layer and to allow for the cellular and tissue response of bone remodeling. These examples emphasize that nanophase materials deserve more attention in improving orthopedic implant failure rates. However, to reduce surface energy, all nano-sized materials tend to agglomerate, and to avoid self-aggregation of  $\text{CaPO}_4$  nano-sized particles [164–167], special precautions might be necessary [29, 35, 168–171].

Finally, yet importantly, nano-sized crystals of CDHA obtained by precipitation methods in aqueous solutions were shown to exhibit physicochemical characteristics rather similar to those of bone apatite [172]. In particular, their chemical composition departs from stoichiometry by calcium and hydroxide ions deficiency, leading to an increased solubility, and in turn bioresorption rate in vivo [115, 173, 174]. The nano-sized crystals of CDHA have also a property to evolve in solution (maturation) like bone crystals. Namely, freshly precipitated CDHA has been shown to be analogous to embryonic bone mineral crystals, whereas aged precipitates resemble bone crystals of old vertebrates [172].

## 9.4 Nano-scaled $\text{CaPO}_4$ in Calcified Tissues of Mammals

### 9.4.1 *Bones*

Bone is the most typical calcified tissue of mammals, and it comes in all sorts of shapes and sizes in order to achieve various functions of protection and mechanical support for the body. The major inorganic component of bone mineral is a biological apatite, which might be defined as a poorly crystalline, nonstoichiometric, and ion-substituted CDHA [2–5, 173–175]. From the material point of view, bone can be considered as an assembly of distinct levels of nine hierarchical structural units from macro- to micro- and to nanoscale (Fig. 9.1) to meet numerous functions [176]. Furthermore, all these levels of bones permanently interact with cells and biological macromolecules. At the nanostructural level, tiny platelike crystals of biological apatite in bone occur within the discrete spaces within the collagen fibrils and grow with specific crystalline orientation along the *c*-axes, which are roughly parallel to the long axes of the collagen fibrils [177]. Type I collagen molecules are self-assembled into fibrils with a periodicity of ~67 nm and ~40 nm gaps between the ends of their molecules, into which the apatite nano-sized crystals are placed. A biocomposite of these two constituents forms mineralized fibers. The fibers also may be cross-linked, which provides a highly dynamic system capable of modification through the selection of different amino acids to allow for different mechanical



**Fig. 9.1** A schematic illustration of the hierarchical organization of bones. Up to level V, the hierarchical levels can be divided into the ordered material (*green*) and the disordered material (*blue*). At level VI, these two materials combine in lamellar bone and parallel-fibered bone. Other members of the bone family still need to be investigated with respect to the presence of both material types; hence, they are depicted in a *box* without color. Level VII depicts the lamellar packets that make up trabecular bone material and the cylindrically shaped lamellar bone that makes up osteonal bone. The fibrolamellar unit comprises the primary hypercalcified layer, parallel-fibered bone, and lamellar bone. *Abbreviations: c-HAP* carbonated HA, *GAGs* glycosaminoglycans, *NCPs* non-collagenous proteins (Reprinted from Ref.[176] with permission. Copyright © 2014 Acta Materialia Inc. Published by Elsevier Ltd)

properties for different biomaterial applications [178]. This is why bone is usually termed a fiber-reinforced composite of a biological origin, in which nanometer-sized hard inclusions are embedded into a soft protein matrix [179]. Though dimensions of biological apatite crystals reported in the literature vary due to different treatment methods and analytical techniques, it is generally around the nanometric level with values in the ranges of 30–50 nm (length), 15–30 nm (width), and 2–10 nm (thickness) [180]. Some details on the stability reasons of nanodimensional apatites in bones are available in literature [181, 182].

Why does the nanoscale appear to be so important to bones? It was demonstrated that natural biocomposites exhibit a generic mechanical structure in which the nanometer sizes of mineral particles are used to ensure the optimum strength and maximum tolerance of flaws [183, 184]. Furthermore, nano-scaled apatite has another crucial function for organisms. It is a huge reservoir of calcium and orthophosphate ions necessary for a wide variety of metabolic functions, which offer or consume calcium and orthophosphate ions through a so-called “remodeling” process because of a continuous resorption and formation of nanodimensional apatite

by osteoclasts and osteoblasts, respectively, in a delicate equilibrium [2, 5]. Additional details on the structure, properties, and composition of bones are available elsewhere [5, 175, 185].

### 9.4.2 *Teeth*

Teeth are another normal  $\text{CaPO}_4$ -based calcified tissue of vertebrates. Unlike bone, teeth consist of a bulk of dentin covered with enamel on the crown and cementum on the root surface. Taking into consideration that dentin and cementum are rather similar, one can claim that teeth consist of two substantially different biominerals [186]. Dental enamel contains up to 98% of biological apatite, ~1% of bioorganic compounds, and up to 2% of water. Typical rods in enamel are composed of rodlike apatite crystals measuring 25–100 nm and an undetermined length of 100–100  $\mu\text{m}$  or longer along the *c*-axis [187–189]. However, the apatite crystals in enamel were found to exhibit regular sub-domains or subunits with distinct chemical properties [190]. This subunit structure reflects an assembly mechanism for such biological crystals [191, 192]. Similar to that for bones (Fig. 9.1), seven levels of structural hierarchy have been also discovered in human enamel; moreover, the analysis of the enamel and bone hierarchical structures suggests similarities of the scale distribution at each level [193]. In enamel, nano-sized crystals of biological apatite at first form mineral nanodimensional fibrils; the latter always align lengthways, aggregating into fibrils and afterward into thicker fibers; further, prism/interprism continua are formed from the fibers. At the microscale, prisms are assembled into prism bands, which present different arrangements across the thickness of the enamel layer. These compositional and structural characteristics endow enamel special properties such as anisotropic elastic modulus, effective viscoelastic properties, much higher fracture toughness, and stress-strain relationships more similar to metals than ceramics [194].

Dentin and cementum contain ~50% of biological apatite, ~30% of bioorganic compounds (chiefly, collagen), and ~20% of water. In dentin, the nanodimensional building blocks (~25 nm width, ~4 nm thickness and ~35 nm length) of biological apatite are smaller than those of enamel. Briefly, dentin and cementum are analogous to bone in many aspects, for example, the inorganic part of dentin has a similar composition and a hierarchical structure up to the level of the bone lamellae [173]; nevertheless, there are some histogenetical differences from bones. Additional details on the structure, properties, and composition of teeth might be found elsewhere [195].

To finalize this topic, one should briefly mention that nano-scaled  $\text{CaPO}_4$  clusters are also present in biological fluids of mammals, such as blood, saliva, milk, etc. [196].

## 9.5 The Structure of the Nano-scaled Apatites

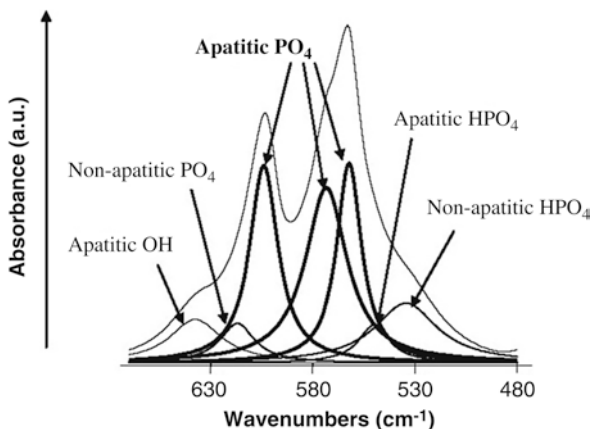
Due to the apatitic structure on natural calcified tissues, apatites appear to be the best investigated compounds among the available  $\text{CaPO}_4$  (Table 9.1). Thus, nano-scaled apatites have been extensively studied by various physicochemical techniques and chemical analysis methods [40, 166, 197–215] with a special attention to the “nano”-effect (i.e., an enhanced contribution of the surface against the volume). Computer simulations of the nano-scaled apatites are performed as well [216]. Unfortunately, no publications on the structure of other nanodimensional and/or nanocrystalline  $\text{CaPO}_4$  were found in the available literature.

Due to a nanocrystalline nature, various diffraction techniques have not yet given much information on the fine structural details related to apatite nano-sized crystals (assemblies of nano-sized particles give only broad diffraction patterns, similar to ones from an amorphous material) [197, 198]. Nevertheless, the diffraction studies with electron microprobes of  $35 \pm 10$  nm in diameter clearly indicated a crystalline character of the nano-sized particles in these assemblies. Furthermore, high-resolution transmission electron microscopy results revealed that nano-sized particles of HA behaved a fine monocrystalline grain structure [166, 197].

Therefore, a recent progress on the structure investigations of the precipitated apatites (nano-scaled CDHA) has relied mainly on diverse spectroscopic methods, which are sensitive to disturbances of the closest environments of various ions [213]. Namely, the structure analysis revealed an existence of structural disorder at the particle surface, which was explained by chemical interactions between the orthophosphate groups and either adsorbed water molecules or hydroxyl groups located at the surface of nano-sized apatites [199]. More to the point, infrared (FTIR) spectra of nanocrystalline apatites, in the  $\nu_4$   $\text{PO}_4$  domain, revealed the existence of additional bands of orthophosphate ions which could not be assigned to an apatitic environment and which were not present in well-crystallized apatites (Fig. 9.2). These bands were assigned to non-apatitic environments of  $\text{PO}_4^{3-}$  and  $\text{HPO}_4^{2-}$  ions of the nano-sized crystals. Thus, FTIR spectra can be used to provide a sufficiently accurate evaluation of the amounts of such environments. Furthermore, the non-apatitic environments were found to correspond to hydrated domains of the nano-sized crystals, which were distinct from the apatite domains [201, 213]. Hence, precipitated crystals of nano-sized apatite appeared to have a hydrated surface layer containing labile ionic species, which easily and rapidly could be exchanged by ions and/or macromolecules from the surrounding fluids [199, 200, 208]. For the as-precipitated apatites, such a layer appears to constitute mainly by water molecules coordinated to surface  $\text{Ca}^{2+}$  ions, approximately in the 1: 1 ratio, while the OH groups account only for ~20% of the surface hydration species. The FTIR data indicated that water molecules, located at the surface of nanodimensional apatites, are coordinated to surface cations and experience hydrogen bonding significantly stronger than that in liquid water [207]. The surface hydrated layer is very delicate and becomes progressively transformed into a more stable apatitic lattice upon aging in aqueous media. Furthermore, it irreversibly altered upon drying



**Fig. 9.2** FTIR spectrum for a nanocrystalline apatite sample, around the  $\nu_4(\text{PO}_4)$  vibrational region (Reprinted from Ref. [213] with permission. Copyright © 2012 Elsevier Ltd)



[201]. Outgassing at increasing temperatures up to  $\sim 300^\circ\text{C}$  resulted in a complete surface dehydration, accompanied by a decrease of the capability to readsorb water. Combination of these data with rehydration tests suggested that a significant part of the surface  $\text{Ca}^{2+}$  ions, once dehydrated, could undergo a relaxation inward the surface, more irreversibly as the outgassing temperature increased [206].

In another study, elongated nano-sized crystals of CDHA of  $\sim 10$  nm thick and of  $\sim 30$ – $50$  nm length were synthesized followed by investigations with X-ray diffraction and nuclear magnetic resonance techniques. The nano-sized crystals of CDHA were shown to consist of a crystalline core with the composition close to the stoichiometric HA and a disordered (amorphous) surface layer of 1–2 nm thick [205, 206] with the composition close to DCPD [204]. Based on the total Ca/P ratio, on the one hand, and the crystal shape, on another hand, a thickness of the DCPD surface layer along the main crystal axis was estimated to be  $\sim 1$  nm [204], which is close to dimensions of the unit cells (Table 9.2). A similar structure of a crystalline core with the composition of the stoichiometric HA and a disordered (amorphous) surface layer was found by other researchers [217]. Furthermore, in a study devoted to nanodimensional carbonate apatites, the same core/surface layer structure was proposed as well [48]; however, this model was not confirmed in another study on carbonate apatites [218]. Perhaps, this discrepancy could be explained by the presence of dopants. A lack of hydroxide in nanodimensional apatites was detected; an extreme nanocrystallinity was found to place an upper bound on  $\text{OH}^-$  possible in apatites [219]. Interestingly, that dry milling of HA powders was found to result in a concentration decreasing of structural hydroxyl groups due to the crystal size decreasing with simultaneous increasing of the total water content due to an increasing of the surface area of crystallites [214]. The presence of nonstoichiometric surfaces coexisting in nanodimensional HA was noticed in still another study [210].

However, it is possible to address the structure of surface terminations of HA nano-sized particles to be amorphous or crystalline by properly selecting the preparation parameters and, in particular, the temperature; thus, nanodimensional HA

**Table 9.2** Crystallographic data of calcium orthophosphates [240, 241]

Compound	Space group	Unit cell parameters	Z <sup>a</sup>	Density, g/cm <sup>3</sup>
MCPM	Triclinic $P\bar{1}$	$a = 5.6261(5)$ , $b = 11.889(2)$ , $c = 6.4731(8)$ Å,	2	2.23
		$\alpha = 98.633(6)^\circ$ , $\beta = 118.262(6)^\circ$ , $\gamma = 83.344(6)^\circ$		
MCPA	Triclinic $P\bar{1}$	$a = 7.5577(5)$ , $b = 8.2531(6)$ , $c = 5.5504(3)$ Å,	2	2.58
		$\alpha = 109.87(1)^\circ$ , $\beta = 93.68(1)^\circ$ , $\gamma = 109.15(1)^\circ$		
DCPD	Monoclinic $Ia$	$a = 5.812(2)$ , $b = 15.180(3)$ , $c = 6.239(2)$ Å, $\beta = 116.42(3)^\circ$	4	2.32
DCPA	Triclinic $P\bar{1}$	$a = 6.910(1)$ , $b = 6.627(2)$ , $c = 6.998(2)$ Å,	4	2.89
		$\alpha = 96.34(2)^\circ$ , $\beta = 103.82(2)^\circ$ , $\gamma = 88.33(2)^\circ$		
OCP	Triclinic $P\bar{1}$	$a = 19.692(4)$ , $b = 9.523(2)$ , $c = 6.835(2)$ Å, $\alpha = 90.15(2)^\circ$ , $\beta = 92.54(2)^\circ$ , $\gamma = 108.65(1)^\circ$	1	2.61
$\alpha$ -TCP	Monoclinic $P2_1/a$	$a = 12.887(2)$ , $b = 27.280(4)$ , $c = 15.219(2)$ Å, $\beta = 126.20(1)^\circ$	24	2.86
$\beta$ -TCP	Rhombohedral $R3cH$	$a = b = 10.4183(5)$ , $c = 37.3464(23)$ Å, $\gamma = 120^\circ$	21 <sup>b</sup>	3.08
HA	Monoclinic $P2_1/b$ or hexagonal $P6_3/m$	$a = 9.84214(8)$ , $b = 2a$ , $c = 6.8814(7)$ Å, $\gamma = 120^\circ$ (monoclinic)	4	3.16
		$a = b = 9.4302(5)$ , $c = 6.8911(2)$ Å, $\gamma = 120^\circ$ (hexagonal)	2	
FA	Hexagonal $P6_3/m$	$a = b = 9.367$ , $c = 6.884$ Å, $\gamma = 120^\circ$	2	3.20
OA	Hexagonal $P\bar{6}$	$a = b = 9.432$ , $c = 6.881$ Å, $\alpha = 90.3^\circ$ , $\beta = 90.0^\circ$ , $\gamma = 119.9^\circ$	1	~3.2
TTCP	Monoclinic $P2_1$	$a = 7.023(1)$ , $b = 11.986(4)$ , $c = 9.473(2)$ Å, $\beta = 90.90(1)^\circ$	4	3.05

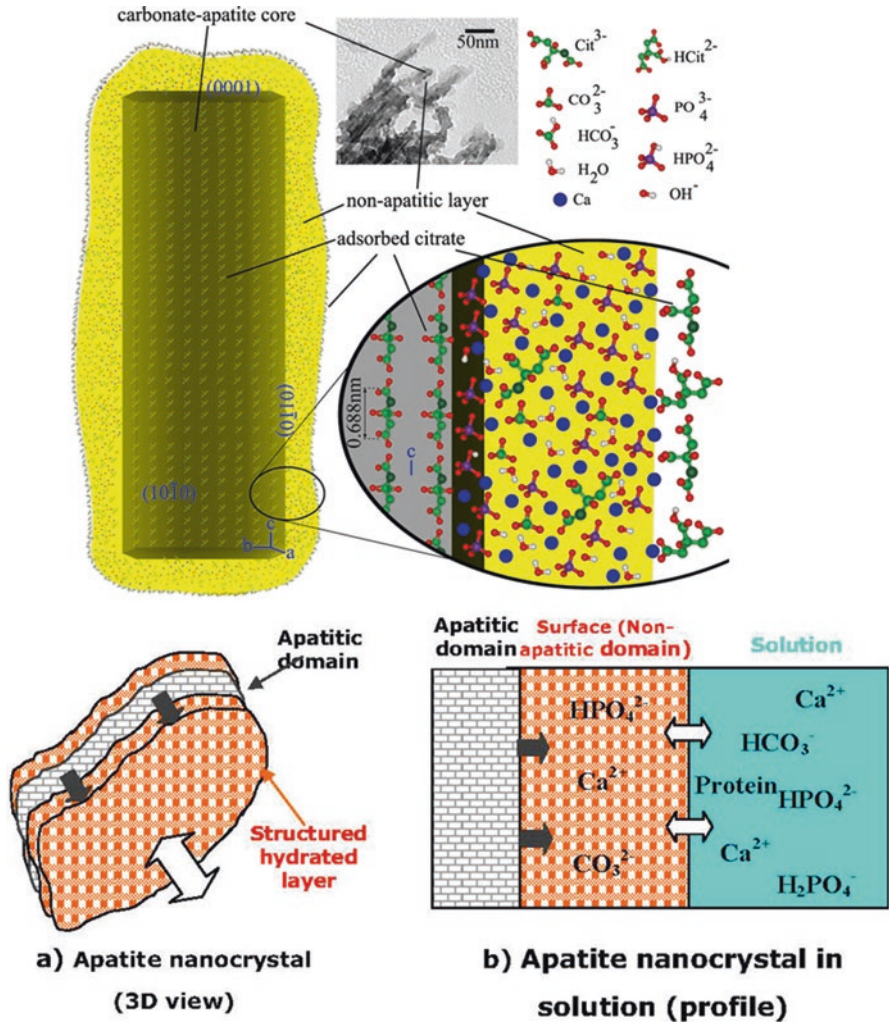
<sup>a</sup>Number of formula units per unit cell<sup>b</sup>Per the hexagonal unit cell

without the amorphous layer on the surface was prepared [220, 221]. The two types of surfaces (amorphous or crystalline) of nanodimensional HA appeared to be quite similar in terms of their first hydration layer, as well as Lewis acid strength of exposed Ca<sup>2+</sup> ions. Both features have a strong dependence on the local structure of surface sites (well probed by small molecules, such as H<sub>2</sub>O and CO) that appeared essentially unaffected by the organization at a longer range. Interestingly, that for the as-synthesized material, it was found that the first hydration layer was essentially made up of H<sub>2</sub>O molecules, strongly bound to surface Ca<sup>2+</sup> cations in the 1: 1 ratio. However, once treated at 573 K, the crystalline surfaces of nanodimensional HA were found to adsorb multilayers of water in a larger extent than the amorphous ones [220, 221].

Nevertheless, after summarizing the available data, the following statements on the structure of nano-sized crystals of apatites have been made:

1. They involve non-apatitic anionic and cationic chemical environments (in another study, the researchers mentioned on “ordered and disordered HA” [205]).
2. At least part of these environments are located on the surface of the nano-sized crystals and are in strong interaction with hydrated domains.
3. Immature samples show FTIR band fine substructure that is altered upon drying without leading to long-range order (LRO) modifications.
4. This fine substructure shows striking similarities with the FTIR spectrum of OCP [202].

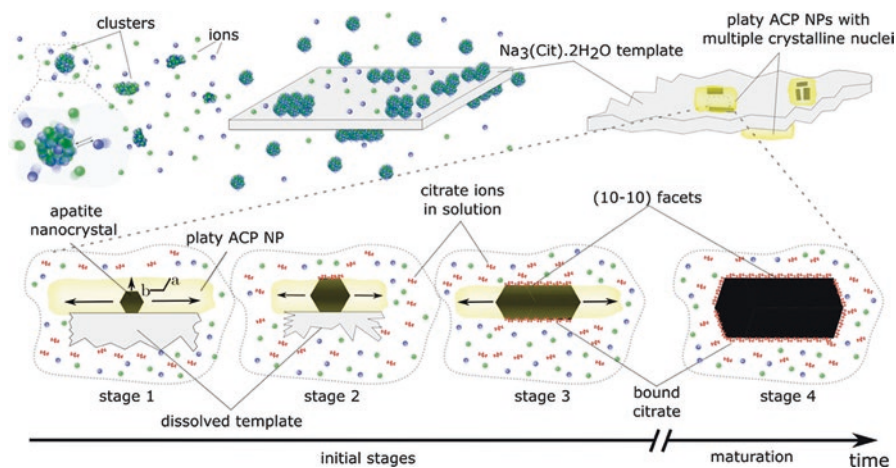
All these elements favor a model in which nano-sized crystals of apatites are covered with a rather fragile but structured surface hydrated layer containing relatively mobile ions (mainly, bivalent anions and cations:  $\text{Ca}^{2+}$ ,  $\text{HPO}_4^{2-}$ ,  $\text{CO}_3^{2-}$ ) in “non-apatitic” sites (Fig. 9.3) [40, 202], which is supposed to be ACP [40] or of either OCP or DCPD structure [202]. Obviously, the properties (structure, thickness, chemical composition, etc.) of this hydrated layer depend on the experimental conditions of apatite preparation, which strongly complicates its characterization (regrettably, as the hydrated layer cannot be isolated, it is not possible to standardize the methods for detailed studies) [202, 204–206]. Nevertheless, it is known that the surface layer might adsorb considerable amounts of foreign compounds (molecules and ions) in the percent mass range [222]. In 2014, based on this model, a formation mechanism of nano-scaled platelike apatite crystals similar to those found in bones was proposed [223]. According to this mechanism, sodium citrate crystals are thought to act as a template surface, which, through adsorption of ionic species ( $\text{Ca}^{2+}$ ,  $\text{HPO}_4^{2-}$ , and  $\text{OH}^-$ , neglecting the minor ones), might trigger the heterogeneous nucleation process through surface formation of  $\text{CaPO}_4$  clusters that, laterally aggregating, form nano-scaled ACP particles with unusual platy morphology. The presence of adsorbed citrate on the surface of ACP platelets slows down their thickening by inhibiting both further ion adsorption and mutual aggregation, while biomimetic apatite crystals start to grow from multiple nuclei within each ACP platelet (Fig. 9.4) [223]. Thus, according to this model, the surface hydrated layer shown in Fig. 9.3 might represent an untransformed ACP or any other precursor of apatite crystallization, while the progressive growth of apatite domains at the expense of the surface hydrated layer is referred to as maturation. The maturation process (Fig. 9.5) is thought to be linked to the metastability of such poorly crystallized non-apatitic sites, which steadily evolve in solution toward stoichiometry and better crystallinity. According to another opinion: “The hydrated layer shall not be considered as a Stern double layer but a result of the precipitation process of biomimetic apatites. This layer is believed to decrease the water-crystal interfacial energy and to favor the formation of the nanocrystals in aqueous media” [224, p. 66]. Strictly speaking, all the aforementioned apply to both biological apatite of calcified tissues [225] and micron-sized apatites as well [226]; nonetheless, in nano-sized crystals, the composition of the hydrated surface layer contributes to the global



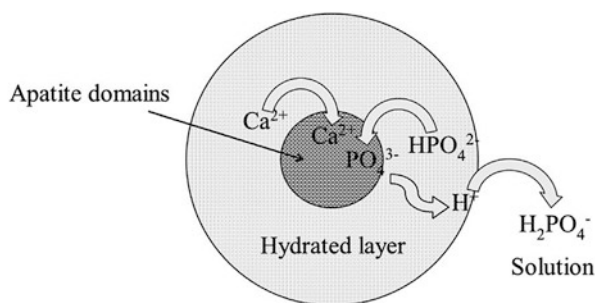
**Fig. 9.3** Two schematic drawings of a surface hydrated layer model for carbonate apatite nanocrystals, consisting of a well-ordered apatite core covered by a non-apatitic hydrated layer composed of various ionic species (including citrate (Cit) for the top scheme) and structural water. A TEM image shows this layered structure (Reprinted from Ref. [40] (top) and Ref. [202] (bottom) with permission. Copyright © 2012 Acta Materialia Inc. Published by Elsevier Ltd)

composition for a non-negligible proportion. The results of electron state spectroscopy of nanostructural HA bioceramics are available elsewhere [227, 228].

The hydrated surface layer confers unexpected properties to nano-sized apatite, is responsible for most of the properties of apatites, and, for example, can help to explain the regulation by biological apatites of the concentration in mineral ions in body fluids (homeostasis) [229]. These properties are important for living organ-



**Fig. 9.4** A schematic representation of a possible formation mechanism of nano-scaled bonelike apatite platelets due to an ACP-to-CDHA transformation. A time scale of minutes applies to the initial stages and hours to the maturation process. *NP* means nano-scaled particle, *Cit* means citrate (Reprinted from Ref. [223] with permission. Copyright © 2014 WILEY-VCH Verlag GmbH & Co. KGaA, Weinheim)



**Fig. 9.5** A schematic representation of a maturation process for a nano-scaled bonelike apatite. The Ca/P ratio in the hydrated layer (containing essentially  $\text{Ca}^{2+}$  and  $\text{HPO}_4^{2-}$ ) is lower than that in the apatite domain. The growth of the apatite domains (the driving force of maturation) induces an uptake of  $\text{Ca}^{2+}$  ions larger than that of orthophosphate ions. The release of protons in the hydrated layer and the excess of orthophosphate lead to a release of  $\text{H}_2\text{PO}_4^-$  and eventually a rather acidic solution (non-congruent dissolution) (Reprinted from Ref. [224] with permission (HAL, open access))

isms; therefore, they need to be used in both material science and biotechnology [201]. The consideration of this type of surface state can help understanding and explaining the behavior of biological apatites in participating in homeostasis due to a very high specific surface area of bone crystals and in constituting an important ion reservoir with an availability that depends on the maturation state. The important consequences are that the surface of nanodimensional apatites has nothing in common with the bulk composition and that the chemistry of such materials (e.g.,

binding of protein molecules) must be reconsidered [202, 204]. Interestingly, in response to an electrical potential, the surface of nano-sized HA bioceramics was found to exhibit dynamic changes in interfacial properties, such as wettability. The wettability modification enabled both a sharp switching from hydrophilic to hydrophobic states and a microscopic wettability patterning of the HA surface, which may be used for fabrication of spatially arrayed HA for biological cell immobilization or gene transfer [230].

Furthermore, dry powders of nanodimensional HA were found to contain an X-ray amorphous portion with an unspecified location [231]. After mixing of an initial nano-sized HA powder with a physiological solution (aqueous isotonic 0.9% NaCl solution for injections), this amorphous portion was fully converted into the crystalline phase of HA. The initial crystallite average size (~35 nm) was enlarged by a factor of about 4 within the first 100 min after mixing the powder with the physiological solution, and no more structural changes were detected during the following period [231]. In the light of the aforementioned studies, presumably, the discovered X-ray amorphous component of the initial powder was located on the surface of nanodimensional HA.

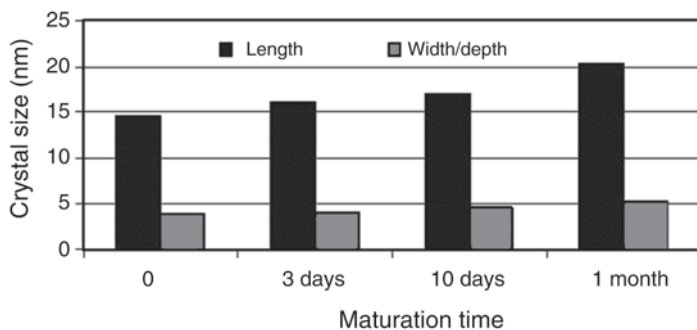
To conclude this section, one should mention studies devoted to the investigations of nano-scaled  $\text{CaPO}_4$ /water interface [232].

## 9.6 Synthesis of the Nano-scaled $\text{CaPO}_4$

### 9.6.1 General Approaches of Nanotechnology

The synthesis of nanoscale materials has received considerable attention, and their novel properties can find numerous applications, for example, in the biomedical field. This has encouraged the invention of chemical, physical, and biomimetic methods by which such nano-sized materials can be obtained [100]. Generally, all approaches for preparation of nano-scaled materials can be categorized as “bottom-up” and “top-down” ones [108, 233]. The bottom-up approach refers to the buildup of a material from the bottom, i.e., atom by atom, molecule by molecule, or cluster by cluster, and then assembles them into the final nanostructured material. An example is production of a nano-sized powder and its compaction into the final product (e.g., hot-pressed or sintered nanostructured ceramics). The top-down approach starts from a bulk material and then, via different dimension decreasing techniques, such as milling, slicing, or successive cutting, leads to the formation of nanodimensional materials [100]. Using this approach, a novel two-dimensional carbon material graphene of just 1 atom thick has been prepared from bulk graphite. Furthermore, environmentally friendly methodologies of nanostructure synthesis have been summarized into a special review [234].

Concerning  $\text{CaPO}_4$ , the original creator of the nano-scaled structures, undoubtedly, must be honored to the nature (see Sect. 9.4 above). Presumably, all known



**Fig. 9.6** Variation of nanocrystalline apatite dimensions with maturation time (Reprinted from Ref. [202] with permission. Copyright © 2007 Nova Science Publishers)

CaPO<sub>4</sub> (Table 9.1) somehow might be manufactured in a nanodimensional and/or a nanocrystalline state; however, not all of them (especially those with low Ca/P ionic ratios) have been prepared yet. The details on the available preparation techniques are given below.

### 9.6.2 Nano-scaled Apatites

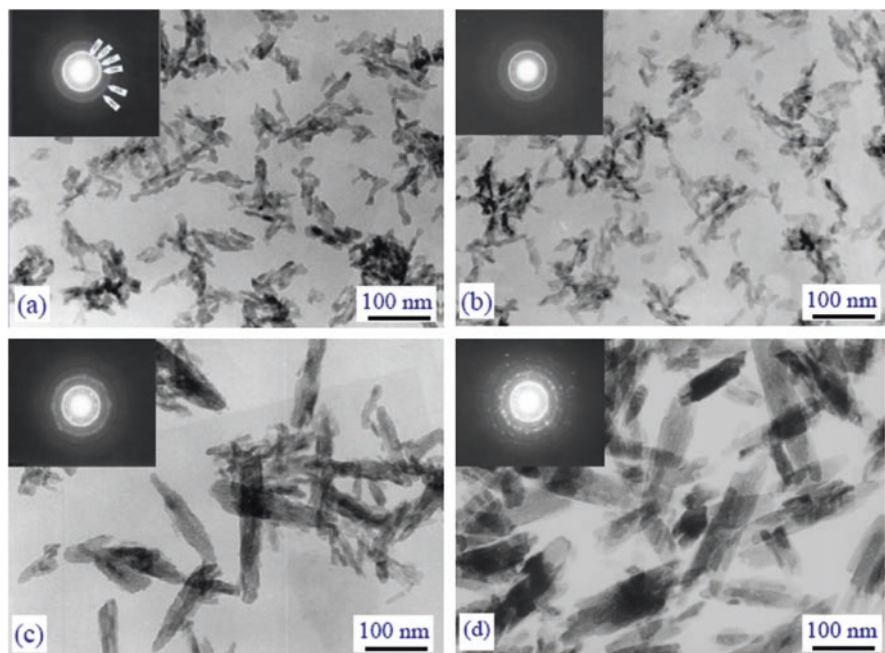
First of all, one should stress that the stoichiometric HA with well-resolved X-ray diffraction patterns might be prepared mostly at temperatures exceeding ~700 °C either by calcining of CDHA with the Ca/P molar ratio very close to 1.67 or by solid-state reactions of other CaPO<sub>4</sub> with various chemicals (e.g., DCPA + CaO). Thus, with the exception of a hydrothermal synthesis [235–237], in aqueous solutions, only CDHA could be prepared [115, 173, 174, 235–241]. As apatites (CDHA, HA, and FA) belong to the sparingly soluble compounds (Table 9.1), simple mixing of calcium- and orthophosphate-containing aqueous solutions at pH >9 results in the formation of extremely supersaturated solutions and, therefore, a very fast precipitation of the tremendous amounts of very fine crystals [242], initially of ACP, and those afterward are recrystallized into apatites [173, 174, 243–246]. The dimensions of the precipitated nano-sized crystals might be slightly increased by the Ostwald ripening approach (maturation), that is, by boiling and/or ambient aging in the mother liquid (Fig. 9.6) [121, 135, 172, 202, 236, 245–250]. Heat treatment of ACP might be applied as well [251]. Therefore, preparation of nano-scaled apatites is not a problem at all and has been known for many years [123, 124, 252–254]; however, a prefix “nano” had not been used before 1994. On the contrary, with the exception of a thermally stable FA (thus, big crystals of FA might be produced by a melt-growth process [255, 256]), manufacturing of big crystals of both CDHA and HA still is a challenge.

Many different methodologies have been proposed to prepare nano-scaled structures [257–265]. Prior to describing them, it is important to stress that in the vast

majority of the available literature on apatites, the authors do not tell the difference between CDHA and HA. Therefore, getting through scientific papers, an attentive reader often finds statements, as: “Because natural bone is composed of both organic components (mainly type I collagen) and inorganic components (HA), ...” [88, p. 357], “The HA nanorods are synthesized via a wet precipitation process ...” [133, p. 2364], “... (TTCP) has been shown previously to be an essential component of self-setting calcium phosphate cements that form hydroxyapatite (HA) as the only end-product. ...” [266, abstract], etc. The matter with distinguishing between CDHA and HA becomes even much more complicated, when researchers deal with nanodimensional and/or nanocrystalline apatites because the assemblies of nano-sized particles give only broad diffraction patterns, similar to ones from an amorphous material [197, 198]. While composing this chapter, I always tried to specify whether each cited study dealt with CDHA or HA; unfortunately, the necessary data were found in just a few papers. Therefore, in many cases, I was forced to mention just “apatites” without a further clarification. Thus, the readers are requested to be understandable on this uncertainty.

The greater part of the published reports on synthesizing of nano-scaled apatites is focused on the bottom-up approach. Among the available preparation techniques, a wet-chemical precipitation is the most popular one [132–135, 144, 170, 172, 252, 267–306]. This process might occur in the presence of various (bio)organic additives [269, 277, 282, 293–298, 301, 306], including ionic liquids [303, 304] and complexing agents [302]. In the vast majority of the cases, the obtained precipitates are aggregates of low crystallinity particles. Various authors discussed the effects of synthesis parameters, such as temperature [270–273, 283], time [271], calcium ion concentration [273], solution pH [301], presence of surfactants [275–277], calcination [271], and the use of various reagents [290] on the morphological properties of nanodimensional apatites. In general, the shape, stoichiometry, dimensions, and specific surface area of nano-sized apatites appeared to be very sensitive to both the reaction temperature (Fig. 9.7) and the reactant addition rate [270, 280, 283]. Namely, particle sizes of nanodimensional apatites were observed to increase in a linear correlation with temperature [272, 283], which is a good indication that sizes of nanodimensional apatites can possibly be tailored. Furthermore, the initial pH values and reaction temperatures both play important roles in the morphology of the precipitated apatites, as well as on the phase formation and degree of crystallinity [286]. For example, significant differences in the chemical composition, morphology, and amorphous character of nano-sized CDHA produced through the reaction between aqueous solutions of  $\text{Ca}(\text{NO}_3)_2$  and  $(\text{NH}_4)_2\text{HPO}_4$  can be induced, simply by changing the pH of the reactant hydrogen phosphate solution [287]. Thus, the solvent systems, dispersant species, and drying methods appear to have effects on the particle size and dispersibility. However, some conflicting results have been obtained on how certain synthesis parameters can affect the morphological properties of these nano-sized particles. Nevertheless, it was commonly observed that nano-sized crystals of apatites synthesized through the chemical precipitation were often highly agglomerated; however, these agglomerates could be clusters of ultrafine primary particles [274]. The prepared nano-scaled apatites might be consolidated to transparent bioceramics [289].





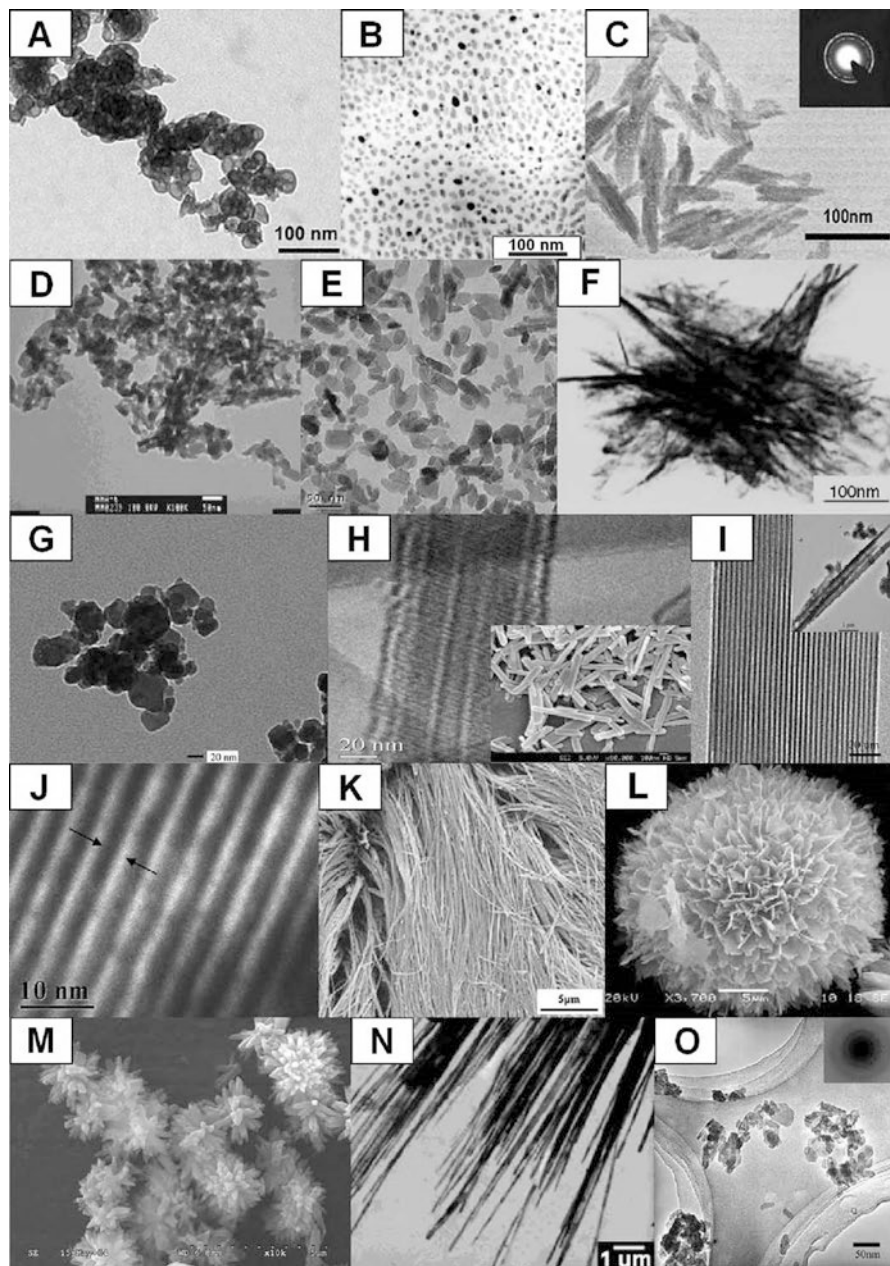
**Fig. 9.7** The influence of the reaction temperature on the crystal dimensions of precipitated CDHA: (a) 25 °C, (b) 37 °C, (c) 55 °C, (d) 75 °C

A hydrothermal synthesis [123, 124, 236, 237, 283, 284, 307–332] seems to be the second most popular preparation technique of the nano-scaled apatites. The term “hydrothermal” refers to a chemical reaction of substances in a sealed heated solution above ambient temperature and pressure [333], and this process allows synthesis of highly pure fine-grained single crystals, with controlled morphology and narrow size distribution [307]. Extraneous additives, such as EDTA [316], surfactants [317, 328, 329, 334], anionic starburst dendrimer [318], nanodimensional liposomes [327], alginate [332], sodium citrate [330, 331], etc., might be utilized to modify the morphology of nano-scaled apatites during the synthesis. Most of these techniques produced rodlike crystals or whiskers, while platelike shapes were obtained in just a few studies [309, 313, 314]. Nevertheless, nano-sized particles, wires, and hollow spheres were successfully synthesized on a large scale via a facile hydrothermal treatment of similarly structured hard precursors [322]. In addition, nano-sized rings of HA with an inner diameter of  $\sim 70$  nm were grown by a combined high gravity and hydrothermal approach [324].

Other preparation methods of nano-scaled apatites of various states, shapes, and sizes comprise sol-gel [155, 198, 199, 248, 288, 335–348], coprecipitation [249, 307, 308, 349–353], mechanochemical approach (ball milling) [205, 214, 227, 354–367], mechanical alloying [368, 369], radio-frequency induction plasma [370, 371], vibro-milling of bones [372], flame spray pyrolysis [373, 374], liquid-solid-solution synthesis [375], electro-crystallization [125, 376, 377], electrochemical deposition

[378] and synthesis [379], microwave processing [307, 308, 321, 380–388], hydrolysis of other  $\text{CaPO}_4$  [389–395], double-step stirring [396], and emulsion-based [278, 315, 397–410], steam-assistant [411], sonochemical [412–414], and solvo-thermal [415, 416] syntheses. However, still other preparation methods [114, 121, 253, 320, 417–448], as well as various combined processes, such as sol-gel-hydrothermal [449, 450], mechanochemical-hydrothermal [451–453], chemical precipitation-hydrothermal [454], high-gravity reactive precipitation-hydrothermal [455], and a combination of electrospinning with sol-gel [456], are also known. For example, there is a Pechini-based method, a type of homogeneous solid-state technique, in which a mixture of nanodimensional HA and CaO matrix was first prepared under nonstoichiometric conditions ( $\text{Ca/P}$  molar ratio  $\gg 1.67$ ) at  $1000^\circ\text{C}$  and then the CaO matrix was removed by washing to obtain well-dispersible nanodimensional HA [444]. Continuous preparation techniques are also available [169, 457–460]. Application of both ultrasound [281, 335, 461–469] and viscous systems [470, 471] could be helpful. Furthermore, nanodimensional HA might be manufactured by a laser-induced fragmentation of HA targets in water [472–476] and in solvent-containing aqueous solutions [312, 339, 477], while dense nanocrystalline HA films might be produced by radio-frequency magnetron sputtering [478, 479]. An interesting approach using a sitting drop vapor diffusion technique should be mentioned as well [480–482]. A comparison between the sol-gel synthesis and wet-chemical precipitation technique was performed, and both methods appeared to be suitable for synthesis of nanodimensional apatite [288]. By means of these methods, a variety of nanodimensional  $\text{CaPO}_4$  building blocks with various structures and morphologies have been synthesized, including needlelike, spherical, fibrous, and mesoporous nano-sized crystals, as well as nano-sized rods, hollow spheres, layered structures, and flowers as shown in Fig. 9.8 [432, 445, 483–487]. However, nanodimensional and/or nanocrystalline apatites with sphere and rod structures prepared by the simple and low-cost synthetic methods are usually available for practical applications. Those with sophisticated structures, such as hollow spheres, although are endowed with specific functions (e.g., the hollow spheres can become the drug carrier) due to their structural advantages, have limited applications due to both a low yield and a high cost resulted from their synthetic process.

Table 9.3 presents some data on the chronological development of synthesis of nanodimensional apatites for the period of 1995–2004 [114]. Among the methods described, the thinnest crystals of apatite ( $60 \times 15 \times 0.69$  or  $0.84$  nm) have been prepared by Melikhov et al. and have been called “two-dimensional crystalline HA” [267], while the smallest ones (size between 2.1 and 2.3 nm, i.e., around two times the HA unit cell parameters) have been found by Biggemann et al. [166]. Liu et al. [493, 494] and Han et al. [492] synthesized nano-sized HA via a template-mediated and a non-template-mediated sol-gel techniques, respectively. Alkylphosphates, such as triethylphosphate [493, 494], might be used to produce nanocrystalline apatites. Besides, nanodimensional ion-substituted CDHA might be precipitated from both a synthetic [350] and a simulated [495] body fluids. A relatively simple sol-gel process using ethanol and/or water as a solvent was also reported to produce the stoichiometric, nanocrystalline single-phase HA [339].



**Fig. 9.8** A variety of nanoscale  $\text{CaPO}_4$  with different structures and morphologies synthesized by: (a, b) sol-gel processing, (c) coprecipitation, (d) emulsion technique, (e) hydrothermal process, (f) ultrasonic technique, (g) mechanochemical method, (h–l) template method, (m) microwave processing, (n) emulsion-hydrothermal combination, (o) microwave-hydrothermal combination (Reprinted from Ref. [432] with permission. Copyright © 2010 Published by Elsevier B.V)

**Table 9.3** Synthesis of nanodimensional apatites – a chronological development [114]

Year	Process	References
1995	Synthesis of nanocrystalline HA (particle size ~20 nm) for the first time using calcium nitrate and diammonium hydrogen orthophosphate as precursors by solution spray dry method	[488]
2000	Synthesis of biomimetic nanosized CDHA powders (~50 nm) at 37 °C and pH of 7.4 from calcium nitrate tetrahydrate and diammonium hydrogen orthophosphate salts in synthetic body fluid using a novel chemical precipitation technique	[350]
2002	Preparation of nanosized HA particles and HA/chitosan nanocomposite	[489]
2002	Direct precipitation from dilute calcium chloride and sodium orthophosphate solutions	[490]
2003	Radio-frequency plasma spray process employing fine spray-dried HA powders (average size ~15 μm) as a feedstock	[370]
2003	Sol-gel process using equimolar solutions of calcium nitrate and diammonium hydrogen orthophosphate dissolved in ethanol	[339]
2003	Chemical precipitation through aqueous solutions of calcium chloride and ammonium hydrogen orthophosphate	[271]
2003	Mechanochemical synthesis of nanosized HA and β-TCP powders using DCPD and CaO as starting materials	[357]
2003	Synthesis of nanopowders via sucrose-templated sol-gel method using calcium nitrate and diammonium hydrogen orthophosphate as precursor chemicals	[491]
2004	Hydrolysis method of DCPD and CaCO <sub>3</sub> by 2.5 M NaOH (aq)	[389]
2004	Citric acid sol-gel combustion process using calcium nitrate tetrahydrate, diammonium hydrogen orthophosphate, and citric acid	[492]

A combustion technique was employed as well. The attractive features of this method were to synthesize materials with a high purity, a better homogeneity, and a high surface area in a single step [492, 496]. Namely, nanocrystalline HA powder was synthesized at a low calcination temperature of 750 °C by the citric acid sol-gel combustion method [492]. An array of highly ordered HA nano-sized tubes of uniform length and diameter was synthesized by sol-gel auto-combustion method with porous anodic aluminum oxide template [338]. In another study, nano-sized HA was synthesized by a polymeric combustion method and a self-propagating combustion synthesis by using novel body fluid solutions [497]. In a still another study, nanodimensional HA was synthesized by combustion in the aqueous system containing calcium nitrate + diammonium hydrogen orthophosphate with urea and glycine as fuels [498]. Furthermore, nano-sized particles of both FA and β-TCP might be synthesized by a simultaneous combustion of calcium carboxylate- and tributylphosphate-based precursors in a flame spray reactor [499]. Nano-scaled HA, FA, and chlorapatite [500], as well as nano-scaled HA, β-TCP, and biphasic calcium phosphate (BCP) consisting of HA + β-TCP [501], were prepared as well. Both a flame-based technique [502] and a spray-drying approach [89, 503] might be applied as well. Furthermore, crystalline and phase pure nano-sized HA and CDHA were synthesized in a continuous hydrothermal flow system using supercritical water at  $t < 400$  °C and 24 MPa pressure [310].

Nanodimensional powders of the stoichiometric HA of ~20 nm particle size were synthesized by hydrolysis of a mixture of DCPD and CaCO<sub>3</sub> performed with 2.5 M aqueous solution of NaOH at 75 °C for 1 h. The only product synthesized was nanocrystalline HA, and its crystallinity was improved with increasing annealing temperature [389]. Similar results were obtained in other studies [390–392]. Furthermore, Xu et al. used radio-frequency plasma spray process to synthesize nanodimensional HA powders with particle size in the range of 10–100 nm [370]. Kuriakose et al. synthesized nanocrystalline HA of size ~1.3 nm that was thermally stable until 1200 °C [339]. Nanocrystalline plate-shaped particles of HA were directly precipitated at ambient temperature and pH ~7.4 from dilute aqueous solutions of calcium chloride and sodium orthophosphate. The direct precipitation of nano-sized HA was achieved by submitting the aqueous suspension to microwave irradiation immediately after mixing [490]. A simple and easy approach for synthesizing thermally stable nanostructured stoichiometric HA powder under invariant pH conditions of 7.5, known as the NanoCaP process, was developed. Under these conditions, the synthesized HA not only remained in the nanostructured state but also did not exhibit any compositional fluctuations that were observed in conventional approaches for synthesizing HA [12]. Other preparation techniques of nano-sized apatite might be found elsewhere [253]. Bulk bioceramics made of nanocrystalline HA with a grain size of no more than 50 nm and a near-theoretical density might be prepared by application of a high (~3.5 GPa) pressure in uniaxial compaction of nanodimensional powders with subsequent sintering at 640 °C [134]. A similar approach was reported by another research group [380].

Mechanochemical processing is another compelling method to produce nanostructured apatites in the solid state [205, 214, 227, 354–367]. For example, Yeong et al. used the appropriate amounts of DCPA and calcium oxide. The initial stage of mechanical activation resulted in a significant refinement in crystallite and particle sizes, together with a degree of amorphization in the starting powder mixture. This was followed by steady formation and subsequent growth of HA crystallites with increasing degree of mechanical activation. Finally, a single-phase HA of an average particle size of ~25 nm, a specific surface area of ~76 m<sup>2</sup>/g, and a high crystallinity was attained after 20 h of mechanical activation [355].

The use of macromolecules as templating agents to manipulate the growth of inorganic crystals has been realized in many biological systems. Namely, in the presence of biological macromolecules (such as collagen), nucleation and growth of nanocrystalline apatite to form highly organized bone minerals are one of the most fascinating processes in nature. These processes might be simulated. For example, layers of nanocrystalline apatite were formed in situ on the surface of various films at soaking them in aqueous solutions containing ions of calcium and orthophosphate. The in situ synthesized particles were found to be less agglomerated which was believed to be the result of nucleation of apatite crystallites on the regularly arranged side groups located on polymer chains [504, 505]. Another approach comprises precipitation of nanodimensional apatites from aqueous solutions in the presence of dissolved high molecular weight polyacrylic acid [506, 507] that acts as an inhibitor for the crystallization of apatite crystals [508, 509]. A similar inhibiting

effect was found for dimethyl acetamide [510], polyvinyl alcohol [269], and several other (bio)polymers [511, 512]. This type of synthesis is expected to lead to the formation of nanodimensional biocomposites, which might be structurally more comparable to bones with closely related mechanical and biological properties. Furthermore, a control of particle size of aqueous colloids of apatite nano-sized particles was described involving a presence of amino acids [513, 514]. The amino acids ensured effective growth inhibition by a predominant adsorption onto the Ca-rich surfaces during the initial stages of crystallization. Thus, the nano-sized particles were formed by an oriented aggregation of primary crystallite domains along the *c*-axis direction. The size of the domains was shown to be governed by the interactions with the amino acid additives, which restricted the growth of the primary crystallites [513, 514]. Furthermore, nanodimensional apatites might be precipitated from aqueous solutions of gelatin. The development of nano-sized apatite in aqueous gelatin solutions was highly influenced by the concentration of gelatin: namely, a higher concentration of gelatin induced the formation of tiny ( $4 \times 9$  nm) nano-sized crystals, while a lower concentration of gelatin contributed to the development of bigger ( $30 \times 70$  nm) nano-sized crystals. In this experiment, a higher concentration of gelatin supplied abundant reaction sites containing groups such as carboxyl, which could bind with calcium ions. This leads to the formation of a very large number of nuclei and creation of a large number of tiny nano-sized crystals [515].

Although each of the reported approaches to produce nanodimensional apatites has both a scientific and a practical relevance, little attention has been dedicated to the physicochemical details involved in the careful control of the particle size distribution and particle shape. Indeed, in the case of particle size distribution, most of the reported ways to synthesize nanodimensional apatites really produced a particle mixture with a wide size distribution from tens to hundreds of nanometers. Moreover, the control of particle shape is another problem for these methods, which commonly result in pin-like or irregular particles. It is well known that bone consists of homogeneous platelike crystals of biological apatite of 15–30 nm wide and 30–50 nm long, while enamel consists of rodlike crystals of biological apatite of 25–100 nm thick and lengths of 100 nm to microns [2, 5, 175, 176, 185, 193, 195]. The study of higher-level biomineralization and biomimetic assembly involves a search for advanced methods so that the synthesis of nano-sized apatite can be accurately controlled [516]. Namely, the size-controlled synthesis of materials can be achieved by using limited reaction spaces. For example, microemulsions have been shown to be one of the few techniques, which is able to produce particle sizes in the range of nanometers and with minimum agglomeration [517]. Thus, microemulsions [315, 399–410], micelles [518], and reverse (inverse) micelles [311, 519–522] have been successfully applied to synthesize nanodimensional apatites with minimal agglomeration. It was found that experimental conditions, such as aqueous/organic phase volume ratio, pH, aging time, aging temperature, and ion concentration, in the aqueous phase can affect the crystalline phase, surface area, particle size, and morphology of nanodimensional apatites.

In some cases, special polymers can be used as spatial reaction vessels for fabrication of CDHA. For example, a poly(allylamine hydrochloride)/ $\text{PO}_4^{3-}$  complex was employed as a source of orthophosphate anions to capture calcium cations and make them react in the capsule volume [523]. A spherical-like nanocrystalline CDHA powder with particle diameters of  $\sim 30$  and  $\sim 50$  nm was synthesized using the emulsion route [401]. Furthermore, nano-sized crystals of apatite might be aggregated into microspheres [418, 524]. Cetyltrimethylammonium bromide (CTAB) was selected as an efficient surfactant to modulate formation of CDHA nano-sized particles [519, 520]. For example, three different types of spherical particles of nano-sized CDHA with average diameters of  $20 \pm 5$ ,  $40 \pm 10$ , and  $80 \pm 12$  nm were fabricated using a series of CTAB concentrations to control the particle size. The experimental results revealed that the dimensions of the prepared nano-sized CDHA were relatively uniform. In the presence of STAB, rodlike particles with lengths of hundreds of nanometers and width of tens of nanometers were prepared as well [525]. Colloidal formulations are known as well [29, 35, 171]. The nano-sized apatites were found to perform crystalline to amorphous phase transformation when powders were aged for 5 months in 30% relative humidity [526].

To conclude this part, one should mention that an analysis of the existing literature reveals that the low-temperature methods seem to be the optimal routes to synthesize nano-scaled apatites analogous to the biogenic ones. Since biogenic apatites always contain dopants, a synthesis of bone-mimic apatites should be performed in the presence of additives. As an alternative, bone-mimic apatites could be prepared from a big variety of natural sources [527]. Furthermore, nano-scaled apatites might be functionalized and/or doped by various compounds (even by quantum dots [528, 529]) to provide new important properties [29, 35, 513, 530–542], e.g., fluorescence [534, 535] and luminescence [29, 35, 528, 536, 537, 540]. Both fluorescence and luminescence can be used as a tracking property for the nano-sized particles to give an observable indication of agent delivery, while the particles are served to protect the agent in vivo until it has reached the destination. Additional details on the preparation techniques of nano-scaled apatites are available in a topical review [543].

### 9.6.3 Nano-scaled TCP

Many researchers have formulated synthesis of nanodimensional  $\beta$ -TCP. For example, Bow et al. synthesized  $\beta$ -TCP powders of  $\sim 50$  nm particle diameter at room temperature in anhydrous methanol as a solvent [544]. With increase in aging time, the phase transformation was found to take place from initial DCPA to intermediate ACP phases and then to final  $\beta$ -TCP. The authors observed that incorporation of carbonates helped in suppressing the formation of ACP phases with apatitic structure and its transformation into poorly crystalline (almost amorphous) CDHA and favored the formation of  $\beta$ -TCP phase [544]. Nano-sized particles of both FA and  $\beta$ -TCP were synthesized by a simultaneous combustion of calcium carboxylate- and tributylphosphate-based precursors in a flame spray reactor [499]. The same

technique was used to synthesize nano-sized particles of amorphous TCP of 25–60 nm size [545–548]; those after calcinations transformed into  $\alpha$ -TCP or  $\beta$ -TCP. Nanodimensional  $\beta$ -TCP powders with an average grain size of  $\sim$ 100 nm [138, 549] and less [550] were prepared by wet precipitation methods, followed by calcining at elevated temperatures. Similarly, nano-scaled  $\alpha$ -TCP was prepared by calcining of previously prepared ACP at temperatures between 700 and 800 °C, followed by cooling [551]. Furthermore, a sol-gel technique [552], a reverse micelle-mediated synthesis [553], and a polystyrene template method [554] are also applicable. In wet precipitation techniques, dialysis might be applied as a separation method [549]. When wet precipitation methods are used, initially nanodimensional CDHA with Ca/P ratio of  $\sim$ 1.50 is precipitated, which is further transformed into nano-sized  $\beta$ -TCP at calcining [555, 556].

To synthesize nano-sized TCPs, other techniques, such as milling [557, 558], a high-temperature flame spray pyrolysis [559, 560], mechanochemical synthesis [561], and pulsed laser ablation [562], might be employed as well. Afterward, the nanodimensional  $\beta$ -TCP powders can be compacted into 3D specimens, followed by sintering to achieve the appropriate mechanical strength [138]. The maximal values of the bending strength, elastic modulus, Vickers hardness, and compressive strength of the samples fabricated from nano-sized  $\beta$ -TCP powders were more than two times higher as compared to those of bioceramics obtained from micron-sized  $\beta$ -TCP powders. However, the degradability of bioceramics sintered from nanodimensional powders was just about one fourth of that sintered from micron-sized powders. Thus, the degradability of  $\beta$ -TCP bioceramics could be additionally regulated by the particle dimensions [138].

Nano-sized whiskers of several  $\text{CaPO}_4$  (HA,  $\beta$ -TCP and BCP (HA +  $\beta$ -TCP)) were produced by using a novel microwave-assisted “combustion synthesis (autoignition)/molten salt synthesis” hybrid route. Aqueous solutions containing  $\text{NaNO}_3$ ,  $\text{Ca}(\text{NO}_3)_2$ , and  $\text{KH}_2\text{PO}_4$  (with or without urea) were irradiated in a household microwave oven for 5 min at 600 watts of power. The as-synthesized precursors were then simply stirred in water at room temperature for 1 h to obtain the nano-sized whiskers of the desired  $\text{CaPO}_4$  [563]. Similar results were obtained in another study [501]. Furthermore, nanostructured and/or nano-sized biphasic (HA +  $\beta$ -TCP) bioceramics was successfully prepared by other techniques, such as microwave synthesis [564–566], a polymer matrix-mediated process [567], and in situ in polyvinyl alcohol [568]. Good cellular activities of the biphasic bioceramics have been reported.

Layrolle and Lebugle developed a synthesis route of nano-sized FA and other  $\text{CaPO}_4$ , using calcium diethoxide ( $\text{Ca}(\text{OEt})_2$ ) and  $\text{H}_3\text{PO}_4$  [121] (+  $\text{NH}_4\text{F}$  to prepare FA [569]) as the initial reagents and anhydrous ethanol as a solvent. By a simple variance of the ratio of reagents,  $\text{CaPO}_4$  of various chemical compositions were precipitated in ethanol. The precipitates were characterized and the results indicated that those  $\text{CaPO}_4$  were amorphous and nanodimensional. Furthermore, they had large specific surface areas and possessed a high reactivity [121, 569].



### 9.6.4 Other Nano-scaled $\text{CaPO}_4$

Nano-sized crystals of DCPD (with some amount of CDHA and ACP) of a relatively high monodispersity could be synthesized from aqueous solutions of calcium nitrate and  $\text{H}_3\text{PO}_4$  in the presence of 2-carboxyethylphosphonic acid. They are produced in a discoid shape with a diameter of 30–80 nm and a height of less than ~5 nm. They form stable colloidal solutions displaying minimal agglomeration [570]. Nano-sized rods and fibers of DCPD with average diameters of  $25 \pm 5$  nm (aspect ratio ~6) and  $76 \pm 20$  nm (aspect ratio ~40), respectively, were synthesized by sucrose ester-based reverse microemulsion technique [571]. A similar approach was used in another study [405]. Nanodimensional crystals of both DCPD and DCPA were prepared by EDTA-assisted hydrothermal method [316]. In addition, nanocrystalline DCPD was prepared by a reverse microemulsion technique with surfactin [572]. Further, nano-scaled DCPD, functionalized with triethylene glycol dimethacrylate (added to one of the reacting solutions, with the purpose of reducing agglomeration and improving the compatibility with vinyl-based resin matrices), was synthesized at room temperature by sol-gel process through the stoichiometric reaction between  $(\text{NH}_4)_2\text{HPO}_4$  and  $\text{Ca}(\text{NO}_3)_2 \cdot 4\text{H}_2\text{O}$  [573].

An interesting approach comprises precipitation of  $\text{CaPO}_4$  inside nano-sized pores of another material. For example, nanodimensional clusters DCPD were immobilized into pores of an oxide network by immersion of this network into an acidic ( $\text{pH} = 2.7$ )  $\text{CaPO}_4$  solution at  $50^\circ\text{C}$  [574]. The acid-base reaction between the  $\text{CaPO}_4$  solution and the hydroxyl groups of the oxide network resulted in formation of nanodimensional clusters of DCPD immobilized inside the oxide pores. Interestingly, the immobilized nanodimensional clusters of DCPD were further converted into those of ACP and CDHA by supplementary treatment of the oxide network in alkaline solutions [574]. Hollow nano-sized shells of undisclosed  $\text{CaPO}_4$  (presumably, of ACP) with a size distribution of  $(120\text{--}185) \pm 50$  nm and predictable mean shell thickness from 10 to 40 nm were prepared by crystallization onto the surface of nanodimensional liposomes [575, 576]. Both the suspension stability and shell thickness control were achieved through the introduction of carboxyethylphosphoric acid. Variation of shell thickness and stoichiometry may be a way of manipulating the dissolution kinetics of ACP coating to control the release of encapsulated materials, necessary for drug delivery purposes [575, 576]. Other types of  $\text{CaPO}_4$  shells with Ca/P ratios of 0.97 (DCPD or DCPD-like ACP) and 1.45 (CDHA or ACP) were prepared using liposome templates [577]. Furthermore, nanodimensional  $\text{CaPO}_4$  with DCPD as the major phase have been synthesized by an inverse microemulsion system using kerosene as the oil phase, a cationic surfactant, and a nonionic surfactant [578]. A little bit later, phase pure, stable nanocrystalline DCPD with average dimensions in the range of 23–87 nm were obtained by the same technique [579]. Microskeletal constructions might be synthesized as well [580]. Finally, yet importantly, nano-scaled DCPD was prepared in a continuous flow tube reactor [460].

Concerning preparation of nano-scaled DCPA, roughly spherical particles of approximately 50–100 nm in sizes were synthesized via a spray-drying technique [89, 581–583], while ribbonlike fibers were prepared upon hydrolysis in urea [391]. In addition, nano-scaled crystals of DCPA containing pores of 1–30 nm in diameter were prepared by an energy-efficient microwave method [584]. Furthermore, nanodimensional DCPA might be synthesized galvanostatically [585] and in reverse micelles [586].

When it comes to precipitated ACPs, they are nanodimensional in the vast majority of cases. Approximately spherical nano-sized particles of ACP with a diameter of about 50 nm can be prepared by rapid precipitation from water [587] and subsequent colloidal stabilization by coating with polymers [588]. Nano-sized clusters of ACP [589] or those comprising a spherical core of  $355 \pm 20$  DCPD units with density of  $2.31 \text{ g/cm}^3$  and radius of  $2.30 \pm 0.05 \text{ nm}$  surrounded by  $49 \pm 4$  peptide chains with a partial specific volume of  $0.7 \text{ cm}^3/\text{g}$ , forming a tightly packed shell with an outer radius of  $4.04 \pm 0.15 \text{ nm}$ , were prepared by precipitation using 10 mg/ml of the 25-amino-acid N-terminal tryptic phosphopeptide of bovine  $\beta$ -casein as a stabilizing agent [590]. Nano-sized particles of ACP were prepared by mixing of solutions of  $\text{Ca}(\text{NO}_3)_2 \cdot 4\text{H}_2\text{O}$  (450 mmol/L) in acetone and  $(\text{NH}_4)_2\text{HPO}_4$  (30 mmol/L) in deionized water at pH within 10.0–11.0 [591]. Furthermore, nanodimensional particles of ACP might be prepared by microwave-assisted synthesis [592], microwave-assisted hydrothermal synthesis [593, 594], electrostatic spray pyrolysis [595, 596], pulsed laser ablation [562], mechanochemical synthesis [597], spray drying [89], as well as by flame spray synthesis [437]. By means of the latter technique, one can produce nanodimensional ACPs with a broad Ca/P ratio within 0.5–1.5 [437].

Self-assembled shell cross-linked poly(acrylic acid-*b*-isoprene) micelles and/or cross-linked poly(acrylic) acid nano-sized cages in aqueous solutions might be used as templates for preparation of polymer/ $\text{CaPO}_4$  nanodimensional capsules of 50–70 nm in diameter, which consisted of spherical polymer nano-sized particles enclosed within a continuous 10–20 nm thick surface layer of ACP [598]. Synthesis of hollow spherical  $\text{CaPO}_4$  nano-sized particles using polymeric templates has been also reported by other researchers [599–601]. Furthermore, bundles of surfactant-coated ACP nanodimensional filaments of  $\sim 2 \text{ nm}$  in width and  $>300 \mu\text{m}$  in length were synthesized in reverse micelles [602]. Bundles of the nanodimensional filaments were stable in the reverse micelle phase up to around 5 days, after which they transformed into 5-nm-wide surfactant-coated CDHA rods. Discrete filaments of  $100\text{--}500 \times 10\text{--}15 \text{ nm}$  in size and a linear superstructure based on the side-on stacking of surfactant-coated ACP nano-sized rods were also prepared [508]. A double reverse micelle strategy was realized to synthesize amine and carboxylate- and polyethylene glycol surface-functionalized  $\text{CaPO}_4$  nano-sized particles of an undisclosed nature [603]. Furthermore, the reverse micelle technique might be applied to prepare nanodimensional DCPA [519, 604].

Concerning nano-scaled OCP, it was prepared in a continuous flow tube reactor [460]. In addition, an oriented growth of nano-scaled belts of OCP with a clean surface was achieved by wet-chemical approach using cetyltrimethylammonium bromide [605]. Pulsed laser deposition technique was employed to obtain thin films

of nanocrystalline OCP on pure Ti substrates [606]. The deposition was performed by a pulsed UV laser source in a flux of hot water vapors. High-resolution electron microscopy and X-ray diffraction at grazing incidence investigations indicated that the coatings were made of nanocrystalline OCP (unfortunately, the dimensions were not indicated). In vitro tests proved that both fibroblasts and osteoblasts adhered, reached a normal morphology, proliferated, and remained viable when cultured on the nanocrystalline OCP coatings, supporting a good biocompatibility and absence of any toxicity [606].

Agglomerates of spherical well-ordered nano-sized (10–18 nm) particles of TTCP were prepared by solid-state reactions between  $\text{CaCO}_3$  and MCPM powders mixed in a molar ratio of 3: 1 and suspended in *n*-heptane for 16 h, followed by filtration, drying, sintering at 1450–1500 °C for 6–12 h, and rapid quenching to room temperature [607]. Nanodimensional powders of BCP (both HA +  $\beta$ -TCP [608–612] and HA +  $\alpha$ -TCP [613]) have been fabricated as well. To get the details, the interested readers are referred to the original publications.

Similar to that for apatites (see above), nano-scaled particles of other types of  $\text{CaPO}_4$  might be functionalized and/or doped by various compounds to provide new important properties [169, 542, 603, 613–621], such as fluorescence [616, 617, 621], luminescence [619], or a good dispersibility in organic solvents [613]. Furthermore, nano-sized  $\text{CaPO}_4$  might be used as templates to manufacture nanodimensional capsules [622].

To conclude this part, one should mention a review on patents on the subject [623]. Unfortunately, no information on the preparation of nanodimensional or nanocrystalline MCPM, MCPA, OA, and TTCP was found in literature. Hopefully, they will be manufactured in a near future.

### 9.6.5 *Biomimetic Construction Using Nanodimensional Particles*

Morphological control of bioinorganic materials is another interesting issue in biomineralization, by which inorganic materials with complex morphologies can be produced. Complex forms or patterns with a hierarchical structure over several length scales are important features of biomineralization. Pattern formation in biomineralization is a process in which self-assembled organic templates are transformed by a material's replication into organized inorganic structures. Needless to mention, researchers try to reproduce these processes in laboratories. For example, Chen et al. reported a way to create enamel-like structures by modifying synthetic nano-sized rods of apatite with a surfactant, bis(2-ethylhexyl)sulfosuccinate salt that allowed the nano-sized rods to self-assemble into prism-like structures at the water/air interface [191]. A nanometer-scale rod array of apatite having preferred orientation to the *c*-axis was successfully prepared simply by soaking calcium-containing silicate glass substrates in  $\text{Na}_2\text{HPO}_4$  aqueous solution at 80 °C for

various periods [624]. A biomimetic bottom-up route to obtain the first hierarchical level of bone was reported [178]. A pH-induced self-assembly of peptide amphiphile to make a nanostructured fibrous scaffold reminiscent of extracellular bone matrix was obtained. After the cross-linking of the scaffold, the fibers were able to direct mineralization of CDHA to form a biocomposite, in which the crystallographic *c*-axes of the nano-sized crystals of CDHA were aligned with the long axes of the fibers. This alignment was similar to that observed between collagen fibrils and crystals of biological apatite in bones [178]. Other attempts to fabricate artificial materials having bone-like both nanostructure and chemical composition were performed, and several significant achievements were obtained [625, 626].

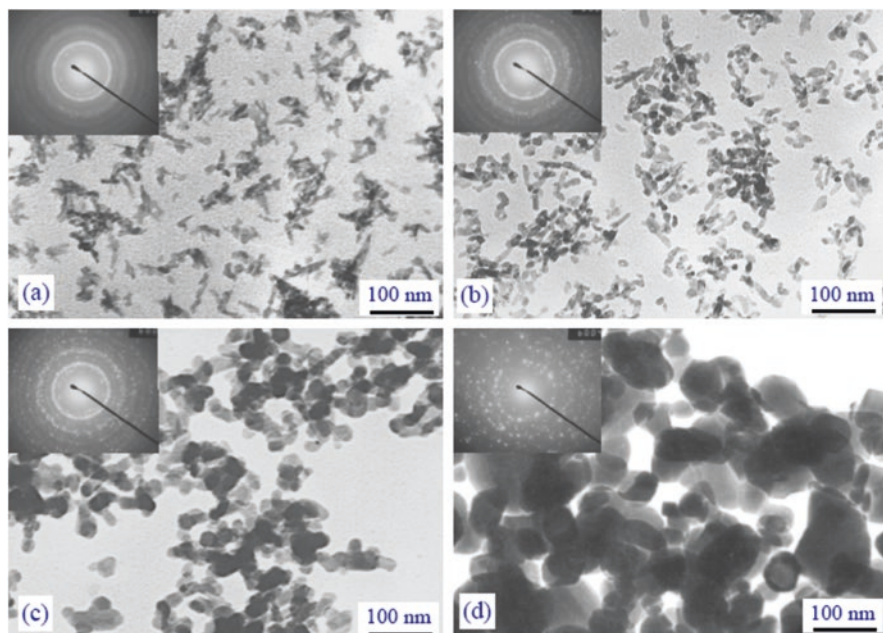
The classical model of biomineralization considers mineral formation as an amplification process in which individual atoms or molecules are added to existing nuclei or templates [1, 2, 627]. This process occurs in the presence of various bioorganic molecules, which deterministically modify nucleation, growth, and facet stability. A model involving aggregation-based growth [628] recently challenged this conventional concept for the crystal growth. Inorganic nano-sized crystals were found to aggregate into ordered solid phases via oriented attachment to control the reactivity of nanophase materials in nature [19, 629]. A model of “bricks and mortar” was suggested to explain the biological aggregation of nano-sized apatite [630]. In this model, ACP acts as “mortar” to cement the crystallized “bricks” of nano-sized HA. Meanwhile, biological molecules control the construction process. By using nanodimensional spheres of HA as the building blocks, highly ordered enamel-like and bone-like apatites were hierarchically constructed in the presence of glycine and glutamate, respectively. It is interesting that, during the evolution of biological apatite, the amorphous “mortar” can be eventually turned into the “brick” by phase-to-phase transformation to ensure the integrity of biominerals [630].

## 9.7 Biomedical Applications of the Nano-scaled $\text{CaPO}_4$

### 9.7.1 Bone Repair

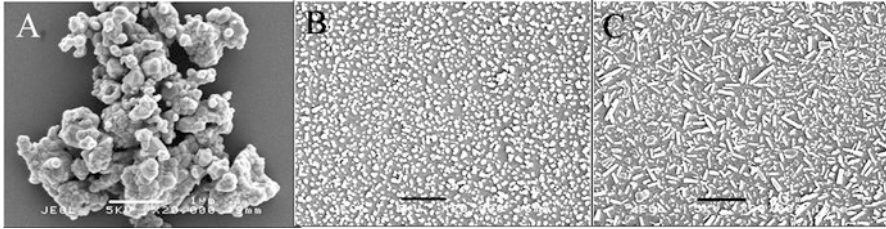
Due to advances in surgical practice and a fast aging of the population, there is a permanently increasing demand for bone grafts [631]. Modern grafts should not only replace the missing bones but also should be intrinsically osteoinductive by acting as scaffolds for guided bone growth. Furthermore, an ability to form a biologically active apatite layer to bond to living bone is an essential requirement to modern biomaterials [632]. In addition, a good graft should provide a framework to support new blood vessels and soft tissues in forming a bridge to existing bones [631].

$\text{CaPO}_4$  bioceramics of micron dimensions have been used in dentistry, orthopedics, and surgery for over 30 years because of their chemical similarity to calcified tissues of mammals and, therefore, excellent biocompatibility [115, 173, 174, 238–



**Fig. 9.9** Particle sizes and crystallinity of HA powders after a heat treatment at various temperatures: (a) 300 °C, (b) 500 °C, (c) 700 °C, (d) 900 °C

241]. Due to a rapid development of nanotechnology, the potential of nanodimensional and nanocrystalline forms of  $\text{CaPO}_4$  has received a considerable attention [18] because they produce favorable results in repair of bone defects [633–641]. For example, due to an improved sinterability, an enhanced densification, and a better bioactivity than coarser crystals, they might be chosen as the major components of self-setting bone cements [14, 545, 546, 642–645]. However, there is a study in which an increase of particle and crystallite sizes of TCP did not prolong but shortened the induction time until the cement setting reaction started [548], which was against the common physical rules (generally, smaller particles or crystallites should enhance reactivity). Nevertheless, two general directions of the biomedical application of nanodimensional and nanocrystalline  $\text{CaPO}_4$  can be outlined: (i) using them in powder form as filling materials to impart bioactivity to various biocomposites and hybrid biomaterials [52–76, 145, 646–651] and (ii) manufacturing of either dense compacts or porous scaffolds, possessing the sufficient mechanical properties [625, 626, 652–655]. As nano-scaled  $\text{CaPO}_4$  tend to agglomerate at heating (Fig. 9.9) [165, 279, 656–658], normally a low-temperature [135, 289, 339, 659] and/or a rapid consolidation [135, 237, 284, 660–666] techniques must be employed. The low-temperature approach comprises gel hardening (at 4 °C) [339] and uniaxial pressing at 150–200 °C [135]. In addition, HA plates with nano-sized pores inside the plates could be prepared by drying an aqueous dispersion of nanodimensional HA on a liquid substrate at 60 °C without binder [289, 659]. The rapid consolidation



**Fig. 9.10** HA powders calcined (a) without additives and (b, c) with anti-sintering agents for (a, b) spherical and (c) rod-shaped nano-sized particles. Bar is 1  $\mu\text{m}$  (Reprinted from Ref. [420] with permission. Copyright © 2012 National Institute for Materials Science)

techniques comprise spark plasma sintering [135, 237, 284, 660–666], pressure sintering [661], and microwave sintering over the temperature range 1000–1300 °C, using a rapid sintering schedule [664–666]. Besides, a two-step sintering process might be applied as well [667, 668]. Furthermore, nanodimensional crystals of calcined HA might be fabricated by calcination at 800 °C for 1 h with an anti-sintering agent surrounding the original nano-sized CDHA particles (Fig. 9.10). During sintering, this agent prevents the contacts among the particles and, after sintering, the agent is subsequently removed by washing [669–671]. These consolidation approaches provided a limited alteration of the initial nano-sized crystals, while the final bioceramics possessed the mechanical properties similar to those reached with sintered stoichiometric HA.

Already in 1990s, implants prepared from nanodimensional apatites, as well as biocomposites of nanodimensional apatite with organic compounds, were tested *in vivo* [672–674]. Cylinders made of both pure nanodimensional apatite and organoapatite containing a synthetic peptide were analyzed 28 days after implantation into spongy bones of Chinchilla rabbits. Both implant types were well incorporated, and interface events were found to be similar to those observed on human bone surfaces with regard to resorption by osteoclast-like cells and bone formation by osteoblasts. That study revealed a suitability of such materials for both bone replacement and drug release purposes [672]. Similar results were obtained in other studies [673, 674].

Among the available commercial formulations, NanOss™ bone void filler from Angstrom Medica, Inc., is considered as the first nanotechnological medical device to have received the clearance by the US Food and Drug Administration (FDA) in 2005 [675]. It is prepared by precipitation of nano-sized  $\text{CaPO}_4$  from aqueous solutions, and the resulting white powder is then compressed and heated to form a dense, transparent, and nanocrystalline material. NanOss™ mimics the microstructure, composition, and performance of human bone, as well as it is mechanically strong and osteoconductive. It is remodeled over time into human bone with applications in sports medicine, trauma, and spine and general orthopedics markets [675].

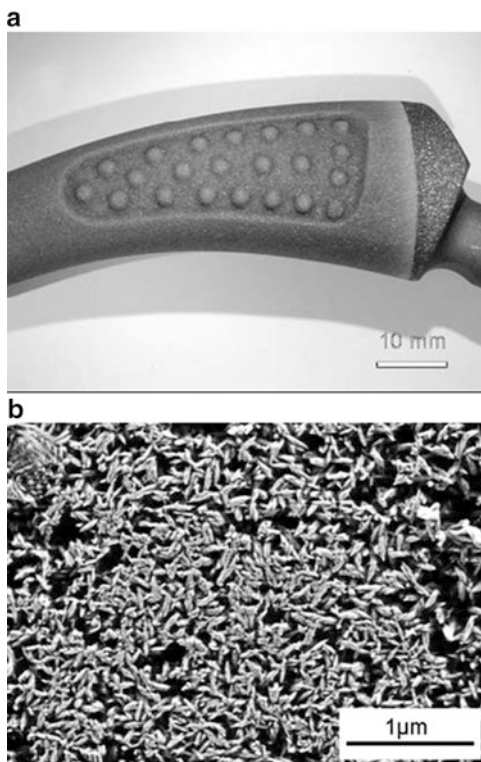
Ostim® (Osartis GmbH & Co. KG, Obernburg, Germany) is another popular commercial formulation. This ready-to-use injectable paste received CE (Conformite Europeenne) approval in 2002. Ostim® is a suspension of synthetic nanocrystalline

HA (average crystal dimensions:  $100 \times 20 \times 3 \text{ nm}^3$  (a needlelike appearance), specific surface area  $\sim 100 \text{ m}^2/\text{g}$ ) in water, prepared by a wet-chemical reaction [676]. After completion, the HA content in the paste is  $\sim 35\%$ . Ostim<sup>®</sup> does not harden when mixed with blood or spongiosa, so it is highly suitable for increasing the volume of autologous or homologous material. Simultaneously, its viscosity enables its applications to form-fit in close contact with the bone. Ostim<sup>®</sup> can be used in metaphyseal fractures and cysts, alveolar ridge augmentation, acetabulum reconstruction, and periprosthetic fractures during hip prosthesis exchange operations, osteotomies, filling cages in spinal column surgery, etc. [675–689]. It can be incorporated into bones and a new bone formation is visible after only 3 months [690]. For a number of clinical applications, Ostim<sup>®</sup> can be combined with other types of  $\text{CaPO}_4$  bioceramics, e.g., with a HA bioceramic core (Cerabone<sup>®</sup>) [676, 691] or with biphasic ( $\beta$ -TCP + HA) granules (BoneSaves<sup>®</sup>) [692]. Application of such combinations of a nanocrystalline Ostim<sup>®</sup> with the microcrystalline  $\text{CaPO}_4$  bioceramics appeared to be an effective method for treatment of both tibia head compression fractures [676] and metaphyseal osseous volume defects in the metaphyseal spongiosa [691]. Besides, such combinations might be used for acetabular bone impaction grafting procedures [692]. Interestingly, that self-setting formulations might be prepared by replacement of water by a neutral ( $\text{pH} = 7$ ) phosphate buffer solution [693].

Cui et al. developed nano-sized HA/collagen biocomposites, which mimicked the nanostructure of bones [176, 694]. After implantation, such biocomposites can be incorporated into bone metabolism. Due to processing difficulties and poor mechanical properties of bulk  $\text{CaPO}_4$ , their applications are currently confined to non-load-bearing implants and porous bodies/scaffolds. Porous 3D biocomposites of nanodimensional HA with collagen or other (bio)polymers (chitin, chitosan, gelatin, etc.) mimic bones in composition and microstructure and can be employed as a matrix for the tissue engineering of bone.

Owing to their low mechanical properties, the use of  $\text{CaPO}_4$  in load-bearing applications is rather limited:  $\text{CaPO}_4$  are too stiff and brittle for such use. Today's solutions for weight-bearing applications rely mostly on biologically friendly metals, like cobalt-chromium alloys, titanium and its alloys, as well as stainless steel 316L, but problems with stress-shielding and long-term service can cause failures. All these metals, although nontoxic, are always bioinert and cannot bond to bone directly. In order to improve the biological properties of the metallic implants, nanostructured  $\text{CaPO}_4$  (mainly, apatites) are deposited on their surface to accelerate bone growth and enhance bone fixation [152, 153, 419, 606, 695–703]. There are about 50 deposition techniques to put down  $\text{CaPO}_4$  onto the surface of various substrates [704], and in the case of apatites, the deposits are commonly composed from uniform nanodimensional particles or crystals (Fig. 9.11). They are capable of performing bone formation and promoting direct osseointegration with juxtaposed bone [707–710]. For example, an enhanced new bone formation can be clearly seen on nanophase HA-coated tantalum compared to microscale HA-coated tantalum and non-coated tantalum (see Fig. 9.2 in Ref. [88]). Furthermore, nanostructured  $\text{CaPO}_4$  might be used as a coating material to impart surface bioactivity to other

**Fig. 9.11** (a) A photo of a titanium implant coated with electrochemically deposited HA at 37 °C (Cenos® BoneMaster); (b) a micrograph of a titanium implant surface coated with electrochemically deposited HA at 37 °C (Reprinted from Ref. [705] with permission. Copyright © 2007 Carl Hanser Verlag GmbH & Co. KG; other micrographs of nanodimensional CDHA coatings biomimetically deposited on NaOH-treated Ti6Al4V surfaces might be found in Ref. [706])



materials, e.g., glasses [711], polymers [712, 713], xenografts [714], and even other types of  $\text{CaPO}_4$  [715]. Finally, but yet importantly, such coatings might be patterned, e.g., by laser direct writing [624] or electrohydrodynamic atomization spraying technique [716]. However, the deposition of nano-sized  $\text{CaPO}_4$  on the implant surfaces does not always improve early tissue integration [717, 718].

### 9.7.2 Nano-scaled $\text{CaPO}_4$ and Cells

It is well accepted that bone-related cells (especially, osteoblasts and osteoclasts) play the key roles in the physiological formation of calcified tissues. Bone-related cells not only are speculated to take part in the formation of biominerals and macrostructure constructions of bones, but they also continuously modulate the density, regeneration, and degradation of bones. Therefore, understanding the relationship between the bone-related cells and nano-sized  $\text{CaPO}_4$  has been paid much attention in order to elucidate the formation mechanism of bones, to prevent and cure bone-related diseases, and to design novel biomaterials. Better structural biomimicry and osteoconductivity can be achieved using nano-scaled  $\text{CaPO}_4$  [144, 145, 151, 152, 719–723]. Biocompatibility of such biomaterials is the key question for their



application possibility for clinical use. For example, adhesion, proliferation, and differentiation of mesenchymal stem cells were studied on nano-sized HA/polyamide biocomposite scaffolds. The results indicated that such biocomposites exhibited a good biocompatibility and an extensive osteoconductivity with host bone *in vitro* and *in vivo* and proved that nano-sized HA/polyamide scaffolds had a potential to be used in orthopedic, reconstructive, and maxillofacial surgery [724–726].

Most results demonstrate that nanostructured  $\text{CaPO}_4$  can improve cell attachment and mineralization *in vivo*, which suggests that they may be a better candidate for clinical use in terms of bioactivity [151, 152, 157, 727–732]. The size effects of nanodimensional HA on bone-related cells, as well as the influence of crystallinity of nano-sized HA, were studied [733–736]. Namely, different nano-sized particles of HA, typically of  $20 \pm 5$ ,  $40 \pm 10$ , and  $80 \pm 12$  nm in diameter, were prepared, and their effects on the proliferation of two types of bone-related cells, bone marrow mesenchymal stem cells (MSCs) and osteosarcoma cells (U2OS and MG63), were studied. The cell culture experiments showed an improved cytophilicity of the nano-phase HA if compared to the submicron-sized HA. A greater cell viability and proliferation of MSCs were measured for nano-sized HA, remarkably for 20-nm-sized particles. However, the opposite phenomenon occurred for bone tumor cells when nano-sized HA were cocultured with cells. Nano-sized HA can inhibit proliferation of U2OS and MG63 cells, and the inhibited strengths were inversely proportional to the particle size, i.e., smaller particles possessed a greater ability to prevent cell proliferation. This suggests that nano-sized HA can exhibit favorable cell proliferation to optimize biological functionality, in which the particle dimensions are believed to play a key role. These *in vitro* findings are of a great significance for the understanding of cytophilicity and biological activity of nano-sized particles during biomineralization [733]. Furthermore, an early osteogenic signal expression of rat bone marrow stromal cells appeared to be influenced by nanodimensional HA content [737]. On the other hand, there is a study on early bone healing, in which an importance of nanometer-thick coatings of nanodimensional HA on titanium implants appeared to be insignificant if compared to the control [738]. In addition, it was found that large quantities of nano-sized HA entered into cells and damaged their morphology; therefore, it was concluded that not all the types of nano-sized HA could be considered for clinical applications [735].

In still another study, an interaction mechanism of nano-scaled HA with cells was investigated [739]. A real-time polymerase chain reaction analysis revealed that the expression of bone morphogenetic protein BMP-2 increased upon stimulation with nano-scaled HA in both dose- and time-dependent manners. Concentrations of calcium and orthophosphate ions in culture supernatants were found to be unchanged, suggesting that nano-scaled HA functioned as just nanoparticles rather than as a source for extracellular releasing of the ions. This novel interaction mechanism could be important for the rational design of future periodontal regeneration [739].

Studies confirmed that nano-sized ACP had an improved bioactivity if compared to nano-sized HA since a better adhesion and proliferation of osteogenic cells had been observed on the ACP substrates. However, in order to understand the influence

of crystallinity of the nano-sized  $\text{CaPO}_4$  on the osteogenic cells correctly, it was critical to use nano-sized ACP and HA of the same size distribution [734]. Thus, ACP and HA particles of ~20 nm size were synthesized, and the effects of crystallinity were studied. The adhesion, proliferation, and differentiation of MSC cells were measured on both ACP and HA films and compared at the same size scale. Surprisingly, more cells were adsorbed and proliferated on the films of the well-crystallized nano-sized HA than those on the films of nano-sized ACP. Alkaline phosphatase activity assay and RT-PCR assay were also used to evaluate the differentiation of MSC cells. The results showed that the differentiation of MSC cells from osteoblasts was promoted significantly by nano-sized HA. These experimental phenomena clearly demonstrate that the crystallized phase of HA provides a better substrate for MSC cells than ACP, when the factor of size effect is removed. This new view on the relationship between the crystallinity of  $\text{CaPO}_4$  and the responses of cells emphasized the importance of both size and phase control in the application of biomedical materials [734–738].

On the other hand, the chemical composition of the samples appears to be important. Interestingly, in spite of the fact that the biological apatite of bones contains the substantial amount of carbonates, among investigated samples of nanocrystalline apatites, osteoclastic differentiation was found to be constrained on carbonate-rich samples, leading to smaller numbers of osteoclast-like cells and fewer resorption pits. Furthermore, the highest resorption rate was found for nanodimensional HA with a low carbonate content, which strongly stimulated the differentiation of osteoclast-like cells on its surface [740].

Cells are sufficiently sensitive and nanoscale alterations in topography might elicit diverse cell behavior [741–743]. How cells can recognize the particle size and other very small differences in the properties of nano-sized HA in these experiments remains unclear. Actually, determining the mechanisms whereby nano-sized particles of  $\text{CaPO}_4$  and their sizes exert effects on bone-related cells will require further systematic studies.

To conclude this part, one should note that the entire aforementioned is devoted to bone-related cells. However, nanodimensional  $\text{CaPO}_4$  start to be applied to other parts of the bodies. For example, a possible protective effect of nano-sized HA was investigated against nerve injury, and it appeared to be not neurotoxic for the electrophysiology activity of cells [744]. Additional details on the interactions between nano-scaled  $\text{CaPO}_4$  and cells are available elsewhere [484].

### 9.7.3 *Dental Applications*

Dental caries is an ubiquitous and worldwide oral disease. At the initial stage of caries lesions, bacteria cause damage of dental enamel, which is the exterior coating of teeth and possesses remarkable hardness and resistance. As the most highly mineralized structure in vertebrate bodies, enamel is composed of numerous needlelike apatite crystals of nanodimensional sizes, which are bundled in parallel ordered

prisms to ensure unique mechanical strength and biological protection. As a nonliving tissue, the main constituent (~97 wt.%) of mature enamel is inorganic nanodimensional apatite so that enamel is scarcely self-repaired by living organisms after substantial mineral loss. Filling with artificial materials is a conventional treatment to repair damaged enamel. However, secondary caries frequently arise at the interfaces between the tooth and foreign materials [745].

Nanodimensional HA and CDHA are often considered as model compounds of dental enamel due to the chemical and phase similarities [115, 173]. Therefore, enamel remineralization by using nanodimensional apatite or other  $\text{CaPO}_4$  is suggested in dental research [746]. For example, toothpastes containing nanodimensional apatite could promote a partial remineralization of demineralized enamel [747–752], as well as possess some whitening effect [753]. Furthermore, nano-sized HA might be added to methacrylate-based root canal sealers [754], as well as to mouth rinses [752, 755]. A remineralization potential of sports drink, containing nano-sized HA, was also investigated [756, 757]. A positive influence of addition of nanodimensional  $\beta$ -TCP against acid demineralization and promoted remineralization of enamel surface was detected as well [758]. In addition, nanodimensional ACP could be added to various dental biocomposites to reduce secondary caries [759–761]. Unfortunately, these chemically analogous compounds of enamel are not widely applied in clinical practices. The native structure of dental enamel is too complex to be remodeled, and the synthesized apatite crystallites often have different dimensions, morphologies, and orientations from the natural ones, which result in a poor adhesion and mechanical strength during dental restoration. Recent advances in biomineralization also indicate that features of smaller particles of nano-sized HA might approximate features of biological apatite more closely than features of the larger HA particles that are conventionally used [13]. For example, it has been demonstrated that nano-sized HA can be self-assembled to form enamel-like structures in the laboratory [191]. Therefore, a biomimetic technique is suggested as follows: the localized repair of the enamel surface can be improved by nano-sized HA (dimension of ~20 nm), analogues to the basic building blocks of enamel rods. Furthermore, it is found that nano-sized HA can adsorb onto the enamel surface strongly and can even be integrated into the natural enamel structure [762].

It is surprising that nano-sized HA of ~20 nm can inhibit significantly a mineral loss from the enamel surface [194]. Without any treatment, the demineralization of the natural enamel surface was remarkable in acidic solution (pH  $\sim 4.5 \pm 0.1$ , experimental period of 2 days), and damaged sites were observed. The mass loss rate was about  $0.12 \pm 0.04$  mg/mm<sup>2</sup> per day. In contrast, a layer of nano-sized HA on the treated enamel surface was almost unchanged in acidic solution. The rate of mass loss of enamel coated by nano-sized HA approached zero ( $< 0.02$  mg/mm<sup>2</sup> per day), which was beyond the sensitivity of the detection methods. Since the coating by nano-sized HA appeared to be insensitive to dissolution, the underlying enamel surface was well protected under slightly acidic conditions. Furthermore, the enamel surface coated by ~20-nm-sized HA had a hardness of  $4.6 \pm 0.4$  GPa and an elastic modulus of  $95.6 \pm 8.4$  GPa. These data appeared to be very similar to those of natural enamel samples, which are  $4.2 \pm 0.2$  and  $94.1 \pm 5.4$  GPa, respectively [194].

The similarity between ~20-nm-sized HA and building blocks of dental enamel results in a good fixation of artificial biomaterials to natural tissues. Moreover, the enamel structure appears to be reinforced by nano-sized HA since secondary caries formation is suppressed and hardness is retained [745, 763, 764]. This strategy may have prospective applications in dentistry as it offers an easy but effective method to reconstruct tooth enamel that is suffering from mineral losses. Generally, these studies also suggest that analogues of nanodimensional building blocks of biominerals should be highlighted in the entire subject of biomineralization.

In the case of nanodimensional DCPA, decreasing of DCPA particle dimensions was found to increase the Ca and PO<sub>4</sub> ion releases from DCPA-based biocomposites. Therefore, biocomposites based on nano-sized DCPA, possessing both a high strength and good release of Ca and PO<sub>4</sub> ions, may provide the needed and unique combination of stress-bearing and caries-inhibiting capabilities suitable for dental applications [583]. Further details on dental applications of CaPO<sub>4</sub> might be found in topical reviews [748, 765].

### 9.7.4 *Other Biomedical Applications*

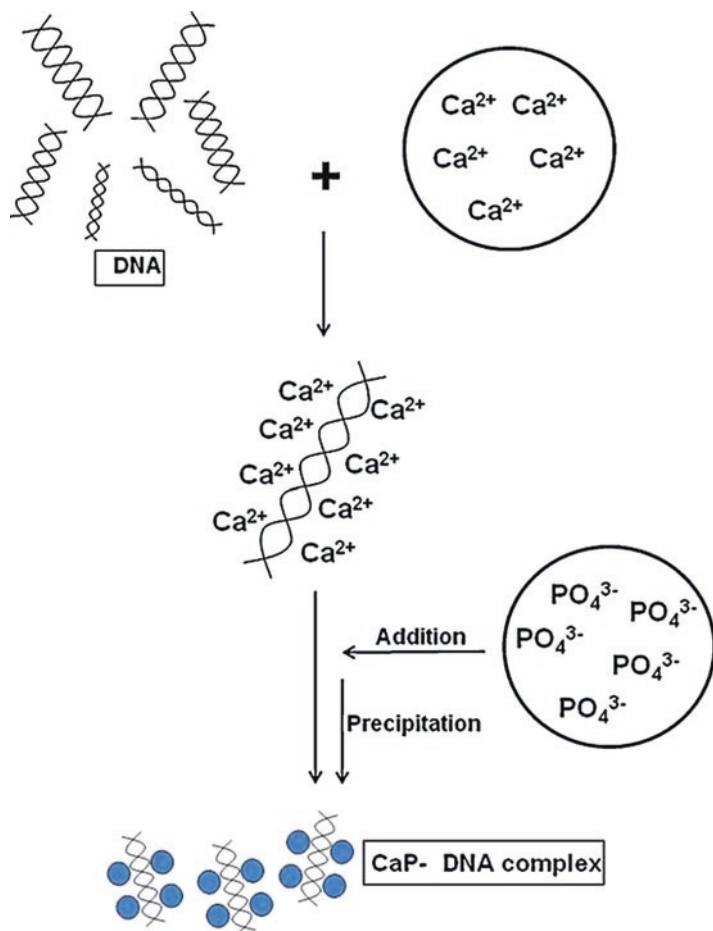
Several other biomedical applications of nano-scaled CaPO<sub>4</sub> are in progress, some of which are described here. For example, there is a report on a successful preparation of a multimodal contrast agent based on nano-sized crystals of HA, which was engineered to show simultaneous contrast enhancement for three major molecular imaging techniques such as magnetic resonance imaging, X-ray imaging, and near-infrared fluorescence imaging [766]. Furthermore, various compositions based on nanodimensional CaPO<sub>4</sub> have been already tested for cancer treatment [35, 168, 319, 617, 767–778]. For example, a relationship between the suppression and apoptosis of osteosarcoma cells and the size of the HA nanoparticles was established [772]. In another study, biocomposites consisting of a nano-sized HA core with a combination of an oleic acid and 1,2-distearoyl-sn-glycero-3-phosphoethanolamine-N-[carboxy(polyethylene glycol)-2000] lipid shell were studied as delivery vehicles for docetaxel in the treatment for hormone-refractory prostate cancer. The study reported cytotoxicity of the formulations in both the PC3 and DU145 prostate cancer cell lines [771]. Besides, nanodimensional HA was found to be effective for proliferation inhibition of highly malignant melanoma cells [779] and human chronic myeloid leukemia K562 cells [780].

Surface modification of nanodimensional CaPO<sub>4</sub> was performed in order to modulate their colloid stability, prevent dissolution in the case of low pH, avoid inflammation, serve as an intermediate layer to allow strong bond formation between CaPO<sub>4</sub> and polymer matrices, and potentially enhance its bioactivity or improve its conjugation ability with special functional groups [12, 781–790]. Such surface-modified nano-sized particles might be applied for oral insulin delivery [791].

In another aspect, many strategies have been employed to load various agents, i.e., therapeutic, bio-imaging, etc., to nanodimensional CaPO<sub>4</sub> (mainly, apatites)

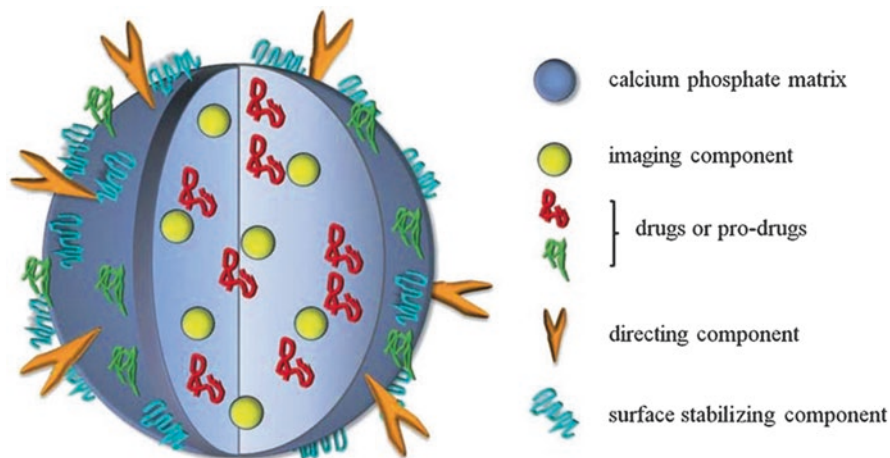
[792]. In summary, these strategies can be broadly categorized into two main approaches. One approach is to load these agents during the synthesis – the so-called *in situ* loading. This is done by adding the desired agent(s) to the reaction mixture before the formation of a nanodimensional  $\text{CaPO}_4$  is completed. The second approach is to load the agent(s) only after a nanodimensional  $\text{CaPO}_4$  has been fully synthesized or, in other words, after the synthesis process – the so-called *ex situ* loading. This is mainly done through surface adsorption where the agents are adsorbed onto the surfaces of pre-synthesized nanodimensional particles [793]. The Coulomb force between  $-\text{COO}^-$  groups of proteins and  $\text{Ca}^{2+}$  of solid HA appears to be the main adsorption mechanism [794]. Therefore, due to established biocompatibility, ease of handling, and notorious adsorption affinity, nano-sized  $\text{CaPO}_4$  have been applied as nonviral carriers for drug delivery and gene therapy [97, 172, 268, 285, 530, 576, 603, 767, 795–812]. After loading with genes and/or drugs, nanodimensional  $\text{CaPO}_4$  provide a protective environment that shields them from degradation while providing a convenient pathway for cell membrane penetration and controlled release of the genes or drugs [531]. The experimental results proved that nanodimensional  $\text{CaPO}_4$  possessed a higher penetration rate into cell membranes, and their transfection efficiency could be 25-fold higher than that of the micron-sized particles. Namely, the size increase from 100 nm in length and 20 nm in diameter to 150 nm in length and 50 nm in diameter yields zero uptake of HA particles [813]. Furthermore, due to the larger specific surface areas, nanodimensional  $\text{CaPO}_4$  can hold larger load amounts of drugs than coarser particles. These results indicate the potential of nano-sized  $\text{CaPO}_4$  in gene delivery and as drug carriers [531, 813–819]. Since a charge of the particles influences their ability to pass through the cellular membrane and a positive charge is beneficial [788], positively charged nano-sized particles of  $\text{CaPO}_4$ /polymer biocomposites were successfully applied for photodynamic therapy [820]. Furthermore, nanodimensional  $\text{CaPO}_4$  can be stably loaded with radioisotopes [800, 821].

A transfer of functional foreign nucleic acids (DNA or RNA) into nuclei of living cells (transfection) with the aim of repairing missing cell function and providing means to enhance or silence gene expression is currently used extensively in the laboratory and is fastly becoming a therapeutic reality. Since DNA and RNA are negatively charged, the electrostatic repulsion with the anionic cell membrane reduces their transfection efficiency [822]; efficient carriers are required [823, 824]. Nanodimensional  $\text{CaPO}_4$  can be represented as a unique class of the nonviral vectors, which can serve as efficient and alternative nucleic acid carriers for targeted delivery of genes [268, 768, 792, 798, 825–841] and cells [614, 842–851]. For example, by means of nanodimensional  $\text{CaPO}_4$ , an efficient and safe strategy to introduce suicide genes into colon cancer cells was developed [770]. In addition, the pH-dependent solubility profiles of  $\text{CaPO}_4$  make this class of nano-sized particles especially useful for *in vitro* and *in vivo* delivery purposes. Therefore, after transfection, these particles dissociate into calcium and orthophosphate ions, i.e., physiological components found in every cell. The standard transfection method using  $\text{CaPO}_4$ , first introduced by Graham and van der Eb in 1973 [849], is still used in biochemistry. It involves a straightforward *in situ* coprecipitation of  $\text{CaPO}_4$ /DNA

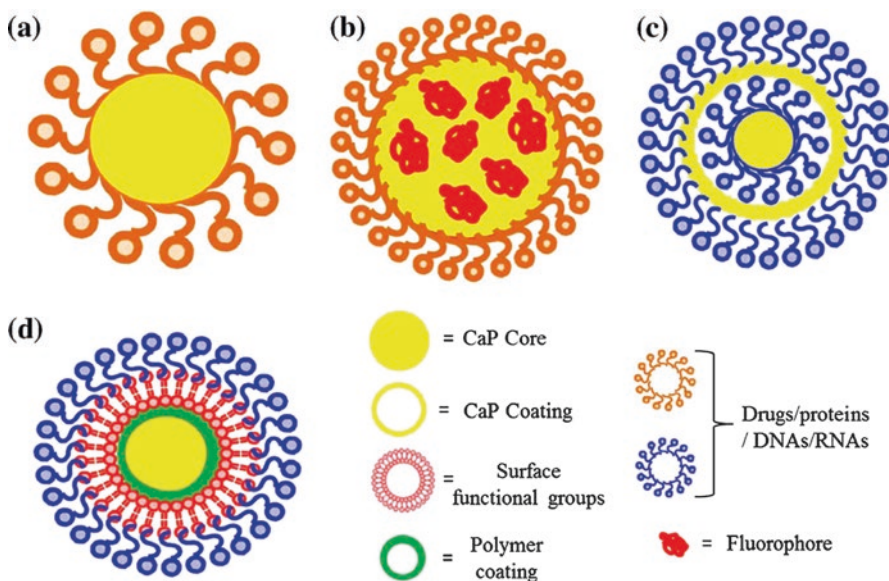


**Fig. 9.12** Schematics of the formation of CaPO<sub>4</sub>/DNA complexes via coprecipitation method. Calcium ions readily bind to anionic DNA and forms Ca-DNA complexes. As orthophosphate anions are mixed into the solution, Ca-DNA complexes react with the anions and form CaP-DNA complexes by precipitation as the DNAs are condensed into and around the calcium phosphate particulates (Reprinted from Ref. [832] with permission. Copyright © 2012 John Wiley & Sons, Inc)

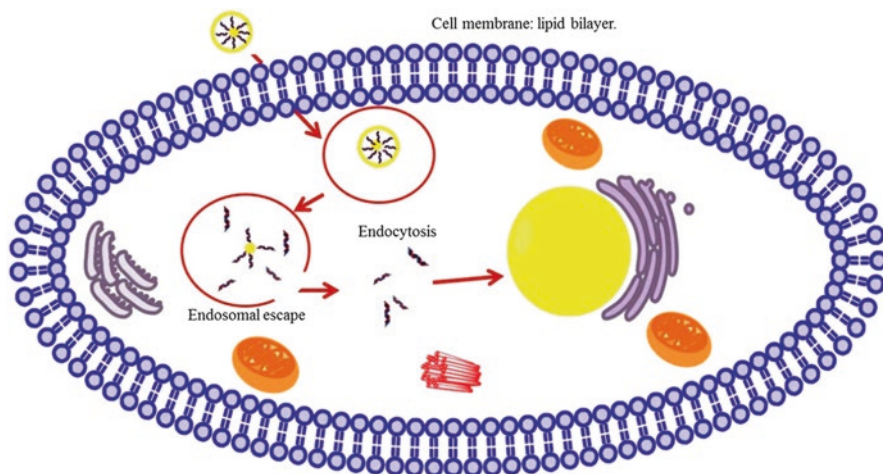
aggregates (Fig. 9.12) [832]. During this process, DNA gets readily condensed and adsorbed onto the precipitate and thereby changes the characteristics of the particles. A similar experimental approach is used to load CaPO<sub>4</sub> by drugs [804]. Schematic drawings of the various types of functionalized nano-sized CaPO<sub>4</sub> particles suitable for both imaging and drug delivery purposes are shown in Fig. 9.13 [852] and Fig. 9.14 [853], while a schematic representation of a gene delivery process into the cell nucleus through a double-shell nano-sized CaPO<sub>4</sub> particles is shown in Fig. 9.15 [854]. It is interesting to note that nano-sized CaPO<sub>4</sub> appear to be applicable for DNA extraction from cell lysates [855].



**Fig. 9.13** A generalized schematic setup of a nanodimensional particle of a  $\text{CaPO}_4$  suitable for both imaging and drug delivery purposes (Reprinted from Ref. [852] with permission. Copyright © 2010 Royal Society of Chemistry)



**Fig. 9.14** A schematic of  $\text{CaPO}_4$  (CaP) nanodimensional particles for drug delivery applications: single shell (a, b), multi-shell (c), and surface functionalization approach (d). Fluorophore agents can be entrapped/doped into  $\text{CaPO}_4$  core as shown in (b) for imaging. The multi-shell approach (c) is more effective for nuclear transfection than the single shell as in (a). Drugs or biomolecules that are poorly adsorbed on  $\text{CaPO}_4$  can also be adsorbed on the surface-functionalized polymer coating as shown in (d) (Reprinted from Ref. [853] with permission. Copyright © 2011 Acta Materialia Inc. Published by Elsevier Ltd)



**Fig. 9.15** A schematic of transfection/intracellular delivery of drugs and biomolecules by nanodimensional  $\text{CaPO}_4$ . Cellular uptake of nanodimensional  $\text{CaPO}_4$  loaded with DNAs/RNAs is caused by endocytosis through lipid bilayer cellular membrane. Afterward, DNAs or RNAs escape from the endosome following the dissolution of  $\text{CaPO}_4$  in an acidic environment of the endocytic vesicle (Reprinted from Ref. [853] with permission. Copyright © 2011 Acta Materialia Inc. Published by Elsevier Ltd. Additional schematic illustrations of this process are available in literature [832])

When these particles are added to the cells, the pH of the medium defines the degree of saturation and hence the fate of the precipitate, which normally gets endocytosed by cells within  $\sim 1$  h after contact. Furthermore, after being delivered inside cells, it is hypothesized that dissolution of nanodimensional  $\text{CaPO}_4$  particles occurs. Large quantities of  $\text{Ca}^{2+}$  and orthophosphate ions are released into the endosomal mixture inside vesicles. As a result, rapid increase of osmotic pressure inside the vesicle ensues leading to massive influx of water into the vesicles, which ruptures the vesicle, and the nucleic acids into the cytosol [832, 853]. Interestingly, the transfection efficiency of nanodimensional  $\text{CaPO}_4$  was found to depend on Ca/P ionic ratio: namely,  $\text{CaPO}_4$  with Ca/P = 1.30 ratio exhibited a fourfold increase in the transfection efficiency over the ones with Ca/P = 1.65 ratio composition [268]. This data emphasizes the importance of understanding the interaction between  $\text{CaPO}_4$  and DNA to optimize the DNA uptake and its channeling to the nucleus of the cell. Besides, it has been demonstrated that surface-modified particles of nano-sized  $\text{CaPO}_4$  can be used *in vivo* to target genes specifically to a liver [855]. Attachment of galactose moiety onto the particle surface has increased the targetability of the nano-sized particles. Furthermore, this surface modification makes it possible for site-specific gene delivery [855, 856]. Assemblies of block-copolymer/nano-sized  $\text{CaPO}_4$  were prepared and used for cell transfection; a high biocompatibility of this system was emphasized [857]. Structures that are even more complex are known as well [858–860]. Furthermore, vaccination to protect against human infectious diseases may be enhanced by using adjuvants that can selectively stimulate immuno-



regulatory responses, and nano-sized particles of  $\text{CaPO}_4$  were found to be suitable for such purposes [861, 862].

In all these new applications of nano-sized  $\text{CaPO}_4$ , knowledge of the exact internalization pathways into the cells represents the first necessary step toward the detailed investigation and optimization of the functional mechanisms [863]. The main groups of pathways into the cell are diffusion, passive and active transport, as well as a number of endocytic mechanisms [767]. Bigger particles of far above 10 nm are internalized by eukaryotic cells through the endocytic pathways including phagocytosis, macropinocytosis, clathrin-mediated endocytosis, and non-clathrin-mediated endocytosis such as internalization via caveolae. To date, the exact internalization pathway of nano-sized  $\text{CaPO}_4$  into cells has not been determined, and there are many questions that remain to be answered, particularly, concerning possible interactions of  $\text{CaPO}_4$  with nucleic acids. Furthermore, the mechanisms of cellular uptake and transport to the cell nucleus of  $\text{CaPO}_4$ /DNA nanodimensional complexes remain unclear either. Therefore, there is a need to conduct a focused study on the synthesis of various forms of nano-sized  $\text{CaPO}_4$  that could elucidate the mechanisms of binding, transport, and release of attached plasmid DNA for understanding the gene delivery method. Research is also warranted to understand the tracking of DNA intracellularly [846] to understand the release and transport of DNA into cellular nuclei.

Concerning the healing abilities of nano-sized  $\text{CaPO}_4$ , an *in vitro* inhibiting effect and even apoptotic action of un-functionalized nano-sized HA of about 50 nm diameter on a hepatoma cell line in the concentration range of 50–200 mg/l were reported [864]. Similar effects were discovered for nano-sized HA particles, which appeared to cause inhibition and/or apoptosis of leukemia P388 cells, C6 cells [865], macrophages [866, 867], and osteoblasts [720, 868]. This effect might be due to a harmful increase in the intracellular calcium concentration. However, the correlation between the particle dimensions and the apoptotic action of nano-sized  $\text{CaPO}_4$  appears not to be straightforward. Namely, the apoptosis efficacy of nanodimensional particles of HA of various sizes was found to decrease in the order of 45 nm > 26 nm > 78 nm > 175 nm [869]. Furthermore, the needle-shaped and the short rodlike particles induced greater cellular injury than the spherical and long rodlike particles, respectively [868].

Hollow nano-sized structures are extremely attractive constructions because they can greatly enhance the load quantity. Though these novel biomaterials can improve the total intake of drugs, they also bring new problems, e.g., uncontrolled release kinetics and unreasonable metabolism pathway of the carriers [870]. In order to solve these problems,  $\text{CaPO}_4$  were selected as suitable biomaterials to construct nanodimensional spheres [167, 575, 576, 802, 871–874] and ellipsoidal capsules [875] hollow inside. Such hollow structures with dimensions ranging from 110 to 180 nm were synthesized by an ultrasonic-assisted wet-chemical reaction in the presence of a modifier [876]. In addition, they might be prepared through emulsions [877] and by electrophoresis [878]. Transmission electron microscopy investigations revealed that the uniform nanodimensional spheres were formed, and they were well dispersed in the solutions. Thickness of the shells was about 45 nm; thus,

they always had  $\sim 60$ -nm-sized internal cavities, which could be used to load drugs. The hollow spheres appeared to be stable in both air and aqueous solutions without ultrasonic application. However, when an ultrasonic treatment (40 kHz, 150 W) was applied, the hollow structures deconstructed to form pin-like nano-sized crystals of  $\text{CaPO}_4$  [876]. During this transformation, the encapsulated drugs and chemicals are released [603, 876]. Different from a free and slow diffusion of encapsulated drugs from the cavity through the shells [168], the release kinetics in this system was triggered and controlled by ultrasound. Furthermore, the power density of ultrasound can conveniently regulate the release dynamics. Besides, the formed pin-like nano-sized crystals of  $\text{CaPO}_4$  had similar behavior to the biological apatite of bones. Thus, a combination of the hollow  $\text{CaPO}_4$  nanospheres and ultrasonic treatment might provide a good system for drug delivery and release [876].

To conclude this part, one should note that nanodimensional  $\text{CaPO}_4$  seem to be the only inorganic materials that are biocompatible, bioresorbable, and benignly cleared from the body. Therefore, the use of them, particularly combined with drug and imaging agents already FDA approved, likely faces far fewer regulatory hurdles than new materials, either organic or inorganic. Obviously, in the near future, bio-composites based on nano-sized  $\text{CaPO}_4$  will begin clinical trials for both bioimaging and drug delivery with a high probability of positive outcomes for the diagnosis and treatment of human diseases [879–881].

## 9.8 Non-biomedical Applications of the Nano-scaled $\text{CaPO}_4$

Not many publications are yet available on non-biomedical applications of the nano-scaled  $\text{CaPO}_4$  [450, 882–903]. For example,  $\text{CaPO}_4$  particles with a mean size of  $150 \pm 20$  nm filled with a solution containing luminol, hematin, and fluorescein were found to improve the ease and accuracy of  $\text{H}_2\text{O}_2$  sensing [882]. Other examples of sensors based on nano-scaled  $\text{CaPO}_4$  are known as well [896–898]. Besides, nanodimensional HA particles were tested as a component of a green slow-release fertilizer composition [883]. Also, addition of nano-scaled HA remarkably inhibits desorption of heavy metals from soils, which increases their geochemical stability in metal-contaminated soils [884]. Furthermore, nano-scaled HA was found to hold a great potential to remove cationic metal species [885–891] and some organic compounds [900] from industrial wastewater, as well as fluorides from drinking water [450, 902, 903]. Finally, yet importantly, nanodimensional and nanocrystalline  $\text{CaPO}_4$  might possess a catalytic activity [892–895] and be used in gas sensors [896] and ion detectors [901].

## 9.9 Summary and Perspectives

As the basic building blocks of calcified tissues of mammals, nano-sized  $\text{CaPO}_4$  of the apatitic structure play an important role in the construction of these biominerals. Therefore, they appear to be almost the ideal biomaterials due to their good

biocompatibility and bioresorbability. Even more enhanced applications are expected in drug delivery systems [904]. However, there is still an unanswered question concerning their structure: whether the majority of nanodimensional  $\text{CaPO}_4$  appear to be almost amorphous (according to numerous results of X-ray diffraction studies) due to their nanoscopic dimensions of well-crystallized structures or due to a really amorphous (i.e., retaining only a short-range order at the scale of few atomic neighbors) matter? A good attempt to discuss this topic is available in literature [905], where the interested readers are referred to.

In the future, an ability to functionalize surfaces with different molecules of varying nature and dimensions by means of their attachment to cells will enable them to act selectively on biological species such as proteins and peptides. The capability of synthesizing and processing of nanodimensional and nanocrystalline  $\text{CaPO}_4$  with the controlled structures and topographies, in attempts to simulate the basic units of bones and teeth, will provide a possibility of designing novel proactive bioceramics necessary for enhanced repair efficacy. The various primary positive results on the biocompatibility and biomimicity of novel nanostructured bioceramics merit further confirmations. Namely, much work remains to be undertaken to address the following key challenges and critical issues of nanodimensional and nanocrystalline  $\text{CaPO}_4$  [906]:

- Consistency of the processing technologies
- Optimization the structure and properties mimicking bones
- Matching the strength of nanodimensional and nanocrystalline constructs with those of bones in order to provide a uniform distribution of stresses (load sharing)
- Optimizing bioresorption without comprising the mechanical properties
- Assessing the inflammatory response to validate their biosafety

Furthermore, substantial research efforts are required in the analysis of cells and their different behaviors with regard to their interactions with nanodimensional and nanocrystalline  $\text{CaPO}_4$  [906]. An important but still unsolved question is how the cells can recognize the particle dimensions and crystallinity of nano-sized  $\text{CaPO}_4$ . What is the signal for nanodimensional biomaterials to promote cell proliferation and differentiation and how can the pathways be found out? According to the experiment results on transfection, nano-sized particles can enter into cells readily, but many details of this process remain unclear. Namely, the pathways for the nano-sized particles to enter the cells through the membranes should be revealed [907]. A greater influence of the hydrated surface layer with labile ionic species of smaller particles and crystals (see Sect. 9.5. “The Structure of the Nano-scaled Apatites” for the details) might be another possible option, to be confirmed experimentally. Then, it is important to examine the metabolism process of nano-sized  $\text{CaPO}_4$  inside cells, so the existing forms of these particles during the biological processes could be understood. Further, a critical step will be the investigation of possible changes of gene or protein expression in the absence and presence of various nano-sized  $\text{CaPO}_4$ , which may directly be related to cell proliferation and differentiation [13].

Understanding of the interactions between nano-sized particles and living cells is still a great challenge [906]. Namely, elucidating mechanisms, by which cells internalize and process nanodimensional particles, is of great importance for understanding their potential toxicity and for improving the targeted delivery of nanodimensional particles for biomedical applications. Already, some data are available that clathrin-mediated endocytosis might be responsible for the uptake of nano-sized HA [767]. In another study, nanodimensional particles of HA were sequestered within a specialized membrane-bound surface-connected compartment, directly connected to the extracellular space [908]. Future studies will focus on (1) the detailed interfacial structure of nanodimensional  $\text{CaPO}_4$  and the specific adsorption of proteins [909] or other matrices, (2) uptake processes of the nano-sized particles by cells, and (3) metabolism of nano-sized  $\text{CaPO}_4$  inside the cells and its possible interference with physiological reactions. Another important topic is a biological security of nano-sized particles in general [111, 112, 910, 911] and those of  $\text{CaPO}_4$  in particular [144, 343, 735, 912, 913]. For example, toxicity of nano-sized HA was found to vary considerably, which was related to their physicochemical properties [914, 915]. Besides, the toxicity of nano-sized HA appears to be both crystal shape and cell dependent [914]. Toxicity of an undisclosed nano-scaled TCP was detected as well [867]. Furthermore, cell death correlates strongly with the load of nano-sized particles. Namely, the biological effects of rod-shaped apatite, 50–80 nm in length, were investigated on human monocyte-derived macrophages [144]. High concentrations of apatite (200 nano-sized particles per cell) were incubated for 24 h with the macrophages in both serum and serum-free conditions. This induced high levels of lactate dehydrogenase release, which is an indicator of cellular damage. However, lower concentrations (20 and 2 nano-sized particles per cell) of the rod-shaped apatite did not affect the cell viability similarly to the control group that did not contain nano-sized apatite [144]. Similarly, intracellular dissolution of nano-sized HA as a function of time suggests that increased cytoplasmic calcium load is likely to be the cause of cell death [912]. Furthermore, nano-sized  $\text{CaPO}_4$  were found to interfere with cell cycle of cultured human ovarian granulosa cells, thus increasing cell apoptosis [916]. That pilot study suggested that effects of nano-sized particles on ovarian function should be extensively investigated. A time-dependent toxicological effect of inhaled nanodimensional HA on a natural pulmonary surfactant lining layer was noticed [917]. A biotoxicity of nano-scaled HA to the plant growth was detected as well [918]. Additional examples of cytotoxicity experiments of nanodimensional  $\text{CaPO}_4$  are well described in a special review [793].

To finalize this topic, one should stress that *in vivo* evaluation of nano-sized particles includes the particle's activity, biodistribution, and pharmacokinetic properties [919]. Ultimately, all these properties are determined by dimensions, surface charge, morphology, and surface chemistry. Furthermore, it is very important and necessary to trace and clarify the localizations of nanodimensional  $\text{CaPO}_4$  *in vivo* [920]. It is already known that nano-sized particles penetrate and leave biological organisms more readily using a number of pathways. Namely, very small (<10 nm) particles are generally eliminated from the body via renal clearance, i.e., being fil-

tered through the kidneys and eliminated through urine, while nano-sized particles of larger dimensions are phagocytized by tissue macrophages of the reticuloendothelial system in the liver and spleen [797]. For example, intravenously administered nanodimensional (~40 nm and ~200 nm) rod-shaped crystals of apatite showed clearance from the bloodstream within 2 h, with ~90% of them being cleared in the first 10 min postinjection; those nanodimensional crystals of apatite were observed primarily in the liver with a minority seen in the spleen [800]. These results indicate that bloodstream clearance occurs rapidly for a wide range of nanodimensional sizes. The accumulation of nanodimensional (50–100 nm in size) apatite in the liver was also noted in another study [528].

Thus, understanding the biological influence of nano-sized and nanocrystalline  $\text{CaPO}_4$  is essential for a future development of bionanotechnologies, which are modeled after biological substances and structures or combine nanomaterials with biological substances. They include materials such as biochips, drug release systems, nanofibers, hybrid nanobiodevices, molecular electronics, and biomimetics (synthetic genes, proteins, and viruses) [921]. This interdisciplinary approach is very complicated, and the effective collaboration of scientists from different disciplines is the key [13].

## 9.10 Conclusions

With a high surface area, un-agglomerated nano-scaled particles are of interest for many applications including injectable or controlled setting bone cements, high-strength porous or nonporous synthetic bone grafts, and the reinforcing phase in biocomposites that attempt to mimic both the complex structure and superior mechanical properties of bone. Therefore, nano-sized and nanocrystalline  $\text{CaPO}_4$  have already gained much regard in the biomedical field due to their superior biocompatibility and biomechanical properties. This is easily seen from a permanent increasing of the amount of publications. At present, apatites (HA and CDHA) and  $\beta$ -TCP are the major  $\text{CaPO}_4$  used in clinics. Currently, nanodimensional apatites are used primarily as bioactive coatings on bioinert materials like titanium and its alloys, in bone tissue repairs and implants, as well as for drug delivery purposes. The nano-sized  $\beta$ -TCP exhibits a significant biological affinity and activity and responds very well to the physiological environment. A lot of research is expected for much enhanced applications of the nanodimensional and nanocrystalline  $\text{CaPO}_4$  for both drug delivery systems and as resorbable scaffolds that can be replaced by the endogenous hard tissues with the passage of time [114, 922].

Although the nanostructured biomaterials may have many potential advantages in the context of promoting bone cell responses [564, 565, 567, 743], it is important to remember that studies on nanophase materials have only just begun; there are still many other issues regarding human health that must be answered. Since particles of very low size have higher reactivity and effectiveness, a rapid technical development of nanometer-scaled particles in the biomedical field leads to concerns regard-

ing the unknown risks of such materials [910, 911]. These nano-sized particles might induce inflammatory reactions [923], cytotoxicity, oxidative stresses, or thrombogenesis when injected for drug delivery purposes. Namely, nano-sized particles may enter the human body through pores and may accumulate in the cells of the respiratory or other organ systems (when becoming dislodged through wear debris), and the health effects are yet to be largely known. This could happen during commercial-scale processing of the nano-sized particles as well as using these materials as implants [924]. Besides, nano-sized particles might be the objects whose existence has not been assumed by living body defense system [18, 111, 112]. Up to now, only a small number of short-term and small-scale health effects of single nanodimensional materials have been examined in toxicological studies, usually of the lungs [911]. Therefore, prior to clinical applications, any toxicity concerns of the nanophase materials in general [925–930] and nano-scaled  $\text{CaPO}_4$  in particular [931, 932] need to be overcome. Namely, the European Union's Scientific Committee on Consumer Safety (SCCS) opinion on hydroxyapatite (nano), adopted 16 October 2015, concludes: "Based on the information available, SCCS considers that the safety of nano-hydroxyapatite materials ... when used up to a concentration of 10% in oral cosmetic products, cannot be decided on the basis of the data submitted ... and that retrieved from literature search. The available information indicates that nano-hydroxyapatite in needle form is of concern in relation to potential toxicity. Therefore, needle-shaped nano-hydroxyapatite should not be used in cosmetic products" [932].

In summary, despite the challenges that lie ahead, significant evidences now exist elucidating that nanophase biomaterials represent an important growing area of research that may improve bonding between the implants and the surrounding tissues. It has proven to be a versatile approach that can increase bone cell functions on a wide range of orthopedic implant chemistries. Even if the nanodimensional and nanocrystalline  $\text{CaPO}_4$  do not provide the ultimate answer for increasing bone cell responses (due to some potential problems as mentioned above), researchers have learned a tremendous amount of information concerning bone cell recognition with nanostructured surfaces that will most certainly aid in improving orthopedic implant efficacy [111, 112].

## References

1. Mann S (2001) *Biom mineralization principles and concepts in bioinorganic materials chemistry*. Oxford University Press, New York
2. Lowenstam HA, Weiner S (1989) *On biomineralization*. Oxford University Press, New York
3. Vallet-Regí M, González-Calbet JM (2004) Calcium phosphates as substitution of bone tissues. *Prog Solid State Chem* 32:1–31
4. Weiner S, Addadi L (1997) Design strategies in mineralized biological materials. *J Mater Chem* 7:689–702
5. Weiner S, Wagner HD (1998) The material bone: structure-mechanical function relations. *Annu Rev Mater Sci* 28:271–298

6. Pasteris JD, Wopenka B, Valsami-Jones E (2008) Bone and tooth mineralization: why apatite? *Elements* 4:97–104
7. Giachelli CM (1999) Ectopic calcification: gathering hard facts about soft tissue mineralization. *Am J Pathol* 154:671–675
8. Kirsch T (2006) Determinants of pathological mineralization: crystal deposition diseases. *Curr Opin Rheumatol* 18:174–180
9. Christian RC, Fitzpatrick LA (1999) Vascular calcification. *Curr Opin Nephrol Hypertens* 8:443–448
10. Dorozhkin SV (2012) Nanodimensional and nanocrystalline calcium orthophosphates. *AM J Biomed Eng* 2(3):48–97
11. Alivisatos AP (2000) Enhanced naturally aligned nanocrystals. *Science* 289:736–737
12. Narayan RJ, Kumta PN, Sfeir C, Lee DH, Choi D, Olton D (2004) Nanostructured ceramics in medical devices: applications and prospects. *JOM* 56:38–43
13. Cai Y, Tang R (2008) Calcium phosphate nanoparticles in biomineralization and biomaterials. *J Mater Chem* 18:3775–3787
14. Ginebra MP, Driessens FCM, Planell JA (2004) Effect of the particle size on the micro and nanostructural features of a calcium phosphate cement: a kinetic analysis. *Biomaterials* 25:3453–3462
15. <http://www.nano.gov/nanotech-101/what/definition>. Accessed in Dec 2016
16. Karch J, Birringer R, Gleiter H (1987) Ceramics ductile at low temperature. *Nature* 330:556–558
17. Webster TJ (2001) Nanophase ceramics: the future of orthopedic and dental implant material. In: Ying JY (ed) *Nanostructured materials*. Academic, New York, pp 125–166
18. Tasker LH, Sparey-Taylor GJ, Nokes LD (2007) Applications of nanotechnology in orthopaedics. *Clin Orthop Relat Res* 456:243–249
19. Banfield JF, Welch SA, Zhang H, Ebert TT, Penn RL (2000) Aggregation-based crystal growth and microstructure development in natural iron oxyhydroxide biomineralization products. *Science* 289:751–754
20. Cölfen H (2007) Bio-inspired mineralization using hydrophilic polymers. *Top Curr Chem* 271:1–77
21. Oaki Y, Imai H (2005) Nanoengineering in echinoderms: the emergence of morphology from nanobricks. *Small* 2:66–70
22. Lee SH, Shin H (2007) Matrices and scaffolds for delivery of bioactive molecules in bone and cartilage tissue engineering. *Adv Drug Deliv Rev* 59:339–359
23. Ben-Nissan B (2004) Nanoceramics in biomedical applications. *MRS Bull* 29:28–32
24. Rehman I (2004) Nano bioceramics for biomedical and other applications. *Mater Technol* 19:224–233
25. Cacciotti I, Bianco A, Lombardi M, Montanaro L (2009) Mg-substituted hydroxyapatite nanopowders: synthesis, thermal stability and sintering behaviour. *J Eur Ceram Soc* 29:2969–2978
26. Bianco A, Cacciotti I, Lombardi M, Montanaro L (2009) Si-substituted hydroxyapatite nanopowders: synthesis, thermal stability and sinterability. *Mater Res Bull* 44:345–354
27. Capuccini C, Torricelli P, Boanini E, Gazzano M, Giardino R, Bigi A (2009) Interaction of Sr-doped hydroxyapatite nanocrystals with osteoclast and osteoblast-like cells. *J Biomed Mater Res A* 89A:594–600
28. Jiang H, Li Y, Zuo Y, Yang W, Zhang L, Li J, Wang L, Zou Q, Cheng L, Li J (2009) Physical and chemical properties of superparamagnetic Fe-incorporated nano hydroxyapatite. *J Nanosci Nanotechnol* 9:6844–6850
29. Al-Kattan A, Dufour P, Dexpert-Ghys J, Drouet C (2010) Preparation and physicochemical characteristics of luminescent apatite-based colloids. *J Phys Chem C* 114:2918–2924
30. Hou CH, Chen CW, Hou SM, Li YT, Lin FH (2009) The fabrication and characterization of dicalcium phosphate dihydrate-modified magnetic nanoparticles and their performance in hyperthermia processes in vitro. *Biomaterials* 30:4700–4707

31. Hanifi A, Fathi MH, Sadeghi HMM, Varshosaz J (2010) Mg<sup>2+</sup> substituted calcium phosphate nano particles synthesis for non viral gene delivery application. *J Mater Sci Mater Med* 21:2393–2401
32. Stojanović Z, Veselinović L, Marković S, Ignjatović N, Uskoković D (2009) Hydrothermal synthesis of nanosize pure and cobalt-exchanged hydroxyapatite. *Mater Manuf Process* 24:1096–1103
33. Veselinović L, Karanović L, Stojanović Z, Bračko I, Marković S, Ignjatović N, Uskoković D (2010) Crystal structure of cobalt-substituted calcium hydroxyapatite nanopowders prepared by hydrothermal processing. *J Appl Crystallogr* 43:320–327
34. Evis Z, Webster TJ (2011) Nanosize hydroxyapatite: doping with various ions. *Adv Appl Ceram* 110:311–320
35. Al-Kattan A, Girod-Fullana S, Charvillat C, Ternet-Fontebasso H, Dufour P, Dexpert-Ghys J, Santran V, Bordère J, Pipy B, Bernard J, Drouet C (2012) Biomimetic nanocrystalline apatites: emerging perspectives in cancer diagnosis and treatment. *Int J Pharm* 423:26–36
36. Kafak A, Kolodziejski W (2011) Complementary information on water and hydroxyl groups in nanocrystalline carbonated hydroxyapatites from TGA, NMR and IR measurements. *J Mol Struct* 990:263–270
37. Kafak A, Ślósarczyk A, Kolodziejski W (2011) A comparative study of carbonate bands from nanocrystalline carbonated hydroxyapatites using FT-IR spectroscopy in the transmission and photoacoustic modes. *J Mol Struct* 997:7–14
38. Li Y, Widodo J, Lim S, Ooi CP (2012) Synthesis and cytocompatibility of manganese (II) and iron (III) substituted hydroxyapatite nanoparticles. *J Mater Sci* 47:754–763
39. Tampieri A, d’Alessandro T, Sandri M, Sprio S, Landi E, Bertinetti L, Panseri S, Pepponi G, Goettlicher J, Bañobre-López M, Rivas J (2012) Intrinsic magnetism and hyperthermia in bioactive Fe-doped hydroxyapatite. *Acta Biomater* 8:843–851
40. Delgado-López JM, Iafisco M, Rodríguez I, Tampieri A, Prat M, Gómez-Morales J (2012) Crystallization of bioinspired citrate-functionalized nanoapatite with tailored carbonate content. *Acta Biomater* 8:3491–3499
41. Peetsch A, Greulich C, Braun D, Stroetges C, Rehage H, Siebers B, Köller M, Epple M (2013) Silver-doped calcium phosphate nanoparticles: synthesis, characterization, and toxic effects toward mammalian and prokaryotic cells. *Colloids Surf B Biointerfaces* 102:724–729
42. Han Y, Wang X, Da H, Li S (2013) Synthesis and luminescence of Eu<sup>3+</sup> doped hydroxyapatite nanocrystallines: effects of calcinations and Eu<sup>3+</sup> content. *J Lumin* 135:281–287
43. Hayakawa S, Kanaya T, Tsuru K, Shirosaki Y, Osaka A, Fujii E, Kawabata K, Gasqueres G, Bonhomme C, Babonneau F, Jäger C, Kleebe HJ (2013) Heterogeneous structure and in vitro degradation behavior of wet-chemically derived nanocrystalline silicon-containing hydroxyapatite particles. *Acta Biomater* 9:4856–4867
44. Kheradmandfard M, Fathi MH (2013) Fabrication and characterization of nanocrystalline Mg-substituted fluorapatite by high energy ball milling. *Ceram Int* 39:1651–1658
45. Alshemary AZ, Goh YF, Akram M, Razali IR, Kadir MRA, Hussain R (2013) Microwave assisted synthesis of nano sized sulphate doped hydroxyapatite. *Mater Res Bull* 48:2106–2110
46. Liu Z, Wang Q, Yao S, Yang L, Yu S, Feng X, Li F (2014) Synthesis and characterization of Tb<sup>3+</sup>/Gd<sup>3+</sup> dual-doped multifunctional hydroxyapatite nanoparticles. *Ceram Int* 40:2613–2617
47. Ignjatovic N, Ajdukovic Z, Rajkovic J, Najman S, Mihailovic D, Uskokovic D (2015) Enhanced osteogenesis of nanosized cobalt-substituted hydroxyapatite. *J Bionic Eng* 12:604–612
48. Ma J, Qin J (2015) Graphene-like zinc substituted hydroxyapatite. *Cryst Growth Des* 15:1273–1279
49. Zheng X, Liu M, Hui J, Fan D, Ma H, Zhang X, Wang Y, Wei Y (2015) Ln<sup>3+</sup>-doped hydroxyapatite nanocrystals: controllable synthesis and cell imaging. *Phys Chem Chem Phys* 17:20301–20307
50. Ciobanu G, Bargan AM, Luca C (2015) New bismuth-substituted hydroxyapatite nanoparticles for bone tissue engineering. *JOM* 67:2534–2542



51. AlHammad MS (2016) Nanostructure hydroxyapatite based ceramics by sol gel method. *J Alloys Compd* 661:251–256
52. Wilberforce SI, Finlayson CE, Best SM, Cameron RE (2011) The influence of the compounding process and testing conditions on the compressive mechanical properties of poly(D,L-lactide-co-glycolide)/ $\alpha$ -tricalcium phosphate nanocomposites. *J Mech Behav Biomed Mater* 4:1081–1089
53. Wilberforce SI, Finlayson CE, Best SM, Cameron RE (2011) A comparative study of the thermal and dynamic mechanical behaviour of quenched and annealed bioresorbable poly-L-lactide/ $\alpha$ -tricalcium phosphate nanocomposites. *Acta Biomater* 7:2176–2184
54. Tolmachev DA, Lukasheva NV (2012) Interactions binding mineral and organic phases in nanocomposites based on bacterial cellulose and calcium phosphates. *Langmuir* 28:13473–13484
55. Frohbergh ME, Katsman A, Botta GP, Lazarovici P, Schauer CL, Wegst UGK, Lelkes PI (2012) Electrospun hydroxyapatite-containing chitosan nanofibers crosslinked with genipin for bone tissue engineering. *Biomaterials* 33:9167–9178
56. Liang YH, Liu CH, Liao SH, Lin YY, Tang HW, Liu SY, Lai IR, Wu KCW (2012) Cosynthesis of cargo-loaded hydroxyapatite/alginate core-shell nanoparticles (HAP@Alg) as pH-responsive nanovehicles by a pre-gel method. *ACS Appl Mater Interfaces* 4:6720–6727
57. Son KD, Kim YJ (2013) Morphological structure and characteristics of hydroxyapatite/ $\beta$ -cyclodextrin composite nanoparticles synthesized at different conditions. *Mater Sci Eng C* 33:499–506
58. Thien DVH, Hsiao SW, Ho MH, Li CH, Shih JL (2013) Electrospun chitosan/hydroxyapatite nanofibers for bone tissue engineering. *J Mater Sci* 48:1640–1645
59. Abdal-Hay A, Sheikh FA, Lim JK (2013) Air jet spinning of hydroxyapatite/poly(lactic acid) hybrid nanocomposite membrane mats for bone tissue engineering. *Colloids Surf B: Biointerfaces* 102:635–643
60. Soltani Z, Ziaie F, Ghaffari M, Afarideh H, Ehsani M (2013) Mechanical and thermal properties and morphological studies of 10MeV electron beam irradiated LDPE/hydroxyapatite nano-composite. *Radiat Phys Chem* 83:79–85
61. Sahni G, Gopinath P, Jeevanandam P (2013) A novel thermal decomposition approach to synthesize hydroxyapatite-silver nanocomposites and their antibacterial action against GFP-expressing antibiotic resistant *E. coli*. *Colloids Surf B: Biointerfaces* 103:441–447
62. Aminzare M, Eskandari A, Baroonian MH, Berenov A, Hesabi ZR, Taheri M, Sadnezhaad SK (2013) Hydroxyapatite nanocomposites: synthesis, sintering and mechanical properties. *Ceram Int* 39:2197–2206
63. Zhang H, Fu QW, Sun TW, Chen F, Qi C, Wu J, Cai ZY, Qian QR, Zhu YJ (2015) Amorphous calcium phosphate, hydroxyapatite and poly(D,L-lactic acid) composite nanofibers: electrospinning preparation, mineralization and in vivo bone defect repair. *Colloids Surf B: Biointerfaces* 136:27–36
64. Kollath VO, Mullens S, Luyten J, Traina K, Cloots R (2015) Protein-calcium phosphate nanocomposites: benchmarking protein loading via physical and chemical modifications against co-precipitation. *RSC Adv* 5:55625–55632
65. Hannora AE, Ataya S (2016) Structure and compression strength of hydroxyapatite/titania nanocomposites formed by high energy ball milling. *J Alloys Compd* 658:222–233
66. Garai S, Sinha A (2016) Three dimensional biphasic calcium phosphate nanocomposites for load bearing bioactive bone grafts. *Mater Sci Eng C* 59:375–383
67. Pan Y, Xiong D, Chen X (2007) Mechanical properties of nanohydroxyapatite reinforced poly(vinyl alcohol) gel composites as biomaterial. *J Mater Sci* 42:5129–5134
68. Deng C, Weng J, Lu X, Zhou SB, Wan JX, Qu SX, Feng B, Li XH, Cheng QY (2008) Mechanism of ultrahigh elongation rate of poly(D,L-lactide)-matrix composite biomaterial containing nano-apatite fillers. *Mater Lett* 62:607–610
69. Meng YH, Tang CY, Tsui CP, Chen DZ (2008) Fabrication and characterization of needle-like nano-HA and HA/MWNT composites. *J Mater Sci Mater Med* 19:75–81

70. Lin J, Zhu J, Gu X, Wen W, Li Q, Fischer-Brandies H, Wang H, Mehl C (2011) Effects of incorporation of nano-fluorapatite or nano-fluorohydroxyapatite on a resin-modified glass ionomer cement. *Acta Biomater* 7:1346–1353
71. Gemelli E, de Jesus J, Camargo NHA, de Soares GDA, Henriques VAR, Nery F (2012) Microstructural study of a titanium-based biocomposite produced by the powder metallurgy process with TiH<sub>2</sub> and nanometric  $\beta$ -TCP powders. *Mater Sci Eng C* 32:1011–1015
72. Liu D, Zuo Y, Meng W, Chen M, Fan Z (2012) Fabrication of biodegradable nano-sized  $\beta$ -TCP/Mg composite by a novel melt shearing technology. *Mater Sci Eng C* 32:1253–1258
73. Zheng F, Wang S, Wen S, Shen M, Zhu M, Shi X (2013) Characterization and antibacterial activity of amoxicillin-loaded electrospun nano-hydroxyapatite/poly(lactic-co-glycolic acid) composite nanofibers. *Biomaterials* 34:1402–1412
74. Li H, Fu Y, Niu R, Zhou Z, Nie J, Yang D (2013) Study on the biocomposites with poly(ethylene glycol) dimethacrylate and surfaced-grafted hydroxyapatite nanoparticles. *J Appl Polym Sci* 127:1737–1743
75. Jia L, Duan Z, Fan D, Mi Y, Hui J, Chang L (2013) Human-like collagen/nano-hydroxyapatite scaffolds for the culture of chondrocytes. *Mater Sci Eng C* 33:727–734
76. Viswanathan K, Rathish P, Gopinath VP, Janice R, Raj GD (2014) *In ovo* delivery of Newcastle disease virus conjugated hybrid calcium phosphate nanoparticle and to study the cytokine profile induction. *Mater Sci Eng C* 45:564–572
77. Dorozhkin SV (2015) Calcium orthophosphate-containing biocomposites and hybrid biomaterials for biomedical applications. *J Funct Biomater* 6:708–832
78. Williams DF (2008) The relationship between biomaterials and nanotechnology. *Biomaterials* 29:1737–1738
79. Feynman RP (1992) There's plenty of room at the bottom. *J Microelectromech Syst* 1:60–66
80. European Commission, Scientific Committee on Emerging and Newly Identified Health Risks (SCENIHR) (n.d.) Opinion on “the scientific aspects of the existing and proposed definitions relating to products of nanoscience and nanotechnologies”. Adopted Brussels: European Commission. 29 November 2007
81. [http://ec.europa.eu/environment/chemicals/nanotech/faq/definition\\_en.htm](http://ec.europa.eu/environment/chemicals/nanotech/faq/definition_en.htm). Accessed in Dec 2016
82. Moriarty P (2001) Nanostructured materials. *Rep Prog Phys* 64:297–381
83. Webster TJ, Ahn ES (2006) Nanostructured biomaterials for tissue engineering bone. *Adv Biochem Eng Biotechnol* 103:275–308
84. Streicher RM, Schmidt M, Fiorito S (2007) Nanosurfaces and nanostructures for artificial orthopedic implants. *Nanomedicine* 2:861–874
85. Havancsak K (2003) Nanotechnology at present and its promises in the future. *Mater Sci Forum* 414–415:85–94
86. Duncan R (2004) Nanomedicines in action. *Pharm J* 273:485–488
87. Williams DF (2009) On the nature of biomaterials. *Biomaterials* 30:5897–5909
88. Liu H, Webster TJ (2007) Nanomedicine for implants: a review of studies and necessary experimental tools. *Biomaterials* 28:354–369
89. Sun L, Chow LC, Frukhtbeyn SA, Bonevich JE (2010) Preparation and properties of nanoparticles of calcium phosphates with various Ca/P ratios. *J Res Natl Inst Stand Technol* 115:243–255
90. Sylvie J, Sylvie TD, Pascal PM, Fabienne P, Hassane O, Guy C (2010) Effect of hydroxyapatite and  $\beta$ -tricalcium phosphate nanoparticles on promonocytic U937 cells. *J Biomed Nanotechnol* 6:158–165
91. Sokolova V, Knuschke T, Kovtun A, Buer J, Epple M, Westendorf AM (2010) The use of calcium phosphate nanoparticles encapsulating toll-like receptor ligands and the antigen hemagglutinin to induce dendritic cell maturation and T cell activation. *Biomaterials* 31:5627–5633
92. Wu HC, Wang TW, Bohn MC, Lin FH, Spector M (2010) Novel magnetic hydroxyapatite nanoparticles as non-viral vectors for the glial cell line-derived neurotrophic factor gene. *Adv Funct Mater* 20:67–77

93. Gergely G, Wéber F, Lukács I, Illés L, Tóth AL, Horváth ZE, Mihály J, Balázs C (2010) Nano-hydroxyapatite preparation from biogenic raw materials. *Cent Eur J Chem* 8:375–381
94. Ergu C, Evis Z, Webster TJ, Sahin FC (2011) Synthesis and microstructural characterization of nano-size calcium phosphates with different stoichiometry. *Ceram Int* 37:971–977
95. Ge X, Leng Y, Ren F, Lu X (2011) Integrity and zeta potential of fluoridated hydroxyapatite nanothick coatings for biomedical applications. *J Mech Behav Biomed Mater* 4:1046–1056
96. Wang J, Chen X, Yang X, Xu S, Zhang X, Gou Z (2011) A facile pollutant-free approach toward a series of nutritionally effective calcium phosphate nanomaterials for food and drink additives. *J Nanopart Res* 13:1039–1048
97. Sokolova V, Knuschke T, Buer J, Westendorf AM, Epple M (2011) Quantitative determination of the composition of multi-shell calcium phosphate-oligonucleotide nanoparticles and their application for the activation of dendritic cells. *Acta Biomater* 7:4029–4036
98. Mostaghaci B, Loretz B, Haberkorn R, Kickelbick G, Lehr CM (2013) One-step synthesis of nanosized and stable amino-functionalized calcium phosphate particles for DNA transfection. *Chem Mater* 25:3667–3674
99. Lee DSH, Pai Y, Chang S, Kim DH (2016) Microstructure, physical properties, and bone regeneration effect of the nano-sized  $\beta$ -tricalcium phosphate granules. *Mater Sci Eng C* 58:971–976
100. Traykova T, Aparicio C, Ginebra MP, Planell JA (2006) Bioceramics as nanomaterials. *Nanomedicine* 1:91–106
101. Grainger DW, Castner DG (2008) Nanobiomaterials and nanoanalysis: opportunities for improving the science to benefit biomedical technologies. *Adv Mater* 20:867–877
102. Nelson KG (1972) The Kelvin equation and solubility of small particles. *J Pharmacol Sci* 61:479–480
103. Fan C, Chen J, Chen Y, Ji J, Teng HH (2006) Relationship between solubility and solubility product: the roles of crystal sizes and crystallographic directions. *Geochim Cosmochim Acta* 70:3820–3829
104. Sato M, Webster TJ (2004) Nanobiotechnology: implications for the future of nanotechnology in orthopedic applications. *Expert Rev Med Dev* 1:105–114
105. Hahn H (2003) Unique features and properties of nanostructured materials. *Adv Eng Mater* 5:277–284
106. Aronov D, Karlov A, Rosenman G (2007) Hydroxyapatite nanoceramics: basic physical properties and biointerface modification. *J Eur Ceram Soc* 27:4181–4186
107. Ramsden JJ, Freeman J (2009) The nanoscale. *Nanotechnol Percept* 5:3–25
108. Rempel AA (2007) Nanotechnologies. Properties and applications of nanostructured materials. *Russ Chem Rev* 76:435–461
109. Thomas V, Dean DR, Vohra YK (2006) Nanostructured biomaterials for regenerative medicine. *Curr Nanosci* 2:155–177
110. Catledge SA, Fries MD, Vohra YK, Lacefield WR, Lemons JE, Woodard S, Venugopalan R (2002) Nanostructured ceramics for biomedical implants. *J Nanosci Nanotechnol* 2:1–20
111. Balasundarama G, Webster TJ (2006) A perspective on nanophase materials for orthopedic implant applications. *J Mater Chem* 16:3737–3745
112. Balasundarama G, Webster TJ (2006) Nanotechnology and biomaterials for orthopedic medical applications. *Nanomedicine* 1:169–176
113. Padilla S, Izquierdo-Barba I, Vallet-Regí M (2008) High specific surface area in nanometric carbonated hydroxyapatite. *Chem Mater* 20:5942–5944
114. Kalita SJ, Bhardwaj A, Bhatt HA (2007) Nanocrystalline calcium phosphate ceramics in biomedical engineering. *Mater Sci Eng C* 27:441–449
115. LeGeros RZ (1991) Calcium phosphates in oral biology and medicine. Karger, Basel
116. Mann S (1986) The study of biominerals by high resolution transmission electron microscopy. *Scan Electron Microsc Pt* 2:393–413
117. Katsura N (1990) Nanospace theory for biomineralization. *Dent Jpn (Tokyo)* 27:57–63

118. Cuisinier FJG, Voegel JC, Yacaman J, Frank RM (1992) Structure of initial crystals formed during human amelogenesis. *J Cryst Growth* 116:314–318
119. Cuisinier FJG, Steuer P, Senger B, Voegel JC, Frank RM (1993) Human amelogenesis: high resolution electron microscopy of nanometer-sized particles. *Cell Tissue Res* 273:175–182
120. Brès EF, Moebus G, Kleebe HJ, Pourroy G, Werkmann J, Ehret G (1993) High resolution electron microscopy study of amorphous calcium phosphate. *J Cryst Growth* 129:149–162
121. Layrolle P, Lebugle A (1994) Characterization and reactivity of nanosized calcium phosphate prepared in anhydrous ethanol. *Chem Mater* 6:1996–2004
122. Cui FZ, Wen HB, Zhang HB, Ma CL, Li HD (1994) Nanophase hydroxyapatite-like crystallites in natural ivory. *J Mater Sci Lett* 13:1042–1044
123. Li YB, de Wijn J, Klein CPAT, de Meer SV, de Groot K (1994) Preparation and characterization of nanograde osteoapatite-like rod crystals. *J Mater Sci Mater Med* 5:252–255
124. Li YB, de Groot K, de Wijn J, Klein CPAT, de Meer SV (1994) Morphology and composition of nanograde calcium phosphate needle-like crystals formed by simple hydrothermal treatment. *J Mater Sci Mater Med* 5:326–331
125. ShirkHzanadeh M (1994) X-ray diffraction and Fourier transform infrared analysis of nanophase apatite coatings prepared by electrocrystallization. *Nanostruct Mater* 4:677–684
126. Webster TJ, Ergun C, Doremus RH, Siegel RW, Bizios R (2000) Specific proteins mediate enhanced osteoblast adhesion on nanophase ceramics. *J Biomed Mater Res* 51:475–483
127. Chan CK, Kumar TSS, Liao S, Murugan R, Ngiam M, Ramakrishnan S (2006) Biomimetic nanocomposites for bone graft applications. *Nanomedicine* 1:177–188
128. Mukhopadhyay A, Dasgupta AK, Chattopadhyay D, Chakrabarti K (2012) Improvement of thermostability and activity of pectate lyase in the presence of hydroxyapatite nanoparticles. *Bioresour Technol* 116:348–354
129. Okada M, Furukawa K, Serizawa T, Yanagisawa Y, Tanaka H, Kawai T, Furuzono T (2009) Interfacial interactions between calcined hydroxyapatite nanocrystals and substrates. *Langmuir* 25:6300–6306
130. Mikołajczyk T, Rabiej S, Bogun M (2006) Analysis of the structural parameters of polyacrylonitrile fibers containing nanohydroxyapatite. *J Appl Polym Sci* 101:760–765
131. Wilberforce SIJ, Finlayson CE, Best SM, Cameron RE (2011) The influence of hydroxyapatite (HA) microparticles (m) and nanoparticles (n) on the thermal and dynamic mechanical properties of poly-L-lactide. *Polymer* 52:2883–2890
132. Sung YM, Lee JC, Yang JW (2004) Crystallization and sintering characteristics of chemically precipitated hydroxyapatite nanopowder. *J Cryst Growth* 262:467–472
133. Wang J, Shaw LL (2007) Morphology-enhanced low-temperature sintering of nanocrystalline hydroxyapatite. *Adv Mater* 19:2364–2369
134. Fomin AS, Barinov SM, Ievlev VM, Smirnov VV, Mikhailov BP, Belonogov EK, Drozdova NA (2008) Nanocrystalline hydroxyapatite ceramics produced by low-temperature sintering after high-pressure treatment. *Dokl Chem* 418:22–25
135. Drouet C, Bosc F, Banu M, Largeot C, Combes C, Dechambre G, Estournes C, Raimbeaux G, Rey C (2009) Nanocrystalline apatites: from powders to biomaterials. *Powder Technol* 190:118–122
136. Ramesh S, Tan CY, Bhaduri SB, Teng WD, Sopyan I (2008) Densification behaviour of nanocrystalline hydroxyapatite bioceramics. *J Mater Process Technol* 206:221–230
137. Skorokhod VV, Solonin SM, Dubok VA, Kolomiets LL, Katashinski VP, Shinkaruk AV (2008) Pressing and sintering of nanosized hydroxyapatite powders. *Powder Metall Metal Ceram* 47:518–524
138. Lin K, Chang J, Lu J, Wu W, Zeng Y (2007) Properties of  $\beta$ -Ca<sub>3</sub>(PO<sub>4</sub>)<sub>2</sub> bioceramics prepared using nanosized powders. *Ceram Int* 33:979–985
139. Lin K, Chen L, Qu H, Lu J, Chang J (2011) Improvement of mechanical properties of macroporous  $\beta$ -tricalcium phosphate ceramic scaffolds with uniform and interconnected pore structures. *Ceram Int* 37:2397–2403

140. Tanaka Y, Hirata Y, Yoshinaka R (2003) Synthesis and characteristics of ultra-fine hydroxyapatite particles. *J Ceram Process Res* 4:197–201
141. Wang J, Shaw LL (2009) Nanocrystalline hydroxyapatite with simultaneous enhancements in hardness and toughness. *Biomaterials* 30:6565–6572
142. Stupp SI, Ciegler GW (1992) Organoapatites: materials for artificial bone. I. Synthesis and microstructure. *J Biomed Mater Res* 26:169–183
143. Webster TJ, Ergun C, Doremus RH, Siegel RW, Bizios R (2001) Enhanced osteoclast-like cell functions on nanophase ceramics. *Biomaterials* 22:1327–1333
144. Huang J, Best SM, Bonfield W, Brooks RA, Rushton N, Jayasinghe SN, Edirisinghe MJ (2004) In vitro assessment of the biological response to nanosized hydroxyapatite. *J Mater Sci Mater Med* 15:441–445
145. Kim HW, Kim HE, Salih V (2005) Stimulation of osteoblast responses to biomimetic nanocomposites of gelatin-hydroxyapatite for tissue engineering scaffolds. *Biomaterials* 26:5221–5230
146. Webster TJ, Siegel RW, Bizios R (1999) Osteoblast adhesion on nanophase ceramics. *Biomaterials* 20:1221–1227
147. Webster TJ, Ergun C, Doremus RH, Siegel RW, Bizios R (2000) Enhanced functions of osteoblast on nanophase ceramics. *Biomaterials* 21:1803–1810
148. Smith IO, McCabe LR, Baumann MJ (2006) MC3T3-E1 osteoblast attachment and proliferation on porous hydroxyapatite scaffolds fabricated with nanophase powder. *Int J Nanomedicine* 1:189–194
149. Nelson M, Balasundaram G, Webster TJ (2006) Increased osteoblast adhesion on nanoparticulate crystalline hydroxyapatite functionalized with KRSR. *Int J Nanomedicine* 1:339–349
150. Liu H, Yazici H, Ergun C, Webster TJ, Bermek H (2008) An in vitro evaluation of the Ca/P ratio for the cytocompatibility of nano-to-micron particulate calcium phosphates for bone regeneration. *Acta Biomater* 4:1472–1479
151. Sato M, Sambito MA, Aslani A, Kalkhoran NM, Slamovich EB, Webster TJ (2006) Increased osteoblast functions on undoped and yttrium-doped nanocrystalline hydroxyapatite coatings on titanium. *Biomaterials* 27:2358–2369
152. Thian ES, Huang J, Best SM, Barber ZH, Brooks RA, Rushton N, Bonfield W (2006) The response of osteoblasts to nanocrystalline silicon-substituted hydroxyapatite thin films. *Biomaterials* 27:2692–2698
153. Palin E, Liu H, Webster TJ (2005) Mimicking the nanofeatures of bone increases bone-forming cell adhesion and proliferation. *Nanotechnology* 16:1828–1835
154. Smoak M, Hogan K, Krieger L, Chen C, Terrell LKB, Qureshi AT, Monroe TW, Gimble JM, Hayes DJ (2015) Modulation of mesenchymal stem cell behavior by nano- and micro-sized  $\beta$ -tricalcium phosphate particles in suspension and composite structures. *J Nanopart Res* 17:182–196
155. Sun W, Chu C, Wang J, Zhao H (2007) Comparison of periodontal ligament cells responses to dense and nanophase hydroxyapatite. *J Mater Sci Mater Med* 18:677–683
156. Ergun C, Liu H, Webster TJ, Olcay E, Yılmaz Ş, Sahin FC (2008) Increased osteoblast adhesion on nanoparticulate calcium phosphates with higher Ca/P ratios. *J Biomed Mater Res A* 85A:236–241
157. Lewandrowski KU, Bondre SP, Wise DL, Trantolo DJ (2003) Enhanced bioactivity of a poly(propylene fumarate) bone graft substitute by augmentation with nano-hydroxyapatite. *Biomed Mater Eng* 13:115–124
158. Zhou DS, Zhao KB, Li Y, Cui FZ, Lee IS (2006) Repair of segmental defects with nano-hydroxyapatite/collagen/PLA composite combined with mesenchymal stem cells. *J Bioact Compat Polym* 21:373–384
159. Khanna R, Katti KS, Katti DR (2011) Bone nodules on chitosan-polygalacturonic acid-hydroxyapatite nanocomposite films mimic hierarchy of natural bone. *Acta Biomater* 7:1173–1183

160. Xu Z, Sun J, Liu CS, Wei J (2009) Effect of hydroxyapatite nanoparticles of different concentrations on rat osteoblast. *Mater Sci Forum* 610–613:1364–1369
161. Okada S, Nagai A, Oaki Y, Komotori J, Imai H (2011) Control of cellular activity of fibroblasts on size-tuned fibrous hydroxyapatite nanocrystals. *Acta Biomater* 7:1290–1297
162. Kalia P, Vizcay-Barrena G, Fan JP, Warley A, di Silvio L, Huang J (2014) Nanohydroxyapatite shape and its potential role in bone formation: an analytical study. *J R Soc Interface* 11:20140004. (11 pages)
163. Bansal M, Kaushik M, Khattak BBP, Sharma A (2014) Comparison of nanocrystalline hydroxyapatite and synthetic resorbable hydroxyapatite graft in the treatment of intrabony defects: a clinical and radiographic study. *J Indian Soc Periodontol* 18:213–219
164. Krut'ko VK, Kulak AI, Lesnikovich LA, Trofimova IV, Musskaya ON, Zhavnerko GK, Paribok IV (2007) Influence of the dehydration procedure on the physicochemical properties of nanocrystalline hydroxylapatite xerogel. *Russ J Gen Chem* 77:336–342
165. Severin AV, Komarov VF, Bozhevol'nov VE, Melikhov IV (2005) Morphological selection in suspensions of nanocrystalline hydroxylapatite leading to spheroidal aggregates. *Russ J Inorg Chem* 50:72–77
166. Biggemann D, da Silva MHP, Rossi AM, Ramirez AJ (2008) High-resolution transmission electron microscopy study of nanostructured hydroxyapatite. *Microsc Microanal* 14:433–438
167. Hagemeyer D, Ganesan K, Ruesing J, Schunk D, Mayer C, Dey A, Sommerdijk NAJM, Epple M (2011) Self-assembly of calcium phosphate nanoparticles into hollow spheres induced by dissolved amino acids. *J Mater Chem* 21:9219–9223
168. Kester M, Heakal Y, Fox T, Sharma A, Robertson GP, Morgan TT, Altinoğlu EI, Tabaković A, Parette MR, Rouse SM, Ruiz-Velasco V, Adair JH (2008) Calcium phosphate nanocomposite particles for in vitro imaging and encapsulated chemotherapeutic drug delivery to cancer cells. *Nano Lett* 8:4116–4121
169. Welzel T, Meyer-Zaika W, Epple M (2004) Continuous preparation of functionalised calcium phosphate nanoparticles with adjustable crystallinity. *Chem Commun* 1204–1205
170. Nichols HL, Zhang N, Zhang J, Shi D, Bhaduri S, Wen X (2007) Coating nanothickness degradable films on nanocrystalline hydroxyapatite particles to improve the bonding strength between nanohydroxyapatite and degradable polymer matrix. *J Biomed Mater Res A* 82A:373–382
171. Bouladjine A, Al-Kattan A, Dufour P, Drouet C (2009) New advances in nanocrystalline apatite colloids intended for cellular drug delivery. *Langmuir* 25:12256–12265
172. Rey C, Hina A, Tofighi A, Glimcher MJ (1995) Maturation of poorly crystalline apatites: chemical and structural aspects in vivo and in vitro. *Cell Mater* 5:345–356
173. Dorozhkin SV (2015) Calcium orthophosphate bioceramics. *Ceram Int* 41:13913–13966
174. Elliott JC (1994) Structure and chemistry of the apatites and other calcium orthophosphates. Elsevier, Amsterdam
175. Olszta MJ, Cheng X, Jee SS, Kumar R, Kim YY, Kaufman MJ, Douglas EP, Gower LB (2007) Bone structure and formation: a new perspective. *Mater Sci Eng R* 58:77–116
176. Reznikov N, Shahar R, Weiner S (2014) Bone hierarchical structure in three dimensions. *Acta Biomater* 10:3815–3826
177. Rubin MA, Jasiuk I, Taylor J, Rubin J, Ganey T, Apkarian RP (2003) TEM analysis of the nanostructure of normal and osteoporotic human trabecular bone. *Bone* 33:270–282
178. Hartgerink JD, Beniash E, Stupp SI (2001) Self-assembly and mineralization of peptide-amphiphile nanofibers. *Science* 294:1684–1688
179. Ji B, Gao H (2006) Elastic properties of nanocomposite structure of bone. *Compos Sci Technol* 66:1212–1218
180. Wang L, Nancollas GH, Henneman ZJ, Klein E, Weiner S (2006) Nanosized particles in bone and dissolution insensitivity of bone mineral. *Biointerphases* 1:106–111
181. Xie B, Nancollas GH (2011) How to control the size and morphology of apatite nanocrystals in bone. *Proc Natl Acad Sci U S A* 107:22369–22370

182. Hu YY, Rawal A, Schmidt-Rohr K (2011) Strongly bound citrate stabilizes the apatite nanocrystals in bone. *Proc Natl Acad Sci U S A* 107:22425–22429
183. Gao H, Ji B, Jager IL, Arz E, Fratzl P (2003) Materials become insensitive to flaws at nanoscale: lessons from nature. *Proc Natl Acad Sci U S A* 100:5597–5660
184. Gupta HS, Seto J, Wagermaier W, Zaslansky P, Boesecke P, Fratzl P (2006) Cooperative deformation of mineral and collagen in bone at the nanoscale. *Proc Natl Acad Sci U S A* 103:17741–17746
185. Currey JD (2006) *Bones: structure and mechanics*. Princeton University Press, Princeton
186. Porter AE, Nalla RK, Minor A, Jinschek JR, Kisielowski C, Radmilovic V, Kinney JH, Tomsia AP, Ritchie RO (2005) A transmission electron microscopy study of mineralization in age-induced transparent dentin. *Biomaterials* 26:7650–7660
187. Kirkham J, Brookes SJ, Shore RC, Wood SR, Smith DA, Zhang J, Chen H, Robinson C (2002) Physico-chemical properties of crystal surfaces in matrix-mineral interactions during mammalian biomineralisation. *Curr Opin Colloid Interface Sci* 7:124–132
188. Daculsi G, Mentanteau J, Kerbel LM, Mitre D (1984) Length and shape of enamel crystals. *Calcif Tissue Int* 36:550–555
189. Robinson C, Connell S, Kirkham J, Shorea R, Smith A (2004) Dental enamel – a biological ceramic: regular substructures in enamel hydroxyapatite crystals revealed by atomic force microscopy. *J Mater Chem* 14:2242–2248
190. Chen H, Tang Z, Liu J, Sun K, Chang SR, Peters MC, Mansfield JF, Czajka-Jakubowska A, Clarkson BH (2006) Acellular synthesis of a human enamel-like microstructure. *Adv Mater* 18:1846–1851
191. Chen H, Clarkson BH, Sun K, Mansfield JF (2005) Self-assembly of synthetic hydroxyapatite nanorods into an enamel prism-like structure. *J Colloid Interface Sci* 288:97–103
192. Robinson C (2007) Self-oriented assembly of nano-apatite particles: a subunit mechanism for building biological mineral crystals. *J Dent Res* 86:677–679
193. Cui FZ, Ge J (2007) New observations of the hierarchical structure of human enamel, from nanoscale to microscale. *J Tissue Eng Regen Med* 1:185–191
194. He LH, Swain MV (2007) Enamel – a “metallic-like” deformable biocomposite. *J Dent* 35:431–437
195. Nelson SJ (2009) *Wheeler’s dental anatomy, physiology and occlusion*, 9th edn. W. B. Saunders, Philadelphia
196. Lenton S, Nylander T, Teixeira SCM, Holt C (2015) A review of the biology of calcium phosphate sequestration with special reference to milk. *Dairy Sci Technol* 95:3–14
197. Suvorova EI, Buffat PA (1999) Electron diffraction from micro- and nanoparticles of hydroxyapatite. *J Microsc* 196:46–58
198. Panda RN, Hsieh MF, Chung RJ, Chin TS (2001) X-ray diffractometry and X-ray photoelectron spectroscopy investigations of nanocrystalline hydroxyapatite synthesized by a hydroxide gel technique. *Jpn J Appl Phys* 40:5030–5035
199. Panda RN, Hsieh MF, Chung RJ, Chin TS (2003) FTIR, XRD, SEM and solid state NMR investigations of carbonate-containing hydroxyapatite nano-particles synthesized by hydroxide-gel technique. *J Phys Chem Solids* 64:193–199
200. Eichert D, Sfihi H, Combes C, Rey C (2004) Specific characteristics of wet nanocrystalline apatites. Consequences on biomaterials and bone tissue. *Key Eng Mater* 254-256:927–930
201. Rey C, Combes C, Drouet C, Sfihi H, Barroug A (2007) Physico-chemical properties of nanocrystalline apatites: implications for biominerals and biomaterials. *Mater Sci Eng C* 27:198–205
202. Eichert D, Drouet C, Sfihi H, Rey C, Combes C (2007) Nanocrystalline apatite-based biomaterials: synthesis, processing and characterization. In: Kendall JB (ed) *Biomaterials research advances*. Nova Science Publishers, New York, pp 93–143
203. Aronov D, Rosenman G (2007) Trap state spectroscopy studies and wettability modification of hydroxyapatite nanobioceramics. *J Appl Phys* 101:034701. (5 pages)

204. Jäger C, Welzel T, Meyer-Zaika W, Epple M (2006) A solid-state NMR investigation of the structure of nanocrystalline hydroxyapatite. *Magn Reson Chem* 44:573–580
205. Isobe T, Nakamura S, Nemoto R, Senna M, Sfihi H (2002) Solid-state double nuclear magnetic resonance of calcium phosphate nanoparticles synthesized by wet-mechanochemical reaction. *J Phys Chem B* 106:5169–5176
206. Bertinetti L, Tampieri A, Landi E, Ducati C, Midgley PA, Coluccia S, Martra G (2007) Surface structure, hydration, and cationic sites of nanohydroxyapatite: UHR-TEM, IR, and microgravimetric studies. *J Phys Chem C* 111:4027–4035
207. Bertinetti L, Tampieri A, Landi E, Bolis V, Busco C, Martra G (2008) Surface structure, hydration and cationic sites of nanohydroxyapatite. *Key Eng Mater* 361–363:87–90
208. Bertinetti L, Drouet C, Combes C, Rey C, Tampieri A, Coluccia S, Martra G (2009) Surface characteristics of nanocrystalline apatites: effect of Mg surface enrichment on morphology, surface hydration species, and cationic environments. *Langmuir* 25:5647–5654
209. Gopi D, Indira J, Prakash VCA, Kavitha L (2009) Spectroscopic characterization of porous nanohydroxyapatite synthesized by a novel amino acid soft solution freezing method. *Spectrochim Acta A* 74A:282–284
210. Ospina CA, Terra J, Ramirez AJ, Farina M, Ellis DE, Rossi AM (2012) Experimental evidence and structural modeling of nonstoichiometric (010) surfaces coexisting in hydroxyapatite nano-crystals. *Colloids Surf B: Biointerfaces* 89:15–22
211. Song K, Kim YJ, Kim YI, Kim JG (2012) Application of theta-scan precession electron diffraction to structure analysis of hydroxyapatite nanopowder. *J Electron Microsc* 61:9–15
212. Bian S, Du LW, Gao YX, Huang J, Gou BD, Li X, Liu Y, Zhang TL, Wang K (2012) Crystallization in aggregates of calcium phosphate nanocrystals: a logistic model for kinetics of fractal structure development. *Cryst Growth Des* 12:3481–3488
213. Gómez-Morales J, Iafisco M, Delgado-López JM, Sarda S, Drouet C (2013) Progress on the preparation of nanocrystalline apatites and surface characterization: overview of fundamental and applied aspects. *Prog Cryst Growth Charact Mater* 59:1–46
214. Pajchel L, Kolodziejcki W (2013) Solid-state MAS NMR, TEM, and TGA studies of structural hydroxyl groups and water in nanocrystalline apatites prepared by dry milling. *J Nanopart Res* 15:1868. (15 pages)
215. Sakhno Y, Ivanchenko P, Iafisco M, Tampieri A, Martra G (2015) A step toward control of the surface structure of biomimetic hydroxyapatite nanoparticles: effect of carboxylates on the {010} P-rich/Ca-rich facets ratio. *J Phys Chem C* 119:5928–5937
216. Ospina CA, Terra J, Ramirez AJ, Ellis DE, Rossi AM (2012) Simulations of hydroxyapatite nanocrystals for HRTEM images calculations. *Key Eng Mater* 493–494:763–767
217. Rossi AM, da Silva MHP, Ramirez AJ, Biggemann D, Caraballo MM, Mascarenhas YP, Eon JG, Moure GT (2007) Structural properties of hydroxyapatite with particle size less than 10 nanometers. *Key Eng Mater* 330–332:255–258
218. Ramirez CAO, Costa AM, Bettini J, Ramirez AJ, da Silva MHP, Rossi AM (2009) Structural properties of nanostructured carbonate apatites. *Key Eng Mater* 396–398:611–614
219. Pasteris JD, Wopenka B, Freeman JJ, Rogers K, Valsami-Jones E, van der Houten JAM, Silva MJ (2004) Lack of OH in nanocrystalline apatite as a function of degree of atomic order: implications for bone and biomaterials. *Biomaterials* 25:229–238
220. Sakhno Y, Bertinetti L, Iafisco M, Tampieri A, Roveri N, Martra G (2010) Surface hydration and cationic sites of nanohydroxyapatites with amorphous or crystalline surfaces: a comparative study. *J Phys Chem C* 114:16640–16648
221. Bolis V, Busco C, Martra G, Bertinetti L, Sakhno Y, Ugliengo P, Chiatti F, Corno M, Roveri N (2012) Coordination chemistry of Ca sites at the surface of nanosized hydroxyapatite: interaction with H<sub>2</sub>O and CO. *Phil Trans A Math Phys Eng Sci* 37:1313–1336
222. Zyman ZZ, Epple M, Rokhmistrov D, Glushko V (2009) On impurities and the internal structure in precipitates occurring during the precipitation of nanocrystalline calcium phosphate. *Mater Wiss Werkst* 40:297–301



223. Delgado-López JM, Frison R, Cervellino A, Gómez-Morales J, Guagliardi A, Masciocchi N (2014) Crystal size, morphology, and growth mechanism in bio-inspired apatite nanocrystals. *Adv Funct Mater* 24:1090–1099
224. Rey C, Combes C, Drouet C, Cazalbou S, Grossin D, Brouillet F, Sarda S (2014) Surface properties of biomimetic nanocrystalline apatites; applications in biomaterials. *Prog Cryst Growth Charact Mater* 60:63–73
225. Cazalbou S, Combes C, Eichert D, Rey C (2004) Adaptive physico-chemistry of bio-related calcium phosphates. *J Mater Chem* 14:2148–2153
226. Eichert D, Salomé M, Banu M, Susini J, Rey C (2005) Preliminary characterization of calcium chemical environment in apatitic and non-apatitic calcium phosphates of biological interest by X-ray absorption spectroscopy. *Spectrochim Acta B* 60B:850–858
227. Rosenman G, Aronov D, Oster L, Haddad J, Mezinskis G, Pavlovska I, Chaikina M, Karlov A (2007) Photoluminescence and surface photovoltage spectroscopy studies of hydroxyapatite nano-bio-ceramics. *J Lumin* 122–123:936–938
228. Melikhov IV, Teterin YA, Rudin VN, Teterin AY, Maslakov KI, Severin AV (2009) An X-ray electron study of nanodisperse hydroxyapatite. *Russ J Phys Chem A* 83:91–97
229. Wu CY, Young D, Martel J, Young JD (2015) A story told by a single nanoparticle in the body fluid: demonstration of dissolution-reprecipitation of nanocrystals in a biological system. *Nanomedicine (London)* 10:2659–2676
230. Aronov D, Rosenman G, Karlov A, Shashkin A (2006) Wettability patterning of hydroxyapatite nanobioceramics induced by surface potential modification. *Appl Phys Lett* 88:163902. (3 pages)
231. Rau JV, Generosi A, Ferro D, Minozzi F, Paci B, Albertini VR, Dolci G, Barinov SM (2009) In situ time-resolved X-ray diffraction study of evolution of nanohydroxyapatite particles in physiological solution. *Mater Sci Eng C* 29:1140–1143
232. Zhao W, Xu Z, Yang Y, Sahai N (2014) Surface energetics of the hydroxyapatite nanocrystal–water interface: a molecular dynamics study. *Langmuir* 30:13283–13292
233. Arora A (2004) Ceramics in nanotech revolution. *Adv Eng Mater* 6:244–247
234. Mao Y, Park TJ, Zhang F, Zhou H, Wong SS (2007) Environmentally friendly methodologies of nanostructure synthesis. *Small* 3:1122–1139
235. Ioku K, Yoshimura M (1991) Stoichiometric apatite fine single crystals by hydrothermal synthesis. *Phosphorus Res Bull* 1:15–20
236. Chen JD, Wang YJ, Wei K, Zhang SH, Shi XT (2007) Self-organization of hydroxyapatite nanorods through oriented attachment. *Biomaterials* 28:2275–2280
237. Guo X, Xiao P, Liu J, Shen Z (2004) Fabrication of nanostructured hydroxyapatite via hydrothermal synthesis and spark plasma sintering. *J Am Ceram Soc* 88:1026–1029
238. Brown PW, Constantz B (eds) (1994) Hydroxyapatite and related materials. CRC Press, Boca Raton
239. Amjad Z (ed) (1997) Calcium phosphates in biological and industrial systems. Kluwer Academic Publishers, Boston
240. Dorozhkin SV (2012) Calcium orthophosphates: applications in nature, biology, and medicine. Pan Stanford, Singapore
241. Dorozhkin SV (2016) Calcium orthophosphate-based bioceramics and biocomposites. Wiley-VCH, Weinheim
242. Komarov VF, Kibalchitz V (1979) Precipitation of apatite through highly saturated solutions. *Moscow Univ Bull Chem Dic* 2680–2685
243. Prakash KH, Kumar R, Ooi CP, Cheang P, Khor KA (2006) Conductometric study of precursor compound formation during wet-chemical synthesis of nanocrystalline hydroxyapatite. *J Phys Chem B* 110:24457–24462
244. Tao J, Pan H, Wang J, Wu J, Wang B, Xu X, Tang R (2008) Evolution of amorphous calcium phosphate to hydroxyapatite probed by gold nanoparticles. *J Phys Chem C* 112:14929–14933
245. Chane-Ching JY, Lebugle A, Rousselot I, Pourpoint A, Pelle F (2007) Colloidal synthesis and characterization of monocrySTALLINE apatite nanophosphors. *J Mater Chem* 17:2904–2913

246. Zyman ZZ, Rokhmistrov DV, Glushko VI (2010) Structural and compositional features of amorphous calcium phosphate at the early stage of precipitation. *J Mater Sci Mater Med* 21:123–130
247. Wei M, Ruys AJ, Milthorpe BK, Sorrell CC (1999) Solution ripening of hydroxyapatite nanoparticles: effects on electrophoretic deposition. *J Biomed Mater Res* 45:11–19
248. Zhu X, Eibl O, Berthold C, Scheideler L, Geis-Gerstorfer J (2006) Structural characterization of nanocrystalline hydroxyapatite and adhesion of pre-osteoblast cells. *Nanotechnology* 17:2711–2721
249. Rusu VM, Ng CH, Wilke M, Tiersch B, Fratzl P, Peter MG (2005) Size-controlled hydroxyapatite nanoparticles as self-organized organic-inorganic composite materials. *Biomaterials* 26:5414–5426
250. Wang YJ, Lai C, Wei K, Tang SQ (2005) Influence of temperature, ripening time and cosurfactant on solvothermal synthesis of calcium phosphate nanobelts. *Mater Lett* 59:1098–1104
251. Li YB, Li D, Weng W (2008) Preparation of nano carbonate-substituted hydroxyapatite from an amorphous precursor. *Int J Appl Ceram Technol* 5:442–448
252. Zhang S, Gonsalves KE (1997) Preparation and characterization of thermally stable nanohydroxyapatite. *J Mater Sci Mater Med* 8:25–28
253. Ferraz M, Monteiro FJ, Manuel CM (2004) Hydroxyapatite nanoparticles: a review of preparation methodologies. *J Appl Biomater Biomech* 2:74–80
254. Ahn ES, Gleason NJ, Nakahira A, Ying JY (2001) Nanostructure processing of hydroxyapatite-based bioceramics. *Nano Lett* 1:149–153
255. Mazelsky R, Hopkins RH, Kramer WE (1968) Czochralski-growth of calcium fluorophosphates. *J Cryst Growth* 3–4:260–264
256. Loutts GB, Chai BHT (1993) Growth of high-quality single crystals of FAP ( $\text{Ca}_5(\text{PO}_4)_3\text{F}$ ) and its isomorphs. *Proc SPIE Int Soc Opt Eng* 1863:31–34
257. Siegel RW (1996) Creating nanophase materials. *Sci Am* 275:42–47
258. Hu J, Odum TW, Lieber CM (1999) Chemistry and physics in one dimension: synthesis and properties of nanowires and nanotubes. *Acc Chem Res* 32:435–445
259. Schmidt HK (2000) Nanoparticles for ceramic and nanocomposite processing. *Mol Cryst Liq Cryst* 353:165–179
260. Cushing BL, Kolesnichenko VL, O'Connor CJ (2004) Recent advances in the liquid-phase syntheses of inorganic nanoparticles. *Chem Rev* 104:3893–3946
261. Wang X, Zhuang J, Peng Q, Li Y (2005) A general strategy for nanocrystal synthesis. *Nature* 437:121–124
262. Yin Y, Alivisatos AP (2005) Colloidal nanocrystal synthesis and the organic-inorganic interface. *Nature* 437:664–670
263. de Mello Donegá C, Liljeroth P, Vanmaekelbergh D (2005) Physicochemical evaluation of the hot-injection method, a synthesis route for monodisperse nanocrystals. *Small* 1:1152–1162
264. Ma MG, Zhu JF (2010) Recent progress on fabrication of calcium-based inorganic biodegradable nanomaterials. *Rec Pat Nanotechnol* 4:164–170
265. Chen F, Zhu Y, Wu J, Huang P, Cui D (2012) Nanostructured calcium phosphates: preparation and their application in biomedicine. *Nano Biomed Eng* 4:41–49
266. Takagi S, Chow LC, Ishikawa K (1998) Formation of hydroxyapatite in new calcium phosphate cements. *Biomaterials* 19:1593–1599
267. Melikhov IV, Komarov VF, Severin AV, Bozhevol'nov VE, Rudin VN (2000) Two-dimensional crystalline hydroxyapatite. *Dokl Phys Chem* 373:355–358
268. Kumta P, Sfeir C, Lee DH, Olton D, Choi D (2005) Nanostructured calcium phosphates for biomedical applications: novel synthesis and characterization. *Acta Biomater* 1:65–83
269. Mollazadeh S, Javadpour J, Khavandi A (2007) In situ synthesis and characterization of nanosized hydroxyapatite in poly(vinyl alcohol) matrix. *Ceram Int* 33:1579–1583
270. Bouyer E, Gitzhofer F, Boulos MI (2000) Morphological study of hydroxyapatite nanocrystal suspension. *J Mater Sci Mater Med* 11:523–531

271. Pang YX, Bao X (2003) Influence of temperature, ripening time and calcination on the morphology and crystallinity of hydroxyapatite nanoparticles. *J Eur Ceram Soc* 23:1697–1704
272. Kumar R, Prakash KH, Cheang P, Khor KA (2004) Temperature driven morphological changes of chemically precipitated hydroxyapatite nanoparticles. *Langmuir* 20:5196–5200
273. Cao LY, Zhang CB, Huang JF (2005) Influence of temperature,  $[Ca^{2+}]$ , Ca/P ratio and ultrasonic power on the crystallinity and morphology of hydroxyapatite nanoparticles prepared with a novel ultrasonic precipitation method. *Mater Lett* 59:1902–1906
274. Afshar A, Ghorbani M, Ehsani N, Saeri MR, Sorrell CC (2003) Some important factors in the wet precipitation process of hydroxyapatite. *Mater Des* 24:197–202
275. Liu Y, Hou D, Wang G (2004) A simple wet chemical synthesis and characterization of hydroxyapatite nanorods. *Mater Chem Phys* 86:69–73
276. Saha SK, Banerjee A, Banerjee S, Bose S (2009) Synthesis of nanocrystalline hydroxyapatite using surfactant template systems: role of templates in controlling morphology. *Mater Sci Eng C* 29:2294–2301
277. Shanthi PMSL, Ashok M, Balasubramanian T, Riyasdeen A, Akbarsha MA (2009) Synthesis and characterization of nano-hydroxyapatite at ambient temperature using cationic surfactant. *Mater Lett* 63:2123–2125
278. Phillips MJ, Darr JA, Luklinska ZB, Rehman I (2003) Synthesis and characterization of nanobiomaterials with potential osteological applications. *J Mater Sci Mater Med* 14:875–882
279. Ramesh S, Tan CY, Sopyan I, Hamdi M, Teng WD (2007) Consolidation of nanocrystalline hydroxyapatite powder. *Sci Technol Adv Mater* 8:124–130
280. Shi HB, Zhong H, Liu Y, Gu JY, Yang CS (2007) Effect of precipitation method on stoichiometry and morphology of hydroxyapatite nanoparticles. *Key Eng Mater* 330–332:271–274
281. Poinern GE, Brundavanam RK, Mondinos N, Jiang ZT (2009) Synthesis and characterisation of nanohydroxyapatite using an ultrasound assisted method. *Ultrason Sonochem* 16:469–474
282. Doğan Ö, Öner M (2008) The influence of polymer architecture on nanosized hydroxyapatite precipitation. *J Nanosci Nanotechnol* 8:667–674
283. Loo SCJ, Siew YE, Ho S, Boey FYC, Ma J (2008) Synthesis and hydrothermal treatment of nanostructured hydroxyapatite of controllable sizes. *J Mater Sci Mater Med* 19:1389–1397
284. Guo X, Gough JE, Xiao P, Liu J, Shen Z (2007) Fabrication of nanostructured hydroxyapatite and analysis of human osteoblastic cellular response. *J Biomed Mater Res A* 82A:1022–1032
285. Iafisco M, Palazzo B, Marchetti M, Margiotta N, Ostuni R, Natile G, Morpurgo M, Gandin V, Marzano C, Roveri N (2009) Smart delivery of antitumoral platinum complexes from biomimetic hydroxyapatite nanocrystals. *J Mater Chem* 19:8385–8392
286. Wang P, Li C, Gong H, Jiang X, Wang H, Li K (2010) Effects of synthesis conditions on the morphology of hydroxyapatite nanoparticles produced by wet chemical process. *Powder Technol* 203:315–321
287. Leskiv M, Lagoa ALC, Urch H, Schwiertz J, da Piedade MEM, Epple M (2009) Energetics of calcium phosphate nanoparticle formation by the reaction of  $Ca(NO_3)_2$  with  $(NH_4)_2HPO_4$ . *J Phys Chem C* 113:5478–5484
288. Rodrigues LR, Motisuke M, Zavaglia CAC (2009) Synthesis of nanostructured hydroxyapatite: a comparative study between sol-gel and aqueous solution precipitation. *Key Eng Mater* 396–398:623–626
289. Okada M, Furuzono T (2011) Low-temperature synthesis of nanoparticle-assembled, transparent, and low-crystallized hydroxyapatite blocks. *J Colloid Interface Sci* 360:457–462
290. Alobeedallah H, Coster H, Dehghani F, Ellis J, Rohanizadeh R (2011) The preparation of nanostructured hydroxyapatite in organic solvents for clinical applications. *Trends Biomater Artif Organs* 25:12–19
291. Lagno F, Rocha SDF, Katsarou L, Demopoulos GP (2012) Supersaturation-controlled synthesis of dicalcium phosphate dihydrate and nanocrystalline calcium-deficient hydroxyapatite. *Ind Eng Chem Res* 51:6605–6612

292. Shafiei F, Behroozibakhsh M, Moztaarzadeh F, Haghbin-Nazarpak M, Tahriri M (2012) Nanocrystalline fluorine-substituted hydroxyapatite  $[\text{Ca}_5(\text{PO}_4)_3(\text{OH})_{1-x}\text{F}_x]$  ( $0 \leq x \leq 1$ ) for bio-medical applications: preparation and characterization. *Micro Nano Lett* 7:109–114
293. Khalid M, Mujahid M, Amin S, Rawat RS, Nusair A, Deen GR (2013) Effect of surfactant and heat treatment on morphology, surface area and crystallinity in hydroxyapatite nanocrystals. *Ceram Int* 39:39–50
294. Iyyappan E, Wilson P (2013) Synthesis of nanoscale hydroxyapatite particles using triton X-100 as an organic modifier. *Ceram Int* 39:771–777
295. Gao S, Sun K, Li A, Wang H (2013) Synthesis and characterization of hydroxyapatite nanofiber by chemical precipitation method using surfactants. *Mater Res Bull* 48:1003–1006
296. Mohandes F, Salavati-Niasari M, Fathi M, Fereshteh Z (2014) Hydroxyapatite nanocrystals: simple preparation, characterization and formation mechanism. *Mater Sci Eng C* 45:29–36
297. Pokale P, Shende S, Gade A, Rai M (2014) Biofabrication of calcium phosphate nanoparticles using the plant *Mimusops elengi*. *Environ Chem Lett* 12:393–399
298. Ji X, Su P, Liu C, Song J, Liu C, Li J, Tan H, Wu F, Yang L, Fu R, Tang C, Cheng B (2015) A novel ethanol induced and stabilized hierarchical nanorods: hydroxyapatite nanopenanut. *J Am Ceram Soc* 98:1702–1705
299. Roche KJ, Stanton KT (2014) Measurement of fluoride substitution in precipitated fluorhydroxyapatite nanoparticles. *J Fluor Chem* 161:102–109
300. Stanić V, Dimitrijević S, Antonović DG, Jokić BM, Zec SP, Tanasković ST, Raičević S (2014) Synthesis of fluorine substituted hydroxyapatite nanopowders and application of the central composite design for determination of its antimicrobial effects. *Appl Surf Sci* 290:346–352
301. Palanivelu R, Saral AM, Kumar AR (2014) Nanocrystalline hydroxyapatite prepared under various pH conditions. *Spectrochim Acta A* 131:37–41
302. Mohandes F, Salavati-Niasari M, Fereshteh Z, Fathi M (2014) Novel preparation of hydroxyapatite nanoparticles and nanorods with the aid of complexing agents. *Ceram Int* 40:12227–12233
303. Bi YG, Xu XS (2014) Study on nano-hydroxyapatite assisted preparing by ionic liquids. *Adv Mater Res* 1015:501–504
304. Sundrarajan M, Jegatheeswaran S, Selvam S, Sanjeevi N, Balaji M (2015) The ionic liquid assisted green synthesis of hydroxyapatite nanoplates by *Moringa oleifera* flower extract: a biomimetic approach. *Mater Des* 88:1183–1190
305. Gentile P, Wilcock CJ, Miller CA, Moorehead R, Hatton PV (2015) Process optimisation to control the physico-chemical characteristics of biomimetic nanoscale hydroxyapatites prepared using wet chemical precipitation. *Materials* 8:2297–2310
306. Karimi M, Hesaraki S, Alizadeh M, Kazemzadeh A (2016) Synthesis of calcium phosphate nanoparticles in deep-eutectic choline chloride-urea medium: investigating the role of synthesis temperature on phase characteristics and physical properties. *Ceram Int* 42:2780–2788
307. López-Macipe A, Gómez-Morales J, Rodríguez-Clemente R (1998) Nanosized hydroxyapatite precipitation from homogeneous calcium/citrate/phosphate solutions using microwave and conventional heating. *Adv Mater* 10:49–53
308. Siddharthan A, Seshadri SK, Kumar TSS (2005) Rapid synthesis of calcium deficient hydroxyapatite nanoparticles by microwave irradiation. *Trends Biomater Artif Organs* 18:110–113
309. Ioku K, Yamauchi S, Fujimori H, Goto S, Yoshimura M (2002) Hydrothermal preparation of fibrous apatite and apatite sheet. *Solid State Ionics* 151:147–150
310. Chaudhry AA, Haque S, Kellici S, Boldrin P, Rehman I, Khalid FA, Darr JA (2006) Instant nano-hydroxyapatite: a continuous and rapid hydrothermal synthesis. *Chem Commun* 21:2286–2288
311. Cao M, Wang Y, Guo C, Qi Y, Hu C (2004) Preparation of ultrahigh-aspect-ratio hydroxyapatite nanofibers in reverse micelles under hydrothermal conditions. *Langmuir* 20:4784–4786
312. Guo X, Xiao P (2006) Effects of solvents on properties of nanocrystalline hydroxyapatite produced from hydrothermal process. *J Eur Ceram Soc* 26:3383–3391

313. Xin R, Yu K (2009) Ultrastructure characterization of hydroxyapatite nanoparticles synthesized by EDTA-assisted hydrothermal method. *J Mater Sci* 44:4205–4209
314. Zhang HB, Zhou KC, Li ZY, Huang SP (2009) Plate-like hydroxyapatite nanoparticles synthesized by the hydrothermal method. *J Phys Chem Solids* 70:243–248
315. Sun Y, Guo G, Tao D, Wang Z (2007) Reverse microemulsion-directed synthesis of hydroxyapatite nanoparticles under hydrothermal conditions. *J Phys Chem Solids* 68:373–377
316. Xin R, Ren F, Leng Y (2010) Synthesis and characterization of nano-crystalline calcium phosphates with EDTA-assisted hydrothermal method. *Mater Des* 31:1691–1694
317. Yan L, Li Y, Deng Z, Zhuang J, Sun X (2005) Surfactant-assisted hydrothermal synthesis of hydroxyapatite nanorods. *Int J Inorg Mater* 2001(3):633–637
318. Zhang F, Zhou Z, Yang S, Mao L, Chen H, Yu X (2005) Hydrothermal synthesis of hydroxyapatite nanorods in the presence of anionic starburst dendrimer. *Mater Lett* 59:1422–1425
319. Pathi SP, Lin DD, Dorvee JR, Estroff LA, Fischbach C (2011) Hydroxyapatite nanoparticle-containing scaffolds for the study of breast cancer bone metastasis. *Biomaterials* 32:5112–5122
320. Zhu A, Lu Y, Si Y, Dai S (2011) Fabricating hydroxyapatite nanorods using a biomacromolecule template. *Appl Surf Sci* 257:3174–3179
321. Wang YZ, Fu Y (2011) Microwave-hydrothermal synthesis and characterization of hydroxyapatite nanocrystallites. *Mater Lett* 65:3388–3390
322. Lin K, Liu X, Chang J, Zhu Y (2011) Facile synthesis of hydroxyapatite nanoparticles, nanowires and hollow nano-structured microspheres using similar structured hard-precursors. *Nanoscale* 3:3052–3055
323. Ren F, Ding Y, Ge X, Lu X, Wang K, Leng Y (2012) Growth of one-dimensional single-crystalline hydroxyapatite nanorods. *J Cryst Growth* 349:75–82
324. Nathanael AJ, Hong SI, Mangalaraj D, Ponpandian N, Chen PC (2012) Template-free growth of novel hydroxyapatite nanorings: formation mechanism and their enhanced functional properties. *Cryst Growth Des* 12:3565–3574
325. Nathanael AJ, Mangalaraj D, Hong SI, Masuda Y, Rhee YH, Kim HW (2013) Influence of fluorine substitution on the morphology and structure of hydroxyapatite nanocrystals prepared by hydrothermal method. *Mater Chem Phys* 137:967–976
326. Nagata F, Yamauchi Y, Tomita M, Kato K (2013) Hydrothermal synthesis of hydroxyapatite nanoparticles and their protein adsorption behavior. *J Ceram Soc Jpn* 121:797–801
327. Ramedani A, Yazdanpanah A, Moztaarzadeh F, Mozafari M (2014) On the use of nanoliposomes as soft templates for controlled nucleation and growth of hydroxyapatite nanocrystals under hydrothermal conditions. *Ceram Int* 40:9377–9381
328. Nga NK, Giang LT, Huy TQ, Viet PH, Migliaresi C (2014) Surfactant-assisted size control of hydroxyapatite nanorods for bone tissue engineering. *Colloids Surf B: Biointerfaces* 116:666–673
329. Taheri MM, Kadir MRA, Shokuhfar T, Hamlekhan A, Assadian M, Shirdar MR, Mirjalili A (2015) Surfactant-assisted hydrothermal synthesis of fluoridated hydroxyapatite nanorods. *Ceram Int* 41:9867–9872
330. Jin X, Zhuang J, Zhang Z, Guo H, Tan J (2015) Hydrothermal synthesis of hydroxyapatite nanorods in the presence of sodium citrate and its aqueous colloidal stability evaluation in neutral pH. *J Colloid Interface Sci* 443:125–130
331. Jin X, Chen X, Cheng Y, Wang L, Hu B, Tan J (2015) Effects of hydrothermal temperature and time on hydrothermal synthesis of colloidal hydroxyapatite nanorods in the presence of sodium citrate. *J Colloid Interface Sci* 450:151–158
332. Wang Y, Ren X, Ma X, Su W, Zhang Y, Sun X, Li X (2015) Alginate-intervened hydrothermal synthesis of hydroxyapatite nanocrystals with nanopores. *Cryst Growth Des* 15:1949–1956
333. Byrappa K, Haber M (2002) Handbook of hydrothermal technology: a technology for crystal growth and materials processing. Noyes Publications, New Jersey
334. Yu-Song P (2011) Surface modification of nanocrystalline hydroxyapatite. *Micro Nano Lett* 6:129–132

335. Gopi D, Govindaraju KM, Victor CAP, Kavitha L, Rajendiran N (2008) Spectroscopic investigations of nanohydroxyapatite powders synthesized by conventional and ultrasonic coupled sol-gel routes. *Spectrochim. Acta A Mol Biomol Spectrosc* 70:1243–1245
336. Rajabi-Zamani AH, Behnamghader A, Kazemzadeh A (2008) Synthesis of nanocrystalline carbonated hydroxyapatite powder via nonalkoxide sol-gel method. *Mater Sci Eng C* 28:1326–1329
337. Sopyan I, Toibah AR, Natasha AN (2008) Nanosized bioceramic hydroxyapatite powders via sol-gel method. *Int J Mech Mater Eng* 3:133–138
338. Yuan Y, Liu C, Zhang Y, Shan X (2008) Sol-gel auto-combustion synthesis of hydroxyapatite nanotubes array in porous alumina template. *Mater Chem Phys* 112:275–280
339. Kuriakose TA, Kalkura SN, Palanichamy M, Arivuoli D, Dierks K, Bocelli G, Betzel C (2004) Synthesis of stoichiometric nano crystalline hydroxyapatite by ethanol-based sol-gel technique at low temperature. *J Cryst Growth* 263:517–523
340. Sanosh KP, Chu MC, Balakrishnan A, Lee YJ, Kim TN, Cho SJ (2009) Synthesis of nano hydroxyapatite powder that simulate teeth particle morphology and composition. *Curr Appl Phys* 9:1459–1462
341. Darroudi M, Eshtiaqh-Hosseini H, Housaindokht MR, Youssefi A (2010) Preparation and characterization of fluorohydroxyapatite nanopowders by nonalkoxide sol-gel method. *Dig J Nanomater Biostruct* 5:29–33
342. Jadalannagari S, More S, Kowshik M, Ramanan SR (2011) Low temperature synthesis of hydroxyapatite nano-rods by a modified sol-gel technique. *Mater Sci Eng C* 31:1534–1538
343. Montazeri N, Jahandideh R, Biazar E (2011) Synthesis of fluorapatite-hydroxyapatite nanoparticles and toxicity investigations. *Int J Nanomedicine* 6:197–201
344. Vijayalakshmi U, Rajeswari S (2012) Influence of process parameters on the sol-gel synthesis of nano hydroxyapatite using various phosphorus precursors. *J Sol-Gel Sci Technol* 63:45–55
345. Salimi MN, Bridson RH, Grover LM, Leeke GA (2012) Effect of processing conditions on the formation of hydroxyapatite nanoparticles. *Powder Technol* 218:109–118
346. Rogoan R, Andronescu E, Ghitulica C, Birsan M, Voicu G, Stoleriu S, Melinescu A, Ianculescu A (2012) Analysis of the structure and morphology of hydroxyapatite nanopowder obtained by sol-gel and pirosol methods. *Adv Mater Res* 590:63–67
347. Bakan F, Laçin O, Sarac H (2013) A novel low temperature sol-gel synthesis process for thermally stable nano crystalline hydroxyapatite. *Powder Technol* 233:295–302
348. Kurgan N, Karbivskyy V, Kasyanenko V (2015) Morphology and electronic structure of nanoscale powders of calcium hydroxyapatite. *Nanoscale Res Lett* 10:41. (5 pages)
349. Li B, Wang XL, Guo B, Xiao YM, Fan HS, Zhang XD (2007) Preparation and characterization of nano hydroxyapatite. *Key Eng Mater* 330–332:235–238
350. Tas AC (2000) Synthesis of biomimetic Ca-hydroxyapatite powders at 37°C in synthetic body fluids. *Biomaterials* 21:1429–1438
351. Wu YS, Lee YH, Chang HC (2009) Preparation and characteristics of nanosized carbonated apatite by urea addition with coprecipitation method. *Mater Sci Eng C* 29:237–241
352. Swain SK, Sarkar D (2011) A comparative study: hydroxyapatite spherical nanopowders and elongated nanorods. *Ceram Int* 37:2927–2930
353. Martínez-Pérez CA, García-Montelongo J, García Casillas PE, Farias-Mancilla JR, Romero MH (2012) Preparation of hydroxyapatite nanoparticles facilitated by the presence of  $\beta$ -cyclodextrin. *J Alloys Compd* 536(Suppl 1):S432–S436
354. Rameshbabu N, Kumar TSS, Murugan R, Rao KP (2005) Mechanochemical synthesis of nanocrystalline fluorinated hydroxyapatite. *Int J Nanosci* 4:643–649
355. Yeong KCB, Wang J, Ng SC (2001) Mechanochemical synthesis of nanocrystalline hydroxyapatite from CaO and CaHPO<sub>4</sub>. *Biomaterials* 22:2705–2712
356. Coreno JA, Coreno OA, Cruz RJJ, Rodriguez CC (2005) Mechanochemical synthesis of nanocrystalline carbonate-substituted hydroxyapatite. *Opt Mater* 27:1281–1285

357. el Briak-Ben Abdeslam H, Mochales C, Ginebra MP, Nurit J, Planell JA, Boudeville P (2003) Dry mechanochemical synthesis of hydroxyapatites from dicalcium phosphate dihydrate and calcium oxide: a kinetic study. *J Biomed Mater Res A* 67A:927–937
358. Nakamura S, Isobe T, Senna M (2001) Hydroxyapatite nano sol prepared via a mechanochemical route. *J Nanopart Res* 3:57–61
359. Nasiri-Tabrizi B, Honarmandi P, Ebrahimi-Kahrizsangi R, Honarmandi P (2009) Synthesis of nanosize single-crystal hydroxyapatite via mechanochemical method. *Mater Lett* 63:543–546
360. Sharifah A, Iis S, Mohd H, Singh R (2011) Mechanochemical synthesis of nanosized hydroxyapatite powder and its conversion to dense bodies. *Mater Sci Forum* 694:118–122
361. Fereshteh Z, Fathi M, Mozaffarinia R (2014) Synthesis and characterization of fluorapatite nanoparticles via a mechanochemical method. *J Clust Sci* 26:1041–1053
362. Silva CC, Graça MPF, Valente MA, Sombra ASB (2007) Crystallite size study of nanocrystalline hydroxyapatite and ceramic system with titanium oxide obtained by dry ball milling. *J Mater Sci* 42:3851–3855
363. Zahrani EM, Fathi MH (2009) The effect of high-energy ball milling parameters on the preparation and characterization of fluorapatite nanocrystalline powder. *Ceram Int* 35:2311–2323
364. Mochales C, Wilson RM, Dowker SEP, Ginebra MP (2011) Dry mechanosynthesis of nanocrystalline calcium deficient hydroxyapatite: structural characterization. *J Alloys Compd* 509:7389–7394
365. Nasiri-Tabrizi B, Fahami A, Ebrahimi-Kahrizsangi R (2013) Effect of milling parameters on the formation of nanocrystalline hydroxyapatite using different raw materials. *Ceram Int* 39:5751–5763
366. Fahami A, Nasiri-Tabrizi B (2014) Mechanochemical behavior of  $\text{CaCO}_3\text{-P}_2\text{O}_5\text{-CaF}_2$  system to produce carbonated fluorapatite nanopowder. *Ceram Int* 40:14939–14946
367. Mandal T, Mishra BK, Garg A, Chaira D (2014) Optimization of milling parameters for the mechanosynthesis of nanocrystalline hydroxyapatite. *Powder Technol* 253:650–656
368. Fathi MH, Zahrani EM (2009) Fabrication and characterization of fluoridated hydroxyapatite nanopowders via mechanical alloying. *J Alloys Compd* 475:408–414
369. Fathi MH, Zahrani EM (2009) Mechanical alloying synthesis and bioactivity evaluation of nanocrystalline fluoridated hydroxyapatite. *J Cryst Growth* 311:1392–1403
370. Xu JL, Khor KA, Dong ZL, Gu YW, Kumar R, Cheang P (2004) Preparation and characterization of nanosized hydroxyapatite powders produced in a radio frequency (rf) thermal plasma. *Mater Sci Eng A* 374:101–108
371. Xu JL, Khor KA, Kumar R, Cheang P (2006) RF induction plasma synthesized calcium phosphate nanoparticles. *Key Eng Mater* 309–311:511–514
372. Ruksudjarit A, Pengpat K, Rujijanagul G, Tunkasiri T (2008) Synthesis and characterization of nanocrystalline hydroxyapatite from natural bovine bone. *Curr Appl Phys* 8:270–272
373. Cho JS, Kang YC (2008) Nano-sized hydroxyapatite powders prepared by flame spray pyrolysis. *J Alloys Compd* 464:282–287
374. Cho JS, Rhee SH (2013) Formation mechanism of nano-sized hydroxyapatite powders through spray pyrolysis of a calcium phosphate solution containing polyethylene glycol. *J Eur Ceram Soc* 33:233–241
375. Wang X, Zhuang J, Peng Q, Li Y (2006) Liquid-solid-solution synthesis of biomedical hydroxyapatite nanorods. *Adv Mater* 18:2031–2034
376. ShirkHzadeh M (1998) Direct formation of nanophase hydroxyapatite on cathodically polarized electrodes. *J Mater Sci Mater Med* 9:67–72
377. Montalbert-Smith R, Palma CA, Arias JD, Montero ML (2009) Formation of hydroxyapatite nanosized and other apatites by electrolysis process. *Key Eng Mater* 396–398:579–582
378. Gao JH, Guan SK, Chen J, Wang LG, Zhu SJ, Hu JH, Ren ZW (2011) Fabrication and characterization of rod-like nano-hydroxyapatite on MAO coating supported on Mg–Zn–Ca alloy. *Appl Surf Sci* 257:2231–2237

379. Nur A, Rahmawati A, Ilmi NI, Affandi S, Widjaja A, Setyawan H (2014) Electrochemical synthesis of nanosized hydroxyapatite by pulsed direct current method. *AIP Conf Proc* 1586:86–91
380. Krishna DSR, Siddharthan A, Seshadri SK, Kumar TSS (2007) A novel route for synthesis of nanocrystalline hydroxyapatite from eggshell waste. *J Mater Sci Mater Med* 18:1735–1743
381. Lak A, Mazloumi M, Mohajerani MS, Zanganeh S, Shayegh MR, Kajbafvala A, Arami H, Sadmezhaad SK (2008) Rapid formation of mono-dispersed hydroxyapatite nanorods with narrow-size distribution via microwave irradiation. *J Am Ceram Soc* 91:3580–3584
382. Kalita SJ, Verma S (2010) Nanocrystalline hydroxyapatite bioceramic using microwave radiation: synthesis and characterization. *Mater Sci Eng C* 30:295–303
383. Mishra VK, Srivastava SK, Asthana BP, Kumar D (2012) Structural and spectroscopic studies of hydroxyapatite nanorods, formed via microwave-assisted synthesis route. *J Am Ceram Soc* 95:2709–2715
384. Smolen D, Chudoba T, Malka I, Kedzierska A, Lojkowski W, Swieszkowski W, Kurzydowski KJ, Kolodziejczyk-Mierzynska M, Lewandowska-Szumiel M (2013) Highly biocompatible, nanocrystalline hydroxyapatite synthesized in a solvothermal process driven by high energy density microwave radiation. *Int J Nanomedicine* 8:653–668
385. Amer W, Abdelouahdi K, Ramanarivo HR, Zahouily M, Fihri A, Djessas K, Zahouily K, Varma RS, Solhy A (2014) Microwave-assisted synthesis of mesoporous nano-hydroxyapatite using surfactant templates. *Cryst Eng Comm* 16:543–549
386. Nabyouni M, Zhou H, Luchini TJJ, Bhaduri SB (2014) Formation of nanostructured fluorapatite via microwave assisted solution combustion synthesis. *Mater Sci Eng C* 37:363–368
387. Shavandi A, Bekhit AEDA, Ali A, Sun Z (2015) Synthesis of nano-hydroxyapatite (nHA) from waste mussel shells using a rapid microwave method. *Mater Chem Phys* 149:607–616
388. Hassan MN, Mahmoud MM, El-Fattah AA, Kandil S (2016) Microwave-assisted preparation of nano-hydroxyapatite for bone substitutes. *Ceram Int* 42:3725–3744
389. Shih WJ, Chen YF, Wang MC, Hon MH (2004) Crystal growth and morphology of the nanosized hydroxyapatite powders synthesized from  $\text{CaHPO}_4 \cdot 2\text{H}_2\text{O}$  and  $\text{CaCO}_3$  by hydrolysis method. *J Cryst Growth* 270:211–218
390. Furuichi K, Oaki Y, Imai H (2006) Preparation of nanotextured and nanofibrous hydroxyapatite through dicalcium phosphate with gelatin. *Chem Mater* 18:229–234
391. Zhang Y, Lu J (2008) The transformation of single-crystal calcium phosphate ribbon-like fibres to hydroxyapatite spheres assembled from nanorods. *Nanotechnology* 19:155608. (10 pages)
392. Ito H, Oaki Y, Imai H (2008) Selective synthesis of various nanoscale morphologies of hydroxyapatite via an intermediate phase. *Cryst Growth Des* 8:1055–1059
393. Hajiloo N, Ziaie F, Mehtieva SI (2012) Gamma-irradiated EPR response of nano-structure hydroxyapatite synthesised via hydrolysis method. *Radiat Prot Dosim* 148:487–491
394. Chen F, Zhu Y (2015) Microwave-assisted synthesis of calcium phosphate nanostructured materials in liquid phase. *Prog Chem* 27:459–471
395. Wang MC, Chen HT, Shih WJ, Chang HF, Hon MH, Hung IM (2015) Crystalline size, microstructure and biocompatibility of hydroxyapatite nanopowders by hydrolysis of calcium hydrogen phosphate dihydrate (DCPD). *Ceram Int* 41:2999–3008
396. Yoruç ABH, Koca Y (2009) Double step stirring: a novel method for precipitation of nanosized hydroxyapatite powder. *Dig J Nanomater Biostruct* 4:73–81
397. Jarudilokkul S, Tanthapanichakoon W, Boonamnuyvittaya V (2007) Synthesis of hydroxyapatite nanoparticles using an emulsion liquid membrane system. *Colloids Surf A Physicochem Eng Asp* 296:149–153
398. Guo G, Sun Y, Wang Z, Guo H (2005) Preparation of hydroxyapatite nanoparticles by reverse microemulsion. *Ceram Int* 31:869–872
399. Lim GK, Wang J, Ng SC, Gan LM (1999) Formation of nanocrystalline hydroxyapatite in nonionic surfactant emulsions. *Langmuir* 15:7472–7477



400. Sun Y, Guo G, Wang Z, Guo H (2006) Synthesis of single-crystal HAP nanorods. *Ceram Int* 32:951–954
401. Bose S, Saha SK (2003) Synthesis and characterization of hydroxyapatite nanopowders by emulsion technique. *Chem Mater* 15:4464–4469
402. Jiang FX, Lu XY, Zhang ML, Weng J (2008) Regulating size, morphology and dispersion of nano-crystallites of hydroxyapatite by pH value and temperature in microemulsion system. *Key Eng Mater* 361–363:195–198
403. Li H, Zhu MY, Li LH, Zhou CR (2008) Processing of nanocrystalline hydroxyapatite particles via reverse microemulsions. *J Mater Sci* 43:384–389
404. Koetz J, Baier J, Kosmella S (2007) Formation of zinc sulfide and hydroxylapatite nanoparticles in polyelectrolyte-modified microemulsions. *Colloid Polym Sci* 285:1719–1726
405. Lim HN, Kassim A, Huang NM (2010) Preparation and characterization of calcium phosphate nanorods using reverse microemulsion and hydrothermal processing routes. *Sains Malaysiana* 39:267–273
406. Furuzono T, Walsh D, Sato K, Sonoda K, Tanaka J (2001) Effect of reaction temperature on the morphology and size of hydroxyapatite nanoparticles in an emulsion system. *J Mater Sci Lett* 2:111–114
407. Sadjadi MAS, Akhavan K, Zare K (2011) Preparation of hydroxyapatite nanoparticles by reverse microemulsions and polyelectrolyte-modified microemulsions. *Res J Chem Environ* 15:959–962
408. García C, García C, Paucar C (2012) Controlling morphology of hydroxyapatite nanoparticles through hydrothermal microemulsion chemical synthesis. *Inorg Chem Commun* 20:90–92
409. Fan T, Sun Y, Ma L (2013) Controllable synthesis of spheroid hydroxyapatite nanoparticles by reverse microemulsion method. *Adv Mater Res* 602–604:227–230
410. Amin S, Siddique T, Mujahid M, Shah SS (2015) Synthesis and characterization of nano hydroxyapatite using reverse micro emulsions as nano reactors. *J Chem Soc Pak* 37:79–85
411. Shen SC, Chia L, Ng WK, Dong YC, Tan RBH (2010) Solid-phase steam-assisted synthesis of hydroxyapatite nanorods and nanoparticles. *J Mater Sci* 45:6059–6067
412. Jevtić M, Mitrić M, Škapin S, Jančar B, Ignjatović N, Uskoković D (2008) Crystal structure of hydroxyapatite nano-rods synthesized by sonochemical homogenous precipitation. *Cryst Growth Des* 8:2217–2222
413. Utara S, Klinkaewnarong J (2015) Sonochemical synthesis of nano-hydroxyapatite using natural rubber latex as a templating agent. *Ceram Int* 41:14860–14867
414. Cóta LF, Licona KPM, Lunz JN, Ribeiro AA, Morejón L, de Oliveira MV, Pereira LC (2016) Hydroxyapatite nanoparticles: synthesis by sonochemical method and assessment of processing parameters via experimental design. *Mater Sci Forum* 869:896–901
415. Wang YJ, Lai C, Wei K, Chen X, Ding Y, Wang ZL (2006) Investigations on the formation mechanism of hydroxyapatite synthesized by the solvothermal method. *Nanotechnology* 17:4405–4412
416. Chen F, Zhu YJ, Wang KW, Zhao KL (2011) Surfactant-free solvothermal synthesis of hydroxyapatite nanowire/nanotube ordered arrays with biomimetic structures. *Cryst Eng Comm* 13:1858–1863
417. Cao LY, Zhang CB, Huang JF (2005) Synthesis of hydroxyapatite nanoparticles in ultrasonic precipitation. *Ceram Int* 31:1041–1044
418. Liu J, Wu Q, Ding Y (2005) Self-assembly and fluorescent modification of hydroxyapatite nanoribbon spherulites. *Eur J Inorg Chem* 20:4145–4149
419. Huang J, Jayasinghe SN, Su X, Ahmad Z, Best SM, Edirisinghe MJ, Brooks RA, Rushton N, Bonfield W (2006) Electrostatic atomisation spraying: a novel deposition method for nano-sized hydroxyapatite. *Key Eng Mater* 309–311:635–638
420. Okada M, Furuzono T (2012) Hydroxylapatite nanoparticles: fabrication methods and medical applications. *Sci Technol Adv Mater* 13:064103. (14 pages)

421. Uota M, Arakawa H, Kitamura N, Yoshimura T, Tanaka J, Kijima T (2005) Synthesis of high surface area hydroxyapatite nanoparticles by mixed surfactant-mediated approach. *Langmuir* 21:4724–4728
422. Chu M, Liu G (2005) Preparation and characterization of hydroxyapatite/liposome core – shell nanocomposites. *Nanotechnology* 16:1208–1212
423. Huang F, Shen Y, Xie A, Zhu J, Zhang C, Li S, Zhu J (2007) Study on synthesis and properties of hydroxyapatite nanorods and its complex containing biopolymer. *J Mater Sci* 42:8599–8605
424. Wang A, Liu D, Yin H, Wu H, Wada Y, Ren M, Jiang T, Cheng X, Xu Y (2007) Size-controlled synthesis of hydroxyapatite nanorods by chemical precipitation in the presence of organic modifiers. *Mater Sci Eng C* 27:865–869
425. Ye F, Guo H, Zhang H (2008) Biomimetic synthesis of oriented hydroxyapatite mediated by nonionic surfactants. *Nanotechnology* 19:245605. (7 pages)
426. Han Y, Wang X, Li S (2009) A simple route to prepare stable hydroxyapatite nanoparticles suspension. *J Nanopart Res* 11:1235–1240
427. Tseng YH, Kuo CS, Li Y, Huang CP (2009) Polymer-assisted synthesis of hydroxyapatite nanoparticle. *Mater Sci Eng C* 29:819–822
428. Klinkaewnarong J, Swatsitang E, Maensiri S (2009) Nanocrystalline hydroxyapatite powders by a chitosan-polymer complex solution route: synthesis and characterization. *Solid State Sci* 11:1023–1027
429. Li Y, Li D, Xu Z (2009) Synthesis of hydroxyapatite nanorods assisted by Pluronic. *J Mater Sci* 44:1258–1263
430. Nayar S, Sinha MK, Basu D, Sinha A (2006) Synthesis and sintering of biomimetic hydroxyapatite nanoparticles for biomedical applications. *J Mater Sci Mater Med* 17:1063–1068
431. Yao X, Yao H, Li G, Li Y (2010) Biomimetic synthesis of needle-like nano-hydroxyapatite templated by double-hydrophilic block copolymer. *J Mater Sci* 45:1930–1936
432. Hong Y, Fan H, Li B, Guo B, Liu M, Zhang X (2010) Fabrication, biological effects, and medical applications of calcium phosphate nanoceramics. *Mater Sci Eng R* 70:225–242
433. Mostaghaci B, Fathi MH, Sheikh-Zeinoddin M, Soleimani-Zad S (2009) Bacterial synthesis of nanostructured hydroxyapatite using *Serratia marcescens* PTCC 1187. *Int J Nanotechnol* 6:1015–1030
434. Nathanael AJ, Hong SI, Mangalaraj D, Chen PC (2011) Large scale synthesis of hydroxyapatite nanospheres by high gravity method. *Chem Eng J* 173:846–854
435. Parisi M, Stoller M, Chianese A (2011) Production of nanoparticles of hydroxy apatite by using a rotating disk reactor. *Chem Eng Trans* 24:211–216
436. Yuan J, Wu Y, Zheng Q, Xie X (2011) Synthesis and characterization of nano hydroxylapatite by reaction precipitation in impinging streams. *Adv Mater Res* 160–162:1301–1308
437. Mohn D, Doebelin N, Tadier S, Bernabei RE, Luechinger NA, Stark WJ, Bohner M (2011) Reactivity of calcium phosphate nanoparticles prepared by flame spray synthesis as precursors for calcium phosphate cements. *J Mater Chem* 21:13963–13972
438. Kandori K, Kuroda T, Togashi S, Katayama E (2011) Preparation of calcium hydroxyapatite nanoparticles using microreactor and their characteristics of protein adsorption. *J Phys Chem B* 115:653–659
439. He W, Kjellin P, Currie F, Handa P, Knee CS, Bielecki J, Wallenberg LR, Andersson M (2012) Formation of bone-like nanocrystalline apatite using self-assembled liquid crystals. *Chem Mater* 24:892–902
440. Chandanshive BB, Rai P, Rossi AL, Ersen O, Khushalani D (2013) Synthesis of hydroxyapatite nanotubes for biomedical applications. *Mater Sci Eng C* 33:2981–2986
441. Mousa S, Hanna A (2013) Synthesis of nano-crystalline hydroxyapatite and ammonium sulfate from phosphogypsum waste. *Mater Res Bull* 48:823–828
442. Wang X, Qian C, Yu X (2014) Synthesis of nano-hydroxyapatite via microbial method and its characterization. *Appl Biochem Biotechnol* 173:1003–1010

443. Zhang Y, Wang J, Sharma VK (2014) Designed synthesis of hydroxyapatite nanostructures: bullet-like single crystal and whiskered hollow ellipsoid. *J Mater Sci Mater Med* 25:1395–1401
444. Omori Y, Okada M, Takeda S, Matsumoto N (2014) Fabrication of dispersible calcium phosphate nanocrystals via a modified Pechini method under non-stoichiometric conditions. *Mater Sci Eng C* 42:562–568
445. He W, Fu Y, Andersson M (2014) Morphological control of calcium phosphate nanostructures using lyotropic liquid crystals. *J Mater Chem B* 2:3214–3220
446. Holopainen J, Santala E, Heikkilä M, Ritala M (2015) Electrospinning of calcium carbonate fibers and their conversion to nanocrystalline hydroxyapatite. *Mater Sci Eng C* 45:469–476
447. Okada M, Matsumoto T (2015) Synthesis and modification of apatite nanoparticles for use in dental and medical applications. *Jpn Dent Sci Rev* 51:85–95
448. Peng H, Wang J, Lv S, Wen J, Chen JF (2015) Synthesis and characterization of hydroxyapatite nanoparticles prepared by a high-gravity precipitation method. *Ceram Int* 41:14340–14349
449. Costa DO, Dixon SJ, Rizkalla AS (2012) One- and three-dimensional growth of hydroxyapatite nanowires during sol-gel-hydrothermal synthesis. *ACS Appl Mater Interfaces* 4:1490–1499
450. He J, Zhang K, Wu S, Cai X, Chen K, Li Y, Sun B, Jia Y, Meng F, Jin Z, Kong L, Liu J (2016) Performance of novel hydroxyapatite nanowires in treatment of fluoride contaminated water. *J Hazard Mater* 303:119–130
451. Shuk P, Suchanek WL, Hao T, Gulliver E, Riman RE, Senna M, TenHuisen KS, Janas VF (2001) Mechanochemical-hydrothermal preparation of crystalline hydroxyapatite powders at room temperature. *J Mater Res* 16:1231–1234
452. Suchanek WL, Shuk P, Byrappa K, Riman RE, TenHuisen KS, Janas VF (2002) Mechanochemical-hydrothermal synthesis of carbonated apatite powders at room temperature. *Biomaterials* 23:699–710
453. Abdel-Aal EA, El-Midany AA, El-Shall H (2008) Mechanochemical-hydrothermal preparation of nano-crystallite hydroxyapatite using statistical design. *Mater Chem Phys* 112:202–207
454. Ji Y, Wang A, Wu G, Yin H, Liu S, Chen B, Liu F, Li X (2015) Synthesis of different sized and porous hydroxyapatite nanorods without organic modifiers and their 5-fluorouracil release performance. *Mater Sci Eng C* 57:14–23
455. Yang Q, Wang JX, Guo F, Chen JF (2010) Preparation of hydroxyapatite nanoparticles by using high-gravity reactive precipitation combined with hydrothermal method. *Ind Eng Chem Res* 49:9857–9863
456. Song X, Ling F, Li H, Gao Z, Chen X (2012) Tuned morphological electrospun hydroxyapatite nanofibers via pH. *J Bionic Eng* 9:478–483
457. Tadic D, Veresov A, Putlayev VI, Epple M (2003) In-vitro preparation of nanocrystalline calcium phosphates as bone substitution materials in surgery. *Mater Wiss Werkst* 34:1048–1051
458. Yang Q, Wang JX, Shao L, Wang QA, Guo F, Chen JF, Gu L, An YT (2010) High throughput methodology for continuous preparation of hydroxyapatite nanoparticles in a microporous tube-in-tube microchannel reactor. *Ind Eng Chem Res* 49:140–147
459. Liu K, Qin J (2013) Droplet-fused microreactors for room temperature synthesis of nanoscale needle-like hydroxyapatite. *Nanotechnology* 24:125602. (7 pages)
460. Fujii E, Kawabata K, Shirosaki Y, Hayakawa S, Osaka A (2015) Fabrication of calcium phosphate nanoparticles in a continuous flow tube reactor. *J Ceram Soc Jpn* 123:101–105
461. An GH, Wang HJ, Kim BH, Jeong YG, Choa YH (2007) Fabrication and characterization of a hydroxyapatite nanopowder by ultrasonic spray pyrolysis with salt-assisted decomposition. *Mater Sci Eng A* 448–451:821–824
462. Qiu Y, Xia H, Jiang H (2010) Fabrication of nano-hydroxyapatite using a novel ultrasonic atomization precipitation method. *J Nanosci Nanotechnol* 10:2213–2218
463. Rouhani P, Taghavinia N, Rouhani S (2010) Rapid growth of hydroxyapatite nanoparticles using ultrasonic irradiation. *Ultrason Sonochem* 17:853–856

464. Giardina MA, Fanovich MA (2010) Synthesis of nanocrystalline hydroxyapatite from  $\text{Ca}(\text{OH})_2$  and  $\text{H}_3\text{PO}_4$  assisted by ultrasonic irradiation. *Ceram Int* 36:1961–1969
465. Girija EK, Kumar GS, Thamizhavel A, Yokogawa Y, Kalkura SN (2012) Role of material processing on the thermal stability and sinterability of nanocrystalline hydroxyapatite. *Powder Technol* 225:190–195
466. Gopi D, Indira J, Kavitha L, Sekar M, Mudali UK (2012) Synthesis of hydroxyapatite nanoparticles by a novel ultrasonic assisted with mixed hollow sphere template method. *Spectrochim Acta A* 93:131–134
467. Kojima Y, Kitazawa K, Nishimiya N (2012) Synthesis of nano-sized hydroxyapatite by ultrasound irradiation. *J Phys Conf Ser* 339:12001. (4 pages)
468. Zhang YG, Zhu YJ, Chen F, Wu J (2015) Ultralong hydroxyapatite nanowires synthesized by solvothermal treatment using a series of phosphate sodium salts. *Mater Lett* 144:135–137
469. Brundavanam S, Poinern GEJ, Fawcett D (2015) Synthesis of a hydroxyapatite nanopowder via ultrasound irradiation from calcium hydroxide powders for potential biomedical applications. *Nanosci Nanoeng* 3:1–7
470. Sadjadi MS, Meskinfam M, Sadeghi B, Jazdarreh H, Zare K (2010) In situ biomimetic synthesis, characterization and in vitro investigation of bone-like nanohydroxyapatite in starch matrix. *Mater Chem Phys* 124:217–222
471. Pandi K, Viswanathan N (2015) In situ precipitation of nano-hydroxyapatite in gelatin poly-matrix towards specific fluoride sorption. *Int J Biol Macromol* 74:351–359
472. Mhin SW, Ryu JH, Kim KM, Park GS, Ryu HW, Shim KB, Sasaki T, Koshizaki N (2009) Simple synthetic route for hydroxyapatite colloidal nanoparticles via a Nd:YAG laser ablation in liquid medium. *Appl Phys A Mater Sci Process* 96A:435–440
473. Musaeov OR, Dusevich V, Wieliczka DM, Wrobel JM, Kruger MB (2008) Nanoparticle fabrication of hydroxyapatite by laser ablation in water. *J Appl Phys* 104:084316. (5 pages)
474. Boutinguiza M, Lusquiños F, Riveiro A, Comesaña R, Pou J (2009) Hydroxylapatite nanoparticles obtained by fiber laser-induced fracture. *Appl Surf Sci* 255:5382–5385
475. Boutinguiza M, Pou J, Lusquiños F, Comesaña R, Riveiro A (2011) Production of calcium phosphate nanoparticles by laser ablation in liquid. *Phys Procedia* 12:54–59
476. Boutinguiza M, Comesaña R, Lusquiños F, Riveiro A, Pou J (2011) Production of nanoparticles from natural hydroxylapatite by laser ablation. *Nanoscale Res Lett* 6:1–5
477. Zuo Y, Li YB, Wei J, Yan Y (2003) Influence of ethylene glycol on the formation of calcium phosphate nanocrystals. *J Mater Sci Technol* 19:628–630
478. Barinov SM, Belonogov EK, Ievlev VM, Kostyuchenko AV, Putlyaev VI, Tret'yakov YD, Smirnov VV, Fadeeva IV (2007) Synthesis of dense nanocrystalline hydroxyapatite films. *Dokl Phys Chem* 412:15–18
479. Mello A, Mavropoulos E, Hong Z, Ketterson JB, Rossi AM (2009) Nanometer coatings of hydroxyapatite characterized by glancing-incidence X-ray diffraction. *Key Eng Mater* 396–398:369–372
480. Nassif N, Martineau F, Syzgantseva O, Gobeaux F, Willinger M, Coradin T, Cassaignon S, Azaïs T, Giraud-Guille MM (2010) In vivo inspired conditions to synthesize biomimetic hydroxyapatite. *Chem Mater* 22:3653–3663
481. Iafisco M, Morales JG, Hernández-Hernández MA, García-Ruiz JM, Roveri N (2010) Biomimetic carbonate-hydroxyapatite nanocrystals prepared by vapor diffusion. *Adv Eng Mater* 12:B218–B223
482. Iafisco M, Delgado-López JM, Gómez-Morales J, Hernández-Hernández MA, Rodríguez-Ruiz I, Roveri N (2011) Formation of calcium phosphates by vapour diffusion in highly concentrated ionic micro-droplets. *Cryst Res Technol* 46:841–846
483. Rivera-Muñoz EM, Velázquez-Castillo R, Huirache-Acuña R, Cabrera-Torres JL, Arenas-Alatorre J (2012) Synthesis and characterization of hydroxyapatite-based nanostructures: nanoparticles, nanoplates, nanofibers and nanoribbons. *Mater Sci Forum* 706–709:589–594
484. Zhou C, Hong Y, Zhang X (2013) Applications of nanostructured calcium phosphate in tissue engineering. *Biomater Sci* 1:1012–1028

485. Zhao H, Zhu YD, Sun J, Wei D, Wang KF, Liu M, Fan HS, Zhang XD (2014) Synthesis of hollow hydroxyapatite nanospheres by the control of nucleation and growth in a two phase system. *Chem Commun* 50:12519–12522
486. Lee JH, Kim YJ (2014) Hydroxyapatite nanofibers fabricated through electrospinning and sol-gel process. *Ceram Int* 40:3361–3369
487. Hui J, Wang X (2014) Hydroxyapatite nanocrystals: colloidal chemistry, assembly and their biological applications. *Inorg Chem Front* 1:215–225
488. Luo P, Nieh TG (1995) Synthesis of ultrafine hydroxyapatite particles by a spray dry method. *Mater Sci Eng C* 3:75–78
489. Chen F, Wang ZC, Chang JL (2002) Preparation and characterization of nanosized hydroxyapatite particles and hydroxyapatite/chitosan nano-composite for use in biomedical materials. *Mater Lett* 57:858–861
490. Sarig S, Kahana F (2002) Rapid formation of nanocrystalline apatite. *J Cryst Growth* 237–239:55–59
491. Bose S, Saha SK (2003) Synthesis of hydroxyapatite nanopowders via sucrose-templated sol-gel method. *J Am Ceram Soc* 86:1055–1057
492. Han Y, Li S, Wang X, Chen X (2004) Synthesis and sintering of nanocrystalline hydroxyapatite powders by citric acid sol-gel combustion method. *Mater Res Bull* 39:25–32
493. Liu DM, Yang Q, Troczynski T, Tseng WJ (2002) Structural evolution of sol-gel-derived hydroxyapatite. *Biomaterials* 23:1679–1687
494. Liu DM, Troczynski T, Tseng WJ (2001) Water-based sol-gel synthesis of hydroxyapatite: process development. *Biomaterials* 22:1721–1730
495. Wang F, Li MS, Lu YP, Ge SS (2005) Synthesis of nanocrystalline hydroxyapatite powders in stimulated body fluid. *J Mater Sci* 40:2073–2076
496. Wang J, Shaw LL (2009) Synthesis of high purity hydroxyapatite nanopowder via sol-gel combustion process. *J Mater Sci Mater Med* 20:1223–1227
497. Varma HK, Kalkura SN, Sivakumar R (1998) Polymeric precursor route for the preparation of calcium phosphate compounds. *Ceram Int* 24:467–470
498. Ghosh SK, Roy SK, Kundu B, Datta S, Basu D (2011) Synthesis of nano-sized hydroxyapatite powders through solution combustion route under different reaction conditions. *Mater Sci Eng B* 176:14–21
499. Loher S, Stark WJ, Maciejewski M, Baiker A, Pratsinis SE, Reichardt D, Maspero F, Krumeich F, Günther D (2005) Fluoro-apatite and calcium phosphate nanoparticles by flame synthesis. *Chem Mater* 17:36–42
500. Zheo J, Dong X, Bian M, Zhao J, Zhang Y, Sun Y, Chen J, Wang X (2014) Solution combustion method for synthesis of nanostructured hydroxyapatite, fluorapatite and chlorapatite. *Appl Surf Sci* 314:1026–1033
501. Wagner DE, Lawrence J, Bhaduri SB (2013) Microwave-assisted solution combustion synthesis of high aspect ratio calcium phosphate nanoparticles. *J Mater Res* 28:3119–3129
502. Trommer RM, Santos LA, Bergmann CP (2009) Nanostructured hydroxyapatite powders produced by a flame-based technique. *Mater Sci Eng C* 29:1770–1775
503. Chow LC, Sun L, Hockey B (2004) Properties of nanostructured hydroxyapatite prepared by a spray drying technique. *J Res Natl Inst Stand Technol* 109:543–551
504. Li J, Chen YP, Yin Y, Yao F, Yao K (2007) Modulation of nano-hydroxyapatite size via formation on chitosan-gelatin network film in situ. *Biomaterials* 28:781–790
505. Zhai Y, Cui FZ, Wang Y (2005) Formation of nano hydroxyapatite on recombinant human like collagen fibrils. *Curr Appl Phys* 5:429–432
506. Liou SC, Chen SY, Liu DM (2003) Synthesis and characterization of needlelike apatitic nanocomposite with controlled aspect ratios. *Biomaterials* 24:3981–3988
507. Liou SC, Chen SY, Liu DM (2005) Manipulation of nanoneedle and nanosphere apatite/poly(acrylic acid) nanocomposites. *J Biomed Mater Res B Appl Biomater* 73B:117–122
508. Amjad Z (1995) Performance of polymeric additives as HA crystal growth inhibitors. *Phosphorus Res Bull* 5:1–12

509. Kamitahara M, Kawashita M, Kokubo T, Nakamura T (2001) Effect of polyacrylic acid on the apatite formation of a bioactive ceramic in a simulated body fluid: fundamental examination of the possibility of obtaining bioactive glass-ionomer cements for orthopedic use. *Biomaterials* 22:3191–3196
510. Wang X, Li Y, Wei J, de Groot K (2002) Development of biomimetic nano-hydroxyapatite/poly(hexamethylene adipamide) composites. *Biomaterials* 23:4787–4791
511. Sinha A, Nayar S, Agrawal AC (2003) Synthesis of nanosized and microporous precipitated hydroxyapatite in synthetic polymers and biopolymers. *J Am Ceram Soc* 86:357–359
512. Liao S, Watari F, Zhu Y, Uo M, Akasaka T, Wang W, Xu G, Cui F (2007) The degradation of the three layered nano-carbonated hydroxyapatite/collagen/PLGA composite membrane in vitro. *Dent Mater* 23:1120–1128
513. Gonzalez-McQuire R, Chane-Ching JY, Vignaud E, Lebugle A, Mann S (2004) Synthesis and characterization of amino acid-functionalized hydroxyapatite nanorods. *J Mater Chem* 14:2277–2281
514. Rosseeva EV, Golovanova OA, Frank-Kamenetskaya OV (2007) The influence of amino acids on the formation of nanocrystalline hydroxyapatite. *Glas Phys Chem* 33:283–286
515. Zhan J, Tseng YH, Chan JCC, Mou CY (2005) Biomimetic formation of hydroxyapatite nanorods by a single-crystal-to-single-crystal transformation. *Adv Funct Mater* 15:2005–2010
516. Xu AW, Ma Y, Cölfen H (2007) Biomimetic mineralization. *J Mater Chem* 17:415–449
517. Pileni M (2003) The role of soft colloidal templates in controlling the size and shape of inorganic nanocrystals. *Nat Mater* 12:145–150
518. Wu Y, Bose S (2005) Nanocrystalline hydroxyapatite: micelle templated synthesis and characterization. *Langmuir* 21:3232–3234
519. Wei K, Lai C, Wang Y (2006) Solvothermal synthesis of calcium phosphate nanowires under different pH conditions. *J Macromol Sci A* 43A:1531–1540
520. Lai C, Tang SQ, Wang YJ, Wei K, Zhang SY (2005) Insight into shape control mechanism of calcium phosphate nanoparticles in reverse micelles solution. *Synth React Inorg Met Met Org Nano Metal Chem* 35:717–725
521. Banerjee A, Bandyopadhyay A, Bose S (2007) Hydroxyapatite nanopowders: synthesis, densification and cell-materials interaction. *Mater Sci Eng C* 27:729–735
522. Han JY, Tan TTY, Loo JSC (2011) Utilizing inverse micelles to synthesize calcium phosphate nanoparticles as nano-carriers. *J Nanopart Res* 13:3441–3454
523. Shchukin DG, Sukhorukov GB, Möhwald H (2003) Biomimetic fabrication of nanoengineered hydroxyapatite/polyelectrolyte composite shell. *Chem Mater* 15:3947–3950
524. Mateus AYP, Ferraz MP, Monteiro FJ (2007) Microspheres based on hydroxyapatite nanoparticles aggregates for bone regeneration. *Key Eng Mater* 330–332:243–246
525. Nguyen NK, Leoni M, Maniglio D, Migliaresi C (2012) Hydroxyapatite nanorods: soft-template synthesis, characterization and preliminary in vitro tests. *J Biomater Appl* 28:49–61
526. Mossaad C, Tan MC, Starr M, Payzant EA, Howe JY, Riman RE (2011) Size-dependent crystalline to amorphous uphill phase transformation of hydroxyapatite nanoparticles. *Cryst Growth Des* 11:45–52
527. Šupová M (2014) Isolation and preparation of nanoscale bioapatites from natural sources: a review. *J Nanosci Nanotechnol* 14:546–563
528. Guo Y, Shi D, Lian J, Dong Z, Wang W, Cho H, Liu G, Wang L, Ewing RC (2008) Quantum dot conjugated hydroxyapatite nanoparticles for in vivo imaging. *Nanotechnology* 19:175102. (6 pages)
529. Wang X, Fang Z, Liu J, Zhong X, Ye B (2010) High sensibility of quantum dots to metal ions inspired by hydroxyapatite microbeads. *Chin J Chem* 28:1005–1012
530. Liu Q, de Wijn JR, de Groot K, van Blitterswijk CA (1998) Surface modification of nanoapatite by grafting organic polymer. *Biomaterials* 19:1067–1072
531. Palazzo B, Iafisco M, Laforgia M, Margiotta N, Natile G, Bianchi CL, Walsh D, Mann S, Roveri N (2007) Biomimetic hydroxyapatite-drug nanocrystals as potential bone substitutes with antitumor drug delivery properties. *Adv Funct Mater* 17:2180–2188

532. Lee HJ, Choi HW, Kim KJ, Lee SC (2006) Modification of hydroxyapatite nanosurfaces for enhanced colloidal stability and improved interfacial adhesion in nanocomposites. *Chem Mater* 18:5111–5118
533. Lee SC, Choi HW, Lee HJ, Kim KJ, Chang JH, Kim SY, Choi J, Oh KS, Jeong YK (2007) In-situ synthesis of reactive hydroxyapatite nanocrystals for a novel approach of surface grafting polymerization. *J Mater Chem* 17:174–180
534. Li L, Liu YK, Tao JH, Zhang M, Pan HH, Xu XR, Tang RK (2008) Surface modification of hydroxyapatite nanocrystallite by a small amount of terbium provides a biocompatible fluorescent probe. *J Phys Chem C* 112:12219–12224
535. Neumeier M, Hails LA, Davis SA, Mann S, Epple M (2011) Synthesis of fluorescent core-shell hydroxyapatite nanoparticles. *J Mater Chem* 21:1250–1254
536. Wang W, Shi D, Lian J, Guo Y, Liu G, Wang L, Ewing RC (2006) Luminescent hydroxylapatite nanoparticles by surface functionalization. *Appl Phys Lett* 89:183106. (3 pages)
537. Liu H, Xi P, Xie G, Chen F, Li Z, Bai D, Zeng Z (2011) Biocompatible hydroxyapatite nanoparticles as a redox luminescence switch. *J Biol Inorg Chem* 16:1135–1140
538. Saoiabi S, El Asri S, Laghzizil A, Masse S, Ackerman JL (2012) Synthesis and characterization of nanoapatites organofunctionalized with aminotriphosphonate agents. *J Solid State Chem* 185:95–100
539. Sharma R, Pandey RR, Gupta AA, Kar S, Dhayal M (2012) In situ amino acid functionalization and microstructure formation of hydroxyapatite nanoparticles synthesized at different pH by precipitation route. *Mater Chem Phys* 133:718–725
540. Escudero A, Calvo ME, Rivera-Fernández S, de la Fuente JM, Ocaña M (2013) Microwave-assisted synthesis of biocompatible europium-doped calcium hydroxyapatite and fluoroapatite luminescent nanospindles functionalized with poly(acrylic acid). *Langmuir* 29:1985–1994
541. Parthiban SP, Kim IY, Kikuta K, Ohtsuki C (2013) Formation of serrated nanorods of hydroxyapatite through organic modification under hydrothermal processing. *J Nanopart Res* 15:1657. (10 pages)
542. Sharma S, Verma A, Teja BV, Pandey G, Mittapelly N, Trivedi R, Mishra PR (2015) An insight into functionalized calcium based inorganic nanomaterials in biomedicine: trends and transitions. *Colloids Surf B: Biointerfaces* 133:120–139
543. Sadat-Shojai M, Khorasani MT, Dinpanah-Khoshdargi E, Jamshidi A (2013) Synthesis methods for nanosized hydroxyapatite with diverse structures. *Acta Biomater* 9:7591–7621
544. Bow JS, Liou SC, Chen SY (2004) Structural characterization of room-temperature synthesized nanosized  $\beta$ -tricalcium phosphate. *Biomaterials* 25:3155–3161
545. Brunner TJ, Bohner M, Dora C, Gerber C, Stark WJ (2007) Comparison of amorphous TCP nanoparticles to micron-sized  $\alpha$ -TCP as starting materials for calcium phosphate cements. *J Biomed Mater Res B Appl Biomater* 83B:400–407
546. Brunner TJ, Grass RN, Bohner M, Stark WJ (2007) Effect of particle size, crystal phase and crystallinity on the reactivity of tricalcium phosphate cements for bone reconstruction. *J Mater Chem* 17:4072–4078
547. Döbelin N, Brunner TJ, Stark WJ, Eggimann M, Fisch M, Bohner M (2009) Phase evolution of thermally treated amorphous tricalcium phosphate nanoparticles. *Key Eng Mater* 396–398:595–598
548. Bohner M, Brunner TJ, Döbelin N, Tang R, Stark WJ (2008) Effect of thermal treatments on the reactivity of nanosized tricalcium phosphate powders. *J Mater Chem* 18:4460–4467
549. Liu YH, Zhang SM, Liu L, Zhou W, Hu W, Li J, Qiu ZY (2007) Rapid wet synthesis of nanosized  $\beta$ -TCP by using dialysis. *Key Eng Mater* 330–332:199–202
550. Abdel-Fattah WI, Reicha FM, Elkhooly TA (2008) Nano-beta-tricalcium phosphates synthesis and biodegradation: 1. Effect of microwave and  $\text{SO}_4^{2-}$  ions on  $\beta$ -TCP synthesis and its characterization. *Biomed Mater* 3:034121. (13 pages)
551. Vecbiskena L, Gross KA, Riekstina U, Yang TCK (2015) Crystallized nano-sized alpha-tricalcium phosphate from amorphous calcium phosphate: microstructure, cementation and cell response. *Biomed Mater* 10:025009

552. Sanosh KP, Chu MC, Balakrishnan A, Kim TN, Cho SJ (2010) Sol-gel synthesis of pure nano sized  $\beta$ -tricalcium phosphate crystalline powders. *Curr Appl Phys* 10:68–71
553. Dasgupta S, Bandyopadhyay A, Bose S (2009) Reverse micelle-mediated synthesis of calcium phosphate nanocarriers for controlled release of bovine serum albumin. *Acta Biomater* 5:3112–3121
554. Xia C, Deng X, Lin YH, Nan CW (2010) Preparation and characterisation of nano-sized beta-tricalcium phosphate with a ps template method. *Int J Mater Prod Technol* 37:257–262
555. Bucur AI, Bucur R, Vlase T, Docă N (2012) Thermal analysis and high-temperature X-ray diffraction of nano-tricalcium phosphate crystallization. *J Therm Anal Calorim* 107:249–255
556. Hoonnivathana E, Pankaew P, Klumdoung P, Limsuwan P, Naemchanthara K (2012) Synthesis of nanocrystalline  $\beta$ -tricalcium phosphate from chicken eggshells by precipitation method. *Adv Mater Res* 506:86–89
557. Choi D, Kumta PN (2007) Mechano-chemical synthesis and characterization of nanostructured  $\beta$ -TCP powder. *Mater Sci Eng C* 27:377–381
558. Nikčević I, Maravić D, Ignjatović N, Mitrić M, Makovec D, Uskoković D (2006) The formation and characterization of nanocrystalline phases by mechanical milling of biphasic calcium phosphate/poly-L-lactide biocomposite. *Mater Trans* 47:2980–2986
559. Cho JS, Jung DS, Han JM, Kang YC (2009) Nano-sized  $\alpha$  and  $\beta$ -TCP powders prepared by high temperature flame spray pyrolysis. *Mater Sci Eng C* 29:1288–1292
560. Ataol S, Tezcaner A, Duygulu O, Keskin D, Machin NE (2015) Synthesis and characterization of nanosized calcium phosphates by flame spray pyrolysis, and their effect on osteogenic differentiation of stem cells. *J Nanopart Res* 17:95. (14 pages)
561. Nasiri-Tabrizi B, Fahami A (2014) Production of poorly crystalline tricalcium phosphate nanopowders using different mechanochemical reactions. *J Ind Eng Chem* 20:1236–1242
562. Boutinguiza M, Pou J, Lusquinos F, Comesaña R, Riveiro A (2011) Laser-assisted production of tricalcium phosphate nanoparticles from biological and synthetic hydroxyapatite in aqueous medium. *Appl Surf Sci* 257:5195–5199
563. Jalota S, Tas AC, Bhaduri SB (2004) Microwave-assisted synthesis of calcium phosphate nanowhiskers. *J Mater Res* 19:1876–1881
564. Rameshbabu N, Rao KP (2009) Microwave synthesis, characterization and in-vitro evaluation of nanostructured biphasic calcium phosphates. *Curr Appl Phys* 9:S29–S31
565. Li B, Chen X, Guo B, Wang X, Fan H, Zhang X (2009) Fabrication and cellular biocompatibility of porous carbonated biphasic calcium phosphate ceramics with a nanostructure. *Acta Biomater* 5:134–143
566. Pasand EG, Nemati A, Solati-Hashjin M, Arzani K, Farzadi A (2012) Microwave assisted synthesis & properties of nano HA-TCP biphasic calcium phosphate. *Int J Miner Metall Mater* 19:441–445
567. Guha AK, Singh S, Kumaresan R, Nayar S, Sinha A (2009) Mesenchymal cell response to nanosized biphasic calcium phosphate composites. *Colloids Surf B: Biointerfaces* 73:146–151
568. Reddy S, Wasnik S, Guha A, Kumar JM, Sinha A, Singh S (2013) Evaluation of nano-biphasic calcium phosphate ceramics for bone tissue engineering applications: in vitro and preliminary in vivo studies. *J Biomater Appl* 27:565–575
569. Layrolle P, Lebugle A (1996) Synthesis in pure ethanol and characterization of nanosized calcium phosphate fluoroapatite. *Chem Mater* 8:134–144
570. Andres C, Sinani V, Lee D, Gun'ko Y, Kotov N (2006) Anisotropic calcium phosphate nanoparticles coated with 2-carboxyethylphosphonic acid. *J Mater Chem* 16:3964–3968
571. Lim H, Kassim A, Huang N, Hashim R, Radiman S, Khiew P, Chiu W (2009) Fabrication and characterization of 1D brushite nanomaterials via sucrose ester reverse microemulsion. *Ceram Int* 35:2891–2897
572. Maity JP, Lin TJ, Cheng HP, Chen CY, Reddy AS, Atla SB, Chang YF, Chen HR, Chen CC (2011) Synthesis of brushite particles in reverse microemulsions of the biosurfactant surfactin. *Int J Mol Sci* 12:3821–3830



573. Rodrigues MC, Hewer TLR, de Souza Brito GE, Arana-Chavez VE, Braga RR (2014) Calcium phosphate nanoparticles functionalized with a dimethacrylate monomer. *Mater Sci Eng C* 45:122–126
574. ShirkHzanadeh M, Sims S (1997) Immobilization of calcium phosphate nano-clusters into alkoxy-derived porous TiO<sub>2</sub> coatings. *J Mater Sci Mater Med* 8:595–601
575. Schmidt HT, Ostafin AE (2002) Liposome directed growth of calcium phosphate nanoshells. *Adv Mater* 14:532–535
576. Schmidt HT, Gray BL, Wingert PA, Ostafin AE (2004) Assembly of aqueous-cored calcium phosphate nanoparticles for drug delivery. *Chem Mater* 16:4942–4947
577. Yeo CH, Zein SHS, Ahmad AL, McPhail DS (2012) Comparison of DOPA and DPPA liposome templates for the synthesis of calcium phosphate nanoshells. *Ceram Int* 38:561–570
578. Singh S, Bhardwaj P, Singh V, Aggarwal S, Mandal UK (2008) Synthesis of nanocrystalline calcium phosphate in microemulsion – effect of nature of surfactants. *J Colloid Interface Sci* 319:322–329
579. Singh S, Singh V, Aggarwal S, Mandal UK (2010) Synthesis of brushite nanoparticles at different temperatures. *Chem Pap* 64:491–498
580. Walsh D, Mann S (1996) Chemical synthesis of microskeletal calcium phosphate in bicontinuous microemulsions. *Chem Mater* 8:1944–1953
581. Xu HHK, Sun L, Weir MD, Antonucci JM, Takagi S, Chow LC, Peltz M (2006) Nano DCPA – whisker composites with high strength and Ca and PO<sub>4</sub> release. *J Dent Res* 85:722–727
582. Xu HHK, Weir MD, Sun L, Takagi S, Chow LC (2007) Effects of calcium phosphate nanoparticles on Ca-PO<sub>4</sub> composite. *J Dent Res* 86:378–383
583. Xu HHK, Weir MD, Sun L (2007) Nanocomposites with Ca and PO<sub>4</sub> release: effects of reinforcement, dicalcium phosphate particle size and silanization. *Dent Mater* 23:1482–1491
584. Reardon PJT, Huang J, Tang J (2015) Mesoporous calcium phosphate bionanomaterials with controlled morphology by an energy-efficient microwave method. *J Biomed Mater Res A* 103A:3781–3789
585. Djošić MS, Mišković-Stanković VB, Kačarević-Popović ZM, Jokić BM, Bibić N, Mitrić M, Milonjić SK, Jančić-Heinemann R, Stojanović J (2009) Electrochemical synthesis of nanosized monetite powder and its electrophoretic deposition on titanium. *Colloids Surf A Physicochem Eng Asp* 341:110–117
586. Wei K, Lai C, Wang Y (2007) Formation of monetite nanoparticles and nanofibers in reverse micelles. *J Mater Sci* 42:5340–5346
587. Ma Z, Chen F, Zhu YJ, Cui T, Liu XY (2011) Amorphous calcium phosphate/poly(D,L-lactic acid) composite nanofibers: electrospinning preparation and biomineralization. *J Colloid Interface Sci* 15:371–379
588. Urch H, Vallet-Regí M, Ruiz L, Gonzalez-Calbet JM, Epple M (2009) Calcium phosphate nanoparticles with adjustable dispersability and crystallinity. *J Mater Chem* 19:2166–2171
589. Holt C, Wahlgren NM, Drakenberg T (1996) Ability of a  $\beta$ -casein phosphopeptide to modulate the precipitation of calcium phosphate by forming amorphous dicalcium phosphate nanoclusters. *Biochem J* 314:1035–1039
590. Holt C, Timmins PA, Errington N, Leaver J (1998) A core-shell model of calcium phosphate nanoclusters stabilized by  $\beta$ -casein phosphopeptides, derived from sedimentation equilibrium and small-angle X-ray and neutron-scattering measurements. *Eur J Biochem* 252:73–78
591. Duan B, Wang M, Zhou WY, Cheung WL (2008) Synthesis of Ca-P nanoparticles and fabrication of Ca-P/PHBV nanocomposite microspheres for bone tissue engineering applications. *Appl Surf Sci* 255:529–533
592. Zhou H, Bhaduri S (2012) Novel microwave synthesis of amorphous calcium phosphate nanospheres. *J Biomed Mater Res B Appl Biomater* 100B:1142–1150
593. Zhao J, Zhu YJ, Cheng GF, Ruan YJ, Sun TW, Chen F, Wu J, Zhao XY, Ding GJ (2014) Microwave-assisted hydrothermal rapid synthesis of amorphous calcium phosphate nanoparticles and hydroxyapatite microspheres using cytidine 5'-triphosphate disodium salt as a phosphate source. *Mater Lett* 124:208–211

594. Ding GJ, Zhu YJ, Qi C, Sun TW, Wu J, Chen F (2015) Amorphous calcium phosphate nanowires prepared using beta-glycerophosphate disodium salt as an organic phosphate source by a microwave-assisted hydrothermal method and adsorption of heavy metals in water treatment. *RSC Adv* 5:40154–40162
595. Hwang KS, Jeon KO, Jeon YS, Kim BH (2006) Hydroxyapatite forming ability of electrostatic spray pyrolysis derived calcium phosphate nano powder. *J Mater Sci* 41:4159–4162
596. Hwang KS, Jeon KO, Jeon YS, Kim BH (2007) Hydroxyapatite forming ability of electrostatic spray pyrolysis derived calcium phosphate nano powder. *J Mater Sci Mater Med* 18:619–622
597. Nasiri-Tabrizi B, Fahami A (2013) Mechanochemical synthesis and structural characterization of nano-sized amorphous tricalcium phosphate. *Ceram Int* 39:8657–8666
598. Perkin KK, Turner JL, Wooley KL, Mann S (2005) Fabrication of hybrid nanocapsules by calcium phosphate mineralization of shell cross-linked polymer micelles and nanocages. *Nano Lett* 5:1457–1461
599. Tjandra W, Ravi P, Yao J, Tam KC (2006) Synthesis of hollow spherical calcium phosphate nanoparticles using polymeric nanotemplates. *Nanotechnology* 17:5988–5994
600. Ye F, Guo H, Zhang H, He X (2010) Polymeric micelle-templated synthesis of hydroxyapatite hollow nanoparticles for a drug delivery system. *Acta Biomater* 6:2212–2218
601. Jiang SD, Yao QZ, Zhou GT, Fu SQ (2012) Fabrication of hydroxyapatite hierarchical hollow microspheres and potential application in water treatment. *J Phys Chem C* 116:4484–4492
602. Sadasivan S, Khushalani D, Mann S (2005) Synthesis of calcium phosphate nanofilaments in reverse micelles. *Chem Mater* 17:2765–2770
603. Morgan TT, Muddana HS, Altinoglu EI, Rouse SM, Tabakovic A, Tabouillot T, Russin TJ, Butler PJ, Eklund P, Yun JK, Kester M, Adair JH (2008) Encapsulation of organic molecules in calcium phosphate nanocomposite particles for intracellular imaging and drug delivery. *Nano Lett* 8:4108–4115
604. Lai C, Wang YJ, Wei K (2008) Nucleation kinetics of calcium phosphate nanoparticles in reverse micelle solution. *Colloids Surf A Physicochem Eng Asp* 315:268–274
605. Yang X, Gao X, Gan Y, Gao C, Zhang X, Ting K, Wu BM, Gou Z (2010) Facile synthesis of octacalcium phosphate nanobelts: growth mechanism and surface adsorption properties. *J Phys Chem C* 114:6265–6271
606. Socol G, Torricelli P, Bracci B, Iliescu M, Miroiu F, Bigi A, Werckmann J, Mihailescu IN (2004) Biocompatible nanocrystalline octacalcium phosphate thin films obtained by pulsed laser deposition. *Biomaterials* 25:2539–2545
607. Fathi AM, Abd El-Hamid HK, Radwan MM (2016) Preparation and characterization of nanotetracalcium phosphate coating on titanium substrate. *Int J Electrochem Sci* 11:3164–3178
608. de Campos M, Müller FA, Bressiani AHA, Bressiani JC, Greil P (2004) Comparative study of sonochemical synthesized  $\beta$ -TCP- and BCP-nanoparticles. *Key Eng Mater* 254–256:923–926
609. Lee BT, Youn MH, Paul RK, Lee KH, Song HY (2007) In situ synthesis of spherical BCP nanopowders by microwave assisted process. *Mater Chem Phys* 104:249–253
610. Cho JS, Ko YN, Koo HY, Kang YC (2010) Synthesis of nano-sized biphasic calcium phosphate ceramics with spherical shape by flame spray pyrolysis. *J Mater Sci Mater Med* 21:1143–1149
611. Farzadi A, Solati-Hashjin M, Tahmasebi-Birgani Z, Aminian A (2010) Microwave-assisted synthesis and characterization of biphasic calcium phosphate nanopowders. *Ceram Trans* 218:59–65
612. Farzadi A, Solati-Hashjin M, Bakhshi F, Aminian A (2011) Synthesis and characterization of hydroxyapatite/ $\beta$ -tricalcium phosphate nanocomposites using microwave irradiation. *Ceram Int* 37:65–71
613. Pan L, Li Y, Zou C, Weng W, Cheng K, Song C, Du P, Zhao G, Shen G, Wang J, Han G (2007) Surface modification of nanosized biphasic  $\alpha$ -TCP/HA powders. *Key Eng Mater* 330–332:223–226

614. Urch H, Franzka S, Dahlhaus D, Hartmann N, Hasselbrink E, Epple M (2006) Preparation of two-dimensionally patterned layers of functionalised calcium phosphate nanoparticles by laser direct writing. *J Mater Chem* 16:1798–1802
615. Sokolova V, Prymak O, Meyer-Zaika W, Cölfen H, Rehage H, Shukla A, Epple M (2006) Synthesis and characterization of DNA functionalized calcium phosphate nanoparticles. *Mater Wiss Werkst* 37:441–445
616. Muddana HS, Morgan TT, Adair JH, Butler PJ (2009) Photophysics of Cy3-encapsulated calcium phosphate nanoparticles. *Nano Lett* 9:1559–1566
617. Altinoğlu EI, Russin TJ, Kaiser JM, Barth BM, Eklund PC, Kester M, Adair JH (2008) Near-infrared emitting fluorophore-doped calcium phosphate nanoparticles for in vivo imaging of human breast cancer. *ACS Nano* 2:2075–2084
618. Schwiertz J, Wiehe A, Gräfe S, Gitter B, Epple M (2009) Calcium phosphate nanoparticles as efficient carriers for photodynamic therapy against cells and bacteria. *Biomaterials* 30:3324–3331
619. Chen F, Zhu YJ, Zhang KH, Wu J, Wang KW, Tang QL, Mo XM (2011) Europium-doped amorphous calcium phosphate porous nanospheres: preparation and application as luminescent drug carriers. *Nanoscale Res Lett* 6:1–9
620. Haynes MT, Huang L (2014) Lipid-coated calcium phosphate nanoparticles for nonviral gene therapy. *Adv Genet* 88:205–229
621. Haedicke K, Kozlova D, Gräfe S, Teichgräber U, Epple M, Hilger I (2015) Multifunctional calcium phosphate nanoparticles for combining near-infrared fluorescence imaging and photodynamic therapy. *Acta Biomater* 14:197–207
622. Schwiertz J, Meyer-Zaika W, Ruiz-Gonzalez L, González-Calbet JM, Vallet-Regí M, Epple M (2008) Calcium phosphate nanoparticles as templates for nanocapsules prepared by the layer-by-layer technique. *J Mater Chem* 18:3831–3834
623. Cai Y, Liu P, Tang R (2008) Recent patents on nano calcium phosphates. *Recent Pat Mater Sci* 1:209–216
624. Hayakawa S, Li Y, Tsuru K, Osaka A, Fujii E, Kawabata K (2009) Preparation of nanometer-scale rod array of hydroxyapatite crystal. *Acta Biomater* 5:2152–2160
625. Liao SS, Cui FZ, Zhang W, Feng QL (2004) Hierarchically biomimetic bone scaffold materials: nano-HA/collagen/PLA composite. *J Biomed Mater Res B Appl Biomater* 69B:158–165
626. Thomas V, Dean DR, Jose MV, Mathew B, Chowdhury S, Vohra YK (2007) Nanostructured biocomposite scaffolds based on collagen co-electrospun with nanohydroxyapatite. *Biomacromolecules* 8:631–637
627. de Yoreo JJ, Vekilov PG (2003) Principles of crystal nucleation and growth. *Rev Mineral Geochem* 54:57–93
628. Liao S, Xu G, Wang W, Watari F, Cui F, Ramakrishna S, Chan CK (2007) Self-assembly of nano-hydroxyapatite on multi-walled carbon nanotubes. *Acta Biomater* 3:669–675
629. Penn RL, Banfield JF (1998) Imperfect oriented attachment: dislocation generation in defect-free nanocrystals. *Science* 281:969–971
630. Tao J, Pan H, Zeng Y, Xu X, Tang R (2007) Roles of amorphous calcium phosphate and biological additives in the assembly of hydroxyapatite nanoparticles. *J Phys Chem B* 111:13410–13418
631. Hing KA (2004) Bone repair in the twenty-first century: biology, chemistry or engineering? *Phil Trans R Soc Lond A* 362:2821–2850
632. Kokubo T, Kim HM, Kawashita M (2003) Novel bioactive materials with different mechanical properties. *Biomaterials* 24:2161–2175
633. Fu JM, Miao B, Jia LH, Lü KL (2009) Nano-hydroxyapatite for repair of rabbit jaw bone defect: bone mineral density analysis. *J Clin Rehabil Tissue Eng Res* 13:2387–2390
634. Zhou H, Lee J (2011) Nanoscale hydroxyapatite particles for bone tissue engineering. *Acta Biomater* 7:2769–2781

635. Wang L, Li J, Xie Y, Yang P, Liao Y, Guo G (2012) Effect of nano biphasic calcium phosphate bioceramics on periodontal regeneration in the treatment of alveolar defects. *Adv Mater Res* 486:422–425
636. Ghanaati S, Barbeck M, Willershausen I, Thimm B, Stuebinger S, Korzinskas T, Obreja K, Landes C, Kirkpatrick CJ, Sader RA (2013) Nanocrystalline hydroxyapatite bone substitute leads to sufficient bone tissue formation already after 3 months: histological and histomorphometrical analysis 3 and 6 months following human sinus cavity augmentation. *Clin Implant Dent Relat Res* 15:883–892
637. Wang L, Hou H, Zhang J, Sun Z, Yang P, Liao Y (2012) Assessing the effect of nano biphasic calcium phosphate on acute alveolar bone defects in beagle dogs using micro-computed tomography imaging. *Adv Mater Res* 465:132–135
638. Wu X, Xu W, Zeng ZL, Hu X, Xi B, Zhou YF, Su JC (2012) Application of nanometer calcium phosphate ceramic artificial bone in percutaneous kyphoplasty; a short-term clinical observation. *Acad J Second Mil Med Univ* 33:1151–1153
639. Tavakol S, Nikpour MR, Amani A, Soltani M, Rabiee SM, Rezayat SM, Chen P, Jahanshahi M (2013) Bone regeneration based on nano-hydroxyapatite and hydroxyapatite/chitosan nanocomposites: an in vitro and in vivo comparative study. *J Nanopart Res* 15:1373
640. Robbins S, Laurysen C, Songer MN (2016) Use of nanocrystalline hydroxyapatite with autologous BMA and local bone in the lumbar spine: a retrospective CT analysis of posterolateral fusion results. *Clin Spine Surg*. doi:10.1097/BSD.000000000000091
641. Pang KM, Lee JK, Seo YK, Kim SM, Kim MJ, Lee JH (2015) Biologic properties of nano-hydroxyapatite: an in vivo study of calvarial defects, ectopic bone formation and bone implantation. *Biomed Mater Eng* 25:25–38
642. Barralet JE, Lilley KJ, Grover LM, Farrar DF, Ansell C, Gbureck U (2004) Cements from nanocrystalline hydroxyapatite. *J Mater Sci Mater Med* 15:407–411
643. Lilley KJ, Gbureck U, Wright AJ, Farrar DF, Barralet JE (2005) Cement from nanocrystalline hydroxyapatite: effect of calcium phosphate ratio. *J Mater Sci Mater Med* 16:1185–1190
644. Neira IS, Kolen'ko YV, Lebedev OI, van Tendeloo G, Gupta HS, Matsushita N, Yoshimura M, Guitián F (2009) Rational synthesis of a nanocrystalline calcium phosphate cement exhibiting rapid conversion to hydroxyapatite. *Mater Sci Eng C* 29:2124–2132
645. Dorozhkin SV (2013) Self-setting calcium orthophosphate formulations. *J Funct Biomater* 4:209–311
646. Leitune VCB, Collares FM, Trommer RM, Andrioli DG, Bergmann CP, Samuel SMW (2013) The addition of nanostructured hydroxyapatite to an experimental adhesive resin. *J Dent* 41:321–327
647. Fricain JC, Schlaubitz S, le Visage C, Arnault I, Derkaoui SM, Siadous R, Catros S, Lalande C, Bareille R, Renard M, Fabre T, Cornet S, Durand M, Léonard A, Sahraoui N, Letourneur D, Amédée J (2013) A nano-hydroxyapatite – pullulan/dextran polysaccharide composite macroporous material for bone tissue engineering. *Biomaterials* 34:2947–2959
648. Venkatesan J, Kim SK (2014) Nano-hydroxyapatite composite biomaterials for bone tissue engineering – a review. *J Biomed Nanotechnol* 10:3124–3140
649. Jayasree R, Kumar TSS (2015) Acrylic cement formulations modified with calcium deficient apatite nanoparticles for orthopaedic applications. *J Compos Mater* 49:2921–2933
650. Munarin F, Petrini P, Gentilini R, Pillai RS, Dirè S, Tanzi MC, Sglavo VM (2015) Micro- and nano-hydroxyapatite as active reinforcement for soft biocomposites. *Int J Biol Macromol* 72:199–209
651. Kang X, Zhang W, Yang C (2016) Mechanical properties study of micro- and nano-hydroxyapatite reinforced ultrahigh molecular weight polyethylene composites. *J Appl Polym Sci* 133:42869
652. Strnadova M, Protivinsky J, Strnad J, Vejsicka Z (2008) Preparation of porous synthetic nanostructured HA scaffold. *Key Eng Mater* 361–363:211–214

653. Kim JY, Lee JW, Lee SJ, Park EK, Kim SY, Cho DW (2007) Development of a bone scaffold using HA nanopowder and micro-stereolithography technology. *Microelectron Eng* 84:1762–1765
654. Naga SM, El-Maghraby HF, Sayed M, Saad EA (2015) Highly porous scaffolds made of nanosized hydroxyapatite powder synthesized from eggshells. *J Ceram Sci Technol* 6:237–243
655. Roh HS, Myung SW, Jung SC, Kim BH (2015) Fabrication of 3D scaffolds with nano-hydroxyapatite for improving the preosteoblast cell-biological performance. *J Nanosci Nanotechnol* 15:5585–5588
656. Rodrigues LR, d'Ávila MA, Monteiro FJM, de Zavaglia CAC (2012) Synthesis and characterization of nanocrystalline hydroxyapatite gel and its application as scaffold aggregation. *Mater Res* 15:974–980
657. Krylova IV, Ivanov LN, Bozhevol'nov VE, Severin AV (2007) Self-organization processes and phase transitions in nanocrystalline hydroxyapatite according to exoemission data. *Russ J Phys Chem A* 81:241–245
658. Veljovic D, Jokic B, Jankovic-Castvan I, Smiciklas I, Petrovic R, Janackovic D (2007) Sintering behaviour of nanosized HAP powder. *Key Eng Mater* 330–332:259–262
659. Uehira M, Okada M, Takeda S, Matsumoto N (2013) Preparation and characterization of low-crystallized hydroxyapatite nanoporous plates and granules. *Appl Surf Sci* 287:195–202
660. Zhang F, Lin K, Chang J, Lu J, Ning C (2008) Spark plasma sintering of macroporous calcium phosphate scaffolds from nanocrystalline powders. *J Eur Ceram Soc* 28:539–545
661. Grossin D, Banu M, Sarda S, Martinet-Rollin S, Drouet C, Estournès C, Champion E, Rossignol F, Combes C, Rey C (2010) Low temperature consolidation of nanocrystalline apatites toward a new generation of calcium phosphate ceramics. *Ceram Eng Sci Proc* 30:113–126
662. Chaudhry AA, Yan H, Gong K, Inam F, Viola G, Reece MJ, Goodall JBM, ur Rehman I, McNeil-Watson FK, Corbett JCW, Knowles JC, Darr JA (2011) High-strength nanograined and translucent hydroxyapatite monoliths via continuous hydrothermal synthesis and optimized spark plasma sintering. *Acta Biomater* 7:791–799
663. Eriksson M, Liu Y, Hu J, Gao L, Nygren M, Shen Z (2011) Transparent hydroxyapatite ceramics with nanograin structure prepared by high pressure spark plasma sintering at the minimized sintering temperature. *J Eur Ceram Soc* 31:1533–1540
664. Kutty MG, Loertscher J, Bhaduri S, Bhaduri SB, Tinga WR (2001) Microwave sintering of nanocrystalline hydroxyapatite. *Ceram Eng Sci Proc* 22:3–10
665. Vijayan S, Varma H (2002) Microwave sintering of nanosized hydroxyapatite powder compacts. *Mater Lett* 56:827–831
666. Ramesh S, Tan CY, Bhaduri SB, Teng WD (2007) Rapid densification of nanocrystalline hydroxyapatite for biomedical applications. *Ceram Int* 33:1363–1367
667. Lin K, Chen L, Chang J (2012) Fabrication of dense hydroxyapatite nanobioceramics with enhanced mechanical properties via two-step sintering process. *Int J Appl Ceram Technol* 9:479–485
668. Feng P, Niu M, Gao C, Peng S, Shuai C (2014) A novel two-step sintering for nano-hydroxyapatite scaffolds for bone tissue engineering. *Sci Rep* 4:5599. (10 pages)
669. Okada M, Furuzono T (2006) Fabrication of high-dispersibility nanocrystals of calcined hydroxyapatite. *J Mater Sci* 41:6134–6137
670. Okada M, Furuzono T (2007) Nanosized ceramic particles of hydroxyapatite calcined with an anti-sintering agent. *J Nanosci Nanotechnol* 7:848–851
671. Okada M, Furuzono T (2007) Calcination of rod-like hydroxyapatite nanocrystals with an anti-sintering agent surrounding the crystals. *J Nanopart Res* 9:807–815
672. Müller-Mai CM, Stupp SI, Voigt C, Gross U (1995) Nanoapatite and organoapatite implants in bone: histology and ultrastructure of the interface. *J Biomed Mater Res* 29:9–18
673. Du C, Cui FZ, Feng QL, Zhu XD, de Groot K (1998) Tissue response to nano-hydroxyapatite/collagen composite implants in marrow cavity. *J Biomed Mater Res* 42:540–548

674. Du C, Cui FZ, Zhu XD, de Groot K (1999) Three-dimensional nano-HAp/collagen matrix loading with osteogenic cells in organ culture. *J Biomed Mater Res* 44:407–415
675. Paul W, Sharma CP (2006) Nanoceramic matrices: biomedical applications. *Am J Biochem Biotechnol* 2:41–48
676. Huber FX, McArthur N, Hillmeier J, Kock HJ, Baier M, Diwo M, Berger I, Meeder PJ (2006) Void filling of tibia compression fracture zones using a novel resorbable nanocrystalline hydroxyapatite paste in combination with a hydroxyapatite ceramic core: first clinical results. *Arch Orthop Trauma Surg* 126:533–540
677. Smeets R, Jelitte G, Heiland M, Kasaj A, Grosjean M, Riediger D, Yildirim M, Spiekermann H, Maciejewski O (2008) Hydroxylapatit-Knochenersatzmaterial (Ostim®) bei der Sinusbodenelevation. *Schweiz Monatsschr Zahnmed* 118:203–208
678. Gerlach KL, Niehues D (2007) Die Behandlung der Kieferzysten mit einem neuartigen nanopartikelären Hydroxylapatit. *Mund Kiefer Gesichtschir* 11:131–137
679. Schwarz F, Bieling K, Latz T, Nuesry E, Becker J (2006) Healing of intrabony periimplantitis defects following application of a nanocrystalline hydroxyapatite (Ostim™) or a bovine-derived xenograft (Bio-Oss™) in combination with a collagen membrane (Bio-Gide™). A case series. *J Clin Periodontol* 33:491–499
680. Strietzel FP, Reichart PA, Graf HL (2007) Lateral alveolar ridge augmentation using a synthetic nano-crystalline hydroxyapatite bone substitution material (Ostim®). Preliminary clinical and histological results. *Clin Oral Implants Res* 18:743–751
681. Spies C, Schnürer S, Gotterbarm T, Breusch S (2008) Tierexperimentelle Untersuchung des Knochenersatzstoffs Ostim™ im knöchernen Lager des Göttinger Miniaturschweins. *Z Orthop Unfall* 146:64–69
682. Thorwarth M, Schultze-Mosgau S, Kessler P, Wiltfang J, Schlegel KA (2005) Bone regeneration in osseous defects using a resorbable nanoparticulate hydroxyapatite. *J Oral Maxillofac Surg* 63:1626–1633
683. Brandt J, Henning S, Michler G, Schulz M, Bernstein A (2008) Nanocrystalline hydroxyapatite for bone repair. *Key Eng Mater* 361–363:35–38
684. Huber FX, Hillmeier J, Herzog L, McArthur N, Kock HJ, Meeder PJ (2006) Open reduction and palmar plate-osteosynthesis in combination with a nanocrystalline hydroxyapatite spacer in the treatment of comminuted fractures of the distal radius. *J Hand Surg (Br)* 31B:298–303
685. Huber FX, Hillmeier J, McArthur N, Kock HJ, Meeder PJ (2006) The use of nanocrystalline hydroxyapatite for the reconstruction of calcaneal fractures: preliminary results. *J Foot Ankle Surg* 45:322–328
686. Laschke MW, Witt K, Pohlemann T, Menger MD (2007) Injectable nanocrystalline hydroxyapatite paste for bone substitution: in vivo analysis of biocompatibility and vascularization. *J Biomed Mater Res B Appl Biomater* 82B:494–505
687. Spies CKG, Schnürer S, Gotterbarm T, Breusch S (2009) The efficacy of Biobon™ and Ostim™ within metaphyseal defects using the Göttinger Minipig. *Arch Orthop Trauma Surg* 129:979–988
688. Chitsazi MT, Shirmohammadi A, Faramarzie M, Pourabbas R, Rostamzadeh AN (2011) A clinical comparison of nano-crystalline hydroxyapatite (Ostim) and autogenous bone graft in the treatment of periodontal intrabony defects. *Med Oral Patol Oral Cir Bucal* 16:448–453
689. Canuto RA, Pol R, Martinasso G, Muzio G, Gallesio G, Mozzati M (2012) Hydroxyapatite paste Ostim®, without elevation of full-thickness flaps, improves alveolar healing stimulating BMP- and VEGF-mediated signal pathways: an experimental study in humans. *Clin Oral Implants Res Suppl A* 100:42–48
690. Huber FX, Belyaev O, Hillmeier J, Kock HJ, Huber C, Meeder PJ, Berger I (2006) First histological observations on the incorporation of a novel nanocrystalline hydroxyapatite paste OSTIM® in human cancellous bone. *BMC Musculoskelet Disord* 7:50. (14 pages)
691. Huber FX, Berger I, McArthur N, Huber C, Kock HP, Hillmeier J, Meeder PJ (2008) Evaluation of a novel nanocrystalline hydroxyapatite paste and a solid hydroxyapatite

- ceramic for the treatment of critical size bone defects (CSD) in rabbits. *J Mater Sci Mater Med* 19:33–38
692. Arts JJC, Verdonschot N, Schreurs BW, Buma P (2006) The use of a bioresorbable nanocrystalline hydroxyapatite paste in acetabular bone impaction grafting. *Biomaterials* 27:1110–1118
693. Varma NP, Garai S, Sinha A (2012) Synthesis of injectable and cohesive nano hydroxyapatite scaffolds. *J Mater Sci Mater Med* 23:913–919
694. Zhang W, Liao SS, Cui FZ (2003) Hierarchical self-assembly of nano-fibrils in mineralized collagen. *Chem Mater* 15:3221–3226
695. Li X, Huang J, Edirisinghe MJ (2008) Development of nano-hydroxyapatite coating by electrohydrodynamic atomization spraying. *J Mater Sci Mater Med* 19:1545–1551
696. Hahn BD, Park DS, Choi JJ, Ryu J, Yoon WH, Kim KH, Park C, Kim HE (2009) Dense nanostructured hydroxyapatite coating on titanium by aerosol deposition. *J Am Ceram Soc* 92:683–687
697. Narayanan R, Kwon TY, Kim KH (2008) Direct nanocrystalline hydroxyapatite formation on titanium from ultrasonated electrochemical bath at physiological pH. *Mater Sci Eng C* 28:1265–1270
698. Yousefpour M, Afshar A, Yang X, Li X, Yang B, Wu Y, Chen J, Zhang X (2006) Nanocrystalline growth of electrochemically deposited apatite coating on pure titanium. *J Electroanal Chem* 589:96–105
699. Mendes VC, Moineddin R, Davies JE (2009) Discrete calcium phosphate nanocrystalline deposition enhances osteoconduction on titanium-based implant surfaces. *J Biomed Mater Res A* 90A:577–585
700. Barkarmo S, Wennerberg A, Hoffman M, Kjellin P, Breiding K, Handa P, Stenport V (2013) Nano-hydroxyapatite-coated PEEK implants: a pilot study in rabbit bone. *J Biomed Mater Res A* 101A:465–471
701. Iskandar ME, Aslani A, Tian Q, Liu H (2015) Nanostructured calcium phosphate coatings on magnesium alloys: characterization and cytocompatibility with mesenchymal stem cells. *J Mater Sci Mater Med* 26:189. (18 pages)
702. Feng G, Cheng X, Xie D, Wang K, Zhang B (2016) Fabrication and characterization of nano prism-like hydroxyapatite coating on porous titanium substrate by combined biomimetic-hydrothermal method. *Mater Lett* 163:134–137
703. Bral A, Mommaerts MY (2016) In vivo biofunctionalization of titanium patient-specific implants with nano hydroxyapatite and other nano calcium phosphate coatings: a systematic review. *J Craniomaxillofac Surg* 44:400–412
704. Dorozhkin SV (2015) Calcium orthophosphate deposits: preparation, properties and biomedical applications. *Mater Sci Eng C* 55:272–326
705. Nies B, Rößler S, Reinstorf A (2007) Formation of nano hydroxyapatite – a straightforward way to bioactivate bone implant surfaces. *Int J Mater Res (Formerly Z Metallkd)* 98:630–636
706. Jalota S, Bhaduri SB, Tas AC (2006) Effect of carbonate content and buffer type on calcium phosphate formation in SBF solutions. *J Mater Sci Mater Med* 17:697–707
707. Chen F, Lam WM, Lin CJ, Qiu GX, Wu ZH, Luk KDK, Lu WW (2007) Biocompatibility of electrophoretical deposition of nanostructured hydroxyapatite coating on roughen titanium surface: in vitro evaluation using mesenchymal stem cells. *J Biomed Mater Res B Appl Biomater* 82B:183–191
708. Thian ES, Ahmad Z, Huang J, Edirisinghe MJ, Jayasinghe SN, Ireland DC, Brooks RA, Rushton N, Bonfield W, Best SM (2008) The role of electro sprayed nanoapatites in guiding osteoblast behaviour. *Biomaterials* 29:1833–1843
709. Bigi A, Nicoli-Aldini N, Bracci B, Zavan B, Boanini E, Sbaiz F, Panzavolta S, Zorzato G, Giardino R, Facchini A, Abatangelo G, Cortivo R (2007) In vitro culture of mesenchymal cells onto nanocrystalline hydroxyapatite coated Ti13Nb13Zr alloy. *J Biomed Mater Res A* 82A:213–221

710. Bigi A, Fini M, Bracci B, Boanini E, Torricelli P, Giavaresi G, Aldini NN, Facchini A, Sbaiz F, Giardino R (2008) The response of bone to nanocrystalline hydroxyapatite-coated Ti13Nb11Zr alloy in an animal model. *Biomaterials* 29:1730–1736
711. Thian ES, Huang J, Ahmad Z, Edirisinghe MJ, Jayasinghe SN, Ireland DC, Brooks RA, Rushton N, Best SM, Bonfield W (2008) Influence of nanohydroxyapatite patterns deposited by electrohydrodynamic spraying on osteoblast response. *J Biomed Mater Res A* 85A:188–194
712. Furuzono T, Masuda M, Okada M, Yasuda S, Kadono H, Tanaka R, Miyatake K (2006) Increase in cell adhesiveness on a poly(ethylene terephthalate) fabric by sintered hydroxyapatite nanocrystal coating in the development of an artificial blood vessel. *ASAIO J* 52:315–320
713. Yanagida H, Okada M, Masuda M, Ueki M, Narama I, Kitao S, Koyama Y, Furuzono T, Takakuda K (2009) Cell adhesion and tissue response to hydroxyapatite nanocrystal-coated poly(L-lactic acid) fabric. *J Biosci Bioeng* 108:235–243
714. Moon JW, Sohn DS, Heo JU (2015) Histomorphometric analysis of maxillary sinus augmentation with calcium phosphate nanocrystal-coated xenograft. *Implant Dent* 24:333–337
715. Hu J, Yang Z, Zhou Y, Liu Y, Li K, Lu H (2015) Porous biphasic calcium phosphate ceramics coated with nano-hydroxyapatite and seeded with mesenchymal stem cells for reconstruction of radius segmental defects in rabbits. *J Mater Sci Mater Med* 26:257. (12 pages)
716. Li X, Huang J, Edirisinghe MJ (2008) Development of template-assisted electrohydrodynamic atomization spraying for nanoHA patterning. *Key Eng Mater* 361–363:585–588
717. Abrahamsson I, Linder E, Larsson L, Berglund T (2013) Deposition of nanometer scaled calcium-phosphate crystals to implants with a dual acid-etched surface does not improve early tissue integration. *Clin Oral Implants Res* 24:57–62
718. Alghamdi HS, van Oirschot BAJA, Bosco R, van den Beucken JJ, Aldosari AAF, Anil S, Jansen JA (2013) Biological response to titanium implants coated with nanocrystals calcium phosphate or type 1 collagen in a dog model. *Clin Oral Implants Res* 24:475–483
719. Kasaj A, Willershausen B, Reichert C, Rohrig B, Smeets R, Schmidt M (2008) Ability of nanocrystalline hydroxyapatite paste to promote human periodontal ligament cell proliferation. *J Oral Sci* 50:279–285
720. Shi ZL, Huang X, Cai YR, Tang RK, Yang DS (2009) Size effect of hydroxyapatite nanoparticles on proliferation and apoptosis of osteoblast-like cells. *Acta Biomater* 5:338–345
721. Liu Y, Wang G, Cai Y, Ji H, Zhou G, Zhao X, Tang R, Zhang M (2009) In vitro effects of nanophasic hydroxyapatite particles on proliferation and osteogenic differentiation of bone marrow-derived mesenchymal stem cells. *J Biomed Mater Res A* 15A:1083–1091
722. Zhu X, Eibl O, Scheideler L, Geis-Gerstorfer J (2006) Characterization of nano hydroxyapatite/collagen surfaces and cellular behaviors. *J Biomed Mater Res A* 79A:114–127
723. Zhu W, Zhang X, Wang D, Lu W, Ou Y, Han Y, Zhou K, Liu H, Fen W, Peng L, He C, Zeng Y (2010) Experimental study on the conduction function of nano-hydroxyapatite artificial bone. *Micro Nano Lett* 5:19–27
724. Wang H, Li Y, Zuo Y, Li J, Ma S, Cheng L (2007) Biocompatibility and osteogenesis of biomimetic nano-hydroxyapatite/polyamide composite scaffolds for bone tissue engineering. *Biomaterials* 28:3338–3348
725. Zhang YF, Cheng XR, Chen Y, Shi B, Chen XH, Xu DX, Ke J (2007) Three-dimensional nanohydroxyapatite / chitosan scaffolds as potential tissue engineered periodontal tissue. *J Biomater Appl* 21:333–349
726. Huang YX, Ren J, Chen C, Ren TB, Zhou XY (2008) Preparation and properties of poly(lactide-*co*-glycolide) (PLGA)/nano-hydroxyapatite (NHA) scaffolds by thermally induced phase separation and rabbit mscs culture on scaffolds. *J Biomater Appl* 22:409–432
727. Thian ES, Ahmad Z, Huang J, Edirisinghe MJ, Jayasinghe SN, Ireland DC, Brooks RA, Rushton N, Bonfield W, Best SM (2007) Bioactivity of nanoapatite produced by electrohydrodynamic atomization. *J Bionanosci* 1:60–63



728. Pezzatini S, Solito R, Morbidelli L, Lamponi S, Boanini E, Bigi A, Ziche M (2006) The effect of hydroxyapatite nanocrystals on microvascular endothelial cell viability and functions. *J Biomed Mater Res A* 76A:656–663
729. Pezzatini S, Morbidelli L, Solito R, Paccagnini E, Boanini E, Bigi A, Ziche M (2007) Nanostructured HA crystals up-regulate FGF-2 expression and activity in microvascular endothelium promoting angiogenesis. *Bone* 41:523–534
730. Macmillan AK, Lamberti FV, Moulton JN, Geilich BM, Webster TJ (2014) Similar healthy osteoclast and osteoblast activity on nanocrystalline hydroxyapatite and nanoparticles of tricalcium phosphate compared to natural bone. *Int J Nanomedicine* 9:5627–5637
731. Pilloni A, Pompa G, Saccucci M, di Carlo G, Rimondini L, Brama M, Zeza B, Wannenes F, Migliaccio S (2014) Analysis of human alveolar osteoblast behavior on a nano-hydroxyapatite substrate: an in vitro study. *BMC Oral Health* 14:22. (7 pages)
732. Ha SW, Jang HL, Nam KT, Beck GR (2015) Nano-hydroxyapatite modulates osteoblast lineage commitment by stimulation of DNA methylation and regulation of gene expression. *Biomaterials* 65:32–42
733. Cai Y, Liu Y, Yan W, Hu Q, Tao J, Zhang M, Shi Z, Tang R (2007) Role of hydroxyapatite nanoparticle size in bone cell proliferation. *J Mater Chem* 17:3780–3787
734. Hu Q, Tan Z, Liu Y, Tao J, Cai Y, Zhang M, Pan H, Xu X, Tang R (2007) Effect of crystallinity of calcium phosphate nanoparticles on adhesion, proliferation, and differentiation of bone marrow mesenchymal stem cells. *J Mater Chem* 17:4690–4698
735. Liu X, Zhao M, Lu J, Ma J, Wei J, Wei S (2012) Cell responses to two kinds of nanohydroxyapatite with different sizes and crystallinities. *Int J Nanomedicine* 7:1239–1250
736. d'Elía NL, Mathieu C, Hoemann CD, Laiuppa JA, Santillán GE, Messina PV (2015) Bone-repair properties of biodegradable hydroxyapatite nano-rod superstructures. *Nanoscale* 7:18751–18762
737. Kim K, Dean D, Lu A, Mikos AG, Fisher JP (2011) Early osteogenic signal expression of rat bone marrow stromal cells is influenced by both hydroxyapatite nanoparticle content and initial cell seeding density in biodegradable nanocomposite scaffolds. *Acta Biomater* 7:1249–1264
738. Svanborg LM, Hoffman M, Andersson M, Currie F, Kjellin P, Wennerberg A (2011) The effect of hydroxyapatite nanocrystals on early bone formation surrounding dental implants. *Int J Oral Maxillofac Surg* 40:308–315
739. Suto M, Nemoto E, Kanaya S, Suzuki R, Tsuchiya M, Shimauchi H (2013) Nanohydroxyapatite increases BMP-2 expression via a p38 MAP kinase dependent pathway in periodontal ligament cells. *Arch Oral Biol* 58:1021–1028
740. Detsch R, Hagemeyer D, Neumann M, Schaefer S, Vortkamp A, Wuelling M, Ziegler G, Epple M (2010) The resorption of nanocrystalline calcium phosphates by osteoclast-like cells. *Acta Biomater* 6:3223–3233
741. Stevens MM, George JH (2005) Exploring and engineering the cell surface interface. *Science* 310:1135–1138
742. Martínez E, Engel E, Planell JA, Samitier J (2009) Effects of artificial micro- and nano-structured surfaces on cell behaviour. *Ann Anat* 191:126–135
743. Lee DH, Han JS, Yang JH, Lee JB (2009) MC3T3-E1 cell response to pure titanium, zirconia and nano-hydroxyapatite. *Int J Mod Phys B* 23:1535–1540
744. Liu M, Zhou G, Song W, Li P, Liu H, Niu X, Fan Y (2012) Effect of nano-hydroxyapatite on the axonal guidance growth of rat cortical neurons. *Nanoscale* 4:3201–3207
745. Onuma K, Yamagishi K, Oyane A (2005) Nucleation and growth of hydroxyapatite nanocrystals for nondestructive repair of early caries lesions. *J Cryst Growth* 282:199–207
746. Huang S, Gao S, Cheng L, Yu H (2011) Remineralization potential of nano-hydroxyapatite on initial enamel lesions: an in vitro study. *Caries Res* 45:460–468
747. Roveri N, Battistella E, Bianchi CL, Foltran I, Foresti E, Iafisco M, Lelli M, Naldoni A, Palazzo B, Rimondini L (2009) Surface enamel remineralization: biomimetic apatite nanocrystals and fluoride ions different effects. *J Nanomater* 2009:746383. (9 pages)

748. Dorozhkin SV (2016) Calcium orthophosphates (CaPO<sub>4</sub>) and dentistry. *Bioceram Dev Appl* 6:96
749. Jeong SH, Jang SO, Kim KN, Kwon HK, Park YD, Kim BI (2006) Remineralization potential of new toothpaste containing nano-hydroxyapatite. *Key Eng Mater* 309–311:537–540
750. Tschoppe P, Zandim DL, Martus P, Kielbassa AM (2011) Enamel and dentine remineralization by nano-hydroxyapatite toothpastes. *J Dent* 39:430–437
751. Wang CJ, Zhang YF, Wei J, Wei SC (2011) Repair of artificial enamel lesions by nano fluorapatite paste containing fluorin. *J Clin Rehabil Tiss Eng Res* 15:6346–6350
752. Kovtun A, Kozlova D, Ganesan K, Biewald C, Seipold N, Gaengler P, Arnold WH, Epple M (2012) Chlorhexidine-loaded calcium phosphate nanoparticles for dental maintenance treatment: combination of mineralising and antibacterial effects. *RSC Adv* 2:870–875
753. Kim BI, Jeong SH, Jang SO, Kim KN, Kwon HK, Park YD (2006) Tooth whitening effect of toothpastes containing nano-hydroxyapatite. *Key Eng Mater* 309–311:541–544
754. Collares FM, Leitune VCB, Rostirolla FV, Trommer RM, Bergmann CP, Samuel SMW (2012) Nanostructured hydroxyapatite as filler for methacrylate-based root canal sealers. *Int Endod J* 45:63–67
755. Kim MY, Kwon HK, Choi CH, Kim BI (2007) Combined effects of nano-hydroxyapatite and NaF on remineralization of early caries lesion. *Key Eng Mater* 330–332:1347–1350
756. Lee HJ, Min JH, Choi CH, Kwon HG, Kim BI (2007) Remineralization potential of sports drink containing nano-sized hydroxyapatite. *Key Eng Mater* 330–332:275–278
757. Min JH, Kwon HK, Kim BI (2011) The addition of nano-sized hydroxyapatite to a sports drink to inhibit dental erosion – in vitro study using bovine enamel. *J Dent* 39:629–635
758. Hong YW, Kim JH, Lee BH, Lee YK, Choi BJ, Lee JH, Choi HJ (2008) The effect of nano-sized  $\beta$ -tricalcium phosphate on remineralization in glass ionomer dental luting cement. *Key Eng Mater* 361–363:861–864
759. Weir MD, Chow LC, Xu HHK (2012) Remineralization of demineralized enamel via calcium phosphate nanocomposite. *J Dent Res* 91:979–984
760. Melo MAS, Cheng L, Weir MD, Hsia RC, Rodrigues LKA, Xu HHK (2013) Novel dental adhesive containing antibacterial agents and calcium phosphate nanoparticles. *J Biomed Mater Res B Appl Biomater* 101:620–629
761. Melo MAS, Weir MD, Rodrigues LKA, Xu HHK (2013) Novel calcium phosphate nanocomposite with caries-inhibition in a human in situ model. *Dent Mater* 29:231–240
762. Li L, Pan HH, Tao JH, Xu XR, Mao CY, Gu XH, Tang RK (2008) Repair of enamel by using hydroxyapatite nanoparticles as the building blocks. *J Mater Chem* 18:4079–4084
763. Meng X, Lv K, Zhang J, Qu D (2007) Caries inhibitory activity of the nano-HA in vitro. *Key Eng Mater* 330–332:251–254
764. Li BG, Wang JP, Zhao ZY, Sui YF, Zhang YX (2007) Mineralizing of nano-hydroxyapatite powders on artificial caries. *Rare Metal Mater Eng* 36:128–130
765. Choi AH, Ben-Nissan B, Matinlinna JP, Conway RC (2013) Current perspectives: calcium phosphate nanocoatings and nanocomposite coatings in dentistry. *J Dent Res* 92:853–859
766. Ashokan A, Menon D, Nair S, Koyakutty M (2010) A molecular receptor targeted, hydroxyapatite nanocrystal based multi-modal contrast agent. *Biomaterials* 31:2606–2616
767. Bauer IW, Li SP, Han YC, Yuan L, Yin MZ (2008) Internalization of hydroxyapatite nanoparticles in liver cancer cells. *J Mater Sci Mater Med* 19:1091–1095
768. Czapryna J, Tsourkas A (2006) Suicide gene delivery by calcium phosphate nanoparticles. A novel method of targeted therapy for gastric cancer. *Cancer Biol Ther* 5:1691–1692
769. Pareta RA (2009) Calcium phosphate nanoparticles: toxicology and lymph node targeting for cancer metastasis prevention. In: Webster TJ (ed) *Safety of nanoparticles. From manufacturing to medical applications*. Springer, New York
770. Zhang G, Liu T, Chen YH, Chen Y, Xu M, Peng J, Yu S, Yuan J, Zhang X (2009) Tissue specific cytotoxicity of colon cancer cells mediated by nanoparticle-delivered suicide gene in vitro and in vivo. *Clin Cancer Res* 15:201–207

771. Luo Y, Ling Y, Guo W, Pang J, Liu W, Fang Y, Wen X, Wei K, Gao X (2010) Docetaxel loaded oleic acid-coated hydroxyapatite nanoparticles enhance the docetaxel-induced apoptosis through activation of caspase-2 in androgen independent prostate cancer cells. *J Control Release* 147:278–288
772. Shi Z, Huang X, Liu B, Tao H, Cai Y, Tang R (2010) Biological response of osteosarcoma cells to size-controlled nanostructured hydroxyapatite. *J Biomater Appl* 25:19–37
773. Iafisco M, Palazzo B, Martra G, Margiotta N, Piccinonna S, Natile G, Gandin V, Marzano C, Roveri N (2012) Nanocrystalline carbonate-apatites: role of Ca/P ratio on the upload and release of anticancer platinum bisphosphonates. *Nanoscale* 4:206–217
774. Chu SH, Feng DF, Ma YB, Li ZQ (2012) Hydroxyapatite nanoparticles inhibit the growth of human glioma cells in vitro and in vivo. *Int J Nanomedicine* 7:3659–3666
775. Iafisco M, Delgado-Lopez JM, Varoni EM, Tampieri A, Rimondini L, Gomez-Morales J, Prat M (2013) Cell surface receptor targeted biomimetic apatite nanocrystals for cancer therapy. *Small* 9:3834–3844
776. Han Y, Li S, Cao X, Yuan L, Wang Y, Yin Y, Qiu T, Dai H, Wang X (2014) Different inhibitory effect and mechanism of hydroxyapatite nanoparticles on normal cells and cancer cells in vitro and in vivo. *Sci Rep* 4:7134. (7 pages)
777. Yin M, Yin Y, Chen H, Han Y, Dai H, Li S (2015) Effect of hydroxyapatite nanoparticles on the growth potential of hepatoma cells in nude mice. *J Nanosci Nanotechnol* 15:3816–3822
778. Xiong H, Du S, Ni J, Zhou J, Yao J (2016) Mitochondria and nuclei dual-targeted heterogeneous hydroxyapatite nanoparticles for enhancing therapeutic efficacy of doxorubicin. *Biomaterials* 94:70–83
779. Li B, Guo B, Fan H, Zhang X (2008) Preparation of nano-hydroxyapatite particles with different morphology and their response to highly malignant melanoma cells in vitro. *Appl Surf Sci* 255:357–360
780. Dai H, Pei C, Han Y, Xinyu W, Li S (2011) Inhibitory effect of hydroxyapatite nanoparticles on K562 cells. *Mater Sci Forum* 685:352–356
781. Borum L, Wilson OC (2003) Surface modification of hydroxyapatite. Part II Silic. *Biomater* 24:3681–3688
782. Lee HJ, Kim SE, Choi HW, Kim CW, Kim KJ, Lee SC (2007) The effect of surface-modified nano-hydroxyapatite on biocompatibility of poly( $\epsilon$ -caprolactone)/hydroxyapatite nanocomposites. *Eur Polym J* 43:1602–1608
783. Wilson OC, Hull JR (2008) Surface modification of nanophase hydroxyapatite with chitosan. *Mater Sci Eng C* 28:434–437
784. Liao JG, Wang XJ, Zuo Y, Zhang L, Wen JQ, Li YB (2008) Surface modification of nano-hydroxyapatite with silane agent. *J Inorg Mater* 23:145–149
785. Wang Y, Xiao Y, Huang X, Lang M (2011) Preparation of poly(methyl methacrylate) grafted hydroxyapatite nanoparticles via reverse ATRP. *J Colloid Interface Sci* 15:415–421
786. Deng C, Xiao X, Yao N, Yang XB, Weng J (2011) Effect of surface modification of nano-hydroxyapatite particles on in vitro biocompatibility of poly( $\epsilon$ -caprolactone)-matrix composite biomaterials. *Int J Polym Mater* 60:969–978
787. Jensen T, Baas J, Dolathshahi-Pirouz A, Jacobsen T, Singh G, Nygaard JV, Foss M, Bechtold J, Bünger C, Besenbacher F, Søballe K (2011) Osteopontin functionalization of hydroxyapatite nanoparticles in a PDLLA matrix promotes bone formation. *J Biomed Mater Res A* 99A:94–101
788. Chen L, Mccrate JM, Lee JCM, Li H (2011) The role of surface charge on the uptake and biocompatibility of hydroxyapatite nanoparticles with osteoblast cells. *Nanotechnology* 22:105708. (10 pages)
789. Dai Y, Xu M, Wei J, Zhang H, Chen Y (2012) Surface modification of hydroxyapatite nanoparticles by poly(l-phenylalanine) via ROP of l-phenylalanine N-carboxyanhydride (Pha-NCA). *Appl Surf Sci* 258:2850–2855

790. Feng G, Cheng X, Xie D, Wang K, Zhang B (2016) Synthesis of nano-hydroxyapatite and its rapid mediated surface functionalization by silane coupling agent. *Mater Sci Eng C* 58:675–681
791. Ramachandran R, Paul W, Sharma CP (2009) Synthesis and characterization of PEGylated calcium phosphate nanoparticles for oral insulin delivery. *J Biomed Mater Res B Appl Biomater* 88B:41–48
792. Uskoković V, Uskoković DP (2010) Nanosized hydroxyapatite and other calcium phosphates: chemistry of formation and application as drug and gene delivery agents. *J Biomed Mater Res B Appl Biomater* 96B:152–191
793. Loo SC, Moore T, Banik B, Alexis F (2010) Biomedical applications of hydroxyapatite nanoparticles. *Curr Pharm Biotechnol* 11:333–342
794. Dong X, Shao C (2013) The dynamic behaviors and structure conservation of protein BMP-2 on hydroxyapatite nano surfaces. *Adv Mater Res* 601:115–119
795. Fu H, Hu Y, McNelis T, Hollinger JO (2005) A calcium phosphate-based gene delivery system. *J Biomed Mater Res A* 74A:40–48
796. Liu TY, Chen SY, Liu DM, Liou SC (2005) On the study of BSA-loaded calcium-deficient hydroxyapatite nano-carriers for controlled drug delivery. *J Control Release* 107:112–121
797. Cheng XG, Kuhn LT (2007) Chemotherapy drug delivery from calcium phosphate nanoparticles. *Int J Nanomedicine* 2:667–674
798. Maitra A (2005) Calcium phosphate nanoparticles: second-generation nonviral vectors in gene therapy. *Expert Rev Mol Diagn* 5:893–905
799. Yang XC, Walboomers XF, van den Dolder J, Yang F, Bian Z, Fan MW, Jansen JA (2008) Non-viral bone morphogenetic protein 2 transfection of rat dental pulp stem cells using calcium phosphate nanoparticles as carriers. *Tissue Eng A* 14:71–81
800. Ong HT, Loo JSC, Boey FYC, Russell SJ, Ma J, Peng KW (2008) Exploiting the high-affinity phosphonate – hydroxyapatite nanoparticle interaction for delivery of radiation and drugs. *J Nanopart Res* 10:141–150
801. Altinoğlu EI, Adair JH (2009) Calcium phosphate nanocomposite particles: a safer and more effective alternative to conventional chemotherapy? *Future Oncol* 5:279–281
802. Joyappa DH, Kumar CA, Banumathi N, Reddy GR, Suryanarayana VVS (2009) Calcium phosphate nanoparticle prepared with foot and mouth disease virus P1-3CD gene construct protects mice and guinea pigs against the challenge virus. *Vet Microbiol* 139:58–66
803. Dreesen IAJ, Lüchinger NA, Stark WJ, Fussenegger M (2009) Tricalcium phosphate nanoparticles enable rapid purification, increase transduction kinetics, and modify the tropism of mammalian viruses. *Biotechnol Bioeng* 102:1197–1208
804. Tang QL, Zhu YJ, Wu J, Chen F, Cao SW (2011) Calcium phosphate drug nanocarriers with ultrahigh and adjustable drug-loading capacity: one-step synthesis, in situ drug loading and prolonged drug release. *Nanomedicine* 7:428–434
805. Pittella F, Zhang M, Lee Y, Kim HJ, Tockary T, Osada K, Ishii T, Miyata K, Nishiyama N, Kataoka K (2011) Enhanced endosomal escape of siRNA-incorporating hybrid nanoparticles from calcium phosphate and PEG-block charge-conversional polymer for efficient gene knockdown with negligible cytotoxicity. *Biomaterials* 32:3106–3114
806. Behera T, Swain P (2011) Antigen adsorbed calcium phosphate nanoparticles stimulate both innate and adaptive immune response in fish, *Labeo rohita* H. *Cell Immunol* 271:350–359
807. Jiang JL, Li YF, Fang TL, Zhou J, Li XL, Wang YC, Dong J (2012) Vancomycin-loaded nano-hydroxyapatite pellets to treat MRSA-induced chronic osteomyelitis with bone defect in rabbits. *Inflamm Res* 61:207–215
808. Varoni EM, Iafisco M, Rimondini L, Prat M (2012) Development of a targeted drug delivery system: monoclonal antibodies adsorption onto bonelike hydroxyapatite nanocrystal surface. *Adv Mater Res* 409:175–180
809. Rout SR, Behera B, Maiti TK, Mohapatra S (2012) Multifunctional magnetic calcium phosphate nanoparticles for targeted platinum delivery. *Dalton Trans* 41:10777–10783

810. Knuschke T, Sokolova V, Rotan O, Wadwa M, Tenbusch M, Hansen W, Staeheli P, Epple M, Buer J, Westendorf AM (2013) Immunization with biodegradable nanoparticles efficiently induces cellular immunity and protects against influenza virus infection. *J Immunol* 190:6221–6229
811. Kozlova D, Sokolova V, Zhong M, Zhang E, Yang J, Li W, Yang Y, Buer J, Westendorf AM, Epple M, Yan H (2014) Calcium phosphate nanoparticles show an effective activation of the innate immune response in vitro and in vivo after functionalization with flagellin. *Virol Sin* 29:33–39
812. Barros J, Grenho L, Fernandes MH, Manuel CM, Melo LF, Nune OC, Monteiro FJ, Ferraz MP (2015) Anti-sessile bacterial and cytocompatibility properties of CHX-loaded nanohydroxyapatite. *Colloids Surf B: Biointerfaces* 130:305–314
813. Chu TC, He Q, Potter DE (2002) Biodegradable calcium phosphate nanoparticles as a new vehicle for delivery of a potential ocular hypotensive agent. *J Ocul Pharmacol Ther* 18:507–514
814. Paul W, Sharma CP (2001) Porous hydroxyapatite nanoparticles for intestinal delivery of insulin. *Trends Biomater Artif Organs* 14:37–38
815. Victor SP, Kumar TSS (2008) Tailoring calcium-deficient hydroxyapatite nanocarriers for enhanced release of antibiotics. *J Biomed Nanotechnol* 4:203–209
816. Kilian O, Alt V, Heiss C, Jonuleit T, Dingeldein E, Fleisch I, Fidorra U, Wenisch S, Schnettler R (2005) New blood vessel formation and expression of VEGF receptors after implantation of platelet growth factor-enriched biodegradable nanocrystalline hydroxyapatite. *Growth Factors* 23:125–133
817. Tabaković A, Kester M, Adair JH (2012) Calcium phosphate-based composite nanoparticles in bioimaging and therapeutic delivery applications. *WIREs Nanomed Nanobiotechnol* 4:96–112
818. Fox K, Tran PA, Tran N (2012) Recent advances in research applications of nanophase hydroxyapatite. *Chem Phys Chem* 13:2495–2506
819. Madhumathi K, Kumar TSS (2014) Regenerative potential and anti-bacterial activity of tetracycline loaded apatitic nanocarriers for the treatment of periodontitis. *Biomed Mater* 9:035002
820. Klesing J, Wiehe A, Gitter B, Grafe S, Epple M (2010) Positively charged calcium phosphate/polymer nanoparticles for photodynamic therapy. *J Mater Sci Mater Med* 21:887–892
821. Ling JY, Loo SC, Phung NT, Boey F, Ma J (2008) Controlled size and morphology of EDTMP-doped hydroxyapatite nanoparticles as model for <sup>153</sup>Samarium-EDTMP doping. *J Mater Sci Mater Med* 19:2993–3003
822. Reischl D, Zimmer A (2009) Drug delivery of siRNA therapeutics: potentials and limits of nanosystems. *Nanomedicine* 5:8–20
823. Jordan M, Schallhorn A, Wurm FM (1996) Transfecting mammalian cells: optimization of critical parameters affecting calcium-phosphate precipitate formation. *Nucleic Acids Res* 24:596–601
824. Sokolova VV, Epple M (2008) Inorganic nanoparticles as carriers of nucleic acids into cells. *Angew Chem Int Ed* 47:1382–1395
825. Chowdhury EH (2007) pH-sensitive nano-crystals of carbonate apatite for smart and cell-specific transgene delivery. *Expert Opin Drug Deliv* 4:193–196
826. Wu GJ, Zhou LZ, Wang KW, Chen F, Sun Y, Duan YR, Zhu YJ, Gu HC (2010) Hydroxylapatite nanorods: an efficient and promising carrier for gene transfection. *J Colloid Interface Sci* 345:427–432
827. Zhou C, Yu B, Yang X, Huo T, Lee LJ, Barth RF, Lee RJ (2010) Lipid-coated nano-calcium-phosphate (LNCP) for gene delivery. *Int J Pharm* 392:201–208
828. Giger EV, Puigmartí-Luis J, Schlatter R, Castagner B, Dittrich PS, Leroux JC (2011) Gene delivery with bisphosphonate-stabilized calcium phosphate nanoparticles. *J Control Release* 28:87–93

829. Olton DY, Close JM, Sfeir CS, Kumta PN (2011) Intracellular trafficking pathways involved in the gene transfer of nano-structured calcium phosphate-DNA particles. *Biomaterials* 32:7662–7670
830. Do TNT, Lee WH, Loo CY, Zavgorodniy AV, Rohanizadeh R (2012) Hydroxyapatite nanoparticles as vectors for gene delivery. *Ther Deliv* 3:623–632
831. Naqvi S, Maitra AN, Abdin MZ, Akmal M, Arora I, Samim M (2012) Calcium phosphate nanoparticle mediated genetic transformation in plants. *J Mater Chem* 22:3500–3507
832. Lee D, Upadhye K, Kumta PN (2012) Nano-sized calcium phosphate (CaP) carriers for non-viral gene delivery. *Mater Sci Eng B* 177:289–302
833. Wu X, Ding D, Jiang H, Xing X, Huang S, Liu H, Chen Z, Sun H (2012) Transfection using hydroxyapatite nanoparticles in the inner ear via an intact round window membrane in chin-chilla. *J Nanopart Res* 14:708. (13 pages)
834. Chernousova S, Klesing J, Soklakova N, Epple M (2013) A genetically active nano-calcium phosphate paste for bone substitution, encoding the formation of BMP-7 and VEGF-A. *RSC Adv* 3:11155–11161
835. He P, Takeshima SN, Tada S, Akaike T, Ito Y, Aida Y (2014) pH-sensitive carbonate apatite nanoparticles as DNA vaccine carriers enhance humoral and cellular immunity. *Vaccine* 32:6199–6205
836. Lee MS, Lee JE, Byun E, Kim NW, Lee K, Lee H, Sim SJ, Lee DS, Jeong JH (2014) Target-specific delivery of siRNA by stabilized calcium phosphate nanoparticles using dopa-hyaluronic acid conjugate. *J Control Release* 192:122–130
837. Alhaji SY, Chowdhury EH, Rosli R, Hassan F, Abdullah S (2014) Gene delivery potential of biofunctional carbonate apatite nanoparticles in lungs. *Biomed Res Int* 2014:646787
838. Zeng B, Shi H, Liu Y (2015) A versatile pH-responsive platform for intracellular protein delivery using calcium phosphate nanoparticles. *J Mater Chem B* 3:9115–9121
839. Jebali A, Kalantar SM, Hekmatimoghaddam S, Saffarzadeh N, Sheikha MH, Ghasemi N (2015) Surface modification of tri-calcium phosphate nanoparticles by DOPE and/or anti-E6 antibody to enhance uptake of antisense of E6 mRNA. *Colloids Surf B: Biointerfaces* 126:297–302
840. Jung H, Kim SA, Yang YG, Yoo H, Lim SJ, Mok H (2015) Long chain microRNA conjugates in calcium phosphate nanoparticles for efficient formulation and delivery. *Arch Pharm Res* 38:705–715
841. Zhang J, Sun X, Shao R, Liang W, Gao J, Chen J (2015) Polycation liposomes combined with calcium phosphate nanoparticles as a non-viral carrier for siRNA delivery. *J Drug Deliv Sci Technol* 30:1–6
842. Chowdhury EH, Sasagawa T, Nagaoka M, Kundu AK, Akaike T (2003) Transfecting mammalian cells by DNA/calcium phosphate precipitates: effect of temperature and pH on precipitation. *Anal Biochem* 314:316–318
843. Jordan M, Wurm F (2004) Transfection of adherent and suspended cells by calcium phosphate. *Methods* 33:136–143
844. Welzel T, Radtke I, Meyer-Zaika W, Heumann R, Epple M (2004) Transfection of cells with custom-made calcium phosphate nanoparticles coated with DNA. *J Mater Chem* 14:2213–2217
845. Sokolova VV, Radtke I, Heumann R, Epple M (2006) Effective transfection of cells with multi-shell calcium phosphate-DNA nanoparticles. *Biomaterials* 27:3147–3153
846. Sokolova VV, Kovtun A, Heumann R, Epple M (2007) Tracking the pathway of calcium phosphate/DNA nanoparticles during cell transfection by incorporation of red-fluorescing tetramethylrhodamine isothiocyanate-bovine serum albumin into these nanoparticles. *J Biol Inorg Chem* 12:174–179
847. Sokolova VV, Kovtun A, Prymak O, Meyer-Zaika W, Kubareva EA, Romanova EA, Oretskaya TS, Heumann R, Epple M (2007) Functionalisation of calcium phosphate nanoparticles by oligonucleotides and their application for gene silencing. *J Mater Chem* 17:721–727

848. Neumann S, Kovtun A, Dietzel ID, Epple M, Heumann R (2009) The use of size-defined DNA-functionalized calcium phosphate nanoparticles to minimise intracellular calcium disturbance during transfection. *Biomaterials* 30:6794–6802
849. Graham FL, van der Eb AJ (1973) A new technique for the assay of infectivity of human adenovirus 5 DNA. *Virology* 52:456–467
850. Kovtun A, Heumann R, Epple M (2009) Calcium phosphate nanoparticles for the transfection of cells. *Biomed Mater Eng* 19:241–247
851. Hu J, Kovtun A, Tomaszewski A, Singer BB, Seitz B, Epple M, Steuhl KP, Ergün S, Fuchsluger TA (2012) A new tool for the transfection of corneal endothelial cells: calcium phosphate nanoparticles. *Acta Biomater* 8:1156–1163
852. Epple M, Ganesan K, Heumann R, Klesing J, Kovtun A, Neumann S, Sokolova V (2010) Application of calcium phosphate nanoparticles in biomedicine. *J Mater Chem* 20:8–23
853. Bose S, Tarafder S (2012) Calcium phosphate ceramic systems in growth factor and drug delivery for bone tissue engineering: a review. *Acta Biomater* 8:1401–1421
854. Shan Z, Li X, Gao Y, Wang X, Li C, Wu Q (2012) Application of magnetic hydroxyapatite nanoparticles for solid phase extraction of plasmid DNA. *Anal Biochem* 425:125–127
855. Roy I, Mitra S, Maitra A, Mozumdar S (2003) Calcium phosphate nanoparticles as novel non-viral vectors for targeted gene delivery. *Int J Pharm* 250:25–33
856. Li J, Chen YC, Tseng YC, Mozumdar S, Huang L (2010) Biodegradable calcium phosphate nanoparticle with lipid coating for systemic siRNA delivery. *J Control Release* 142:416–421
857. Kakizawa Y, Kataoka K (2002) Block copolymer self-assembly into monodisperse nanoparticles with hybrid core of antisense DNA and calcium phosphate. *Langmuir* 18:4539–4543
858. Wang KW, Zhou LZ, Sun Y, Wu GJ, Gu HC, Duan YR, Chen F, Zhu YJ (2010) Calcium phosphate/PLGA-mPEG hybrid porous nanospheres: a promising vector with ultrahigh gene loading and transfection efficiency. *J Mater Chem* 20:1161–1166
859. Epple M, Kovtun A (2010) Functionalized calcium phosphate nanoparticles for biomedical application. *Key Eng Mater* 441:299–305
860. Sokolova V, Neumann S, Kovtun A, Chernousova S, Heumann R, Epple M (2010) An outer shell of positively charged poly(ethyleneimine) strongly increases the transfection efficiency of calcium phosphate/DNA nanoparticles. *J Mater Sci* 45:4952–4957
861. He Q, Mitchell AR, Johnson SL, Wagner-Bartak C, Morcol T, Bell SJD (2000) Calcium phosphate nanoparticle adjuvant. *Clin Diagn Lab Immunol* 7:899–903
862. He Q, Mitchell AR, Morcol T, Bell SJD (2002) Calcium phosphate nanoparticles induce mucosal immunity and protection against herpes simplex virus type 2. *Clin Diagn Lab Immunol* 9:1021–1024
863. Yang D, Sun E (2012) Fabrication of hydroxyapatite and observation of nanoparticles entering into cells. *Adv Mater Res* 366:451–455
864. Liu ZS, Tang SL, Ai ZL (2003) Effects of hydroxyapatite nanoparticles on proliferation and apoptosis of human hepatoma BEL-7402 cells. *World J Gastroenterol* 9:1968–1971
865. Xu J, Xu P, Li Z, Huang J, Yang Z (2012) Oxidative stress and apoptosis induced by hydroxyapatite nanoparticles in C6 cells. *J Biomed Mater Res A* 100A:738–745
866. Sun J, Ding T (2009) P53 reaction to apoptosis induced by hydroxyapatite nanoparticles in rat macrophages. *J Biomed Mater Res A* 88A:673–679
867. Huang Z, Ding T, Sun J (2012) Study of effect on cell proliferation and hemolysis of HAP and TCP nanometer particles. *Adv Mater Res* 378–379:711–714
868. Xu Z, Liu C, Wei J, Sun J (2012) Effects of four types of hydroxyapatite nanoparticles with different nanocrystal morphologies and sizes on apoptosis in rat osteoblasts. *J Appl Toxicol* 32:429–435
869. Yuan Y, Liu C, Qian J, Wang J, Zhang Y (2010) Size-mediated cytotoxicity and apoptosis of hydroxyapatite nanoparticles in human hepatoma HepG2 cells. *Biomaterials* 31:730–740
870. Allen TM, Cullis PR (2004) Drug delivery systems: entering the mainstream. *Science* 303:1818–1822

871. Schmidt HT, Kroczyński M, Maddox J, Chen Y, Josephs R, Ostafin AEJ (2006) Antibody-conjugated soybean oil-filled calcium phosphate nanoshells for targeted delivery of hydrophobic molecules. *Microencapsulation* 23:769–781
872. Ferraz MP, Mateus AY, Sousa JC, Monteiro FJ (2007) Nanohydroxyapatite microspheres as delivery system for antibiotics: release kinetics, antimicrobial activity, and interaction with osteoblasts. *J Biomed Mater Res A* 81A:994–1004
873. Yeo CH, Zein SHS, Ahmad AL, McPhail DS (2012) Investigation into the role of NaOH and calcium ions in the synthesis of calcium phosphate nanoshells. *Braz J Chem Eng* 29:147–158
874. Shao F, Liu L, Fan K, Cai Y, Yao J (2012) Ibuprofen loaded porous calcium phosphate nanospheres for skeletal drug delivery system. *J Mater Sci* 47:1054–1058
875. Ma MY, Zhu YJ, Li L, Cao SW (2008) Nanostructured porous hollow ellipsoidal capsules of hydroxyapatite and calcium silicate preparation and application in drug delivery. *J Mater Chem* 18:2722–2727
876. Cai Y, Pan H, Xu X, Hu Q, Li L, Tang R (2007) Ultrasonic controlled morphology transformation of hollow calcium phosphate nanospheres: a smart and biocompatible drug release system. *Chem Mater* 19:3081–3083
877. Zhou WY, Wang M, Cheung WL, Guo BC, Jia DM (2008) Synthesis of carbonated hydroxyapatite nanospheres through nanoemulsion. *J Mater Sci Mater Med* 19:103–110
878. Kamitakahara M, Kimura K, Ioku K (2012) Synthesis of nanosized porous hydroxyapatite granules in hydrogel by electrophoresis. *Colloids Surf B: Biointerfaces* 97:236–239
879. Wang P, Zhao L, Liu J, Weir MD, Zhou X, Xu HHK (2014) Bone tissue engineering via nanostructured calcium phosphate biomaterials and stem cells. *Bone Res* 2:14017. (13 pages)
880. Loomba L, Sekhon BS (2015) Calcium phosphate nanoparticles and their biomedical potential. *J Nanomater Mol Nanotechnol* 4:1. (12 pages)
881. Uskoković V, Wu VM (2016) Calcium phosphate as a key material for socially responsible tissue engineering. *Materials* 9:434. (27 pages)
882. Wingert PA, Mizukami H, Ostafin AE (2007) Enhanced chemiluminescent resonance energy transfer in hollow calcium phosphate nanoreactors and the detection of hydrogen peroxide. *Nanotechnology* 18:295707. (7 pages)
883. Kottegoda N, Munaweera I, Madusanka N, Karunaratne V (2011) A green slow-release fertilizer composition based on urea-modified hydroxyapatite nanoparticles encapsulated wood. *Curr Sci* 101:73–78
884. Chen JH, Wang YJ, Zhou DM, Cui YX, Wang SQ, Chen YC (2010) Adsorption and desorption of Cu(II), Zn(II), Pb(II), and Cd(II) on the soils amended with nanoscale hydroxyapatite. *Environ Prog Sustain Energy* 29:233–241
885. Wang D, Chu L, Paradelo M, Peijnenburg WJ, Wang Y, Zhou D (2011) Transport behavior of humic acid-modified nano-hydroxyapatite in saturated packed column: effects of Cu, ionic strength, and ionic composition. *J Colloid Interface Sci* 15:398–407
886. Mobasherpour I, Salah E, Pazouki M (2012) Comparative of the removal of Pb<sup>2+</sup>, Cd<sup>2+</sup> and Ni<sup>2+</sup> by nano crystallite hydroxyapatite from aqueous solutions: adsorption isotherm study. *Arab J Chem* 5:439–446
887. Handley-Sidhu S, Renshaw JC, Yong P, Kerley R, Macaskie LE (2011) Nano-crystalline hydroxyapatite bio-mineral for the treatment of strontium from aqueous solutions. *Biotechnol Lett* 33:79–87
888. Gandhi RM, Kousalya GN, Meenakshi S (2011) Removal of copper (II) using chitin/chitosan nano-hydroxyapatite composite. *Int J Biol Macromol* 48:119–124
889. Manocha LM, Disher IA, Manocha S (2011) Sorption of cadmium ions on (AB-type) carbonated hydroxyapatite nanoparticles. *Adv Sci Lett* 4:44–50
890. Gok C (2014) Neodymium and samarium recovery by magnetic nano-hydroxyapatite. *J Radioanal Nucl Chem* 301:641–651
891. Fernando MS, de Silva RM, de Silva KMN (2015) Synthesis, characterization, and application of nano hydroxyapatite and nanocomposite of hydroxyapatite with granular activated carbon for the removal of Pb<sup>2+</sup> from aqueous solutions. *Appl Surf Sci* 351:95–103



892. Ma'mani L, Heydari A, Shiroodi RK (2009) Nanohydroxyapatite microspheres as a biocompatible and recoverable catalyst for synthesis of carbon-phosphorous bond formation. *Curr Org Chem* 13:758–762
893. Liu Y, Zhong H, Li L, Zhang C (2010) Temperature dependence of magnetic property and photocatalytic activity of Fe<sub>3</sub>O<sub>4</sub>/hydroxyapatite nanoparticles. *Mater Res Bull* 45:2036–2039
894. Viswanadham N, Debnath S, Sreenivasulu P, Nandan D, Saxena SK, Al-Muhtaseb AH (2015) Nano porous hydroxyapatite as a bi-functional catalyst for bio-fuel production. *RSC Adv* 5:67380–67383
895. Wang H, Wang C, Xiao ZL, Zhang J, Zhu Y, Guo X (2016) The hydroxyapatite nanotube as a promoter to optimize the HDS reaction of NiMo/TiO<sub>2</sub> catalyst. *Catal Today* 259:340–346
896. Khairnar RS, Mene RU, Munde SG, Mahabole MP (2011) Nano-hydroxyapatite thick film gas sensors. *AIP Conf Proc* 1415:189–192
897. Viswanathan K, Vadivoo VS, Raj GD (2014) Rapid determination of hydrogen peroxide produced by *Lactobacillus* using enzyme coupled rhodamine isocyanide/calcium phosphate nanoparticles. *Biosens Bioelectron* 61:200–208
898. Xu J, Shen X, Jia L, Zhang M, Zhou T, Wei Y (2017) Facile ratiometric fluorapatite nanoprobe for rapid and sensitive bacterial spore biomarker detection. *Biosens Bioelectron* 87:991–997
899. Wang D, Bradford SA, Paradelo M, Peijnenburg WJGM, Zhou D (2012) Facilitated transport of copper with hydroxyapatite nanoparticles in saturated sand. *Soil Sci Soc Am J* 76:375–388
900. Wei W, Sun R, Jin Z, Cui J, Wei Z (2014) Hydroxyapatite-gelatin nanocomposite as a novel adsorbent for nitrobenzene removal from aqueous solution. *Appl Surf Sci* 292:1020–1029
901. Lu Y, Jiang H, Zhang NQ, Zhang M, Liu JK (2014) Assembly and copper ions detection of highly sensible and stable hydroxyapatite nanocomposite fluorescence probe. *Micro Nano Lett* 9:127–131
902. Sternitzke V, Kaegi R, Audinot JN, Lewin E, Hering JG, Johnson CA (2012) Uptake of fluoride from aqueous solution on nano-sized hydroxyapatite: examination of a fluoridated surface layer. *Environ Sci Technol* 46:802–809
903. Yu X, Tong S, Ge M, Zuo J (2013) Removal of fluoride from drinking water by cellulose@hydroxyapatite nanocomposites. *Carbohydr Polym* 92:269–275
904. Yih TC, Al-Fandi M (2006) Engineered nanoparticles as precise drug delivery systems. *J Cell Biochem* 97:1184–1190
905. Celotti G, Tampieri A, Sprio S, Landi E, Bertinetti L, Martra G, Ducati C (2006) Crystallinity in apatites: how can a truly disordered fraction be distinguished from nanosize crystalline domains? *J Mater Sci Mater Med* 17:1079–1087
906. Christenson EM, Anseth KS, van den Beucken JJJP, Chan CK, Ercan B, Jansen JA, Laurencin CT, Li WJ, Murugan R, Nair LS, Ramakrishna S, Tuan RS, Webster TJ, Mikos AG (2007) Nanobiomaterial applications in orthopedics. *J Orthop Res* 25:11–22
907. Schmidt SM, Moran KA, Kent AMT, Slosar JL, Webber MJ, McCready MJ, Deering C, Veranth JM, Ostafin A (2008) Uptake of calcium phosphate nanoshells by osteoblasts and their effect on growth and differentiation. *J Biomed Mater Res A* 87A:418–428
908. Motskin M, Müller KH, Genoud C, Monteith AG, Skepper JN (2011) The sequestration of hydroxyapatite nanoparticles by human monocyte-macrophages in a compartment that allows free diffusion with the extracellular environment. *Biomaterials* 32:9470–9482
909. Mohsen-Nia M, Bidgoli MM, Behrashi M, Nia AM (2012) Human serum protein adsorption onto synthesis nano-hydroxyapatite. *Protein J* 31:150–157
910. Powell MC, Kanarek MS (2006) Nanomaterials health effects – part 1: background and current knowledge. *Wis Med J* 105:16–20
911. Powell MC, Kanarek MS (2006) Nanomaterials health effects – part 2: uncertainties and recommendations for the future. *Wis Med J* 105:18–23
912. Motskin M, Wright DM, Muller K, Kyle N, Gard TG, Porter AE, Skepper JN (2009) Hydroxyapatite nano and microparticles: correlation of particle properties with cytotoxicity and biostability. *Biomaterials* 30:3307–3317

913. Wang J, Wang L, Fan Y (2016) Adverse biological effect of TiO<sub>2</sub> and hydroxyapatite nanoparticles used in bone repair and replacement. *Int J Mol Sci* 17:798. (14 pages)
914. Zhao X, Ng S, Heng BC, Guo J, Ma L, Tan TTY, Ng KW, Loo SJ (2013) Cytotoxicity of hydroxyapatite nanoparticles is shape and cell dependent. *Arch Toxicol* 87:1037–1052
915. Ding T, Xue Y, Lu H, Huang Z, Sun J (2012) Effect of particle size of hydroxyapatite nanoparticles on its biocompatibility. *IEEE Trans Nanobiosci* 11:336–340
916. Liu X, Qin D, Cui Y, Chen L, Li H, Chen Z, Gao L, Li Y, Liu J (2010) The effect of calcium phosphate nanoparticles on hormone production and apoptosis in human granulosa cells. *Reprod Biol Endocrinol* 8:32. (8 pages)
917. Fan Q, Wang YE, Zhao X, Loo JS, Zuo YY (2011) Adverse biophysical effects of hydroxyapatite nanoparticles on natural pulmonary surfactant. *ACS Nano* 5:6410–6416
918. Jiang H, Liu JK, Wang JD, Lu Y, Zhang M, Yang XH, Hong DJ (2014) The biotoxicity of hydroxyapatite nanoparticles to the plant growth. *J Hazard Mater* 270:71–81
919. Li S, Huang L (2008) Pharmacokinetics and biodistribution of nanoparticles. *Mol Pharm* 5:496–504
920. Zhou W, Zheng J (2012) Direct observation of hydroxyapatite nanoparticles in vivo. *Adv Mater Res* 503–504:688–691
921. Moghimi SJ, Hunter AC, Murray JC (2005) Nanomedicine: current status and future prospects. *FASEB J* 19:311–330
922. Xu HHK, Weir MD, Simon CG Jr (2008) Injectable and strong nano-apatite scaffolds for cell/growth factor delivery and bone regeneration. *Dent Mater* 24:1212–1222
923. Pujari-Palmer S, Chen S, Rubino S, Weng H, Xia W, Engqvist H, Tang L, Ott MK (2016) In vivo and in vitro evaluation of hydroxyapatite nanoparticle morphology on the acute inflammatory response. *Biomaterials* 90:1–11
924. Watari F, Abe S, Tamura K, Uo M, Yokoyama A, Totsuka Y (2008) Internal diffusion of micro/nanoparticles inside body. *Key Eng Mater* 361–363:95–98
925. Oberdorster G, Oberdorster E, Oberdorster J (2005) Nanotoxicology: an emerging discipline evolving from studies of ultrafine particles. *Environ Health Perspect* 113:823–839
926. Nel A, Xia T, Mädler L, Li N (2006) Toxic potential of materials at the nanolevel. *Science* 311:622–627
927. Jahnen-Dechent W, Simon U (2008) Function follows form: shape complementarity and nanoparticle toxicity. *Nanomedicine* 3:601–603
928. Singh N, Manshian B, Jenkins GJS, Griffiths SM, Williams PM, Maffei TGG, Wright CJ, Doak SH (2009) NanoGenotoxicology: the DNA damaging potential of engineered nanomaterials. *Biomaterials* 30:3891–3914
929. Dhawan A, Sharma V, Parmar D (2009) Nanomaterials: a challenge for toxicologists. *Nanotoxicology* 3:1–9
930. Dwivedi PD, Misra A, Shanker R, Das M (2009) Are nanomaterials a threat to the immune system? *Nanotoxicology* 3:19–26
931. Liu Z, Xiao Y, Chen W, Wang Y, Wang B, Wang G, Xu X, Tang R (2014) Calcium phosphate nanoparticles primarily induce cell necrosis through lysosomal rupture: the origination of material cytotoxicity. *J Mater Chem B* 2:3480–3489
932. Scientific Committee on Consumer Safety (SCCS) Opinion on Hydroxyapatite (nano). SCCS/1566/15, adopted 16 October 2015. [http://ec.europa.eu/health/scientific\\_committees/consumer\\_safety/docs/sccs\\_o\\_191.pdf](http://ec.europa.eu/health/scientific_committees/consumer_safety/docs/sccs_o_191.pdf)

# Chapter 10

## Calcium Phosphate-Silk Fibroin Composites: Bone Cement and Beyond

Fengxuan Han, Chen Shi, Huilin Yang, and Bin Li

**Abstract** Calcium phosphate cements (CPCs) are promising substitute materials for current nonbiodegradable poly(methyl methacrylate)-based bone cements due to their outstanding biocompatibility, biodegradability, and osteoconductivity. However, the applications of calcium phosphates (CaPs) are relatively limited due to the inferior mechanical strength. Silk fibroin (SF), a natural fibrous protein that originated from silkworm or spider which has good biocompatibility, biodegradability, and mechanical properties, has been used to reinforce the mechanical properties and improve the performance of CPCs. In addition to bone cement, CaP-SF composites have also been used as bone-repairing materials and carrier systems. In this chapter, we aim to provide a brief overview of recent progress in the use of CaP-SF composites as bone cement and for other purposes. The properties, processing techniques, and applications of CaPs and SF are first introduced, and the emerging challenges for CPCs are also discussed. Then the application of CaP-SFs as reinforced bone cements as well as the reinforcing mechanisms is reviewed. Finally, other applications of CaP-SF composites in bone tissue engineering are also discussed. We also provide our perspectives on the future development of CaP-SF composites for clinical applications.

**Keywords** Calcium phosphate • Silk fibroin • Composite • Bone cement • Bone regeneration

---

Fengxuan Han and Chen Shi contributed to the chapter equally.

F. Han • H. Yang • B. Li (✉)

Orthopedic Institute, Soochow University (South Campus),  
708 Renmin Rd, Rm 308 Bldg 1, Suzhou, Jiangsu 215007, China

Department of Orthopaedics, The First Affiliated Hospital of Soochow University,  
Suzhou, Jiangsu, China

e-mail: [binli@suda.edu.cn](mailto:binli@suda.edu.cn)

C. Shi

Department of Chemical and Materials Engineering, University of Alberta,  
Edmonton, Canada

## 10.1 Introduction

Aging-related osteoporosis prevalence has gradually evolved into a global concern because of the improved life expectancy. Especially, the osteoporosis with subsequent vertebral compression fractures (VCFs) has become a serious worldwide healthcare problem. For example, the annual incidence of osteoporotic fractures exceeds 1.5 million in the USA, with more than 50% being VCFs, which is almost twice the incidence of hip fractures [1]. About 20% of individuals over 50 years old and 45% of women over 50 experience osteoporotic VCFs (OVCFs). If left untreated, OVCFs may result in dramatic physical, functional, and psychological consequences which significantly impair the life quality of patients [2]. OVCF patients usually suffer from severe back pain. Moreover, restrictive lung diseases may develop if there are multiple thoracic fractures [3]. In the worst cases, female OVCF patients may have a 23% higher mortality rate compared to those without OVCFs [4]. Besides conservative treatments, two minimally invasive surgery procedures to treat OVCFs, vertebroplasty (VP) and kyphoplasty (KP), have been developed to reduce the morbidity of patients with acute OVCFs. An essential component of VP and KP treatments includes the injection of bone cement to stabilize the fractured vertebrae.

In general, bone cements as the filling material are self-curing compounds that can be injected in flowing state and subsequently fully harden in the body. They should have considerable mechanical strength and toughness to achieve long-term sustainability as well as appropriate setting time and injectability for conducting surgeries. In addition, radiopacity and clear contrast under fluoroscopy are also important features of bone cements. Currently, the two main categories of bone cements are nondegradable acrylic bone cements (ABCs) and biodegradable calcium phosphate cements (CPCs). To date, the most popular bone cements are poly(methyl methacrylate) (PMMA)-based ABCs. However, the application of PMMA-based ABCs is highly limited due to several drawbacks including nonbiodegradability, monomer toxicity, heat generation during curing, and leakage of monomer. Moreover, while bone cements are often combined with antibiotics that are released systematically or locally at the affected site to treat chronic bone infection caused by the implants, PMMA bone cements show only limited antibiotic release due to incompatibility with many antimicrobial agents [5].

To overcome the disadvantages of PMMA-based bone cements, CPCs and other types of biodegradable bone cements have been developed. The first kind of CPCs was invented by Brown and Chow in the early 1980s [6]. Compared to ABCs, CPCs are biocompatible and osteoconductive materials with great potential in orthopedic applications. The interest in this material is still rapidly rising for the following reasons. First, the need for CPCs in dental and orthopedic applications is increasing as the life expectancy of the population increases [7]. Second, CPC powder can be mixed with other liquid to form a paste that can intimately adapt to the neighboring bone at the defects and then harden *in vivo* without generating heat [8, 9]. Third, implants with bone-like calcium phosphate (CaP) minerals may beneficially bond to

host bone because the biomimetic CaP minerals can act as a preferred substrate for cell attachment and proliferation of osteoblastic cells [10]. Especially for vertebral augmentation, CPCs can be used as biodegradable fillers to achieve balanced cement resorption and new bone formation, avoiding the potential risks of traditional non-biodegradable PMMA-based bone cements. Interestingly, the compressive strength of CPC-treated vertebra was reported to continuously increase, whereas PMMA-treated VBs presented decreasing compressive strength, indicating both short-term and intermediate effects of CPC injection on treating vertebral defects [11]. Hence, CPC is considered as a highly promising candidate material for bone tissue engineering for its outstanding moldability, in situ self-setting ability, and excellent osteoconductivity.

On the other hand, the relatively poor fracture toughness, tolerance to damage, and mechanical reliability of CPCs compared to natural bone tissue and other types of bone cements significantly limit their wide applications in bone tissue repairing, especially in repairing high load-bearing bone defects [6]. Therefore, mechanical reinforcement of CPCs to meet or exceed clinical requirements is of the highest research priority in CPCs development. Recently, compositing CPCs with natural and synthetic polymers provides a new strategy to meet this challenge. Among them, silk fibroin (SF), a natural fibrous protein produced from silkworms and spiders, appears to be a promising material due to the remarkable mechanical properties and biocompatibility.

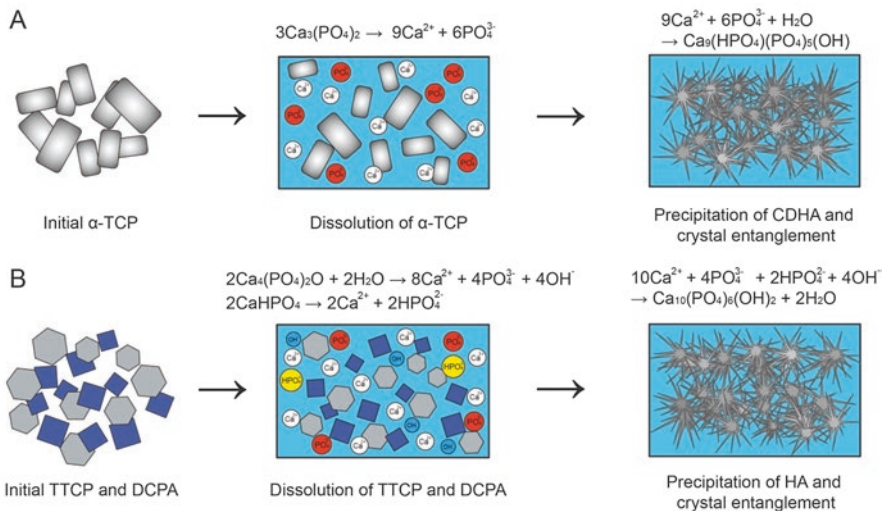
## 10.2 Calcium Phosphate Cements

In general, CPCs are produced by mixing a powder phase, which contains a combination of different CaP compounds, and a liquid phase of water- or calcium- or phosphate-containing aqueous solutions [12]. Calcium orthophosphates are the most commonly used CaPs in CPCs (Table 10.1) [13–16]. Upon mixing, the two-phase mixture forms a semisolid paste and progressively cures into a solid mass.

Despite numerous formulations, all CPC systems share the same setting chemistry, dissolution-precipitation, and entanglement of precipitated crystals [6]. Depending on the pH of the paste, the final products of CPCs can be categorized into apatite (HA or CDHA, formed at pH >4.2) and brushite (DCPD, formed at pH <4.2) [16, 17]. At a physiological pH, apatite is thermodynamically more stable than brushite [15]. As brushite cement has short setting time, low mechanical strength, and inferior injectability, its application in bone tissue engineering is much limited compared to apatite [18]. Figure 10.1a illustrates the synthesis of CPCs by hydrolyzing  $\alpha$ -TCP powder, a component in most commercialized CPC formulations. Upon contact with water,  $\alpha$ -TCP dissolves and releases  $\text{Ca}^{2+}$  and  $\text{PO}_4^{3-}$ , whose concentration exceeds the solubility of CDHA. Therefore, the solution is supersaturated with respect to CDHA, resulting in the precipitation of CDHA crystals. These precipitated CDHA crystals entangle with each other and gradually form a solid paste. A different combination of calcium phosphates forms various CPCs. As an

**Table 10.1** Characteristics of generally used CaPs in CPCs [14–16]

Compound	Formula	Ca/P ratio	Solubility at 25 °C, $-\log(K_s)$
Amorphous calcium phosphate (ACP)	$\text{Ca}_{10-x}\text{H}_{2x}(\text{PO}_4)_6(\text{OH})_2$	1.2–2.2	Highly soluble
Calcium-deficient hydroxyapatite (CDHA)	$\text{Ca}_{10-x}(\text{HPO}_4)_x(\text{PO}_4)_{6-x}(\text{OH})_{2-x}$	1.5–1.67	~85
Dicalcium phosphate anhydrous (DCPA)	$\text{CaHPO}_4$	1.0	~6.9
Dicalcium phosphate dihydrate (DCPD)	$\text{CaHPO}_4 \cdot 2\text{H}_2\text{O}$	1.0	~6.59
Hydroxyapatite (HA)	$\text{Ca}_{10}(\text{PO}_4)_6(\text{OH})_2$	1.67	~116.8
Monocalcium phosphate anhydrous (MCPA)	$\text{Ca}(\text{H}_2\text{PO}_4)_2$	0.5	~1.14
Monocalcium phosphate monohydrate (MCPM)	$\text{Ca}(\text{H}_2\text{PO}_4)_2 \cdot \text{H}_2\text{O}$	0.5	~1.14
Octacalcium phosphate (OCP)	$\text{Ca}_8(\text{HPO}_4)_2(\text{PO}_4)_4 \cdot 5\text{H}_2\text{O}$	1.33	~96.6
Tetracalcium phosphate (TTCP)	$\text{Ca}_4(\text{PO}_4)_2\text{O}$	2.0	~44
$\alpha$ -Tricalcium phosphate ( $\alpha$ -TCP)	$\alpha\text{-Ca}_3(\text{PO}_4)_2$	1.5	~25.5
$\beta$ -Tricalcium phosphate ( $\beta$ -TCP)	$\beta\text{-Ca}_3(\text{PO}_4)_2$	1.5	~28.9

**Fig. 10.1** Schematics of (a) synthesis of CDHA cements using  $\alpha$ -TCP and (b) synthesis of HA cements using TTCP and DCPA

example, a mixture of equimolar TTCP and DPCA will lead to the formation of HA crystals (Fig. 10.1b). Since the first CPC was commercialized in the 1990s, there have been many CPCs with different compositions being developed and made commercially available.

### ***10.2.1 CPCs as Bone Cements***

The application of CPCs as bone cements can be traced back to the 1980s [19, 20]. To date, CPCs are still attracting research interest as cement materials for dental [21, 22], craniofacial [23], orthopedic [24, 25], and VP and KP applications [14, 26]. Numerous previous studies have demonstrated the biocompatibility and osteogenic properties of CPCs [27]. Although CPC products specific for VP and KP purposes are not yet commercially available, there have been many off-label uses of CPCs for vertebral augmentation and spinal fusion. It was reported that CPCs could restore the strength but not the stiffness of vertebra when vertebra was filled with CPCs by VP/KP procedures [28]. In the treatment of fractured vertebra, CPCs could restore the strength and stiffness and result in similar anterior vertebral height restoration [29]. Using a canine VP model, Turner et al. found that CPCs were well integrated to vertebra bone tissue and remarkable vascular invasion and bone ingrowth happened, demonstrating that CPCs had excellent biocompatibility and osteoconductivity [11].

In some applications, CPCs were also loaded with drugs and used as bone cements. CPCs were abundant in nano-/micro-sized pores with approximately 30–50% porosity [30]. This porous structure enables fluid exchange and inclusion of growth factors, matrix proteins, and cells. Due to their inherent porosity, CPCs have also been used as carriers for controlled drug delivery [30, 31]. To improve the osteogenesis performance of CPCs, some supplements were added into them [32, 33]. In a research, recombinant bone morphogenetic protein-2 (BMP-2) was incorporated into CPC/SF cement, and the materials showed excellent osteoconduction and osteoinduction capability [32]. Recently, we found that  $\alpha$ -TCP/SF cement could sustain controlled release of an osteogenic reagent, N-Acetyl cysteine (NAC) [33]. It should be noted that the porosity may also become a limitation for CPCs to be used in high load-bearing sites as high porosity weakens the mechanical strength of CPCs [34].

### ***10.2.2 CPCs for Bone Regeneration***

With CaP crystals resembling the HA in native bone tissue, CPCs are also utilized as biocompatible and osteoconductive materials for bone regeneration. The osteoconductivity of CPCs can facilitate attachment, proliferation, and phenotypic expression of bone cells at the implant site, eventually leading to formation of new bone. In addition, the bone-like elastic modulus of CPCs can help prevent stress shielding as well as maintain adequate toughness to prevent fatigue fracture under cyclic loading [35]. Yi et al. incorporated electrospun ultrafine polymer fibers into CPCs for bone regeneration [36]. The incorporated fibers were shown to form a connected channel-like structure in the CPCs, and interconnected channel-like pores could be achieved after degradation of the fibers. CPCs were also combined

with alginate to form a porous 3D matrix for bone regeneration in another study [37]. Mesenchymal stem cells (MSCs) cultured on the CPCs/alginate scaffold demonstrated active proliferation and subsequent osteogenic differentiation. In vivo study also showed that CPCs/alginate scaffolds promoted new bone formation. Moreover, with the intrinsic micropores, CPCs can also be used as a delivery system for controlled release of bioactive substances or cells, making it a promising material for bone regeneration [32, 33].

When implanted, CPCs may undergo passive and/or active resorption in vivo. The passive absorption mainly depends on the solubility and dispersion of the materials, while the active resorption is largely determined by the activity of osteoclasts. For successful bone regeneration, a balance between CPC resorption and new bone formation is required, and new bone tissue is expected to form along with the resorption of CPCs. By controlling the characteristics of CPCs, complete bone regeneration at the implanted site can be achieved within a few months to a couple of years [38]. However, the inconsistently reported degradability of CPCs, possibly due to the composition complexity, setting chemistry, and environment, may present a major challenge toward their clinical applications. For example, BoneSource was observed to be stable with little resorption after several years of implantation [39]. In contrast, Turner et al. found evident degradation of implanted BoneSource in a canine VP model [11]. In another study, replacement of approximately 30% of BoneSource with new bone tissue was observed 40 weeks after implantation [40].

### ***10.2.3 Emerging Challenges with CPCs***

Clinically, the mechanical strength of ideal bone cement should be similar to or greater than that of bone tissue at the defect site. The mechanical properties of CPCs can be affected by a number of factors including chemical composition, granularity, crystal type, powder/liquid ratio, and porosity. For example, decreasing the porosity of CPCs by compacting the cement paste prior to hydration could significantly boost their mechanical properties, while high pore density and size contributed to mechanical strength loss [41]. High porosity could also lead to poor injectability, making it difficult to be used in minimally invasive surgery procedures [6]. However, when the porosity of CPC reached a critical level (~30%), the enhancement effect was no longer apparent [42]. Therefore, optimizing the balance among mechanical properties, porosity, handling convenience, and bone replacement performance is still an important challenge for the development of CPCs. Recently, compositing CPCs with natural and synthetic polymers provides a new strategy to deal with this challenging issue.



### 10.2.4 CaP-Based Composites

To improve the performance of CPCs, various CaP-based composites were prepared. Incorporation with organic additives, biocompatible polymers, proteins, polysaccharides, and inorganic materials like bioceramics, bioglass, and fiber has been proven to effectively improve the mechanical properties of CPCs. For example, citrate ions could facilitate the sliding and dispersion of apatite crystals. Adding citric acid into apatite cement paste, therefore, increased both the injectability and strength of CPCs [43]. In another study, addition of a silanized-hydroxypropyl methylcellulose (Si-HPMC) hydrogel was also found to improve the mechanical and handling properties of CPCs [44].

Compositing with fibers is an effective approach to improve the mechanical properties of CPCs, probably through a crack-arresting mechanism [6, 45]. Commonly used fibers include nondegradable ones like polyamides, carbon fibers, and glass fibers and biodegradable ones including natural biomolecules like proteins and polysaccharides and synthetic polymers such as poly(glycolic acid) (PGA), polylactide (PLA), poly(lactic-co-glycolic acid) (PLGA), and polycaprolactone (PCL). In a previous study, absorbable polyglactin fibers were added at a volume fraction of 25% to reinforce CPC. The flexural strength increased from ~5 to 13 MPa at a powder/liquid mass ratio of 2, and it further increased to 25 MPa at a powder/liquid mass ratio of 3 [17]. In another study, the flexural strength of CPC reached 26 MPa with addition of 15% chitosan and 20% polyglactin fibers [16]. It has been demonstrated that the fiber length, volume fraction, and fiber strength are the key microstructural parameters determining the mechanical properties of CPC composites. In a study, four different fibers, including aramid, carbon, E-glass, and polyglactin, with fiber length ranging from 3 to 200 mm and fiber volume fraction of 1.9–9.5%, were used to reinforce CPCs [46]. The ultimate strength of unreinforced CPC was  $13 \pm 3$  MPa while that of the composites increased to  $62 \pm 16$  MPa,  $59 \pm 11$  MPa,  $29 \pm 8$  MPa, and  $24 \pm 4$  MPa with addition of 5.7 vol% 75 mm-long aramid, carbon, E-glass, and polyglactin fibers, respectively. Fiber length is also an important factor. For composites containing 5.7% aramid fibers, the ultimate strength increased with fiber length [46]. We also prepared CPC/SF composites in which the supplement of SF markedly improved the mechanical strength and wash-out resistance of CPCs [33].

CPC-based composites containing whiskers made of HA, calcium carbonate, silicon nitride, silicon carbide, or bioglass have also been fabricated, which show substantially improved mechanical properties [47, 48]. CPCs with gelatin microspheres were formulated to comply with mechanical stability, osteoconductivity, biodegradability, and porosity. The in vitro degradation study revealed that degradation of microspheres first started at the surface of composite and gradually proceeded to the inner part, resulting in the in situ generation of macropores in CPCs after complete microsphere degradation [49].

## 10.3 Silk Fibroin

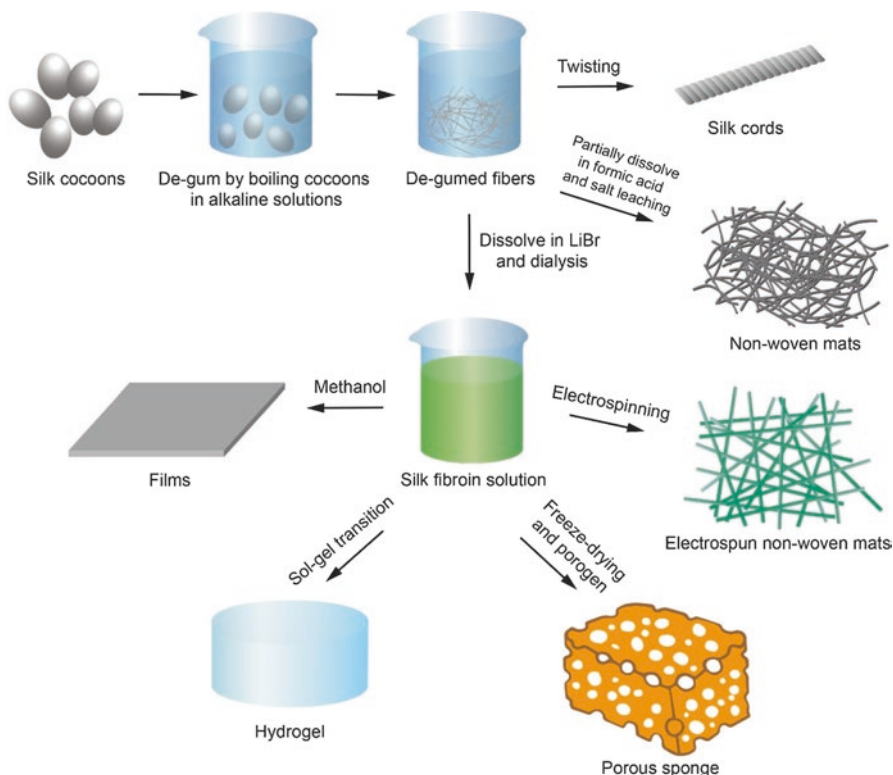
SF, a type of fibrous protein produced from silkworms and spiders with remarkable mechanical properties and biocompatibility, has been used as biomedical materials, especially as sutures, for centuries. In natural silk, SF is coated with hydrophilic proteins called sericin [50], which constitute 25–30% of the silk cocoon mass. Sericin may cause immunological response in the body [51], and thereby they are usually removed through the degumming process by boiling silk cocoons in an alkaline solution. Afterward, the degummed or purified silk fibers can be fabricated into silk cords by twisting [51] or nonwoven silk mats by partial dissolution in formic acid and salt-leaching treatment [52]. Regeneration and purification of SF solutions by degumming process significantly broaden its application as biomaterials [50]. SF can also be dissolved in lithium bromide solution, dialyzed, and formed into aqueous SF solution for further preparation of biomaterials with different morphologies (Fig. 10.2) [53]. Till now, SF has been prepared into biomaterials including films [54], hydrogels [55], nonwoven fabrics [56], and 3D porous scaffolds [57] by various methods, e.g., freeze-drying [53], salt leaching [58], gas foaming [53], and electrospinning [59].

The spider silk is also an attractive material for biomedical applications for its outstanding mechanical properties [60]. However, the insolubility and unique properties hinder the purification and preparation of silk protein and limit its applications. In recent studies, hexafluoro-2-propanol and concentrated formic acid were used to dissolve and purify spider SF. Electrospun spider SF-poly(D,L-lactide) composite nonwoven mats were successfully prepared using this method [61, 62].

### 10.3.1 Characteristics of SF

The domesticated silkworm SF fibers are about 10–25  $\mu\text{m}$  long in diameter and consist of light chain proteins (~26 kDa) and heavy chain proteins (~390 kDa) linked by disulfide bond [63]. The primary amino acid composition of SF is ~43% glycine (Gly), ~30% alanine (Ala), and ~12% serine (Ser) [50]. Silks generally consist of  $\beta$ -sheet structures for the abundance of hydrophobic domains formed by short side chain amino acids in the primary sequence. The combination of large hydrophobic domains and interspaced small hydrophilic domains facilitates the assembly of silk and evidently promotes the strength of silk fibers [64]. Surface modification of SF can be achieved by chemical reaction with the amino acid side chains, which can be used to immobilize cellular growth factors and improve the cell recognition and mineralization properties of SF [50].

SF derived from silkworm cocoon has good biocompatibility and biodegradability, remarkable humidness, excellent air permeability, and satisfactory mechanical properties. Aside from properties as above, controlled hydroxyapatite mineralization on SF has also been reported [65]. For example, SF that blended with



**Fig. 10.2** Degumming process of silk to obtain purified silk fibroin and fabrication of silk fibroin into biomaterials with different morphologies

poly(L-aspartate) was successfully used as a template for the growth of apatite crystals [65]. Besides, enhanced attachment and proliferation of different kinds of cells including human skin fibroblasts, keratinocytes, and human MSCs were also reported for SF scaffolds [66, 67].

Control over the degradation rate is essential for tissue reconstruction, such that the rate of scaffold degradation should match the rate of tissue growth. SF is a long-term degradable biomaterial. SF is susceptible to proteolytic degradation as a function of a foreign body response *in vivo*, and it has been reported to lose the majority of the mechanical strength within 1 year *in vivo* after implantation and fail to be recognized at the implantation site after 2 years [67]. Degradation rate of SFs can be controlled for specific applications by manipulating the scaffold design and surface modification [68]. A previous study modified the surface of SF by covalent coupling of arginine-glycine-aspartic acid to enhance the cell-SF interactions. This strategy likely altered the degradation rate as a function of macrophage/cell recognition and binding [69]. The degradability of SF can also be controlled by the processing procedures and the resultant percentage of  $\beta$ -sheet crystallinity. SF degrades via the action of proteases, and its degradation rate depends upon the morphology, structure,

and mechanical and biological environment. Several types of proteolytic enzymes including protease,  $\alpha$ -chymotrypsin, and collagenases were proved to effectively degrade SF films or fibers in vitro [68, 70]. Interestingly, a cocoon shell-associated trypsin inhibitor (CSTI) isolated from the water-soluble extract from silkworm cocoons was shown to protect the light chain of SF against tryptic degradation [71], which could be a useful tool to control the degradation of SF. The morphology and structure also affect the degradation rate of SF. When exposed to similar enzymes, SF films were shown to degrade faster than SF fibers [70]. Porous SF sponges also showed different degradation rate depending on the processing conditions. In a report, solvent-processed SF sponges degraded at a slower rate than the water-processed systems with similar pore sizes, which might be attributed to increased surface roughness or different content or distribution of crystallized phase [72]. The degradation rate of SF could also be modulated by changing crystallinity, porosity, and molecular weight distribution (MWD) [73]. For example, decrease in MWD may disrupt ordered structures and reduce cross-links, potentially resulting in faster degradation. In general, SF may be an advantageous material over rapidly degrading biomaterials such as collagen and polyester synthetics as it can maintain tissue integrity while continually and gradually transferring the load-bearing burden to developing tissue.

Sericin from the original silk cocoon is known to cause hypersensitivity [51], but purified SF by degumming shows little immunological response. The inflammatory response of SF in vitro showed less adhesion to immunocompetent cells compared to polystyrene and poly(2-hydroxyethyl methacrylate) [74]. In another study, SF films were found to induce weaker inflammatory response in vivo than collagen films and PLA films [75]. Invasion by lymphocytes was not observed in vivo 6 months after implantation, and upregulation of inflammatory pathways was negligible at the implantation site [52]. Compared with other fibrous protein such as collagen [76], SF was also easier to sterilize using autoclaving [77, 78], ethylene oxide [51], and  $\gamma$ -radiation or ethanol [79, 80].

### ***10.3.2 SF for Bone Regeneration***

SF can be used as biomaterials for bone regeneration. Osteoblast-like cells cultured on SF hydrogels demonstrated excellent cell adherence [81]. Electrospun nonwoven SF mats implanted in calvarial defects of rabbits also contributed to complete bone healing within 12 weeks [82]. When SF hydrogels were injected at critical-sized femur defects of rabbits, greater trabecular bone volume and thickness, significantly higher mineralization, and faster bone formation were seen compared to injection with PLGA [83]. Porous SF scaffolds were also loaded with human BMP-2 gene-activated MSCs to promote bone regeneration [84]. In vitro test showed the scaffold supported the osteogenic differentiation of MSCs, and successful regeneration of bone tissues at critical defects was observed by in vivo experiments. While these studies suggested the potential of SF for applications in bone regeneration, SF is

more often composited with inorganics or other natural or synthetic polymers to achieve improved performance. As an example, electrospun SF scaffolds containing hydroxyapatite nanoparticles showed upregulation of BMP-2 gene expression and significant osteogenesis [80].

### ***10.3.3 SF as a Reinforcing Material***

Due to the excellent biocompatibility, degradability, and mechanical properties, SF is also usually used as reinforcing materials to strengthen the mechanical properties of other materials. For example, the mechanical properties of electrospun spider SF-poly(D,L-lactide) (PDLLA) composite fibers improved with the content of SF as a result of the formation of more helix structure and retention of  $\beta$ -sheets [62]. SF was also used to enhance chitosan, resulting in the improvement of tensile strength from 5 to 13 MPa and decrease of strain at break from 22.5% to 8.3%. This is likely due to the strong hydrogen-bonding interactions between chitosan and SF [85]. Micro-sized SF fibers were also applied to reinforce a porous silk scaffold to fabricate a bone composite material with compressive strength as high as  $\sim$ 13 MPa [86]. The scaffold showed an optimal combination of roughness, porosity, and mechanical strength and significantly promoted osteogenic differentiation of MSCs.

## **10.4 CaP-SF Composites as Bone Cements**

Natural bone is a typical inorganic/organic composite composed of approximately 80% HA and 20% collagen matrix. Therefore, a growing interest has been focused on compositing HA ceramics with biocompatible polymers, such as gelatin [87], polylactic acid [88], and SF [89–91] for bone defect repair and bone regeneration. CaP-SF composites are promising bone cement materials with good biocompatibility. For example, CPCs combining SF and  $\alpha$ -TCP promoted the adhesion, spreading, and proliferation of MSCs. They also markedly promoted improved osteogenic differentiation of MSCs, as shown by the upregulated gene expression of alkaline phosphatase (ALP), collagen type I, and osteocalcin [92]. Recently, our group prepared injectable SF/CPC composites supplemented with HA-SF complex, which showed good biocompatibility both in vitro and in vivo [93]. In another study, SF/nano-CaP composites showed decent self-mineralization capability and no cytotoxicity [94].

### 10.4.1 *Injectability*

The injectability is essential for the clinical applications of CaP-SF composites as bone cements. The setting time is a critical parameter of bone cements. Prolonged setting may cause cement leakage and insufficient mechanical strength, while too rapid setting may result in difficulty during injection. Ideally, the initial setting time is 3–8 min, and the final setting time should be less than 15 min [95]. Faster setting within acceptable range is more desirable because the graft can attain geometric integrity and enhanced mechanical strength within a short period of time. While the setting time and microstructure of CPC are largely affected by the ratio between Ca and P [96], addition of SF may accelerate the hydrolysis process and therefore shorten both the initial and final setting times of  $\alpha$ -TCP [33]. However, further addition of N-acetyl cysteine (NAC) led to slightly extended setting time of  $\alpha$ -TCP/SF composites by rupturing the disulfide bonds to increase the fluidity of SF [33]. Increasing the concentration of NAC in 6% SF solution was found to produce negative effects on the initial and final setting time of  $\alpha$ -TCP/SF-NAC cements. Increasing the NAC concentration to 50 mM was found to increase the initial setting time from about  $18.61 \pm 1.09$  min to approximately  $23.47 \pm 1.34$  min and the final setting time from  $28.96 \pm 1.11$  min to  $35.01 \pm 1.32$  min.

The anti-washout property is another property affecting the application of CPCs. During procedures, direct contact between cements and blood or other body fluid may lead to cement collapse and leakage, which can result in severe complications such as fatal pulmonary embolism [97]. The addition of SF was demonstrated to significantly enhance the anti-washout property of CPCs [33]. In a previous study, our group applied a coprecipitation method to synthesize HA-SF complex and supplemented it to an injectable CPC/SF composite [93]. The setting time of CPC/HA-SF/SF composites was found to decrease with increasing HA-SF content, and no apparent effect on injectability was observed [93]. The initial setting time and final setting time of CPC/HA-SF/SF composites with 3 wt% were  $25.9 \pm 0.8$  min and  $32.5 \pm 0.5$  min, respectively [93]. This optimized injectability and setting times make CPC/HA-SF/SF composites suitable VP/KP filler materials.

SFs, by promoting HA formation and reducing fluid penetration, can improve the stability of CPCs in fluids. For instance, SF was reported to induce HA deposition at 37 °C in 1.5 SBF, and the authors evaluated the effect of pH and initial  $\text{Ca}^{2+}$ - $\text{H}_2\text{PO}_4^-$  (CaP) concentration on the crystal growth of HA on the surface of SF [90]. They demonstrated that a pH of 7 promoted the transition of DCPD to HA. Kong et al. found that SF could accelerate the phase transmittance of amorphous calcium phosphate to the crystal hybrid between DCPD and HA [98]. Li et al. prepared SF/calcium phosphate composite with addition of a different amount of  $\text{Na}_2\text{SiO}_3$  to assess the effect of silicon on the HA formation in the composite [99]. And the HA crystal formation was revealed to be significantly accelerated in the presence of silicon. H. Zhu et al. prepared SF/Wollastonite composite scaffolds via freeze-drying method. The composite scaffold was shown to be in vitro bioactive, because it induced the formation of carbonated HA on the surface after soaking in SBF for

5 days [100]. SF can also regulate the mineralization process of HA and form fibroin-HA nanocomposites with better gelation properties by bonding with HA. The incorporation of SF reinforced the cohesion of CPC and consequently reduced the risk of cardiovascular complications in VP/KP treatments [101].

### 10.4.2 Reinforcing Effect

With excellent bone replacement capability and osteoconductivity, CPC is of promising potential for a wide range of clinical applications in bone regeneration. Unfortunately, however, the application of CPC is currently limited to non-stress-bearing defects due to its relatively low mechanical strength and high susceptibility to brittle catastrophic fracture. SF was believed to supplement excellent biomechanical properties to CPC. Recently, we found that supplementing SF to CPCs could improve the mechanical strength and washout resistance of CPCs [32]. In another study, SF was added into  $\alpha$ -tricalcium phosphate cements, and the flexural strength of prepared CPC/SF scaffold ( $8.9 \pm 1.8$  MPa) was significantly higher than that of pure CPC ( $5.2 \pm 0.3$  MPa) [92], which exceeded the tensile strength of cancellous bone (3.5 MPa) [102]. Reinforced by SF, the compressive strength of  $\alpha$ -TCP/SF reached  $29.86 \pm 4.66$  MPa, which was much higher than that of pure  $\alpha$ -TCP ( $11.59 \pm 3.50$  MPa) [33]. Interestingly, addition of NAC in the cements also enhanced the mechanical property of  $\alpha$ -TCP and  $\alpha$ -TCP/SF. And the highest compressive strength of  $24.25 \pm 4.86$  MPa and  $42.41 \pm 7.99$  MPa for  $\alpha$ -TCP and  $\alpha$ -TCP/SF were reached in the presence of 50 mM NAC [33].

Although the mechanical strength of CPCs could be improved by supplementing with SF, the compressive strength of CPC/SF composites required further enhancement especially for VP/KP purposes, which needed compressive strength around 50–90 MPa [32, 103]. Interfacial adhesion between incompatible phases is believed to be a critical factor which largely determines the mechanical properties of inorganics-polymer hybrid composites [104, 105]. Hence, improving interfacial compatibility between CPC and SF phases may further reinforce their mechanical properties. To enhance the interfacial integration between the inorganic and organic phases, a mineralized HA-SF complex prepared through coprecipitation method was supplemented to CPC/SF composites as an interfacial coupling reagent [93]. Even at a small amount, the complex remarkably improved the mechanical strength of the composite, likely because of the enhanced interfacial integrity and more oriented growth of hydroxyapatite crystals in the composite. The compressive strength of the CPC/HA-SF/SF composite increased with increasing HA-SF content within 3 wt%, and the highest compressive strength of CPC/HA-SF/SF could reach  $50.2 \pm 1.9$  MPa which was obviously larger than that of CPC/SF without HA-SF ( $33.4 \pm 0.9$  MPa) [93]. Further, we developed stronger CPCs using calcium hydroxide-treated silk fibroin as curing solution, the mechanical strength of which was found to dramatically improve with increasing pH.

### 10.4.3 Reinforcement Mechanisms

Since silk is the strongest fiber known in nature with a strength up to 4.8 GPa [106], SF can provide high mechanical properties when applied as a reinforcement material. Several mechanisms have been proposed for reinforcement of CaP-SF composite bone cements. For CPC/HA-SF/SF, the addition of HA-SF evidently increased the mechanical properties compared with CPC/SF, and optimal reinforcement of CPC/SF was achieved with addition of about 3 wt% HA-SF [93]. Functioning as a coupling agent, the HA-SF complex containing both organic and inorganic components can bridge the incompatible CPC and SF phases. Moreover, the HA-SF complex may also act as nucleation seeds to improve the crystallinity of HA in CPC [93]. With a small amount of apatite seeds such as HA-SF, precipitating apatite would preferentially nucleate around the seeds, and the oriented growth would enhance the mechanical strength of the CPC/HA-SF/SF composite. However, excessive HA seeds might limit the dissolution rate of TTCP or DCPA, resulting in weak mechanical strength [93].

It has been reported that NAC could be used to improve the mechanical properties of CPC. For example, the highest compressive strength of  $42.41 \pm 7.99$  MPa was achieved at the presence of 50 mM NAC [33]. The mechanism of reinforcement might be the oriented HA crystal growth induced by the interactions among NAC, SF, and  $\alpha$ -TCP [33]. The presence of NAC with SF induces oriented growth of HA crystals, and NAC can further expand the three-dimensional networks of SF, which can restrict and tightly bond with HA crystals [33].

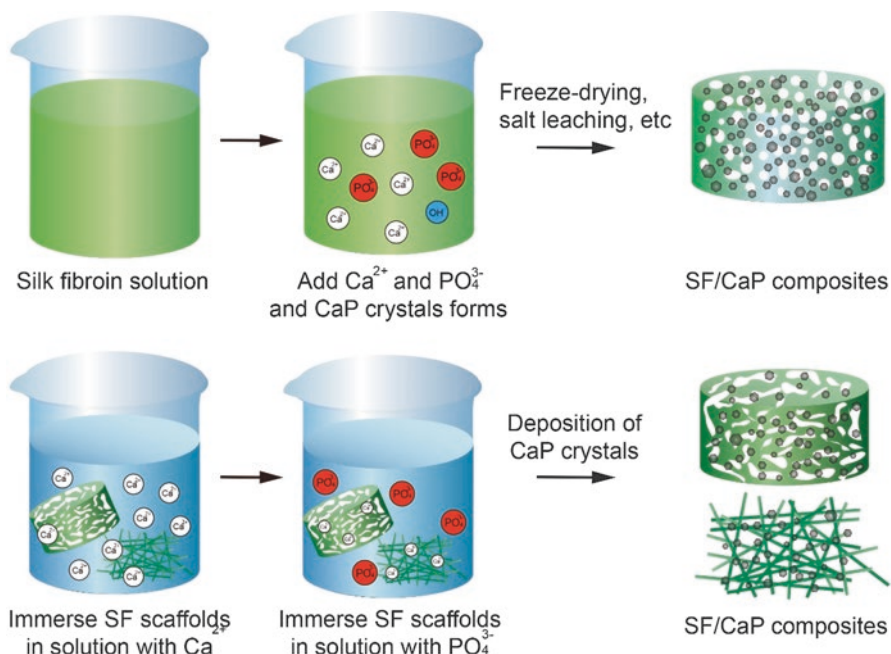
In addition, the reinforcement mechanisms of SF fibers to CPCs were suggested to be (1) bridging of the cracks to resist their further propagation, (2) friction between SF and CPC matrix, and (3) stretching of SF during pullout [92]. A relationship was found between fiber strength and composite strength, and the strength of CPC-fiber scaffold was found to increase linearly with the fiber strength [46].

## 10.5 CaP-SF Composites as Bone Tissue Engineering Scaffolds

### 10.5.1 Preparation of CaP-SF Composites

CaP-SF composites in various forms such as microspheres and porous scaffolds are promising candidates for bone tissue engineering applications. Various techniques have been applied to fabricate CaP-SF composites, including in situ crystallization of CaPs and deposition of CaPs on SF scaffolds (Fig. 10.3). Strong chemical interactions were observed between HA and SF, and these bonds could be detected from the blue shift of amide II bond [78]. Based on that, silk powder/HA nanocomposites could be prepared with a coprecipitation method [91, 107]. For instance, Wang et al. applied this method to deposit HA on SF microspheres, and the prepared composites





**Fig. 10.3** Fabrication of CaP-SF composites by in situ CaP crystallization (*upper*) and direct deposition of CaP crystals (*lower*)

showed 3D network morphology and increased hardness [107]. SF scaffolds with highly dispersed CaP nanoparticles in the matrix were also successfully developed for bone tissue engineering [94]. In this study, nano-CaP was synthesized in situ in a concentrated aqueous SF solution (16 wt%), and then a salt-leaching/lyophilization approach was applied to fabricate silk/nano-CaP scaffolds [94]. In another study, macro-/microporous silk/nanosized calcium phosphate scaffolds (SC16) and silk fibroin scaffolds (S16) were prepared for bone tissue engineering with SC16 scaffolds showing better bioactivity than the S16 scaffolds [108]. New bioactive nanocomposite scaffolds based on silk fibroin nanofiber, porous starch, and calcium phosphate were presented for potential bone tissue regeneration in another study. SF electrospun nanofibers were first fabricated and then chopped. The chopped SF nanofibers for inducing calcium phosphate deposition were then incorporated into the starch matrix to obtain composites of porous starch-silk fibroin nanofiber-calcium phosphate followed by particulate leaching and freeze-drying [109]. Kong et al. demonstrated that SF could promote HA nucleation and crystal growth on the fiber surfaces in simulated body fluid (SBF) solution to directly form a SF/HA nanocomposite, and the nucleated HA crystals are carbonate-substituted HA ( $\text{CO}_3\text{HA}$ ) [89]. In a report, composites of SF and calcium phosphate silicate (CPS) ceramic in the  $15\text{CaO}-6\text{SiO}_2-0.5\text{P}_2\text{O}_5$  system were prepared by mixing CPS powder with SF solutions. High concentration of HA phase was observed on the

composite surfaces after in vitro soaking test in SBF, demonstrating the enhanced in vitro bioactivity with incorporation of CPS ceramic powder [19].

### ***10.5.2 Degradation and Mechanical Properties of CaP-SF Composites***

The in vitro degradation behavior of a silk/nano-CaP composite in isotonic saline solution was evaluated in a report [94]. About 5% weight loss after 30 days was observed for the composites. Another study evaluated the in vitro biodegradation of a biphasic calcium phosphate (BCP) scaffold coated with nanofibrous SF and PCL in simulated body fluid [110]. Nanosized holes were observed on the scaffold surface after 14 days, and surface nanofibrous SF layer became disrupted after 28 days. The weight loss of the scaffold after 28 days was measured to be ~10%, which was significantly less than that of pure BCP (~30%).

Composting CaP with SF is an effective approach to fabricate materials for bone regeneration with improved mechanical properties. Our group previously fabricated CPC/HA-SF/SF composite, and the highest compressive strength of CPC/HA-SF/SF was measured to be  $50.2 \pm 1.9$  MPa with addition of 3 wt% HA-SF, compared to that of HA-SF ( $33.4 \pm 0.9$  MPa) [93]. Jiao et al. investigated the mechanical properties of BCP scaffolds with multiple silk coatings [111]. BCP scaffolds with more than five layers of silk coating demonstrated significant improvement in mechanical properties, exhibiting greatly improved elastic behavior and toughness than pure BCP. The hMSCs cultured on silk-coated BCP scaffolds in vitro also showed enhanced osteogenic responses. Andrew et al. fabricated macroporous SF/CaP scaffolds by infiltrating a frozen phosphate-containing SF gel with calcium chloride solution and cross-linking using hexamethylene diisocyanate [112]. These scaffolds demonstrated excellent tolerance and ductile deformation under compressive loading, suggesting its potential application in repairing load-bearing bone defects.

### ***10.5.3 In Vitro Osteogenesis of CaP-SF Composites***

The biocompatibility and osteogenesis capacity of a semaphorin 3A-loaded chitosan microspheres/SF/ $\alpha$ -TCP (CMs/SF/ $\alpha$ -TCP) composite were evaluated in a study. The MC3T3-E1 cells were shown to well spread and present an elongated shape on the surface of the composite, and ALP activity and the osteogenic-related gene expression indicated promoted osteoblastic differentiation of MC3T3-E1 cells on Sema3A CMs/SF/ $\alpha$ -TCP composite than those on CMs/SF/ $\alpha$ -TCP and SF/ $\alpha$ -TCP composites [113]. A porous bilayer scaffold integrating an SF layer and a silk-nano calcium phosphate (silk-nano-CaP) layer for osteochondral defect regeneration was developed [114]. In vitro test by culturing rabbit bone marrow mesenchymal

stromal cells (RBMSCs) demonstrated good adhesion and proliferation of the RBMSCs on both the surface of the silk layer and the silk-nano-CaP layer. And the interface was also fully covered by the cells and the extracellular matrix. In vitro tests in osteogenic conditions showed increasing ALP activity from day 7 to day 14, with significantly higher ALP activity observed on the silk-nano-CaP layer than the silk layer.

#### ***10.5.4 In Vivo Osteoconductivity of CaP-SF Composites***

CaP-SF composites also demonstrate outstanding in vivo osteoconductive capacities. In a study, the in vivo bone formation ability of porous SF and SF/nano-CaP was evaluated by implantation into the rat femur defects for 3 weeks [108]. Regenerated bone with higher density was observed on the SC16 surface than S16 scaffolds, demonstrating that the osteoconductivity of SC16 hybrid scaffolds as potential candidates for bone tissue engineering [108]. Another study reported the evaluation of in vivo bone regeneration of an injectable calcium phosphate cement/silk fibroin/human recombinant bone morphogenetic protein-2 composite (CPC/SF/rhBMP-2) using an ovine interbody fusion model [32]. The fusion rates of CPC/SF/rhBMP-2 composites attained 55.56% and 77.78% at 6 and 12 months, respectively, and at the same stiffness, the autograft was reached in 12 months. Besides that, significantly smaller ceramic residue volume was observed for CPC/SF/rhBMP-2 composite compared with CPC/SF and CPC/rhBMP-2, demonstrating that more degradation occurred along with new bone formation. These results indicated the excellent osteoconduction and osteoinduction capacities and balanced degradation and osteogenesis of CPC/SF/rhBMP-2 composite for applications in bone regeneration. Yan et al. evaluated the in vivo bone formation performance of a bilayer silk/silk-nano-CaP scaffold [114]. After implantation in a rabbit knee critical size osteochondral defect model for 4 weeks, the bilayer silk/silk-nano-CaP was found to well integrate with the host tissue from the macroscopic images, and micro-CT analysis also showed less void space and more regular morphology at the bilayer-scaffold-filled defect sites compared with the control. Histological and immunohistochemical analysis also demonstrated presence of collagen II-positive cartilage and glycosaminoglycan regeneration in the silk layer, as well as the formation of new bone and vessel in the silk-nano-CaP layer. These suggested the potential of these bilayer scaffolds for osteochondral defect regeneration. In another study, the in vivo osteogenetic capacities of pure silk and hybrid CaP/silk scaffolds were evaluated by implanting them in osteoporotic defects of Wistar rats [115]. More significantly increased regeneration of bone tissue and mineralization were detected at the defects filled with hybrid CaP/silk scaffolds compared to pure silk scaffolds, together with dynamic scaffold degradation and reduced osteoclastic bone resorption.

### ***10.5.5 Other Applications of CaP-SF Composites***

In addition to being used as bone cement, CaP-SF composites have also been used as an effective carrier system for delivering cells and drugs to facilitate bone regeneration. Different kinds of osteoconductive drugs have been incorporated into CaP-SF cements. For instance, in a report, Sema3A-loaded chitosan microspheres (SLCM) and silk fibroin (SF) mixed with calcium sulfate cement (CSC) were applied as drug carriers for bone repairing [116]. Cumulative drug release rate of 44.62% was observed for CSC/SF/0.5SLCM in 28 days, and the scaffold was also found to support the growth of MC3T3 cells. Three other osteogenic supplements ( $\beta$ -glycerophosphate, ascorbic acid, and dexamethasone) were also reported to be successfully incorporated into CPC/SF scaffolds [92]. An injectable CPC/SF composite incorporated with rhBMP-2 showed excellent osteoconductive and osteoinductive performance and balanced degradation and osteogenesis [32]. We have also incorporated N-Acetyl cysteine (NAC), a water-soluble aminothiol containing carboxyl and acylamino groups and possessing diverse functionality including osteogenic property, into  $\alpha$ -TCP/SF cement, in which sustained release of NAC was achieved [33].

### ***10.5.6 Further Supplementation to CaP-SF Composites***

Although compositing CaP materials with SF has been one of the most effective strategies to obtain bone materials with improved mechanical properties and bone regeneration performance, further supplementations to CaP-SF composites to endow them with properties, like better osteoinductivity, anti-washout property, antimicrobial activity, and immunomodulation, are still needed for their development toward clinical applications. The osteoinductivity of CaPs can be enhanced with appropriate morphology, especially high porosity with macro- and micropores [16, 17]. In a study, CaPs with varying physicochemical and structural properties were synthesized, and the CaPs with the highest microporosity exhibited the highest propensity to induce bone formation in vivo [19]. Modification of CPC with magnesium was reported to modulate the behaviors of bone marrow stromal cells. This strategy demonstrated the feasibility to regulate the adhesion and osteogenic differentiation of BMSCs by changing the content of magnesium in the CPC [20]. To improve the anti-washout performance, several gelling agent for rheological control, including xanthan gum hydroxypropyl methylcellulose, lactic acid, and glycerol, was added also into CPCs in previous reports [21, 22, 27]. Antimicrobial activity was incorporated within CaPs by doping with silver or antimicrobial peptides [23, 24]. Addition of magnesium was also reported to modulate the activity of macrophage and the interaction between immune cells and bone cells to achieve improved osteogenesis [25]. Recently, strontium attracts much interest due to its capability to stimulate bone regeneration and inhibit bone resorption [26]. Various

methods have been applied to modify CPCs with strontium to combine the advantages of both materials. All the approaches above for CPCs can possibly be applied to CaP-SF composites to render them with desired characteristics for bone tissue engineering.

## 10.6 Concluding Remarks

To date, a broad range of CaP-SF composites have been developed as bone cements or bone regeneration materials. However, the mechanical properties of CaP-SF composites still need more reinforcement for bone tissue engineering applications, especially for repairing the bone defects at high load-bearing sites. Despite the improved biodegradability, osteoconductivity, and moldability of CaP-SF composites compared to CPCs, further enhancement of the properties, including osteogenesis, osteoinductivity, antimicrobial activity, and immunomodulation, is still highly desirable. Not only are these cements required to be accepted by the body with little risk of side effects, they should also act as resorbable scaffolds for the formation of new bone at the defect sites. Further studies in this area should target at controllable degradation, mechanical reinforcement, and osteoinductive enhancement for bone regeneration applications.

**Acknowledgments** The authors are grateful to the funding support from the National Natural Science Foundation of China (81471790, 31530024, 31500779, 81672213), Jiangsu Provincial Special Program of Medical Science (BL2012004), China Postdoctoral Science Foundation (2016M590500, 2017T100398), Jiangsu Planned Projects for Postdoctoral Research Funds (1601269C), the Priority Academic Program Development (PAPD) of Jiangsu Higher Education Institutions, and the Natural Science Foundation of the Jiangsu Higher Education Institutions of China (15KJB310021).

## References

1. Mitchell BD, Streeten EA (2013) Clinical impact of recent genetic discoveries in osteoporosis. *Appl Clin Genet* 6:75–85
2. Marcucci G, Brandi ML (2010) Kyphoplasty and vertebroplasty in the management of osteoporosis with subsequent vertebral compression fractures. *Clin Cases Miner Bone Metab* 7:51–60
3. Longo UG, Loppini M, Denaro L et al (2012) Osteoporotic vertebral fractures: current concepts of conservative care. *Br Med Bull* 102:171–189
4. Kado DM, Browner WS, Palermo L et al (1999) Vertebral fractures and mortality in older women: a prospective study. Study of Osteoporotic Fractures Research Group. *Arch Intern Med* 159:1215–1220
5. Inzana JA, Schwarz EM, Kates SL et al (2016) Biomaterials approaches to treating implant-associated osteomyelitis. *Biomaterials* 81:58–71
6. Zhang J, Liu W, Schnitzler V et al (2014) Calcium phosphate cements for bone substitution: chemistry, handling and mechanical properties. *Acta Biomater* 10:1035–1049

7. Laurencin CT, Ambrosio AM, Borden MD et al (1999) Tissue engineering: orthopedic applications. *Annu Rev Biomed Eng* 1:19–46
8. Sun L, Xu HHK, Takagi S et al (2007) Fast setting calcium phosphate cement-chitosan composite: mechanical properties and dissolution rates. *J Biomater Appl* 21:299–315
9. Khairoun I, Magne D, Gauthier O et al (2002) In vitro characterization and in vivo properties of a carbonated apatite bone cement. *J Biomed Mater Res* 60:633–642
10. Yao J, Li X, Bao C et al (2010) Ectopic bone formation in adipose-derived stromal cell-seeded osteoinductive calcium phosphate scaffolds. *J Biomater Appl* 24:607–624
11. Turner TM, Urban RM, Singh K et al (2008) Vertebroplasty comparing injectable calcium phosphate cement compared with polymethylmethacrylate in a unique canine vertebral body large defect model. *Spine J* 8:482–487
12. Bose S, Tarafder S (2012) Calcium phosphate ceramic systems in growth factor and drug delivery for bone tissue engineering: a review. *Acta Biomater* 8:1401–1421
13. Dorozhkin SV (2011) Calcium orthophosphates: occurrence, properties, biomineralization, pathological calcification and biomimetic applications. *Biomaterials* 1:121–164
14. Tomita S, Kin A, Yazu M et al (2003) Biomechanical evaluation of kyphoplasty and vertebroplasty with calcium phosphate cement in a simulated osteoporotic compression fracture. *J Orthop Sci* 8:192–197
15. Dorozhkin SV (2008) Calcium orthophosphate cements for biomedical application. *J Mater Sci* 43:3028–3057
16. He Z, Zhai Q, Hu M et al (2015) Bone cements for percutaneous vertebroplasty and balloon kyphoplasty: current status and future developments. *J Orthop Transl* 3:1–11
17. Krüger R, Groll J (2012) Fiber reinforced calcium phosphate cements-on the way to degradable load bearing bone substitutes? *Biomaterials* 33:5887–5900
18. Dorozhkin SV (2012) Biphasic, triphasic and multiphasic calcium orthophosphates. *Acta Biomater* 8:963–977
19. Ellinger RF, Nery E, Lynch K et al (1986) Histological assessment of periodontal osseous defects following implantation of hydroxyapatite and biphasic calcium phosphate ceramics: a case report. *Int J Periodontics Restorative Dent* 6:22–23
20. LeGeros R (1988) Calcium phosphate materials in restorative dentistry: a review. *Adv Dent Res* 2:164–180
21. Sugawara A, Fujikawa K, Kusama K et al (2002) Histopathologic reaction of a calcium phosphate cement for alveolar ridge augmentation. *J Biomed Mater Res* 61:47–52
22. Noetzel J, Özer K, Reissbauer B-H et al (2006) Tissue responses to an experimental calcium phosphate cement and mineral trioxide aggregate as materials for furcation perforation repair: a histological study in dogs. *Clin Oral Investig* 10:77–83
23. Šiniković B, Kramer F-J, Swennen G et al (2007) Reconstruction of orbital wall defects with calcium phosphate cement: clinical and histological findings in a sheep model. *Int J Oral Maxillofac Surg* 36:54–61
24. Liverneaux P (2005) Osteoporotic distal radius curettage-filling with an injectable calcium phosphate cement. A cadaveric study. *Eur J Orthop Surg Traumatol* 15:1–6
25. Simpson D, Keating J (2004) Outcome of tibial plateau fractures managed with calcium phosphate cement. *Injury* 35:913–918
26. Libicher M, Hillmeier J, Liegibel U et al (2006) Osseous integration of calcium phosphate in osteoporotic vertebral fractures after kyphoplasty: initial results from a clinical and experimental pilot study. *Osteoporos Int* 17:1208–1215
27. Link DP, Van den Dolder J, Wolke JG et al (2007) The cytocompatibility and early osteogenic characteristics of an injectable calcium phosphate cement. *Tissue Eng* 13:493–500
28. Tomita S, Molloy S, Jasper LE et al (2004) Biomechanical comparison of kyphoplasty with different bone cements. *Spine (Phila Pa 1976)* 29:1203–1207
29. Bai B, Jazrawi LM, Kummer FJ et al (1999) The use of an injectable, biodegradable calcium phosphate bone substitute for the prophylactic augmentation of osteoporotic vertebrae and the management of vertebral compression fractures. *Spine (Phila Pa 1976)* 24:1521–1526

30. Espanol M, Perez RA, Montufar EB et al (2009) Intrinsic porosity of calcium phosphate cements and its significance for drug delivery and tissue engineering applications. *Acta Biomater* 5:2752–2762
31. Ginebra M-P, Canal C, Espanol M et al (2012) Calcium phosphate cements as drug delivery materials. *Adv Drug Deliv Rev* 64:1090–1110
32. Gu Y, Chen L, Yang HL et al (2011) Evaluation of an injectable silk fibroin enhanced calcium phosphate cement loaded with human recombinant bone morphogenetic protein-2 in ovine lumbar interbody fusion. *J Biomed Mater Res A* 97:177–185
33. Feng T, Pi B, Li B et al (2015) N-Acetyl cysteine (NAC)-mediated reinforcement of alpha-tricalcium phosphate/silk fibroin ( $\alpha$ -TCP/SF) cement. *Colloids Surf B Biointerfaces* 136:892–899
34. Low KL, Tan SH, Zein SH et al (2010) Calcium phosphate-based composites as injectable bone substitute materials. *J Biomed Mater Res B Appl Biomater* 94:273–286
35. Lewis G et al (2006) Injectable bone cements for use in vertebroplasty and kyphoplasty: state-of-the-art review. *J Biomed Mater Res B Appl Biomater* 76:456–468
36. Zuo Y, Yang F, Wolke JG et al (2010) Incorporation of biodegradable electrospun fibers into calcium phosphate cement for bone regeneration. *Acta Biomater* 6:1238–1247
37. Lee G-S, Park J-H, Shin US et al (2011) Direct deposited porous scaffolds of calcium phosphate cement with alginate for drug delivery and bone tissue engineering. *Acta Biomater* 7:3178–3186
38. Tsai C-H, Lin R-M, Ju C-P et al (2008) Bioresorption behavior of tetracalcium phosphate-derived calcium phosphate cement implanted in femur of rabbits. *Biomaterials* 29:984–993
39. Friedman CD, Costantino PD, Takagi S et al (1998) BoneSource™ hydroxyapatite cement: a novel biomaterial for craniofacial skeletal tissue engineering and reconstruction. *J Biomed Mater Res* 43:428–432
40. Rupprecht S, Merten H-A, Kessler P et al (2003) Hydroxyapatite cement (BoneSource™) for repair of critical sized calvarian defects—an experimental study. *J Cranio Maxill Surg* 31:149–153
41. Lopez-Heredia MA, Sariibrahimoglu K, Yang W et al (2012) Influence of the pore generator on the evolution of the mechanical properties and the porosity and interconnectivity of a calcium phosphate cement. *Acta Biomater* 8:404–414
42. Ishikawa K, Asaoka K et al (1995) Estimation of ideal mechanical strength and critical porosity of calcium phosphate cement. *J Biomed Mater Res* 29:1537–1543
43. Sarda S, Fernández E, Nilsson M et al (2002) Kinetic study of citric acid influence on calcium phosphate bone cements as water-reducing agent. *J Biomed Mater Res* 61:653–659
44. Liu W, Zhang J, Rethore G et al (2014) A novel injectable, cohesive and toughened Si-HPMC (silanized-hydroxypropyl methylcellulose) composite calcium phosphate cement for bone substitution. *Acta Biomater* 10:3335–3345
45. Canal C, Ginebra M (2011) Fibre-reinforced calcium phosphate cements: a review. *J Mech Behav Biomed Mater* 4:1658–1671
46. Xu HH, Eichmiller FC, Giuseppetti AA (2000) Reinforcement of a self-setting calcium phosphate cement with different fibers. *J Biomed Mater Res* 52:107–114
47. Kon M, Hirakata LM, Miyamoto Y et al (2005) Strengthening of calcium phosphate cement by compounding calcium carbonate whiskers. *Dent Mater J* 24:104–110
48. Xu HHK, Quinn JB et al (2001) Whisker-reinforced bioactive composites containing calcium phosphate cement fillers: effects of filler ratio and surface treatments on mechanical properties. *J Biomed Mater Res* 57:165–174
49. Habraken WJ, Wolke JG, Mikos AG et al (2009) Porcine gelatin microsphere/calcium phosphate cement composites: an in vitro degradation study. *J Biomed Mater Res B Appl Biomater* 91:555–561
50. Vepari C, Kaplan DL (2007) Silk as a biomaterial. *Prog Polym Sci* 32:991–1007
51. Altman GH, Diaz F, Jakuba C et al (2003) Silk-based biomaterials. *Biomaterials* 24:401–416

52. Dal Pra I, Freddi G, Minic J et al (2005) De novo engineering of reticular connective tissue in vivo by silk fibroin nonwoven materials. *Biomaterials* 26:1987–1999
53. Nazarov R, Jin HJ, Kaplan DL (2004) Porous 3-D scaffolds from regenerated silk fibroin. *Biomacromolecules* 5:718–726
54. Gil ES, Panilaitis B, Bellas E et al (2013) Functionalized silk biomaterials for wound healing. *Adv Healthc Mater* 2:206–217
55. Zhong T, Xie Z, Deng C et al (2013) Copolymer-induced silk-based hydrogel with porous and nanofibrous structure. *J Appl Polym Sci* 127:2019–2024
56. Chutipakdeevong J, Ruktanonchai UR, Supaphol P (2013) Process optimization of electrospun silk fibroin fiber mat for accelerated wound healing. *J Appl Polym Sci* 130:3634–3644
57. Asakura T, Saotome T, Aytemiz D et al (2014) Characterization of silk sponge in the wet state using  $^{13}\text{C}$  solid state NMR for development of a porous silk vascular graft with small diameter. *RSC Adv* 4:4427–4434
58. Chung YG, Algarrahi K, Franck D et al (2014) The use of bi-layer silk fibroin scaffolds and small intestinal submucosa matrices to support bladder tissue regeneration in a rat model of spinal cord injury. *Biomaterials* 35:7452–7459
59. Khan MMR, Tsukada M, Zhang X et al (2013) Preparation and characterization of electrospun nanofibers based on silk sericin powders. *J Mater Sci* 48:3731–3736
60. Vollrath F, Knight DP (2001) Liquid crystalline spinning of spider silk. *Nature* 410:541–548
61. Lewis RV, Hinman M, Kothakota S et al (1996) Expression and purification of a spider silk protein: a new strategy for producing repetitive proteins. *Protein Expr Purif* 7:400–406
62. Zhou S, Peng H, Yu X et al (2008) Preparation and characterization of a novel electrospun spider silk fibroin/poly(D,L-lactide) composite fiber. *J Phys Chem B* 112:11209–11216
63. Zhou CZ, Confalonieri F, Medina N et al (2000) Fine organization of *Bombyx mori* fibroin heavy chain gene. *Nucleic Acids Res* 28:2413–2419
64. Bini E, Knight DP, Kaplan DL (2004) Mapping domain structures in silks from insects and spiders related to protein assembly. *J Molecul Biol* 335:27–40
65. Li C, Jin H-J, Botsaris GD (2005) Silk apatite composites from electrospun fibers. *J Mater Res* 20:3374–3384
66. Sasaki M, Kato Y, Yamada H (2005) Development of a novel serum-free freezing medium for mammalian cells using the silk protein sericin. *Biotechnol Appl Biochem* 42:183–188
67. Altman GH, Horan RL, Lu HH et al (2002) Silk matrix for tissue engineered anterior cruciate ligaments. *Biomaterials* 23:4131–4141
68. Horan RL, Antle K, Collette AL et al (2005) In vitro degradation of silk fibroin. *Biomaterials* 26:3385–3393
69. Chen J, Altman GH, Karageorgiou V et al (2003) Human bone marrow stromal cell and ligament fibroblast responses on RGD-modified silk fibers. *J Biomed Mater Res A* 67:559–570
70. Arai T, Freddi G, Innocenti R et al (2004) Biodegradation of *Bombyx mori* silk fibroin fibers and films. *J Appl Polym Sci* 91:2383–2390
71. Kurioka A, Yamazaki M, Hirano H (1999) Primary structure and possible functions of a trypsin inhibitor of *Bombyx mori*. *Eur J Biochem* 259:120–126
72. Kim U-J, Park J, Joo Kim H et al (2005) Three-dimensional aqueous-derived biomaterial scaffolds from silk fibroin. *Biomaterials* 26:2775–2785
73. Minoura N, Tsukada M, Nagura M (1990) Physico-chemical properties of silk fibroin membrane as a biomaterial. *Biomaterials* 11:430–434
74. Santin M, Motta A, Freddi G et al (1999) In vitro evaluation of the inflammatory potential of the silk fibroin. *J Biomed Mater Res* 46:382–389
75. Meinel L, Hofmann S, Karageorgiou V et al (2005) The inflammatory responses to silk films in vitro and in vivo. *Biomaterials* 26:147–155
76. Sugihara A, Sugiura K, Morita H et al (2000) Promotive effects of a silk film on epidermal recovery from full-thickness skin wounds. *Proc Soc Exp Biol Med* 225:58–64
77. Furuzono T, Kishida A, Tanaka J et al (2004) Nano-scaled hydroxyapatite/polymer composite I. Coating of sintered hydroxyapatite particles on poly(gamma-methacryloxypropyl



- trimethoxysilane)grafted silk fibroin fibers through chemical bonding. *J Mater Sci Mater Med* 15:19–23
78. Meinel L, Hofmann S, Karageorgiou V et al (2004) Engineering cartilage-like tissue using human mesenchymal stem cells and silk protein scaffolds. *Biotechnol Bioeng* 88:379–391
  79. Karageorgiou V, Meinel L, Hofmann S et al (2004) Bone morphogenetic protein-2 decorated silk fibroin films induce osteogenic differentiation of human bone marrow stromal cells. *J Biomed Mater Res A* 71:528–537
  80. Li C, Vepari C, Jin HJ et al (2006) Electrospun silk-BMP-2 scaffolds for bone tissue engineering. *Biomaterials* 27:3115–3124
  81. Motta A, Migliaresi C, Faccioni F, Torricelli P, Fini M, Giardino R et al (2004) Fibroin hydrogels for biomedical applications: preparation, characterization and in vitro cell culture studies. *J Biomater Sci Polym Ed* 15:851–864
  82. Kim K-H, Jeong L, Park H-N et al (2005) Biological efficacy of silk fibroin nanofiber membranes for guided bone regeneration. *J Biotechnol* 120:327–339
  83. Fini M, Motta A, Torricelli P et al (2005) The healing of confined critical size cancellous defects in the presence of silk fibroin hydrogel. *Biomaterials* 26:3527–3536
  84. Meinel L, Hofmann S, Betz O et al (2006) Osteogenesis by human mesenchymal stem cells cultured on silk biomaterials: comparison of adenovirus mediated gene transfer and protein delivery of BMP-2. *Biomaterials* 27:4993–5002
  85. Guang S, An Y, Ke F et al (2015) Chitosan/silk fibroin composite scaffolds for wound dressing. *J Appl Polym Sci* 132:42503
  86. Mandal BB, Grinberg A, Gil ES et al (2012) High-strength silk protein scaffolds for bone repair. *P Natl Acad Sci* 109:7699–7704
  87. Liu X, Smith LA, Hu J et al (2009) Biomimetic nanofibrous gelatin/apatite composite scaffolds for bone tissue engineering. *Biomaterials* 30:2252–2258
  88. Cai X, Tong H, Shen X et al (2009) Preparation and characterization of homogeneous chitosan-poly(lactic acid)/hydroxyapatite nanocomposite for bone tissue engineering and evaluation of its mechanical properties. *Acta Biomater* 5:2693–2703
  89. Kong XD, Cui FZ, Wang XM et al (2004) Silk fibroin regulated mineralization of hydroxyapatite nanocrystals. *J Cryst Growth* 270:197–202
  90. Ren Y, Sun X, Cui F et al (2007) Effects of pH and initial  $\text{Ca}^{2+}$ - $\text{H}_2\text{PO}_4^-$  concentration on fibroin mineralization. *Front Mater Sci China* 1:258–262
  91. Fan C, Li J, Xu G et al (2010) Facile fabrication of nano-hydroxyapatite/silk fibroin composite via a simplified coprecipitation route. *J Mater Sci* 45:5814–5819
  92. Qu Y, Yang Y, Li J et al (2011) Preliminary evaluation of a novel strong/osteoinductive calcium phosphate cement. *J Biomater Appl* 26:311–325
  93. Cao C, Li H, Li J et al (2014) Mechanical reinforcement of injectable calcium phosphate cement/silk fibroin (SF) composite by mineralized SF. *Ceram Int* 40:13987–13993
  94. Yan LP, Silva-Correia J, Correia C et al (2013) Bioactive macro/micro porous silk fibroin/nano-sized calcium phosphate scaffolds with potential for bone-tissue-engineering applications. *Nanomedicine (Lond)* 8:359–378
  95. Kong X, Sun X, Cui F et al (2006) Effect of solute concentration on fibroin regulated biomimetalization of calcium phosphate. *Mater Sci Eng C* 26:639–643
  96. Li L, Wei K-M, Lin F et al (2008) Effect of silicon on the formation of silk fibroin/calcium phosphate composite. *J Mater Sci Mater Med* 19:577–582
  97. Zhu H, Shen J, Feng X et al (2010) Fabrication and characterization of bioactive silk fibroin/wollastonite composite scaffolds. *Mater Sci Eng C* 30:132–140
  98. Ding T, Yang H, Maltenfort M et al (2010) Silk fibroin added to calcium phosphate cement to prevent severe cardiovascular complications. *Med Sci Monit* 16:Hy23–Hy26
  99. Ginebra MP, Fernandez E, Boltong MG et al (1994) Compliance of an apatitic calcium phosphate cement with the short-term clinical requirements in bone surgery, orthopaedics and dentistry. *Clin Mater* 17:99–104

100. Vlad MD, Gómez S, Barracó M et al (2012) Effect of the calcium to phosphorus ratio on the setting properties of calcium phosphate bone cements. *J Mater Sci Mater Med* 23:2081–2090
101. Song H-Y, Esfakur Rahman AHM, Lee B-T (2009) Fabrication of calcium phosphate-calcium sulfate injectable bone substitute using chitosan and citric acid. *J Mater Sci Mater Med* 20:935–941
102. Krebs J, Aebli N, Goss BG et al (2007) Cardiovascular changes after pulmonary embolism from injecting calcium phosphate cement. *J Biomed Mater Res B Appl Biomater* 82:526–532
103. Damien CJ, Parsons JR (1991) Bone graft and bone graft substitutes: a review of current technology and applications. *J Appl Biomater* 2:187–208
104. Yang HL, Zhu XS, Chen L et al (2012) Bone healing response to a synthetic calcium sulfate/ $\beta$ -tricalcium phosphate graft material in a sheep vertebral body defect model. *J Biomed Mater Res B Appl Biomater* 100:1911–1921
105. Low KL, Zein SHS, Tan SH et al (2011) The effect of interfacial bonding of calcium phosphate cements containing bio-mineralized multi-walled carbon nanotube and bovine serum albumin on the mechanical properties of calcium phosphate cements. *Ceram Int* 37:2429–2435
106. Hong Z, Zhang P, He C et al (2005) Nano-composite of poly(L-lactide) and surface grafted hydroxyapatite: mechanical properties and biocompatibility. *Biomaterials* 26:6296–6304
107. Rising A, Nimmervoll H, Grip S et al (2005) Spider silk proteins-mechanical property and gene sequence. *Zool Sci* 22:273–281
108. Wang L, Nemoto R, Senna M (2004) Effects of alkali pretreatment of silk fibroin on microstructure and properties of hydroxyapatite-silk fibroin nanocomposite. *J Mater Sci Mater Med* 15:261–265
109. Yan LP, Salgado AJ, Oliveira JM et al (2013) De novo bone formation on macro/microporous silk and silk/nano-sized calcium phosphate scaffolds. *J Bioact Compat Polym* 28:439–452
110. Hadisi Z, Nourmohammadi J, Mohammadi J (2015) Composite of porous starch-silk fibroin nanofiber-calcium phosphate for bone regeneration. *Ceram Int* 41:10745–10754
111. Roohani-Esfahani S, Lu Z, Li J et al (2012) Effect of self-assembled nanofibrous silk/poly-caprolactone layer on the osteoconductivity and mechanical properties of biphasic calcium phosphate scaffolds. *Acta Biomater* 8:302–312
112. Li JJ, Gil ES, Hayden RS et al (2013) Multiple silk coatings on biphasic calcium phosphate scaffolds: effect on physical and mechanical properties and in vitro osteogenic response of human mesenchymal stem cells. *Biomacromolecules* 14:2179–2188
113. Collins AM, Skaer NJ, Gheysens T et al (2009) Bone-like resorbable silk-based scaffolds for load-bearing osteoregenerative applications. *Adv Mater* 21:75–78
114. Wang J-N, Pi B, Wang P et al (2015) Sustained release of Semaphorin 3A from  $\alpha$ -tricalcium phosphate based cement composite contributes to osteoblastic differentiation of MC3T3-E1 cells. *Front Mater Sci* 9:282–292
115. Yan L-P, Silva-Correia J, Oliveira MB et al (2015) Bilayered silk/silk-nanoCaP scaffolds for osteochondral tissue engineering: in vitro and in vivo assessment of biological performance. *Acta Biomater* 12:227–241
116. Cheng N, Dai J, Cheng X et al (2013) Porous CaP/silk composite scaffolds to repair femur defects in an osteoporotic model. *J Mater Sci Mater Med* 24:1963–1975

# Chapter 11

## Importance of Biomaterials In Vivo Microenvironment pH ( $\mu\text{e-pH}$ ) in the Regeneration Process of Osteoporotic Bone Defects

Wenlong Liu, Xiuli Dan, William Weijia Lu, and Haobo Pan

**Abstract** In scenario of osteoporotic fracture, significantly higher activity of osteoclasts than osteoblasts may lead to continuous loss of bone in fracture/defect site. Impaired bone regeneration efficiency is the major barrier that influences endosseous implants to get a better performance, and this substantially increases the risk of a second fracture, nonunion, and aseptic implant loosening. Although great effects have been made, there are still no clinically approved biomaterials specifically tailored for applications in osteoporotic bones. The key issue for developing such biomaterials is to reestablish normal bone regeneration at the fracture site. Acid-base property could directly influence the behavior of bone cells, thus making it an important factor to modulate the unbalanced activity between osteoclast and osteoblast in osteoporotic conditions. More importantly, it is adjustable through implant biodegradation. Therefore, a rational strategy to reconstruct the regeneration balance in the fracture site is to regulate the microenvironmental pH ( $\mu\text{e-pH}$ ) through the application of biodegradable materials. The present chapter provides an overview on how pH change influences bone cells behaviors as well as recent development on revealing the role of  $\mu\text{e-pH}$  in guiding the localized bone regeneration. We proposed that the  $\mu\text{e-pH}$  is an important and accessible factor which should be taken into consideration in the development of orthopedic biomaterials, in particular for repair of osteoporotic bone fracture/defect.

---

W. Liu • H. Pan (✉)

Research Center for Human Tissue and Organs Degeneration, Institute of Biomedicine and Biotechnology, Shenzhen Institutes of Advanced Technology, Chinese Academy of Sciences, Shenzhen, China

e-mail: [hb.pan@siat.ac.cn](mailto:hb.pan@siat.ac.cn)

X. Dan

School of Biomedical Sciences, Faculty of Medicine, The Chinese University of Hong Kong, Shatin, Hong Kong

W.W. Lu

Department of Orthopaedics and Traumatology, Faculty of Medicine, The University of Hong Kong, Pok Fu Lam, Hong Kong

**Keywords** Osteoporotic bone fracture/defect • Bioactive glass/ceramic • Biodegradable materials • Microenvironment pH • Bone regeneration • Acid-base bone homeostasis

## 11.1 Biomaterials for Osteoporotic Bone Defect/Fracture

Osteoporosis is a disease characterized by low bone mass with deterioration of bone microstructure; it leads to nearly nine million fractures annually worldwide [1]. In osteoporotic bone, the unbalanced activity of osteoblasts and osteoclasts generates a hostile microenvironment, which in turn causes the continuous loss of bone mineral [2]. Pharmaceutical therapies are suggested after the surgeries in the treatment of osteoporotic fracture, since they could modulate the unbalanced osteoblasts and osteoclasts activities. Anti-osteoporotic agents applied in pharmacological therapy may work either by reducing bone resorption rate or by directly stimulating the increase of bone mass [3]. For example, bisphosphonates are antiresorptive compounds which are capable of suppressing the activation of osteoclast [4], whereas recombinant human parathyroid hormone (PTH) is a parathyroid hormone that could strongly stimulate bone formation and increase bone mass [5]. Besides, some of the anti-osteoporotic agents may contribute to bone remodeling by both increasing bone formation and decreasing bone resorption, such as strontium ranelate [6]. Depending on the drug and patient populations, the intervention of treatment could decrease the risk of vertebral fracture by 30–70% and nonvertebral fractures by 15–20% [7, 8].

Though various treatments have been developed to reduce the impact of bone fragility, no effective alternatives to recover bone strength have been proposed [9]. Current pharmaceutical therapies for osteoporosis appear to rely on modulating the communication between osteoblasts and osteoclasts, generally by focusing on one or the other while ignoring their microenvironment. In this context, implants generate their own milieu through biodegradation, that is, control of this might be used to influence favorably the bone remodeling microenvironment. Also, drugs used for osteoporosis treatment are not suitable for postfracture rehabilitation use, that is to say, the efficiency of systematic administration of osteoporotic drugs toward bone defect regeneration is expected to be very low. One of the reasons is that these drugs are not developed with the capability to target the fracture/defect region – the most fragile region requiring early recovery. It is documented that PTH treatment exhibits no effect on trabecular bone formation without mechanical stimulation [10]. This is of particular importance, because when the defect region suffers from immobilization, the most efficient place for the drug may be coordinated to other load-bearing regions [11].

Clinically, the challenges for the treatment of osteoporotic fractures come from two aspects which are, respectively, mechanical and biological concerns. Mechanical problems are mainly attributed to the weakness of bone mechanical strength,

deteriorated microstructure, comminuted fracture, and trabecular collapse. Biologically, in osteoporotic bones, the osteoblastic differentiation capacity of mesenchymal stem cells and the angiogenesis ability in the fracture regions are usually attenuated, whereas the activities of osteoclasts are enhanced. Based on these facts, the following two conditions are required in the application of biomaterials in clinical practice: (1) the materials could provide appropriate mechanical support to allow adequate movements of patients as soon as possible after the operation, and (2) the materials could contribute to a fast restoration of fractured bones.

In the aspect of materials, metallic materials are able to provide good mechanical support for the fracture. Unfortunately, they are basically bio-inert. On the contrary, ceramic materials may not possess such superior mechanical properties, but they could be developed with a bioactive property. Moreover, their bioactivity could be modulated by their compositions and stimulate the recovery of fractured bones by promoting osteogenesis and angiogenesis. Composite materials are then accordingly designed by spreading ceramic materials (e.g., by plasma spray) on the surface of metallic materials to combine their advantages. The present fact is that, although great effects have been made, there are still no clinically approved biomaterials specifically tailored for applications in osteoporotic bones [9]. The main problems are that in short terms, the unstable osteoporotic bone microstructure strongly impairs the primary stability of implants; in long terms, biomaterials develop poor biological fixation with osteoporotic bone. The reason for these problems may be the impaired tissue response to the biomaterial under osteoporotic condition, such as insufficient osteogenesis around the implant [12].

In order to realize this objective, we believe that a proper design of ceramic materials with outstanding surface properties for bone recovery is one of the most fundamental and important points. Considering that implants could generate their own milieu through biodegradation and the degradation products (debris, loaded drugs, ions, etc.) may directly influence the defect regeneration process, we proposed to control this microenvironment by properly designed material surface to induce favorable effect on regeneration-related cells.

## **11.2 Acid-Base Balance in Bone Homeostasis**

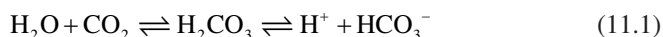
### ***11.2.1 Acid-Base Balance in Human Body***

The human body has the ability to maintain and regulate pH at different levels in different organs, which allows optimal function of most cellular enzymes. Acid-base balance of tissues/organs is maintained by different buffering systems, respiratory exchange, and renal compensation. The circulation blood and interstitial pHs usually stay in a narrow range from 7.35 to 7.45 under normal circumstance. At the same time, in order to keep normal cellular function, the pH of intracellular matrix should be strictly regulated by transmembrane ion exchange with extracellular environment [13].

**Table 11.1** Responses of bone toward systematical acid-base imbalance

	pH	HCO <sub>3</sub> <sup>-</sup>	CO <sub>2</sub>	Bone response
Metabolic acidosis	↓	↓	-	Calcium efflux (++) [14, 15]
				Protons influx (++)
				PTH (+)
Metabolic alkalosis	↑	↑	-	Calcium efflux(-) [16, 17]
				PTH (-)
Respiratory acidosis	↓	-	↑	Calcium efflux (+) [14, 15]
				No protons influx
				PTH (+)
Respiratory alkalosis	↑	-	↓	Calcium efflux(-) [17]
				PTH (-)

Among different H<sup>+</sup> buffering systems for extracellular pH equilibration (e.g., phosphate buffered, protein buffered, etc.), CO<sub>2</sub>/HCO<sub>3</sub><sup>-</sup> buffering system is the most general one which accounts for 80–90% of total metabolic acid buffering. Acid-base balance of the human body that is accommodated by CO<sub>2</sub>/HCO<sub>3</sub><sup>-</sup> buffering system could be expressed by the following equation:



Based on this system, systematically acid-base disorders could be classified into four categories: metabolic acidosis, respiratory acidosis, metabolic alkalosis, and respiratory alkalosis (Table 11.1). Respiratory acidosis/alkalosis is caused by an increase/decrease level of CO<sub>2</sub>, while metabolic acidosis is generally caused by decreased H<sup>+</sup> excretion, increased H<sup>+</sup> load, or loss/dilution of bicarbonate. In addition, acidosis can also happen locally, which is influenced by inflammation, infection, or wound healing process [18]. The relationships between acidosis/alkalosis and bone response play crucial roles in calcium equilibration of the human body.

### 11.2.2 Role of Bone in Regulation of Acid-Base Balance

Bone is an active organ which has the capability to modulate systematical pH both in cellular level and in physicochemical level. Studies carried out on neonatal mouse calvaria by Bushinsky show that acute metabolic acidosis induces a net influx of protons into the bone and a calcium efflux out of the bone [14, 19]. This trend is not the same with respiratory acidosis which shows no proton influx and less calcium efflux from the bone, indicating a lower buffering capability of bone under respiratory acidosis condition. Furthermore, impaired bone formation and improved bone resorption are observed under acidosis condition [20, 21]. On the contrary, alkalosis decreases bone calcium efflux, and it is correlated with a decreased osteoclastic β-glucuronidase production and an increased osteoblastic collagen synthesis [16].

However, compared with acidosis, fewer studies are conducted regarding the effect of alkalosis on buffering compatibility of bone. The responses of bone toward systematic acid-base imbalance are listed in Table 11.1.

Parathyroid hormone (PTH) and calcitonin (CT) are peptide hormones that work reversely in calcium homeostasis. They also play important roles in regulating the function of bone cells [22]. PTH increases blood calcium level by stimulating bone turnover rate; conversely, CT could bind to its receptors on osteoclasts and inhibit their bone resorption activity [23]. Interestingly, both PTH and CT have been approved for clinical use for osteoporosis, and this may be because different PTH-delivery ways generate different tissue response toward bone [24].

Escolastico's group used dogs as animal models and demonstrated the role of PTH in response to acid-base disorder. They found that the PTH level was markedly decreased under acute metabolic/respiratory alkalosis [17] and was increased under acute metabolic/respiratory acidosis [15] (Table 11.1). It is reasonable to suspect that the increased/decreased PTH level will further influence the activity of osteoblasts/osteoclasts, so that the level of calcium remains relatively constant.

### ***11.2.3 Bone Cells in Response to Extracellular pH Change***

#### **11.2.3.1 Osteoblasts**

Bushinsky's group revealed that chronic metabolic acidosis completely prevented the increase of matrix Gla and osteopontin mRNA levels of primary bone cells [25]. Similarly, the research group of Timothy found that acidosis generated progressively reduced primary osteoblast mineralization. More than 90% of osteoblastic ALP activity was lost when they were cultured in pH 6.9 in comparison with that in pH 7.4 [20]. The differentiation of osteoblasts was negatively correlated with concentrations of protons but was independent of the change of extracellular bicarbonate [26].

On the contrary, bone formation process is postulated to happen in a relatively high local pH condition [27]. Study shows that mouse osteoblastic collagen synthesis is increased in alkalosis condition [28]. Similarly, in human osteoblast, collagen synthesis, ALP activity, and thymidine incorporation are increased when pH is raised from 7.0 to 7.6 [29]. Furthermore, when bone marrow stromal cells are cultured in higher pH culturing conditions for 48 h, ALP activity, collagen gene expression, and collagen synthesis are found to be significantly increased [30]. In addition, ALP activity toward inorganic pyrophosphatase is optimized at pH 8.5 (about 67% increase compared with a "physiological" value of pH 7.5) [31].

#### **11.2.3.2 Osteoclast**

The calcium efflux under elevated  $[\text{H}^+]$  conditions is demonstrated to be mediated mainly by osteoclastic bone resorption activity [32]. It is documented that osteoclasts are almost inactivated at physiological pH level of 7.4, while bone resorption

increases apparently as pH decreases and reaches the peak near pH 7.0 [33]. Rat osteoclastic activity is sharply increased when pH value of the culturing media drops from pH 7.25 to pH 7.15, presenting a “switch on/off” response pattern in vitro [34]. This elevated osteoclastic activity in response to pH decrease continues throughout a culture time of 7 days or more. Arnett believes that  $\text{HCO}_3^-$  acidification mainly acts on mature osteoclasts instead of promoting new osteoclasts formation [35].

The elevated osteoclast activity could be explained by a higher activity of matrix catabolic enzymes and increased osteoclasts sensitivity toward stimulation factors. The mRNA levels of carbonic anhydrase II (CA II) and calcitonin receptor of osteoclasts are upregulated by acid stimuli [36], increasing the sensitivity of osteoclasts toward resorptive signals. Upregulated level of TRAP and enhanced activity of cathepsin K, a collagenolytic enzyme secreted by osteoclast, on organic matrix are achieved at slightly acidic pH [33, 37]. Another explanation suggests that since osteoclasts could be activated by RANKL (secreted by osteoblastic lineage cells), they could also respond indirectly to a pH change through communication with osteoblast via RANK/RNKL/OPG signaling. During this process, transcription factor NFATc1 is expected to play an important role [38].

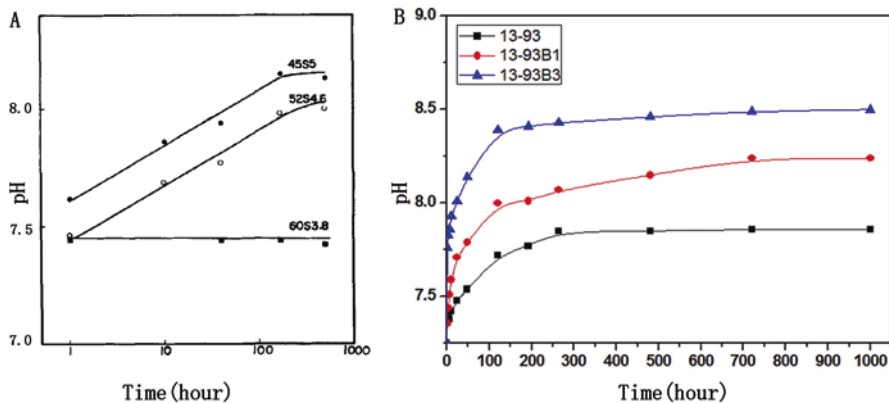
Researchers have also tried to find out the effect of proton and bicarbonate on the activity of osteoclasts during process of acid stimulation, respectively, and the results demonstrated an increased osteoclasts activity could be directly stimulated by proton [39]. Furthermore, by replacing  $\text{CO}_2$  buffering system with HEPE buffering system, a more recent study demonstrated proton concentration is actually playing the major and independent role in regulating osteoclasts/osteoblast differentiation [26]. On the contrary, alkalosis inhibits osteoclastic resorption activity and inhibits its  $\beta$ -glucuronidase secretion of osteoclast [28].

### 11.3 Implication from Biomaterial Extraction pH

One of the advantages of utilizing ceramic/glass materials for the treatment of osteoporotic bone defect is that these materials are capable of releasing beneficial elements throughout their biodegradation process. By adulterating different types of ions (e.g.,  $\text{Mg}^{2+}$ ,  $\text{Sr}^{2+}$ ,  $\text{Zn}^{2+}$ ,  $\text{Si}^{4+}$ , etc.) into silicate/phosphate framework, these materials usually acquire promoting effect toward bone defect regeneration. However, previous studies usually attribute these effects to the released ions, while less effort has been put into evaluating the microenvironment change after material implantation. For example, due to the blood/tissue fluid circulation, the concentration of the released ion at implant surface may be significantly different from that examined by a static in vitro extraction system. In addition, the  $\mu\text{-pH}$  level may also be significantly influenced by these released products, whereas the effect of this localized extracellular pH change on bone cells behaviors has seldom been discussed.

45S5 glass was developed by LL Hench in the 1970s. It shows the capability to form an apatite-like layer which binds directly to the bone on the surface [40]. This





**Fig. 11.1** (a) Time-dependent pH change of solutions exposed to 45S5, 52S4.6, or 60S3.8 glass (Tris buffer; figure is reproduced from Ref. [42] by permission of John Wiley and Sons). (b) Time-dependent pH change of solutions exposed to 13-93, 13-93B1, or 13-93B3 glass (Simulated body fluid; figure is reproduced from Ref. [43] by permission of Elsevier)

may be realized by its ability to release alkaline ions which drive the nucleation of the apatitic material by raising the local pH [41]. The change of pH in the extracts of  $\text{SiO}_2\text{-Na}_2\text{O-CaO-P}_2\text{O}_5$  glass system influences the formation of a calcium phosphate film as well as the viability and differentiation of osteoblast. The pH value of homogeneous bulk extraction increases with time in 45S5 (46.1%  $\text{SiO}_2$ , 2.6%  $\text{P}_2\text{O}_5$ , 26.9%  $\text{CaO}$ , and 24.4%  $\text{Na}_2\text{O}$ ) and 52S4.6 (52.1%  $\text{SiO}_2$ , 2.6%  $\text{P}_2\text{O}_5$ , 23.8%  $\text{CaO}$ , and 21.5%  $\text{Na}_2\text{O}$ ) glasses (Fig. 11.1a); and when the pH reaches a value higher than 7.9, the formation of calcium phosphate film on their surface could be detected by IRRS. At the same time, the pH value of 60S3.8 (60.1%  $\text{SiO}_2$ , 2.6%  $\text{P}_2\text{O}_5$ , 19.6%  $\text{CaO}$ , and 17.7%  $\text{Na}_2\text{O}$ ) remains constant throughout the immersion period (Fig. 11.1a), and it is not sufficient to form a stable calcium phosphate film on its surface [42]. In addition, when the concentration of  $\text{P}_2\text{O}_5$  in a  $\text{SiO}_2\text{-Na}_2\text{O-CaO-P}_2\text{O}_5$  system increases, the pH values of their extracts are decreased [44]. The downregulated osteoblast viability and differentiation in the presence of higher  $\text{P}_2\text{O}_5$  incorporation (lower  $\mu\text{e-pH}$ ) are recorded in another study [45]. Similarly, in the borosilicate glass system ( $\text{SiO}_2\text{-Na}_2\text{O-K}_2\text{O-MgO-CaO-P}_2\text{O}_5\text{-B}_2\text{O}_3$ -based glass), a higher  $\text{B}_2\text{O}_3$  content generates a higher pH value (Fig. 11.1b) and possesses better new bone formation ability when examined in vivo [46]. Our previous study also indicates that a weakly alkaline surface pH of borosilicate shows the potential to stimulate osteoblast viability and activity, thus further facilitating apatite nucleation [47].

It seems that a higher in vitro pH generated by biomaterial degradation (with similar degradation products) is associated with a better in vivo performance; and at the same time, this trend is consistent with the behavior of bone cells cultured in pH-adjusted media (discussed in Sect. 11.2.3). Therefore, it is reasonable to hypothesize that change of in vivo  $\mu\text{e-pH}$  during materials biodegradation process may play a critical role in the bone regeneration process. In order to verify this hypothesis, techniques for direct detecting pH values at material surface are necessary;

also, considering that  $\mu\text{-pH}$  changes influenced by materials biodegradation could not be simply explained by the concentration change of proton and/or  $\text{HCO}_3^-$ , their effect should be evaluated in different material systems, specifically.

## 11.4 Techniques for Detecting Biomaterial Interfacial pH

In vitro/in vivo pH detection is important for a better understanding of organ/tissue metabolism under normal or pathological conditions. In material science, in vitro leaching method is widely used to predict change of implants pH in vivo [48, 49]. However, interaction between implants and surrounding tissues may generate a cascade of tissue responses and makes it impossible to predict in vivo result by in vitro simulation, so that a direct in vivo detection is necessary. Also, ordinary bulky glass pH electrode is not suitable for measuring material interfacial pH due to its large sensor size. There is a great need for developing pH sensors with good biocompatibility, short response time, high precision, and continuous monitoring properties for in vivo  $\mu\text{-pH}$  detection.

It has been said to be difficult to evaluate rapid  $\mu\text{-pH}$  change near the surface of biomaterials [50], and the knowledge of material  $\mu\text{-pH}$  change after implantation remains sketchy. Currently, techniques used for in vivo pH detection are of three kinds [51]: electrochemical (e.g., convention glass pH electrode [52]), gravimetric [53], and spectroscopic (e.g., nuclear magnetic resonance (NMR)-based spectroscopy [54]; near-infrared (NIR)-based fluorescence spectroscopy [55, 56]). The gravimetric pH detection system is based on precise detection of mass changes following concentration changes but has the drawback of a long response time, which limits its wide application [51]; besides, NMR-based pH monitoring systems are too sophisticated to be employed for routine detection [51]. In this section, we mainly discuss fluorescence- and electrode-based pH detection systems used for in vivo/in vitro pH detection.

### 11.4.1 *Noninvasive pH Monitoring System: NIR Fluorescence Dye*

Fluorescence spectroscopy provides better spatial and temporal in vitro images when compared with NMR or microelectrode monitor systems. It is sensitive and requires simple operation. Most importantly, it is nondestructive to cells. The pH-sensitive NIR fluorescence dyes play important roles in the detection of in vivo/in vitro pH distributions [57–59]. The principle of qualitative fluorescent pH indicators is that they could be activated when pH changes to a specific threshold. However, they may also be influenced by the length of optical path, change of temperature, alteration of excitation intensities, and emission collection efficiencies [60]. There

are two main ways to avoid these errors: fluorescence ratio imaging and fluorescence lifetime imaging.

Ratiometric method requires that fluorescence molecular probe should be excited at a specific wavelength range and has at least two emission wavelengths [61, 62]. The two emission wavelengths are carefully chosen according to their enhanced and diminished pattern in relevance to pH change. The fluorescent intensities of these two signals are recorded, and the ratio between which is calibrated. This ratio is expected to correlate with pH value in a restricted pH region [60]. Take carboxy seminaphthorhodafluor (SNARF)-1 and LysoSensor Yellow/Blue DND-160 as examples, when carboxy SNARF-1 is excited at 488 nm, the emission wavelengths which are sensitive to pH change are typically at about 580 nm and 640 nm, while LysoSensor Yellow/Blue DND-160 shows characteristic emission wavelengths at about 440 nm and 540 nm when it is excited at 360 nm. In addition, different probes have different pH detecting ranges, and a pilot estimation is needed before choosing appropriate probes for specific detections. Most used near-neutral pH indicators include SNARF [63] and 8-hydroxypyrene-1,3,6-trisulfonic acid (HPTS), while LysoSensor Yellow/Blue dye is usually employed as an acidic pH indicator [64]. Another choice to overcome uncertainties in the calibration of responses toward pH (e.g., probe concentration, heterogeneities medium) is the use of time-resolved fluorescence pH probe [65]. Fluorescence lifetime imaging is based on the measurement of fluorescence decay time at respective spatially resolvable location. The fluorescence lifetime of a pH probe is pH dependent and could be converted into a pH map of the detected tissue accordingly [66].

The *in vitro* pH distribution in polymer microspheres could be monitored by blending pH-sensitive fluorescence dye with polymers. The probe-enraptured microspheres are prepared by a w/o/w double emulsion-solvent evaporation microencapsulation method [63, 64]. Different probes are chosen at different pH levels. Based on our knowledge, there is at least one attempt that uses the optical method to detect biomaterial local pH in a subcutaneous implantation region. The tissue pH surrounding the implant was monitored indirectly but noninvasively by a fluorescence dye, seminaphthorhodafluor (SNARF) [67]. Using ratiometric method, the study compared *in vitro* and *in vivo* fluorescence ratio change by SNARF-1 in response to a standard pH solution or in response to subcutaneously implanted Mesofol (acid degradation products) or magnesium hydroxide (alkaline degradation products) powders. Hairless but immunocompetent mice were used as the animal model to avoid autofluorescence signals [68], and the fluorescent dye was injected intravenously in their system. The authors concluded their method was noninvasive and suitable for studies on interaction between degrading biomaterials and the tissue environment. However, due to the low sensitivity, the result is far from satisfactory.

At last, pH detection based on fluorescence ratio imaging microscopy is susceptible to photo-bleaching and variation in light scattering, since the interaction of pH indicators with intracellular proteins may change the fluorescence intensity ratio [66], thus introducing bias in the results of pH measurement. Besides, there is a lack of data on longtime *in vivo* biological toxicity and biocompatibilities for these small molecular probes. These drawbacks strongly limit their experimental and clinical applications.

### 11.4.2 Direct pH Monitoring System: pH Microelectrode

Direct pH measurement by a pH electrode would get rid of most of the drawbacks of optical-based pH detecting systems. The pH-sensitive membrane-solution interface of a pH electrode could respond to the concentration change of hydrogen ions in the detected solution. A pH-sensitive membrane separates the standard solution from the test solution, and the potential  $E$  across the membrane is determined by the Nernst equation:

$$E = \text{constant} + (RT / F) \ln [H^+] \quad (11.2)$$

where  $R$  represents gas constant,  $T$  represents temperature (K),  $F$  represents Faraday constant, and  $[H^+]$  represents hydrogen ion concentration (mol/L). According to  $\text{pH} = -\log [H^+]$ , Eq. 11.2 changes to a form as follows:

$$E = -(2.303RT / F) \text{pH} + \text{constant} \quad (11.3)$$

where  $-(2.303RT/F)$  is the slope of the line and is 59.16 mV/pH at 298 K. According to this calibration equation, the relationship between solution pH and potential could be calibrated in standard solution, while the constant could be determined by adding a reference electrode [69]. The electrode sensitivity (in mV/pH) is determined by the slope, and generally, the absolute value of the slope gets lower after longtime use or get contaminated [70].

The linear response range of a pH electrode is generally from a pH of 2 to 9. Acid error occurs when the electrode is used to detect high  $[H^+]$  (low pH; pH = 2) solution. At high pH (low  $[H^+]$ ; pH = 8–11), alkaline ions (e.g.,  $\text{Na}^+$  or  $\text{K}^+$ ) interfere the final reading, and the electrode gives a lower result than the actual pH. Therefore, there may be small variations between individual calibration slopes at different pH levels, and it is suggested to calibrate the slope by a two-point calibration that is close to the detection range.

However, ordinary bulky glass pH is not suitable for in vivo detection, especially for the detection in a small microenvironment. Table 11.2 lists some primary parameters of commercially available glass-made pH microelectrode or electrode. The diameter of a pH microelectrode sensor is about one-tenth of that of ordinary glass electrode, so that the minimum test volume could be three orders of magnitude smaller, which makes the detection of a  $\mu\text{e-pH}$  possible. The minimum response volume of the detection solution is calculated by the equation as follows:

$$V_{\min} = 8R^3 - 4\pi R^3 / 3 \quad (11.4)$$

where  $R$  means the radius of the electrode or microelectrode. Therefore only a small amount ( $\sim 1 \mu\text{L}$ ) of the solution is needed for each detection with a pH microelectrode.

**Table 11.2** A comparison between commercially available glass-made pH electrode and pH microelectrode

	Needle (sensor) diameter	Minimum immersion depth	Response time	Theoretical minimum response volume
pH electrode	12 mm	20 mm	<20 s	823.68 $\mu\text{L}$
pH microelectrode	1.3 mm	1 mm	5–15 s	1.047 $\mu\text{L}$

The sensitivity, response time, reproducibility, selectivity, stability, and reliability are most important parameters for a good pH microelectrode. Furthermore, there are two more factors that should be considered for *in vivo* detection: one is the biocompatibility of the sensor-tissue interface, which could be achieved by encapsulating the sensor with biocompatible materials [71, 72]; the other one is that the salts and proteins in the biological fluid make *in vivo* test solution a corrosive environment which may shorten the life of the device [73, 74]. A cleaning procedure to remove adherent proteins is suggested after each test, and this will prolong the working life of the microelectrodes.

Based on the format of pH-sensitive materials, the pH microelectrodes could be classified into glass-based pH microelectrodes, polymer membrane-based pH microelectrodes, silicon-based pH microelectrodes, metal/metal oxide-based pH microelectrodes, and so on [51]. Glass breakage [75] and miniaturization [76] are the major limitations of glass-based pH microelectrodes, while polymer membrane-based pH microelectrodes have the problem of poor biocompatibility [77]. Compared with glass-based pH microelectrodes and polymer membrane-based pH microelectrodes, the ion-sensitive field-effect transistor (ISFET) which is a kind of silicon (Si) water-based pH sensors has some unique features, such as dry storage, fast response, and capability of miniaturization [78]. It finds continuing applications in detecting bacterial activity [79] and pH gradient across a cell membrane [80]. It is also widely applied in areas of food, cosmetic, pharmaceutical, and water purification industries. Even though, ISFET pH sensor is still confronted with the challenges of encapsulation of Si sensor chip and dissolution of gate material for detection of corrosive *in vivo* tissue fluid, especially when it is employed for long-term *in vivo* pH detection or as an implantable sensor [51].

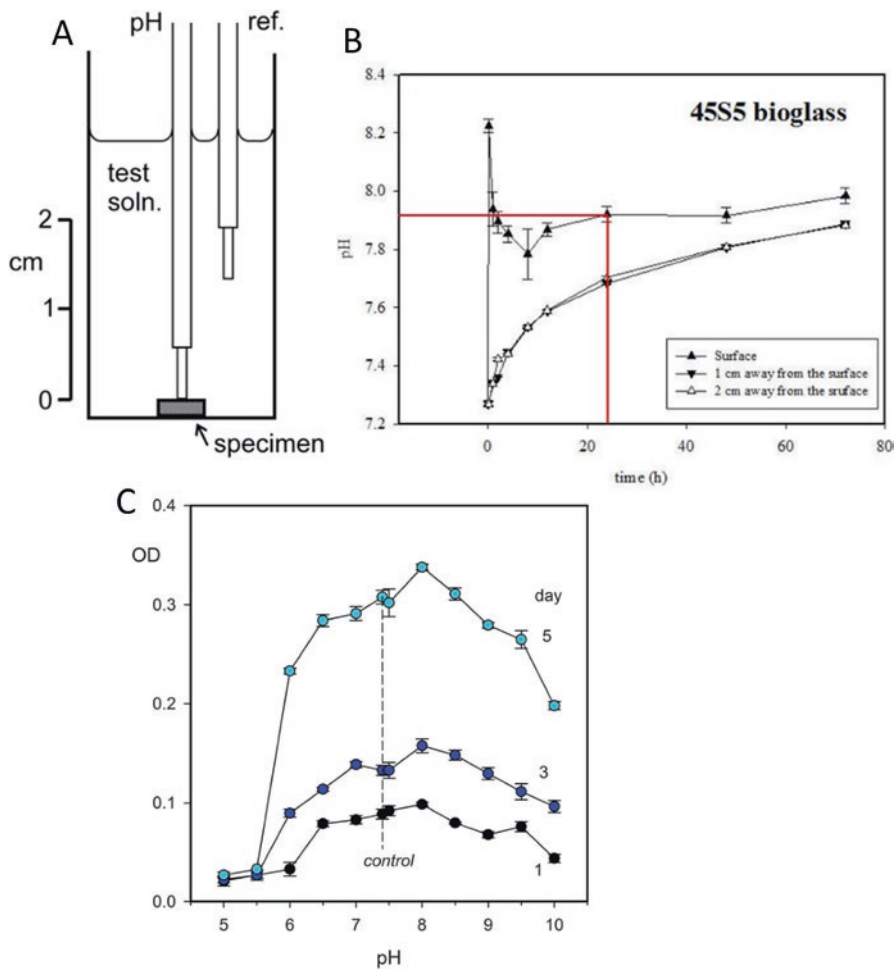
The pH microelectrode is a reliable detection technique widely applied in detection pH of normal tissue (e.g., brain [81], heart [82], skin [83], eyes [84], etc.) or diseased tissue (e.g., cancer [85]). Using a pH microelectrode, Chakkalakal et al. detected changes of tissue pH during the bone healing process and concluded that the pH of repair tissue fluids may play a regulatory role in bone healing and mineralization process [86]. However, the change pattern of  $\mu\text{e-pH}$  of different biodegradable implants during tissue regeneration and its influence on the performance of biomaterials remain uncertain.

## 11.5 Influence of Biomaterial $\mu$ -pH on Bone Regeneration

By employing pH microelectrode, the detection of orthopedic artificial biomaterials interfacial pH has been realized both in vitro and in vivo. In vitro, there is a significant difference between pH at the surface of a material and that of a homogeneous bulk extract at an early stage [47, 87]. For example, the interfacial pH of a well-studied biomaterial developed in the 1970s, 45S5 bioactive glass, is found to be appreciably higher than that of the bulk medium and the “standard” physiological value of 7.4 (Fig. 11.2a, b). The surface pHs of a series of Sr-B-Si-based glasses are further checked by the same method, and the results indicate that although there is no significant difference between borosilicate glasses with (SrBSi) or without (BSi) 6% Sr adulteration at any time points, the pH difference is apparent between material surface and their bulk solutions (Fig. 11.3a) within 24 h. The bulk pH increases steadily and becomes indistinguishable from the surface value by about 24 h. It is believed that this  $\mu$ -pH change, instead of a diluted bulk extraction pH, may directly influence the behavior of the surrounding bone cells.

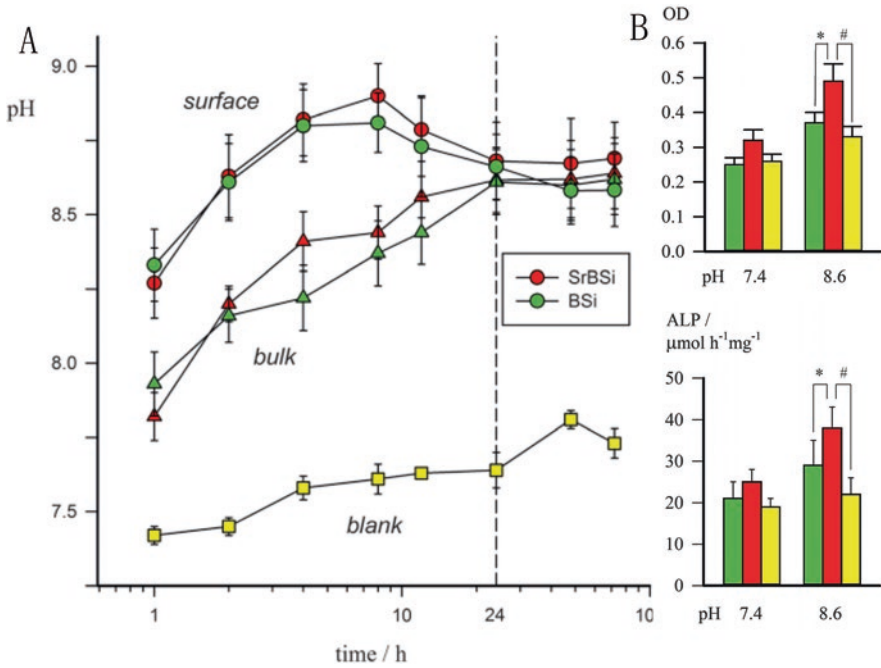
By adjusting extraction solutions of a series of Sr-containing  $\text{CaCO}_3$  to their interfacial pH values (pH >8), both proliferation and alkaline phosphatase (ALP) activity of MG-63 cells are significantly enhanced [87]. In addition, pH 8 has a distinct effect on promoting MC3T3-E1 pre-osteoblast proliferation, compared with the control at pH 7.4 (Fig. 11.2c). After that, effect of beneficial elements, such as Sr, Si, and B, is examined in different pH-adjusted media. According to the results, both strontium and silicon enhance cell proliferation at pH 7.4, with peak values at 5 and 1  $\text{mmol}\cdot\text{L}^{-1}$ , respectively, while boron has no beneficial effect at any concentration at pH 7.4 (Fig. 11.4). The promoting effect of pH (at pH 8–8.5) on the viability of MC3T3-E1 is not significant in 1  $\text{mmol}\cdot\text{L}^{-1}$  Si-containing medium but is detectable at 5  $\text{mmol}\cdot\text{L}^{-1}$  Sr-containing medium ( $p = 0.047$  vs. pH 7.4) and at 1  $\text{mmol}\cdot\text{L}^{-1}$  B-containing medium ( $p = 0.035$  vs. pH 7.4) (Fig. 11.3). At last, by culturing cells into the extraction of Sr-B-Si-based glasses, both OD and ALP activities for the SrBSi extracts are significantly higher than that for BSi at pH 8.6 but lose their significance at pH 7.4 (Fig. 11.3b).

The activity of osteoporotic bone marrow stromal cells (oBMSCs) and RAW 264.7 osteoclast precursors that influenced by  $\mu$ -pH change has been further checked by a recent work. Osteoporotic bone marrow stromal cells are extracted from the established ovariectomized (OVX) rat model [88], and their proliferation is significantly inhibited when they are cultured in either a higher or a lower pH condition in the extract of 10% strontium-substituted calcium silicate (Sr-CS) in  $\alpha$ -MEM (200 mg/mL and 1:16 diluted) (Fig. 11.5a). The alkaline-adjusted osteogenesis medium with Sr-CS extract (pH 7.57–7.73) shows higher ALP activity after a culture time of 1 week (Fig. 11.5b). With increasing culture medium pH, the proliferation of RAW 264.7 cells is significantly suppressed (Fig. 11.5c). The osteoclast-formation capability of RAW 264.7 cells, examined by a RANKL stimulating test, is decreased and vanished in the extreme alkaline condition (pH  $8.00 \pm 0.04$ ) (Fig. 11.5d). All these results indicate that both chemistry and  $\mu$ -pH of the solid-liquid interface are critical factors that influence the bone cell behaviors.



**Fig. 11.2** (a) The measurement of in vivo  $\mu\text{-pH}$  on the surface of biomaterials. (b) Time-dependent surface pH change of 45S5 glass in vitro. (c) Effect of pH on the MC3T3-E1 viability (Figure is reproduced from Ref. [47, 87] with the permission of American Chemical Society and The Royal Society of Chemistry)

The in vivo  $\mu\text{-pH}$  detection of different biomaterials is realized by placing the sensing tip of the microelectrode on the surface of the blood-saturated packed powders. The average of the stable values is used for analysis. Protein contamination on the sensor is removed after each measurement by immersing the sensor in enzymatic detergent (1% Tergazyme). As shown in Fig. 11.6, after implantation, in vivo  $\mu\text{-pH}$  for  $\beta$ -tricalcium phosphate ( $\beta$ -TCP), calcium silicate (CS), and 10% strontium-substituted calcium silicate (Sr-CS) increase immediately in comparison with the Blank group ( $7.42 \pm 0.02$ ), with CS ( $8.17 \pm 0.06$ ) and Sr-CS ( $9.16 \pm 0.11$ )



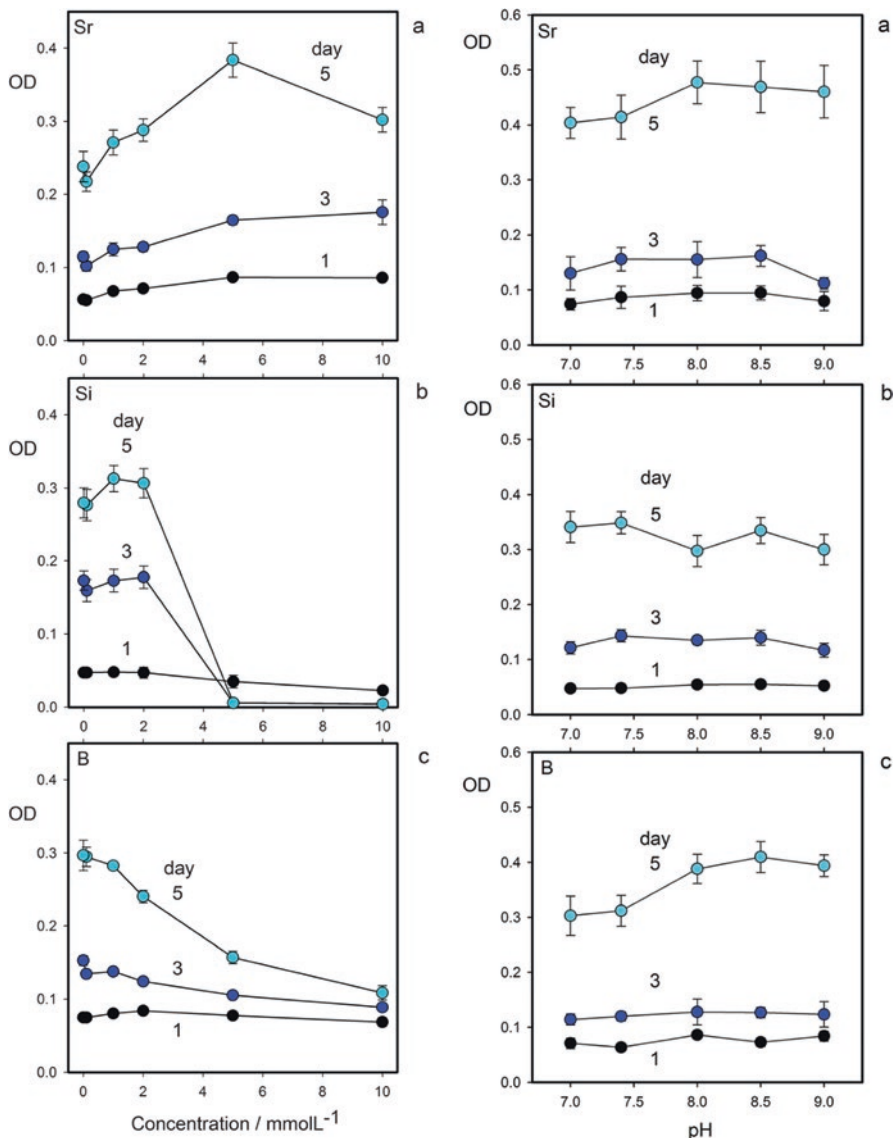
**Fig. 11.3** (a) Interfacial and bulk pH variation of the medium in contact with the SrBSi and BSi scaffolds. (b) Proliferation (*top*) and ALP activity (*bottom*) of MC3T3-E1 with respect to pH and scaffold material in contact. Significant comparisons: \*  $p < 0.05$ ,  $p < 0.01$  (Figure is reproduced from Ref. [47] with the permission of The Royal Society of Chemistry)

giving a significantly higher value compared with  $\beta$ -TCP ( $7.77 \pm 0.15$ ) ( $P < 0.01$ ), that is, Sr-CS  $>$  CS  $>$   $\beta$ -TCP (Fig. 11.6). The significant elevation of  $\mu$ e-pH persists to day 3 ( $P < 0.05$ ) but has faded by 9 weeks, so that the early stage may be the most important stage for  $\mu$ e-pH change to take effect. Besides, Sr-CS has higher  $\mu$ e-pH values than both CS and  $\beta$ -TCP at all time points (Fig. 11.6).

According to the histological examination, there is significantly more new bone (NB) that formed in defect regions in the higher  $\mu$ e-pH conditions (CS and Sr-CS) at week 9; also, during material degradation, an intermediate (assumed apatitic) calcium phosphate layer, but without osteocyte lacunae, is also observed in these groups (Fig. 11.7a). For  $\beta$ -TCP, TRAP<sup>+</sup> osteoclast-like cells are found as early as week 1 and then reach the highest levels at week 4, whereas in the higher  $\mu$ e-pH groups, a late response of TRAP<sup>+</sup> osteoclast-like cells is observed: none is found at week 1, appearing at week 4, and could still be seen at week 9 (Fig. 11.7b).

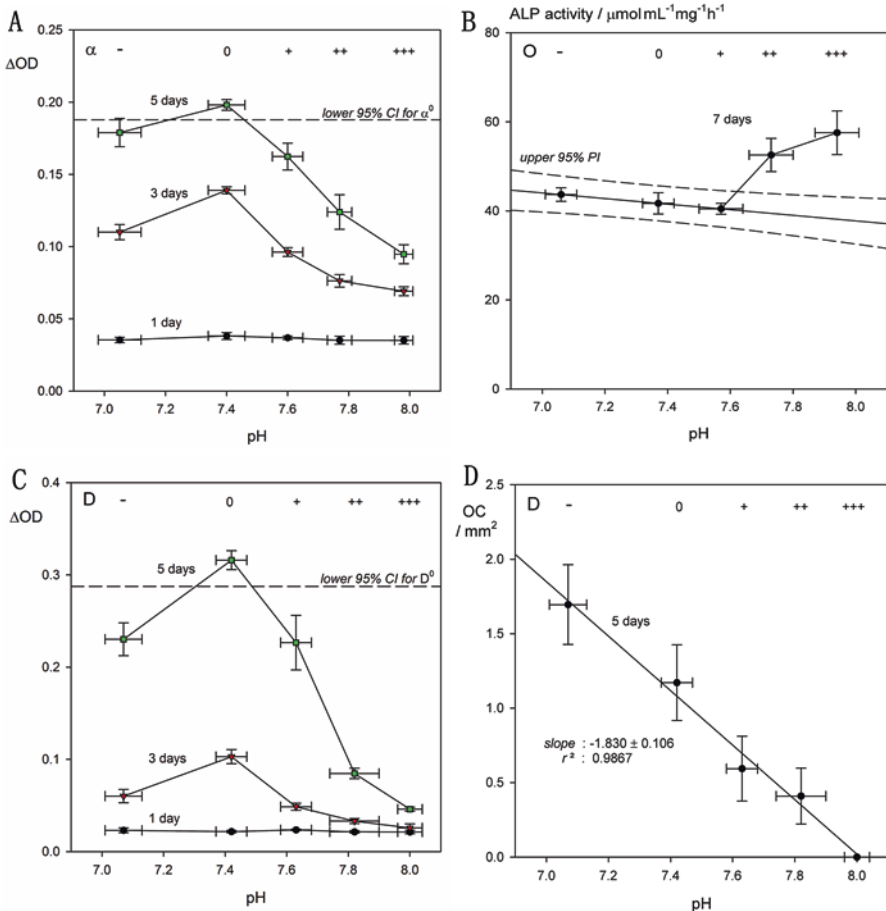
The *in vivo*  $\mu$ e-pH could be influenced by, but not restricted to, biodegradation of implants, formation of apatite, tissue fluid, and blood circulation. Therefore, it should notice that the  $\mu$ e-pH is an intermediate variable that different materials could generate a similar  $\mu$ e-pH by releasing different types of ions. The influence from beneficial ions released from biomaterial extraction *in vitro* has been widely





**Fig. 11.4** Effect of the concentration of solution Sr, Si, and B and pH on the MC3T3-E1 osteoblast activity (Figure is reproduced from Ref. [47] with the permission of The Royal Society of Chemistry)

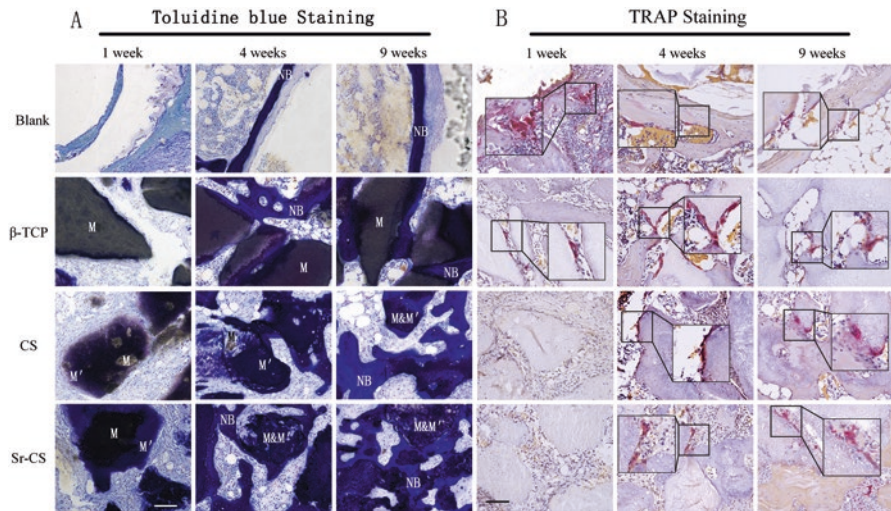
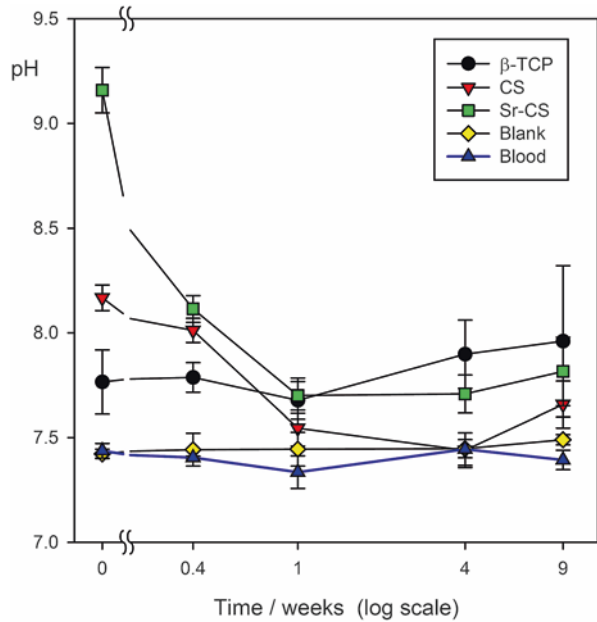
reported, whereas the present works demonstrate the importance of  $\mu\text{e-pH}$  during the bone regeneration under osteoporosis conditions. Since both of degradation products and  $\mu\text{e-pH}$  are critical to guarantee a fast bone regeneration process, biomaterials should be carefully designed with proper composition ions to provide a favorable  $\mu\text{e-pH}$  without generating any adverse effects.



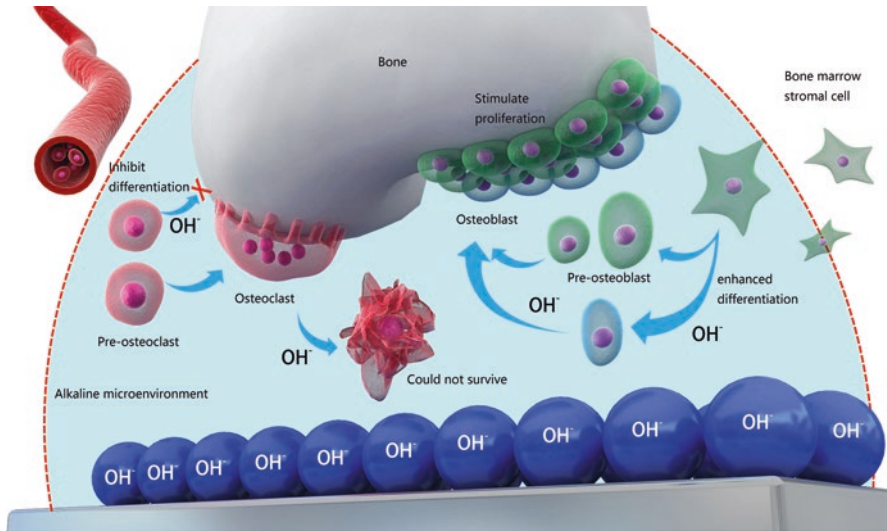
**Fig. 11.5** (a) oBMSC proliferation in  $\alpha$ -MEM by MTT assay (optical density difference,  $\Delta OD = OD_{650} - OD_{570}$ );  $n = 5$ . (b) oBMSC differentiation in osteogenesis medium by ALP activity in terms of rate of  $p$ -nitrophenol production ( $\mu\text{mol}\cdot\text{mL}^{-1}\cdot\text{mg}^{-1}\cdot\text{hour}^{-1}$ ;  $n = 4$ ; 95% prediction interval for linear regression on  $-$ ,  $0$ , and  $+$  points shown dashed). (c) RAW 264.7 proliferation in DMEM by MTT assay (optical density difference,  $\Delta OD = OD_{650} - OD_{570}$ );  $n = 5$ . (d) Semiquantitative image analysis for osteoclast surface area (OC/mm<sup>2</sup>);  $n = 5$  (Figure is reproduced from Ref. [89] with the permission of Springer)

To summarize, the detection of in vitro/in vivo  $\mu\text{e-pH}$  is realized by utilizing a pH microelectrode. The impaired regeneration process under osteoporotic or immobilized conditions may be ameliorated by adjusting the materials to generate a weakly alkaline microenvironment, since it has the effects on promoting osteoblast differentiation and inhibiting osteoclast formation. It has been demonstrated that the  $\mu\text{e-pH}$  differs from that of the homogeneous peripheral blood and exhibits variations over time particular to each biodegradable material. Higher  $\mu\text{e-pH}$  is associated with better overall performances: greater new bone formation and a later

**Fig. 11.6** Variation of  $\mu\text{e-pH}$  with time postimplantation. Data are expressed as the mean  $\pm$  standard deviation;  $n = 4$  (Figure is reproduced from Ref. [89] with the permission of Springer)



**Fig. 11.7** (a) Undecalcified tissue section results, Toluidine Blue staining. Implant materials (M) appear black or gray; new bone (NB) is stained blue (osteocyte lacunae can be clearly observed). “Apatitic” intermediate layer (M’), lacking lacunae, found for CS and Sr-CS. Scale bar: 100  $\mu\text{m}$ . (b) In TRAP staining, TRAP-positive osteoclast-like cells (magnified view) were stained red-purple. The osteoclast-like cells are multinucleated, attached to the bone or implant surface, and TRAP positive. None were found for CS and Sr-CS at 1 week. Scale bar: 100  $\mu\text{m}$  (Figure is reproduced from Ref. [89] with the permission of Springer)



**Fig. 11.8** Sketch map of the  $\mu\text{e-pH}$  and the performance of biomaterials

response of TRAP<sup>+</sup> osteoclast-like cells as well as the formation of an intermediate “apatitic” layer. Therefore, alkaline biodegradable materials with a  $\mu\text{e-pH}$  higher than physiological condition are advocated for better regeneration, in particular, for osteoporotic bone defect regeneration.

Finally, it is proposed that the scheme of the general tissue response process that is influenced by  $\mu\text{e-pH}$  change appears to be as follows, given that osteoclast activity is higher than normal in the context of osteoporotic bone (Fig. 11.8). Initially, fibroblasts attach to the surface of the implant and develop the fibrous capsule. Mesenchymal stem cells then migrate to the bone defect under some biochemical cue, proliferate, and differentiate into osteoblasts which then attach to the surface of the implant, secreting bone matrix (osteoid). These osteoblasts are embedded in that matrix, becoming osteocytes, and the matrix is mineralized, with this new bone growing out and attaching to the trabecular bone. If the implant material is biodegradable, it is gradually replaced by new bone, along with remodeling of the existing structures by osteoclasts. All these processes are considered to be influenced by the change of biomaterials'  $\mu\text{e-pH}$  spatiotemporally, whereas the present works only demonstrated the effect of  $\mu\text{e-pH}$  on oBMSCs, osteoblast, and osteoclasts at the early stage after their implantation. Further studies on how  $\mu\text{e-pH}$  is taking its effect throughout this process are needed, and it is suggested that the  $\mu\text{e-pH}$  should be used as one of the indices for biomaterial evaluation to better guide the design of biomaterials used for osteoporotic patients.

During the bone regeneration process of osteoporotic bone defect/fracture, a weak-alkaline  $\mu\text{e-pH}$  that is created by biodegradable material implantation may suppress the abnormal osteoclasts activity, stimulate osteoblast differentiation from BMSCs, and thus reestablish the normal bone regeneration process for these patients.

**Acknowledgments** This work was supported by grants from the National Natural Science Foundation of China (No. 81672227; 51372170), Shenzhen Peacock Program (No. 110811003586331), Highlight research of frontier science, Chinese academy of sciences (No. QYZDB-SSW-JSC030), Shenzhen Science and Technology Research funding (No. CXZZ20150401152251209; JSGG2015103014032514; JSGG20150331154931068, CXZZ20140417113430716, JCYJ20170413162104773) and Youth Innovation Promotion Association CAS.

## References

1. Johnell O, Kanis JA (2006) An estimate of the worldwide prevalence and disability associated with osteoporotic fractures. *Osteoporos Int* 17(12):1726–1733. doi:[10.1007/s00198-006-0172-4](https://doi.org/10.1007/s00198-006-0172-4)
2. Feng X, McDonald JM (2011) Disorders of bone remodeling. *Annu Rev Pathol* 6:121–145. doi:[10.1146/annurev-pathol-011110-130203](https://doi.org/10.1146/annurev-pathol-011110-130203)
3. Italian Society of Osteoporosis MM, Skeletal D, Italian Society of R, Varenna M, Bertoldo F, Di Monaco M, Giusti A, Martini G, Rossini M (2013) Safety profile of drugs used in the treatment of osteoporosis: a systematical review of the literature. *Reumatismo* 65(4):143–166. doi:[10.4081/reumatismo.2013.143](https://doi.org/10.4081/reumatismo.2013.143)
4. Fleisch H (2003) Bisphosphonates in osteoporosis. *Eur Spine J* 12(Suppl 2):S142–S146. doi:[10.1007/s00586-003-0622-z](https://doi.org/10.1007/s00586-003-0622-z)
5. Neer RM, Arnaud CD, Zanchetta JR, Prince R, Gaich GA, Reginster JY, Hodsman AB, Eriksen EF, Ish-Shalom S, Genant HK, Wang O, Mitlak BH (2001) Effect of parathyroid hormone (1-34) on fractures and bone mineral density in postmenopausal women with osteoporosis. *N Engl J Med* 344(19):1434–1441. doi:[10.1056/NEJM200105103441904](https://doi.org/10.1056/NEJM200105103441904)
6. Meunier PJ, Slosman DO, Delmas PD, Sebert JL, Brandi ML, Albanese C, Lorenc R, Pors-Nielsen S, de Vernejoul MC, Roces A, Reginster JY (2002) Strontium ranelate: dose-dependent effects in established postmenopausal vertebral osteoporosis – a 2-year randomized placebo controlled trial. *J Clin Endocrinol Metab* 87(5):2060–2066
7. Black DM, Delmas PD, Eastell R, Reid IR, Boonen S, Cauley JA, Cosman F, Lakatos P, Leung PC, Man Z, Mautalen C, Mesenbrink P, Hu H, Caminis J, Tong K, Rosario-Jansen T, Krasnow J, Hue TF, Sellmeyer D, Eriksen EF, Cummings SR, Trial HPF (2007) Once-yearly zoledronic acid for treatment of postmenopausal osteoporosis. *N Engl J Med* 356(18):1809–1822. doi:[10.1056/NEJMoa067312](https://doi.org/10.1056/NEJMoa067312)
8. Kanis JA, Burlet N, Cooper C, Delmas PD, Reginster JY, Borgstrom F, Rizzoli R, European Society for C, Economic Aspects of O, Osteoarthritis (2008) European guidance for the diagnosis and management of osteoporosis in postmenopausal women. *Osteoporos Int* J Established Result Cooperation Between Eur Found Osteoporos National Osteoporos Found USA 19(4):399–428. doi:[10.1007/s00198-008-0560-z](https://doi.org/10.1007/s00198-008-0560-z)
9. Arcos D, Boccaccini AR, Bohner M, Diez-Perez A, Epple M, Gomez-Barrena E, Herrera A, Planell JA, Rodriguez-Manas L, Vallet-Regi M (2014) The relevance of biomaterials to the prevention and treatment of osteoporosis. *Acta Biomater* 10(5):1793–1805. doi:[10.1016/j.actbio.2014.01.004](https://doi.org/10.1016/j.actbio.2014.01.004)
10. Kim CH, Takai E, Zhou H, Von Stechow D, Muller R, Dempster DW, Guo XE (2003) Trabecular bone response to mechanical and parathyroid hormone stimulation: the role of mechanical microenvironment. *J Bone Miner Res* 18(12):2116–2125. doi:[10.1359/jbmr.2003.18.12.2116](https://doi.org/10.1359/jbmr.2003.18.12.2116)
11. Leblanc AD, Schneider VS, Evans HJ, Engelbretson DA, Krebs JM (1990) Bone-mineral loss and recovery after 17 weeks of bed rest. *J Bone Miner Res* 5(8):843–850
12. Fini M, Giavaresi G, Torricelli P, Krajewski A, Ravaglioli A, Belmonte MM, Biagini G, Giardino R (2001) Biocompatibility and osseointegration in osteoporotic bone. *J Bone Joint Surg Br* 83(1):139–143

13. Boron WF (2004) Regulation of intracellular pH. *Adv Physiol Educ* 28(4):160–179. doi:[10.1152/advan.00045.2004](https://doi.org/10.1152/advan.00045.2004)
14. Bushinsky DA, Ori Y (1993) Effects of metabolic and respiratory acidosis on bone. *Curr Opin Nephrol Hypertens* 2(4):588–596
15. Lopez I, Aguilera-Tejero E, Felsenfeld AJ, Estepa JC, Rodriguez M (2002) Direct effect of acute metabolic and respiratory acidosis on parathyroid hormone secretion in the dog. *J Bone Miner Res* 17(9):1691–1700. doi:[10.1359/jbmr.2002.17.9.1691](https://doi.org/10.1359/jbmr.2002.17.9.1691)
16. Bushinsky DA (1996) Metabolic alkalosis decreases bone calcium efflux by suppressing osteoclasts and stimulating osteoblasts. *Am J Phys* 271(1 Pt 2):F216–F222
17. Lopez I, Rodriguez M, Felsenfeld AJ, Estepa JC, Aguilera-Tejero E (2003) Direct suppressive effect of acute metabolic and respiratory alkalosis on parathyroid hormone secretion in the dog. *J Bone Miner Res* 18(8):1478–1485. doi:[10.1359/jbmr.2003.18.8.1478](https://doi.org/10.1359/jbmr.2003.18.8.1478)
18. Arnett T (2003) Regulation of bone cell function by acid-base balance. *Proc Nutr Soc* 62(2):511–520
19. Bushinsky DA, Krieger NS, Geisser DI, Grossman EB, Coe FL (1983) Effects of pH on bone calcium and proton fluxes in vitro. *Am J Phys* 245(2):F204–F209
20. Brandao-Burch A, Utting JC, Orriss IR, Arnett TR (2005) Acidosis inhibits bone formation by osteoblasts in vitro by preventing mineralization. *Calcif Tissue Int* 77(3):167–174. doi:[10.1007/s00223-004-0285-8](https://doi.org/10.1007/s00223-004-0285-8)
21. Bushinsky DA (2001) Acid-base imbalance and the skeleton. *Eur J Nutr* 40(5):238–244. doi:[10.1007/s394-001-8351-5](https://doi.org/10.1007/s394-001-8351-5)
22. Carter PH, Schipani E (2006) The roles of parathyroid hormone and calcitonin in bone remodeling: prospects for novel therapeutics. *Endocr Metab Immune Disord Drug Targets* 6(1):59–76
23. Eastell R (1998) Treatment of postmenopausal osteoporosis. *N Engl J Med* 338(11):736–746
24. Morley P, Whitfield JF, Willick GE (2001) Parathyroid hormone: an anabolic treatment for osteoporosis. *Curr Pharm Des* 7(8):671–687
25. Frick KK, Bushinsky DA (1998) Chronic metabolic acidosis reversibly inhibits extracellular matrix gene expression in mouse osteoblasts. *Am J Phys* 275(5 Pt 2):F840–F847
26. Kato K, Matsushita M (2014) Proton concentrations can be a major contributor to the modification of osteoclast and osteoblast differentiation, working independently of extracellular bicarbonate ions. *J Bone Miner Metab* 32(1):17–28. doi:[10.1007/s00774-013-0462-9](https://doi.org/10.1007/s00774-013-0462-9)
27. Kaunitz JD, Yamaguchi DT (2008) TNAP, TrAP, TrAP, Ecto-purinergic signaling, and bone remodeling. *J Cell Biochem* 105(3):655–662. doi:[10.1002/Jcb.21885](https://doi.org/10.1002/Jcb.21885)
28. Bushinsky DA (1996) Metabolic alkalosis decreases bone calcium efflux by suppressing osteoclasts and stimulating osteoblasts. *Am J Physiol Renal Fluid Electrolyte Physiol* 271(1):F216–F222
29. Kaysinger KK, Ramp WK (1998) Extracellular pH modulates the activity of cultured human osteoblasts. *J Cell Biochem* 68(1):83–89. doi:[10.1002/\(Sici\)1097-4644\(19980101\)68:1<83::Aid-Jcb8>3.0.Co;2-S](https://doi.org/10.1002/(Sici)1097-4644(19980101)68:1<83::Aid-Jcb8>3.0.Co;2-S)
30. Kohn DH, Sarmadi M, Helman JI, Krebsbach PH (2002) Effects of pH on human bone marrow stromal cells in vitro: implications for tissue engineering of bone. *J Biomed Mater Res* 60(2):292–299
31. Harada M, Udagawa N, Fukasawa K, Hiraoka BY, Mogi M (1986) Inorganic pyrophosphatase activity of purified bovine pulp alkaline-phosphatase at physiological pH. *J Dent Res* 65(2):125–127. doi:[10.1177/00220345860650020601](https://doi.org/10.1177/00220345860650020601)
32. Goldhaber P, Rabadjija L (1987) H<sup>+</sup> stimulation of cell-mediated bone-resorption in tissue-culture. *Am J Phys* 253(1):E90–E98
33. Arnett TR (2008) Extracellular pH regulates bone cell function. *J Nutr* 138(2):415S–418S
34. Arnett TR, Spowage M (1996) Modulation of the resorptive activity of rat osteoclasts by small changes in extracellular pH near the physiological range. *Bone* 18(3):277–279. doi:[10.1016/8756-3282\(95\)00486-6](https://doi.org/10.1016/8756-3282(95)00486-6)

35. Meghji S, Morrison MS, Henderson B, Arnett TR (2001) pH dependence of bone resorption: mouse calvarial osteoclasts are activated by acidosis. *Am J Physiol Endocrinol Metab* 280(1):E112–E119
36. Biskobing DM, Fan D (2000) Acid pH increases carbonic anhydrase II and calcitonin receptor mRNA expression in mature osteoclasts. *Calcif Tissue Int* 67(2):178–183. doi:[10.1007/S00223001107](https://doi.org/10.1007/S00223001107)
37. Bromme D, Okamoto K, Wang BB, Biroc S (1996) Human cathepsin O2, a matrix protein-degrading cysteine protease expressed in osteoclasts. Functional expression of human cathepsin O2 in *Spodoptera frugiperda* and characterization of the enzyme. *J Biol Chem* 271(4):2126–2132
38. Komarova SV, Pereverzev A, Shum JW, Sims SM, Dixon SJ (2005) Convergent signaling by acidosis and receptor activator of NF-kappaB ligand (RANKL) on the calcium/calcineurin/NFAT pathway in osteoclasts. *Proc Natl Acad Sci U S A* 102(7):2643–2648. doi:[10.1073/pnas.0406874102](https://doi.org/10.1073/pnas.0406874102)
39. Arnett TR, Dempster DW (1986) Effect of pH on bone resorption by rat osteoclasts in vitro. *Endocrinology* 119(1):119–124. doi:[10.1210/endo-119-1-119](https://doi.org/10.1210/endo-119-1-119)
40. Hench LL (2006) The story of bioglass (R). *J Mater Sci-Mater M* 17(11):967–978. doi:[10.1007/s10856-006-0432-z](https://doi.org/10.1007/s10856-006-0432-z)
41. Huang WH, Day DE, Kittiratanapiboon K, Rahaman MN (2006) Kinetics and mechanisms of the conversion of silicate (45S5), borate, and borosilicate glasses to hydroxyapatite in dilute phosphate solutions. *J Mater Sci Mater Med* 17(7):583–596. doi:[10.1007/s10856-006-9220-z](https://doi.org/10.1007/s10856-006-9220-z)
42. Ogino M, Ohuchi F, Hench LL (1980) Compositional dependence of the formation of calcium-phosphate films on bioglass. *J Biomed Mater Res* 14(1):55–64. doi:[10.1002/jbm.820140107](https://doi.org/10.1002/jbm.820140107)
43. Rahaman MN, Day DE, Bal BS, Fu Q, Jung SB, Bonewald LF, Tomsia AP (2011) Bioactive glass in tissue engineering. *Acta Biomater* 7(6):2355–2373. doi:[10.1016/j.actbio.2011.03.016](https://doi.org/10.1016/j.actbio.2011.03.016)
44. O'Donnell MD, Watts SJ, Hill RG, Law RV (2009) The effect of phosphate content on the bioactivity of soda-lime-phosphosilicate glasses. *J Mater Sci Mater Med* 20(8):1611–1618. doi:[10.1007/s10856-009-3732-2](https://doi.org/10.1007/s10856-009-3732-2)
45. Lossdorfer S, Schwartz Z, Lohmann CH, Greenspan DC, Ranly DM, Boyan BD (2004) Osteoblast response to bioactive glasses in vitro correlates with inorganic phosphate content. *Biomaterials* 25(13):2547–2555. doi:[10.1016/j.biomaterials.2003.09.094](https://doi.org/10.1016/j.biomaterials.2003.09.094)
46. Bi LX, Jung S, Day D, Neidig K, Dusevich V, Eick D, Bonewald L (2012) Evaluation of bone regeneration, angiogenesis, and hydroxyapatite conversion in critical-sized rat calvarial defects implanted with bioactive glass scaffolds. *J Biomed Mater Res A* 100A(12):3267–3275. doi:[10.1002/jbm.a.34272](https://doi.org/10.1002/jbm.a.34272)
47. Shen YH, Liu WC, Wen CY, Pan HB, Wang T, Darvell BW, Lu WW, Huang WH (2012) Bone regeneration: importance of local pH-strontium-doped borosilicate scaffold. *J Mater Chem* 22(17):8662–8670
48. Ruan CS, Hu N, Hu Y, Jiang LX, Cai QQ, Wang HY, Pan HB, Lu WW, Wang YL (2014) Piperazine-based polyurethane-ureas with controllable degradation as potential bone scaffolds. *Polymer* 55(4):1020–1027. doi:[10.1016/j.polymer.2014.01.011](https://doi.org/10.1016/j.polymer.2014.01.011)
49. Fu Q, Rahaman MN, Bal BS, Bonewald LF, Kuroki K, Brown RF (2010) Silicate, borosilicate, and borate bioactive glass scaffolds with controllable degradation rate for bone tissue engineering applications. II. In vitro and in vivo biological evaluation. *J Biomed Mater Res A* 95(1):172–179. doi:[10.1002/jbm.a.32823](https://doi.org/10.1002/jbm.a.32823)
50. Korostynska O, Arshak K, Gill E, Arshak A (2008) Review paper: materials and techniques for in vivo pH monitoring. *IEEE Sensors J* 8(1–2):20–28. doi:[10.1109/Jsen.2007.912522](https://doi.org/10.1109/Jsen.2007.912522)
51. Zhou DD (USA, 2008) Microelectrodes for in-vivo determination of pH. In: Zhang XJ, Ju HX, Wang J (eds) *Electrochemical sensors, biosensors and their biomedical applications*. Academic, pp 261–305
52. Pandolfino JE, Ghosh S, Zhang Q, Heath M, Bombeck T, Kahrilas PJ (2006) Slimline vs. glass pH electrodes: what degree of accuracy should we expect? *Aliment Pharmacol Ther* 23(2):331–340. doi:[10.1111/j.1365-2036.2006.02750.x](https://doi.org/10.1111/j.1365-2036.2006.02750.x)

53. Ruan CM, Zeng KF, Grimes CA (2003) A mass-sensitive pH sensor based on a stimuli-responsive polymer. *Anal Chim Acta* 497(1–2):123–131. doi:10.1016/j.aca.2003.08.051
54. Bock C, Sartoris FJ, Wittig RM, Portner HO (2001) Temperature-dependent pH regulation in stenothermal Antarctic and eurythermal temperate eelpout (Zoaridae): an in-vivo NMR study. *Polar Biol* 24(11):869–874. doi:10.1007/s003000100298
55. Lee H, Akers W, Bhushan K, Bloch S, Sudlow G, Tang R, Achilefu S (2011) Near-infrared pH-activatable fluorescent probes for imaging primary and metastatic breast tumors. *Bioconjug Chem* 22(4):777–784. doi:10.1021/bc100584d
56. Pirkebner D, Fuetsch M, Wittmann W, Weiss H, Haller T, Schramek H, Margreiter R, Amberger A (2004) Reduction of intracellular pH inhibits constitutive expression of cyclooxygenase-2 in human colon cancer cells. *J Cell Physiol* 198(2):295–301. doi:10.1002/jcp.10408
57. Hilderbrand SA, Weissleder R (2007) Optimized pH-responsive cyanine fluorochromes for detection of acidic environments. *Chem Commun (Camb)* 26:2747–2749. doi:10.1039/b703764c
58. Luo S, Zhang E, Su Y, Cheng T, Shi C (2011) A review of NIR dyes in cancer targeting and imaging. *Biomaterials* 32(29):7127–7138. doi:10.1016/j.biomaterials.2011.06.024
59. Gerweck LE, Seetharaman K (1996) Cellular pH gradient in tumor versus normal tissue: potential exploitation for the treatment of cancer. *Cancer Res* 56(6):1194–1198
60. Han JY, Burgess K (2010) Fluorescent indicators for intracellular pH. *Chem Rev* 110(5):2709–2728. doi:10.1021/cr900249z
61. Ge FY, Chen LG (2008) pH fluorescent probes: chlorinated fluoresceins. *J Fluoresc* 18(3–4):741–747. doi:10.1007/s10895-007-0305-y
62. Giuliano KA, Gillies RJ (1987) Determination of intracellular Ph of Balb/C-3t3 cells using the fluorescence of pyranine. *Anal Biochem* 167(2):362–371. doi:10.1016/0003-2697(87)90178-3
63. Li L, Schwendeman SP (2005) Mapping neutral microclimate pH in PLGA microspheres. *J Control Release* 101(1–3):163–173. doi:10.1016/j.jconrel.2004.07.029
64. Ding AG, Schwendeman SP (2008) Acidic microclimate pH distribution in PLGA microspheres monitored by confocal laser scanning microscopy. *Pharm Res* 25(9):2041–2052. doi:10.1007/s11095-008-9594-3
65. Orte A, Alvarez-Pez JM, Ruedas-Rama MJ (2013) Fluorescence lifetime imaging microscopy for the detection of intracellular pH with quantum dot nanosensors. *ACS Nano* 7(7):6387–6395. doi:10.1021/nn402581q
66. Zhang XM, Lin YX, Gillies RJ (2010) Tumor pH and its measurement. *J Nucl Med* 51(8):1167–1170. doi:10.2967/jnumed.109.068981
67. Bartsch I, Willbold E, Rosenhahn B, Witte F (2014) Non-invasive pH determination adjacent to degradable biomaterials in vivo. *Acta Biomater* 10(1):34–39. doi:10.1016/j.actbio.2013.08.047
68. Benavides F, Oberszyn TM, VanBuskirk AM, Reeve VE, Kusewitt DF (2009) The hairless mouse in skin research. *J Dermatol Sci* 53(1):10–18. doi:10.1016/j.jdermsci.2008.08.012
69. Buck RP, Rondinini S, Covington AK, Baucke FGK, Brett CMA, Camoes MF, Milton MJT, Mussini T, Naumann R, Pratt KW, Spitzer P, Wilson GS (2002) Measurement of pH. Definition, standards, and procedures. *Pure Appl Chem* 74(11):2169–2200. doi:10.1351/pac200274112169
70. Rundle C (2015) A beginner's guide to ion-selective electrode measurements. <http://www.nico2000.net/Book/Guide1.htm>. 2015
71. Kanda Y, Aoshima R, Takada A (1981) Blood compatibility of components and materials in silicon integrated-circuits. *Artif Organs* 5(3):307–307
72. Frost MC, Batchelor MM, Lee YM, Zhang HP, Kang YJ, Oh BK, Wilson GS, Gifford R, Rudich SM, Meyerhoff ME (2003) Preparation and characterization of implantable sensors with nitric oxide release coatings. *Microchem J* 74(3):277–288. doi:10.1016/S0026-265x(03)00033-X
73. Ziaie B, VonArx JA, Dokmeci MR, Najafi K (1996) A hermetic glass-silicon micropackage with high-density on-chip feedthroughs for sensors and actuators. *J Microelectromech Syst* 5(3):166–179. doi:10.1109/84.536623



74. Guth U, Oelssner W, Vonau W (2001) Investigation of corrosion phenomena on chemical microsensors. *Electrochim Acta* 47(1–2):201–210. doi:[10.1016/S0013-4686\(01\)00545-X](https://doi.org/10.1016/S0013-4686(01)00545-X)
75. Schoning MJ, Brinkmann D, Rolka D, Demuth C, Poghossian A (2005) CIP (cleaning-in-place) suitable “non-glass” pH sensor based on a Ta<sub>2</sub>O<sub>5</sub>-gate EIS structure. *Sensors Actuators B Chem* 111:423–429. doi:[10.1016/j.snb.2005.03.053](https://doi.org/10.1016/j.snb.2005.03.053)
76. Vonau W, Gabel J, Jahn H (2005) Potentiometric all solid-state pH glass sensors. *Electrochim Acta* 50(25–26):4981–4987. doi:[10.1016/j.electacta.2005.02.084](https://doi.org/10.1016/j.electacta.2005.02.084)
77. Espadastorre C, Meyerhoff ME (1995) Thrombogenic properties of untreated and poly(ethylene oxide)-modified polymeric matrices useful for preparing intraarterial ion-selective electrodes. *Anal Chem* 67(18):3108–3114. doi:[10.1021/Ac00114a003](https://doi.org/10.1021/Ac00114a003)
78. Martinoia S, Massobrio G, Lorenzelli L (2005) Modeling ISFET microsensor and ISFET-based microsystems: a review. *Sensors Actuators B Chem* 105(1):14–27. doi:[10.1016/j.snb.2004.02.046](https://doi.org/10.1016/j.snb.2004.02.046)
79. Pourciel-Gouzy ML, Sant W, Humenyuk I, Malaquin L, Dollat X, Temple-Boyer P (2004) Development of pH-ISFET sensors for the detection of bacterial activity. *Sensors Actuators B Chem* 103(1–2):247–251. doi:[10.1016/j.snb.2004.04.056](https://doi.org/10.1016/j.snb.2004.04.056)
80. Lehmann M, Baumann W, Brischwein M, Ehret R, Kraus M, Schwinde A, Bitzenhofer M, Freund I, Wolf B (2000) Non-invasive measurement of cell membrane associated proton gradients by ion-sensitive field effect transistor arrays for microphysiological and bioelectronic applications. *Biosens Bioelectron* 15(3–4):117–124. doi:[10.1016/S0956-5663\(00\)00065-8](https://doi.org/10.1016/S0956-5663(00)00065-8)
81. Jabre A, Bao YC, Spatz EL (2000) Brain pH monitoring during ischemia. *Surg Neurol* 54(1):55–58. doi:[10.1016/S0090-3019\(00\)00238-X](https://doi.org/10.1016/S0090-3019(00)00238-X)
82. Khabbaz KR, Zankoul F, Warner KG (2001) Intraoperative metabolic monitoring of the heart: II. Online measurement of myocardial tissue pH. *Ann Thorac Surg* 72(6):S2227–S2233. doi:[10.1016/S0003-4975\(01\)03284-2](https://doi.org/10.1016/S0003-4975(01)03284-2)
83. Harrison DK, Walker WF (1979) Microelectrode measurement of skin pH in humans during ischemia, hypoxia and local hypothermia. *J Physiol-London* 291:339–350
84. Padnick-Silver L, Linsenmeier RA (2002) Quantification of in vivo anaerobic metabolism in the normal cat retina through intraretinal pH measurements. *Vis Neurosci* 19(6):793–806. doi:[10.1017/S095252380219609x](https://doi.org/10.1017/S095252380219609x)
85. Jahde E, Rajewsky MF, Baumgartl H (1982) pH distributions in transplanted neural tumors and normal-tissues of bdx rats as measured with pH microelectrodes. *Cancer Res* 42(4):1498–1504
86. Chakkalakal DA, Mashoof AA, Novak J, Strates BS, McGuire MH (1994) Mineralization and pH relationships in healing skeletal defects grafted with demineralized bone matrix. *J Biomed Mater Res* 28(12):1439–1443. doi:[10.1002/jbm.820281209](https://doi.org/10.1002/jbm.820281209)
87. Shen YH, Liu WC, Lin KL, Pan HB, Darvell BW, Peng SL, Wen CY, Deng LF, Lu WW, Chang JA (2011) Interfacial pH: a critical factor for osteoporotic bone regeneration. *Langmuir* 27(6):2701–2708. doi:[10.1021/La104876w](https://doi.org/10.1021/La104876w)
88. Zhu H, Guo ZK, Jiang XX, Li H, Wang XY, Yao HY, Zhang Y, Mao N (2010) A protocol for isolation and culture of mesenchymal stem cells from mouse compact bone. *Nat Protoc* 5(3):550–560. doi:[10.1038/nprot.2009.238](https://doi.org/10.1038/nprot.2009.238)
89. Liu W, Wang T, Yang C, Darvell BW, Wu J, Lin K, Chang J, Pan H, Lu WW (2016) Alkaline biodegradable implants for osteoporotic bone defects-importance of microenvironment pH. *Osteoporos Int* 27(1):93–104. doi:[10.1007/s00198-015-3217-8](https://doi.org/10.1007/s00198-015-3217-8)

# Chapter 12

## 3D Printing of Calcium Phosphate Bio-scaffolds for Bone Therapy and Regeneration

Hongshi Ma, Jiang Chang, and Chengtie Wu

**Abstract** Bone cancer brings patients great sufferings and puts an end to normal activities in life. In clinic, the most common treatment for bone cancer is the combination of surgery and chemo-/radiotherapy. However, surgery is difficult to eliminate tumor cells completely and results in large bone defect. Chemo-/radiotherapy is associated with chemo-/radioresistance and evident short-/long-term toxic effects. Therefore, the development of a novel bio-scaffold for local treatment of residual tumor cells and regeneration of bone defect induced by surgery has become a very urgent need. Some progress has been made in the development of scaffolds with the ability of both tumor therapy and bone regeneration. These scaffolds function as local agents and selectively kill the tumor cells via photothermal/magnetothermal therapy or local chemotherapy. Compared with traditional treatment, they have no side effects. In addition, scaffolds possess satisfactory biocompatibility, stimulating the migration, adhesion, proliferation, and differentiation of bone marrow stroma cells. Furthermore, they can promote gene expression of BMSCs and formation of new bone. Therefore, to bone tumor-suffering patients, it is a very meaningful progress in the biomedical application. Hopefully, more efforts and progress will be made in the development of scaffolds for the treatment of tumor-induced bone defects, and more research will continue to inform and guide this field.

**Keywords** 3D printing • Bio-scaffold • Tumor therapy • Bone regeneration • Biocompatibility

---

H. Ma • J. Chang • C. Wu (✉)

State Key Laboratory of High Performance Ceramics and Superfine Microstructure, Shanghai Institute of Ceramics, Chinese Academy of Sciences, Shanghai 200050, China  
e-mail: [chentiewu@mail.sic.ac.cn](mailto:chentiewu@mail.sic.ac.cn)

© Springer Nature Singapore Pte Ltd. 2018

C. Liu, H. He (eds.), *Developments and Applications of Calcium Phosphate Bone Cements*, Springer Series in Biomaterials Science and Engineering 9,  
DOI 10.1007/978-981-10-5975-9\_12

497

## **12.1 Introduction**

### ***12.1.1 Origin of Bone Cancer***

Cancer is a serious threat to people's health. Malignancies in the bone can be of different origin. The bone cancer cells are either derived from the bone tissue or marrow itself or are affected by metastatic cancer. The most common sorts of primary bone cancer are osteosarcoma, chondrosarcoma, and Ewing's sarcoma [1]. Although primary bone cancers are rare events, once settled, a complicated process is started including a large amount of factors and interactions.

The bone is the most favored organ for metastatic cancer, especially for breast cancer and prostate cancer. The metastatic process involves highly specific interactions between tumor cells and the bone microenvironment [2, 3]. Stephen Paget first proposed "soil and seed" concept that the environment of the bone supplied a fertile ground for the aggressive behavior and growth of the tumor cells [4]. In the bone microenvironment, tumor cells overproduce osteoclast-activating factors, leading to osteoclastic bone resorption [5]. Resorbed bone releases active growth factors, thereby stimulating the proliferation of tumor cells and production of the osteoclast-activating factors, which, in turn, results in more bone resorption [6, 7]. In this way, a "vicious cycle" is set up between the bone and tumor cells. Ever since the "seed and soil" [8] and the "vicious cycle" conceptions, scientists have made great efforts to get a lot more insight into the complicated interactions between the bone and metastatic tumor.

### ***12.1.2 The Treatment of Bone Cancer in Clinic***

#### **12.1.2.1 The Treatment of Primary Bone Cancer in Clinic**

The current treatment in clinic for newly diagnosed primary bone cancer mainly comprises neoadjuvant chemotherapy followed by surgical resection of the primary tumor tissue and then adjuvant chemotherapy after surgery [9]. Current surgery concentrates on refining the scope and nature of resection to preserve healthy bone tissues [10]. Despite advances in imaging techniques, it has been reported that the local recurrence rate got to 2–3% after amputation and 5–7% after conservative surgery [11, 12]. Indeed, it is difficult to remove tumor tissue completely with clear margins due to the site of origin or the extension of tumor [13]. In addition, surgery intervention results in large bone defects, which are very difficult to be healed by itself. Although autologous bone grafting is the most effective and safest treatment, it has obvious limitation in clinic due to insufficient amount of donor tissue and followed by donor-site morbidity [14]. On the other hand, xenogeneic or allogeneic bone grafts are limited by immunological rejection in the host recipient [15].

Therefore, surgical strategy needs to focus on the adoption of bioactive materials with optimized function to repair the large bone defects [16].

The preoperative chemotherapeutic treatment provides sufficient time for planning conservative surgery and reconstructive procedures [17]. However, the chemotherapy treatment of bone cancer is associated with evident short-/long-term toxic effects, such as myelosuppression, alopecia, nausea, vomiting, and mucositis [18]. Additionally, 35–45% of patients may be not suitable of this treatment because tumors are inherently resistant to these agents or become unresponsive to chemotherapy drugs [19, 20].

For some patients, the combination of chemotherapy and radiotherapy may achieve the aim of long-term remission and prolong survival [21]. However, like chemotherapy, radiotherapy also has the problems of radioresistance and side effect [22]. Moreover, the radiotherapy induces apoptosis of the bone and endothelial cells, causing a decrease of blood flow and matrix and reduction of relative amounts of phosphorus and calcium, which lead to bone atrophy [23–25].

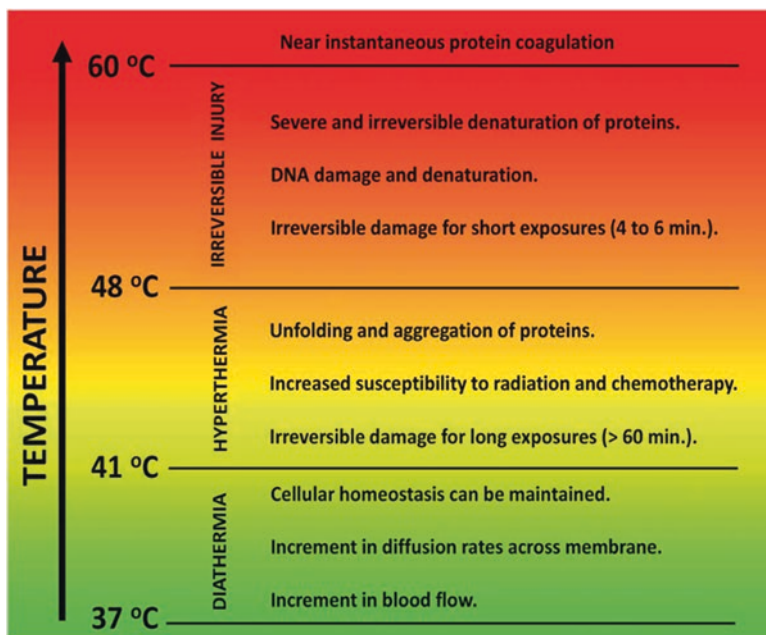
### **12.1.2.2 The Treatment of Metastatic Bone Cancer in Clinic**

There is still no final agreement on the optimum treatment of metastatic bone cancer. Although the management of metastatic bone cancer is primarily palliative, surgery still deserved to be adopted according to the possible complications and the expected life quality of the patients [26]. In some patients, skeletal complications, including bone pains, pathological fracture, hypercalcemia, and dural compression, result in the final death and significantly decline the quality of life [27]. Since the improvements in oncological treatment, there are more and more long-term survival of patients suffering from skeletal complications [28]. Therefore, for patients with metastatic bone cancer, the aims of surgery are to relieve pain, improve function, and prolong survival. Overtreatment of deadly ill patients should be avoided; however, if patients may benefit greatly from surgery and survive for some years with less pain, it deserves to adoption of an operation.

Conventional surgery intervention with the assistance of chemo-/radiotherapy is effective to improve the survival of patients. However, it has reached a plateau phase and there exist a lot of problems. Therefore, more effects need to be made in continuing exploration into novel therapeutic modalities and target-selective treatment to achieve more efficient therapy.

### **12.1.3 Development of Thermal Therapy**

In the nineteenth century, the benefits of thermal therapy were first observed, and it is based on increasing the temperature of a part of the body beyond its normal degree for a certain period of time. It was found that a partial tumor regression would be caused by the administration of living bacteria to cancer patients, only

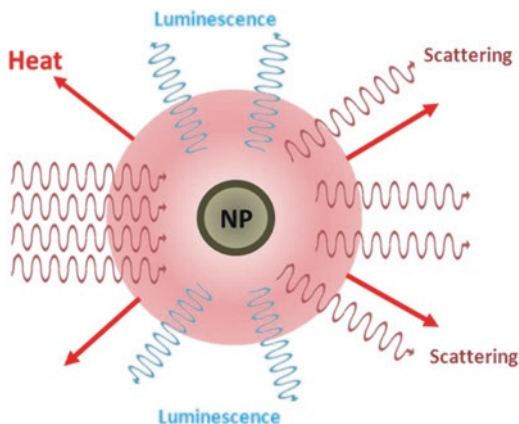


**Fig. 12.1** Schematic diagram of the variety of effects caused by the different thermal treatments as classified by the corresponding operating temperature (Reproduced from Ref. [31] by permission of The Royal Society of Chemistry)

when the bacteria infected in the patients resulting in the appearance of fever [29]. At the same time, the treatment of uterine cervix cancer was successfully achieved when fixed with circulating heat water [30]. However, the applications of thermal therapy in clinic were not accomplished because the rate of success and reproducibility of such treatments was reduced by the fact that temperature-measuring technologies and heating methods were not advanced enough at that time [31]. In the 1980s, the interest of understanding and development of novel thermal therapy was reactivated [32]. For the last few years, great efforts have been made in the development of novel techniques for localized and controlled heating and further exploring the mechanism of thermal therapy based on temperature-induced cell ablation [33–35].

The magnitude of the temperature increase and the duration of the treatment are considered to be two main factors of the efficacy of thermal treatments [36]. Slightly higher temperature (41–45 °C) results in irreversible cell damage only after exposure for a very prolong time (from 30 to 60 min), and the increased blood flow causes the increment of reactive oxygen species, which further lead to oxidative damage to proteins, lipids, and nucleic acids [37]. When the tumor temperature is above 50 °C, a drastic activation of cell death is achieved resulting from cell membrane collapse, a halt in enzyme activity, protein denaturation, DNA polymerase function, and mitochondrial dysfunction [37] (shown in Fig. 12.1).

**Fig. 12.2** Schematic representation of the different processes activated when a light beam interacts with a nanoparticle. The presence of scattering, luminescence, and heat generation is included. Heat and luminescence occur as a result of light absorption (Reproduced from Ref. [31] by permission of The Royal Society of Chemistry)



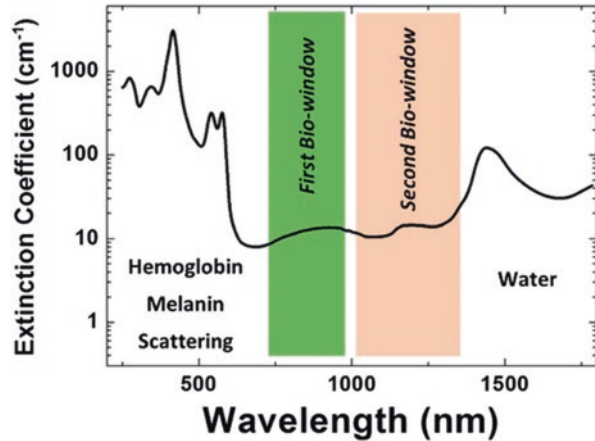
### 12.1.3.1 Mechanism of Photothermal Therapy

As a noninvasively or minimally therapeutic method, photothermal therapy has attracted great attentions in recent years [38, 39]. Compared with traditional chemo-/radiotherapeutic approaches, the well-designed phototherapeutic agents could selectively ablate tumor cells via either active or passive tumor targeting [40–42]. And the light beam could be spatially and temporally controlled to irradiate only the tumor site, without damaging the surrounding healthy tissue. Such selectivity offered by phototherapy could significantly reduce the systemic toxicity.

When a photothermal agent is irradiated by laser, some of the incident photons are absorbed, while others are scattered by the nanoparticle (shown in Fig. 12.2). The energy absorbed by the photothermal agent can be released by emission of luminescence and production of heat. For the purpose of large light-to-heat conversion efficiency, photothermal agents with low luminescence quantum yields and large absorption efficiency are expected to obtain efficient photothermal therapy effect [31].

Because of the limitation of penetration depth, considerable attention is attracted on the so-called biological windows, where tissues become partially transparent due to a reduction in both absorption and scattering [43, 44]. In the first biological window (700–980 nm light), absorption strongly reduces, while optical extinction still exists because of the residual scattering. The second biological window extends from 1000 to 1400 nm. In this spectrum, although optical absorption does not vanish entirely, optical scattering is minimized due to the longer wavelengths with respect to the first biological window (Fig. 12.3). Therefore, an ideal photothermal agent should have large absorption and light-to-heat conversion efficiency in the spectrum of first or second biological window.

**Fig. 12.3** Extinction coefficient of a representative tissue. The different effects leading to light attenuation (such as the presence of hemoglobin, water and optical scattering) have been indicated. The spectral extensions of the two biological windows are also indicated (Reproduced from Ref. [31] by permission of The Royal Society of Chemistry)

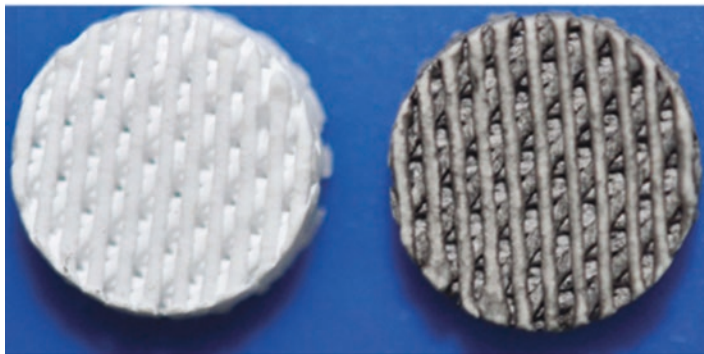


### 12.1.3.2 Mechanism of Magnetothermal Therapy

In 1957, Gilchrist et al. first outlined the concept of magnetic therapy treatment based on  $\gamma$ -Fe<sub>2</sub>O<sub>3</sub> magnetic nanoparticles [45]. Under oscillating magnetic field, the mechanisms of heat generation in magnetic nanoparticles include hysteresis loss, Brown relaxation, and Néel relaxation [46]. When these magnetothermal agents are introduced into the tumor sites, they interact with the magnetic field to generate heat on the basis of any of mentioned mechanisms above [47, 48]. Compared with photothermal therapy, magnetothermal therapy has no limitation on penetrating depth in the application of bone tumor therapy.

## 12.2 Preparation and Properties of Bio-scaffolds with the Ability of Tumor Therapy

With the improvement of people's quality of life, the traditional amputation of bone tumor surgery has been inclined to shift to the limb salvage surgery and comprehensive treatment model which center on surgery and combine postoperative chemotherapy and radiotherapy; however, the postoperative tumor recurrence and the induced bone defect influence the treatment effects of bone tumor surgery and constrain the development of bone tumor surgery. With the rapid development of nanotechnology in the past decade, various nanomaterials with excellent photothermal or magnetothermal effect have been designed and fabricated to enhance therapeutic efficacy, showing great promise in the treatment of cancer. However, in the application of bone cancer, these nanomaterials are difficult to fill the bone defects and further stimulate new bone formation after the surgical resection of bone tumors. Therefore, the development of a new scaffold for bone regeneration and local treatment of tumor has become a very urgent need. However, there are still few researches



**Fig. 12.4** Photograph of 3D-printing  $\beta$ -TCP scaffold and GO-TCP scaffold with well-designed morphology (Reproduced from Ref. [49] by permission of John Wiley & Sons Ltd)

on scaffolds with the ability of both killing the residual tumor cells and repairing bone defects after surgery.

Ideal bio-scaffolds for the treatment of tumor-induced tissue defects had better possessed the following characteristics: (1) ablating tumor cells selectively via tumor targeting, (2) having lower side effect and better biosafety compared with traditional treatments, (3) exhibiting excellent mechanical strength and longtime stability, and (4) having satisfactory biological biocompatibility and osteogenic activities, stimulating the migration, adhesion, proliferation, and differentiation of bone mesenchymal stem cells and, further, promoting the formation of new bone.

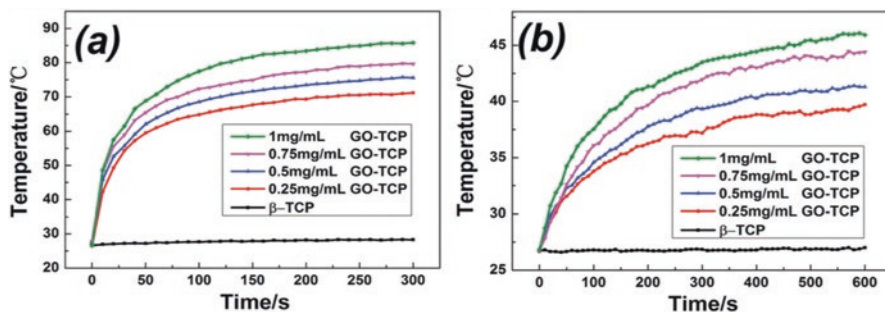
The research and development of biomaterials aim to organically integrate the ability of the local treatment of bone tumors and bone regeneration so that in surgery process, possible residual tumor cells are also killed, which can avoid postoperative systemic chemotherapy and radiotherapy, prevent tumor recurrence, improve the quality of life of patients, and prolong survival.

## ***12.2.1 Bio-scaffolds with Photothermal Therapy Ability***

### **12.2.1.1 Fabrication of 3D-Printing Bio-scaffolds**

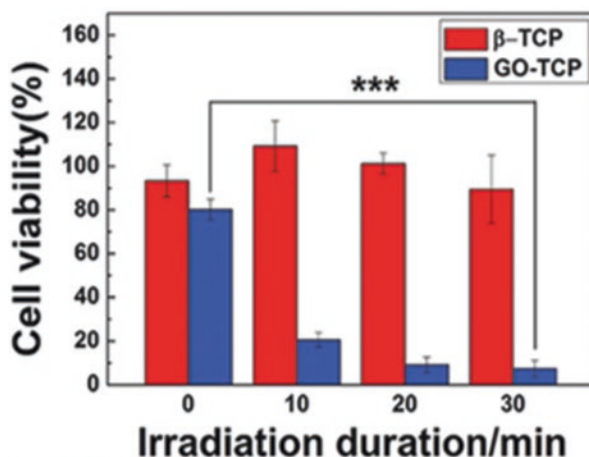
Wu group outlined an idea that combines the photothermal therapy with tissue engineering to repair the large bone defects after surgery and kill the possibly residual tumor cells [49]. And a bio-scaffold with excellent photothermal effect and osteogenic activity is prepared. First, pure  $\beta$ -TCP scaffolds were fabricated by 3D-printing method, and then graphene oxide (GO) was introduced to modify the surface of  $\beta$ -TCP scaffolds by soaking method. As shown in Fig. 12.4, the obvious wrinkles of GO can be observed on the surface of the scaffolds, due to the formation of valence bond between  $\text{COO}^-$  in GO and  $\text{Ca}^{2+}$  in  $\beta$ -TCP [50, 51].





**Fig. 12.5** Heating curves of  $\beta$ -TCP scaffolds and GO-TCP scaffolds with different concentration of GO solution in dry state (a) and in PBS (b) with 808 nm laser irradiation, exhibiting excellent photothermal effect of GO-TCP scaffolds (Reproduced from Ref. [49] by permission of John Wiley & Sons Ltd)

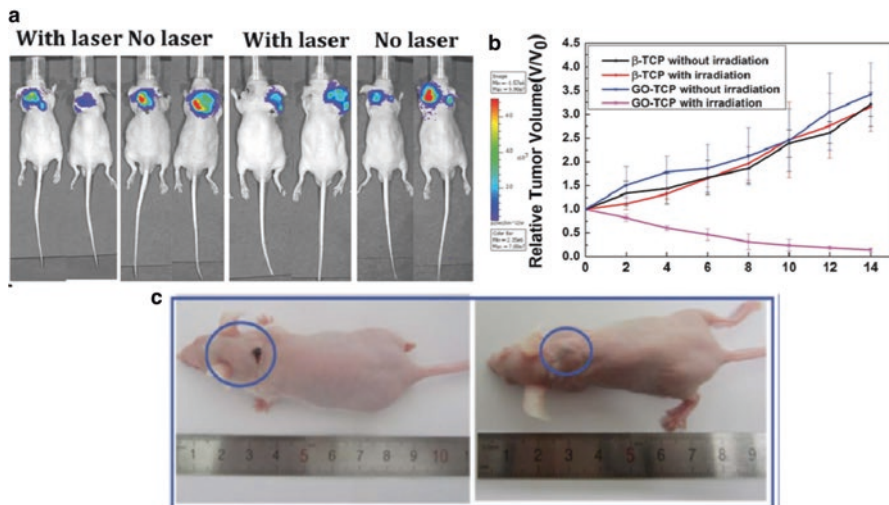
**Fig. 12.6** Relative viability of MG-63 cells in  $\beta$ -TCP and GO-TCP scaffolds treated with different irradiation duration (Reproduced from Ref. [49] by permission of John Wiley & Sons Ltd)



GO-TCP scaffolds exhibited excellent photothermal performance due to the strong absorption and high thermal conversion of graphene oxide in near-infrared light (700–900 nm) [52–54]. With the increase of concentration of graphene oxide (0.25, 0.5, 0.75, 1 mg/mL), the final temperature of the GO-TCP scaffolds also increased (Fig. 12.5), while pure  $\beta$ -TCP maintained room temperature under the irradiation at the power density of 0.36 W/cm<sup>2</sup>. The scaffold also exhibits power-density, soaking-time dependent photothermal effect.

### 12.2.1.2 Photothermal Effect for Killing Bone Tumor Cells

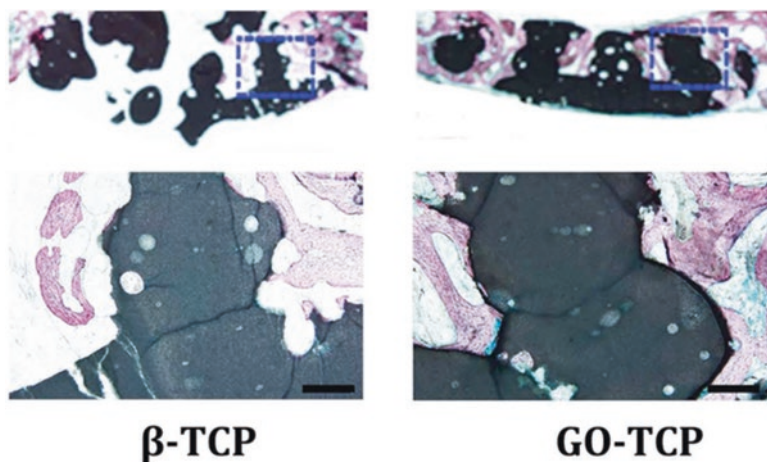
Benefiting from the high temperature induced by GO-TCP under the NIR laser irradiation, the viability of bone tumor cells (MG-63) in GO-TCP scaffolds decreased by 80% after irradiation for 10 min at the power density of 0.36 W/cm<sup>2</sup>



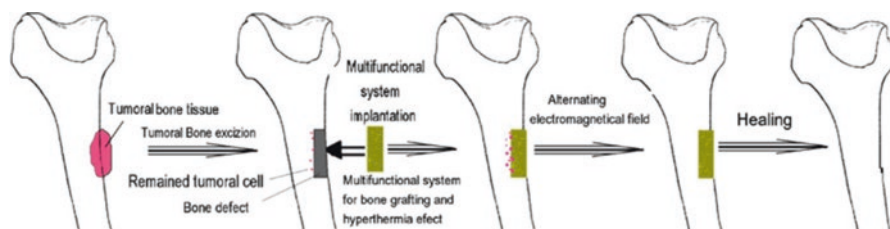
**Fig. 12.7** (a) The whole-body fluorescence imaging of tumor in four groups (GO-TCP with or without irradiation,  $\beta$ -TCP with or without irradiation, respectively.) at day 0 and day 7; (b) Relative tumor volume changes with increasing days in four groups. (c) Photograph of Saos-2 tumor-bearing mice implanted with GO-TCP scaffolds at day 0 and day 14 (Reproduced from Ref. [49] by permission of John Wiley & Sons Ltd)

(Fig. 12.6). In comparison, there were still a large amount of MG-63 cells presenting active morphology with affluent pseudopods in pure  $\beta$ -TCP without irradiation, GO-TCP scaffolds without irradiation, and GO-TCP scaffolds with irradiation. As the irradiation duration extended, the photothermal effect of GO-TCP scaffolds on viability of tumor cells was enhanced.

The photothermal therapy effect *in vivo* is assessed by implanting the scaffolds in the center site of the tumor tissue of the nude mice. As shown in Fig. 12.7, the intensity of bioluminescent and area of the tumor in GO-TCP scaffolds with irradiation group were obviously decreased at day 7 in comparison with the other three control groups ( $\beta$ -TCP without irradiation, GO-TCP scaffolds without irradiation, and GO-TCP scaffolds with irradiation). The high temperature of GO-TCP scaffolds under irradiation effectively inhibited the growth of tumor tissue. Further hematoxylin and eosin (H&E)-stained images showed that the nucleus of tumor cells in GO-TCP scaffolds disappeared after NIR laser (Fig. 12.8). Due to the excellent photothermal effect of GO-TCP scaffolds and fast heat conduction, the high temperature spread and covered almost the whole tumor tissues, resulting in long-term cell inactivation, and thus the obvious photothermal therapy effect was achieved.



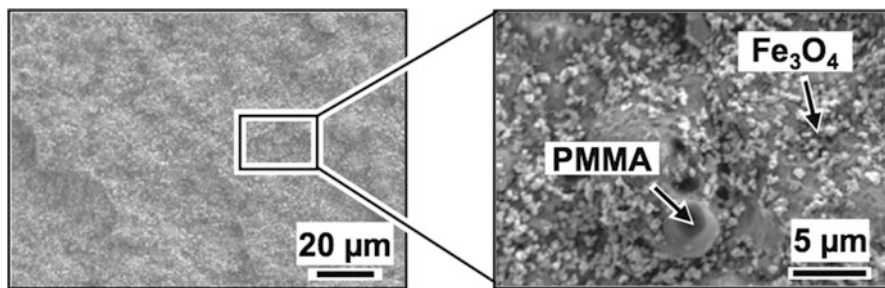
**Fig. 12.8** Histological analysis of bone formation ability in vivo for  $\beta$ -TCP and GO-TCP scaffolds after implanted in rabbits for 8 weeks. GO-TCP promoted the in vivo bone formation as compared to  $\beta$ -TCP. The scale bar is 100  $\mu$ m (Reproduced from Ref. [49] by permission of John Wiley & Sons Ltd). Therefore, in this work, the selectivity of a bio-scaffold was achieved by localized photothermal agents (implanted GO-TCP scaffolds) and the controlled laser irradiation. In comparison with traditional chemo-/radiotherapy, photothermal therapy of GO-TCP scaffolds is an effective treatment of bone tumor disease without side effects. Simultaneously, the bio-scaffolds enhanced bone-forming activity by promoting osteogenic differentiation of rBMSCs and in vivo bone formation



**Fig. 12.9** Schematic illustration for the process of magnetic bio-scaffolds for the treatment of tumor-induced bone defect (Reprinted from Ref. [60], with kind permission from Springer)

### 12.2.1.3 Osteogenic Activity In Vitro and In Vivo

For the treatment of bone tumor-induced defects, as a bio-scaffold, bone-forming ability in vitro and in vivo is an important issue. GO-TCP scaffolds exhibited satisfactory cytocompatibility. rBMSCs attached and proliferated well with spread morphology on the pore walls of both  $\beta$ -TCP and GO-TCP scaffolds (Fig. 12.9). In contrast with the blank control and  $\beta$ -TCP scaffolds, GO-TCP scaffolds obviously stimulated the specific ALP activity and bone-related gene expression of rBMSCs (Runx2, OCN, and BSP), which are related to bone mineralization [55, 56].



**Fig. 12.10** SEM photographs of the cross-sectional areas of the magnetic cement sample with the composition of 50%  $\text{Fe}_3\text{O}_4$ , 20%PMMA, and 30%MMA (wt.%) (Reprinted from Ref. [61], Copyright 2012, with permission from Elsevier)

The further *in vivo* study confirmed that TCP scaffolds modified with graphene oxide promoted more new bone formation than  $\beta$ -TCP scaffolds (Fig. 12.8). Bioactive groups,  $\text{OH}^-$  and  $\text{COO}^-$  in GO, are one of the main factors to stimulate the differentiation of stem cells [57]. In addition, through hydrophobic and electrostatic interactions, proteins in the culture media adhered to the surface of GO-TCP scaffold [58, 59]. Thus, the specific bioactive groups and protein absorbance of GO resulted in the improved osteogenic differentiation of rBMSCs, seeding in GO-TCP scaffolds, and further led to the enhancement of *in vivo* formation of new bone.

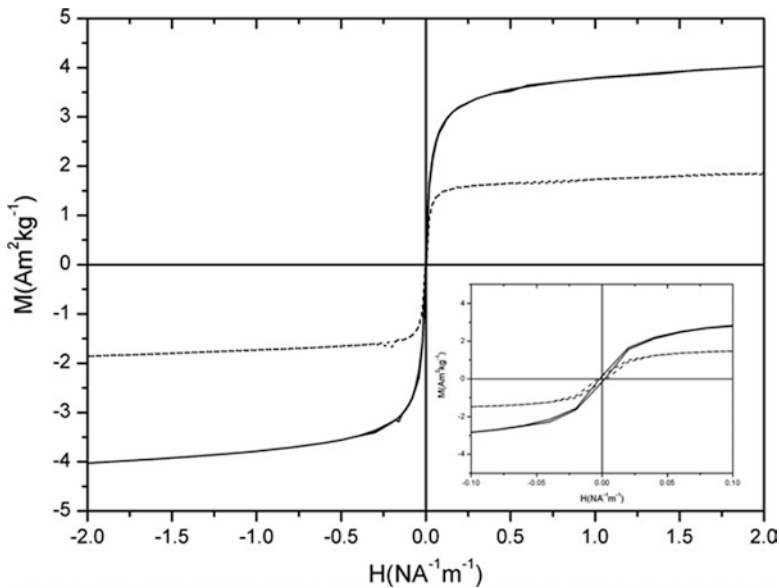
## 12.2.2 Bio-scaffolds with Magnetothermal Therapy Ability

Implantable magnetic scaffolds can be designed to prevent tumor recurring after tumor resection via magnetothermal therapy. As shown in Fig. 12.9, the success of fabricating superparamagnetic scaffolds makes it possible to kill the residual tumor cells locally under an oscillating magnetic field, without damaging the healthy tissue. In addition, magnetic scaffolds can support the adhesion, proliferation, and differentiation of BMSCs and further promote the formation of new bone.

### 12.2.2.1 Traditional Preparation Methods of Magnetic Scaffolds

With the aim of exploring new biomaterials that combine magnetic function and biological compatibility, PMMA-based bone cements were fabricated by casting the mixture of PMMA,  $\text{Fe}_3\text{O}_4$  powder, MMA, benzoyl peroxide, and N,N-dimethyl-p-toluidine into cylindrical mold (Fig. 12.10). PMMA-based bone cements with high mechanical strength would be useful for magnetothermal therapy of bone tumors, especially for tumors occurring in vertebrae [61].

Benefiting from biological properties of natural biomaterials like hydroxyapatite (HA), magnetic scaffolds were synthesized by chemically doping of HA scaffolds



**Fig. 12.11** Magnetic curves in function of the applied magnetic field up to  $2\text{NA}^{-1}\text{m}^{-1}$  for Fe-HA synthesized by simultaneous addition (*continue line*) and by oxidative process (*dotted line*) at  $T = 300\text{ K}$  (Reprinted from Ref. [62], Copyright 2012, with permission from Elsevier)

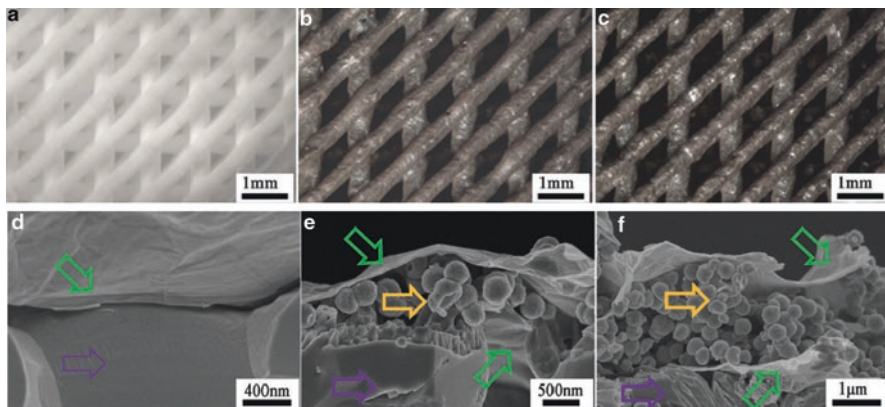
crystal nanostructure with Fe ions [62]. This approach of synthesizing magnetic scaffolds led to a rather low-crystalline apatite. The superparamagnetic-like behavior of the Fe-HA nanopowders was typical of single-domain magnetic nanoparticles (shown in Fig. 12.11).

On the basis of production of Fe-HA, nanocomposite substrate was designed by embedding Fe-HA nanoparticles into a poly( $\epsilon$ -caprolactone) (PCL) matrix via molding and solvent casting method. The saturation magnetization values of PCL/Fe-HA were strictly proportional to Fe-HA content [63].

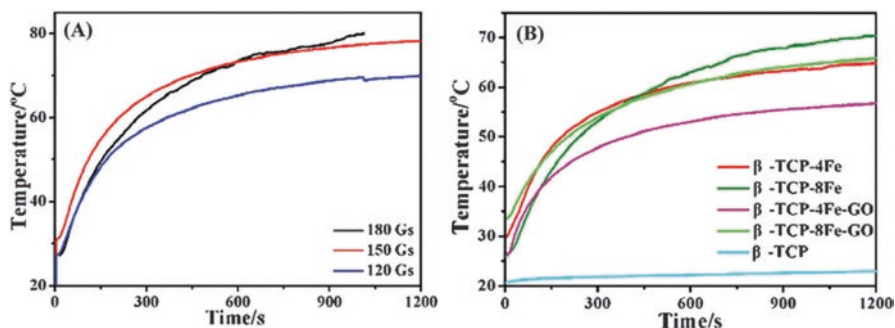
### 12.2.2.2 3D Printing of Magnetic Bio-scaffolds

Compared with conventional approaches to prepare magnetic bio-scaffolds, 3D-printing technique is more beneficial to control mechanical strength and pore structure of the scaffolds. The interconnected macropores of 3D-printing scaffolds are essential to provide sufficient space for nutrient transport, bone cell penetration, adhesion, and proliferation, further leading to bone ingrowth and vascularization after implantation [64].

Polycaprolactone-based magnetic scaffolds can be printed by 3D printing with a mixture of polycaprolactone and functionalized magnetic Fe-HA and then heated at the temperature of  $110\text{--}130\text{ }^\circ\text{C}$  to harden the scaffolds [65] (Fig. 12.12).



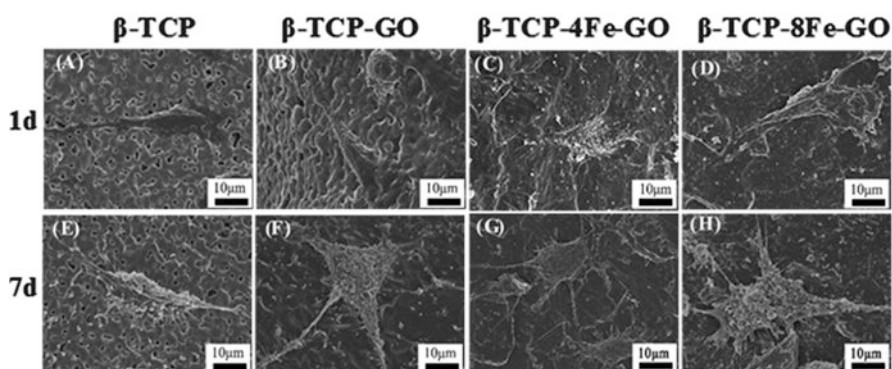
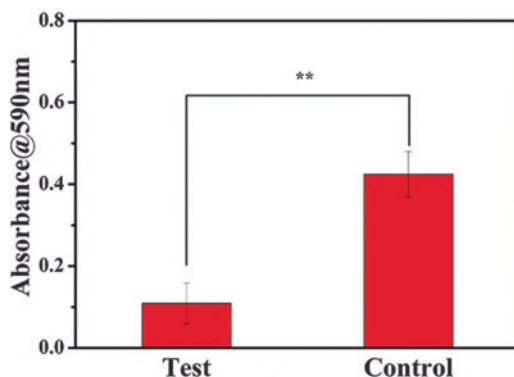
**Fig. 12.12** Optical micrographs of  $\beta$ -TCP (a),  $\beta$ -TCP-4Fe-GO (b), and  $\beta$ -TCP-8Fe-GO (c) scaffolds. The fracture surface of  $\beta$ -TCP-GO (d),  $\beta$ -TCP-4Fe-GO (e), and  $\beta$ -TCP-8Fe-GO (f) scaffolds showed that the magnetic scaffolds had sandwich-like layers. The *green arrows* show the GO layer of thickness of about 100 nm. The *yellow arrows* show the  $\text{Fe}_3\text{O}_4/\text{GO}$  particles layer of thickness of about 1  $\mu\text{m}$  (Reproduced from Ref. [66] by permission of The Royal Society of Chemistry)



**Fig. 12.13** Magnetothermal curves of  $\beta$ -TCP-Fe-GO scaffolds in an alternating magnetic field (a) the influence of different magnetic field intensities on the magnetothermal ability of  $\beta$ -TCP-8Fe-GO scaffolds, (b) the influence of graphene oxide on the magnetothermal ability of different scaffolds (Reproduced from Ref. [66] by permission of The Royal Society of Chemistry)

Considering the shielding effect of the bulk matrix on Fe-doped scaffolds, magnetic scaffolds modified with a sandwich layer of  $\text{GO}-\text{Fe}_3\text{O}_4-\text{GO}$  was fabricated via a layer-by-layer self-assembly method (Fig. 12.13) [66]. Compared with incorporating Fe into scaffolds, this sandwich-like scaffold exhibited superior magnetothermal effects with only a small amount of  $\text{Fe}_3\text{O}_4$  on the surface of the scaffolds (Fig. 12.14). In addition, the existence of GO on the strut surface of the scaffolds is beneficial to transport the heat to inner parts due to its excellent thermal conductivity.

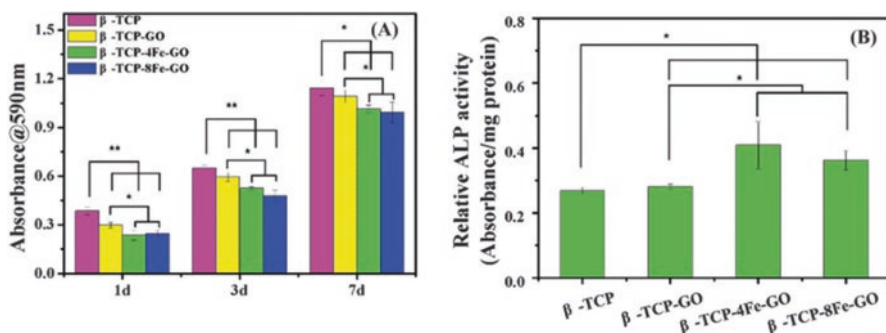
**Fig. 12.14**  $\beta$ -TCP-8Fe-GO scaffold-induced magnetothermal effects distinctively killed bone tumor cells. (\*\* $P < 0.01$ ) (Reproduced from Ref. [66] by permission of The Royal Society of Chemistry)



**Fig. 12.15** SEM images of rBMSCs after seeding on  $\beta$ -TCP (a and e),  $\beta$ -TCP-GO (b and f),  $\beta$ -TCP-4Fe-GO (c and g), and  $\beta$ -TCP-8Fe-GO (d and h) scaffolds for 1 day (a–d) and 7 days (e–h) (Reproduced from Ref. [66] by permission of The Royal Society of Chemistry)

### 12.2.2.3 Magnetothermal Effect for Killing Tumor Cells

Benefiting from the excellent magnetothermal effect of superparamagnetic scaffolds, the viability of tumor cell decreased by 75% after magnetothermal treatment for 20 min, and the morphology of the tumor cells had been damaged because of the changes of the disruption and permeability of the plasma membrane (Fig. 12.15). In addition, hyperthermia induced DNA repair deficiency and apoptosis in tumor cells. All above suggest superparamagnetic scaffolds are promising biomaterials for bone tumor therapy.



**Fig. 12.16** The proliferation of rBMSCs on the scaffolds containing different Fe contents (a). The ALP activity of rBMSCs cultured on scaffolds at day 7 (b). (\*\* $P < 0.01$ , \* $p < 0.05$ ) (Reproduced from Ref. [66] by permission of The Royal Society of Chemistry)

#### 12.2.2.4 Osteogenic Activity In Vitro and In Vivo

Compared to pure HA, the magnetic Fe-HA substrate maintained satisfactory biocompatibility for osteoblasts [62]. In addition, the inclusion of Fe nanoparticles modified the topography of the scaffolds and induced cell response. Fe ions promoted the attachment, proliferation, and osteogenic differentiation of rBMSCs and hBMSCs; the cell proliferation and differential can be guided by magnetic forces (Figs. 12.16 and 12.17) [67, 68]. Furthermore, magnetic forces generated in the vicinity and inside the scaffold may control specific processes at cell level, resulting in transportation of growth factors (BMPs and VEGF) and biomolecules by magnetic carriers, and further stimulate vascular remodeling and bone regeneration [65].

Therefore, 3D-printed magnetic bio-scaffolds possess excellent magnetic and osteogenic capabilities and have a great potential application in the bone tumor therapy and regeneration of large bone defects induced by surgery. Compared with NIR laser, magnetic field has no limit on penetration depth; thus magnetic scaffolds show the unique advantage in the treatment of tumor-induced large bone defects.

### 12.2.3 Bio-scaffolds with Chemotherapy Ability

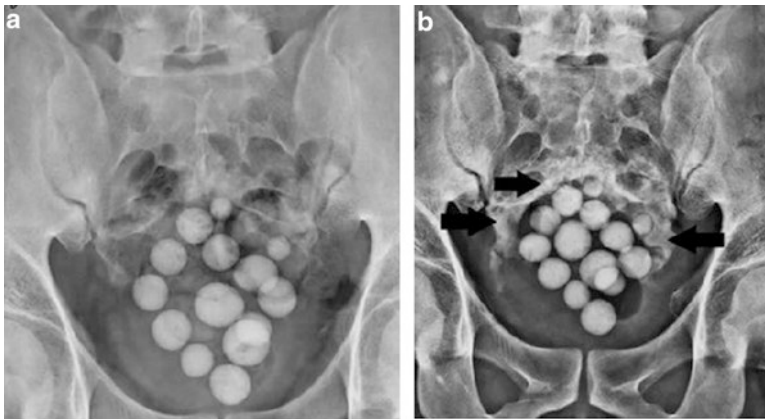
In many cases, due to nonspecific release and the limited absorption by the target cancer tissue, large doses of the drug have to be applied [69, 70]. This problem is also the risk of chemotherapy in oncological diseases. Biomaterials, which consist of robust tunable matrices with the ability to repair the bone defect induced by resection of tumor tissue, can be regarded as a carrier locally delivering chemotherapy drugs to improve therapeutic effects and reduce the side effect.

Zoledronic acid (ZOL) is the common anticancer drug used to control tumor progression and prevent skeletal complications [71]. Kun et al. managed to prepare





**Fig. 12.17** A photograph showing that the zoledronic acid-loaded bone cement was handmade into ball shapes of unequal sizes, approximately 1–2 cm<sup>3</sup> (Reprinted from Ref. [72], with kind permission from Springer ). Those ZOL-loaded balls were placed into the bone defects of the sacrum after the tumor had been removed by surgery. After 28 months of following investigation, all four patients who suffered from cauda equina syndrome recovered after intralesional curettage of tumor with mean tumor volume approximately of 472.8 cm<sup>3</sup>. The recurrence of the tumor was successfully inhibited, and new bone formation was observed on radiograph



**Fig. 12.18** (a) Sacral anteroposterior radiograph taken postoperatively. (b) Sacral anteroposterior radiograph 28 months postoperative showing new bone regeneration and increased bone density (black arrow) (Reprinted from Ref. [72], with kind permission from Springer )

a drug-loaded bone cement as a local adjuvant therapy to avoid the high recurrence rate after the intralesional curettage of the giant cell tumor and repair of the large bone defect [72]. The zoledronic acid-loaded bone cement realizes targeted drug delivery and hence improves the efficacy of drugs and reduces the toxicity of drugs. The ZOL-loaded cement containing ZOL, bone cement, vancomycin, and PMMA was mixed with their hands under sterile conditions without vacuum and then was shaped into balls of approximately 1–2 cm<sup>3</sup> (Fig. 12.18).

## 12.3 Conclusion and Perspective

With the improvement of people's quality of life, more and more attention has been focused on the novel and efficient treatment of bone cancer. Since the problems of tumor recurrence and large bone defects induced by surgery, it is of great importance to design and develop novel biomaterials for killing the residual bone tumor cells via a safe and effective protocol and simultaneously repairing the large bone defect after surgical resection of bone tumor by harnessing the bioactivity of biomaterials.

Some progress has been made in the development of bio-scaffolds. These bio-scaffolds function as local agents and selectively kill the tumor cells via photothermal/magnetothermal therapies or local chemotherapy. Compared with traditional treatments, they have no side effects. In addition, bio-scaffolds possess satisfactory biocompatibility, stimulating the migration, adhesion, proliferation, and differentiation of bone marrow stroma cells. Furthermore, they can promote gene expression of BMSCs and formation of new bone. Therefore, to bone tumor-suffering patients, it is very a meaningful progress in the biomedical application.

However, there are still some limitations at present and a great need for further investigation. First, the application of bio-scaffolds in different sites of bone calls for the fabrication of novel scaffolds with specific functionalities. Second, some other therapy treatments, such as photodynamic therapy and immunotherapy, can also be explored and introduced to bio-scaffolds. Different therapy methods can be considered to function simultaneously to pursue more efficient tumor therapy effect. Third, the idea that combines tumor therapy and tissue regeneration can also be expanded to skin cancer, meaning the fabrication of biomaterials with the ability of both skin cancer therapy and skin wound healing. Hopefully, more efforts and progress will be made in the development of bio-scaffolds for the treatment of tumor-induced bone defects, and more research will continue to inform and guide this field.

**Acknowledgments** Funding for this study was provided by the Recruitment Program of Global Young Talent, China (Dr. Wu), National Key Research and Development Program of China (2016YFB0700803), the National High Technology Research and Development Program of China (863 Program, SS2015AA020302), Natural Science Foundation of China (Grant 81430012, 31370963), Key Research Program of Frontier Sciences, CAS (QYZDB-SSW-SYS027), and Program of Shanghai Outstanding Academic Leaders (15XD1503900).

## References

1. Driel M, Leeuwen JPTM (2014) Cancer and bone: a complex complex. *Arch Biochem Biophys* 561:159–166
2. Mundy GR (2002) Metastasis: metastasis to bone: causes, consequences and therapeutic opportunities. *Nat Rev Cancer* 2:584–593

3. Buenrostro D, Mulcrone PL, Owens P, Sterling JA (2016) The bone microenvironment: a fertile soil for tumor growth. *Curr Osteoporos Rep* 14:151–158
4. Paget S (1889) The distribution of secondary growths in cancer of the breast. *Lancet* 1:571–573
5. Guise TA, Yin JJ, Taylor SD et al (1996) Evidence for a causal role of parathyroid hormone-related protein in the pathogenesis of human breast cancer-mediated osteolysis. *J Clin Invest* 98:1544–1549
6. Yin JJ, Selander K, Chirgwin JM et al (1999) TGF- $\beta$  signaling blockade inhibits PTHrP secretion by breast cancer cells and bone metastases development. *J Clin Invest* 103:197–206
7. Hiraga T, Williams PJ, Mundy GR, Yoneda T (2001) The bisphosphonate ibandronate promotes apoptosis in MDA-MB-231 human breast cancer cells in bone metastases. *Cancer Res* 61:4418–4424
8. Fidler IJ (2003) The pathogenesis of cancer metastasis: the ‘seed and soil’ hypothesis revisited. *Nat Rev Cancer* 3:453–458
9. Chou AJ, Geller DS, Gorlick R (2008) Therapy for osteosarcoma: where do we go from here? *Paediatr Drugs* 10:315–327
10. Yasko AW (2009) Surgical management of primary osteosarcoma. *Cancer Treat Res* 152:125–145
11. Marulanda GA, Henderson ER, Johnson DA, Letson GD, Cheong D (2008) Orthopedic surgery options for the treatment of primary osteosarcoma. *Cancer Control* 15:13–20
12. Errani C, Longhi A, Rossi G et al (2011) Palliative therapy for osteosarcoma. *Expert Rev Anticancer Ther* 11:217–227
13. Grimer RJ, Taminiou AM, Cannon SR (2002) Surgical outcomes in osteosarcoma. *J Bone Joint Surg Br* 84-B:395–400
14. Healy KE, Guldberg RE (2007) Bone tissue engineering. *J Musculoskelet Neuronal Interact* 7(4):328–330
15. Bird JE (2014) Advances in the surgical management of bone tumors. *Curr Oncol Rep* 16:392–397
16. Chao P-HG, Grayson W, Vunjak-Novakovic G (2007) Engineering cartilage and bone using human mesenchymal stem cells. *J Orthop Sci* 12:398–404
17. Smeland S, Bruland ØS, Hjorth L et al (2011) Results of the Scandinavian Sarcoma Group XIV protocol for classical osteosarcoma. *Acta Orthop* 82:211–216
18. Janeway KA, Grier HE (2010) Sequelae of osteosarcoma medical therapy: a review of rare acute toxicities and late effects. *Lancet Oncol* 11:670–678
19. Chou AJ, Gorlick R (2014) Chemotherapy resistance in osteosarcoma: current challenges and future directions. *Expert Rev Anticancer Ther* 6:1075–1085
20. Hattinger CM, Pasello M, Ferrari S et al (2010) Emerging drugs for high-grade osteosarcoma. *Expert Opin Emerg Dr* 15:615–634
21. Ozaki T, Flege S, Liljenqvist U et al (2002) Osteosarcoma of the spine. *Cancer* 94:1069–1077
22. Meijer TWH, Kaanders JHAM, Span PN, Bussink J (2012) Targeting hypoxia, HIF-1, and tumor glucose metabolism to improve radiotherapy efficacy. *Clin Cancer Res* 18:5585–5594
23. Zhuang Q, Zhang Z, Fu H et al (2011) Does radiation-induced fibrosis have an important role in pathophysiology of the osteoradionecrosis of jaw? *Med Hypotheses* 77:63–65
24. Da Cunha SS, Sarmiento V, Ramalho LMP et al (2007) Effect of laser therapy on bone tissue submitted to radiotherapy: experimental study in rats. *Photomed Laser Surg* 25:197–204
25. Rabelo GD, Beletti ME, Dechichi P (2010) Histological analysis of the alterations on cortical bone channels network after radiotherapy: a rabbit study. *Microsc Res Tech* 73:1015–1018
26. Mavrogenis AF, Angelini A, Vottis C et al (2016) Modern palliative treatments for metastatic bone disease. *Clin J Pain* 32:337–350
27. Böhm P, Huber J (2002) The surgical treatment of bony metastases of the spine and limbs. *J Bone Joint Surg (Br)* 84-B:521–529
28. Harrington KD (1997) Orthopedic surgical management of skeletal complications of malignancy. *Cancer* 80:1614–1627

29. Habash RW, Bansal R, Krewski D, Alhafid HT (2006) Thermal therapy, part 2: hyperthermia techniques. *Crit Rev Bioeng* 34:491–542
30. Wunderlich CA, Woodman WB (1871) On the temperature in diseases: a manual of medical thermometry. The New Sydenham Society, London
31. Jaque D, Maestro LM, del Rosal B et al (2014) Nanoparticles for photothermal therapies. *Nanoscale* 6:9494–9530
32. Habash RW, Bansal R, Krewski D, Alhafid HT (2006) Thermal therapy, part 1: an introduction to thermal therapy. *Crit Rev Bioeng* 34:459–489
33. Hildebrandt B, Wust P, Ahlers O, Dieing A et al (2002) The cellular and molecular basis of hyperthermia. *Crit Rev Oncol Hemat* 43:33–56
34. Fisher JW, Sarkar S, Buchanan CF et al (2010) Photothermal response of human and murine cancer cells to multiwalled carbon nanotubes after laser irradiation. *Cancer Res* 70:9855–9864
35. Takahashi HT, Nariai A, Niidome Y, Yamada S (2006) Photothermal reshaping of gold nanorods prevents further cell death. *Nanotechnology* 17:4431–4435
36. Oleson JR, Samulski TV, Leopold KA, Clegg ST et al (1993) Sensitivity of hyperthermia trial outcomes to temperature and time: implication for thermal goals of treatment. *Radiat Oncol Biol Phys* 25:289–297
37. Chu KF, Dupuy DE (2014) Thermal ablation of tumours: biological mechanisms and advances in therapy. *Nat Rev Cancer* 14:199–208
38. Chen Q, Wen J, Li H et al (2016) Recent advances in different modal imaging-guided photothermal therapy. *Biomaterials* 106:144–166
39. Young JK, Figueroa ER, Drezek RA (2012) Tunable nanostructures as photothermal theranostic agents. *Ann Biomed Eng* 40:438–459
40. Cheng L, Wang C, Feng L et al (2014) Functional nanomaterials for phototherapies of cancer. *Chem Rev* 114:10869–10939
41. Wang Z, Huang P, Jacobson O et al (2016) Biomineralization-inspired synthesis of Copper Sulfide–Ferritin Nanocages as cancer theranostics. *ACS Nano* 10:3453–3460
42. Yang Y, Liu J, Liang C et al (2016) Nanoscale metal–organic particles with rapid clearance for magnetic resonance imaging-guided photothermal therapy. *ACS Nano* 10:2774–2781
43. Smith AM, Mancini MC, Nie S (2009) Bioimaging: second window for in vivo imaging. *Nat Nanotechnol* 4:710–711
44. Weissleder R (2001) A clearer vision for in vivo imaging. *Nat Biotechnol* 19:316–317
45. Gilchrist RK, Medall R, Shorey WD, Hanselman RC et al (1957) Selective inductive heating of lymph nodes. *Ann Surg* 146:596–606
46. Pankhurst QA, Connolly J, Jones SK, Dobson J (2003) Applications of magnetic nanoparticles in biomedicine. *J Phys D Appl Phys* 36:167–181
47. Mornet SP, Vasseur SB, Grasset F, Duguet E (2004) Magnetic nanoparticle design for medical diagnosis and therapy. *J Mater Chem* 14:2161–2175
48. Hergt R, Dutz S, Röder M (2006) Effects of size distribution on hysteresis losses of magnetic nanoparticles for hyperthermia. *J Phys Condens Matter* 18:2919–2934
49. Ma H, Jiang C, Zhai D et al (2016) A bifunctional biomaterial with photothermal effect for tumor therapy and bone regeneration. *Adv Funct Mater* 26:1197–1208
50. Zhang Y, Nayak TR, Hong H, Cai W (2012) Graphene: a versatile nanoplatform for biomedical applications. *Nanoscale* 4:3833–3842
51. Lee WC, Lim CHYX, Shi H et al (2011) Origin of enhanced stem cell growth and differentiation on graphene and graphene oxide. *ACS Nano* 5:7334–7341
52. Yang K, Zhang S, Zhang G et al (2010) Graphene in mice: ultrahigh in vivo tumor uptake and efficient photothermal therapy. *Nano Lett* 10:3318–3323
53. Robinson JT, Tabakman SM, Liang Y et al (2011) Ultrasmall reduced graphene oxide with high near-infrared absorbance for photothermal therapy. *J Am Chem Soc* 133:6825–6831
54. Gonçalves G, Vila M, Portolés M-T et al (2013) Nano-graphene oxide: a potential multifunctional platform for cancer therapy. *Adv Healthc Mater* 2:1072–1090

55. Ivaska KK, Hentunen TA, Vaaraniemi J et al (2004) Release of intact and fragmented osteocalcin molecules from bone matrix during bone resorption in vitro. *J Biol Chem* 279:18361–18369
56. Alford AI, Hankenson KD (2006) Matricellular proteins: extracellular modulators of bone development, remodeling, and regeneration. *Bone* 38:749–757
57. Wu C, Xia L, Han P et al (2015) Graphene-oxide-modified  $\beta$ -tricalcium phosphate bioceramics stimulate in vitro and in vivo osteogenesis. *Carbon* 93:116–129
58. Hong J, Shah NJ, Drake AC et al (2012) Graphene multilayers as gates for multi-week sequential release of proteins from surfaces. *ACS Nano* 6:81–88
59. La W-G, Park S, Yoon H-H et al (2013) Delivery of a therapeutic protein for bone regeneration from a substrate coated with graphene oxide. *Small* 9:4051–4060
60. Andronescu E, Fikai M, Voicu G et al (2010) Synthesis and characterization of collagen/hydroxyapatite: magnetite composite material for bone cancer treatment. *J Mater Sci Mater Med* 21:2237–2242
61. Kawashita M, Kawamura K, Li Z (2010) PMMA-based bone cements containing magnetite particles for the hyperthermia of cancer. *Acta Biomater* 6:3187–3192
62. Tampieri A, D'Alessandro T, Sandri M et al (2012) Intrinsic magnetism and hyperthermia in bioactive Fe-doped hydroxyapatite. *Acta Biomater* 8:843–851
63. Gloria A, Russo T, D'Amora U et al (2013) Magnetic poly( $\epsilon$ -caprolactone)/iron-doped hydroxyapatite nanocomposite substrates for advanced bone tissue engineering. *J R Soc Interface* 10:20120833
64. Wei G, Ma PX (2008) Nanostructured biomaterials for regeneration. *Adv Funct Mater* 18:3568–3582
65. Bañobre-López M, Pineiro-Redondo Y, Sandri M et al (2014) Hyperthermia induced in magnetic scaffolds for bone tissue engineering. *IEEE Trans Magn* 50:1–7
66. Zhang Y, Zhai D, Xu M et al (2016) 3D-printed bioceramic scaffolds with a Fe<sub>3</sub>O<sub>4</sub>/graphene oxide nanocomposite interface for hyperthermia therapy of bone tumor cells. *J Mater Chem B* 4:2874–2886
67. Zhang J, Zhao S, Zhu M et al (2014) 3D-printed magnetic Fe<sub>3</sub>O<sub>4</sub>/MBG/PCL composite scaffolds with multifunctionality of bone regeneration, local anticancer drug delivery and hyperthermia. *J Mater Chem B* 2:7583–7595
68. Wu C, Fan W, Chang J (2013) Functional mesoporous bioactive glass nanospheres: synthesis, high loading efficiency, controllable delivery of doxorubicin and inhibitory effect on bone cancer cells. *J Mater Chem B* 1:2710–2718
69. Tsai HC, Chang WH, Lo CL et al (2010) Graft and diblock copolymer multifunctional micelles for cancer chemotherapy and imaging. *Biomaterials* 31:2293–2301
70. Verstappen CCP, Heimans JJ, Hoekman K, Postma TJ (2003) Neurotoxic complications of chemotherapy in patients with cancer. *Drugs* 63:1549–1563
71. Meazza C, Scanagatta P (2016) Metastatic osteosarcoma: a challenging multidisciplinary treatment. *Expert Rev of Anticancer* 16:543–556
72. Chen KH, Po-Kuei Wu PK, Chen CF, Chen WM (2015) Zoledronic acid-loaded bone cement as a local adjuvant therapy for giant cell tumor of the sacrum after intralesional curettage. *Eur Spine J* 24:2182–2188

# Chapter 13

## Development of Biodegradable Bone Graft Substitutes Using 3D Printing

Zhidao Xia, Yunsong Shi, Hongyan He, Yuanzhong Pan, and Changsheng Liu

**Abstract** New manufacturing technologies using rapid prototyping or 3D printing enable the fabrication of free-form biomaterials/scaffolds for tissue regeneration. The printing technology can produce materials with computer-aided design of architecture, additives of inorganic/organic compositions, and connective pores with suitable pore sizes that are particularly important for bone tissue ingrowth and vascularization. Therefore, the available 3D printing techniques including vat polymerization (VP), powder bed fusion (PBF), material extrusion, and binder jetting are summarized in this chapter. The potential biomaterials for 3D printing are also discussed. Finally, 3D printing techniques are applied for various medical applications. Obviously, such techniques have paved ways in bone tissue engineering and regeneration and also in personalized medicine of clinical orthopedic and orthodontic practices.

**Keywords** Rapid prototyping/3D printing • Bone graft substitutes • Biodegradation • Bone tissue engineering

### 13.1 Introduction

Bone tumor, diseases, and trauma may cause various bone loss issues including delayed unions, nonunions, and malunions and other problems, which severely affect life quality and even lead to disability of the human body [1]. To solve these

---

Z. Xia (✉) • Y. Shi

Centre for Nanohealth, Swansea University Medical School, Singleton Park, Swansea, UK  
e-mail: [z.xia@swansea.ac.uk](mailto:z.xia@swansea.ac.uk)

H. He (✉) • Y. Pan

Engineering Research Center for Biomedical Materials of Ministry of Education, East China University of Science and Technology, Shanghai 200237, China  
e-mail: [hyhe@ecust.edu.cn](mailto:hyhe@ecust.edu.cn)

C. Liu

Key Laboratory for Ultrafine Materials of Ministry of Education, East China University of Science and Technology, Shanghai 200237, China

skeletal issues and make the effective treatment, the orthopedic surgeon currently has several options: auto-, allo-, and xeno-bone graft as well as artificial bone substitutes [2]. Although autogenous graft has remained to be the golden standard in restoring bone defects, the insufficient bone donor, a certain amount of morbidity, or potential risk of infection in harvesting limit its applications [3, 4]. The allo- and xeno-options are also restricted due to the risks of disease transmission by viruses or bacteria [5, 6]. With the development of biomaterials and biological analysis, the artificial bone grafts become more promising for improved compatibility at graft sites and hold great potential for bone regeneration due to their mimic composition and structure of natural bone. Typically, artificial bone materials do not contain any pathogens or alloantigens. Although they lack osteoinductive or osteogenic properties at the initial stage, synthetic biomaterials and substitutes are already used in clinical practice.

In the process of bone regeneration, scaffold-assisted bone tissue engineering aims to rebuild the configuration of defected bone tissues and its physiological functions [7]. Degradable scaffolds with 3D porous structures have received numerous attentions. For instance, it has been reported that demineralized bone matrix (DBM) and collagen were used as bone graft extenders for the minimal structural support [8]. A number of synthetic bone substitutes have been provided in the market, mainly including bioglass ceramics and calcium phosphate cements (CPCs) [8, 9]. Especially, CPCs have absorbed much attraction for many years [10, 11]. A calcium phosphate cement formed by tetracalcium phosphate [TTCP,  $\text{Ca}_4(\text{PO}_4)_2\text{O}$ ] and dicalcium phosphate anhydrous (DCPA,  $\text{CaHPO}_4$ ) or dicalcium phosphate dihydrate (DCPD,  $\text{CaHPO}_4 \cdot 2\text{H}_2\text{O}$ ) can produce hydroxyapatite (HA) as the final product [12, 13]. This property has led to the development of injectable CPC. Moreover, CPC has demonstrated the excellent osteoconductive response in animal models [14–16] and therefore has been used for a wider range of clinical applications [17, 18]. Our group developed a series of novel CPC products with unique advantages of self-setting and easily shaped capability. Under physiological conditions, the CPC is able to set and harden to form HA after mixed with aqueous solution [19]. The mechanical strength of CPC is improved due to the formation of HA [20]. However, the low degradation rate of HA might hinder the fast formation and restoration of a new bone after implanted in the human body [21].

For certain clinical applications, it is highly desirable for a scaffold with fast new bone formation and matchable resorption rate. Therefore, it is better to develop new CPC-based biomaterials with higher degradation rate. There are many strategies available for achieving the faster biodegradation of CPCs. The most important one is the macroporosity, the key factor for controlling CPC biodegradation/resorbability [22]. Macroporous CPC scaffolds can be prepared by conventional approaches including sintering, fiber bonding, solvent casting and particulate leaching, membrane lamination, melt molding, and gas foaming [23–26]. However, these techniques might be limited by such drawbacks as high sintering temperature, low mechanical strength, long fabrication periods, poor repeatability and labor intensity, incomplete removal of residuals in the polymer matrix, irregularly shaped pores, and insufficient interconnectivity of pores. Moreover, most of these methods bear

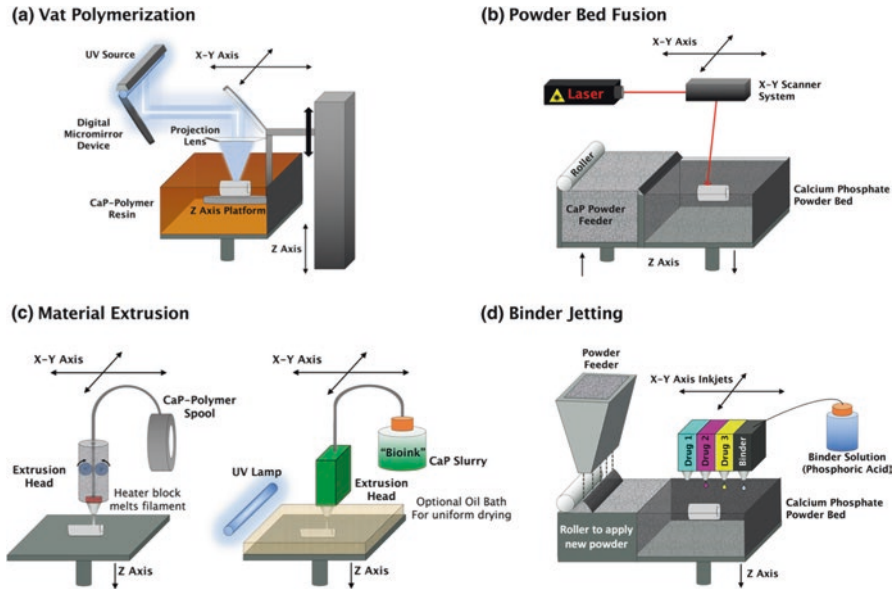
restrictions on the shape control. For example, casting is dependent on the shape of the mold and may not suit the resultant scaffold architecture, porosity, or pore size of the scaffolds [27]. Therefore, it is necessary to develop new manufacturing processes to overcome some of these disadvantages and to fulfill the requirement of the desired scaffolds.

Three-dimensional (3D) printing has been developed in the medical field including porous scaffolds, with extensive research objectives focusing on the development of multi-functionality and the reduction of costs [28]. As additive manufacturing, 3D printing holds great advantages over the traditional techniques: creation of complex design, well-controlled spatial heterogeneity, customized structures, excellent repeatability, and short fabrication periods. Therefore, this technique has been used to fabricate CPC scaffolds with controllable porous structure directly from powder materials [29, 30]; however, the entrapped powder and mechanical strength still remain the issues. It is well known that low strength along with brittleness makes the porous scaffolds difficult to handle and even undermine their biologic performances. Other issues also include limited processible materials, questionable accuracy, and difficulty in small size. Therefore, the typical 3D printing techniques are first reviewed in this chapter. The chapter also discusses the major materials used in 3D printing, focusing on the CaP-based scaffolds for tissue engineering. It also summarizes the applications of 3D printing for artificial bone substitutes, with the demonstration of therapeutic performances *in vitro* and *in vivo*.

## 13.2 Three-Dimensional (3D) Printing Technology

3D printing (3DP) technologies, as rapid prototyping (RP) techniques, are a group of advanced manufacturing processes and can produce custom-made objects directly from computer data such as computer-aided design (CAD), computed tomography (CT), and magnetic resonance imaging (MRI) data [31–33]. This revolutionary technology can be applied to produce three-dimensional objects directly from 3D models primarily through a material additive process, where successive layers of material are laid down and stacked under computer control. Generally, the available 3DP techniques include vat polymerization (VP), powder bed fusion (PBF), material extrusion, and binder jetting [34–37]. Their schematics have been summarized in Fig. 13.1 [38]. These processes have been widely used for the traditional manufacturing applications and also absorbed great attention for their medical uses and clinical applications [39]. In the beginning, 3DP technique was mainly used to fabricate drug delivery devices [40]. Recently, this capability of creating 3D structures has attracted tissue engineers to apply it to design and fabricate tissue scaffolds. Both constructions with controllable design and complex internal architecture with appropriate mechanical properties fabricated by using 3DP have demonstrated the scaffold potential of the 3DP technology [41].





**Fig. 13.1** Schematic depiction of the major technologies used in 3D printing of pure or composite calcium phosphate (*CaP*) scaffolds for bone regeneration and drug delivery (Reproduced from Ref. [38] by permission. Copyright © 2016 Biomedical Engineering Society)

### 13.2.1 Vat Polymerization (VP)

Vat polymerization, or stereolithographic processes, represents a group of additive manufacturing techniques. This technique can be applied to convert photocurable liquid polymers into solid and highly cross-linked structures under a radiation of a low-power ultraviolet light [42]. Since the process uses liquids to produce objects, there is no structural support from the material during the building phase. As the curable polymer is selectively polymerized on the surface of a vat, correlated with down-moving of the z-axis, a thin layer of material is formed. This process is repeated until a desired solid is built. To accelerate the printing process, Tumbleston et al. [43] developed continuous liquid interface production (CLIP) 3D printing as a novel vat polymerization technique. Besides the UV laser as photo-curator, oxygen was introduced to create a non-polymerized dead zone, which made it possible to project continuous solid objects without the lamination.

Vat polymerization techniques have been widely explored for creating various products in medical applications (i.e., bone tissue engineering) due to their high accuracy, fine resolution, well-controlled stiffness of scaffold, and ability to process the biological molecules and even living cells in a pretty short time. However, VP technique is restricted to photosensitivity of the liquid polymers.

### 13.2.2 Powder Bed Fusion

Different from vat polymerization using liquid polymers, powder bed fusion (PBF) employs solid particles of various materials to print. In order to bind the particles to a mass material, this process needs laser or electron beam to achieve selective thermal binding of materials of each layer, through complete melting, partial melting, or sintering. The candidate materials for PBF are not limited to liquid-phase polymers. Rather, biopolymers, bioceramics, biomedical composites, and even titanium alloys are all suitable for processing [44–46]. Because of the ability of selective bounding, PBF can be applied for achieving fine-tuning of pattern and flexible structure. The strong strength is also an attractive characteristic of PBF process, while its resolution is correlated with the diameter of the laser or electron beam for bounding. PBF process includes the following commonly used techniques: direct metal laser sintering (DMLS), electron beam melting (EBM), selective heat sintering (SHS), selective laser melting (SLM), and selective laser sintering (SLS).

For nonbiodegradable polymers, polyetheretherketone (PEEK) [47] and ultra-high molecular weight polyethylene (UHMWPE) [48] have been successfully sintered into scaffolds. Since these polymers are nonbiodegradable, they are used for permanent implantation, such as PEEK for maxillofacial, cranial, or dental defects and UHMWPE for joint replacement. Biodegradable polymers, including PCL [44] and PLLA [49], have also been processed into 3D scaffolds. To improve the mechanical/biofunctional properties of scaffolds, biodegradable polymers combined with bioactive ceramics were successfully processed into composite scaffolds (i.e., HAP/PCL, HA/PLGA, and  $\beta$ -TCP/PLGA) by using SLS technique [50, 51]. SLS technology has been used for fabricating osteoconductive, nanocomposite scaffolds for tissue engineering without the introduction of cells or growth factors. Just like other PBF techniques, high-energy involvement leads to the high local temperature during processing, inhibiting the simultaneous incorporation of other bioactive factors such as cells, growth factors, and other heat-labile molecules, which are commonly used to enhance the functions of the scaffolds.

A modified and enhanced SLS procedure, namely, surface-selective laser sintering (SSLS), was also developed to prevent the degradation of the biopolymer and to facilitate the incorporation of bioactive agents or cells [52, 53]. This technique utilizes specific laser irradiation parameters, in which the most part of polymer particles is not heated during polymer sintering. For example, Duan et al. [54] used SSLS technique to prepare two types of nanocomposite scaffolds. The benign process conditions in SSLS allowed the maintenance of the biological properties of biomaterials, which was experimentally demonstrated in terms of the improved cell proliferation and alkaline phosphatase activity for the scaffolds.

### 13.2.3 *Material Extrusion*

Material extrusion refers to processes depositing materials as continuous strands through a nozzle or a dispensing orifice, followed by solidification of the material. The techniques are one of the most commonly used 3D printing strategies for tissue engineering and related regenerative fields. A spate of material extrusion techniques have been described by such growing terminologies as 3D plotting, dispense plotting, or bioprinting. Due to the mild condition and highly detailed pattern with essential and sacrificial contents, living cells and bioactive molecules can be included during the process [55]. Therefore, a number of materials have been adaptable to bone applications via extrusion-based techniques. These materials involve synthetic polymers (i.e. polyester), natural polymers, polymer/ceramic composites, and photo-curable hydrogels [56, 57].

These techniques not only offer the ability to manufacture matrices with complex structures such as defect site matched outer shape, as well as designed internal channel network to mimic bone structures, but also process the bioactive materials, including biological factors and even cells. However, post-processing is sometimes required to fully complete the item formation. For example, when ceramics are involved, a secondary heat treatment or sintering may be needed. The resolution of extrusion-based methods depends on the diameter of the dispensing nozzles and the stability of the material after extrusion.

### 13.2.4 *Binder Jetting*

The binder jetting (BJ) process uses particulate raw materials and a binder. The binder in liquid form acts as an adhesive between powder layers. Instead of fusing the materials with relatively high-energy sources, proper solutions are sprayed from the inkjet in a layer-by-layer way. As can be seen in Fig. 13.1d, the printhead moves horizontally along the x and y axes of the machine and deposits alternating layers of the build material and the binding material. After each layer, the object being printed is lowered on its build platform [58].

CaP-based materials (i.e., TCP and HA) are the widely used powder phase in bone repairing and regenerating grafts, and the binding solutions for CaP are usually an aqueous solution, i.e., dilute phosphoric acid with a concentration range of 5–30 wt.%. Another research group used a 12 wt.% PVA aqueous solution as the binder and successfully fabricated porous calcium silicate ( $\text{CaSiO}_3$ , CS) scaffolds by using 3D biojetting technique [59]. The result indicated that the mechanical strength of the porous scaffold was improved because of the viscosity of polyvinyl alcohol aqueous and the increased density of the paste. Since the binder for CaP-based materials is usually an aqueous solution, the solubility of CaP in the binder significantly inferences their printability. Introduction of reactive minerals, selection

of more soluble CaP materials, and regulation of powder size may be the feasible strategies for improving the printability.

Binder jetting can print pure CaP scaffolds simultaneously with other bioactive factors such as growth factors in ink cartridges. Therefore, this technique holds great potential for bone tissue engineering. However, it is still challenging to print the cells directly via using BJ technique. Moreover, due to the method nature of binding, the material characteristics are not always suitable for structural parts, and despite the relative speed of printing, additional post-processing can add significant time to the overall process.

### 13.3 Potential Materials in 3D Printing

Since biomaterials strongly influence the overall properties of a scaffold, it is necessary to comprehend their individual characteristics to allow for appropriate selection in specific applications. Biomaterials not only offer the different printable ability but also show the different affinity to cells, which affects adhesion, growth, proliferation, and the overall regeneration performance. Thus, several categories of potential biomaterials for 3D printing are summarized as follows.

#### 13.3.1 *CaP-Based Materials*

For bone repairing and regenerating applications, one of the most important biomaterials is calcium phosphate bioceramics, which are inorganic biomaterials constituting different categories. CaP bioceramics mainly include hydroxyapatite, tricalcium phosphate, and biphasic calcium phosphate, all of which can also be in the form of injectable materials that are moldable and easy to handle and harden in situ [60]. Combined with their other excellent characteristics, injectable and easy handling ability makes them more attractive in bone regeneration.

With the development of rapid prototyping, numerous research groups would like to integrate these “old” materials with 3D techniques to endow these materials with well-controlled structures and better biological performances. The most widely used CPC in bone tissue engineering is HAp, which positively influences adhesion and proliferation of osteoblasts. However, due to the slow degradation, applications of crystalline HAp are being eventually substituted by amorphous hydroxyapatite with a faster degradation rate. Modification of HAp degradation rate can be achieved by its combination with other biomaterials of faster kinetics or foaming agents for microporosity enhancement [61].

$\beta$ -tricalcium phosphate ( $\beta$ -TCP) is also the widely studied CaP-based material, because of its ability to form a strong bone-calcium phosphate bond and its improved degradation rate. Interestingly, when tricalcium phosphate is combined with HAp, a mixture termed biphasic calcium phosphate (BCP) is produced. In comparison to

other calcium phosphate ceramics, BCP has significant advantages in terms of controlled bioactivity and stability, while promoting bone ingrowth especially in large bone defects, and controllable degradation rate as BCP has a higher degradation rate than HAp, yet slower than that of  $\beta$ -TCP [62, 63]. Although calcium phosphate bioceramics have attractive properties, they are extremely brittle and difficult to shape into the desired structures. They also have weak mechanical strength, which limits their applications to non-load-bearing areas. To improve their properties and extend their applications, combination with mechanically strong biomaterials (i.e., nanoparticle of synthetic polyesters) might be the potential way.

### 13.3.2 *Biodegradable Polymers*

Collagens and gelatins are widely used natural biomaterials in pharmaceutical applications and tissue engineering [64]. Collagen is the most copious protein present in the human body being the major component of skin and musculoskeletal tissues. Gelatin is a denatured collagen and is typically isolated from bovine or porcine skin or bone by acid or base extraction. Gelatin and collagen have been employed to generate 3D scaffolds. These inorganic/organic materials can be used alone or as composition to produce 3D printing bone graft substitutes. However, low bioactivity and weak mechanical properties may limit their applications.

Apart from the natural materials, there are many synthetic biodegradable materials and/or polymers used for bone graft substitutes as well. Saturated poly- $\alpha$ -hydroxy esters are the most commonly used biodegradable synthetic polymers for 3D printing scaffolds, including poly(lactic acid) (PLA), poly(glycolic acid) (PGA), poly(lactic-co-glycolide) (PLGA), and poly- $\epsilon$ -caprolactone (PCL) [65, 66, 67].

In general, PLGA degrades faster than PLA; their degradation rates decrease in the following order: PLGA>PLLA>PCL. PLA, PLGA, and PGA have been used for preparing various medical products and devices, such as degradable sutures that have been approved by the US Food and Drug Administration [65]. PLA and PGA can be easily processed and their degradation rates; physical and mechanical properties can be adjusted over a wide range by using various molecular weights and copolymers. The racemic mixture of D,L-PLA (PDLLA) has excellent implant performance which has been extensively investigated as a biomedical coating orthopedic material [68].

Besides the materials discussed above, PCL is also an important member of the aliphatic polyester family and an excellent candidate for bone tissue engineering applications due to its biocompatibility, suitability for various scaffold fabrication techniques, remarkably slow degradation rate, and mechanical stability. Especially, the latter two traits might allow for a better maintenance of generated bone volume and its contour over time. However, PCL is hydrophobic in nature, which is responsible for the inferior cell affinity and poor cellular responses and interactions to the surface [54]. In general, aliphatic polyesters display a slow degradation rate in correlation with natural polymers and bioceramics. Most of the available polyesters

degrade by the bulk degradation, while the size is maintained for a considerable amount of time. This feature is considered appealing for scaffold utilization as a bone graft substitute and less suitable for drug delivery purposes. Moreover, aliphatic polyesters are easily moldable for fabrication into the required shapes and have good mechanical properties.

### ***13.3.3 Supplementing Materials***

#### **13.3.3.1 Drugs and Proteins**

In clinical use, the osteoconductivity and osteoinductivity of the CaP itself are often not sufficient to rapidly complete the reparation and regeneration. Therefore, certain drugs, biomolecules, and proteins are sometimes introduced to improve the bioactivity of the printed scaffolds. These cofactors could be, but not limited to, antibiotics that can prevent infection, growth factors that can promote cell proliferation and differentiation and regulate local inflammation, and inorganic compounds that can serve as source of ions helping regeneration. It is a feasible way to absorb growth factors and drugs onto the 3D-printed CaP scaffolds after post-processing. This approach normally results in burst release of the surface-absorbed molecules, unable to prolong the release to a desirable period [69, 70]. This elicits the necessity of incorporating drugs in a homogeneous volumetric way or creating a spatial gradients or site-specific drug localization using 3D printing techniques. Specifically, biological molecules including proteins are highly sensitive to the surrounding conditions. The harsh fabrication conditions, such as high temperature, organic solvent, or acidic/basic may lead to denaturation, degradation, or loss of bioactivity. Therefore, it is highly required to choose the appropriate fabrication approach and well control the process conditions.

Bone morphogenetic proteins belong to the large transforming growth factor-beta (TGF- $\beta$ ) superfamily of structurally related signaling proteins. To date, more than 20 members have been identified in humans with varying functions during developmental and physiological processes. Among these growth factors, BMP-2 and BMP-7 (also called osteogenic protein-1) have been largely used as recombinant proteins for their ability to repair bone defects in different animal models [71, 72]. Liu et al. [73] have elucidated the exact mechanism by which BMPs affect MSCs. These proteins generate the transcription factor Smads by combining with type I or II serine/threonine receptor on the MSC membrane to activate 203 gene loci which control the osteoblast differentiation of MSCs. Thus, introduction of BMP-2 in 3D-printed scaffolds with well-designed structures can significantly enhance the bone ingrowth, osteointegration, and vascularization. Vascular endothelial growth factor (VEGF) is also a commonly used factor in 3D-printed scaffolds for its potent effect on angiogenesis, which is pivotal for bone growth and achievement of full bone function. It has been confirmed that fast release of VEGF protein in vivo was less effective, and a slow release formulation of VEGF applied

locally at the site of bone damage could be an effective therapy to promote human bone repair [74]. Thus, it needs to take the consideration for the distribution and location of VEGF with the scaffold matrix.

Depending on the medical applications, there are many drugs available for incorporating into 3D-printed scaffolds. The amount of drug loading and its release kinetics hinge on the CaP phase and the approach used for drug loading. To maintain the bioactivity and enhance the mechanical strength of scaffolds, other materials in microsphere or microcapsule form can be incorporated into scaffolds and serve as carriers or controllers for highly manipulated control of biomolecular drugs. These materials mainly involve PLGA, gelatin, and poly(trimethylene carbonate) [75, 76]. Combined with 3D printing techniques, biomolecular drugs with the assistance of these degradable materials can be directly incorporated into scaffolds during printing or during post-processing.

### 13.3.3.2 Living Cells

Instead of drugs, loading cells into material scaffolds can serve as an artificial organ to achieve bone repairing and tissue regeneration. It has been reported to introduce living cells into 3D-printed repairing materials [77]. Mesenchymal stem cells and osteoblasts are potential candidate cells that are considered to be helpful in this context. However, compared with the case of drugs or proteins, printing process involving cells is more challenging since it is very difficult to maintain the required microenvironment for cell survival and bioactivity stability. As a result, despite several attempts, direct incorporation of living cells in 3D printing is still a great challenge for many researchers. The feasible way used is seeding cells on the scaffolds after printing prior to implantation.

## 13.4 Applications of 3D Printing Techniques

A variety of 3D printing techniques have been used to produce artificial bone graft substitutes, which are summarized in Table 13.1. Each technique requires specific manufacturing processes and materials and holds some advantages and disadvantages.

**Table 13.1** The application of 3D printing techniques for artificial bone graft substitutes

Technique	Process details	Processed materials for bone tissue engineering	Advantages (+) and disadvantages (-)	References
3D plotting/direct ink writing	Extrude paste/viscous material (in fluid form) based on the designed structure	PCL Hydroxyapatite (HAp) Bioactive glasses Mesoporous bioactive glass/alginate composite	+	[78, 79, 80, 81, 82, 83]
	Build designed structure layer by layer under specific pressure and moving speed	Poly(lactic acid (PLA)/polyethylene glycol (PEG) PLA/(PEG)/G5 glass Poly(hydroxymethylglycolide-co-caprolactone) (PHMGCL) Bioactive 6P53B glass	- Heating process needed which restricts the biomolecule incorporation	
Laser-assisted bioprinting (LAB)	Loading the chosen material on transparent quartz disk	HAp	+	[84, 85, 86, 87]
		Zirconia	Ambient condition	
	HAp/MG63 osteoblast-like cell	Applicable for mild materials including cells		
	Nano-HAp	-		
	Deposition control by laser pulse energy	Human osteoprogenitor cell	Homogeneous ribbons needed	
	Resolution control by distance between ribbon, substrate, layer thickness, and laser scan mode	Human umbilical vein endothelial cell		

(continued)



Table 13.1 (continued)

Technique	Process details	Processed materials for bone tissue engineering	Advantages (+) and disadvantages (-)	References
SLS	Preparing the working space	PCL Nano-HAp	+ No support needed Strong structure	[44, 54, 55, 88, 89]
	Sintering powder layer by layer according to designed structure.	Calcium phosphate (CaP)/poly (hydroxybutyrate-co-hydroxyvalerate) (PHBV)	- • Feature resolution and strength of product depend on particle size and laser spot size	
		Carbonated hydroxyapatite (CHAp)/poly(L-lactic acid) (PLLA) PLLA [78, 79] b-Tricalcium phosphate (b-TCP) PHBV		
SLA	Loading working space with photopolymer liquid	Poly(propylene fumarate) (PPF)/diethyl fumarate (DEF)	+ Fast building speed with complex structure	[90, 91, 92, 93]
	Exposure photopolymer layer by layer according to designed structure			
	Polymer solidifying after exposure, nonexposed polymer remains liquid,	PF/DEF-HAp PDLA/HAp $\beta$ -TCP	Loading growth factors, proteins, and cell patterning in materials is available - Materials limited, only photopolymer allowed	

FDM	Extrude filaments by melting the nozzle to build designed structure layer by layer	Tricalcium phosphate (TCP)/PLA	+ Short working time when building simple structure - Only thermoplastic allowed	[32, 94, 95, 96, 97, 98]
		TCP/polypropylene (PP)		
		PCL		
		TCP/PCL		
Robotic-assisted deposition/robocasting	Building designed structure with fluid materials	HA/p/PLA	+ No axis limit, more accurate than other 3D printing technology No platform/support needed - Material restriction	[99]
		HA/p/PCL		
		6P53B glass/PCL		

### **13.4.1 Basic Requirements for 3D Printing**

#### **13.4.1.1 3D Structure Design**

3D structure design can be obtained by both software (such as CAD and ProE) and image acquisition such as multidetector computed tomography (MDCT) and magnetic resonance imaging (MRI). The 3D scaffold designed for bone substitute requires a high porosity (75% and 90%) and inner interconnecting pores. The pore size between 250 and 500  $\mu\text{m}$  has been reported ideal for bone cell attachment and vascularization [100]. Image acquisition can be achieved at ultrahigh spatial resolution (400–600  $\mu\text{m}$ ). MDCT or MRI data can be transferred into 3D images by segmentation tools if needed [101]. MDCT gives more details of calcified hard tissue, whereas MRI provides balanced details of both soft and hard tissues.

#### **13.4.1.2 Materials**

The ultimate target for 3D-printed bone graft substitutes is mimicking the bone structure and composition. Calcium phosphate, the component in natural bone, is probably still the best material for 3D printing of bone graft substitutes. By combining with suitable binders, working temperature and correct parameters are applied and optimized for 3D printing techniques. Take examples, the choice of suitable particles is important in SLS and bioplotter. In SLS, particle sizes between 25 and 100  $\mu\text{m}$  are preferable so that the particles can flow freely. Smooth powder flowing to form new layers is required in SLS processing [102]. The more uniformed the particle size and shape, the better the produce specimen. Irregular particles may reduce the binding strength and generate brittle products with lower mechanical integrity in SLS. Besides, a thorough mixing of the particles and binders plays an important role in mechanical strength of the produced scaffolds [102].

#### **13.4.1.3 Biodegradation**

Biodegradation in vivo is a combination of material solubilization in body fluid and resorption by macrophage/osteoclast. Even though it is desirable to produce a bone graft substitute which can be biodegraded completely after implantation, the control of the period of biodegradation to match bone remodeling cycle is still a challenging subject which needs further study and optimization. The biodegradation of synthetic bone graft substitutes is primarily determined by material composition. Adding the water-soluble molecules may change the composition of raw materials and thus enhance the resorption behavior of produced scaffolds. Controlling the porous structure and adding the degradable polymers can also accelerate the biodegradation.

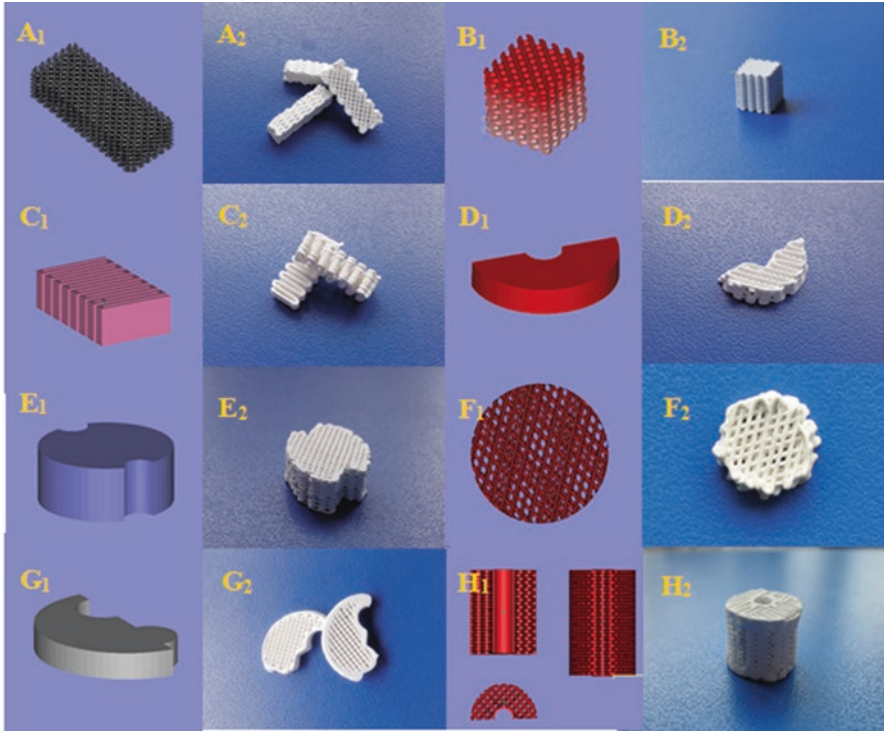
### 13.4.2 3D-Printed Scaffolds Based on CaP Materials for Bone Regeneration

As we discussed in Sect. 2, CaP-based scaffolds can be fabricated via thermal material extrusion and binder jetting at high temperatures. These processes, together with the post-processing techniques, allow the printed scaffolds with enhanced mechanical strength. However, it is very challenging to incorporate biological molecules or cells with stable bio-functions at high temperature. Usually, the CaP-based scaffolds were 3D printed and then evaluated for their biological performances in terms of biocompatibility, cell proliferation, and differentiation *in vitro* and *in vivo*. A number of different cells have been applied for these kinds of studies.

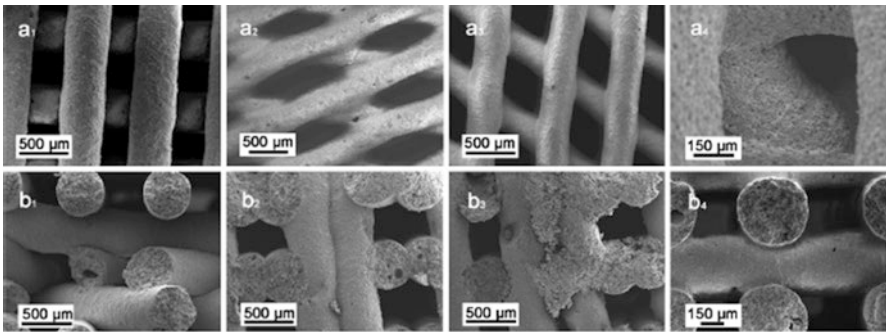
Many research groups have reported the good biocompatibility of CaP-based scaffolds. For instance, Castilho et al. [103] demonstrated the enhanced viability and proliferation of osteoblasts seeded on the biphasic TCP and HA scaffolds produced by binder jetting, compared to pure TCP scaffolds. Once the scaffolds produced at high temperature were implanted *in vivo*, the biocompatibility and enhanced mechanical properties have been confirmed. However, the 3D-printed pure scaffolds did not show the comparable osteoconductivity as the autologous grafts. To improve the osteoconductivity potential, osteoinductive agents or surface modification was proposed for treating 3D-printed scaffolds. The osteoinductive agents include inorganic ions (i.e., calcium, silicate, magnesium, zinc, strontium, manganese, copper, or ferrum), mesoporous glass, and some compounds of ECM.

As comparison, there are many techniques available for fabricating the scaffolds at low temperature (desirable at room temperature). These techniques involve binder jetting approaches and some processes in material extrusion. By choosing the appropriate binder solution, CaP powders can be made the pure scaffold at low temperature, while CaP slurries or cements are extruded through a non-heated nozzle under mild conditions in material extrusion. Typically, post-fabrication treatments are required for solidifying the extruded materials. For example, Liu group fabricated CPC scaffolds incorporated mesoporous calcium silicate (MCS) by using micro-droplet jetting (MDJ) at room temperature. The architectures of the scaffold including pore structure, pore size, and porosity were designed by turning the operation parameters and nozzle sizes. Figure 13.2 shows CAD-designed images (A1–H1) and corresponding printed photograph of MCS/CPC scaffolds with different geometries (A2–H2).

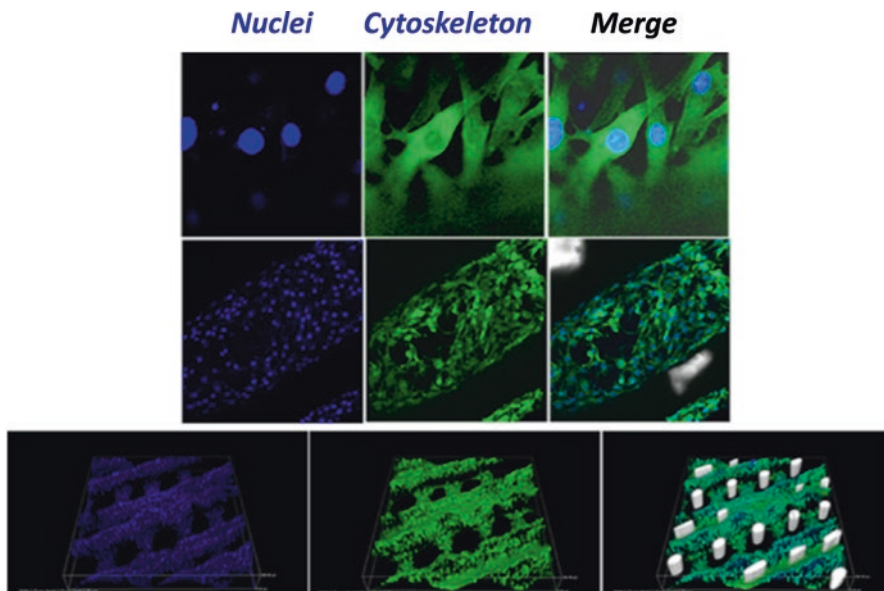
With the addition of MCS, the printable time of MCS/CPC extended to about 120 min, in comparison with 10 min of pure CPC. The longer printable time made MCS/CPC paste extruded continuously and homogeneously. The inner pore shape of the MCS/CPC scaffold was first controlled by adjusting the angle of the process pattern. Figure 13.3a1–a4 presents diverse pore structures of MCS/CPC scaffolds with  $-15^{\circ}/15^{\circ}$ ,  $-30^{\circ}/30^{\circ}$ ,  $-45^{\circ}/45^{\circ}$ , and  $-45^{\circ}/45^{\circ}/0^{\circ}/90^{\circ}$  patterns in X-Y direction. It can be clearly seen that the macropores in the scaffold were uniform and completely open. In addition, scaffolds with different pore structures in Z direction were prepared precisely in Fig. 13.3b1–b4. With 12 wt.% PVA aqueous solution as



**Fig. 13.2** CAD-designed images (A1–H1) and corresponding printed photograph of MCS/CPC scaffolds with different outer architectures (A2–H2) (This figure is kindly provided by Prof. Changsheng Liu and the copyright is held by East China University of Science and Technology)



**Fig. 13.3** SEM images of MCS/CPC scaffolds printed with different angles of the process pattern (Reproduced from Ref. [100] by permission. Copyright © 2015 Springer Science+Business Media, New York)



**Fig. 13.4** Observation of cytoskeleton stained with FITC phalloidin (*green*) and nuclei stained with DAPI (*blue*) of C2C12 cells after 3 days of culture on the MCS/CPC scaffold. *White* columns inside the scaffold were caused by the light that penetrated the macropores from confocal laser scanning microscope (Reproduced from Ref. [105] by permission. Copyright @ 2015 Springer Science+Business Media, New York)

the binder, tight bonding within different layers was observed from the cross section of scaffolds. To meet a wide range of individual needs, MCS/CPC scaffolds with different outer architectures were designed and fabricated successfully (Fig. 13.2A2–H2).

In binder jetting techniques, additives to the binder solution or CaP powders have played an important role on the cell behavior. As described in [105], mixing MCS with CaP powder not only increased the mechanical strength and extended the printable time but also speed up the degradation behavior of the composite scaffold and increased the cell viability. This has been experimentally confirmed by Liu group [104]. As can be seen in Fig. 13.4, C2C12 cells spread well with an intimate contact on the scaffold surface and almost covered the whole surface of the MCS/CPC strands. Combined with other evaluations, the MCS/CPC scaffolds with pore size of 350  $\mu\text{m}$  showed properly interconnected macropores via MDJ approach, high mechanical strength due to MCS addition, fast degradation rate, and good cytocompatibility. Another research reported that mixing CaP powder with alginate could enhance both cell viability and cell proliferation, while vacuum infiltration of alginate into the printed scaffold reduced both cell viability and proliferation of the osteoblastic cell line MG63 [105].

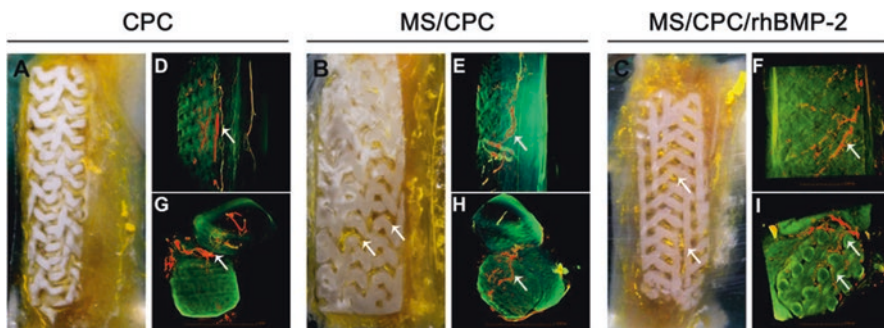
CaP bone grafts fabricated by using 3DP at low temperatures have been confirmed to be osteoconductive *in vivo*. The osteoconductivity of the binder jetting

3D-printed TCP scaffolds has been shown to be better than that of HA scaffolds [106]. However, the CaP-based scaffolds still showed lower osteoconductivity than autologous grafts. To further improve the bone regeneration *in vivo*, one feasible way is to incorporate the functional biomolecules (i.e., growth factors) or even living cells into scaffold structures. It is known that biomolecules (protein, growth factor, hormone, etc.) can maintain their structures and bioactivities under the physiological conditions. The closer the process condition is to the physiological environment, the more stable the biomolecule is. Thus, the 3D printing techniques operated at low temperature hold the potential to directly print the drugs, proteins, and even the living cells suspended in printable inks.

### ***13.4.3 3D-Printed Scaffolds Incorporating Drugs or Proteins for Bone Regeneration***

As just discussed, 3D printing techniques at high temperature have limitation of incorporating biomolecules and cells. To solve the issues, additional post-processing steps are typically required to introduce an osteoinductive element by physical absorption or surface modifications (i.e., chemical binding, surface coating). The most popular growth factor, rhBMP-2, has been widely studied and applied during the post-processing for repairing the bone defects. In several studies, rhBMP-2 molecules were absorbed on the SLS-printed CaP construct surface via heparin surface modifications [54] or on the BJ-silicon-doped CaP via physical absorption [107]. The *in vivo* data demonstrated the bone ingrowth, osseointegration, and vascularization of the bone construct due to the combination of rhBMP-2. In contrast with the high temperature techniques with several post-processing steps, 3D printing at low temperature seems easy to use and biomolecule-friendly.

Theoretically, CaP scaffolds produced by 3DP at low temperature can realize the incorporation of bioactive molecules for localized and sustained delivery. Just like other techniques at high temperature, biomolecules are able to adsorb onto the CaP scaffolds at low temperature during the post-processing step. Li et al. [109] developed a CPC-based scaffold combining the properties of mesoporous silica (MS) with rhBMP-2. 3D printing techniques in mild conditions allowed the scaffolds with a defined macroporous structure and optimized silicon ion release profile to promote the ingrowth of vascular tissue at an early stage after implantation, which can be demonstrated in Fig. 13.5. As can be seen, abundant vessels labeled by yellow-colored Microfil (the radiopaque contrast agent, Flowtech, USA) were vividly displayed inside the macropores of the MS/CPC and MS/CPC/rhBMP-2 scaffolds and around the defects, whereas few blood vessels were seen inside the CPC scaffolds. The 3D reconstructed images of new blood vessels (red and yellow) formed in the macropores and around the scaffolds (green) are presented in Fig. 13.5d–i. From the top view, the newly formed vessels could be seen to have grown straight along the pore structure and deep inside the middle of the MS/CPC



**Fig. 13.5** The (a–c) digital camera photographs of PMMA-embedded blocks from longitudinal sections and 3D reconstructed  $\mu$ CT images of blood vessels from (d–f) side view and (g–i) top view of CPC, MS/CPC, and MS/CPC/rhBMP-2 scaffolds after 4 weeks of implantation. *White arrow*: newly formed blood vessels (Reproduced from Ref. [108] by permission. Copyright © 2017 Nature Publishing Group)

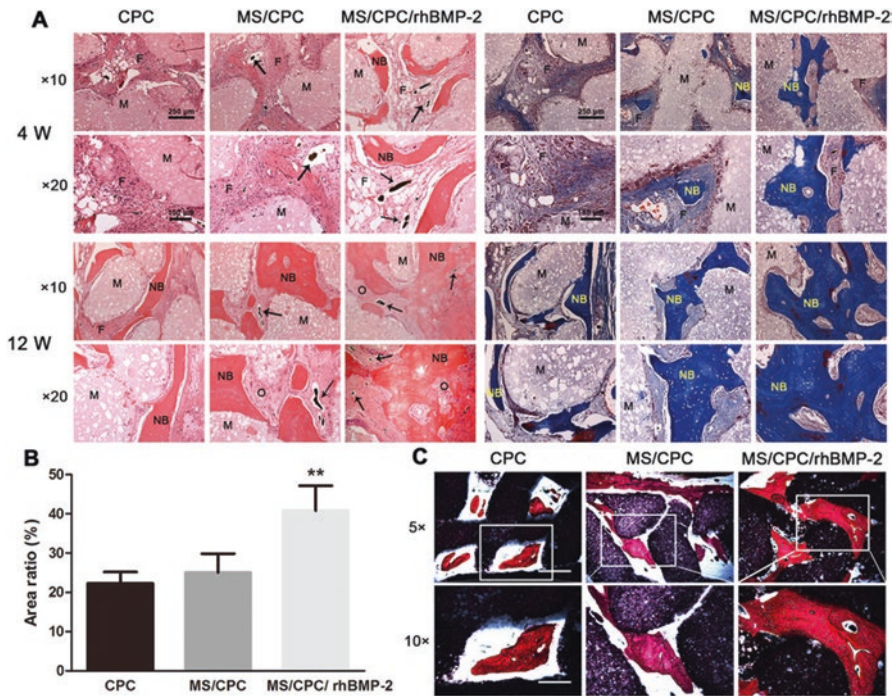
and MS/CPC/rhBMP-2 scaffolds, while from the side view, to have grown through the entire MS-doped scaffolds from top to bottom.

The absorbed rhBMP-2 on the scaffold microstructure was released in a controlled manner, which in turn significantly stimulated the osteogenesis of human bone marrow stromal cells (BMSC) *in vitro* and of bone regeneration *in vivo* in a rabbit femur defect repair model. As shown in Fig. 13.6, during the regeneration process, newly formed bone tissue grew gradually into the central region as well as into most macropores of the scaffolds and bound tightly with the material. After implantation for 12 weeks, MS/CPC/rhBMP-2 scaffolds showed a greater quantity of new bone formation than the other two groups ( $P < 0.01$ ). Moreover, newly formed blood vessels could be clearly observed inside the macropores of MS/CPC and MS/CPC/rhBMP-2 scaffolds. Combined HE staining, Masson trichrome staining, with VG staining, it is confirmed that MS/CPC/rhBMP-2 scaffolds displayed the best osteogenesis in comparison to the other groups without rhBMP-2 molecules [108].

However, the burst release of the surface-adsorbed biomolecules is still a critical issue for medical applications. To minimize the burst effect and extend the therapeutic time, the biomolecules are highly desirable to be entrapped homogeneously or localized specifically within a scaffold with well-control geometry. Take examples, antibiotics were mixed with  $\alpha$ -TCP and then directly binder-jetted along with special binder to form scaffolds [109]. *In vitro* data confirmed the reduced burst effect and sustained release behavior due to the homogenous incorporation of bioactive molecules.

In material extrusion, drugs or biomolecules can be easily mixed with slurries or raw cements and then extruded at the physiological conditions. After harden and self-setting, these additives can be homogeneously entrapped into the matrix. This kind of 3D printing technique has been utilized for loading rhBMP-2, BSA, VEGF, and various antibiotics. Akkineni et al. [110] fabricated  $\alpha$ -TCP-based scaffold by





**Fig. 13.6** Histological evaluation of longitudinal sections of orthotopic bone formation within CPC, MS/CPC, and MS/CPC/rhBMP-2 scaffolds. (a) HE and Masson trichrome staining ( $\times 10$ ,  $\times 20$ ) after 4 and 12 weeks of implantation. *M* materials, *NB* newly formed bones, *F* fibrous tissue, *O* osteoid, *Black arrow*: newly formed blood vessels. (b) Quantitative analysis of the new bone area in HE stained sections after 12 weeks of implantation.  $**P < 0.01$ , MS/CPC/rhBMP-2 vs. CPC and MS/CPC scaffolds. (c) VG staining ( $\times 5$ : bar = 500  $\mu\text{m}$ ,  $\times 10$ : bar = 250  $\mu\text{m}$ ) after 12 weeks of implantation (Reproduced from [108] by permission. Copyright © 2017 Nature Publishing Group)

extruding the CaP cement premixed with chitosan/dextran sulfate microparticles encapsulating VEGF and BSA. The cytocompatibility of the scaffolds was successfully demonstrated by the viability and alkaline phosphatase activity of mesenchymal stem cells cultivated for up to 21 days. And the maintenance of the VEGF bioactivity during the fabrication procedure was confirmed in the culture experiments with endothelial cells. Obviously, the mild conditions of the 3D printing techniques allow the precise and localized integration of biological components without change of structures and loss of bioactivities. However, the consideration related to the printing resolution should be taken for some specific designs, since the high viscosity of raw material mixture usually requires a printed head or nozzle with large size.

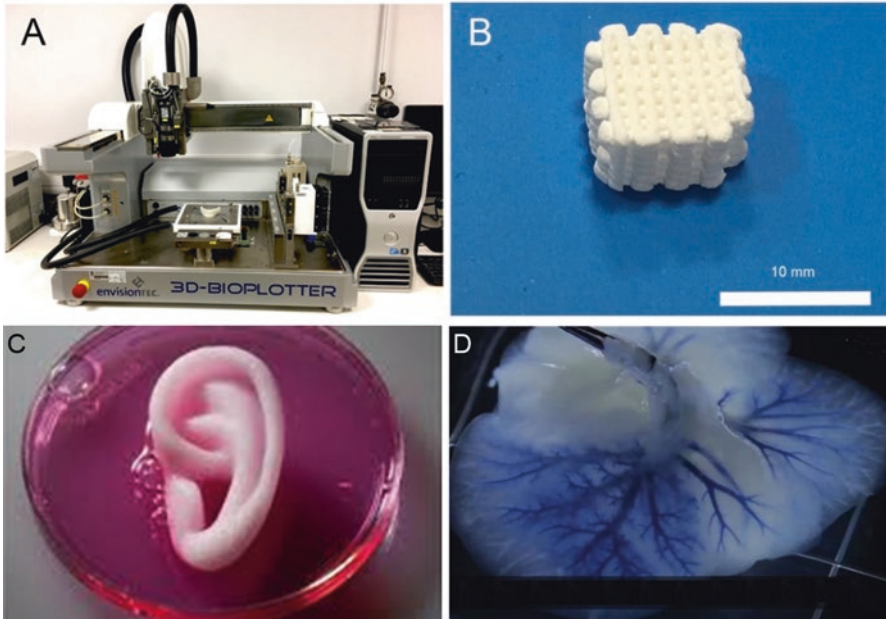
### ***13.4.4 3D-Printed Scaffolds Incorporating Living Cells for Bone Regeneration***

Some researchers have found that pre-loading living cells into scaffold matrix may be favorable to activate the biological response of surrounding cells at the implanted sites. Therefore, a variety of cells was introduced into the raw printable “inks” or patterned scaffolds before implantation. The large porous structure and interconnectivity of the scaffold allow the easy seeding of cells and enough transport of nutrients for cell survival. However, it is very difficult to ensure the homogeneous distribution and good attachment of cells or achieve the multi-seeding of different cells. Many researchers have made attempts to precisely layout cells in “layer-by-layer” assembly in turn bio-mimicking the bone tissues by using bioprinters. One of the typical bioprinters is 3D bioplotter (EnvisionTEC GmbH, Germany) showed in Fig. 13.7, which enables to fabricate scaffolds with suitable porosity and strong mechanical properties for mimicking human organs [111]. Theoretically, bioplotter can print two types of materials at very different temperature and mechanical properties, when two nozzles containing different materials are printed sequentially or simultaneously. Thus, this bioprinter can be extended for medical applications, such as combination with stem cells, growth factors/cytokines, and other reagents to promote bone regeneration/induction.

The generation of bio-artificial bone using 3D printing technique requires isolation of autologous cells, which is then proliferated in the laboratory to obtain the desired cell numbers followed by layering of cells via a 3D bioprinter. Gao’s group loaded human mesenchymal stem cells (hMSCs) into different bioinks and investigated the effect of the ink composition on the cell viability. According to the experiments, the hMSC viability was highest in a mixed bioink of PEG-dimethacrylate and HA, while PEGDMA-BG had a pretty lower cell viability. Moreover, the presence of HA enhanced the differentiation toward the osteoblastic lineage [77]. Obviously, the composition of bioinks played a vital role on the viability and function of hMSCs cells, which should be suspended in bioinks with low viscosity.

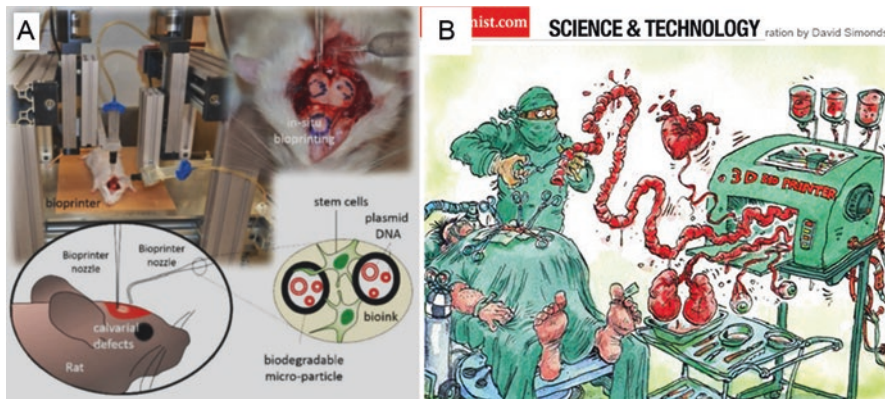
Bioprinting of living cells has offered the promising possibility in the area of bone regeneration and drug screening and held such advantages as the ability to organize the cell distribution within the scaffold, enhancement of cell attachment and biological ability, and improvement of bone defect management. However, the delicate characteristics of living cells, especially for human cells, require the cell-friendly operation conditions and experienced technical skills.

To further achieve the precise placement of blood vessels, nerves, or muscles during the surgery, *in situ* bioprinting is proposed to treat the injured patients for using in hospitals and clinics for civilians. This special technique can directly print the bioactive tissue constructs with porous structures in the defects or lesions. Because of completely matchable architectures and precise placement of construct at the injured sites, this technique can facilitate the repair of large bone defects through better media exchange, tissue engraftment, and vascularization [113].



**Fig. 13.7** (a) A typical bioprinter, Envision Bioplotter, (b) a porous scaffold produced containing calcium phosphate cement, (c) 3D-printed external ear, and (d) artificial human liver tissues produced by Wake Forest Institute for Regenerative Medicine (Figs. (c) and (d) are reproduced from the website [112] with open access)

Prof. Ozbolat and coworkers developed a novel approach to print multi-tissue constructs into calvarial defects for bone regeneration (shown in Fig. 13.8a). BMSCs and plasmid DNA were bioprinted within a bioink composing collagen and block copolymer F-127. In this design, plasmid DNA can transfect BMSCs and encode the different growth factors, which promote the differentiation of BMSCs into functional components of bones at the deposited site. Moreover, the collagen matrix also can improve the proliferation and differentiation of BMSCs. Thus, highly promising results were achieved in the regeneration of bony tissues in critical-sized calvarial defects *in vivo* [114]. The great hope of transplant surgeons is that they will be able to order replacement body parts on demand (shown in Fig. 13.8b). To achieve this ultimate goal, many researchers and scientists are working on the *in situ* bioprinting area. However, there still exist challenging problems. More research and further clinical studies are needed for integrating biomaterial characteristics, design of printed architectures, and 3D printing techniques in operation room for bone regeneration.



**Fig. 13.8** (a) In situ bioprinting in operation rooms, where a composite bioink loaded with plasmid DNA and stem cells is printed for cranial bone regeneration, (b) a machine that prints organs is coming to the market, which is illustrated by David Simonds (Here, Fig. (a) is reproduced from [115] by permission. Copyright © 2016 Quintessence Publishing, UK, and Fig. (b) is reproduced from the website [116] with open access)

### 13.5 Conclusion and Perspectives

The 3D printing technology has the potential to pave a way in producing biodegradable bone graft substitutes to suit the mechanical property, porosity, surface structure, cellular attachment, and differentiation. The interconnective porous 3D structure is essential for cell ingrowth and vascularization. The printed materials are expected to be designed and fabricated to fit with the structure of patients' bone defects. Traditional modeling methods failed on building such specific structures, whereas 3D printing can produce personalized, tailor-made bone implants loaded with bifunctional components, in particular at desired microstructure entrapped drugs, proteins, and even living cells.

There are also certain issues of currently used 3D printing technology, such as poor biomechanical properties, relatively low resolution for bioplotting, unmatched degradation behavior, burst release of drugs and proteins, and integration of functional components. Future perspectives of the application of this technology are expected to be on the development of more sophistic image analytic tools and computer-aided design, simplified modeling for printing processes, and bioink/material mixture formulations with improved composition to mimic the physiochemical as well as mechanical properties of natural bone.

## References

1. Cornell CN, Lane JM (1992) Newest factors in fracture healing. *Clin Orthop Relat Res* 277:297–311
2. Jahangir AA, Nunley RM, Mehta S, Sharan A (2008) Bone-graft substitutes in orthopaedic surgery. *AAOS Now* 2(1):35–37
3. Langer R, Vacanti JP (1993) Tissue engineering. *Science* 260:920–926
4. Banwart JC, Asher MA, Hassanein RS (1995) Iliac crest bone graft harvest donor site morbidity: a statistical evaluation. *Spine* 20(9):1055–1060
5. Khan MT, Stockley I, Ibbotson C (1998) Allograft bone transplantation: a Sheffield experience. *Ann Roy Coll Surg* 80(2):150
6. Heiple KG, Kendrick RE, Herndon CH, Chase SW (1967) A critical evaluation of processed calf bone. *J Bone Joint Surg Am* 49(6):1119–1127
7. Luo Y, Lode A, Sonntag F et al (2013) Well-ordered biphasic calcium phosphate–alginate scaffolds fabricated by multi-channel 3D plotting under mild conditions. *J Mater Chem B* 1(33):4088–4098
8. Giannoudis PV, Dinopoulos H, Tsiridis E (2005) Bone substitutes: an update. *Injury* 36:S20–S27
9. Finkemeier CG (2002) Bone-grafting and bone-graft substitutes. *J Bone Joint Surg Am* 84(3):454–464
10. Lee G-S, Park J-H, Shin US, Kim H-W (2011) Direct deposited porous scaffolds of calcium phosphate cement with alginate for drug delivery and bone tissue engineering. *Acta Biomater* 7(8):3178–3186
11. Bohner M (2007) Reactivity of calcium phosphate cements. *J Mater Chem* 17(38):3980–3986
12. Brown WE, Chow LC (1986) US Patent No 4,612,053. US Patent and Trademark Office, Washington, DC
13. Chow LC (1991) Development of self-setting calcium phosphate cements. *J Ceram Soc Jpn* 99(10):954–964
14. Chohayeb AA, Chow LC, Tsaknis PJ (1987) Evaluation of calcium phosphate as a root canal sealer-filler material. *J Endod* 13(8):384–387
15. Costantino PD, Friedman CD, Jones K et al (1991) Hydroxyapatite cement: I basic chemistry and histologic properties. *Arch Otolaryngol–Head Neck Surg* 117(4):379–384
16. Friedman CD, Costantino PD, Jones K et al (1991) Hydroxyapatite cement: II obliteration and reconstruction of the cat frontal sinus. *Arch Otolaryngol–Head Neck Surg* 117(4):385–389
17. Miyamoto Y, Ishikawa K, Fukao H et al (1995) In vivo setting behaviour of fast-setting calcium phosphate cement. *Biomaterials* 16(11):855–860
18. Ishikawa K, Takagi S, Chow LC, Ishikawa Y (1995) Properties and mechanisms of fast-setting calcium phosphate cements. *J Mater Sci Mater Med* 6(9):528–533
19. Liu C, Gai W, Pan S, Liu Z (2003) The exothermal behavior in the hydration process of calcium phosphate cement. *Biomaterials* 24(18):2995–3003
20. Liu C, Huang Y, Zheng H (1999) Study of the hydration process of calcium phosphate cement by AC impedance spectroscopy. *J Am Ceram Soc* 82(4):1052–1057
21. Liu C, Shen W, Chen J (1999) Solution property of calcium phosphate cement hardening body. *Mater Chem Phys* 58(1):78–82
22. Martin RB, Chapman MW, Holmes BE et al (1989) Effects of bone ingrowth on the strength and non-invasive assessment of a coralline hydroxyapatite material. *Biomaterials* 10(7):481–488
23. Barralet JE, Grover L, Gaunt T, Wright AJ, Gibson IR (2002) Preparation of macroporous calcium phosphate cement tissue engineering scaffold. *Biomaterials* 23(15):3063–3072
24. Deville S (2008) Freeze-casting of porous ceramics: a review of current achievements and issues. *Adv Eng Mater* 10(3):155–169
25. Hesarak S, Zamanian A, Moztaaradeh F (2008) The influence of the acidic component of the gas-foaming porogen used in preparing an injectable porous calcium phosphate cement

- on its properties: acetic acid versus citric acid. *J Biomed Mater Res Part B: Appl Biomater* 86B(1):208–216
26. Miao X, Hu Y, Liu J, Wong AP (2004) Porous calcium phosphate ceramics prepared by coating polyurethane foams with calcium phosphate cements. *Mater Lett* 58(3):397–402
  27. Huttmacher DW (2000) Scaffolds in tissue engineering bone and cartilage. *Biomaterials* 21(24):2529–2543
  28. Yeong WY, Chua CK, Leong KF, Chandrasekaran M (2004) Rapid prototyping in tissue engineering: challenges and potential. *Trend Biotechnol* 22(12):643–652
  29. Klammert U, Reuther T, Jahn C et al (2009) Cytocompatibility of brushite and monetite cell culture scaffolds made by three-dimensional powder printing. *Acta Biomater* 5(2):727–734
  30. Habibovic P, Gbureck U, Doillon CJ et al (2008) Osteoconduction and osteoinduction of low-temperature 3D printed bioceramic implants. *Biomaterials* 29(7):944–953
  31. Leong KF, Cheah CM, Chua CK (2003) Solid freeform fabrication of three-dimensional scaffolds for engineering replacement tissues and organs. *Biomaterials* 24(13):2363–2378
  32. Tsang VL, Bhatia SN (2004) Three-dimensional tissue fabrication. *Adv Drug Deliver Rev* 56(11):1635–1647
  33. Huttmacher DW, Sittinger M, Risbud MV (2004) Scaffold-based tissue engineering: rationale for computer-aided design and solid free-form fabrication systems. *Trend Biotechnol* 22(7):354–362
  34. Popov VK, Evseev AV, Ivanov AL et al (2004) Laser stereolithography and supercritical fluid processing for custom-designed implant fabrication. *J Mater Sci Mater Med* 15(2):123–128
  35. Tan KH, Chua CK, Leong KF et al (2003) Scaffold development using selective laser sintering of polyetheretherketone–hydroxyapatite biocomposite blends. *Biomaterials* 24(18):3115–3123
  36. Sherwood JK, Riley SL, Palazzolo R et al (2002) A three-dimensional osteochondral composite scaffold for articular cartilage repair. *Biomaterials* 23(24):4739–4751
  37. Ang TH, Sultana FSA, Huttmacher DW et al (2002) Fabrication of 3D chitosan–hydroxyapatite scaffolds using a robotic dispensing system. *Mater Sci Eng C* 20(1):35–42
  38. Trombetta R, Inzana JA, Schwarz EM et al (2017) 3D printing of calcium phosphate ceramics for bone tissue engineering and drug delivery. *Ann Biomed Eng* 45(1):23–44
  39. Maruthappu M, Keogh B (2014) How might 3D printing affect clinical practice? *BMJ* 349:g7709
  40. Wu BM, Borland SW, Giordano RA et al (1996) Solid free-form fabrication of drug delivery devices. *J Control Release* 40(1–2):77–87
  41. Kim SS, Utsunomiya H, Koski JA et al (1998) Survival and function of hepatocytes on a novel three-dimensional synthetic biodegradable polymer scaffold with an intrinsic network of channels. *Ann Surg* 228(1):8–13
  42. da Silva Bartolo PJ, de Lemos ACS, Pereira AMH et al (eds) (2013) High value manufacturing: advanced research in virtual and rapid prototyping: proceedings of the 6th international conference on advanced research in virtual and rapid prototyping. CRC Press, Leiria., 1–5 October
  43. Tumbleston JR, Shirvanyants D, Ermoshkin N et al (2015) Continuous liquid interface production of 3D objects. *Science* 347(6228):1349–1352
  44. Williams JM, Adewunmi A, Schek RM et al (2005) Bone tissue engineering using polycaprolactone scaffolds fabricated via selective laser sintering. *Biomaterials* 26(23):4817–4827
  45. Van der Stok J, Van der Jagt OP, Amin Yavari S et al (2013) Selective laser melting-produced porous titanium scaffolds regenerate bone in critical size cortical bone defects. *J Orthop Res* 31(5):792–799
  46. Xia Y, Zhou P, Cheng X et al (2013) Selective laser sintering fabrication of nano-hydroxyapatite/poly- $\epsilon$ -caprolactone scaffolds for bone tissue engineering applications. *Int J Nanomedicine* 8:4197–4213
  47. Schmidt M, Pohle D, Rechtenwald T (2007) Selective laser sintering of PEEK CIRP. *Ann Manuf Tech* 56(1):205–208

48. Rimell JT, Marquis PM (2000) Selective laser sintering of ultra high molecular weight polyethylene for clinical applications. *J Biomed Mater Res* 53(4):414–420
49. Kang HW, Lee SJ, Ko IK et al (2016) A 3D bioprinting system to produce human-scale tissue constructs with structural integrity. *Nat Biotechnol* 34(3):312–319
50. Wu C, Luo Y, Cuniberti G et al (2011) Three-dimensional printing of hierarchical and tough mesoporous bioactive glass scaffolds with a controllable pore architecture, excellent mechanical strength and mineralization ability. *Acta Biomater* 7(6):2644–2650
51. van der Stok J, Wang H, Amin Yavari S et al (2013) Enhanced bone regeneration of cortical segmental bone defects using porous titanium scaffolds incorporated with colloidal gelatin gels for time-and dose-controlled delivery of dual growth factors. *Tissue Eng Part A* 19(23–24):2605–2614
52. Kanczler JM, Mirmalek-Sani SH, Hanley NA et al (2009) Biocompatibility and osteogenic potential of human fetal femur-derived cells on surface selective laser sintered scaffolds. *Acta Biomater* 5(6):2063–2071
53. Antonov EN, Bagratashvili VN, Whitaker MJ et al (2005) Three-dimensional bioactive and biodegradable scaffolds fabricated by surface-selective laser sintering. *Adv Mater* 17(3):327–330
54. Duan B, Wang M, Zhou WY et al (2010) Three-dimensional nanocomposite scaffolds fabricated via selective laser sintering for bone tissue engineering. *Acta Biomater* 6(12):4495–4505
55. Tan KH, Chua CK, Leong KF et al (2005) Selective laser sintering of biocompatible polymers for applications in tissue engineering. *Biomed Mater Eng* 15(1–2):113–124
56. Wiria FE, Leong KF, Chua CK, Liu Y (2007) Poly- $\epsilon$ -caprolactone/hydroxyapatite for tissue engineering scaffold fabrication via selective laser sintering. *Acta Biomater* 3(1):1–12
57. Simpson RL, Wiria FE, Amis AA et al (2008) Development of a 95/5 poly (L-lactide-co-glycolide)/hydroxyapatite and  $\beta$ -tricalcium phosphate scaffold as bone replacement material via selective laser sintering. *J Biomed Mater Res Part B: Appl Biomater* 84(1):17–25
58. <http://www.lboro.ac.uk/research/amrg/about/the7categoriesofadditivemanufacturing/binderjetting/>
59. Wu C, Fan W, Zhou Y et al (2012) 3D-printing of highly uniform CaSiO<sub>3</sub> ceramic scaffolds: preparation, characterization and in vivo osteogenesis. *J Mater Chem* 22(24):12288–12295
60. Lin L, Huang X, Hu Q, Fang M (2006) Fabrication of tissue engineering scaffolds via rapid prototyping machine. *International Technology and Innovation Conference (ITIC 2006)*, pp 1280–1285
61. Hesarakı S, Sharifi D (2007) Investigation of an effervescent additive as porogenic agent for bone cement macroporosity. *BioMed Mater Eng* 17(1):29–38
62. Tedder ME, Simionescu A, Chen J, et al. (2010) Assembly and testing of stem cell-seeded layered collagen constructs for heart valve tissue engineering. *Tissue Eng Part A* 17(1–2): 25–36
63. Schaefermeier PK, Szymanski D, Weiss F et al (2009) Design and fabrication of three-dimensional scaffolds for tissue engineering of human heart valves. *Eur Surg Res* 42(1):49–53
64. Sodian R, Schaefermeier P, Abegg-Zips S et al (2010) Use of human umbilical cord blood-derived progenitor cells for tissue-engineered heart valves. *Ann Thorac Surg* 89(3):819–828
65. Mano JF, Sousa RA, Boesel LF et al (2004) Bioinert, biodegradable and injectable polymeric matrix composites for hard tissue replacement: state of the art and recent developments. *Compos Sci Technol* 64(6):789–817
66. Ratner BD, Hoffman AS, Schoen FJ, Lemons JE (2006) Biomaterials science: an introduction to materials in medicine. *MRS Bull*:31–59
67. Kumar MNVR (2000) Nano and microparticles as controlled drug delivery devices. *J Pharm Pharm Sci* 3(2):234–258
68. Gollwitzer H, Thomas P, Diehl P et al (2005) Biomechanical and allergological characteristics of a biodegradable poly (D, L-lactic acid) coating for orthopaedic implants. *J Orthop Res* 23(4):802–809
69. Gbureck U, Hölzel T, Klammert U et al (2007) Resorbable dicalcium phosphate bone substitutes prepared by 3D powder printing. *Adv Funct Mater* 17(18):3940–3945

70. Gbureck U, Vorndran E, Barralet JE (2008) Modeling vancomycin release kinetics from microporous calcium phosphate ceramics comparing static and dynamic immersion conditions. *Acta Biomater* 4(5):1480–1486
71. Sellers RS, Peluso D, Morris EA (1997) The effect of recombinant human bone morphogenetic protein-2 (rhBMP-2) on the healing of full-thickness defects of articular cartilage. *J Bone Joint Surg Am* 79(10):1452–1463
72. Sellers RS, Zhang R, Glasson SS et al (2000) Repair of articular cartilage defects one year after treatment with recombinant human bone morphogenetic protein-2 (rhBMP-2). *J Bone Joint Surg Am* 82(2):151–160
73. Liu H, Peng H, Wu Y et al (2013) The promotion of bone regeneration by nanofibrous hydroxyapatite/chitosan scaffolds by effects on integrin-BMP/Smad signaling pathway in BMSCs. *Biomaterials* 34(18):4404–4417
74. Street J, Bao M, Bunting S et al (2002) Vascular endothelial growth factor stimulates bone repair by promoting angiogenesis and bone turnover. *Proc Natl Acad Sci* 99(15):9656–9661
75. Poldervaart MT, Wang H, van der Stok J, Weinans H, Leeuwenburgh SC, Öner FC, Alblas J (2013) Sustained release of BMP-2 in bioprinted alginate for osteogenicity in mice and rats. *PLoS One* 8(8):e72610
76. Inzana JA, Trombetta RP, Schwarz EM et al (2015) 3D printed bioceramics for dual antibiotic delivery to treat implant-associated bone infection. *Eur Cells Mater* 30:232–247
77. Gao G, Schilling AF, Yonezawa T et al (2014) Bioactive nanoparticles stimulate bone tissue formation in bioprinted three-dimensional scaffold and human mesenchymal stem cells. *Biotechnol J* 9:1304–1311
78. Luo Y, Wu C, Lode A, Gelinsky M (2012) Hierarchical mesoporous bioactive glass/alginate composite scaffolds fabricated by three-dimensional plotting for bone tissue engineering. *Biofabrication* 5(1):015005
79. Sobral JM, Caridade SG, Sousa RA et al (2011) Three-dimensional plotted scaffolds with controlled pore size gradients: effect of scaffold geometry on mechanical performance and cell seeding efficiency. *Acta Biomater* 7(3):1009–1018
80. Detsch R, Uhl F, Deisinger U, Ziegler G (2008) 3D-Cultivation of bone marrow stromal cells on hydroxyapatite scaffolds fabricated by dispense-plotting and negative mould technique. *J Mater Sci Mater Med* 19(4):1491–1496
81. Wu C, Luo Y, Cuniberti G et al (2011) Three-dimensional printing of hierarchical and tough mesoporous bioactive glass scaffolds with a controllable pore architecture, excellent mechanical strength and mineralization ability. *Acta Biomater* 7(6):2644–2650
82. Serra T, Planell JA, Navarro M (2013) High-resolution PLA-based composite scaffolds via 3-D printing technology. *Acta Biomater* 9(3):5521–5530
83. Seyednejad H, Gawlitta D, Kuiper RV et al (2012) In vivo biocompatibility and biodegradation of 3D-printed porous scaffolds based on a hydroxyl-functionalized poly ( $\epsilon$ -caprolactone). *Biomaterials* 33(17):4309–4318
84. Catros S, Fricain JC, Guillotin B et al (2011) Laser-assisted bioprinting for creating on-demand patterns of human osteoprogenitor cells and nano-hydroxyapatite. *Biofabrication* 3(2):025001
85. Doraiswamy A, Narayan RJ, Harris ML et al (2007) Laser microfabrication of hydroxyapatite-osteoblast-like cell composites. *J Biomed Mater Res Part A* 80(3):635–643
86. Harris ML, Doraiswamy A, Narayan RJ et al (2008) Recent progress in CAD/CAM laser direct-writing of biomaterials. *Mater Sci Eng C* 28(3):359–365
87. Guillotin B, Souquet A, Catros S et al (2010) Laser assisted bioprinting of engineered tissue with high cell density and microscale organization. *Biomaterials* 31(28):7250–7256
88. Pereira TF, Silva MAC, Oliveira MF et al (2012) Effect of process parameters on the properties of selective laser sintered poly (3-hydroxybutyrate) scaffolds for bone tissue engineering: this paper analyzes how laser scan spacing and powder layer thickness affect the morphology and mechanical properties of SLS-made scaffolds by using a volume energy density function. *Virt Phys Prototyp* 7(4):275–285



89. Shuai C, Gao C, Nie Y et al (2011) Structure and properties of nano-hydroxyapatite scaffolds for bone tissue engineering with aselective laser sintering system. *Nanotechnology* 22(28):285703
90. Lan PX, Lee JW, Seol YJ, Cho DW (2009) Development of 3D PPF/DEF scaffolds using micro-stereolithography and surface modification. *J Mater Sci Mater Med* 20(1):271–279
91. Lee JW, Ahn G, Kim DS, Cho DW (2009) Development of nano-and microscale composite 3D scaffolds using PPF/DEF-HA and micro-stereolithography. *Microelectron Eng* 86(4):1465–1467
92. Ronca A, Ambrosio L, Grijpma DW (2013) Preparation of designed poly (D, L-lactide)/nanosized hydroxyapatite composite structures by stereolithography. *Acta Biomater* 9(4):5989–5996
93. Bose S, Vahabzadeh S, Bandyopadhyay A (2013) Bone tissue engineering using 3D printing. *Mater Today* 16(12):496–504
94. Kalita SJ, Bose S, Hosick HL, Bandyopadhyay A (2003) Development of controlled porosity polymer-ceramic composite scaffolds via fused deposition modeling. *Mater Sci Eng C* 23(5):611–620
95. Lam CX, Savalani MM, Teoh SH, Huttmacher DW (2008) Dynamics of in vitro polymer degradation of polycaprolactone-based scaffolds: accelerated versus simulated physiological conditions. *Biomed Mater* 3(3):034108
96. Lam CX, Teoh SH, Huttmacher DW (2007) Comparison of the degradation of polycaprolactone and polycaprolactone-( $\beta$ -tricalcium phosphate) scaffolds in alkaline medium. *Polym Inter* 56(6):718–728
97. Schantz JT, Huttmacher DW, Lam CXF et al (2003) Repair of calvarial defects with customised tissue-engineered bone grafts II evaluation of cellular efficiency and efficacy in vivo. *Tissue Eng* 9(4, Supplement 1):127–139
98. Lam CX, Huttmacher DW, Schantz JT et al (2009) Evaluation of polycaprolactone scaffold degradation for 6 months in vitro and in vivo. *J Biomed Mater Res Part A* 90(3):906–919
99. Russias J, Saiz E, Deville S et al (2007) Fabrication and in vitro characterization of three-dimensional organic/inorganic scaffolds by robocasting. *J Biomed Mater Res Part A* 83(2):434–445
100. Zeltinger J, Sherwood JK, Graham DA et al (2001) Effect of pore size and void fraction on cellular adhesion, proliferation, and matrix deposition. *Tissue Eng* 7:557–572
101. Frakes DH, Smith MJ, Parks J et al (2005) New techniques for the reconstruction of complex vascular anatomies from MRI images. *J Cardiovasc Magn Reson* 7:425–432
102. Chung H, Das S (2008) Functionally graded Nylon-11/silica nanocomposites produced by selective laser sintering. *Mater Sci Eng A* 487:251–257
103. Castilho M, Moseke C, Ewald A et al (2014) Direct 3D powder printing of biphasic calcium phosphate scaffolds for substitution of complex bone defects. *Biofabrication* 6:015006
104. Li C, Gao L, Chen F, Liu C (2015) Fabrication of mesoporous calcium silicate/calcium phosphate cement scaffolds with high mechanical strength based on rapid prototyping. *J Mater Sci* 50:7182–7191
105. Castilho M, Rodrigues J, Pires I et al (2015) Fabrication of individual alginate-TCP scaffolds for bone tissue engineering by means of powder printing. *Biofabrication* 7:015004
106. Igawa K, Mochizuki M, Sugimori O et al (2006) Tailor-made tricalcium phosphate bone implant directly fabricated by a three-dimensional ink-jet printer. *J Artif Organs* 9:234–240
107. El-Ghannam A, Hart A, White D, Cunningham L (2013) Mechanical properties and cytotoxicity of a resorbable bioactive implant prepared by rapid prototyping technique. *J Biomed Mater Res A* 101:2851–2861
108. Li C, Jiang C, Deng Y et al (2017) RhBMP-2 loaded 3D-printed mesoporous silica/calcium phosphate cement porous scaffolds with enhanced vascularization and osteogenesis properties. *Sci Rep* 7:41331
109. Inzana JA, Trombetta RP, Schwarz EM et al (2015) 3D printed bioceramics for dual antibiotic delivery to treat implant-associated bone infection. *Eur Cell Mater* 30:232–247

110. Akkineni AR, Luo Y, Schumacher M et al (2015) 3D plotting of growth factor loaded calcium phosphate cement scaffolds. *Acta Biomater* 27:264–274
111. Kim GH, Son JG (2009) 3D polycaprolactone (PCL) scaffold with hierarchical structure fabricated by a piezoelectric transducer (PZT) -assisted bioplotter. *Appl Phys A* 94: 781–785
112. <http://www.wakehealth.edu/WFIRM/>
113. Ozbolat I, Hospodiuk M (2016) Current advances and future perspectives in extrusion-based bioprinting. *Biomaterials* 76:321–343
114. Ozbolat IT, Chen H, Yu Y (2014) Development of “Multi-arm Bioprinter” for hybrid biofabrication of tissue engineering constructs. *Robot Comput Integr Manuf* 30:295–304
115. Hellera M, Bauerb HK, Goetzec E et al (2016) Materials and scaffolds in medical 3D printing and bioprinting in the context of bone regeneration. *Int J Comput Dent* 19(4):301–321
116. <http://www.economist.com/node/15543683>

# Chapter 14

## Preparation of Collagen/Calcium Phosphate Coatings and Evaluation of Their Biological Performances

Cheng Kui, Jun Lin, and Wenjian Weng

**Abstract** Collagen/calcium phosphate nanocomposite coating similar to the natural bone structure is a promising material in surface modification of metallic implants to accelerate the osseointegration. In this chapter, electrochemical deposition was utilized to prepare collagen/calcium phosphate coating on titanium substrates successfully. A modified method called alternating potential-assisted electrochemical deposition (AP-ECD) was further proposed to modulate coating microstructures, making it possible to effectively achieve a controlled preparation of the collagen/calcium phosphate coating for different purposes. In vitro tests demonstrated that the desired cytocompatibility, loading/release behavior, and antibacterial property of the coatings were realized, intensifying its biological role as differentiation inducer and promoting the osteogenic differentiation. In vivo tests further confirmed that the implant with the collagen/calcium phosphate coatings showed higher new bone density and pull out strength, and the significantly accelerated osseointegration was realized. The AP-ECD method could provide a basis for function design and controlled preparation of collagen/calcium phosphate composite coatings, favoring for different biological applications.

**Keywords** Collagen/calcium phosphate • Nanocomposite coating • Electrochemical deposition • Osteogenic differentiation • Osseointegration

---

C. Kui • J. Lin • W. Weng (✉)

School of Materials Science and Engineering, Zhejiang University, Hangzhou 310027, China  
e-mail: [wengwj@zju.edu.cn](mailto:wengwj@zju.edu.cn)

© Springer Nature Singapore Pte Ltd. 2018

C. Liu, H. He (eds.), *Developments and Applications of Calcium Phosphate Bone Cements*, Springer Series in Biomaterials Science and Engineering 9,  
DOI 10.1007/978-981-10-5975-9\_14

547

## 14.1 Introduction

### 14.1.1 *Surface Modification of Metallic Implants*

The increasing number of cases of hard tissue replacements and repair due to bone lesions and damages make it necessary to seek suitable biomaterials. Initial research focused on the substitute biomaterials required to bear and transfer the load. Medical metals such as stainless steel, Co-base alloys, and titanium alloys are the most widely applied replacement materials in the clinical surgery because of their good mechanical properties and resistance performance. Among these metals, titanium and its alloys have relatively low modulus; good fatigue strength, formability, machinability, and corrosion resistance; as well as good biocompatibility; they are widely used in biomedical devices and components, especially as hard tissue replacements.

However, the “native” surface of titanium is bio-inert, which is clearly not appropriate for osseointegration. Since the biomaterial surface plays an extremely important role in the response of the biological environment to the artificial implants, surface modifications are often required for better biological integration. The methods of surface modifications are classified into chemical and physical methods according to the formation mechanism of the modified layers on the material surface.

The physical modification refers to the changes of surface properties, such as surface morphology, microstructure, roughness, and so on. The surface roughness is one of the principle factors that has influence on the biological effects of biomaterials. Rough surface with large specific surface area is able to promote cell adhesion, to enhance the bonding strength between implants and host bone. Nanoscale surface roughness with higher surface energy accelerates protein adsorption, cell proliferation, and differentiation and finally improves the osseointegration ability of biomaterials. Blasting, plasma spraying, acid etching, and anodic oxidation are the common methods to change the surface roughness. However, changing the roughness of titanium is often accompanied by the changes in the chemical composition of the surface, forming a new structure.

Constructing micro-/nanostructures such as TiO<sub>2</sub> nanodots and nanorods on the titanium implant surface is a research hotspot of titanium surface modification nowadays, which can regulate the microenvironment around the implants, make the osteoblasts interact with more sites, and facilitate their attachment and proliferation. Puckett et al. [1] prepared TiO<sub>2</sub> with different nanostructures and sizes by anodic oxidation on the surface of titanium and found that these micro-/nanostructured surfaces could not only promote adsorption and proliferation of osteoblasts but also had the ability to kill bacteria, which provided a good way for titanium surface modification.

Chemical modification refers to preparation of bioactive coatings on the implants by some technologies, such as sol-gel and electrochemical deposition, which accelerate osseointegration between implants and host bone. Inorganic coatings, organic

coatings, and composite coatings of inorganic and organic polymer are often applied in the surface modification of implants. Calcium phosphate is the primary inorganic component in the hard tissue of the human body, and calcium phosphate bioceramics coatings are proven to promote osseointegration very well because of its good biological activity and biocompatibility. Pan et al. [2] prepared a CaP coating on the metallic implant by micro-arc oxidation in the solution containing Ca and P. When immersed in the SBF, the implant with CaP coating further formed needlelike or spherical CaP again compared to the implant without coating on its surface, which revealed that the bioactivity was enhanced by preparing a CaP coating on the implant surface. In addition, bioglass and bioceramics with CaO-SiO<sub>2</sub> as the main component also raised extensive attention. Bioglass and bioceramics react with the body fluid and tissue around the implant, forming the Si-OH groups that are conceived to nucleation and growth of calcium phosphate, and cells will respond to the released silicon ions, promoting osseointegration.

Although the abovementioned inorganic coatings are bioactive, they still have limits, such as low toughness and lack of communication with cells, which greatly restrict the application of inorganic coating.

In the process of contact between osteoblasts and implant, cells will selectively communicate with extracellular substances through the receptors on the membranes, further activate a series of physiological and biochemical reactions intracellularly, and finally accomplish osseointegration. In recent years, surface modification researches increasingly focus on the relationship between the surface substances of implants and signal pathways of osteocytes. Receptors on the surface of undifferentiated pre-osteoblasts are capable of recognizing and selectively binding to signaling molecules. When combined with a ligand, signaling molecules convert the extracellular signal into intracellular chemical and physical signal-by-signal transduction, followed by synthesis of osteoblast-associated proteins, and finally pre-osteoblasts differentiate into osteoblasts.

Bioactive macromolecules can provide pre-osteoblasts with the corresponding signal substances and can be divided into growth factor and cell adhesion molecules. Growth factors include bone morphogenetic protein (BMP-2), transforming growth factor, fibroblast growth factor, etc. For promoting cell proliferation and differentiation, they play an important role in the osteogenesis process. Cell adhesion molecules include fibronectin, osteopontin, and vitronectin, containing arginine, glycine, and aspartic acid (RGD) sequences, which regulate cells, serum, and extracellular matrix protein adhesion on the surface of implants. To accelerate the required biological reaction process, titanium modification needs to realize the specifically adsorption of beneficial proteins. Hence, a typical surface biochemical modification strategy is to immobilize specific proteins, enzymes, or polypeptides onto the surfaces of titanium implants with micro-/nanostructures to induce specific cell differentiation and tissue transformation. Compared to other modification methods, this approach focuses on the application of the biologically active macromolecules, the decisive organic components of bone formation, to control tissue response, because bone integration is primarily dependent on the adhesion, proliferation, and differentiation of osteoblasts to promote new bone formation.

Therefore, to accelerate the integration of the implant with the host bone, the bioactive coating on the implant surface needs to provide the corresponding signaling molecules besides the conditions required for the proliferation and adhesion of osteoblasts, so the protein synthesis related to osteoblast differentiation can be promoted, and ultimately the growth of new bone to complete the process of osseointegration is accelerated.

### ***14.1.2 The Function of Extracellular Matrix (ECM)***

The primary microenvironment that cells connect with is extracellular matrix (ECM). ECM plays a key role in the induction and promotion of bone growth, and its main components are collagen, fibronectin, laminin, elastin, aminoglycan, and proteoglycan. ECM is not only the framework surrounding cells but also regulates cell morphology, growth, division, differentiation, and apoptosis by changing its three-dimensional structure and composition.

The ECM of bone tissue is composed of one-third of the organic and two-thirds of inorganic substances, and collagen I is accounted for 80–90% of organic substance, which is crucial to maintain integrity of bone structure and its biomechanical properties. The three-dimensional network structure of collagen fibers, as the scaffold of bone growth, provides a natural three-dimensional space for cell proliferation, differentiation, and bone formation in bone healing process. As the main component of bone, type I collagen, which contains a variety of molecular amino acid residues that are crucial for the cell adhesion, is an ideal active substance that carries and transmits biological signals [3] by combining with other signal molecules, which can effectively promote cell adhesion, proliferation, and differentiation. Meanwhile, because of its high porosity, excellent hydrophilicity, low immunogenicity, and easy absorption by the human body, collagen I is considered as a good biomaterial. Therefore, how to introduce collagen onto the implant surface to create imitational extracellular matrix environment has been widespread concerned.

### ***14.1.3 Grafting of Collagen on the Surface of Metallic Materials***

The study of imitational extracellular matrix coatings on the surface of implants focuses on how to graft the collagen onto the surface of metal implants in order to obtain better cell compatibility and cell responsiveness and ultimately accelerate bone integration. There are a few ways to introduce collagen onto the surface of metal implants, which can be divided into physical and chemical methods. Because of the denaturation of collagen, the usual physical introduction of collagen is

essentially physical adsorption. Stefan Rammelt et al. [4] centrifuged and sedimented the collagen solution, then the titanium rod was placed in the precipitate for 15 min, and then a collagen layer in 3–6  $\mu\text{g}/\text{cm}^2$  was formed on the titanium rod. Four days after implantation into the mice, better proliferation of osteoblasts was found on the surface of the implanted collagen-coated implant compared with the titanium implant without the collagen coating; after 4 and 7 days of implantation, a larger number of osteoblasts were observed around the coating. The BIC (bone-to-implant contact) value of a group with collagen coating increased significantly after 4 weeks of implantation compared with the group without the collagen layer, and the results of micro-CT showed a collagen-coated group had a higher bone density.

Organic grafting and inorganic grafting are the conventional chemical methods. Organic grafting methods include sol-gel method, electrostatic adsorption method, and so on. Stefan Rammelt et al. [5] prepared a pure collagen coating on the titanium implant surface by sol-gel method and implanted it into mice. Four weeks after implantation, there were more nascent bone structures around the implanted collagen-coated implants than titanium implants, with higher BIC values for the implant and the host bone, resulting in faster bone integration. Morra et al. [6] first introduced a layer of hydrocarbon onto the surface of the titanium implant by plasma spraying, followed by introducing a layer of acrylic acid. Finally, the collagen was immobilized onto the surface of the titanium by electrostatic coupling with a pore size of 1–2  $\mu\text{m}$ . Bone marrow mesenchymal stem cells' (BMSCs) culture results indicated that the collagen coating promoted adhesion and proliferation of BMSCs. The collagen-coated samples were implanted into the fibula of New Zealand white rabbits for 4 weeks. It was found that the collagen-coated implants showed a higher BIC value.

However, neither the physical method nor the organic grafting in the chemical method can construct a similar structure to the human bone tissue on the implant surface. Since bone is composed of collagen fibers and hydroxyapatite (HA) in a form of mineralized collagen composition, a mineralized collagen or HA/collagen composite coating is suggested as a feasible method to introduce collagen onto the implant surface.

The main methods of preparing HA/collagen composite coatings are spray coating, bionic deposition, sol-gel, electrochemical deposition, etc. Jonge et al. [7] obtained HA/collagen coating on the Ti substrate by electrostatic spraying deposition. The coating had strong adhesion strength with the substrate, and the thickness of the coating could be adjusted by controlling the electrostatic spraying time. The results showed that the coating could significantly improve the osteoblast differentiation on the implant surface. Cai et al. [8] prepared apatite/collagen fiber coating using biomimetic deposition by immersing the NiTi shape memory alloy in collagen-contained SBF solution for 3–7 days. Manara et al. [9] prepared HA/collagen coating and carbonate-apatite/collagen coating on the surface of titanium substrate by electrochemical deposition. Good biological activity was proved by comparing the binding strength between the coating and fibronectin. Wang et al. [10] prepared HA/collagen coating on the surface of titanium with  $\text{TiO}_2$  bioactive

layer on it, and TiO<sub>2</sub> bioactive layer can effectively promote the formation of HA/collagen coating. In vitro study showed good biological activity. Above results indicated that the HA/collagen coating on the surface of metal implants confers rich biological signals on the surface of metal implants and improves the bioactivity significantly, which induces and promotes bone tissue growth.

## 14.2 Controllable Preparation of Collagen/Calcium Phosphate Coating with Electrochemical Deposition

Because of the instability of collagen, a lot of coating technologies cannot be applied to the preparation of mineralized collagen coating. At present, the modest deposition of collagen and calcium phosphate coating methods include electrochemical deposition [10], spin coating [11], and bionic deposition [12]. Electrochemical deposition generally includes two types, electrophoretic deposition and electrolytic deposition. The preparation process of calcium phosphate/collagen composite coating combines the electrophoretic deposition of collagen molecules and the electrolytic deposition of calcium phosphate. Substrate conductivity is only required in this method for preparation of mineralized collagen coating, without strict control of the substrate surface biological activity, solution supersaturation, or pre-calcium phosphate particles. The preparation process is efficient with simple equipment and operation and takes generally only 10 min to an hour for a more uniform coating. At the same time, since a small pH gradient is generated around the cathode during the electrolytic deposition, it is possible to achieve a high pH near the metal substrate while keeping the bulk pH of the solution small, which is advantageous for co-deposition of the biomolecule (such as collagen, chitosan) that dissolves only at low pH and calcium phosphate crystal that nucleates and precipitates at high pH. Therefore, the electrochemical deposition is a very efficient method for preparing mineralized collagen coating. Researches showed that the mineralized collagen coating prepared by this method has good biocompatibility, which could promote cell adhesion, proliferation, and differentiation and induce new bone formation.

The microstructure and composition of the implant surface have a very significant effect on cell adhesion and tissue formation [13]. Therefore, in order to further optimize the biological response of the mineralized collagen coating, it is necessary to realize the controllable preparation of the coating. Studies have shown that certain surface porosity and roughness of the implants assist the new bone tissue to grow into the surface of the implant, facilitating the osseointegration process at the implant/host tissue interface [14]. The chemical composition of the surface also has important implications for protein adsorption, cell adhesion, and proliferation during osseointegration. As to mineralized collagen coating, the surface morphology and chemical composition will be changed by the different preparation methods and preparation parameters, thus affecting the biological effects of coating. For example, the degree of mineralization of the coating is directly related to the relative ratio



of collagen and calcium phosphate, which is present in a variety of different phases that have different biological responsiveness.

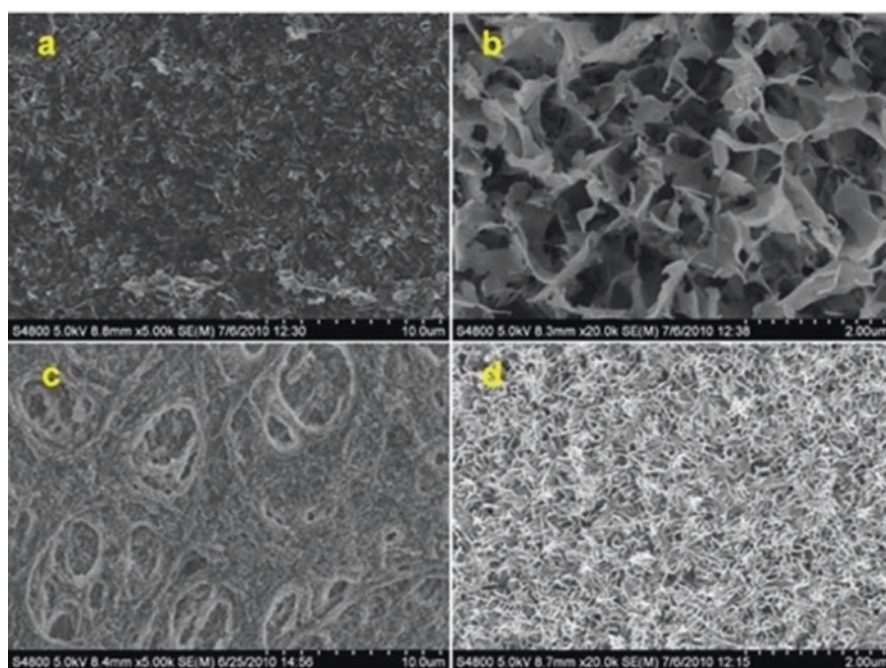
In addition to the high biological responsiveness of the implant coating, it is necessary to have favorable drug/growth factor loading and release capacity, and growth factors (such as BMP) promote cell differentiation by sustained release; sustained release of drugs (antimicrobial drugs) is to eliminate biological interference (such as fungi) during the bone formation, with the aim of establishing an excellent biological environment, promoting bone formation, thereby speeding up the process of osseointegration. Biological coatings, due to their thin and porous properties, limit the loading ability of drug and present burst release in spite of high biological responsiveness. There are a number of reasons for the poor performance of thin-layer materials to carry and release drugs/growth factors, but they can be divided into two main aspects: (1) limited spatial distribution and single diffusion path of the drug/growth factor during the release process and (2) poor affinity of the coatings for the drug/growth factor. At present, the ways to optimize the loading/release capability of coatings are as follows: (1) improving the distribution of drugs/growth factors in the coatings, which requires a highly controllable fabrication technique and a suitable micro-/nanostructure of the coating and (2) enhancing the affinity of the coating for the drugs/growth factor, which reduces their diffusion rate. For thin coatings, enhancing the affinity of the coating for the drug/growth factor and loading the nano-sized drug/growth factor carrier into the coating will be excellent choices. Therefore, it is a key scientific and technical problem how to realize the controllable preparation of micro-/nanostructure of mineralized collagen and the controllable loading of drug/growth factor carrier, thus archiving controlled distribution of drug/growth factor and maximizing the bio-efficiency of coatings in accelerating osseointegration.

Depending on the parameters, the electrochemical deposition can be carried out under constant voltage or constant current conditions. Electrochemical deposition parameters include environmental factors (temperature, humidity, etc.), the value of current and voltage, and electrolyte composition (pH, ion concentration, additives, etc.). The crystal phase, morphology, and composition of the coating can be adjusted by controlling the parameters to achieve controllable preparation. For example, altering voltage can significantly adjust pore size and mineralization degree of collagen in the network structure, and programmed application of voltage can control the deposition of different constituents. These changes in microstructure and composition will affect the ability of inducing bone formation and drug release behavior of the coatings.

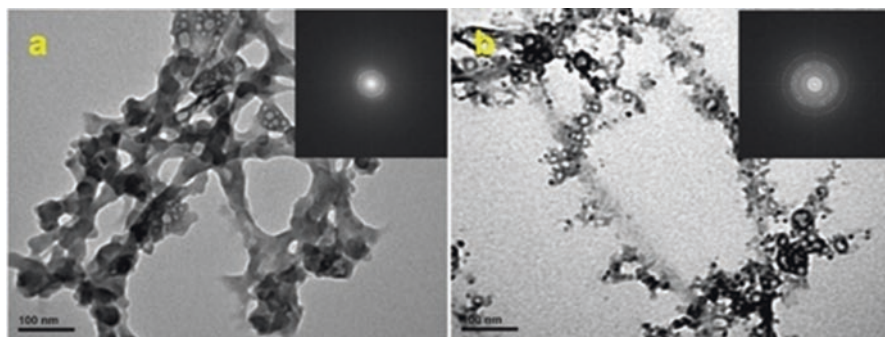
## 14.2.1 Mechanism of Electrochemical Deposition

### 14.2.1.1 Mechanism of Constant Potential Electrochemical Deposition (ECD)

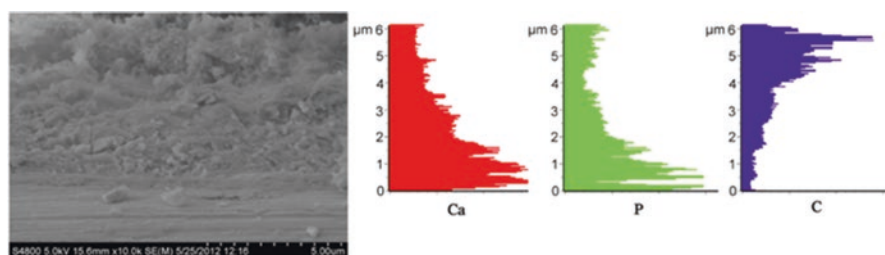
To reveal the microstructure of the porous mineralized collagen coating, it was torn off from the titanium substrate, and the peeled coating and the remaining coating on the titanium substrate were observed (Fig. 14.1) [15]. For the dense coating, the layer near the titanium substrate after stripping still had dense morphology, and compared with the outermost layer, collagen bundles were more unapparent in this layer. The residual layer on the titanium substrate was a calcium phosphate layer. For the porous coating, the peeling surface still had a porous structure with high mineralization degree of collagen near the bottom layer. Residual calcium phosphate on titanium substrate had smaller grain size, which indicated faster deposition rate of calcium phosphate, and mineralized collagen might combine with the substrate by the mineralized bonding between underlying calcium phosphate layer and the mineral on the collagen bundles.



**Fig. 14.1** Dense and porous coating morphology. (a) The reverse side of stripping layer of dense coating, (b) the residual layer of dense coating. (c) the reverse side of stripping layer of porous coating, (d) the residual layer of porous coating (Reprinted from Ref. [15], with kind permission from Springer)



**Fig. 14.2** TEM images of dense (a) and porous (b) coatings

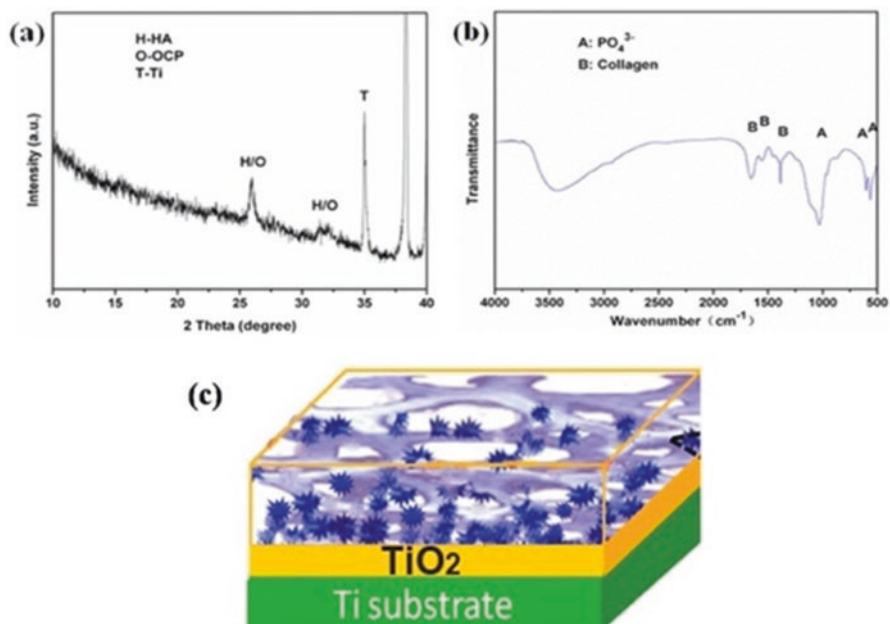


**Fig. 14.3** The cross-section morphology of mineralized collagen coating and the corresponding energy spectrum analysis

Two types of coatings were observed by TEM to study the differences in the mineralization of collagen fibers. Figure 14.2 showed the TEM and SAED images for dense and porous coatings. Dense coating showed low mineralization degree, close combination of collagen, and less nucleation of calcium phosphate on the collagen fibers with weak diffraction peak of calcium phosphate on the electron diffraction pattern, while the mineralization degree of collagen in the porous coating was higher, which was accompanied with obvious calcium phosphate diffraction peaks and single mineralized collagen fibers. Calcium phosphate particles could be seen on the surface of collagen fibers with distinct macroscopic porous structure.

After electrodeposition, the cross section of the coating was characterized by EDS, and the compositional distribution of the coating in the longitudinal direction was obtained (shown in Fig. 14.3). The mineralized collagen coating formed by electrochemical deposition was composed of calcium phosphate and collagen (Fig. 14.4). The bottom layer contained a large amount of calcium and phosphorus, mainly calcium phosphate. The carbon content was relatively large in the mineralized collagen layer, and the relative content of collagen and calcium phosphate presented a gradient distribution.

According to the synthesis and characteristics of mineralized collagen coating, the structure of the coating obtained by electrochemical deposition on a titanium substrate was shown in Fig. 14.4c. The coating consisted of a layer of calcium



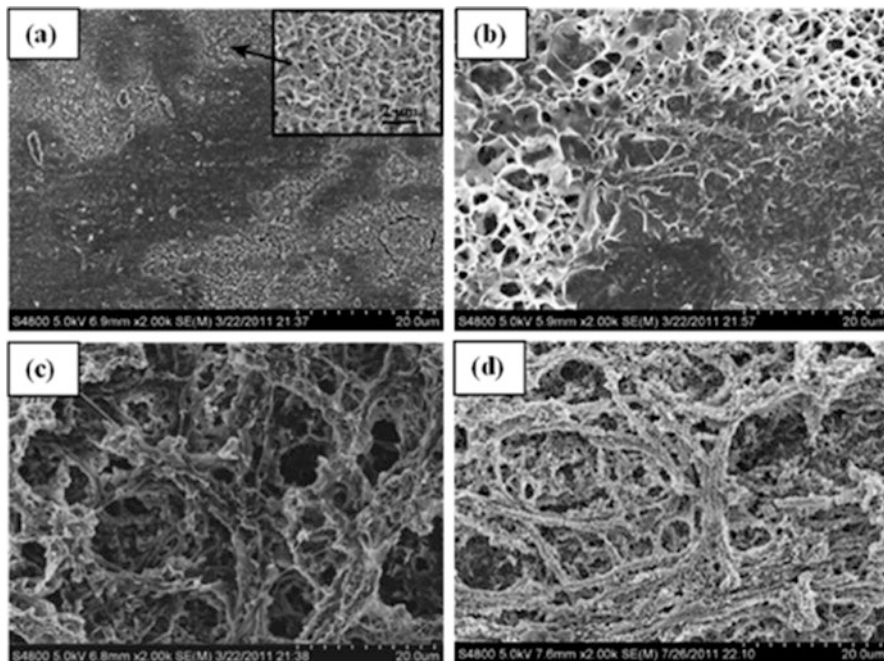
**Fig. 14.4** (a) XRD pattern, (b) FTIR pattern, (c) schematic diagram of the mineralized collagen coating

phosphate in close contact with the titanium substrate and mineralized collagen layer that connected with calcium phosphate layer. The distribution of elements in the mineralized collagen layer showed a certain mineralization gradient. From the calcium phosphate layer to the surface of the coating, the mineralization was weakened, and the content of calcium phosphate gradually reduced with organic substance content gradually increased.

Figure 14.5 showed the morphologies of the coatings deposited on the Ti substrates with different deposition times [16]. In the early ECD period, CaP crystals first nucleated and grew on the cathode, and few collagen fibers had attached to the cathode (Fig. 14.5a, b). As the deposition continued, collagen fibers with a few CaP crystals, which were weakly mineralized collagen, were deposited on the substrates (Fig. 14.5c), and then the collagen was gradually wrapped by calcium phosphate with the final diameter of 1–2  $\mu\text{m}$  (Fig. 14.5d).

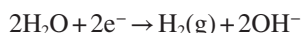
The morphologies (Fig. 14.6) of collagen localized to the cathode in the electrolyte at different deposition times demonstrated that the collagen had self-assembled into interconnected fibers (with an average diameter of 200–400 nm) or sheets (Fig. 14.6a, b), and the mineralization characteristic appeared as the deposition time increased (Fig. 14.6c).

Based on the above experimental results, an ECD process for mineralized coating preparation is proposed to have five steps: initial CaP deposition (Fig. 14.7a), collagen fibril self-assembly (Fig. 14.7b) and mineralization (Fig. 14.7c) near the cathode, mineralized collagen deposition (Fig. 14.7d), and post-growth of mineral-

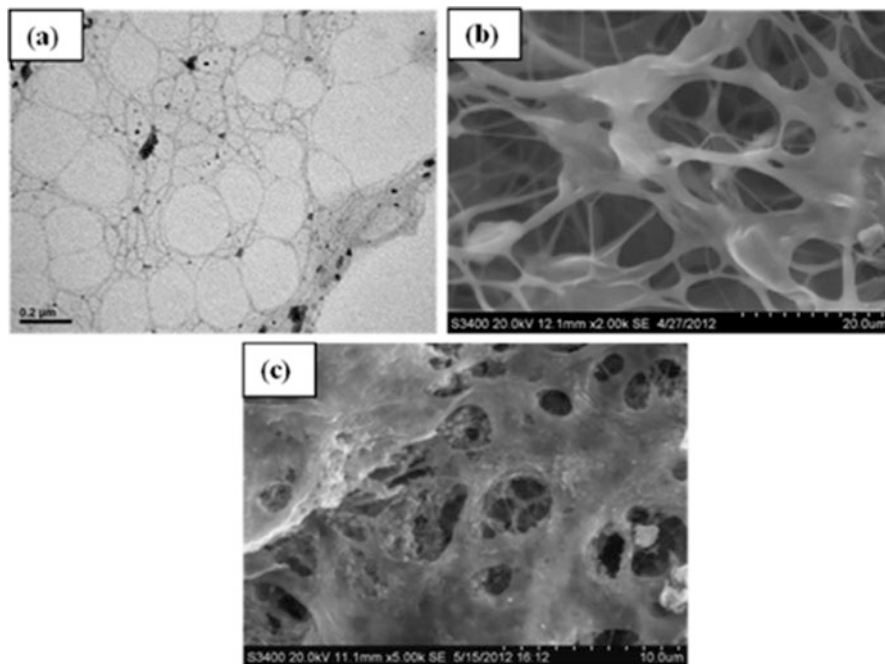


**Fig. 14.5** SEM images of coatings deposited on the Ti substrates for (a) 1 min, (b) 5 min, (c) 30 min, (d) 60 min (Reprinted from Ref. [16], with kind permission from Springer [16])

ized collagen in the coating (Fig. 14.7e). When an electric field is activated, the pH local to the cathode increases due to  $\text{OH}^-$  generation according to the following electrolytic reaction:



A pH gradient is spontaneously produced near the cathode. CaP crystals are easy to nucleate and grow on the cathode due to their high sensitivity to increases in pH, and the initial CaP deposition is shown in Fig. 14.7a. Collagen fibrils are originally positively charged in the electrolyte with pH 4.5 and are driven toward the cathode. The collagen fibrils adjacent to the cathode begin to self-assemble into fibers or sheets (Fig. 14.7b) due to the isoelectric point [15] that resulted from the pH increase. Since the negatively charged carboxylate groups of collagen serve as key nucleation sites for CaP crystals, the high pH near the cathode leads to the mineralization in the collagen fibers or sheets (Fig. 14.7c). Subsequently, the deposition of the mineralized collagen fibers or sheets onto the cathode (Fig. 14.7d) takes place under the electrical field. It is suggested that CaP in the mineralized collagen after deposition continues to grow due to the existence of Ca and phosphate ions as well as the appropriate pH value. This post-growth results in the connection of as-deposited collagen with the bottom CaP layer or other mineralized collagens, forming a well-constructed coating (Fig. 14.7e).



**Fig. 14.6** Morphologies of collagen fibrils near the cathode from the electrolyte after electric field activation. (a) 0 min, TEM image of the collagen fibrils as a raw material. (b), (c) SEM images of the collagen fibrils of the coatings after 1 min and 5 min, respectively (Reprinted from Ref. [16], with kind permission from Springer)

#### 14.2.1.2 Mechanism of Alternating Potential-Assisted Electrochemical Deposition (AP-ECD)

Figure 14.8 revealed that the degree of mineralization (Fig. 14.8a-1) of the coating was higher when the last stage deposition potential was negative (Fig. 14.8a-2) [17]. This showed that positive potential was conducive to reducing the degree of mineralization coating. It was also found that the surface porosity decreased with the increase of positive potential time (Fig. 14.8b), which indicated that combining negative potential deposition with positive potential effectively reduced the porosity of the coating surface as well as the degree of mineralization of the coating as a whole.

Figure 14.9 showed the surface morphology of the coating at each deposition stage. It revealed that the weakly mineralized collagen layer was deposited on the calcium phosphate coating after the first positive potential application (Fig. 14.9a) followed by the highly mineralized collagen depositing after applying negative potential (Fig. 14.9b). When the positive potential was applied again, the weakly mineralized collagen layer deposited again, and the subsequent negative potential resulted in highly mineralized collagen layer deposits (Fig. 14.9c).

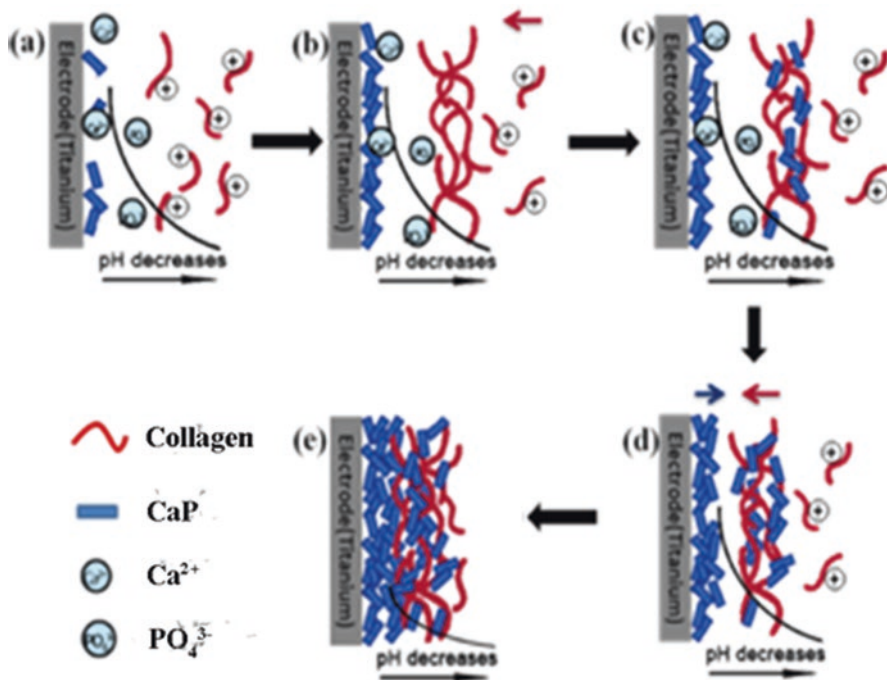
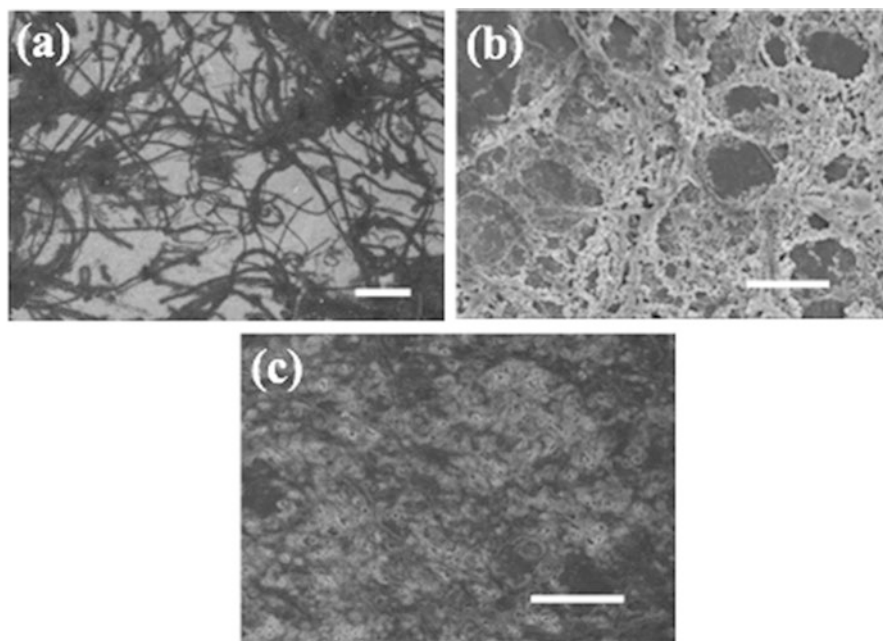


Fig. 14.7 Mineralized collagen coating formation process by ECD (Reprinted from Ref. [16], with kind permission from Springer)

The strong mineralized dense collagen coating (blue arrow) was sandwiched between two weakly mineralized collagen coatings (red arrows), as seen from the cracks in the coating (Fig. 14.10a-1). The alternating positive and negative potentials made the mineralized collagen deposit to form a sandwich structure (Fig. 14.10a-2). In order to further explore the way of mineralized collagen assembly, different coatings were subjected to decalcification treatment (Fig. 14.10b); we could see that the diameter of highly mineralized collagen fibers deposited by the negative potential was significantly larger than the weakly mineralized ones, indicating that the highly mineralized collagen fibers underwent a higher degree of assembly, while the weakly mineralized collagen had no obvious self-assembly process. Comparing the diameter of weakly mineralized collagen layer after decalcification and the original sediment (Fig. 14.10c), it was found that they are of comparable size, which further demonstrated that the collagen fibers in the weakly mineralized collagen layer had not undergone significant self-assembly.

The scratches on the coatings showed that there was only one acoustic signal in the coating obtained by the constant potential method, while the coatings that obtained by the alternating potential-assisted method showed many acoustic signals before the fracture (Fig. 14.11). It revealed that the internal structure of the coating was not homogeneous compared with the coating obtained by the constant potential



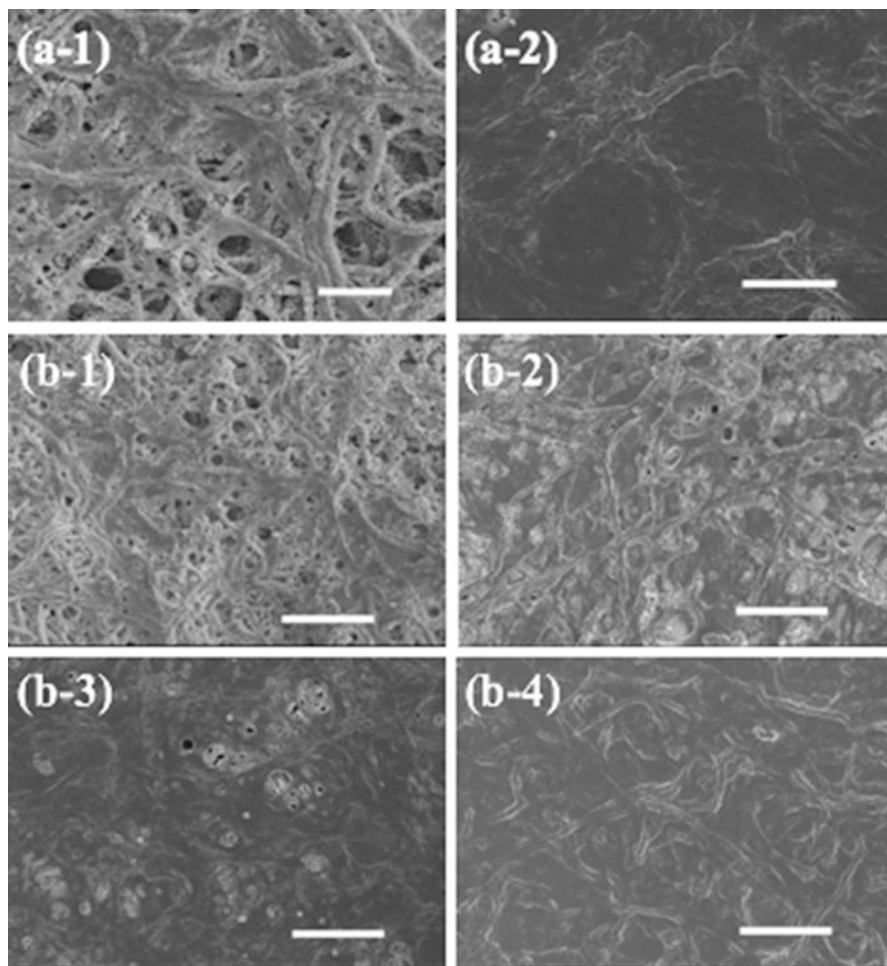
**Fig. 14.8** SEM images of the coating prepared with different parameters. **a** The coating prepared with negative (**a-1**) and positive (**a-2**) potential at the last deposition stage, respectively. Scale bar, 10  $\mu\text{m}$ . **b** The coating prepared with different deposition time of the penultimate deposition stage with positive potential, (**b-1**) 0 min, (**b-2**) 8 min, (**b-3**) 10 min, (**b-4**) 12 min. Scale bar, 25  $\mu\text{m}$  (Reprinted from Ref. [17] with permission, Copyright © Elsevier 2012)

method, which indirectly confirmed that the coating obtained by the AP-ECD had a multilayer structure.

For the deposition by negative potential, the mechanism has been put forward in our previous work. Firstly, pH near the electrode increases due to cathode electrolysis, subsequently collagen self-assembly and mineralization occur, and finally the mineralized collagens are deposited onto the electrode (substrate) to form mineralized collagen coatings.

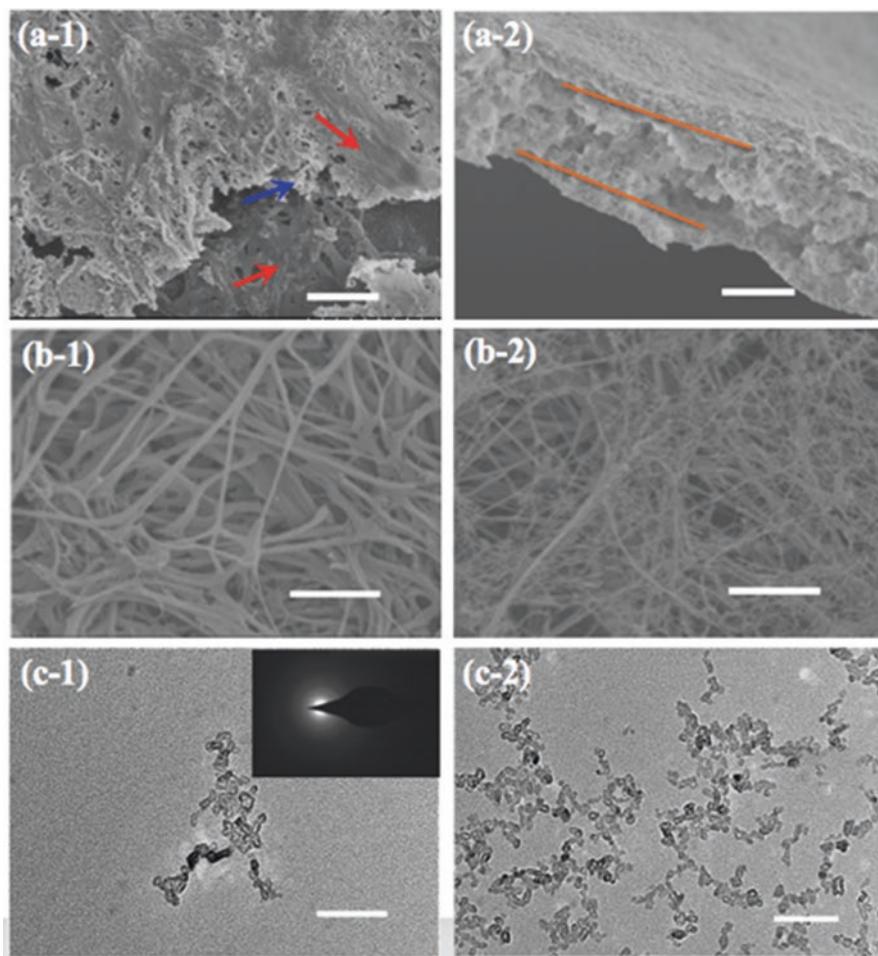
Since the increasing pH induced by cathode electrolysis is gradient, negatively charged collagen fibrils in the vicinity of the substrate will appear when the pH is higher than the isoelectric point. In the deposition at negative potential, these negatively charged collagen fibrils are repelled from the substrate to a location with a relative lower pH, i.e., the isoelectric point, and the collagen fibrils undergo self-assembly, mineralization, and deposition. If these negatively charged collagen fibrils under positive potential are directly deposited on the substrate without self-assembly, low mineralized collagens should be increased in the resulting coatings. When an alternating potential-assisted electrochemical deposition is adopted, the resulting coatings show an increase in low mineralized collagens as expected, and the low mineralized collagens appear in the coating in a multilayer form, consistent with applying alternative potentials.





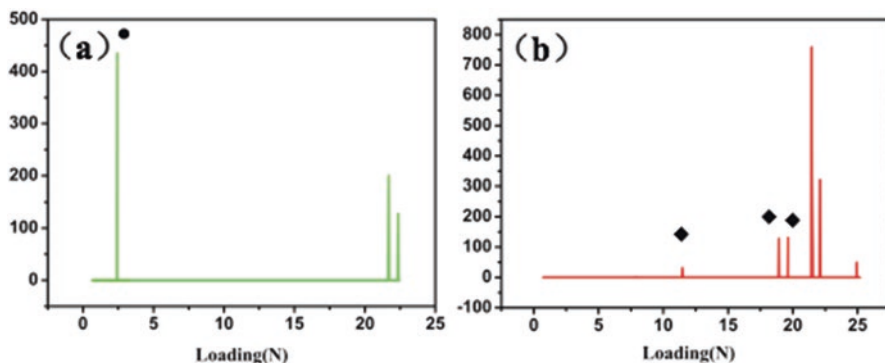
**Fig. 14.9** SEM images of the coating deposited at different stages. After first deposition at positive potential (a), after second deposition at negative potential (b), after third deposition at positive potential again (c). Scale bar, 25  $\mu\text{m}$  (Reprinted from Ref. [17], Copyright 2012, with permission from Elsevier)

Here, the alternating potential-assisted electrochemical deposition process is proposed as below. When an electrode is applied with negative potential, increase in pH near the electrode appears due to cathode electrolysis. The pH increase firstly results in nucleation and growth of apatite onto the electrode due to their high sensitivity to increase in pH to form an initial apatite layer (Fig. 14.12a). Although collagen fibrils are originally positively charged in the electrolyte with pH 4.5, near the electrode, they tend to be uncharged or even become negatively charged because of the pH increase with a gradient curve. For the uncharged collagen fibrils, they began to self-assemble and mineralize to form a highly mineralized collagen layer



**Fig. 14.10** (a) SEM images of coating showed layers with different microstructures, (a-1) crack of the coating showed weakly mineralized collagen layer (red arrow) and highly mineralized collagen layer (yellow arrow). Scale bar, 10  $\mu\text{m}$ . (a-2) The cross section of the coating. Scale bar, 25  $\mu\text{m}$ . (b) SEM images of the collagen after decalcification of the coating from (b-1) highly mineralized layer. (b-2) weakly mineralized layer. Scale bar, 5  $\mu\text{m}$ . (c) TEM image of the collagen in the weakly mineralized layer (c-1), the collagen in the initial electrolyte (c-2). Scale bar, 100 nm. (For interpretation of the references to color in this figure legend, the reader is referred to the web version of this article) (Reprinted from Ref. [17], Copyright 2012, with permission from Elsevier)

as proven in Fig. 14.12b. When a positive potential is applied, the negatively charged collagen fibrils are difficult to self-assemble and mineralize because they move to the substrate which is kept away from the isoelectric point and then deposit onto the electrode to form a weakly mineralized collagen layer directly as proven in Fig. 14.12c, of which the decalcified collagen fiber diameter becomes the same as the original one in electrolyte solution. Since the highest pH exists nearest the elec-



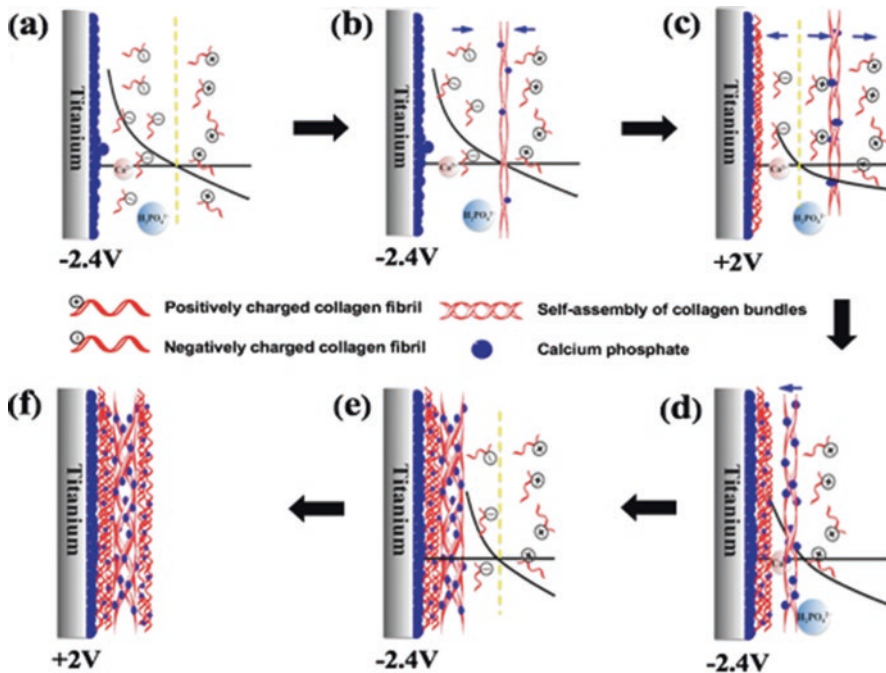
**Fig. 14.11** Scratch testing of coatings prepared using constant potential (a) and alternating potential (b) method. One dot presents that just one and three acoustic signals appeared in the scratch testing of coatings prepared by constant potential and alternating potential, respectively (Reprinted from Ref. [17], Copyright 2012, with permission from Elsevier)

trode during the positive potential, the weakly mineralized collagen fibrils are deposited on the CaP layer constantly, along with the formation of highly mineralized collagen layer at the location of isoelectric point (Fig. 14.12c). Next, the negative potential makes the highly mineralized collagen layer deposit on the substrates, which are shown in Fig. 14.12d, e. If the cycle of the potential change repeats, the weakly and highly mineralized collagen layers are deposited again, and a multilayer structured coating is formed (Fig. 14.12f).

## 14.2.2 Regulation of Micro-/Nanostructures of Coating

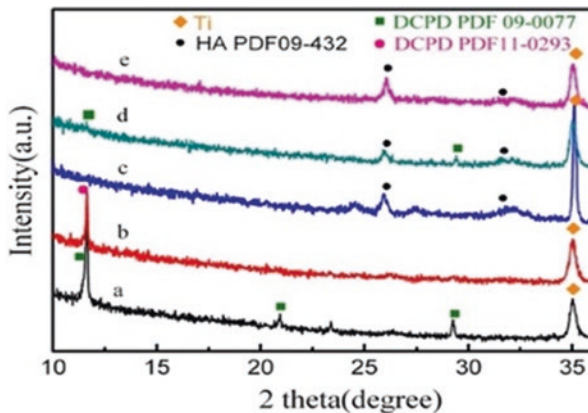
### 14.2.2.1 Regulation of Crystal Phase of CaP

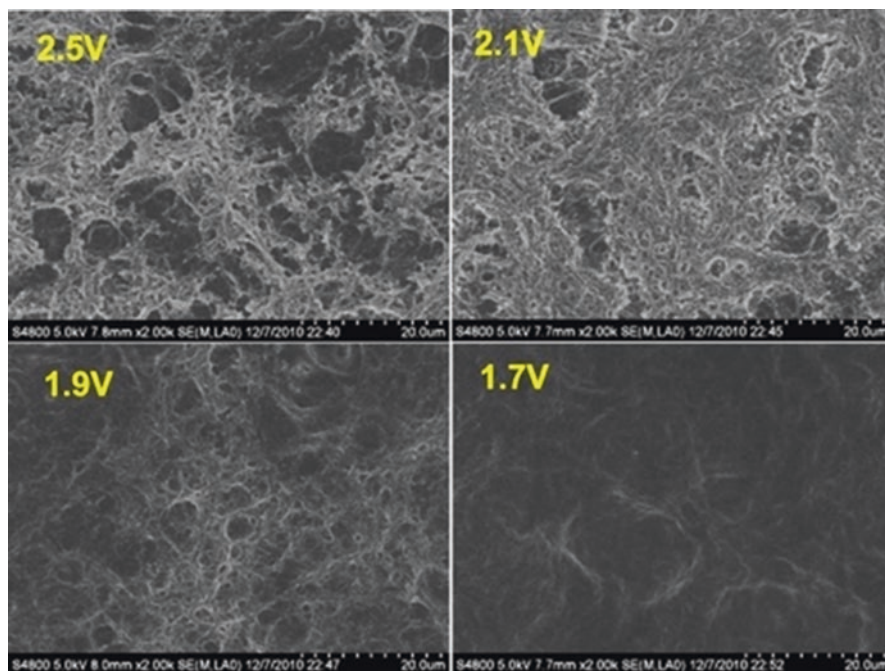
The temperature had a great influence on the crystal phase of calcium phosphate in the coating. Figure 14.13 showed that the primary phase of calcium phosphate was dicalcium phosphate dihydrate (DCPD) at 20 °C. When the temperature reached 30 °C, the main phase was brushite and HA phase appeared at 37 °C. The characteristic peak of the (002) plane presented that HA grew along the c axis of collagen. When the temperature rose to a higher level, the main phase was HA. The results showed that the temperature had a significant effect on the electrochemical deposition of the mineralized collagen coating. Collagen is loosely packed with the calcium phosphate layer, resulting in a few collagen molecules deposited on the substrate at low temperature, while high temperature failed collagen and calcium phosphate co-deposition [15].



**Fig. 14.12** A proposal mechanism of AP-ECD method. (a) When negative potential is applied first, pH gradient appeared next to the substrate and CaP began to deposit on the substrate. (b) The uncharged collagen fibrils began to self-assemble at the location of isoelectric point. (c) The moment that positive potential is enforced, negatively charged collagen fibrils move to the substrate and deposited on the substrate forming a weakly mineralized collagen layer. (d) When a negative potential is applied again, mineralized collagen bundles are enlarged and a little CaP is deposited on the weakly mineralized collagen layer. (e) Mineralized collagen bundles are deposited on the substrate forming a highly mineralized collagen layer. (f) When a positive potential is enforced again, weakly mineralized collagen layer is deposited in the same way (Reprinted from Ref. [17], Copyright 2012, with permission from Elsevier)

**Fig. 14.13** XRD patterns of coatings prepared at different deposition temperatures: (a) 20 °C, (b) 30 °C, (c) 37 °C, (d) 40 °C, (e) 50 °C (Reprinted from Ref. [15], with kind permission from Springer)





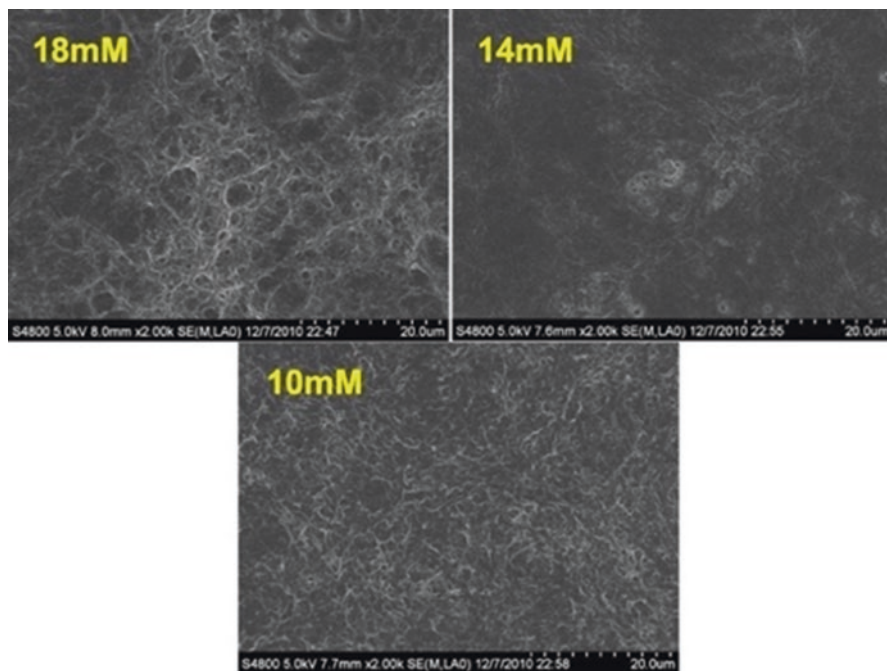
**Fig. 14.14** Different voltage deposition results with 18 mM hydrogen peroxide (Reprinted from Ref. [16], with kind permission from Springer)

### 14.2.2.2 Regulation of Mineralization Degree

#### 14.2.2.2.1 Regulation of Electrolyte on the Degree of Mineralization

Changing the type of cathodic reaction is an important method to regulate the pH gradient of cathode. Adding redox agent in the electrolyte, which increases the electron transfer rate of the cathode, will enlarge the pH gradient, and the redox agent does not modify the collagen molecules and the calcium phosphate in the electrolytic solution.  $\text{H}_2\text{O}_2$  is a strong oxidant, and its decomposition rate is greater than water in the electrolysis conditions, without modification on the collagen, so we chose  $\text{H}_2\text{O}_2$  as redox agent that added to the electrolyte. Figure 14.14 showed that the degree of collagen mineralization was high, showing porous structure when the deposition potential was 2.1–2.5 V.

Considering the introduction of  $\text{H}_2\text{O}_2$  and the regulation of potential control and the self-assembly behavior of collagen by the change of the pH gradient of the cathode, different concentrations of  $\text{H}_2\text{O}_2$  also had an effect on mineralized collagen deposition. Figure 14.15 showed the morphology of the coating at different concentrations of  $\text{H}_2\text{O}_2$ . The coating showed a porous structure with visible mineralized collagen bundles on the surface under high concentration of  $\text{H}_2\text{O}_2$ . As  $\text{H}_2\text{O}_2$



**Fig. 14.15** Different deposition results with hydrogen peroxide at different concentrations (Reprinted from Ref. [16], with kind permission from Springer)

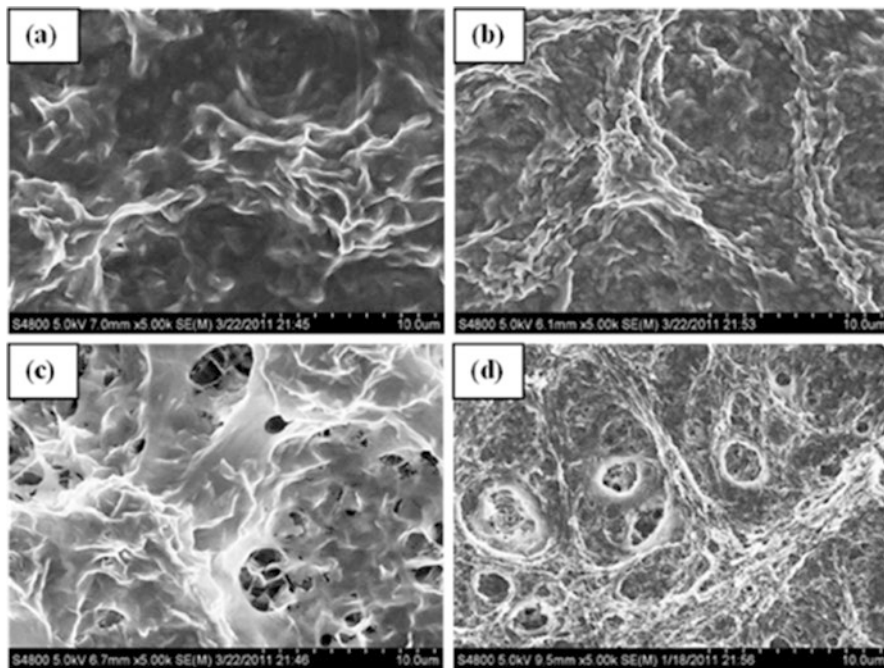
concentration decreases, the mineralization of collagen in the coating was weakened obviously.

#### 14.2.2.2.2 Regulation of Potential on the Degree of Mineralization

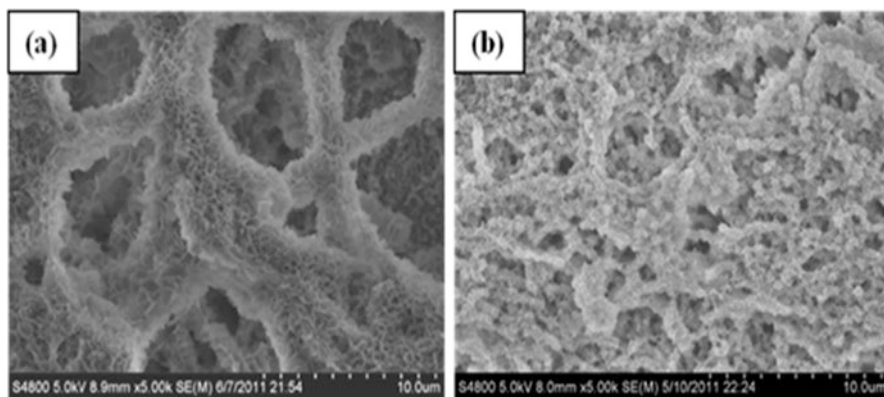
Figure 14.16 showed the morphology of the mineralized collagen coating under deposition potential of 1.9–2.3 V, when the deposition temperature and the composition of the electrolyte were kept unchanged. It could be seen that the mineralized collagen coating became porous and the degree of mineralization increased with the deposition potential increasing, accompanied by the decreased amount of collagen fibers exposed on the surface.

#### 14.2.2.2.3 Regulation of Deposition Time on Mineralization Degree

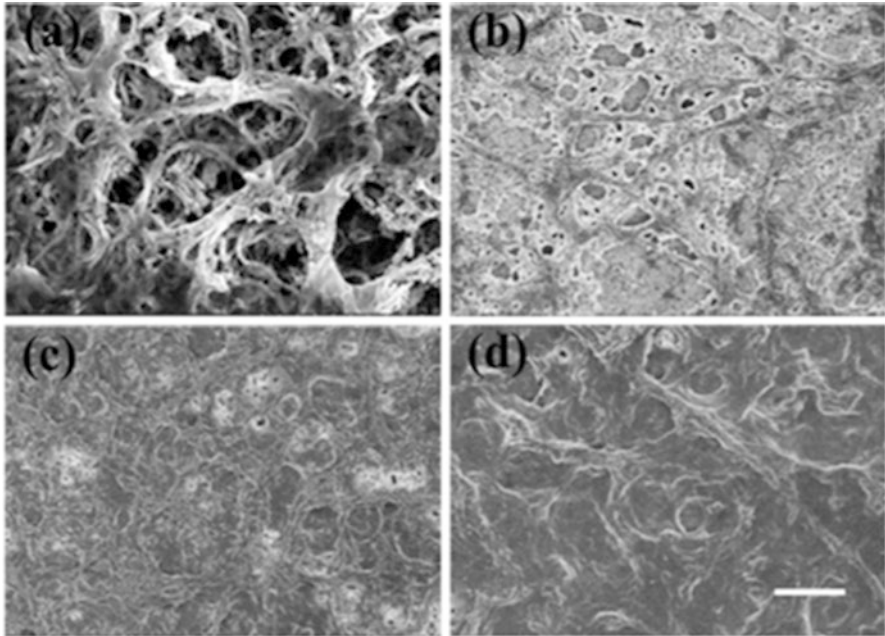
Figure 14.17 showed the morphology of the coating with deposition potential of 2.3 V and deposition time of 45 min and 60 min, respectively. With the deposition time increased, the coating was still porous, but the degree of mineralization was further aggravated. The relative content of calcium phosphate on the surface of the coating increased, but the pore size of the coating decreased.



**Fig. 14.16** SEM micrographs of mineralized collagen coatings with different deposition voltages, (a) 1.7 V, (b) 1.9 V, (c) 2.1 V, (d) 2.3 V



**Fig. 14.17** SEM images of mineralized collagen coating at different deposition times (deposition potential 2.3 V), (a) 45 min, (b) 60 min



**Fig. 14.18** The morphology of coating prepared with different molar ratios of BSA and collagen (a) 0, (b) 1:5, (c) 1:20, (d) 1:10 (Reprinted from Ref. [18], Copyright 2012, with permission from Elsevier)

#### 14.2.2.2.4 Regulation of Bovine Serum Albumin (BSA) on the Mineralization Degree

Figure 14.18 showed the morphology of the coatings prepared with the molar ratio of BSA and collagen in the electrolyte solution at 0, 1:20, 1:10, 1:5, and 1:2.5, respectively, when the deposition temperature was kept constant; the deposition potential was kept at 2.5 V and the deposition time was 30 min. It could be seen from the SEM images that the addition of BSA weakened the degree of mineralization. Mineralized collagen without BSA showed a porous morphology with visible collagen bundles. However, the porosity of the coating decreased after the addition of BSA. With the increase of BSA concentration, the degree of mineralization was further weakened with the porous structure gradually disappeared, and the exposed bare collagen gradually increased until it was completely covered with naked collagen [18].

#### 14.2.2.3 Regulation of Composition Distribution of Coating

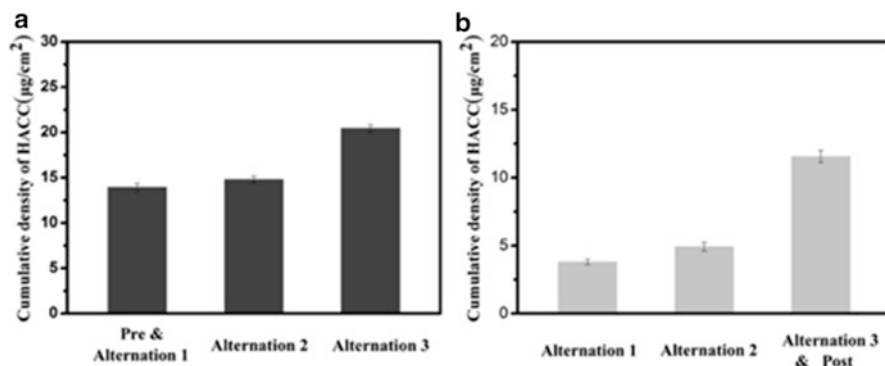
The controllable distribution of the bioactive factors can be realized by the alternating potential-assisted deposition method [19].



**Table 14.1** Deposition parameters of HACC-IN and HACC-OUT

Stage	Samples							
	Pre	Alternation 1		Alternation 2		Alternation 3		Post
HACC-IN	-1.5 V	-2.4 V	2 V	-2.4 V	2 V	-2.4 V	2 V	-
	60 s	120 s	60 s	480 s	120 s	720 s	180 s	
HACC-OUT	-	-2.4 V	2 V	-2.4 V	2 V	-2.4 V	2 V	-2.4 V
		120 s	60 s	360 s	120 s	480 s	180 s	480 s

Reprinted from Ref. [19], Copyright 2012, with permission from Elsevier

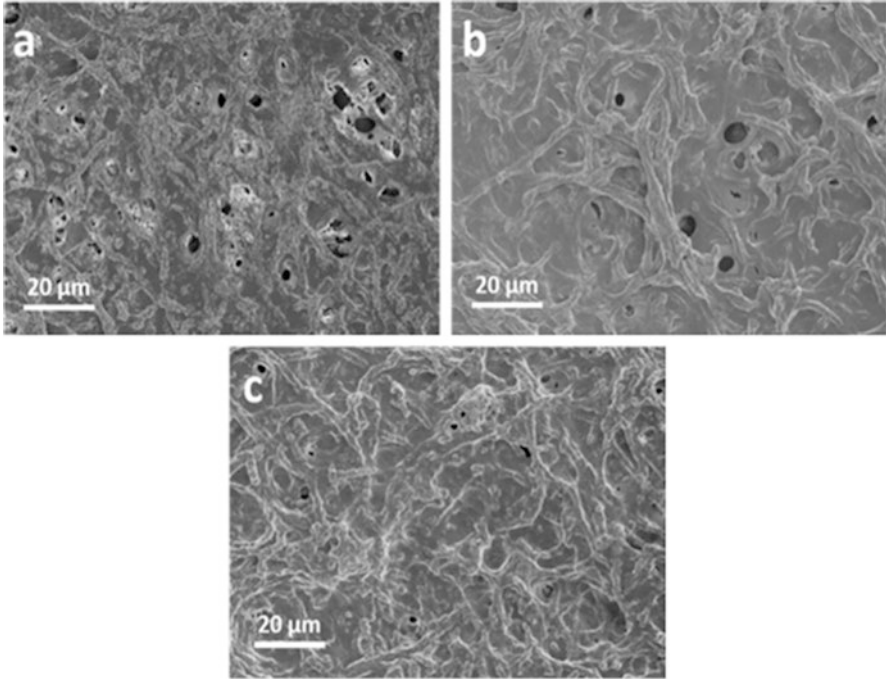


**Fig. 14.19** Cumulative density of HACC in coatings after different deposition stages: (a) HACC-IN64, (b) HACC-OUT64 (Reprinted from Ref. [19], Copyright 2012, with permission from Elsevier)

During AP-ECD process, the deposition parameters including potential values and negative/positive alternations and their durations were designed as shown in Table 14.1. Three alternations were set to ensure the sufficient coating thickness so that the spatial distribution of HACC can be controlled.

Relatively, longer negative potential durations in alternations led HACC to exist in the inner part of coating, while shorter ones to repulse more HACC and locate them in the outer part. HACC concentrations in electrolyte at 48, 64, and 80 M were chosen to prepare coatings. According to deposition manner (producing different HACC locations) and HACC concentrations, the coatings obtained via AP-ECD were labeled as HACC-IN48/64/80 and HACC-OUT48/64/80. The COL coating prepared following our previous work was used as control [20].

Based on measurements of HACC density in the coatings for each alternation (Fig. 14.19), HACC-IN64 coating showed that HACC density only increased by 27.5% after the second and third alternation (Fig. 14.19a), while HACC-OUT64 coating showed that HACC density increased obviously by 57.4% after the third alternation and post-alternation (Fig. 14.19b). This indicates effective control on the spatial distribution of HACC has been realized.



**Fig. 14.20** (a) SEM images of COL coating, (b) HACC-IN64 coating, and (c) HACC-OUT64 coating (Reprinted from Ref. [19], Copyright 2012, with permission from Elsevier)

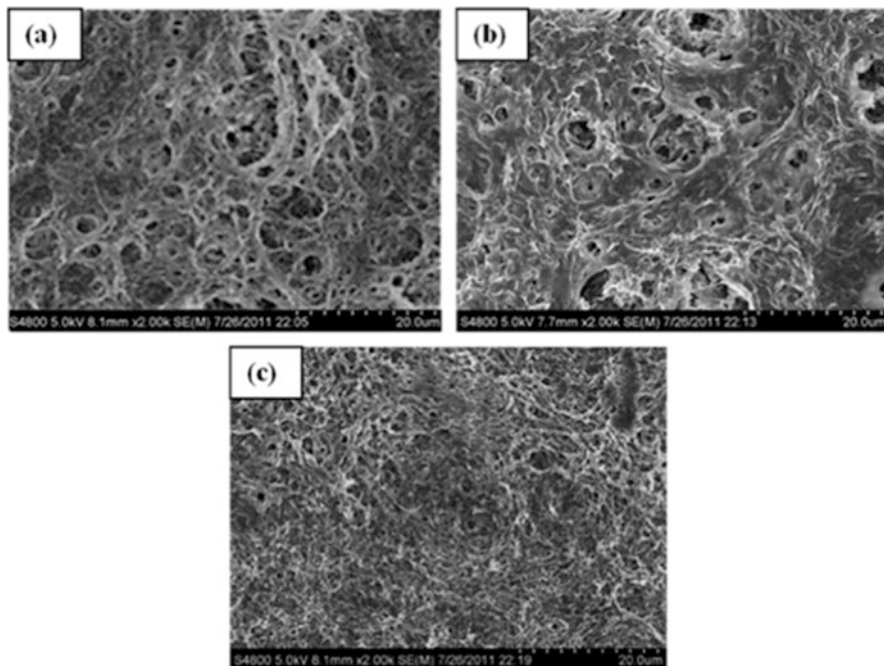
HACC-IN and HACC-OUT coatings showed a similar porous morphology (Fig. 14.20), demonstrating that HACC incorporation and different locations hardly influence the coating morphology. The XRD patterns indicated that both of the coatings contained apatite phases (Fig. 14.20d). Hence, the coatings with different HACC locations have similar surface morphology and mineralization.

### **14.3 Loading/Release Behaviors of Collagen/Calcium Phosphate Coatings**

#### **14.3.1 Drug Loading/Release Properties of Mineralized Collagen Coatings**

##### **14.3.1.1 Drug Release Behavior of Mineralized Collagen/PLGA-PEG-PLGA Coatings**

PLGA-PEG-PLGA nanocomposites have excellent drug delivery/drug release properties and can be used to improve the drug loading/release behavior of mineralized collagen coatings [21]. Micelles can be prepared by direct dissolution (Dis) or

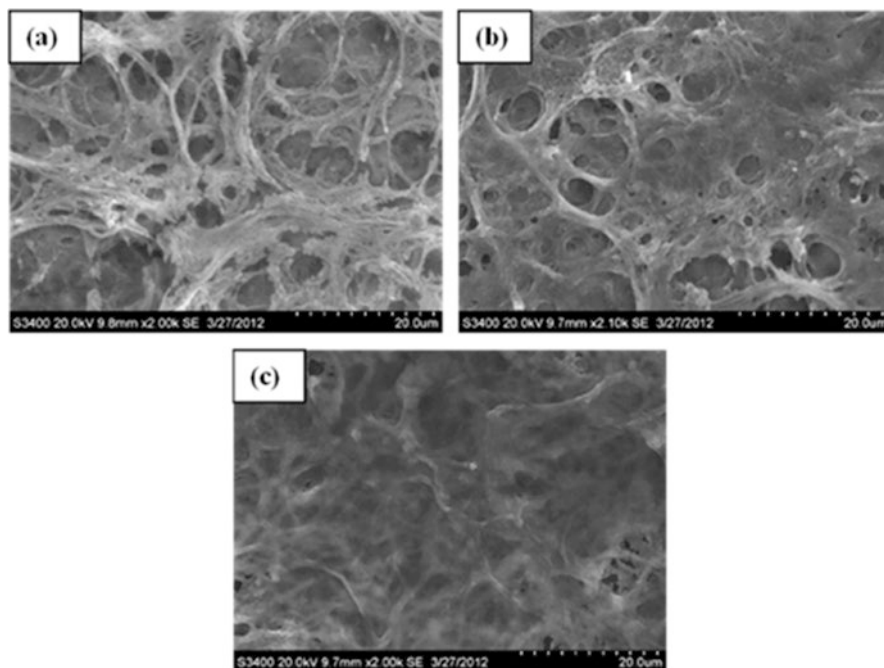


**Fig. 14.21** Morphology of the coatings with different PLGA-PEG-PLGA concentration micelles were assembled into mineralized collagen (micelles were prepared by direct dissolution method), (a) MC+Dis P1, (b) MC+Dis P2, (c) MC+Dis P3 (Reproduced from Ref. [21] by permission of John Wiley & Sons Ltd)

solvent-dialysis (Dia). Drug-loaded micelles were obtained by dissolving the vancomycin hydrochloride (VH) in the micellar solution (Dia Pi,  $i = 1, 2, 3$  and Dis Pi,  $i = 1, 2, 3$ , respectively) and ensuring the concentration of the drug was 4 mg/mL. Mineralized collagen/PLGA-PEG-PLGA coating was obtained by dropping 50- $\mu$ L-drug-loaded PLGA-PEG-PLGA micelles onto the mineralized collagen coating.

Figure 14.21 showed the morphology of the coating (MC + Dis Pi,  $i = 1, 2, 3$ ) obtained by assembling different PLGA-PEG-PLGA micelles into mineralized collagen. When the PLGA-PEG-PLGA concentration was appropriate, the coating remained porous (Fig. 14.21a, b). However, as the concentration of PLGA-PEG-PLGA increased, the micelles might accumulate, covering the surface of the mineralized collagen coating, resulting in a denser structure (Fig. 14.21c).

Figure 14.22 showed the morphology of the coating (MC + Dia Pi,  $i = 1, 2, 3$ ) obtained by assembling different PLGA-PEG-PLGA micelles that is prepared by the solvent-dialysis method into mineralized collagen. Similar to the micelles prepared by direct dissolution method, increasing the concentration of PLGA-PEG-PLGA micelles prepared by the solvent-dialysis method, the coating changed from porous to dense morphology.



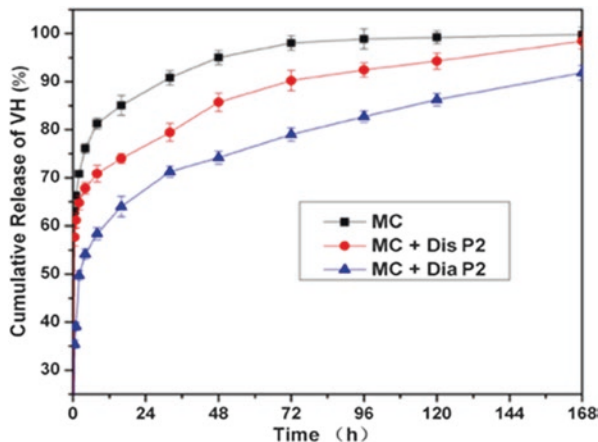
**Fig. 14.22** Morphology of the coating obtained by assembling micelles of PLGA-PEG-PLGA at different concentrations into mineralized collagen (micelle was prepared by solvent-dialysis method), (a) MC+Dia P1, (b) MC+Dia P2, (c) MC+Dia P3 (Reproduced from Ref. [21] by permission of John Wiley & Sons Ltd)

Figure 14.23 showed the *in vitro* release profiles of VH from different coatings. The MC coatings showed an early burst release of nearly 81% of the total VH loaded in 8 h. This serious burst effect led to the result that the following sustained release of the remaining VH only lasted for about 3 days. In comparison, approximately 70.8% and 58% of the total VH released from the dissolved-micelle-immobilized and dialyzed-micelle-immobilized coatings in 8 h, respectively, and the sustained release continued for at least 7 days. Thus, by the regulation of the micelles, the release behaviors could be controlled.

#### 14.3.1.2 Drug Release Behavior of Chitosan/Mineralized Collagen Coatings

Chitosan is the only basic polysaccharide in many natural polysaccharides. It has many advantages, such as rich source, nontoxic, easy chemical modification, good biocompatibility and reproducibility, and unique molecular structure. The chitosan microspheres can be embedded into the mineralized collagen coating to improve its

**Fig. 14.23** Release behaviors of mineralized collagen/PLGA-PEG-PLGA coating prepared by different methods (Reproduced from Ref. [21] by permission of John Wiley & Sons Ltd)

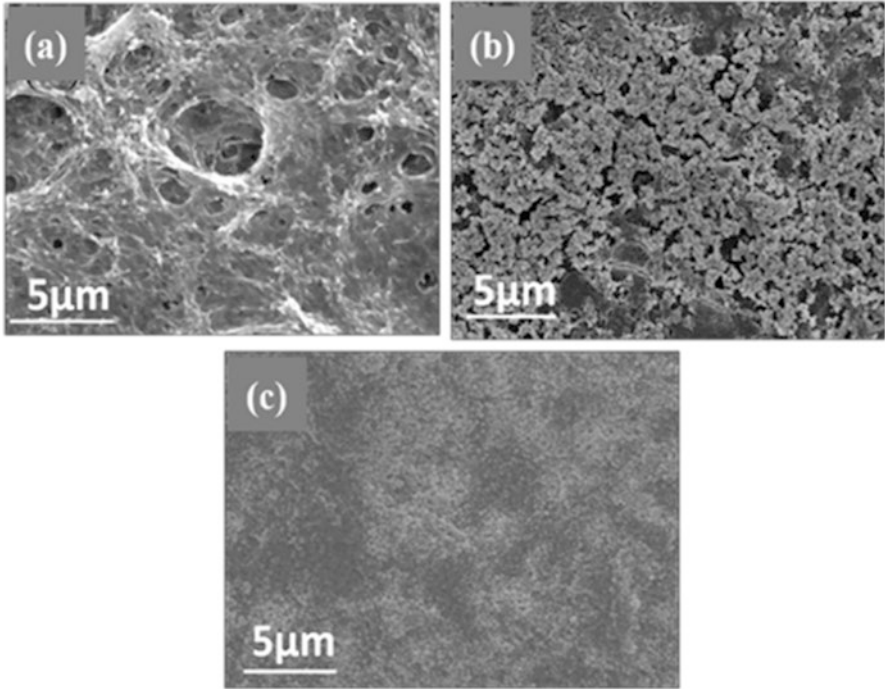


drug-loading and drug-releasing properties by utilizing the large specific surface area of the chitosan microspheres and the excellent binding ability to the drug and collagen fibers [22].

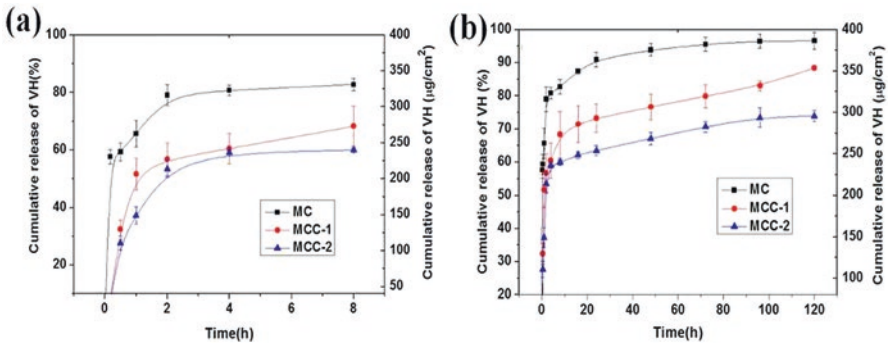
Different concentrations of chitosan microspheres (0.04 mg/mL, 0.24 mg/mL) were prepared by ion-gel method. The electrochemical co-deposition process was used to prepare chitosan microspheres by ion-gel method and then mixed with collagen solution; a coating of chitosan/mineralized collagen was prepared on the surface of the titanium substrate by electrochemical co-deposition and VH was added to the coating by drowsed addition (Fig. 14.24).

The morphology of the coatings prepared under different concentrations of microspheres was observed. The coatings with different chitosan concentrations (0, 0.04, 0.24 mg/mL) were abbreviated as MC, MCC-1, and MCC-2, respectively. It could be seen that the content of chitosan microspheres in the mineralized collagen coating increased with the increasing of the content of chitosan microspheres in the electrolyte under the same deposition conditions. The microspheres mainly adhered to the collagen fibers with low mineralization. On the other hand, the porosity of the originally porous mineralized collagen coating was reduced by the introduction of microspheres.

The VH released from the unincorporated (MC) and the incorporated coatings (MCC-1 and MCC-2) were shown in Fig. 14.25. In the first 24 h, significant differences were observed as a result of the incorporation of chitosan nanospheres. During the first 1 h, the overall released of VH from unincorporated coatings was nearly 65%, and the extent of release was reduced greatly with the addition of chitosan nanospheres. When the weight ratio of chitosan nanospheres to collagen was 0.1:1, the overall release percentage was 51.6%, and this percentage was reduced to 37.2% when the weight ratio was 0.6:1. It is well known that the drug-loading capacity of chitosan is better than that of collagen. As more nanospheres were incorporated into the coating, the release rate of VH was reduced. After 24 h, the released VH from



**Fig. 14.24** SEM images of the coatings, (a) mineralized collagen coating (MC), (b) mineralized collagen coating (MCC-1) with less microspheres, (c) mineralized collagen coating (MCC-2) with more microspheres.



**Fig. 14.25** Comparative drug release kinetics of VH from MC, MCC-1, and MCC-2 coatings. (a) Burst release, (b) sustained release. Data shown are means  $\pm$  SD of triplicate assays (Reprinted from Ref. [22], Copyright 2012, with permission from Elsevier)

MC coating was nearly 100%, whereas the incorporated coatings showed sustained release during the following days. After 96 h, release of VH from incorporated coatings could still be observed.

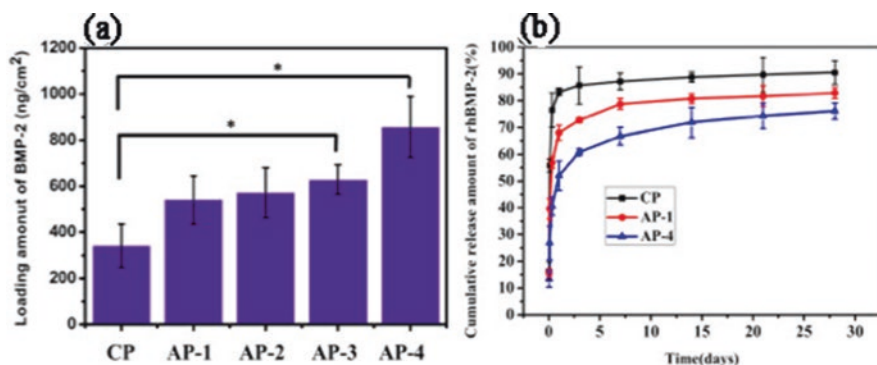
### 14.3.2 *RhBMP-2 Loading/Release Behavior of Composite Coatings*

#### 14.3.2.1 *RhBMP-2 Loading/Release Behavior of Mineralized Collagen Coatings*

The rhBMP-2 loading/release behavior showed that the higher content of weakly mineralized collagen resulted in the increasing loading of rhBMP-2 (Fig. 14.26a). It was also due to the presence of naked collagen, which improved the binding ability of the coating and rhBMP-2, thus improving its release behavior (Fig. 14.26b). The combination of weakly mineralized collagen and rhBMP-2 effectively inhibited the burst release of the coating. The above work not only shows the need for controlled preparation of the coating but also provides a basis for assembling the auxiliary additives into the coating subsequently [17].

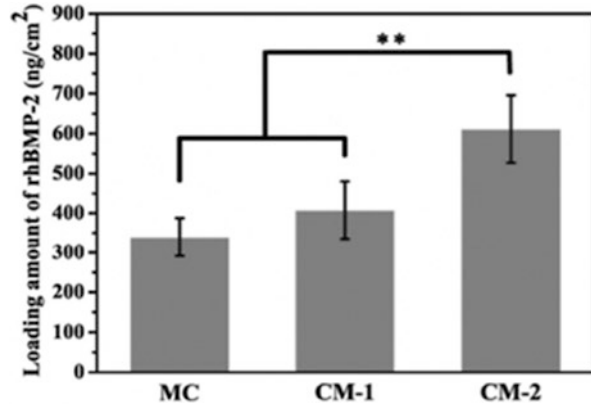
#### 14.3.2.2 *RhBMP-2 Loading/Release Behavior of BSA/Mineralized Collagen Coatings*

The rhBMP-2 was loaded into the BSA/mineralized collagen coating by soaking. As can be seen from Fig. 14.27, the loading amount of rhBMP-2 was gradually promoted with the increasing of BSA content in the coating, which effectively improved the rhBMP-2 carrying capacity of the coating [18].



**Fig. 14.26** (a) Evaluation of the rhBMP-2 loading capacity of the mineralized collagen, (b) rhBMP-2 release behavior from the mineralized collagen (Reprinted from Ref. [17], Copyright 2012, with permission from Elsevier)

**Fig. 14.27** RhBMP-2 loading capacity of BSA/mineralized collagen coating (Reprinted from Ref. [18], Copyright 2012, with permission from Elsevier)



### 14.3.2.3 RhBMP-2 Loading/Release Behavior of Chitosan/Mineralized Collagen Coatings

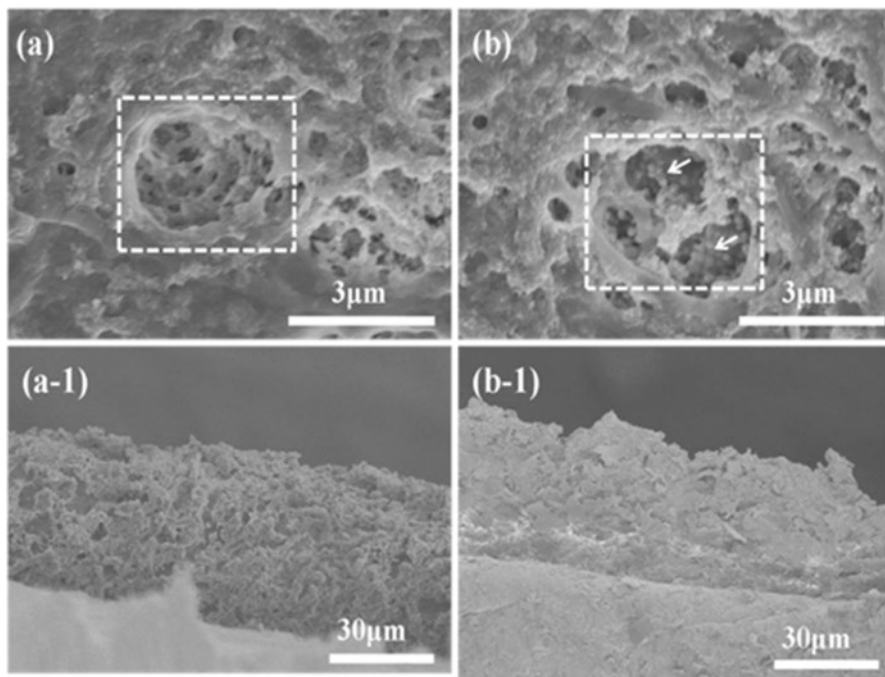
The chitosan microspheres-rhBMP-2 mixed solution with rhBMP-2 concentration of 2  $\mu\text{g/mL}$  was prepared by ion-gel method. The implants that are coated with mineralized collagen were used as electrode cathodes, so that the chitosan microspheres loaded with rhBMP-2 moved from the anode to the cathode under the action of potential and finally assembled into the mineralized collagen coating [23].

The as-prepared mineralized collagen coating was porous in morphology and approximately 40–50  $\mu\text{m}$  in thickness (Fig. 14.28a, a-1). After electrophoretic injection, chitosan nanospheres were incorporated into the pores of the mineralized collagen coating by electrophoresis (Fig. 14.28b), and the morphology and thickness of the resulting coating were not markedly changed (Fig. 14.28b, b-1), which proved that the chitosan nanospheres fully entered into the inner pores of the mineralized collagen rather than just stayed on the surface of the coating.

As shown in Fig. 14.29, the loading amount of rhBMP-2 in the Col/BMP coating was approximately 446  $\text{ng/cm}^2$ , but in the Col/Cs/BMP coating, it increased 2.7-fold to reach 1,186  $\text{ng/cm}^2$  with the addition of chitosan nanospheres.

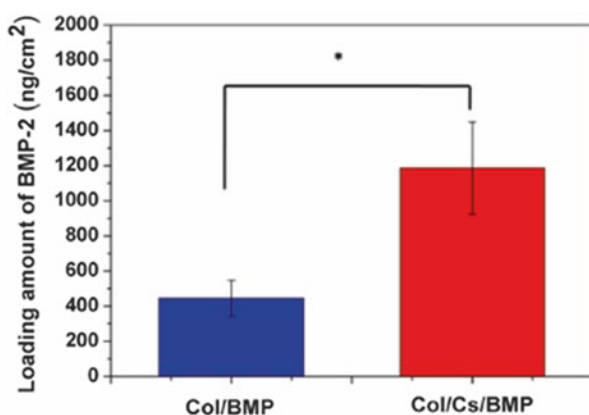
The release behavior of rhBMP-2 has a great influence on the process of osteogenesis. The emergency of burst release of rhBMP-2 may cause ectopic osteogenesis. If the release amount of rhBMP-2 is not enough, the implant and host bone will not complete the osseointegration process at short notice. After soaking for 11 days, approximately 58.5% of the rhBMP-2 had been released from the Col/BMP coating, while only 39.5% was released from the Col/Cs/BMP coating, demonstrating that this coating showed sustained release behavior (Fig. 14.30).

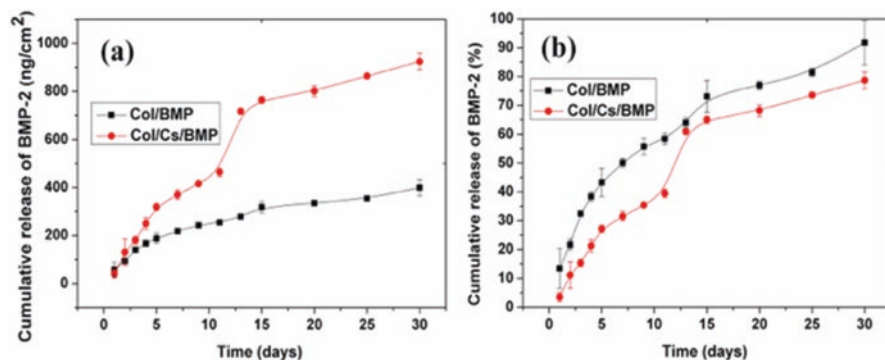




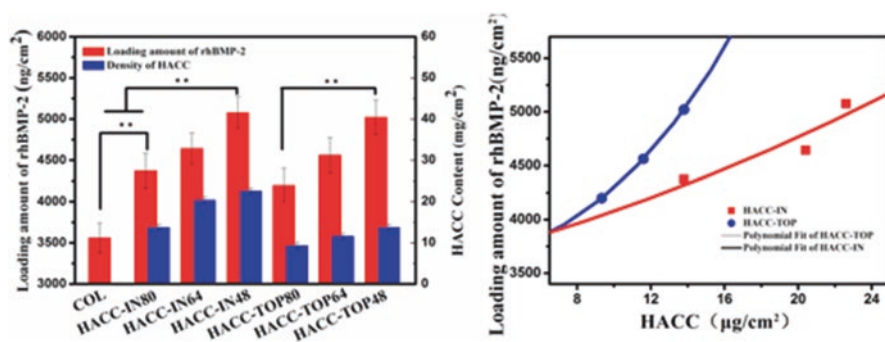
**Fig. 14.28** SEM images of the coatings: (a) surface morphology of Col/BMP coating, (a-1) cross-section morphology of Col/BMP coating, (b) surface morphology of Col/Cs/BMP coating, (b-1) cross-section morphology of Col/Cs/BMP coating. The arrows point to chitosan nanospheres (Reproduced from Ref. [23] by permission of The Royal Society of Chemistry)

**Fig. 14.29** RhBMP-2 loading amount in Col/BMP and Col/Cs/BMP coatings. Data shown are means $\pm$ SD of triplicate assays. Asterisks denote significant differences between different coatings (\*  $P < 0.05$ ) (Reproduced from Ref. [23] by permission of The Royal Society of Chemistry)





**Fig. 14.30** Cumulative release profiles of rhBMP-2 of Col/BMP and Col/Cs/BMP coatings: (a) release profile ( $\text{ng}/\text{cm}^2$ ) of rhBMP-2 from the coatings, (b) release profile (%) of rhBMP-2 from the coatings (Data shown are means  $\pm$ SD of triplicate assays. Reproduced from Ref. [23] by permission of The Royal Society of Chemistry)

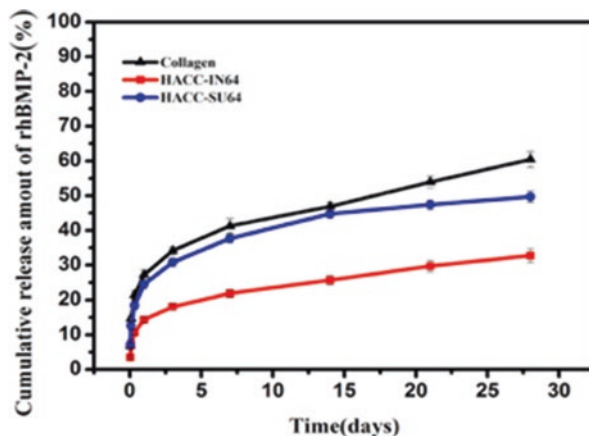


**Fig. 14.31** RhBMP-2 loading capability evaluation (Reprinted from Ref. [19], Copyright 2012, with permission from Elsevier)

#### 14.3.2.4 RhBMP-2 Loading/Release Behavior of HACC/Mineralized Collagen Coatings

The HACC density in both HACC-IN and HACC-OUT coatings increased along with the concentration of HACC in the electrolyte (Fig. 14.31), and HACC-IN manner showed higher HACC incorporation efficiency than HACC-OUT manner. As shown in Fig. 14.31, a higher HACC density in the coatings favored rhBMP-2 loading. Considering the loading amount per HACC content incorporated, HACC in HACC-OUT coatings presented more contribution to rhBMP-2 loading than that in HACC-IN coating. Interestingly, the differences in HACC incorporation efficiency and HACC contribution to the rhBMP-2 loading resulted in that HACC-IN64 ( $4,644 \text{ ng}/\text{cm}^2$ ) and HACC-OUT64 ( $4,563 \text{ ng}/\text{cm}^2$ ) coatings had a similar rhBMP-2 loading amount, and the two coatings were adopted to evaluate releasing behavior [19].

**Fig. 14.32** rhBMP-2 release behavior of the HACC/mineralized collagen coating (Reprinted from Ref. [19], Copyright 2012, with permission from Elsevier)



As shown in Fig. 14.32, HACC-IN64 coating exhibited a more sustained releasing behavior than HACC-OUT64 and COL coatings; 14% (667 ng/cm<sup>2</sup>) rhBMP-2 was released at the first day and as low as 25% (1,191 ng/cm<sup>2</sup>) was released for 14 days, while HACC-OUT64 and COL coatings exhibited burst release with 24% (967 ng/cm<sup>2</sup>) and 27% (1,116 ng/cm<sup>2</sup>) for the first day, and a relatively fast release of 44% (1,670 ng/cm<sup>2</sup>) and 47% (2,044 ng/cm<sup>2</sup>) was induced for 14 days. This demonstrated that the HACC distribution had a significant influence on rhBMP-2 loading/release behavior, and the HACC located in the inner part facilitated a persistent and expected performance.

## 14.4 Biological Performance of Collagen/Calcium Phosphate Coatings

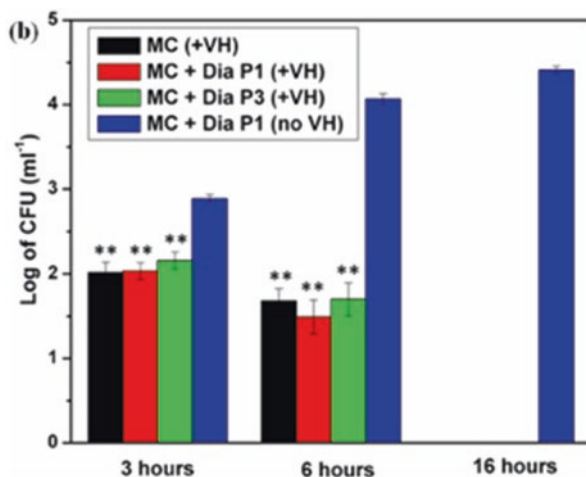
### 14.4.1 Antibacterial Properties and Osteoblast Response of Composite Coatings

#### 14.4.1.1 Antibacterial Properties of Composite Coatings

##### 14.4.1.1.1 Antibacterial Properties of PLGA-PEG-PLGA/Mineralized Collagen Coating

Compared with other means, drug-loaded coatings not only could inhibit bacterial adhesion and proliferation but also could effectively kill the bacteria. Antimicrobial test was designed to evaluate anti-infection ability of the present VH-loaded coatings. The amount of colonies of *S. aureus* cultured on the VH-loaded coatings were significantly less than that on the negative control group in the first 3 and 6 h, and almost disappeared after 16 h (Fig. 14.33), which indicated that the released VH

**Fig. 14.33** Antimicrobial activity of coatings cultured for (a) 3 h and 6 h, (b) 16 h. Asterisks (\*\*) indicate significant differences ( $p < 0.01$ ) compared with samples without VH (Reproduced from Ref. [21] by permission of John Wiley & Sons Ltd)

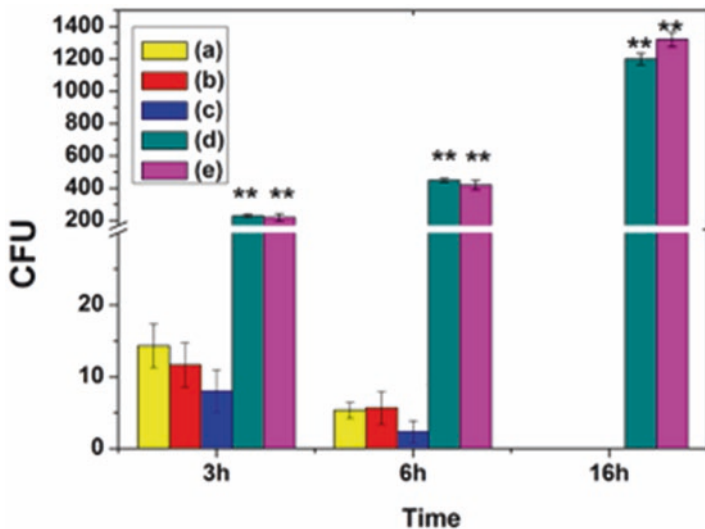


had exerted antimicrobial activity. On the other hand, the PLGA-PEG-PLGA micelle-modified coating slowed the initial release of VH and decreased the amount of drug released at the same time. From the results of antimicrobial experiments, it was found that the initial drug release did not significantly affect the initial antibacterial effect of the coating. The sustained drug release ability of the coating is strengthened, which will be beneficial to inhibit the adhesion and proliferation of the bacterial in the later stage of implantation, so as to effectively prevent the occurrence of infection and improve the success rate and quality of the implantation operation [21].

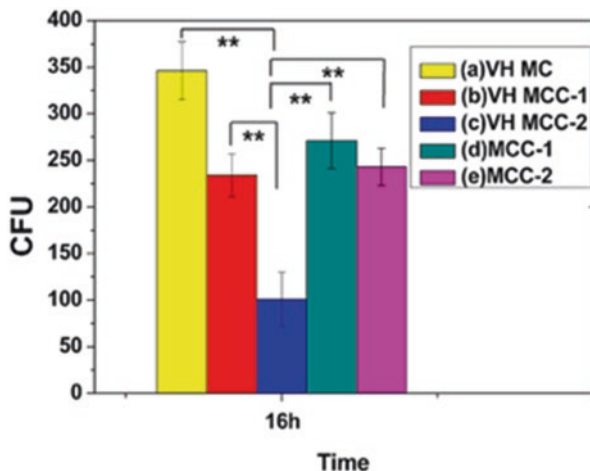
#### 14.4.1.1.2 Antibacterial Properties of Chitosan/Mineralized Collagen Coatings

As can be seen from Fig. 14.34, in the first 3 h and 6 h after incubation, the colonies of *S. aureus* were significantly less in the culture capsule of the VH-loaded coatings than that of the control, whereas the amount of colonies exceeded 1000 CFUs on the coatings with no antibiotic. After an incubation for 16 h, the colonies of *S. aureus* disappeared in the case of VH-loaded coatings, whereas the amount of colonies exceeded 1000 CFUs on the coatings without VH. From this result, it can be concluded that the VH loaded in the chitosan nanosphere-incorporated coating could inhibit the growth of the *S. aureus* in vitro in the first 16 h and that the local concentration of the VH released from the coating exceeded the minimal inhibitory concentration (MIC) of the *S. aureus* [22].

The results in Fig. 14.35 showed that the colonies of *S. aureus* in the case of chitosan nanosphere-incorporated coatings (MCC-1, MCC-2), especially the MCC-2 coatings, were less than those in the plain coatings (MC). These results indicated that the sustained release amount of the antibiotic (VH) from the chitosan



**Fig. 14.34** Antibacterial results of different coatings: (a) MC coating loaded with VH, (b) MCC-1 coating loaded with VH, (c) MCC-2 coating loaded with VH, (d) MCC-1 coating with no VH, (e) MCC-2 coating with no VH. Data shown are means  $\pm$  SD of triplicate assays (*S. aureus* suspension dilution ratio: 1:10,000) (Reprinted from Ref. [22], Copyright 2012, with permission from Elsevier)



**Fig. 14.35** Antibacterial results of different coatings after a 48-h immersion in PBS: (a) MC coating loaded with VH, (b) MCC-1 coating loaded with VH, (c) MCC-2 coating loaded with VH, (d) MCC-1 coating with no VH, (e) MCC-2 coating with no VH. The data shown are means  $\pm$  SD of triplicate assays. Asterisks denote significant differences between (d) and (a–c) and (e) (\*\* $p < 0.01$ ) (*S. aureus* suspension dilution ratio:  $1:2 \times 10^9$ ) (Reprinted from Ref. [22], Copyright 2012, with permission from Elsevier)

nanosphere-incorporated coatings (MCC-1 and MCC-2) could also exert an antibacterial effect after the initial burst release (following immersion in a PBS solution for 48 h before seeding the *S. aureus*).

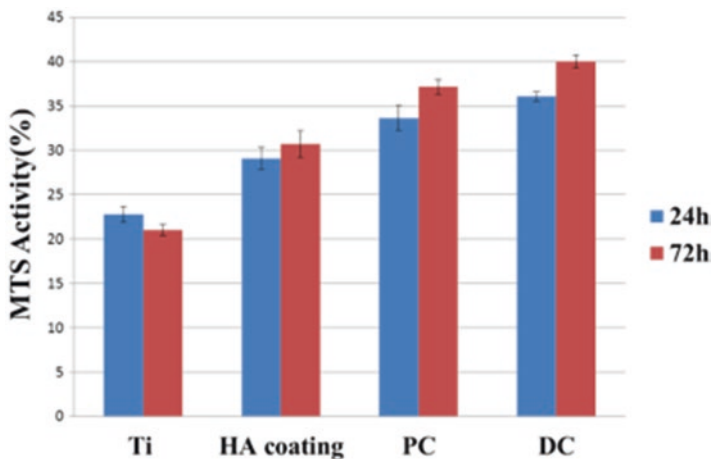
The antibacterial test showed that the mineralized collagen coatings with incorporated chitosan nanospheres could be used for loading and releasing antibiotics such as VH to kill specific bacteria during implantation. In combination with the VH release tests, it can be concluded that the incorporation of nanospheres into coatings is a good way to slow down the release rate and extend the antibacterial effect.

#### 14.4.1.2 Osteoblast Response to Composite Coatings

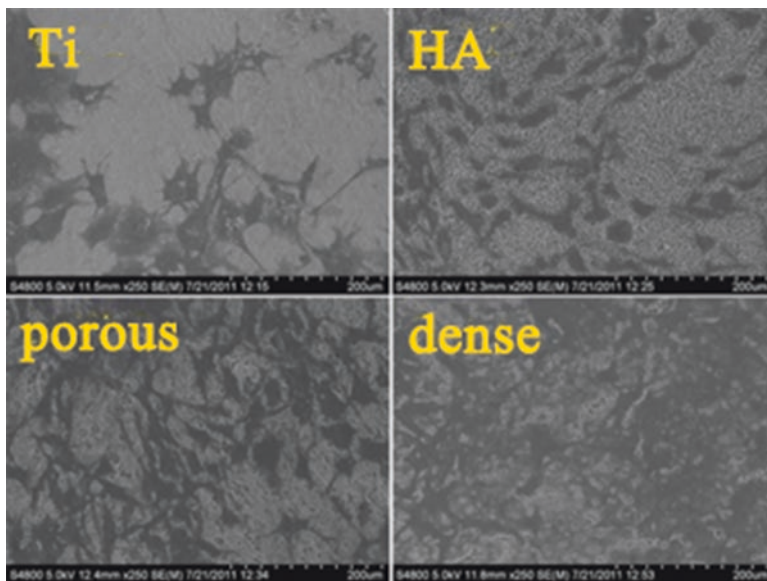
##### 14.4.1.2.1 Osteoblast Response to the Mineralized Collagen Coating

When the sample is implanted in the body, the first reaction with the tissue is cell adhesion and proliferation. Figure 14.36 showed that after 1 day of culture, the MTS relative value of the collagen-coated experimental group was higher than that of the pure Ti and HA coating groups. As demonstrated by the adhesion of the pre-osteoblast to the substrate (Fig. 14.37), the amount of cells on the dense and the porous coating was also relatively high, indicating that the weakly mineralized collagen coating facilitated early cell adhesion. After 72 h of incubation, mineralized collagen coating also had a higher MTS value, revealing that collagen coating can promote cell proliferation.

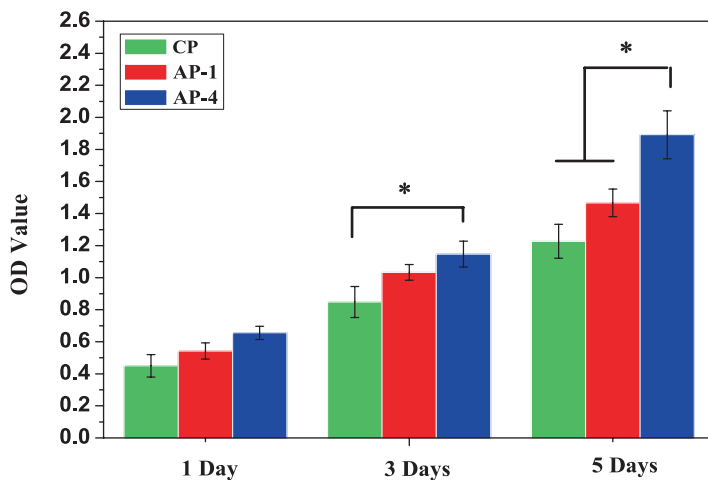
The cytocompatibility of mineralized collagen coating prepared by alternating potential-assisted electrochemical deposition was shown in Fig. 14.38. The multi-



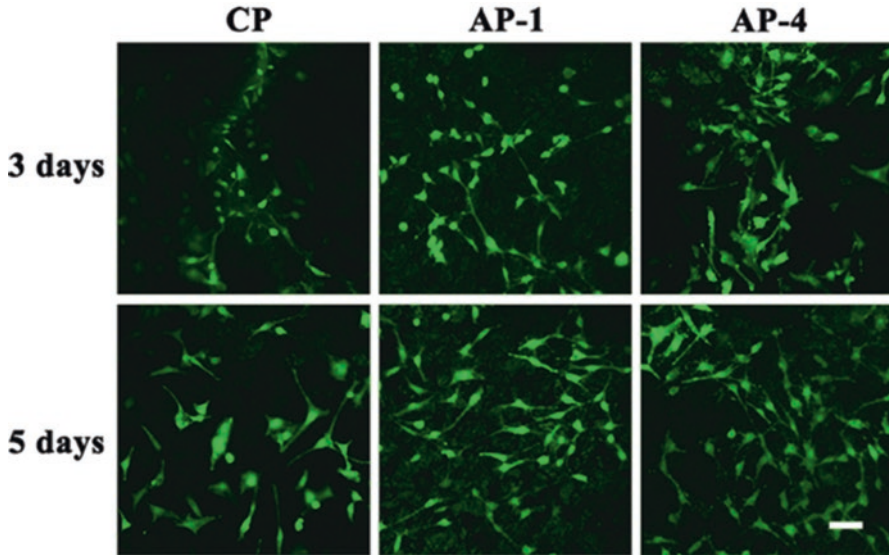
**Fig. 14.36** Bioactivity test mineralized collagen coating (MTS method) *Ti* Ti metal substrate, *HA* hydroxyapatite coating, *PC* porous mineralized collagen coating, *DC* dense mineralized collagen coating (Reprinted from Ref. [15], with kind permission from Springer)



**Fig. 14.37** Cell attachment on different substrates after 1 day of incubation (Reprinted from Ref. [15], with kind permission from Springer)

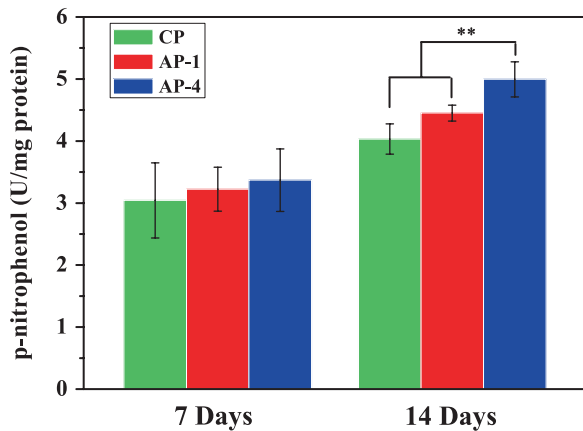


**Fig. 14.38** CCK-8 activity after incubation for 1, 3, and 5 days of different groups (Reprinted from Ref. [17], Copyright 2012, with permission from Elsevier)



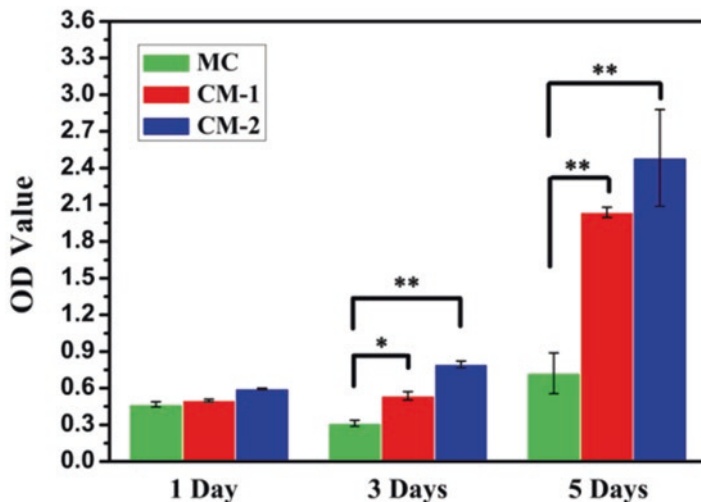
**Fig. 14.39** The CLSM images of cells on different coatings. Scale bar, 100  $\mu\text{m}$  (Reprinted from Ref. [17], Copyright 2012, with permission from Elsevier)

**Fig. 14.40** Alkaline phosphatase expressed levels of MC3T3-E1 cells cultured on different coatings after culture for 7 days and 14 days, respectively (Reprinted from Ref. [17], Copyright 2012, with permission from Elsevier)



layered mineralized collagen contributed to an increase in cellular responsiveness (Figs. 14.38 and 14.39). Higher content of weakly mineralized collagen was conducive to the promotion of cell proliferation because the naked collagen would expose more active site that can be identified by cells. The coating with high content of weakly mineralized collagen was more favorable for cell spreading and pseudopod extension, which further indicated that the coating prepared by our method could promote the cell proliferation (Fig. 14.40), and the effect was enhanced with the increased content of weakly mineralized collagen.





**Fig. 14.41** Cytocompatibility of different coatings (Reprinted from Ref. [18], Copyright 2012, with permission from Elsevier)

#### 14.4.1.2.2 Osteoblast Response to the BSA/Mineralized Collagen Coatings

Figure 14.41 showed that the adhesion behavior of cells on the coating had no obvious difference as the BSA content increases, but the cell proliferation of coatings with high content of BSA was significantly better than that of coating with lower BSA content and pure mineralized collagen coating, which was caused by the release behavior of BSA. BSA was mainly located in the bottom layer of the coating. With the prolongation of cell culture, the BSA in the coating was gradually released, so the difference of cell behavior was more obvious in the period of proliferation. This was also illustrated by the amount and the morphology of the cells on different samples (Fig. 14.42).

#### 14.4.1.2.3 Osteoblast Response to the HACC/Mineralized Collagen Coatings

The cytocompatibility of mineralized collagen coatings could be controlled by different distributions of HACC. As shown in Fig. 14.43, the higher concentration of HACC in the electrolyte decreased the cell compatibility of the coating, but when the HACC was distributed to the inner layer of the coating, the cell compatibility was improved and even exceeded that of the collagen coating. For HACC-IN64 and HACC-OUT64 coatings soaked in cell culture medium for 7 h before cell culture, the CCK-8 results were showed in Fig. 14.43b. The OD values of HACC-IN64 and HACC-OUT64 coatings increased by 40% and approximately twofold after soaking, respectively, higher than COL coatings. This suggested that HACC in the coatings

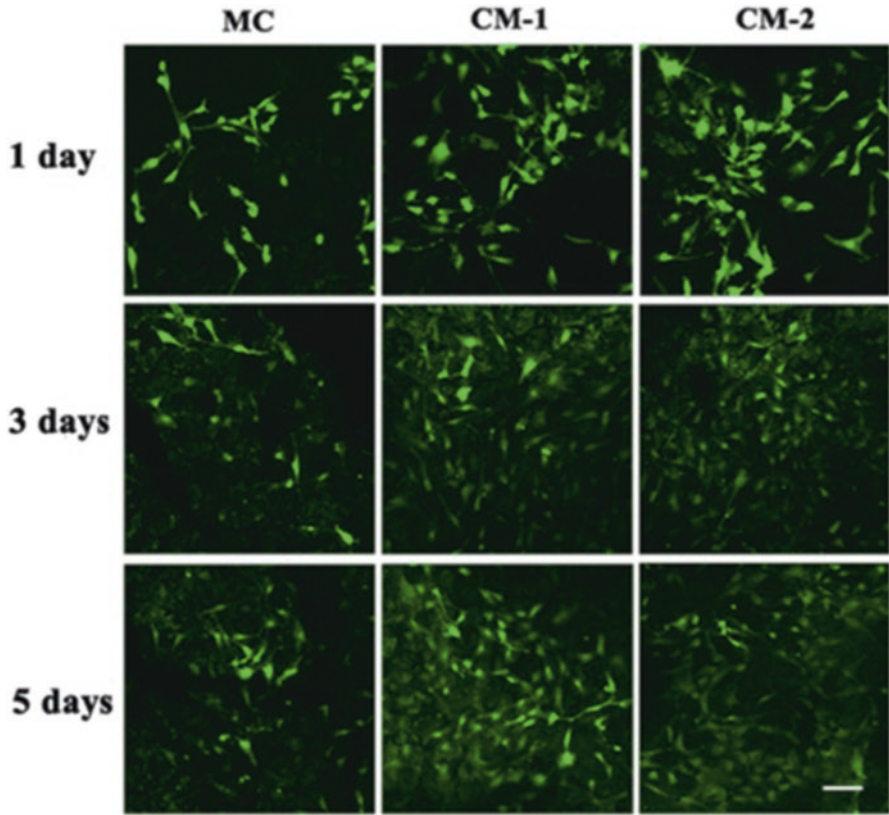


Fig. 14.42 The CLSM images of cells on different coatings (Reprinted from Ref. [18], Copyright 2012, with permission from Elsevier)

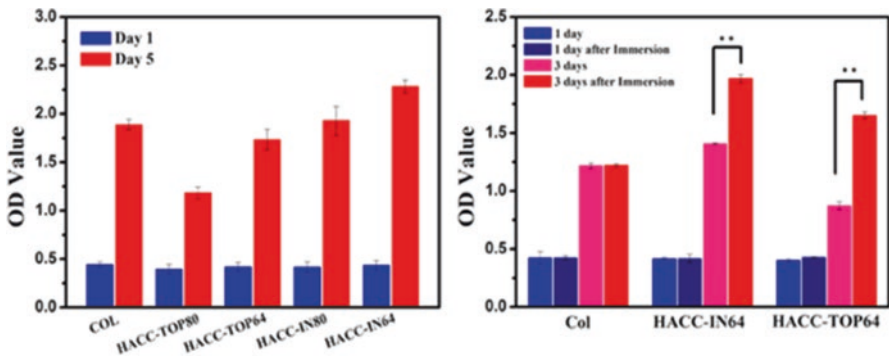
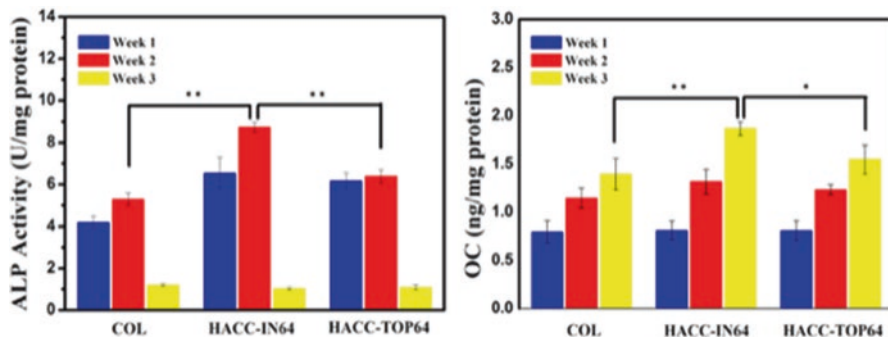


Fig. 14.43 Cytocompatibility of the coatings with different treatments (Reprinted from Ref. [19], Copyright 2012, with permission from Elsevier)



**Fig. 14.44** Osteogenic differentiation evaluations (Reprinted from Ref. [19], Copyright 2012, with permission from Elsevier)

had a strong ability to interact with proteins from culture medium, and consequently the negative influence on initial cytocompatibility could be eliminated.

HACC-IN64 and HACC-OUT64 coatings with similar rhBMP-2 loading amount showed differences in ALP expression levels. The level of 2-week cultured cells on HACC-IN64 coatings was increased by 37% compared with that on HACC-OUT64 coatings. The ALP levels of the cells cultured on rhBMP-2-loaded HACC-IN64 and HACC-OUT64 coatings were higher than that on rhBMP-2-loaded COL coatings. OCN expressions of the cells cultured on all coatings for 1 week presented no significant difference. However, for the 2- and 3-week cultured cells, the expressions of OCN on rhBMP-2-loaded HACC-IN64 coating were increased by 7% and 21% compared with that on rhBMP-2-loaded HACC-OUT64 (Fig. 14.44). The findings above suggest that the coating with HACC located at the inner part supports rhBMP-2 to create a remarkable osteogenic differentiation.

#### 14.4.1.2.4 Osteoblast Response to Chitosan/Mineralized Collagen Coatings

Figure 14.45 showed the proliferation behavior of cells (measured by the MTS test) in the presence of the coatings. After 6 h, 24 h, and 2 days of incubation with the cells, the incorporated coatings (MCC-1, MCC-2) resulted in higher OD values than that of the unincorporated coatings (MC). After 5 days of culture, the different coatings (MC, MCC-1, MCC-2) produced no obvious difference in the OD values. These results showed that the incorporation of chitosan nanospheres had no obvious influence on the proliferation of cells on mineralized collagen coatings.

The initial attachment of the cells to the different coatings (MC, MCC-1, MCC-2) was shown in Fig. 14.46. The SEM images showed that the pre-osteoblastic cells were all well spread and that the pseudopodia of the cells penetrated fully into the coatings. This observation indicated that the incorporation of chitosan nanospheres did not affect the initial attachment of the cells to the coatings.

Figure 14.47 showed the adhesion and proliferation of cells on the different coatings. Cells were cultured for 6 and 24 h in order to observe differences in cell

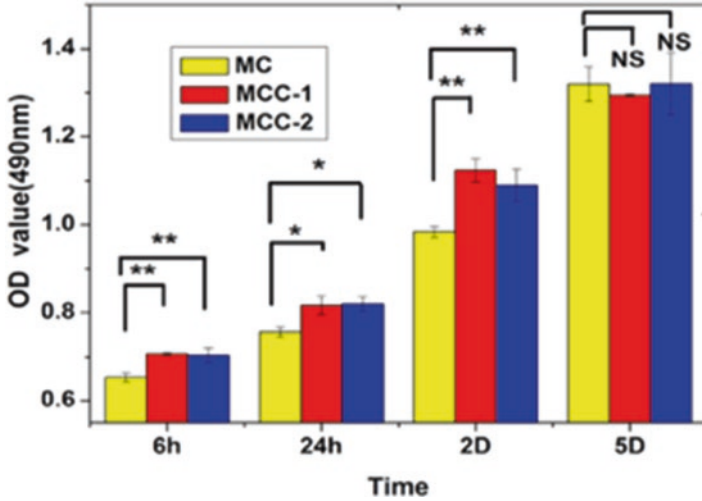


Fig. 14.45 MTS results for different coatings

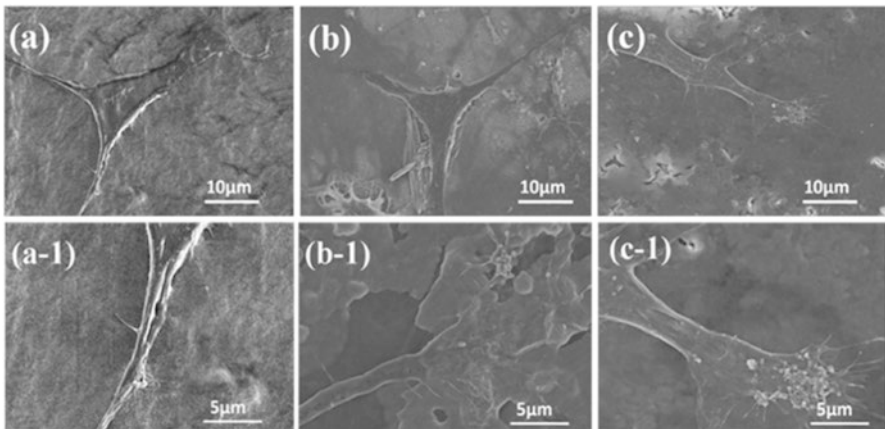
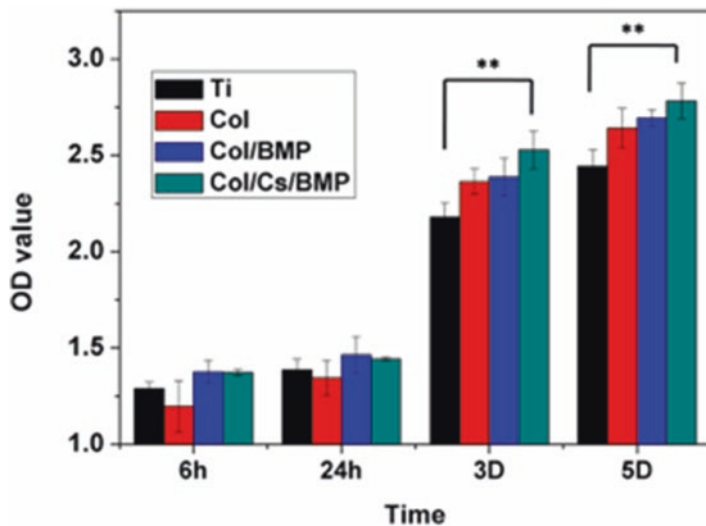


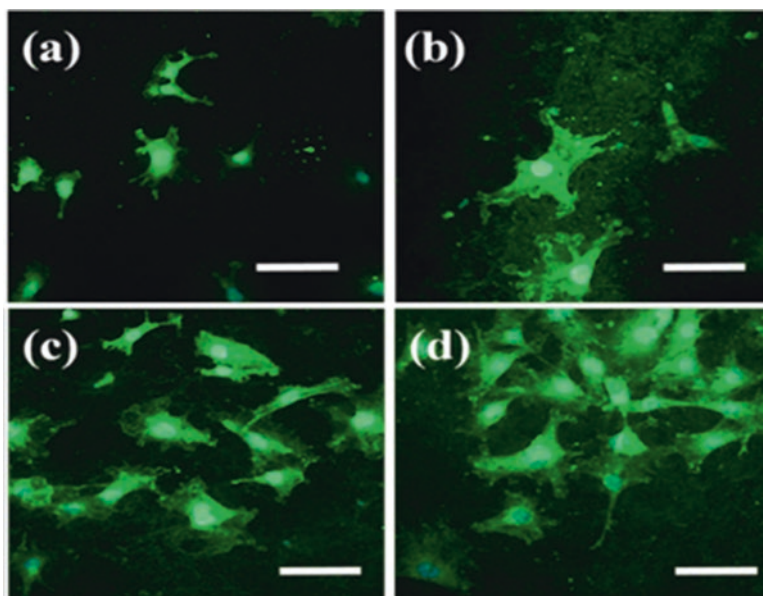
Fig. 14.46 MC3T3-E1 adhesion on different coatings for 3 h, (a) MC coating, (b) MCC-1 coating, (c) MCC-2 coating

attachment and for 3 days and 5 days to observe differences in cell proliferation. When incubated for 6 and 24 h, there was no obvious difference in cell attachment among the different groups. After culture for 3 and 5 days, the OD value of the cells cultured on the coatings increased with rhBMP-2 loading, with the Col/Cs/BMP coating showing the highest OD value.

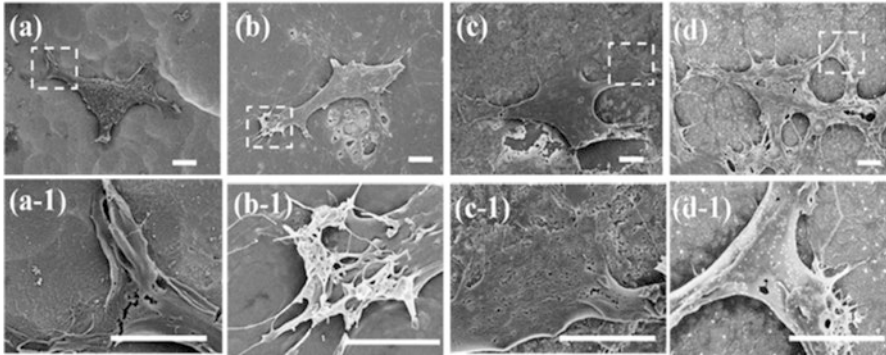
Intensive and extensive vinculin expression signals appeared within the cytoplasm and around the edges of cells grown on the Col coating (Fig. 14.48b), and the



**Fig. 14.47** Cck-8 activity in 6 h, 24 h, 72 h, 3 days, and 5 days for different groups. Data shown are means  $\pm$  SD of triplicate assays. Asterisks denote significant differences between different groups ( $* P < 0.05$ ) (Reproduced from Ref. [23] by permission of The Royal Society of Chemistry)

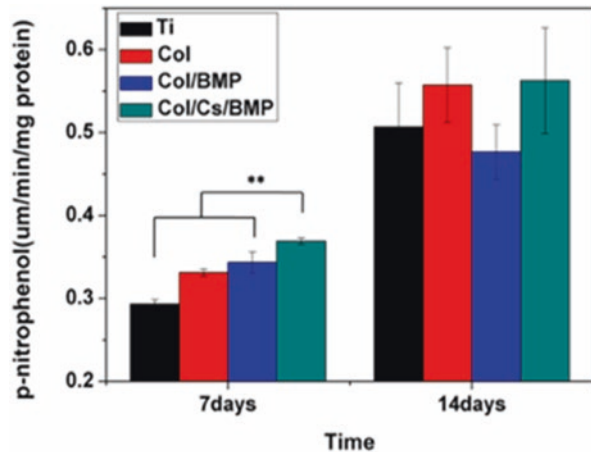


**Fig. 14.48** Representative vinculin fluorescence images of cells on different groups: (a) Ti, (b) Col coating, (c) Col/BMP coating, (d) Col/Cs/BMP coating (the scale bar is 10  $\mu$ m) (Reproduced from Ref. [23] by permission of The Royal Society of Chemistry)



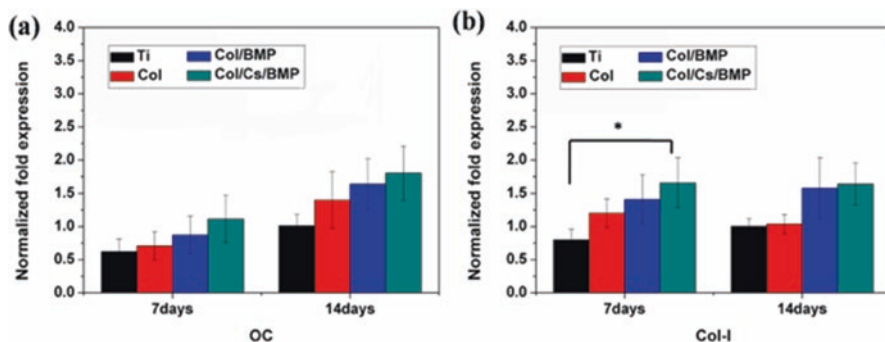
**Fig. 14.49** SEM images of cell morphology on different groups: (a) Ti, (b) Col coating, (c) Col/BMP coating, (d) Col/Cs/BMP coating (the scale bar is 5  $\mu\text{m}$ ) (Reproduced from Ref. [23] by permission of The Royal Society of Chemistry)

**Fig. 14.50** Alkaline phosphatase expressed level of MC3T3-E1 cells cultured on different groups after culture for 7 and 14 days, respectively; data shown are means  $\pm$  SD of triplicate assays. Asterisks denote significant differences between different groups (\*\*  $P < 0.01$ ) (Reproduced from Ref. [23] by permission of The Royal Society of Chemistry)



cells spread well with filopodia embedded into the coating (Fig. 14.49b, b-1). On Col/BMP and Col/Cs/BMP coatings, vinculin was also well distributed in the cells (Fig. 14.48c, d), with filopodia embedded deeply into the coatings (Fig. 14.49c-1, d-1), which implies that cell attachment was good. In contrast, only weak vinculin expression (Fig. 14.48a) and discrete cells with no extended pseudopodia could be observed on the Ti surface (Fig. 14.49a, a-1).

As can be seen from Fig. 14.50, the level of ALP expressed by cells cultured on all coatings increased over the period from 7 to 14 days. The ALP expression level of cells cultured on the Col/Cs/BMP coating for 7 days was significantly higher (by approximately 20%) than that of cells on Col alone and approximately 50% higher than those grown on Ti ( $P < 0.01$ ), and this increase in ALP expression indicated the



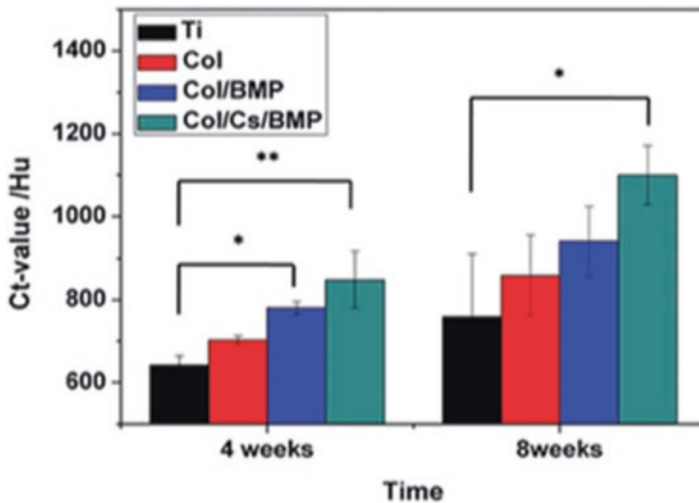
**Fig. 14.51** Relative mRNA expression of different groups: (a) osteocalcin, (b) Col I. The value was normalized to GAPDH. Data shown are means  $\pm$  SD of triplicate assays. Asterisks denote significant differences between different groups ( $*P < 0.05$ ) (Reproduced from Ref. [23] by permission of The Royal Society of Chemistry)

increased differentiation of cells cultured on the Col/Cs/BMP coating. However, there were no significant differences among cells cultured on the different coatings for 14 days, which could be attributed to the fact that ALP is an early marker of differentiation, indicating that cells on the Col/Cs/BMP coating differentiated more rapidly but that cells on the other coatings later caught up so that the difference weakened with time. For the later indicators of differentiation osteocalcin (OC) and collagen I (Col I), the expression of OC in cells cultured on the Col/Cs/BMP coating for 7 and 14 days was higher than that of cells cultured on Col or Col/BMP coatings or Ti control (Fig. 14.51a). The Col/Cs/BMP coating also resulted in a higher level of expression of Col I than any of the other groups (Fig. 14.51b).

## 14.4.2 In Vivo Tests of Composite Coatings

### 14.4.2.1 In Vivo Tests of Chitosan/Mineralized Collagen Coatings

To evaluate the role of different coatings in the growth of bone tissue on implants, spiral CT was employed to characterize bone density around the implant, a parameter which is considered to be the key to the assessment of new bone formation after implantation. As shown in Fig. 14.52, the bone density around the implant increased with time, and the density around the implants with Col, Col/BMP, and Col/Cs/BMP coatings was higher than that around Ti implants after 4 and 8 weeks. The density around the Col-/Cs-/BMP-coated implants at both 4 and 8 weeks after implantation demonstrated significant differences ( $P < 0.01$  and  $P < 0.05$ ) from the Ti group at the same time points. Although the artifacts of implants were present, the results here were only to show the enhancement trend of the osseointegration process with the help of chitosan nanospheres.

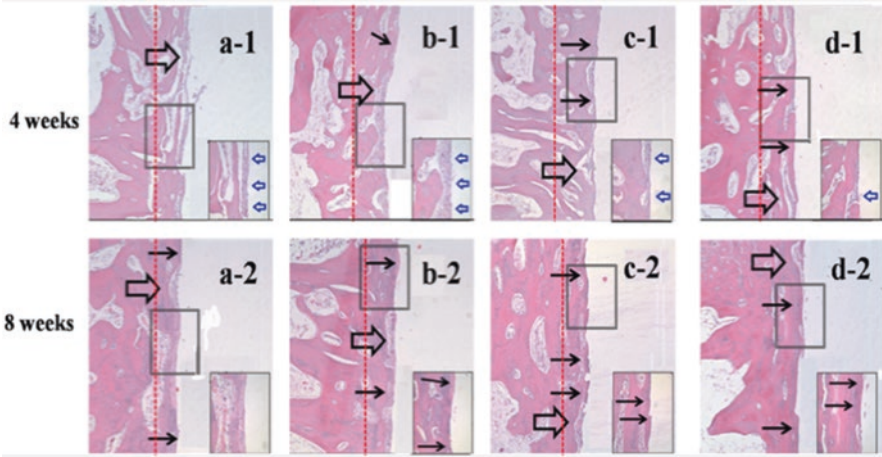


**Fig. 14.52** CT values of different groups. Data shown are means  $\pm$  SD of triplicate assays. Asterisks denote significant differences between different groups (\*  $P < 0.05$ , \*\*  $P < 0.01$ ) (Reproduced from Ref. [23] by permission of The Royal Society of Chemistry)

Hematoxylin and eosin (H&E) staining of decalcified samples was employed to evaluate osteogenesis at the interface between the implant and the host bone. After implantation for 4 weeks, a mass of fibrous and non-connective tissues could be seen around the implant in the Ti (Fig. 14.53a-1) and Col groups (Fig. 14.53b-1), while these tissues were replaced by a dense bone matrix (fewer small blue arrows and more small black arrows) in the groups with Col/BMP (Fig. 14.53c-1) and Col/Cs-/BMP-coated implants (Fig. 14.53d-1). After implantation for 8 weeks, the density of the bone matrix increased in all groups in comparison with the results at 4 weeks; however, the bone matrix (stained red at the interface) was still sparse in the Ti group (Fig. 14.53a-2), while the connective and compact bone matrix could be seen in the Col, Col/BMP, and Col/Cs/BMP groups (Fig. 14.53b-2, c-2 and d-2). The results also show that no ectopic bone formation was observed in any of the groups. Importantly, the boundary between the host bone and the new bone disappeared 8 weeks after implantation (Fig. 14.53d-2), indicating that osseointegration had been basically completed.

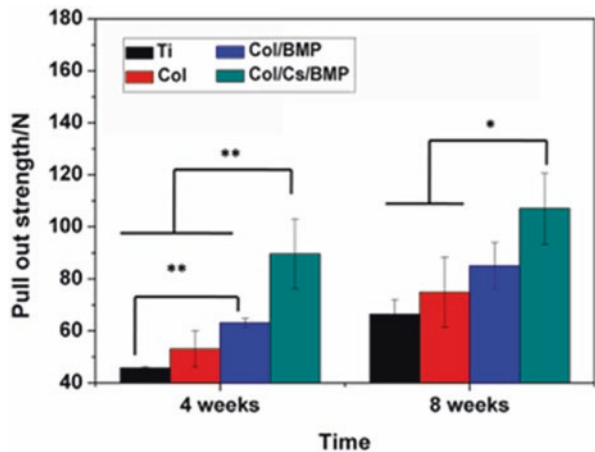
The biomechanical properties of an implant are key parameters affecting osseointegration after surgical implantation. In biomechanics, the maximum pull-out force is often used to mechanically evaluate the bone bonding strength between the bone and the implant. In this study, the pull-out test results revealed that the pull-out force increased over time for all groups (Fig. 14.54). Col coating on the implant resulted in a greater bonding strength between the implant and the bone (53.09 N at 4 weeks and 74.89 N at 8 weeks) compared to the Ti group (45.80 N at 4 weeks and 74.89 N at 8 weeks). When rhBMP-2 was incorporated into the coatings, the pull-out force increased (63.13 N at 4 weeks and 85.13 N at 8 weeks), while enhanced





**Fig. 14.53** Histological observations (H&E staining): (a) Ti, (b) Col, (c) Col/BMP, (d) Col/Cs/BMP. Large picture, 100; inset picture, 400. The *blank part* represented the location of the implant. The *big arrows* point to the fracture of the plant pitter. The *small black arrows* point to the dense bone matrix. The *small blue arrows* point to the unconnective tissues. The *red line* represents the boundary of the new bone and the old bone (Reproduced from Ref. [23] by permission of The Royal Society of Chemistry)

**Fig. 14.54** Pull-out strength of different groups after 4 weeks and 8 weeks of implantation. Data shown are means  $\pm$  SD of triplicate assays. *Asterisks* denote significant differences between different groups (\* $P < 0.05$ , \*\* $P < 0.01$ ) (Reproduced from Ref. [23] by permission of The Royal Society of Chemistry)



rhBMP-2 loading resulted in the coating with the highest pull-out strength (89.67 N at 4 weeks and 107.01 N at 8 weeks). This increase of pull-out strength in comparison with the Ti control group (48.92% increase at 4 weeks and 30.16% increase at 8 weeks) indicates a significant effective improvement in osseointegration compared with the previous work.

The aim of incorporating rhBMP-2 is to accelerate new bone formation. In *in vivo* tests, the quantity of new bones formed was found to significantly increase

with increasing rhBMP-2 loading. The boundary between the host bone and new bone disappeared in 8 weeks after implantation in the Col/Cs/BMP group, indicating that the implant had basically become integrated with the host bone. Here, the coating was biodegradable and finally the coating would be biologically transformed into the new bone. The results of pull-out tests showed that the degree of osseointegration was enhanced dramatically with rhBMP-2 loading, with the increase in pull-out strength being greater after 4 weeks of implantation than that after 8 weeks. This implies that the incorporation of chitosan nanospheres with rhBMP-2 could make a significant contribution to early bone formation (4 weeks) and that this plays an important role in shortening the osseointegration process to almost 8 weeks. The new bone growth would be extremely limited after the completion of the osseointegration process as the space for tissue growing around coating was very limited. The BMP loading-dependent increase in the pull-out strength could imply that the BMP released from the coating played the key role in osseointegration. The Col/Cs/BMP coating group demonstrates good ability to induce bone formation at its surface.

Based on the results from both *in vitro* and *in vivo* tests, the enhanced amount of loaded rhBMP-2 of 1,186 ng/cm<sup>2</sup> in the Col/Cs/BMP coating not only shows the highest loading value in this work but also demonstrates that it is necessary to reach a desired value range in order to significantly accelerate the osseointegration process, which is essential to shorten recovery time after implantation surgeries.

## 14.5 Summary and Outlook

Applying the electrochemical deposition method, a collagen/calcium phosphate nanocomposite coating similar to the natural bone structure can be prepared on the surface of the metal implant, and an ameliorate electrochemical deposition method called alternating potential-assisted electrochemical deposition method can be designed by programmatically changing the deposition potential and time. The alternating deposition of highly and weakly mineralized collagen and the controllable distribution of the active carriers make it possible to effectively achieve a controlled preparation of the collagen/calcium phosphate composite coating. The results of cell culture show that the collagen/calcium phosphate nanocomposite coating had a good biological response, which could obviously promote the adhesion, proliferation, and differentiation of osteoblasts and finally accelerate the osseointegration process. In addition, the collagen/calcium phosphate coating can act as an antibacterial drug or growth factor carrier, so as to prolong the effective antibacterial time on the implant surface and further accelerate the implant-host osteoconjunction process.

In summary, collagen/calcium phosphate composite coating is a promising bone implant material; in addition to its osteoinductive compositions, the use of optimal preparation techniques can realize the purposeful control of its structure and components, such as in line with different disease needs; the porous structure can load

the corresponding drug or growth factor, so as to achieve the purpose of effective treatment. In addition, the utilization of electrochemical deposition technology is expected to achieve the assembly between protein and protein or protein and gene, by which the function of mineralized collagen is optimized to enhance the ability of the coating at the molecular level to promote osteogenesis. Taking an insight into the process of bone formation, the role of implanted coating materials and the way of regulation will provide guidance for the functional design and preparation of the coating, which is in favor of further enhancing the biological function of implants.

## References

1. Puckett SD, Taylor E, Raimondo T et al (2010) The relationship between the nanostructure of titanium surfaces and bacterial attachment. *Biomaterials* 31:706–713
2. Pan YK, Chen CZ, Wang DG et al (2013) Preparation and bioactivity of micro-arc oxidized calcium phosphate coatings. *Mater Chem Phys* 141:842–849
3. Cui FZ, Li Y, Ge J (2007) Self-assembly of mineralized collagen composites. *Mater Sci Eng R* 57:1–27
4. Rammelt S, Schulze E, Bernhardt R et al (2004) Coating of titanium implants with type-I collagen. *J Orthop Res*. 2004 22:1025–1034
5. Rammelt S, Illert T, Bierbaum S et al (2006) Coating of titanium implants with collagen, RGD peptide and chondroitin sulfate. *Biomaterials* 27:5561–5571
6. Morra M, Cassinelli C, Cascardo G et al (2006) Collagen I-coated titanium surfaces: mesenchymal cell adhesion and in vivo evaluation in trabecular bone implants. *J Biomed Mater Res A* 78:449–458
7. De Jonge LT, Leeuwenburgh SCG, van den Beucken JJJP et al (2010) The osteogenic effect of electrosprayed nanoscale collagen/calcium phosphate coatings on titanium. *Biomaterials* 31:2461–2469
8. Cai YL, Liang CY, Zhu SL, Cui ZD, Yang XJ (2006) Formation of bonelike apatite–collagen composite coating on the surface of NiTi shape memory alloy. *Scripta Mater* 54:89–92
9. Manara S, Paolucci F, Palazzo B et al (2008) Electrochemically-assisted deposition of biomimetic hydroxyapatite–collagen coatings on titanium plate. *Inorg Chim Acta* 361:1639–1645
10. Fan Y, Duan K, Wang R (2005) A composite coating by electrolysis-induced collagen self-assembly and calcium phosphate mineralization. *Biomaterials* 26:1623–1632
11. Hu K, Yang XJ, Cai YL et al (2006) Preparation of bone-like composite coating using a modified simulated body fluid with high ca and P concentrations. *Surf Coat Technol* 201:1902–1906
12. Teng SH, Lee EJ, Park CS et al (2008) Bioactive nanocomposite coatings of collagen/hydroxyapatite on titanium substrates. *J Mater Sci: Mater Med* 19:2453–2461
13. Dalby MJ, Riehle MO, Sutherland DS et al (2004) Use of nanotopography to study mechanotransduction in fibroblasts—methods and perspectives. *Eur J Cell Biol* 83:159–169
14. Park CH, Rios HF, Jin Q et al (2012) Tissue engineering bone-ligament complexes using fiber-guiding scaffolds. *Biomaterials* 33:137–145
15. Tu J, Yu M, Lu Y et al (2012) Preparation and antibiotic drug release of mineralized collagen coatings on titanium. *J Mater Sci: Mater Med* 23:2413–2423
16. Ling T, Lin J, Tu J et al (2013) Mineralized collagen coatings formed by electrochemical deposition. *J Mater Sci: Mater Med* 24:2709–2718
17. Zhuang J, Lin J, Li J et al (2015) Alternating potentials assisted electrochemical deposition of mineralized collagen coatings. *Colloids Surf B Biointerfaces* 136:479–487
18. Zhuang J, Lin J, Li J et al (2016) Electrochemical deposition of mineralized BSA/collagen coating. *Mater Sci Eng C* 66:66–76

19. Chen L, Lin J, Li J et al (2016) Spatially-controlled distribution of HACC in mineralized collagen coatings for improving rhBMP-2 loading and release behavior. *Colloids Surf B Biointerfaces* 145:114–121
20. Lee YJ, Elosegui-Artola A, Le KHT et al (2013) Morphological cues for regulation of cell adhesion and motility with tailored electrospun scaffolds of PCL and PCL/PVP blends. *Cell Mol Bioeng* 6:482–495
21. Ling T, Yu M, Weng W et al (2013) Improvement of drug elution in thin mineralized collagen coatings with PLGA-PEG-PLGA micelles. *J Biomed Mater Res A* 101:3256–3265
22. Kong Z, Yu M, Cheng K et al (2013) Incorporation of chitosan nanospheres into thin mineralized collagen coatings for improving the antibacterial effect. *Colloids Surf B Biointerfaces* 111:536–541
23. Kong Z, Lin J, Yu M et al (2014) Enhanced loading and controlled release of rhBMP-2 in thin mineralized collagen coatings with the aid of chitosan nanospheres and its biological evaluations. *J Mater Chem C* 2:4572–4582

# Chapter 15

## Preclinical and Clinical Assessments of Calcium Phosphate Bone Cements

Lingyan Cao, Deliang Zeng, Shuxian Lin, Xiao Wang, Xiangkai Zhang,  
Ao Zheng, Jie Wang, and Xinquan Jiang

**Abstract** With the increasing development of biomaterials and tissue engineering, many novel biomaterials have been successfully explored. Before they are put into clinical applications, it is obligatory to appropriately and adequately evaluate the biocompatibility/biological performance in vitro and in vivo. Calcium phosphate cement (CPC), a bioactive and biodegradable grafting substance, has attracted great attention in recent years because of its self-setting and hardening after mixing the powder with a liquid phase to form a viscous paste. In order to fulfill the requirements in the clinical applications, it is necessary to make the preclinical and clinical assessments of CPC-based materials. Hence, the preclinical and clinical evaluations of biomaterials as medical devices are introduced in this chapter. The related testing protocols, standards, and guidelines are also summarized. Specifically, the biocompatibility of CPCs is evaluated and discussed in detail. Moreover, the actual and potential clinical applications of CPCs are highlighted, particularly in the fields of oral and maxillofacial repair, cranioplasty, orthopedic applications, as well as other usages including as a drug delivery carrier and medical biosensors.

**Keywords** Biomaterials • Clinical assessments • Calcium phosphate cement • Biocompatibility • Bioresorbability

---

L. Cao • D. Zeng • S. Lin • X. Wang • X. Zhang • A. Zheng • J. Wang • X. Jiang (✉)  
Department of Prosthodontics, Ninth People's Hospital, Shanghai JiaoTong University School  
of Medicine, No. 639, Zhizaoju Road, Shanghai 200011, China

Shanghai Key Laboratory of Stomatology & Shanghai Research Institute of Stomatology,  
National Clinical Research Center of Stomatology, No. 639, Zhizaoju Road,  
Shanghai 200011, China  
e-mail: [xinquanj@aliyun.com](mailto:xinquanj@aliyun.com)

## 15.1 Introduction

In the past half century, an explosive growth concerning the clinical use of medical implants has been witnessed by clinicians, researchers, patients, and industry. Orthopedic, plastic, and oral maxillofacial/dental surgeons are the typical examples of the medical specialties in which implantable devices are applied for millions of patients every year. The economic burden of treating the related diseases and problems has been estimated to exceed US\$39 billion in the United States alone [1]. In China, the treatment expenses are also expected to increase rapidly due to the fast growth of the aging population and an increase in life expectancy. Thus, tissues and organs may be forced to function longer than they may be able to independently withstand, and more artificial tissues/organs with adequate biological responses have to be developed for clinical applications.

In order to solve these issues, the scientists and researchers in the fields of materials, chemical engineering, pharmaceutical engineering, etc. have made numerous efforts in recent years. They have built a close collaboration with medical doctors for monitoring and evaluating the performances of biomaterials *in vitro* and *in vivo*. These evaluations provide the essential information about biological responses, gauge efficacy, and the stability over time of biomaterials, which enable the optimization of the biomaterials and implants, and realize the desirable bone substitutes. Therefore, it is necessary to understand what the basic evaluations of biomaterials/medical devices are in the preclinical and clinical studies. Moreover, the related test protocols, standards, and guidelines are discussed in this chapter. Take calcium phosphate cement (CPC) as a typical biomaterial example. Its biocompatibility and characteristics of the CPCs are evaluated and discussed in detail. The potential clinical applications of CPC are highlighted in this chapter.

Calcium phosphate (CP)-based materials are relatively “old” but attractive biomaterials, which have also experienced great development throughout the years. It has been hypothesized that the implants/medical devices composed of calcium and phosphate at a proportion similar to the one of the bone tissues would not be rejected by the organism; the ability of CP-based materials to trigger bone formation in biological systems continues to be unmatched by other recently developed biomaterials. However, there still exist limitations of CPC in clinical applications. To achieve complete substitution and fulfill the regeneration of a damaged or lost tissue, it still needs more optimization work on CP-based biomaterials as well as in-depth clinic assessments.

## 15.2 Preclinical Evaluations of Biomaterials and Medical Devices

In a medical sense, biocompatibility is used to refer to the ability for the materials to interact with the body without causing damages. Thus, it is necessary for materials to be tested for the biocompatibility before medical applications. As a desired property of a product, biocompatibility covers many features of the product and the biological response from the host. The materials/medical devices have to meet the

basic requirements of the biocompatibility. If the biomaterials/medical device shows the adverse effects on the host, it indicates the biocompatibility deficiency. An attempt has been made in this section to give a summary over the anticipated major hazards during the production and sourcing phase. The existing guidelines and standards concerning safety evaluation of medical device and the individual components of biomaterials are also reviewed.

One of major goals of a scaffold is to offer proper structure support for cells. Recent attention has been focused on the role of a scaffold in mimicking the natural microenvironment of the cells. The more similarities between the natural extracellular matrix and a scaffold, the more possibility it will achieve biocompatibility. Typically, a scaffold can be made with the combination of synthetic materials (i.e., polylactic-co-glycolic acid, polylactic acid) and natural materials (such as fibronectin, collagen, elastin, and hyaluronic acid derivatives). Such natural materials possess a relative high variation of the characteristics, influencing the quality of the final product. For instance, these materials hold the advantages in terms of degradability, physiological properties, and also the inherent ability to contact with the receptors and proteins on cells and in the natural extracellular matrix, while the synthetic materials could reduce the variation of the materials characteristics.

Any significant host responses or immunological reactions, such as the irritation and sensitization of the materials and additives (i.e., coupling agents, blowing agents, and ceramic fillers), are supposed to be determined [1, 2]. Furthermore, it is necessary to evaluate the short-term and long-term influence of the materials over the living tissue at both the macroscopic and microscopic levels. There are some parameters which should be taken into account, including presence of necrosis, distribution and number of inflammatory cell types, degeneration, extent of fibrosis, and tissue ingrowth.

Toxicity is another required biological parameter for biomaterial evaluation. The release of substances and materials are supposed to be examined for systemic and local toxicity. The degradation products might compose metabolites with non-immunogenic and toxic effects. The biological responses of mammalian cells to toxic agents are evaluated by using the cytotoxicity assays. Some endpoints, such as cellular metabolism, cell proliferation, and cell damage, can be then determined. After determining the reproductive and developmental toxicity, carcinogenicity and possible genotoxicity need to be taken into consideration. The blood compatibility will be created through a set of testing over particular categories like complement, hematology, platelets, coagulation, and thrombosis, once the scaffold interacts with the blood. The tests are supposed to be selected according to the intended application and duration of the contact.

It is also of great importance to consider pyrogenicity testing. The presence of bacterial endotoxins serves as the major cause for the pyrogenic reactions. And some evidences have shown that there are some material-related pyrogens. The limulus amoebocyte lysate (LAL) is the most exclusively applied assay to examine bacterial endotoxins. However, the material-related pyrogens cannot be detected in the assay. Moreover, interferences impose great suffer to LAL, resulting in either false-negative or false-positive outcomes. Thus, some other tests have to be carried out. Taking the rabbit pyrogen test as an example, the pyrogens in both assays are supposed to be eluted, while materials should be firmly attached by pyrogens. For

solid materials, there is “Human Whole Blood Pyrogen Assay,” which is based on the pro-inflammatory cytokine interleukin  $1\beta$ 's production after being exposed to pyrogens. However, this is still under validation now [3].

The structure features of scaffolds including pore size and porosity also affect their biological performances since the vascularization and the ingrowth of host cells mainly rely on the porous features. The biological behavior of the host cells will be impacted by the transmission of the mechanical forces via the scaffold [4]. The resorption and degradation process for both synthetic and natural materials will be helpful for the regeneration of host tissues. Ideally, the implanted material is resorbed during controlled time period, which hence makes it possible for the host cells to establish a new extracellular matrix with adequate structural strength. Eventually, the materials can be degraded and removed instead of accumulating in the body. Therefore, it is necessary to determine the effect of the excretion of degraded products on human body and the metabolism process.

By using related animal models, the implantation studies over the final product can offer the information what the researchers need. However, these researches are impeded by the fact that a xenogeneic immune response will be induced by the human cellular components. This issue can be solved by performing studies in immunocompromised mice which are reconstituted with human leukocytes and immune-privileged sites [5].

## 15.3 Test Protocols for Preclinical Evaluations

Generally, test protocols can be divided into short-term and long-term tests. Normally, the safety evaluations of medical devices are carried out to determine the risk of adverse effect on health. As the exposure of the materials will lead to adverse effects, preclinical evaluation of toxic potential for these materials is required, and hence the potential hazard to the patient can be minimized. The potential range for biological hazards is pretty wide and can be determined through the testing shown in Table 15.1.

### 15.3.1 Short-Term Tests

According to the Wikipedia Website, acute toxicity represents the adverse effects of a biomaterial exposing to animal models in a short period of time. In contrast, chronic toxicity describes the adverse health effects from repeated exposures over a longer time period (months or years). Experimentally, nonpolar, polar, and other extracting media can be injected in mice by either the intraperitoneal (IP) route or the intravenous (IV) route. Observations of such toxicity signs are immediately made in 24-, 48-, and 72-h intervals. Because of the ethical issues, most acute toxicity data are collected from animal testing or on similar substances.



**Table 15.1** Typical test protocols for preclinical evaluations

Test Classification	Testing	Notes
Short-term tests	Thrombogenicity	Tendency of forming a thrombus or clot in contact with the blood
	Sensitization	Progressive amplification of a response
	Hemolysis	Rupturing red blood cells
	Irritation	Skin irritation for the sake of the edema and erythema
	Toxicity	Acute toxicity via IV route
Long-term tests	Sensitization	Maximization test and closed patch test
	Genotoxicity	Genetic damages
Supplementary tests	Subchronic and chronic toxicity	Adverse effects for long term
	Carcinogenicity	Agents involving in causing cancer

For medical devices, pyrogenicity testing is required because of the contaminant, surface characteristics, immune reaction of the host cells, and batch dependence. However, the risk of febrile reaction has been limited by a program test to acceptable level of patients as an outcome of administration through the injection of the product's extraction. The test includes the measurement of the temperature increase in rabbits after the IV injection of the test solution. Every 30 interval, the temperature is recorded, and then the temperature change will be compared.

The hemolytic potential is assessed through the hemolytic properties. The materials used for medical devices interact with the blood. Under static or dynamic conditions, rabbit blood serves as the test specimens, in comparison with the control materials. Changes in the plasma hemoglobin are measured for indicating the hemolytic properties.

To evaluate the intracutaneous/intradermal reactivity, the nonpolar and polar extracts are intradermally injected on both sides of rabbits at 24, 48, and 72 h. Observations are immediately made after the injection. Then, tissue reaction is graded for edema and erythema. To examine the skin irritation, the researchers use albino rabbits of either a single strain or sex. After closing and clipping of the dorsal side, the material is covered with and applied with a dressing, which is nonocclusive for 4 h. Skin will be observed at 24, 48, and 72 h for the sake of the edema and erythema.

### 15.3.2 Long-Term Tests

The skin sensitization in guinea pigs can be determined through various methods. The most exclusively used methods for delayed hypersensitivity include maximization test (MT) and closed patch test (CPT). In MT, the guinea pigs are administered by injections of test material extracts followed by the induction phase just after 7 days. The challenge phase with the test material just starts after 14 days of

injection. The sensitization potential of the test compound is then observed at 24, 48, and 72 h. For CPT testing, the test material extract has been applied in the dorsal area of guinea pigs or rabbits. This procedure is conducted weekly repeatedly in 3 weeks. After 14 days of the last application, the challenge phase with test material begins. The sites are then tested in 24 h, 48 h, and 72 h for the sensitization potential of the materials.

To examine the biological safety of the materials at the local site, the specimens are implanted in living animals for achieving the abnormal response of the tissues. Depending on the specific site, the specimens have different dimensions. As subcutaneously implanted, the material specimen has a millimeter dimension ranging from 10 to 12 mm in length and from 0.3 to 1 mm in thickness. The animals are then examined and euthanized for any response and reaction. The material specimen with 10 mm in length and 1–3 mm in width is also implanted in muscle. The following steps are then carried out:

1. If there is any infection in the presence of the sample, it would be recorded.
2. Assessment of tissues for giant cell proliferation, fibro-endothelial proliferation, plasma cell proliferation, eosinophil proliferation, and inflammation.
3. Muscle sample has been taken for the microscopic examination.
4. Observations for the appearance of the muscle surrounding the implant.

For bone implantation, the size of specimen depends on the size of the animal. Cylindrical implants with 6 mm in length and 2 mm in diameter are placed in the fibula and femur. The implantation is conducted by intermittent drilling with profuse irrigation at a low drilling speed via saline suction, hence avoiding the local tissue necrosis.

Genotoxicity describes the property of materials that damages the genetic information within a cell. The exclusively used genotoxicity tests for the medical devices involve *in vitro* and *in vivo* testing. The former one includes a number of assays: reverse mutation assay (*Salmonella typhimurium*), reverse mutation assay (*Escherichia coli*), *in vitro* sister chromatid exchange, *in vitro* mammalian cell gene mutation, and *in vitro* mammalian cytogenetic tests, while *in vivo* testing includes mouse heritable translocation assay, mouse spot test, chromosomal aberration analysis, germ cell cytogenetic assay, and micronucleus test.

### 15.3.3 Supplementary Tests

For medical devices, it is required to ensure the safety issues and no toxicity for long term. Thus, repeated doses have been given to these animals during the part of their life span (within 10%). This test has offered the information on the impact over the estimate of a no-effect level, the possibilities of accumulation, and target organs. And the appropriate dose levels are then determined for the following chronic studies. Besides, the safety criteria should be established for human exposure. The effects of single and multiple exposures to materials and devices are evaluated

during the entire life span of the test animals for chronic toxicity (more than 90 days in rats).

To evaluate the potential of carcinogenicity, some specific tests are carried out to assess whether either single implant or multiple implants have effects on tumorigenicity and chronic toxicity during a part of the total life span of the tested animals. When the devices have the potential to impact the reproductive system, it is recommended to carry out the developmental and reproductive toxicity studies, which could provide the evidences about the impact over reproduction function, embryonic development (teratogenicity/malformations), and the fetus early and prenatal developmental toxicity.

## 15.4 Clinical Evaluations of Biomaterials and Medical Devices

Since there still exist some issues with regard to effectiveness and safety, which cannot be confirmed adequately by laboratory or preclinical testing, a series of clinical trials are performed to evaluate these characteristics of implantable biomaterials/medical devices. The clinical evaluation is most closely connected with the prospective and randomized clinical trials. Depending on the requirements for safety or effectiveness with a device, the investigation might cover lots of clinical literatures and double-blind, prospective, randomized, and multicenter studies.

Historically, two kinds of clinical trials are available for manufacturing a device. The first actually is a feasibility study or a pilot study. Its goal is to collect safety data over the device in some human subjects. Usually, these trials should include 10–40 patients. For the device with significant risk, an investigational device exemption (IDE) must be approved by FDA. Otherwise, it's not allowed to be used in a clinical study for collecting safety and effectiveness data. By building the safety profile of the device to FDA, the device can be applied to a comparatively larger study afterward.

Pivotal trial serves as the following stage of the clinical trials, allowing a manufacturer to collect enough data and hence to support their marketing submission. Usually, it would be a premarket approval. This research is powered to illustrate some statistical assurance which can guarantee that the investigational device performs very rather good or at least much better in comparisons with the control. A pivotal trial should be 100–1000 patients. The trial is designed to illustrate the effectiveness and safety of the device based on the pre-specified endpoints. Finally, the subject number is based upon the difference in clinically relevant endpoints and the power of the study from the control and the subject device. Placebos have been used by the pharmaceutical world to control the investigational drugs. There is more flexibility in the device in terms of trial design. It is rather common to adopt historical data or the device non-operational version as the control.

The FDA has approved the introduction of a new clinical trial modality. This stage serves as the first step in the early feasibility studies or in human. There are five to ten subjects being in the first-in-human study. It gives manufacturers a chance to characterize and understand their device in an earlier during the development phase compared with what was possible previously. It is required to illustrate whether the device is safe (for instance, preclinical data in vivo analysis). However, the total amount of data needed in the test might be less than that of data in the feasibility study. Such kind of study is especially useful for biomaterial manufacturers. This program actually is a pilot one during the publication time. The Center for Device and Radiological Health (CDRH) has selected a handful of devices. It would be a rather exciting new option if the pilot program actually goes well. This can be very beneficial to the new products.

The development stage of the clinical trials between devices and drugs begins to become parallel because of the introduction of the first-in-human clinical trial option. The general process is analogous even though the objectives of the stage dramatically differ between the device models and drugs. One growing difference from the model for the pharmaceutical development is that the clinical trials do not have to be linear. Without conducting a feasibility study, manufacturers could ask for launching a pivotal research with no any other experience with humans. If successful, clearance with a single investigation can be achieved.

It is of great importance to conform to the expectations of the FDA before initiating any kind of clinical evaluation if the objective is to launch some products on the US market. Guidance documents have been published by the FDA on clinical trial expectations for various devices. As the guidance document might be absent, it is necessary to have direct feedback from the agency. Early contact with the FDA serves as a key to collect sufficient safety data and tackle the concerns of FDA before the approval of IDE application. Frequently, insufficient bench and/or pre-clinical tests may lead to the failures of the IDE applications in the USA. The early contact with the FDA can be realized via a formal pre-IDE meeting or informal discussions with the FDA representatives. Regardless of the method, all discussions actually are non-binding and hence are supposed to be adopted to confirm the current thinking and expectations of the agency. A final guidance document has been issued by the agency over the pre-submission meetings. This document can be seen from their website.

The agency is going to be very helpful to solve questions together with the manufacturers in terms of both protocol development and trial design. However, a request might be turned down, and remarkets will be provided through an e-mail because of overwhelming demand and limited resources. CDRH has over 400 pre-IDE meetings every year per division. Useful information has also been provided by this draft on pre-submission conferences which involve over one center (for instance, the Center for Biologics Evaluation and Research (CBER)). During the pre-submission meeting, the guidance collected from the agency serves as not binding. However, it has been stated by the agency that it will try to obey the agreements and then make decisions where the desired indication has been changed by the manufacturer for the

adoption of the pre-submission meeting or if new safety questions have come up during the clinical research.

## 15.5 Standards and Guidelines

Standards and guidelines supporting a regulatory system for biomaterials or medical devices should contain requirements for performance and safety evaluation of products. Methods should be described identifying and evaluating potential adverse effects. Depending on the specifications of the standards and guidelines, general techniques or specific assays may be assigned as tools for the identification and quantification of the associated risks.

To evaluate and identify the possible adverse effects of medical products, appropriate approaches are supposed to be used. Specific assays or general techniques might be taken as tools in the quantification and identification course, depending on the specifications of standards and guidelines. Related parties like physicians, government, and manufacturers could reach a consensus over the testing type that is about to be implemented. Besides, they need to reach a consensus about the standards they are going to set before the entering of the product into the market. These requirements of the product can be set in the international or the national standards. At this moment, standards that are designed specifically for the products loading with viable cells are still not released yet. As increasing innovative products are put on the market, harmonization of biocompatibility-related aspects has shown a pretty important role. This has been shown from the case that EUCOMED, who stands for the interest of most of the non-pharmaceutical European medical technology industry, published a position paper, which focuses on the need of the entire European market according to these products' risk/benefit approach.

Besides the safety and quality aspects of the biocompatibility, the standardization related to the product safety needs to be discussed. EN ISO 10993 series is very helpful for the assessment of the biocompatibility aspects. The medical device directive is supported by the standard norms, which have been published by European Committee for Standardization (CEN) and the International Organization for Standardization (ISO). It has been classified into 20 different parts, and each division is based upon the duration and frequency of the implant, the application site, as well as many other factors. Part 1 depicts how the appropriate examinations are selected, and the following parts depict particular testing or evaluation types. This standard applicability adopted in medical devices and biomaterials is at the moment hampered by the fact that scaffolds adopted in the tissue engineering are intended mostly to degrade with the passing of time. The specific guidance for the biocompatibility testing of the biodegradable materials has been started quite recently in the EN ISO 1993 framework. The evaluation of undesired pyrogenic, immunological, or toxicological reactions of nonviable animal tissues and their derivatives is provided in the 12,442 series standard.

The majority of the existing European documents have covered the safety and quality issues of the biomolecules because Council Directive 65/65/EEC marketed these biomolecules as medical products. These documents described the requirements for these biomolecules published by the ICH or CPMP. The ICH and the COMP documents concentrate on the safety evaluation for pharmaceutical-deriving biotechnologies. Besides, it also focuses on the impurities and contaminations of the product, the characterization specifications, and the selection of other related animal models for the immunogenicity and toxicity testing. The genetic tests are not involved in the description of these documents. Apart from ICH and CPMP guidance, the European Pharmacopoeia includes monographs depicting a great of test methods and quality requirements for some biologically active compounds, taking growth factors and interferon as examples.

One of the pioneers for the biomaterial standardization is the division on the Committee F04 on the Medical and Surgical Devices and Materials under the supervision of ASTM (American Society for Testing and Materials). This division has about 40 different task groups, covering the quality and safety issues of medical devices and biomaterials. These task groups include biomolecules and normal biology, tissue characterization, as well as many other things terminology. Usually, the terminology, classifications, and test methods should be adopted in a consensus process featured by input from the government, manufacturers, academic, and other interested parties.

The CEN Healthcare Forum (CHeF) has established a task group to explore the demands of the shareholders for the European standard development in terms of human tissues. The start of standardization over the horizontal subjects is connected with the medical devices or biomaterials like microbiological safety, biological safety, quality system, risk management system, and terminology. Standards such as CEN/TC 285-Non-active surgical implants, CEN/TC206-Biocompatibility of medical and dental materials and devices and CEN/TC206-Biocompatibility of medical and dental materials and devices, have been established by the technical committees (TCs). Apart from the ISO/TC 150, the necessity to promote the standards specifically was discussed by the task force that was gathered by the “implants for surgery.” According to their conclusion, the standardization activities of other organizations should be closely followed by the ISO, taking the CEN and the ASTM as examples. On the contrary, the ISO should not start any activity at its own.

Moreover, EMEA forecasted the increasing amount of products containing viable cells through Points to Consider document, which focuses on therapy products of human somatic cell (which serve as viable somatic cell preparation used suitably for the transfer), when the cells have been subjected to a specialized facility manufacturing process.

The process is supposed to be in those cases which encompasses expansion or over minimal manipulation which are designed to change the functional, physiological, and biological features of the resulting cells. It has been demonstrated that the combination of the noncellular matrix might be concluded in this manipulation. In addition, the resulting cell product is supposed to be definable in lights of quantitative

and qualitative composition. This draft document focuses on characterization, source, and suitability of other materials adopted in the manufacturing course, such as antibiotics and immunoglobulin as well as the cell culture procedures with no description over the generic tests. Note for guidance is closely connected with this subject in terms of the gene-transferred medical products. It has been deemed that the genetically modified cells will grow in appropriate matrices. It demonstrates that the separate components and final product's quality are supposed to be documented and characterized.

At last, provisions concerning the clinical trials especially connecting with the performing of the good clinical practice are established by Council Directive 2001/20/EEC. This directive demonstrates that the competent written authorization is supposed to be required before the commencement over the clinical trials about somatic cell therapy. This legal framework can then be adopted to prepare extra guidelines for the preclinical safety and quality assessment.

## **15.6 Biocompatibility Evaluation of Calcium Phosphate Cements**

Calcium phosphate cements have attracted great attention due to their excellent biological behavior (e.g., biocompatibility, bioactivity, and osteoconductivity). The biocompatibility of CPC has been investigated systematically, including the implant histological evaluation, the DNA damage assay (unscheduled DNA synthesis test), chromosome aberration assay (micronucleus test), gene mutation assay (Ames test), and cell culture cytotoxicity assay. The outcomes illustrated that CPC had been proven having no toxicity. Moreover, all tests for potential carcinogenicity of CPC are negative. The femurs of rabbits were implanted with CPC in a no-load condition. The histology of the specimen suggested that the implant actually joined the surrounding bone slightly. Quite a limited histological inflammatory reaction took place. Therefore, CPC serves as a very biocompatible material. Its application in humans seems to be safe [6].

The FDA has approved some CPC formulations which are used in the clinical sector [7, 8]. The Conformance Européenne (CE) also marked the same formulations for specific maxillofacial indications and also for the adoption of the bone-void filler in particular non-load-bearing orthopedic indications [9]. The major properties of these formulations actually are available. A variety of bone fillers and cements have been listed in the review [9]. Moreover, there are more cement formulations which are still in experimental stages.

## 15.7 In Vivo Appraisalment and Clinical Applications of CPCs

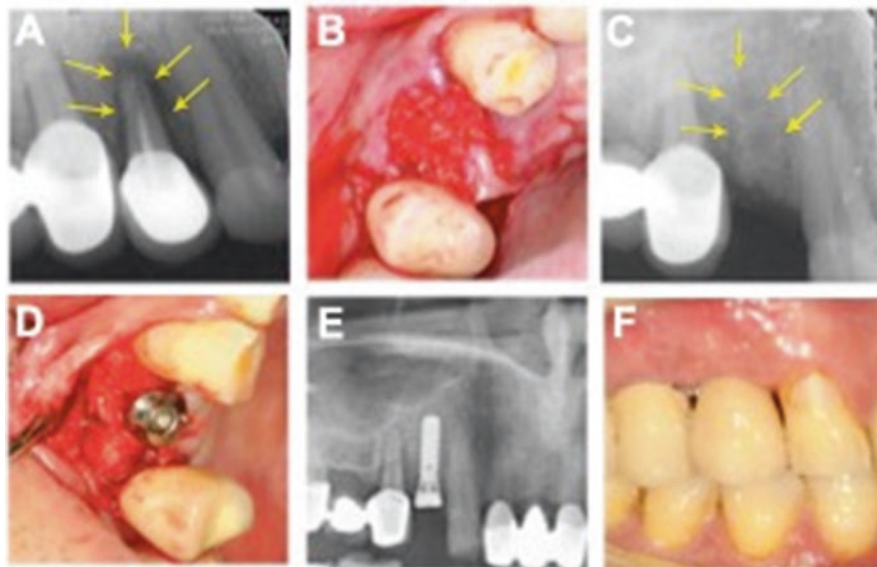
Many researches have already proved that CPCs are quite biocompatible as osteoconductive materials used to regenerate tissues [7, 10]. With available references so far, since 1987, CPCs have been investigated in vivo using different animal models [11–13] to validate the function variety and some typical medical applications.

### 15.7.1 Oral and Maxillofacial Applications

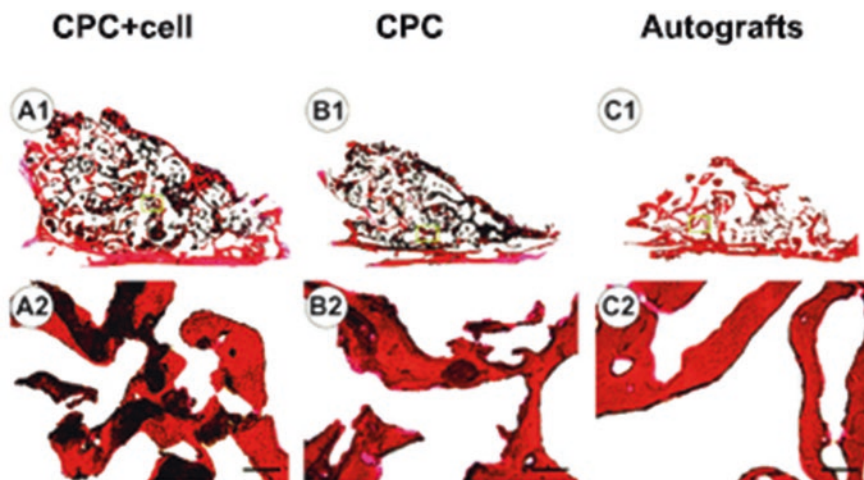
As bone filling materials, the injectable CPCs have been used to block up the gaps surrounding the oral implants. Although there was non-obvious resorption occurring, this kind of CPC induced excellent formation of new bone surrounding the oral implants [14]. Within the artificially created periodontal defects, CPCs acted as scaffolds for bone formation and provided histocompatible healing of periodontal tissues [15]. CPC blocks have also been applied for alveolar bone repair. Generally, the animal model is built by extraction of beagles' mandibular premolar teeth followed by a 1-month healing. The alveolar bone was then reduced to make space for the implants with being healed for another month [16]. It has reported that [16, 17] HA implants with coronal half embedded into the CPC block induced new bone formation within the initial cement areas at 1 month post-operation and showed pretty fixed attachment with the natural bone. The identical elemental distribution with natural bone was found within CPC site after 6 months detected by electron microanalysis and fluorescent labeling analysis. Our group has already started the clinical study on CPC scaffold loaded with BMP-2 for functional recovery of dental implant (Fig. 15.1), which displayed effective bone repair capacity on patients. Moreover, applying CPCs to pulp capping [18], maxillary sinuses' lifting, defects' repair of buccal dehiscence and atrophic areas [19], and root canal fillers [20, 21] were also reported. Some studies showed that CPCs would generate a secondary dentin within 24 weeks when used for pulp capping [22].

Utility of CPCs in oral and maxillofacial applications significantly reduced the use of autologous grafts and alloplastic implants [23]. High bioresorbability and biocompatibility of CPCs were also illustrated with none or little inflammation [24–31]. CPCs osteoconduction make them function feasibly as mandibular augmentation devices to induce subperiosteal and endosteal osteonal bone formation [32]. In clinic, CPCs have already been applied for 38 patients with reconstruction of front facial skeleton and frontal sinus. According to the report [33], the success rate was 82% for the reconstruction by the calcium phosphate cement, superior than acrylic implants. Our unpublished data also showed CPC scaffolds loaded with osteoblast cells have been already successfully applied in vivo for maxillofacial bone regeneration and segmental bone defect repair (Fig. 15.2). CPC doped with magnesium phosphate was also used in the maxillary sinus floor elevation in vivo. The great

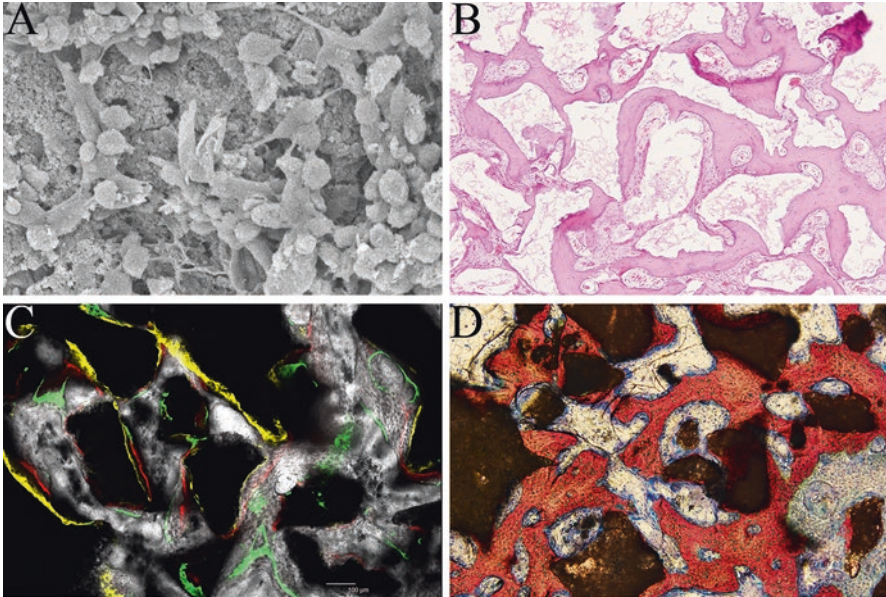




**Fig. 15.1** Clinical trials of CPC scaffolds loaded with BMP-2 for alveolar site preservation and functional recovery of dental implant. (a) X-ray tooth film of alveolar resorption. (b, c) After dental extraction, the extraction socket was immediately filled by BMP-2 loading CPC scaffolds for alveolar site preservation. (d, e) After 6 months, the dental implant was implanted at the preserved site. (f) At 3 months post-implantation, the custom crown is cemented onto the implant



**Fig. 15.2** In vivo application of CPC scaffolds for bone repair: (A1, A2) Osteoblast cells loaded CPC, (B1, B2) CPC, and (C1, C2) autologous bone grafts were, respectively, implanted for maxillofacial bone regeneration in dogs. The zoomed in views of top row images were showed in the bottom row



**Fig. 15.3** Maxillary sinus floor elevation with calcium-magnesium phosphate cement (CMPC) and bone mesenchymal stem cells (BMSCs) in rabbits. (a) Scanning electron microscopic images of BMSCs attached on CMPC in vitro; (b) HE staining image of newly formed bone in CMPC/BMSCs group at 8 weeks after operation; (c) Sequential fluorescent labeling was used to determine the rate of bone formation and mineralization in CMPC/BMSCs group. The rabbits were injected with the fluorescent labeling reagent, respectively, at 2, 4, and 8 weeks after operation; (d) microscopic view of bone formation in the maxillary sinus from non-decalcified slide in CMPC/BMSCs group at 8 weeks after operation

biodegradability and excellent osteoconductivity exemplified the CPC as a potential alternative graft for maxillofacial bone regeneration (Fig.15.3) [34].

### 15.7.2 Cranioplasty

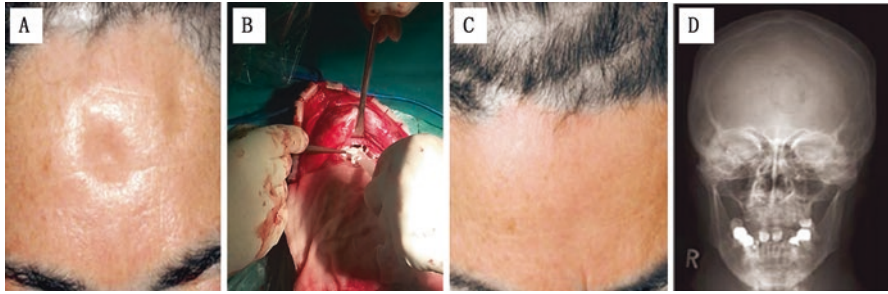
CPCs have been examined at cranial defects in many animal models. It's reported that modified CPC combined with a PLA mesh underlay was applied to repair 10-mm diameter full-thickness calvarial defects of Yorkshire pigs and displayed extensive bony ingrowth at 6 months after implantation without compromise to its biocompatibility, osteoconductivity, or remodeling capacity [35]. Kim et al. [36] surgically created bilateral subcritical-sized (8-mm diameter) defects in the parietal bones of each rabbit and randomly filled either the new fiber-reinforced CPCs or conventional CPCs (positive control). The results indicated that there was no severe inflammatory response or osteolysis but new dural and pericranial bone formation along the implants and excellent bone-to-implant interfaces in all of the CPC-filled

defects. Eight-millimeter cranial defects of rats were repaired with human umbilical vein endothelial cells (hUVECs) co-cultured with human umbilical cord MSCs (hUCMSCs), MSCs from induced pluripotent stem cells (hiPSC-MSCs), MSCs from embryonic stem cells (hESC-MSCs), and human bone marrow MSCs (hBM-SCs) delivered via CPC scaffold [37]. Finally, the complex scaffold achieved excellent osteogenic and angiogenic capabilities *in vivo*. Apart from cells, CPC scaffolds with suitable modification, such as improving the porous structure [38], also could load growth factor or composited with polymers to accomplish the defect regeneration. Actually, the molding capacity of CPC material at placement possesses a great advantage [8]. For instance, BoneSource™, as one kind of the commercial product of hydroxyapatite cement, has already been introduced for the fixation of cranial defects like contiguous craniotomy cut and neurosurgical burr holes, whose defect surface area is less than 25 cm<sup>2</sup>. In dogs, the supraorbital ridge was supplemented by BoneSource™, and hence the skull base defect was augmented [39].

In clinical studies, CPCs were applied to parietal craniotomies to avoid the temporal depression. Excellent findings were obtained from more than 100 human patients when a CPC was applied in the treatment of cranial defects. After 6 years, the cement's success ratio increased to 97% [40]. Rebone Gutai® (CPC-based powders) (Shanghai Rebone Biomaterials Co., Shanghai, China) developed by Prof. Changsheng Liu has also been used for filling and adhering to the skull defect. Figure 15.4 shows the clinic case treated with Rebone Gutai powders. As can be seen, the male patient (53 years old) had a skull defect on the forehead. After the craniotomy, Rebone Gutai powders were applied to fill the bone deflection with negative pressure drainage. The patient had good postoperative conditions without irritation locally. After 1 year, the digital and X-ray images showed the perfectly filled skull.

To compare the complication rates of CPCs and Ti-mesh cranioplasty in patients, Foster et al. [41] reviewed the clinical data from 672 consecutive patients who underwent retromastoid craniectomy at a single institution for microvascular decompression or tumor resection. For Ti-mesh group, there were 38 complications (11.4%) related to the surgical site, while 2 patients (0.6%) experienced wound infection, no patients (0%) had CSF leak, and 2 patients (0.6%) had other wound complications for the CPC cement cranioplasty group. Obviously, the CPC cement cranioplasty could significantly decrease the rate of wound infection and CSF leak and holds great potentials as an alternative replacing the titanium cranioplasty with better patient satisfaction.

However, there was significant heterogeneity in the estimated rate of major complications, infection, and reoperation ( $p < 0.001$ ), while minor complications and secondary contour correction had less heterogeneity ( $p = 0.58$  and  $p = 0.78$ , respectively), which was showed in the clinical meta-analysis on CPCs in skull reconstruction [42]. Using methyl methacrylate or autogenous bone, calcium phosphate fared no better, and sometimes fared worse, when mean complication rate and complication range of CPCs were compared with the other large cranioplasty studies than these other modalities. Calcium phosphate, therefore, should only be used



**Fig. 15.4** Skull defect filled with Rebone Gutai powders: (a) before operation, (b) in surgery, (c) 1-year follow-up of post-operation, and (d) X-ray image of 1-year follow-up

selectively, and prospective long-term studies are needed to further refine its role in skull reconstruction.

Recently, the three-dimensional printing (3DP) technique enables the production of a properly fitting implant with complicated shape and personalized design for craniofacial defects. Klammert et al. generated CPC-based skull specimen as precise patient-oriented craniofacial implants by using a 3D powder printing system. Since the original human cadaver skulls were mirror-imaged into the printed skull via using computer-aided designed, the individual implants showed a high degree of accuracy and suitable physical/mechanical characteristics [43]. Therefore, combination of CPC materials with these flexible manufacturing processes will realize the patient-specific implantable parts for various clinical applications.

### 15.7.3 Orthopedic Applications

#### 15.7.3.1 Restoration of Metaphyseal Defects

The application of CPCs in bone reconstruction has been detailed and elaborated in Chap. 1. Treating bone defects in the proximity of joints still remains as a challenge in the field of orthopedic surgeons, especially for those aged patients. Internal fixation of metaphyseal fractures may be difficult because of the low strength in the cancellous bone that makes up the major part of the metaphysis. In addition, the fragment closest to the joint is often short, and the fracture frequently has an intra-articular component. Two factors frequently complicate stabilization of metaphyseal fractures. The first is the crushing of subchondral cancellous bone by depressed articular fragments at the time of injury. Reducing the fracture during surgery creates a metaphyseal defect that must be filled to prevent the joint surface from subsiding when the bone is subjected to loading. Most commonly, the subchondral void is filled with autologous bone graft. However, this procedure has serious drawbacks, such as donor site morbidity and the limited immediate mechanical stability afforded by cancellous autograft. The second factor is the presence of osteoporosis, which

increases the risk that a fracture will become displaced before it heals. Formulation improvement allows CPC a better candidate in bone regeneration. It has been reported [44] when applied to supracondyle hole defect (5 mm in diameter) in the femurs of New Zealand white rabbits, CPC could induce  $12.4 \pm 2.7\%$  of new bone formation within 12 months, while that of its composite group containing addition of chitosan fiber and gelatin was  $46.5 \pm 3.2\%$  ( $p < 0.05$ ). Both CPC and the composite had osteoconductive characteristics and good biocompatibility with no adverse response. Strontium modification to CPC (SrCPC) is also an effective way to induce the enhanced new bone formation in a critical-size metaphyseal defect in the femur of ovariectomized rats [45, 46].

#### 15.7.3.1.1 Hip Fractures

Surgical treatment is generally accepted for patients with hip fracture. However, the stability of internal fixation of displaced femoral neck fractures is often poor since most patients who experience a hip fracture are elderly and suffering from osteoporosis. Apart from improvement of deficient blood flow, good primary stability is also helpful with reducing the complications of internal fixation. For trochanteric fractures, generally referring to the two-part fractures, healing is often not difficult. As to the multifragmentary fracture, it is indeed a technological challenge. The demand for mechanical properties prompts solutions when attempting to achieve the fracture stability. A sliding screw device in combination with CPC was applied to treat the trochanteric fractures with a detached minor trochanter in a cadaver model for the mechanical evaluation [47, 48]. The CPC-augmented group showed significantly higher stiffness, stability, and strength and less shortening at the fracture site. Moreover, the CPC-augmented group showed closer strain on the medial bone surface to normal than that of the metal device alone group. CPC has also been evidenced to be useful for augmentation of unstable trochanteric fractures in a prospective, randomized multicenter clinical trial [49]. Surgical fixation using a conventional sliding screw system together with CPC filling was adopted for patients with a trochanteric fracture including a detached posteromedial fragment. The results demonstrated that augmentation with CPC might be an attractive option for better fracture stability and reduced pain during the early phase of the rehabilitation compared with using sliding screw system alone, when treating severely unstable trochanteric fractures.

However, although the treatment of CPC augmentation combined with cannulated screws fixation can significantly enhance stability in the cement-augmented fractures, CPC was still not recommended for void filling agent to patients with displaced femoral neck fractures [50]. The possible reason is that the cement inserted at the fracture void might harm the vulnerable circulation to the femoral head and lead to an increased risk of complications.

### 15.7.3.1.2 Proximal Humerus

It often needs no operation for majority of fractures through the proximal humerus. However, minimally invasive techniques are required for reduction and fixation to reduce the risk for further impairment of the blood circulation to the humeral head caused by the trauma. As there is an inadequate fixation, secondary displacement becomes the common problem. One possible reason for the infrequent secondary displacement is the lack of cancellous bone support due to the bone defect and the void created behind the reduced humeral head. In a case series [51], CPCs were filled into the subchondral voids in 29 patients with severely impacted valgus fractures with open reduction. Besides, fixation by either screw or a buttress plate was adopted. The results showed that all fractures united and all the reductions were maintained. Until final follow-up at between 1 and 2 years, no patient had any signs of osteonecrosis of the humeral head.

### 15.7.3.1.3 Distal Radius

In clinic, closed reduction and plaster are often used to heal fractures of the distal end of the radius. However it usually shows notable curative effect on patients who have little initial displacement, limited comminution, and good bone quality. Plaster alone may lead to a high risk for secondary displacement and malunion since its poor stabilization of fractures with severe comminution, bone loss at the fracture site, or involving osteoporotic bone. Hence, injectable CPCs may be a good choice to fill the metaphyseal defect, improve fracture stability, and reduce immobilization time.

Fresh fractures of distal radius have been treated with CPC [52, 53]. Enough filling of the fracture void by CPC can be achieved by means of percutaneous injection. A significantly faster gain in grip strength and range of movement at 8 weeks was found in the group treated by CPC augmentation combined with a short period of plaster immobilization compared with conventional external fixation. Fractures to be displaced after primary treatment with closed reduction and plaster are also indications for CPC [54]. It is recommended that an open cementing technique, which includes evacuating the organized hematoma before injecting the cement, should be applied to patients who need a secondary procedure after redislocation while wearing a plaster cast. Clinical researches have illustrated 76% success rate of brushite cements during reconstruction of distal radial metaphyseal fractures. It has been found the leakages of the cement in some adjacent tissues. However, it has been resorbed eventually with nondramatic complications. Besides, clinical failures in these processes have been found to have close connections with poor bone quality, lack of stable fixation, and contact between joint and cement [55].

#### 15.7.3.1.4 Calcaneus

It is still controversial to take surgical treatment for restoring the anatomy of the subtalar joints because of the technical difficulties. The challenges of such surgeries are often related with the unstable metal fixation on the fracture fragments. The crushed cancellous bone usually made calcaneus fractures worse by reducing cancellous bone density. Hence, it is beneficial for patients to choose injectable, bioactive cements for curing calcaneal fractures. In a clinical study, 36 calcaneal fractures with joint depression were treated with a combination of internal fixation and CPC [56]. The shortest time to full weight bearing was 3 weeks after surgery, and the patient showed no radiological evidence of loss of reduction, while the recommended time to full weight bearing for traditional surgery is 8–12 weeks. In another clinical series, a similar technique using conventional metal hardware and CPC to fill in the defect below the posterior facet after open reduction was adopted on the 15 patients with displaced intra-articular calcaneal fractures [57]. No patient had any visible loss of reduction based on radiographs until healing. Obviously, augmentation with CPC holds the potential to provide a more stable fixation compared with metal fixation alone.

#### 15.7.3.1.5 Tibial Plateau

For fractures of the tibial plateau, surgery is often necessary to elevate the depressed articular fragments and restore the joint stability. The metaphyseal void outlined by crushed cancellous bone is usually filled with autologous or allogenic bone graft or with preformed blocks or granules composed of sintered, highly crystalline hydroxyapatite. Although autograft is the clinical golden standard with desirable osteoconductive and osteogenic properties, its mechanical stability is not adequate for the full weight bearing during the healing process of the fracture. The injectable bioactive cements such as CPCs can fill the defect perfectly and provide good stability with enough compressive strength. Compared with bone graft filling, CPCs can help patients to get earlier active joint motion and shorter time to full weight bearing [58]. A clinic study including 30 patients with a lateral tibial plateau fracture was carried out by filling either autologous bone or CPC into the subchondral void to evaluate the stability of the elevated articular fragment until healing and also to determine the actual weight bearing [59]. The results showed that patients treated with CPC got earlier full weight bearing (6 weeks) than the bone-grafted group (12 weeks).

#### 15.7.3.2 Ligament Anchor

The ligaments, muscles, tendons, and bones actually belong to the musculoskeletal tissues, which possess various kinds of properties. The physiological interfaces that connected such tissues have been adapted to permit the minimal injury's force

transmission. Current approaches to tissue-engineered ligaments and tendons do not involve such interfaces, constraining their future success. Recent studies *in vitro* have evaluated the potential of brushite cements in getting the ligaments anchored over the bone. Therefore, a mechanical suitable interface is generated [60]. To realize this goal, the shape of the anchor system and the cement composition need to be optimized carefully. Thus, more researches conducted recently have explored the application of 3D printing techniques so that it can be used to optimize the cement ligament sinews. The 3D technology is used to print the monetite and brushite brackets for one-ligament-bone replacement. The monetite brackets and brushite have been checked *in vitro* and showed a great compressive force being alike to the artificial brackets [61].

Another method to prepare ligament sinews is to connect the ceramic anchor of the cast brushite with a fibrin gel, which is contained in the fibroblasts. It is reported that the interface between the sinew and ceramic became more powerful with the passing of time because of the production of collagen and cellular proliferation. The tensile forces were resisted by 42 kPa. The Young's modulus of this sinew type could increase to 5.5 MPa when the cells have been surrounded by growth factors. The bone-tendon interface is anchored through the brushite cements in the reconstruction of anterior cruciate in rabbits. An implanted tendon has been secured in the tunnel, which is perforated via this technique. It has been shown that placing the brushite cement in the tunnel indeed reduced the number of intratunnel mechanical failures and promoted the bone-tendon interface strength [62].

### 15.7.3.3 Reinforcement of Osteosynthesis Screws

It is obvious that the stability of the osteosynthesis screws is of great importance in realizing successful treatment in patients who suffer from serious complicated bone fractures. The fixation of the osteosynthesis screws indeed poses a great challenge to victims whose bone quality is poor. Taking those patients who have to suffer osteoporosis as examples, there is a therapy treating this disease, which is to use polymer cement (PMMA, named polymethyl methacrylate) to stabilize the screws. However, this cement is in exothermic setting and is not resorbable *in vivo*. Considering the reasons above, brushite cements have been deemed as another choice. Landuyt et al. [63] have conducted the research *in vitro* to evaluate the pull-out power of the removed osteosynthesis screw. The pullout force of brushite cement was found to be increased by three times. CPCs have also been used for augmentation of anterior vertebral screw fixation [64]. Its pullout force was enhanced by  $50 \pm 37\%$  compared with the untreated group. In eight cases of CPC-augmented vertebral arch, only one case occurred as vertebral fracture. It indicates there is pretty feasibility of applying CPC to strengthen the osteoporotic vertebral screw.



### 15.7.3.4 Vertebroplasty and Kyphoplasty

Vertebroplasty and kyphoplasty are two surgical procedures that have been introduced to medically manage of osteoporosis-induced vertebral compression fractures. Both procedures involve injection of self-setting CPC pastes into the fractured vertebral for a faster healing [40, 65–71]. With a canine model, Turner TM and colleagues claimed that CPCs served as viable alternatives to PMMA cements, which can be applied into the treatment of large vertebral defects [72]. Positive results would be obtained with no complications if the vertebroplasty procedures were conducted with amount of CPC, namely, the correct powder to liquid ratio [72–74]. CPCs have been applied successfully in kyphoplasty which promoted patient mobility, reduced pain, and increased vertebral height [75]. As filling materials, brushite cement was injected to the body to fix the osteoporotic damaged vertebrae. According to cadaver studies, brushite cement is capable to promote the density of the mineral in the bone with a rate of 20–50%. The vertebral stiffness was increased by 120% and the maximum force was 113% after the vertebrae was injected with the brushite cement. Cement extrusion occurred in 12% of cases. However, the cement had no dramatic impact over healthy vertebra [68]. Nowadays, injectable CPCs are used widely in clinics in china, showing good cure effect. The detailed results can be found in Chap. 3.

In order to obtain a desirable clinical effect, surgical technique is important, including selection of indications as well as operation protocol, which should be paid more attention. Uncorrected operation will result in the cement leakage of vertebroplasty [76], even aggravating the cardiovascular deterioration in pulmonary cement embolism through the stimulation of coagulation [77]. Research efforts should be devoted to improving cohesion of CaP cements in an aqueous environment for future clinical applications such as vertebral body augmentation.

In addition, CPCs were also used in wrist arthrodesis [78], thoracolumbar burst fractures' reinforcement [79], and restoration of pedicle screw fixation [80]. Moreover, CPCs serve as a reliable subchondral replacement material next to the articular cartilage [81]. For all these cases, CPC addition allows the achievements of some advantages, including no complications and radiological consolidation for 23-month follow-up, augmented anterior column stability, or enhanced pedicle screw fixation. Clearly, CPCs may offer an alternative to currently used materials for the enhancement of fixation clinically.

### 15.7.4 Other Applications

Calcium phosphate cement can act as a carrier of drugs, having the capacity of providing accommodation for the drugs. It also has the ability to deliver this drug with time in neighboring tissues and keep it in a specific site. CPCs are biodegradable and injectable, which offered many advantages over other materials, such as self-setting at ambient temperature, having a large surface area and neutral pHs [82, 83].

Such properties held by CPCs, making them very active as the carriers of drugs, growth factors like morphogenetic proteins of bone [84–87], hormones [88], cytokines [89], anti-inflammatory drugs [90, 91], anticancer drugs [92], antibiotics [93–102], therapeutic peptides [103], etc. Although the majority of materials currently applied as carriers of drugs are polymers, CPCs possess added value because of their injectability and bioactive character in the sector of pharmacological treatment over skeletal disorders.

Injectable CPCs could work as fillers to block up the defects of the bone, which are generated by pathological tumors. The defects of the bone existed in the distal femoral condyle. According to *in vivo* studies, the formation of the bone was achieved via the brushite cements, superior to the formation obtained via the PMMA cements and collagen gels [104].

Amperometric biosensors can quantify and detect specific molecules in small numbers in either solutions or gases. The typical sensitive amperometric biosensors are mainly based upon the reactions over the enzyme. Judging from this perspective, brushite cements possess two critical properties, allowing it as an interesting device: (1) the capacity on electricity conduction via a mechanism, which is also named as proton conduction, and (2) the capacity in protein adsorption. Correspondingly, there are two recent studies concerning brushite-based biosensors. One study focuses on the glucose detection via the glucose oxidase of enzyme [105], while the other focuses on the phenol detection through the combination of the enzyme tyrosinase and the cement [106]. These two biosensors have been proven to have higher sensitivity and faster signaling compared with the traditional biosensor systems in terms of clay or polymeric matrices, which create more possibilities for future development of these devices.

## 15.8 Summary and Perspectives

To be summarized, there are truly impressive advances achieved in the past years in the field of CPCs for clinical applications. Not only did the knowledge of fundamental investigations assessing preclinical and clinical performances for CPC-based biomaterials/devices grow tremendously but also their applications as synthetic bone graft substitutes and delivery vehicles have demonstrated to be very important. CPCs have already been established for implanting/injecting/filling of voids in various types of bone defects. Especially, with the development of rapid manufacturing techniques and new functional additives in CPC formulations, much more attentions have been paid on these “old” biomaterials again in recent years because of excellent clinic performances, user-friendly, personalized design, etc. These materials will most certainly be part of the future armory when dealing with bone-related treatment. However, lots of efforts have to be devoted to the preclinical and clinical assessments of CPC-related products for achieving the diversity applications to their maximum extent since numerous researchers are developing/optimizing the material properties and exploring their potentials. It is really important

and highly challenging to devise or revise the biological response tests, which can appropriately, adequately, and rapidly identify biological responses to CPC biomaterials and CPC-engineered scaffolds which may contain various components such as new materials, cells, and proteins. With the technological developments by interdisciplinary experts, it is believed that CPC-based research and development will be marched to the next step, which fits well for damaged and diseased bone in our aging population.

## References

1. Hutmacher DW (2000) Scaffolds in tissue engineering bone and cartilage. *Biomaterials* 21(24):2529–2543
2. Gomes ME, Reis RL, Cunha AM, Blitterswijk CA, de Bruijn JD (2001) Cytocompatibility and response of osteoblastic-like cells to starch-based polymers: effect of several additives and processing conditions. *Biomaterials* 22(13):1911–1917
3. Fennrich S, Wendel A, Hartung T (1999) New applications of the human whole blood pyrogen assay (PyroCheck). *ALTEX* 16(3):146–149
4. Cima LG, Vacanti JP, Vacanti C, Ingber D, Mooney D, Langer R (1991) Tissue engineering by cell transplantation using degradable polymer substrates. *J Biomech Eng* 113(2):143–151
5. Boehncke WH (1999) The SCID-hu xenogeneic transplantation model: complex but telling. *Arch Dermatol Res* 291(7):367–373
6. Liu C, Wang W, Shen W, Chen T, Hu L, Chen Z (1997) Evaluation of the biocompatibility of a nonceramic hydroxyapatite. *J Endod* 23(8):490–493
7. Schmitz JP, Hollinger JO, Milam SB (1999) Reconstruction of bone using calcium phosphate bone cements: a critical review. *J Oral Maxillofac Surg* 57(9):1122–1126
8. Ambard AJ, Mueninghoff L (2006) Calcium phosphate cement: review of mechanical and biological properties. *J Prosthodont* 15(5):321–328
9. Weiss DD, Sachs MA, Woodard C (2003) Calcium phosphate bone cements: a comprehensive review. *J Long-Term Eff Med Implants* 13:41–47
10. Claes L, Hoellen I, Ignatius A (1997) Resorbable bone cements. *Orthopade* 26(5):459–462
11. Mirtchi AA, Lemaître J, Munting E (1989) Calcium phosphate cements: action of setting regulators on the properties of the beta-tricalcium phosphate-monocalcium phosphate cements. *Biomaterials* 10(7):475–480
12. Costantino PD, Friedman CD, Jones K, Chow LC, Pelzer HJ, Sr SG (1991) Hydroxyapatite cement I basic chemistry and histologic properties. *Arch Otolaryngol Head Neck Surg* 117(4):379–384
13. Hong YC, Wang JT, Hong CY, Brown WE, Chow LC (1991) The periapical tissue reactions to a calcium phosphate cement in the teeth of monkeys. *J Biomed Mater Res A* 25(4):485–498
14. Comuzzi L, Ooms E, Jansen JA (2002) Injectable calcium phosphate cement as a filler for bone defects around oral implants: an experimental study in goats. *Clin Oral Implants Res* 13(3):304–311
15. Shirakata Y, Oda S, Kinoshita A, Kikuchi S, Tsuchioka H, Ishikawa I (2002) Histocompatible healing of periodontal defects after application of an injectable calcium phosphate bone cement a preliminary study in dogs. *J Periodontol* 73(9):1043–1053
16. Sugawara A, Fujikawa K, Kusama K, Nishiyama M, Murai S, Takagi S, Chow LC (2002) Histopathologic reaction of a calcium phosphate cement for alveolar ridge augmentation. *J Biomed Mater Res* 61(1):47–52
17. Fujikawa K, Sugawara A, Kusama K, Nishiyama M, Murai S, Takagi S, Chow LC (2002) Fluorescent labeling analysis and electron probe microanalysis for alveolar ridge augmentation using calcium phosphate cement. *Dent Mater J* 21(4):296–305

18. Zhang W, Walboomers XF, Jansen JA (2008) The formation of tertiary dentin after pulp capping with a calcium phosphate cement, loaded with PLGA microparticles containing TGF-beta1. *J Biomed Mater Res A* 85(2):439–444
19. Tamimi F, Torres J, Lopezcarcos E, Bassett DC, Habibovic P, Luceron E, Barralet JE (2009) Minimally invasive maxillofacial vertical bone augmentation using brushite based cements. *Biomaterials* 30(2):208–216
20. Sugawara A, Chow LC, Takagi S, Chohayeb H (1990) In vitro evaluation of the sealing ability of a calcium phosphate cement when used as a root canal sealer-filler. *J Endod* 16(4):162–165
21. Noetzel J, Ozer K, Reissbauer BH, Anil A, Rossler R, Neumann K, Kielbassa AM (2006) Tissue responses to an experimental calcium phosphate cement and mineral trioxide aggregate as materials for furcation perforation repair: a histological study in dogs. *Clin Oral Investig* 10(1):77–83
22. Chaung HM, Hong CH, Chiang CP, Lin SK, Kuo YS, Lan WH, Hsieh CC (1996) Comparison of calcium phosphate cement mixture and pure calcium hydroxide as direct pulp-capping agents. *J Formos Med Assoc* 95(7):545–550
23. Dorozhkin SV (2008) Calcium orthophosphate cements for biomedical application. *J Mater Sci* 43(9):3028
24. Theiss F, Apelt D, Brand B, Kutter A, Zlinszky K, Bohner M, Matter S, Frei C, Auer JA, Rechenberg BV (2005) Biocompatibility and resorption of a brushite calcium phosphate cement. *Biomaterials* 26(21):4383–4394
25. Stallmann HP, Faber C, Bronckers AL, Nieuw Amerongen AV, Wuisman PI (2004) Osteomyelitis prevention in rabbits using antimicrobial peptide hLF1-11- or gentamicin-containing calcium phosphate cement. *J Antimicrob Chemother* 54(2):472–476
26. Chae SK, Kim HY, Lee HY, Lee CH, Seo KM (2003) Calcium phosphate artificial bone as osteoconductive and biodegradable bone substitute material, US Patent No. CA2401194A1
27. Silva RV, Camilli JA, Bertran CA, Moreira NH (2005) The use of hydroxyapatite and autogenous cancellous bone grafts to repair bone defects in rats. *Int J Oral Maxillofac Surg* 34(2):178–184
28. Yuan H, Li Y, de Bruijn JD, de Groot K, Zhang X (2000) Tissue responses of calcium phosphate cement: a study in dogs. *Biomaterials* 21(12):1283–1290
29. Friedman CD, Costantino PD, Takagi S, Chow LC (1998) BoneSource hydroxyapatite cement: a novel biomaterial for craniofacial skeletal tissue engineering and reconstruction. *J Biomed Mater Res* 43(4):428–432
30. Kuemmerle JM, Oberle A, Oechslin C, Bohner M, Frei C, Boecken I, Von RB (2005) Assessment of the suitability of a new brushite calcium phosphate cement for cranioplasty – an experimental study in sheep. *J Craniomaxillofac Surg* 33(1):37–44
31. Fortier S, Labelle D, Sina A, Moreau R, Annabi B (2000) Tissue reaction against a self-setting calcium phosphate cement set in bone or outside the organism. *J Mater Sci Mater Med* 11(12):811–815
32. Bifano CA, Edgin WA, Colleton C, Bifano SL, Constantino PD (1998) Preliminary evaluation of hydroxyapatite cement as an augmentation device in the edentulous atrophic canine mandible. *Oral Surg Oral Med Oral Pathol Oral Radiol Endod* 85(5):512–516
33. Friedman CD, Costantino PD, Synderman CH, Chow LC, Takagi S (2000) Reconstruction of the frontal sinus and frontofacial skeleton with hydroxyapatite cement. *Arch Facial Plast Surg* 2(2):124–129
34. Zeng D, Xia L, Zhang W, Huang H, Wei B, Huang Q, Wei J, Liu C, Jiang X (2012) Maxillary sinus floor elevation using a tissue-engineered bone with calcium-magnesium phosphate cement and bone marrow stromal cells in rabbits. *Tissue Eng Part A* 18(7–8):870–881
35. Losee JE, Karmacharya J, Gannon FH, Slemper AE, Ong G, Hunenko O, Gorden AD, Bartlett SP, Kirschner RE (2003) Reconstruction of the immature craniofacial skeleton with a carbonated calcium phosphate bone cement: interaction with bioresorbable mesh. *J Craniofac Surg* 14(1):117–124

36. Kim J, McBride S, Fulmer M, Harten R, Garza Z, Dean DD, Sylvia VL, Doll B, Wolfgang TL, Gruskin E, Hollinger JO (2012) Fiber-reinforced calcium phosphate cement formulations for cranioplasty applications: a 52-week duration preclinical rabbit calvaria study. *J Biomed Mater Res Part B, Appl Biomater* 100(4):1170–1178
37. Chen W, Xian L, Chen Q, Bao C, Liang Z, Zhu Z, Xu HHK (2017) Angiogenic and osteogenic regeneration in rats via calcium phosphate scaffold and endothelial cell coculture with hBM-SCs, hUCMSCs, hiPSC-MSCs and hESC-MSCs. *J Tissue Eng Regen Med*. doi:[10.1002/term.2395](https://doi.org/10.1002/term.2395)
38. Lee K, Weir MD, Lippens E, Mehta M, Wang P, Duda GN, Kim WS, Mooney DJ, Xu HH (2014) Bone regeneration via novel macroporous CPC scaffolds in critical-sized cranial defects in rats. *Dent Mater* 30(7):199–207
39. Shindo ML, Costantino PD, Friedman CD, Chow LC (1993) Facial skeletal augmentation using hydroxyapatite cement. *Arch Otolaryngol Head Neck Surg* 119(2):185–190
40. Vlad MD, del Valle LJ, Poeta I, Barracó M, López J, Torres R, Fernández E (2008) Injectable iron-modified apatitic bone cement intended for kyphoplasty: cytocompatibility study. *J Mater Sci Mater Med* 19(12):3575–3583
41. Foster KA, Shin SS, Prabhu B, Fredrickson A, Sekula RF Jr (2016) Calcium phosphate cement cranioplasty decreases the rate of cerebrospinal fluid leak and wound infection compared with titanium mesh cranioplasty: retrospective study of 672 patients. *World Neurosurg* 95:414–418
42. Afifi AM, Gordon CR, Pryor LS, Sweeney W, Papay FA, Zins JE (2010) Calcium phosphate cements in skull reconstruction: a meta-analysis. *Plast Reconstr Surg* 126(4):1300–1309
43. Klammert U, Gbureck U, Vorndran E, Rödiger J, Meyer-Marcotty P, Kübler AC (2010) 3D powder printed calcium phosphate implants for reconstruction of cranial and maxillofacial defects. *J Craniomaxillofac Surg* 38(8):565–570
44. Pan Z, Jiang P (2008) Assessment of the suitability of a new composite as a bone defect filler in a rabbit model. *J Tissue Eng Regen Med* 2(6):347–353
45. Thormann U, Ray S, Sommer U, Elkhassawna T, Rehling T, Hundgeburth M, Henß A, Rohnke M, Janek J, Lips KS (2013) Bone formation induced by strontium modified calcium phosphate cement in critical-size metaphyseal fracture defects in ovariectomized rats. *Biomaterials* 34(34):8589–8598
46. Seemun R (2014) Effects of strontium loaded calcium phosphate cement on osteoporotic fracture defect healing. Doctor Dissertation, Justus-Liebig-Universität Gießen
47. Elder S, Frankenburg E, Goulet J, Yetkinler D, Poser R, Goldstein S (2000) Biomechanical evaluation of calcium phosphate cement-augmented fixation of unstable intertrochanteric fractures. *J Orthop Trauma* 14(6):386–393
48. Yetkinler DN, Goodman SB, Reindel ES, Carter D, Poser RD, Constantz BR (2002) Mechanical evaluation of a carbonated apatite cement in the fixation of unstable intertrochanteric fractures. *Acta Orthop* 73(2):157–164
49. Mattsson P, Alberts A, Sohlman M, Dahlberg G, Hyldahl HC, Larsson S (2005) Resorbable cement for augmentation of internally fixed unstable trochanteric fractures: a prospective randomised multicenter study. *J Bone Joint Surg* 87(9):1203–1209
50. Mattsson P, Larsson S (2006) Calcium phosphate cement for augmentation did not improve results after internal fixation of displaced femoral neck fractures: a randomized study of 118 patients. *Acta Orthop* 77(2):251–256
51. Robinson CM, Page RS (2003) Severely impacted valgus proximal humeral fractures results of operative treatment. *J Bone Joint Surg Am* 85-A(9):1647–1655
52. Jupiter JB, Winters S, Sigman S, Lowe C, Pappas C, Ladd AL, Van WM, Smith ST (1997) Repair of five distal radius fractures with an investigational cancellous bone cement: a preliminary report. *J Orthop Trauma* 11(2):110–116
53. Sanchez-Sotelo J, Munuera L, Madero R (2000) Treatment of fractures of the distal radius with a remodelable bone cement: a prospective, randomised study using Norian SRS. *J Bone Joint Surg (Br)* 82(6):856–863

54. Kopylov P, Runnqvist K, Jonsson K, Aspenberg P (1999) Norian SRS versus external fixation in redisplaced distal radial fractures A randomized study in 40 patients. *Acta Orthop* 70(1):1–5
55. Ryf C, Goldhahn S, Radziejowski M, Blauth M, Hanson B (2009) A new injectable brushite cement: first results in distal radius and proximal tibia fractures. *Eur J Trauma Emerg Surg* 35(4):389–396
56. Schildhauer TA, Bauer TW, Josten C, Muhr G (2000) Open reduction and augmentation of internal fixation with an injectable skeletal cement for the treatment of complex calcaneal fractures. *J Orthop Trauma* 14(5):309–317
57. Thordarson DB, Bollinger M (2005) SRS cancellous bone cement augmentation of calcaneal fracture fixation. *Foot Ankle Int* 26(5):347–352
58. Yetkinler DN, McClellan RT, Reindel ES, Carter D, Poser RD (2001) Biomechanical comparison of conventional open reduction and internal fixation versus calcium phosphate cement fixation of a central depressed tibial plateau fracture. *J Orthop Trauma* 15(3):197–206
59. Mattsson P, Larsson S (2004) Unstable trochanteric fractures augmented with calcium phosphate cement A prospective randomized study using radiostereometry to measure fracture stability. *Scand J Surg SJS Off Organ Finn Surg Soc Scand Surg Soc* 93(3):223
60. Paxton JZ, Donnelly K, Keatch RP, Baar K, Grover LM (2010) Factors affecting the longevity and strength in an in vitro model of the bone-ligament interface. *Ann Biomed Eng* 38(6):2155–2166
61. Mehrban N, Paxton JZ, Bowen J, Bolarinwa A, Vorndran E, Gbureck U, Grover LM (2011) Comparing physicochemical properties of printed and hand cast bioceramics designed for ligament replacement. *Adv Appl Ceram* 110(3):162–167
62. Paxton JZ, Grover LM, Baar K (2010) Engineering an in vitro model of a functional ligament from bone to bone. *Tissue Eng Part A* 16(11):3515–3525
63. Landuyt PV, Peter B, Beluze L, Lemaître J (1999) Reinforcement of osteosynthesis screws with brushite cement. *Bone* 25(25):95S–98S
64. Liu ZG, Liu Y, Liu CS, Fu CF (2005) In vitro study of improving the strength of vertebral nail fixation via using CPC cement. *Chin J Bone Joint Inj* 20(9):614–616
65. Lewis G (2006) Injectable bone cements for use in vertebroplasty and kyphoplasty: state-of-the-art review. *J Biomed Mater Res* 76(2):456–468
66. Lim TH, Brebach GT, Renner SM, Kim WJ, Kim JG, Lee RE, Andersson GB, An HS (2002) Biomechanical evaluation of an injectable calcium phosphate cement for vertebroplasty. *Spine* 27(12):1297–1302
67. Belkoff SM, Mathis JM, Jasper LE, Deramond H (2001) An ex vivo biomechanical evaluation of a hydroxyapatite cement for use with vertebroplasty. *Spine* 26(26):1542–1546
68. Heini PF, Berlemann U, Kaufmann M, Lippuner K (2001) Augmentation of mechanical properties in osteoporotic vertebral bones – a biomechanical investigation of vertebroplasty efficacy with different bone cements. *Eur Spine J* 10(2):164–171
69. Tomita S, Kin A, Yazu M, Abe M (2003) Biomechanical evaluation of kyphoplasty and vertebroplasty with calcium phosphate cement in a simulated osteoporotic compression fracture. *J Orthop Sci* 8(2):192–197
70. Libicher M, Hillmeier J, Liegibel U, Sommer U, Pyerin W (2006) Osseous integration of calcium phosphate in osteoporotic vertebral fractures after kyphoplasty: initial results from a clinical and experimental pilot study. *Osteoporos Int* 17(8):1208–1215
71. Khanna AJ, Lee S, Villarraga M, Gimbel J, Steffey D, Schwardt J (2008) Biomechanical evaluation of kyphoplasty with calcium phosphate cement in a 2-functional spinal unit vertebral compression fracture model. *Spine J* 8(5):770–777
72. Turner TM, Urban RM, Singh K, Hall DJ, Renner SM, Lim TH, Tomlinson MJ, An HS (2008) Vertebroplasty comparing injectable calcium phosphate cement compared with polymethylmethacrylate in a unique canine vertebral body large defect model. *Spine J* 8(3):482–487

73. Nakano M, Hirano N, Zukawa M, Suzuki K, Hirose J, Kimura T, Kawaguchi Y (2012) Vertebroplasty using calcium phosphate cement for osteoporotic vertebral fractures: study of outcomes at a minimum follow-up of two years. *Asian Spine J* 6(1):34–42
74. Ishiguro S, Kasai Y, Sudo A, Iida K, Uchida A (2010) Percutaneous vertebroplasty for osteoporotic compression fractures using calcium phosphate cement. *J Orthop Surg* 18(3):346–351
75. Kasperk C, Hillmeier J, Nöldge G, Grafe IA, Dafonseca K, Raupp D, Bardenheuer H, Libicher M, Liegibel UM, Sommer U (2005) Treatment of painful vertebral fractures by kyphoplasty in patients with primary osteoporosis: a prospective nonrandomized controlled study. *J Bone Miner Res* 20(4):604–612
76. Schmidt R, Cakir B, Mattes T, Wegener M, Puhl W, Richter M (2005) Cement leakage during vertebroplasty: an underestimated problem? *Eur Spine J* 14(5):466–473
77. Krebs J, Aebli N, Goss BG, Sugiyama S, Bardyn T, Boecken I, Leamy PJ, Ferguson SJ (2007) Cardiovascular changes after pulmonary embolism from injecting calcium phosphate cement. *J Biomed Mater Res B Appl Biomater* 82(2):526–532
78. Liverneaux P, Khallouk R (2006) Calcium phosphate cement in wrist arthrodesis: three cases. *J Orthop Sci* 11(3):289–293
79. Mermelstein LE, McLain RF, Yerby SA (1998) Reinforcement of thoracolumbar burst fractures with calcium phosphate cement. *Spine* 23(6):664–670
80. Moore DC, Maitra RS, Farjo LA, Graziano GP, Goldstein SA (1997) Restoration of pedicle screw fixation with an in situ setting calcium phosphate cement. *Spine* 22(15):1696–1705
81. Hisatome T, Yasunaga Y, Ikuta Y, Fujimoto Y (2002) Effects on articular cartilage of subchondral replacement with polymethylmethacrylate and calcium phosphate cement. *J Biomed Mater Res A* 59(3):490–498
82. Ginebra MP, Traykova T, Planell JA (2006) Calcium phosphate cements: competitive drug carriers for the musculoskeletal system? *Biomaterials* 27(10):2171–2177
83. Ginebra MP, Traykova T, Planell JA (2006) Calcium phosphate cements as bone drug delivery systems: a review. *J Control Release* 113(2):102–110
84. Fei Z, Hu Y, Wu D, Wu H, Lu R, Bai J, Song H (2008) Preparation and property of a novel bone graft composite consisting of rhBMP-2 loaded PLGA microspheres and calcium phosphate cement. *J Mater Sci Mater Med* 19(3):1109–1116
85. Ruhé PQ, Kroese-Deutman HC, Wolke JG, Spauwen PH, Jansen JA (2004) Bone inductive properties of rhBMP-2 loaded porous calcium phosphate cement implants in cranial defects in rabbits. *Biomaterials* 25(11):2123–2132
86. Bodde EWH, Boerman OC, Russel FGM, Mikos AG, Spauwen PHM, Jansen JA (2008) The kinetic and biological activity of different loaded rhBMP-2 calcium phosphate cement implants in rats. *J Biomed Mater Res A* 87(3):780–791
87. Perrier M, Yan LU, Nemke B, Kobayashi H, Peterson A, Markel M (2008) Acceleration of second and fourth metatarsal fracture healing with recombinant human bone morphogenetic protein-2/calcium phosphate cement in horses. *Vet Surg* 37(7):648–655
88. Li DX, Fan HS, Zhu XD, Tan YF, Xiao WQ, Lu J, Xiao YM, Chen JY, Zhang XD (2007) Controllable release of salmon-calcitonin in injectable calcium phosphate cement modified by chitosan oligosaccharide and collagen polypeptide. *J Mater Sci Mater Med* 18(11):2225–2231
89. Le ND, Hacking SA, Gbureck U, Komarova SV, Barralet JE (2008) The use of RANKL-coated brushite cement to stimulate bone remodelling. *Biomaterials* 29(22):3253–3259
90. Otsuka M, Matsuda Y, Suwa Y, Fox JL, Higuchi WI (1994) A novel skeletal drug delivery system using self-setting calcium phosphate cement 2 physicochemical properties and drug release rate of the cement-containing indomethacin. *J Pharm Sci* 83(5):611–615
91. Panzavolta S, Torricelli P, Bracci B, Fini M, Bigi A (2009) Alendronate and Pamidronate calcium phosphate bone cements: setting properties and in vitro response of osteoblast and osteoclast cells. *J Inorg Biochem* 103(1):101–106
92. Otsuka M, Matsuda Y, Suwa Y, Fox JL, Higuchi WI (1994) A novel skeletal drug delivery system using a self-setting calcium phosphate cement 5 drug release behavior from a heterogeneous drug-loaded cement containing an anticancer drug. *J Pharm Sci* 83(11):1565–1568

93. Yu D, Wong J, Matsuda Y, Fox JL, Higuchi WI, Otsuka M (1992) Self-setting hydroxyapatite cement: a novel skeletal drug-delivery system for antibiotics. *J Pharm Sci* 81(6):529–531
94. Bohner M, Lemaître J, Landuyt PV, Zambelli PY, Merkle HP, Gander B (1997) Gentamicin-loaded hydraulic calcium phosphate bone cement as antibiotic delivery system. *J Pharm Sci* 86(5):565–572
95. Bohner M, Lemaître J, Merkle HP, Gander B (2000) Control of gentamicin release from a calcium phosphate cement by admixed poly(acrylic acid). *J Pharm Sci* 89(10):1262–1270
96. Ratier A, Freche M, Lacout JL, Rodriguez F (2004) Behavior of an injectable calcium phosphate cement with added tetracycline. *Int J Pharm* 274(1–2):261–268
97. Kisanuki O, Yajima H, Umeda T, Takakura Y (2007) Experimental study of calcium phosphate cement impregnated with dideoxy-kanamycin B. *J Orthop Sci* 12(3):281–288
98. McNally A, Sly K, Lin S, Bourges X, Daculsi G (2008) Release of antibiotics from macroporous injectable calcium phosphate cement. *Key Eng Mater* 361–363:359–962
99. Hofmann MP, Mohammed AR, Perrie Y, Gbureck U, Barralet JE (2009) High-strength resorbable brushite bone cement with controlled drug-releasing capabilities. *Acta Biomater* 5(1):43–49
100. Faleh T, Jesús T, Ruggero B, Francesca R, Carmen R, Manuel LP, Enrique LC (2008) Doxycycline sustained release from brushite cements for the treatment of periodontal diseases. *J Biomed Mater Res A* 85(3):707–714
101. Young AM, Ng PYJ, Gbureck U, Nazhat SN, Barralet JE, Hofmann MP (2008) Characterization of chlorhexidine-releasing, fast-setting, brushite bone cements. *Acta Biomater* 4(4):1081–1088
102. Hesaraki S, Nemati R (2009) Cephalexin-loaded injectable macroporous calcium phosphate bone cement. *J Biomed Mater Res B Appl Biomater* 89(2):342–352
103. Otsuka M, Matsuda Y, Suwa Y, Fox JL, Higuchi WI (1994) A novel skeletal drug-delivery system using self-setting calcium phosphate cement 3 physicochemical properties and drug-release rate of bovine insulin and bovine albumin. *J Pharm Sci* 83(2):255–258
104. Pasquier G, Lemaitre J, Flautre B, Ikenaga M, Hardouin P (1998) Development of a bone defect model for testing injectable bone substitutes and evaluation of a calcium phosphate cement. *Bull Acad Nat Méd* 182(9):1851–1865
105. López SP, López-Ruiz B (2011) A sensitive glucose biosensor based on brushite, a biocompatible cement. *Electroanalysis* 23(1):280–286
106. Sánchezpaniagua LM, Tamimi F, Lópezcabarcos E, Lópezruiz B (2009) Highly sensitive amperometric biosensor based on a biocompatible calcium phosphate cement. *Biosens Bioelectron* 24(8):2574–2579